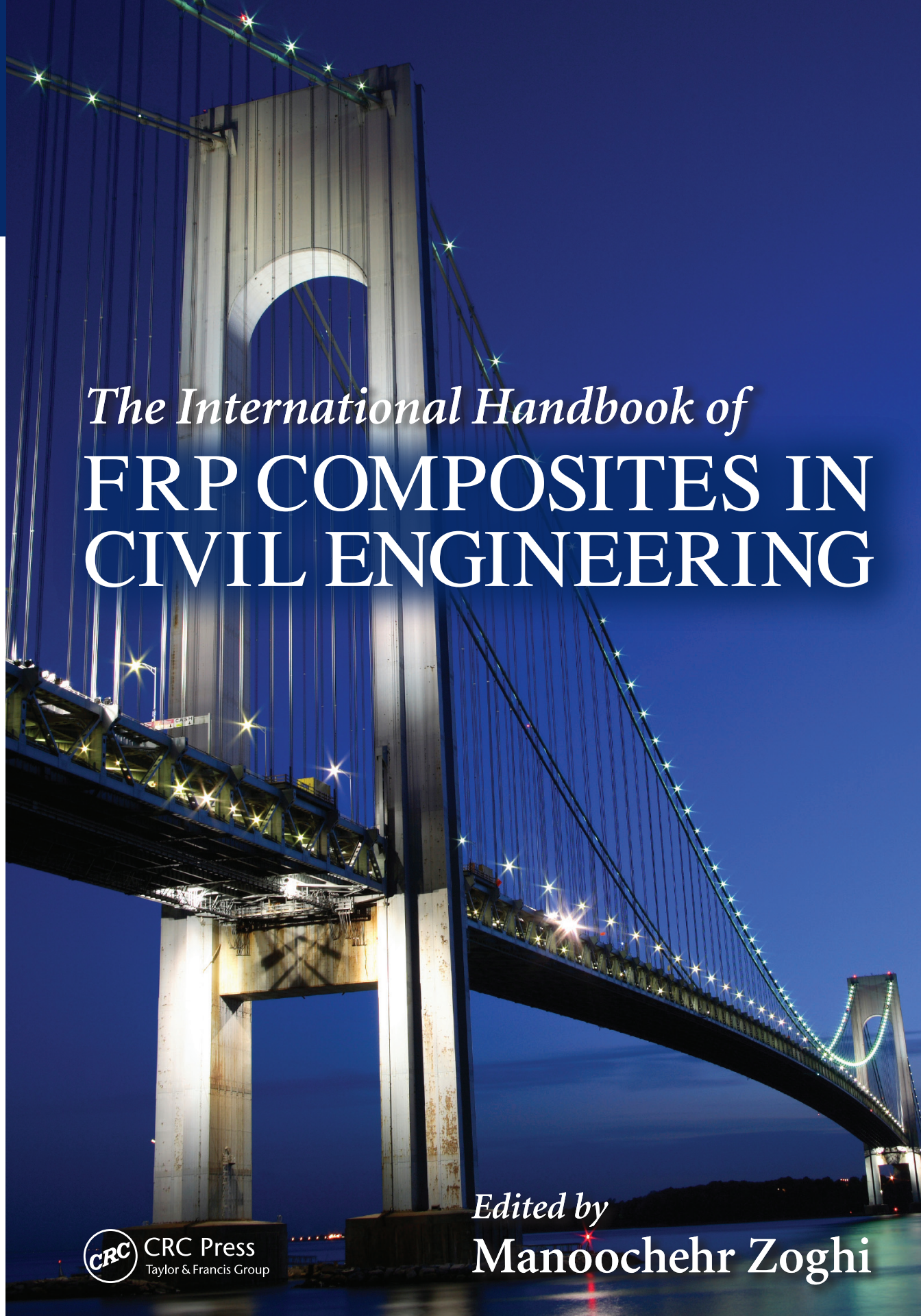
The International Handbook of
FRP COMPOSITES IN CIVIL ENGINEERING
Edited by
Manoochehr Zoghi
CRC Press
Taylor & Francis Group

The International Handbook of

FRP COMPOSITES IN CIVIL ENGINEERING

The International Handbook of

FRP COMPOSITES IN CIVIL ENGINEERING

Edited by

Manoochehr Zoghi

CRC Press
Taylor & Francis Group
Boca Raton London New York

CRC Press is an imprint of the
Taylor & Francis Group, an **informa** business

CRC Press
Taylor & Francis Group
6000 Broken Sound Parkway NW, Suite 300
Boca Raton, FL 33487-2742

Version Date: 20130906

International Standard Book Number-13: 978-1-4200-0374-1 (eBook - PDF)

In memory of my father and two brothers

and

To my beloved mother,
who has been a guiding light and has continuously given me
hope, courage, and unconditional love throughout my life

and

To my dearest wife and our two wonderful sons, Shayan
and Shervin, the true gifts of our lives

Everything should be made as simple as possible, but not simpler

Einstein

Contents

PART VII Glossary

Robert L. Sierakowski

Foreword

In the very long history of civil construction, the idea of combining two or more different materials resulting in a new material with improved properties has fascinated mankind. Giant grain silos and tubes for water pipelines and aggressive wastewater were some of the first important practical applications of fiber-reinforced polymer (FRP) in the 1970s. The practical knowledge for the design, fabrication, and construction of FRP was passed over generations from old experienced masters to their apprentices in a similar manner to the knowledge transferred by master builders of huge cathedrals in the Middle Ages. This knowledge was considered top secret, and there were no written documents available. This trend changed, however, in the ensuing decades. Some companies delivering raw material, like E-glass or unsaturated polyester resins, started to write recommendations and specifications for the use of their products. However, most of these documents were very limited in scope.

In the 1980s, composite bridges, tendons, stays, reinforcing bars, and poststrengthening components made of FRP were envisioned, and in the following decade research about such topics increased manifold. Thousands of publications related to FRP in civil constructions appeared, making it difficult for researchers and practitioners to have an overview and to use this valuable but widespread information in their daily work.

In the twenty-first century, advanced FRP composite materials will witness steady and widespread growth in the civil infrastructure arena. The recent launch of new design codes and the development of new products for civil construction will create new opportunities for the composite industry. Advanced FRP composite materials are poised to become an integral part of civil infrastructure, especially in relation to the concrete repair and reinforcement and seismic retrofit, bridge deck repair and new installation, composite-hybrid technology, piling products and systems for marine waterfront structures, and sustainable, energy-efficient housing. The latest development in nearly all aspects of FRP composites, their applications in civil engineering, and state-of-the-art technologies for nondestructive evaluation and structural health monitoring of FRP have been expounded in this comprehensive book, which is the result of collaboration among top experts from around the world.

The civil and FRP engineering communities should be very thankful to the editor in chief, Prof. Dr. Manoochehr Zoghi, the coeditors, and all the authors for their outstanding work. The famous French writer and aviator Antoine de Saint-Exupéry wrote: “As for the future, your task is not to foresee it, but to enable it.” This book will enable FRP in civil engineering and lead it to a very bright future.

Prof. Dr. h.c. Urs Meier
EMPA
Swiss Federal Laboratories for Materials Science and Technology

Preface

In 2008, the National Academy of Engineering identified 14 grand challenges of the twenty-first century for engineering. The grand challenges address complex social issues that affect our quality of life, which require innovative and systematic approaches to solve (NAE, 2008). One of the 14 grand challenges is to restore and improve urban infrastructure. It is widely known that America's infrastructure, along with those of many other countries, has been on the brink of crisis. Engineers of the twenty-first century face the formidable challenge of revitalizing the aging infrastructure in view of insufficient funding. The American Society of Civil Engineers (ASCE) has given an overall grade of "D+" to U.S. infrastructure (ASCE, 2013a). In its most recent report, "Failure to act: The impact of current infrastructure investment on America's economic future," ASCE stated that if infrastructure investment remains at current levels, the nation will face losses of $3.1 trillion in gross domestic product (GDP) and $1.1 trillion in trade by the year 2020, costing the average household $3100 per year in disposable income (ASCE, 2013b). Concerning raising the grades, ASCE recommends the following five key solutions: (1) increase federal leadership; (2) promote sustainability and resilience; (3) develop federal, regional, and state infrastructure plans; (4) address life-cycle costs (LCCs) and ongoing maintenance; and (5) increase and improve infrastructure investment from all stakeholders (ASCE, 2013a).

Clearly, infrastructure renewals that are based on the same practices, processes, technologies, and materials that were developed and employed in the twentieth century will most likely yield the same results (NRC, 2009). These involve familiar long-standing incidences of service disruptions, increased operating and repair costs, and catastrophic failures such as Minnesota's I-35W Bridge collapse. To paraphrase Albert Einstein, "we can't solve problems by using the same kind of thinking we used when we created them." To implement the five key solutions stated earlier, a new paradigm for the renewal of critical infrastructure systems is needed, which is efficient, reliable, and cost effective.

Extensive research has yielded innovative technologies and materials that could prolong and extend service lives of existing infrastructure while providing opportunities for the design and construction of highly durable new structures. Today, new technologies are available that enable monitoring the condition and performance of infrastructure systems, while self-diagnosing, self-healing, and self-repairing systems can be designed to afford greater resiliency, fewer long-term service disruptions, and lower LCCs of infrastructure systems (Amin and Stringer, 2008).

Fiber-reinforced polymer (FRP) composite technology, developed primarily for the aerospace, defense, and marine industries, possesses many of the features mentioned earlier for infrastructure applications. Christened "the materials of the twenty-first century," the application of FRP composite technology has resulted in a paradigm shift in material usage due to its inherent superior properties. The numerous advantages of FRP composites over conventional construction materials such as steel, concrete, and wood are well known. There have been myriad successful applications of FRP composites for repairing and retrofitting existing infrastructure systems as well as for new construction over the last three decades. FRP composites are no longer considered the "space-age" structures used exclusively for stealth bombers or space shuttles (ACMA, 2004). They have become an integral part of the construction industry because of their versatility, enhanced durability and fatigue characteristics, noncorrosiveness, high strength-to-weight ratio, accelerated construction feature, lower maintenance, and LCCs. Many more composite products are being actively developed and are emerging for civil infrastructure applications, which is considered to be potentially the largest market for FRP composites (ACMA, 2004). There have been a number of professional organizations and technical committees worldwide involved in developing and preparing codes,

standards, test methods, and specifications regarding FRP composites for construction. In addition, there are a variety of regional, national, and international conferences and trade exhibitions organized regularly that cover all aspects of FRP composites for construction and showcase new ideas and innovations, emerging technologies, best practices, and case studies. It is the goal of this handbook to capture important features of FRP composites, in relation to civil infrastructure applications, in a single volume.

This handbook is not intended to serve as a textbook. There have been several outstanding textbooks published such as Barbero (2011), Bank (2006), and Hollaway and Head (2001). By and large, the mission of *The International Handbook of FRP Composites in Civil Engineering* is to provide a single, comprehensive, ready-to-use reference source for the practicing engineer to keep abreast of advances in materials, techniques, practices, and structural health monitoring (SHM) of FRP composites in civil infrastructure. The main focus is on professional applications, including design formulas, tables, and charts that could provide immediate answers to questions from practical work. This handbook will also provide an invaluable reference for undergraduate and graduate students, researchers, and seasoned professionals. Although the primary audience will be the civil engineering community, other engineering disciplines including architectural, materials, and aerospace engineering will benefit from this single-volume source as well. The state-of-the-practice information that are presented herein will be useful for manufacturers and suppliers of high-performance fiber-reinforced polymer composites as well as for engineering firms, the construction industry, and state departments of transportation.

This handbook is divided into seven parts. Each part, including multiple chapters, focuses on different aspect and/or application of FRP composites. Part I, "Composites Primer," is intended to provide a brief overview of FRP, comprising historical perspective, codes and standards, manufacturing processes, constituent materials, mechanics of composite materials, and LCCs. Historically, FRP composite has not been a required course as part of the undergraduate civil engineering curriculum. Thus, the majority of practicing civil engineers have not had any background in composites. The aim of this part is to bridge this gap and to provide a basic understanding of the fundamentals of FRP composites in relation to civil infrastructure applications. In addition, a brief introduction concerning the LCC, along with sustainability and environmental implications of FRP composites, has been provided herein.

FRP composite modular bridge decks offer viable alternative solutions to conventional materials such as reinforced concrete and steel bridges, which are prone to corrosion. FRP decks have intrinsic characteristics that enable them to be suitable for the Federal Highway Administration's (FHWA's) "Bridge of the Future" program (FHWA, 2013). Their primary benefits include durability (i.e., highly resistant to corrosion and fatigue), lightweight, high strength, rapid installation, lower or competitive LCC, and high-quality manufacturing processes under controlled environments (ACMA, 2004, 2013). In recent years, there have been numerous successful bridge deck installations worldwide utilizing FRP composites. The main focus of Part II, "All-Composite Structures and Components," is to present an overview of bridge deck applications along with several case studies. There is also a chapter dedicated to the critical topic of connection design for FRP structural members.

Chapters in Part III, "Externally Bonded FRP Composite Systems for Rehabilitation," deal with external reinforcement for rehabilitation, unstressed and prestressed flexural and shear strengthening of reinforced concrete structures, unstressed and prestressed near surface mounted reinforcement, confinement of concrete columns, strengthening of masonry, wood and metallic structures, and durability issues. In addition, several numerical examples are included to demonstrate the design procedure for each case.

Part IV, "FRP Composites for Reinforcement of Concrete Structures," focuses on FRP composites, which has been growing rapidly in recent years. In addition to material characteristics, design procedures, codes and standards, and state of the practice related to the internal reinforcement for concrete columns as well as FRP prestressed concrete applications have been discussed

in detail. Furthermore, specific durability issues along with quality assurance–quality control (QA/QC) issues have been discussed.

Part V, "Hybrid FRP Composite Systems," presents the topic of FRP composite hybrid systems, with an emphasis on design considerations of axial, flexural, and axial–flexural hybrid members. In addition, construction considerations along with QA/QC and repair of hybrid structures have been discussed. Several relevant examples and case studies are also included.

Part VI, "Nondestructive Testing and Evaluation," elaborates on the applications of nondestructive testing and evaluation for SHM of FRP composites. In order to assure the structural integrity and long-term reliability of structures retrofitted via FRP composites, it is critical to identify any potential defects during and following the application of FRP throughout the structure's service life. State-of-the-art technologies for nondestructive evaluation and SHM are expounded in this part. The case studies specifically refer to bridge engineering applications. Moreover, an entire chapter is devoted to the important topic of smart composites. Smart materials can actively sense, respond, and occasionally control the environment and internal states. The chapter provides up-to-date information as it relates to FRP composites.

Finally, Part VII, "Glossary," includes several appendices involving lists of FRP-related books, journals, conference proceedings and symposiums, organizations, and typical research papers in selected areas.

The impetus for this handbook originated several years ago when I was involved in a couple of FRP-related bridge research projects. One of the projects was sponsored by the FHWA through the Innovative Bridge Research and Construction (IBRC) initiative and administered by the Office of Bridge Technology, Infrastructure Core Business Unit. The IBRC initiative promotes the use of innovative materials and materials technologies in bridge applications (FHWA, 2013). As part of this program, two severely deteriorated long-span, precast, prestressed concrete box girder bridges were strengthened utilizing advanced carbon fiber–reinforced polymer (CFRP) composite strips, post-tensioned via the stress head system that was developed and patented in Switzerland (Zoghi et al., 2006). SHM and a series of full-scale live-load tests were also incorporated in the rehabilitation plan. The technique, the first of its type in the United States, entailed a collaboration between government, academia, and industry from the United States and Switzerland. As the principal investigator (PI) of the project, I recognized the need for a single-volume source throughout the design, construction, nondestructive testing and evaluation, and SHM stages.

The second project that was the impetus for the publication of this handbook was in relation to an all-composite vehicular bridge constructed in July 1997, rechristened Tech 21 (BCEO, 2001). The two-lane, short-span bridge deck, supported on three trapezoidal beams fabricated using E-glass fibers with polyester resin, was manufactured utilizing sandwich configuration with a center core made by bonding orthotropic fiberglass and polyester tubes (Zoghi et al, 2003). Tech 21, the third all-composite vehicular bridge and first fully instrumented of its type in the United States comprised of an extensive health-monitoring system installed during its fabrication. The structure was designed and manufactured by Martin Marietta Materials, Inc. This project was also a joint venture between government, industry, and academia. Intimately involved in various aspects of the research, including durability study, finite-element modeling, full-scale live-load testing, and structural health monitoring, I became aware of the lack of a comprehensive yet quick reference handbook that would provide answers to pertinent practical questions.

Evidently, the idea of a need for *The International Handbook of FRP Composites in Civil Engineering* was born through preceding personal experiences and international collaboration. From the inception of the project, the editors of CRC Press, Michael Slaughter (executive commissioning editor), Allison Shatkin (senior commissioning editor), and Theresa Gutierrez (editorial project development), wholeheartedly embraced the proposal and have since provided their unwavering support throughout this very long process. Their continued support is greatly appreciated. Also, Amy Blalock (project coordinator), Robert Sims (project editor), and Mythili Gopi (project manager) and their associates worked diligently to bring this handbook to realization. I am forever grateful to them for their hard work and dedication.

Paraphrasing Sir Isaac Newton, "If I have seen further it is by standing on the shoulders of giants." This is indeed the case regarding the publication of the present handbook. The editorship of each individual part was carried out by the designated associate editor(s), who administered the tasks of recruiting respective authors to prepare chapters and adhere to publication guidelines and deadlines, along with completion of the review process. In addition, several associate editors drafted numerous chapters in their respective parts. I would like to express my appreciation to all the associate editors and authors for preparing the highest quality manuscripts that constitute the crux of this handbook and for their invaluable contributions and commitment. Finally, my heartfelt gratitude to my family for their continued support and encouragement.

Manoochehr Zoghi
Fresno, California

REFERENCES

ACMA, 2004, Why use FRP composites? http://www.mdacomposites.org/mda/why_frp.html (accessed on January 10, 2013).

ACMA, 2013, http://www.acmanet.org/ (accessed on January 10, 2013).

Amin, M. and Stringer, J., 2008, The electric power grid: Today and tomorrow, *MRS Bulletin*, vol. 33. www. mrs.org/bulletin (accessed on January 15, 2013).

ASCE (American Society of Civil Engineers), 2013a, ASCE report card for America's infrastructure. http://www.infrastructurereportcard.org/ (accessed on March 29, 2013).

ASCE (American Society of Civil Engineers), 2013b, Failure to act: The impact of current infrastructure investment on America's economic future. http://www.asce.org/economicstudy/ (accessed on January 10, 2013).

Bank, L.C., 2006, *Composites for Construction: Structural Design with FRP Materials*, John Wiley & Sons, Inc., Hoboken, NJ, 551pp.

Barbero, E.J., 2011, *Introduction to Composite Materials Design,* 2nd edn., CRC Press, Taylor & Francis Group, Boca Raton, FL, 520pp.

BCEO (Butler County Engineer's Office), 2001, Technology—A composite bridge; Ohio's 1st all-composite bridge. http://www.bceo.org/technology.html (accessed on March 12, 2001).

FHWA—Extra! http://www.fhwa.dot.gov/bridge/frp/frp1298.cfm

FHWA (Federal Highway Administration), 2013, Fiber reinforced polymer composite bridge technology, Current practice, http://www.fhwa.dot.gov/bridge/frp/frppract.cfm (accessed on January 15, 2013).

Hollaway, L.C. and Head, P.R., 2001, *Advanced Polymer Composites and Polymers in the Civil Infrastructure*, Elsevier, Amsterdam, the Netherlands, 336pp.

National Academy of Engineering, Grand Challenges for Engineering, 2008. http://www.engineeringchallenges.org/ (accessed on January 15, 2013).

NRC (National Research Council), 2009, *Sustainable Critical Infrastructure Systems—A Framework for Meeting 21st Century Imperatives*, The National Academies Press, Washington, DC. www.nap.edu (accessed on January 12, 2013).

Zoghi, M. and Bowman, D.R., 2003, Structural health monitoring of the tech 21 all-composite vehicular bridge, Final Report, 14716-FR, Submitted to the Ohio Department of Transportation, March 2003.

Zoghi, M. and Foster, D.C., 2006, Post-strengthening prestressed concrete bridges via post-tensioned CFRP laminates, *SAMPE Journal*, Infrastructure/Civil Engineering Technology Issue, March/April 2006.

Editor

Manoochehr Zoghi, a registered professional engineer, received his bachelor of science and master of engineering degrees in civil engineering from the J.B. Speed School of Engineering at the University of Louisville, Kentucky, in 1979 and 1981, respectively. He received a doctor of philosophy in civil engineering from the School of Advanced Structures at the University of Cincinnati, Ohio, in 1988. He is currently pursuing his MBA in sustainability from San Francisco Institute of Architecture.

Dr. Zoghi has had extensive academic, administrative, and consulting experiences. He has served as a faculty and the graduate program director of the Department of Civil and Environmental Engineering and Engineering Mechanics at the University of Dayton; founding chair and professor of the Department of Civil and Environmental Engineering at Idaho State University; interim chair of the Department of Mechanical Engineering at California State University (CSU), Fresno; and is currently the associate dean and professor of the Lyles College of Engineering at CSU, Fresno. Prior to joining the academe, he worked as a structural engineer for a consulting firm of Lockwood, Jones and Beals, Inc., in Dayton, Ohio, where he was instrumental in research and development of the patented CON/SPAN® Bridge Systems.

Professor Zoghi has taught a wide variety of civil engineering, engineering mechanics, and construction management courses and has conducted research in interdisciplinary areas of infrastructure revitalization, nondestructive evaluation and structural health monitoring, soil–structure interaction, geohazards, and geotechnical engineering. He has received numerous awards for his teaching, research, and community service, including the Ohio Society of Professional Engineers' Outstanding Engineering Educator Award and the International Concrete Repair Institute's Award of Excellence in the transportation category for his collaborative bridge repair and rehabilitation project, sponsored through the Federal Highway Administration's Innovative Bridge Research and Construction program.

A fellow of the American Society of Civil Engineers, a Coleman Fellow, and a diplomate of geotechnical engineering, Professor Zoghi has been cited in several who's who indexes and is a Golden Key International honorary member. He is a member of the American Society of Engineering Education, past president of the ASCE-Dayton Section, and an ABET (Accreditation Board for Engineering and Technology, Inc.) program evaluator (PEV). He also serves on multiple national technical committees as well as the Board of Trustees of the California Homebuilding Foundation.

A prolific author, Dr. Zoghi has published widely. He serves as an associate editor of the ASCE's *Journal of Materials in Civil Engineering*, an associate editor of the ASCE's *Journal of Professional Issues in Engineering Education and Practice*, and is an editorial advisory panel member of the UK's Institution of Civil Engineers' flagship journal.

Contributors

Sreenivas Alampalli
Structures Evaluation Services Bureau
New York State Department of Transportation
Albany, New York

Brahim Benmokrane
Department of Civil Engineering
University of Sherbrooke
Sherbrooke, Quebec, Canada

Luke A. Bisby
Institute for Infrastructure and Environment
School of Engineering
University of Edinburgh
Edinburgh, United Kingdom

Alexander Bogdanovich
College of Textiles
North Carolina State University
Raleigh, North Carolina

Lee Canning
Sinclair Knight Mertz
Salford, United Kingdom

Yi Chen
Shaffer, Wilson, Sarver & Gray
Reston, Virginia

Lijuan "Dawn" Cheng
Department of Civil Engineering Technology
University of California, Davis
Davis, California

Ching Chiaw Choo
Department of Civil and Geomatics Engineering
California State University
Fresno, California

Christoph Czaderski
Empa—Swiss Federal Laboratories for Materials Science and Technology
Duebendorf, Switzerland

Julio F. Davalos
Department of Civil Engineering
The City College of New York
New York

Arya Ebrahimpour
Department of Civil and Environmental Engineering
College of Science and Engineering
Idaho State University
Pocatello, Idaho

Ehab El-Salakawy
Department of Civil Engineering
University of Manitoba
Winnipeg, Manitoba, Canada

Ahmed K. El-Sayed
Department of Civil Engineering
King Saud University
Riyadh, Saudi Arabia

Hector Estrada
Department of Civil Engineering
School of Engineering and Computer Science
University of the Pacific
Stockton, California

Mohammed M. Ettouney
Weidlinger Associates, Inc.
New York

Amir Fam
Department of Civil Engineering
Queen's University
Kingston, Ontario, Canada

Nestore Galati
Structural Technologies
Elkridge, Maryland

Hota GangaRao
College of Engineering and Mineral Resources
West Virginia University
Morgantown, West Virginia

Kumar K. Ghosh
California Department of Transportation
Diamond Bar, California

Osman Hag-Elsafi
Consultant
Fort Lauderdale, Florida

Issam Harik
Kentucky Transportation Center
College of Engineering
University of Kentucky
Lexington, Kentucky

Andrin Herwig
Empa—Swiss Federal Laboratories for Materials Science and Technology
Duebendorf, Switzerland

Clem Hiel
Composite Support & Solutions Inc.
San Pedro, California

Dryver R. Huston
Department of Mechanical Engineering
University of Vermont
Burlington, Vermont

Kerstin Lang
Baudirektion Kanton Zürich
Zürich, Switzerland

Luke S. Lee
Department of Civil Engineering
School of Engineering and Computer Science
University of the Pacific
Stockton, California

Stijn Matthys
Magnel Laboratory for Concrete Research
Department of Structural Engineering
Ghent University
Ghent, Belgium

Amir Mirmiran
College of Engineering and Computing
Florida International University
Miami, Florida

Masoud Motavalli
Structural Engineering Laboratory
Empa—Swiss Federal Laboratories for Materials Science and Technology
Duebendorf, Switzerland

Pedram Sadeghian
Civil Engineering Program
School of Science, Engineering, and Technology
Pennsylvania State University, Harrisburg
Middletown, Pennsylvania

Marco P. Schoen
Department of Mechanical Engineering
College of Science and Engineering
Idaho State University
Pocatello, Idaho

Ann Schumacher
dsp Ingenieure & Planer
Greifensee, Switzerland

Robert L. Sierakowski
Air Force Research Laboratory
Eglin Air Force Base, Florida

Khaled Soudki
Department of Civil Engineering
University of Waterloo
Waterloo, Ontario, Canada

Gustavo Tumialan
Simpson Gumpertz & Heger, Inc.
Boston, Massachusetts

Glenn A. Washer
Department of Civil and Environmental Engineering
University of Missouri, Columbia
Columbia, Missouri

Brea Williams
Department of Civil Engineering Technology
Red River College
Winnipeg, Manitoba, Canada

Lei Zhao
Alabama Metal Industries Corporation
Gibraltar Industries
Birmingham, Alabama

Aixi Zhou
Department of Engineering Technology
University of North Carolina at Charlotte
Charlotte, North Carolina

Olesya I. Zhupanska
Department of Mechanical and Industrial Engineering
Center for Computer-Aided Design
University of Iowa
Iowa City, Iowa

Paul Ziehl
Department of Civil and Environmental Engineering
University of South Carolina
Columbia, South Carolina

Part I

Composites Primer

Luke S. Lee and Hector Estrada

1 Introduction

Hota GangaRao

CONTENTS

HISTORIC PERSPECTIVE

Fiber-reinforced polymer (FRP) composites are composed of at least two constituent materials differing in terms of thermomechanical properties, with combined properties engineered to be superior to the constituent materials. A key feature of composites is that the constituent materials remain separate and distinct in the final product, that is, the reinforcement (generally a fibrous material) remains distinct from the matrix (a resin generally in the form of a polymer), which helps bond fibers, fabrics or fibrous particulates.

The history of FRP composites can be traced back thousands of years to Mesopotamia (present-day Iraq), including the use of mud and straw in bricks and asphaltic bonded copper sheets and decorated inlays set with natural resins. Halfway into the second millennium, decorative pieces made of cloisonnes (a kind of enamel decoration) were produced in Asia and Europe. All the aforementioned have one important thing in common, that is, they were made with at least two distinctly different constituent materials combined into one final product of improved performance. Even thousands of years ago, organic polymers from tree and plant secretions, fossilized resins, bituminous materials and those prepared from fish and animal offal were used in practice (Seymour and Deanin, 1986).

As the knowledgebase kept expanding, fine copper wires were most prevalent and even gold alloy filaments have been used effectively coupled with polymeric fibers such as silk for decorative purposes. Textiles and metal fibers woven as fabrics have been preserved under dry conditions for thousands of years (Sinopoli, 2003). Cotton, wool, and linen are natural organic fibers that have been decorated with fine gold threads as has been utilized in India. The inclusions of metallic wires to reinforce nonmetallic applications are many. For example, decorative organic plastic and paper pulp were used to make canes and umbrella handles in the late nineteenth century in Europe (Seymour and Deanin, 1986).

Sophisticated applications of composites have been identified in nature from time immemorial, and man-made composite applications such as straw-reinforced adobe or brick in Tulou houses of

FIGURE 1.1 Tulou house. (From Liang, R. et al., SGER: Material and structural response of historic Hakka rammed earth structures, Final Report No. 0908199, National Science Foundation, Morgantown, WV, 2011.)

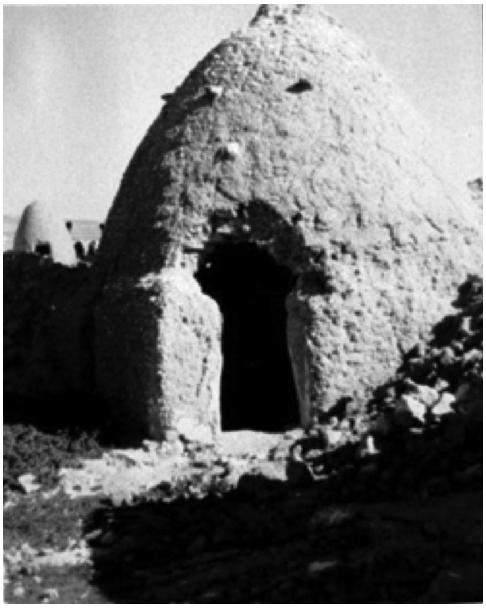

FIGURE 1.2 Beehive house.

China (Figure 1.1) (Liang et al., 2011) and beehives (Figure 1.2) (Chernick, 2009) have been identified over several thousands of years ago. Typical beehive house of a high-domed structure with adobe brick was found to be extremely durable and provide excellent service as a significant heat sink due to favorable thermal properties for hot countries.

More sophisticated composites appeared in ensuing years including Damascus steel (Figure 1.3) using wootz steel imported from India. Recent research discoveries (Inman, 2006) revealed that nanowires and carbon nanotubes in a blade were forged from Damascus steel. This discovery provides a lesson that it is preferable to incorporate nanomaterials as an integral means of mass manufacturing for their maximum effect on properties as opposed to the conventional wisdom of using nanomaterials as additives to enhance chemo-thermomechanical properties. A few additional examples of recent origins of polymer composites are reinforced rubber tires, aerospace components, laminated polymer parts, laminated electroplated components, and others. Similarly, polymer-coated metal hardware appeared in the markets in the last 70–80 years such

FIGURE 1.3 Damscus steel.

FIGURE 1.4 Soybean car.

as polymer-insulated copper wires. Henry Ford first exhibited a finished soybean car (Figure 1.4) in 1941 at the Dearborn Days Festival in Dearborn, MI (Soybean Car, 2012). Ford invested millions of research and development (R&D) dollars developing quarter-inch-thick plastic car panels reinforced with tubular steel, but he could not make an economically viable automobile at the time. Other notable examples made of composites appeared in thousands of household washing machines, refrigerators, drains, etc.

The stiffness and strength of these FRP composite materials are to be designed and produced as to sustain the water and chemical resistance of the relatively thick polymer coatings. More recently, FRP composites are formed as load bearing structural components for aircraft and marine structures. The surfaces of marine structures are protected through a class of polymer coatings including sacrificial coatings (lead or silver). For example, the protection of ship hulls against marine growth has been accomplished through these novel coatings. As recently as 2012, the U.S. Navy and Air Force (SERDP and ESTCP, 2012) are demonstrating a novel protective coating to reduce wear on

compressor airfoils on gas turbine engines significantly increasing fuel efficiency and reducing maintenance requirements. These coatings are made of multilayer ceramic–metal matrix composites using vapor deposition process.

After World War II, U.S. manufacturers began producing fiberglass and polyester resin composite boards and the automotive industry introduced the first composite vehicle bodies in the early fifties (Tang, 2011). The obvious reasons for moving in the direction of polymer composites are because of their corrosion and magnetic transparency, high strength-to-weight ratio and the ease of shaping. Modern composites are made primarily of glass, carbon, and/or aramid reinforcements. However, natural fiber composites are just beginning to make some inroads into high-volume applications. These fibers are bound together with a variety of resin systems such as esters, urethanes, and phenolics. In addition, a variety of additives and fillers are used in composites to improve performance such as the bonding characteristics between the fiber and resin, manufacturing process improvement, colors, fire protection, and cost reductions.

DESIGN PHILOSOPHIES

In general, the design community of FRP composites currently utilizes two primary design philosophies: (1) allowable stress design (ASD) and (2) load and resistance factor design (LRFD). While ASD methods have been used in FRP composite design for many years, LRFD is a relatively new methodology.

For the most part, ASD methods are based on extending elastic theory from the elementary principles of strength of materials to complex linear and nonlinear finite element analyses. However, material properties of FRP composites in different directions have to be properly accounted for in the analyses as well as the design. ASD methods are still widely used in the design of FRP composites in aerospace industry as well as marine and civil structural industries. Designs are carried out based on anisotropic material properties under service loads. The induced stresses in composite components are limited to the maximum allowable stresses, that is, by providing a factor of safety against the strength at first ply failure. This implies that safe design can be attained by making sure that externally applied load-induced stresses must be a fraction of failure stresses where failure stress may be defined as a first ply or last ply failure or even the failure stress may be obtained by testing a composite coupon to failure. It is worthwhile to highlight that certain design communities do not feel comfortable to theoretically establish failure strengths at the present time and hence rely heavily on test data. Failure stresses are defined differently for different materials including FRP composites depending on the modes of failure, stress or strain concentration factors, materials and structural system behavior, and combined load conditions. It must be noted for design purposes that residual stresses are not accounted for in an ASD method unless incorporated in a direct or indirect manner, that is, subtract the residual stress effect from allowable design stress values specified by the engineer in charge of the project.

To overcome the inherent limitations of ASD, especially in terms of safety related to variability of applied loads and strengths of FRPs and the probability of failure, LRFD has been introduced in recent years for the design of structures made of FRP composites. The central theme of the LRFD approach is to make sure that the product of the nominal resistance of a material and statistically derived (characteristic value) resistance factor is greater than the sum of the products of different load factors and the corresponding load types. Typical resistance factors correspond to uncertainties in constituent material properties and manufacturing processes in addition to accuracy of equations predicting different strengths induced in a structure as well as the consequences of failure. Similarly, uncertainties in load factors in any design consider type and magnitude of external loads acting on a structure and their combinations. For example, proper accounting of statistical design data for static, wind, and earthquake forces acting simultaneously at peak design magnitudes is a design challenge. Additionally, the design limit states in LRFD account for service limit states (limits on deformations and vibrations), fatigue and fracture limit states, and strength and extreme

event limit states. Typically, probability of failure is arrived at using the safety index, commonly known as "beta (β)." The LRFD code equations including load and resistance factors are calibrated using reliability theories as well as fitting these factors based on experimental data and also on practices adopted by other codes.

Preliminary Analysis

Analysis of structural response is required to proportion structural composite components. However, for initial conceptualization of a design, approximate analysis based on statics may be adopted for preliminary proportioning of structural member sizes. Once the preliminary proportioning is done, more sophisticated analysis will be adopted and the member size refined accordingly. Highly approximate analyses of elastic structural responses of an idealized structural element can be a valuable tool to calculate internal forces under simple static conditions. Viscoelastic behavior needs to be accounted for in the preliminary analysis and design using viscoelastic constants (e.g., rate of decrease of elastic modulus with time, temperature, or stress) to enable the use of readily available elastic formulae. For example, the elastic modulus needs to be appropriately adjusted to account for sustained stresses. Also anisotropic material properties as well as section properties including orientation of fibers have to be preliminarily approximated as orthotropic or even as isotropic materials. Similarly, element configuration and load distribution are to be idealized to conform to available structural response solutions. The structural response in a preliminary sense is determined in terms of internal member stress, deformation and stability of a structural system, and even that of a member. Some preliminary design aids related to structural elements under different load conditions including time and temperature effects including aging have to be properly integrated into the design. The designer must use certain understanding of structural behavior to make appropriate modifications to the results of simplified analyses of preliminary design before carrying out more refined analyses. Some of the approximations used in practical analysis are (1) adjusting the material properties for varying time and temperature ranges including physical and chemical aging, (2) approximating multilayer FRP laminates as non-layered materials with orthotropic material properties that may be determined through coupon testing of samples extracted from composites or through lamination theories, (3) determining in a preliminary sense the edge and interior stiffening rib support as a type of boundary condition (i.e., simple, fixed, or semirigid support) based on their strength and stiffness (bending, tensile, torsional, shear, and combinations) in these elements, and (4) approximating buckling and dynamic responses of a complex shape by a beam element or an equivalent plate or shell element of simple geometry such as cylindrical shell, that is, a longitudinally loaded double-curved cylindrical shell.

Simplifications for Common Laminate Analyses

In commonly used laminates, recent composite constructions are using directional symmetry in order to simplify governing equations and to attempt to eliminate warping effects and coupling terms. For example, for thin laminates, in composite plates, only properties within the plane of the laminate will be used in the elastic analysis. Therefore, their elastic constants are only defined for 2D structural elements. Stress–strain relations for planar orthotropic materials are defined by four important elastic constants (moduli in longitudinal and transverse directions, in-plane shear modulus and Poisson's ratio). Typically reinforcement directions are symmetrically balanced with respect to the middle surface of the laminate so that coupling terms vanish; thus, the ensuing analysis can be simplified.

In laminates comprised of plies having directional orientation, both axial stiffness and bending stiffness can be computed for the overall laminate in different directions based on the orthotropic properties in each ply. But a less accurate approach is to estimate the overall stiffness and cross-sectional properties for balanced symmetric laminates and use the transformed

section method. Normally plies are fabricated using glass or carbon fabric, woven roving, or filament winding, and elastic properties of individual plies are not determined. Instead, overall tension, compression, torsional and flexural stiffnesses are determined from direct tests on the full laminate in the directions of the principal axes of reinforcement. Alternatively, stiffness properties of a 2D structural member in different directions can be found from the laminate properties using classical lamination theory in the two (primary) principal directions. Equations corresponding to complex laminates are given in Chapter 6 of the *ASCE Structural Plastics Design Manual* (ASCE, 1984).

Summary of Design

Typical design of an FRP structural component has three broad steps as follows:

1. Identify structural and performance requirements: size and shape of a component that is subjected to static and other loads including thermal, wind, and seismic forces.
2. Identify service environment: corrosion resistance, fire safety, UV degradation rate, moisture uptake, abrasion resistance, electrical and magnetic transparencies, etc.
3. Establish production and cost targets: volume and production rates, fabrication and installation anomalies if any, strength-to-weight ratio including cost per unit structural performance, etc.

Based on the preceding evaluations, an FRP system configuration is selected for a structure and preliminary design is carried out including the selection of constituent materials, manufacturing process, structural response computations targeting design criteria before proportioning structural components, and developing details for final analyses and design. After developing the final design of components, a detailed evaluation has to be carried out including full-scale prototype structural testing, that is, check for any such work was done in the past, under a given service environment. In the design of any structural system made of FRP composites, the critical aspect is the joining mechanism and various concerns exist in the design community regarding a total reliance on chemical or adhesive bonding (joining) as opposed to mechanical fastening. An extensive amount of work was done by Hart-Smith, Mosallam, and others in suggesting innovative ways of bonding and jointing design methodologies (Hart-Smith, 1994; Mosallam, 2011). The *Design Guide for FRP Composite Connections* by ASCE (Mosallam, 2011) has many excellent references for the design of FRP composite connections.

CODES AND STANDARDS

Historically FRP components were designed, manufactured, fabricated, and repaired utilizing general codes issued by standard specifying bodies (ASCE, EUROCOMP, CEN, etc.) with in-depth design manuals published by individual companies based upon the typical products they manufacture following strenuous testing and evaluation. The ASCE *Structural Plastics Design Manual* was the standard for pultruded profiles in the United States, but is no longer in print. For designs in Europe, the following guides are extensively used while others are available to a lesser extent: *Structural Design of Polymer Composites—EUROCOMP Design Code and Handbook* (Clark, 1986), *Reinforced Plastic Composites: Specifications for Pultruded Profiles* by the European Committee for Standardization (CEN, 2002), and *Guide for the Design and Construction of Structures Made of Thin FRP Pultruded Elements* by the National Research Council of Italy (CRN, 2008). Additional standards exist depending on the country/jurisdiction and application (i.e., pultruded components, wraps, concrete reinforcement including ACI Committee 440, 2006; ACMA, 2012; ASCE, 1984; CEN, 2002; CRN DT 205/2007, 2008; CUR, 2003; Kutz, 2011; Ramkumar et al., 1987; Clark, 1996).

Manufacturer design manuals are available from nearly every producer, including Extren, Creative Pultrusions, Fiberline, and Bedford Reinforced Plastics. A draft Pre-Standard for Load and Resistance Factor Design (LRFD) of Pultruded Fiber Reinforced Polymer (FRP) Structures is nearing public release from ASCE at this time (ACMA, 2012). As FRP codes and standards are rapidly evolving, any codes, standards, or design guides should be verified for their current applicability before use.

FUTURE PERSPECTIVES

FRP composite research efforts recently have been focused on marine, aerospace, civil, and military infrastructure applications such as deckhouses for ships, airplane components (Figure 1.5), wind turbine blades, cold-water pipes for Ocean Thermal Energy Conversion (OTEC) (Figure 1.6), high-pressure composite pipes for natural gas transmission (Figure 1.7), carbon-cored aluminum alloy conductor electric transmission lines, and utility poles up to 120 ft in height (Figure 1.8), modular housing construction, and so on. Some of the current and future application details were reported by GangaRao (2011).

FIGURE 1.5 DDG1000.

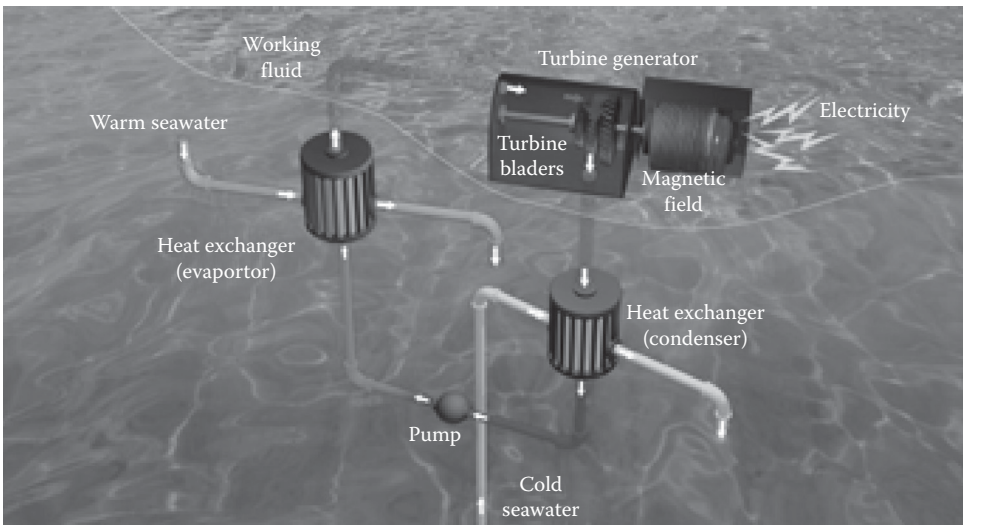

FIGURE 1.6 Lockheed OTEC.

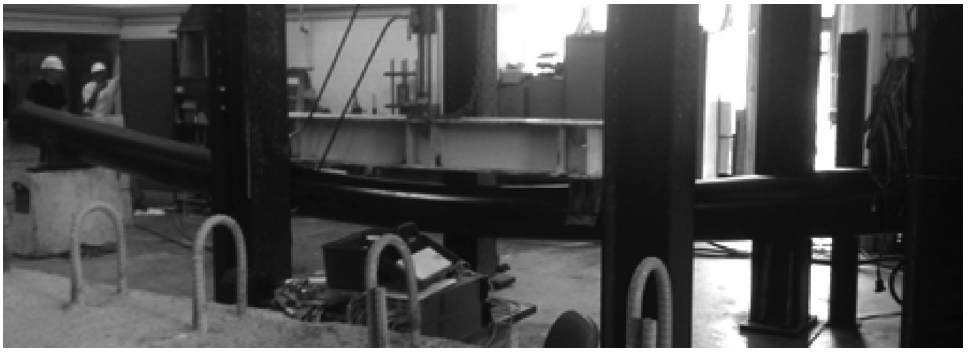

FIGURE 1.7 Pipe section during testing. (From *Applied Plastics Engineering Handbook—Processing and Materials*, GangaRao, H.V.S., Infrastructure applications of fiber-reinforced polymer composites, Copyright 2011, from Elsevier.)

FIGURE 1.8 Utility pole.

Bridging

FRP composites can be floating bridges, underwater bridges, and even folding/unfolding bridges. Movable bridges of 10 lb/ft^2 self-weight can be developed in a cost-competitive manner. However, some of these bridging systems have to be either anchored or balanced with dampers for stability. For example, a novel rolling bridge system (Figure 1.9) was designed by Thomas Heatherwick Studio, London in 2005. Similar advances made by the U.S. Army in lightweight bridging with rapid deployment capabilities such as the Wolverine Heavy Assault Bridge System (FAS: MAN, 2000) and new developments in composite bridging are being pursued by USDOD (ONR BAA 04-009) in terms of lightweight expeditionary bridging capability.

Smart Materials

The community of advanced composites development has been constantly assessing for self-healing materials, including coatings as sensors and also self-cleaning functionality. For example, certain surface coatings can reduce or even eliminate any algae growth on marine structures. Similarly paints containing nano-bubbles can heal wall paints that might be damaged due to accidents. Recent developments using carbon fibers as sensing and healing damage through polymers housed in nano-fibers are another excellent example of the future research trends. Similarly, electrically conductive coatings with wireless networks are being developed to detect fire and other structural hazards. Examples of smart materials with shape memory (Figure 1.10) are being developed by Cornerstone Research Group (CRG Technology Overviews, 2011). As fundamental R&D matures in shape

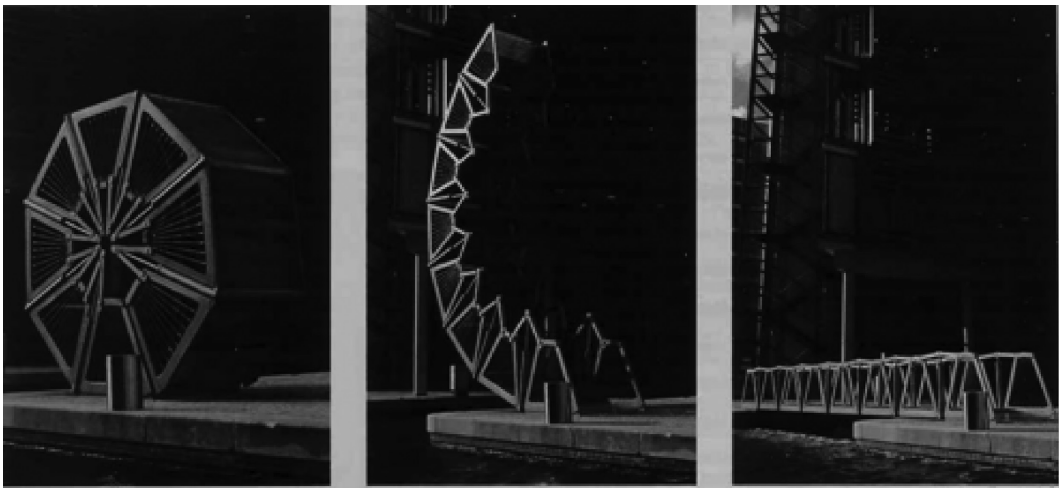

FIGURE 1.9 Rolling bridge. (Photo courtesy of Steve Speller.)

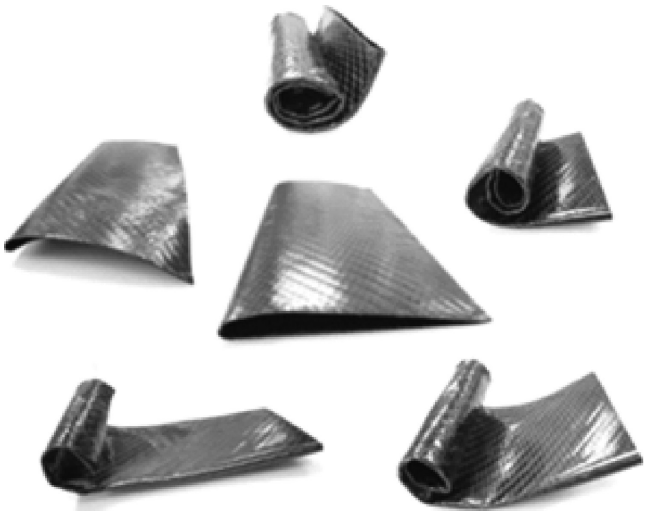

FIGURE 1.10 Shape memory polymers.

memory polymers, a wide range of applications can open up for structural health monitoring and even in the fields of health care, security, and altering and controlling human behavior patterns. For example, a polymer that releases slow doses of insulin (commonly known as Humulin) is being marketed extensively to control diabetes.

Fire

Fire-retardant properties of composites have to be quantified with special emphasis on chemical reaction (including toxicity) of polymers to fire (ignition, flame spread, and heat release rate). This is especially important when composites are filled with nanoparticles such as nanoclay or carbon nanotubes or filaments and even traditional additives such as halogens or phosphorus. Even non-toxic inorganic fillers are used to minimize smoke output and to retard the burn rate through the thickness of a composite laminate. These additives can alter the mechanical and physical properties of polymers as well as composites. Therefore, protective coatings against fire using innovative

materials are being considered. For example, nanofiber sheets in the form of coatings are being researched by Zhao et al. (2009). These coatings have "bilayer structure," with the top layer being thermally conductive and expected to redirect the heat flux on the surface. Since the in-plane heat flux is of several magnitudes higher than the through-thickness flux, fire-induced heat is dissipated through the outer thin layer. The thermally insulated bottom layer will turn into char (silicon oxide) due to an immense heat buildup from the top layer to the bottom; thus, the silicon oxide layer protects the polymer composite. In a somewhat similar manner, researchers are working on the use of graphite to alter thermal properties of composites (Yu et al., 2007). Intertek testing services NA, Inc has successfully conducted fire testing (ASTM E119) for WVU-CFC on a composite wall panel consisting of intumescent coating and noise barriers in addition to gypsum board and natural resin based FRP sheathings. The fire test results revealed a rating of 60 min. The ASTM E119 is expensive and we need economical fire test methods.

Natural Fiber Composites

Natural fibers with excellent specific mechanical properties cost around 40%–60% of the cost of common E-glass fiber, require only 20%–40% of the embodied (production) energy, and are sustainable. Even though several limitations of natural fibers are well documented (Dittenber and GangaRao, 2012), many researchers have been advancing the state of the art of natural fiber composites focusing on surface treatments of fibers and improving the fiber–matrix interfacial bond strength properties. Advances in natural fiber composites are being made in such a way that a class of natural fiber composites are yielding better mechanical properties than typical glass fiber composites, albeit more expensive than GFRPs (Netravali et al., 2007; Dittenber, 2013). However, research is being focused to reduce costs and improve performance characteristics so that they can compete directly with GFRPs.

SUMMARY

Composites are composed of two or more constituent materials that remain distinct in the final form but bond to create a product that has superior properties to the constituent materials. Composite use dates back to the earliest civilizations, but the use of engineered composites has dramatically increased in the last century. Codes and specifications are rapidly evolving to keep up with the recent growth of composites in civil infrastructure; often the most detailed guides are provided by manufacturers based on their testing and experience for specific products. With the properties that can be completely customized to fit specific needs, the future prospects of FRP composites are limitless.

REFERENCES

ACI Committee 440. (2006). *440.1R-06: Guide for the Design and Construction of Structural Concrete Reinforced with FRP Bars*. Farmington Hills, MI: American Concrete Institute.

ACMA. (2013). Pre-standards for pultruded products. Retrieved May 16, 2012, from http://www.acmanet.org/resources/lrfd.cfm

ASCE. (1984). In Gray, E. F. Jr. (Ed.), *Structural Plastics Design Manual*. New York: Task Committee on Design of the Structural Plastics Research Council of the Technical Council on Research of the American Society of Civil Engineers. doi:978-0-87262-391-0.

CEN. (2002). *Reinforced Plastic Composites: Specifications for Pultruded Profiles Parts 1–3 EN 13706*. Brussels, Belgium: European Committee for Standardization (CEN).

Chernick, K. (2009). Traditional Syrian beehive houses kept heat out the natural way. Retrieved May 11, 2012, from http://www.greenprophet.com/2009/07/syrian-beehive-houses/

Clark, J. L. (Ed.). (1996). *Structural Design of Polymer Composites: Eurocomp Design Code and Background Document*. London, U.K.: E & FN Spon.

CRG Technology Overviews. (2011). Retrieved May 15, 2012, from http://www.crgrp.com/technology/overviews/morphing.shtml

CRN DT 205/2007. (2008). *Guide for the Design and Construction of Structures Made of Thin FRP Pultruded Elements*. Rome, Italy: National Research Council of Italy (CNR).

CUR. (2003). *CUR Recommendation 96: Fiber Reinforced Plastics in Civil Engineering Structures*. Amsterdam, the Netherlands: CUR.

Dittenber, D. B. (2013). Natural composites for infrastructural applications. PhD dissertation, West Virginia University, Morgantown, WV.

Dittenber, D. B. and GangaRao, H. V. S. (2012). Critical review of recent publications on use of natural composites in infrastructure. *Composites Part A: Applied Science and Manufacturing,* 43(8), 1419–1429.

FAS: MAN. (2000). XM104 wolverine: Heavy assault bridge system H82510. Retrieved May 15, 2012, from http://www.fas.org/man/dod-101/sys/land/wolverine.htm

GangaRao, H. V. S. (2011). Infrastructure applications of fiber-reinforced polymer composites. In Kutz, M. (Ed.), *Applied Plastics Engineering Handbook—Processing and Materials*. New York: Elsevier. Retrieved from http://www.knovel.com/web/portal/browse/display?_EXT_KNOVEL_DISPLAY_bookid=4606

Hart-Smith, L. J. (1994). The key to designing efficient bolted composite joints. *Composites,* 25(8), 835–837.

Heatherwick Studio. (2005). Rolling bridge, London, U.K. Retrieved from http://www.heatherwick.com/rolling-bridge/ (March 1, 2013).

Inman, M. (2006). Legendary swords' sharpness, strength from nanotubes, study says. Retrieved May 15, 2012, from http://news.nationalgeographic.com/news/2006/11/061116-nanotech-swords.html

Kutz, M. (2011). *Applied Plastics Engineering Handbook—Processing and Materials*. New York: Elsevier. Retrieved from http://www.knovel.com/web/portal/browse/display?_EXT_KNOVEL_DISPLAY_bookid=4606

Liang, R., GangaRao, H. V. S., and Stanislawski, D. (2011). SGER: Material and structural response of historic Hakka rammed earth structures. Final Report No. 0908199. Morgantown, WV: National Science Foundation.

Mosallam, A. S. (2011). *Design Guide for FRP Composite Connections*. Reston, VA: American Society of Civil Engineers. Retrieved from http://books.google.com/books?id=-M-Yz0FXCeAC

Netravali, A. N., Huang, X., and Mizuta, K. (2007). Advanced 'green' composites. *Advanced Composite Materials: The Official Journal of the Japan Society of Composite Materials*, 16(4), 269–282.

Ramkumar, R. L., Bhatia, N. M., Labor, J. D., and Wilkes, J. S. (1987). *Handbook: An Engineering Compendium on the Manufacture and Repair of Fiber-Reinforced Composites*. Atlantic City International Airport, Atlantic City, NJ: Prepared for Department of Transportation FAA Technical Center.

SERDP and ESTCP. (2012). Erosion resistant coating improves engine efficiency. Retrieved May 16, 2012, from http://www.serdp.org/News-and-Events/In-the-Spotlight/Erosion-Resistant-Coating-Improves-Engine-Efficiency

Seymour, R. B. and Deanin, R. D. (1986). History of polymeric composites. In *Proceedings of the Symposium Held during the 192nd ACS National Meeting*, Anaheim, CA.

Sinopoli, C. M. (2003). *The Political Economy of Craft Production: Crafting Empire in South India*. England, U.K.: Cambridge University Press.

Soybean Car. (2012). Retrieved May 11, 2012, from http://en.wikipedia.org/wiki/Soybean_Car

Tang, B. (2011). Fiber reinforced polymer composites applications in USA. Retrieved May 11, 2011, from http://www.fhwa.dot.gov/bridge/frp/frp197.cfm

Yu, A., Ramesh, P., Itkis, M. E., Bekyarova, E., and Haddon, R. C. (2007). Graphite nanoplatelet—Epoxy composite thermal interface materials. *The Journal of Physical Chemistry C,* 111(21), 7565–7569. doi:10.1021/jp071761s.

Zhao, Z., Gou, J., Bietto, S., Ibeh, C., and Hui, D. (2009). Fire retardancy of clay/carbon nanofiber hybrid sheet in fiber reinforced polymer composites. *Composites Science and Technology*, 69(13), 2081–2087. doi:10.1016/j.compscitech.2008.11.004.

2 Manufacturing Processes and QA/QC

Kumar K. Ghosh, Luke S. Lee, and Hector Estrada

CONTENTS

INTRODUCTION

Fiber-reinforced polymer (FRP) composites are a combination of two discrete phases: a matrix that is often a resin and a fibrous reinforcing system. Along with the type and orientation of the fibers used and the relative proportions of the constituent materials (matrix and fibers), the manufacturing process plays an equally important role in determining the characteristics of the final composite product. Hence, it is necessary to judiciously choose the manufacturing process that would result in optimal properties of the composite as well as improved economics. The choice of the manufacturing process will also depend on the user needs, performance and appearance requirements, size and surface complexity of the desired product, production rate and available equipment/tooling assembly. There are several manufacturing processes, which may be broadly classified into three categories:

1. *Manual processes*, including methods such as wet lay-up and contact molding
2. *Semi automated processes*, including methods such as compression molding and resin infusion
3. *Automated processes*, including methods such as pultrusion, filament winding, and injection molding

All these manufacturing processes can also be fine-tuned by the manufacturer in terms of the total cost involved in fabricating the composite part, the level of precision involved to obtain the desired quality, varying degrees of compaction provided by the tools and pre-/post-cure of the resin.

MANUAL MANUFACTURING PROCESSES

Wet Lay-Up and Prepreg

The wet lay-up process is one of the oldest and simplest techniques used in the manufacturing of polymer composites. In this process, resins are impregnated by hand into fibers that may be in the form of woven, knitted, stitched, or bonded fabrics placed on a mold. The resin may be sprayed, poured, or brushed onto the mold, which may be made of wood, sheet metal, plaster, or FRP composites, as shown in Figure 2.1. An FRP composite mold that is shaped and fabricated from a wooden master mold is most desirable since it can be made into any shape, has a good surface finish, has no corrosion problems, and can be used over a long period of time. The mold may be of male (plug) or female (cavity) types depending on the desired shape of the part.

In the wet lay-up process, a mold release agent is first applied to the mold to prevent the composite from sticking to the mold. Next, the fabric is placed on the mold and impregnated with resin using a roller until it conforms to the surface of the mold and is "wet out" with additional resin if needed. Third, entrapped air and excess resin is rolled or brushed out and the process is repeated by building layer upon layer (referred to as laminate construction) depending on the required thickness and mechanical properties of the composite part. Finally, the composite part is then cured at room temperature or external heating is used to accelerate the curing process. A promoter may also be mixed with the resin just before application of the resin to speed up the curing of the composite.

There are three types of laminate construction: (1) sandwich lamination in which two high-stiffness and high-strength outer layers are laminated over a lightweight and low-strength sandwiched core, which is usually foam, aluminum honeycomb cells, or balsa core; (2) all laminated construction consisting of high-stiffness and high-strength layers bonded to each other; and (3) fabric laminates bonded to a structural member to upgrade its properties or to retrofit the member for increased demand. In all cases, the quality of the bond between the composite layers is the key element in obtaining the required mechanical properties.

Given the increased use of polymer composites in retrofitting and strengthening civil infrastructure, the wet lay-up process can be used in order to bond the composite directly onto the surface of the structure being rehabilitated or upgraded, as shown in Figure 2.2. In such instances, it is imperative that the surface to which the composite is being bonded be properly prepared through sanding, grinding, and cleaning so that the composite can adhere to the surface. The wet lay-up

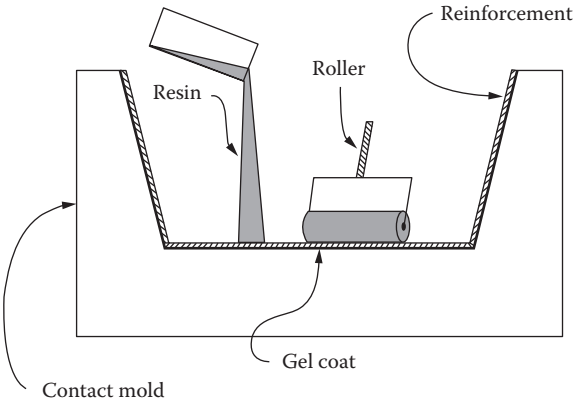

FIGURE 2.1 Schematic of the hand lay-up manufacturing process.

FIGURE 2.2 Bonding of FRP composites to a reinforced concrete bridge deck.

process is currently being used extensively in the flexure/shear upgrading of strength and/or seismic retrofitting of deficient civil structures because of its low cost compared to other processes, flexible manufacturing in field conditions, and relatively low-precision and technical know-how required for manufacturing. Also in applications where the composite part may be exposed to harsh environmental conditions or fire/blast hazards, a resin-rich gel coat mixed with suitable admixtures may be applied on the exposed surface of the composite. The gel coats may also be used in instances where aesthetic requirements may need the composite part to be of a particular finish or color. It is noted that the interface bond between the fibers and resin matrix or between two fiber layers is the key to the strength and mechanical properties of the composite part, and hence, a gel coat should be chosen that does not compromise the strength of the composite through chemical reaction with the fibers or the resin.

The main advantages of using the wet lay-up are as follows:

- The processing cost is relatively low since no expensive tooling assembly is required.
- The parts can be made into any shape or size by choosing the proper mold over which the material is layered.
- This method gives the designer the flexibility to use any fiber–resin combination and fiber orientation.
- The start-up lead time and cost are minimal for the manufacturer because there is no requirement for highly skilled technicians or worker training.

However, the inherent advantages of this method also result in some shortcomings:

- The method has a low production rate and the quality of the manufactured composite is dependent on the skill of the technician.
- It can be a labor-intensive process with the cure times being governed by the environment.
- There can be a considerable waste of materials, particularly the resin, depending on the skill of the technician.
- It is very difficult to maintain consistent composite properties for multiple parts manufactured using wet lay-up. Quality control becomes a major part of this process to ensure that defects and voids are not left in the composite part.

A variation of the wet lay-up process is the *prepreg* method. In this method, the composite fibers are pre-impregnated with the resin, either through solvent impregnation or through hot-melt impregnation. In the solvent impregnation method, the dry fibers are passed through a resin bath and excess

FIGURE 2.3 Impregnation of dry fabric via a resin bath.

resin is squeezed out, as shown in Figure 2.3. The impregnated fibers are passed through a drying chamber and the prepreg is partially cured and rolled up on a drum. In the hot-melt method, the resin is cast into a film and this film is applied on the dry fiber strips. The fiber strips and the resin are then subjected to heat and pressure impregnating the resin into the fibers. Vacuum bagging and sometimes autoclaving (discussed later) are often used with the prepreg method to drive out air voids and excess resin. The rolled up prepreg composite strips can be directly laid out on the mold or slightly melted with a blower before application. Prepregs usually have limited shelf life since the resin starts to cure once it is applied on the dry fibers. The shelf life can be extended by including additives in the resin that can slow the curing process or by keeping the prepregs refrigerated. A better quality composite part can be manufactured using this process as compared to wet lay-up and a higher production rate can be achieved. However, it still suffers from the inherent disadvantages of the wet lay-up method as compared to automated composite manufacturing methods.

Contact Molding

In this method, improved composite properties can be obtained as compared to the wet lay-up or prepreg process by encapsulating the molding and the composite part inside a vacuum (polymer) membrane and applying up to 1 atm pressure on the membrane by pulling a vacuum. This extracts the air along with excess resin and produces better compaction of the composite part, resulting in fewer defects and voids. Figure 2.4 provides a schematic of a composite manufactured using a vacuum bagging process.

In the contact molding technique, a mold release agent is placed on the mold and a perforated release film such as peel-ply sheet is placed above and below the composite part to release the part

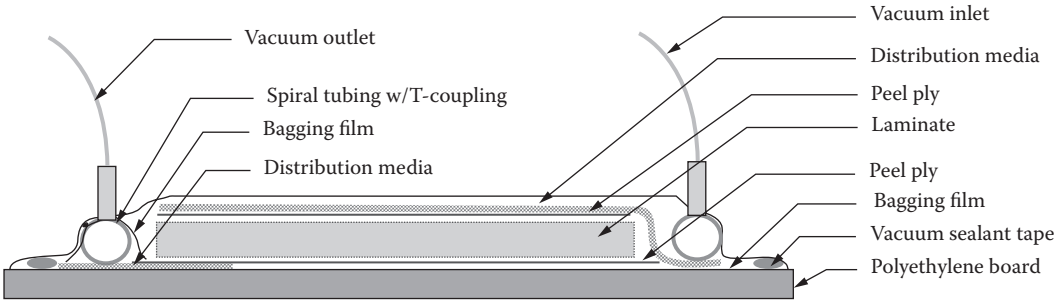

FIGURE 2.4 Cross section of the vacuum bagging process.

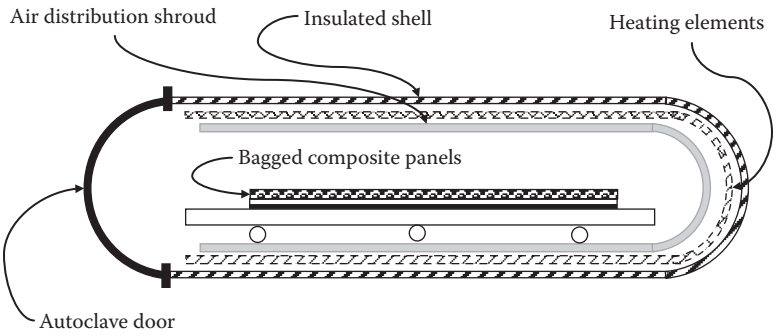

FIGURE 2.5 Configuration and elements of an autoclave.

and to allow the excess resin to pass through. A bleeder felt membrane with good absorption properties is placed between the peel ply and the vacuum bag to absorb the excess resin. A barrier layer or resin trap may be used to prevent the resin from flowing into the vacuum tubes. A good seal around the mold is necessary to obtain an airtight system. A leak caused by improper sealing or damage to the vacuum bag is the most common problem with this method. Also uneven pressure over the surface of the composite can impede the vacuum bag or bleeder membrane from conforming around the composite part resulting in bridging, which results in nonuniform compaction of the part. Even though in some instances vacuum bag composite parts are cured at room temperature, for most high-production manufacturing, the composites are cured at elevated temperatures to reduce the curing time and to improve properties of the composite. Also in order to avoid the recurring cost of the expendable polymeric vacuum bag, some manufacturers use reusable silicone vacuum bags.

If used properly, a mix fiber–resin ratio by weight of about 55% can be achieved through this process. A mix fiber–resin ratio by weight of about 65% can be achieved by applying a pressure of about 3 atm in what is called a *pressure bag* process. An even higher pressure of about 6 atm can be applied in an *autoclave* process, which can result in a mix fiber–resin ratio by weight of about 70% and considerable reduction of the voids and defects through better compaction. An autoclave is usually a pressure chamber that can simultaneously apply heat and pressure, as shown in Figure 2.5. A compatible mold, vacuum bag, and special tooling that can withstand such high pressures are necessary. The desired quality of the composite in terms of mechanical properties, aesthetics, and related economics will determine which contact bagging method will be used by the manufacturer.

SEMIAUTOMATED MANUFACTURING PROCESSES

Resin Infusion under Flexible Tooling

Resin infusion under flexible tooling (RIFT) is a variation of the injection molding or resin transfer molding (RTM) that will be described later in the section "Automated Manufacturing Processes." In this process, one of the mold faces is replaced by a polymer film or by a thin composite "splash" mold tool to reduce the high tooling costs associated with RTM for large composite parts. This process is also an improvement over the hand lay-up or vacuum bag processes in terms of limited styrene emissions from the uncured resins, resulting in a better work environment and worker health and safety. The basic principle is to infuse resin material into a dry fiber reinforcement placed inside an evacuated vacuum-bagged tool that consists of a rigid male mold tool on one side and a semi-flexible female tool on the outer surface. The infusion of the resin under partial vacuum conditions results in good saturation of the dry fibers due to increased flow rate of the resin. The flexible tool can either be a silicone rubber or nylon diaphragm bag, aluminum sheet metal, or glass-reinforced polymer sheet. The choice of the flexible mold/bag material is a key parameter in this process; the flexible tool should be reusable, tear resistant, heat resistant, and moisture resistant and should be

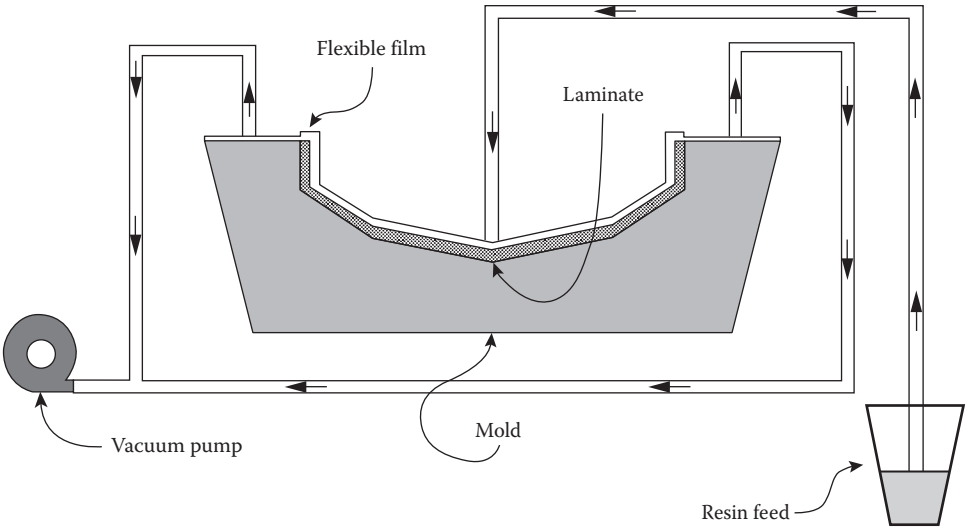

FIGURE 2.6 Schematic of the SCRIMP manufacturing process.

able to elongate and conform to the shape of the composite part. The use of a silicone or nylon bag is the most suitable for this process. However, nylon bags are sensitive to moisture, while silicone bags have poor solvent resistance and high cost. Some manufacturers have used a flexible resin distribution membrane with an embossed pattern, thus eliminating the need for bleeder and breather peel plies and thus increasing the production speed of the process.

There are several patented variations of the RIFT process, the most notable being the *Seemann Composites Resin Infusion Manufacturing Process* (*SCRIMP*) and *Vacuum Assisted Resin Transfer Molding* (*VARTM*). In the SCRIMP, the fiber preform is placed between a mold and a nylon vacuum bag. The patented system includes a resin distribution mesh that is placed between the fiber and the vacuum bag, thus eliminating the need to place a breather layer. The mesh also helps to uniformly distribute the resin over the surface of the fiber. The SCRIMP process most commonly uses a nylon vacuum bag that has to be replaced along with all the hoses, peel ply, and resin distribution membrane after each resin infusion process as illustrated in Figure 2.6. However, some manufacturers may use a reusable elastomeric vacuum bag that incorporates a built-in resin distribution membrane and resin inlet tube. The VARTM is similar to the SCRIMP process and consists of a patented textured polyester high-temperature vacuum bagging film with an embossed pattern that eliminates the need for a breather or bleeder membrane. The resin is often cured with UV light with the areas needing secondary bonding being cured less as compared to other areas of the composite part.

The RIFT method offers improved economics as compared to RTM while producing composite components with better mechanical properties as compared to hand lay-up. It also uses a closed molding technique to reduce the styrene emissions. However, this process is not fully automated, and thus, variability in the process can result from variations in the fiber compaction or flow rate of the resin through the fibers. Also, the process has a much lower production rate as compared to the fully automated processes, such as filament winding or pultrusion, which will be described later.

Compression Molding

Compression molding is a manufacturing process where the molding material is placed in an open, heated mold cavity along with a thermosetting resin. The molding materials include unidirectional preform tapes, woven fabrics, randomly oriented fiber mat, or chopped strand. Even though this process can be fully automated, manufacturers usually tend to use a combination of automation and human workman to keep the manufacturing costs down by minimizing the use of expensive

automated tooling equipment. The thermosetting resin is usually in a partially cured stage, either in the form of granules, putty-like masses, or preforms. Depending on the type of molding material used, the compression molding process is referred to as *preform*, *sheet molding compound* (*SMC*), or *bulk molding compound* (*BMC*) molding. In *preform molding*, either a stitched or braided fiber mat or chopped rovings held together by water-soluble binder are preformed into the desired shape of the composite part and is placed inside the molds. In *SMC molding*, a sheet material is first produced by compacting chopped fibers between two polyurethane films treated with a resin filler paste. The sheet material may also be partially cured, stored, and then shipped to a separate facility where the material can then be used between the molds for compression molding after removing the polyurethane film backing. In *BMC molding* the chopped fibers and the resin/filler paste are formed into a bulk dough that can either be preformed or made at the time of placing the material into the molds. In order to ensure good and uniform fiber volume over the composite part, it is necessary to choose a resin of proper viscosity and flowability so that the dough paste can be molded uniformly without any voids or resin-/fiber-rich areas.

In the compression molding process, illustrated in Figure 2.7, the molding material is first placed between the molds. Then, the mold is closed with a top force applied by a hydraulic ram, which compresses and conforms the molding material to the mold shape. Generally the molds are made of hard metal and are highly polished or are chromium plated. Next, platens hold the two sides of the mold in place, while heat and pressure are maintained until the curing reaction occurs. Once fully cured, the part is ejected from the mold. Quality compression molding results from the even distribution of the molding material over the surface of the mold itself. The mold is then opened and the part is removed from it by means of the ejector pin. If a thermosetting resin is used, the mold may be opened in the hot state since the composite part can maintain its shape and dimension. If a thermoplastic is molded, the mold and the molded part need to be cooled before opening. Also, if a condensation type cross-linking is used for molding condensation polymers such as phenolics, the molds have to be opened to allow the gases to escape.

The main advantage of compression molding is that it is a high-volume, high-pressure method suitable for molding complex, high-strength fiberglass reinforcements into flat or moderately curved parts. Since a finished male–female tool combination is used, the composite part will have good inside and outside finished surfaces. The inexpensive overhead involved with compression molding, and the comparatively little waste material that results from the manufacturing process, makes

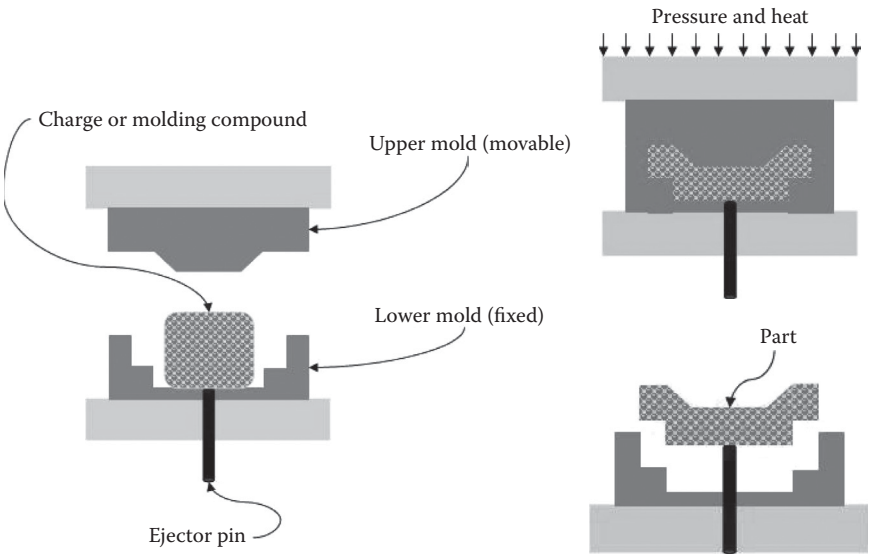

FIGURE 2.7 Compression molding manufacturing process.

compression molding a preferred manufacturing method. Also, compression molding produces fewer knit lines and less fiber-length degradation than injection molding. However, the molding cycle time, which is usually about 5 min, is longer than the injection molding cycle. Also, the equipment needed makes the process more costly to operate than the hand lay-up or RIFT processes.

AUTOMATED MANUFACTURING PROCESSES

Pultrusion Process

The pultrusion technique is a fully automated closed mold continuous process in which continuous fiber, rovings, or mats are passed through a resin bath, drawn through a preforming die to form the composite into a strip, and cured in a heated die. The various stages and components of the pultrusion process are illustrated in Figure 2.8. The automated process is designed such that the fibers are uniformly distributed over the section of the composite, the fibers are completely wetted out with the resin, and the composite is compacted in the die eliminating most voids and defects. The pultrusion process usually uses thermosetting polymers such as polyester, vinyl ester, or epoxy resins as the matrix. The choice of the resin is guided by the tool, speed settings, and cure die temperature. Usually a resin is chosen that can cure rapidly, has low viscosity, and shrinks little during curing to aid in releasing the composite part from the die. Polyester with controlled styrene content is usually the resin of choice in the pultrusion process because of its low shrinkage and ease of release from the die. Epoxy resins, on the other hand, required the use of release agents or viscosity modifiers to prevent the resin from adhering to the dies. Also several mechanical pulleys, usually in the form of double clamp pullers, are used to direct the rovings through the resin bath and to maintain the required tension. In some manufacturing processes, the fibers are injected through port holes in the heated die as the continuous fibers pass through them. This process is usually used when the desired shape of the pultruded part is not straight or if the rovings are pulled around heated mandrels to form a hollow part. In such cases, the infusion of resin at the final stage has the advantage that the fibers are in their final form before being wetted out.

The curing of the composite can be done either inside or outside a die. If the curing is done inside a die, called *die curing*, a resin is used that can cure very fast and the die is heat controlled so that curing of the composite part can occur as the composite passes through the die. Ceramic dies with microwaves may be used to aid the curing process, but this tends to increase the manufacturing cost. Also mechanical properties are often sacrificed when quick curing systems are used. More commonly the composite is cured outside the die by passing it through a temperature-controlled *tunnel oven*. The composite is passed continuously through the oven with the length of the oven being determined by the type of resin, part application, part size and thickness, and the speed at which the composite passes through the oven.

Continuity and automation make the pultrusion process a high-production technique for quality manufactured composite parts with very little waste of materials. This process also results in

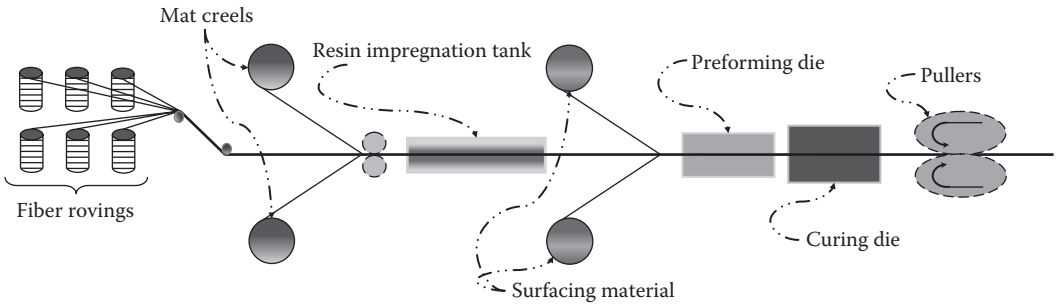

FIGURE 2.8 Components and stages of the pultrusion manufacturing process.

high-fiber-content, high-quality (little defects and voids) parts. However, the parts must have constant cross sections for every batch, and the rovings must be drawn in a predetermined pattern resulting in composite parts of unidirectional fiber architecture, which tend to have low transverse strength. Therefore, these parts have limited applicability for loading other uniaxial. One solution to this problem is to impart transverse strength; a mat or stitched fabric may be folded into the material package before it enters the die. A surface veil is usually incorporated to provide a resin-rich exterior surface to protect the unidirectional fibers. A modified *pull winding* process has been developed to counter these disadvantages, in which a pull winder is used in conjunction with the pultrusion process. The winding machine is designed with heads to wind angled fibers around a spindle between layers of unidirectional fibers pulled by the regular pultrusion machine. However, these manufacturing techniques and tools are limited to very specific applications.

Filament Winding

Filament winding is an automated process in which continuous spools of dry fiber (tows) are pulled in a predetermined pattern by computer-controlled winding machines. Filament winding equipment comes in a variety of sizes and configurations characterized by capacity, single/multiple spindles, and a multi-axis carriage and payout eye. The spools of rovings are usually supported by a creel and the fibers are maintained under constant tension. This tension is read by a computer as a signal and is interpreted into the pattern and speed at which the winding machine pulls the fibers from the creel. Automated monitoring of the tension ensures that the composite part is manufactured with the desired fiber volume and without any voids or defects. The rovings are passed through a resin bath that "wets" out the fibers; the wet fibers are then fed through a comb and payout eye and wound on specially designed mandrel tool. It is necessary to choose a resin that is low in volatile content and has the necessary viscosity so that the fibers can be completely wetted out without sticking to the payout eye. Polyesters and epoxy resins are generally the material of choice for this process. Though less common, a *dry filament winding* process is sometimes used in which instead of wetting the dry fiber rovings through a resin bath, a pre-impregnated tow is used. The tow may be heated during winding to improve its tackiness so that they do not slip when woven over the mandrel. Overall the dry winding process is more expensive since the pre-impregnated tows are more costly. However, the need for resin preparation and handling is eliminated and the quality of the composite part can be better controlled.

The filament winding process, illustrated in Figure 2.9, is very flexible in terms of the geometric shape of the composite part, depending on the shape of the tool, which can be manufactured from a variety of materials including steel, aluminum, ceramics, and composites. For tubular structures, the mandrel is typically a steel or aluminum cylinder that has a carefully machined outer diameter with a precision-polished surface to ensure easy extraction of the composite tube. The filament winding machine can lay the fibers on the mandrel in any geometrical pattern designated by the designer. Thus, it enables the designer to custom engineer components by developing optimized materials, geometry, fiber–resin weight/volume ratios and fiber pattern that result in the desired mechanical properties of the composite part. A typical filament winding pattern consists of both helical and circumferential layers. The circumferential winding gives hoop or radial strength to the composite part, while the helical winding gives axial, shear, and torsion strengths as necessary based on the design of the component. The mandrel is held under tension and is spun at precise rates to ensure proper winding, while a carriage containing the wet fiber spools travels back and forth along the length of the mandrel. The tension control is important to ensure that the fibers are properly wetted out and are then wound with minimum possible voids or defects. Successive layers at the same or different winding angles are added until the composite part reaches the desired thickness. Other than the initial start-up where an operator may manually splay the fibers onto the mandrel and monitor the fiber bandwidth and part diameter, the process is fully automated.

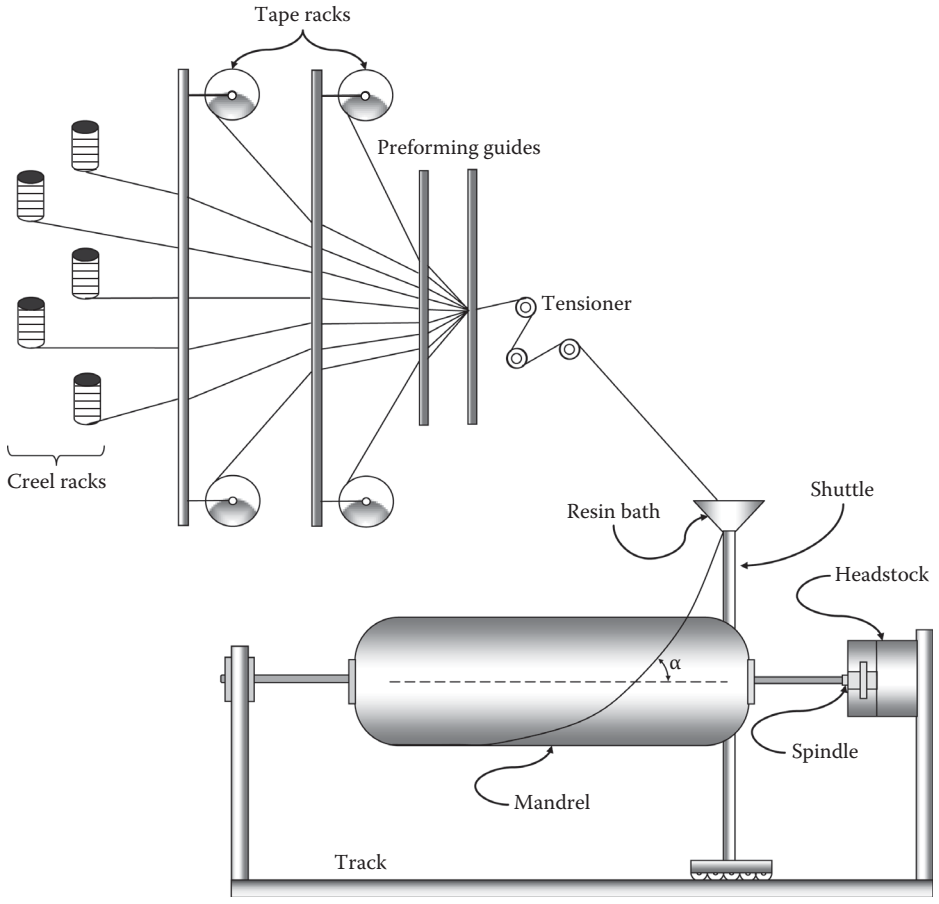

FIGURE 2.9 Schematic of the filament winding manufacturing process.

Upon completion of the winding process a nonstick polyurethane film may be wrapped under tension around the composite part to provide additional compaction to the composite. The composite is then cured, either at room temperature or in a computer-controlled oven depending on the type of resin used in the process. Also, for some composite parts, an autoclave may be used to attain further compaction of the part. The heating profiles are preprogrammed to incrementally ramp and hold the oven temperature throughout various temperature cycles until the composite is fully cured. Following the monitored cure, the mandrel is stripped out from the composite part using specialized machinery that protects both the composite and the tooling. A collapsible metal mandrel with proper release agents is usually preferred. For complex geometrical shapes where it might be difficult to take out a mandrel, an inflatable mandrel may be used, which can either be deflated and taken out or left inside as a liner material. Such mandrels can also exert an internal pressure during the winding process so that the inner windings can stay under tension.

Filament winding is one of the most cost-effective methods for mass production of lightweight and strong composite parts. The full automation of the process helps to reproduce identical components at a very fast rate without compromising product quality. In fact, the automation leads to the robust quality control as well as material and cost optimization. By using low-cost materials and automation, the cost to reproduce components in bulk is substantially reduced. The process involves less material, less labor, and less transportation costs than many other manufacturing methods. The process also gives the designer full flexibility to use different techniques of winding and curing

to achieve any winding pattern and fiber layout, including fabrication of complex engineered noncircular composite parts. The process, however, requires careful programming and close quality monitoring and control through the entire process.

Resin Transfer Molding

RTM is a fully automated version of the RIFT process discussed earlier. A schematic configuration and typical components in the RTM process are shown in Figure 2.10. In this process, a preformed dry fiber part is placed on a tool or inside a mold cavity with rigid surfaces on both sides of the composite part, and the whole assembly is encapsulated in a reusable vacuum bag. Thermosetting resin is injected under pressure into the mold so that it wets out the dry fibers and fills the mold. Vacuum is applied, which draws out the air voids and excess resin and compacts the composite part. Reinforcements placed in the mold are usually in the form of binder-bound chopped mat, random continuous strand-stitched mat, or woven cloth. The primary requirement is that the fiber be preformed to the desired shape of the composite part. Resins with low viscosity are required in order to be pumped in automatically; these resins included epoxy, vinyl ester, methyl methacrylate, polyester, and phenolic. The mold has to be carefully designed so that it will allow the resin to flow and wet out the fibers at a steady rate without disturbing the fibers. The success of the process depends on the uniform distribution of resin throughout the composite part in a timely manner before the onset of gelation. Proper venting should also be incorporated in the mold design so as to drive out entrapped air and excess resin. Like the other processes, after the process is completed, the part can be cured either at room temperature or inside an oven.

RTM allows production for intermediate volume applications in a wide range of sizes and shapes and with different types, level, and orientation of fibers. The RTM process can provide considerably faster molding cycles than open molding techniques, while achieving lower tooling and equipment cost compared to conventional compression or injection molding. As a closed mold process, RTM produces both highly reproducible part thicknesses and good surface aesthetics. The rapid introduction of the resin also allows faster gel and cure compared to open molding processes. A faster curing cycle allows a high rate of output per RTM mold, compared to a hand lay-up mold. Environmentally, the RTM system is also inherently cleaner than open mold techniques and release of styrene vapors

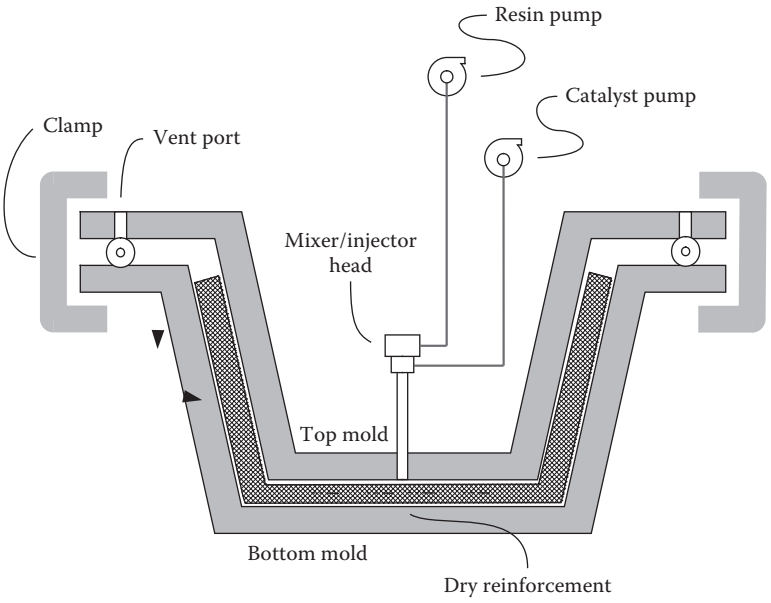

FIGURE 2.10 Components and representative configuration in the RTM process.

during RTM is lower. When necessary, this process allows for cores, inserts, or attachments inside the fiber, before infusion of the resin. However, the primary disadvantage of this process is that the mold has to be designed so that the resin can be uniformly distributed. The edges of the composite parts often tend to be rich in resin and have to be trimmed out. Parts produced by this method tend to have better mechanical properties and surface finish compared to wet lay-up; however, the properties are usually not as good as filament winding or pultrusion.

QUALITY ASSURANCE AND QUALITY CONTROL

Composites are unique in that their mechanical properties and surface aesthetics depend on the design and manufacturing process as well as on the quality of the equipment, tooling, and inspection equipment used during the manufacturing process. Quality assurance and quality control (QA/QC) thus form an integral and significant part of the manufacturing process in order to obtain high-quality composite parts. An effective quality assurance for composite parts depends on careful and systematic monitoring of the design process, the manufacturing tools and equipment, and finished quality of the manufactured part.

The first step of quality assurance begins with validation of the critical design, geometric, material and manufacturing parameters assumed by the designer, and by comparing those parameters with the tooling, assembly, equipment, and labor constraints in the manufacturing plant. Weight, cost, and productivity concerns are weighed to ensure that an optimized design and manufacturing methodology has been chosen. The second step of QA involves verification of the tooling and mold dimensional tolerances, equipment and controller calibrations, assembly stability and fabrication/handling processes. Component tests on the tooling assembly may include tests to validate aerodynamics, vibroacoustic, mechanical, and thermal loading conditions during the manufacturing process. Tests on subcomponent tool parts may include tensile and compressive coupon tests and damage tolerance tests. The third step of quality assurance, which is the focus of this section, includes quality control of the manufactured composite part through inspections and/or destructive/nondestructive testing (NDT) over the entire manufacturing process. The main components of this step included (1) validation and characterization of the properties of the raw materials used to produce the composite part, (2) monitoring the cure process and post-cure machining, and (3) validating the physical and mechanical properties of the cured composite part. Visual inspection is used to inspect bond lines that are visible in the various bond stages and to detect any visible surface discontinuities and/or delaminations. Mechanical inspection and testing are used to verify design dimensions and mechanical properties of the individual constituents as well as the manufactured composite part as a whole. Numerical simulation and study of cure kinematics may be performed to monitor the curing process. Nondestructive evaluation is used for determining defects and anomalies in the composite part and can be used as the final quality control tool before the part is shipped out. The aforementioned quality control is deemed necessary to ensure that the manufactured part consistently meets the design specifications and is necessary in order to obtain ISO 9000 certification for the product.

Visual and Mechanical Inspection

In most cases, the manufacturer of the composite part obtains the raw material components such as fibers, resins, and additives from separate suppliers, who will generally provide the mechanical properties of the components. Thus, a visual inspection of the components can be used to observe presence of visual defects, such as fiber fraying, breakage or twisting, yarn nonuniformity and misalignment of fibers, uneven weight, and weaving characteristics. Fabric mats may be inspected for distortions, fuzz balls, broken fibers, and stitching pattern. Visual inspections are also carried out periodically over the manufacturing process to ensure proper mixing of the resin components, wet out or pre-impregnation of the fibers, curing of the composite, and finished surface aesthetics. A visual inspection can often be the precursor for carrying out further mechanical tests or nondestructive evaluation.

Visual inspections may be supplemented with mechanical inspections to determine density, volume fractions, and component characteristics. The *density* of the fibers provided by the supplier is often accurate enough to be used directly by the manufacturer. However, the density of the matrix provided by the supplier is usually that of the unreinforced bulk resin. For thermosets and semi-crystalline thermoplastics that crystallize more readily when used to wet out fibers, the bulk resin density is usually lower than that found in a composite matrix of the same material. Also many resins consist of two parts that need to be mixed in specific proportions to produce the matrix. Thus, the density of the matrix may need to be determined for use in calculations of constituent fractions. ASTM D2734 (Standard Test Method for Void Content of Reinforced Plastics) and ISO 1183 (Plastics—Methods for Determining the Density and Relative Density of Non-Cellular Plastics) test standards are commonly used for determining the density of the matrix and the fibers. *Matrix burn-off* and *matrix digestion* are two of the tests most commonly used to determine the constituent fractions of the composite. In matrix burn-off, the matrix is removed from the composite sample through burning, while in the matrix digestion, the matrix is removed through chemical dissolution. Based on the weights of the dry fiber and the original composite sample, the weight fractions of the fiber and the matrix can be obtained. The corresponding volume fractions can be obtained based on the weight fractions and the densities. ASTM D2584 (Standard Test Method for Ignition Loss of Cured Reinforced Resins) and ASTM D3171 (Standard Test Method for Fiber Content of Resin-Matrix Composites by Matrix Digestion) are the recommended standards. The appropriate method is chosen depending on how fibers are affected by oxidation or high temperatures during burning such as carbon or aramid fibers, for which the matrix digestion method needs to be used. *Microscopy* may also be used to determine the constituent fractions and for accurate determination of void content. In this method, a composite sample with a very highly polished surface is placed under a microscope that is often mounted with a video camera to record the image. This image may then be analyzed using specific automated image processing programs and image enhancement techniques to determine fiber area fractions, void content and distribution, characteristics of any defects, fiber damage, and matrix-rich areas.

Mechanical Testing

Mechanical or destructive testing is often carried out on representative composite samples cut out from larger laminates to determine several mechanical properties of the composite part or that of its constituents, such as tensile, compressive, flexural, toughness, and shear properties. *Tensile tests* are used to determine the tensile modulus, Poisson's ratio, tensile strength, and ultimate tensile strains. Specific details of the tensile test can be found in ASTM D3039, ASTM D638, and ISO 3268 standard tensile testing protocols. The mode of failure will usually be in fiber fracture or fiber pullout when the sample is tested with fibers in the longitudinal direction, while matrix or fiber–matrix interface failure will usually govern with fibers tested in the transverse direction. The tensile, compressive, flexural, toughness, and shear properties can be obtained from a record of the tensile load-displacement test data.

Compressive tests are used to determine the compressive modulus, Poisson's ratio, compressive strength, and ultimate compressive strains. The compressive tests can be carried out per ASTM D3410, ASTM D695, and ISO 8515 testing standards. Depending on the type and modulus of the matrix system used, the mode of failure can be (1) microbuckling of fibers, (2) transverse tension failure or fiber splitting, and (3) compression failure of the reinforcement. The compressive properties are obtained using compressive load–displacement test data. Compressive tests may also be carried out on test specimens that have been subjected to prior impact load to determine the effect of delaminations caused by such loads.

Shear tests are used to determine the shear modulus, shear strength, and ultimate shear strains. The most commonly used shear test is the short-beam shear test per ASTM D2344 and ISO 4585.

The desired failure mode for this test is due to interlaminar shear failure between the plies, which usually occurs for a specimen support span/thickness ratio of around 4 to 5, with the specimen loaded in three-point bending. However, since the specimen is not loaded in uniform shear, it is difficult to reliably determine the shear properties and is used more as a quality control test to determine interlaminar shear strengths between specimens. Other shear tests used to determine shear properties of composites include double-notched shear test (ASTM D5379), double-cantilever beam test, and rail shear test (ASTM D4255).

Flexure tests are used to determine the flexural strength and modulus of the composite. The test is similar to the interlaminar shear test, carried out using a three- or four-point fixture (ASTM D790). However, the support span/thickness ratio is usually much larger to reduce the interlaminar shear deformation and to ensure failure is in flexure. Since a flexural failure is due to a combination of tensile and compressive forces, it is difficult to extract any inherent properties from the flexure tests and they are used more as a quality control tool.

Toughness tests may be carried out for quality control and to estimate the crack propagation and delamination characteristics of a composite sample under impact loads. The Izod and Charpy pendulum impact tests and the falling dart impact test are most commonly used.

Monitoring Cure Kinematics and Durability

The ultimate strength and mechanical properties of the composite part depends to a considerable extent on effective curing of the resin either under ambient conditions or inside controlled temperature and/or pressure chambers such as autoclaves. During the cure process if heat is applied particularly for thermoset and epoxy resins, there will be an initial decrease of viscosity for the matrix. However, as the chemical cross-linking is initiated, the viscosity of the matrix will start rising, which will eventually lead to gelation and produce the composite part in its desired shape. Polyester resins are usually cured under ambient conditions since the curing reactions for these resins are exothermic causing the temperature to rise initially.

The curing process of the resin may be monitored using thermocouples through methods such as *differential scanning calorimetry* (*DSC*), *dynamic mechanical analysis* (*DMA*), and *thermomechanical analysis* (*TMA*). In the DSC method, the resin or composite sample is placed in a heating chamber along with a reference material, and the difference in the amount of heat required to increase the temperature of a sample and reference is measured as a function of temperature. Whenever there is a phase change of the resin, referred to as the glass transition temperature (T_g), there is a change in the heat capacity of the resin and thus either an exotherm (heat given off) or endotherm (heat taken in) reaction will occur. Over the cure process of the resin, the T_g advances to higher temperatures and becomes fixed when the cure is complete. Thus, once the complete cure T_g of a particular resin has been determined, the extent of cure during the manufacturing of the composite part can be monitored by monitoring the T_g. In the DMA method, the sample is subjected to sinusoidal loading and the displacement is monitored. The T_g of the sample is taken as the point of loading at which there is a considerable change in the storage modulus or loss modulus. In the TMA method, the sample is subjected to sustained loading and change in length or thickness of sample is recorded as function of temperature.

Although the short-term mechanical properties of composites are well researched and documented, long-term durability information is not always readily available. This is because the use of composites is relatively new as compared to other materials such as steel, aluminum, and concrete. Also different types of composite deteriorate at different rates under different environmental and loading conditions depending on their physical and mechanical characteristics. Experimental observations indicate that for most fiber-reinforced plastics, long-term strengths are only a fraction of the short-term strength. Parts made from glass and aramid FRPs will usually degrade in direct contact with concrete, in the presence of moisture, and when subjected to UV radiation. Thus, this

degradation has to be taken into account while designing the composite part for a particular design life. Even though durability assessment is rarely performed by the manufacturer and is usually the responsibility of the designer and the material supplier, the manufacturer may in some cases need to include this information as part of the material data sheet for specific applications. The most common durability tests are to expose the composite parts to high temperatures, moisture, UV radiation, and flammability in controlled environmental chambers. The degradation in the composite properties caused by the environmental exposures over time is monitored through mechanical tests. Since it is not possible to determine the deterioration of the composites over its entire life span, usually the baseline tests are run for a year to 2 years and the properties at the end of the life span of the composite are extrapolated to design life using theoretical models.

Nondestructive Testing

Since it is usually not feasible to carry out any of the mechanical tests on finished composite parts because of size and shape constrains, nondestructive tests are ideally suited for quality control on the factory floor. Even though most of the nondestructive tests are subjective and aim at detecting anomalies and defects rather than quantifying them, these tests are very useful quality control tools. Also with considerable advances in electronic recording, data processing, and image and acoustic enhancement along with detailed numerical analysis and modeling, it is possible to use these nondestructive methods as quantitative tools to determine the effects of any defects or anomalies on the performance of the composite part.

Ultrasonic testing is the most common method for detecting defects, such as delaminations, voids, disbonds, presence of foreign particles, and flaws in fiber orientation or thickness. In this method, the part is subjected to ultrasonic waves and the reflected (pulse echo) or transmitted waves are recorded and then compared to reference waves sent through a defect-free sample. The presence of a defect acts as a material of lower density changing the wave pattern and its speed. Water is usually used as a coupling medium between the transducer producing the wave and the composite part so that very little energy is lost during transmission of the wave from the transducer to the composite, which clearly identifies a void or a defect. However, this is also a drawback of this method, since a testing chamber is needed to immerse the composite part in the coupling medium.

Vibrational (*modal*) *inspection* uses the natural frequency and modal characteristics of the composite to locate defects. The composite part is subjected to continuous or pulse excitation, through an automated shaker or impact hammer, and accelerations are recorded, which can then be converted into a natural frequency spectrum and mode shapes using vibrational analysis methodologies. These can then be compared to reference frequencies and mode shapes of defect-free sample to qualitatively determine the presence of defects. If the information is recorded over the entire surface of the part through well-placed accelerometers, the reference and actual vibrational characteristics can be processed by automated NDT defect detection algorithms and numerical procedures to locate a defect and quantify its damage severity.

Radiographic inspection is carried out by subjecting the composite part to radiation, most commonly using x-rays and neutron radiation. The flaws and defects can be detected by virtue of the difference in absorption of radiation between defect-free composite parts compared to that with defects due to the density differences between the two. The unabsorbed radiation is either detected by a photographic film or through a camera. However, since many composites are transparent to x-rays, low-energy rays need to be used and in some instances an opaque liquid penetrant may need to be introduced into a defect. The radiography process is usually very expensive and may not be suitable for use as a quality control tool for periodic inspection.

Thermographic inspection relies on the rate of thermal diffusion to locate a defect. In this inspection, the composite part is first subjected to heat on the surface either through a high-intensity flash

heat impulse (such as a xenon flashbulb) or through gradual heating using a lightbulb or ambient heating. The sample may also be heated uniformly in an oven and the loss of heat upon cooling may be monitored. The flash impulse heating is usually preferred since the amount of heat input can be monitored and replicated between samples. It also uses a portable system that can be used for periodic inspection during the manufacturing process. The rate of diffusion of heat is different through different materials and depends on the density of the material through which it passes. Thus, in the presence of a defect that has a different density than that of the composite, there will either be a buildup of heat (hot spot) in defects such as air voids or an absorption of heat (cold spot) at locations of defects such as uncured resin or entrapped moisture. The thermal gradients over the surface of the composite can be recorded by a thermographic camera. The presence of defects can be identified by peaks or troughs in the thermal gradient. Using image processing software that captures the data from the camera over a period of time, it is possible to quantitatively determine the location and severity of the defect. The resolution of the thermographic image is usually lower than that of ultrasonic or radiographic inspections, particularly for unidirectional fiber composites in which the heat conductivity in the fiber direction is much greater than that in the thickness direction. However, the portability of the system and the relative ease of using it in a factory setting make it an attractive tool for quality control of composites.

Acoustic emission inspection detects defects by "listening" to sounds emitted by the composite sample when it is stressed either through mechanical or thermal loading. The sounds are emitted due to micro-failures such as individual fiber fractures and progressive matrix micro-cracking. The number of acoustic events over sustained loading will be much greater for a composite part with defects. However, currently it is very difficult to quantify the location and severity of defects using this method particularly in a factory setting.

CONCLUSIONS

The manufacturing processes, quality control of these processes, and the conceptual design of the composite part are of equal importance. Careful consideration of quality control and the conceptual design is necessary to determine the manufacturing process most suitable for a particular application in terms of constructability, economics, production speed, and desired quality. Similarly, an appropriate quality control methodology has to be developed by the manufacturer to ensure a quality product and to serve as a prerequisite for obtaining certifications from many government and commercial certification agencies. This chapter is intended to give the reader an overview of different manufacturing processes and quality control tools available for composites.

For additional information and details on manufacturing processes, quality control, and evaluation of FRP composites, see Astrom (1997), Peters (1998), and Mazumdar (2002).

REFERENCES

Astrom, B.T. *Manufacturing of Polymer Composites*. London, U.K.: Chapman & Hall, 1997.

Mazumdar, S.K. *Composites Manufacturing—Materials, Product, and Process Engineering*. Boca Raton, FL: CRC Press, 2002.

Peters, S.T. (Ed.). *Handbook of Composites*, 2nd edn. London, U.K.: Chapman & Hall, 1998.

3 FRP Composite Constituent Materials

Hector Estrada and Luke S. Lee

CONTENTS

INTRODUCTION

A composite material is a material consisting of two or more distinct parts. By this broad definition, nearly all materials occurring in nature can be classified as a composite material. Even atoms can be considered a composite being composed of electrons, protons, and neutrons. A narrower definition of a composite material is one where two or more chemically distinct and mechanically separable materials, on the macroscale, having a distinct interface separating them, are combined to give desirable overall properties. For example, concrete and steel are combined to form reinforced concrete taking advantage of the high compressive strength of concrete and the high tensile strength of steel. In the case of advanced composite materials, the matrix or fiber materials alone have a limited structural value. The matrix of a composite serves to bind reinforcement together to form a composite structure and protect reinforcement from physical damage and chemical attack, while the fibers provide strength and stiffness. Therefore, the combination of fiber and matrix materials provides a synergistic effect on the overall mechanical properties.

In civil infrastructure, the increasing use of composite materials has paralleled technological development and advances in materials. Advanced systems and components such as suspension bridges, aircraft, and even microcomputers are dependent on available materials with characteristics to withstand service conditions and prevent failure. Irrespective of the industry or application,

the final limitation on advancement depends on availability of materials. Composites can address this limitation with their tailorable characteristics and properties to satisfy design criteria of any complex engineered systems.

The existence of composite materials is arguably as old as life itself, with examples occurring in nature, such as wood and bone. Man-made composites can be traced back in time to approximately 4000 BC, where biblical references in the Book of Exodus state "do not give them straw for their bricks, make them find their own straw," indicating that straw was mixed with clay to manufacture straw-reinforced bricks. This practice was so successful in ancient Egypt that it is still in use in many parts of the world today. Later, ancient Romans invented concrete and built many structures and monuments with it, including the Pantheon in Rome, which was constructed more than 2000 years ago and stands to this day. Contemporary examples of man-made composites include reinforced concrete and advanced composites such as those discussed in this handbook.

CHARACTERISTICS OF COMPOSITE MATERIALS

A composite material consists of one or more discontinuous phases (reinforcement) embedded in a continuous phase (matrix) with an interface between them; that is, a composite consists of reinforcement in a matrix with the interface acting as the bond between them. Table 3.1 lists the description of each of the three composite constituents.

The performance specific design of composite materials suggests that a wide range of factors influence the properties of a composite. The following list provides a summary of possible factors that can alter composite properties and influence performance:

- Properties of composite constituent materials
- Distribution of constituent materials
- Interaction (bonding) among constituents
- Geometry of the reinforcement, specifically its shape, size, and size distribution
- Reinforcement concentration or volume
- Homogeneity or uniformity of the composite system
- Orientation of constituents

MATRIX CONSTITUENTS

The matrix of a composite material serves to bind the reinforcement together, transfers loads to the reinforcement, and acts as a barrier to minimize damage from environmental attack or during handling. The matrix material also has the largest influence on the shear, transverse, and compressive

TABLE 3.1
Description of Constituent Materials

Composite Constituent	Description
Reinforcement	This is the discontinuous phase, which is strong and/or stiff and typically lightweight
Matrix	This is the continuous phase that transfers the load among reinforcement, provides protection to reinforcement, and is typically lightweight
Interface	This provides bond between reinforcement and matrix and can be strong or weak, depending on application

FIGURE 3.1 Temperature range for different matrix materials.

strength of the composite. Matrices are typically polymers (thermosets or thermoplastics), metals, or ceramics. The selection of matrix material is often influenced by the required temperature performance of the composite; polymers are usually selected for lower temperatures and ceramics are used in high-temperature applications. Figure 3.1 shows temperature ranges associated with typical matrix materials.

Metal and ceramic matrices have not been used in civil infrastructure applications because of cost. Polymers are the most commonly used form of matrix in civil infrastructure applications. Advantages of polymer matrices include their low cost, ease of processing, low density, and good chemical resistance. Disadvantages associated with the polymer matrix include low strength and stiffness, low operating temperature, deterioration due to ultraviolet radiation exposure, and degradation of mechanical properties due to moisture absorption.

Polymer matrices are classified into thermosets and thermoplastics, based on the way they respond to heat. When heated, thermosets undergo permanent reactions, while thermoplastics only undergo temporary physical change. Thermosets are formed by irreversible chemical reactions between polymer chains (cross-linking), while thermoplastics are composed of long polymer chains that can be heated, deformed, and cooled, with no chemical reaction occurring. A detailed discussion of these two general classes of polymers follows in the ensuing sections.

Thermosets

Thermosets are cross-linked polymers that have undergone an irreversible chemical reaction to permanently connect all molecular chains with covalent bonds. This material sets (or cures) into shape by adding a catalyst (or by heating). The processing of a thermoset involves an exothermic reaction where the catalyst (or curing agent) is mixed with a polymer resin—both are generally liquid. The resulting mixture is liquid and it begins to set (or gel). As the polymer gels, it undergoes an irreversible chemical reaction to form a 3-D network of cross-links, gaining a higher degree of rigidity. During the cooling period, which follows the exothermic reaction, residual and shrinkage stresses can occur. The properties of the matrix are dependent upon the degree of cross-linking and their density. It is important to note that the rigid, 3-D molecular structure will not regain processability under any circumstances; it has transformed permanently.

Typical thermosets include epoxy, polyester, and phenolic resins. This class of polymers is the most widely used in civil infrastructure applications because they outperform thermoplastics in terms of mechanical properties, chemical resistance, thermal stability, and overall durability. Also, thermoset matrices have a stronger interface bond between polymeric chains. The disadvantages include long cure times, not recyclable, and brittle behavior.

Temperature plays an important role in the properties of all polymer materials. In the case of thermosets, exposure to elevated temperatures (close to but below the glass transition temperature, T_g) greatly influences the mechanical properties and durability of the matrix. The glass transition temperature, T_g, is the temperature at which a material transitions from a hard and brittle state into a soft and rubberlike state. Therefore, when the exposure temperature reaches T_g of the matrix, a dramatic reduction in stiffness is observed as illustrated in Figure 3.2.

The mechanical properties of thermosets are not only temperature dependent but also time dependent. This makes the material viscoelastic, with stress–strain behavior, as shown in Figure 3.3. This viscoelastic behavior makes polymer matrices susceptible to creep effects.

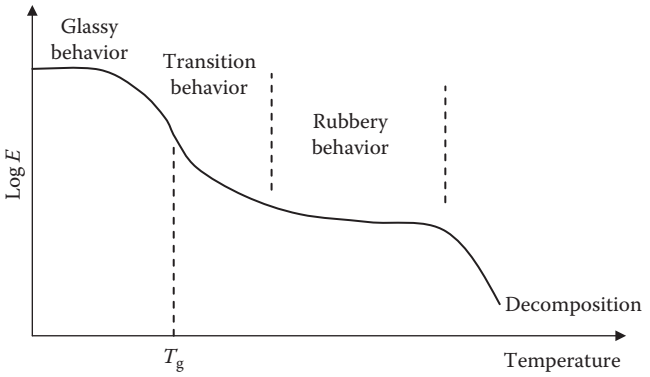

FIGURE 3.2 Logarithm of stiffness versus temperature for a thermoset matrix.

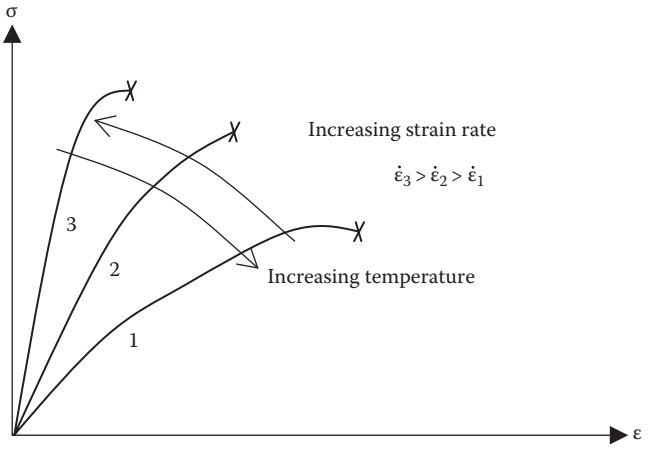

FIGURE 3.3 Load-rate- and temperature-dependent stress–strain behavior of thermoset matrices.

Thermoplastics

Thermoplastics are linear or branched polymers, with molecular chains that are connected or formed by weak intermolecular bonds (van der Waals bonds). Unlike thermosets, thermoplastics do not cure or set when heated; in fact, they soften and become more fluid as the temperature increases. The processing of thermoplastics therefore involves softening/melting by applying heat; as the material cools, it hardens into the shape of the mold containing it. There is no chemical reaction or cross-linking as with thermosets; the material changes are entirely physical. Because the changes are reversible, thermoplastics can be recycled and reprocessed, although after many recycling iterations, the polymer tends to degrade.

The properties of thermoplastics are strongly dependent on crystallinity, temperature, and time. Like thermosets, the stress–strain behavior of thermoplastics is viscoelastic, as shown in Figure 3.4. In general, thermoplastics are more ductile than thermosets, as presented in Figure 3.4. Thermoplastics can display failure strains much greater than 100%, whereas the failure strains of thermosets are typically less than 10%. As displayed in Figure 3.4, the strength of a thermoplastic is dependent on strain rate and temperature.

Typical thermoplastics include polyethylene, polycarbonate, nylon, polyether–ether ketone resins. This class of polymers is rarely used in civil infrastructure applications because of their poor chemical resistance, unknown processing for composites properties, high shrinkage (as much as 20%), and

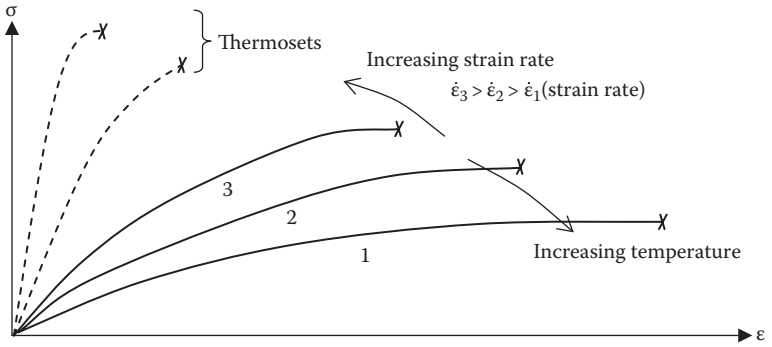

FIGURE 3.4 Load-rate- and temperature-dependent stress–strain behavior of thermoplastic matrices.

TABLE 3.2
Typical Properties of Thermoset and Thermoplastic Polymers

Property	Epoxy	Polycarbonate
Density, ρ (g/cm^3)	1.2–1.3	1.0–1.2
Modulus of elasticity, E (GPa)	3–4	2.2–2.4
Ultimate strength, σ_{ult} (MPa)	55–130	45–70
Thermal expansion, α (10^{-6}/°C)	45–65	70
Failure strain, ε_f	1–8	50–100

poor durability (i.e., moisture plasticizes or softens the polymer chains). Also a comparison of the properties of a thermoset (epoxy) and a thermoplastic (polycarbonate) shows that thermoplastics have much lower stiffness and strength than thermosets (see Table 3.2). The advantages of a thermoplastic, as compared to thermosets, include short melting times, easy processing (no catalysts needed during processing), recyclable, and good fracture toughness (ductility).

Thermoplastics can be amorphous and semicrystalline. The stiffness of thermoplastics also depends on temperature, with significant decreases in stiffness observed with exposure to temperatures at or greater than the glass transition temperature, T_g. This dependence however is most pronounced for amorphous than semicrystalline thermoplastics as exhibited in Figures 3.5 and 3.6.

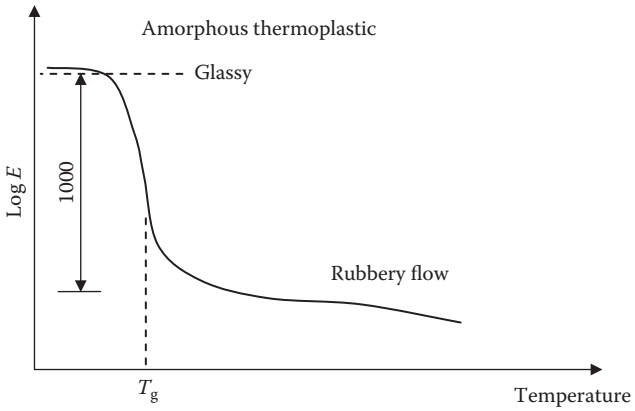

FIGURE 3.5 Logarithm of stiffness versus temperature for an amorphous thermoplastic matrix.

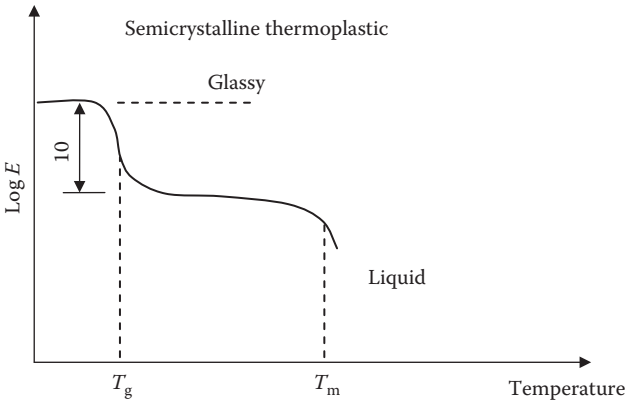

FIGURE 3.6 Logarithm of stiffness versus temperature for a semicrystalline thermoplastic matrix.

That is, the loss of stiffness at the glass transition temperature is not as severe in a semicrystalline thermoplastic, which displays a distinct melting temperature, T_m. There is no noticeable T_m for amorphous thermoplastics (see Figure 3.5).

REINFORCEMENT CONSTITUENTS

As previously mentioned, improved properties over parent constituent materials are the most desirable characteristic of composites, for example, strength, stiffness, and toughness. These properties are actually highly dependent on the type and geometry of the reinforcement. Composites are generally classified based on reinforcement geometry into fiber-reinforced composites or particulate-reinforced composites. Fiber-reinforced, or fibrous, composites have their properties derived primarily from the reinforcement. As with the reinforcement, fibrous composites are typically strong, stiff, and tough and can perform well at elevated temperatures. Particulate composite properties, on the other hand, are primarily derived from the matrix. In this section, we discuss a number of reinforcement materials, with particular emphases on those used in civil infrastructure composite applications.

Most of the materials used as reinforcement for composite materials consist of elements found in the first two rows of the periodic table. The elements include beryllium (Be), boron (B), carbon (C), magnesium (Mg), aluminum (Al), and silicon (Si). These elements are considered strong, stiff, and light; they form covalent bonds and are brittle, which makes them sensitive to flaws. The specific reinforcement and chemical composition include

- Glass (silica, SiO_2; calcium oxide, CaO; etc.)
- Carbon (graphite, C)
- Kevlar®, Spectra® (organic, carbon based)
- Silicon carbide (SiC)
- Aluminum (Al_2O_3)
- Boron (B)
- Beryllium (Be), which is highly toxic

The three most popular reinforcing materials are glass, carbon, and silicon carbide—in that order—which directly correlate with cost. Glass and carbon are the most widely used reinforcement materials for civil infrastructure composite applications because of cost. For applications that require large amounts of materials, glass is the most popular because it is the least expensive; for example, most FRP structural sections fabricated by pultrusion are reinforced with fiberglass. However, there are a number of applications where carbon is more cost effective because of its superior strength

and stiffness as compared to glass. These applications include seismic retrofit of concrete columns using carbon fiber wrapping to enhance concrete confinement, where light weight and high strength is required.

Fibrous Reinforcement

Fibrous reinforcement includes continuous fibers, discontinuous fibers, whiskers, and carbon nanotubes (CNTs). The most common types of fibrous reinforcement are glass, carbon, and aramid fibers—other types of fibers include boron, silicon carbide (SiC), alumina, and sapphire, all of which are used in special applications. The choice of fiber for a specific application depends on the desired mechanical and environmental properties, but the most important deciding factor is typically cost. Also, there a number of compatibility issues that must be taken into account when combining these various types of reinforcement with matrix materials; the typical matrix selected for different fibers is shown in Table 3.3.

Continuous fibers are available in long continuous fiber bundles, also known as yarns, tows, strands, and rovings, with individual fibers having a length-to-diameter ratio that approaches infinity and a diameter on the order of 10 μm (Astrom, 1997). For reinforcement, fibers are used in bundles, configured as unidirectional, woven, or braided fabrics; these configurations also affect the properties of the composite, with unidirectional being the most desirable based on strength and stiffness, while the other two being more desirable from fabrication and handling perspectives.

One advantage of using continuous fiber reinforcement is the reduction in the number of flaws and flaw sizes in the material, both of which help the composite approach its theoretical strength. On average, the theoretical longitudinal strength of a fiber is approximately $\sigma_{th} \cong E/2\pi \cong E/6.3$, whereas the typical measured strength of a fiber is approximately $\sigma_{me} \cong E/15$, where E is a fiber's longitudinal modulus of elasticity (Felbeck and Atkins, 1984). There are some material geometries that approach the theoretical strength, for example, iron whiskers with a theoretical strength of $\sigma_{th} \cong 200$ GPa/6.3 = 31.7 GPa and measured strength of $\sigma_{me} \cong 14$ GPa. Note that measured strength is approximately half of the theoretical strength in this case (Felbeck and Atkins, 1984). Another example is multiwall CNTs, which contain walls with about 15 graphene layers (a single layer of carbon atoms in hexagonal arrangement) forming a cylinder of 10–15 nm outside diameter, 2–4 nm inside diameter, and about 10–20 μm long, capable of reaching a strength of 150 GPa and elastic modulus of 800–900 GPa because of the defect-free structure.

An examination of fibers at the crystal level is useful when examining the results of theoretical strength values. In an unstressed condition, the repulsive and attractive forces between atoms in a crystal are in equilibrium for a given spacing of atoms. If a crystal is strained, however, the net force resisting the external pulling force increases from zero as the atoms move away from equilibrium positions. Eventually, a maximum force is reached and the force between atoms decreases as the spacing between atoms increases. The ideal strength of the material in terms of cohesion is related to that maximum value. Figure 3.7 depicts a typical curve for applied force or stress versus distance at the atomic level—the springs represent the bond between two atoms.

TABLE 3.3
Fiber Choice for Different Matrix Materials

Matrix	Fiber Choice
Polymer	Glass, carbon, aramid (Kevlar, etc.)
Metal	Silicon carbide, boron, alumina (large diameter)
Ceramic	Silicon carbide, alumina, and sapphire

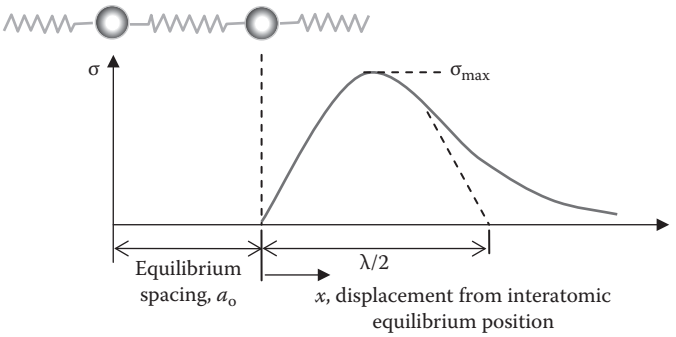

FIGURE 3.7 Applied stress versus displacement at the atomic level.

Since the force or stress, σ, is periodic, the relationship between stress and displacement can be expressed as follows:

$$\sigma = \sigma_{max} \sin\left(\frac{2\pi x}{\lambda}\right) \tag{3.1}$$

where

λ is an artificial wavelength

x is the displacement relative to the interatomic equilibrium spacing, a_o, during a unidirectional tensile loading condition

For small displacements, x, the crystal strain is defined as $d\varepsilon = dx/a_o$. In the elastic region around the origin, from Hooke's law, $d\sigma/d\varepsilon = E$. Substituting the strain definition into Hooke's law yields the following:

$$\frac{d\sigma}{dx} = \frac{E}{a_o} \tag{3.2}$$

From Equation 3.1,

$$\frac{d\sigma}{dx} = \frac{2\pi}{\lambda}\sigma_{max} \cos\left(\frac{2\pi x}{\lambda}\right)$$

Since $2\pi x/\lambda \ll 1.0$, $\cos(2\pi x/\lambda) \approx 1.0$. Therefore, for small values of x/λ, combining Equations 3.1 and 3.2 results in a maximum theoretical fiber strength of

$$\sigma_{max} = \frac{\lambda E}{2\pi a_o}$$

If it is assumed that λ and a_o are approximately the same size (i.e., $\lambda \cong a_o$), then

$$\sigma_{max} \cong \frac{E}{2\pi}$$

The discrepancies between theoretical and measured tensile strength of brittle fibers can be attributed to the presence of microcracks or flaws within the fiber. Statistically, a flaw of a given size is less likely to occur in a small lump of material as opposed to a larger quantity of the same material. For instance, the size effect is evidenced by lower measured tensile strengths of thick rods versus thin fibers. Flaws in the fiber act as stress concentrations that raise local stresses around the flaws to the theoretical maximum although stresses remain relatively low away from flaw locations.

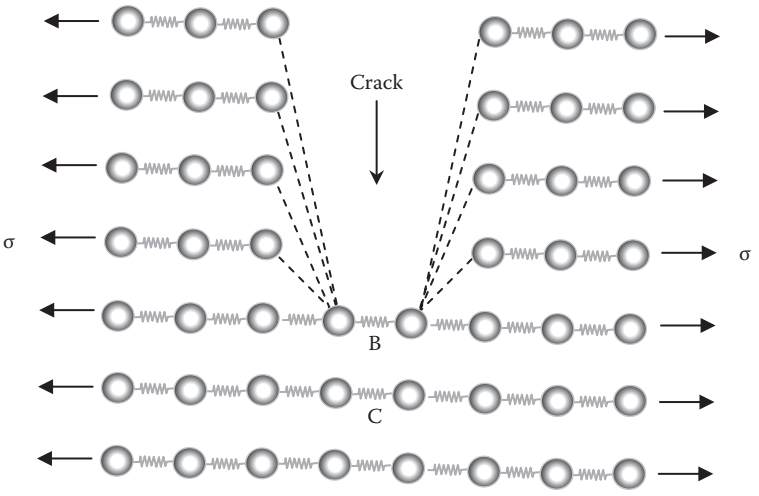

FIGURE 3.8 Effect of cracks on atomic bonds.

Bonds adjacent to a flaw or crack tip can be broken, and crack opening occurs as illustrated in Figure 3.8. All missing bonds due to crack opening are redirected to the two atoms adjacent to point B at the crack tip giving rise to a stress concentration, as shown in Figure 3.8.

Fiber reinforcement does not follow a classification system based on physical properties (like matrices); rather, fibers are classified based on their material composition. As indicated earlier, there are a number of materials that have been used to produce fibers. A detailed discussion of the most important fiber materials ensues in the following sections.

Glass Fibers

Glass fibers are typically used in low-cost applications of polymer matrix composites. The primary advantages of glass fibers are their low cost and high strength, along with typical glass properties such as hardness, corrosion resistance, and chemical inertness. However, glass fibers also possess some disadvantages, including

- Low modulus of elasticity, typical of all glass fibers.
- Poor abrasion resistance, where rubbing of fibers together results in surface flaws, thus lowering strength. Consequently, glass fibers are manufactured with various protective coatings.
- Poor adhesion to polymer matrix resins, especially in the presence of moisture. The poor adhesion requires the use of chemical coupling agents such as silane.

There are different types of glass fiber available for various applications, including "A" or "AR" glass for alkaline resistant, "C" glass for corrosion resistance, "E" glass with enhanced electrical properties, "S" and "R" glass for high strength and stiffness, and some other specialized compositions. E-glass offers high tensile strength and excellent durability characteristics, which is the reason it serves as a general purpose grade of glass fiber and is the most widely used type of glass (Astrom, 1997). S- and R-glass display higher strength, stiffness, and temperature tolerance when compared to E-glass; however, the cost of S- and R-glass can be three to four times that of E-glass. Table 3.4 provides an overview of the properties of various glass-fiber types. All glass fibers are composed of an amorphous silicon oxide, SiO_2 (or silica), as the main constituent molecule. Other constituent molecules include those listed in Table 3.5. These constituent oxides typically have a 3-D isotropic structure (unlike carbon and organic fibers, which are discussed later) that gives glass its strength and stiffness.

Structure of glass is based on a silicon dioxide, SiO_2, backbone in the form of $(SiO_4)_n$ tetrahedral because SiO_2 molecules analogous to carbon dioxide molecules do not exist. Instead, in nature, SiO_2 is often found as a crystalline solid with the structure shown in Figure 3.9.

TABLE 3.4
Typical Properties of Glass Fibers

Properties	E-Glass	A-Glass	S-Glass	C-Glass	R-Glass	D-Glass	High Modulus
Density, ρ (g/cm³)	2.54	2.45	2.49	2.45	2.58	2.14	2.89
Tensile strength, σ_{ult} (GPa)[a]	3.45	3.30	4.58	3.31	4.40	2.50	3.40
Elastic modulus, *E* (GPa)	72.4	69.0	85.5	69.0	84.8	55.0	110.4
Diameter, *d* (μm)	3–20	—	8–13	—	—	—	—
Thermal expansion, α (10^{-6}/°C)	5.0	—	2.9	6.3	—	3.1	—
Max operation temp. (°C)	550	—	650	600	—	477	—

Sources: Adpated from Chawla, K.K., *Composite Materials: Science and Engineering*, 2nd edn., Springer-Verlag, New York, 1998; Agarwal, B.D. and Broutman, L.J., *Analysis and Performance of Fiber Composites*, 2nd edn., John Wiley & Sons, New York, 1990; Hull, D. and Clyne, T.W., *An Introduction to Composite Materials*, 2nd edn., Cambridge University Press, New York, 1996; Tsai, S.W., *Composite Design*, 4th edn., Think Composites, Dayton, OH, 1988; Mathews, F.L. and Rawlings, R.D., *Composite Materials: Engineering and Science*, 2nd edn., Woodhead Publishing Limited, Boca Raton, FL, 1999.

[a] Virgin strength values of fresh-drawn fibers (measured by ASTM D3379) can yield up to 3.5 GPa for E-glass and 4.8 GPa for S-glass, but actual values are only 1.74 GPa for E-glass and 2.1 GPa for S-glass (which constitutes about 50% reduction) because of damage produced during the various stages of processing.

TABLE 3.5
Typical Composition of Different Types of Glass Fibers

	% Weight			
Material	A-Glass	C-Glass	E-Glass	S-Glass
Silicon oxide (SiO_2)	64	65	54	64
Aluminum oxide (Al_2O_3)	1	4	15	25
Zirconium oxide (ZrO_2)	13	—	—	—
Calcium oxide (CaO)	5	14	17	—
Magnesium oxide (MgO)	—	3	5	10
Sodium oxide (Na_2O)	14	8	0.6	0.3
Boron oxide (B_2O_3)	—	5	8	—
Titanium oxide (TiO_2)	3	—	—	0.2

Sources: Adpated from Chawla, K.K., *Composite Materials: Science and Engineering*, 2nd edn., Springer-Verlag, New York, 1998; Agarwal, B.D. and Broutman, L.J., *Analysis and Performance of Fiber Composites*, 2nd edn., John Wiley & Sons, New York, 1990; Hull, D. and Clyne, T.W., *An Introduction to Composite Materials*, 2nd edn., Cambridge University Press, New York, 1996.

Every silicon atom is bonded to four oxygen atoms tetrahedrally; thus, every oxygen atom is bonded to two silicon atoms. SiO_2 in this crystalline form is called silica, which is often identified as quartz (large crystals) or sand (miniscule crystals). In order to manufacture glass, silica particles are heated until melting and then cooled down quickly. During the melting process, the silica and oxygen atoms break out of their crystal structure. If the cooling process is slow, the atoms slowly line up back into their crystalline arrangement, whereas in a quick cool down, silica atoms are stopped in their current position and are unable to return to the crystalline arrangement. For structural application,

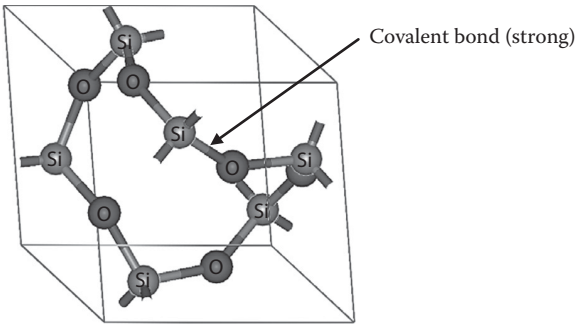

FIGURE 3.9 Silica glass network structure.

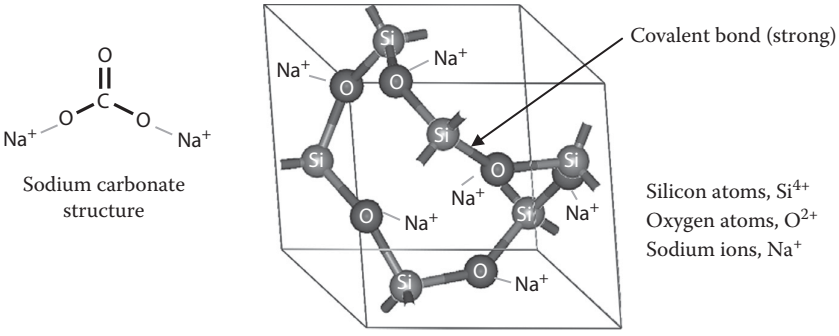

FIGURE 3.10 Silica glass network structure after sodium carbonate (Na_2O) is added.

most glass fibers are manufactured by melting sand and adding sodium carbonate. The sodium ions are ionically linked to the oxygen atoms but are not part of the network, as shown in Figure 3.10.

Glass can be tailored to various applications with the addition of oxides to the basic composition, as shown in Table 3.4. The typical materials used to produce glass are sand, limestone, and alumina. These materials are melted in a refractory furnace at 1260°C, and at this stage the glass is also refined. The melted glass then passes through platinum bushings so as to form the fibers. Next, the fiber surface is chemically treated with a protective coating and a chemical coupling agent, called size, to promote adhesion to the matrix material. The chemically treated glass fibers are then wound onto a spool at a high speed or, in some cases, chopped for further processing.

The chemical treatment is necessary to reduce damage sustained when fibers rub against one another during processing. The protective coating or size, in addition to helping minimize fiber damage, also improves adhesion between fiber and matrix. Two general types of sizes are available for glass fibers: starch–oil sizes that are temporary and compatibility sizes that serve as coupling agents. A temporary size acts as a lubricant to prevent abrasive wear during processing and imparts antistatic properties and must be removed prior to bonding with matrix materials. A compatibility size acts as a coupling agent and protects the glass fiber from moisture effects. Organo-functional silanes, $X_3Si(CH_2)_nY$, are commonly used as compatibility sizes that are chemically linked between the glass surface and the matrix. As shown in Figure 3.11, the organo-functional group, Y, is intended to react with a polymer matrix to form strong covalent bonds and may also form physical bonds or van der Waals bonds. The hydrolysable group, X, is essential for generating intermediate silanols to establish hydrogen bonds with the glass-fiber surface. Basically, X bonds to the glass fiber, while Y bonds to the matrix (Agarwal and Broutman, 1990).

Glass-Fiber Terminology

Composite glass-fiber reinforcement is available in bundles of individual fibers or filaments called strands or ends, which consists of 204 filaments. The strands are further bundled into groups

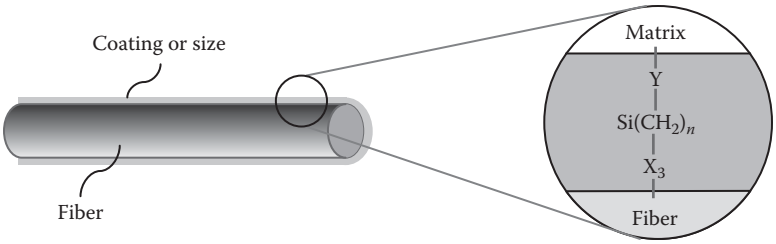

FIGURE 3.11 Interface between glass fibers and matrix.

called rovings, which are wound onto a spool for packaging. These rovings are then stitched together to form a band used in composite fabrication. Rovings can also be used directly in composite fabrication, particularly pultrusion, filament winding, and other manufacturing techniques, which are discussed in Chapter 2. For some manufacturing techniques, it is more practical to use glass fibers in forms other than bands and rovings, including chopped strands, chopped strand mat, and woven fabric or cloth, woven fabric being one of the most commonly used forms.

Woven fabrics are constructed of interlaced yarns (rovings or bands) usually in a planar structure. Typical glass-fiber fabrics are manufactured by interlacing warp (lengthwise direction) yarns and fill (crosswise direction, also known as weft) yarns on conventional weaving looms (see Figure 3.12). These fabrics can be woven into a variety of structures with exact control over thickness, weight, and strength. The main factors that define a given fabric structure are weave, density of yarns in the fabric, fabric count, characteristics of warp and fill yarn, characteristics of fibers, and factors introduced during weaving, such as yarn crimp. The fabric count refers to the number of warp yarns per inch (ends) and the number of fill yarns per inch (picks). The weave of fabric refers to how warp and fill yarns are interlaced. Weave determines the appearance and some of the handling characteristics of a fabric. Among the most popular weave patterns are plain, twill, crowfoot satin, leno, and unidirectional.

There are two general categories of fabrics used in composites: woven and unidirectional. Woven fabrics combine warp yarns along the major axis and fill yarns across the fabric (Figure 3.12). Unidirectional fabrics have most of the yarns along the warp direction and only nominal fibers in the fill direction to keep the longitudinal fibers in a plane, with specific properties controlled by varying the number of filament ends per inch and type of yarn.

Properties of woven fabric can also affect the type of weave used. Although woven fabrics are more expensive than unidirectional fabrics or tape, significant cost savings can be realized in applications with complex molding operation because labor requirements are reduced. Complex shaped part requiring careful positioning of the reinforcement can benefit from the use of the more workable woven forms of fiber (see Figure 3.13). The plain weave is the most cost-effective of the fabric

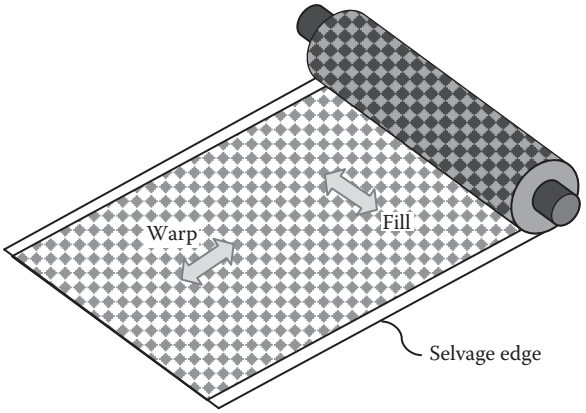

FIGURE 3.12 Glass-fiber fabric weaving directions.

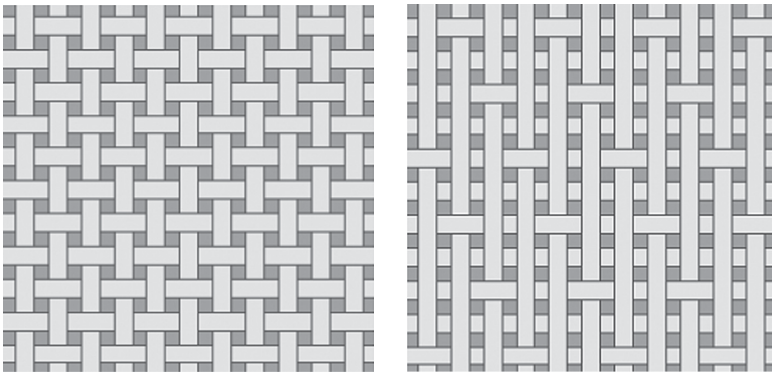

FIGURE 3.13 (a) Plain and (b) satin weaves.

types because it has superior stiffness properties and is more open, which is useful when infusing resin. However, the satin (crowfoot or multi-harness) weave provides better draping for conforming to contoured surfaces than plain weave.

Carbon Fibers

Compared to glass fibers, carbon fibers have found only limited application in construction. Carbon fibers are characterized by high specific strength, high specific stiffness, and high cost; the first two attributes make these fibers ideal where lightweight is important, such as aerospace applications. Despite the high cost, carbon fiber–based composites have been used in many critical civil infrastructure applications, including seismic rehabilitation, retrofitting, and repair of structural systems such as concrete beams and columns.

This type of fiber is classified as graphite- or carbon-based on the corresponding elemental carbon content. Fibers containing 90% or more elemental carbon are identified as graphite fibers, whereas carbon fibers are those containing 80%–90% elemental carbon—the second type being far more abundant. The carbon content in a fiber is a function of the heat-treatment temperature during processing. The processing temperature also controls the internal structure of the fibers. Carbon fibers are anisotropic with higher strength and stiffness in the longitudinal direction of the fiber compared to the transverse direction. They are composed of small crystallites of turbostratic graphite. In each graphite single crystal, the carbon atoms are arranged in hexagonal arrays, as shown in Figure 3.14. Atoms in the basal planes are held together by strong covalent bonds, while weak van der Waals forces exist

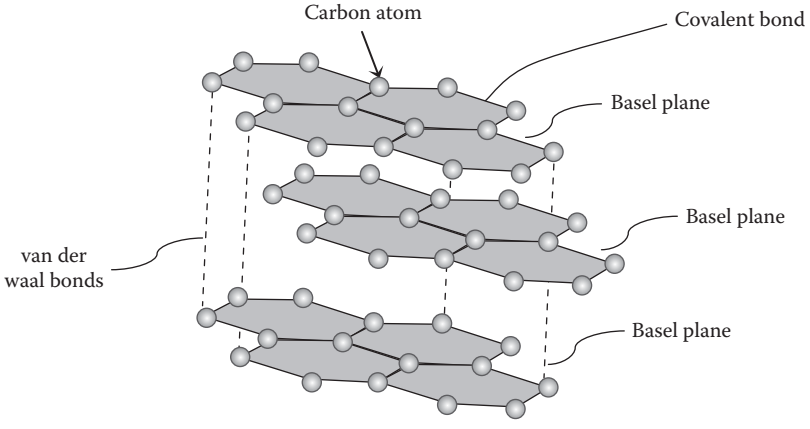

FIGURE 3.14 Lattice structure of graphite.

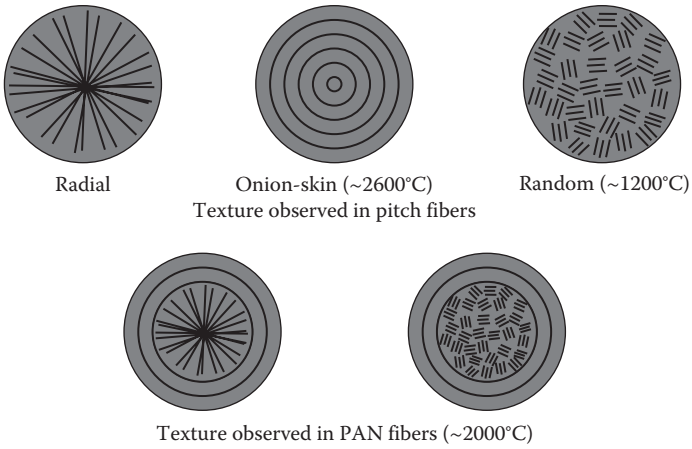

FIGURE 3.15 Cross-sectional structure of carbon fibers.

between layers. This indicates that the basic crystal unit in a fiber is anisotropic. Carbon fibers display a high modulus in the plane of the basal planes, depending on the degree of alignment, and lower modulus transverse to the basal planes in the direction of the van der Waals bonds. Consequently, the longitudinal fiber modulus of elasticity, E_{fL}, ranges from 250 to 390 GPa and the transverse fiber modulus of elasticity, E_{fT}, ranges from 12 to 20 GPa. High strength of carbon fibers is achieved by good alignment of the basal planes in the fiber direction. Also, the arrangement of layer planes in the cross section influences the transverse and shear properties of the fiber. Figure 3.15 illustrates the cross-sectional structure of several types of carbon fibers. Fiber structure is highly influenced by fabrication method.

Carbon fibers are categorized by fabrication method. Fabrication of carbon fibers involves thermal decomposition (pyrolysis) of the raw material (or precursor). Common precursors for carbon fiber are polyacrylonitrile (PAN), rayon, or pitch, the latter being a complex mixture of thousands of different species of hydrocarbon and heterocyclic molecules. These raw materials are primarily derived from petroleum and asphalt by-products.

To fabricate PAN carbon fibers, first the PAN precursor is spun into a fiber and stretched to produce molecular alignment. The stretched fiber is then heat treated in an oxygen-rich environment. Next, carbonization takes place at 1500°C to drive out non-carbon elements and form a carbon ring structure. Finally, graphitization takes place at 3000°C to convert carbon to turbostratic graphite. The modulus and strength of the fiber depend on this final heat treatment, which governs the crystallite size and alignment. Similar to the fabrication process for glass fibers, the carbon fiber surface is chemically treated with a protective coating and a chemical coupling agent before any further processing. The chemically treated carbon fibers are then wound onto a spool, or in some cases, the matrix is applied to the fibers to produce unidirectional prepregs that can be used in the manufacturing of composite components. These prepregs typically are pre-impregnated with a thermoset and frozen to slow down the setting process.

The pitch fibers are produced by spinning the molten pitch. The orientation of the fibers depends on the spinning conductions. The fibers are oxidized and carbonized at temperatures around 2000°C. Crystal size is greater than in PAN-based fibers. Rayon-based fibers are oriented by stretching during graphitization. Carburized fibers of rayon, pitch, or PAN are stretched during the graphitization stage at very high temperatures. Graphite layers slide over each other and further orient the layers.

Carbon fiber properties can be optimized for a specific application through processing. Type I PAN fibers are graphitized to give maximum stiffness, while Type II PAN fibers are graphitized to give maximum strength. There is a trade-off between strength and stiffness, which is influenced by heat treatment, as shown in Figure 3.16. However, the strength and stiffness of these fibers are well below theoretical values due to poor alignment and flaws introduced during manufacturing. Also, carbon fiber strength has high variability and follows a Weibull distribution. A list of properties for carbon fibers is given in Table 3.6.

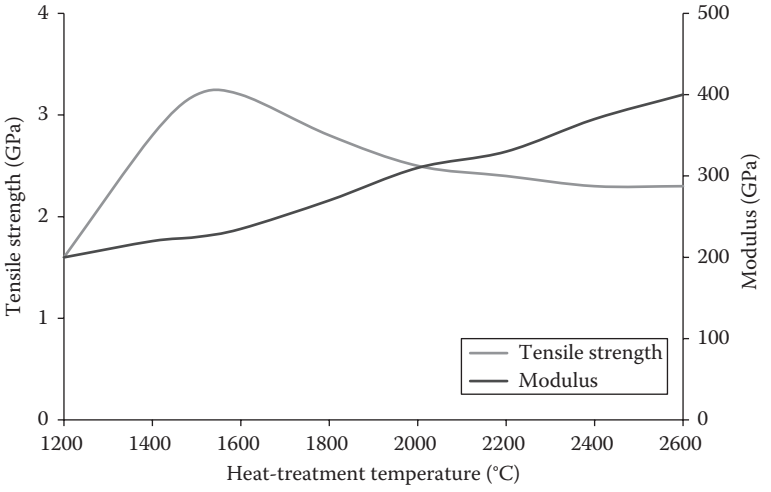

FIGURE 3.16 Heat-treatment effects on strength and stiffness of carbon fibers.

TABLE 3.6
Typical Properties of Carbon Fibers

	PAN			
Properties	**Type I**	**Type II**	**Pitch**	**Rayon**
Density, ρ (g/cm^3)	1.95	1.75	2.0	1.7
Tensile strength, σ_{ult} (GPa)[a]	2.4–2.7	3.4–4.5	1.55	2.50
Long. elastic modulus, E_L (GPa)	380	230	380	500
Trans. elastic modulus, E_T (GPa)	12	20	—	—
Diameter, d (μm)	7–10	8–9	10–11	6.5
Long. thermal expansion, α_L (10^{-6}/°C)	−0.5	−0.5	−1.0	−0.9
Trans. thermal expansion, α_T (10^{-6}/°C)	7–12	7–12	8	7.8

Sources: Adpated from Chawla, K.K., *Composite Materials: Science and Engineering*, 2nd edn., Springer-Verlag, New York, 1998; Agarwal, B.D. and Broutman, L.J., *Analysis and Performance of Fiber Composites*, 2nd edn., John Wiley & Sons, New York, 1990; Hull, D. and Clyne, T.W., *An Introduction to Composite Materials,* 2nd edn., Cambridge University Press, New York, 1996.

[a] Virgin strength value of fresh drawn fibers, measured in single fiber tests may yield up to 3.5 GPa for E-glass and 4.8 GPa for S-glass; however, the values cannot be realized due to fiber damage during processing. Actual values are 1.75 GPa for E-glass and 2.10 GPa for S-glass.

Carbon Fiber Terminology

Composite carbon fiber reinforcement is available in bundles of individual fibers or filaments called tows, which consists of 12,000 filaments for PAN fibers and 2,000 for pitch fibers. These tows are then stitched together to form a band used in composite fabrication, such as pultrusion, filament winding, or other manufacturing techniques discussed in Chapter 2.

Organic Fibers

Aramid fibers are the best known organic fibers, and of these, Kevlar® (produced by DuPont) is the most commercially recognized brand. Others include Spectra®, Technora, and Twaron. All aramid

TABLE 3.7
Typical Properties of Kevlar Fibers

Properties	K29	K49	K68	K119	K129	K149
Density, ρ (g/cm^3)	1.44	1.44	1.44	1.44	1.45	1.47
Tensile strength, σ_{ult} (GPa)	2.9	3.0	2.8	3.0	3.4	2.4
Long. elastic modulus, E_L (GPa)	70.5	112.4	101	55	100	147
Diameter, d (μm)	12	12	12	12	12	12
Long. thermal expansion, α_L (10^{-6}/°C)	−4.0	−4.9	—	—	—	—

Sources: Adapted from Chawla, K.K., *Composite Materials: Science and Engineering*, 2nd edn., Springer-Verlag, New York, 1998; Mathews, F.L. and Rawlings, R.D., *Composite Materials: Engineering and Science*, 2nd edn., Woodhead Publishing Limited, Boca Raton, FL, 1999; Tsai, S.W., *Composite Design*, 4th edn., Think Composites, Dayton, OH, 1988; Hull, D. and Clyne, T.W., *An Introduction to Composite Materials*, 2nd edn., Cambridge University Press, New York, 1996; Agarwal, B.D. and Broutman, L.J., *Analysis and Performance of Fiber Composites*, 2nd edn., John Wiley & Sons, New York, 1990.

fibers are characterized by high toughness, which makes them ideal for impact and ballistic protection applications. It is a low-density fiber offering high strength-to-weight and high stiffness-to-weight ratios. The disadvantages of aramid fibers are similar to those of the parent polymers, namely, low compressive strength, susceptibility to creep, moisture absorption, sensitivity to UV light, temperature-dependent mechanical properties, and high cost.

Organic fibers are produced by an extrusion or spinning process. First, an acid solution of polymer is extruded through a hot die, which has small holes to evaporate the solvent. Next, the polymers are stretched to improve the strength and stiffness. Kevlar is an aromatic polyamide polymer (paraphenylene terephthalamide) with stiff polymer chains that align along the fiber axis in a radial fashion as sheets. Like in the case of carbon fibers, weak bonds exist between sheets. This implies transverse anisotropy, which leads to low compressive strength. Table 3.7 provides a summary of the properties of various grades of Kevlar. Spectra fibers are made from ultralightweight polyethylene by a solution and gel spinning fabrication process, which results in very light, low-density fibers. Unfortunately, these fibers have a low melting point (150°C) with a maximum useful temperature of 100°C. However, the most important property of aramid fibers is their high toughness resulting from their high ductility.

Organic Fiber Terminology

Composite Kevlar fiber reinforcement is available in bundles of individual fibers or filaments called ends (or yarns), which consists of 768 filaments. Four yarns are further bundled to form a roving, which are wound onto a spool for packaging. These rovings are then stitched together to form a band used in composite fabrication.

Comparison of Various Types of Fibers

In this section, the specific tensile strength, specific modulus, thermal stability, and strain to failure of the various fibers addressed in this section are compared. With respect to compression properties, all fibers have lower compressive strength compared to tensile strength; Kevlar has the lowest compressive strength, while glass typically has the highest.

Specific Strength and Stiffness

Figure 3.17 graphically shows plots of the specific strength versus specific stiffness of various fiber types. The data are given in Table 3.8 along with a summary of other important properties. It is clear from Table 3.8 and Figure 3.17 that fibrous materials are much stronger than bulk materials (steel, aluminum, and titanium). More importantly, Figure 3.17 shows that when the properties are

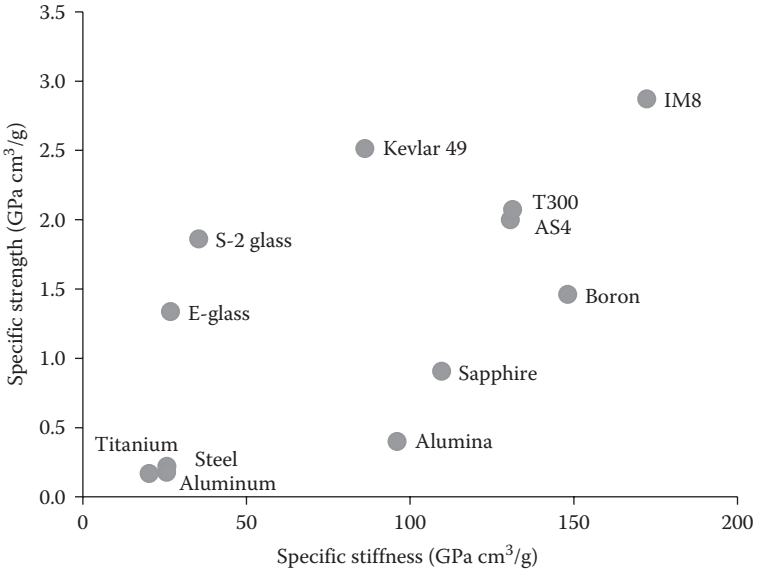

FIGURE 3.17 Comparison of specific properties of various materials.

TABLE 3.8
Typical Properties of Fibers[a]

Material	Density, ρ (g/cm^3)	Modulus, E_L (GPa)	Poisson's Ratio, ν_L	Strength, σ_{ult} (GPa)	Specific Stiffness, E/ρ (GPa cm^3/g)	Specific Strength, σ_{ult}/ρ (GPa cm^3/g)	Thermal Expansion, α_L (10^{-6}/°C)
Steel	7.80	200	0.32	1.72	25.64	0.22	12.8
Aluminum	2.70	69	0.33	0.48	25.56	0.18	23.4
Titanium	4.50	91	0.36	0.76	20.22	0.17	8.8
AS4[b]	1.80	235	0.20	3.60	130.56	2.00	−0.8
T300[b]	1.76	231	0.20	3.65	131.25	2.07	−0.5
IM8[b]	1.80	310	0.20	5.17	172.22	2.87	−1
Boron	2.60	385	0.21	3.80	148.08	1.46	8.3
Kevlar 49	1.44	124	0.34	3.62	86.11	2.51	−2.0
Alumina	3.95	379	0.25	1.58	95.95	0.40	7.5
S-2 glass	2.46	87	0.23	4.58	35.37	1.86	1.6
E-glass	2.58	69	0.22	3.45	26.74	1.34	5.4
Sapphire	3.97	435	0.28	3.6	109.57	0.91	8.8

Sources: Adapted from Chawla, K.K., *Composite Materials: Science and Engineering*, 2nd edn., Springer-Verlag, New York, 1998; Mathews, F.L. and Rawlings, R.D., *Composite Materials: Engineering and Science*, 2nd edn., Woodhead Publishing Limited, Boca Raton, FL, 1999; Tsai, S.W., *Composite Design*, 4th edn., Think Composites, Dayton, OH, 1988; Hull, D. and Clyne, T.W., *An Introduction to Composite Materials*, 2nd edn., Cambridge University Press, New York, 1996; Agarwal, B.D. and Broutman, L.J., *Analysis and Performance of Fiber Composites*, 2nd edn., John Wiley & Sons, New York, 1990.

[a] Please note that the sources for the data contained in this chapter include fiber manufacturers' brochures, the list of references at the end of the chapter, and other industry sources generally available to the public through the Internet. The authors have not performed independent studies to warrant the validity or accuracy of these data. Use caution when using these data for any application. The authors selected the most commonly used products or representative classes of products for this chapter. Our selection of any product does not represent an endorsement on our part.

[b] Carbon-based fibers.

TABLE 3.9
Thermal Stability of Fibers

Fiber	Spectra	Kevlar	E-Glass	C-Glass	S-Glass	Carbon
T_{max} (°C)	100	250	500	600	650	2000[a]

[a] If oxygen is present, T_{max} = 500°C.

normalized with respect to the density, bulk materials are much heavier than fibrous materials, which is the most important advantage fiber-reinforced composite materials have over traditional materials.

Thermal Stability

Table 3.9 shows the thermal stability of fibers based on the temperature at which the mechanical properties of the fiber start to change drastically, T_{max}. Based on these values, carbon fibers are an excellent choice for high-temperature applications (in an inert atmosphere); however, in the presence of air, carbon starts to oxidize at temperatures above 500°C.

Strain to Failure

Table 3.10 provides the ranges of failure strain for various fiber types with the most ductile behavior displayed by Kevlar fibers followed by glass and carbon. Figure 3.18 shows the stress–strain behavior of various reinforcing fibers.

Particulate Reinforcements

Particulate reinforcements are tiny particles that are near spherical, cubic, or tetragonal in shape. This type of reinforcement is often used as filler in composites in order to reduce the volume of matrix and thereby reduce cost, particularly when matrix costs are greater than the particulate costs. In some cases, particulates are able to enhance the stiffness of the composite. Particulate reinforcement is also available in the form of flakes that are available as platelets made of clay particle or metallic. Flakes typically are used in electrical and heating applications. Particulate reinforcement typically is not used where strength is a critical attribute because the particulates induce stress concentrations that reduce the strength of the composite, unless interface bonds between particulate and matrix are strong.

The primary role of particulate reinforcement is to improve the properties of the matrix. Particulate reinforcement can improve thermal and electrical conductivity of composites, increase wear and

TABLE 3.10
Strain to Fracture of Fibers

Fiber	Spectra	Kevlar	E-Glass	C-Glass	S-Glass	Carbon (PAN)
ε_{max} (%)	2.9–3.9	3.0–4.0	4.8	4.8	5.7	0.6–1.1

Sources: Adapted from Chawla, K.K., *Composite Materials: Science and Engineering*, 2nd edn., Springer-Verlag, New York, 1998; Mathews, F.L. and Rawlings, R.D., *Composite Materials: Engineering and Science*, 2nd edn., Woodhead Publishing Limited, Boca Raton, FL, 1999; Tsai, S.W., *Composite Design*, 4th edn., Think Composites, Dayton, OH, 1988; Hull, D. and Clyne, T.W., *An Introduction to Composite Materials*, 2nd edn., Cambridge University Press, New York, 1996; Agarwal, B.D. and Broutman, L.J., *Analysis and Performance of Fiber Composites*, 2nd edn., John Wiley & Sons, New York, 1990.

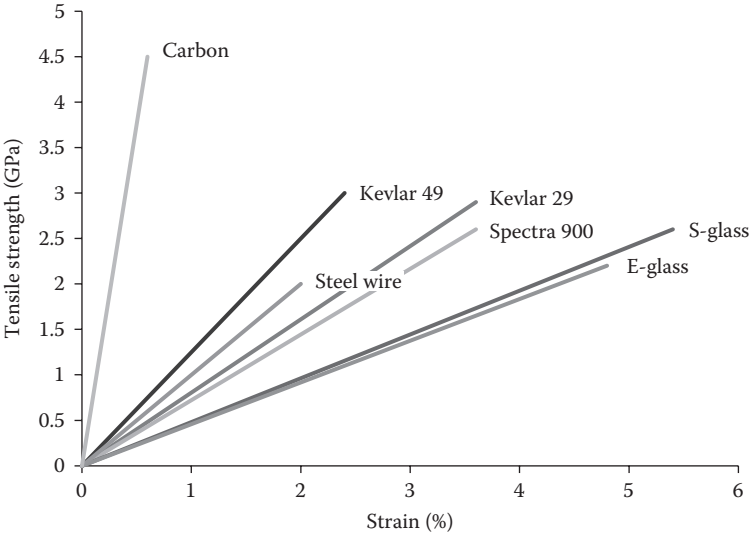

FIGURE 3.18 Stress–strain behavior of various fibers.

abrasion resistance, improve machinability, increase surface hardness, reduce shrinkage, and, most importantly, reduce costs. Discussion on particulate composites will be limited in this chapter since they are typically analyzed with traditional methods for homogeneous, isotropic materials.

Other Types of Reinforcements

There are a number of other types of reinforcement materials that have become available recently, including short fibers, whiskers, and nanomaterials. Short fibers (also known as discontinuous fibers) are obtained by chopping continuous fibers or produced directly as short fibers. Short fibers are defined as those with length-to-diameter ratio of less than 10. Short fibers are sometimes randomly oriented in a composite in order to obtain isotropic behavior. Whiskers are elongated single crystals with diameters less than 1 μm and lengths in the order of 100 μm. Whiskers are characterized by high tensile strength and used in ceramic matrix composites and metal matrix composites. Recently, the development of CNTs has introduced an entirely new class of reinforcement for composite applications. These materials are very strong and possess excellent mechanical and electrical properties. One of the primary challenges to their adoption in civil infrastructure is cost. Dispersing these materials in a matrix is also a considerable obstacle and the topic of much current research as of 2012. As the cost of these materials and the technological challenges are resolved, the potential to make a great impact in the construction industry exists—from electromagnetic interference shielding to ballistic-resistant building components.

REFERENCES

Agarwal, B.D. and Broutman, L.J. (1990). *Analysis and Performance of Fiber Composites*, 2nd edn., John Wiley & sons, New York.

Astrom, B.T. (1997). *Manufacturing of Polymer Composites*, CRC Press, Boca Raton, FL.

Chawla, K.K. (1998). *Composite Materials: Science and Engineering*, 2nd edn., Springer-Verlag, New York.

Felbeck, D.K. and Atkins, A.G. (1984). *Strength and Fracture of Engineering Solids*, Prentice Hall, Upper Saddle River, NJ.

Hull, D. and Clyne, T.W. (1996). *An Introduction to Composite Materials*, 2nd edn., Cambridge University Press, New York.

Mathews, F.L. and Rawlings, R.D. (1999). *Composite Materials: Engineering and Science*, 2nd edn., Woodhead Publishing Limited, Boca Raton, FL.

Tsai, S.W. (1988). *Composite Design*, 4th edn., Think Composites, Dayton, OH.

4 Mechanics of Composite Materials

Hector Estrada and Luke S. Lee

CONTENTS

INTRODUCTION

Recall that a composite is formed by combining reinforcement plus matrix plus interface. Therefore, composite properties depend on the properties of these three constituents as well as the size, shape, orientation, and distribution of reinforcement. Regardless of the constituent properties, the geometry and arrangement of the reinforcement is the most critical characteristic, and is, therefore, used to classify composites into three categories based on the aspect ratio of the reinforcement l/d, where l is the length and d is the diameter:

1. $l/d \rightarrow \infty$, the composite is classified as unidirectional (continuous fibers).
2. $l/d \approx 1$, the composite is classified as particulate.
3. $l/d \leq 500$, the composite is classified as short fiber.

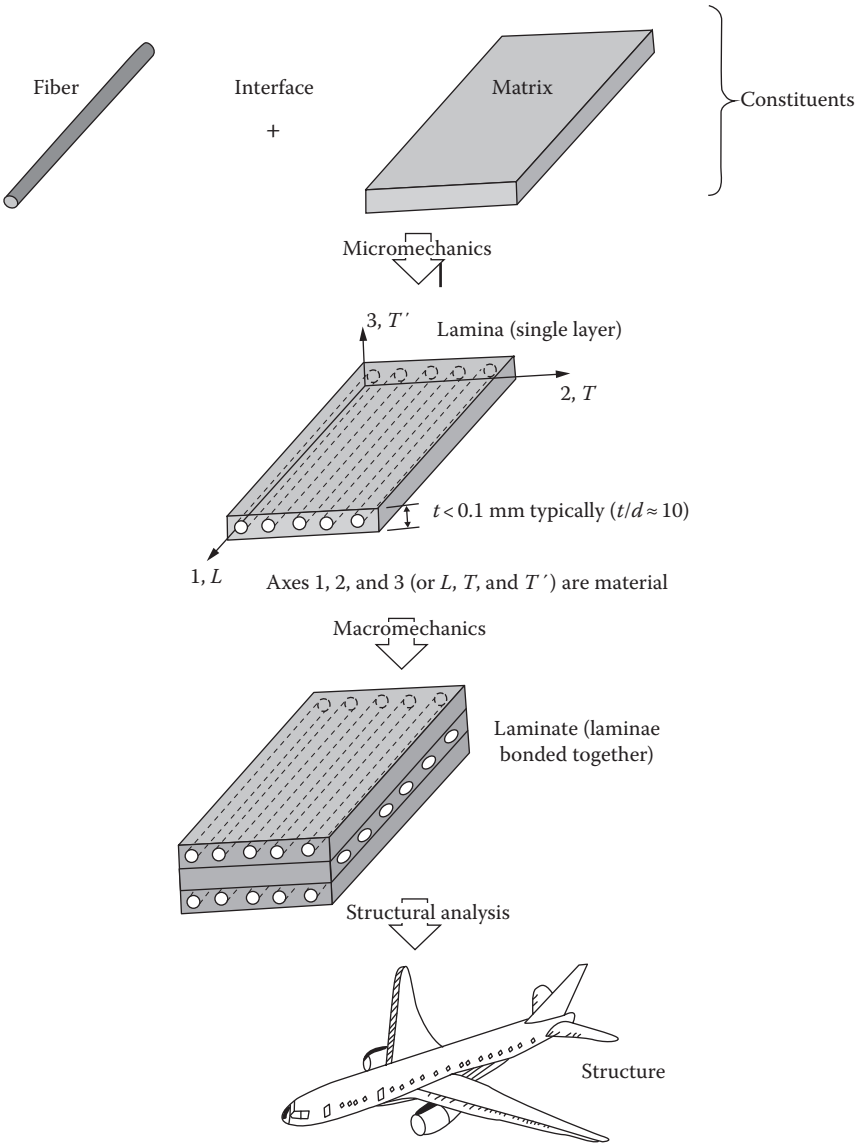

FIGURE 4.1 Levels of analysis for composite materials.

The primary focus of this chapter is on the mechanics of unidirectional composites, since they are the most commonly used in civil infrastructure applications.

The following nomenclature is used in the analysis of unidirectional composites. Figure 4.1 depicts a layer (ply) also known as a lamina (plural is laminae), which is the combination of matrix and fiber constituent materials and the interface between the two—the analysis of the lamina is based on micromechanics. A combination of several laminae, stacked in a specified sequence of orientation, form a "laminate" that will meet design strength and stiffness requirements (see Figure 4.1)—the analysis of which is based on macromechanics.

Notice, in Figure 4.1, that the structure of the composite lamina shows different properties in the direction along the fiber (longitudinal direction denoted with *L*) and the direction transverse to the fiber (transverse direction denoted with *T*). This is an orthotropic material system with principal axes 1, 2, and 3. However, this is not a fully 3-D orthotropic material system; it is a transversely isotropic system.

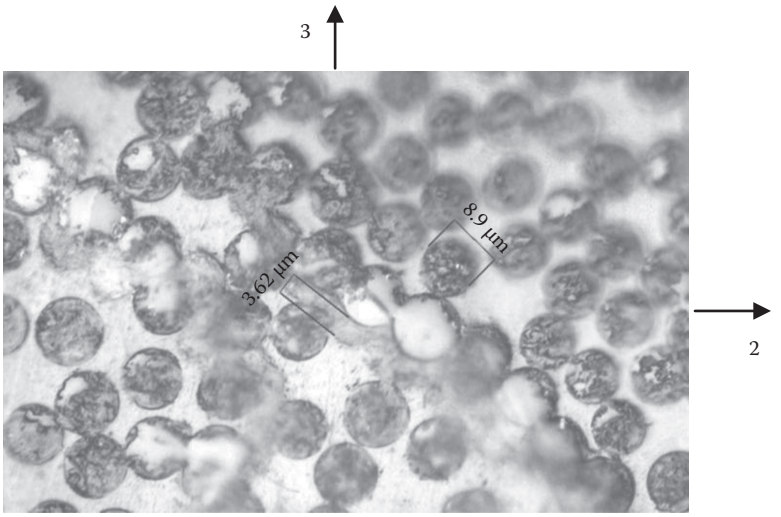

FIGURE 4.2 Lamina transverse isotropy.

The behavior in the 2 and 3 directions is nearly equal and different than the behavior along the longitudinal direction. Figure 4.2 shows the transverse isotropy of a lamina. It is clear that the fiber distribution in the lamina is nonuniform, which makes it difficult to distinguish between directions 2 and 3.

MICROMECHANICS OF COMPOSITES

In this section, properties of unidirectional composite in terms of the individual constituent material properties are discussed; in particular, properties pertaining to stiffness, strength, and hygrothermal effects are covered. First, an issue that is common to all micromechanical properties is introduced, the relative proportions of constituent materials based on a representative volume element.

Volume (and Weight) Fractions

The most important factors governing the properties of a composite are the relative proportions of fiber and matrix (and to a lesser extent voids). These relative fractions of material used in theoretical analysis are based on volume fractions of the constituent materials; however, it is more convenient to obtain the weight fraction obtained through experimental procedures. The process entails determining the weights of individual materials by the chemical matrix digestion method (ASTM D-3171) or the burn-off method (ASTM D-2584) (in both methods the matrix is consumed leaving only fibers, the weight of which is then determined). The volume fraction of the fibers is computed from

$$V_f = \frac{\rho_m w_f}{\rho_f w_m + \rho_m w_f} \tag{4.1}$$

where

$V_f = v_f/v_c$ is the fiber volume fraction
w_f is the weight of fiber material
ρ_m is the density of matrix material
ρ_f is the density of fiber material
v_f is the volume of fiber material
v_c is the volume of composite material

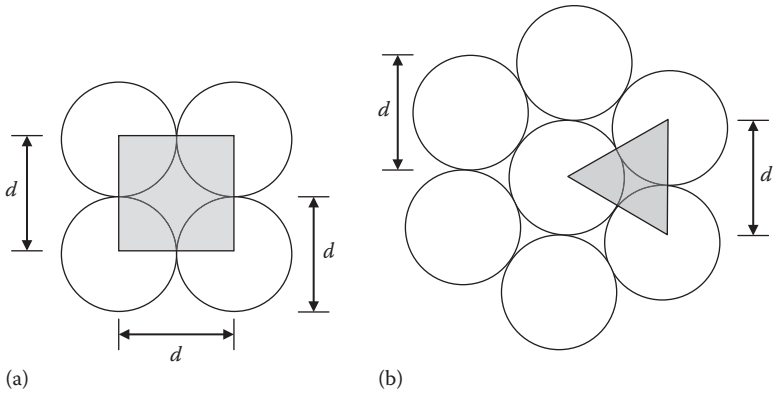

FIGURE 4.3 (a) Square and (b) hexagonal fiber packing configurations.

Also, the matrix volume fraction is given by $V_m = v_m/v_c$, where v_m is the volume of matrix material. The volume fractions of all constituents and voids are given as follows:

$$V_f + V_m + V_v = 1.0 \tag{4.2}$$

where V_v is the volume fraction of voids or defects and can consist of 5% of the total volume or more depending on the quality of the processing technique. Voids are formed in the composite because of gasses and volatiles trapped in the matrix during fabrication. The void content can be obtained from the difference in the measured and theoretical composite densities according to ASTM D-2734. Or V_v can be obtained in terms of densities and weights using Equation 4.2:

$$V_v = 1 - \frac{\left(w_f/\rho_f + w_m/\rho_m\right)\rho_c}{w_c} \tag{4.3}$$

Here the weight of the composite, w_c, and the density of the composite, ρ_c, must be accurately measured.

The upper bound of the fiber volume fraction may be determined using a theoretical fiber packing analysis. As an example, two packing models are presented, square and hexagonal—representative composite area (shaded area in Figure 4.3) is used instead of volumes, given that the length of the fibers and matrix is equal. For the square packing, the area of the fibers enclosed by the shaded square is equal to the area of a single fiber, $\pi d^2/4$, and the area of the square is d^2; therefore, the fiber volume fraction $V_f \leq (\pi d^2/4)/d^2 = \pi/4 \approx 0.785$. For the hexagonal packing, the area of the fibers enclosed by the shaded triangle is equal to the area of a half of a single fiber (given that the interior angles must be 60°), $\pi d^2/8$, and the area of the triangle is $\sqrt{3}d^2/4$; therefore, the fiber volume fraction $V_f \leq (\pi d^2/8)/(\sqrt{3}d^2/4) = \pi/2\sqrt{3} \approx 0.907$. Theoretically, the maximum fiber volume fraction attainable is 90.7%; in practice, V_f is lower than this—in the range of 10%–60%, depending on the manufacturing process.

Density of Composites

The density of a composite can be estimated using the volume fractions and densities of the constituent materials. Recall that density is given by the mass of a body divided by the volume it occupies. As discussed earlier, the mass of a composite is a combination of the masses of the constituent

materials, while the volume is the sum of the volumes of the constituent materials plus that of any voids. Thus, composite density can be obtained as follows:

$$\rho_c = \frac{M}{V} = \frac{(\rho_f v_f + \rho_m v_m)}{V} = \rho_f V_f + \rho_m V_m \tag{4.4}$$

Micromechanical Properties of Lamina

Unidirectional continuous fiber composite properties depend on constituent material properties, distribution of constituents (volume fractions), and physical and chemical interactions between constituents (which is dominated by the interface constituent). Two formulations are common, theoretical and semiempirical; both are relatively accurate for longitudinal properties but give poor correlation for transverse properties when compared to experimentally obtained properties.

Stresses and Strains

Composite stresses, σ_i, and strains, ε_i, can be obtained by averaging the constituent stresses and strains over the composite volume:

$$\sigma_i = \sigma_{fi} V_f + \sigma_{mi} V_m \tag{4.5}$$

$$\varepsilon_i = \varepsilon_{fi} V_f + \varepsilon_{mi} V_m \tag{4.6}$$

where
the subscripts *f* and *m* represent fiber and matrix, respectively
the subscript *i* represents any given load step

Constitutive Constants

There are several expressions within the framework of linear elasticity to characterize the constitutive behavior of a material: anisotropic behavior requires different properties in different directions, orthotropic behavior that has three mutually orthogonal planes of material property symmetry, transversely isotropic (laminated composites) behavior that has infinite planes of material property symmetry about one axis, and isotropic behavior that has infinite planes of material property symmetry. The constitutive behavior of an isotropic material can be fully characterized using two independent constants, Young's modulus, E, and Poisson's ratio, ν—sometimes the shear modulus is used in mechanics, which may be derived from the two independent properties as follows: $G = E/2(1 + \nu)$. The other extreme is an anisotropic material, which requires 21 independent constants to characterize its constitutive behavior; composites are a special case of anisotropic materials, requiring only 9 independent constants in their most general form—orthotropic. Fortunately, unidirectional continuous fiber composites behave transversely isotropic and their constitutive behavior can be fully characterized with five independent constants, including the longitudinal modulus of elasticity, E_1; the transverse modulus of elasticity, E_2; the in-plane shear modulus, G_{12}; and two Poisson's ratios, ν_{12} and ν_{23}. The other four properties can be derived from the five independent quantities as follows: $E_3 = E_2$, $G_{13} = G_{12}$, $\nu_{13} = \nu_{12}$, and the transverse shear modulus, $G_{23} = E_2/2(1 + \nu_{23})$. As discussed previously, the notation used in this chapter is one of two popular notations used to represent the constitutive properties of a transversely isotropic material; the other uses subscripts L, T, and T' for directions 1, 2, and 3, respectively (see Figure 4.1), that is, the longitudinal modulus of elasticity, E_L; the transverse modulus of elasticity, E_T; the shear modulus, G_{TL}; and the two Poisson's ratios, ν_{TL} and $\nu_{TT'}$.

The constitutive properties of a composite also depend on the properties of its constituent ingredients and distribution. Experimental methods to determine properties may be used to obtain composite properties; however, many tests are needed to fully characterize each variable. On the other hand, theoretical methods and semiempirical methods can be used to predict properties using constituent properties. There are many proposed property prediction theories, including the following: netting analysis; mechanics of materials approach; elasticity solutions (which include bounding techniques, exact solution, and self-consistent method); statistical, discrete element; and semiempirical methods. The general assumptions used in these theories include the following:

1. Each ply is macroscopically homogeneous, linear elastic, and generally orthotropic.
2. The matrix and the fibers are linear elastic and homogeneous.
3. Matrix and fibers are free of voids.
4. The interface between matrix and fibers provides a perfect bond.
5. Each ply is initially in a stress-free state.
6. The fibers are uniform in properties and diameter, continuous and parallel throughout.

A reasonably accurate prediction of the longitudinal stiffness properties is given by a simple mechanics of materials model—assuming iso-strains ($\varepsilon_L = \varepsilon_f = \varepsilon_m$), for example, constituents loaded in parallel to obtain the longitudinal modulus of elasticity:

$$E_1 = E_f V_f + E_m V_m \tag{4.7}$$

where

E_f is the modulus of elasticity of the fibers
E_m is the modulus of elasticity of the matrix

This relationship is based on the so-called rule of mixtures, which can be used to obtain other properties. This rule of mixture relationship gives the upper limit for the modulus of elasticity, which may be proven from the principle of minimum potential energy (Jones, 1998). Notice that depending on the volume fraction, V_f, the stress–strain diagram for the composite may follow that of the fibers or that of the matrix. For low fiber volume fractions, it would be expected that the composite behavior would be nonlinear since the stress–strain behavior for the matrix is typically nonlinear. However, the composite behavior can always be assumed to be linear because of the dominate behavior of the fibers.

One other property that can be predicted with the rule of mixtures is the major Poisson's ratio:

$$\nu_{12} = \nu_f V_f + \nu_m V_m = \nu_{13} \tag{4.8}$$

This model, however, fails to predict the shear modulus and transverse properties accurately when compared to experimental results. A semiempirical model, more specifically the Halpin–Tsai model, provides a more accurate prediction for these properties:

$$P_c = P_m \frac{1 + \xi \eta V_f}{1 - \eta V_f} \tag{4.9}$$

where

$$\eta = \frac{P_f / P_m - 1}{P_f / P_m + \xi} \tag{4.10}$$

and P can take either of the properties E_2 or G_{12}. The parameter ξ depends on the fiber geometry, packing geometry, and loading conditions. For circular fibers, the following estimates have been proposed: for E_2, $\xi = 2$, and for G_{12}, $\xi = 1$. These values were obtained by comparing the results of Equation 4.9 with exact elasticity solutions (Jones, 1998). This relationship predicts values for E_2 and G_{12} quite adequately for practical volume fractions less than 0.7. Notice that the Halpin–Tsai relationship can also be used to obtain the rule of mixtures; as ξ goes to infinity, Equation 4.9 approaches the rule of mixtures.

The transverse Poisson's ratio can be obtained from Poisson's ratio of the matrix, ν_m, as follows:

$$\nu_{23} = \nu_m \tag{4.11}$$

Also, Poisson's ratio relating the longitudinal and transverse strains when the composite is loaded in the transverse direction is known as the minor Poisson's ratio, ν_{21}, and is given by

$$\nu_{21} = \nu_{12} \frac{E_2}{E_1} \tag{4.12}$$

Earlier, the upper limit on the modulus of elasticity was introduced as the value given by Equation 4.7, the rule of mixtures. The lower limit for the modulus of elasticity is given by a relationship obtained from mechanics of materials assuming iso-stresses ($\sigma_T = \sigma_f = \sigma_m$); that is, constituents are loaded in series:

$$\frac{1}{E_{ll}} = \frac{V_f}{E_f} + \frac{V_m}{E_m} \tag{4.13}$$

The proof for this case is based on the principle of minimum complementary energy (Jones, 1998). All perditions of the modulus of elasticity will fall between the upper and lower limits given by Equations 4.7 and 4.13, respectively. Lastly, there are a number of restrictions on these constants to ensure that they are thermodynamically admissible; see Jones (1998) for details.

Lamina Constitutive Relations

The stress–strain relations for a transversely isotropic material are given as $\{\sigma\} = [Q]\ \{\varepsilon\}$; that is, there are six stress components, six strain components, and the constitutive matrix, $[Q]$, which is six by six. Since composite laminae are rather thin, a state of plane stress is applicable, which in contracted notation is given as

$$\begin{Bmatrix} \sigma_1 \\ \sigma_2 \\ \tau_{12} \end{Bmatrix} = \begin{bmatrix} Q_{11} & Q_{12} & 0 \\ Q_{12} & Q_{22} & 0 \\ 0 & 0 & Q_{66} \end{bmatrix} \begin{Bmatrix} \varepsilon_1 \\ \varepsilon_2 \\ \gamma_{12} \end{Bmatrix} \tag{4.14}$$

where

σ_1 and σ_2 represent the normal stresses
τ_{12} is the shear stress
ε_1 and ε_2 represent the normal strains
γ_{12} is the shear strain

The constitutive matrix components are given as

$$\left.\begin{aligned} Q_{11} &= \frac{E_1}{1-\nu_{12}\nu_{21}} \\ Q_{12} &= \frac{\nu_{21}E_1}{1-\nu_{12}\nu_{21}} \\ Q_{22} &= \frac{E_2}{1-\nu_{12}\nu_{21}} \\ Q_{66} &= G_{12} \end{aligned}\right\} \tag{4.15}$$

Strength Properties

Predicting composite strength from constituent materials is much more difficult than predicting stiffness properties. Strength is highly dependent on the failure mode of the composite—and there are many failure modes for each type of loading. For this reason, composite strength is usually determined experimentally, using composite specimens with layups similar to those for the intended application. However, for routine applications, this is cost prohibitive, and an estimate of the strength must be established using constituent strength properties. In composites, internal material failure generally initiates before any macroscopic appearance or behavior change.

Different strength values are associated with different loading conditions. For transversely isotropic materials (plane stress), the following five different loadings are of interest: longitudinal tension and compression, transverse tension and compression, and shear. The strength associated with each of these five loadings is influenced by a number of factors, including misalignment of fibers, fibers of nonuniform strength, discontinuous fibers, and residual stresses. FRP composites have excellent longitudinal tensile strength (and stiffness) because fibers generally carry most of the load in this direction. For the other four loading conditions, the load is about equally shared between fibers and matrix. The strengths associated with these load cases are highly dependent on the matrix strength since it tends to be much lower than that of the fibers. Also, the interface between constituents plays a major role in strength because in order to achieve material failure, stresses must be much higher compared to stresses involved in determining stiffness properties. In cases with equal load sharing between constituents of unequal stiffness, the interface may become the weakest link and fail prematurely, governing the overall strength of the composite.

Longitudinal tensile strength, σ_{1TU}, can be determined using the rule of mixtures, accounting for the appropriate stress level in the constituent materials. Depending on V_f, FRP composites can fail when fibers are loaded to their fracture strain (when the fracture strain for the fiber is less than that for the matrix) or for low values of V_f when the matrix strength is exceeded. When loaded in axial longitudinal tension, most composites will behave linear up to fracture, which indicates fiber-controlled failure, and the longitudinal strength can be estimated as follows:

$$\sigma_{1TU} = \sigma_{fU}V_f + \sigma_{mf}V_m \tag{4.16}$$

where

σ_{fU} is the strength of the fiber

σ_{mf} is the matrix stress at the fiber fracture strain

For the matrix-controlled case (very low V_f values), there is actually polymer strength degradation caused by stress concentrations resulting from the constraint placed on the matrix by the fibers. So, in order to strengthen the polymer, the following minimum critical fiber volume fraction must be provided:

$$V_{fcrit} = \frac{\sigma_{mU} - \sigma_{mf}}{\sigma_{fU} - \sigma_{mf}} \tag{4.17}$$

This formulation assumes that all fibers are making up the composite fracture at the same stress level and longitudinal position. However, since the fibers act in a bundle in parallel and are prone to random imperfections, fiber strength varies statistically and is usually characterized with a Weibull distribution. See Jones (1998) for further details on statistical analysis of longitudinal tensile strength.

Longitudinal compressive strength, σ_{1CU}, can be estimated based on one of the following failure modes:

1. Transverse tensile failure in the matrix or interface. This is caused by transverse tensile strain resulting from Poisson's effect. When the transverse strain exceeds the matrix failure strain, cracks form at the interface in the matrix. The longitudinal compressive strength can be estimated by

$$\sigma_{1CU} = \frac{E_1}{\nu_{12}} \varepsilon_{mu} \left(1 - V_f^{1/3}\right) \tag{4.18}$$

   This mode tends to happen first and the strength predicted by Equation 4.18 correlates well with experimental results (Agarwal and Broutman, 1990).
2. Fibers act as long columns on an elastic foundation and microbuckle in phase (all fibers buckle in the same direction) or out of phase (fibers buckle in a mirror image of each other). Either case may happen depending on the relative volume content of fibers; for low V_f, the fibers microbuckle out of phase, while inphase microbuckling happens when V_f is high. The out-of-phase case is similar to the last failure more, in that transverse extension causes longitudinal cracking of the matrix. The longitudinal compressive strength for the out-of-phase case is governed by an extension failure and can be estimated as

$$(\sigma_{1CU})_{ext} = 2V_f \sqrt{\frac{0.63 E_m E_f V_f}{3(1 - V_f)}} \tag{4.19}$$

   The 0.63 factor has been added to obtain a better correlation with experimental data and is theorized to account for the inelastic behavior of the matrix (Jones, 1998). This factor may vary depending on the fiber architecture and can be as high as 0.97 for fiberglass cloth.

   The inphase case results in shear failure in the matrix. The longitudinal compressive strength for the inphase case is caused by a shear failure and can be estimated as

$$(\sigma_{1CU})_{shear} = \frac{0.63 G_m}{1 - V_f} \tag{4.20}$$

   The longitudinal compressive strength is the smallest value obtained from Equations 4.18 through 4.20.

Transverse tensile strength, σ_{2TU}, is assumed to be controlled by the strength of the matrix. There are several failure modes that can be used to estimate σ_{2TU}; matrix tensile failure is the most common, for which the transverse tensile strength can be estimated as

$$\sigma_{2TU} = \frac{\sigma_{mU}}{S} \tag{4.21}$$

where S is a strength reduction factor and is always greater than one. This factor depends on the relative properties of the constituent matrix and fibers, as well as the fiber volume fraction. From a mechanics of materials standpoint, neglecting Poisson's effect, S can be considered a stress-concentration factor given as

$$S = \frac{1 - V_f(1 - E_m/E_f)}{1 - \sqrt{4V_f/\pi}(1 - E_m/E_f)} \tag{4.22}$$

This semiempirical equation may yield inaccurate predictions. However, because transverse loading is not as critical as longitudinal loading, little research has been devoted to finding a more accurate formulation for this case (nor the transverse compressive strength, which is discussed next).

Transverse compressive strength, σ_{2CU}, is assumed to be controlled by matrix shear failure (in some cases accompanied by fiber crushing and fiber–matrix interface failure). None of the empirical formulations give good results when compared to experimentally obtained data. For design, either use the compressive strength of the matrix, $\sigma_{2CU} = \sigma_{mcu}$, or determine the strength experimentally. Barbero (1999) gives the following relationship:

$$\sigma_{2CU} = \sigma_{mcu}\left(1 - \sqrt{\frac{4V_v}{\pi(1 - V_f)}}\right)\left(1 - V_f^{1/3}\right)\frac{E_2}{E_m} \tag{4.23}$$

This relationship could also be used to determine σ_{2TU} by replacing the matrix compressive strength with its tensile strength.

Shear strength, τ_{12U}, is assumed to be controlled by matrix shear failure and/or constituent debonding. Again, none of the empirical formulations give good results when compared to experimentally obtained data. For shear strength, a clear distinction must be made between the various shear stress components, τ_{23}, τ_{12}, and τ_{31}. The stress component of interest is the in-plane shear stress, τ_{12}. For design, either use the in-plane shear strength of the matrix, $\tau_{12U} = \tau_{mu}$, or determine the strength experimentally. Barbero (1999) gives the following relationship:

$$\tau_{12U} = \tau_{mu}\left(1 - \sqrt{\frac{4V_v}{\pi(1 - V_f)}}\right)\left[1 + \left(V_f - \sqrt{V_f}\right)\left(1 - \frac{G_m}{G_f}\right)\right] \tag{4.24}$$

Expansion Properties

Two expansion agents are of interest, temperature and moisture. Any change of either of these agents produces a proportional change in dimensions of the body. The associated expansion is characterized by a material-dependent constant, and since composites are orthotropic, these constants are direction dependent, similar to other composite properties.

Thermal expansion is characterized with the thermal expansion coefficient, α, which is the change in linear dimensions of the body per unit initial length, per unit change in temperature. The strain

associated with this change in length is the thermal strain and is obtained by multiplying α by the change in temperature. Thermal behavior of transversely isotropic composites can be characterized with two constants, the longitudinal thermal expansion coefficient, α_L, and the transverse thermal expansion coefficient, α_T. α_L is highly influenced by the fiber thermal expansion coefficient, α_f, while α_T is mostly influenced by the matrix thermal expansion coefficient, α_m; therefore, α_L is smaller than α_T because $\alpha_f < \alpha_m$.

Assuming free expansion and no mechanical strains, a reasonably accurate prediction of α_L is given by a simple mechanics of materials model based on a parallel response of the fibers and matrix—iso-strain response ($\varepsilon_L = \varepsilon_f = \varepsilon_m$). The result is

$$\alpha_L = \frac{1}{E_1}(V_f E_f \alpha_f - V_m E_m \alpha_m) \tag{4.25}$$

Note that since α_f and α_m are different, some residual stresses will be induced because of the bond between the matrix and the fibers. These residual stresses are usually small and can be neglected in estimating the strength.

A prediction of α_T based on a self-consistent model was derived by Schapery using the principle of minimum potential energy (the simple mechanics of materials model results do not correlate well with experimental data). Schapery's relationship is

$$\alpha_T = (1+\nu_f)\alpha_f V_f + (1+\nu_m)\alpha_m V_m - \alpha_L \nu_{12} \tag{4.26}$$

This equation satisfies the elasticity field equations and correlates well with experimental data.

Moisture expansion is characterized with the hygroscopic (or hygral) expansion coefficient, β, which is the change in linear dimensions of the body per unit initial length, per unit change in moisture concentration. The strain associated with this change in length is the hygral strain and is obtained by multiplying β by the change in moisture concentration. The hygral behavior of transversely isotropic composites is characterized with two constants, the longitudinal hygral expansion coefficient, β_L, and the transverse hygral expansion coefficient, β_T. The effect of moisture is usually determined experimentally by obtaining the moisture concentration in the material, C, which is the weight of the moisture present divided by the weight of the dry body—this is discussed further in the "Transport Properties" section. Moisture expansion is analogous to thermal expansion and the equations for α_L and α_T apply. However, there is an important difference; inorganic fibers (most fibers) do not absorb moisture, that is, $\beta_f \approx 0$. Also, since $E_m/E_1 \ll 1.0$, Equation 4.25 for hygral expansion reduces to

$$\beta_L = 0 \tag{4.27}$$

The presence of moisture causes most of the swelling in the matrix (which may be as high as 8% for epoxies), so a reasonably accurate prediction of β_T can be derived using Schapery's equation earlier (Equation 4.26). The result is

$$\beta_T = \beta_m V_m (1+\nu_m) \tag{4.28}$$

Transport Properties

Transport phenomena such as heat conduction, moisture permeability, and electric conductivity are generally important in the design of composites. The first two (the only ones discussed here) are particularly important in assessing the durability of composites used in civil infrastructure applications. The associated effects of these phenomena are characterized by material-dependent

constants, heat conduction for thermal conductivity, and moisture permeability for mass diffusivity. Thermal conductivity is a measure of how quickly a material can transfer heat, while mass diffusivity is a measure of how quickly moisture concentration changes inside the host solid. These constants are direction dependent since composites are orthotropic, similar to other composite properties. Therefore, transport phenomena constants can be determined using constituent properties.

Heat conduction of transversely isotropic composites can be characterized with two constants, the longitudinal thermal conductivity, C_1, and the transverse thermal conductivity, C_2 (the through-thickness conductivity, C_3, is equal to C_2). C_i can be determined from the thermal conductivities of the composite constituent and the fiber volume fraction as outlined in Agarwal and Broutman (1990). A reasonably accurate prediction of C_1 is given by the rule of mixtures:

$$C_1 = V_f C_f + V_m C_m \tag{4.29}$$

where
C_f is the thermal conductivity of the fiber material
C_m is that of the matrix material

The Halpin–Tsai relationship, with $\xi = 1$, gives a reasonable prediction for C_2. That is,

$$C_2 = C_m \frac{1 + \xi \eta V_f}{1 - \eta V_f} \tag{4.30}$$

where

$$\eta = \frac{C_f / C_m - 1}{C_f / C_m + \xi} \tag{4.31}$$

Moisture diffusivity of transversely isotropic composites can be characterized with two constants, the moisture diffusivity, D_1, and the transverse moisture diffusivity, D_2 (the through-thickness diffusivity, D_3, is equal to D_2). D_i can be determined from the moisture diffusivity of the matrix and the fiber volume fraction as outlined in Agarwal and Broutman (1990). A reasonably accurate prediction of D_1 is given by the rule of mixtures:

$$D_1 = V_f D_f + V_m D_m \tag{4.32}$$

where
D_f is the moisture diffusivity of the fiber material
D_m is that of the matrix material

The Halpin–Tsai relationship, with $\xi = 1$, gives a reasonable prediction for D_2. That is,

$$D_2 = D_m \frac{1 + \xi \eta V_f}{1 - \eta V_f} \tag{4.33}$$

where

$$\eta = \frac{D_f / D_m - 1}{D_f / D_m + \xi} \tag{4.34}$$

MACROMECHANICS OF COMPOSITES

The individual plies (or laminae) are usually too thin to be useful in an engineering system; therefore, a number of laminae are bonded together to create a laminate. The properties of each lamina can be chosen such that they meet the laminate design requirements (which must meet the structural design requirements). Laminate properties can be predicted from the properties of the constituent laminae, which can be obtained using micromechanics as discussed earlier. For each ply k, we have ply properties E_{1k} (fiber-direction stiffness), E_{2k} (transverse stiffness), ν_{12k} (major Poisson's ratio), G_{12k} (shear stiffness), α_{11k} (fiber-direction coefficient of thermal expansion [CTE]), α_{22k} (transverse CTE), β_{11k} (fiber-direction moisture expansion coefficient [MEC]), and β_{22k} (transverse MEC). Collectively, these properties characterize the constitutive behavior of a transversely isotropic material through the constitutive matrix $[Q]$, which relates the stresses to the strains (see Equation 4.14). This relationship is for a lamina oriented in principle direction of orthotropy (the natural axis of the material or lamina coordinates), which may not coincide with the structural coordinates (coordinate directions that are geometrically natural to the solution to the problem). In general, fibers may be aligned at an angle θ_k to the structural x-axis, as shown in Figure 4.4. Therefore, the material properties must be transformed from lamina coordinates to structural coordinates. Also, the structural coordinates serve as a common coordinate system for all laminae. First though, the stresses and the strains are transformed using tensor transformation laws. The stresses are transformed as follows:

$$\begin{Bmatrix} \sigma_x \\ \sigma_y \\ \tau_{xy} \end{Bmatrix} = \begin{bmatrix} \cos^2\theta & \sin^2\theta & -2\sin\theta\cos\theta \\ \sin^2\theta & \cos^2\theta & 2\sin\theta\cos\theta \\ 2\sin\theta\cos\theta & -2\sin\theta\cos\theta & \cos^2\theta - \sin^2\theta \end{bmatrix} \begin{Bmatrix} \sigma_1 \\ \sigma_2 \\ \tau_{12} \end{Bmatrix} \tag{4.35}$$

This equation can be written in matrix form as $\{\bar{\sigma}\} = [T]^{-1}\{\sigma\}$. Similarly, the strains can be transformed as

$$\begin{Bmatrix} \varepsilon_x \\ \varepsilon_y \\ \frac{\gamma_{xy}}{2} \end{Bmatrix} = \begin{bmatrix} \cos^2\theta & \sin^2\theta & -2\sin\theta\cos\theta \\ \sin^2\theta & \cos^2\theta & 2\sin\theta\cos\theta \\ 2\sin\theta\cos\theta & -2\sin\theta\cos\theta & \cos^2\theta - \sin^2\theta \end{bmatrix} \begin{Bmatrix} \varepsilon_1 \\ \varepsilon_2 \\ \frac{\gamma_{12}}{2} \end{Bmatrix} \tag{4.36}$$

In matrix form, $\{\bar{\varepsilon}'\} = [T]^{-1}\{\varepsilon'\}$.

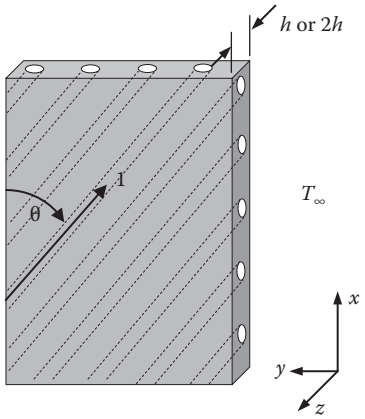

FIGURE 4.4 Composite plate.

The ½ factor for the shear strain in Equation 4.36 is required in order to transform the engineering shear strain using the same transformation relationship as stress; the factor is a result of the fundamental difference between the definitions of engineering and tensorial strains. The following relationship is typically used to simplify the transformation process:

$$\begin{Bmatrix} \varepsilon_x \\ \varepsilon_y \\ \gamma_{xy} \end{Bmatrix} = \begin{bmatrix} 1 & 0 & 0 \\ 0 & 1 & 0 \\ 0 & 0 & 2 \end{bmatrix} \begin{Bmatrix} \varepsilon_x \\ \varepsilon_y \\ \dfrac{\gamma_{xy}}{2} \end{Bmatrix} \tag{4.37}$$

This equation can be written in matrix form as $\{\bar{\varepsilon}\} = [R]\,\{\bar{\varepsilon}'\}$. And

$$\begin{Bmatrix} \varepsilon_1 \\ \varepsilon_2 \\ \gamma_{12} \end{Bmatrix} = \begin{bmatrix} 1 & 0 & 0 \\ 0 & 1 & 0 \\ 0 & 0 & 2 \end{bmatrix} \begin{Bmatrix} \varepsilon_1 \\ \varepsilon_1 \\ \dfrac{\gamma_{12}}{2} \end{Bmatrix} \tag{4.38}$$

In matrix form, $\{\varepsilon\} = [R]\{\varepsilon'\}$. Combining Equations 4.14 and 4.35 through 4.38, we attain the stress–strain relations for a lamina of arbitrary orientation as

$$\begin{Bmatrix} \sigma_x \\ \sigma_y \\ \tau_{xy} \end{Bmatrix} = \begin{bmatrix} \bar{Q}_{11} & \bar{Q}_{12} & \bar{Q}_{16} \\ \bar{Q}_{12} & \bar{Q}_{22} & \bar{Q}_{26} \\ \bar{Q}_{16} & \bar{Q}_{26} & \bar{Q}_{66} \end{bmatrix} \begin{Bmatrix} \varepsilon_x \\ \varepsilon_y \\ \gamma_{xy} \end{Bmatrix} \tag{4.39}$$

where

$$\begin{aligned}
\bar{Q}_{11} &= Q_{11}\cos^4\theta + 2(Q_{12} + 2Q_{66})\sin^2\theta\cos^2\theta + Q_{22}\sin^4\theta \\
\bar{Q}_{12} &= (Q_{11} + Q_{22} - 4Q_{66})\sin^2\theta\cos^2\theta + Q_{12}(\sin^4\theta + \cos^4\theta) \\
\bar{Q}_{22} &= Q_{11}\sin^4\theta + 2(Q_{12} + 2Q_{66})\sin^2\theta\cos^2\theta + Q_{22}\cos^4\theta \\
\bar{Q}_{16} &= (Q_{11} - Q_{12} - 2Q_{66})\sin\theta\cos^3\theta + (Q_{12} - Q_{22} + 2Q_{66})\sin^3\theta\cos\theta \\
\bar{Q}_{26} &= (Q_{11} - Q_{12} - 2Q_{66})\sin^3\theta\cos\theta + (Q_{12} - Q_{22} + 2Q_{66})\sin\theta\cos^3\theta \\
\bar{Q}_{66} &= (Q_{11} + Q_{22} - 2Q_{12} - 2Q_{66})\sin^2\theta\cos^2\theta + Q_{66}(\sin^4\theta + \cos^4\theta)
\end{aligned} \tag{4.40}$$

In matrix form, $\{\bar{\sigma}\} = [\bar{Q}]\{\bar{\varepsilon}\}$ and $[\bar{Q}] = [T]^{-1}[Q][T]^{-T}$.

Classical Lamination Theory

A laminate is formed from two or more laminae bonded together to act as a homogeneous structural element. The principal material orientation, thickness, and material type for each lamina can be specified so as to produce a structural element with any desired properties. This information may be conveyed in compact form following a convention for stocking sequence, discussed in the next section.

Laminate Orientation Codes

The description of a laminate construction, individual layer thickness, principal material property orientations, and overall stacking sequence may be represented in a simple concise fashion using the following codes:

- For regular laminates, with equal thickness layers, a listing of the laminae and their orientation suffices. For example, [0°/90°/45°] represents a laminate with three layers of equal thickness, oriented at 0°, 90°, and 45°, from top to bottom.
- For irregular laminates with layers with different thicknesses, the layer thicknesses must be appended to the laminate stacking notation. For example, $\left[0^{\circ}_{t}/90^{\circ}_{2t}/45^{\circ}_{3t}\right]$ represents a three-layer laminate with the thickness appended to the orientation angles as subscripts.
- Laminates that are symmetric about the midplane can be represented with the top half of the stacking sequence and the symmetry indicated with a subscript *s* after the closing bracket. For example, [0°/90°/45°/45°/90°/0°] can be represented as $[0°/90°/45°]_s$.
- Laminates with reoccurring ply orientation can be contracted, as shown in the next example. For example, [0°/0°/0°/90°/90°] can be represented as $\left[0^{\circ}_{3}/90^{\circ}_{2}\right]$.
- Laminates with repeated sequences of laminae can be contracted, as shown in the next example. For example, [0°/90°/45°/0°/90°/45°] can be represented as $[0°/90°/45°]_2$.

Laminate Constitutive Relations

The mechanical response of a laminate can be characterized with a set of equations relating the stress resultants (forces and moments) to the in-plane deformations (strains and midplane curvatures). These relations are derived by combining equilibrium, kinematics (strain–displacement relations), and stress–strain relations (Equation 4.39). The results are a set of force–strain–curvature relationships

$$\begin{Bmatrix} N_x \\ N_y \\ N_{xy} \end{Bmatrix} = \begin{bmatrix} A_{11} & A_{12} & A_{13} \\ A_{21} & A_{22} & A_{23} \\ A_{31} & A_{32} & A_{33} \end{bmatrix} \begin{Bmatrix} \varepsilon'_x \\ \varepsilon'_y \\ \gamma'_{xy} \end{Bmatrix} + \begin{bmatrix} B_{11} & B_{12} & B_{13} \\ B_{21} & B_{22} & B_{23} \\ B_{31} & B_{32} & B_{33} \end{bmatrix} \begin{Bmatrix} \kappa_x \\ \kappa_y \\ \kappa_{xy} \end{Bmatrix} \tag{4.41}$$

and a set of moment–strain–curvature

$$\begin{Bmatrix} M_x \\ M_y \\ M_{xy} \end{Bmatrix} = \begin{bmatrix} B_{11} & B_{12} & B_{13} \\ B_{21} & B_{22} & B_{23} \\ B_{31} & B_{32} & B_{33} \end{bmatrix} \begin{Bmatrix} \varepsilon'_x \\ \varepsilon'_y \\ \gamma'_{xy} \end{Bmatrix} + \begin{bmatrix} D_{11} & D_{12} & D_{13} \\ D_{21} & D_{22} & D_{23} \\ D_{31} & D_{32} & D_{33} \end{bmatrix} \begin{Bmatrix} \kappa_x \\ \kappa_y \\ \kappa_{xy} \end{Bmatrix} \tag{4.42}$$

These two sets can be written in matrix form as $\{N\} = [A]\{\varepsilon'\} + [B]\{\kappa\}$ and $\{M\} = [B]\{\varepsilon'\} + [D]\{\kappa\}$

where

$\{N\}$ is the force stress resultant (or force) vector, N
$\{M\}$ is the moment stress resultant (or moment) vector, N m
$\{\varepsilon'\}$ is the midplane laminate strain vector
$\{\kappa\}$ is the curvature vector, 1/m

$$[A] = A_{ij} = \sum_{k=1}^{N} \bar{Q}_{ij}^{k}(h_k - h_{k-1}) \text{ is the extension stiffness matrix, N/m}$$

$$[B] = B_{ij} = \frac{1}{2}\sum_{k=1}^{N} \bar{Q}_{ij}^{k}\left(h_k^2 - h_{k-1}^2\right) \text{ is the coupling stiffness matrix, N}$$

$$[D] = D_{ij} = \frac{1}{3}\sum_{k=1}^{N} \bar{Q}_{ij}^{k}\left(h_k^3 - h_{k-1}^3\right) \text{ is the bending stiffness matrix, N m}$$

Note that when the laminate is stretched, the [*B*] matrix causes curvatures (stretching/curvature coupling), and when the laminate is bended, the [*B*] matrix causes extensions (bending/extension coupling). Also, A_{16} and A_{26} cause shear–extension coupling, while D_{16} and D_{26} cause bend–twist coupling. B_{16} and B_{26} further couple stretching to twisting and bending to shearing. The coupling between bending and extension caused by [*B*] is a phenomenon not found at the lamina level, while the shear–extension coupling from A_{16} and A_{26} is analogous to that caused by the 16 and 26 components of $[\bar{Q}]$ at the lamina level. These coupling effects are usually undesirable and can be eliminated by selecting special layups. Some of these layups include

- Symmetric laminates, which do not in general have extension–bending or bending–stretching coupling. That is, $B_{ij} = 0$.
- Cross-ply laminates, $[0°/90°]_N$, have $A_{16} = A_{26} = D_{16} = D_{26} = 0$.
- So, symmetric cross-ply laminates, $[0°/90°]_s$, have no coupling.
- Unidirectional laminates $[0°]_N$ behave like symmetric cross-ply laminates and experience no coupling.
- Angle-ply laminates (also known as balanced or antisymmetric), $[\pm\theta]_N$, only have bending–twisting coupling, $B_{16} \neq B_{26} \neq 0$.
- Quasi-isotropic laminates have no coupling, and the [*A*] matrix is isotropic. For this case, $A_{11} = A_{22}$, $A_{66} = ½(A_{11} - A_{12})$, and $A_{16} = A_{26} = 0$. For the laminate to behave quasi-isotropic, it must be constructed with three or more plies; each ply must have identical stiffness properties and thickness, and layers must be oriented at equal angles (the angle between two adjacent plies must be π/N, where N is the total number of plies).

We can solve Equations 4.41 and 4.42 for the strains and curvatures (which can then be used to find the laminae stresses)

$$\begin{Bmatrix} \varepsilon' \\ \kappa \end{Bmatrix} = \begin{bmatrix} A & B \\ B & D \end{bmatrix}^{-1} \begin{Bmatrix} N \\ M \end{Bmatrix} \tag{4.43}$$

With the midplane strains {ε} and curvatures {κ}, lamina stresses in general coordinates at the top and bottom of each lamina can be determined as (say for lamina k of N laminae)

$$\begin{Bmatrix} \sigma_x \\ \sigma_y \\ \tau_{xy} \end{Bmatrix}_k = \begin{bmatrix} \bar{Q}_{11} & \bar{Q}_{12} & \bar{Q}_{16} \\ \bar{Q}_{21} & \bar{Q}_{22} & \bar{Q}_{26} \\ \bar{Q}_{61} & \bar{Q}_{62} & \bar{Q}_{66} \end{bmatrix}_k \begin{Bmatrix} \varepsilon_x' + z\kappa_x \\ \varepsilon_y' + z\kappa_y \\ \gamma_{xy}' + z\kappa_{xy} \end{Bmatrix}_k \tag{4.44}$$

where z is the distance to the top or bottom of laminae k, measured from the midplane h_k. The stresses in principal material directions can be obtained using Equation 4.35. That is,

$$\begin{Bmatrix}\sigma_1\\ \sigma_2\\ \tau_{12}\end{Bmatrix}_k = \begin{bmatrix}\cos^2\theta & \sin^2\theta & 2\sin\theta\cos\theta\\ \sin^2\theta & \cos^2\theta & -2\sin\theta\cos\theta\\ -2\sin\theta\cos\theta & 2\sin\theta\cos\theta & \cos^2\theta-\sin^2\theta\end{bmatrix}_k \begin{Bmatrix}\sigma_x\\ \sigma_y\\ \tau_{xy}\end{Bmatrix}_k \tag{4.45}$$

Hygrothermal Expansion Stresses

Recall that a change in temperature (ΔT) or moisture content (ΔC) in a lamina causes a change in its dimensions. The change in dimensions is proportional to the change in temperature or moisture content, the initial dimensions, and the coefficients of thermal and moisture expansion (Equations 4.25 through 4.28). These dimensional changes can be quantified with unit deformations, strains, both thermal and hygroscopic strains—$\varepsilon^T = \alpha\Delta T$ and $\varepsilon^H = \beta\Delta C$, respectively. These strains in principal material directions are

$$\left.\begin{aligned}\varepsilon_1^T &= \alpha_L\Delta T\\ \varepsilon_2^T &= \alpha_T\Delta T\\ \varepsilon_1^H &= \beta_L\Delta C = 0\\ \varepsilon_2^H &= \beta_T\Delta C\end{aligned}\right\} \tag{4.46}$$

These strains can be transformed to arbitrary coordinates using the transformation relations. First, the total strains are a combination of the mechanical strains caused by load and the hygrothermal strains:

$$\begin{Bmatrix}\varepsilon_1\\ \varepsilon_2\\ \gamma_{12}\end{Bmatrix}^{Total} = \begin{Bmatrix}\varepsilon_1\\ \varepsilon_2\\ \gamma_{12}\end{Bmatrix}^{Mechanical} + \begin{Bmatrix}\varepsilon_1\\ \varepsilon_2\\ 0\end{Bmatrix}^{Hygro\text{-}thermal} \tag{4.47}$$

Recall Equation 4.36, $\{\bar{\varepsilon}'\} = [T]^{-1}\{\varepsilon'\}$, which is used to transform the total strains. This relationship can also be used to transform the hygrothermal strains. The result for the thermal strains yields the coefficients of thermal expansion in laminate coordinates:

$$\left.\begin{aligned}\alpha_x &= \alpha_L\cos^2\theta + \alpha_T\sin^2\theta\\ \alpha_y &= \alpha_L\sin^2\theta + \alpha_T\cos^2\theta\\ \alpha_{xy} &= 2\sin\theta\cos\theta(\alpha_L - \alpha_T)\end{aligned}\right\} \tag{4.48}$$

Similarly for the MECs,

$$\left.\begin{aligned}\beta_x &= \beta_L\cos^2\theta + \beta_T\sin^2\theta = \beta_T\sin^2\theta\\ \beta_y &= \beta_L\sin^2\theta + \beta_T\cos^2\theta = \beta_T\cos^2\theta\\ \beta_{xy} &= 2\sin\theta\cos\theta(\beta_L - \beta_T) = 2\beta_T\sin\theta\cos\theta\end{aligned}\right\} \tag{4.49}$$

Hygrothermal strains do not produce stresses when the body is completely free to expand, bend, and twist, but deformation restraint occurs because of the difference in coefficients between laminae. From constitutive relationships, the total stresses (including hygrothermal effects) in the *k*th laminae are

$$\begin{Bmatrix} \sigma_x \\ \sigma_y \\ \tau_{xy} \end{Bmatrix}_k = \begin{bmatrix} \bar{Q}_{11} & \bar{Q}_{12} & \bar{Q}_{16} \\ \bar{Q}_{21} & \bar{Q}_{22} & \bar{Q}_{26} \\ \bar{Q}_{61} & \bar{Q}_{62} & \bar{Q}_{66} \end{bmatrix}_k \begin{Bmatrix} \varepsilon'_x + z\kappa_x - \alpha_x \Delta T - \beta_x \Delta C \\ \varepsilon'_y + z\kappa_y - \alpha_y \Delta T - \beta_y \Delta C \\ \gamma'_{xy} + z\kappa_{xy} - \alpha_{xy} \Delta T - \beta_{xy} \Delta C \end{Bmatrix}_k \tag{4.50}$$

From a stress result analysis similar to that used to derive the classical lamination theory (CLT) equations, we arrive at the resultant thermal forces and moments:

$$\begin{Bmatrix} N_x^T \\ N_y^T \\ N_{xy}^T \end{Bmatrix} = \Delta T \sum_{k=1}^{N} \bar{Q}_{ij}^k \begin{Bmatrix} \alpha_x \\ \alpha_y \\ \alpha_{xy} \end{Bmatrix}_k (h_k - h_{k-1}) \tag{4.51}$$

$$\begin{Bmatrix} M_x^T \\ M_y^T \\ M_{xy}^T \end{Bmatrix} = \frac{\Delta T}{2} \sum_{k=1}^{N} \bar{Q}_{ij}^k \begin{Bmatrix} \alpha_x \\ \alpha_y \\ \alpha_{xy} \end{Bmatrix}_k \left(h_k^2 - h_{k-1}^2\right) \tag{4.52}$$

The resultant hygroscopic forces and moments are

$$\begin{Bmatrix} N_x^H \\ N_y^H \\ N_{xy}^H \end{Bmatrix} = \Delta C \sum_{k=1}^{N} \bar{Q}_{ij}^k \begin{Bmatrix} \beta_x \\ \beta_y \\ \beta_{xy} \end{Bmatrix}_k (h_k - h_{k-1}) \tag{4.53}$$

$$\begin{Bmatrix} M_x^H \\ M_y^H \\ M_{xy}^H \end{Bmatrix} = \frac{\Delta C}{2} \sum_{k=1}^{N} \bar{Q}_{ij}^k \begin{Bmatrix} \beta_x \\ \beta_y \\ \beta_{xy} \end{Bmatrix}_k \left(h_k^2 - h_{k-1}^2\right) \tag{4.54}$$

Therefore, the total stress resultants (forces and moments) are

$$\{N\} = [A]\{\varepsilon'\} + [B]\{\kappa\} - \{N^T\} - \{N^H\} \text{ and } \{M\} = [B]\{\varepsilon'\} + [D]\{\kappa\} - \{M^T\} - \{M^H\}$$

Laminate Strength

For design purposes, the load-carrying capacity of a structure or component must be estimated. This can be done by comparing the stresses computed using Equation 4.45 to the strengths of the material using a failure criterion. Two of the most popular criteria include the *maximum stress theory* and the *maximum work theory*, both of which examine the onset of failure in the structure—but not the failure mode.

The *maximum stress theory* postulates that failure will occur when one (or all) of the stresses reaches a respective maximum value of ultimate strength, which can be estimated experimentally as discussed earlier. The criterion states that failure initiates when any one of the following inequalities is false or violated:

$$\left.\begin{aligned}\sigma_1 &< \sigma_{1TU}\\ \sigma_2 &< \sigma_{2TU}\\ \tau_{12} &< \tau_{12U}\end{aligned}\right\} \quad \text{Normal stresses are tensile} \tag{4.55}$$

When the longitudinal or transverse stresses are compressive, the corresponding ultimate compressive strengths are used. There is no interaction among modes of failure with this theory. This criterion is popular with designers because of its simplicity of concept and ease of use, not its validity.

The *maximum work theory* was derived by Tsai from a yield criterion for anisotropic materials proposed by Hill, which is often referred to as Tsai–Hill criterion in literature. This criterion is more accurate than the maximum stress criterion. The theory is based on the maximum distortional energy, and it postulates that ply failure initiates when the following inequality is false or violated:

$$I_f < 1 \tag{4.56}$$

where

$$I_f = \sqrt{\left(\frac{\sigma_1^k}{\sigma_{LU}}\right)^2 - \frac{\sigma_1^k \sigma_2^k}{(\sigma_{LU})^2} + \left(\frac{\sigma_2^k}{\sigma_{TU}}\right)^2 + \left(\frac{\tau_{12}^k}{\tau_{LTU}}\right)^2}, \quad \text{the Tsai–Hill failure index}$$

When the stress in the lamina for the transverse or longitudinal direction is compressive, the appropriate ultimate compressive value should be used. When Equation 4.56 is violated, the ply under consideration has failed. The advantages of this theory over the maximum stress (1) include relatively consistent agreement between theory and experimental results, (2) consider the interaction between failure strengths producing lower strength than the maximum stress criterion, and (3) offer a simple equation with strength parameters that can be determined experimentally without the need for complex experimental techniques required by other theories, such as the Tsai–Wu theory, which requires biaxial testing to determine some strength parameters.

Progressive Failure

Progressive failure analysis accounts for the strength of all the laminae in a laminate to determine the laminate strength. The strength analysis in the previous section is usually referred to as first-ply-failure (FPF) analysis. However, FPF does not provide the ultimate strength of a laminate because after FPF, it is likely that reserved capacity in the remaining laminae exists to continue carrying additional load. This means that failure of a single ply does not necessarily constitute failure of the entire laminate, despite the fact that the laminate will experience a significant change in stiffness.

This type of analysis requires knowledge of the stress state in each lamina throughout the analysis process. Stress analyses need to be repeated several times as different plies fail and relinquish their stiffness contribution, until the laminate is unable to carry higher loads. After each lamina fails, there are several approaches to account for ply failure, such as the *total ply discount* and the *ply failure distribution. Total ply discount* is a conservative approach that assumes a failed ply only contributes volume to the laminate and no stiffness properties. To determine the state of stress after

ply discounting, the CLT A_{ij}, B_{ij}, and C_{ij} matrices are modified by setting Q_{ij} for this lamina equal to zero. In *ply failure distribution*, knowledge of the failure mechanism of the ply is assumed to be known. For example, when matrix failure occurs in a ply, the transverse properties of that ply are omitted, and when fiber failure occurs in a ply, that ply can be treated as having zero stiffness for the subsequent analysis—as in the *total ply discount* approach.

Regardless of the approach to account for ply failure, the analysis process entails the following steps:

1. Determine the load (normal forces and moments) at which FPF occurs assuming that the response of the laminate is linear (between two-layer failures).
2. Modify the A_{ij}, B_{ij}, and C_{ij} matrices to account for the FPF by setting the Q_{ij} for this lamina equal to zero (say, for the total ply discount case). That is, a new set of A_{ij}, B_{ij}, and C_{ij} matrices is obtained using $Q_{ij}(\text{FPF}) = 0$:

$$[\bar{A}] = \bar{A}_{ij} = -\bar{Q}_{ij}(\text{FPF}) + \sum_{k=1}^{N} \bar{Q}_{ij}^{k}(h_k - h_{k-1})$$

$$[\bar{B}] = \bar{B}_{ij} = -\frac{1}{2}\bar{Q}_{ij}(\text{FPF})\left[\left(h_{top}^{\text{FPF}}\right)^2 - \left(h_{bottom}^{\text{FPF}}\right)^2\right] + \frac{1}{2}\sum_{k=1}^{N} \bar{Q}_{ij}^{k}\left(h_k^2 - h_{k-1}^2\right)$$

$$[\bar{D}] = \bar{D}_{ij} = -\frac{1}{3}\bar{Q}_{ij}(\text{FPF})\left[\left(h_{top}^{\text{FPF}}\right)^3 - \left(h_{bottom}^{\text{FPF}}\right)^3\right] + \frac{1}{3}\sum_{k=1}^{N} \bar{Q}_{ij}^{k}\left(h_k^3 - h_{k-1}^3\right)$$

3. With the modified matrices, the load increment that causes the second ply to fail is computed:

$$\begin{Bmatrix} \Delta N \\ \Delta M \end{Bmatrix}_2 = \begin{bmatrix} \bar{A} & \bar{B} \\ \bar{B} & \bar{D} \end{bmatrix} \begin{Bmatrix} \Delta\varepsilon' \\ \Delta\kappa \end{Bmatrix}_2$$

4. The total load after the second ply fails is computed by adding the load from step 1 and the load increment from step 3.
5. The midplane strains and curvatures can then be computed by adding the strain and curvature at FPF from step 1 and the increment in strain computed in step 3.
6. Steps 2–5 are then repeated for all subsequent plies until the change in load is relatively small; at that point, the laminate is considered to have failed.

The ultimate load of a laminate based on progressive failure analysis correlates well with experimental data. The deflection, however, is larger in the experimental data. The reason for this is the progressive failure analysis discussed here does not account for the increase in deflection that occurs when each ply fails and relinquishes its stiffness.

Transport Properties

Thermal conductivity transforms in the same manner as stresses and strains, via tensor transformation rules. Therefore, the thermal conductivity tensor, k_{ij}, for a laminate (layup of N laminae) can be calculated from ply thermal conductivities (longitudinal, C_1; transverse, C_2; and through thickness, C_3, discussed earlier); the tensor consists of four nonzero elements, k_{xx} (or k_x for short), k_y, k_z,

and k_{xy}. In order to combine the thermal conductivities of each ply to obtain k_x and k_y (since rotation is about z-axis, k_z does not change), C_1 and C_2 must be transformed to global coordinates by transforming the heat flux from the balance of energy (McManus and Springer, 1992). Then the laminate conductivities can be obtained as follows:

$$k_x = C_1 \frac{\sum_{j=1}^{N} h_j \cos^2 \theta_j}{\sum_{j=1}^{N} h_j} + C_2 \frac{\sum_{j=1}^{N} h_j \sin^2 \theta_j}{\sum_{j=1}^{N} h_j}$$

$$k_y = C_1 \frac{\sum_{j=1}^{N} h_j \sin^2 \theta_j}{\sum_{j=1}^{N} h_j} + C_2 \frac{\sum_{j=1}^{N} h_j \cos^2 \theta_j}{\sum_{j=1}^{N} h_j}$$

$$k_z = C_3 \tag{4.57}$$

where

h_j is the individual ply thicknesses, mm

θ_j is the ply orientation with respect to the fiber direction, positive counterclockwise

The thermal conductivity coupling term $k_{xy} = \sin \theta_j \cos\theta_j(C_1 - C_2)$ will usually be equal to zero. *Moisture diffusivity* also transforms in the same manner as stresses and strains, via tensor transformation rules. Therefore, the moisture diffusivity tensor, k_{ij}^m, for a laminate (layup of N laminae) can be calculated from ply moisture diffusivities (longitudinal, D_1; transverse, D_2; and through thickness, D_3, discussed earlier); the tensor consists of four nonzero elements, k_{xx}^m (or k_x^m for short), k_y^m, k_z^m, and k_{xy}^m. In order to combine the moisture diffusivities of each ply to obtain k_x^m and k_y^m (since rotation is about z-axis, k_z^m does not change), D_1 and D_2 must be transformed to global coordinates using a balance of mass (McManus and Springer, 1992). Then the laminate diffusivities can be obtained as follows:

$$k_x^m = D_1 \frac{\sum_{j=1}^{N} h_j \cos^2 \theta_j}{\sum_{j=1}^{N} h_j} + D_2 \frac{\sum_{j=1}^{N} h_j \sin^2 \theta_j}{\sum_{j=1}^{N} h_j}$$

$$k_y^m = D_1 \frac{\sum_{j=1}^{N} h_j \sin^2 \theta_j}{\sum_{j=1}^{N} h_j} + D_2 \frac{\sum_{j=1}^{N} h_j \cos^2 \theta_j}{\sum_{j=1}^{N} h_j}$$

$$k_z^m = D_3 \tag{4.58}$$

where

h_j is the individual ply thickness, mm

θ_j is the ply orientation with respect to the fiber direction, positive counterclockwise

The moisture diffusivity coupling term $k_{xy}^m = \sin \theta_j \cos \theta_j (D_1 - D_2)$ will usually be equal to zero.

TRANSPORT PHENOMENA

Transport phenomena are important in the study of composite durability and life prediction analyses. There are a number of degradation mechanisms that depend on transport agents, such as moisture and temperature, to cause permanent damage of the materials. In this section, we present the analysis required to determine the temperature and moisture concentration in a composite material for the given hygrothermal environmental conditions.

Thermal Analysis

Temperature is assumed to be governed by anisotropic transient heat conduction. The general 3-D relation is

$$\frac{\partial T}{\partial t} = \frac{\partial}{\partial x_i}\left(\frac{k_{ij}}{\rho c}\frac{\partial T}{\partial x_j}\right) \tag{4.59}$$

where

T is the temperature, °C
ρ is the density of the material, kg/m^3
c is the specific heat of material, J/kg · °C
x_i, x_j are the material directions x, y, or z, as shown in Figure 4.4
k_{ij} is the thermal conductivity tensor of material, given earlier, W/m · °C

Typical laminated structures are much longer (and wider) compared to the thickness, $L_x \gg h$, where L_x is the length of the structure. As a result, thermal gradients through the thickness, 1-D, are of primary interest. The geometry–orthotropy nondimensional parameter $\mathcal{L}_{xz}$ (also known as the Lauren parameter) is used to assess if modeling of lengthwise diffusion is needed. From Crews and McManus (1997),

$$\mathcal{L}_{xz} = \frac{k_z L_x^2}{k_x h^2} \tag{4.60}$$

If $\mathcal{L}_{xz}$ is much less than 1.0, the geometry can be modeled as 1-D. If the width (y direction size) needs to be considered, use Equation 4.60 with x replaced by y in all subscripts. Note that this is true for most structures. Therefore, a simplified 1-D (through thickness) solution is sufficiently accurate in most cases. This solution can be found in Kreith and Bohn (1986) and is summarized in the following paragraphs.

For 1-D with constant thermal conductivity, Equation 4.59 reduces to the form (Fourier's equation)

$$\frac{\partial T}{\partial t} = \alpha \frac{\partial^2 T}{\partial z^2} \tag{4.61}$$

where $\alpha = k_z/\rho c$ is the thermal diffusivity (represents a measure of the rate at which temperature changes inside the material), m^2/s.

To solve this equation, we need boundary conditions, which can be convective or adiabatic (insulated), depending on the condition at the surfaces. The front face of the composite is always assumed to be convective, while the back face can be either convective or insulated (no heat flow).

The convective boundary condition at the surface is expressed by setting the heat convected into the surface equal to the heat conducted into the surface, that is,

$$h_c(T_{surface} - T_\infty) = -k_z \frac{\partial T}{\partial z}$$

where

h_c is the convective heat transfer coefficient, W/m$^2 \cdot$ °C

T_∞ is the temperature of convective environment, °C

The adiabatic boundary condition at an insulated surface for a flat plate exposed on one side (or the midsurface of a flat plate exposed on both sides) is expressed by the specified surface (or midsurface) temperature.

The analytical solution to Equation 4.61 (temperature distribution through the thickness as time changes) is derived in Kreith and Bohn (1986) as

$$T(z,t) = T_\infty + \sum_{n=1}^{\infty} e^{-\delta_n^2 \mathrm{Fo}} A_n \cos(\delta_n \xi) \tag{4.62}$$

where

$\delta_n \tan(\delta_n) = \mathrm{Bi}$ (this is a transcendental equation with an infinite number of discrete values of δ_n satisfying it)

$\mathrm{Bi} = h_c h/k$ = Biot number, nondimensional

$\mathrm{Fo} = \alpha t/h^2$ = Fourier number, nondimensional

$\xi = z/h$, nondimensional

$$A_n = \frac{2(T_i - T_\infty)\sin(\delta_n)}{\delta_n + \sin(\delta_n)\cos(\delta_n)}$$

T_i is the initial temperature of the body, °C

h is the thickness

Note that the temperature $T(z,t)$ is expressed in terms of dimensionless quantities, Fo, Bi, and ξ. This relationship can be used to determine the through-thickness temperature distribution of a flat plate with thickness h exposed on one side or a plate of thickness $2h$ exposed on both sides (for this case, we need to replace h with $2h$ earlier).

A practical issue for analyzing the thermal state of composite structures is deciding if a full heat transfer analysis is necessary. The Biot nondimensional parameter, Bi, physically represents the ratio of internal (conduction) thermal resistance to the surface (convection) thermal resistance. Bi can be used to assess the through-thickness temperature variation as a structure is heated or cooled over time using a thermal gradient applied to its surface.

If the thermal response of the structure is considerably faster than the changes expected in the thermal environment, transient (or cyclic) thermal analyses will not be required. That is, the temperature of the structure can be assumed to track the temperature of the environment. If the condition that $\mathrm{Bi} < 0.1$ is satisfied, then the structure can be assumed to have a constant internal temperature, but a simple calculation is required to determine the temperature lag between the structure and the environment. The temperature lag can be calculated from a simple transient thermal analysis, the lumped-heat-capacity analysis

$$T(t) = (T_i - T_\infty)e^{-\mathrm{Bi}\,\mathrm{Fo}} + T_\infty \tag{4.63}$$

The time constant associated with the lag is approximately

$$\tau = \frac{hc\rho}{h_c} \quad \text{for Bi} < 0.1 \quad \text{and} \quad \tau = \frac{4h^2 c\rho}{\pi^2 k_z} \quad \text{for Bi} > 0.1 \tag{4.64}$$

If the environment temperature varies with time interval, Δt, and the condition $\tau \ll \Delta t$ is satisfied, the structure can be assumed to track the environment temperature, and no thermal analysis is required. If this condition is not satisfied, a full thermal gradient calculation using Equation 4.62 is required to obtain the temperature of the material. The implication of a uniform temperature distribution throughout the laminate (even with varying surface temperature) is that changes in surface temperature propagate through the material rapidly and stresses caused by through-thickness thermal gradients are negligible.

When a full analysis is required, it can also be simplified depending on the value of the Fourier nondimensional parameter, Fo, which physically represents the ratio of the rate of internal (conduction) heat transfer to the rate of energy storage in the system. For Fo greater than approximately 0.2, Equation 4.62 can be reduced to only the first term without loss of accuracy:

$$T(z,t) = T_\infty + e^{-\delta_1^2 \text{Fo}} A_1 \cos(\delta_1 \xi) \tag{4.65}$$

In order to conduct a full thermal analysis, a set of parameters must first be determined. Depending on the importance of the parameters, their value may be assumed, estimated from available data for a similar material/condition, or may need to be determined experimentally.

Hygral Analysis

The diffusion of moisture into the composites (amount of moisture as a fraction of the dry mass) is assumed to be governed by Fick's second law and is discussed in Tsai (1988). The 3-D relation is

$$\frac{\partial C_m}{\partial t} = \frac{\partial}{\partial x_i}\left(k_{ij}^m \frac{\partial C_m}{\partial x_j}\right) \tag{4.66}$$

where

C_m is the moisture concentration, dimensionless—usually expressed as a percentage of the dry mass of the host solid

x_i, x_j are material directions x, y, or z, as shown in Figure 4.4

k_{ij}^m is the moisture diffusivity tensor (which represents a measure of how fast moisture concentration changes inside the host solid), given earlier, m^2/s

A practical issue for analyzing a composite structure is deciding if a full moisture transport analysis is necessary. Similar to heat transfer analysis, a number of nondimensional parameters are used to evaluate the accuracy of the simplifying assumptions. Moisture gradients will always exist for some period of time; therefore, there is no need for analog Biot or Fourier numbers. The relevant nondimensional parameters for this case include the moisture diffusion time constant

$$\tau^m = \frac{h^2}{\pi^2 k_z^m} \tag{4.67}$$

and the geometry–orthotropy parameter (also known as the Lauren parameter)

$$\mathcal{L}_{xz}^{m} = \frac{k_z^m L_x^2}{k_x^m h^2} \tag{4.68}$$

These parameters were developed by analogy to the aforementioned thermal parameters by Seth et al. (2007). If the time constant is much less than the time interval of interest, moisture transient calculations can be omitted, and the moisture can be assumed to be in equilibrium with the environment. If not, transient moisture calculations must be carried out, which is usually the case. Also, for $\mathcal{L}_{xz}^{m} \gg 1$, the geometry can be modeled as 1-D. If width (y direction size) needs to be considered, Equation 4.68, with x replaced by y in all subscripts, applies.

The platelike geometry of the model used in the code, along with the assumption that the through-thickness temperature and surface moisture exposure are constant, allows us to use a 1-D analysis to determine the moisture gradient through the thickness (Foch, 1997). Equation 4.66 in 1-D is

$$\frac{\partial C_m}{\partial t} = k_z^m \left(\frac{\partial^2 C_m}{\partial z^2} \right) \tag{4.69}$$

The through-thickness moisture diffusivity k_z^m is assumed independent of time, does not vary through the thickness, and is dependent on temperature according to an Arrhenius exponential equation:

$$k_z^m = k_0^m \exp\left(\frac{-E_A^m}{RT} \right) \tag{4.70}$$

where

k_0^m is the reference diffusion constant, m^2/s

E_A^m is the activation energy, J/mol; given that k_z^m strongly depends on temperature, the results from at least two different temperatures are fit to Equation 4.70 in order to obtain the temperature this factor

R is the gas constant, 8.3143 J/mol · K

T is the absolute temperature in Kelvin, K

The moisture transport properties (reference diffusion constant, k_0^m, and the activation energy) needed to obtain the moisture diffusivity, k_z^m, as a function of temperature using Equation 4.70 can be reduced by measuring specimen weight gain per ASTM D-5229. First, the pre-saturation data are plotted against the square root of time and the slopes extracted by a linear fit. Equation 4.75 can then be used to obtain the moisture diffusivity for different temperatures. The coefficients in Equation 4.70 are then fit using a least-squares error criterion.

Notice that the form of Equation 4.69 is the same as that of Equation 4.61. Given the dependence of k_z^m on temperature, the two equations appear to be coupled. However, temperature reaches equilibrium much faster (at a rate of 10^6) than moisture concentration (ASTM D-5229) since for most composite applications, the thermal diffusivity, α, is about six orders of magnitude greater than k_z^m. Thus, material temperature can be assumed to track the environmental temperature—decoupling the two equations.

The initial and boundary conditions for a plate exposed to the same moisture environment on two sides are as follows:

$$\text{For } t \le 0,\ C_m = C_{mi} \text{ (assumed uniform throughout)}$$

$$\text{For all } t > 0,\ C_m(z = 0,\ t) = C_\infty(t) \quad \text{and} \quad C_m(z = h,\ t) = C_\infty(t)$$

where h is the thickness of the plate.

The following analytical solution to Equation 4.69 is given by Shen and Springer (1976):

$$C_m(z,t) = C_{mi} + (C_\infty - C_{mi})\left[1 - \frac{\pi}{4}\sum_{j=0}^{\infty}\frac{1}{2j+1}\sin\frac{(2j+1)\pi z}{h}\exp\left(-\frac{(2j+1)^2\pi^2 k_z^m t}{h^2}\right)\right] \tag{4.71}$$

This equation can be used to determine the moisture distribution through the thickness of a flat plate as a function of time. However, of great practical importance is the total moisture content (or weight gain), which can be used to obtain the through-thickness moisture diffusivity empirically. First, the average moisture concentration is obtained by integrating Equation 4.71 over the thickness:

$$\begin{aligned}\bar{C}_m(t) &= \frac{1}{h}\int_0^h C_m(t,z)dz \\ &= C_m + (C_\infty - C_{mi})\left[1 - \frac{8}{\pi^2}\sum_{j=0}^{\infty}\frac{1}{(2j+1)^2}\exp\left(-\frac{(2j+1)^2\pi^2 k_z^m t}{h^2}\right)\right]\end{aligned} \tag{4.72}$$

Note that at $t = 0$, $\bar{C}_m = C_{mi}$ because we assumed C_{mi} to be uniform through the thickness, and at $t = \infty$, $\bar{C}_m = C_\infty$, which is the moisture equilibrium state. The series in this relationship converges slowly for short times ($t \approx \tau^m$); however, for sufficiently large values of t, the relationship may be approximated by the first term of the series. An approximate solution to Equation 4.72 for short times is given by Tsai and Hahn (1980):

$$\bar{C}_m(t) = C_{mi} + 4(C_\infty - C_{mi})\left(\frac{k_z^m t}{\pi h^2}\right)^{1/2} \tag{4.73}$$

If we multiply both sides of this relationship by the thickness h for plates exposed on two sides (or by thickness $2h$ for plates exposed on one side only), we arrive at the moisture content of the material; that is, $M_m = \bar{C}_m \cdot h$, $M_{mi} = C_{mi} \cdot h$, and $M_\infty = C_\infty \cdot h$. Rearranging Equation 4.73 in terms of moisture content,

$$\frac{\bar{C}_m - C_{mi}}{C_\infty - C_{mi}} = \frac{M_m - M_{mi}}{M_\infty - M_{mi}} = 4\left(\frac{k_z^m}{\pi h^2}\right)^{1/2}\sqrt{t} \tag{4.74}$$

Obviously plotting $(M_m - M_{mi})/(M_\infty - M_{mi})$ vs. $\sqrt{t}$ will result in a straight line, the slope of which can be used to obtain the through-thickness moisture diffusivity, k_z^m. Per ASTM D-5229, the slope can

be obtained by using two weight gain points and the square root of the corresponding times. The following relation is then used to determine the diffusivity using experimental data:

$$k_z^m = \pi\left(\frac{h}{4M_m}\right)^2\left(\frac{M_2 - M_1}{\sqrt{t_2} - \sqrt{t_1}}\right)^2 \tag{4.75}$$

where

M_m is the effective moisture equilibrium content (the maximum moisture uptake), %

$(M_2 - M_1/\sqrt{t_2} - \sqrt{t_1})$ is the slope of moisture absorption in the linear portion of the curve in $\sqrt{time}^{-1}$

The two points used to find M_1 and M_2 must be based on at least five specimen weighings per condition, with a minimum time interval specified in ASTM D-5229.

The maximum moisture uptake depends on the moisture content of the environment and may be obtained following the procedure listed in ASTM D-5229 (essentially by measuring the average moisture content until it changes by less than 0.01%) or from the following relationship:

$$M_m = A\Phi^B \tag{4.76}$$

where

Φ is the environmental concentration (usually expressed as a relative humidity)

B is the material constant, may be assumed to be 1.0

A is the constant that represents the percent moisture in the material at equilibrium with a saturated (Φ = 100%) environment, also referred to as the saturation moisture concentration

A and B can be determined by conducting a series of tests at different relative humidities and plotting M_m as a function of Φ, on a logarithmic scale, $\ln(M_m) = B \cdot \ln(\Phi) + \ln(A)$.

In order to conduct a full hygral analysis, a set of parameters must first be determined. Depending on the importance of the parameters, their value may be assumed, estimated from available data for a similar material/condition, or may need to be determined experimentally.

SUMMARY

In this chapter, we presented relationships that can be used to predict the properties of FRP composite materials using the properties of individual constituents. Also presented are relationships for hygroscopic and thermal transport properties. These relationships in conjunction with the material properties should assist the infrastructure engineer in the design of FRP composite systems for construction. For additional information, a number of resources are cited in the reference list that can provide in-depth guidance on topics discussed in this chapter.

REFERENCES

Agarwal, B.D. and Broutman, L.J. 1990. *Analysis and Performance of Fiber Composites*, 2nd edn., John Wiley & sons, New York.

Barbero, E.J. 1999. *Introduction to Composite Materials Design*, 2nd edn., CRC, Boca Raton, FL.

Crews, L.K. and McManus, H.L. 1997. Modeling the high-temperature degradation of graphite/epoxy, *Proceedings of the American Society for Composites 12th Technical Conference on Composite Materials*, Detroit, MI, October 1997, pp. 1123–1132.

Foch, B.J. 1997. Integrated degradation models for polymer matrix composites, MSc thesis, Massachusetts Institute of Technology, Cambridge, MA, May 1997.

Jones, R.M. 1998. *Mechanics of Composite Materials*, 2nd edn., Taylor & Francis Group, Philadelphia, PA.

Kreith, F. and Bohn, M. 1986. *Principles of Heat Transfer*, 4th edn., Harper & Row, New York, pp. 101–107.

McManus, H.L. and Springer, G.S. 1992. High temperature thermomechanical behavior of carbon-phenolic and carbon-carbon composites, I. Analysis, *Journal of Composite Materials*, 26(2), 206–229.

Seth, S.K., McManus, H.L., and Hyer, M.W. (2007). Service life assessment methodology for composites, *Proceedings of the 22nd Annual Technical Conference of the American Society for Composites*, Seattle, WA, September 17–19, 2007, Paper ASC-2007 #020.

Shen, C.H. and Springer, G.S. 1976. Moisture absorption and desorption of composite materials, *Journal of Composite Materials*, 10, 2–20.

Tsai, S.W. 1988. *Composite Design*, 4th edn., Think Composites, Dayton, OH.

Tsai, S.W. and Hahn, H.T. 1980. *Introduction to Composite Materials*, Technomic, Westport, CT.

5 Overview of Electroactive Polymers

Marco P. Schoen and Arya Ebrahimpour

CONTENTS

INTRODUCTION

Polymers have found at an ever-increasing rate their places in the engineering world. Nowadays, polymers are used in civil structures, automobiles, aircrafts, and even kitchen appliances. This expansion of applications of polymers has come at the expense of often heavier materials, such as steel, die cast, and aluminum alloys. It is not surprising that polymers themselves have evolved over time and represent a current popular research area. In this chapter, we look at special types of polymers, electroactive polymers (EAPs), that have some interesting features and a lot of promise for future applications not only in civil engineering but also in other fields of engineering. As these polymers find their way into the daily engineering world, it is important that civil engineering practitioners have basic understanding of these materials. We will highlight properties of a few selected EAPs and provide some key performance data. In addition, we attempt to provide a glimpse into the future and forecast potential applications civil engineering practitioners may find in the near future.

In this chapter, we will first review some of the basic terms and definitions fundamental to the understanding of the operation of EAPs. In the "Classification of EAPs" section, we discuss basic operational functionality and properties of two classes of EAPs: ionic EAPs and electric EAPs. As examples for the first category can be listed ionic polymer–metal composites (IPMCs) and carbon

nanotubes (CNTs), while to the second category belong liquid crystal elastomers (LCEs) and electrostrictive graft elastomers (EGEs). The "Future Application of EAPs" section discusses future potential application of these materials in the field of civil engineering.

FUNDAMENTALS

The polymers we are presenting in this chapter are considered primarily to be of use in a dynamic environment. By this we mean that dynamic properties such as shape or simple dimensional changes due to input to the polymers are used to address dynamic problems commonly found in engineering. For example, consider structural vibration, which is either human-induced, machinery-generated, or caused due to environmental interaction. Mitigation of such dynamics can be achieved in many different ways, one of which is the use of smart materials. EAPs belong to the class of smart materials. The term smart material is defined by the ability of the material to drastically auto-alter one or more of its properties. In addition, this change in property is controlled by physical events, such as electrical or mechanical stimuli. There are a number of different smart materials (some of which have made their mark in everyday engineering application), such as piezoelectric materials, shape memory alloys (SMAs), and magneto- and electrorheological fluids. Commonly, smart materials not only have the property of actuating and therefore interacting with its environment but also have the ability to sense changes such as deformation, charge, etc.

In this section, we will establish some of the basic fundamentals that can be used to characterize properties that allow a material to be classified as a smart material. Further, we will restrict ourselves to properties that are descriptive of EAPs.

Dipoles

One of the key driving elements for some of the EAPs is based on dipole moments. In this section, we will briefly review the concept of an electric dipole and how it affects the functionality of some EAPs. Considering a positive and a negative charge q separated by a distance L (Figure 5.1a), applying an electric field E (Figure 5.1b) results into forces at each charge in accordance with the field, as depicted in Figure 5.1c.

The magnitude of the force generated is $q \times E$, and hence, the moment generated by the dipole is equal to

$$M = d \times qE \sin(\theta) \tag{5.1}$$

Polarization

Considering the resulting electric dipole of some material, the polarization is defined as the vector describing the direction and magnitude of the moment per unit volume. If no electric field E is applied to the specimen, the polarization results in the charge per unit surface area of the material (Kim and Tadokora, 2007).

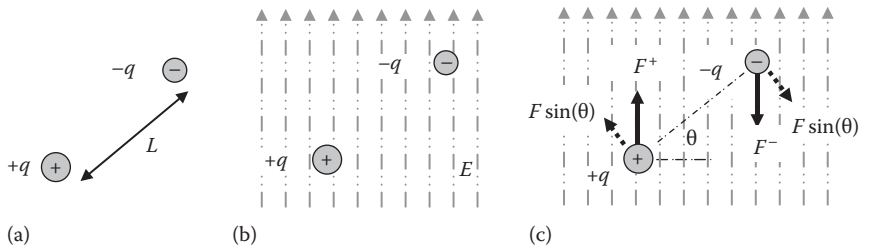

FIGURE 5.1 Dipole illustration, (a) positive and negative charge, (b) applied electric field E, and (c) resulting forces.

Piezoelectricity

A number of materials including EAPs have the property of piezoelectricity, that is, the ability to respond to electrical stimuli when deforming its shape and vice versa: generating an electrical charge due to external forces that cause the material to deform. Thus, this reversible effect can be utilized as a sensing device and as an actuation mechanism. For example, in actively engaging and changing the behavior of some civil structures to control structural vibration, for which case, it is most advantageous to have sensor and actuator collocated. The collocation avoids the inclusion of an additional transfer function, thus making the control problem simpler and more efficient. A common piezoelectric material used in structural vibration control is the lead zirconate titanate crystal, also commonly known by its abbreviation PZT.

Consider the electric displacement D, given by $D = \varepsilon E$, where ε is the permittivity (ability of a material to polarize in response to an applied field) and E is the applied electric field. We can quantify the piezoelectric effect using Hook's law, which is presented here in a slightly different form than the standard form by utilizing the compliance s (measure of flexibility): $S = sT$, where S is the strain and T corresponds to the stress. This effect is given by relating S and T coupled with E and D:

$$S = E \times d \quad \text{and} \quad D = T \times d \tag{5.2}$$

where d is the piezoelectric coefficient. Now using Hook's law to relate the two equations, we arrive at the piezoelectric constitutive equations:

$$\begin{aligned} S_{ij} &= d_{kij}E_k + s^E_{ijkl}T_{kl} \\ D_i &= \varepsilon^T_{ik}E_k + d_{ikl}T_{kl} \end{aligned} \tag{5.3}$$

This formulation (Nye, 1987) is in tensor form where the superscript indicates the condition under which the constant was evaluated. For example, the exponent E indicates that the measurement was conducted under a constant electric field, while T indicates constant stress. The indexes i, j, k, and l are set from 1 to 3, corresponding to the tensor notation. Also note that the permittivity has F/m as units, the piezoelectric coefficient is given in m/V, and the elastic coefficient (compliance) is given in m^2/N.

It is quite useful to view relationships (5.3) in matrix notation, by converting the tensor indices (ij) and (kl) into matrix indices p and q. This can be easily accomplished using Table 5.1:

In this form, Equations 5.3 will transform into

$$D_i = \varepsilon^T_{ik}E_k + d_{iq}T_q \tag{5.4}$$

and

$$S_p = d_{pk}E_k + s^E_{pq}T_q \tag{5.5}$$

TABLE 5.1
Conversion between Tensor and Matrix Notation

ij or kl	11	22	33	23 or 32	31 or 13	12 or 21
p or q	1	2	3	4	5	6

To illustrate the use of these two equations, we utilize a PZT material. The compliance matrix s, piezoelectric coefficient matrix d, and the permittivity matrix of PZT are given as follows:

$$s_{pq}^{E} = \begin{bmatrix} s_{11} & s_{12} & s_{13} & 0 & 0 & 0 \\ s_{12} & s_{11} & s_{13} & 0 & 0 & 0 \\ s_{13} & s_{13} & s_{33} & 0 & 0 & 0 \\ 0 & 0 & 0 & s_{44} & 0 & 0 \\ 0 & 0 & 0 & 0 & s_{44} & 0 \\ 0 & 0 & 0 & 0 & 0 & 2(s_{11} - s_{12}) \end{bmatrix} \quad d_{iq} = \begin{bmatrix} 0 & 0 & 0 & 0 & d_{15} & 0 \\ 0 & 0 & 0 & d_{15} & 0 & 0 \\ d_{31} & d_{31} & d_{33} & 0 & 0 & 0 \end{bmatrix}$$

and

$$\varepsilon_{ik}^{E} = \begin{bmatrix} \varepsilon_{11} & 0 & 0 \\ 0 & \varepsilon_{22} & 0 \\ 0 & 0 & \varepsilon_{33} \end{bmatrix}$$

The coefficient matrix d entails the properties of a PZT used to specify the material. Using a simplified version of the equation earlier, we can compute the estimated change in dimension of the piezoelectric material:

$$\Delta L = \pm E \times d_{ij} \times L_o \tag{5.6}$$

where L_o is the original length. Hence, the direction of polarization and use of the material will determine which index of the piezoelectric coefficient matrix d is to be used. For example, d_{33} is used to describe the strain parallel to the polarization vector—or thickness—of the ceramics; d_{31} corresponds to the strain orthogonal to the polarization vector—that is, the width.

Supramolecular Assemblies

In supramolecular chemistry, one is concerned about bonding interactions of molecules, where the chemical bonding mechanism is between macromolecules rather than sharing of electrons.

Amorphous

Many polymers are described as amorphous materials. The adjective indicates that the material is not organized in a thermodynamically favorable crystalline state. This is often accomplished by rapid cooling of the material or by adding chemicals that prevent the position of the atoms to form in a long-range order.

Joule Heating

Heat is generated when an electric current flows through a conductor. This process is called Joule heating. The name can be traced back to Joule's first law, where heat produced is proportional to the electric resistance in the conductor. The physical mechanism of heating in this process is based on the movement of electrons and atomic ions within the conductor. Joule heating is sometimes also called ohmic heating or resistive heating. Joule heating is used to activate LCEs.

Ions

If a group of atoms lose or gain electrons, they become charged. For example, losing an electron makes the group negatively charged. Ions play a fundamental role in IPMCs, as we will discuss in the next section.

Nematic Liquid Crystal

These crystals have their molecules more or less aligned along a common axis.

CLASSIFICATION OF EAPs

As mentioned earlier, only a brief segment of the vast area of smart materials is covered in this chapter; even within EAPs, there is a wide variety of different configurations and working principles. A comprehensive comparison of all EAPs is difficult because of the various material specifications. This chapter is intended to be a short overview of EAPs, and as such, we can only compare these materials with some of the more popular smart materials. In Table 5.2, we compare EAPs with other popular smart materials such as SMAs and piezoelectric materials.

As discussed earlier, EAPs can be classified into two categories depending on their activation mechanisms: electronic and ionic (Bar-Cohen, 2001). Ionic polymers require low driving voltages (less than 7 V) to achieve large strains (more than 300%) but need to be kept hydrated for its electromechanical operation. In contrast to the electronic type, this class of materials cannot sustain direct current (DC)-induced displacements (Bar-Cohen, 2004). Examples of such materials include conductive polymers/polyaniline actuators, CNTs, IPMCs, and ionic gels (Bar-Cohen et al., 2001). Electronic-type polymers are dry and have greater mechanical energy density and can be operated in air, vacuum, or water in a wide temperature range with no major constraints (Bar-Cohen, 2001). Also, these materials require high voltages (>100 MV/m) to achieve longitudinal deformations of order 4%–360% (Bar-Cohen et al., 2001). Unlike ionic polymers, electronic polymers can be made to hold the induced displacement under activation of a DC voltage, which makes them prime candidates for civil applications (Bar-Cohen, 2004). This category includes piezoelectric, electrostrictive, and ferroelectric materials (Bar-Cohen et al., 2001). In the next two sections, we provide a more detailed overview of these two types of polymers.

Ionic EAPs

Within the ionic EAPs, we will briefly describe properties and working principles of IPMCs and CNTs.

Ionic Polymer–Metal Composites

IPMCs are an interesting class of EAPs that promises a wide variety of potential applications because they exhibit very large bending strains (>10%) under relatively low applied voltages (1–7 V), as shown in Figure 5.2; they are lightweight (density 1–2.5 g/cc), have minimal energy consumption, and are electromechanically efficient (>25% for actuation and >90% for sensing) (Bar-Cohen, 2004). Though there are several different types of IPMC, all of these materials are manufactured in a similar manner (Bar-Cohen, 2001; Shahinpoor and Kim, 2001). The process entails taking an ionic polymer such as Nafion®, soaking it in an ionic salt solution of an

TABLE 5.2
Key Properties Comparison for Smart Materials and EAPs

Property	PZT	SMA	EAP	
Strain achieved (%)	<0.1	<8	>300	
Force generated (MPa)	>100	200	<40	
Voltage required (V)	>50 V	5 V	Ionic EAP <7 V	Electronic EAP <150 V/μm

Source: Bar-Cohen, Y., *Electroactive Polymer (EAP) Actuators as Artificial Muscles: Reality, Potential, and Challenges*, 2nd Edn., SPIE Press, Bellingham, WA, 2004.

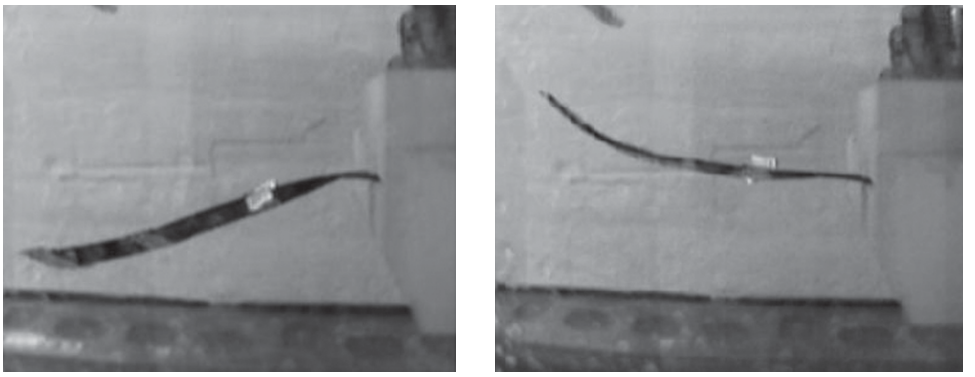

(a) (b)

FIGURE 5.2 IPMC before (a) and after (b) application of a 2 V step input.

appropriate metal (such as platinum), and then chemically reducing it to draw the metal to the surface of the polymer yielding a composite that consists of the polymer sandwiched between two thin sheets of metal. The large bending strains that are observed in Figure 5.2 are driven by ion exchange within the polymer as cations are attracted to the cathode surface of the polymer under an applied voltage.

While this bending characteristic has been demonstrated many times, it has also been shown that a linear relationship exists between the voltage output and the displacement applied at the tip of an IPMC strip (Shahinpoor, 1999). Given these characteristics, IPMCs have the potential to be useful in a variety of different applications, albeit primarily sensing and actuating. Some examples that are currently under investigation for IPMC as actuators are mechanical lightweight robotic grippers, 3D beam actuators, morphing actuators, fluid flow actuators (such as in a robotic fish), linear actuators, contractile serpentine actuators, diaphragm mini pumps, MEMS actuators, nonmagnetic electromechanical relay switches, and continuous variable aperture mirrors and antenna dishes (Shahinpoor and Kim, 2005). In the area of biomedical engineering, a variety of future applications are possible, including artificial ventricular- or cardiac-assist muscles, surgical tools, peristaltic pumps, artificial smooth muscle actuators, artificial sphincter and ocular muscles, and aiding refractive error correction of the human eye (Shahinpoor and Kim, 2005). Great steps have been taken since the discovery of this novel material toward devising a system to characterize and accurately control the response of an IPMC to an input voltage (Mallavarapu and Donald Leo, 2001; Bar-Cohen et al., 2002; Bhat and Won-jong, 2003; Richardson et al., 2003; Lavu et al., 2005). However, the actuation of IPMCs remains relatively simple, consisting of a voltage applied at a single point at the edge or at some central location on the polymer surface, which results in a simple cantilever motion such as the motion observed in Figure 5.2.

The main drawbacks of IPMCs are that these materials do not offer an appreciable power output (estimated at 10 W/kg) (Wax and Sands, 1999) as compared with the natural muscle (1000 W/kg), pneumatic, piezoelectric, or hydraulic components; operation at higher voltages is prohibited due to concomitant electrolysis of water, which in turn may contaminate an operating platform; presence of a hydrated environment for operation, lack of which curtails the migration of cation species; sample contamination from competing cationic species; lack of consistency of processing of these materials; and the manufacturing cost, which is quite high (Bar-Cohen, 2004).

Carbon Nanotubes

CNTs are a very recent addition to the field of EAPs (though not technically a polymer, though when added to polymers can render the host materials conductive, provided that the CNT

loading is above the percolation threshold). This particular configuration of CNT-loaded polymers is a very promising material because of their superior mechanical and electrical properties. Applications of CNTs will be plentiful in the near future, spanning from nanosized actuation and sensing systems to reinforced composite materials. CNTs belong to the class of allotropes, where the most popular allotrope is probably the diamond. The CNT's walls can be as small as one atom thick; the cylindrical shape can have diameters in the nanometer scale, that is, 1/50,000 of a human hair—hence the name carbon nanotubes. This carbon configuration can have length to diameter ratios of over 10,000 (the length can reach several millimeters), resulting in a high-strength nanostructure possessing desirable electrical, mechanical, and thermal properties. There are two types of CNTs, single-walled nanotubes (SWNTs) and multi-walled nanotubes (MWNTs).

Single-Walled Nanotubes

SWNTs are the more promising of the two types of CNTs. This form of the material is more difficult to achieve due to impurities such as amorphous and graphitic forms of carbon and carbon-encapsulated catalytic metal nanoparticles. Impurities have degenerative results on the array of applications of SWNTs; that is, the quality of SWNTs is crucial for applications in nanostructured composite materials (Zhou et al., 2002).

The structure of the one-atom-thick SWNT is made up of benzene rings, which are hexagonal carbon units. There is a double bond between two atoms, a single bond on the other side of the atom and one free bond per atom (see Figure 5.3). Since CNTs are very receptive of van der Waals forces, they tend to align themselves into chains and can structure themselves to substantial lengths.

Multi-Walled Nanotubes

MWNTs appear in two different configurations. One configuration has several SWNTs aligned in concentric cylinders, each SWNT with a different diameter. The other configuration of MWNTs is by rolling an SWNT in itself (similar to a gift paper roll). For either model, the distance between the cylinders or layers is in the order of 3.3 Å. MWNTs are in general easier to produce than SWNTs. A particular MWNT is the double-walled nanotube (DWNT), which has a specific advantage over the other MWNTs and the SWNTs. A DWNT has the capacity to alter its chemical functionality without changing much of its carbon structure. This is accomplished by chemically altering (grafting chemicals to the sheet of graphite). SWNTs and other MWNTs are susceptible to damage in the form of "holes" in their carbon structure due to breaking of some of the carbon bonds; however, DWNTs provide a more robust structure for the grafting since only the outer wall is modified.

Since CNTs are relatively new materials, the potential applications of these materials will be explored as neat material as well as a material that can be used in combination with others. In Table 5.3, the basic properties of CNTs and other commonly found material in civil engineering practice are compared based on the most common mechanical properties.

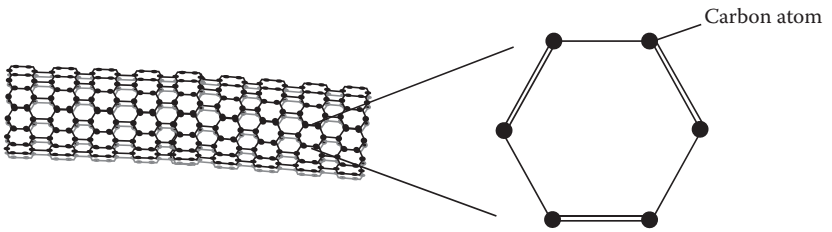

FIGURE 5.3 Benzene rings that function as the fundamental building block for SWNTs.

TABLE 5.3
Basic Properties of Carbon Nanotubes Compared with Some Other Materials

Material	Young's Modulus (GPa)	Tensile Strength (GPa)	Density (g/cm³)
SWNT	1054	150	—
MWNT	1200	150	2.6
Steel	208	0.4	7.8
Wood	16	0.008	0.6
Epoxy	3.5	0.005	1.25

Electronic EAPs

In contrast to ionic EAPs, electric EAPs are driven by either an electric field or coulomb forces. We will focus on electric-field-activated EAPs. In general, electronic EAPs require high activation electric fields (>150 V/μm) and are capable of holding their shape/displacement with a constant electric field, in contrast to ionic EAPs. Also, another advantage over ionic EAPs is the lack of hydration for electronic EAP materials. Their main application currently is in solid-state electromechanical actuators and motion sensors. There are numerous electric EAPs, including ferroelectric polymers, which are driven by the field-induced dipole action; dielectric elastomers, the motions of which are governed by Maxwell stresses; electrostrictive paper, which is in essence silver laminated paper activated by a strong electric field; and electroviscoelastic elastomers, which are a special form of electrorheological. In this section, two of the more commonly electronic EAPs will be reviewed, LCEs and EGEs.

Liquid Crystal Elastomers

LCEs have piezoelectric properties and can be set in motion through Joule heating. These materials are in general supramolecular ordered assemblies made of a monodomain nematic LCE with conductive polymers spread within the network structure (Bar-Cohen, 2004). The Joule heating causes phase changes, which in turn have the effect of alignment changes of the liquid crystals and ultimately produce stresses within the LCE that make the polymer change its shape. Figure 5.4 depicts the actuation mechanism of LCEs. The main limitation of these materials is based on the

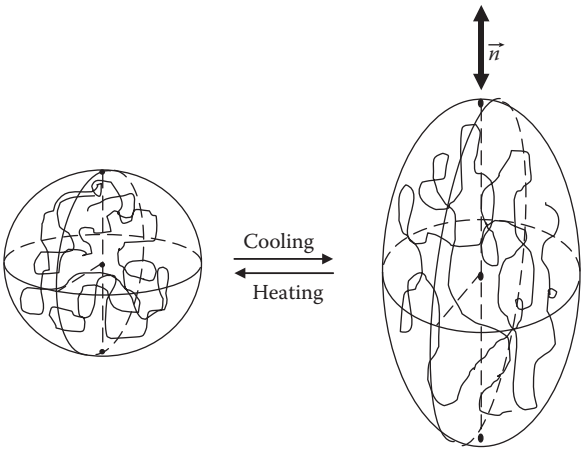

FIGURE 5.4 LCE response to thermal activation.

TABLE 5.4
Basic Electrical Properties of LCEs

	Response Time (ms)	Strain (%)	Blocked Stress Value (kPa)	Appl. Elec. Field (MV/m)	Film Thickness (μm)
LCE	~10	>400	460	1.5–25	>1

Sources: Springer Science + Business Media: *Electroactive Polymers for Robotic Applications: Artificial Muscles and Sensors*, 2007, Kim, K.J. and Tadokora, S.; Bar-Cohen, Y., *Electroactive Polymer (EAP) Actuators as Artificial Muscles: Reality, Potential, and Challenges*, 2nd Edn., SPIE Press, Bellingham, WA, 2004.

thermodynamics occurring within the actuation mechanism. In particular, the heat transfer time constant limits the rate of change. A rough (rule of thumb)-type relationship between the time constant and the thickness is given by Kim and Tadokora (2007) as

$$\tau = c\frac{1}{t^2}$$

where
- τ is the time constant
- c a proportionality coefficient
- t the thickness of the LCE

From this, we see that the thicker the material is, the smaller the time constant. Another factor is related to the application of heat to one or both sides of the LCE, which in the latter case can reduce the time constant drastically. LCEs are in general spherical in the isotropic state and stretch when they are thermally activated to the nematic state. The vector $\vec{n}$ (nematic) points along the long axis of the shaped spheroid (Warner and Terentjev, 2003) (see Figure 5.4).

Some basic response-based properties of LCEs are given in Table 5.4.

Electrostrictive Graft Elastomers

Electrostrictivity refers to change of shape in electrically nonconducting material due to applied fields; hence, EGEs belong to the class of electronic EAPs. The basic components are given by flexible macromolecular chains and crystallizable side chains that can be attached or "grafted" to the flexible macromolecular chains. Figure 5.5 illustrates the basic configuration of the EGEs.

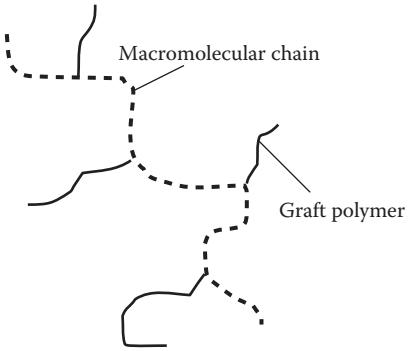

FIGURE 5.5 Electrostrictive graft elastomer molecular structure.

TABLE 5.5
Common Properties of EGEs

	Strain (%)	Young's Modulus (MPa)	Output Power (MPa)	Energy Density (J/kg)	Dielectric Constant
Graft elastomer	4	550	22	247	11

Source: Su, J. et al., *Proc. IEEE Int. Symp. Appl. Ferroelectr.*, 2, 811, 2000.

The grafted elastomers linked to the macromolecular chain can crystallize and form physical cross-linkages, which result in electric-field-sensitive polar crystal domains. These domains rotate while exposed to an electric field and align with the field due to dipole action. This alignment causes the macromolecular chains to change shape and thus change the EGE's shape as well. Some of the electromechanical properties of this material are given in Table 5.5.

FUTURE APPLICATION OF EAPs

EAPs are best suited for dynamic environments. The inherent damping properties of these polymers and their adaptive nature make them ideal for vibration attenuation. In the field of structural engineering, research is currently being conducted for drag/oscillation reduction of large shell structures (EMPA, 2007a). Another potential application is the use of EAPs in long-span, lightweight bridge structures (EMPA, 2007b). The bridge vibrations caused by traffic, rain, and wind are best controlled by adaptive systems that may include integration of distributed EAPs in the structural system. For example, by using EAPs, it may be possible to alter the structural natural frequency to avoid resonance at a given loading frequency or dissipate energy through excitation of higher modes that may not cause damage or disturb the occupants (e.g., in the case of long-span pedestrian bridges). Piezoelectric polymer sensors such as polyvinylidene fluoride (PVDF) have also been recently developed for structural health monitoring. These sensors are capable of identifying defects as well as dynamic changes in structures (Gu et al., 2005; Vinogradov et al., 2005).

Since civil engineers may be involved in design of aerospace structures, we will briefly mention applications in this area. Ongoing work includes development of novel propulsion system for blimp structures that are used for transportation, observation, and stratospheric platforms (WW-EAP Newsletter, 2006). With the help of electrically activated elastic polymer films, the blimp surface can change shape by bending and stretching, simulating motion of a fish in a stream. In another application, controllable inflated EAP reflectors were proposed for use with lightweight optical and microwave systems that are placed in low-gravity space environment (Bao et al., 2005). Changes in temperature or slight defects in fabrication make the surface of such systems (e.g., a space mirror) distorted; thus, the use of EAPs is proposed to correct for these deviations.

Conclusions

This chapter's discussion of EAPs is intended to provide some ideas about the future potential of these materials. As polymers continue replacing some traditional engineering materials, EAPs will inevitably become options as well. In the area of civil infrastructure, they have a great potential to affect the dynamics of civil structures, particularly when coupled with other technologies such as control systems. In many instances, EAP can provide actuation and sensing mechanisms that may be used to alter a structure's property with little intrusion or added weight.

REFERENCES

Bao, X., Bar-Cohen, Y., Chang, Z., Sherrit, S., and Badescu, M. (2005). Wirelessly controllable inflated electroactive polymer (EAP) reflectors. *Proceedings of the SPIE Smart Structures Conference*, San Diego, CA, pp. 5759–5752, March 7–10, 2005.

Bar-Cohen, Y. (2001). *Electroactive Polymer (EAP) Actuators as Artificial Muscles: Reality, Potential, and Challenges*. SPIE—The International Society for Optical Engineering, Bellingham, WA.

Bar-Cohen, Y. (2004). *Electroactive Polymer (EAP) Actuators as Artificial Muscles: Reality, Potential, and Challenges*. 2nd Edn. SPIE Press, Bellingham, WA.

Bar-Cohen, Y., Bao, X., Sherrit, S., and Lih, S.S. (2002). Characterization of the electromechanical properties of ionomeric polymer–metal composite (IPMC). *SPIE Smart Structures and Materials Symposium*, San Diego, CA.

Bar-Cohen, Y., Sherrit, S., and Lih, S.-S. (2001). Characterization of the electromechanical properties of EAP materials. *Proceedings of SPIE—Smart Structures and Materials*, 4329: 319–327.

Bhat, N. and Won-jong, K. (2003). System identification and control of ionic polymer metal composite. *Proceedings of SPIE, Smart Structures and Materials*, San Diego, CA.

EMPA. Civil and Mechanical Engineering. (2007a). Adaptive Systems, http://www.empa.ch/plugin/template/empa/51/*/ (July 17, 2007).

EMPA. Research Group of Laboratory for Materials and Engineering. (2007b). Electroactive polymer (EAP) actuators, http://www.empa.ch/plugin/template/empa/*/56570/ (July 17, 2007).

Gu, H., Zhao, Y., and Wang, L.M. (2005). A wireless smart PVDF sensor for structural health monitoring. *Structural Control and Health Monitoring*, 12(3–4): 329–343.

Kim, K.J. and Tadokora, S. (2007). *Electroactive Polymers for Robotic Applications: Artificial Muscles and Sensors*. Springer Verlag, London, U.K.

Lavu, B.C., Schoen, M.P., and Mahajan, A. (2005). Adaptive intelligent control of ionic polymer–metal composites. *Smart Materials and Structures*, 14: 466–474.

Mallavarapu, K. and Donald Leo, J. (2001). Feedback control of ionic polymer actuators. *Journal of Intelligent Material Systems and Structure*, 12: 143–155.

Nye, F.J. (1987). *Physical Properties of Crystals*. Clarendon Press, Oxford, U.K.

Richardson, R.C., Levesley, M.C., Brown, M.D., Hawkes, J.A., Watterson, K., and Walter, P.G. (2003). Control of ionic polymer metal composites. *IEEE/ASME Transactions on Mechatronics*, 8(2): 245–253.

Shahinpoor, M. (1999). Electro-mechanics of iono-elastic beams as electrically controllable artificial muscles. *Proceedings of the SPIE—Smart Structures and Materials*, 3669: 109–121.

Shahinpoor, M. and Kim, K.J. (2001). Ionic polymer–metal composites: I. Fundamentals. *Smart Materials and Structures*, 10: 819–833.

Shahinpoor, M. and Kim, K.J. (2005). Ionic polymer–metal composites: IV. Industrial and medical applications. *Smart Materials and Structures*, 14: 197–214.

Su, J., Harrison J.S., and St. Chair, T. (2000). Novel polymeric elastomers for actuation. *Proceedings of IEEE International Symposium on Application of Ferroelectrics*, 2: 811–819.

Vinogradov, A., Su, J., Jenkins, C., and Bar-Cohen, Y. (2005). State-of-the-art developments in the field of electroactive polymers. *Proceedings of the Materials Research Society*, Boston, MA, November 28, 2005.

Warner, M. and Terentjev, E.M. (2003). *Liquid Crystal Elastomers*, Clarendon Press, Oxford, U.K.

Wax, S.G. and Sands, R.R. (1999). Electroactive polymer actuators and devices. *SPIE Conference on Electroactive Polymer Actuators and Devices*, San Diego, CA.

WW-EAP Newsletter. (2006). Development of a blimp with bionic propulsion based on electro active polymers. *Worldwide Electroactive Polymers*, 8(2), July 17, 2007.

Zhou, O., Shimoda, H., Gao, B., Oh, S., Fleming, L., and Yue, G. (2002). Materials science of carbon nanotubes: Fabrication, integration and properties of macroscopic structures of carbon nanotubes. *Accounts of Chemical Research*, 35: 1045–1053.

6 Life Cycle Costs of Composite Materials

Hector Estrada and Luke S. Lee

CONTENTS

INTRODUCTION

Civil infrastructure provides the basic framework for a functioning society. It has directly and indirectly influenced our civilization with the sole purpose of raising our standards of living through increased global interaction. However, infrastructure systems are under increasing strain because of rapid population growth, system aging, and natural disasters, all of which have resulted in increased demands on performance and cost, even without consideration for the environmental and social impacts associated with construction and infrastructure maintenance management. For example, the fabrication of cement results in large quantities of CO_2 emissions (Kendall, 2004) that amounted to 71.3 million metric tons in 2008 (van Oss, 2010). To mitigate the effects of emissions, new materials and production methods are under development, such as engineered cementitious materials and fiber-reinforced polymer (FRP) composites.

In many countries, the strain on civil infrastructure has been exacerbated by increasing population and a disparate investment pace in new infrastructure systems; in many cases, maintenance needs are not sustained consistently with the rate of population growth. These conditions require entities responsible for construction, repair, maintenance, and rehabilitation of infrastructure systems to choose between various competing systems. In order to prioritize the replacement, repair, or maintenance of systems, engineers must have tools available to ensure safety and optimize cost. One such tool is life cycle cost (LCC) analysis. Also, the true total cradle-to-grave cost of systems must include environmental and social cost along with monetary cost. This is typically referred to as the triple bottom line, which is one of the fundamental pillars of sustainability. The costs associated with environmental and social impact are rather tenuous but are beginning to be quantified and documented in the literature. This has been driven by the so-called green building movement and can prove to be beneficial in the financial decision-making processes.

The increased use of FRP composites in infrastructure is primarily driven by the investments made in research to develop applications for composites. During the first few decades of this research, it is estimated that the American federal government spent $30 million developing composites for use in infrastructure applications (Mu et al., 2006). Although the use of FRP materials in infrastructure is relatively recent, composites have a long history (since World War II) in a number of other commercial industries, such as the aerospace and sporting goods industries. Many of the attributes that make composites ideal in these industries can also benefit civil infrastructure. For instance, some of the advantages of composites over traditional infrastructure materials include high specific properties (strength-to-weight and stiffness-to-weight ratios), corrosion resistance, and low-cost erection/maintenance. A more detailed description of each of these advantages is provided as follows:

- *High specific properties* are particularly important in civil infrastructure; for example, FRP bridge decks weigh approximately 20% of the weight of an equivalent reinforced concrete deck. This allows a reduction in dead load requirements, which in turn reduces the strength requirements for the sub- and superstructural elements. For existing bridges, a replacement FRP deck with a high strength-to-weight ratio can increase the live-to-dead load ratio, potentially resulting in adjustments to any imposed bridge load restrictions. Also, in seismic prone regions, a lighter system will generate smaller seismic forces on the supporting systems.
- *Corrosion resistance* is critically important in infrastructure systems exposed to corrosive and deicing chemicals. In fact, corrosion of steel reinforcement is the primary cause of structural deficiency in reinforced concrete infrastructure systems. Since FRP composites are not susceptible to degradation at the same rate as steel, the use of FRP materials should result in a longer service life and lower maintenance costs, all of which contribute to lower associated LCCs (Nelson, 2005).
- *Low-cost erection/maintenance* is important for highly trafficked bridges, where the indirect costs from traffic delays and lost productivity are estimated at 10 times the direct costs (Nelson, 2005). FRP bridge decks can be installed in approximately half the time of an equivalent reinforced concrete bridge deck (Nelson, 2005). The faster installation time results in a lower economic impact.

There are also some disadvantages associated with using FRP materials:

- *Material unit cost* when compared to reinforced concrete is much higher. The range of costs found for composites is two to three times higher compared to concrete. Although, there is potential cost savings over the extended service life of FRP materials, engineers are always hesitant to change designs to an unfamiliar material (Nelson, 2005).
- *Low ductility* results in little to no warning of failure, which can be potentially catastrophic (Nelson, 2005). Properly detailed reinforced concrete provides system ductility allowing some warning before failure; this can be seen in routine inspections, for example, as excessive deflections (Nelson, 2005). Due to this danger, inspections of FRP bridges are conducted every year as opposed to every 2 years for bridge decks of accepted material characteristics (Telang et al., 2006).

While the advantages and disadvantages of composite materials are well defined with respect to mechanical and hygrothermal properties, the challenge of characterizing the LCC of a material requires integrating environmental, social, and economic factors with traditional engineering measures of safety and performance. In this chapter, the LCC of composite materials is examined. First, sustainability is introduced in the context of FRP composites and the need for life

cycle analysis is described; then, an overview of environmental impacts of FRP composites that focuses on the effects of constituent materials is examined; and finally, the theoretical framework of LCC analysis is presented.

SUSTAINABILITY AND FRP COMPOSITES

The sustainability concept, as described in the Common Future (World Commission on Environment and Development, 1987), states that:

> Sustainable development is a process of change in which the exploitation of resources, the direction of investments, the orientation of technological development, and institutional change are all in harmony and enhance both current and future potential to meet human needs and aspirations. Sustainable development "… meets the needs of the present without compromising the ability of future generations to meet their own needs."

While numerous metrics have been developed to assess the sustainability of materials and systems, in general, each emphasizes or weighs factors for the following characteristics:

1. Minimum resources use
2. Low environmental impact
3. Low human and environmental health risks
4. Sustainable site design strategies
5. Higher performance

The ideal sustainable material or system would have a closed life cycle where renewable energy and resources are used with zero waste and zero social impact. Certainly, there are few materials that could qualify as ideal sustainable materials and still satisfy structural performance requirements. Even more challenging are the demands of sustainable design, which essentially seeks to achieve tailored design, construction, and maintenance plans depending on impact priorities, regional issues, and economic requirements.

Composite Material Sustainability

The fabrication of constituent materials for FRP composites, namely, matrix and fiber, is the primary area of concern when considering that most polymers (excluding biopolymers) are derived from crude oil, natural gas, chlorine, and nitrogen (Gerdeen et al., 2006). The most commonly used fiber reinforcements in civil infrastructure, glass and carbon fibers, require high temperatures (1400°C for glass; 1200°C–2400°C for carbon) during production and in some cases require petroleum byproducts as precursors. However, it is worth noting that the production of traditional civil engineering materials (cement and steel) is accompanied by high environmental costs as well (Hollaway, 2010). During the manufacture of cement, intense heat is required, as high as 1870°C, fueled by coal and natural gas that are used to transform raw materials into clinker. In steel, the refining process involves the use of a blast furnace using coke and limestone to heat iron ore to a temperature of 1600°C.

When considering only energy and material resources, on the surface, it appears that the argument for FRP composites in a sustainable built environment is questionable. However, such a conclusion needs to be evaluated in terms of the potential advantages of FRP composites related to considerations such as the following:

- Higher strength
- Lighter weight
- Higher performance

- Longer life
- Rehabilitating existing structures to extend their life
- Seismic retrofits
- Defense systems unique requirements
- Space systems
- Ocean and other highly corrosive environments

In the case of FRP composites, environmental concerns appear to be a barrier to its feasibility as a sustainable material, especially when considering fossil fuel depletion, air pollution, smog, and acidification associated with their production. In addition, the ability to recycle FRP composites is limited, and unlike steel and timber, structural components cannot be reused to perform a similar function in another structure. However, quantifying the benefits of FRP composites in infrastructure applications through a life cycle analysis may potentially balance adverse environmental impacts.

Life Cycle Assessment

The life cycle assessment of a material, component, or system involves examining the inputs and outputs from design, fabrication, operation, and decommissioning. There are five categories to consider when ascertaining the life of an asset or the selection of material (Woodward, 1997):

1. *Functional life*: period of time for which the asset is needed
2. *Physical life*: period of time the asset is expected to last without replacement or major rehabilitation
3. *Technological life*: period until it is determined that the asset is obsolete and a new superior alternative is needed
4. *Economic life*: period until the state of the economy dictates that a lower-cost alternative is needed
5. *Social and legal life*: period until human desire or legal requirement dictates a replacement

The initial costs of a material or structure involve capital resources, environmental, and social impact resulting from a material's production and installation. While lower initial costs might be attractive in the present, capital and environmental resources used as well as the social impact during maintenance and replacement of a material must also be considered. It is important to note that the selection of FRP composites will not be governed by the economic, environmental, or social impacts of the material alone; rather, the selection of FRP composites will depend on the contribution of the material to reducing the overall LCCs associated with an entire structural system.

Perhaps the best solution for a sustainable environment is not to rebuild or replace an existing structure but to extend its physical life, thereby minimizing energy use and waste production that result from demolition of the existing structure and construction of a new structure. This scenario lends itself to the use of FRP composites for repair and strengthening of existing structures so that they can continue serving their function or support changes in use requirements. The development of new FRP or hybrid infrastructure systems requires a design that considers the useful life of the system in every phase of design and maintenance. A key aspect to life cycle assessment of rehabilitated or new infrastructure systems is the ability to estimate the service life integrating durability data. An estimation of service life is integral to evaluating performance, economic, environmental, and social LCCs associated with any material or system. Figure 6.1 provides an illustration of how performance of a rehabilitated system can be integrated with time-dependent parameters to select materials or designs based on remaining service life of options a, b, and c.

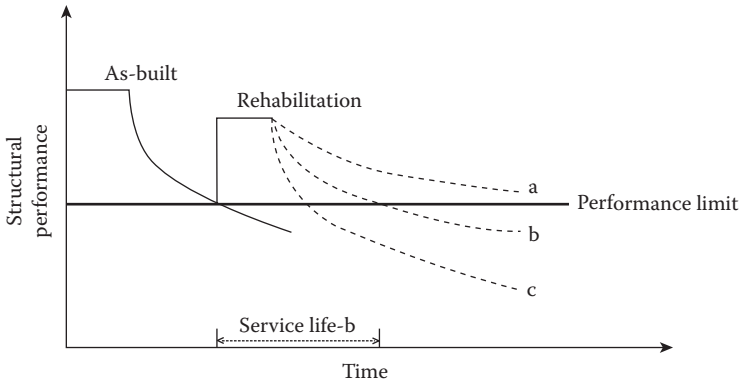

FIGURE 6.1 Service life estimation based on a measure of structural performance.

ENVIRONMENTAL IMPLICATIONS OF FRP COMPOSITES

Significant advantages in FRP composites exist over conventional materials; however, since FRP materials are synthetic, doubt exists about how manufacturing these materials will affect the environment. The primary environmental concerns include health, safety, emission of volatile organic compounds (VOCs), energy consumption, and toxicity. Most fabrication and manufacturing processes consist of multiple steps that result in the use of energy, materials, and water resources, generating large air, water, and land emissions. Each phase of the manufacturing process from material choice, mold preparation, preparation of materials, application of materials, mold operations and consolidation, curing and post curing, and trimming the component to cleaning and disposal of equipment needs to be considered for adverse environmental impact. It is worth noting that only through a comparative life cycle analysis from cradle to grave of a specific material or system that a judgment can be rendered on the superiority of a material. The intent here is to draw attention to the manufacturing and processing aspects of composite materials in civil infrastructure applications that are likely to result in adverse environmental impacts. The remainder of this section highlights areas associated with the manufacturing of constituent materials and methods of processing of composite materials that are prevalent in civil infrastructure and presents the most significant sources of environmental impact of FRP composites.

Environmental Impacts of the Matrix

The three most common thermosetting resins used in infrastructure applications are polyester, vinylester, and epoxy. Due to the use of fossil-based materials, polymers are often the primary cause of environmental impact because of the considerable environmental impact associated with raw material extraction; fibers have a much lower impact (Anderson et al., 2004). Table 6.1 summarizes

TABLE 6.1
Summary of Matrix Environmental Impacts

Matrix	Environmental Impact
Polyester	Use of fossil fuels, peroxide, and styrene
Vinylester	Use of peroxide and styrene
Epoxy	Use of fossil fuels, use of hardeners

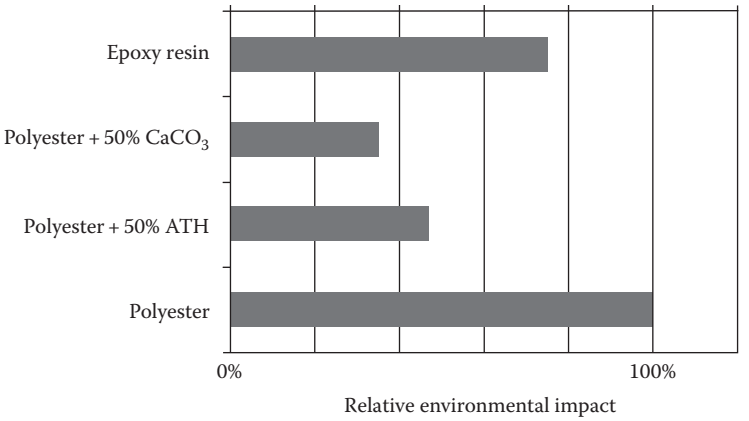

FIGURE 6.2 Relative environmental impact of resins compared to polyester. (From Anderson, J. et al., *Green Guide to Composites: An Environmental Profiling System for Composite Materials and Products*, BRE Bookshop, Hertfordshire, U.K., 2004.)

environmental concerns for matrices that are prevalent in civil infrastructure. Curing and polymerization of resins, which is the process of bonding monomers to form polymers or long chains of monomers, requires high amounts of energy input. Much of this energy requirement results from the necessity of high heats for production.

Polyester is used for its low cost and high corrosion resistance and can serve as a fire retardant. The polymerization reaction for polyester usually takes place in the presence of a catalyst, such as peroxide (Bank, 2006). Peroxide is toxic and can irritate eyes and skin. Styrene, a cross-linking agent, poses health concerns since it evaporates and can be inhaled during the mixing and application of the resin (Anderson et al., 2004). In addition, prolonged exposure can lead to brain damage and changes in blood cells (Astrom, 1997). Figure 6.2 provides relative comparisons of environmental impact between polyester, epoxy, and polyester with two different types of fillers.

Vinylester is a premium resin that has advantages with respect to high heat and moisture resistance and is highly effective in corrosive environments. In addition, vinylester resin is very workable, cures quickly, and is known to develop good bond characteristics with fibers. During production of vinylester resins, styrene and a peroxide catalyst have similar emission and health concerns as in polyester production (Bank, 2006).

Epoxies are one of the more expensive types of resin but are attractive because of their workability, adhesive properties, low shrinkage, and environmental durability. Epoxy resins are typically supplied in two parts, resin and hardener. The resin itself is known to be toxic, while the hardeners are known to cause disease and damage to the liver and kidneys (Astrom, 1997). Table 6.2 provides a summary of environmental impact during production of a typical epoxy resin (Joshi et al., 2004).

Environmental Impacts of the Fiber

The three most common types of fibers used in FRP composite materials are glass, carbon, and aramid fibers. Depending on the manufacturing process, the fiber volume fraction of composites ranges from 10% to 65%. In general, the production of fibers is associated with high temperatures, and both carbon and aramid fibers require the use of petroleum by-products as precursors. Table 6.3 provides a brief summary of the environmental impacts during fiber production.

TABLE 6.2
Environmental Impact of Production of Epoxy Resin

Environmental Impact	Epoxy Resin
Energy use (MJ/kg)	140.71
Carbon dioxide emissions (kg/kg)	5.90
CO emissions (kg/kg)	2.20
SO_x emissions (g/kg)	19.00
NO_x emissions (g/kg)	35.00
Particulate matter (g/kg)	15.0
BOD to water (mg/kg)	1,200
COD to water (mg/kg)	51,000
Nitrates to water (mg/kg)	1
Phosphates to water (mg/kg)	220

Source: Joshi, S.V. et al., *Compos. Part A*, 35, 371, 2004.

TABLE 6.3
Summary of Fiber Environmental Impacts

Fiber	Environmental Impact
Carbon	Use of petroleum pitch, high energy use
Glass	Dusty processing, high energy use, use of fossil fuels
Aramid	High energy use, use of petroleum by-products

Carbon fibers are manufactured from three different constituents: rayon, polyacrylonitrile (PAN), and petroleum pitch. Fibers are initially drawn and oxidized at temperatures below 400°C. After this process, the fibers undergo pyrolysis (heated above 800°C). Finally, graphitization is carried out with fibers heated to temperatures in excess of 1000°C. Clearly, carbon fibers require high temperatures to manufacture; therefore, compared to glass and aramid fibers, carbon fibers have the greatest environmental impact due to energy requirements during production. However, it should be noted that due to their excellent properties, a lower quantity of material is often needed to achieve the same performance for a longer duration than glass or aramid fibers, which may potentially offset their adverse environmental impact (Anderson et al., 2004).

Glass fibers include E-glass and S-glass, two commonly used types of glass fibers. The primary material of glass fibers is silica; to effectively produce these fibers, the ingredients must be melted in a furnace at temperatures of about 1370°C. Like carbon fibers, glass fibers require high temperatures to manufacture, using large quantities of energy and fossil fuels. To produce a glass fiber mat, a total of 54.7 MJ/kg of nonrenewable energy is used (Joshi et al., 2004). This includes energy used for each step, including raw materials extraction, mixture, transport, melting, spinning, and mat production. In addition, glass processing is dusty, which makes the production of glass fibers a contributor to air pollution (Daniel and Nagtegaal, 2001). In order to assess the sustainability of glass fibers, the amount of carbon emission and by-products produced during manufacturing needs to be quantified for all fibers and all other basic construction materials.

Glass fibers are a popular choice as reinforcement due to their low cost and many advantageous properties, such as high strength (tensile strength of approximately 3.40 GPa) and tolerance to high temperatures and corrosive environments. However, glass fibers have a relatively low stiffness. Typically, values of stiffness for glass fibers range from approximately 70 to 90 GPa, whereas the stiffness of carbon fiber can range from 230 to 830 GPa. Additionally, glass fibers are very sensitive to moisture; in a study conducted by Abdel-Magid et al. (2005), the strength of a glass fiber specimen decreased by 35% (767–499 MPa) when exposed to water at room temperature while under a constant tensile load. This is a concern if glass fibers are to be considered for areas that are particularly humid.

Environmental Impacts of Production

It has been emphasized throughout this chapter that an adequate comparison of environmental impacts due to material choice requires a life cycle analysis that depends on the component or system being constructed over its entire expected service life. Each material choice is characterized by its respective production stages. Figure 6.3 illustrates a typical production process for a component or system constructed of FRP composites within the framework of life cycle assessment. Most composite manufacturing processes require the use of energy, raw materials, and water resources

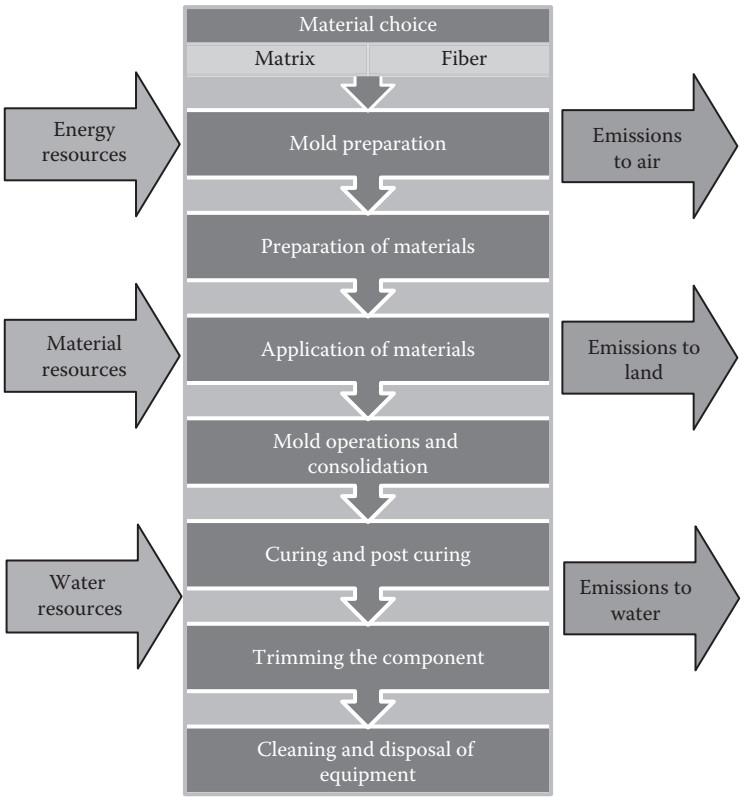

FIGURE 6.3 Overview of composite manufacturing process. (From Anderson, J. et al., *Green Guide to Composites: An Environmental Profiling System for Composite Materials and Products*, BRE Bookshop, Hertfordshire, U.K., 2004.)

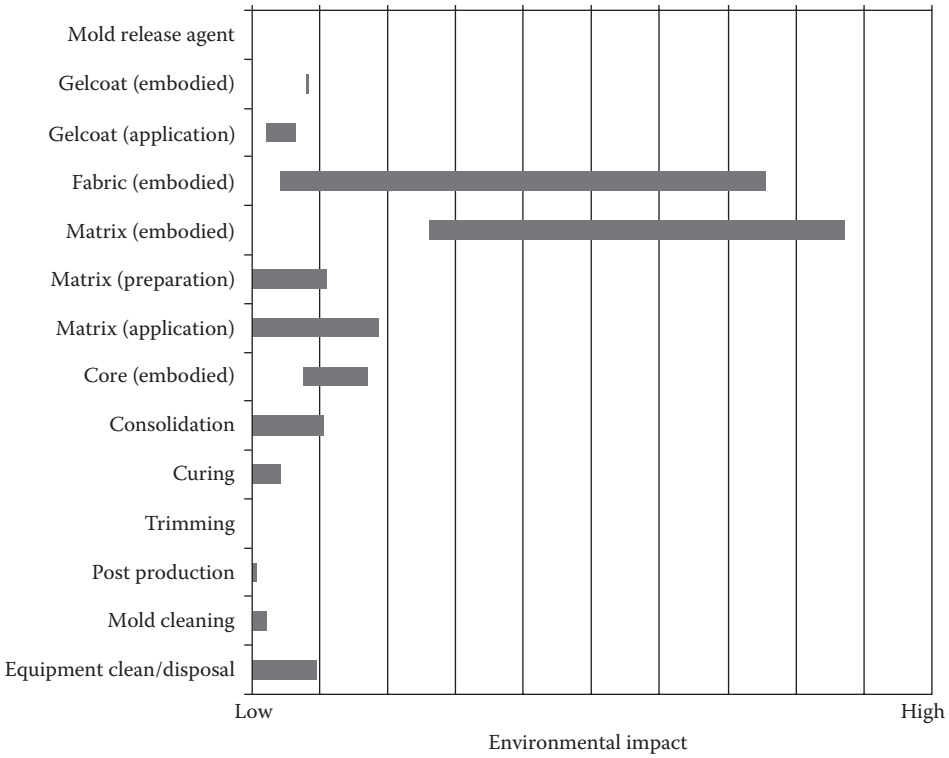

FIGURE 6.4 Range of environmental impact of composite production phases. (From Anderson, J. et al., *Green Guide to Composites: An Environmental Profiling System for Composite Materials and Products*, BRE Bookshop, Hertfordshire, U.K., 2004.)

and can result in various forms of emissions to air, land, and water. Each stage of the manufacturing process has an environmental impact that contributes to the total impact of the composite component; there are multiple options in each manufacturing stage that results in varying magnitude and range of environmental impact (Anderson et al., 2004). Figure 6.4 provides a qualitative chart illustrating the varying magnitude and range of environmental impacts for each step in the manufacturing process.

While Figures 6.3 and 6.4 provide a qualitative guide to material selection for composite materials from a life cycle context, the need exists for quantitative analyses regarding input resources and emissions for all materials for a given product in order to maximize the sustainability of civil infrastructure components and systems. Some researchers have initiated the process of comparing the economic, environmental, and social costs of constructing civil infrastructure systems using FRP composites versus conventional materials such as steel and concrete (Daniel and Nagtegaal, 2001; Halliwell, 2010). For instance, Daniel and Nagtegaal (2001) compared initial construction costs, maintenance costs, embodied energy, and environmental impact for the replacement of a corroded steel pedestrian bridge. Five materials (structural steel, stainless steel, glass FRP composites, aluminum, and concrete) were analyzed and compared to find the material that offered the most sustainable solution. It was found that for combined initial construction and maintenance costs, structural steel was the least expensive followed by FRP composites, aluminum, and stainless steel. In terms of embodied energy, the FRP composite consumed the least amount of energy at 120,000 MJ, while all other material options consumed at least twice as much. The FRP composite was also found to have the least environmental impact in terms of emissions to air and water.

The study by Daniel and Nagtegaal (2001) substantiates the competitiveness of FRP composites in a specific application compared to traditional materials. In general, materials that compete with composites are more susceptible to degradation, which can lead to more maintenance or the need for frequent material replacement. This clearly indicates that composites have a lower adverse impact on the environment compared to their competitors, since they require less energy due to a lower need for replacement. FRP bridge decks, for example, have three times greater service life, on average, than that of concrete (Hollaway, 2010). Therefore, less waste is generated from FRP composites because replacement is necessary after a longer duration of time.

The lower density of FRP composites helps facilitate installation by minimizing the need for heavy equipment. In addition, FRP composite components for structural systems are manufactured in factories as opposed to cast-in-place. This allows for the quality of the composite to be monitored, unpleasant weather to be avoided, and use of light lifting cranes. Other benefits of heavy equipment not being required are that much energy, time, and costs are saved (Hollaway, 2010). Less labor (included in cost) and traffic control are needed than for using competitor materials. Also, fewer emissions are released to the environment because the equipment will be used for shorter durations, if used at all.

LIFE CYCLE COST ANALYSIS

We can define LCC as the total costs (including direct and indirect costs) of a system or component from cradle to grave. The time period from cradle to grave is defined as the life cycle of the system or component. For cost comparisons, the life cycle can be assumed to be the period of time over which the investment in the system/component is evaluated as compared to a comparable alternative. In this context, a key aspect of the LCC analysis is determining the financial performance of the competing systems in order to rank the different alternatives. The different competing systems will have different streams of costs and benefits over a set time horizon, which when monetized can be expressed as cash flows. In order to compare and rank different systems that may be proposed for a project, the concept of the net present value is useful. To be able to perform a net present-value analysis, any future costs or revenues must be discounted to their present value, which requires consideration of the time value of money. There are a number of reasons why money will be less valuable in the future, versus today, particularly, opportunity cost, inflation, and risks. To account for these factors and adjust the value of money over time, we usually use the discount rate, which is the fraction (in percent) of the reduction of future cash flows (costs and revenues) at present value. Therefore, the discount rate can be used to precisely relate the future value of a cash flow to its present value as follows:

$$C_{PV} = \frac{C_{CP}}{(1+r)^n}$$

where

C_{PV} is the cost discounted to present value
C_{CP} is cost at current price
n is the time period in years
$(1 + r)^{-n}$ is known as the discount factor
r is the discount rate (Biondini and Frangopol, 2008)

The choice of discount rate is the most important factor in LCC analysis of projects with large initial investments where benefits are achieved over a long period of time. The relationship between C_{PV} and C_{CP} yields exponentially diminishing returns as the discount rate or the period increases. That is, the present value for a given future value decreases exponentially with discount rate, period, or both.

The discount rate is also used to quantify the actual return on the investment of anything that can be monetized and depends on the time horizon of a particular investor. In this context, the discount rate is considered the minimum acceptable rate of return (MARR). Therefore, an entrepreneur will only invest in a project if its MARR is attractive compared to other potential investments. For instance, government agencies typically invest in projects that are not expected to have a large return on the investment over any specific time period but rather provide a benefit to the public they serve. Private investors on the other hand expect a significant return on their investment over relatively short periods of time because of the large number of competing investment ventures available, some of which can yield very large returns over very short periods of time. For both groups, there are four key dates of the life cycle, the baseline date (beginning of the investment), the service date (beginning of operation), the maintenance date (date of major reinvestment to keep the system at an acceptable performance level), and the end date (end of investment period at which point the system is replaced and the cycle must be restarted).

For investments by government agencies, the discount rate may be defined as the difference between the rate of return on a risk-free investment (such as the interest rate on 1 year Treasury bills) and the inflation rate (Chen and Lui, 2005). An analysis provided in Chen and Lui (2005) uses historical discount rates from years 1962 to 2002, with an average discount rate of 2.1%. Other publications quote values 5%–10% (Martland, 2012). For a more detailed discussion of discount rate and life cycle analysis, see Martland (2012).

LCC analyses are used to evaluate the economic performance of different options, which can be assessed based on total cost of different construction, inspection, maintenance repair, and rehabilitation expenditures that are incurred at different points in time, along with any revenue over the same period of time. The present-value LCC (C_{PVLC}) can be used to compare the alternatives over a given life cycle (N) over which different expenditures (C_i) are incurred at different points in time (t_1, t_2, t_3, … t_i), assuming a constant discount rate (r). The relationship that gives C_{PVLC} is (Hawk, 2003)

$$C_{PVLC} = C_0 + \sum_{t_i=1}^{N} \frac{C_i(t_i)}{(1+r)^{t_i}} - \frac{R_v}{(1+r)^N}$$

where

C_0 is the initial construction cost (including design costs)
$C_i(t_i)$ is the ith expenditure at time t_i (inspection, maintenance, repair, demolition, and disposal costs)
r is the discount rate
N is the life cycle
R_v is the residual (or salvage) value at the end of the life cycle

In competing cases where the service lives are of different periods, the life cycle for analysis purpose should be taken over a common period, either the longest service life or a common multiple of the two service lives. That is, in the first case, the shortest service life system is assumed to be replaced with a similar system at the end of its service life. In all cases, there is a residual (salvage) value for some components that are taken as negative value in LCC calculations.

For a detailed comparison of LCCs to evaluate the economic feasibility of an FRP bridge deck compared to a steel-reinforced concrete (SRC) bridge deck, see Kawahara et al. (2012). The study is focused on short-span bridges with a total span less than 10 m, which make up over half of all bridges in the United States. The FRP bridge deck consists of four self-supporting FRP honeycomb sandwich panels. Though the comparison is made for the deck only (the supports and foundations are assumed to be identical), the lighter FRP composite deck would require a smaller foundation, leading to a lower cost than that for the SRC deck.

SUMMARY

In this chapter, the sustainability concept was introduced with an emphasis on the factors that are critical in understanding the role that FRP composites can have in a sustainable built environment. The assessment for material selection for new designs or rehabilitation requires examining the LCCs of an engineered system that considers performance, economic, environmental, and social factors.

An overview of the environmental implications of FRP composites was also provided in this chapter with respect to constituent materials and production processes for composites. While it was noted in this chapter that evidence exists showing FRP composite systems to have minimal emissions to air and water versus conventional materials, the high heats of production for fibers, the use of materials derived from crude oil, and human health factors will call into question the viability of FRP composites as a sustainable alternative. The widespread adoption and integration of FRP composites in sustainable infrastructure is predicated on evaluating materials and systems based on resource use, environmental impact, public health, sustainable design, and performance throughout their life cycle. Currently, there are numerous studies in literature regarding the structural feasibility of composite materials in civil infrastructure; however, the need exists for extensive quantitative research on the economic, environmental, and social feasibility of these materials from the perspective of a life cycle approach.

REFERENCES

Abdel-Magid, B., Ziaee, S., Gass, K., and Schneider, M. (2005). The combined effects of load, moisture and temperature on the properties of E-glass/epoxy composites. *Composite Structures*, 71(3–4), 320–326.

Anderson, J., Jansz, A., Steele, K., Thistlethwaite, P., Bishop, G., and Black, A. (2004). *Green Guide to Composites: An Environmental Profiling System for Composite Materials and Products*. Hertfordshire, U.K.: BRE Bookshop.

Astrom, B. T. (1997). *Manufacturing of Polymer Composites*. New York: Chapman & Hall.

Bank, L. C. (2006). *Composites for Construction: Structural Design with FRP Materials*. Hoboken, NJ: John Wiley & Sons, Inc.

Biondini, F. and Frangopol, D. M. (2008). *Life-Cycle Civil Engineering*. Boca Raton, FL: CRC Press.

Chen, W. and Lui, E. M. (2005). *Handbook of Structural Engineering*, 2nd Edn. Boca Raton, FL: CRC Press.

Daniel, R. A. and Nagtegaal, G. (2001). Pedestrian bridge of pultruded sections as result of ecological design. *Proceedings of the EPTA Seminar*, Roermond, Holland, October, pp. 42–44.

Gerdeen, J. C., Lord, H. W., and Rorrer, R. A. L. (2006). *Engineering Design with Polymers and Composites*. Boca Raton, FL: CRC Press.

Halliwell, S. (2010). FRPs—The environmental agenda. *Advances in Structural Engineering*, 13(5), 783–791.

Hawk, H. (2003). Bridge life-cycle cost analysis. NCHRP Report 483, Transportation Research Board, Washington, DC.

Hollaway, L. C. (2010). A review of the present and future utilization of FRP composites in the civil infrastructure with reference to their important in-service properties. *Construction and Building Materials*, 24, 2419–2445.

Joshi, S. V., Drzal, L. T., Mohanty, A. K., and Arora, S. (2004). Are natural fiber composites environmentally superior to glass fiber. *Composites: Part A*, 35, 371–376.

Kawahara, B., Estrada, H., and Lee, L. S. (2012). Life-cycle cost comparison for steel reinforced concrete and fiber reinforced polymer bridge decks, in *Fiber Reinforced Polymer (FRP) Composites for Infrastructure Applications: Focusing on Innovation, Technology Implementation and Sustainability*, R. Jain and L. Lee (eds.), Dordrecht, the Netherlands: Springer, pp. 237–273.

Kendall, A. (2004). A dynamic life cycle assessment tool for comparing bridge deck designs. Center for Sustainable Systems, University of Michigan, Report No. CSS04–12. http://css.snre.umich.edu/css_doc/CSS04–12.pdf, accessed February 2, 2011.

Martland, C. D. (2012). *Toward more Sustainable Infrastructure: Project Evaluation for Planners and Engineers*. Hoboken, NJ: John Wiley & Sons, Inc.

Mu, B., Wu, H., Yan, A., Warnemuende, K., Fu, G., Gibson, R. F., and Kim, D. (2006). FEA of complex bridge system with FRP composite deck. *Journal of Composites for Construction*, 10, 79–86.

Nelson, J. L. (2005). Behavior of GFRP bridge decks for highway bridges. MS thesis, Civil Engineering, North Carolina State University, Raleigh, NC, September 2005.

van Oss, H. G. (2010). Cement, in *United States Geological Survey 2010 Minerals Yearbook*, US Department of the Interior, US Geological Survey. Retrieved from http://minerals.usgs.gov/minerals/pubs/commodity/cement/myb1-2010-cemen.pdf, accessed April 18, 2013.

Telang, N. M., Dumlao, C., Mehrabi, A. B., Ciolko, A. T., and Gutierrez, J. (2006). Field inspection of in-service FRP bridge decks. National Cooperative Highway Research Program (NCHRP). Transportation Research Board, http://onlinepubs.trb.org/onlinepubs/nchrp/nchrp_rpt_564.pdf, accessed June 12, 2010.

Woodward, D. G. (1997). Life cycle costing—Theory, information acquisition and application. *International Journal of Project Management*, 15(6), 335–344.

World Commission on Environment and Development. (1987). *Our Common Future*. Oxford, U.K.: Oxford University Press.

Part II

All-Composite Structures and Components

Aixi Zhou and Lijuan "Dawn" Cheng

7 Materials and Manufacturing

Clem Hiel

CONTENTS

MATERIALS

Between 2002 and 2007, the price for steel rose 200% and the price for aluminum increased 187%. These cost trends had driven equipment prices up by 60%–90% during that time period. This upward cost trend may stabilize, but with the volatility of the world oil prices, it will definitely continue to fluctuate.

These dynamic market forces have altered the existing market segmentation in the composites industry and have created new and favorable conditions for all composite structures and components. This section will provide a basic background on materials, on the main manufacturing processes for thermoset materials, and it will give a bird's-eye overview of thermoplastic manufacturing processes.

Example 7.1

A rectangular strip with dimensions 101 × 4.82 × 500 mm (4 in. × 0.19 in. × 19.7 in.) needs to be manufactured of E-glass fiber and vinylester resin.

An important element, as seen from a manufacturing point of view, is whether 2 or 20,000 of these components are needed. This will be discussed in the "Manufacturing Processes" section, which specifically deals with composite manufacturing.

Although a rectangular strip is an example of a greatly simplified component, this example serves to bring out the profound differences between designing and manufacturing composites as opposed to their metal counterparts with which most engineers are more familiar.

Figure 7.1a shows a shop drawing of a desired 101 × 4.82 mm (4 in. × 0.19 in.) rectangular section in steel, whereas Figure 7.1b shows the drawing of that same part, with the same dimensions, but this time for fabrication in E-glass fiber and vinylester resin.

Material legend

Mat. type	Orientation	Composition weight % orientation	Weight		Information (vender/style)
			(g/m^2)	(oz/yd^2)	
A	Veil/mat	100	308	13.1	Reemay 2014/1 oz/ft^2 mat
B	Mat	Continuous	305	9.0	1 oz/FT2 mat
C	0	100	?	13.0	A130/
D	Woven(0/90)	50/50	?	26.63	WR18 7×5 or E-LT 1808–7

Note:

2014 Reemay thickness = 0.005*
A130A thickness = 0.014*
WR18 thickness = 0.019*
1 0z/FT2 Mat thickness = 0.022*
E-LTM 1808–7 thickness = 0.036*

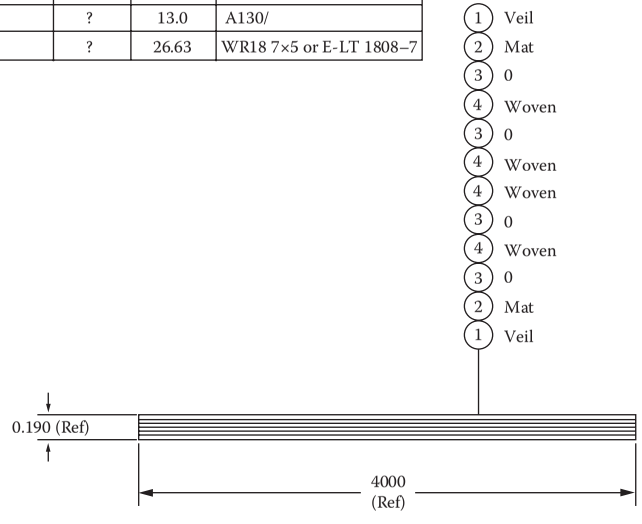

(a) Test sample (upstream view)

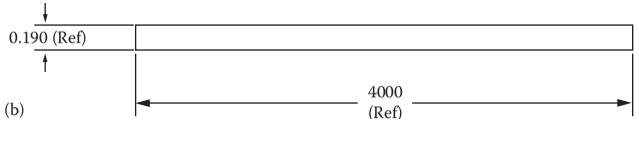

Resin information
Resin manufacturer: dow
Name: Derakane momentum 640–900 (vinylester)

Ply schedule legend

Ply#	Mat. task	Qty.	Mat.type	Orientation	Net width (n.)	Slited mat. neck down factor
1		2	A	Veil	4.0	4.08
2		2	B	Mat	4.0	4.08
3		4	C	0	4.0	4.08
4		4	D	Woven	4.0	4.08

Ply#	Qty.	Mat. type	Area (ln^2)	Number of ends		
				113 yield	250 yield	110 yield (EP620 [bulked])

FIGURE 7.1 Shop drawing for (a) a desired rectangular section in steel and (b) a rectangular composite section. (Courtesy of CSSI, San Pedro, CA.)

It should be noted that E-glass fiber-reinforced resins are expected to be at best one-quarter of the stiffness of equal-size aluminum and barely one-tenth as stiff as equal-size steel parts. For this reason, the industry will use many other fibers such as S-glass, HM-carbon and HS-carbon, and Kevlar. The use of these other fibers and possibly of other resins does not change the fundamentals of the underlying discussion.

It is striking that the shop drawing for the metal part is very simple since it only needs to give the dimensions, the tolerances, the surface roughness, the steel alloy, and the number of parts that are needed. Once this drawing is released to manufacturing, the raw material bar stock can be purchased from a supplier, and the strips can be cut and/or machined to the right dimensions and surface roughness requirements.

The drawing shown in Figure 7.1b is strikingly more complex. Not only are the dimensions and their tolerances specified but also the details of a dozen fiber-reinforced layers of different kinds that make up the cross section. In other words, whereas for the steel part, the designer only needs to specify the steel alloy, for the composite, he or she also needs to design and build the material itself on the basis of a designer-selected number of plies of various types. These ply types are determined by the type of loading the part is being designed for, and this suggests an integrated design approach of the ply-level materials for the load conditions at hand. Since the materials bloc in Figure 7.1b is too small for this level of details, it is provided in tables, which are positioned on the main body of the drawing.

Figure 7.2 is an enlargement of the rectangular composite strip for which the designer has chosen 12 layers of 4 different types of material (1 = surfacing veil, 2 = mat, 3 = 0° roving, 4 = woven fabric).

Each material has a fiber type (i.e., glass fiber, carbon fiber, Kevlar) and a thickness, expressed in grams per square meter or ounces per square yard. Additionally, a glass fiber orientation is specified as explained later.

Good handbooks to assist the designers in selection of fibers and fabrics are provided by the suppliers [1,2].

Material #1 shown in Figure 7.3a is identified in the composites industry as a surfacing veil.

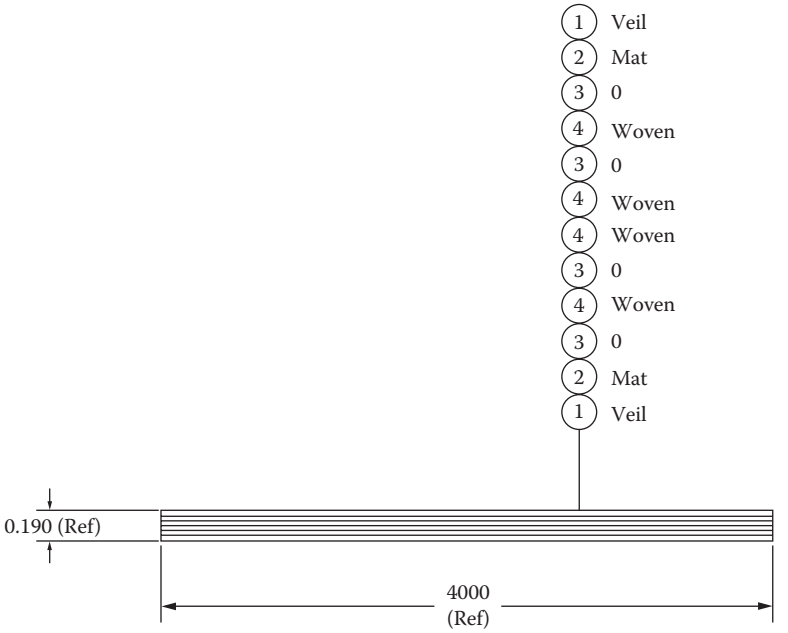

FIGURE 7.2 Twelve individual glass fiber layers identified. (Courtesy of CSSI, San Pedro, CA.)

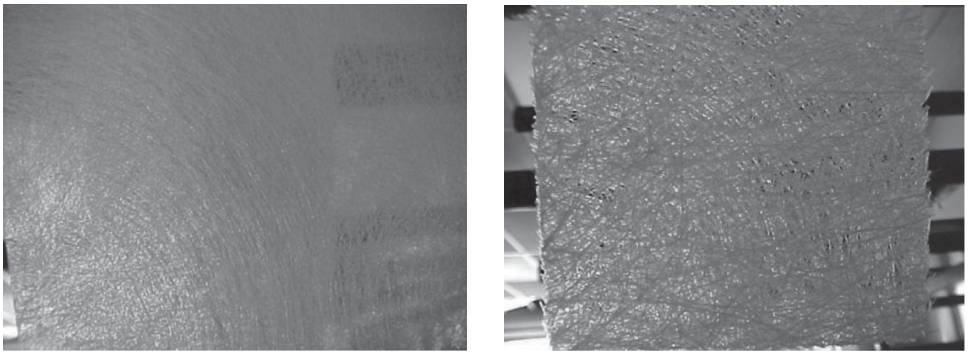

(a) (b)

FIGURE 7.3 Materials #1 and #2. (a) Material #1 = surfacing veil and (b) material #2 = continuous strand mat. (Photo courtesy of Dr. Clem Hiel, CSSI, San Pedro, CA.)

One will note from the laminate identification in Figure 7.2 that this veil is only used for the top and bottom surface of the strip. The function of the veil is to provide a smooth surface appearance and prevent print-through of the underlying layers. The veil is rich in resin, which is the key to its texture blocking capability. In other applications, the designers may elect to use a gel coat in order to create a desired smooth surface appearance.

Material #2, shown in Figure 7.3b, is called a "continuous strand mat," which means that the fibers are randomly swirling in the plane but do not have a preferential direction. It is common practice to use this layer either next to a layer of veil or next to a gel coat layer. Similar material exists in the form of chopped strand mats. This material consists of fibers that are chopped into short lengths and held together with a resin-soluble binder. The saturation of the mat with resin dissolves the binder and allows the mat to conform to tight curvatures and other specific mold details.

Material #3 is unidirectional (UD) glass fiber roving, as shown in Figure 7.4a. The transverse (horizontal) glass threads that are shown function to keep the UD material together.

It is these UD tows that form the "muscle" of the laminated strip. Figure 7.4 also shows that one cannot look through the layer because it is dense with UD tows.

Material #4 is bidirectional also called woven, as shown in Figure 7.4b. This ply is also not transparent because it contains a heavy 2D distribution of fibers.

In many instances, one will use a layer of mat to separate each of the layers of woven fabric and UD material.

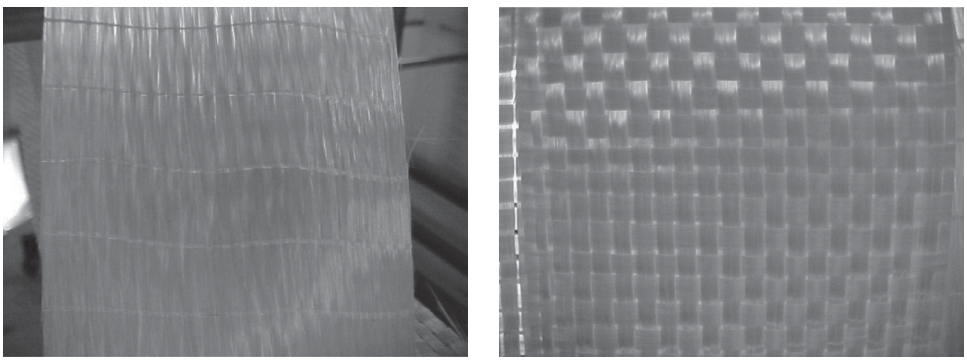

(a) (b)

FIGURE 7.4 Materials #3 and #4. (a) Material #3 = UD roving and (b) material #4 = fabric. (Photo courtesy of Dr. Clem Hiel, CSSI, San Pedro, CA.)

TABLE 7.1
Individual Aerial Weights of Each of the 12 Layers

Ply#	Type	Mass (oz/yd²)	Mass (g/m²)	Fiber Density (g/cm³)	2.52	
1	Veil	1	34	Panel thickness	4.83	mm
2	Mat	9	305	Resin density	1.22	g/cm³
3	0	13	441			
4	Woven	26.63	903			
5	0	13	441			
6	Woven	26.63	903			
7	Woven	26.63	903			
8	0	13	441			
9	Woven	26.63	903			
10	0	13	441			
11	Mat	9	305			
12	Veil	1	34			
	Total	178.52	6053			
		Volume fraction	0.50			
		Mass fraction	0.67			
		Density composite	1.87			

Table 7.1 provides the overview of the individual weights of each of the 12 layers.

The table adds up all the weights of the individual plies to a total of 6053 g/m². This weight allows us to determine the volume fraction on the basis of the following formula:

$$V_f = \frac{\text{Total mass of fiber}}{1000\rho_f t}$$

where

ρ_f is the fiber density (g/cm³)

t is the laminate thickness (mm)

Thus,

$$V_f = \frac{6053}{1000(2.52)(0.19 \times 25.4)}$$

$$V_f = 0.50$$

The significance of a 50% volume fraction can be appreciated from the following approximate formula:

$$d = D\left(\frac{1}{2}\sqrt{\frac{\pi}{V_f}} - 1\right)$$

where

D is the fiber diameter

d is the distance between fibers

TABLE 7.2
Material Microstructure Details

Fiber diameter, D (μm)	22
Volume fraction, V_f	0.5
Distance, d (μm)	5.57

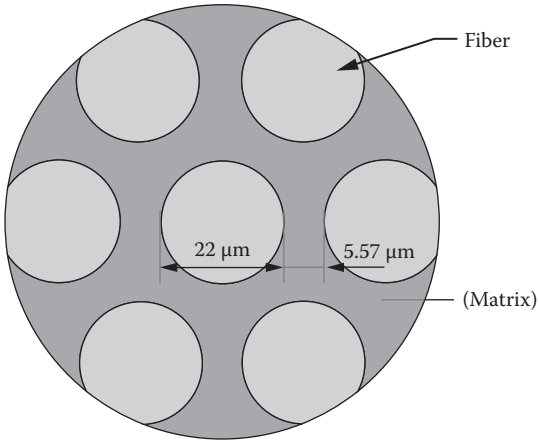

FIGURE 7.5 Material microstructure.

Table 7.2 indicates that the spacing between 22 μm fibers is only 5.57 μm for a volume fraction of 0.5.

This conclusion has formidable consequences for the manufacturing process as illustrated in Figure 7.5.

Shown is the cross-sectional configuration for the 50% volume fraction composite, which we looked at previously. This creates a fiber-to-fiber distance of no more than 5.57 μm. These are the dimensions between the fibers in which the polymer resin needs to be transported by using one of several manufacturing processes. This will not be done perfectly except in laboratory conditions. The degree of imperfection is measured by the void content in the microstructure.

The void content is a measure for how well the manufacturing process has accomplished this ideal goal. For aerospace parts, this is typically less than 1%, whereas for civil engineering construction, it is desirable to be less than 5%.

The matrix material selected was a vinylester with a density of 1.22 g/cm^3. The mass fraction of fibers can be obtained as follows:

$$m_f = \frac{V_f \rho_f}{\rho_r + V_f(\rho_f - \rho_r)}$$

where ρ_r is the resin density (g/cm^3)
Thus,

$$m_f = \frac{0.50(2.52)}{1.22 + 0.50(2.52 - 1.22)}$$

$$m_f = 0.67$$

The density of the laminate is given by the following formula:

$$\rho_{comp} = \rho_f V_f + \rho_r (1 - V_f)$$

$$\rho_{comp} = 2.52(0.50) + 1.22(1 - 0.50)$$

$$\rho_{comp} = 1.88\ (\text{g/cm}^3)$$

The density of the composite laminate is thus only one-fourth of the density of steel!

An interesting picture emerges if we estimate the number of fibers that is actually aligned with the load and as such is determined. For the case of the tensile strip from Figure 7.1, the number of fibers that participates in carrying the load is found by the following formula:

$$N = \frac{4V_f t_0 w}{\pi D^2}$$

$$V_f = 0.5$$

$$t_0 = 2.79 \times 10^{-3}\ \text{m}$$

$$w = 101.6 \times 10^{-3}\ \text{m}$$

$$D = 22 \times 10^{-6}\ \text{m}$$

$$N = \frac{4(0.5)(2.79 \times 10^{-3})(101.6 \times 10^{-3})}{\pi(22 \times 10^{-6})^2}$$

$$N = 372{,}850$$

$$\text{For } D = 10 \times 10^{-6}\ \text{m}$$

$$N = 1{,}804{,}590$$

This simple exercise indicates that sizable structural engineering members may easily have billions of fibers contained in their cross section. The manufacturing challenge is to manage the process of starting from dry fibers and create a fully cured fiber-reinforced cross section, with all the fibers pointing in the right direction and being fully supported and surrounded by resin with no or virtually no voids to interrupt this support.

A first estimate of the tensile strength of the laminate is given by the following formula:

$$\sigma_{tc} = \sigma_f V_f k + \sigma_r (1 - V_f k)$$

$$\sigma_{tc} = 115(0.50)(0.58)$$

$$\sigma_{tc} = 34\ (\text{kg/mm}^2) \text{ or } 340\ \text{MPa}$$

where

σ_f is the fiber tension strength

k is the fraction of zero degree fibers parallel to applied load (=58%)

σ_r is the resin tension strength (neglecting the second term)

In comparison the tensile strength of steel would be 551 MPa. Therefore, a tensile member with twice the cross section of steel would weigh only half as much and carry 123% of the load that steel would be able to carry.

The following problem provides a more formal way for the designer in trading of weight and cost.

PROBLEM 7.1

The glass fiber/vinylester tensile structural member needs to support a failure load of 166,710 N over a length of 0.5 m, as illustrated in Figure 7.6.

The material purchase cost of the glass fiber composite is $2.5/kg. What is the mass required to use glass fiber composite for this application, and what is the cost?
The formula for the mass is

$$\text{mass} = \text{Load} \cdot \text{Length} \frac{\rho_{comp}}{\sigma_{comp}}$$

$$\text{mass} = 166,710(0.5) \frac{1.88}{340}$$

$$\text{mass} = 0.46\,\text{kg}$$

The cost of the support member is

$$\text{Cost} = 0.46\ \text{kg} \frac{\$2.50}{\text{kg}} = \$1.52$$

The cross section would be 490 mm^2 (0.15 in. × 4 in.), which is exactly the size of the sample that is shown in Figure 7.1b. Figure 7.7 shows that part weighing out at about 460 g.

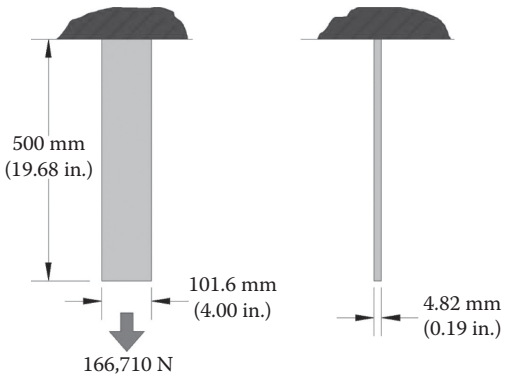

FIGURE 7.6 Glass fiber/vinylester tensile member subject to 166,710 N.

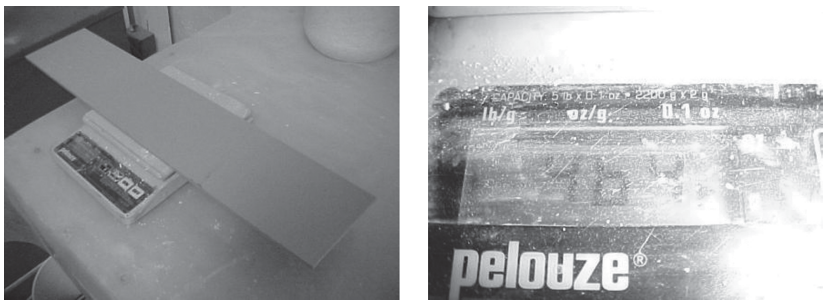

(a) (b)

FIGURE 7.7 Glass fiber/Vinylester strip of Figure 7.6 (a) placed on a precision balance and (b) readout of the weight (640 g). (Photo courtesy of Dr. Clem Hiel, CSSI, San Pedro, CA.)

As we calculated earlier, this cross section has 372,850 filaments, which are each 22 μm in diameter to help support the tensile load. The contact area between the resin and the filaments is obtained from the following formula:

$$A_{contact} = 4\frac{V_f}{D} wt_0 l$$

$$A_{contact} = 4\frac{0.5}{22\times10^{-6}}(101.6\times10^{-3})(2.79\times10^{-3})(0.5)$$

$$A_{contact} = 12.88\,\text{m}^2$$

$$\text{for } D = 10\times10^{-6}\,\text{m}$$

$$A_{contact} = 28.34\,\text{m}^2$$

This derivation indicates that as the fiber diameter decreases to 10 μm, the contact area between fibers and resin tends quickly to the square footage of a 40 ft shipping container (320 ft^2).

The same problem earlier when using galvanized construction steel would come out as follows:

$$\text{Mass} = 166,710(0.5)\frac{7.8}{551}$$

$$\text{Mass} = 1.18\,\text{kg}$$

$$\text{The cost of the support member is}$$

$$\text{Cost} = 1.18\,\text{kg}\frac{\$1.1}{\text{kg}} = \$1.30$$

The needed cross section is now only 302 mm^2. As shown in Figure 7.8, the galvanized steel member could have the same thickness, but the needed width would only be 62.5 mm (2.46 in.).

The mass of the composite is thus 41% (0.46/1.18 × 100) of the mass of steel. The designer is now in a position to trade-off mass against other performance properties such as fatigue life. A quick check

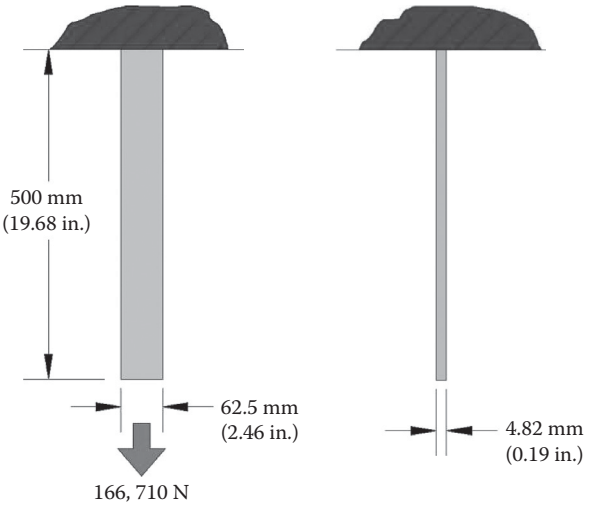

FIGURE 7.8 Steel tensile member subjected to a load of 166,710 N.

confirms that the composite part as drawn in Figure 7.6 does not have comparative fatigue life with the steel part drawn in Figure 7.8. However, when doubling the thickness of the composite strip, we still save 20% in weight relative to the steel strip, but the composite outperforms the steel by almost an order of magnitude in fatigue performance. This is shown in Figure 7.9 in which the relative scale, at which the tensile members are drawn, indicates the more bulky nature of the composite strength member.

In the design trends, compactness and greater load transmission opportunities are provided for more exotic fibers such as carbon and Kevlar fibers.

The fatigue performance is very much tied to the "sizing" of the fibers. The "sizing" means that a submicron thick layer on the fibers applied at the time they were manufactured. It determines the level of adhesion between the fibers and the resin. Over the years, as the sizing types were developed, the number of fatigue cycles went from tens of thousands to hundreds of thousands, and subsequently to millions. An interesting anecdote illustrates this aspect of composite part manufacturing. One company had bought

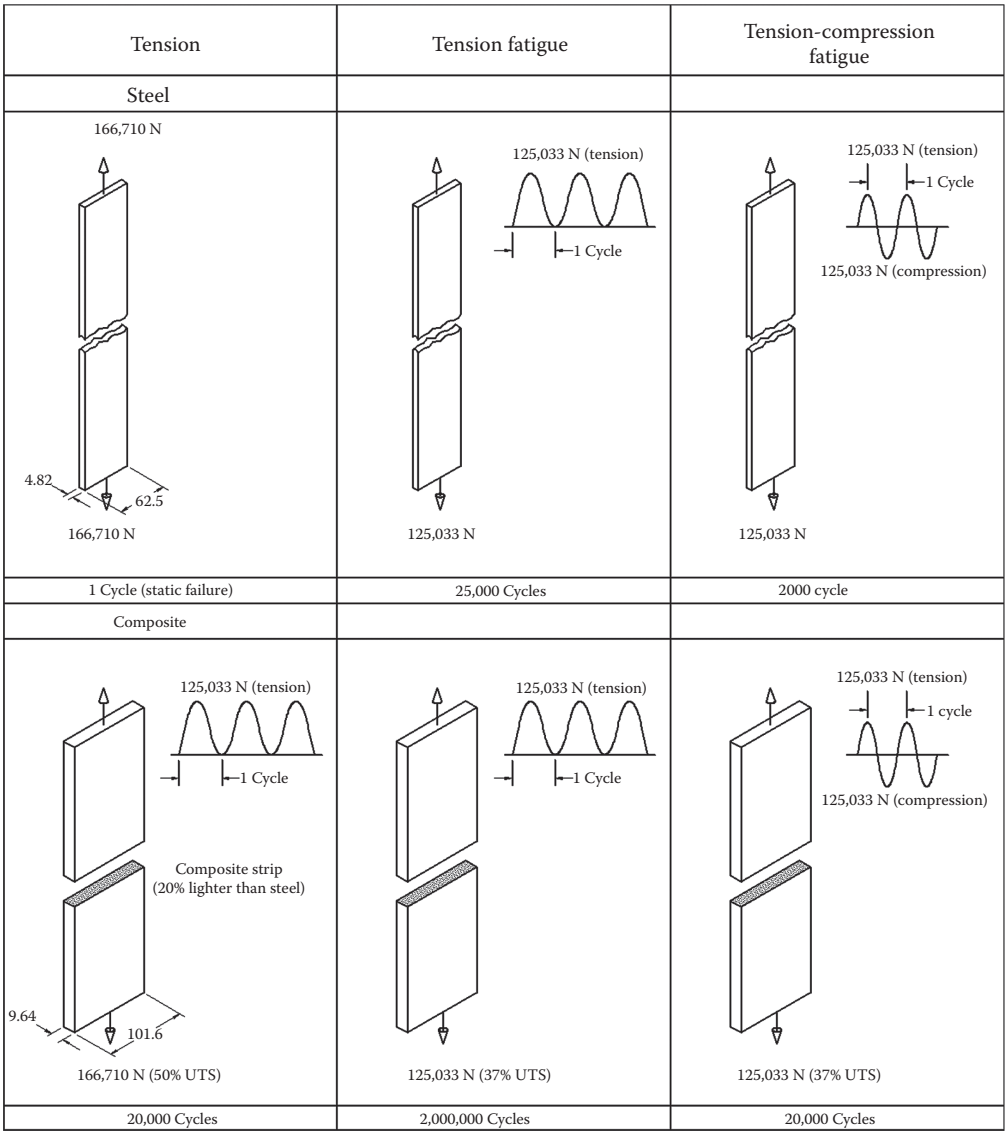

FIGURE 7.9 Fatigue performance illustrates a 20% lighter glass vinylester tensile member outperforming a steel member by almost and order of magnitude.

several hundred square feet of surplus glass fiber fabric at an auction. The fabric was old and had several dirty coal or grease-like spots on its surface. The new owner decided to "steam clean" the glass before using it in his production. By doing this, he unknowingly took off the fiberglass sizing, thereby building a finished part that had grossly inadequate performance when subject to moisture and fatigue.

The data in Figure 7.9 also explain the underlying reason for the replacement of metal helicopter rotor blades by fiberglass blades. The trade-off of weight versus fatigue performance becomes especially advantageous when replacing aluminum alloys, which do not have the benefit of the "Wohler plateau" that mild steel has.

Further weight reduction in combination with improved fatigue performance is obtained by designing with carbon fibers instead of glass fiber. The drawback of carbon fibers is, however, that they are 5–10 times as expensive as glass fiber despite the promise over the years that the cost would come down substantially.

The true design advantage of both glass fiber and carbon fiber composite materials is in integrated components and structures [3–6]. Figure 7.10 shows the example of a truss structure that has been built up from snap-together parts. Figure 7.10a shows a picture of a joint as it engages by utilizing the elasticity of the composite material. The term "structural" applies here because this connection is capable of carrying a 54,500 N tensile load.

Figure 7.10a also illustrates the steps in the engagement of the connection, which is very similar to nonstructural snap fits for plastics. Figure 7.10b shows the commercial pultruded electrical transmission tower application for which this connection was used. This early technology has already been successfully commercialized and continued development and improvement will lead to increasing technical and commercial viability.

The competitive advantage of this structural snap-fit technology over the traditional bolting and riveting is that the assembly takes only 15% of the time and that there are no assembly defects. The entire tower snaps together as a Lego set and is assembled in 20% of the time it takes to assemble a steel tower. In addition, the weight of the composite tower is only one-half of the weight of a steel tower.

Designers need to be well aware that the material properties of the polymer resins may have significant temperature dependence. This dependence is shown for the "workhorse" resins in Figure 7.11.

The corrosion industry, for example, makes extensive use of low styrene emission vinylester resins. Besides these resins, there are a number of higher-temperature and higher-performance resins available from which the designer could choose for specialty applications. These resins come at a higher purchase price and may add significant processing difficulties for the manufacturing engineer.

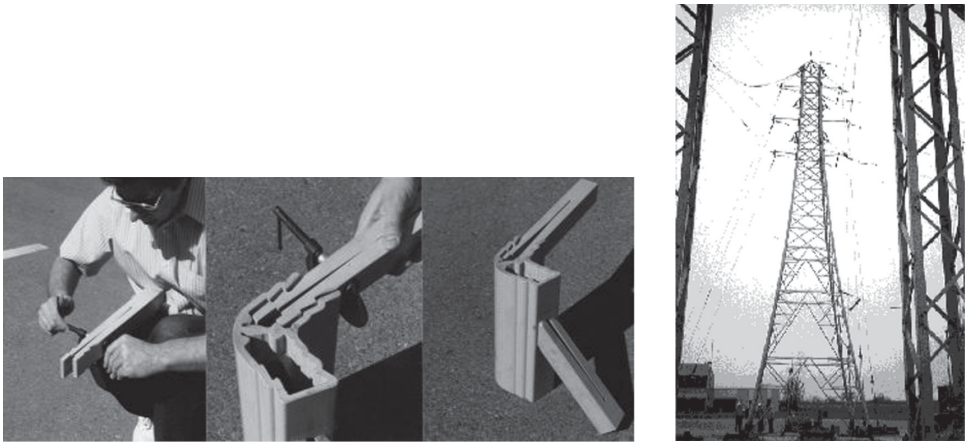

(a) (b)

FIGURE 7.10 "Structural snap-fit" connection. (a) Steps in the snap-fit engagement. (b) Commercial pultruded electrical transmission tower in which the "snap-fit" connection was used. (Photo courtesy of Dr. Clem Hiel, CSSI, San Pedro, CA.)

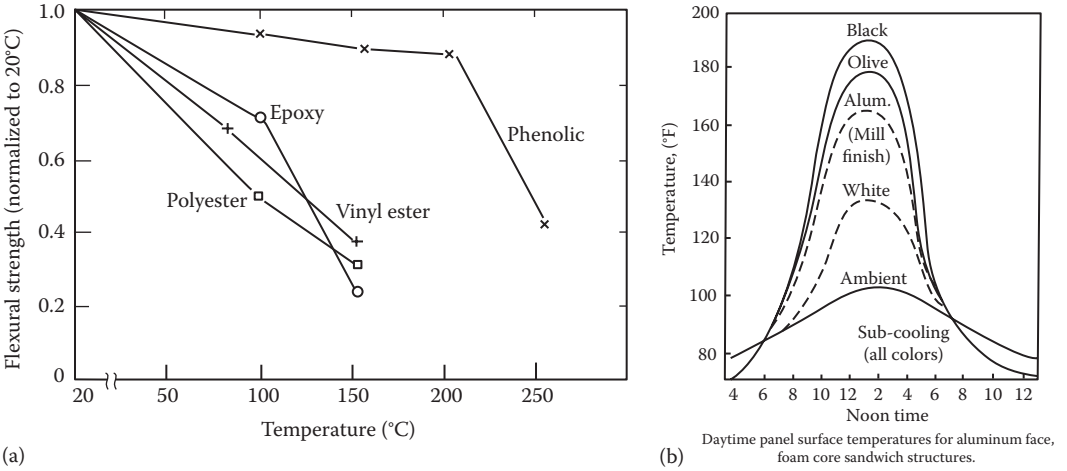

FIGURE 7.11 (a) Resin temperature limits. (b) Temperature rise of a surface exposed to an ambient solar exposure cycle. (Courtesy of Dow Chemical Co., Midland, MI.)

In manufacturing it is important that the cure characteristics of the resin be well understood. For example, certain resins can be applied at room temperature and they will then "cold cure" after a given amount of time. The time during which they can be worked is called the "pot life" of the resin. Once the pot life has been used up, the viscosity of the resin has increased to such an extent that it is no longer fit to create the micron size narrow spaces between the fibers.

MANUFACTURING PROCESSES

The section that follows reviews the manufacturing processes of composites in the following categories:

- Continuous reinforcement processes (pultrusion, filament winding, and braiding)
- Hand layup processes
- Molding processes (matched-die molding, vacuum bagging, autoclave molding)
- Resin injection processes (resin transfer molding, reaction injection molding)
- Processes for thermoplastic composites

Continuous Reinforcement Process

Pultrusion

If the number of strips that needed to be made was in the order of 20,000, then the pultrusion process would be a natural choice. The principles of pultrusion are outlined in Figures 7.12 through 7.16. The process is described in great detail in Refs. [7,8].

The first contributing innovations to the pultrusion process emerged in the late 1940s at one of the fabricators shop floor upon receiving an order for many thousands of feet of structural shape with constant cross section. Continued innovation in reinforcing materials, resins, machinery, and tooling has created the modern process that is described in the following.

Figure 7.12 shows 12 material supply spools, each of which contains 1 of the 4 materials, which we discussed earlier.

One notices that the various materials hang in a catenary shape as they come off the supply rolls and make their way toward the impregnation section and into the pultrusion die.

The next step in manufacturing of the rectangular strip is that the 12 layers of material need to be impregnated with a resin. The type of resin is also specified in the materials bloc. For most commercial applications, this is polyester, vinylester, or epoxy. The precise resin formulation needs to

FIGURE 7.12 Pultrusion infeed with 12 supply spools according to the drawing of Figure 7.1. (Photo courtesy of Dr. Clem Hiel, CSSI, San Pedro, CA.)

be specified in a separate process specification because a resin has curing agents, UV inhibitors, fillers, and other elements in precisely defined concentrations. Therefore, the design of the resin is a separate element in the definition of the manufacturing process.

Figure 7.13 is a view from the top of the impregnation tank as the 12 layers are moving through the tank.

As the individual plies come through the tank, they are wetted and make their way toward the entrance of the pultrusion die. As the plies enter the heated die, they are compressed, and the excess resin is squeezed out. As the laminate proceeds toward the middle of the die, it starts curing and develops an exotherm. Upon curing, the part experiences some thermal shrinkage and pull away from the pultrusion die prior to exiting.

Figure 7.14 shows the actual shape of this simple pultrusion die entrance.

Figure 7.15a through c shows the composite strip as it is exciting the mold.

Once the length of composite is enough, a set of hydraulic grippers take over and pull the material in an automated mode. The pull force for this configuration is about 1200 lb. Specifically Figure 7.16b shows a clear transition from dry glass fiber material to cured material. As the cured composite moves forward, equilibrium is established between the heat necessary to cure the material, and the heat transported out of the mold. Because the pultruded strip has been subject to the confinement of a die upon curing, it exits the pultrusion die with a smooth surface on both sides.

The pultrusion process can be utilized to fabricate components of many different shapes as is shown by the airfoils in aramid fiber (Kevlar) and glass fiber that are emerging from the die, as shown in Figure 7.16.

Pultrusion is basically a process for profiles with constant cross section. There are innovations and adaptations that have attempted to remove this obstacle, but they are not discussed in the realm of this basic description. More information can be found in Ref. [8].

Figure 7.17 shows a hollow pultruded part.

This part is produced by cantilevering two mandrels and depositing all the necessary plies on these mandrels. As the plies proceed, they are impregnated with resin.

The filament winding process that is described later also creates hollow shapes and also makes use of mandrels.

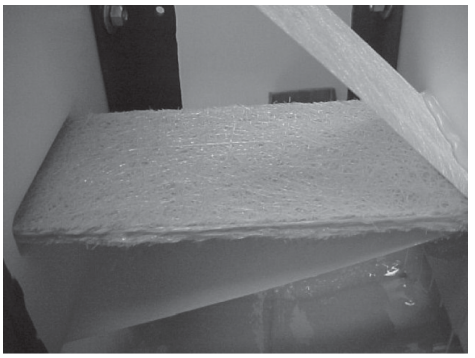

(a)

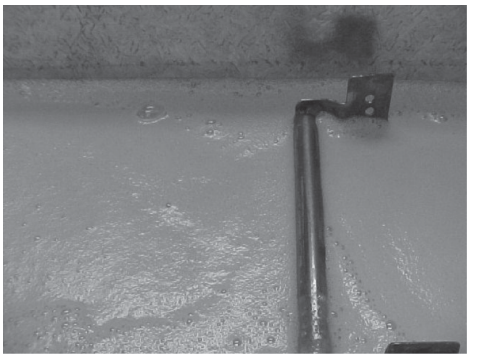

(b)

(c)

FIGURE 7.13 (a) Lamina moving between impregnation stations. (b) Top view of an impregnation station. (c) Final impregnation prior to entering the pultrusion die. (Photo courtesy of Dr. Clem Hiel, CSSI, San Pedro, CA.)

FIGURE 7.14 Cross section of a simple pultrusion die. (Photo courtesy of Dr. Clem Hiel, CSSI, San Pedro, CA.)

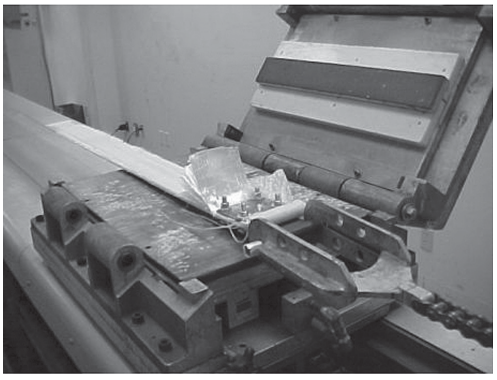

(a)

(b)

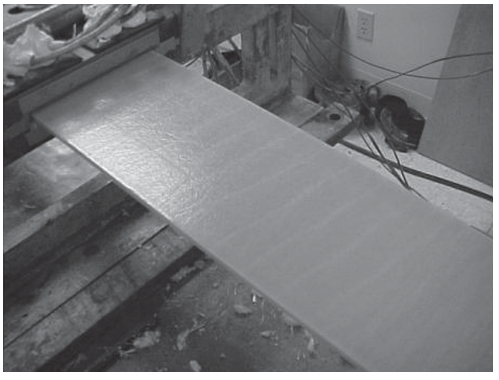

(c)

FIGURE 7.15 (a through c) Composite strip as it is exciting the mold at a rate of 4 ft/min. (Photo courtesy of Dr. Clem Hiel, CSSI, San Pedro, CA.)

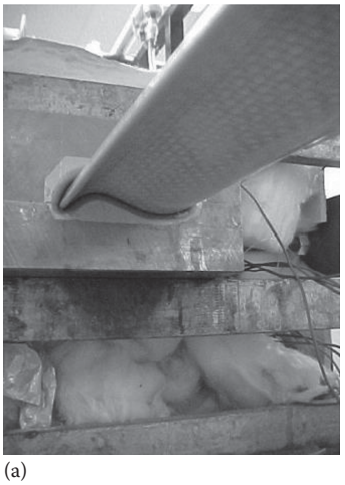

(a)

(b)

FIGURE 7.16 Airfoil parts in (a) Kevlar and (b) glass fiber. (Photo courtesy of Dr. Clem Hiel, CSSI, San Pedro, CA.)

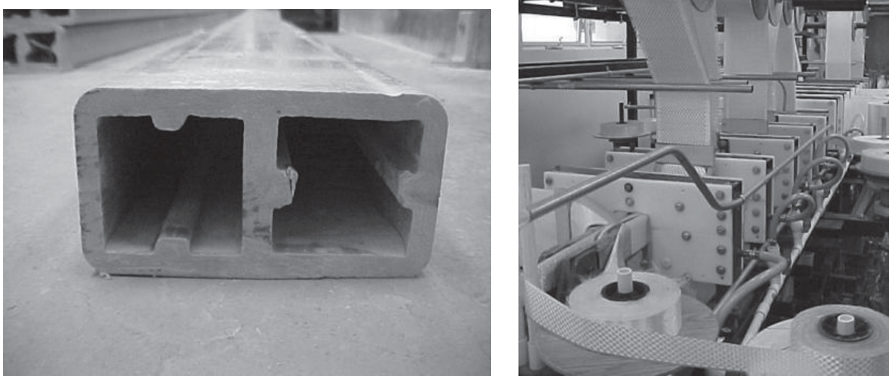

(a) (b)

FIGURE 7.17 (a) Hollow, as produced part. (b) Pultrusion setup to produce the part. (Photo courtesy of Dr. Clem Hiel, CSSI, San Pedro, CA.)

Filament Winding

This process is not a candidate for making rectangular strips but has proven to be very efficient for making hollow cylindrical parts with complex fiber architecture. The process is rapid and capable of laying down hundreds of pounds of composite material per hour. The filament winding process was patented in 1946 by R.E. Young [9,10]. This was part of larger patent umbrella in the development of rocket motors.

Since the late 1930s, gasoline was stored in metal tanks; nevertheless, in the late 1960s and 1970s, Owens Corning produced thousands of filament wound tanks for underground fuel storage and later sold the business to Fluid Containment Inc. of Conroe, Texas.

The principle of this process is illustrated in Figure 7.18.

The best analogy is that of a lathe in which the part that is normally machined is replaced with a rotating mandrel and the cutting tool has been replaced with a fiber delivery eye. It is actually a thin band of fibers that is dispensed onto the mandrel. The fibers either go through a resin bath, which is most common, or are dispensed dry and the resin is added later.

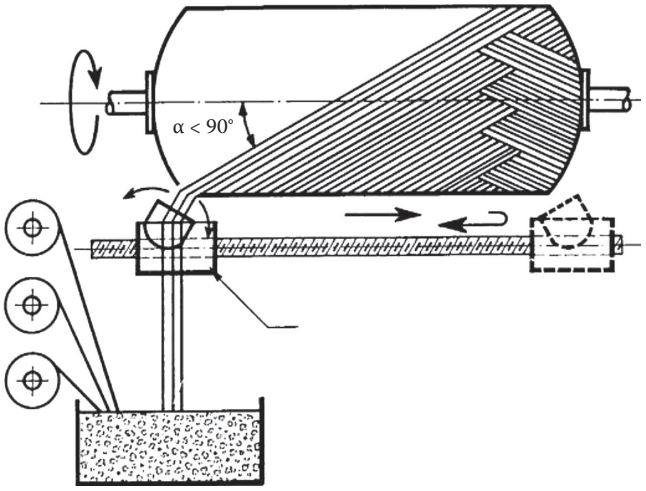

FIGURE 7.18 Principle of filament winding.

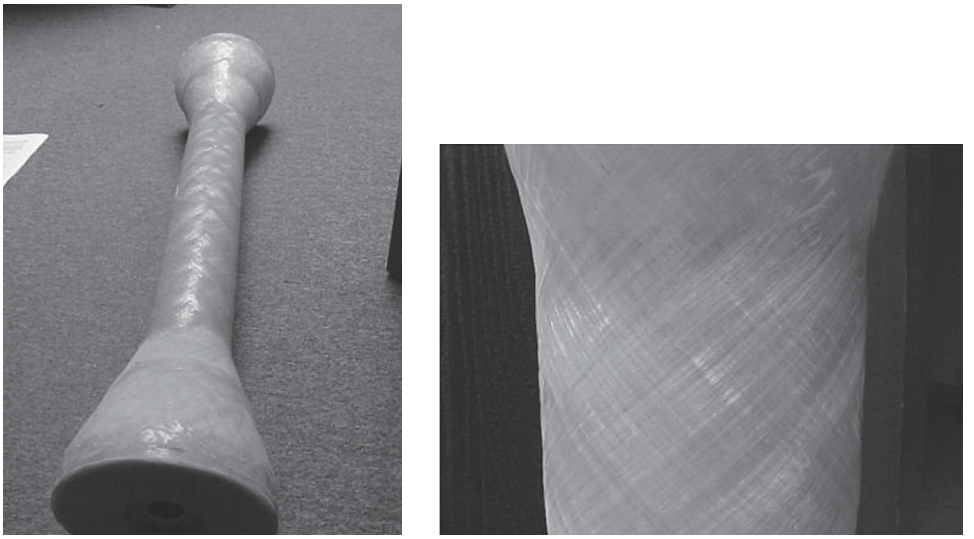

(a) (b)

FIGURE 7.19 (a) Filament wound part, with ropelike surface. (b) Close-up of the surface. (Photo courtesy of Dr. Clem Hiel, CSSI, San Pedro, CA.)

The resins that are used the most are epoxy, vinylester, and unsaturated polyester. Often "heavy" tows consisting of 50,000 individual filaments are used in order to strike a balance between product requirements and processing speed. In most instances, the outer surface of the wound part is left alone, and its smoothness is therefore dependent on the filament tow size that has been used. Larger tows create a ropelike appearance on the outside of the part, as shown in Figure 7.19.

Figure 7.20 is an example of a square filament wound part. Again the ropy surface is shown on this production part.

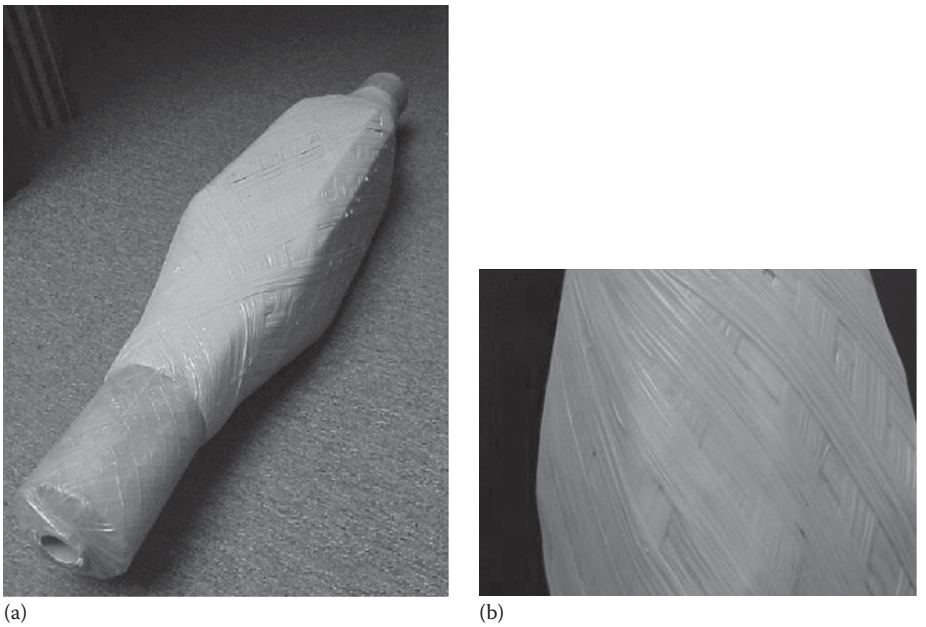

(a) (b)

FIGURE 7.20 (a) Square filament-wound part. (b) Close-up of the surface. (Photo courtesy of Dr. Clem Hiel, CSSI, San Pedro, CA.)

Hand Layup Process

Hand Laminating

Hand laminating is the oldest and cheapest technique available. It could be used if only a limited number of strips would need to be made. The dry plies are placed onto a mold surface one by one and impregnated with resin. This resin may be a "cold cure resin" or one that needs a heat cure cycle. Therefore, the resin-heating requirements will determine the mold and tooling materials that need to be used. In case of a "cold cure" resin, the molds are often made of wood or low from other "cold cure" materials. This allows the manufacturer to create relatively cheap molds with complex curvatures. The drawback of the molds is that they are only good for a limited number of parts and that depending on the complexity and materials used, they need almost continuous repair and maintenance after every molding cycle. The disadvantage of hand laminating is that it is an artisan type process. It is very difficult to train a variety of workers to fabricate a consistent and guaranteed high-performance product in the way this could be done with metal workers.

If the laminating resin needs to be cured at elevated temperature, then the molds need to be metal, high-temperature composites, concrete, ceramic, or other specialty molding materials.

The laminating process as described earlier only provides one smooth surface. If one needs two smooth surfaces, then the matched-die process needs to be employed as discussed later.

If a few hundred strips needed to be made, the most economical way would be to fabricate 4.82 mm (0.19 in.) thick and 1524 mm (60 in.) wide plates, which would later be cut in strips. Figure 7.21 shows what this process would look like.

The 1524 mm (60 in.) width is determined by the commercial width of the roles that are available for the 12 materials that were identified earlier.

Since we needed both sides of the strips smooth, one notices the matched-die press on the right-hand side in Figure 7.21. Since a heat cure resin is used, the platens of the press are capable of being heated at a programmed heating rate.

The dry reinforcements come off the rolls, which are placed at the left in Figure 7.21. As each layer is placed on top of the next, technicians roll in the liquid resin with a roller. As such, this is an open mold process, and the volatile organic compounds (VOCs) that come off the resin are inhaled by the technicians, which is not desirable. It is important that personnel protection be provided when using these processes. It is very important to put technicians through a training class in order to foster their personal hygiene and protection when working with organic resins.

The first step is to coat the mold with a release agent. This coat needs to be sufficient to keep the part from bonding to the mold or being damaged when taken out of the mold. It needs to be sufficiently thin to transfer mold details onto the part. For many elevated temperature applications,

(a)

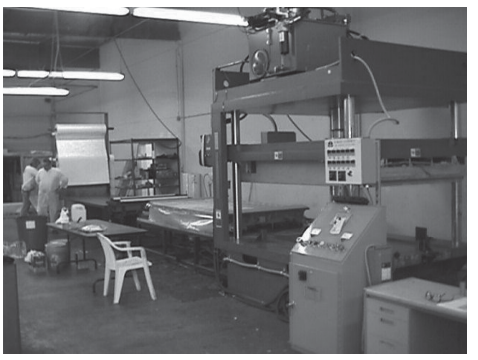

(b)

FIGURE 7.21 (a) Fabrication of panel. (b) Press and layup hardware used for panel fabrication. (Photo courtesy of Dr. Clem Hiel, CSSI, San Pedro, CA.)

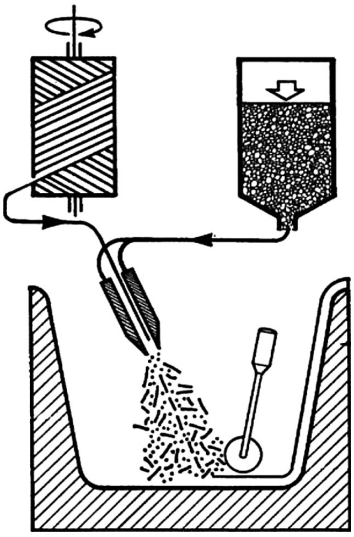

FIGURE 7.22 Spray-up.

the release agent is sprayed or brushed onto the mold and the mold is taken through an elevated temperature "baking" cycle, so that the release agent is "baked onto the mold." Depending on the mold complexity, the release agent will work for 15–50 parts. The design of molds is a specialty, which is too involved to review in the limited space available. Details can be found in Refs. [11,12].

Spray-Up

The basic setup of spray-up equipment is very similar throughout the composites industry. The principle of spray-up is shown in Figure 7.22.

The essential equipment includes

- Pumps for resin and pumps for pressure ports and catalyst
- Chopper gun
- Head for spray gun
- Air regulators, gages, hoses, possibly boom and dolly
- Solvents for flushing the system

Getting the exact glass-to-resin ratio each time is a question of technique and skill. There are best practices available for that industry. The one piece bathtub shower is a typical part that is made by spray-up.

The spray with binder-only approach is excellent for creating a preform. The binder is based on an epoxy or polyester formulation. The preform is then transferred to a closed mold, or a bag is pulled over the perform, to allow a liquid molding phase without the release of VOCs. The binder that was introduced is formulated so that it dissolves into actual resin and wets the material during the liquid molding phase.

A recent adaptation of the spray-up process is known as P4 technology. The spray equipment is mounted onto a computerized robot arm and a thermoplastic powder binder is used. Depending on the mold location that is spayed, the direction and the length of the fibers can be adapted. This process is being developed by the automotive industry, and a more recent adaptation P4A (A for aerospace) has been under development for aerospace use where the short fiber are carbon, rather than glass fiber. The fiber distribution on the mold is a preform that needs to be supplied with resin. This is done by resin transfer molding, which is especially easy because the pressurized resin pumped into the matched-die mold and the short fibers allow easy impregnation.

Molding Process

Matched-Die Molding

Figure 7.23 shows the matched dies as they are ready to close.

The tool used for this particular case is steel, but tools have been built in aluminum, concrete, polymer concrete, composite, and wood. Other tooling materials have been brought to market.

There are troubleshooting procedures available in every plant to adjust to when the molding does not come out correctly.

Once the layers have been impregnated one by one, the mold is moved into a press via a transfer system. This is the compression molding stage and the platens of the press put a predetermined pressure, which is typically 50–200 psi, and go through a heat cycle to cure the part. The advantage of the matched-die process is that the two sides of the part are fully finished. Additionally the compaction pressure squeezes out sufficient resin to reach volume fraction of 50%–60%.

Resin Transfer Molding

Resin transfer molding is a more general term for the technique of placing preformed laminates with long fibers into a matched-die mold and afterward injecting the resin. The resin viscosity is a very important parameter in this process. Once the injection is completed, the mold goes through a heat cycle, and the part cures and is demolded, cleaned up, and eventually further integrated with other parts. As in matched-die molding, both sides of the part will be smooth.

Vacuum Bagging

As discussed earlier, one can fabricate laminated components with high volume fraction by using only one mold half and a vacuum bag as schematically shown in Figure 7.24.

In this case, only the mold surface will be smooth.

The pressure created by the atmospheric air surrounding the vacuum bag pushes the plies together, and fiber volume fraction of 50% can readily be achieved.

This process has the advantage that the equipment costs are relatively low; as such, it is appropriate for low production runs. The work only requires semiskilled labor. A disadvantage is that

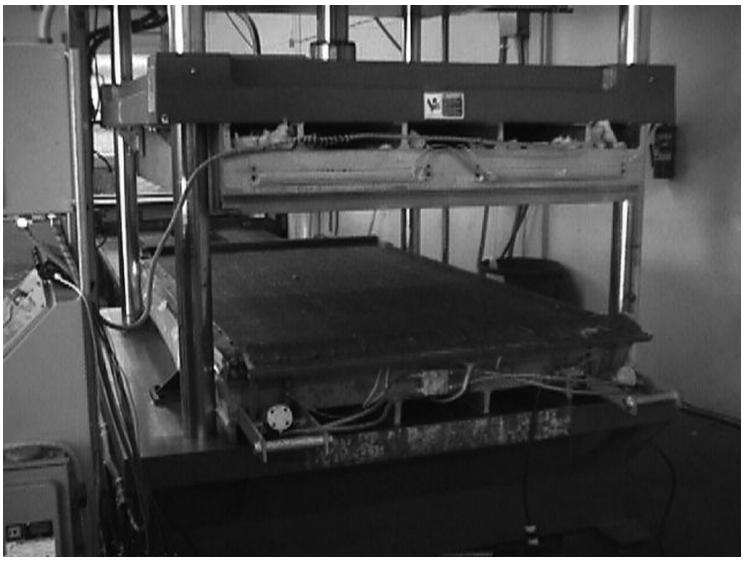

FIGURE 7.23 Contact molding and compression molding. (Photo courtesy of Dr. Clem Hiel, CSSI, San Pedro, CA.)

FIGURE 7.24 Vacuum bag placed over the finished layup. (Photo courtesy of Dr. Clem Hiel, CSSI, San Pedro, CA.)

the process involves a fair amount of waste. As the part comes out of the mold, it may need to be trimmed or be moved to another manufacturing phase for integration and assembly with other parts.

Compression molding can also be used for thermoplastic composites. With these materials it is possible to start out from a flat sheet that has been extruded and the matched die will make it conform. One application is the tailgate of a DaimlerChrysler minivan. An added difficulty in the automotive industry is that an A-class finish is required.

For a number of applications, one makes a "preform."

Vacuum Molding

A flexible sheet or bag is used to cover a single cavity mold that contains either the dry or the wet fiber layup. The edges of the flexible sheet are clamped against the mold to form an envelope and seal the member. A catalyzed liquid plastic resin is introduced into the envelope or bag interior to wet the fiber. A vacuum is applied to the bag interior via a vacuum line to collapse the flexible sheet against the fiber and surface of the mold, while the resin-wetted fiber is pressed and cured to form the fiber-reinforced structure. Resin fumes from the process are prevented from escaping into the ambient workspace.

A vacuum method where the resin is introduced into a preform requires a network of veins or arteries that are embedded between layers of fabric and become an integral part of the final product. Other techniques allow for the artery structure to be broken away from the finished part. The complexity of the part determines the number of resin supply points.

This technique provides a good "void-free" part.

Autoclave Molding

Industry has used autoclaves for the drying of wood and for bonding of wood aircraft components. As the composites aerospace industry emerged, it very quickly embraced the use of the autoclave as a means to provide pressure on a laminate. Many times, the industry uses simultaneous vacuum bagging to assure the possibility of void-free structures. Using an autoclave is a slow process, and it can only be justified for integrated designs in which one composite part replaces hundreds of metal components and thousands of rivets.

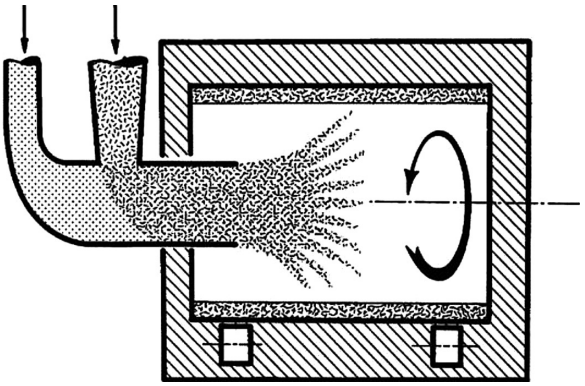

FIGURE 7.25 Centrifugal molding process.

In later years, the aerospace industry has embraced non-autoclave technologies in an effort to increase production speeds and get away from the size limitation of autoclaves.

Centrifugal Molding

An alternate non-autoclave way to provide pressure on a laminate is to spin it around and let the centrifugal pressure move the resin into the laminate plies.

Figure 7.25 illustrates this centrifugal molding process.

First the reinforcement is placed into the mold. One way of doing this is to roll it onto a light stick and bring the stick into the mold cavity. As the mold starts rotating, the dry reinforcement unwinds and starts pressing against the inside of the mold. Once this step is completed, the resin is allowed to enter. The resin impregnates the plies, and since the part has a slight taper, it can be removed from the mold with a slight hammer tap or with a demolding tool, depending on the size of the part.

This creates parts with a smooth surface appearance. Many tubular poles and masts are made using this technique.

Machining

It is very important to realize that glass is a very hard substance. Table 7.3 shows the Mohs scale, indicating that glass is harder than steel.

From a standpoint of hardness, we do know that glass fibers are as hard as steel, as shown in Table 7.3, which is the Mohs scale (from the website of the American Federation of Mineralogical Societies, Inc.: http://www.amfed.org/t_mohs.htm).

This table explains why glass fiber with a Mohs hardness of 7 is capable of scratching a pultrusion die and why a pultrusion die surface needs to be chromed and why regular carbide cutting tools wear

TABLE 7.3
Moh Hardness Scale

2.5	Fingernail
2.5–3	Gold, silver
3	Copper penny
4–4.5	Platinum
4–5	Iron
5.5	Knife blade
6–7	Glass
6.5	Iron pyrite
7+	Hardened steel file

out very quickly. An anecdote related to this is that the president of a pultrusion company noticed the piles of sawdust under the cutoff saws at the end of his machines. One weekend he concocted the idea of using this sawdust as filler for his or her resin. After some days passed, his or her personnel reported that the dimensions of the parts produced on this machine had gone outside the specification range; he or she realized the damage he or she had done. By adding the highly abrasive sawdust, he or she had worn his or her pultrusion die very badly. It suffices to say that he or she never tried this again.

Cutting with a band saw–type setup produces the least dust. Alternatively a diamond-coated rotary cutoff saw with water spray keeps the dust down and is known to give excellent results. Nevertheless, if the part needs to be subsequently bonded, surface coated, or painted, it is advisable to dry the wetted surface, so that all the moisture has been removed prior to secondary processing. Especially when cutting carbon, this dust may short-circuit electrical machinery. It is therefore better to use air tools when trimming and cutting carbon composites.

REFERENCES

1. *Fabric Handbook*, Knytex, New Braunfels, TX, 1994.
2. J. Milewski and H. Katz (eds.), *Handbook of Reinforcements for Plastics*, Van Nostrand Reinhold, New York, 1987 (ISBN 0-442-26475-5).
3. C. Hiel, Composite structures are a snap, *SAMPE Journal*, 34(1), 24–30, January–February 1998.
4. C. Hiel, Analysis methodology for fastenerless joining, in *ASCE Design Handbook*, A. Mosallam (ed.), American Society of Civil Engineers (ASCE), 1999.
5. C. Hiel, Thinking out of the cave, *Composites Technology*, February 2002.
6. C. Hiel, Three design examples with composite materials, Keynote Lecture, *European Conference of Composite Materials*, Bruges, Belgium, June 3–5, 2002.
7. R.W. Meyer, *Handbook of Pultrusion Technology*, Chapman & Hall, New York, 1985 (ISBN 0-412-00761-4).
8. T.F. Star (ed.), *Pultrusion for Engineers*, Woodhead Publishing Limited, Cambridge, U.K., 2000 (ISBN 0-8493-0843-7).
9. S.T. Peters, W.D. Humphrey, and R.F. Foral, *Filament Winding Composite Structure Fabrication*, 2nd edn., SAMPE, Covina, CA.
10. D.V. Rosato and C.S. Grove, Jr., *Filament Winding: Its Development, Manufacture, Applications, and Design*, John Wiley & Sons, New York, 1964.
11. J.J. Morena, *Advanced Composite Mold Making*, Van Nostrand Reinhold, New York, 1988 (ISBN 0-442-26414-3).
12. W.E. Boyes, *Handbook of Jig and Fixture Design*, Society of Manufacturing Engineers, Dearborn, MI, 1989 (ISBN 0-87263-365-9).

8 Analysis of FRP Structural Members

Aixi Zhou

CONTENTS

INTRODUCTION

Basic approaches for design of FRP structural members include allowable stress design (ASD), limit state design (LSD), load and resistance factor design (LRFD), and performance-based design (PBD). All of these approaches require structural analysis for the designed section, member, or structure. FRP composite materials are brittle and exhibit little or no ductility prior to failure. FRP materials also have higher strength-to-stiffness ratio compared to steel or concrete. This implies that when the strength requirements are satisfied for a design, the requirements for stiffness may not be fulfilled. FRP structural members usually exhibit low resistance in the wall's through-thickness direction. In an FRP structure, failure may occur locally due to local bucking or wrinkling or due to local damages such as local delamination or cracking. The design of FRP structures shall take into account the basic material characteristics of FRP composites by ensuring that a serviceability limit state is reached prior to its ultimate limit state for the mode of failure being considered or by providing reasonable and adequate warning of failure prior to reaching an ultimate limit state. This

requires a good understanding of the mechanical and structural behavior of the FRP structure subjected to the design loads and service environment. This chapter provides bases for the mechanical and structural analysis of FRP structural members, including the determination of deformation, stress, strain, stability analysis (buckling analysis), vibration, and delamination.

Some assumptions must be made for the mechanical and structural analysis of FRP materials and structures. In the micro level, fiber-reinforced composite materials are heterogeneous in nature, and the material properties vary from point to point. In macromechanical analysis and structural analysis, we usually deal with a scale that is much larger than the fiber diameter, and the material may be treated as homogeneous with equivalent properties calculated from the fiber and matrix properties through some micromechanics approaches. Micromechanics is the study of a composite's behavior wherein the interaction of the constituent materials (fiber and matrix) is examined in detail as part of the definition of the behavior of the heterogeneous composite, whereas macromechanics and structural mechanics examine its behavior wherein the material is assumed homogeneous, which implies that the properties are taken to be the same at every point and the effects of the constituent materials are detected only as averaged apparent properties of the composite.

The analysis of FRP composite structural members is based on the theory of elasticity of anisotropic body. Under normal and isothermal conditions, FRP materials are considered as ideally elastic, that is, the body recovers its original form completely upon removal of the forces causing the deformation, and there is a one-to-one relationship between the state of stress and the state of strain. This does not include creep at constant stress and stress relaxation at constant strain. The analysis of viscoelastic behavior of FRP composites can be found elsewhere. In this chapter, it assumes that FRP structural members are ideally elastic.

The governing equations describing the motion of a solid body can be classified into four basic categories: kinematics, kinetics, constitutive equations, and thermodynamics. Kinematics studies the geometric changes or deformation (displacement and strains) in a body, with no consideration of forces that cause the geometric changes or deformation. Kinetics studies the static or dynamic equilibrium of forces acting on a body. The constitutive equations describe the constitutive behavior of the body and relate the dependent variables introduced in the kinetic description to those in the kinematic and thermodynamic descriptions. The thermodynamic principles (first and second laws of thermodynamics) describe the conservation of energy and relations among heat, mechanical work, and thermodynamic properties. The mechanical analysis of a solid body is to find solutions to these basic equations supplemented by appropriate boundary and initial conditions of a specific problem. The equations and procedures can be found in various books for isotropic materials and FRP composite materials (Hyer 1998; Jones 1999; Kollár and Springer 2003; Reddy 2004).

COORDINATE SYSTEMS

Continuous FRP composites often have easily identifiable preferred directions associated with their fiber directions or symmetry planes. Each individual ply of an FRP laminate may be an anisotropic body, that is, different values of material property in different directions at a point. Therefore, it is convenient to employ two coordinate systems: a local material coordinate system defined according to the principle directions of reinforcing fibers or the axes of symmetry and a global coordinate system attached to a fixed reference point for ease of understanding for a specific problem. Figure 8.1 shows a lamina with global and local material coordinate systems.

Local coordinate system is often denoted by axis of x_1, x_2, x_3 (or z) or simply 1, 2, 3. Direction x_1 refers to the direction in which highest stiffness or strength exists. Direction x_2 refers to the direction perpendicular to the x_1 direction but remains in the lamina or laminate midplane. Direction x_3 (or z) often refers to the *through-thickness direction*. The x_1 direction is called *longitudinal* (*principal*) *direction*; the x_2 direction is called *transverse direction*; the x_3 direction is called the *vertical*

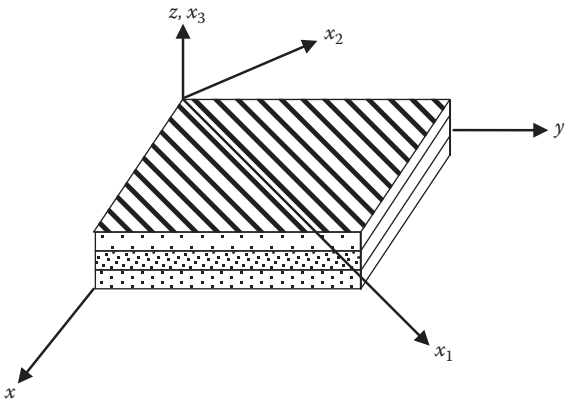

FIGURE 8.1 Global coordinate system (x, y, z) and local coordinate system (x_1, x_2, x_3).

TABLE 8.1
Notations for Strains and Stresses

	Strain Notations		Stress Notations	
	Normal	**Shear**	**Normal**	**Shear**
Global System (x, y, z)				
Tensorial	$\varepsilon_{xx}\ \varepsilon_{yy}\ \varepsilon_{zz}$	$\varepsilon_{yz}\ \varepsilon_{xz}\ \varepsilon_{xy}$	$\sigma_{xx}\ \sigma_{yy}\ \sigma_{zz}$	$\sigma_{yz}\ \sigma_{xz}\ \sigma_{xy}$
Engineering	$\varepsilon_x\ \varepsilon_y\ \varepsilon_z$	$\gamma_{yz}\ \gamma_{xz}\ \gamma_{xy}$	$\sigma_x\ \sigma_y\ \sigma_z$	$\tau_{yz}\ \tau_{xz}\ \tau_{xy}$
Contracted	$\varepsilon_x\ \varepsilon_y\ \varepsilon_z$	$\varepsilon_q\ \varepsilon_r\ \varepsilon_s$	$\sigma_x\ \sigma_y\ \sigma_z$	$\sigma_q\ \sigma_r\ \sigma_s$
Local System (x_1, x_2, x_3)				
Tensorial	$\varepsilon_{11}\ \varepsilon_{22}\ \varepsilon_{33}$	$\varepsilon_{23}\ \varepsilon_{13}\ \varepsilon_{12}$	$\sigma_{11}\ \sigma_{22}\ \sigma_{33}$	$\sigma_{23}\ \sigma_{13}\ \sigma_{12}$
Engineering	$\varepsilon_1\ \varepsilon_2\ \varepsilon_3$	$\gamma_{23}\ \gamma_{13}\ \gamma_{12}$	$\sigma_1\ \sigma_2\ \sigma_3$	$\tau_{23}\ \tau_{13}\ \tau_{12}$
Contracted	$\varepsilon_1\ \varepsilon_2\ \varepsilon_3$	$\varepsilon_4\ \varepsilon_5\ \varepsilon_6$	$\sigma_1\ \sigma_2\ \sigma_3$	$\sigma_4\ \sigma_5\ \sigma_6$

direction or *through-thickness direction*. Because axes x_1 and x_2 are in the midplane of a lamina or laminate, this plane (x_1–x_2) is referred as *in-plane*, the other two planes formed by axes x_1–x_3 and x_2–x_3 are called *out-of-plane*. The displacement field is denoted as (u, v, w) in the global system and (u_1, u_2, u_3) in the local coordinate system. The denotations of strains and stresses in different coordinate systems are shown in Table 8.1.

In analysis of FRP composite, the global coordinate system in general does not coincide with the local (material) coordinate system. In addition, laminates have several layers; each has different orientation of their principal material coordinates with respect to the global laminate coordinate. Thus, there is a need to establish transformation relations among stresses, strains, and material coefficients in one coordinate system to the corresponding quantities in another system.

When we consider two Cartesian coordinate system (x, y, z) and (x', y', z'), the orientation of the primed system with respect to the unprimed system can either be given by nine direction cosines or be specified in terms of three angles that denote consecutive rotations of the primed system about the x-, y-, z-axes (Kollár and Springer 2003).

Constitutive Behavior of FRP Composite Materials

In FRP composites, the fibers may be oriented in a predesigned or arbitrary manner. The material may behave differently in different directions depending on the arrangement of the reinforcing fibers. The constitutive relationships of a generally anisotropic material can be described by

the generalized Hooke's law. By using the contracted notation (see Table 8.1), the stress–strain relationships for a generally anisotropic material in the (x, y, z) global coordinate system can be expressed as

$$\begin{Bmatrix} \sigma_x \\ \sigma_y \\ \sigma_z \\ \tau_{yz} \\ \tau_{xz} \\ \tau_{xy} \end{Bmatrix} = \begin{bmatrix} \bar{C}_{11} & \bar{C}_{12} & \bar{C}_{13} & \bar{C}_{14} & \bar{C}_{15} & \bar{C}_{16} \\ \bar{C}_{21} & \bar{C}_{22} & \bar{C}_{23} & \bar{C}_{24} & \bar{C}_{25} & \bar{C}_{26} \\ \bar{C}_{31} & \bar{C}_{32} & \bar{C}_{33} & \bar{C}_{34} & \bar{C}_{35} & \bar{C}_{36} \\ \bar{C}_{41} & \bar{C}_{42} & \bar{C}_{43} & \bar{C}_{44} & \bar{C}_{45} & \bar{C}_{46} \\ \bar{C}_{51} & \bar{C}_{52} & \bar{C}_{53} & \bar{C}_{54} & \bar{C}_{55} & \bar{C}_{56} \\ \bar{C}_{61} & \bar{C}_{62} & \bar{C}_{63} & \bar{C}_{64} & \bar{C}_{65} & \bar{C}_{66} \end{bmatrix} \begin{Bmatrix} \varepsilon_x \\ \varepsilon_y \\ \varepsilon_z \\ \gamma_{yz} \\ \gamma_{xz} \\ \gamma_{xy} \end{Bmatrix} \tag{8.1}$$

where $\bar{C}_{ij}$ $(i, j = 1, 2, 3, \ldots, 6)$ are elements of the stiffness matrix $[\bar{C}]$ in the global system. The inverse of (8.1) results in the following strain–stress relationship:

$$\{\varepsilon\} = [\bar{S}]\{\sigma\} \tag{8.2}$$

where $\bar{S}_{ij}$ $(i, j = 1, 2, 3, \ldots, 6)$ are elements of the compliance matrix $[\bar{S}]$ in the global system and $[\bar{S}]$ is the inverse of $[\bar{C}]$, that is, $[\bar{S}] = [\bar{C}]^{-1}$. The values of $\bar{S}_{ij}$ can be determined through standard tests (Kollár and Springer 2003). It can be shown that $\bar{S}_{ij} = \bar{S}_{ji}$ and $\bar{C}_{ij} = \bar{C}_{ji}$, and there are only 21 independent elements in both $[\bar{S}]$ and $[\bar{C}]$ matrices. When the elastic coefficients $[\bar{S}]$ or $[\bar{C}]$ at a point remain unchanged for every pair of coordinate systems that are mirror images for each other in a plane, that plane is called a *plane of material symmetry*. Accordingly, FRP composites may be characterized as generally anisotropic, monoclinic, orthotropic, and transversely isotropic (Jones 1999; Reddy 2004).

Equivalent Single-Layer Lamination Theories for FRP Structures

In general, the walls of FRP structural members have their planar dimensions one to two orders of magnitude larger than their thickness. We can call these walls *laminates*. FRP laminates are often treated as plate elements. From solid mechanics point of view, FRP beams or columns can be treated as special 1-D laminated plates. However, the analysis of thick-/thin-walled FRP beams requires special attention. The analysis of FRP laminates or structures has been based on one of the following approaches (Reddy 2004): (1) 2-D equivalent single-layer (ESL) theories, including classical laminate theory and shear deformation laminate theories; (2) 3-D elasticity theories, including traditional 3-D elasticity formulations and layer-wise theories; and (3) hybrid or multiple model 2-D and 3-D methods, including finite element modeling.

The ESL lamination theories are those in which a heterogeneous FRP laminated plate is treated as a statically equivalent, single layer having a complex constitutive behavior. They are derived from the 3-D elasticity theory by making suitable assumptions concerning the kinematics of deformation or stress state through the thickness of the laminate. In general, the ESL theories are developed by assuming the form of displacement field or stress field as a linear combination of unknown functions and the thickness coordinates. The simplest ESL laminate theory is the classical laminated plate theory (CLPT), which is an extension of the Kirchhoff (classical) plate theory to laminated composite plates. Another ESL laminate theory is the first-order shear deformation theory (FSDT), which extends the kinematics of the CLPT by including a gross transverse (or through-thickness) shear deformation, that is, the through-thickness shear strain is assumed to be constant with respect to the thickness coordinate.

In both CLPT and FSDT, the plane-stress state assumption is used and the plane-stress-reduced form of the constitutive law is employed. In both theories, the inextensibility and/or

straightness of transverse (or through-thickness) normals can be removed. Such extensions lead to many second- and higher-order ESL theories (Reddy 2004). The higher-order theories provided a slight increase in accuracy relative to the FSDT solution, at the expense of a significant increase in computational effort. In addition to their inherent simplicity and low computational cost, the CLPT and FSDT theories often provide sufficiently accurate description of global response for thin to moderately thick laminates, for example, global deflection, critical buckling loads, and fundamental vibration frequencies and associated mode shapes. The CLPT is the simplest; however, the accuracy is largely reduced for some moderately thick plates. The FSDT provides the best compromise of solution accuracy, economy, and simplicity. The CLPT applied to FRP beams corresponds to the Euler beam theory and the FSDT applied to FRP beams corresponds to the Timoshenko beam theory.

All-Composite FRP Structural Members in Civil Engineering and Their Material Properties

In the civil engineering domain, most all-composite FRP structural members are manufactured by the pultrusion process. Pultruded members such as rods, grids, beams, columns, plates and panels have been widely used in pedestrian and vehicular bridges, building structures, towers, walkways, and offshore platforms. Standard pultruded FRP structural members include I section beams, T section beams, wide-flange (WF) beams, square tubes, rectangular tubes, circular tubes, channels, angles, plates, and multicellular panels. Customized structural shapes can also be produced, such as double-web beams, sandwich beams, and sandwich plates. By joining simple FRP structural members, primarily through adhesive bonding, one can create secondary structural members: such as the bonding of two C channels or two L channels to form beams or columns with symmetric sections and the bonding of square tubes with skin plates to form multicellular bridge deck panels.

The internal fiber architecture of pultruded FRP members consists of roving bundles, mats, and fabrics and is often arranged such that the laminate is both balanced and symmetric. Such a structural member can be considered as a specially orthotropic laminate. The orthotropic axes of the laminate coincide with the structural axes of the pultruded section. In this case, since no shear–extension coupling and bend–twist and bending–extension couplings exist, the effective laminate stiffness approach can be applied, that is, the laminates can be characterized with effective laminate stiffness, E_x, E_y, G_{xy}, ν_{xy}, etc. Most pultruded FRP structural members can be characterized this way. Therefore, this chapter primarily deals with FRP structural members with orthotropic and symmetrical layup of wall segments.

The effective material properties of structural members can be found in manuals from the material providers. These properties are usually lower bound values to provide safety margins. These properties may be used during the design stage; however, a preferred alternative is to conduct tests according to certain standards on representative specimens. Micromechanics model may be used to estimate material properties. The estimations via micromechanics should be verified by experimental testing. Table 8.2 provides a summary of recommended ASTM testing standards for determining material properties (Bank 2005). Mechanical and structural analysis can be conducted after the required material properties are obtained.

ANALYSIS OF FRP BEAMS

In civil engineering structures, all-composite FRP beams are often thin-walled or sandwich structures. When applying CLPT or Euler–Bernoulli beam theory to the analysis of beams, it is assumed that planes of the beam's cross section remain plane and perpendicular to the mid-axis. For thin-walled and sandwich beams, the assumption that planes of cross section remain plane is

TABLE 8.2
Recommended ASTM Testing Standards for FRP Structural Members

Measured Property	Recommended ASTM Test Methods
Mechanical Properties	
Strength	
Longitudinal tensile strength	D 3039, D 5083, D 638
Longitudinal compressive strength	D 3410, D 695
Longitudinal short beam shear strength	D 2344
Longitudinal bearing strength	D 5961, D 953
In-plane shear strength	D 5379, D 3846
Impact resistance	D 256
Transverse tensile strength	D 3039, D 5083, D 638
Transverse compressive strength	D 3410, D 695
Transverse short beam shear strength	D 2344
Transverse bearing strength	D 5961, D 953
Stiffness	
Longitudinal tensile modulus	D 3039, D 5083, D 638
Longitudinal compressive modulus	D 3410, D 695
Major (longitudinal) Poisson's ratio	D 3039, D 5083, D 638
In-plane shear modulus	D 5379
Transverse tensile modulus	D 3039, D 5083, D 638
Transverse compressive modulus	D 3410, D 695
Physical Properties	
Fiber volume fraction	D 3171, D 2584
Density	D 792
Barcol hardness	D 2583
Glass transition temperature/heat distortion temperature	E 1356, E 1640, D 648, E 2092
Water absorbed when substantially saturated	D 570
Longitudinal coefficient of thermal expansion	E 831, D 696
Transverse coefficient of thermal expansion	E 831, D 696
Flash ignition temperature	D 1929

Source: Revised from Bank, L.C., Fiber-reinforced polymer composites, in *Handbook of Structural Engineering*, W.F. Chen and E.M. Lui, eds., CRC Press, Boca Raton, FL, 2005.

reasonable. The latter part of the assumption may no longer be valid because the cross section does not necessarily remain perpendicular to the axis. Therefore, shear deformation should be included, and FSDT or Timoshenko beam theory should be applied to these orthotropic FRP members.

Structural Analysis of FRP Beams

Axial Tensile Load

We introduce a (x, y, z) coordinate system with its origin at the beam centroid and its x-axis along the beam, as shown in Figure 8.2. We consider orthotropic beams of arbitrary cross sections subjected to axial tensile force N_x (or the stress resultant due to the applied axial tensile forces) at the centroid. The centroid is the point that an acting axial load does not change the curvature of the axis passing

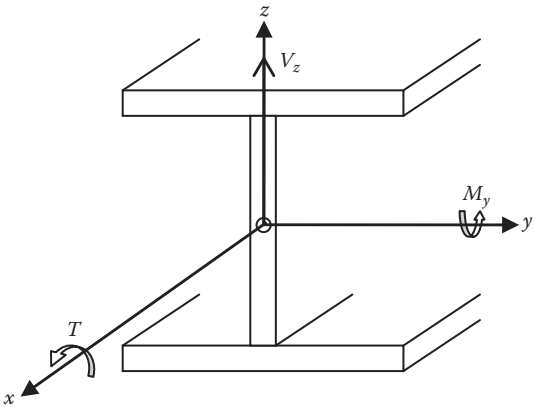

FIGURE 8.2 Coordinates for bending analysis of FRP beams.

through the centroid. Since N_x is applied at the centroid, no eccentricity is considered, and the member is assumed to be under a uniform axial tensile stress σ_x:

$$\sigma_x = \frac{N_x}{A_0} \tag{8.3}$$

where A_0 is the cross-sectional area of the beam.

The relationship between the axial force N_x and the axial strain ε_x is

$$N_x = \overline{EA} \cdot \varepsilon_x \tag{8.4}$$

where $\overline{EA}$ is the beam's tensile stiffness. The tensile stiffnesses of various thin-walled beams are shown in Table 8.3. The axial deformation δ_x is

$$\delta_x = L \cdot \varepsilon_x = \frac{N_x L}{\overline{EA}} \tag{8.5}$$

The critical tensile strength (σ_{cr}) of the beam's gross section is equal to the tensile strength of the material (σ_0). The design stress is calculated using the gross section area. When cutouts are present (e.g., due to the presence of holes for bolting), the critical tensile strength is reduced because of the stress concentration around the cutouts. The stress concentration around cutouts is discussed in detail in Chapter 10. The critical tensile strength for a net section can be in the form of

$$\sigma_{cr} = k\sigma_0 \tag{8.6}$$

where k is a reduction factor and $k < 1$. The factor is taken as 0.9 in the EUROCOMP design code (Clarke 1996). When cutouts are presented, the design stress should be calculated over the net cross-sectional area.

Axial Compressive Load

When an FRP member is loaded by axial compressive forces at the centroid, the calculation of stress, strain, and deformation is the same as provided in (8.3) through (8.6), but the axial force N_x should take a negative sign to distinguish compression from tension. Under axial compression, the member will undergo global or local buckling.

TABLE 8.3
Cross-Sectional Properties of Thin-Walled and Sandwiched FRP Beams

Tensile Stiffness (*EA*), the Coordinates of Centroid (y_c), and Bending Stiffness (*EI*)

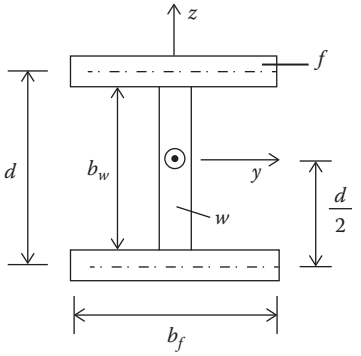

$$EA = \frac{2b_f}{a_{11}^f} + \frac{b_w}{a_{11}^w}; \quad y_c = 0 \text{ (where } f \text{ is flange and } w \text{ is web)}$$

$$EI_{yy} = \frac{b_f}{a_{11}^f}\frac{d^2}{2} + \frac{2b_f}{d_{11}^f} + \frac{b_w^3}{12a_{11}^w}; \quad EI_{zz} = \frac{b_w}{d_{11}^w} + \frac{2b_f^3}{12a_{11}^f}$$

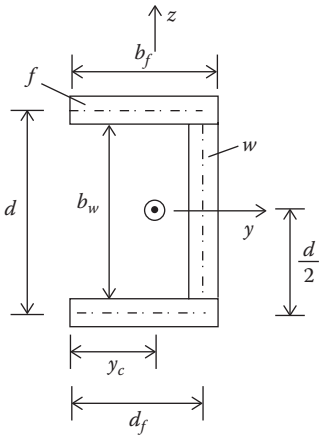

$$EA = \frac{2b_f}{a_{11}^f} + \frac{b_w}{a_{11}^w}; \quad y_c = \frac{1}{EA}\left(\frac{2b_f}{a_{11}^f}\frac{b_f}{2} + \frac{b_w}{a_{11}^w}d_f\right)$$

$$EI_{yy} = \frac{b_f}{a_{11}^f}\frac{d^2}{2} + \frac{2b_f}{d_{11}^f} + \frac{b_w^3}{12a_{11}^w};$$

$$EI_{zz} = \frac{b_w}{d_{11}^w}(d_f - y_c)^2 + \frac{b_w}{d_{11}^w} + \frac{2}{a_{11}^f}\left[\frac{y_c^3}{3} + \frac{(b_f - y_c)^3}{3}\right]$$

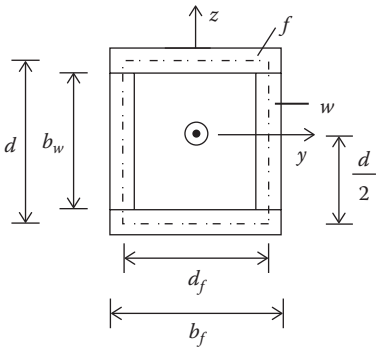

$$EA = \frac{2b_f}{a_{11}^f} + \frac{2b_w}{a_{11}^w}; \; y_c = 0$$

$$EI_{yy} = \frac{b_f}{a_{11}^f}\frac{d^2}{2} + \frac{2b_f}{d_{11}^f} + \frac{2b_w^3}{12a_{11}^w};$$

$$EI_{zz} = \frac{b_w}{a_{11}^w}\frac{d_f^2}{2} + \frac{2b_w}{d_{11}^w} + \frac{2b_f^3}{12a_{11}^f}$$

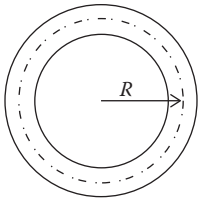

$$EA = \frac{2\pi R}{a_{11}} + \frac{2b_w}{a_{11}^w}; \; y_c = 0$$

$$EI_{yy} = EI_{zz} = \pi\left(\frac{R^3}{a_{11}} + \frac{R}{d_{11}}\right)$$

TABLE 8.3 (continued)
Cross-Sectional Properties of Thin-Walled and Sandwiched FRP Beams

Tensile Stiffness (*EA*), the Coordinates of Centroid (y_c), and Bending Stiffness (*EI*)

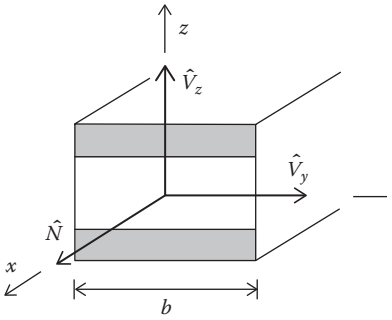

$$EA = \frac{b}{a_{11}^t} + \frac{b}{a_{11}^b}$$ (where superscript *t* is top flange and *b* is bottom flange)

$$z_c = \frac{1}{EA}\frac{bd}{a_{11}^t}$$

$$EI_{yy} = \frac{b}{d_{11}};\ EI_{zz} = \frac{b^3}{12a_{11}^t} + \frac{1}{a_{11}^b}\frac{b^3}{12}$$

Source: Revised from Table A.1, Kollár, L.P. and Springer, G.S., *Mechanics of Composite Structures*, Cambridge University Press, Cambridge, U.K., 2003.

The layup of each wall segment is orthotropic and symmetrical. a_{11} and d_{11} are elements of the compliance matrix of symmetrical laminates, that is, $[a] = [A]^{-1}$, $[d] = [D]^{-1}$ (where $[A]$ is the in-plane stiffness matrix and $[D]$ is the bending stiffness matrix), evaluated at the midsurface.

Global Buckling

In structural design, the cross sections of FRP members are often symmetrical (having one axis of symmetry, say *z*-axis) or doubly symmetrical (having two axes of symmetry, say *y*- and *z*-axes). If the cross section is doubly symmetrical, a beam may undergo flexural bucking in the planes of symmetry as well as torsional buckling. The buckling loads (N_{cry}, N_{crz}, and $N_{cr\psi}$) of beams with doubly symmetrical cross sections are given in Table 8.4.

An orthotropic beam with symmetrical cross section may undergo flexural buckling (or Euler buckling) in the plane of symmetry (*x*–*z* plane) and combined flexural–torsional buckling. The buckling load corresponding to buckling in the plane of symmetry (*x*–*z* plane) is the same as N_{cry}^B in Table 8.4. The buckling loads corresponding to flexural–torsional buckling are the roots of the following equation (when shear deformation is not considered):

$$\left\| \begin{bmatrix} N_{crz}^B & 0 \\ 0 & N_{cr\omega}^B i_\omega^2 \end{bmatrix} - N_{cr} \begin{bmatrix} 1 & z_{SC} \\ z_{SC} & i_\omega^2 \end{bmatrix} \right\| = 0 \tag{8.7}$$

where ‖ denotes the determinant and N_{cry}^B, N_{crz}^B, and $N_{cr\psi}^B$ are given in Table 8.4. The aforementioned equation can be rewritten as

$$N_{cr}^2 \left(i_\omega^2 - z_{SC}^2\right) - N_{cr}\left(N_{crz}^B + N_{cr\psi}^B\right) i_\omega^2 + N_{crz}^B N_{cr\psi}^B i_\omega^2 = 0 \tag{8.8}$$

The two values are approximate when one end of the beam is fixed and the other end is simply supported (SS). The buckling load of interest is the lowest of N_{cry}^B and the two values from (8.8).

TABLE 8.4
Buckling Loads of Slender FRP Beams with Doubly Symmetrical Cross Sections

	Buckling Load	
BCs	**No Shear Deformation**	**With Shear Deformation**
Hinged–hinged	$N_{cr}^{B} = \dfrac{\pi^2 \overline{EI}}{L^2}$	$\dfrac{1}{N_{cr}} = \dfrac{1}{N_{cr}^{B}} + \dfrac{1}{S}$
Fixed–hinged	$N_{cr}^{B} = \dfrac{\pi^2 \overline{EI}}{0.7L^2}$	$\dfrac{1}{N_{cr}} \cong \dfrac{1}{N_{cr}^{B}} + \dfrac{1}{S}$
Fixed–fixed	$N_{cr}^{B} = \dfrac{\pi^2 \overline{EI}}{0.5L^2}$	$\dfrac{1}{N_{cr}} = \dfrac{1}{N_{cr}^{B}} + \dfrac{1}{S}$
Fixed–free	$N_{cr}^{B} = \dfrac{\pi^2 \overline{EI}}{2L^2}$	$\dfrac{1}{N_{cr}} = \dfrac{1}{N_{cr}^{B}} + \dfrac{1}{S}$

Source: Revised from Table B.1, Kollár, L.P. and Springer, G.S., *Mechanics of Composite Structures*, Cambridge University Press, Cambridge, U.K., 2003.

For buckling in the x–z plane, $N_{crz} = N_{cr}$, $\overline{EI} = \overline{EI}_{yy}$, and $S = S_{zz}$; for buckling in the x–y plane, $N_{crz} = N_{cr}$, $\overline{EI} = \overline{EI}_{zz}$, and $S = S_{yy}$; for torsional buckling, $N_{cr\psi} = N_{cr} + \left(\overline{GI}_t / i_\omega^2\right)$, $\overline{EI} = \overline{EI}_\omega / i_\omega^2$, and $S = S_\omega / i_\omega^2$, where i_ω is the polar radius of gyration of the cross section about the shear center, $i_\omega^2 = z_{SC}^2 + y_{SC}^2 + \left[(\overline{EI}_{yy} + \overline{EI}_{zz}) / \overline{EA} \right]$.

When the cross section is unsymmetrical, an orthotropic beam undergoes combined flexural–torsional buckling. The buckling loads are given by the solution of the following equation:

$$\left| \begin{bmatrix} N_{crz}^{B} & 0 & 0 \\ 0 & N_{cry}^{B} & 0 \\ 0 & 0 & N_{cr\psi}^{B} i_\omega^2 \end{bmatrix} - N_{cr} \begin{bmatrix} 1 & 0 & z_{SC} \\ 0 & 1 & -y_{SC} \\ z_{SC} & -y_{SC} & i_\omega^2 \end{bmatrix} \right| = 0 \tag{8.9}$$

The solution results in three values of which the lowest value is of interest. In (8.9), the coordinate systems y and z must be in the principal directions such that $\overline{EI}_{yz} = 0$.

When shear deformation is considered, the buckling load can be obtained using the formulas in the third column provided in Table 8.4 after the corresponding buckling loads without shear deformation are available through (8.8) and (8.9). One can calculate the critical deformation, stress, and strain at buckling according to the equations given in (8.4) through (8.7) when the critical buckling loads are available. Taken from Zureick and Scott (1997) and Zureick and Steffen (2000), Bank (2005) also provided the formulation for the calculation of critical stress for global Euler buckling considering the effect of shear deformation.

Local Buckling

Thin-walled beams can fail due to local buckling of the compressive flange or web. Local buckling of analysis of thin-walled beams is generally performed by modeling the wall segments as long

plates together with assumed boundary conditions (BCs) on the segments' edges. A conservative assumption is to consider the restrained edges as SS. The local buckling resistance $N_{c,d}$ of a cross section is

$$N_{c,d} = A_{eff}\sigma_{cr} \tag{8.10}$$

where

A_{eff} is the effective area of the cross section
σ_{cr} is the least critical buckling resistance (stress) of the individual elements of the section

The buckling resistance of individual elements in a section is determined through the buckling analysis of the plates. The analyses of local buckling of axially loaded thin-walled, closed-section rectangular beam and open-section I beam are illustrated in Kollár and Springer (2003). Bank (2005) provided local buckling analysis of both local compressive flange buckling and local compressive web buckling.

When the restrained edge of a flange is assumed to be SS (and the other opposite edge is free), the critical stress at local buckling for flange elements in compression is

$$\sigma_{cr} = \left(\frac{\pi t_f}{b_f/2}\right)^2 \left[Q_{xx}\left(\frac{b_f/2}{a}\right)^2 + 12\frac{Q_{66}}{\pi^2}\right] \tag{8.11}$$

where

t_f is the flange thickness
b_f is the entire flange width
a is the half wave length of the buckle and is taken as the unbraced length of the flange
Q_{xx} and Q_{66} are stress-reduced stiffnesses of the flange (when it is considered as a plate) and are given in (8.19)

The first term in the square bracket is negligible if the unbraced flange is long.

If the restrained edge is assumed to be fixed, the critical stress can be approximated as

$$\sigma_{cr} = \left(\frac{\pi t_f}{b_f/2}\right)^2 \left[0.935Q_{xx}\sqrt{\frac{E_y}{E_x}} - 0.656\nu_{yx}Q_{xx} + 2.082Q_{66}\right] \tag{8.12a}$$

where

E_x and E_y are the compressive moduli in the longitudinal and width directions, respectively
ν_{yx} is the Poisson's ration in the width direction

The length of the half-buckle wavelength is

$$a = 1.46\frac{b_f}{2}\sqrt[4]{\frac{E_x}{E_y}} \tag{8.12b}$$

It was shown that local buckling stress for I beams is higher than that predicted by this assumption and is lower than predicted by assuming the edges is fixed (Bank et al. 1995). Bank (2005) proposes an approximation that the critical local buckling stress for a compression flange is taken as average of the SS and the fixed conditions given in (8.11) and (8.12).

When both longitudinal edges are restrains, such as box beams, the BCs are assumed to be either SS or fixed on both restrained edges (Bank 2005). When both are assumed SS, the critical buckling stress and the half wavelength are

$$\sigma_{cr} = 2\left(\frac{\pi t_f}{b_f}\right)^2\left[Q_{xx}\sqrt{\frac{E_y}{E_x}} + \nu_{yx}Q_{xx} + 2Q_{66}\right], \quad a = b_f\sqrt[4]{\frac{E_x}{E_y}} \tag{8.13}$$

When both are assumed to be fixed, the critical buckling stress and the half wavelength are

$$\sigma_{cr} = 2.52\left(\frac{\pi t_f}{b_f}\right)^2\left[Q_{xx}\sqrt{\frac{E_y}{E_x}} + 0.543\nu_{yx}Q_{xx} + 1.086Q_{66}\right], \quad a = 0.67b_f\sqrt[4]{\frac{E_x}{E_y}} \tag{8.14}$$

The calculation of critical stress for webs is identical to that of flanges. One only needs to replace the material properties and geometry of the flange with the web.

If the width-to-thickness ratio of the flange or web is small, or the local and global buckling is prevented, the structural member may fail due to compressive crushing of the FRP material. Local compressive crushing of FRP laminates is a complex phenomenon. One simple design criterion is to consider the critical compressive strength of the member equal to the compressive strength of the FRP material in the flange or web.

Transverse Load (Bending)

The applied transverse forces on FRP structural members result in bending moment and transverse shear force in the members. The deflection is due to both bending and shear deformation and can be expressed as

$$\delta = \frac{f_1(x)}{\overline{EI}} + \frac{f_2(x)}{\overline{S}} \tag{8.15}$$

where

$\overline{EI}$ is the bending stiffness

$\overline{S}$ is the shear stiffness of the beam

the functions $f_1(x)$ and $f_2(x)$ depend on loading and BCs

The functions $f_1(x)$ and $f_2(x)$ for some common loading and BCs are provided in Table 8.5.

Assuming loading in the x–y plane and y and z are principal axes, the axial flexural stress σ_x and transverse shear stress can be obtained as

$$\sigma_x = \frac{M_x y}{I_{zz}} \tag{8.16a}$$

TABLE 8.5
Transverse Deflections of FRP Beams

Support Conditions	Deflection, $w_0(x)$	Maximum Deflection
Hinged–Hinged		
Central point load	$\frac{c_1}{48}\left[3\left(\frac{x}{a}\right)-4\left(\frac{x}{a}\right)^3\right]+\frac{s_1}{2}\frac{x}{a}$	$\frac{c_1}{48}+\frac{s_1}{4}$ at $x=\frac{a}{2}$
Uniformly distributed load	$\frac{c_2}{24}\left[\frac{x}{a}-2\left(\frac{x}{a}\right)^3+\left(\frac{x}{a}\right)^4\right]+\frac{s_2}{2}\left[\frac{x}{a}-\left(\frac{x}{a}\right)^2\right]$	$\frac{5c_1}{384}+\frac{s_1}{8}$ at $x=\frac{a}{2}$
Fixed–Fixed		
Central point load	$\frac{c_1}{48}\left[3\left(\frac{x}{a}\right)^2-4\left(\frac{x}{a}\right)^3\right]+\frac{s_1}{2}\frac{x}{a}$	$\frac{c_1}{192}+\frac{s_1}{4}$ at $x=\frac{a}{2}$
Uniformly distributed load	$\frac{c_2}{24}\left[\left(\frac{x}{a}\right)^2-\frac{x}{a}\right]^2+\frac{s_2}{2}\left[\frac{x}{a}-\left(\frac{x}{a}\right)^2\right]$	$\frac{c_1}{384}+\frac{s_1}{8}$ at $x=\frac{a}{2}$
Fixed–Free		
Central point load	$\frac{c_1}{6}\left[3\left(\frac{x}{a}\right)^2-\left(\frac{x}{a}\right)^3\right]+s_1\frac{x}{a}$	$\frac{c_1}{3}+s_1$ at $x=a$
Uniformly distributed load	$\frac{c_2}{24}\left[6\left(\frac{x}{a}\right)^2-4\left(\frac{x}{a}\right)^3+\left(\frac{x}{a}\right)^4\right]+\frac{s_2}{2}\left[2\left(\frac{x}{a}\right)-\left(\frac{x}{a}\right)^2\right]$	$\frac{c_1}{8}+\frac{s_1}{2}$ at $x=a$

Source: Revised from Table 6.3-1, Reddy, J.N., *Mechanics of Laminated Composite Plates: Theory and Analysis*, 2nd edn., CRC Press, Boca Raton, FL, 2004.

$c_1=-F_0ba^3/EI_{yy}$, $c_2=-q_0ba^4/EI_{yy}$, $s_1=-F_0ba/KG_{xz}bh$, and $s_2=-q_0ba^2/G_{xz}bh$, where F_0 is the value of the point load and q_0 is the value of the uniformly distributed load, and K is the shear correction coefficient. For a homogeneous beam with rectangular cross section, $K=5/6$. The K value for a general laminated beam depends on the lamina property and lamination scheme.

$$\tau_{xy}=\frac{V_yQ_z}{I_{zz}t} \tag{8.16b}$$

where

M_x is the resultant moment
y is the distance to the centroid
I_{zz} is the second moment of area with respect to the z-axis
V_y is the resultant transverse force
Q_z is the first moment of area with respect to z-axis
t is the wall thickness

Global and Local Buckling

The critical loads for global flexural, torsional, and combined flexural–torsional buckling of orthotropic beams subjected to transverse loads can be determined in the similar way as presented in the previous section for axially loaded orthotropic beams, that is, Equations 8.3 through 8.9 and Table 8.5. When subjected to transverse load, at certain applied loading level,

the beam can also buckle laterally, while the cross sections of the beam rotate. This phenomenon is called *lateral-torsional buckling*. Equations for studying the lateral-torsional buckling of isotropic beams can be used for orthotropic FRP beams provided the appropriate values of material properties and stiffnesses are used. The equation to determine the critical lateral-torsional buckling stress without shear effect for open-section I or WF beams is given in Equation 16.16 in Bank (2005).

The determination if local compressive buckling in flange or web segments under transverse load is identical to that of members subjected axial compressive load as given in (8.10) through (8.14). When subjected to transverse load, deep webs may be susceptible to flexural buckling in the plane of the web due to the linearly distributed flexural stress along the web, and the vertical web of a WF or box beam may buckle in shear at locations of high shear forces. Bank (2005) provided formulas for web flexural buckling and web shear buckling, though no experimental evidences of these buckling modes were observed in common pultruded FRP structural members.

When the structural member is subjected to a concentrated transverse load, the web or flange segments may crush under the concentrated load. When global or local buckling is prevented, because of either small width-to-thickness ratio or the presence of stiffeners, the flexural member may fail due to compressive crushing or tensile rupture. In these cases, the critical crushing strength can be assumed to be equal to the compressive strength of the material in the web or flange, and the critical tensile strength can be assumed to be the tensile strength of the material in the web or flange. This assumption can also be used for analyzing shear failure in the flange and web, that is, the critical shear strength can be taken as the in-plane shear strength of the FRP material in the web or flange. For flange segments, the interlamina shear strength may be the critical shear strength. In this case, one may calculate the out-of-plane shear stress and compare it to the interlamina shear strength of the material (Bank 2005).

Combined Axial and Transverse Loads

When members are subjected to combined axial and transverse loads, such as combined compression–bending and tension–bending, a linear interaction between the axial and transverse load effects are assumed according to several available codes or manuals.

Vibration

The natural vibration frequencies of double symmetrical cross-sectional orthotropic FRP beams or columns are given in Table 8.6. The fundamental frequencies of beams with unsymmetrical cross section are given by the solution of the following equation (Kollár and Springer 2003):

$$\left\| \begin{bmatrix} \omega_z^2 & 0 & 0 \\ 0 & \omega_y^2 & 0 \\ 0 & 0 & \omega_\psi^2 \frac{\Theta}{\rho} \end{bmatrix} - \omega^2 \begin{bmatrix} 1 & 0 & -(z_G - z_{SC}) \\ 0 & 1 & (y_G - y_{SC}) \\ -(z_G - z_{SC}) & (y_G - y_{SC}) & \frac{\Theta}{\rho} \end{bmatrix} \right\| = 0 \tag{8.17}$$

where

ω_y, ω_z, ω_ψ are given in Table 8.6
y_{SC} and z_{SC} are the coordinates of the shear center
ρ is the mass per unit length
y_G and z_G are the coordinates of the center of mass
Θ is the polar moment of mass about the shear center

TABLE 8.6
Natural Frequencies of FRP Beams with Doubly Symmetrical Cross Sections

$$\frac{1}{w_i^2} = \frac{1}{\left(w_i^B\right)^2} + \frac{1}{\left(w_i^S\right)^2}$$

(i = 1, 2, 3, …, where i = 1 belongs to the First Mode)

BCs	No Shear Deformation $\left(w_i^B\right)^2 = \frac{\overline{EI}}{r}\left(\frac{m_{Bi}}{L}\right)^4$	No Bending Deformation $\left(w_i^S\right)^2 = \frac{\overline{S}}{r}\left(\frac{m_{Si}}{L}\right)^2$
Hinged–hinged	$\mu_{Bi} = i\pi$	$\mu_{Si} = \mu_{Gi} = i\pi$
Fixed–hinged	$\mu_{Bi} \approx (i + 0.25)\pi$	$\mu_{Si} = \mu_{Gi} = i\pi$
Fixed–fixed	$\mu_{B1} = 4.730$, $\mu_{Bi} \approx (i + 0.5)\pi$	$\mu_{Si} = \mu_{Gi} = i\pi$
Fixed–free	$\mu_{B1} = 1.875$, $\mu_{B2} = 4.694$ $\mu_{Bi} \approx (i - 0.5)\pi$	$\mu_{Si} = \mu_{Gi} \approx (i - 0.5)\pi$
Free–free	$\mu_{B1} = 4.730$, $\mu_{Bi} \approx (i + 0.5)\pi$	$\mu_{S1} = \mu_{G1} = 6.283$ $\mu_{S2} = \mu_{G2} = 8.987$ $\mu_{Si} = \mu_{Gi} \approx (i + 1)\pi$

Source: Revised from Table B.2, Kollár, L.P. and Springer, G.S., *Mechanics of Composite Structures*, Cambridge University Press, Cambridge, U.K., 2003.

For vibration in the x–z plane, $\omega_{yi} = \omega_i$, $\overline{EI} = \overline{EI}_{yy}$, and $\overline{S} = \overline{S}_{zz}$; for vibration in the x–y plane, $\omega_{zi} = \omega_i$, $\overline{EI} = \overline{EI}_{zz}$, and $\overline{S} = \overline{S}_{yy}$; for torsional vibration, $(\omega_{\psi i})^2 = \omega_i^2 + (\overline{GI}/\Theta)(\mu_{Gi}/L)^2$, $\overline{EI}/\rho = \overline{EI}_{\omega}/\Theta$, and $\overline{S}/\rho = \overline{S}\,\omega\omega/\Theta$.

ANALYSIS OF FRP PLATES AND PANELS

Introduction

In building and bridge structures, multicellular panels, sandwich plates, and grating panels made with FRP composite material are often used. A plate or panel member is primarily used to resist transverse load. Due to constrains on their boundaries, in-plane and torsional loads can also be present. FRP plate or panel members for civil engineering applications often have unidirectional or cross-ply fiber architecture, especially when the members are produced through the pultrusion process. Therefore, most structural components can be considered as orthotropic. In most cases, bending–extension coupling is undesirable in the design and construction. Therefore, the contribution from bending–extension coupling coefficients B_{ij} can be neglected in structural analysis, that is, we can set $B_{ij} = 0$ when applying laminated plate theories (Reddy 2004).

The analysis of orthotropic FRP plate and panel members can be classified into the analysis of two basic types depending on the bending–twisting coupling coefficients. The first type is referred as *specially orthotropic*, whose global coordinate axes are in coincidence with their principal orthotropic material axes and no bending–twisting coupling exist (i.e., $D_{12} = D_{16} = 0$). The second type can be referred as *generally orthotropic*, where $B_{ij} = 0$ but $D_{12} \neq$, $D_{16} \neq 0$. Most plates and panels (including multicellular FRP panels) for civil engineering applications fall into the first type.

In CLPT, the transverse normal and shear stresses are neglected. The stress field in CLPT is sufficiently accurate for homogeneous and thin plates, but not accurate when plates are relatively thick,

that is, the side-to-thickness ratio $a/h \leq 20$, where h is the plate thickness and a is the minimum in-plane dimension (width or length). For relatively thick plates or panels, it is necessary to use FSDT. Both CLPT and FSDT assume a plate is in a plane-stress state.

The design of FRP structural members is driven by stiffness and serviceability limit states; therefore, the global behavior of FRP members is of primary interest. When detailed local stress and strength analysis is required, numerical efforts through finite element analysis (FEA) can be used.

Analysis of FRP Plates

The analysis of FRP plates presented in this section is based on CLPT, and interested readers can find related information on analysis of FRP plates using FSDT in Reddy (2004). We introduce a single-layer, specially orthotropic FRP plate, with the coordinate system shown in Figure 8.3. The thickness of the plate is h.

Bending of FRP Plates

The governing equation for the static bending of a rectangular, specially orthotropic plate in the absence of hygrothermal effects and in-plane forces, can be expressed as

$$D_{xx}\frac{\partial^4 w_0}{\partial x^4} + 2(D_{xy} + 2D_{66})\frac{\partial^4 w_0}{\partial x^2 \partial y^2} + D_{yy}\frac{\partial^4 w_0}{\partial y^4} = q(x,y) \tag{8.18}$$

where

w_0 is the bending deflection

$q(x,y)$ is the applied transverse load

Q_{ij} are the plane-stress-reduced stiffnesses of the specially orthotropic plate; they are given in terms of the engineering constants (moduli and Poisson's ratios) as

$$Q_{xx} = \frac{E_x}{1-\nu_{xy}\nu_{xy}} \quad Q_{yy} = \frac{E_y}{1-\nu_{xy}\nu_{yx}} \quad Q_{xy} = \nu_{yx}Q_{xx} = \nu_{xy}Q_{yy} \quad Q_{66} = G_{xy} \tag{8.19}$$

Therefore, four independent material properties are required for the bending analysis of specially orthotropic plates using CLPT: E_x, E_y, G_{xy}, and ν_{xy} ($\nu_{xy}/\nu_{yx} = E_x/E_y$ for orthotropic materials). The procedure to obtain the solution to (8.18) depends on the BCs (Reddy 2004).

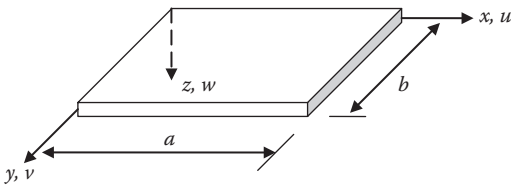

FIGURE 8.3 Coordinates for bending analysis of laminated FRP plates.

Simply Supported FRP Plates

When all the four edges are SS, the solution for an $a \times b$ rectangular plate can be obtained using the Navier method (Lekhnitskii 1968; Reddy 2004), the transverse deflection at the midplane are given as

$$w_0(x,y) = \sum_{n=1}^{\infty}\sum_{m=1}^{\infty} \frac{Q_{mn}}{d_{mn}} \sin \alpha x \sin \beta y \tag{8.20}$$

where

$\alpha = m\pi/a$

$\beta = n\pi/b$

$d_{mn} = \pi^4 \left[(D_{xx} m^4 s^4 + 2(D_{xy} + 2D_{66}) m^2 n^2 s^2 + D_{yy} n^4 \right] / W^4$

$s = W/L$

the coefficients Q_{mn} varies according to loading types as given in Table 8.7

When the plate is subjected to a rectangular patch load q_0, that is, a uniformly distributed load on a $2c \times 2d$ (where c parallel to x-axis and d parallel to y-axis) central rectangular loading patch centered at ($x_0 = L/2$, $y_0 = W/2$),

$$w_0(x,y) = \frac{16q_0}{\pi^2} \sum_{n=1}^{\infty}\sum_{m=1}^{\infty} \frac{1}{mnd_{mn}} \cdot \sin\frac{m\pi x}{L} \cdot \sin\frac{n\pi y}{W} \cdot \sin\frac{m\pi x_0}{L} \cdot \sin\frac{n\pi y_0}{W} \cdot \sin\frac{m\pi c}{L} \cdot \sin\frac{n\pi d}{W} \tag{8.21}$$

The bending moment can be calculated as

$$M_x = \sum_{n=1}^{\infty}\sum_{m=1}^{\infty} (D_{11}\alpha^2 + D_{12}\beta^2) W_{mn} \sin\frac{m\pi x}{a} \sin\frac{n\pi y}{b} \tag{8.22a}$$

TABLE 8.7
Coefficients for Calculating Transverse Deflections of SS FRP Plates

Load $q(x,y)$	Coefficients Q_{mn}
Uniformly distributed load $q = -q_0$	$Q_{mn} = -\dfrac{16q_0}{\pi^2 mn}$ $(m,n = 1,3,5,\ldots)$
Point load $q(x, y) = -Q_0$ at (x_0, y_0)	$Q_{mn} = -\dfrac{4Q_0}{ab} \sin\dfrac{m\pi x_0}{a} \sin\dfrac{n\pi y_0}{b}$ $(m,n = 1,2,3,\ldots)$
Line load $q(x, y) = -q_0$ at $y = y_0$	$Q_{mn} = -\dfrac{4q_0}{\pi bm} \sin\dfrac{n\pi y_0}{b}$ $(m,n = 1,2,3,\ldots)$
Hydrostatic load $q(x,y) = -q_0 \dfrac{y}{b}$	$Q_{mn} = -\dfrac{8q_0}{\pi^2 mn} \cos n\pi$ $(m,n = 1,3,5,\ldots)$

Source: Revised from Table 7.2-1, Reddy, J.N., *Mechanics of Laminated Composite Plates: Theory and Analysis*, 2nd edn., CRC Press, Boca Raton, FL, 2004.

$$M_y = \sum_{n=1}^{\infty}\sum_{m=1}^{\infty}(D_{12}\alpha^2 + D_{22}\beta^2)W_{mn}\sin\frac{m\pi x}{a}\sin\frac{n\pi y}{b} \tag{8.22b}$$

$$M_{xy} = -2\sum_{n=1}^{\infty}\sum_{m=1}^{\infty}\alpha\beta D_{66}W_{mn}\cos\frac{m\pi x}{a}\cos\frac{n\pi y}{b} \tag{8.22c}$$

The in-plane stresses for the kth layer of the laminated plate can be computed as

$$\begin{Bmatrix}\sigma_x\\ \sigma_y\\ \tau_{xy}\end{Bmatrix}^{(k)} = -z\begin{bmatrix}\bar{Q}_{11} & \bar{Q}_{12} & 0\\ \bar{Q}_{12} & \bar{Q}_{22} & 0\\ 0 & 0 & \bar{Q}_{66}\end{bmatrix}^{(k)}\begin{Bmatrix}\dfrac{\partial^2 w_0}{\partial x^2}\\ \dfrac{\partial^2 w_0}{\partial y^2}\\ 2\dfrac{\partial^2 w_0}{\partial x\partial y}\end{Bmatrix} = z\sum_{n=1}^{\infty}\sum_{m=1}^{\infty}\begin{Bmatrix}\left(\bar{Q}_{11}^{(k)}\alpha^2 + \bar{Q}_{12}^{(k)}\beta^2\right)\sin\dfrac{m\pi x}{a}\sin\dfrac{n\pi y}{b}\\ \left(\bar{Q}_{12}^{(k)}\alpha^2 + \bar{Q}_{22}^{(k)}\beta^2\right)\sin\dfrac{m\pi x}{a}\sin\dfrac{n\pi y}{b}\\ -2\alpha\beta\bar{Q}_{66}^{(k)}\cos\dfrac{m\pi x}{a}\cos\dfrac{n\pi y}{b}\end{Bmatrix} \tag{8.23}$$

The maximum normal stresses occur at $(x, y, z) = (a/2, b/2, h/2)$, and the shear stress is maximum at $(x, y, z) = (a, b, -h/2)$.

The interlaminar stresses are identically zero when computed from the constitutive equations in CLPT. However, they can be calculated using 3-D stress-equilibrium equations. For any $-h/2 \le z \le z_{k+1}$, after introducing the stress BCs and considering the continuity of stresses at layer interfaces, we have

$$\begin{Bmatrix}\tau_{xz}\\ \tau_{yz}\\ \sigma_{zz}\end{Bmatrix}^{(k)} = -\begin{Bmatrix}X(z)\displaystyle\sum_{n=1}^{\infty}\sum_{m=1}^{\infty}T_{12}^{(k)}W_{mn}\cos\frac{m\pi x}{a}\sin\frac{n\pi y}{b}\\ Y(z)\displaystyle\sum_{n=1}^{\infty}\sum_{m=1}^{\infty}T_{13}^{(k)}W_{mn}\sin\frac{m\pi x}{a}\cos\frac{n\pi y}{b}\\ Z(z)\displaystyle\sum_{n=1}^{\infty}\sum_{m=1}^{\infty}T_{33}^{(k)}W_{mn}\sin\frac{m\pi x}{a}\sin\frac{n\pi y}{b}\end{Bmatrix} \tag{8.24a}$$

where

$$X(z) = Y(z) = \left(\frac{z^2 - z_k^2}{2}\right)\quad Z(z) = \left[-\frac{h^3}{24} + \frac{z}{6}\left(z^2 - 3z_k^2\right)\right] \tag{8.24b}$$

$$T_{12}^{(k)} = \alpha^3\bar{Q}_{11}^{(k)} + \alpha\beta^2\left(2\bar{Q}_{66}^{(k)} + \bar{Q}_{12}^{(k)}\right),\quad T_{13}^{(k)} = \beta^3\bar{Q}_{22}^{(k)} + \alpha^2\beta\left(2\bar{Q}_{66}^{(k)} + \bar{Q}_{12}^{(k)}\right),$$

$$T_{33}^{(k)} = \alpha T_{12}^{(k)} + \beta T_{13}^{(k)} \tag{8.24c}$$

For single-layer plates, the expression in (8.24a) can be simplified to

$$\begin{Bmatrix}\tau_{xz}\\ \tau_{yz}\\ \sigma_{zz}\end{Bmatrix}=\begin{Bmatrix}\dfrac{h^2}{8}\left[1-\left(\dfrac{2z}{h}\right)^2\right]\displaystyle\sum_{n=1}^{\infty}\sum_{m=1}^{\infty}T_{12}^{(1)}W_{mn}\cos\dfrac{m\pi x}{a}\sin\dfrac{n\pi y}{b}\\ \dfrac{h^2}{8}\left[1-\left(\dfrac{2z}{h}\right)^2\right]\displaystyle\sum_{n=1}^{\infty}\sum_{m=1}^{\infty}T_{13}^{(1)}W_{mn}\sin\dfrac{m\pi x}{a}\cos\dfrac{n\pi y}{b}\\ -\dfrac{h^3}{48}\left\{\left[1+\left(\dfrac{2z}{h}\right)^3\right]-3\left(1+\dfrac{2z}{h}\right)\right\}\displaystyle\sum_{n=1}^{\infty}\sum_{m=1}^{\infty}T_{33}^{(1)}W_{mn}\sin\dfrac{m\pi x}{a}\sin\dfrac{n\pi y}{b}\end{Bmatrix} \tag{8.24d}$$

In integrating the stress-equilibrium equations, it is assumed that the stresses (τ_{xz}, τ_{yz}, σ_{zz}) are zero at the bottom surface of the plate ($z = -h/2$). Because of the assumptions of the laminate plate theory, they will also be zero at $z = h/2$. The transverse shear stress τ_{xz} is the maximum at (x, y, z) = (0, $b/2$, 0), τ_{yz} is the maximum at (x, y, z) = ($a/2$, 0, 0), and the transverse normal stress σ_{zz} is maximum at (x, y, z) = ($a/2$, $b/2$, $h/2$).

Other Types of Boundary Conditions

Plates with two opposite edges SS and the other two edges having arbitrary BCs can be solved using the Levy method (Reddy 2004). The solution to the problem that satisfies SS BCs on edges $y = 0$, W can be represented as

$$w_0(x,y)=\sum_{n=1}^{\infty}W_n(x)\cdot\sin\left(\frac{n\pi y}{W}\right) \tag{8.25}$$

where

$W_n(x) = W_n^h(x) + W_n^p(x)$

$W_n^h(x)$ is the homogeneous solution

$W_n^p(x)$ is the particular solution

The particular solution $W_n^p(x)$ can be determined by expanding the solution and the load as Fourier series. The homogeneous part can be determined as the following:

a. $(D_{xy}+2D_{66})^2 > D_{xx}D_{yy}$: $W_n^h(x)=A_n\cosh\lambda_1 x+B_n\sinh\lambda_1 x+C_n\cosh\lambda_2 x+D_n\sinh\lambda_2 x$

$$\lambda_{1,2}^2=\beta^2\left[(D_{xy}+2D_{66})\pm\sqrt{(D_{xy}+2D_{66})^2-D_{xx}D_{yy}}\right]/D_{xx}$$

b. $(D_{xy}+2D_{66})^2 = D_{xx}D_{yy}$ (isotropic plates): $W_n^h(x)=(A_n+B_n x)\cosh\lambda x+(C_n+D_n x)\sinh\lambda x$

c. $(D_{xy}+2D_{66})^2 < D_{xx}D_{yy}$: $W_n^h(x)=(A_n\cos\lambda_2 x+B_n\sin\lambda_2 x)\cosh\lambda_1 x+(C_n\cos\lambda_2 x+D_n\sin\lambda_2 x)\sinh\lambda_1 x$

$$(\lambda_{1,2})^2=\beta^2\left[\sqrt{D_X^e D_Y^e}\pm\left(D_{XY}^e+2D_{TT}^e\right)\right]\Big/2D_X^e$$

The constants A_n, B_n, C_n, and D_n are determined from the BCs at the other two edges of the plate. Reddy (2004) provides example calculations for the constants A_n, B_n, C_n, and D_n. Detailed and complete calculations for the constants with case (a) and case (c) for all Levy plates were given in Reddy (1999).

There are several other cases of BCs not covered in the solutions provided. For these plates, approximate methods should be used to find solutions, such as the Rayleigh–Ritz Method (Zhou 2002; Reddy 2004).

Buckling and Vibration of FRP Plates

We assume a plate subjected to in-plane compressive forces ($N_{xx} < 0$, $N_{yy} < 0$), and all other mechanical and hygrothermal loads are zero. The equation governing the buckling deflection can be expressed as

$$D_{xx}\frac{\partial^4 w_0}{\partial x^4} + 2(D_{xy} + 2D_{66})\frac{\partial^4 w_0}{\partial x^2 \partial y^2} + D_{yy}\frac{\partial^4 w_0}{\partial y^4} = N_{xx}\frac{\partial^2 w_0}{\partial x^2} + N_{yy}\frac{\partial^2 w_0}{\partial y^2} \tag{8.26a}$$

We denote

$$N_{xx} = -N_0, \quad N_{yy} = -kN_0, \quad k = \frac{N_{yy}}{N_{xx}} \tag{8.26b}$$

When all the edges are SS, we have

$$N_0(m,n) = \frac{d_{mn}}{(\alpha^2 + k\beta^2)} \tag{8.27}$$

where

$\alpha = m\pi/a$

$\beta = n\pi/b$

$d_{mn} = D_{xx}\alpha^4 + 2(D_{xy} + 2D_{66})\alpha^2\beta^2 + D_{yy}\beta^4$

For each choice of m and n, there corresponds a unique value of N_0. The critical buckling load is the smallest of $N_0(m,n)$.

The governing equation for natural vibration of SS specially orthotropic FRP plates is

$$D_{xx}\frac{\partial^4 w_0}{\partial x^4} + 2(D_{xy} + 2D_{66})\frac{\partial^4 w_0}{\partial x^2 \partial y^2} + D_{yy}\frac{\partial^4 w_0}{\partial y^4} + I_0\ddot{w}_0 - I_2\left(\frac{\partial^2 \ddot{w}_0}{\partial x^2} + \frac{\partial^2 \ddot{w}_0}{\partial y^2}\right) = 0 \tag{8.28}$$

where

I_0 and I_2 are the mass moments of inertia

$I_0 = \int_{-h/2}^{h/2} \rho dz$

$I_2 = \int_{-h/2}^{h/2} z^2 \rho dz$

ρ is the density

I_2 is called the rotary inertia, which is neglected in most books, and can contribute to higher-order vibrations (Reddy 2004). The frequency of natural vibration ω can be obtained as

$$\omega_{mn}^2 = \frac{\pi^4}{\hat{I}_0 b^4}\left[D_{xx}m^4\left(\frac{b}{a}\right)^4 + 2(D_{xy} + 2D_{66})m^2n^2\left(\frac{b}{a}\right)^2 + D_{yy}n^4\right] \tag{8.29a}$$

where $\hat{I}_0 = I_0 + I_2[(m\pi/a)^2 + (n\pi/b)^2]$. For different values of m and n, there corresponds a unique frequency and a corresponding mode shape. The rotary inertia I_2 has the effect of reducing the frequency. When it is not zero, it is not simple to find the lowest natural frequency. When it is neglected, the fundamental frequency of a rectangular specially orthotropic plate is

$$\omega_{mn}^2 = \frac{\pi^4}{I_0 b^4}\left[D_{xx}m^4\left(\frac{b}{a}\right)^4 + 2(D_{xy} + 2D_{66})m^2n^2\left(\frac{b}{a}\right)^2 + D_{yy}n^4\right] \tag{8.29b}$$

The buckling and vibration analysis for other types of BCs is more complicated than SS plates. When two parallel edges are SS, the Lévy method can be used (Reddy 2004). For other combination of BCs on the edges, one may use the Rayleigh–Ritz method with similar approximation functions as for bending analysis (Reddy 2004). The solutions for buckling and vibration analyses of SS FRP plates provide conservative design.

Analysis of FRP Panels

Most FRP panels for civil engineering applications have relatively thick multicellular or sandwiched cores. The side-to-thickness ratios range from 5 to 10. In experiments, significant local deformation at locations adjacent to concentrated loads was observed. The structural analysis of these panels is not as simple as single-layer orthotropic plates. Several possible methodologies are available for the analysis of multicellular or sandwiched FRP panels: 2-D equivalent plate modeling, 3-D equivalent continuum modeling, and 3-D detailed modeling through FEA.

The 2-D equivalent plate methods are based on the method of elastic equivalence (MEE). These methods include ESL plate modeling (Aref et al. 2001) and discrete multilayer (DML) modeling (Davalos et al. 2001). The ESL method is a global approximation model that considers the multicellular or sandwich panels as ESL orthotropic plates. The analysis of the ESL plates is performed by using ESL laminated plate theories such as CLPT or FSDT. Single-layer 2-D equivalent plate is the easiest and can provide adequate accuracy for global analysis such as bending, buckling, and vibration. In DML modeling, a multicellular or sandwich panel is divided into three (or more) layers, and piecewise approximations are made in the through-thickness direction in each layer. The core and face sheets can be treated as individual layers (or divided into more layers), and ESL plate theories are then applied to each layer (Davalos et al. 2001).

In 3-D equivalent continuum modeling, a panel's core and face sheets are replaced by equivalent 3-D homogeneous continua. Numerical methods such as FEA are often used to obtain solutions (Davalos et al. 2001). In 3-D detailed modeling, the actual geometry of the multicellular or sandwich core and the face sheet layers can be considered (Zhou 2002; Chiewanichakorn et al. 2003). With the help of layered composite element modeling, 3-D detailed modeling can give information about the layer-wise response in each component (Zhou 2002).

HYGROTHERMAL EFFECTS

In FRP composites, temperature and moisture concentrations can cause change of material state and may reduce the material's strength, and stiffness, therefore, should be investigated. Hygrothermal elasticity deals with the effects of temperature and moisture on the mechanical behavior of the material. In hygrothermal elasticity, the moisture concentration problem is mathematically similar to the heat transfer problem in thermoelasticity. When considering the effects of temperature and

moisture on the mechanical behavior of FRP composites, the principle of linear superposition is often applied to obtain the total strain $\{\varepsilon\}$ in the material as

$$\{\varepsilon\} = [\bar{S}]\{\sigma\} + \{\varepsilon^{ht}\} \quad \text{and} \quad \{\varepsilon^{ht}\} = \{\bar{\alpha}\}(T - T_0) + \{\bar{\beta}\}(c - c_0) \tag{8.30}$$

where

$\{\varepsilon^{ht}\}$ is the vector of strains in an unrestrained composite by uniform temperature and moisture distribution (or vector of hygrothermal strains)
$\{\bar{\alpha}\}$ is the vector of coefficients of thermal expansion
$\{\bar{\beta}\}$ is the vector of coefficients of hygroscopic expansion
T_0 and c_0 are reference values from which the strains and stresses are measured

In the global coordinate system, the strain–stress relationships considering hygrothermal effects of a generally anisotropic material can be expressed as

$$\begin{Bmatrix} \varepsilon_x \\ \varepsilon_y \\ \varepsilon_z \\ \gamma_{yz} \\ \gamma_{xz} \\ \gamma_{xy} \end{Bmatrix} = \begin{bmatrix} \bar{S}_{11} & \bar{S}_{12} & \bar{S}_{13} & \bar{S}_{14} & \bar{S}_{15} & \bar{S}_{16} \\ \bar{S}_{21} & \bar{S}_{22} & \bar{S}_{23} & \bar{S}_{24} & \bar{S}_{25} & \bar{S}_{26} \\ \bar{S}_{31} & \bar{S}_{32} & \bar{S}_{33} & \bar{S}_{34} & \bar{S}_{35} & \bar{S}_{36} \\ \bar{S}_{41} & \bar{S}_{42} & \bar{S}_{43} & \bar{S}_{44} & \bar{S}_{45} & \bar{S}_{46} \\ \bar{S}_{51} & \bar{S}_{52} & \bar{S}_{53} & \bar{S}_{54} & \bar{S}_{55} & \bar{S}_{56} \\ \bar{S}_{61} & \bar{S}_{62} & \bar{S}_{63} & \bar{S}_{64} & \bar{S}_{65} & \bar{S}_{66} \end{bmatrix} \begin{Bmatrix} \sigma_x \\ \sigma_y \\ \sigma_z \\ \tau_{yz} \\ \tau_{xz} \\ \tau_{xy} \end{Bmatrix} + \begin{Bmatrix} \varepsilon_x^{ht} \\ \varepsilon_y^{ht} \\ \varepsilon_z^{ht} \\ \gamma_{yz}^{ht} \\ \gamma_{xz}^{ht} \\ \gamma_{xy}^{ht} \end{Bmatrix} \square \quad \square\square$$

$$\begin{Bmatrix} \varepsilon_x^{ht} \\ \varepsilon_y^{ht} \\ \varepsilon_z^{ht} \\ \gamma_{yz}^{ht} \\ \gamma_{xz}^{ht} \\ \gamma_{xy}^{ht} \end{Bmatrix} = \begin{Bmatrix} \bar{\alpha}_x \\ \bar{\alpha}_y \\ \bar{\alpha}_z \\ \bar{\alpha}_{yz} \\ \bar{\alpha}_{xz} \\ \bar{\alpha}_{xy} \end{Bmatrix} \square\square - \square\square \boxplus \begin{Bmatrix} \bar{\beta}_x \\ \bar{\beta}_y \\ \bar{\beta}_z \\ \bar{\beta}_{yz} \\ \bar{\beta}_{xz} \\ \bar{\beta}_{xy} \end{Bmatrix} \square\square - \square\square \square \tag{8.31}$$

The stress–strain relationship can be obtained by inversing the aforementioned equation. To consider hygrothermal effects through CLPT, we have

$$\begin{Bmatrix} \{N\} \\ \{M\} \end{Bmatrix} = \begin{bmatrix} [A] & [B] \\ [B] & [D] \end{bmatrix} \begin{Bmatrix} \{\varepsilon^0\} \\ \{\kappa\} \end{Bmatrix} - \begin{Bmatrix} \{N^{ht}\} \\ \{M^{ht}\} \end{Bmatrix} \tag{8.32}$$

where $\{N^{ht}\}$ and $\{M^{ht}\}$ are hygrothermal force resultants

$$\{N^{ht}\} = \sum_{k=1}^{n} \int_{z_k}^{z_{k+1}} [\bar{Q}]^{(k)} \{\bar{\alpha}\}^{(k)} \Delta T dz + \sum_{k=1}^{n} \int_{z_k}^{z_{k+1}} [\bar{Q}]^{(k)} \{\bar{\beta}\}^{(k)} \Delta c dz \tag{8.33a}$$

$$\{M^{ht}\} = \sum_{k=1}^{n} \int_{z_k}^{z_{k+1}} [\bar{Q}]^{(k)} \{\bar{\alpha}\}^{(k)} \Delta T \cdot z dz + \sum_{k=1}^{n} \int_{z_k}^{z_{k+1}} [\bar{Q}]^{(k)} \{\bar{\beta}\}^{(k)} \Delta c \cdot z dz \tag{8.33b}$$

and $[\bar{Q}](k)$ are transferred reduced stiffnesses and $\{\bar{\alpha}\}(k)$ are transferred thermal coefficients, with the assumption that temperature and moisture increment varies linearly, consistent with the mechanical strains:

$$\Delta T = T^0(x,y,t) + z \cdot T^1(x,y,t) \quad \text{and} \quad \Delta c = c^0(x,y,t) + z \cdot c^1(x,y,t) \tag{8.34}$$

and the strains in one layer including thermal strains are in the form of

$$\{\varepsilon^0\} = \begin{Bmatrix} \varepsilon_x^0 - \varepsilon_x^{ht0} \\ \varepsilon_y^0 - \varepsilon_y^{ht0} \\ \gamma_{xy}^0 - 2\gamma_{xy}^{ht0} \end{Bmatrix}, \quad \{\kappa\} = \begin{Bmatrix} \kappa_x - \varepsilon_x^{ht1} \\ \kappa_y - \varepsilon_y^{ht1} \\ \kappa_{xy} - 2\gamma_{xy}^{ht1} \end{Bmatrix} \tag{8.35}$$

STRENGTH OF FRP STRUCTURAL MEMBERS: LARGE-SCALE FRP STRUCTURES

The strength of laminated fiber-reinforced composite materials is usually analyzed on the basis of several hypotheses: (1) linear elastic behavior to failure occurs for individual laminae, (2) strengths and stiffnesses of the laminae are the same in tension as in compression, and (3) a certain criterion governs failure of a lamina. A detailed strength analysis of laminated FRP structural members requires the determination of local stresses and strains in the laminae. During the design process, a simplified strength analysis can be carried out by assuming equivalent orthotropic properties of FRP structural members and using appropriate failure criterion for orthotropic materials, such as the maximum stress criterion or maximum strain criterion in different material directions.

For the analysis of large-scale structures made of FRP materials, such as a bridge superstructure, one may choose simplified equivalent method or detailed finite element method (FEM) depending on practical requirements of the analysis. The simplified equivalent method treats the large-scale FRP structures as equivalent orthotropic structures. This method, however, only applies to limited cases when the FRP structures have regular structural shapes so that they can be simplified as equivalent beams or plates and local effects on structural behavior (such as local buckling) are negligible. When using FEM, no geometry limitations exist. Many commercially available FEM programs also support analysis using layered composite elements, and strength analysis can be performed using different failure criteria in the FEM software.

REFERENCES

Aref, A. J., S. Alampalli et al. (2001). Ritz-based static analysis method for fiber reinforced plastic rib core skew bridge superstructure. *Journal of Engineering Mechanics-ASCE* 127(5): 450–458.

Bank, L. C. (2005). Fiber-reinforced polymer composites. In *Handbook of Structural Engineering*. W. F. Chen and E. M. Lui (eds.). Boca Raton, FL: CRC Press, pp. 16-1–16-8.

Bank, L. C., J. S. Yin et al. (1995). Local buckling of pultruded beams—Nonlinearity, anisotropy and inhomogeneity. *Construction and Building Materials* 9(6): 325–331.

Chiewanichakorn, M., A. J. Aref et al. (2003). Failure analysis of fiber-reinforced polymer bridge deck system. *Journal of Composites, Technology and Research* 25(2): 121–129.

Clarke, J. L. (1996). *Structural Design of Polymer Composites: Eurocomp Design Code and Handbook*. London, U.K.: E & FN Spon.

Davalos, J. F., P. Qiao et al. (2001). Modeling and characterization of fiber-reinforced plastic honeycomb sandwich panels for highway bridge applications. *Composite Structures* 52(3–4): 441–452.

Hyer, M. W. (1998). *Stress Analysis of Fiber-Reinforced Composite Materials*. Boston, MA: McGraw-Hill.

Jones, R. M. (1999). *Mechanics of Composite Materials*. Philadelphia, PA: Taylor & Francis Group.

Kollár, L. P. and G. S. Springer. (2003). *Mechanics of Composite Structures*. Cambridge, U.K.: Cambridge, University Press.

Lekhnitskii, S. G. (1968). *Anisotropic Plates*. New York, NY: Gordon and Breach.

Reddy, J. N. (1999). *Theory and Analysis of Elastic Plates*. Philadelphia, PA: Taylor & Francis Group.

Reddy, J. N. (2004). *Mechanics of Laminated Composite Plates: Theory and Analysis* (2nd edn.). Boca Raton, FL: CRC Press.

Zhou, A. (2002). Stiffness and strength of fiber reinforced polymer composite bridge deck systems. Dissertation for PhD, Department of Engineering Science and Mechanics, Virginia Polytechnic Institute and State University, Blacksburg, VA, 233 pp.

Zureick, A. and D. Scott. (1997). Short-term behavior and design of fiber-reinforced polymeric slender members under axial compression. *Journal of Composites for Construction-ASCE* 1(4): 140–149.

Zureick, A. and R. Steffen. (2000). Behavior and design of concentrically loaded pultruded angle struts. *Journal of Structural Engineering-ASCE* 126(3): 406–416.

9 Deck Panels and Girders for Bridge Applications

Lijuan "Dawn" Cheng and Lei Zhao

CONTENTS

ALL-COMPOSITE PANELS FOR BRIDGE DECK APPLICATIONS

Development of bridge decks fabricated entirely from polymer matrix composites has been largely motivated by the modular concept for rapid construction and durability considerations. All-composite panels have shown good potential in bridge deck replacements as well as in new bridge constructions. Their advantages comparing to decks of conventional materials such as reinforced concrete include lightweight, high strength, corrosion resistance, and rapid installation. Many all-composite deck systems are currently available, such as Superdeck, EZ-Span, DuraSpan, Hardcore, Kansas, ASSET, ZellComp, ACCS, X-shaped filament wound, cell core truss, and corrugated-core sandwich systems (Cheng and Karbhari 2006; Hollaway 2010).

Advantages and Challenges

Lightweight: A fiber reinforced polymer (FRP) deck panel typically weighs approximately 20% of a normal weight reinforced concrete deck. A lighter new deck translates to additional load-carrying capacity for the bridge in cases of deck replacement. This advantage could be significant in long span bridges, in which designs are typically governed by dead load, or moveable bridges, which are weight critical.

Corrosion resistance: While most bridges in the United States are typically designed for 75 years, certain portions of the bridges sometimes last significantly shorter. Decks in cold and coastal regions, where chemicals from road salt and seawater are common, have a severe corrosion problem in the steel reinforcement. In some extreme cases, bridge decks have to be replaced every 10 years

due to corrosion. FRP composites have been proven to not corrode, thus has the potential of extending the service life of the bridge.

High strength: Glass FRP (GFRP) used in most composite decks have tensile strengths that are much higher than that of steel and concrete, while its modulus of elasticity is much lower than that of steel but comparable to concrete. Most FRP decks are softer than steel and concrete decks. As a result, most FRP deck designs are stiffness-controlled and typically have significant factors of safety.

Rapid installation: Due to the modular and prefabricated nature of these decks, FRP deck panels can be installed very rapidly, which leads to reduced construction costs and minimal disruption to public traffic.

Challenges: In spite of the attractive features, FRP composite deck panels have their challenges in order to enter the mainstream construction market. The largest challenge is the cost, which is still at least two to three times more expensive than conventional decks. Although they have the potential of lowering the maintenance cost and extending the service life, so far this claim has not been substantiate by sufficient in-service records due to its short history and small number. In some cases, the higher initial costs of FRP decks can be absorbed, particularly when a complete reconstruction is necessary in the absence of a lightweight deck alternative (Bakis et al. 2002). One such example is the potential benefit of replacing damaged open steel grid decks in moveable bridges, which are less skid resistant when wet, damage prone, and expensive to maintain, with FRP decks (Zhao et al. 2006). Furthermore, the current "lowest bid" selection practice adopted in most public works project, not the life-cycle cost, has—to a large extent—hindered the use of FRP decks. In addition to that, the lack of service record on durability of FRP decks and a mature design guideline has also led to a slow adoption of this new technology. There is a need to develop universally accepted material specifications in a non-proprietary manner and design codes (Bakis et al. 2002).

Field Applications

Incremental progress has been made on implementing the FRP materials in deck replacement in many states across the country, some use funding assistance from the Federal Highway Administration through its past Innovative Bridge Research and Construction (IBRC) and the current Innovative Bridge Research and Deployment (IBRD) programs (FHWA 2011a). The all-composite deck systems have been installed in more than a hundred bridges in the field within the United States and around the world (ACMA 2004; FHWA 2011b; Pawel 2011). To name a few, the 1999 Troutville Weigh Station Bridge in Virginia using Strongwell deck, the 1998 Laurel Run Road Bridge in Pennsylvania using Superdeck, the 1999 Salem Ave Bridge in Ohio using Kansas deck, the 2001 Mill Creek Bridge in Delaware using Hardcore deck, and more recently, the 2010 Redstone Arsenal Bridge in Alabama, the 2010 Lunetten Footbridge in the Netherlands, and the 2011 Lleida Footbridge in Spain, etc. Many of these bridges are further instrumented for monitoring the long-term performance of the decks (e.g., Farhey 2004). Periodic field inspection is also recommended for FRP decks in order to collect the important in-service data and help the industrial partners to refine the technology. NCHRP Report 564 provides a detailed in-service inspection manual on field procedures, evaluation guidelines, and reporting standards (NCHRP 2006).

Manufacturing Processes

The typical manufacturing processes of composite panels for bridge deck applications can be divided into the following categories.

Wet layup: The wet layup process is typically labor intensive; quality control on the laminates is often more difficult. Laminates made with the wet layup process have low fiber content and high void

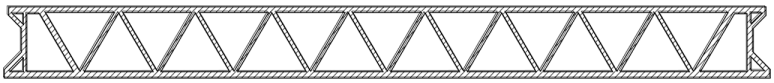

FIGURE 9.1 Deck panel by SCRIMP.

content. Creep and long-term deflection are often the concerns related to the wet layup process. A number of pedestrian bridges built with the wet layup process in the 1980s in China had to be later removed due to excessive creep in the FRP deck panels. On the other hand, the Miyun Bridge in China, which is the first FRP vehicular bridge in the world and made with the wet layup process, did not have creep problems after more than two decades in service (Keller 2003). Typically, wet layup is a useful method for prototyping; its suitability for use in practical bridge structures needs to be further examined.

Vacuum assisted resin transfer molding (*VARTM*): This process involves wrapping dry fabric around preshaped foam core and placing them together. A vacuum bag is then applied to the assembly, which is called "preform." Vacuum is drawn from one side of the bag while resin enters the preform from the other. An example of such construction is shown in Figure 9.1, where SCRIMP is for Seeman Composites Resin Infusion Molding Process, a patented VARTM variation with a highly permeable distribution medium incorporated as a surface layer on the preform. Triangular foam blocks are first individually wrapped with stitched glass fabric and then assembled into a preform of 4.5 m long, 2.4 m wide, and 0.2 m high. Additional fabric is added to the top and bottom flanges to build up additional sectional stiffness. The entire assembly is "bagged" and infused with resin. While this process has shown to produce good quality deck panels, many of which have been in service for more than a decade, quality control problems have been reported. In the Salem Ave Bridge project in Ohio, one of the four decks fabricated by this process showed significant delamination after only 2 months in service and had to be eventually removed, "most likely" due to that the large sizes of the FRP panels did not allow for full flow of resin into all the canals between the foam cores (Shahrooz et al. 2005).

Sandwich construction: Typical sandwich construction panels have two major components: (1) strong, stiff face sheets that carry flexural loads and (2) a low-density, bonded core material that separates the face sheets and ensures composite action of the deck. The design of the face sheet and core materials can be changed in manufacturing to meet various design requirements. E-glass mats and/or roving are commonly used in face sheets. Common core materials are rigid foams (Sopal et al. 2012; Wlasak 2012), thin-walled cellular or honeycomb GFRP (Davalos et al. 2001), filament-wound GFRP tubes (Williams et al. 2003), or corrugated GFRP with internal transverse diaphragms (Ji et al. 2010). Figure 9.2 illustrates some of these design concepts. Changes in details related to materials, orientations, and thickness of the FRP face sheets or core can be determined analytically (Shahawy 2003). While deck panels built with bonding face

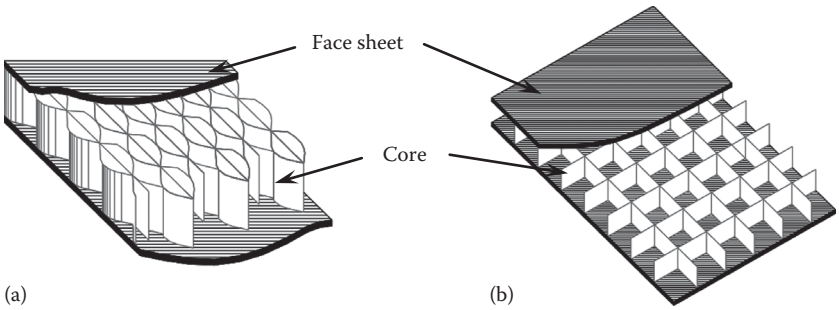

FIGURE 9.2 Examples of sandwich construction. (a) Honeycomb core panel and (b) truss (web) core panel. (Revised from Cheng, L., Steel-free bridge decks reinforced with FRP composites, in R. Jain and L. Lee (eds.), *Fiber Reinforced Polymer (FRP) Composites for Infrastructure Applications*, Springer, New York, 2012, pp. 143–162.)

sheets to corrugated cores have shown sufficient capacity in laboratory testing, their suitability for field installation, especially related to long-term performance, has not been proven. In the Salem Ave Bridge project in Ohio, one of the four decks made from such a sandwich construction with a corrugated core had significant delamination and had to be unfortunately removed, "most likely" due to "fabrication process of hand lay-up in conjunction with poor quality control" (Shahrooz et al. 2005).

Assembly of pultruded section: This is the most common type of all-composite panel construction that has been studied and in use (e.g., Superdeck, DuraSpan, and ASSET). The pultruded elements are typically easy and cheap to fabricate, and of good quality. They are then joined and added with top and/or bottom FRP plates with wet layup, adhesive bonding, mechanical fastening, or combinations thereof. Several examples of FRP deck panels made with this process are shown in Figure 9.3. The pultruded parts allow this type of deck panels to have high strength and stiffness in the longitudinal direction of the panels, consistent and high quality, reduced fabrication time, and relatively low cost due to reduced labor.

Most commercially available deck panels use adhesively bonded top and bottom face sheets to increase the strength and stiffness. The main advantage of such construction is that it allows for an efficient use of the materials in terms of providing the maximum stiffness. It also helps achieving a rapid on-site assembly of the system. However, it results in extra cost of bonding in addition to the pultrusion itself. Difficulty exists related to joining the deck panels to girders due to the top being closed, which also makes the in-service repair difficult. Some deck panel systems, such as that shown in Figure 9.3d, are made of a pultruded bottom panels with several I-sections. Panels are mechanically fastened to adjacent panels and to a top plate on site. The advantages of such designs include

- Low fabrication cost, since all parts are pultruded
- With an open top, grouting connections between the panels and the supporting beams becomes simplified
- In service, if damage occurs to the deck, typically in the top plate or web, the top plate could potentially be removed to allow for easy repair

On the other hand, their disadvantages are

- The need for substantial on-site drilling and mechanical fastening to join the various pieces together
- Durability concerns related to extensive drilling, which could open passages for moisture and salts to invade the laminates
- Stress concentration issues due to the holes, resulting in potential premature failure and high margins of safety in the design

The geometries of the core of the FRP panels have a significant impact on the transverse (perpendicular to the cells) force transfer and distribution. Trapezoidal cores such as Figure 9.3a and b and triangular cores provide good lateral force transfer; allowing a larger area of the panel to participate in load carrying. Rectangular cores such as Figure 9.3c and 3d, on the other hand, have very little capability of lateral force transfer and distribution. Note that a wheel load is primarily carried by the portion of the deck that is directly under the loading points. The designers need to be aware of this difference between decks of different web profiles and calculate deck deflections accordingly.

Properties

All-composite deck panels are made of FRP laminates. The stiffness properties of such laminates can be easily calculated using the Classical Lamination Theory (Jones 1999) or by material testing methods such as ASTM D3039 and ASTM D5379 (ASTM 2005). Analyses using the calculated

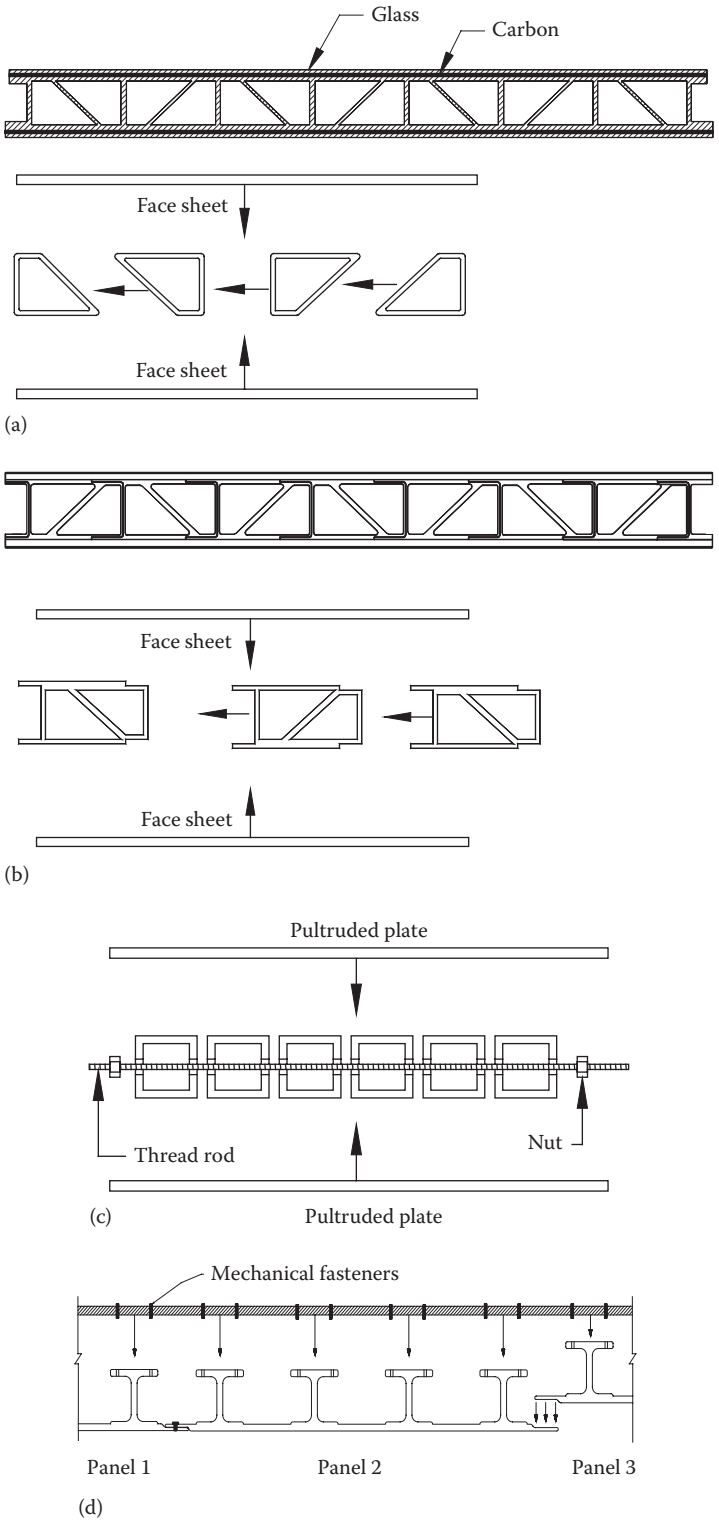

FIGURE 9.3 Assembly examples of pultruded shapes. (a) Lockheed Martin, (b) DuraSpan by Martin Marietta. (c) Virginia Tech by Strongwell (Photo from Strongwell, Bridge components—Fiber reinforced polymer composites), and (d) ZellComp.

stiffness value have been found to be accurate when compared with experiment results. It should be noted that the properties of FRP composite deck panels are highly orthotropic, i.e., the properties of the panels in the longitudinal and transverse directions are very different. The strong (and stiff) direction is typically in that of the cells of the panels.

The strength calculation shall follow the first-ply failure criteria, which assumes that failure of the laminate occurs at the onset of the first ply failure in the laminate. Stress concentration around cutouts in the laminates shall be carefully considered, and the nominal strength of the laminate shall be reduced accordingly (Zhao and Karbhari 2005). Due to limited validation of design equations, all new panel designs shall be experimentally validated, with specific attention paid to local buckling and joint failure.

In general, FRP deck panels have an excellent fatigue resistance with insignificant stiffness degradation. This is partially because most deck designs are stiffness-driven. As a result, fatigue load levels are typically less than 20% of the capacity of the deck panels. However, small fatigue cracking has been seen at the deck's free edges under real field traffic loading conditions. Some fatigue sensitivity has also been reported in negative moment region of the deck and adhesively bonded regions of the panel. The stiffness degradation of FRP decks is found to be more susceptible to the extreme temperatures in the environment than to the cumulative number of load cycles (Kwon et al. 2003). Whether or not the dynamic load allowance factors established for conventional bridges (AASHTO 2012) to all-composite FRP decks is still questionable. A small amount of creep is expected in some FRP decks, especially in parts made with wet layup and/or with low fiber volume contents. For vehicular bridges with FRP superstructures, there have not been reports of creep related problems.

Testing

Material testing: The ASTM Standards have specified procedures for testing FRP laminates for tension per ASTM D3039 (ASTM 2005) and short beam shear per ASTM D2344 (ASTM 2006). However, these tests are typically designed for laminates that are much thinner than those used in the final product of the FRP deck panels. In addition, geometry of the parts of the as-built panels may only allow coupons be made in the direction of pultrusion. The designer should require the deck supplier to provide test results from coupon tests done on the same or equivalent layup designs using the same manufacturing process.

The in-plane mechanical properties of FRP can be accurately calculated following the micromechanics and macromechanics in the Classical Lamination Theory if the fiber volume content is determined. The fiber volume content of glass FRP and carbon FRP (CFRP) can be determine use the burn-off test per ASTM D5630 (ASTM 2006) and the acid digestion test per ASTM D3171 (ASTM 2011), respectively. For GFRP pultruded profiles in structural applications, the European Standard BS EN 13706 (2002) provides more guidelines on testing methods and minimum requirement for technical properties such as strength and stiffness of structural profiles.

Structural testing: Substantial amount of testing has been performed on various FRP deck panel systems under various loading configurations (e.g., Davalos et al. 2001; Aref et al. 2005; Alagusundaramoorthy et al. 2006; Ji et al. 2010). All tests have shown that FRP deck panels typically have no difficulty achieving the AASHTO design loads, while the deflection of such deck panels usually governs the design. Unlike the ductile load-versus-deflection relations of conventional steel reinforced concrete decks, the load-versus-deflection relations of most FRP systems are linear elastic up to failure, after which the load drops significantly. Figure 9.4a illustrates such a comparison on the load-versus-deflection response of a simply supported reinforced concrete deck and that of a FRP deck. However, it has been reported that when a FRP deck is tested in a continuously supported condition, substantial deflection capacity could be developed after the initial load peak (Zhao et al. 2006). As shown in the curve in Figure 9.4b, a two-span continuous deck system has an initial load drop but then quickly regains the load capacity and eventually fails at approximately twice the deflection of that at the initial load drop.

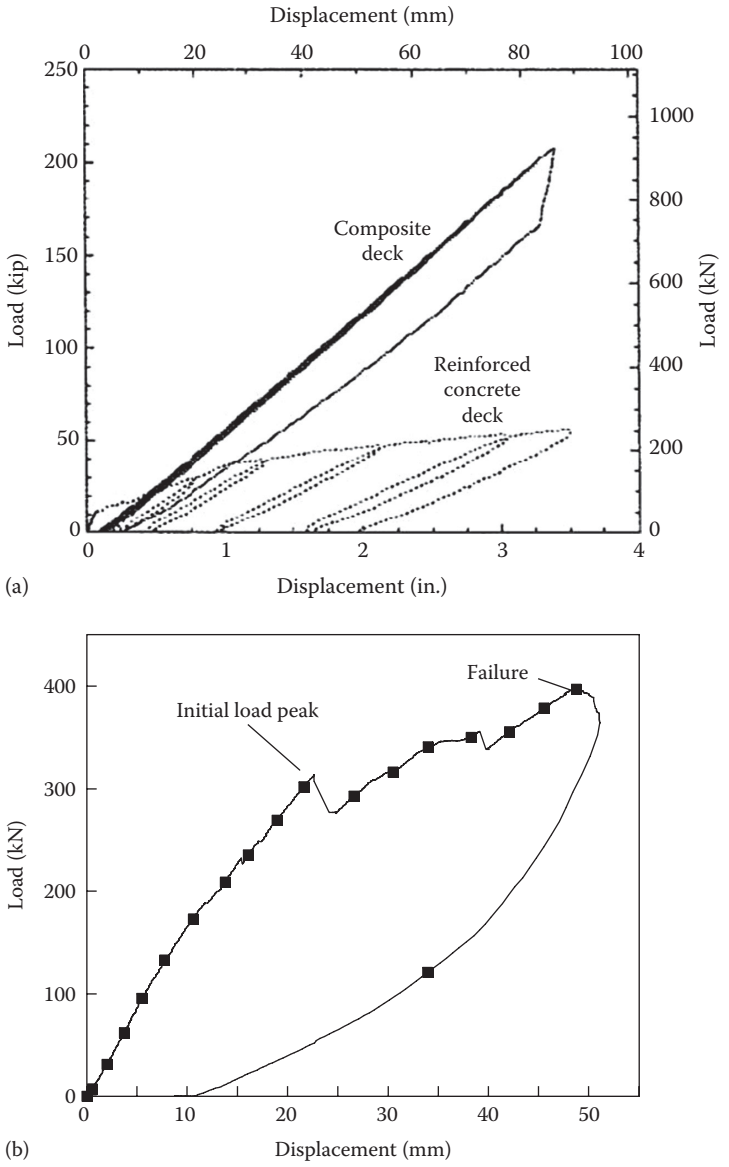

FIGURE 9.4 Load–displacement response of FRP decks. (a) Simply supported (linear elastic). (From Zhao, L. and Karbhari, V.M., Lightweight composite deck systems for renewal, *Engineering Mechanics: A Force for the 21st Century, ASCE 12th Engineering Mechanics Conferences Proceedings*, American Society of Civil Engineers, San Diego, CA, May 17–20, 1998. With permission.) (b) Continuous (some ductility). (From Zhao, L. et al., Testing of a FRP deck system for moveable bridges, *The Third International Conference on FRP Composites in Civil Engineering*, Miami, FL, December 13–15, 2006.)

Wear Surface on FRP Decks

Depending on the volume and characteristics of traffic, the needs for the type of wear surface on a FRP deck are different. In the case of highway bridges that are subjected to heavy traffic, asphalt, asphalt concrete, and resin-based polymer concrete have commonly been used. Earlier applications have shown problems with cracking in the wear surfaces, especially near the panel-to-panel joints. Studies sponsored by the New York DOT (Aboutaha 2005) and the Oregon DOT (Barquist et al. 2005) have reported problems on debonding and cracking. Among all the wear surfaces

systems examined in the studies, some bonded better with FRP, others had better wear resistance but did not bond as well. Workability and odor have also been concerns with some of the systems in both lab tests and field applications.

More testing and field monitoring is necessary for the low-maintenance potential of the FRP decks, which depends—to a large extent—on the durability of the wear surface. To avoid or minimize cracking in the wear surface, special detailing must be considered at the deck-to-deck and deck-to-abutment joints to accommodate nonuniform deflection at the joints. Due to the short history of using FRP decks, the performance of its wear surface has not been well documented. Before selecting a wear surface system, the user is strongly recommended to contact prior users for technical references.

Skew

Many highway bridge decks have a skewed configuration. FRP deck panels can be placed perpendicular to the longitudinal girders, in which case additional pieces will be needed to cover the triangular area near the approach, as shown in Figure 9.5a. This is also the case in a bridge in Maryland (Robert et al. 2002) and a research project (Aref et al. 2005). Another placement approach was experimented in a project in Florida (Zhao et al. 2006), in which case the longitudinal (principal) direction of the deck panel is aligned with that of the skew, as shown in Figure 9.5b, eliminating the need for additional pieces near the approach.

Structural Design

The flexural and torsional stiffness of a FRP deck can be estimated using a simplified method based on an elastic equivalence method and the equivalent orthotropic plate properties (Zhou 2002). The deck's maximum deflections for various boundary and loading conditions can then be calculated using the two-way orthotropic plate bending analysis method. In designing the layup of each deck component, a procedure based on a failure function method and a ply-level strength analysis can be followed for strength and failure of the FRP deck (Zhou 2002). This method considers various failure modes and failure mechanisms of the deck and predictions thus obtained compared well with the test results.

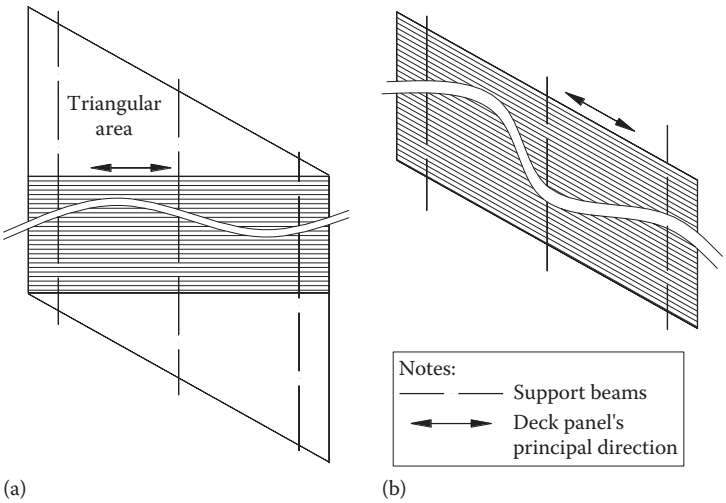

FIGURE 9.5 Deck placement on skewed bridges: (a) Perpendicular placement to girders and (b) Placement aligned with the skew.

The primary (strong) direction of FRP decks is typically placed perpendicular to the girders. When steel or reinforced concrete girders are used, the contribution of the FRP deck to the global stiffness through composite action is small and thus can be conservatively neglected. However, when FRP decks are supported by FRP composite girders, the composite action between the deck and girder should be considered. This is because FRP girders typically have low stiffness and thus cannot satisfy the AASHTO deflection criteria of L/800 on their own. Relaxed deflection criteria have been suggested based on evaluation results (e.g., Neely et al. 2004). Several investigations have also been conducted on the FRP girder load distribution factors (e.g., Moses et al. 2006; Stiller et al. 2006). But all these results have not yet reach the mature state of being codified.

Two common design bases are available in the design of all-composite deck panels: allowable stress design (ASD) and load and resistance factor design (LRFD). The stress levels in the FRP deck under service load shall be no greater than 20% of the rupture stress. The strength reduction factor, φ, shall be determined by the engineer based on factors such as material type, manufacturing process, environmental condition, support condition (simply or continuously supported), and laboratory test results. In addition, the design of the all-composite deck system is seldom governed by punching shear and fatigue. Catastrophic failure has not been reported in any all-composite bridge deck systems studied in research and installed in the field. For all-composite deck systems using pultruded profiles, other design details and requirements are suggested (e.g., Bank 2006; BS EN 13706 2002).

ALL-COMPOSITE GIRDERS FOR BRIDGE STRUCTURES

Bridge girders made of all FRP composites can have a cross section with a circular, I-beam, channel, rectangular, or trapezoidal shape. Materials used have commonly been glass FRP, carbon FRP, or hybrid of the two. However, application of FRP girders in bridge structures is less common than the FRP decks. Due to the lower stiffness of FRP than steel, FRP girders typically need to be very deep or placed very close to one another in order to meet the highway design deflection criteria of L/800 (AASHTO 2012).

While the significant weight saving made possible by using FRP deck panels is well recognized, the weight savings obtained by using FRP girders is not as significant. This is mainly due to that the weight of a typical bridge superstructure is governed by that of the deck rather than the girders. So far, there have not been established economic justifications to replace steel or concrete girders with FRP girders in highway bridge structures. If the girders need replacement, new steel or reinforced concrete girders can be installed as easily. However, there have been some research and field demonstrations in the use of all-composite girders for bridges.

Field Applications

The all-composite girders can be found in nearly 200 bridge field applications in the United States and around the world (Keller 2003; Pawel 2011). The 20 m long single span Miyun Bridge (Seible et al. 1993) used six 1.6 m wide and 1.65 m deep honeycomb box girders placed side-by-side with no gap in between. The 9 m long single span bridge built in Idaho in 1995 and the 10 m long Tech 21 (Smith Road) Bridge constructed in Ohio in 1997 both used large wet layup box girders with inverted hat sections (U-shaped girders that the FRP decks were glued onto). The 6 m long Tom's Creek Bridge in Virginia has twenty-four 0.2 m deep hybrid GFRP/CFRP beams (Strongwell DWB) with 0.3 m spacing (Neely et al. 2004). The same type of girder but with a much deeper section (0.9 m) has also been used with 1 m spacing in the Route 601 Bridge in Virginia (Restrepo et al. 2005). GFRP box section reinforced with a CFRP layer at the bottom was used in a full-scale bridge superstructure in Toowoomba, Australia, in 2002. The bridge has a total length of 10 m and a width of 5 m (Aravinthan and Manalo 2012). A series of bridges and footbridges using FRP girders has been built in Spain in the last decade. Their experience showed that "FRP girder bridges can be

feasible candidates as future bridges in the spans between 20 and 50 m, since they possess many of the characteristics identified such as durability and rapid installation" (Hurtado et al. 2012).

Manufacturing Processes

Several manufacturing methods have been used to produce FRP girders, e.g., wet (hand) layup, filament winding, pultrusion, and resin infusion. Wet layup and pultrusion are by far the most commonly used manufacturing methods.

A hollow rectangular tubular cross section, as shown in Figure 9.6, was used in an experimental investigation into the use of FRP girders as transverse girders for a long span bridge system (Cheng et al. 2005). As a prototype, the wet layup method was employed in the fabrication process. The detailing in the top portion of the cross section is for connecting the girder to a concrete deck that it supports. The primary material used is GFRP in triaxial and unidirectional fabrics with the bottom plate of the section integrated with a 6 mm thick CFRP plate to provide the needed stiffness. Four-point bending test results showed linear-elastic response in the girder and the failure was at a level far exceeding the demand. In a related study, a staged pultrusion concept was proposed for the same section.

Kansas Structural Composites fabricated a honeycomb core girder that is 32 ft long, 31.5 in. high and 1.0 ft wide for the New York DOT (Toillion 2001). It was designed for the HS-25 loading. The tests demonstrated that the girders had an excellent strength. One girder damaged during shipping regained full strength after being repaired.

Pultruded profiles for all-composite girders are produced by many pultrusion manufacturers in the United States and around the world. However, unlike conventional materials such as steel, using FRP girders in bridges is still a very new technology and thus the types and dimensions of girders are very limited. Most of the systems are proprietary. For instance, Strongwell produces an 8 in. deep EXTREN DWB® section, as shown in Figure 9.7a, and a 36 in. deep section, as shown in Figure 9.7b,

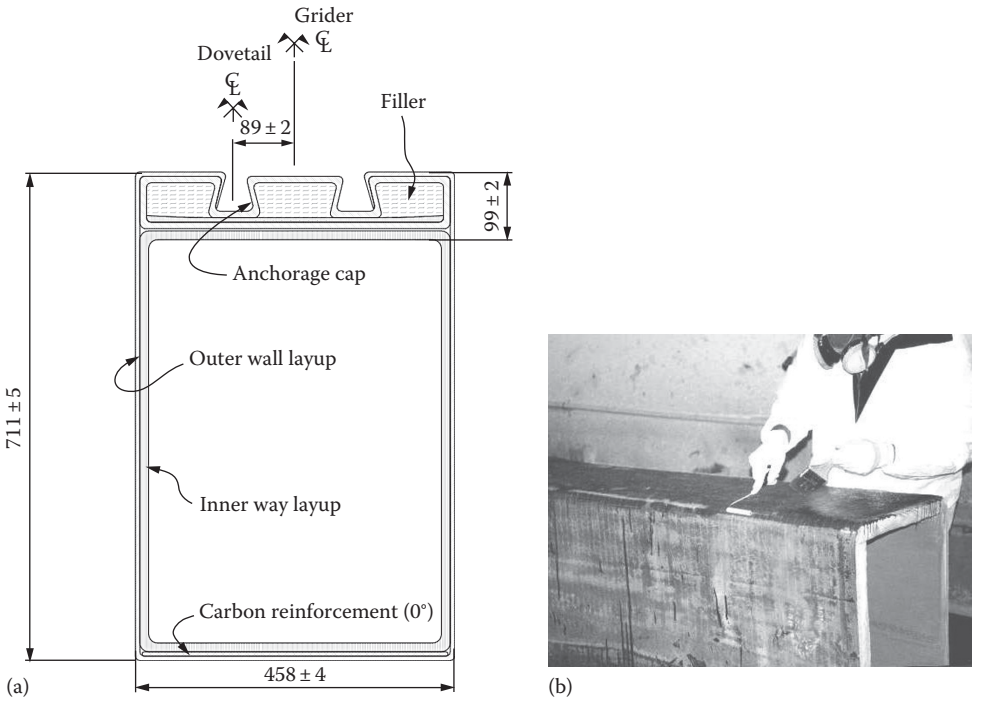

FIGURE 9.6 Hybrid FRP girder with carbon at bottom. (a) Cross section and (b) fabrication. (From Cheng, L. et al., *J. Struct. Eng.*, 131(3), 498, 2005. With permission.)

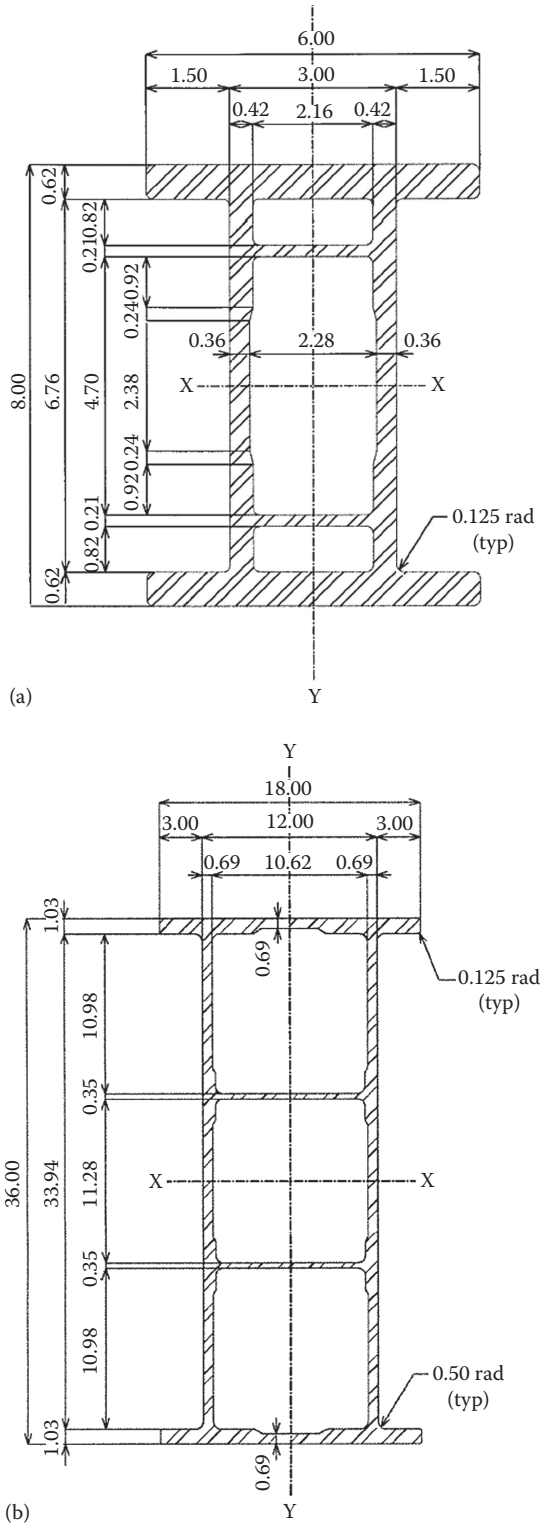

FIGURE 9.7 Strongwell pultruded girders: (a) 8 in. section and (b) 36 in. section. (From Strongwell Corporation, *EXTREN DWB® Design Guide*, Bristol, VA, 2000, available at http://www.strongwell.com/PDFfiles/Extren/EXTREN%20DWB%20Design%20Guide.pdf, accessed on February 14, 2013.)

both have gone through extensive testing and analysis, and have been used in a few field applications (Strongwell 2000). They are pultruded sections and are designed for HS-20 loading. Studies have also been done on other pultruded FRP box beams and girders with H-shape (Salim et al. 1995; Nagaraj and GangaRao 1997; Smith et al. 1998).

Static and fatigue tests of six partially filament-wound GFRP box beams were performed, each with a length of 3 m, a height of 188 mm, and a width of 118 mm (Meier et al. 1983). Good load bearing properties were obtained. Hybrid GFRP/CFRP girders with an open cross-section (trapezoidal shape without top flange) were installed in several bridges in Spain, e.g., Canary Island footbridge (Hurtado et al. 2012). These girders were fabricated using resin infusion process.

Structural Design

Since the technology of FRP girders is still at the stage of research and development, there is not a uniformly accepted design specification. While it has been widely proven that FRP girder can provide excellent strength, its lack of stiffness is typically governing the span length. The properties of FRP depend on the materials and the volume fractions of each component. However, to quickly estimate the weight and section properties of a FRP girder, the materials properties provided in Table 9.1 could be used. It can be seen that the modulus of elasticity of GFRP is approximately 10% of that of steel. Therefore, to achieve stiffness target typical of steel girders, the GFRP sections needs to be much deeper. Fibers are typically oriented primarily in the longitudinal direction of the girder with additional fabrics and mats added to the flanges and webs to increase the properties such as shear in the transverse direction.

For thin-walled sections of pultruded FRP beams, the full-section stiffness (flexural and shear) can be estimated using methodologies similar to the proposed ones (Bank 1989; Minghini et al. 2012). Warping has a negligible effect on the shear stiffness and only at very short spans and very high degrees of orthotropy. The use of the section moduli in a Timoshenko beam theory is attainable in the design where the serviceability limit state shall be checked. Some existing studies on fatigue life models indicate that fatigue will not be a major concern for the selected FRP girders during their life of service (Neely et al. 2004); however, more research is needed to further validate and generalize this claim.

To satisfy the strength limit states in the design, a simplified procedure for strength predictions of a pultruded FRP beam by Hayes (2003) can be referred to. Governing failure modes and mechanisms (such as tension, compression, and delamination) need to be properly identified and carefully considered in the design. For conservativeness, the first-ply failure criteria should be used for the preliminary design of FRP components in the girder. The stiffness

TABLE 9.1
Materials Properties for Estimations of FRP Girders

Property	GFRP	CFRP	Steel
Density (g/cm^3)	1.8	1.3	7.8
Modulus of elasticity (GPa)	20	70	200
Strain at yielding	N.A.[a]	N.A.	0.2%
Strain at rupture	2%	1%	10%–15%

[a] Not applicable.

properties of FRP laminates can be estimated using an approximation for extensional stiffness by neglecting the coupling terms in the following equations:

$$E_x = \frac{1}{hA_{11}^*} \tag{9.1}$$

$$E_y = \frac{1}{hA_{22}^*} \tag{9.2}$$

$$G_{xy} = \frac{1}{hA_{66}^*} \tag{9.3}$$

$$\upsilon_{xy} = \frac{-A_{12}^*}{A_{11}^*} \tag{9.4}$$

where

A_{ij}^* are the extensional compliance stiffness terms that can be calculated using the Classical Lamination Theory

h is the thickness of the laminate

Potential designers should also consult with a fabricator to develop a design that best fits the needs of the project. Some manufacturers actually offer proprietary in-house design manuals to aid the user select their respective profile products based on design concepts, partial safety factors, measured material parameters, etc. Representative examples include the Design Guide by Bedford Reinforced Plastics (2010), the New and Improved Pultex® Pultrusion Design Manual by Creative Pultrusions (2004), the EXTREN DWB® Design Guide by Strongwell (2000), and the Fiberline Design Manual by Fiberline Composites, Corp. (2003).

General guidelines for composite pedestrian bridge design are made available by the AASHTO Guide Specifications for Design of FRP Pedestrian Bridges (AASHTO 2008). Design loads and criteria are specified related to deflection, vibrations, allowable stress limitations, fatigue provisions, minimum thicknesses of structural members, bolted connections, etc.

REFERENCES

AASHTO. *Guide Specifications for Design of FRP Pedestrian Bridges*. American Association of State Highway and Transportation Officials, Washington, DC, 2008.

AASHTO. *LRFD Bridge Design Specifications*, 6th edn., American Association of State Highway and Transportation Officials, Washington, DC, 2012.

Aboutaha RS. Investigation of durability of wearing surfaces for FRP bridge decks. Reported submitted to Transportation Infrastructure Research Consortium, New York State Department of Transportation, Project #C-01-50, Albany, NY, 2005.

ACMA. Global FRP use in bridge applications, American Composites Manufacturers Association, 2004, available at http://www.mdacomposites.org/mda/bridge_statistics.htm, Accessed on February 18, 2013.

Alagusundaramoorthy P, Harik IE, Choo CC. Structural behavior of FRP composite bridge deck panels. *J Bridge Eng* 2006;11(4):384–393.

Aravinthan T, Manalo F. Field applications and case studies of FRP in civil infrastructure: The Australian experience. *Proceedings of the 6th International Conference on FRP Composites in Civil Engineering (CICE-6)*, Rome, Italy, June 13–15, 2012.

Aref AJ, Almpalli S, He Y. Performance of a fiber reinforced polymer web core skew bridge superstructure. Part I: Field testing and finite element simulations. *Compos Struct* 2005;69(4):491–499.

ASTM D2344/D2344M. *Standard Test Method for Short-Beam Strength of Polymer Matrix Composite Materials and Their Laminates*. ASTM International, West Conshohocken, PA, 2006.

ASTM D3039/D3039M. *Standard Test Method for Tensile Properties of Polymer Matrix Composite Materials*. ASTM International, West Conshohocken, PA, 2005.

ASTM D3171. *Standard Test Method for Constituent Content of Composite Materials*. ASTM International, West Conshohocken, PA, 2011.

ASTM D5379/D5379M. *Standard Test Method for Shear Properties of Composite Materials by the V-Notched Beam Method*. ASTM International, West Conshohocken, PA, 2005.

ASTM D5630. *Standard Test Method for Ash Content in Plastics*. ASTM International, West Conshohocken, PA, 2006.

Bakis CE, Bank LC, Brown VL, Cosenza E, Davalos JF, Lesko JJ, Machida A, Rizkalla SH, Triantafillou TC. Fiber-reinforced polymer composites for construction—State-of-the-art review. *J Compos Constr* 2002;6(2):73–87.

Bank, LC. Flexural and shear moduli of full-section fiber reinforced plastic (FRP) pultruded beams. *J Test Eval* 1989;17(1):40–45.

Bank LC. *Composites for Construction: Structural Design with FRP Materials*. John Wiley & Sons, Inc., Hoboken, NJ, 2006.

Barquist G, Lovejoy S, Nelson S, Soltesz S. Evaluation of wearing surface materials for FRP bridge decks. OR-DF-06-02, Oregon Department of Transportation, Salem, OR, 2005, 34 pp.

Bedford Reinforced Plastics, Inc. *Design Guide*, July 2010, available at http://www.bedfordreinforced.com/wp-content/uploads/2011/06/DesignGuide.pdf, Accessed on February 18, 2013.

BS EN 13706. *Reinforced Plastics Composites—Specification for Pultruded Profiles*, The European Standard, BSI, London, U.K., 2002.

Cheng L. Steel-free bridge decks reinforced with FRP composites. In R. Jain and L. Lee (eds.), *Fiber Reinforced Polymer (FRP) Composites for Infrastructure Applications*, Springer, New York, 2012, pp. 143–162.

Cheng L, Karbhari VM. New bridge systems using FRP composites and concrete: A state-of-the-art review. *Prog Struct Eng Mater* 2006;8(4):143–154.

Cheng L, Zhao L, Karbhari VM, Hegemier GA, Seible F. Assessment of a steel-free fiber reinforced polymer-composite modular bridge system. *J Struct Eng* 2005;131(3):498–506.

Creative Pultrusions, Inc. The New and Improved Pultex® Pultrusion Design Manual, 2004, available at http://www.reativepultrusions.com/products-solutions/fabrication-capabilities/pultexc2ae-pultrusion-design-manual1/, Accessed on February 18, 2013.

Davalos JF, Qiao P, Xu XF, Robinson J, Barth KE. Modeling and characterization of fiber-reinforced plastic honeycomb sandwich panels for highway bridge applications. *Compos Struct* 2001;52(3–4):441–452.

Farhey D. Long-term performance monitoring of the Tech 21 all-composite bridge. *J Compos Constr* 2004;9(3):255–262.

FHWA. Innovative bridge research and development program, Federal Highway Administration, July 2011a, http://www.fhwa.dot.gov/bridge/ibrd/, Accessed on February 15, 2013.

FHWA. Current practices in FRP composites technology FRP bridge decks and superstructures, Federal Highway Administration, 2011b, http://www.fhwa.dot.gov/bridge/frp/frppract.cfm, Accessed on February 13, 2013.

Fiberline Composites, Corp. Fiberline Design Manual, 2003, available at http://www.fiberline.com/read-more-about-fiberline-online-tools, Accessed on February 18, 2013.

Hayes M. Structural analysis of a pultruded composite beam: Shear stiffness determination and strength and fatigue life predictions. Ph.D. Dissertation, Virginia Polytechnic Institute and State University, Blacksburg, VA, 2003.

Hollaway LC. A review of the present and future utilization of FRP composites in the civil infrastructure with reference to their important in-service properties. *Constr Build Mater* 2010;24(2):2419–2445.

Hurtado MA, Bansal A, Paulotto C, Primi S. FRP girder bridges: Lessons learned in Spain in the last decade. *Proceedings of the 6th International Conference on FRP Composites in Civil Engineering (CICE-6)*, Rome, Italy, June 13–15, 2012.

Ji HS, Song W, Ma Z. Design, test and field application of a GFRP corrugated-core sandwich bridge. *Compos Struct* 2010;32(9):2814–2824.

Jones RM. *Mechanics of Composite Materials*, 2nd edn. Taylor & Francis Group, Boca Raton, FL, 1999.

Keller T. Use of fibre reinforced polymers in bridge construction. IABSE Structural Engineering Documents, No. 7, Zurich, Switzerland, 2003.

Kwon SC, Dutta PK, Kim YH, Lopez-Anido R. Comparison of the fatigue behaviors of FRP bridge decks and reinforced concrete conventional decks under extreme environment conditions. *KSME Int J* 2003;17(1):1–10.

Meier U, Muller R, Puck A. FRP-box beams under static and fatigue loading. *Proceedings of the International Conference on Testing, Evaluation and Quality Control of Composites*, Butterworth Scientific Ltd., Kent, U.K., pp. 324–336, 1983.

Minghini F, Tullini N, Laudiero F. Full-section properties of pultruded FRP profiles using bending tests. *Proceedings of the 6th International Conference on FRP Composites in Civil Engineering (CICE-6)*, Rome, Italy, June 13–15, 2012.

Moses JP, Harries KA, Earls CJ, Yulismana W. Evaluation of effective width and distribution factors for GFRP bridge decks supported on steel girders. *J Bridge Eng* 2006;11(4):401–409.

Nagaraj V, GangaRao VS. Static behavior of pultruded GFRP beams. *J Compos Constr* 1997;1(3):120–129.

NCHRP. Field inspection of in-service FRP bridge decks. National Cooperative Highway Research Program, Report 564, Transportation Research Board, Washington, DC, 2006.

Neely WD, Cousins TE, Lesko JJ. Evaluation of in-service performance of Tom's Creek Bridge fiber-reinforced polymer superstructure. *J Perform Constr Facil* 2004;18(3):147–158.

Pawel BP. Use of fibre reinforced polymer composites in bridge construction: State of the art in hybrid and all-composite structures. Master thesis, Universitat Politecnica de Catalunya, Barcelona, Spain, 2011.

Restrepo E, Cousins T, Lesko J. Determination of bridge design parameters through field evaluation of the Route 601 Bridge utilizing fiber-reinforced polymer girders. *J Perform Constr Facil* 2005;19(1):17–27.

Robert J, Fu CC, Alayed H. Deck replacement for the skewed truss bridge on MD 24 over Deer Creek in Harford County, Maryland utilizing a fiber-reinforced polymer (FRP) bridge deck. *International Bridge Conference*, Pittsburgh, PA, June 10–12, 2002.

Salim HA, Davalos JF, Qiao P, Barbero EJ. Experimental and analytical evaluation of laminated composite box beams. *The 40th International SAMPE Symposium and Exhibition*, Anaheim, CA, May 8–11, 1995, pp. 532–539.

Seible F, Sun Z, Ma G. Glass fiber composite bridges in China. A state-of-the-art report to the Advanced Composites Technology Transfer Consortium, University of California, San Diego, CA, Report number ACTT-9301, April 1993.

Shahawy MA. Prefabricated bridge elements and systems to limit traffic disruption during construction. NCHRP Synthesis 324, Transportation Research Board, Washington, DC, 2003.

Shahrooz BM, Reising RRMW, Neumann AR, Hunt VJ, Helmicki AJ. Field performance evaluation of multiple fiber reinforced polymer bridge deck systems over existing girders. An Interim Report to Federal Highway Administration and Ohio Department of Transportation, State Job No. 14715(0). University of Cincinnati, Cincinnati, OH, 2005.

Smith SJ, Parsons ID, Hjelmstad KD. Experimental study of the behavior of connections for pultruded GFRP I-beams and rectangular tubes. *Compos Struct* 1998;42(3):281–290.

Sopal G, Rizkalla R, Solomon G. Performance of new 3D GFRP sandwich panels with corrugated GFRP sheets. *Proceedings of the 6th International Conference on FRP Composites in Civil Engineering (CICE-6)*, Rome, Italy, June 13–15, 2012.

Stiller WB, Gergely J, Rochelle R. Testing, analysis, and evaluation of a GFRP deck on steel girders. *J Bridge Eng* 2006;11(4):394–400.

Strongwell Corporation. *EXTREN DWB® Design Guide*, Bristol, VA, 2000, available at http://www.strongwell.com/PDF-files/Extren/EXTREN%20DWB%20Design%20Guide.pdf, Accessed on February 14, 2013.

Toillion SE, FRP Library—Kansas Division documentation report. Federal Highway Administration, October 2001, available at http://www.fhwa.dot.gov/bridge/frp/frptrip.cfm, Accessed on February 13, 2013.

Williams B, Shehata E, Rizkalla SH. Filament-wound glass fiber reinforced polymer bridge deck modules. *J Compos Constr* 2003;7(3):266–273.

Wlasak, L. Development of the concept of composite bridge decks. *Proceedings of the Conference on Civil Engineering Infrastructure Based on Polymer Composites (CECOM)*, Krakow, Poland, November 22–23, 2012.

Zhao L, Karbhari VM. Lightweight composite deck systems for renewal. *Engineering Mechanics: A Force for the 21st Century, ASCE 12th Engineering Mechanics Conferences Proceedings*, American Society of Civil Engineers, San Diego, CA, May 17–20, 1998.

Zhao L, Karbhari VM. An approach for failure analysis of composite bridge deck systems. *Int J Struct Eng Mech* 2005;20(1):123–141.

Zhao L, Vyas JS, Ansley M. Testing of a FRP deck system for moveable bridges. *The Third International Conference on FRP Composites in Civil Engineering*, Miami, FL, December 13–15, 2006.

Zhou A. Stiffness and strength of fiber reinforced polymer composite bridge deck systems. Ph.D. dissertation, Virginia Polytechnic Institute and State University, Blacksburg, VA, 2002.

10 Connection Design for FRP Structural Members

Aixi Zhou and Lei Zhao

CONTENTS

INTRODUCTION

Connections in fiber-reinforced polymer (FRP) composite structures can be classified into three categories according to their functions (Clarke 1996): (1) primary structural connections, which provide major strength and stiffness to an assembly for the whole service life of the structure (the failure of such a connection has a substantial effect on the performance of the assembly and would constitute major structural damage and hazard to life. This connection type demands highest requirements for strength, rigidity, and durability); (2) secondary structural connections, which contribute some strength and stiffness to an assembly (the failure of such a joint would not endanger life or cause major structural damage; the failure would be recognizable and easily repaired); and (3) nonstructural connections, which usually do not provide strength or stiffness (the main purpose of such a connection may be to exclude the external environment or for decorative purposes. The failure of a nonstructural connection will not endanger life or cause structural damage). This chapter deals with the first two types of structural connections.

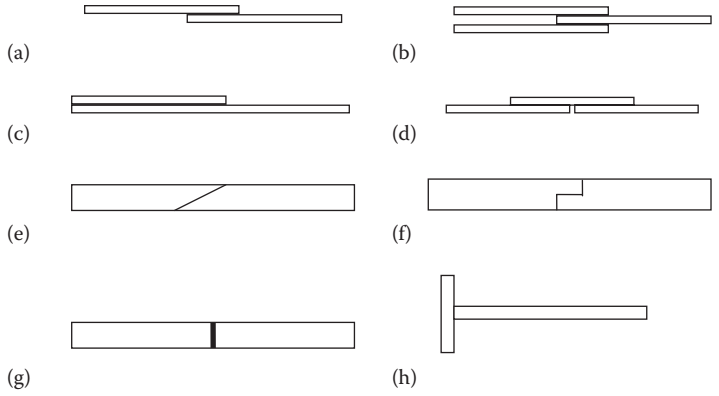

FIGURE 10.1 Typical joint configurations. (a) Single-lap joint (fastened, bonded, or combined), (b) double-lap joint (fastened, bonded, or combined), (c) lap-strap joint (fastened, bonded, or combined), (d) single-strap joint (fastened, bonded, or combined), (e) scarf joint (bonded), (f) stepped joint (fastened, bonded, or combined; stepped region varies), (g) butt joint (bonded), and (h) tee joint (fastened, bonded, or combined; tee region varies).

Many joining techniques have been developed for structural connections involving FRP structural members: mechanical fastening, adhesive bonding, and combined joining technique using both mechanical fastening and adhesive bonding. Some typical joint configurations are shown in Figure 10.1. In this chapter, the connection design of FRP structural members is addressed by types of joining techniques. The "Mechanically Fastened Joints" and "Adhesively Bonded Joints" sections present the fundamentals for design and analysis of composite joints through mechanical fastening and adhesive bonding. The "Joining of Large-Scale FRP Structures" section deals with joining of large-scale FRP structural members, concentrating on connecting bridge structural components.

Typical joint design involves the following procedures: (1) identifying joint design requirements, (2) selecting joint category and joining technique (mechanical, bonded, or combined), (3) selecting joint configuration, (4) detailed joint design, and (5) analysis and design verification.

Design requirements for FRP structural connections vary with the categories of connection and the performance requirements of specific projects. In both primary and secondary structural connections, the main objective is to ensure the integrity of the assembly and the load transfer efficiency between the joined components and the reliability of the connection. A connection should be designed to distribute internal forces and moments and carry the required loads and to satisfy the specified stiffness, strength, stability, fatigue, durability, and reliability requirements. Connections should also be designed for good constructability and ease of inspection (providing warnings of failure) and repair. When all these structural performance requirements are satisfied, economic and aesthetic issues should be considered. The advantages of advanced FRP composites would be lost if the characteristics of the associated joints were not properly understood and the connections were not properly designed.

The selection of joint type is determined by the following factors: (1) the required loads to be transferred and the required joint efficiency, (2) geometry of the members to be connected, (3) suitability of fabrication, (4) lifetime requirement and service environment, (5) the need for disassembly (as bonding is usually good for permanent joints), and (6) the requirements for reliability and issues related to aesthetics and cost. The importance of each factor can vary depending on the specific requirements of a project.

The Structural Plastic Design Manual (SPDM) (ASCE 1984) and European Design Code and Handbook (EDCH) (Clarke 1996) provided some guidelines for connection design of FRP structural members. The EDCH guides are based on the limit state design philosophy. Available approaches for

structural connection design of FRP members include the first principles of mechanics, elastic stress analysis (considering material orthotropy and detailed structural geometry), numerical analysis (mainly finite element analysis [FEA]), and testing of representative design cases or full-size connections.

MECHANICALLY FASTENED JOINTS

Mechanically fastened joints have been used in FRP trusses, beams, and braced frame structures, as well as multicellular FRP bridge deck structures. Both metallic (usually galvanized or stainless steel) and FRP bolts can be used as fasteners. Typical mechanically fastened joints include bolted joints and riveted joints, in which cutouts are required in the FRP components. Mechanical key connections use special design techniques and do not require cutouts. The design approach for mechanical key connections shall be by testing following the principles of the design and verification approach. This section deals with bolted and riveted mechanical joints where at least one of the primary structural components to be joined is made of FRP materials.

Design of Mechanically Fastened Joints

The parameters related to joining design for mechanically fastened joints are summarized in Table 10.1. A connection design shall be validated by either calculation or testing to satisfy the performance requirements. When connecting FRP members using bolts or rivets, the joining area should have solid laminate construction, preferably having balanced symmetrical section and fiber orientations distributed in the laminate plane at different angles and through the thickness (except for some pultruded members). To ensure reliability, there should be not less than two fasteners in a line in the loading direction. Usually the fasteners should have the same diameter. In the design process, any load transferred by friction between the joined members should be neglected. It is assumed that all loads are transferred by the fasteners, and the conditions of equilibrium shall always be fulfilled when determining fastener load distribution and far-field and local stress distributions.

TABLE 10.1
Design Parameters for Mechanically Fastened Joints

Material parameters of the FRP components	(a) Material properties, including anisotropy or orthotropy, inhomogeneity, viscoelasticity, environmental degradation, brittleness
	(b) Fiber type and form, such as unidirectional, woven, random, or fabric
	(c) Resin type, such as polyester, vinyl ester, epoxy, or phenolic resin
	(d) Fiber architecture and scheme, such as stacking sequence and form of construction (laminated or sandwiched)
Design parameters	(a) Geometry, including geometry of the FRP components (thickness, width, length), bolt or rivet size, cutout shape and pattern (circular or oval), cutout size, edge distance, end distance, cutout spacing, and arrangement (pitch and gage values)
	(b) Joint type, such as single lap, double lap, tee joint, or other joint types
	(c) Loading type (tensile, compressive, shear; concentrically loaded or eccentrically loaded)
	(d) Lifetime and environment, including dynamic fatigue loads, environmental effects such as temperature, moisture, and possible chemical solutions
Fabrication parameters	(a) The fastener material (metallic or FRP)
	(b) Fastener type (bolt, rivet, screw)
	(c) Tightening (clamping force or bolting torque, clearance, and washer size)

Several methods can be used for the design of fastened joints, including allowable stress design (ASD), limit state design (LSD), and load and resistance factor design (LRFD). When using the ASD method, the recommended safety factor (γ) for all connection parts is 4.0 (Bank et al. 1996). The EDCH provides guides for the determination of partial safety factors for fastened joints, including the FRP material to be joined and the fasteners. For FRP components forming the joint, the partial safety factor (γ_m) is the material's partial safety factor, which is the product of three basic partial safety coefficients related to the level of uncertainty of material properties from test values ($\gamma_{m,1}$), the material and production process ($\gamma_{m,2}$), and environmental effects and duration of loading ($\gamma_{m,3}$), that is,

$$\gamma_m = \gamma_{m,1}\gamma_{m,2}\gamma_{m,3} \tag{10.1}$$

Section 2.3.3.2 in the EDCH manual (Clarke 1996) specified the ranges of the three basic partial safety coefficients as $1.0 < \gamma_{m,1} < 2.25$ (the higher the level of uncertainty, the greater the $\gamma_{m,1}$ value), $1.1 < \gamma_{m,2} < 2.7$ (the better the manufacturing quality, the smaller the $\gamma_{m,2}$ value), and $1.0 < \gamma_{m,3} < 3.0$ (the longer the duration, the larger the $\gamma_{m,3}$ value). For building structures, the final value of γ_m should be greater than 1.5 and less than 10. For the fasteners, metallic or FRP, the partial safety factors shall be in accordance with their corresponding standards or guides for these materials.

When the LSD philosophy is implemented, specific requirements for serviceability limit state and ultimate limit state shall be satisfied. These requirements are summarized in Table 10.2. Resistance factors through the LRFD method for bolting pultruded FRP members are given by Prabhakaran et al. (1996). They adapted the LRFD procedure developed for bolted steel structures for bolted pultruded composites considering only block shear and net-tension failure modes. The ultimate design load P using LRFD is expressed as

$$P = \gamma_{DL}P_{DL} + \gamma_{LL}P_{LL} \quad \text{and} \quad P \le R \tag{10.2}$$

where

γ_{DL} (and $\gamma_{DL} = 1.2$) is the dead load factor
γ_{LL} (and $\gamma_{LL} = 1.6$) is the live load factor
P_{DL} and P_{LL} are dead and live service loads, respectively

TABLE 10.2
Limit States for Mechanically Fastened Joints

Serviceability limit states	(a) Deformation of the assembly due to slippage of fasteners or excessive deformation of cutouts
	(b) Onset of nonlinear load-deformation behavior of the joint under constant static load
	(c) Onset of increasing deformation under cyclic fatigue loading or environmental effects (esp. the effects of temperature and moisture)
	(d) Fiber debonding or matrix cracking under load or due to fabrication techniques
	(e) Fatigue resistance of FRP members and fasteners
	(f) Weather tightness and durability of unsealed edges
Ultimate limit states	(a) Maximum resistance of the complete joint
	(b) Static failure of joined parts or fasteners
	(c) Progressive failure of cutout edges
	(d) Long-term endurance of FRP members and fasteners (under long-term fatigue loading and environmental effects)

The resistance R is determined by the failure mode of the joint and should be the smallest value calculated from all failure models. For example, for block shear and net-tension failures, we have

$$R_{BS} = \varphi_{BS}(\tau_u A_{ns} + \sigma_u A_{nt}) \tag{10.3a}$$

$$R_{NT} = \varphi_{NT}\, \sigma_u A_{nt} \tag{10.3b}$$

where

τ_u and σ_u are nominal material ultimate shear and normal stresses
terms A_{ns} and A_{nt} are defined as net area subjected to shear and net area subjected to tension, respectively
φ_{BS} and φ_{NT} are set to be 0.50 on a tentative base
statistical variation in τ_u and σ_u values may require an adjustment of the φ values (Prabhakaran et al. 1996)

Failure analysis should be conducted and shall be based on the analysis of detailed stress distribution around cutout regions (Camanho and Matthews 1997). The failure analysis should evaluate the following failure modes: bearing failure, net-section failure, shear-out failure, and the shear failure of fasteners. The analysis should be validated by testing representative connections fabricated according to the design. When testing is not applicable, more rigorous analysis such as finite element analysis should be conducted to ensure the safety and reliability of the design. If the service environment is a concern, measures should be taken to exclude the joint area from the environment; otherwise, durability study should be conducted.

Failure Modes and Critical Limit States

Mechanically fastened FRP structural connections can fail in the fastener or in the joined FRP structural member. For bolted connections, a fastener can fail in the following modes (Figure 10.2): fastener shear failure, fastener tension failure, and bolt or nut thread shear failure. The FRP member can fail in the plane of loading in the following modes: net-section tension failure, bearing failure, shear-out failure, cleavage or splitting failure, or the combinations of the previously mentioned modes. For pultruded FRP members, bearing failure in cutout edges of the FRP material is generally ductile in the pultrusion direction and can lead to progressive shear-out failure. In the transverse direction, however, bearing failure may not be ductile and may lead to brittle net-tension failure of FRP member in the transverse direction. An FRP member can also fail out of the plane of loading due to punching or crushing.

Critical limit states of bolted or riveted connections include (1) bearing failure in FRP member, (2) net-section tensile failure in the FRP member, (3) shear-out failure in the FRP member, and (4) shear failure of fasteners. When FRP threaded fasteners are used in connections, the threads of fasteners can shear off in the longitudinal direction. Such critical limit state is a function of longitudinal shear strength of the fastener used. A general criterion for all these critical limit states is in the form of

$$\sigma_{cr} = k\sigma_{lim} \tag{10.4}$$

where

σ_{cr} is the critical design stress (tensile, compressive, or shear)
σ_{lim} refers to associate strength of material for each critical limit state to be considered
k is a factor considering stress concentrations ($k = 0.9$ for net-section tensile failure through the cutout and $k = 1$ for all other cases)

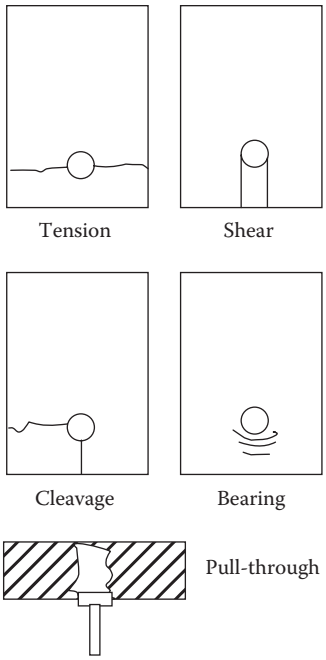

FIGURE 10.2 Typical failure modes in bolted composite joints.

Depending on failure mode considered, σ_{lim} can be the longitudinal or transverse bearing strength, tensile or compressive strength, in-plane shear strength, or shear strength of fasteners.

Stress Analysis for Designing Mechanically Fastened Joints

The stress distribution near a circular hole in composite orthotropic plates under biaxial in-plane loading has been examined by the complex variable mapping approach and the polynomial approximation approach. When the dimension of the cutout is very small compared to the plate, the following equations can be used for calculating the stress concentration factors (Soutis and Filiou 1998):

$$K_A^{orth} = 1 + \lambda - \gamma \cdot \alpha; \quad \text{and} \quad K_B^{orth} = \frac{1}{\alpha}\left[-1 + \gamma \cdot (\alpha + \lambda)\right] \tag{10.5}$$

where

$$\alpha = \sqrt{\frac{E_{xx}}{E_{yy}}}$$

$$\gamma = \frac{q}{p}$$

$$\lambda = \sqrt{2(\alpha - \nu_{xy}) + \frac{E_{xx}}{E_{yy}}}$$

The coordinate system is shown in Figure 10.3. When the effects of finite dimensions are significant, the calculations need to be modified by appropriate correction factors to account for finite width effects (Tan 1994).

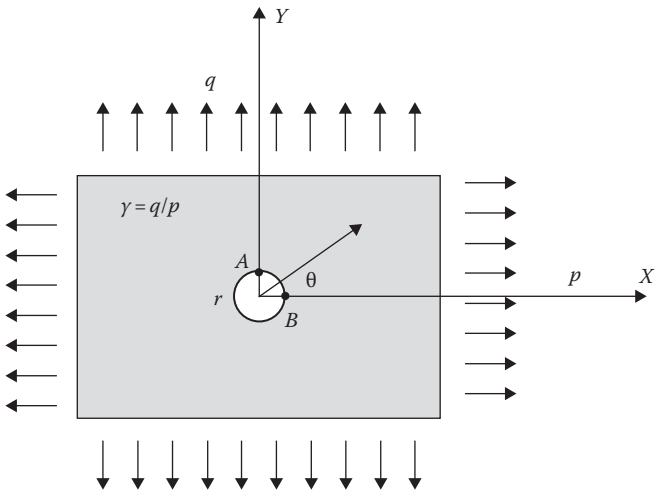

FIGURE 10.3 Coordinates for a circular cutout in an infinite orthotropic flat plate. (From Zhou, A. and Keller, T., *Compos. Struct*., 69(3), 336, 2005. With permission.)

The calculation of stress concentrations is more difficult for FRP members with curved or cylindrical walls than flat ones. For an orthotropic cylindrical shell whose axes of orthotropy (1,2,3) coincide with the cylindrical coordinate lines (r,θ,z) and with a free small circular cutout under uniform in-plane loading (subject to p and q, uniform pressures in r and θ directions respectively), considering the far-field axial stress p as reference stress, the stress concentration factors at two critical locations (θ = 0°,90°) can be approximately obtained as

$$K_{\theta=90^\circ} \approx \left[3+\frac{\pi\beta^2}{2}-\gamma\left(1+\frac{\pi\beta^2}{2}\right)\right]+\frac{(1-\lambda)}{2}\left[(1-\gamma)\left(1-\frac{\pi\beta^2}{2}\right)\right]$$
$$K_{\theta=0^\circ} \approx \left[(3\gamma-1)+\frac{\pi\beta^2}{2}(5\gamma-1)\right]+\frac{(1-\lambda)}{2}\left[(1-\gamma)\left(1-\frac{\pi\beta^2}{2}\right)\right] \quad (10.6)$$

where

$\gamma = q/p$, the ratio of the far-field biaxial uniform pressure loads
$\lambda = E_2/E_1$, the orthotropy ratio
$\beta^2 = \sqrt{3}a^2\sqrt{\lambda(1-\nu_{12}\nu_{21})}/4Rh$
a is the radius of the hole
h is the shell thickness
R is the radius (or curvature) of the cylinder

The previously mentioned approximation was derived for infinite cylindrical shells. In application, it can be used for estimating the stress concentration factors in the initial design stage (Zhou and Keller 2005).

When multiple cutouts are required in a connection design, measures must be taken to reduce the negative effects of the interaction of cutouts. A recommended distance between cutouts would be $L/a \geq 3$ (Zhou and Keller 2005). When close distances cannot be eschewed, measures must be taken to arrange the cutout pattern in a reasonable manner to reduce local stress concentrations and interactions.

ADHESIVELY BONDED JOINTS

Design of Adhesively Bonded Joints

An adhesively bonded joint should be designed and analyzed as a system considering its FRP substrates, adhesive, and the adhesive–adherend interfaces. The design of a bonded joint shall satisfy the following conditions: (1) The failure of a joint should occur either in the adhesive or in its adherends but not in the interfaces, (2) allowable shear stress and peeling stress of adhesive are not exceeded, and (3) allowable through-thickness tensile stress and out-of-plane shear stress should not be exceeded. The through-thickness tensile strength and out-of-plane shear strength of pultruded FRP members are relatively low compared to those of their in-plane values. Therefore, attention should be made on the through-thickness material properties of the adherends when designing adhesively bonded joints with pultruded FRP members. The parameters should be considered in designing adhesively bonded joints, as summarized in Table 10.3. The design of adhesively bonded joints shall be validated by either calculation or testing to verify that the design can fulfill the performance requirements. The limit states shall be satisfied in designing adhesively bonded joints and are provided in Table 10.4.

TABLE 10.3
Design Parameters for Adhesively Bonded Joints

Material parameters of the FRP components	Almost the same as for mechanically fastened joints in Table 10.1. In addition, an important factor that influences the strength of a bonded joint is the properties of the layer adjacent to the adhesive, especially fiber orientation and the presence of reinforcement in the through-thickness direction
Material parameters of structural adhesives	(a) Mechanical properties: brittle or ductile, adhesion properties, requirements for primer and surface preparation, pot life (b) Requirements for curing (c) Resistance to environmental parameters such as temperature and moisture (or water)
Design parameters	(a) Geometry: geometry of the FRP adherends (thickness, width, length), surface area available for bonding, bondline thickness, overlap length (b) Parameters concerning joint type, loading type, and lifetime and environment are the same as for mechanically fastened joints
Fabrication parameters	(a) The preparation before bonding: surface treatment (b) Curing and post-curing: the control of environments, clamping pressure (vacuumed assisted or not)

TABLE 10.4
Limit States for Adhesively Bonded Joints

Serviceability limit states	(a) Deformation of the bonded assembly (b) Onset of nonlinear load-deformation behavior of the joint under constant static load; onset of increasing deformation under cyclic fatigue loading or environmental effects (c) Fatigue resistance of adhesive and FRP members (d) Weather tightness of joints and durability of adhesive
Ultimate limit states	(a) Maximum resistance of the complete joint (b) Static or progressive failure of adhesive joints (c) Long-term endurance of FRP members, adhesives, and interfaces

Structural Adhesives

The properties of structural adhesives are important parameters for selecting adhesive types for a design. These properties include mechanical properties and physical and chemical properties. Structural adhesives can have thermoset or thermoplastic base. Common thermoset adhesives include epoxies, phenolics, and thermoset polyurethanes, while typical thermoplastic structural adhesives are acrylics and thermoplastic polyurethanes. Structural adhesives can be in the form of liquid, paste, and film. The designer should have the following knowledge of the selected adhesives in the design: activation of curing, curing temperature, curing pressure, curing cycle, and post-curing. In practice, thermoset adhesives are usually modified and thermoplastic adhesives are toughened for structural bonding. Table 10.5 summarizes the main strength and weaknesses of commonly used structural adhesives.

Structural adhesives have either brittle or ductile behavior. Thermoset adhesives are usually brittle. They are stiffer and have better creep resistance than thermoplastic adhesives. The most important mechanical properties of structural adhesives include shear modulus and strength, maximum shear strain, tensile modulus and strength, and maximum tensile strain. These properties are usually obtained from the manufacturers. Whenever necessary, tests shall be performed to verify the adhesive material data. Some standard testing methods are available for structural adhesives and bonded joints and are summarized in Table 10.6. Environmental temperature, moisture, and chemicals can affect adhesive mechanical properties considerably. Due to concerns about the long-term performance of adhesives, adhesive bonding has been limited to noncritical structural connections. This situation will change as more research has been devoted to this area, and we will gain better understanding and confidence of the long-term performance of adhesives and bonded joints.

The selection of structural adhesive should be based on previous experience or follow a specific selection process if it is available. Factors to be considered in adhesive selection are (1) adherend materials (such as adhesion compatibility), (2) applied loading, (3) environmental conditions during service, (4) geometry restrictions, (5) bonding and curing processes, and (6) costs and other special requirements including health and personnel safety.

ECDH provided some guidelines about the partial safety factors for structural adhesives. The overall safety factor (γ_m) is the product of four partial safety factors considering the source of adhesive properties ($\gamma_{m,1}$), the method of adhesive application ($\gamma_{m,2}$), the type of loading ($\gamma_{m,3}$), and environmental conditions ($\gamma_{m,4}$):

$$\gamma_m = \gamma_{m,1} \cdot \gamma_{m,2} \cdot \gamma_{m,3} \cdot \gamma_{m,4} \tag{10.7}$$

where the partial safety factors for various situations are provided in Table 10.7 (Clarke 1996).

TABLE 10.5
Advantages and Limitations of Commonly Used Structural Adhesives

Adhesive	Advantages	Limitations
Epoxy	High strength, good solvent resistance, good gap-filling capabilities, good resistance at elevated temperatures, wide range of formulations, relatively low cost	Exothermic reaction, exact proportions needed for optimum properties, short pot life, require special care for storage and cure
Polyurethane	Varying cure times, tough, excellent flexibility even at low temperatures, cure at room temperature or elevated temperature, moderate cost	Moisture sensitive, poor resistance at elevated temperatures, short pot life, special mixing and dispensing equipment required
Acrylic	Good flexibility, goof peel and shear strength, no mixing required, bonding of dirty surfaces possible, room temperature cure, moderate cost	Low strength at elevated temperatures, toxic, flammable, odor, limited open time, dispensing equipment required

Source: Clarke, J.L., *Structural Design of Polymer Composites: Eurocomp Design Code and Handbook*, E & FN Spon, London, U.K., 1996.

TABLE 10.6
Recommended Testing Standards for Adhesively Bonded FRP Composite Joints

Measured Property	Recommended Testing Standard
Adhesive Characterization	
Standard terminology	ASTM D907-05, D4800-94(2005)
Physical properties	ASTM D1084-97(2005), D7149-05, D2556-93a(2005)
Strength and shear modulus	ASTM D3983-98(2004), D4027-98(2004), D905-03, D4896-01
Bonding characteristics	ASTM D5868-01
Environmental aging	ASTM D1183-03
Joint Characterization	
Laminate surface preparation	ASTM D2093-03
Failure mode classification	D5573-99(2005)
Tensile shear loading	ASTM D5868-01, D3163-01, D3164-03, D3165-00; ISO 4587:2003
Tensile loading (butt joint)	ASTM D897-01, D2095-96(2002); ISO 6922: 1987
Peel loading	ASTM D1781-98(2004), D1876-01, D3167-03a(2004), D903-98(2004)
Flexural loading	ASTM D1184-98(2004)
Cleavage loading	ASTM D5041-98(2004), D950-03, D1062-02, D3433-99(2005), D3807-98(2004)
Creep	ASTM D1780-05, D2293-96(2002), D2294-96(2002)
Fatigue	ASTM D3166-99(2005)
Durability	ASTM D1151-00, D1828-01e1, D2918-99(2005), D2919-01e1, D3762-03, D3632-98(2004), D1144-99(2005), D904-99(2005), D896-04

TABLE 10.7
Partial Safety Factors for Adhesively Bonded Joints

Source of Adhesive Properties ($\gamma_{m,1}$)	
Typical or textbook values	1.5
Values obtained by testing	1.25
Method of Adhesive Application ($\gamma_{m,2}$)	
Manual application, no adhesive thickness control	1.5
Manual application, adhesive thickness controlled	1.25
Established procedure with controlled parameters	1.0
Type of Loading ($\gamma_{m,3}$)	
Long-term loading	1.5
Short-term loading	1.0
Environmental Conditions ($\gamma_{m,4}$)	
Service conditions outside the adhesive test conditions	2.0
Adhesive properties determined for service conditions	1.0

Source: Clarke, J.L., *Structural Design of Polymer Composites: Eurocomp Design Code and Handbook*, E & FN Spon, London, U.K., 1996.

10.3.3 Failure Modes and Critical Limit States

A bonded joint, especially the adhesive, may be subjected to the following stresses: (1) shear stresses produced by tensile/compressive, torsional, or shear loads imposed on its adherends; (2) peeling or cleavage stresses at the joint's edges or corners produced by out-of-plane loads acting on adherends or due to unbalanced banding moment; (3) out-of-plane tensile/compressive stresses produced by

out-of-plane tensile/compressive loads; and (4) in-plane tensile/compressive and shear stresses produced by in-plane tensile/compressive and shear loads (depending on joint types). In general, a bonded joint is simultaneously subjected to several of these stresses. Out-of-plane tensile, peeling, and cleavage stresses should be evaluated with great care and should be avoided when possible. A main principle in designing bonded assemblies is to ensure that the joint works in shear and to minimize out-of-plane peeling. For the adhesive layer, a preferred design is that it is primarily stressed in shear or out-of-plane compression.

Failure may occur in the adhesive, the adherend, and their interface. A summary of major failure modes of bonded joints is provided in Figure 10.4. Adhesive failure is the rupture due to separation at the adhesive–adherend interface. This failure is mainly caused by insufficient adhesion, due to either material mismatch or inadequate surface treatment. Failure related to the promoter has similar mechanism as adhesive failure. One of the main design requirements is to ensure that failure in the interface (including the promoter layer) should not happen. Cohesive failure of adhesive occurs when the applied stresses exceed the adhesive strength and cause its failure. Adherends can also fail in the cohesive manner, which is referred as fiber-tear failure to eschew any confusion with the cohesive failure in adhesive. A desirable design is to have a bonded joint that fails in the adherends so that the joint's weakness is only related to the adherend material itself. Stock-break failure in FRP adherends rarely happens in reality. This mode of failure would be the most desirable since the adherend material strength is fully utilized.

According to the discussion earlier, critical limit states for designing adhesively bonded joints include (1) cohesive failure of adhesive due to either shear, peeling, tension (depending on joint type), or their combination, and (2) fiber-tear failure in FRP adherends in the joining area. When long-term performance is a concern, the durability of the joint should be examined.

The adhesive is usually considered as isotropic. Criterion for cohesive failure of adhesive may be described by maximum stress criterion, that is, the maximum shear or tensile (including peeling) stresses (τ_{max}, σ_{max}) in the adhesive shall be equal to or less than the maximum allowable adhesive shear or tensile stresses (τ_{allow}, σ_{allow}):

$$\tau_{max} \le \tau_{allow} \quad \text{and} \quad \sigma_{max} \le \sigma_{allow} \tag{10.8}$$

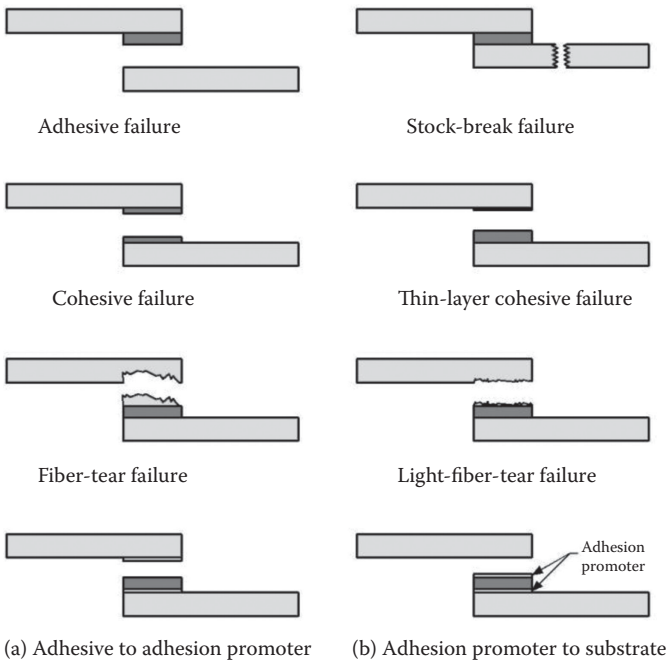

FIGURE 10.4 Typical failure modes in adhesively bonded joints. (a) Concrete-filled FRP girders and (b) steel girders.

FRP adherends have orthotropic (or anisotropic) material properties. The fiber-tear failure of adherends can be considered as delamination in the FRP composites. Criteria for delamination in adherends can be presented by the maximum stress or strain criterion in the through-thickness direction only or by many criteria considering the combined contribution of out-of-plane tension and shear stresses. The maximum stress or strain criterion in the through-thickness direction takes the same form as the second inequality in (10.8). Criteria simultaneously considering out-of-plane tension and shear stresses can be noninteractive type or interaction type. The simplest noninteractive type is

$$\frac{\sigma_z}{\sigma_{z,allow}} + \frac{\tau_{xz}}{\tau_{xz,allow}} = 1 \tag{10.9}$$

where

σ_z is the actual local through-thickness tensile stress at the adherends
τ_{xz} is the actual local out-of-plane shear stress
$\sigma_{z,allow}$ is the through-thickness allowable tensile stress, usually taken as the tensile strength
$\tau_{xz,\text{allow}}$ is the out-of-plane allowable shear stress, usually taken as the out-of-plane shear strength

The determination of out-of-plane tensile and shear strengths is not easy. Tensile strength can be obtained by bonding metal blocks to both faces of a waisted composite specimen and pulling them apart. Shear strength may be obtained by a double-notched specimen as specified in ASTM D5379. Equation 10.9 can be modified to consider the uncertainty of material properties and joint geometry variations. For example, one can use a simple empirical shear–tension interaction criterion of Zhou and Keller (2005):

$$\left(\frac{\sigma_z}{k_\sigma \cdot \sigma_{z,allow}}\right)^2 + \left(\frac{\tau_{xz}}{k_\tau \cdot \tau_{xz,allow}}\right)^2 = 1 \tag{10.10}$$

where factors k_σ and k_τ are introduced to consider the differences of stress states in the joint edges and the real stress states in the specimen when conducting tests to obtain out-of-plane material properties. These factors are mainly related to the geometry of joint such as tapering of the adherends and overlap length. They can be determined through curve fitting from experimental results for specific materials and joint types. There are also other more complex failure criteria such as those using the Tsai–Hill criterion, but these criteria use many material parameters that cannot be easily measured. Criteria using fracture mechanics parameters such as strain energy release rate have also been developed (Camanho and Matthews 1997).

Stress Analysis for the Design of Adhesively Bonded Joints

The analysis of the structural behavior of adhesively bonded joints is often conducted by studying a 2D representation of the joints. A 3D analysis of adhesively bonded joints can only be accomplished using numerical methods such as finite element analysis. In the 2D representation, the behavior and strength of a joint can be described by normal stresses (σ_x and σ_z) and shear stress (τ_{xz}) in the through-thickness plane. The stress analysis of adhesive joints is usually used to describe and determine the normal stresses and shear stress in the through-thickness plane in the adhesive and adherends.

Sources of stresses in adhesive joints include mechanical loading and hygrothermal loading. Mechanical loading can be represented in terms of forces, moments, and torques in the substrates arising from a wide range of external loads. These loads can be quasi-static or transient (including dynamic fatigue and impact loads). Many written works are available for stress analysis of adhesive joints subjected to mechanical loading (Camanho and Matthews 1997). In a 2D representation, the local stress distribution within an adhesive joint can be obtained by considering three loads acting in the FRP substrates at the end of the joint: the axial force, the shear force, and a bending moment.

When considering stresses in the adhesive joints, the out-of-plane normal (or peeling) stress and shear stress are two dominant components of stress.

Hygrothermal loading refers to loads originating from the effects of environmental conditions such as the changes in temperature (thermal stresses) and the absorption of moisture (swelling stresses). The long-term durability is much related to the effects of temperature and moisture. The effect of hygrothermal loading on the mechanical behavior and strength of adhesive joints has gained less attention than that of mechanical loading. Severe thermal stresses can present when the FRP substrates have different coefficient of thermal expansion (CTE). In general, the substrate with higher CTE expands or contracts more and extends or compresses the other substrate. This transmission of load is achieved by introducing a shear stress through the adhesive layer that joins them together. The most significant temperature change often occurs during the manufacturing and curing processes. It is possible that the induced thermal shear stresses can cause joint fracture before any loading is applied. In most cases, however, the FRP substrates have the same CTE, and the main stress in the adhesive is a longitudinal normal stress as the adjacent substrates prevent the free thermal expansion or contraction of the adhesive. These normal stresses are induced by shear stresses along the overlap interface. These shear stresses in the adhesive are much lower than those induced when the FRP substrates have different CTEs.

Swelling stresses play an important role in the mechanical behavior and strength of adhesive joints as both the adhesive and the FRP adherends absorb moisture and swell in a wet environment. The study of swelling stresses can be treated in the same way as thermal stresses by replacing the CTE with the coefficient of swelling and the temperature change with a moisture concentration (see the section "Hygrothermal Effects" in Chapter 8). However, the concentration of moisture within a joint will usually not be uniform as temperature, and the effect of swelling stresses will be more localized than temperature. When the localized moisture effect is significant, stress analysis cannot be carried out by similar procedures as thermal stresses but more general methods such as FEA. In addition to swelling, the absorption of moisture alters the stress distribution by plasticizing the adhesive and the polymer matrix in the FRP adherends. This adds more complexity to the analysis, which is often solved by FEA.

Most available analytical solutions for stress analysis of adhesive joints are for obtaining global stresses or strains. Many local singularities exist in adhesive joints, such as the presence of fillers, voids, and cracks in the adhesive, and the bi-material junctions that occur at the overlap ends or at a substrate corner. In addition, in practice, the geometry of the FRP adherends varies (such as tapering or curved surfaces) in overlap region and spew fillets usually present. It would be too complicated to analyze the stress and strains in an adhesive joint considering its real geometry. It was shown that stresses follow the local singular field up to a distance from the singular point that is of the same order as the geometric irregularity (Adams and Harris 1987). It would be inappropriate to use stresses or strains at such points of singularity as a criterion for failure. It would be more appropriate to characterize the stress filed using stress at a distance or a critical generalized stress intensity.

Combined Fastened–Bonded Joints

The use of combined fastened–bonded joints may be due to (1) manufacturing requirements, such as providing the required clamping pressure during the bonding and curing of adhesive joints; (2) performance requirements, such as using the bonded connection to satisfy the serviceability limit state requirements and the fastened connection to satisfy the ultimate limit state requirements; and (3) enhanced security measures, such as using fasteners to prevent possible service-induced bondline damages or cracks from growing.

The design of fastened–bonded joints assumes that only the bond or the fastener carry the joint load. In general, structural adhesives provide a much stiffer load transfer path than fasteners; thus, the adhesive practically takes all joint loads. When structural adhesives are used, the fastened–bonded joint shall be designed according to the procedures for adhesive joints. When elastomeric adhesives or sealants are used in a fastened–bonded joint, the load is assumed to be taken by fasteners. The joint shall be designed according to the procedures of the corresponding fastened joint.

JOINING OF LARGE-SCALE FRP STRUCTURES

In civil structural applications, such as bridge and building structures, the structural components to be connected are usually large in scale (1–10 m). While the previous sections address the fundamentals of mechanical fastening and adhesive bonding, the connecting of large-scale FRP structural components may be quite different as discussed earlier. The joining of large-scale FRP structures can be performed by mechanical fastening, adhesive bonding, and combined fastening–bonding. Although the basic principles of safety and design requirements are the same as addressed in the previous two sections, joining large-scale FRP structures requires special attention. The following section discusses some important aspects of joining of large-scale FRP structures.

Connecting Composite Girders and Panels to Other Bridge Components

Connecting FRP Bridge Deck Panels to FRP or Steel Girders

FRP bridge deck panels have been used either as replacements for damaged concrete or steel decks or in new constructions. They can be connected to FRP or steel girders by the following approaches: (1) simply resting on girders, (2) adhesive bonding, (3) mechanical fastening, (4) shear studs or dowels, and (5) combinations thereof. Examples of these connection types can be found in the following bridge projects:

The Magazine Ditch Bridge (1997) in Delaware has a foam core deck (by Hardcore DuPont) that is carried by two prestressed concrete girders. The deck panels rest on elastomeric pads placed near the edges of the girders (Chajes et al. 1998).

A bridge at the Idaho National Engineering and Environmental Laboratories (1997) uses three inverted hat sections as girders, which are adhesively bonded to a cellular pultruded deck system (by Lockheed Martin). The Tech 21 Bridge (1997) in Ohio, which is 10 m long and 7.3 m wide, utilizes a similar girder design to that of the Idaho bridge, except that the tops of the hat sections are closed, making them trapezoidal box girders. A similar FRP deck by Martin Marietta Composites is adhesive bonded to the top of the girders (Composites Worldwide 1997). The Laurel Lick Bridge in West Virginia has a pultruded deck (by Creative Pultrusions) adhesively bonded to six pultruded wide-flange FRP stringers (305 × 205 × 13 mm). In the Wickwire Run Bridge (1997), the same deck system is adhesively bonded to four 9.14 m long galvanized steel beams spaced at 1.83 m (Lopez-Anido 1998). In most cases of adhesive bonding connections, mechanical fasteners are also used to close the gaps between the deck and the girder to ensure a good bond (Lopez-Anido et al. 1998).

In high-volume highway bridges, the long-term fatigue and durability of adhesive bonding between FRP deck and girders become questionable. Making connections with steel studs or dowels has been used to address this concern. The King's Stormwater Channel Bridge (2001) in California uses dowels for making the connections, as shown in Figure 10.5a. The dowels are first encased in concrete-filled carbon composite shell girders and then are locally grouted in the cells of an FRP deck (by Martin Marietta Composites) with polymer concrete, which also forms a saddle between the deck and the girder (Zhao 1999). The saddle provides a uniform force transfer between the girder and the deck and minimizes the risk of local stress concentration and fatigue failures. Continuous monitoring has shown an excellent performance by the connection.

Connecting FRP decks to steel girders can be similarly achieved (Zhao 1999) by locally grouting steel studs, which are welded to the top of steel girders, in the cell of the deck panels, as shown in Figure 10.5b.

FRP girders, even when filled with concrete, are typically softer than steel I-girders. Therefore, composite action between FRP decks and FRP girders is needed in order to meet the deflection

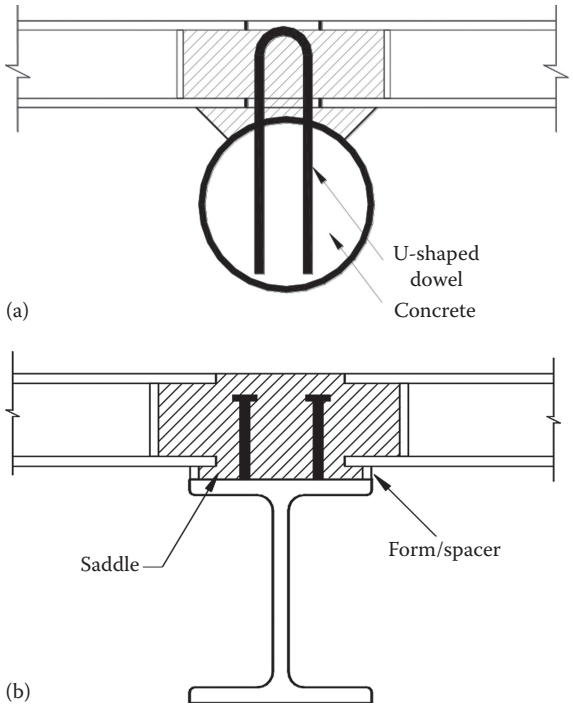

FIGURE 10.5 Connection designs for FRP decks to girders. (a) Concrete filled FRP girders and (b) steel girders. (From Zhao, L., Characterization of deck-to-girder connections in FRP composite superstructures, PhD dissertation, University of California, San Diego, CA, 1999.)

criteria of bridges. Sufficient shear resistance at the deck-to-girder connection is critical to ensuring a composite action. Steel girders, on the other hand, can typically on its own carry the live loads without excessive deflection and thus the composite action is not necessary (Righman et al. 2004).

There is increasing interest of implementing adhesive bonding technology to connect to underneath steel girders (Keller and Zhou 2006). But experiences have been limited to laboratory demonstration.

Connecting FRP Girders to Conventional Decks

FRP girders have been used to support concrete decks. As shown in Figure 10.6, the connection between the girder and the deck can be made with steel dowels, which are first encased in the hollow-shell FRP

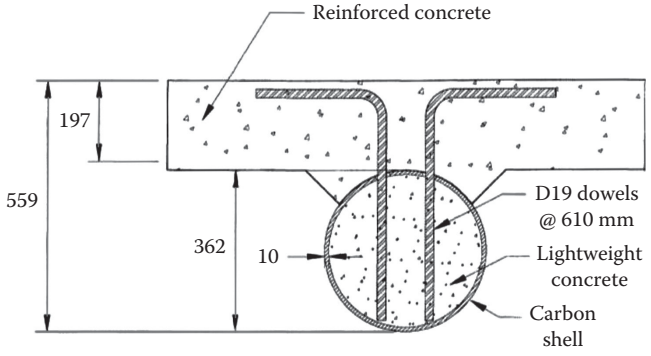

FIGURE 10.6 Concrete-filled carbon composite girder connected to a concrete deck. All dimensions in mm. (From Karbhari, V.M. et al., *Appl. Compos. Mater.*, 7, 151, 2000.)

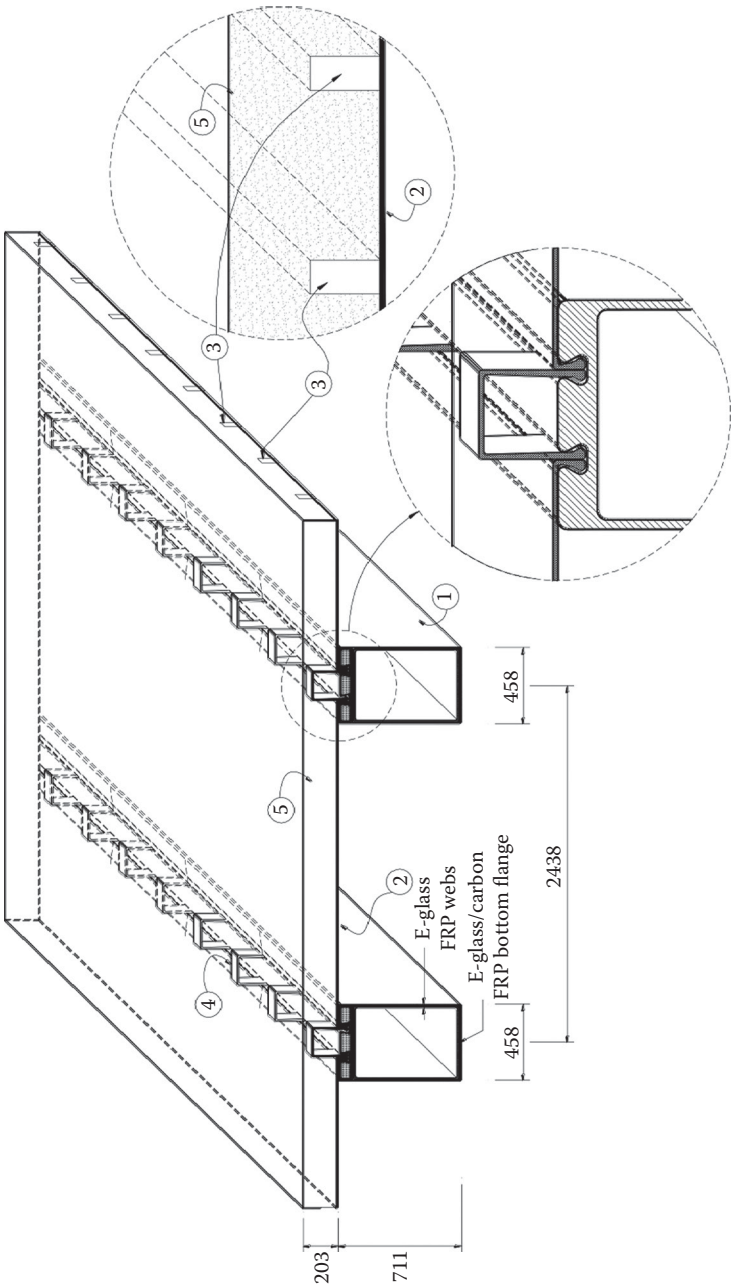

FIGURE 10.7 FRP girders connected to a concrete deck. ① Hybrid girder, ② Bottom skin of deck panel, ③ Stiffened ribs of deck panel embedded in concrete, ④ Shear stirrup, ⑤ Fiber reinforced concrete deck.

girder and then cast in a reinforced concrete deck (Karbhari et al. 2000). The system was able to achieve full composite action at the deck-to-girder interface and meet the strength and deflection criteria.

Carbon composite shear stirrups, which are first grouted in the grooves in the top of an FRP girder and then cast in a concrete deck, have also been used for connecting an FRP girder to a concrete deck, as shown in Figure 10.7 (Zhao et al. 2001).

Other conventional decks, such as a glue-lam deck, can be mechanically fastened to closely spaced pultruded FRP girders. An example of such applications is Tom's Creek Bridge (Lesko et al. 1998) in Virginia. Its girders are made by Strongwell.

Connections between Adjacent FRP Bridge Deck Panels

Connections between adjacent FRP panels can be achieved by (1) pouring grout or polymer concrete into the space between them and form a shear key, as shown in Figure 10.8a, or (2) by engaging each other with interlocking edges, as shown in Figure 10.8b.

Connecting Guardrails to FRP Deck Panels

The function of a guardrail is to prevent an errant vehicle from falling over the deck. The American Association of State Highway and Transportation Officials (AASHTO) Code (AASHTO 1983) requires that the top of a 1.2 m long guardrail section needs to withstand a horizontal force of at least 44.5 kN. As shown in Figure 10.9, a guardrail can be constructed by first grouting "starter bars" in the FRP deck and then casting a standard Jersey-type concrete barrier on the deck. This

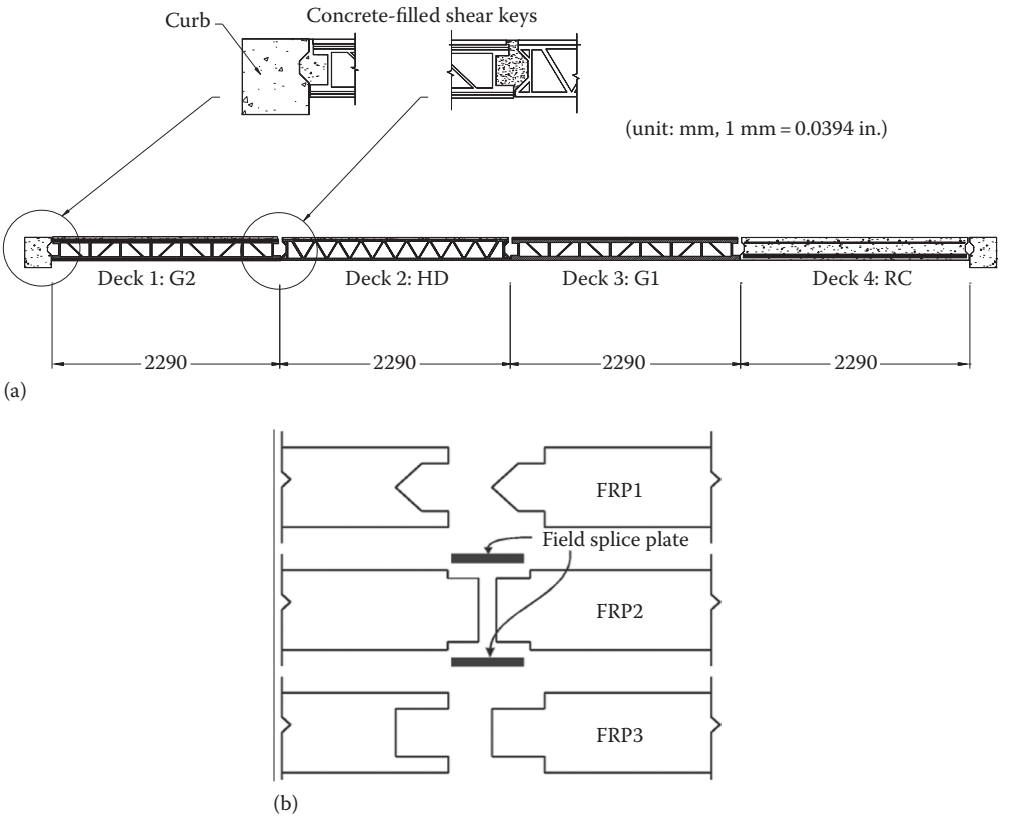

FIGURE 10.8 Deck-to-deck connections. (a) Grout shear keys (From Lopez-Anido, R., Wickwire run bridge: First FRP-deck on steel-stringer bridge, 1998, http://www.umeciv.maine.edu/rla/, accessed on January 16, 2006) and (b) deck interlocking. (From Righman, J.E. et al., *ASCE J. Compos. Constr.*, 8(4), 279, 2004.)

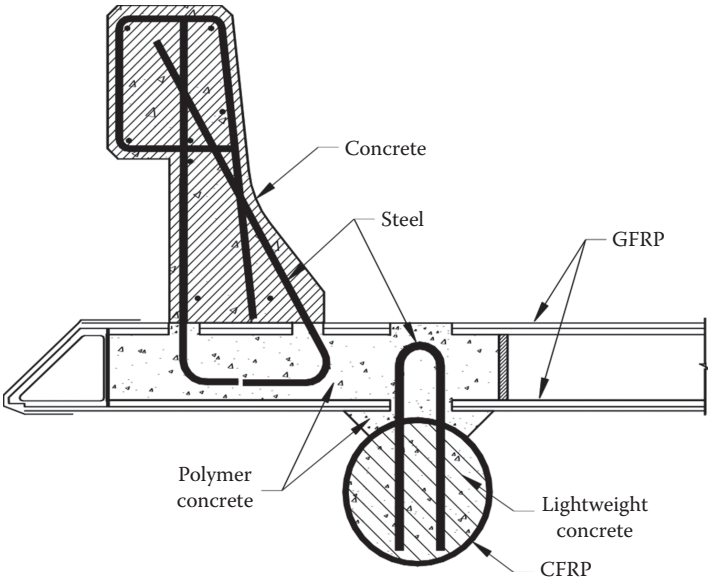

FIGURE 10.9 Guardrail connection to FRP deck/girder.

design was experimentally validated with a full-scale test and then used on King's Stormwater Channel Bridge (Zhao et al. 2004).

On the Tech 21 Bridge in Ohio, a steel barrier rail is connected to the top of the FRP deck by mechanical fasteners that penetrate the depth of the deck (Composites Worldwide 1997). On some other bridges, the guardrails are connected to the steel beams below or built separately with steel or concrete (Chajes et al. 1998; Lesko et al. 1998; Lopez-Anido et al. 1998), thus avoiding the relatively complicated procedure of connecting it to an FRP deck.

It should be noted that in most jurisdictions, a new guardrail system can only be approved for use after it passes the crash test, which typically is a long-drawn process. For guardrails on FRP decks, it is generally easier to receive approval without crash tests if the guardrail sections themselves are standard and widely accepted ones.

REFERENCES

AASHTO. (1983). *Standard Specifications for Highway Bridge* 13th Edn. F. H. Administration, ed., American Association of State Highway and Transportation Officials, Washington, DC.

Adams, R. D. and Harris, J. A. (1987). The influence of local geometry on the strength of adhesive joints. *International Journal of Adhesion and Adhesives*, 7(2), 69–80.

ASCE. (1984). *Structural Plastics Design Manual*. American Society of Civil Engineers, New York.

Bank, L. C., Yin, J. S., Moore, L., Evans, D. J., and Allison, R. W. (1996). Experimental and numerical evaluation of beam-to-column connections for pultruded structures. *Journal of Reinforced Plastics and Composites*, 15(10), 1052–1067.

Camanho, P. P. and Matthews, F. L. (1997). Stress analysis and strength prediction of mechanically fastened joints in FRP: A review. *Composites Part A: Applied Science and Manufacturing*, 28(6), 529–547.

Chajes, M., Gillespie, J., Mertz, D., Shenton, H., and Massarelli, P. (1998). Advanced composite bridges in Delaware. In *2nd International Conference on Composites in Infrastructure*, Tucson, AZ, 645 pp.

Clarke, J. L. (1996). *Structural Design of Polymer Composites: Eurocomp Design Code and Handbook*. E & FN Spon, London, U.K.

Composites Worldwide. (1997). Infrastructure newsletter. *Composites News*, Composites Worldwide, Inc., Solana Beach, CA.

Karbhari, V. M., Seible, F., Burgueno, R., Davol, A., Wernli, M., and Zhao, L. (2000). Structural characterization of fiber-reinforced composite short- and medium-span bridge systems. *Applied Composite Materials*, 7, 151–182.

Keller, T. and Zhou, A. (2006). Fatigue behavior of adhesively bonded joints composed of pultruded GFRP adherends for civil infrastructure applications. *Composites Part A: Applied Science and Manufacturing*, 37(8), 1119–1130.

Lesko, J., Hayes, M., Haramis, J., Hou, J., Cousins, T., and Gomex, J. (1998). Laboratory & field characterization of the Tom's Creak Bridge composite superstructure. In *2nd International Conference on Composites in Infrastructure*, Tucson, AZ, 634 pp.

Lopez-Anido, R. (1998). Wickwire run bridge: First FRP-deck on steel-stringer bridge. http://www.umeciv.maine.edu/rla/ (Accessed January 16, 2006).

Lopez-Anido, R., GangaRao, H. V. S., Troutman, D., and Williams, D. (1998). Design and construction of short-span bridges with modular FRP composite deck. In *2nd International Conference on Composites in Infrastructure*, Tucson, AZ, pp. 634–644.

Prabhakaran, R., Razzaq, Z., and Devara, S. (1996). Load and resistance factor design (LRFD) approach for bolted joints in pultruded composites. *Composites Part B: Engineering*, 27(3–4), 351–360.

Righman, J. E., Barth, K. E., and Davalos, J. F. (2004). Development of an efficient connector system for fiber reinforced polymer bridge decks to steel girders. *ASCE Journal of Composites for Construction*, 8(4), 279–288.

Soutis, C. and Filiou, C. (1998). Stress distributions around holes in composite laminates subjected to biaxial loading. *Applied Composite Materials*, 5(6), 365–378.

Tan, S. C. (1994). *Stress Concentrations in Laminated Composites*. Technomic Publication Corporation, Lancaster, PA.

Zhao, L. (1999). Characterization of deck-to-girder connections in FRP composite superstructures. PhD dissertation, University of California, San Diego, CA.

Zhao, L., Karbhari, V. M., Hegemier, G. A., and Seible, F. (2004). Connection of concrete barrier rails to FRP bridge decks. *Composites Part B: Engineering*, 35(4), 269–278.

Zhao, L., Karbhari, V. M., Seible, F., Burgueño, R., La Rovere, H., Broström, M., and Godonou, P. (2001). *Experimental Investigation of Prototype Transverse System for the Gilman Drive Advanced Technology Overcrossing*. SSRP 2001/04, University of California, San Diego, CA.

Zhou, A. and Keller, T. (2005). Joining techniques for fiber reinforced polymer composite bridge deck systems. *Composite Structures*, 69(3), 336–345.

11 Examples and Case Studies

Lee Canning

CONTENTS

INTRODUCTION

Civil infrastructure is rarely composed entirely of a single material, for technical, practical, and economic reasons. Therefore, the all-composite structures described later are those where the majority of the primary load-bearing elements are of FRP composite, or where FRP components are used. The particular reasons for using FRP composites are discussed, together with the various advantages and disadvantages, as it is considered this will be of interest to students and practicing engineers.

The various schemes described later have been chosen to give a general overview of the different types of FRP composites and construction methods used worldwide; there are currently hundreds of civil structures where FRP components form the majority of the load-bearing components. FRP composite materials have now been used in a wide variety of structures such as bridges, buildings, towers and masts, pressure vessels, gantries, and walkways. A wide variety of structural components are now available such as tubes, beams, cables and tendons, gratings, bars, and nonstructural components such as foot treads, cable trays, enclosures, cladding, etc.

Generally, FRP composite structures and components are more expensive in terms of material cost than those of conventional construction materials. However, in the majority of cases, the greater material cost is offset by reduced installation time and labor cost, reduced maintenance, and whole life cost. In some cases, FRP composites present the only viable technical solution, often due to their lightweight nature and durability in harsh environments.

PEDESTRIAN AND VEHICULAR FRP COMPOSITE BRIDGES

FRP composite bridges are generally fabricated by one of two methods:

1. The combining and joining of proprietary FRP components that are widely available (e.g., beams, decking systems, bars).
2. Manufacture of the primary structural elements as bespoke, project-specific components specially designed for a particular structure.

The first type is described here as "modular" and is currently the more common type of FRP composite bridge. The use of specifically designed FRP composite structural elements for a structure is generally more suitable for relatively large schemes where the premium on design time and cost is less significant in comparison to the total scheme development and installation cost. FRP composite pedestrian footbridges are generally more likely to use bespoke designs—this is mainly due to the fact that these types of bridges do not generally have to be designed for such high concentrated loads and fatigue loads as vehicular bridges; the design of FRP composite components under such loads is complex and is usually required to be proven by testing. Furthermore, as design guidance improves and becomes more widespread, and the civil engineering profession gains experience and confidence with FRP composites, it is likely that the use of project-specific designed FRP composite elements will increase.

Modular FRP Composite Bridges

West Mill Bridge, Oxfordshire, United Kingdom, 2002

The original West Mill Bridge was a nineteenth-century highway bridge over the River Cole in Oxfordshire, United Kingdom, with a span of 7.5 m and width of 3.5 m. The structure consisted of a reinforced concrete deck supported on cast-iron girders and brick abutments. The reconstruction of West Mill Bridge was such that the span was increased to 10 m and the total width of the deck increased to 6.8 m, including the footpaths on each side of the bridge. The new bridge deck comprised pultruded hybrid glass fiber–reinforced polymer/carbon-reinforced polymer (GFRP/CFRP) composite longitudinal beams with a transverse spanning pultruded GFRP cellular deck. Due to the change in span and width, new reinforced concrete abutments were also required.

The first stage in the construction of the new West Mill Bridge was demolition of the existing bridge deck and the abutments, due to the increase in deck width and span. Sheet pile cofferdams were installed on either side of the river using traditional driving methods, to enable the new reinforced concrete abutments to be constructed.

During the abutment construction, the site factory for fabrication of the bridge deck was erected adjacent to the existing bridge site. This comprised a frame of steel and timber beams for the reinforced concrete end diaphragm beams and a tent to ensure that a suitable environment was created for adhesive bonding operations of the advanced composite components (Figure 11.1).

The FRP composite main beams were then located on the hardstanding and the concrete diaphragm beams cast. To enable the safe handling and accurate positioning of the ASSET profile decking system, a lifting beam arrangement either side of the bridge deck was used. The ASSET profiles were transported to site in factory pre-bonded deck panels consisting of seven joined profiles. This reduced the amount of site bonding, a specialist activity, to a minimum. The deck panels were then lifted, positioned, and bonded one at a time, with the required surface preparation (abrading and degreasing) carried out on the main beams and deck panels (Figure 11.2). Regular checks on the site factory environment (cleanliness, temperature, relative humidity) were undertaken, and all bonding operations were closely supervised on site to ensure adequate workmanship. Structural monitoring instruments such as electrical resistance strain gauges and fiber optic sensors were installed during the deck fabrication process.

FIGURE 11.1 Hardstanding and tent for deck fabrication. (Courtesy of Mouchel Parkman, Woking, U.K.)

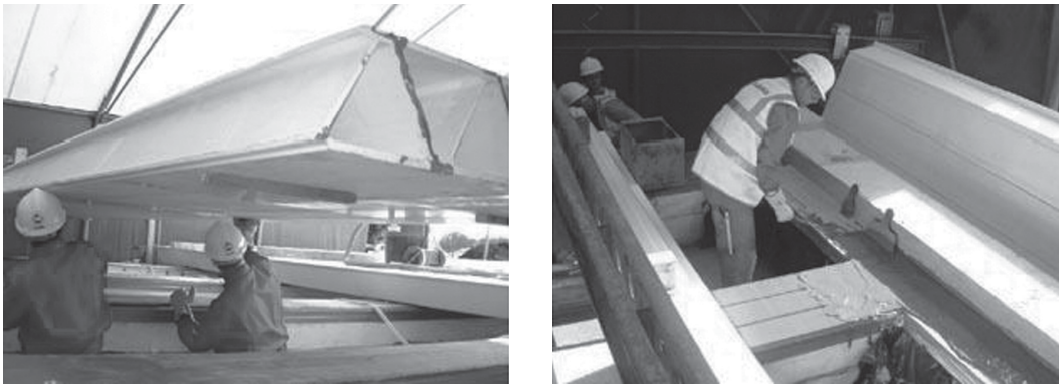

(a) (b)

FIGURE 11.2 (a) Positioning of bonded ASSET deck panels and (b) bonding of ASSET deck panels onto FRP main beams. (Courtesy of Mouchel Parkman, Woking, U.K.)

The final stage of fabrication was locating the composite edge fascia plate on the sides of the bridge deck, bonding of the GFRP composite permanent shuttering for the concrete edge beam, and casting of the concrete edge beams with the parapet post anchor bolts.

Due to the lightweight nature of the bridge deck, weighing approximately 40 ton of which the composite components weighed 12 ton, a relatively small mobile crane was used to lift the bridge deck into position onto the abutment bearing shelf (Figure 11.3). This is approximately one-third of the weight of a comparable reinforced concrete bridge. Following this operation, the polymer concrete and epoxy-based wearing course were applied on the deck to form the running surface. Other associated items such as the parapet barrier, expansions joints, drainage, and earthworks were then completed, and the bridge officially opened on October 29, 2002. The deck fabrication process took approximately 2 weeks to complete during the overall project program of approximately 3 months.

Prior to opening of the bridge, a load test was carried out to confirm the performance of the new structure. In addition, the instrumentation allowed the level of composite action between various components (in the short term) to be assessed, with the possibility of also assessing the level of composite action in the future. Analysis of the load test results showed that a high degree of composite action was present, and this information will aid future design and the creation of design guidelines. West Mill Bridge is also being monitored in the long term to determine its in-service performance and provide further information for the design of FRP composite structures. Further details of the initial and 3 year load test are described in Canning and Luke [1].

(a) (b)

FIGURE 11.3 Lifting of West Mill Bridge deck (a) into position and (b) completed bridge. (Courtesy of Mouchel Parkman, Woking, U.K.)

Tom's Creek Bridge, Blacksburg, Virginia, 1997

The original Tom's Creek Bridge was constructed in 1932 and reconstructed in 1964, with a span of 5.33 m and width of 7.32 m. The bridge superstructure comprised steel stringers supported on concrete abutments, with a timber deck spanning transversely over the stringers. Due to corrosion of the stringers, the bridge was reconstructed in 1997, utilizing FRP composites for the primary structural members. The new bridge retained the existing concrete abutments and used a superstructure comprised of 24 No. 8 in. depth proprietary vinylester resin/glass and carbon hybrid FRP double web beams, supporting a transverse spanning glulam deck of 5 in. depth. The glulam deck was mechanically connected to the FRP beams using a bolted connection, clamping the top flange of the FRP beams to the glulam deck. The surfacing comprises 1.5 in. thick asphalt course on waterproofing, on a 4.5 in. asphalt base course. The crash barriers consisted of glulam sections, with a steel internal face, bolted directly to the edge of the glulam deck using steel angles. A photograph showing the installation of the new Tom's Creek Bridge is shown in Figure 11.4. Further details of the bridge can be found in Hayes [2], Senne [3], and Kassner [4].

It is interesting to note that due to the novelty of the application, and to provide a benchmark, the main elements of the bridge deck (i.e., FRP beams and glulam deck) were connected together and tested in the laboratory prior to final installation.

Bridge deck construction took only 4 days, and instrumentation (strain gauges and deflectometers) was incorporated into the bridge deck to enable short- and long-term monitoring of field structural behavior.

Load testing and structural monitoring of this structure over 3 years, described in Neely [5], have shown that the mechanical connection does not provide a high degree of composite action between the FRP beams and glulam deck; however, the glulam edge barriers do provide a significant stiffening effect to the bridge superstructure. Destructive testing of two of the FRP beams, after 15 months in-service, showed negligible loss of stiffness and strength compared to benchmark tests undertaken prior to construction of the bridge. It was also noted that thermal effects were significant on this type of bridge deck.

Route 601 Bridge, Sugar Grove, Virginia, 2001

This bridge spans 39 ft over Dickey Creek, with a total width of 9.7 m, and replaced a bridge built in 1932 comprising steel stringers and a timber deck. The bridge was reconstructed in 2001, as the original bridge was understrength and in poor condition due to corrosion of the steel stringers. The primary structural members are 36 in. deep hybrid FRP beams of glass/carbon fiber and vinylester resin at 1.1 m spacing, with a glulam timber deck and asphalt surfacing. The glulam timber deck

FIGURE 11.4 Installation of FRP beams for Tom's Creek Bridge. (Courtesy of Strongwell Co., Bristol, VA.)

FIGURE 11.5 Installation of FRP beams on Route 601 Bridge. (Courtesy of Strongwell Co., Bristol, VA.)

was connected to the FRP main beams by a steel bracket bolted connection through the deck and the upper section of the webs of the main beams, avoiding section loss and damage to the top flange of the FRP beams. The superstructure is supported on traditional reinforced concrete abutments. Figure 11.5 shows the installation of the FRP beams. A more detailed description of the bridge and the design methods used are given in Waldron [6].

Wickwire Run Bridge, Taylor County, West Virginia, 1997

Wickwire Run Bridge carries vehicular traffic over a span of 9 m with a deck width of approximately 7 m. The superstructure is comprised of a GFRP transverse spanning deck bonded and mechanically connected to four galvanized steel girders at 1.8 m spacing, supported on reinforced concrete abutments. The GFRP deck is comprised of hexagonal and trapezoidal sections bonded together using polyurethane adhesive, with a 0.5 in. thick polymer concrete surfacing. The GFRP deck was transported to the construction site in four panels and fixed to the steel girders. A number of load tests have been undertaken on the bridge, which has shown that significant composite action occurs between the steel girders and FRP deck. Figure 11.6 shows a general view of Wickwire Run Bridge during installation. A more detailed description of Wickwire Run Bridge is provided in Gangarao et al. [7].

Bentley Creek Bridge, Wellsburg, New York, 2000

Bentley Creek Bridge carries State Route 367 over Bentley Creek Bridge and originally comprised a single span steel truss structure with steel floor beams and stringers, a concrete deck and asphalt surfacing, constructed in 1940. The bridge is 42.7 m long with a width of approximately 7 m and was assessed as understrength due to increases in dead load from surfacing and corrosion to the steelwork. To reduce dead load and provide additional live load capacity from the original structure, the concrete deck was replaced with a lightweight FRP deck system comprising sandwich panels of stitched GFRP fabric faces with an isocycrinate foam core. A total of six prefabricated FRP deck panels were used to replace the concrete deck, connected to the steel beams using bolted and grouted mechanical connections. No composite action between the FRP deck and steel superstructure was assumed, which was shown to generally be the case from load testing, although the connections were designed to resist any existing forces due to composite action. The steelwork was also painted as part of the rehabilitation scheme.

FIGURE 11.6 Wick Wire Run Bridge during installation. (Courtesy of Creative Pultrusions Inc., Alum Bank, PA.)

Broadway Bridge, Portland, Oregon, 2004

Broadway Bridge is the seventh longest bascule bridge in the world. The bridge carries pedestrian and vehicular traffic across the Willamette River and was constructed in 1913, with a total length of approximately 1600 ft and width of 70 ft, and a 278 ft long double-leaf movable span. The superstructure comprised steelwork frames with a steel grating deck, which required replacement. Due to the original lightweight decking system, an alternative durable lightweight deck system was required, and a pultruded FRP decking system was chosen to replace the existing steel grating deck, as alternative concrete or steel options were not feasible. The FRP deck comprises multiple bonded pultruded cellular GFRP components of 5 in. depth. A total of 32 FRP deck panels, each 46 ft long and 8 ft wide, were installed as a replacement to the steel grating, with steel stud and grouted shear connections between the steel beams and FRP deck, and a polymer concrete surfacing. The FRP deck panels were installed in 2 days, causing minimum disruption to traffic and early opening of the bridge to traffic. Figure 11.7 shows installation of the FRP deck panels onto the existing steel superstructure.

FIGURE 11.7 Installation of FRP deck sections onto Broadway Bridge. (Courtesy of Martin Marietta Co., Bethesda, MD.)

Bonds Mill Lift Bridge, Gloucester, United Kingdom, 1994

Bonds Mill Lift Bridge is a single bascule lift bridge that provides pedestrian and vehicular access across a canal linking the rivers Thames and Severn in Gloucester. The bridge superstructure is comprised of bonded multi-cellular GFRP (E-glass fibers, isophthalic polyester resin matrix) box beams, fabricated from the same modular plank and toggle system as in Aberfeldy bridge, with a lightweight epoxy foam filler to the compressive flanges and webs, providing resistance to concentrated wheel loads. The surfacing is comprised of proprietary epoxy-coated panels with gritted surfaces, bolted to the surface of the FRP deck. The use of lightweight components was advantageous in this case as it had a direct effect on the mechanical lifting system (Figure 11.8).

Aberfeldy Bridge, Scotland, United Kingdom, 1992

Aberfeldy Bridge carries pedestrians and golf buggies across a river between two parts of a golf course and is the longest FRP composite bridge in the world with a total length of 113 m. The bridge deck is constructed from pultruded GFRP (E-glass/isophthalic polyester resin) planks that use a bonded and mechanical slotting toggle connection and is supported by aramid cables attached to a GFRP A-frame tower. The individual pultruded components of the bridge deck consist of 610 mm width, 80 mm depth cellular sections; 80 mm width by 80 mm depth toggle sections are used to join together adjacent pultruded planks. Burgoyne [8] provides further information on this structure.

Klipphausen Bridge, German, 2005

Klipphausen Bridge has a span of 6.3 m and width of 6.0 m, carrying a single carriageway and two footpaths, founded on reinforced concrete abutments. Vehicle restraint is provided by steel crash barriers anchored into the FRP deck. The carriageway surfacing comprises a thin polymer concrete screed with an epoxy-based thin wearing course. Previous steel and concrete bridges at this location had suffered severely from corrosion, and an FRP deck was chosen to provide a long-term, low-maintenance solution.

The superstructure comprises 26 pultruded GFRP (E-glass fibers and isophthalic polyester resin) cellular profiles adhesively bonded together, of 225 mm depth, spanning longitudinally across a river. The footpaths are raised, and the edges of the deck stiffened by bonding of additional pultruded GFRP cellular profiles above one another.

FIGURE 11.8 Bonds Mill Lift Bridge.

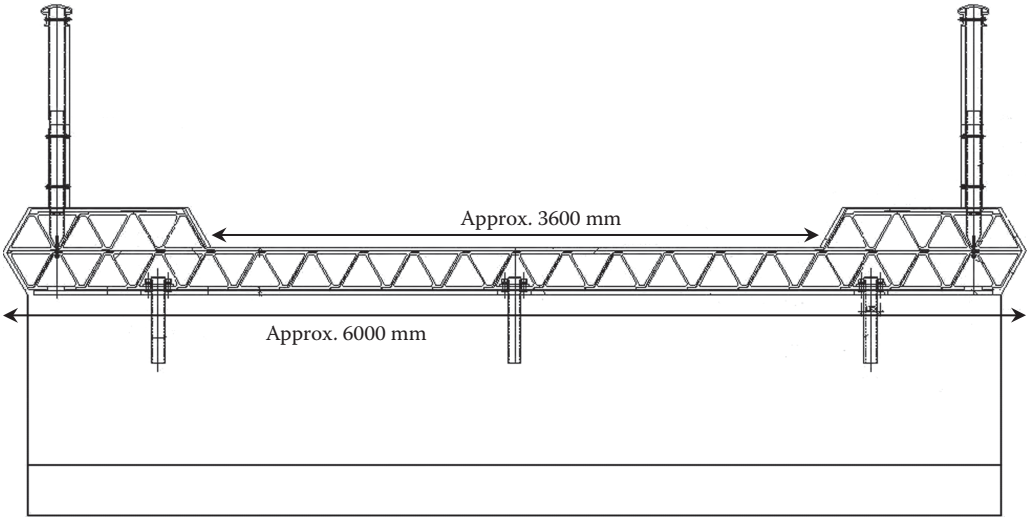

FIGURE 11.9 Cross section of Klipphausen Bridge. (Courtesy of Ingenieurbüro Richter, Hildesheim, Germany; Fiberline Composites Middelfart, Denmark.)

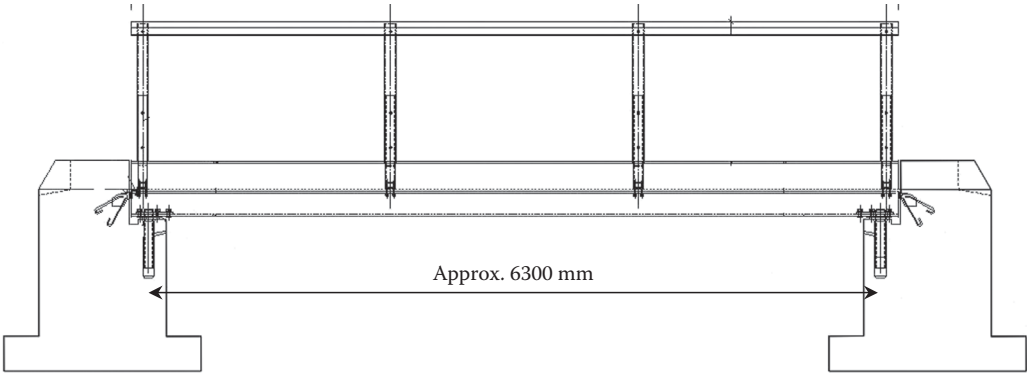

FIGURE 11.10 Side elevation of Klipphausen Bridge. (Courtesy of Ingenieurbüro Richter, Hildesheim, Germany; Fiberline Composites Middelfart, Denmark.)

The FRP bridge deck arrived on site as two separate, completely fabricated sections, which were then installed by crane and site-bonded together. Flooding also occurs at this location, and the bridge deck was secured to the abutments using demountable bolts so that, if required, the bridge could be removed when flooding was expected.

A cross section and elevation of Klipphausen Bridge are shown in Figures 11.9 and 11.10. Figure 11.11 shows the installation of the two parts of the bridge deck.

Bennetts Creek Bridge, New York, 1998

Bennetts Creek Bridge carries New York State Route 248 over Bennetts Creek. The bridge has a span of 23 ft and a width of 33 ft. The superstructure of the bridge comprises a 24.5 in. thick sandwich panel comprising E-glass fiber/vinylester resin composite faces and a foam core. The wearing surface comprises a 10 mm thick epoxy/basalt polymer concrete. The structure was fabricated in two parts widthwise, and a site joint installed to join the two parts of the FRP bridge deck together. The bridge was load tested prior to opening and was shown to be stiffer than predicted by the design. The design and testing of the structure is described in Alampalli et al. [9].

FIGURE 11.11 Installation of Klipphausen Bridge. (Courtesy of Fiberline Composites, Middelfart, Denmark.)

Laurel Lick Bridge, West Virginia, the United States, 1997

Laurel Lick Bridge was reconstructed in May 1997, replacing a traditional steel stringer/timber deck-type bridge, deck spanning over a stream, with an approximately 20 ft span and 10 ft width. FRP components were used both in the substructure and in the superstructure for this particular bridge. The new substructure comprises FRP wide flange columns supporting reinforced concrete capping beams, with pultruded FRP components filling between the FRP columns. The superstructure comprises 6 No. pultruded FRP wide flange beams (vinylester resin/E-glass fiber), each 12 in. wide and 12 in. deep, spanning longitudinally approximately 20 ft and at 0.76 m spacing, with a transverse spanning deck made of pultruded vinylester resin/E-glass FRP cellular sections (Figure 11.12). The pultruded FRP deck was both adhesive bonded and mechanically connected together; a bonded and bolted connection was also used between the FRP deck and FRP main beams. The wearing course comprises a thin polymer concrete overlay of approximately 10 mm thickness. Further details of this structure, and dynamic tests undertaken on the structure, can be found in Jinka [10].

FIGURE 11.12 Installation of Laurel Lick Bridge. (Courtesy of Creative Pultrusions Inc., Alum Bank, PA.)

FIGURE 11.13 General view of Kolding Bridge, Denmark. (Courtesy of Fiberline Composites, Middelfart, Denmark.)

Kolding Bridge, Kolding, Denmark, 1999

Kolding Bridge, at Strandhuse near Kolding, is a cable-stayed pedestrian bridge over a railway and uses GFRP composite pultruded components for all the main structural components in the superstructure. The bridge has a length of 40 m and width of 3.2 m, the length of the bridge comprising two spans of 27 and 13 m. The superstructure comprises 1.5 m deep girders fabricated from pultruded GFRP channel, angle and I-sections, supported by GFRP cables attached to an 18.5 m height pylon fabricated from standard GFRP pultruded components. The superstructure is supported on reinforced concrete abutments. A general view of Kolding Bridge is shown in Figure 11.13.

The total weight of the bridge superstructure was approximately 12.5 ton, which was less than half the weight of a similar steel structure. A cost study of the bridge showed that the material cost of the FRP components used was greater than that for a steel or concrete alternative. This greater cost was partially offset by the reduced cost of installation, and surface treatments, to give a final cost estimated as 5%–10% greater than that of a steel or concrete alternative. Once reduced maintenance and a whole life cost study are taken into account, the bridge was shown to be a cost-effective solution. Further details of the bridge can be found in Braestrup [11].

Pontresina Bridge, Switzerland, 1997

Pontresina footbridge provides access across the Flaz Creek in Pontresina, Switzerland. The bridge consists of two 12.5 m spans of truss form, with the upper chord serving as a handrail. Different joining methods were used for each span: bolted connections on one span and adhesive bonded joints on the other span. One particularly unusual feature of this bridge is that each year, when floodwaters are experienced in the spring, the bridge is lifted out to prevent damage to the bridge superstructure. This is a good example of how lightweight FRP composite structures can be useful in particular circumstances. Testing of each span of the bridge has shown the span with adhesive bonded joints to be slightly stiffer than that utilizing bolted connections. A general view of Pontresina Bridge is shown in Figure 11.14; further details are discussed in Strehler and Kunzle [12].

FIGURE 11.14 Pontresina Bridge, Switzerland. (Courtesy of ETH, Zurich, Switzerland; Fiberline Composites, Middelfart, Denmark.)

Lleida Bridge, Spain, 2004

Lleida Bridge is a pedestrian bridge over a highway and railway line, with a span of approximately 38 m and a width of approximately 3 m. The superstructure comprises a tied-arch system with two arches fabricated from a number of straight pultruded GFRP sections, leaning inwards by 10°, which supports a deck comprising GFRP pultruded planks with a non-slip surfacing. Pultruded GFRP members were connected together using stainless steel fixings.

The bridge was fabricated adjacent to the railway line and then craned into place in a short 3 h period. Figure 11.15 shows a general view of Lleida Bridge.

FIGURE 11.15 Lleida Bridge, Spain. (Courtesy of Pedelta, Barcelona, Spain; Fiberline Composites, Middelfart, Denmark.)

No Name Creek Bridge, Kansas, 1996

No Name Creek Bridge is a 22.5 in. thick sandwich panel structure comprising GFRP faces with a honeycomb core, spanning approximately 7 m and with a total width of approximately 8.5 m. The faces of the sandwich panels are fabricated from 0.75 in. thick GFRP for the lower face, and 0.50 in. thick GFRP for the upper face, with a 0.75 in. thick polymer concrete wearing course of gravel aggregate in a polyester resin. The bridge deck was fabricated from three longitudinal sections of deck, bonded together in situ using in situ wet lay-up of chopped strand mat and supported on steel headers at the ends of the bridge. The edge sandwich panels were fabricated integral with guard rails to minimize site installation time; the entire bridge superstructure was completely installed in 10 h over 2 days.

Bellbird Grove Bridge, Brisbane, Australia, 2006

Bellbird Grove Bridge is a short-span pedestrian bridge comprising an FRP deck and handrails supported on two FRP beams, with a total weight of 2 ton. The fully fabricated bridge was lifted into place by a small crane, over a small stream. Figure 11.16 shows the bridge being craned into place.

Chertanovo Bridge, Chertanovo, Russia, 2005

Chertanovo Pedestrian Bridge crosses a railway line in Moscow, with a length and width of 41 m and 3 m, respectively. The superstructure was fabricated from standard pultruded profiles in three separate sections of 15, 15, and 13 m and transported to the site by road. The three sections were lifted in and connected within a 3 h shutdown of the railway; actual installation took less than 1 h. The installed pedestrian bridge is shown in Figure 11.17 during winter. The reason for choosing an FRP composite superstructure in this case was due to the severe environment and the high maintenance costs associated with steel or concrete solutions.

Kosino Pedestrian Bridge, Moscow, 2005

Kosino Bridge provides pedestrian access over the railway at Kosino station in Moscow. The superstructure is comprised of standard GFRP pultruded sections, shown in Figure 11.18.

FIGURE 11.16 Craning-in of Bellbird Grove Pedestrian Bridge. (Courtesy of Fibre Composite Design and Development Centre, The University of Southern Queensland, Toowoomba, Queensland, Australia.)

FIGURE 11.17 Chertanovo Bridge in Moscow during winter. (Courtesy of ApATeCH, Hertfordshire, U.K.; Fiberline Composites, Middelfart, Denmark.)

FIGURE 11.18 Kosino Station Pedestrian Bridge. (Courtesy of ApATeCH, Hertfordshire, U.K.; Fiberline Composites, Middelfart, Denmark.)

Toowoomba Bridge, Australia, 2002

Toowoomba Bridge was installed in 2002, on a quarry road with a span of 10 m and a width of 5 m, comprising a combination of a concrete top flange with a GFRP box section and un-directional CFRP bottom flange for additional flexural rigidity. A number of these beams are bonded together widthwise using epoxy adhesive to create a deck of 2.5 m width, and an FRP laminate bonded transversely across the bottom flanges to provide transverse stiffness and strength to the deck. Two 2.5 m width sections of deck were transported to site and connected together with a site joint during installation. The total weight of the bridge superstructure is 20 ton. Figure 11.19 shows the bridge during a load test; a more detailed description of the structure can be found in Van Erp and Ayers [13].

FIGURE 11.19 Load test on Toowoomba Bridge, Australia. (Courtesy of Fibre Composite Design and Development Centre, The University of Southern Queensland, Toowoomba, Queensland, Australia.)

Bespoke FRP Composite Bridges

Halgavor Bridge, Cornwall, United Kingdom, 2001

Halgavor Bridge crosses the A30, a busy dual carriageway, in Cornwall and carries pedestrians, cyclists, and equestrians. The bridge superstructure comprises a 48 m span with a steel suspension cable and inclined steel mast system carrying a GFRP composite deck of 3.5 m width and 350 mm depth. The deck surfacing consists of recycled rubber car tires. A GFRP composite deck was proposed due to a required fast installation time (and reduced disruption to the highway network) and good durability with minimal maintenance. Figures 11.20 and 11.21 show the bridge during installation and upon completion. Details of the design and installation of the structure are provided in Firth and Cooper [14].

FIGURE 11.20 Installation of central section of Halgavor Bridge. (Courtesy of Flint & Neill Partnership, London, U.K.)

FIGURE 11.21 Halgavor Bridge crossing the A30 dual carriageway. (Courtesy of Flint & Neill Partnership, London, U.K.)

Cantabrico Motorway Bridge, Spain, 2005

Cantabrico Bridge carries traffic across the Cantabrico Motorway in Spain. The bridge superstructure is comprised of an integral 46 m length reinforced concrete deck with a trapezoidal prepreg CFRP beam with a polyurethane core (also acting as the mold during low-temperature vacuum curing), supported on reinforced concrete piers. The CFRP beams comprise webs with ±45° carbon fibers in an epoxy resin matrix, and top and bottom flanges of ±45° CFRP and unidirectional CFRP. The weight of the complete bridge deck is approximately 15% of an equivalent concrete deck. The installed bridge is shown in Figures 11.22 and 11.23.

Smith Road "Tech 21" Bridge, Butler County, Ohio, 1997

The "Tech 21" Bridge carries two lanes of traffic on Smith Road over a small stream in Butler County, Ohio. The bridge superstructure is comprised of an integral beam and slab system, the "slab" comprising pultruded GFRP tubes with bonded top and bottom GFRP face sheets, supported on hand-laminated GFRP (E-glass/unsaturated polyester) U-beams. The surfacing is asphalt varying from 100 to 150 mm thickness. The bridge spans 33 ft and has a width of 24 ft. Figure 11.24

FIGURE 11.22 Cantabrico Motorway Bridge. (Courtesy of Advanced Composites Group, Derbyshire, U.K.; Acciona S.A., Madrid, Spain.)

FIGURE 11.23 Underside of Cantabrico Motorway Bridge showing CFRP beams. (Courtesy of Advanced Composites Group, Derbyshire, U.K.; Acciona S.A., Madrid, Spain.)

FIGURE 11.24 Transport of deck sections for "Tech 21" Bridge. (Courtesy of Martin Marietta Co., Bethesda, MD.)

shows the combined U-beam and deck sections ready for transport. Figure 11.25 shows the construction of the FRP superstructure.

Taromeo Creek Bridge, Blackbutt, Queensland, Australia, 2005

Taromeo Creek Bridge replaced an old timber bridge with a two-span structure of spans 10 and 12 m, and a width of 10 m, comprising a cellular deck cross section utilizing FRP composite, concrete, and steel fibers. The superstructure consists of a 160 mm thick reinforced concrete deck on FRP composite "webs," each comprising three 100 mm width, 100 mm depth, 5 mm thickness, GFRP box sections bonded vertically, and a 20 mm thick FRP composite/steel fiber resin infused bottom flange.

FIGURE 11.25 Construction of "Tech 21" Bridge. (Courtesy of Martin Marietta Co., Bethesda, MD.)

The deck sections were fabricated as 2.1 and 2.6 m width sections that were installed on site and the longitudinal joints grouted between deck sections in a single day. The total weight of the superstructure was 70 ton compared to an equivalent reinforced concrete deck of 155 ton.

Kings Stormwater Channel Bridge, California, 2000

The Kings Stormwater Channel Bridge comprises a GFRP deck (E-glass fibers, vinylester resin matrix) connected to and supported on six concrete-filled CFRP tubular main beams at approximately 2.3 m spacing. The bridge carries pedestrian and vehicular traffic along the California State Highway near Salton Sea over two spans of 10 m with a deck width of 13 m. The GFRP deck is fabricated from a series of bonded pultruded trapezoidal cellular sections with continuous GFRP face sheets to the top and the bottom, with CFRP tubes comprised of carbon fibers in the longitudinal and hoop direction, stabilized by the concrete core. The CFRP tubes have a ribbed internal surface to enable force transfer between the concrete and CFRP tube. A mechanical U-bar grouted shear connection is used between the GFRP deck and CFRP beams. A thin 13 mm polymer concrete surfacing is used on top of the 152 mm thick GFRP deck. The central pier and abutments are reinforced concrete; however, the central concrete pier is also encased in a CFRP shell. Seible et al. [15] provides further information on the bridge.

OTHER STRUCTURES

Buildings

Severn Visitors Centre, United Kingdom, 1996

The Second Severn Visitors Centre, near the Second Severn Crossing, uses the same pultruded GFRP plank and toggle system used in Aberfeldy Bridge and Bonds Mill Bridge, to form the building structure. Connections in the two-story building are made by bonded lapping plates where required.

Eyecatcher Building, Basel, 1999

The Eyecatcher Building was constructed for the Swissbau 99 exhibition and comprised a frame-type structure with triangular sides of 15 m height and 10 m width, fabricated from standard pultruded GFRP sections with stainless steel bolted connections (Figure 11.26). The building was disassembled and then reassembled into its final location at Munchensteinerstrasse 210, Basel, as an office building.

(a) (b)

FIGURE 11.26 Eyecatcher building: (a) primary structure and (b) lit at night. (Courtesy of ETH, Zurich, Switzerland; Fiberline Composites, Middelfart, Denmark.)

Miscellaneous

Fleetwood RoRo Jetty Refurbishment, United Kingdom, 2005

Fleetwood port is on the Northwestern coast of England and provides ferry services to the Republic of Ireland and further abroad. One of the roll-on roll-off (RoRo) jetties in this port, which provided access from ferries to the road network, comprised a reinforced concrete deck on crossheads supported on steel octagonal piles founded on the seabed. The reinforced concrete crossheads were experiencing considerable spalling to the soffit with corrosion to the steel reinforcement, and the top sections of the steel octagonal piles were corroding. An extensive refurbishment scheme was developed to reinstate the original condition of the bridge deck, comprising cathodic protection to the deck, CFRP wrapping to the tops of the steel piles, and jacking of the concrete crossheads during removal of degraded concrete and reinstatement of reinforcement. Jacking of the deck was enabled by using 36 in. deep proprietary carbon/glass fiber double web beams attached to the octagonal piles by bespoke fabricated steelwork collars with integral brackets as supports for the FRP jacking beam. A general view of the structure and the jacking arrangement is shown in Figures 11.27 and 11.28, respectively. FRP composite beams were proposed, as access to the soffit of the jetty was difficult and lightweight components would be easier to maneuver, would maximize durability in the very severe environment, and were also found to be competitive in cost to steel girders for the same function. Six hybrid FRP beams were jacked simultaneously prior to reinstatement of steel reinforcement and concrete to the crossheads, and monitored until the specified jacking load of 35 ton was achieved and deflection checked. The FRP beams are in the tidal zone and will be subject to storm loads and sever wetting/drying. Further details of the repair and strengthening scheme are provided in Canning and Thoday [16].

FIGURE 11.27 General view of jetty. (Courtesy of Mouchel Parkman, Leicester, U.K.)

FIGURE 11.28 FRP jacking beam and fabricated steelwork brackets. (Courtesy of Mouchel Parkman, Leicester, U.K.)

FRP Composite Waler Beam, Brisbane City Wharf Project, Australia

An 800 m length floating walkway structure on the Brisbane River required a corrosion-resistant connection to tie the separate parts of the floating walkway together. An FRP composite waler beam was developed and installed to meet the required 100 year design life (Figure 11.29).

FRP Composite Walkway and Other Systems, Numerous Worldwide

There are numerous examples of FRP composite products used for walkways, stairways, stair treads, and other minor structural applications; however, this does not reduce their importance for providing

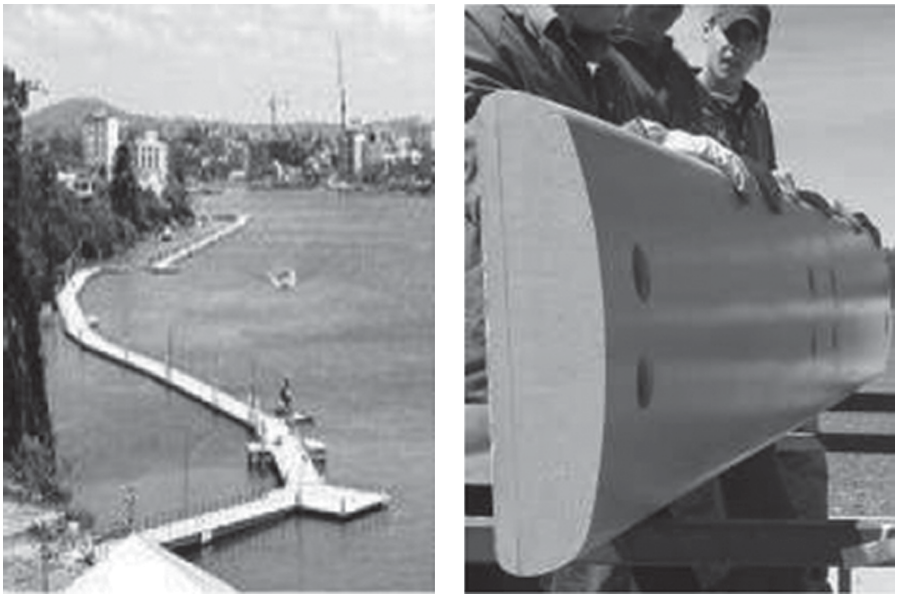

(a) (b)

FIGURE 11.29 (a) Brisbane River Wharf and (b) FRP composite waler beam. (Courtesy of Fibre Composite Design and Development Centre, The University of Southern Queensland, Toowoomba, Queensland, Australia.)

cost-effective solutions. FRP composite walkways are quite common in industrial factories, water purification plants, etc., where the environment is generally too severe for the economic use of concrete and steel components, or where lightweight materials are required such as roof access walkways.

Figures 11.30 through 11.33 show some general applications of FRP composites in these areas. In these cases, the supply and installation cost were less than that for alternatives due to simple installation and handling. In addition, minimal maintenance of the chosen solution was an important factor due to the remote location and/or difficult access.

FIGURE 11.30 Parapet walkways for maintenance/inspection access on the railway. (Courtesy of Pipex px®, Plymouth, U.K.)

FIGURE 11.31 Jetty walkway, Ireland. (Courtesy of Pipex px®, Plymouth, U.K.)

FIGURE 11.32 Roof access walkway, Gatwick Airport. (Courtesy of Pipex px®, Plymouth, U.K.)

CONCEPTS

I-5/Gilman Advanced Technology Bridge, San Diego, California

This bridge concept will provide access between the eastern and western parts of the University of California San Diego campus, over a 137 m span. The conceptual design of the bridge comprises a dual-plane fan type cable-stayed system supporting a lightweight deck. The cables will be manufactured from CFRP composite and will fan from a 58 m tall A-frame pylon fabricated from concrete-filled CFRP tubes. The deck will comprise a polypropylene fiber-reinforced concrete deck on transverse hybrid GFRP/CFRP transverse beams and lightweight concrete-filled CFRP tubular main beams. Seible et al. [15] provide further details on this structure.

FIGURE 11.33 Service walkway on footbridge, Gatwick Airport. (Courtesy of Pipex px®, Plymouth, U.K.)

Sandy Creek Bridge, Nanango, Queensland, Australia

The concept for this bridge is generally similar to that for the previously described Taromeo Creek Bridge; however, the concept uses FRP composite "webs" comprising sandwich panels with an FRP composite bottom flange.

FRP Guided Transport Systems

A number of concepts have been developed for the use of FRP composite monorail or guided transport systems for use in a variety of locations. One such example is an FRP composite guided transport system using one of two options: a "modular" system and a "bespoke" system.

For the "modular" system, standard pultruded GFRP sections with steel or GFRP/CFRP hybrid beams for the superstructure (with an integral gritted deck), supported on steel or concrete-filled GFRP columns, would be used. At the support locations, the FRP deck sections would be filled with polymer grout for adequate shear and direct compression resistance. For the "bespoke" system, a monocoque hybrid CFRP/CFRP structure with an integral gritted surface would be used.
Such a system may provide a number of benefits:

- Ease of installation due to a very lightweight superstructure (~2 kN/m^2) and support system, and prefabricated structural deck sections.
- Highly durable materials with minimal maintenance.

Similar preliminary studies have also been undertaken on FRP composite elevated structures to carry cyclists above, and away, from general road traffic.

"City in the Air," Japan

A number of studies are ongoing in Japan on the use of FRP composites, with other materials, in "mega-structures" for next-generation structure, such as residential and office towers, and general

living areas, of greater than 400 m height and many city blocks wide, due to the premium on footprint space. The lightweight nature of FRP composites would be one particular advantage in this case, to reduce dead load on the foundations and structure in general.

Crash Barriers and Lighting Columns

FRP composite crash barriers for vehicle containment (Figure 11.34) have been under development in the Netherlands and other countries and may give safety and economic benefits due to greater vehicle occupant survivability and low maintenance, respectively. FRP composites can also exhibit good energy absorption characteristics if correctly designed, as crushing, delamination, and fiber pull-out are all effective absorbers of energy.

A similar safety concept has been used for the development of FRP composite lighting columns where the risk of harm to vehicle occupants during collision is reduced due to the directional strength of the lighting column and lower stiffness compared to steel columns, together with reduced maintenance.

Tidal Power Devices

Wave and tidal power devices have the potential to deliver a significant part of the current electricity demand. This is presently an embryonic industry, but is expected to provide a significant market opportunity for the use of composite materials. It is expected that the marine renewable sector will develop rapidly with greater awareness of the need to reduce carbon emissions. It is also expected that composites will be used for primary structures of many devices, offering advantages such as durability and corrosion resistance, lighter weight leading to simplified installation and the ability to mold complex shapes, all leading to more efficient devices.

The majority of the tidal power resource exists in water depths of 40 m or more, and TidalStream are developing a large articulated underwater turbine to harness this energy resource, as shown in

FIGURE 11.34 Prototype FRP composite crash barrier. (Courtesy of Lightweight Structures BV, Delft, the Netherlands.)

FIGURE 11.35 Concept for tidal turbines using FRP composites. (Courtesy of White Young Green and TidalStream, Warwickshire, U.K.)

Figure 11.35. This image shows an articulated structure designed to operate in 60 m water depth, supporting four 1 MW turbines. The blades on each turbine are 10 m long, and the main vertical spar is 60 m long.

SUMMARY

The case studies described earlier are a small selection of the total number of all-FRP composite bridges now installed worldwide, but they give an indication of the wide variety of FRP composite manufacturing methods and structural types that have been designed and constructed, and possible future uses of FRP composites.

The case studies highlight a number of important points:

- FRP composite structures can be installed relatively quickly
- FRP composite structures provide durable, low-maintenance structures
- FRP composite structures are currently most cost-effective when whole life costs or other factors, such as costly major highway and railway closures during installation, severe environments, or poor access requiring lightweight materials, are pertinent
- A wide variety of structural forms and manufacturing methods have been successfully developed and used
- Bespoke designs are becoming more common for new-build FRP composite structures, whereas modular FRP composite components are frequently used for bridge deck replacement

In particular, the increase in bespoke designed FRP composite structures shows that confidence is growing in the design of FRP composites by civil engineers. Figure 11.36 shows the recent trend for the number of bridge structures (where details have been published), among other types of structure, where FRP composites form the primary load-bearing components (i.e., FRP composite beams and/or FRP decks; bridges with FRP cables, tendons, or reinforcement are not included). It can be seen that applications have generally increased, and all-FRP composite structures are

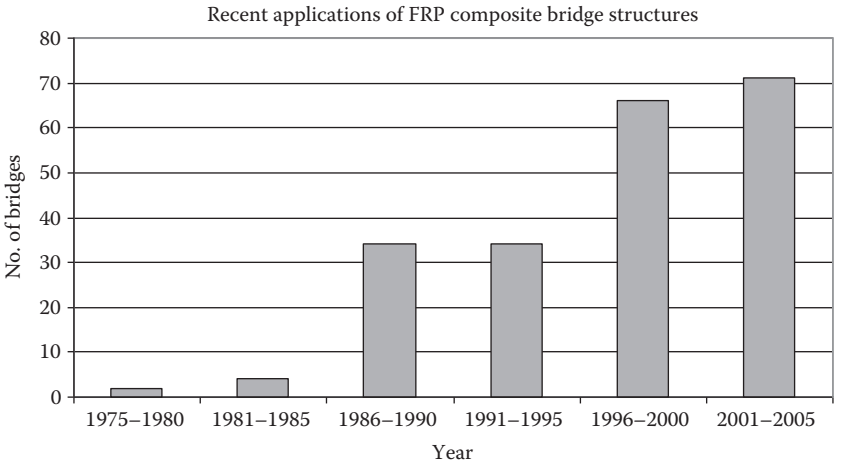

FIGURE 11.36 Recent trends in FRP composite bridge applications.

beginning to show their economic advantages and competitiveness; many initial installations of FRP composite bridges were undertaken as demonstration projects and were not easy to justify solely on economic grounds.

In recent years, there has also been a large increase in the use of lightweight FRP composite decks as replacement for heavier steel and concrete decks on existing structures. This enables dead load to be reduced and the live load capacity of the existing structure to be increased with no other additional major structural renovations. This clearly is advantageous due to the minimal disruption to traffic on highway networks; there have been relatively few applications of this type over, or carrying railways, presumably due to the generally more conservative nature of that industry where safety is paramount, although it would seem that there would be a good economic case for such applications.

ACKNOWLEDGMENTS

The authors would like to thank Fiberline Composites (Denmark), Martin Marietta (the United States), Pipex px (United Kingdom), Creative Pultrusions (the United States), Hardcore Composites (the United States), Strongwell (the United States), Mouchel Parkman (United Kingdom), Flint and Neill (United Kingdom), and Fibre Composite Design and Development (Australia), for various photographs and technical information. The authors would also like to thank David Kendall and Len Hollaway for useful discussion and general information.

REFERENCES

1. Canning, L. and Luke, S., West Mill Bridge—Comparison of initial and long-term structural behaviour, in *Proceedings of the Third International Conference on Bridge Maintenance, Safety and Management*, Porto, Portugal, 2006.
2. Hayes, M., Characterization and modeling of a fiber-reinforced polymeric composite structural beam and bridge structure for use in the Tom's Creek Bridge rehabilitation project, MSc thesis, Virginia Polytechnic Institute and State University, Blacksburg, VA, 1998.
3. Senne, J., Fatigue life of hybrid FRP composite beams, MSc thesis, Virginia Polytechnic Institute and State University, Blacksburg, VA, 2000.
4. Kassner, B., Long-term in-service evaluation of two bridges designed with fibre-reinforced polymer girders, MSc thesis, Virginia Polytechnic Institute and State University, Blacksburg, VA, 2004.
5. Neely, W., Evaluation of the in-service performance of the Tom's Creek Bridge, MSc thesis, Virginia Polytechnic Institute and State University, Blacksburg, VA, 2000.

6. Waldron, C., Determination of the design parameters for the Route 601 Bridge: A bridge containing the Strongwell 36 in. hybrid composite double web beam, MSc thesis, Virginia Polytechnic Institute and State University, Blacksburg, VA, 2001.
7. Gangarao, H., Thippeswamy, H., Shekar, V., and Craigo, C., Development of glass fibre reinforced polymer composite bridge deck, *SAMPE Journal*, 35(4), 12–24, 1999.
8. Burgoyne, C., Advanced composites in civil engineering in Europe, *Structural Engineering International*, 9(4), 267–273, 1999.
9. Alampalli, S., O'Connor, J., and Yannotti, A., Design, fabrication, construction, and testing of an FRP superstructure, Special Report 134, Transport Research and Development Bureau, New York State Department of Transportation, Albany, New York, 2000.
10. Jinka, C., Dynamic response evaluation of fibre reinforced composite bridge decks and bridges, MSc thesis, West Virginia University, Morgantown, WV, 2003.
11. Braestrup, M., Footbridge constructed from glass-fibre-reinforced profiles, Denmark, *Structural Engineering International*, 9(4), 256–258, 1999.
12. Strehler, B. and Kunzle, O., Static and dynamic testing of fibre-reinforced bridge girders, *Structural Engineering International*, 9(4), 300–301, 1999.
13. Van Erp, G. and Ayers, S., A fair dinkum approach to fibre composites in civil engineering, in *Proceedings of the Second International Conference ACIC 2004*, Hollaway, L. and Chryssanthopoulos, M., Eds., Woodhead Publishing Ltd., Cambridge, U.K., 2004.
14. Firth, I. and Cooper, D., New materials for new bridges—Halgavor bridge, U.K., *Structural Engineering International*, 12(2), 80–83, 2002.
15. Seible, F., Karbhari, V., and Burgueno, R., Kings stormwater channel and I-5/Gilman bridges, USA, *Structural Engineering International*, 9(4), 250–253, 1999.
16. Canning, L. and Thoday, N., Refurbishment of fleetwood RoRo jetty, in *Advanced Composites in Construction Conference 2007*, University of Bath, Bath, U.K., 2007.

Part III

Externally Bonded FRP Composite Systems for Rehabilitation

Masoud Motavalli

12 Introduction

Masoud Motavalli

CONTENTS

IMPORTANCE OF FIBER COMPOSITES IN STRUCTURAL REHABILITATION

The deterioration and functional deficiency of existing civil infrastructure represent one of the most significant challenges facing countries in the twenty-first century. In the United States, nearly 11% of the nation's highway bridges are presently structurally deficient and 19% are functionally obsolete. In the United Kingdom, over 10,000 concrete bridges need structural attention (Rizkalla and Hassan 2002). A substantial number of structures in Europe are more than 30 years old. While they require continual maintenance, they also require strengthening due to lack of strength, stiffness, ductility, and durability (Motavalli and Czaderski 2007).

In addition to deterioration and degradation caused through aging, weathering of materials, and accidental damage to structures, traffic and housing/industrial needs have increased dramatically over the past few decades with the transportation of goods and services being conducted on a global, rather than local basis. There is a need for the widening of highway systems to accommodate greater flow of traffic and for the strengthening of existing structures to carry heavier loads at higher speeds. Enhanced understanding of structural response and natural threats such as earthquakes and storms has led to the establishment of new design codes, and the consequent need to rehabilitate existing structures to ensure their continued safety. Conventional materials such as timber, steel, and concrete have a number of advantages, not the least of which is the relatively low cost of the raw materials. However, it is clear that conventional materials and technologies, although suitable in some cases, and with a fairly successful history of past usage, lack longevity in some cases and, in others, are susceptible to rapid deterioration (see Figures 12.1 and 12.2), thereby emphasizing the need for better grades of these materials or newer technologies to supplement the conventional ones used (Karbhari and Seible 2000).

Fiber-reinforced polymers (FRPs), a relatively new class of noncorrosive, high-strength, and lightweight material, have, over the past approximately 15 years, emerged as practical materials for a number of structural engineering applications. The rapid increase in the use of FRP materials for structural engineering applications can be attributed to continuing reductions in cost, to more comprehensive knowledge of the fundamental properties of composites, which enable more specific uses and has reduced safety factors to realistic levels, and to the numerous advantages of FRPs as compared with conventional materials such as concrete and steel. Some of the commonly cited advantages of FRP materials over more conventional materials include (ISIS-Canada 2003) the following:

- High strength-to-weight ratios
- Outstanding durability in a variety of environments
- Ease and speed of installation, flexibility, and application techniques

FIGURE 12.1 Deterioration of reinforced concrete columns due to corrosion. (Taken from ISIS-Canada, *An Introduction to FRP Composites for Construction*, ISIS Canada, Toronto, Ontario, Canada, www.isiscanada.com, 2003.)

FIGURE 12.2 Deteriorated column of a building with low concrete quality and insufficient lateral reinforcement at the bottom of the column.

- Electromagnetic neutrality, which can be important in certain special structures such as magnetic imaging facilities
- The ability to tailor mechanical properties by the appropriate choice and direction of fibers
- Outstanding fatigue characteristics (carbon FRP [CFRP]) and low thermal conductivity

Historical Background

FRPs have been used in the automotive and aerospace industries for more than 50 years in applications where their high strength and lightweight can be used to great advantage. The history of the use of polymers and composites in the construction industry began during the Second World War,

when rapid progress was made with the manufacture of the first radomes to house electronic radar equipment. The main growth interest and technology in the glass fiber/polyester composite in the building and construction industry started in the 1960s (Hollaway 1993). Two major structures were built made of glass fiber–reinforced polymer: the dome structure in Benghazi built in 1968 and the roof structure at Dubai airport built in 1972. By the late 1980s and early 1990s, as the defense market waned, increased importance was placed by fiber and FRP manufacturers on cost reduction for the continued growth of the FRP industry (Bakis et al. 2002). With the decreasing cost of FRP and the increasing need for infrastructure repair and renewal since the early 1990s, interest in the use of FRP materials for structures has also increased steadily, and there are currently hundreds of field applications of FRPs in structures around the world. The Ibach Bridge, located in the Canton of Lucerne in Switzerland, was repaired in 1991 with three CFRP strips making it the first CFRP-reinforced concrete bridge in the world. More in-depth historical background and development overview reports from around the world can be found in Hollaway (1993), Meier (2000), Teng et al. (2002), Bank (2006), GangaRao et al. (2007), and Motavalli and Czaderski (2007).

Part III Contents

The focus in the present discussion is on those FRP materials that are currently used in the rehabilitation of structural engineering applications. That is, although many different material combinations (combinations of fiber and matrix) are possible, only a very small sample of the almost infinite number of possibilities is presented herein. The reader should also keep in mind that several different manufacturing techniques, component shapes, and end-use applications are available for FRP materials, but that only those most relevant to structural engineering are discussed. More comprehensive discussions of FRP materials are available in various composite materials texts (see Eckold 1994; Herakovich 1998; Bank 2006; GangaRao et al. 2007).

The following chapters in Part III introduce composite materials used in rehabilitation, unstressed and prestressed flexural and shear strengthening of reinforced concrete structures, unstressed and prestressed near-surface-mounted reinforcement, confinement of concrete columns, strengthening of masonry, wood and metallic structures, and durability issues. Several simple examples will be presented to show the design procedure of each case.

REFERENCES

Bakis, C. E., L. C. Bank et al. (2002). Fiber-reinforced polymer composites for construction—State-of-the-art review. *Journal of Composites for Construction* 6(2): 73–87.

Bank, L. C. (2006). *Composites for Construction: Structural Design with FRP Materials*, John Wiley & Sons, Inc., Hoboken, NJ.

Eckold, G. (1994). *Design and Manufacture of Composite Structure*, Woodhead Publishing Limited, Cambridge, U.K.

GangaRao, H. V. S., N. Taly et al. (2007). *Reinforced Concrete Design with FRP Composites*, CRC Press, Boca Raton, FL.

Herakovich, C. T. (1998). *Mechanics of Fibrous Composites*, John Wiley & Sons, Inc., New York.

Hollaway, L. (1993). *Polymer Composites for Civil and Structural Engineering*, Blackie Academic & Professional, Glasgow, U.K.

ISIS-Canada (2003). *An Introduction to FRP Composites for Construction*, ISIS Canada, Toronto, Ontario, Canada, www.isiscanada.com

Karbhari, V. M. and F. Seible (2000). Fiber reinforced composites—Advanced materials for the renewal of civil infrastructure. *Applied Composite Materials* 7: 95–124.

Meier, U. (2000). Composite materials in bridge repair. *Applied Composite Materials* 7(2–3): 75–94.

Motavalli, M. and C. Czaderski (2007). *FRP Composites for Retrofitting of Existing Civil Structures in Europe: State-of-the-Art Review*, ACMA, Tampa, FL, October 17–19, 2007.

Rizkalla, S. and T. Hassan (2002). Effectiveness of FRP for strengthening concrete bridges. *Structural Engineering International* 12(2): 89–95.

Teng, J. G., J. F. Chen et al. (2002). *FRP Strengthened RC Structures*, John Wiley & Sons, Ltd., Chichester, U.K.

13 Composite Materials Used in Rehabilitation

Masoud Motavalli

CONTENTS

RAW MATERIALS

Fiber-reinforced polymer (FRP) composite materials are made of three essential constituents: fibers, polymers, and additives. In fibrous polymeric composites, fibers with high strength and high stiffness are embedded in and bonded together by the low-modulus continuous polymeric matrix. In the case of FRP composites, the reinforcing fibers constitute the backbone of the material, and they determine its strength and stiffness in the direction of the fibers. The additives include plasticizers, flame retardants, blowing agents, and coupling agents. Other constituents in small quantities include coatings, pigments, and fillers (GangaRao et al. 2007).

To utilize the full potential of the composites in structural applications, the properties and behavior of its constituents, the fibers and matrices, must be understood.

Fibers

Fibers are used in polymeric composites because they are strong, stiff, and lightweight. Fibers are stronger than the bulk material that constitutes the fibers due to their preferential orientation of molecules along the fiber direction and because of the reduced number of defects present in fibers compared to the bulk material. The desirable structural and functional requirements of the fibers in composites are high elastic modulus for an efficient use of reinforcement; high ultimate strength and low variation of strength between individual fibers; stability of properties during handling and fabrication; uniformity of fiber diameter and surface; high toughness; durability; and availability in suitable forms and acceptable cost. The most common fibers used to make FRP composites are glass, carbon, and aramid. All these fibers exhibit a linear elastic behavior under tensile loading up to failure without showing any yielding (see Figure 13.1). Typical properties of various types of reinforcing fibers are summarized in Table 13.1. Diameters of the fibers are compared in Figure 13.2.

Glass fibers are the most commonly used reinforcing fibers for polymeric matrix composites. Molten glass can be drawn into continuous filaments that are bundled into rovings. During fabrication, fiber surfaces are coated to improve wetting by the matrix and provide better adhesion between

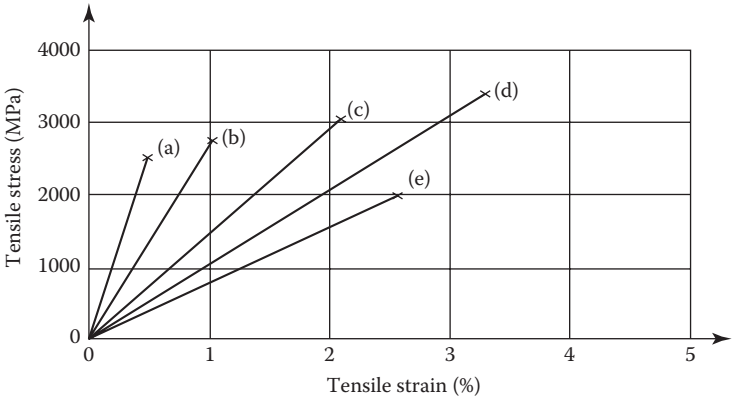

FIGURE 13.1 Stress–strain curves of typical reinforcing fibers (a) carbon (high modulus); (b) carbon (high strength); (c) aramid (Kevlar 49); (d) S-glass; and (e) E-glass.

TABLE 13.1
Typical Properties of Various Types of Reinforcing Fibers

Fiber Type	Density (kg/m³)	Tensile Strength (MPa)	Young Modulus (GPa)	Ultimate Tensile Strain (%)	Thermal Expansion Coefficient (10^{-6}/°C)	Poisson's Coefficient
E-glass	2500	3450	72.4	2.4	5	0.22
S-glass	2500	4580	85.5	3.3	2.9	0.22
Alkali-resistant glass	2270	1800–3500	70–76	2.0–3.0	—	—
ECR	2620	3500	80.5	4.6	6	0.22
Carbon (high modulus)	1950	2500–4000	350–650	0.5	−1.2 to −0.1	0.20
Carbon (high strength)	1750	3500	240	1.1	−0.6 to −0.2	0.20
Aramid (Kevlar 29)	1440	2760	62	4.4	−2.0 longitudinal 59 radial	0.35
Aramid (Kevlar 49)	1440	3620	124	2.2	−2.0 longitudinal 59 radial	0.35
Aramid (Kevlar 149)	1440	3450	175	1.4	−2.0 longitudinal 59 radial	0.35
Aramid (Technora H)	1390	3000	70	4.4	−6.0 longitudinal 59 radial	0.35
Aramid (SVM)	1430	3800–4200	130	3.5	—	—

the composite constituents. Coating the glass fibers with a coupling agent will provide a flexible layer at the interface, the strength of the bond is improved, and the number of voids in the material is reduced. The most common glass fibers are made of E-glass, S-glass, and alkali-resistant (AR) glass. E-glass is the least expensive of all glass types, and it is broadly used in the fiber-reinforced plastics industry. S-glass has a higher tensile strength and higher modulus than E-glass. However, the higher cost of S-glass fibers makes them less popular than E-glass. AR glass fibers, which could help prevent corrosion by alkali attacks in cement matrices, can be produced by adding zirconium. AR glass fibers that are compatible with commonly utilized thermoset resins, however, are not currently available.

The tensile strength of glass fibers reduces at elevated temperatures but can be considered constant for the range of temperatures at which polymer matrices are exposed. The tensile strength also reduces with chemical corrosion and with time under sustained loading.

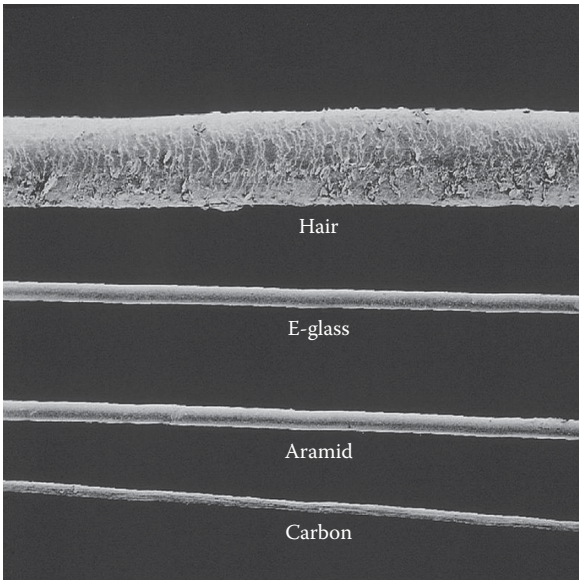

FIGURE 13.2 Comparison of the fiber diameter of three most common fibers to the human hair.

Carbon and graphite fibers are used interchangeably, but there are some significant differences between the two as far as their modular structure is concerned. Most carbon fibers are produced by thermal decomposition of polyacrylonitrile. The carbon atoms are arranged in crystallographic parallel planes of regular hexagons to form graphite, while in carbon, the bonding between layers is weak, so that it has a two-dimensional ordering. The manufacturing process of carbon and graphite fibers consists of oxidation at 200°C–300°C, different stages of carbonization at 1000°C–1500°C and 1500°C–2000°C, and finally graphitization at 2500°C–3000°C. Graphite has a higher tensile modulus than carbon, therefore high-modulus fibers are produced by graphitization. Carbon fibers are commercially available in long and continuous tows, which are bundles of 1,000–160,000 parallel filaments. These fibers exhibit high specific strength and stiffness; in general, as the elastic modulus increases, the ultimate tensile strength and failure elongation decrease (Figure 13.1). The tensile modulus and strength of carbon fibers are stable as temperatures rise; they are also highly resistant to aggressive environmental factors. Carbon fibers behave elastically up to failure and fail in a brittle manner. The greatest disadvantage of carbon fibers is their high cost. They are 10–30 times more expensive than E-glass. The high cost of these fibers is due to the high price of raw materials and the long process of carbonization and graphitization. Moreover, graphite fibers cannot be easily wetted by the matrix; therefore, sizing is necessary before embedding them in a matrix.

Polymeric fibers, using a suitable processing method, can exhibit high strength and stiffness. This happens as a result of the alignment of the polymer chains along the axis of the fiber. Aramid is a generic term for a group of organic fibers that have the lowest specific gravity and the highest tensile strength-to-weight ratio among the current reinforcing fibers. Aramid fibers are currently produced by, for example, DuPont (Kevlar), Teijin (Technora), and Akzo Nobel (Twaron). Kevlar has very good tension fatigue resistance and low creep, and it can withstand relatively high temperatures. The strength and modulus of Kevlar fibers decrease linearly with rising temperatures, but retain more than 80% of their original strength at 180°C. Kevlar fibers absorb some water, the amount of absorbed water depending on the type of the fiber, and are sensitive to UV light. At high moisture content, Kevlar fibers tend to crack internally at the preexisting micro voids and produce longitudinal splitting. Kevlar fibers are resistant to many chemicals, but they can be degraded by some acids and alkalis.

Carbon and aramid fibers are anisotropic with different values of mechanical and thermal properties in the main directions, whereas glass fibers are isotropic (Eckold 1994).

Matrix

The matrix in a polymeric composite can be regarded as both a structural and a protection component. Resin is a generic term used to designate the polymer, polymer precursor material, and/or mixture or formulation thereof with various additives or chemically reactive components. In general, a polymer is referred to as a resin system during processing and a matrix after the polymer has cured. Composite material fabrication and properties are fundamentally affected by the resin, its chemical composition, and physical properties. The matrix materials generally account for between 30% and 60% by volume of a polymeric composite. The main functional and structural requirements of a matrix are to bind the reinforcing fibers together, transfer and distribute the load to the fibers, and protect the fibers from environmental attacks and mechanical abrasion. Hence, the choice of matrix is of paramount importance when designing a composite system and will affect both the mechanical and physical properties of the final product.

There are two basic classes of polymeric matrices used in FRP composites: thermosetting and thermoplastic resins. Thermosetting resins are polymers that are irreversibly formed from low-molecular-weight precursors of low viscosity. These polymers have strong bonds both in the molecules and between the molecules. They develop a network structure that sets them in shape. If they are heated after they have been cured, they do not melt and will retain their shape until they begin to thermally decompose at high temperatures.

Thermoplastics are polymers that do not develop cross-links. They are capable of being reshaped, and repeatedly softened and hardened by subjecting them to temperature cycles reaching values above their forming temperature.

The term epoxy resin defines a class of thermosetting resins prepared by the ring-opening polymerization of compounds containing on average more than one epoxy group per molecule. Prior to adding fibers, small amounts of reactive curing agents are added to liquid resin to initiate polymerization. Cross-links are formed and epoxy liquid resin changes to a solid material. High-performance epoxies have been prepared with a variety of phenolics and aromatic amines. Epoxy resins can be partially cured; thus, the reinforcement can be pre-impregnated with liquid resin and partially cured to give a prepreg.

The main advantages of epoxy resins are good mechanical properties, easy processing, low shrinkage during curing (leading to good bond characteristics when used as adhesives), and good adhesion to a wide variety of fibers. Epoxies have a high corrosion resistance and are less affected by water and heat than other polymeric matrices. Curing of such resins can be achieved at temperatures ranging between 5°C and 150°C. Epoxy resins can be formulated to have a wide range of stiffness and other mechanical properties.

The main disadvantages of epoxy resins are their relatively high cost and long curing period. The cost of epoxies is proportional to their performance and varies over a broad range, but epoxies are generally more expensive than polyesters and vinyl esters. Furthermore, the toughness of the resin and the composite can be controlled by adding additives, including thermoplastics.

Polyester resins are low-viscosity liquids based on unsaturated polyesters, which are dissolved in a reactive monomer, such as styrene. The addition of heat and a free radical initiator, such as organic peroxide, results in a cross-linking reaction, converting the low-viscosity solution into a three-dimensional thermosetting matrix. Cross-linking can also be accomplished at room temperature using peroxides and suitable activators. Polyester resins can be formulated to have good UV resistance and to be used in outdoor applications. There are many glass fiber-reinforced polyester structures that have been in use for more than 30 years, affected only by some discoloration and small loss in strength. Superior durability and resistance to fiber erosion can be obtained when

TABLE 13.2
Some Representative Material Data for Polyester Resins

	Matrix		
Property	**Polyester**	**Epoxy**	**Vinyl Ester**
Density (kg/m^3)	1200–1400	1200–1400	1150–1350
Tensile strength (MPa)	34.5–104	55–130	73–81
Longitudinal modulus (GPa)	2.1–3.45	2.75–4.10	3.0–3.5
Poisson's coefficient	0.35–0.39	0.38–0.40	0.36–0.39
Thermal expansion coefficient (10^{-6}/°C)	55–100	45–65	50–75
Moisture content (%)	0.15–0.60	0.08–0.15	0.14–0.30

styrene is supplemented with methyl methacrylate. The resistance to burning of polyester resins can be achieved by using either filler or a specially formulated flame-retardant polyester resin, depending on the degree of resistance required. Incorporating halogens into a polyester resin has been found to be an effective way of improving fire retardancy. Polyester resins are used in applications requiring corrosion resistance.

Some representative material data for polyester resins are given in Table 13.2. They correspond to unreinforced cast samples of resin. Using any fibrous reinforcement dramatically improves the mechanical properties of the resin. The main disadvantage of polyester resins is their high volumetric shrinkage. This volumetric shrinkage can be reduced by adding a thermoplastic component. Cross-linking can affect the properties of polyester resins in the same manner as for epoxy resins.

Vinyl esters are resins based on methacrylate and acrylate. Some variations contain urethane and ester bridging groups. Due to their chemical structures, these resins have fewer cross-links, and they are more flexible and have a higher fracture toughness than polyesters. They also have very good wet-out and good adhesion when reinforced with glass fibers. Their properties are a good combination of those of epoxy resins and polyesters and make them the preferred choice for the manufacturing of glass fiber-reinforced composites. They exhibit some of the beneficial characteristics of epoxies such as chemical resistance and tensile strength, as well as those of polyesters such as viscosity and fast curing. However, their volumetric shrinkage is higher than that of epoxy and they have only moderate adhesive strength compared to epoxy resins. There is a great variety of vinyl ester resins available for applications up to 170°C. Vinyl ester resins are highly resistant to acids, alkalis, solvents, and peroxides. Brominated versions have high flame retardancy. Typical properties are given in Table 13.2.

Thermoplastic resins are softened from a solid state to be processed hot, whereupon they return to this state after processing is completed and are allowed to cool down. They do not undergo any chemical transformation during processing. Thermoplastics have high viscosity at processing temperatures, making them difficult to process. Since impregnation is impaired by high viscosity, special care must be taken to ensure contact between the fibers and the polymeric resin (Bank 2006; GangaRao et al. 2007).

Composites with thermoplastic matrices can be repaired due to the fact that the transition to the softened state can be achieved any number of times by the application of heat. Polyether ether ketone (PEEK) is the most common thermoplastic resin for high-performance applications. It has high fracture toughness, which is important for the damage tolerance of composites. PEEK has very low water absorption (about 0.5% by weight) at room temperature. Polyphenylene sulfide (PPS) is a thermoplastic with very good chemical resistance. Polysulfone (PSUL) is a thermoplastic with a very high elongation to failure and excellent stability under hot and wet conditions. Some properties of these thermoplastic matrices are given in Table 13.3.

TABLE 13.3
Some Properties of Three Thermoplastic Matrices

	Matrix		
Property	**PEEK**	**PPS**	**PSUL**
Density (kg/m^3)	1320	1360	1240
Tensile strength (MPa)	100	82.7	70.3
Tensile modulus (GPa)	3.24	3.30	2.48
Tensile elongation (%)	50	5	75
Poisson's coefficient	0.40	0.37	0.37
Thermal expansion coefficient (10^{-6}/°C)	47	49	56

FRP Composites for Externally Bonded Reinforcement

In general, for externally bonded reinforcement, fabrics and prefabricated strips are available.

Fabrics have woven or nonwoven fibers in one or more directions (see Figure 13.3). They are applied on the surface through either a "dry" or the "wet" application. The "dry" application means that the impregnation resin is applied on the structure and then the fabric is applied in a dry state to the resin. By using a roller, the fabric is pressed into the resin (Figure 13.4). Any additional layers are applied by again applying impregnation resin and applying the dry fabric.

"Wet" application means that the fabric is pre-impregnated in a saturator machine and then applied in a "wet" state to the surface of the structure.

Prefabricated strips consist of unidirectional fibers in the longitudinal direction of the strips that are embedded in an epoxy matrix (Figure 13.5). They are produced in a pultrusion process. Furthermore, in addition to strips, prefabricated L-shaped strips are available (Figure 13.6). They also have fibers only in the longitudinal direction and are embedded in an epoxy matrix. Due to their shape, however, they

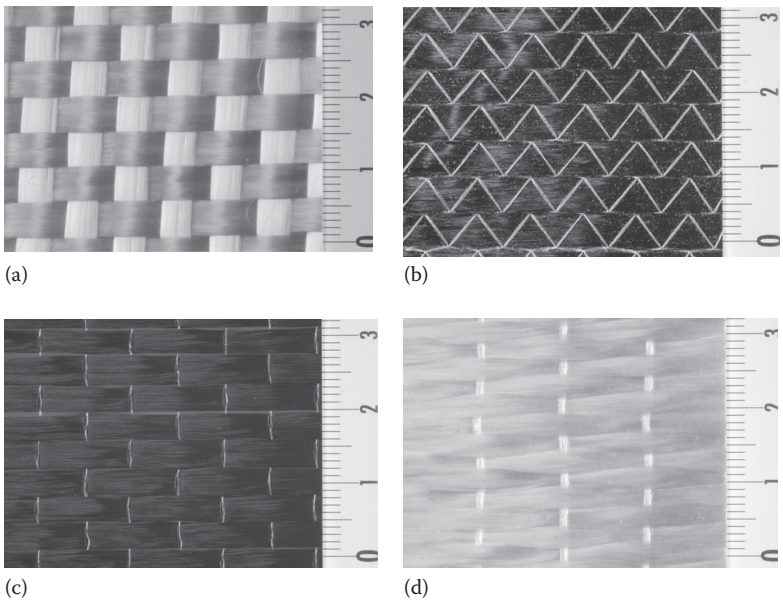

FIGURE 13.3 Different types of fabrics: (a) woven fibers, (b, c, and d) nonwoven fibers. (Photo courtesy of Empa, Dübendorf, Switzerland.)

FIGURE 13.4 Application of fabrics on masonry. (Photo courtesy of Sika AG, Baar, Switzerland.)

FIGURE 13.5 Straight strips produced in a pultrusion process. (Photo courtesy of Empa, Dübendorf, Switzerland.)

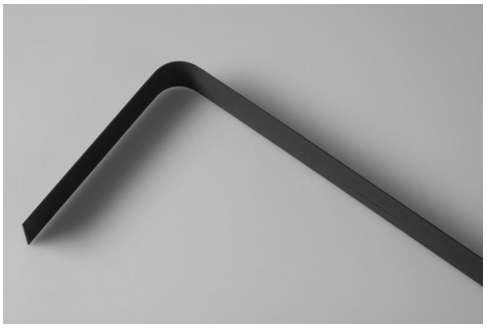

FIGURE 13.6 Prefabricated CFRP L-shaped strips. (Photo courtesy of Empa, Dübendorf, Switzerland.)

cannot be produced by pultrusion and therefore require a special production process. Strips are applied directly on the surface of a structure that is pretreated, for example, by grinding or sandblasting, using a two-component epoxy adhesive. Another technique is the so-called near-surface-mounted reinforcement (NSMR), which means that the strips are embedded into slits in the concrete. NSMR has the advantage that there is a greater bond area between the reinforcement and the concrete (see Chapter 15 in Part III).

If strips or fabrics are applied in a prestressed state, the use of special techniques is necessary. Different products for anchorages using steel or FRP anchors in combinations with special prestressing devices are available on the market and/or under development, see, for example, Kim et al. (2008).

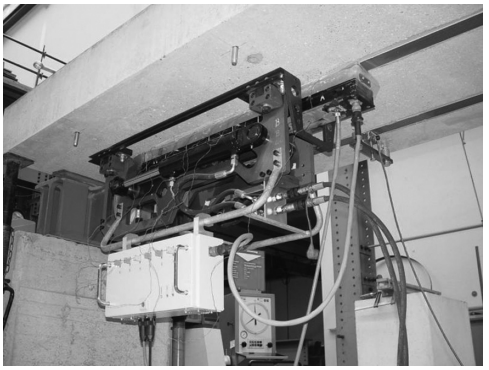

FIGURE 13.7 Prestressing and heating device for producing the gradient anchorage. (Photo courtesy of Empa, Dübendorf, Switzerland.)

All of these anchorage systems, however, must be fixed to the base element with screws or dowels. A method developed at the Swiss Federal Laboratories for Materials Testing and Research (Empa) produces a decrease in the prestressing force at the strip end (see Figure 13.7) and therefore does not require any permanent anchorages and steel pieces (Czaderski and Motavalli 2007; Aram et al. 2008).

Testing Methods

There are several standard testing methods to determine the lamina and laminate properties. The majority of tests conducted on polymer composite materials for structural engineering applications are conducted on coupons cut from as-fabricated FRP composite parts. These tests can be conducted on unidirectional laminas, such as FRP strengthening strips, sheets, or FRP reinforcing bars. Similar tests can be conducted on multilayer laminates cut from as fabricated in situ part. Standard test methods can be found in ASTM, ACI, CSA, JSCE, ISO, ISIS-Canada, and the European codes and guidelines. A comprehensive list of the test methods can be found in Bank (2006), Eckold (1994), GangaRao et al. (2007), Hollaway (1993), ISIS-Canada (2003).

In the following sections, the design of flexural and shear strengthening as well as confinement is described. It shall be noted that these design methods are still under development and that all equations in these sections are presented without safety factors. In an actual design, safety factors must be applied.

Future Developments

The price of carbon fiber is not likely to drop further than it has done in the last 30 years. Increasing expenses for processing energy may even increase the price of the fibers. Modern production techniques for CFRP strips made from thermoplastic polymers rather than thermosetting matrix systems may likewise help to stabilize the likely increasing cost of carbon fibers (Meier 2007). According to Meier (2007), thermoplastic matrices will replace epoxy matrices within the coming decade. Furthermore, more research is needed to investigate the FRP properties and their bond behavior at elevated temperatures. The fire resistance of FRP composites must be improved. Heat-resistant composites for very high temperatures shall be developed. The application of prepregs instead of strips as strengthening material shall be investigated, because prepregs do not require an additional adhesive in order to apply them to the structure, and therefore, their application might be easier and faster.

Nanotubes in polymer composites would serve to increase the stiffness, strength, and toughness, and provide other properties such as electrical and thermal conductivity. Since, at present, nanotubes can be manufactured only at lengths up to the submillimeter scale (thereby falling into

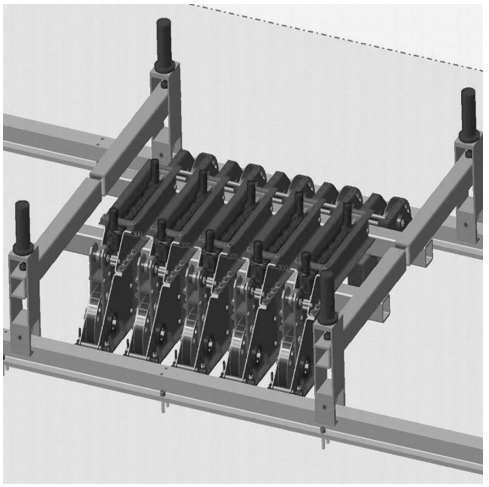

FIGURE 13.8 Automated device for simultaneous application of five pretensioned CFRP strips. (From Meier, U., Is there a future for automated application of CFRP strips for post-strengthening? *FRPRCS-8 Symposium*, University of Patras, Patras, Greece, 2007.)

the short-fiber category), their dominant role in composites is likely to remain as matrix modifiers and providers of multifunctional attributes in the foreseeable future. However, once nanotubes can be efficiently assembled on a macroscopic scale, they could become serious competition for the continuous carbon fibers that are woven and stacked to form load-bearing elements in structural composites used in the building and engineering industries (Ajayan and Tour 2007).

Nanotubes can have diameters ranging from 1 to 100 nm and lengths of up to millimeters. Their densities can be as low as 1.3 g/cm^3 and their Young's moduli are superior to all carbon fibers, with values greater than 1,000,000 MPa. The highest measured strength for a carbon nanotube is 63,000 MPa, which is an order of magnitude stronger than high-strength carbon fibers (Coleman et al. 2006). However, a large amount of work will have to be done before we can really make the most of the exceptional mechanical properties of carbon nanotubes.

Today in construction, only approximately 15% of the potential strength of CFRP strips is used. One important reason for this poor efficiency is that many strengthening tasks are stiffness, and not strength, controlled. The focus of future developments should therefore be on a better exploitation of the potential offered by CFRP composites and on a change to thermoplastic matrix systems in order to reduce cost. A better exploitation is possible when the CFRP strips are pretensioned (Meier 2007). Highly automated flexible track systems will revolutionize rehabilitation work in the construction industry (Figure 13.8).

REFERENCES

Ajayan, P. M. and J. M. Tour. (2007). Nanotube composites. *Nature* 447: 1066–1068.

Aram, M. R., C. Czaderski et al. (2008). Effects of gradually anchored prestressed CFRP strips bonded on prestressed concrete beams. *Journal of Composites for Construction, ASCE* 12(1): 25–34.

Bank, L. C. (2006). *Composites for Construction: Structural Design with FRP Materials*. John Wiley & Sons, Inc., Hoboken, NJ.

Coleman, N., U. Khan et al. (2006). Mechanical reinforcement of polymers using carbon nanotubes. *Advanced Materials* 18: 689–706.

Czaderski, C. and M. Motavalli. (2007). 40-Year-old full-scale concrete bridge girder strengthened with prestressed CFRP plates anchored using gradient method. *Composites Part B: Engineering* 38(7–8): 878–886.

Eckold, G. (1994). *Design and Manufacture of Composite Structure*. Woodhead Publishing Limited, Cambridge, U.K.

GangaRao, H. V. S., N. Taly et al. (2007). *Reinforced Concrete Design with FRP Composites*. CRC Press, Boca Raton, FL.

Hollaway, L. (1993). *Polymer Composites for Civil and Structural Engineering*. Blackie Academic & Professional, Glasgow, U.K.

ISIS-Canada. (2003). *An Introduction to FRP Composites for Construction*. ISIS Canada, Toronto, Ontario, Canada, www.isiscanada.com

Kim, Y. J., R. G. Wight et al. (2008). Flexural strengthening of RC beams with prestressed CFRP sheets: Development of nonmetallic anchor systems. *Journal of Composites for Construction* 12(1): 35–43.

Meier, U. (2007). Is there a future for automated application of CFRP strips for post-strengthening? *FRPRCS-8 Symposium*. University of Patras, Patras, Greece.

14 Flexural and Shear Strengthening of Reinforced Concrete Structures

Christoph Czaderski

CONTENTS

FLEXURAL STRENGTHENING

Introduction and Application Examples

Externally bonded reinforcement (EBR) in the form of carbon fiber–reinforced polymer (CFRP) strips or fabrics is nowadays often used for the flexural strengthening of reinforced concrete (RC) structures such as bridges or buildings because of their lightweight, easy handling, and good durability. Application examples of flexural strengthening of RC slabs are given in Figures 14.1 and 14.2.

FIGURE 14.1 Flexural strengthening with strips. (Photo courtesy of Sika Services AG, Pfäffikon, Switzerland.)

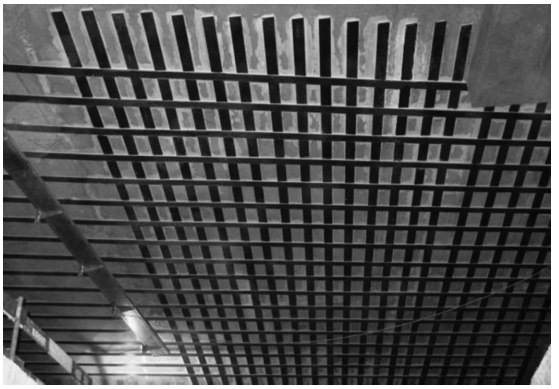

FIGURE 14.2 Flexural strengthening with strips. (Photo courtesy of S&P Clever Reinforcement Company AG, Seewen, Switzerland.)

Design

The most common failure mode of an EBR-strengthened RC structure is debonding of the EBR from the concrete surface in conjunction with the internal steel reinforcement in elastic or rather in yielding state. The failure modes, concrete compression failure and tensile failure of FRP, are more unlikely to occur but possible in some special cases. Many debonding failure mode types are discussed in the literature, for example, in Smith and Teng (2002), Oehlers (2006), Gunes et al. (2009), or Aram et al. (2008a). Figure 14.3 shows the debonding process of an EBR on a test beam. It was photographed with a high-speed camera.
Czaderski et al. (2010), Motavalli et al. (2010) in Pohl (2010), and Czaderski (2012) identified with some simplifications the following three main debonding failure modes, as shown in Figure 14.4:

1. Debonding failure mode 1: Plate-end debonding at the ends of the FRP strip (DM 1a in Figure 14.4) or limited anchorage resistance at the beam ends in the uncracked zone (DM 1b in Figure 14.4).
2. Debonding failure mode 2: Debonding at shear cracks or discontinuities due to high shear stresses between the strip and concrete caused from transverse shear forces or at discontinuities.
3. Debonding failure mode 3: Local debonding at flexural cracks due to high local shear stresses.

The existing guidelines available in different countries, for example, fib (2001), Teng et al. (2002), CNR (2004), SIA166 (2004), TR55 (2004), ISIS (2008), and ACI_440.2R (2008), present different

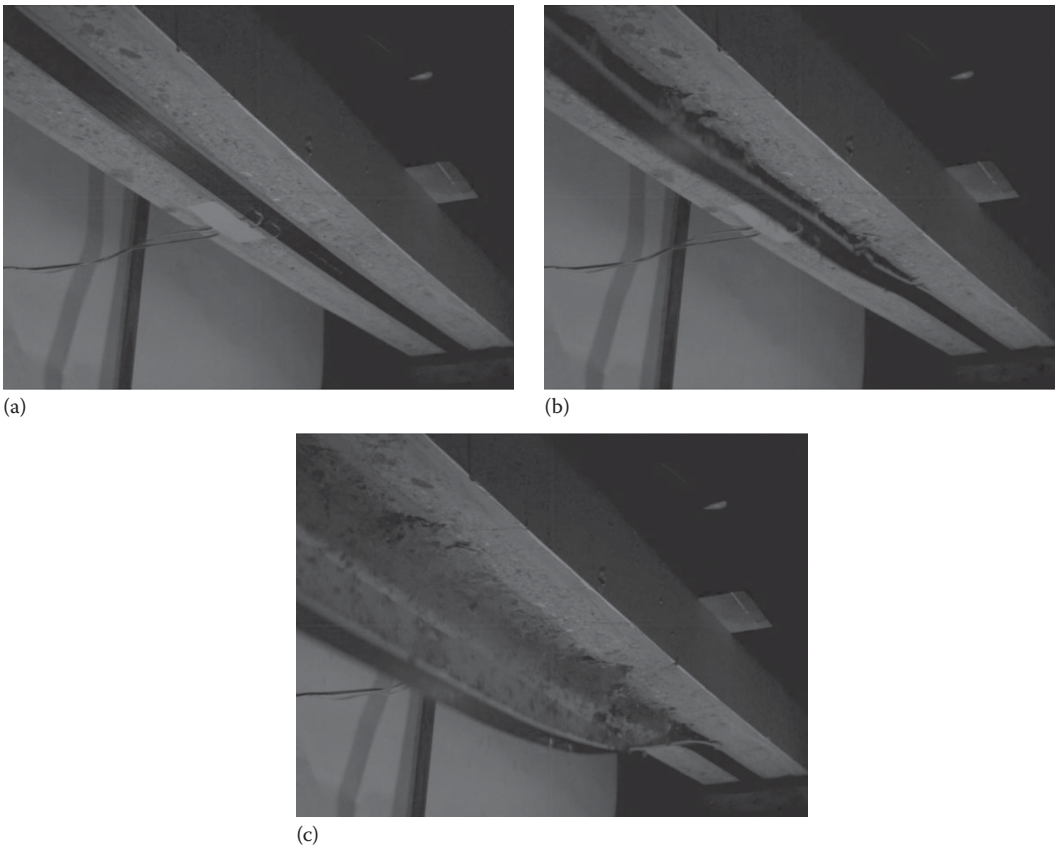

FIGURE 14.3 (a) A strip glued at the bottom face of a RC beam (flexurally strengthening of a test beam), (b) and (c) progressive debonding of the strip. Photos were taken with a high-speed camera. (Photo courtesy of Empa, Dübendorf, Switzerland.)

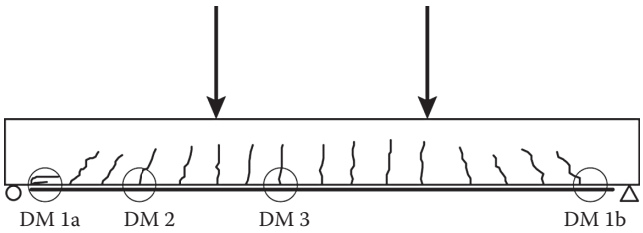

FIGURE 14.4 Types of debonding failure modes (DM: debonding mode) of externally bonded flexural strengthening (EBR).

design equations to avoid debonding of EBR, which indicates that debonding is a complex phenomenon, which is still not fully understood.

However, a proposal on how to avoid debonding is presented in the following sections. It bases on the concept of the Swiss Code (SIA166 2004). This code presents resistance equations for the three debonding failure modes such as the end-anchorage resistance. These resistances should be compared with the existing forces in the structure to find the failure load and failure modes. The existing strains (and therefore also the forces) in the strip can be calculated for certain load levels by using ordinary cross-section analysis. The approach is explained in detail with the help of an example in the "Example of a Flexural Strengthening" section.

In the following sections, the design of flexural strengthening according to SIA166 (2004) is described. Explanations of the design equations according to SIA166 (2004) and comparisons with some other guidelines were already presented in Motavalli et al. (2010), which is a chapter in the book by Pohl (2010). Subsequently, the design equations are very shortly summarized. All equations in these sections are presented without safety factors. In an actual design, safety factors must be applied. The notations are chosen as in Czaderski (2012).

Strip-End Debonding

To avoid debonding at strip end, the existing force in the strip at the last crack (DM 1b in Figure 14.4) should be smaller than the anchorage resistance determined in a lab-shear test with a strip glued on a concrete block with the same bond length. More information on the structural behavior and modeling of lab-shear tests can be found in Czaderski et al. (2010), Martinelli et al. (2011), and Czaderski (2012).

As mentioned before, the strain in the EBR at the last crack and therefore also the force can be determined by using ordinary cross-section analysis.

The anchorage resistance for long bond lengths can be calculated according to SIA166 (2004) with

$$F_{lR} = b_f \sqrt{2G_f E_f t_f} = b_f \sqrt{2\frac{f_{ctH}}{8} E_f t_f} = \frac{b_f}{2}\sqrt{E_f t_f f_{ctH}} \tag{14.1}$$

where

F_{lR} is the maximum anchorage resistance of a strip glued on concrete
G_f is the fracture energy of strip/concrete interface in lab-shear tests
f_{ctH} is the tensile strength of surface concrete
E_f is the elastic modulus
t_f is the thickness
b_f is the width of the strip

The corresponding active bond length l_{ba} for the maximum anchorage resistance F_{lR} is according to SIA166 (2004)

$$l_{ba} = \frac{\pi}{2}\sqrt{2\frac{G_f E_f t_f}{\tau_{f,\max}^2}} \tag{14.2}$$

and

$$\tau_{f,\max} = \frac{4}{3} f_{ctH} \tag{14.3}$$

where, $\tau_{f,max}$ is the maximum bond shear stress.

If a reduced bond length exists (i.e., $l_b < l_{ba}$), the anchorage resistance corresponding to the reduced bond length can be calculated according to SIA166 (2004) with the following equation:

$$F_{lR,s} = b_f \sqrt{2G_f E_f t_f} \cdot \sin\sqrt{\frac{\tau_{f,\max}^2 l_b^2}{2G_f E_f t_f}} \quad l_b \le l_{ba} \tag{14.4}$$

Debonding at Shear Cracks or Discontinuities

To avoid debonding at shear cracks (DM 2 in Figure 14.4), the existing global bond shear stress between the strip and the concrete surface should be smaller than the global bond shear stress resistance, which can be carried from the concrete.

The existing strains in the EBR can again be determined by using ordinary cross-section analysis. The global bond shear stresses can be calculated from the strains using (see Figure 14.6)

$$\tau_{f,gl} = \frac{\Delta\varepsilon_f E_f t_f}{\Delta x} \tag{14.5}$$

where

$\Delta\varepsilon_f$ is the strain change in the strip between two cross sections

Δx is the spacing between these two cross sections

SIA166 (2004) gives the relation

$$\tau_{f,\lim} \le 0.75\sqrt{f_{ck}} \tag{14.6}$$

for the global bond shear stress resistance, where f_{ck} is the characteristic value of cylinder compressive strength of concrete.

Debonding at Flexural Cracks

To avoid local debonding at flexural cracks (DM 3 in Figure 14.4), the maximum existing strain in the strip should be smaller than a limited maximum strain.

The existing strains in the EBR can again be determined by using ordinary cross-section analysis. According to SIA166 (2004), the strains should be limited to

$$\varepsilon_{f,\max} \le \varepsilon_{f,\lim} = 0.8\% \quad \left(\le \varepsilon_{fu}\right) \tag{14.7}$$

where ε_{fu} is the ultimate strain of the FRP.

Verification of Serviceability, Ductility, and Accidental Situation of Flexurally Strengthening

SIA166 (2004) and Motavalli et al. (2010) provide some information about the verification of the serviceability limit state, ductility, and accidental situation of flexural strengthening.

EXAMPLE OF A FLEXURAL STRENGTHENING

Introduction

In order to explain the calculation procedure, the example of a flexurally strengthened four-point bending beam (Figures 14.5 and 14.6) is presented, and the calculations according to SIA166 (2004) are presented in detail. The beam, action effects, simplified strain curve in the strip, and global bond shear stresses are shown in Figure 14.6. It must be noted that this is a test; therefore, real material properties were used for the calculations. Safety factors must be applied and design values of the material properties must be used in the design of EBR for structures such as bridges or buildings.

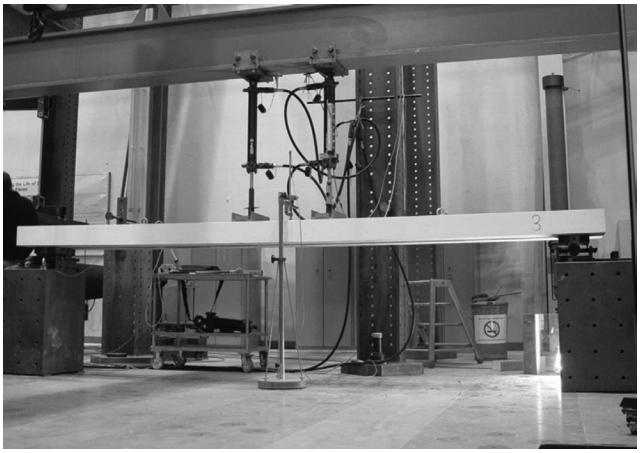

FIGURE 14.5 RC beam flexurally strengthened with a CFRP strip in the test setup. The test beam has a span of 4 m and is loaded under four-point bending (see Figure 14.6). (Photo courtesy of Empa, Dübendorf, Switzerland.)

Parameters

The parameters for the example presented in this chapter are (see Figures 14.5 and 14.6) as follows:

$a = 1.7$ m
$b = 0.5$ m
$l_s = 4.0$ m
$l_{se} = 0.1$ m
$h = 0.15$ m
$d = 0.117$ m
$A_s = 236$ mm^2
$f_y = 551$ N/mm^2
$A_f = 60$ mm^2
$b_f = 50$ mm
$t_f = 1.2$ mm
$E_f = 165$ kN/mm^2
$f_{ck} = 30.9$ N/mm^2
$f_{ct} = 3.0$ N/mm^2
$\varepsilon_{fu} = 1.6\%$

Concrete Tensile Strength

The concrete tensile strength is the most important parameter in the design of a flexural strengthening of a structure. Therefore, special care is necessary when determining this value. It is recommended to define a range of the concrete tensile strength and then to carry out the design for the limiting values. If possible, the tensile strength should be determined with pull-off tests on the structure, which shall be strengthened.

For simplicity, it is assumed in this example that the concrete tensile strength of the concrete surface f_{ctH} is equal to f_{ct} and is set to only one value:

$$f_{ctH} = 3.0\,\text{N/mm}^2$$

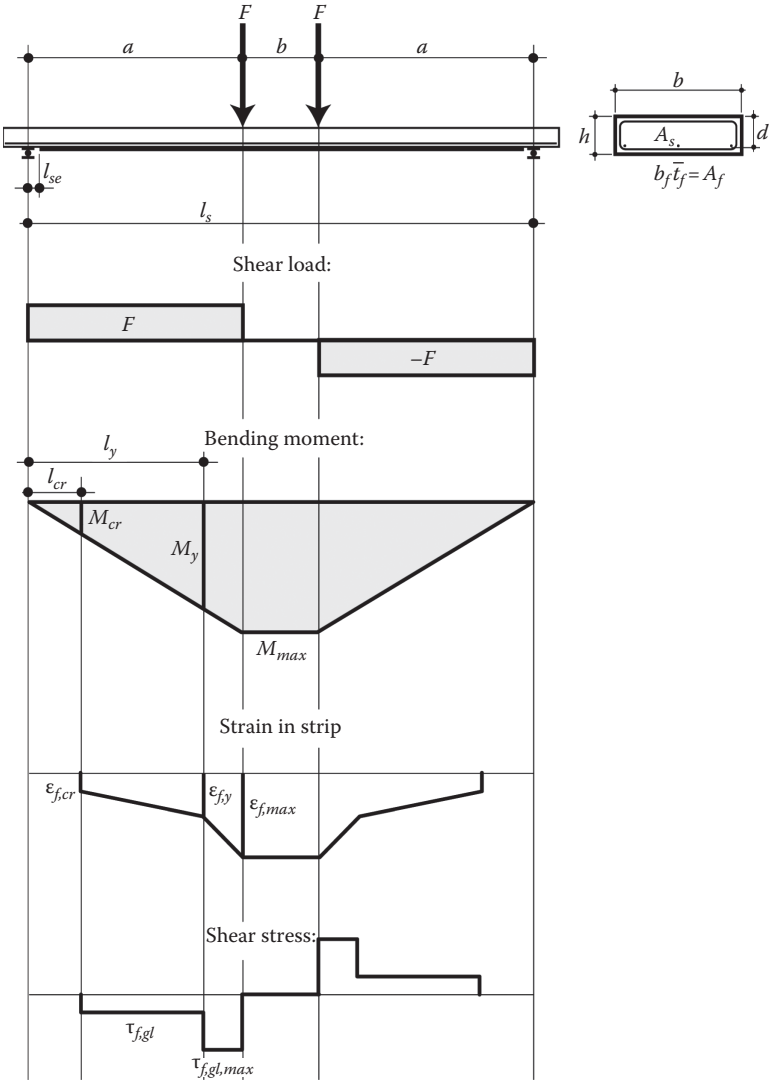

FIGURE 14.6 Example of a four-point bending beam, action effects, simplified strain curve in the strip, and global bond shear stresses.

Calculation of the Resistance Values

By using the concrete tensile strength, the anchorage resistance and the global bond shear stress resistance can be calculated. The values are calculated according to SIA166 (2004) as they were presented in the "Flexural Strengthening" section, and the parameters given earlier are used.

Debonding failure mode 1 (*end-anchorage failure*):
Fracture energy of strip/concrete interface (see Equation 14.1)

$$G_f = \frac{f_{ctH}}{8} = \frac{3.0}{8} = 0.375\,\text{N/mm} \tag{14.8}$$

Maximum bond shear stress (see Equation 14.3)

$$\tau_{f,max} = \frac{4}{3} f_{ctH} = \frac{4}{3} 3.0 = 4.0\,\text{N/mm}^2 \tag{14.9}$$

Maximum anchorage resistance (see Equation 14.1)

$$F_{lR} = 50\sqrt{2 \cdot 0.375 \cdot 165{,}000 \cdot 1.2} = 19.3\,\text{kN} \tag{14.10}$$

Corresponding active bond length (see Equation 14.2):

$$l_{ba} = \frac{\pi}{2} \cdot \sqrt{2 \cdot \frac{0.375 \cdot 165{,}000 \cdot 1.2}{4^2}} = 151\,\text{mm} \tag{14.11}$$

If a reduced bond length of the strip at the last crack exists (i.e., $l_b < l_{ba}$), the anchorage resistance corresponding to the reduced bond length can be calculated using Equation 14.4. Therefore, for the parameters presented earlier, the reduced resistances for reduced bond lengths are thus:

***lb* (mm)**	***FlR,s* (kN)**
10	2.0
20	4.0
30	5.9
40	7.8
50	9.6
60	11.2
70	12.8
80	14.2
90	15.5
100	16.6
110	17.5
120	18.3
130	18.8
140	19.1
150	19.3

Debonding failure mode 2 (*global bond shear stresses between strip and concrete*)
The global bond shear stress resistance is (see Equation 14.6)

$$\tau_{f,\text{lim}} = 0.75 \cdot \sqrt{30.9} = 4.2\,\text{N/mm}^2 \tag{14.12}$$

Debonding failure mode 3 (*local shear stresses at flexural cracks*)
This debonding failure mode is avoided if (see Equation 14.7)

$$\varepsilon_{f,\max} \le 0.8\% \tag{14.13}$$

Dead Load and Existing Loads on the Structure

For simplicity, the dead load is neglected in this example; however, in the real design, it should be considered. The existing stresses in the structure before strengthening are important and can influence the load-carrying behavior.

Cracking Moment

The cracking moment can simply be calculated with

$$M_{cr} = \frac{bh^2}{6} f_{ct} = \frac{500 \cdot 150^2}{6} \cdot 3.0 = 5.6\,\text{kN} \cdot \text{m} \tag{14.14}$$

Yielding Moment

A rough estimation with an assumed strain of $\varepsilon_{f,y} = 0.3\%$ in the FRP at the start of yielding of the internal steel reinforcement and an inner lever arm of 90% of the static height gives the order of magnitude of the yielding moment:

$$\begin{aligned} M_y &= A_s \cdot f_y \cdot 0.9 \cdot d + A_f \cdot \varepsilon_{f,y} \cdot E_f \cdot 0.9 \cdot h \\ &= 236 \cdot 551 \cdot 0.9 \cdot 117 + 60 \cdot 0.003 \cdot 165{,}000 \cdot 0.9 \cdot 150 \\ &= (13.7 + 4)\ \text{kN} \cdot \text{m} = 17.7\,\text{kN} \cdot \text{m} \end{aligned} \tag{14.15}$$

Principle of the Calculation Procedure

Now, an iterative procedure is necessary. Firstly, a loading force F (Figure 14.6) is assumed, and the debonding modes 1–3 are checked by comparing the *existing* with the *resistance* values. If no debonding occurs (i.e., resistance values are all larger as the existing values), the force shall be increased and again the debonding modes checked. This should be continued until one debonding mode occurs, and the failure load and the decisive type of failure mode are found. In the following, for presentation purposes, this is done with several assumptions and simplifications. However, in the design, by using a cross-section analysis software, this could be made more exact.

Calculation of the Existing Strain/Force/Shear Stress in the FRP for an Assumed Load and Comparison with the Resistances

The first estimation of the loading force should be so that the maximum bending moment is larger than the yielding moment. A moment $M_{\max}$ of 24.4 kN · m with a corresponding loading force $F = M/1.7 = 14.4$ kN is used here.

By using M_{cr} and the length from the end of the strip to the support l_{se}, the existing bond length l_b (see Figure 14.6) can be calculated as follows:

$$l_b = \frac{a}{M_{\max}} M_{cr} - l_{se} = \frac{1.7}{24.4} 5.6 - 0.1 = 0.29\,\text{m} \tag{14.16}$$

Therefore, because l_b is larger than l_{ba} (see Equation 14.11), the full anchorage resistance ($F_b = 19.3$kN, see Equation 14.10) can be transferred. The existing force in the strip is roughly estimated here with the relation between the yielding and cracking moments (in design, this should be determined with a real cross-section analysis):

$$\varepsilon_{f,cr} \approx \frac{\varepsilon_{f,y}}{M_y} M_{cr} = \frac{0.003}{17.7} 5.6 = 0.00095 \tag{14.17}$$

The corresponding force is

$$F_f = A_f E_f \varepsilon_{f,cr} = 60 \cdot 165{,}000 \cdot 0.00095 = 9.4\,\text{kN} \tag{14.18}$$

and

$$F_f = 9.4\,\text{kN} < F_b = 19.3\,\text{kN} \tag{14.19}$$

- *Debonding failure mode 1* (end-anchorage failure) does *not* occur.
  By using M_y, the location of the start of the yielding of the internal steel reinforcement can be calculated (see Figure 14.6) as follows:

$$l_y = \frac{a}{M_{\max}} M_y = \frac{1700}{24.4} 17.7 = 1233\,\text{mm} \tag{14.20}$$

  The existing strain $\varepsilon_{f,\max}$ in the strip at $M_{\max}$ can simply be calculated with

$$\varepsilon_{f,\max} = \frac{M_{\max} - A_s \cdot f_y \cdot 0.9 \cdot d}{A_f \cdot E_f \cdot 0.9 \cdot h} = \frac{24.4 \cdot 10^6 - 236 \cdot 551 \cdot 0.9 \cdot 117}{60 \cdot 165{,}000 \cdot 0.9 \cdot 150} = 0.008 \tag{14.21}$$

  The existing shear stress between the strip and the concrete is determined by using the location at the start of yielding of the internal steel reinforcement and the existing strains in the strip (see Figure 14.6):

$$\tau_{f,gl,\max} = \frac{(\varepsilon_{f,\max} - \varepsilon_{f,y}) \cdot E_f \cdot A_f}{b_f (a - l_y)} = \frac{(8.0 - 3.0) \cdot 10^{-3} \cdot 165{,}000 \cdot 60}{50\,(1{,}700 - 1{,}233)} = 2.1\,\text{N/mm}^2 \tag{14.22}$$

$$\tau_{f,gl,\max} = 2.1 < \tau_{f,\lim} = 4.2\,\text{N/mm}^2 \tag{14.23}$$

- *Debonding failure mode 2* (shear stresses between strip and concrete) does *not* occur.

$$\varepsilon_{f,\max} = 0.8\% \geq \varepsilon_{f,\lim} = 0.8\% \quad (\leq \varepsilon_{fu}) \tag{14.24}$$

- *Debonding failure mode 3* (local shear stresses at flexural cracks) *does occur.*
  Therefore, the calculated failure load is 14.4 kN, and the failure mode is debonding due to high local shear stresses at flexural cracks. In the framework of an exercise for students at ETH Zurich in Switzerland, a test at Empa with the geometry and materials presented here had a maximum load of 13.2 kN and strains in the CFRP strip of 0.73% and 0.8% (two strain gauges at mid-span), which shows that the simple calculation presented earlier delivers a reasonable result. The failure mode was debonding; however, the type of debonding was not detected because special measurement techniques would be necessary because of the high speed of the mechanism.

SHEAR STRENGTHENING

Introduction and Applications

Figures 14.7 and 14.8 show different examples of applications of FRP for shear strengthening. Furthermore, in Figure 14.9, a selection of some possibilities of how FRP can be used for shear strengthening of RC is schematically shown. The main problem is to find solutions for the anchorage of the FRP in the flange for the case of T-beams. There are several solutions to this problem, for example, drilling of holes or slits and gluing in the FRP or the use of dowels. A further important point is that the corners must be prepared properly to ensure a good force transfer of the shear strengthening.

For shear strengthening, fabrics that are applied on the entire side of the webs (Figure 14.8), or in the form of sheets with certain spacings, can be used. Prefabricated CFRP L-shaped strips, Figure 13.6 and Figure 14.7, are also an alternative.

Design

Similar as in the shear design of RC, the shear strengthening design of RC is controversially discussed in the literature. In design, usually the well-known truss models are used. In the chapter by Motavalli et al. (2010) in the book by Pohl (2010), such models for the shear strengthening design of RC are given.

FIGURE 14.7 Shear strengthening using prefabricated L-shaped strips. (Photo courtesy of Sika Services AG, Pfäffikon, Switzerland.)

FIGURE 14.8 Shear strengthening using fabrics. (Photo courtesy of Sika Services AG, Pfäffikon, Switzerland.)

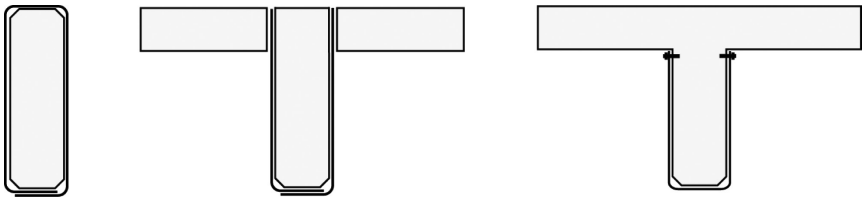

FIGURE 14.9 Some possible shear strengthening principles using FRP.

It is described that with increasing loading of the structures, three states (State I: uncracked, State II: shear cracks exists, internal shear reinforcement in elastic state, State III: shear cracks with yielding of internal shear reinforcement) can be distinguished similar as in flexural strengthening. Furthermore, it is proposed in Motavalli et al. (2010) that the shear resistance of an RC member consists of the contributions of the concrete, internal steel stirrups and the external bonded shear reinforcement (or, if lower, the failure of the compressive struts).

Advices are given on how to estimate the three contributions. Furthermore, some ideas about considering serviceability limit state, accidental situation, and fatigue are described.

PRESTRESSED EXTERNALLY BONDED REINFORCEMENT FOR FLEXURAL STRENGTHENING

Introduction

Prestressing of the EBR has several advantages. Prestressing reduces crack widths and deflections and therefore improves the serviceability and the durability of a structure (Motavalli et al. 2011). Furthermore, prestressed EBR (PEBR) has a greater strengthening effect than EBR because it has also an effect on the existing loads.

As described earlier, debonding of the EBR from the concrete surface is a major failure mode, which means that the strength of the FRP cannot be fully utilized. Therefore, if the EBR is prestressed, a greater amount of its strength can be exploited. Additionally, since for PEBR the initial prestress level can be controlled, it should be possible to change the failure mode from "debonding" to "tensile rupture" of the strip using a clever dimensioning concept.

Anchorage Systems

The prestressing force in the strips must be transferred to the concrete surface at the strip ends. Therefore, in most cases, anchorage systems are used. Two main systems of two different companies are available on the market. One system uses an anchor head made of CFRP. Figures 14.10 and 14.11 show an application example of this system. The anchor heads, its fixing on the concrete, and the stressing are also visible in Figure 14.11. The other anchorage system uses aluminum anchor plates. An application example to strengthen an RC beam is given in Figures 14.12 and 14.13.

More information on both the systems can be found in the Internet (see [Sika] and [S&P]). All of these systems, however, must be fixed to concrete with steel screws or dowels. Furthermore, in some cases, even opening areas in the concrete are necessary.

Gradient Method

A special prestressed concrete technique without an anchorage is utilized in pretensioned concrete. The prestressing force increases from zero at the end of the wires within the anchorage

FIGURE 14.10 Strengthening of a concrete wall with prestressed strips. (Photo courtesy of Sika Services AG, Pfäffikon, Switzerland.)

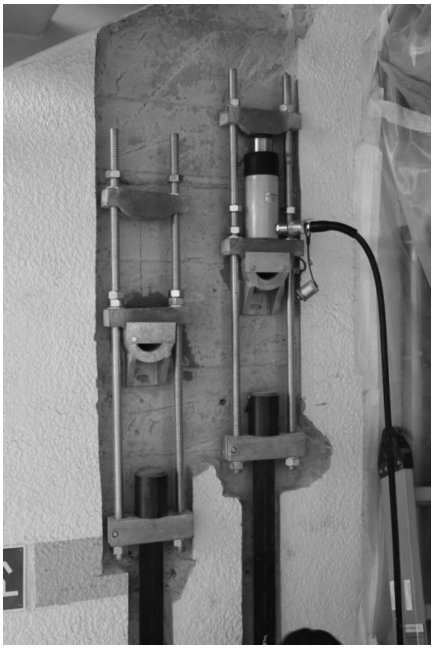

FIGURE 14.11 Details of the prestressed strips and their anchorage using CFRP anchor heads. (Photo courtesy of Sika Services AG, Pfäffikon, Switzerland.)

FIGURE 14.12 Strengthening of a reinforced concrete beam, anchorage details after removing jack during curing. (Photo courtesy of S&P Clever Reinforcement Company AG, Seewen, Switzerland.)

FIGURE 14.13 Details of the finished anchorage using aluminum plates that remain on the structure. (Photo courtesy of S&P Clever Reiforcement Company AG, Seewen, Switzerland.)

length due to activated bond shear stresses. A comparable technique is the PEBR gradient method, which reduces the prestressing force at the strip end to zero by using a special stressing and heating device so that anchorages are no longer needed. The old Empa stressing and heating device was presented in Figure 13.7. The prestressing force is transferred to the concrete gradually using bond shear stresses. The gradient is produced by sector-wise heating of the adhesive and a step-wise release of the force (see the principle in Figure 14.14). This method was developed at Empa (Meier et al. 2002). Prestressed CFRP strips anchored with the gradient method were successfully used and tested on RC test beams with spans of 2.1 m (Stöcklin and

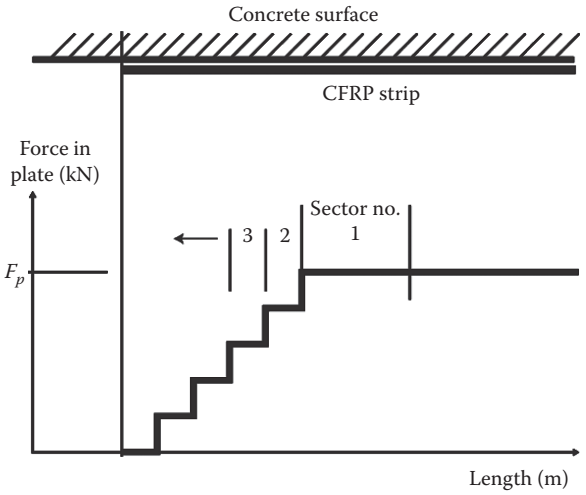

FIGURE 14.14 Principle of the force gradient at the end of the prestressed strips. (Photo courtesy of Sika.)

Meier 2002) and 6.0 m (Meier and Stöcklin 2005). Furthermore, small PC beams were strengthened with EBR and PEBR. In this case, the strengthening effect of the PEBR was similar or even lower than the EBR (Aram et al. 2008b). On the other hand, a 17 m long PC girder taken from a bridge was strengthened flexurally with PEBR (see Figures 14.15 and 14.16) and tested to failure. The load-carrying behavior of the girder was compared with a reference girder and a girder strengthened with EBR. The maximum loads reached with the girders were 24% and 45% higher than that of the reference beam, with EBR and PEBR, respectively (see Czaderski and Motavalli 2007).

A photo of the newly developed device for the production of a prestress force gradient can be seen in Figure 14.17. This project was a collaboration between Empa and the company S&P, Switzerland, with the aim to build a system that is feasible for the usage on site. Detailed descriptions of the development of the device can be found in Czaderski et al. (2011, 2012) and Michels (2012a,b,c).

FIGURE 14.15 Bottom view of a test girder at Empa with applied prestressed strips without any mechanical anchorages. (Photo courtesy of Empa, Dübendorf, Switzerland.)

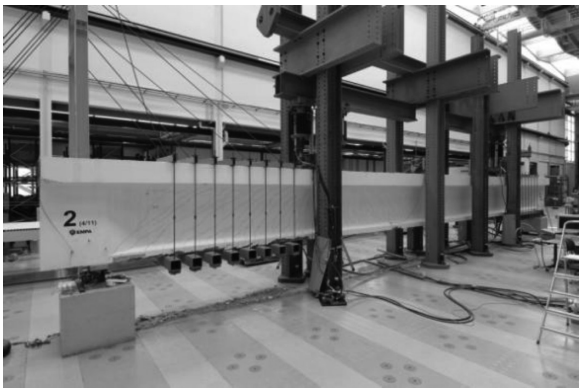

FIGURE 14.16 A 17 m long test girder that was strengthened and tested to failure with prestressed CFRP strips anchored with the gradient method. Note: the visible shear strengthening was not in contact with the strips. (Photo courtesy of Empa, Dübendorf, Switzerland.)

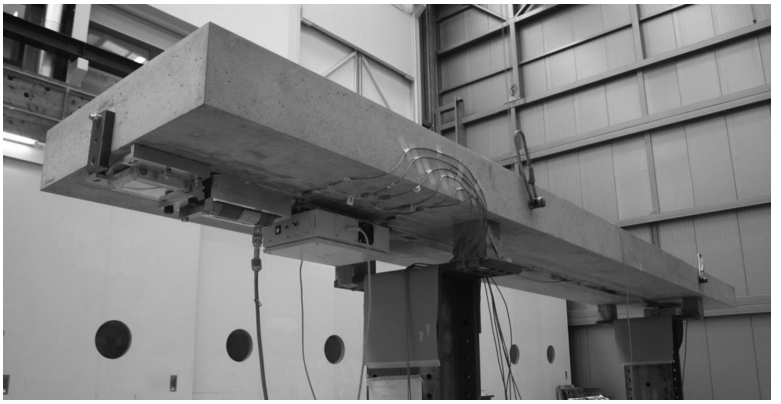

FIGURE 14.17 Beam flexurally strengthened with a prestressed CFRP strip. Visible is the prestressing and heating device for producing the gradient anchorage. (Photo courtesy of Empa, Dübendorf, Switzerland.)

REFERENCES

ACI_440.2R (2008). *Guide for the Design and Construction of Externally Bonded FRP Systems for Strengthening Concrete Structures (ACI 440.2R-08)*. American Concrete Institute, Farmington Hills, MI, p. 80.

Aram, M. R., C. Czaderski, and M. Motavalli (2008a). Debonding failure modes of flexural FRP-strengthened RC beams. *Composites Part B: Engineering* 39(5): 826–841.

Aram, M. R., C. Czaderski, and M. Motavalli (2008b). Effects of gradually anchored prestressed CFRP strips bonded on prestressed concrete beams. *Journal of Composites for Construction, ASCE* 12(1): 25–34.

CNR (2004). *Guide for the Design and Construction of Externally Bonded FRP Systems for Strengthening Existing Structures, CNR-DT 200/2004*. CNR—Advisory Committee on Technical Recommendations for Construction, Rome, Italy, p. 144.

Czaderski, C. (2012). Strengthening of reinforced concrete members by prestressed, externally bonded reinforcement with gradient anchorage. PhD thesis No. 20504. ETH Zurich, Zurich, Switzerland, p. 459.

Czaderski, C., E. Martinelli, J. Michels, and M. Motavalli (2011). Effect of partly cured adhesives on bond-slip-relationship of FRP-concrete interface. *SMAR, First Middle East Conference on Smart Monitoring, Assessment and Rehabilitation of Civil Structures*, Dubai, United Arab Emirates, February 8–10, 2011, p. 8.

Czaderski, C., E. Martinelli, J. Michels, and M. Motavalli (2012). Effect of curing conditions on strength development in an epoxy resin for structural strengthening. *Composites Part B: Engineering* 43(2): 398–410.

Czaderski, C. and M. Motavalli (2007). 40-Year-old full-scale concrete bridge girder strengthened with prestressed CFRP plates anchored using gradient method. *Composites Part B: Engineering* 38(7–8): 878–886.

Czaderski, C., K. Soudki, and M. Motavalli (2010). Front and side view image correlation measurements on FRP to concrete pull-off bond tests. *Journal of Composites for Construction, ASCE* 14(4): 451–463.

fib (2001). Externally bonded FRP reinforcement for RC structures—Bulletin 14, International Federation for Structural Concrete (fib), Lausanne, Switzerland, p. 130.

Gunes, O., O. Buyukozturk, and E. Karaca (2009). A fracture-based model for FRP debonding in strengthened beams. *Engineering Fracture Mechanics* 76(12): 1897–1909.

ISIS (2008). *FRP Rehabilitation of Reinforced Concrete Structures, Design Manual No. 4, Version 2*, ISIS Canada, Toronto, Ontario, Canada, p. 178.

Martinelli, E., C. Czaderski, and M. Motavalli (2011). Modeling in-plane and out-of-plane displacement fields in pull-off tests on FRP strips. *Engineering Structures* 33(12): 3715–3725.

Meier, U. and I. Stöcklin (2005). A novel carbon fiber reinforced polymer (CFRP) system for post-strengthening. *International Conference on Concrete Repair, Rehabilitation and Retrofitting (ICCRRR)*, November 21–23, 2005, Cape Town, South Africa, pp. 477–479.

Meier, U., I. Stöcklin, and A. Winistörfer (2002). Method and device for applying pretensed tension-proof reinforcing strips to a construction. Patent No. US 6,464,811 B1, October 15, 2002, p. 11.

Michels, J., C. Czaderski, R. Brönnimann, and M. Motavalli (2012a). Gradient anchorage method for prestressed CFRP strips—Principle and application. *IABMAS 2012, 6th International Conference on Bridge Maintenance, Safety and Management*, Stresa, Lake Maggiore, Italy, July 8–12, 2012, pp. 1981–1986.

Michels, J., C. Czaderski, R. El-Hacha, R. Brönnimann, and M. Motavalli (2012b). Temporary bond strength of partly cured epoxy adhesive for anchoring prestressed CFRP strips on concrete. *Composite Structures* 94(9): 2667–2676.

Michels, J., C. Czaderski, R. El-Hacha, and M. Motavalli (2012c). Partially cured epoxy adhesive for anchoring prestressed CFRP strips on concrete. *APFIS 2012, The Third Asia-Pacific Conference on FRP in Structures*, Hokkaido University, Hokkaido, Japan, February 2–4, 2012, p. 8.

Motavalli, M., C. Czaderski, and K. Pfyl-Lang (2011). Prestressed CFRP for strengthening of reinforced concrete structures—Recent developments at Empa Switzerland. *Journal of Composites for Construction, ASCE* 15(2): 194–205.

Motavalli, M., C. Czaderski, A. Schumacher, and D. Gsell (2010). Fibre reinforced polymer composite materials for building and construction. In *Textiles, Polymers and Composites for Buildings*. G. Pohl (ed.). Woodhead Publishing Limited, Cambridge U.K., pp. 69–128.

Oehlers, D. J. (2006). FRP plates adhesively bonded to reinforced concrete beams: Generic debonding mechanisms. *Advances in Structural Engineering* 9(6): 737–750.

Pohl, G., Ed. (2010). *Textiles, Polymers and Composites for Buildings*, Woodhead Publishing Limited, Cambridge, U.K.

S&P. S&P Clever Reinforcement Company AG, Seewen, Switzerland. http://www.sp-reinforcement.ch/

SIA166 (2004). Klebebewehrungen (Externally bonded reinforcement). Schweizerischer Ingenieur-und Architektenverein—SIA, Zurich, Switzerland, p. 44.

Sika. Sika Services AG, Pfäffikon, Switzerland. http://che.sika.com/

Smith, S. T. and J. G. Teng (2002). FRP-strengthened RC beams. I: Review of debonding strength models. *Engineering Structures* 24(4): 385–395.

Stöcklin, I. and U. Meier (2002). Strengthening of concrete structures with prestressed and gradually anchored carbon fibre reinforced plastic (CFRP) strips. *IABMAS*, July 14–17, 2002, Barcelona, Spain, pp. 1–8.

Teng, J. G., J. F. Chen, S. T. Smith, and L. Lam (2002). *FRP Strengthened RC Structures*. John Wiley & Sons, Ltd., Chichester, U.K., p. 245.

TR55 (2004). Design guidance for strengthening concrete structures using fibre composite materials, Second edition, Technical Report No. 55 of the Concrete Society, London, U.K., p. 102.

15 Rehabilitation with NSM FRP Reinforcement

Khaled Soudki

CONTENTS

INTRODUCTION

Rehabilitation and strengthening of concrete structures using fiber-reinforced polymer (FRP) reinforcement can be applied as an externally bonded (EB) system or a near-surface mounted (NSM) system. In the EB system, FRP laminates are bonded to the concrete surface using epoxy adhesives. To improve the bond strength between the concrete and the FRP, the concrete surface is usually treated by sandblasting. In the NSM system, FRP bars or plates are inserted into a groove that is made in the concrete surface with a concrete saw. The groove is then filled with epoxy adhesive to bond the FRP to the concrete. The use of NSM steel reinforcement in the rehabilitation of concrete structures dates back to late 1940s (Asplund 1949). Advantages of using FRP reinforcement in NSM strengthening applications are numerous. NSM FRP does not require extensive surface preparation

work and is easy to handle due to their lightweights; better corrosion resistance and less concrete cover is needed; NSM reinforcement inside the epoxied groove is protected from physical damage, fire, or harsh environmental attack.

The practical applications using the NSM system are more limited than the EB system because of the lack of relevant provisions in international guidelines (fib 2001, CNR 2004, SIA166 2004, TR55 2004, ISIS 2008). To address this gap, the international engineering community has carried accelerated research on structural aspects of NSM strengthening of concrete structures: many research work on the bond behavior and flexural strengthening of concrete members with non-prestressed NSM FRP reinforcement has been reported, fewer studies have been carried on prestressed NSM strengthening has been reported in fewer studies, and very limited research has been carried on the shear strengthening with NSM (Badawi and Soudki 2006, El-Hacha and Rizkalla 2004, De Lorenzis and Teng 2007). Recently, ACI 440.2R guide (2008) has included provisions to consider the NSM system.

This chapter will present a synthesis of the existing knowledge and design for the strengthening of concrete structures with NSM reinforcement. Design considerations related to bond and flexural strengthening with non-prestressed and prestressed FRP reinforcement will be discussed. Design examples will be provided to illustrate the concepts presented. The reader should recognize that the procedures will be revised with new developments in NSM FRP systems.

MATERIALS

FRP Reinforcement and Adhesive

Two types of FRP reinforcement are presently used for NSM systems: Carbon FRP (CFRP) and glass FRP (GFRP). CFRPs are characterized by their high longitudinal tensile strength and their high modulus of elasticity (Table 15.1). FRP bars used in NSM applications are commercially available from manufacturers like Sika, Switzerland, Hughes Brothers, the United States, and Pultral, Thetford Mines, Quebec, Canada. Typically, FRP round bars or strips are used depending on the manufacturer. The most common filler material used in the groove for NSM strengthening is the two-part epoxy. The role of the adhesive is to transfer the shear stresses between the FRP reinforcement and the concrete. Typical mechanical properties of the epoxy adhesives are listed in Table 15.1.

Anchorage Systems

In prestressed NSM applications, the FRP reinforcement is gripped by means of clamp- or wedge-type anchors to maintain the prestressing force. Description of the anchors follows.

1. *Clamp anchor*: consists of grooved steel plates held together by bolts clamping the sleeve-encased FRP and transferring the force by shear-friction mechanism.
2. *Split wedge anchor*: consists of a number of wedges fitted into a barrel with a soft metal sleeve encasing the FRP to protect it from notching.

TABLE 15.1
Material Properties of NSM FRP Systems

Material	Specific Gravity	Tensile Strength (MPa)	Tensile Modulus (GPa)	Ultimate Elongation (mm/mm)	Coefficient Therm. Exp (10^{-6}/C)
GFRP	2.40	1379–1724	48–62	0.03–0.045	10.0
CFRP	1.50	2000–2610	142–165	0.01–0.015	0.0
Epoxy	1.1–1.5	50–90	3.0	2–8	—
Steel	7.90	1100–1862	186–200	>0.04	11.7

INSTALLATION

FRP bars or strips are inserted into a groove that is made in the concrete surface with a special concrete saw. Therefore, the soundness of the concrete inside the groove shall be assured before installing FRP bars or plates. The groove is then filled with adhesive material to bond the FRP to the concrete. Since the force should be adequately transferred between the FRP and the concrete, the selection and the application of adhesive materials must be carefully conducted. As such, the bond capacity during installation procedure is critical. For more information about the NSM bond properties, refer to the "Bond Properties" section. In this chapter, the general installation procedure and guidelines for non-prestressed and prestressed NSM strengthening systems are described.

Procedure for Non-Prestressed NSM

The typical procedure for NSM strengthening installation is illustrated in Figure 15.1. The procedure may vary depending on the types of FRP and adhesive; the manufacturers' specifications should be consulted. Installation of the NSM FRP reinforcing bars begins by making the specified grooves in the concrete cover on the tension surface of the concrete member. A special concrete saw with a diamond blade can be used to cut the grooves. Special care is required so that the internal reinforcement is not damaged during this process.

An appropriate groove size shall be selected considering the size of the NSM bar or plate and the concrete cover. Based on research by Lorenzis and Nanni (2002) and Hassan and Rizkalla (2004), larger groove sizes produce higher bond strength than smaller groove sizes. On the other hand, the depth of the groove is limited by the bottom reinforcement, and the width should not be excessive to limit construction costs. Groove size selection is given in the "Bond Properties" section.

After making a groove, the grooves shall be cleaned with compressed air or by other means to remove debris and fine particles to ensure proper bond between the epoxy adhesive and the concrete. Existing excessive cracks or unsound concrete should be repaired. The adhesive material is then applied into the groove before inserting the FRP bars or plates. The groove is half-filled with the epoxy adhesive. The FRP reinforcing bars or plates are inserted in the groove and lightly pressed to displace the epoxy adhesive. The groove is then filled with more paste, and the surface is leveled to prevent the stress concentration due to unevenness of the surface. The adhesive needs to be fully cured to become hardened. The curing time varies depending on the type of adhesive.

Procedure for Prestressed NSM

Installation procedure for NSM prestressing is shown in Figure 15.2. The groove is made in the soffit of the concrete member with the concrete saw, as shown in Figure 15.2a, and the adhesive is applied halfway in the groove (see Figure 15.2b). A prestressing assembly is attached to the concrete member using an anchor system, and the FRP reinforcement is prestressed, as shown

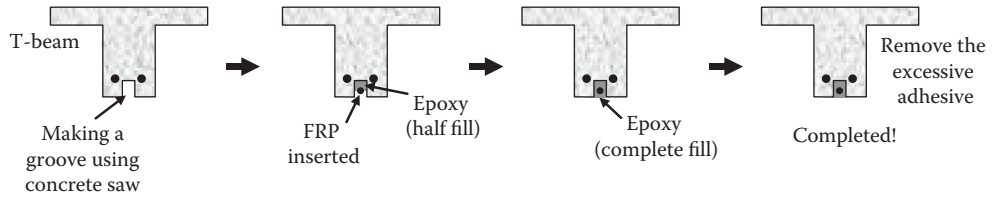

FIGURE 15.1 Installation procedure of non-prestressed NSM-strengthened beams.

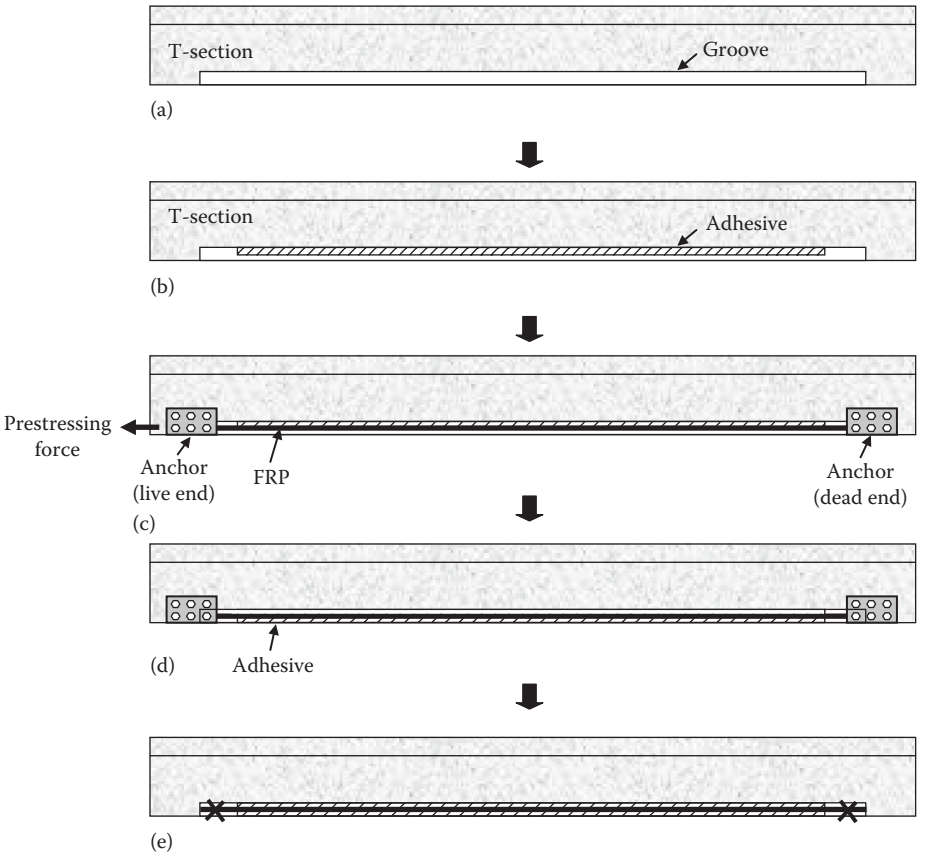

FIGURE 15.2 Prestressing procedure for prestressed NSM system. (a) Make NSM groove, (b) fill halfway of the groove with adhesive, (c) set up prestressing assembly and apply the force, (d) fill the groove completely with adhesive, and (e) remove prestressing assembly and the cut the bar.

in Figure 15.2c. At this stage, the FRP bar is tensioned, and a compressive force is applied to the concrete at the same time. Once the desired prestressing force is reached, the adhesive is completely filled in the groove and the excessive adhesive is cleaned (see Figure 15.2d). After curing of the adhesive, the prestressing assembly is removed and the transfer of force is achieved by bond (Figure 15.2e). Alternatively, the anchors are kept at the ends of the prestressed NSM reinforcement.

BOND PROPERTIES

The bond between an NSM bar and the groove filler plays a key role in ensuring the effectiveness of NSM strengthening. The performance of the bond depends on a number of parameters including the bar cross-sectional shape and surface configuration, the groove dimensions, the shear strength of the groove filler, the degree of roughness of the groove surface, prestress level in the bar, and whether the applied loading is static or fatigue (De Lorenzis and Teng 2007).

The groove filler is specified by the manufacturer of the NSM system. Although research was carried out on both epoxy and cement mortar, the most common type is epoxy. In this regard, ACI 440.2R (2008) recommends that the tensile adhesion strength of the filler should exceed 1.4 MPa and should exhibit failure of the concrete substrate.

TABLE 15.2
Bond Stress for NSM Round Bars in Epoxy

Type of FRP		Surface Texture	k	Bond Strength (MPa)
CFRP	Round	Sandblasted	1.34–2.67	8.6–11.2
	Round	Ribbed	1.33–2.12	11.2–16.6
	Round	Spirally winded	1.5–2.5	18–21.9
	Round	Sand coated	1.5–2.5	18–21.9
GFRP	Ribbed	Ribbed	1.36–2.18	9.1–12.5

The groove dimensions and the bar diameter play an important role in the mode of failure. The ratio between groove size to actual bar diameter is defined as factor k. Table 15.2 lists typical values for k and bond strength for different FRP bars. When the failure is at the filler–concrete interface, the bond strength is calculated from Equation 15.1a, but when failure is by pullout of the bar from the groove filler or by splitting of the cover, the stress is calculated from Equation 15.1b:

$$\tau = \frac{P}{(2d_g + b_g)l} \tag{15.1a}$$

$$\tau = \frac{P}{\pi d_b l} \tag{15.1b}$$

where
τ is the bond strength
P is the force in the bar
d_b is the bar diameter
d_g is the groove depth
b_g is the groove width
l is the bonded length

Regarding the dimension of the groove, ACI 440.2R (2008) recommends that it should be at least 1.5 times the diameter of the FRP bar. For a rectangular bar with an aspect ratio $a \times b$, a minimum groove size of $3.0a \times 1.5b$ is suggested, where a is the smallest bar dimension. For multiple FRP bars, the minimum clear groove spacing for NSM FRP bars should be greater than twice the depth of the NSM groove to avoid overlapping of the tensile stresses around the NSM bars. Also a clear edge distance of four times the depth of the NSM groove should be provided to minimize the edge effects that could accelerate debonding failure (Hassan and Rizkalla 2003).

The development length of an NSM FRP bar is calculated using an average bond strength of 6.9 MPa (ACI 440.2R 2008) as given in Equation 15.2.

$$l = \frac{P}{2(a+b) * \tau} \quad \text{for rectangular bars} \tag{15.2a}$$

$$l = \frac{P}{\pi d_b * \tau} \quad \text{for circular bars} \tag{15.2b}$$

where
- τ is the bond strength
- P is the force in the bar
- d_b is the diameter of the circular bar
- a, b are the dimensions for the rectangular bar
- l is the bonded length

In prestressed NSM application, the release of the force in the prestressing rod creates shear stresses in the surrounding epoxy. Weak bond between the FRP reinforcement and the epoxy results in a longer transfer length. If the bond is weak, the prestressing force may be lost as the member is loaded due to slippage of the bar within the epoxy. The transfer length of CFRP bars in prestressed NSM strengthening, with prestress level 40%–60% of their ultimate capacity, was found to vary between 20 and 40 times bar diameter. The prestressing stress along the NSM CFRP bar in an epoxied groove can be estimated using Equation 15.3 (Badawi et al. 2011):

$$f_s = f_{pre} * (1 - \exp^{-Bx}) \tag{15.3}$$

where
- f_s is the prestress stress in the rod for a given distance (x) from the end of the bonded length
- f_{pre} is the maximum prestressing stress
- B is a factor obtained from best fit of experimental results. This factor accounts for different variables as epoxy type, epoxy thickness, and prestressing level. $B = 0.01$ for CFRP in epoxy
- x is the distance from the end of the bonded length

NON-PRESTRESSED NSM STRENGTHENING

Flexural Strengthening

The capacity condition in flexure that must be satisfied for NSM FRP-strengthened members is that the resisting moment, $M_r(\phi_n M_n)$, shall be greater than the factored moment, $\phi_f M_f$, as follows:

$$M_r \geq \phi_f M_f \tag{15.4}$$

where
- M_n is the nominal moment
- ϕ_f is the load factor
- ϕ_n is the strength reduction factor or material factor

The failure modes of NSM FRP-strengthened members include (1) concrete crushing, (2) FRP rupture, and (3) premature FRP debonding failure. The flexural analysis of NSM-strengthened members shall be performed considering these failure modes.

FRP Strain Limit

In NSM-strengthened members, the occurrence of the debonding failure is reported between approximately 60% and 90% of the ultimate strength (f_{frpu}) or strain of FRP material (ε_{frpu}),

respectively. Therefore, to account for the debonding failure mode, the ultimate FRP strain is reduced by the FRP strain limit factor, ψ_{frp}, to get the effective FRP strain, ε_{fe}, as shown as follows.

$$\varepsilon_{fe} = \psi_{frp} \times \varepsilon_{frpu} \tag{15.5}$$

The FRP strain limit factor, ψ_{frp}, varies depending on many factors such as the types of FRP material and adhesive, concrete soundness near the groove, the geometry of the groove, etc. (see the "Bond Properties" section). ACI 440.2R (2008) recommends using a strain limit factor of 0.7 for NSM systems.

Analysis Assumptions

The basic assumptions for the analysis are as follows:

1. Perfect bond exists between the concrete, adhesive, and the FRP with no slip.
2. Failure is by concrete crushing at ultimate compression strain of 0.003 or FRP failure at an effective FRP strain (set equal 0.7 times the FRP rupture strain) after yielding of the internal steel reinforcement.
3. Strain distribution over section depth is linear (plane section remains plane).
4. Concrete has a parabolic stress–strain relationship in compression. Tensile strength of concrete after cracking is ignored.
5. The stress–strain curve for the steel reinforcement is linear elastic-perfectly plastic.
6. The FRP stress–strain relationship is idealized as linear elastic to failure.

Flexural Analysis

The flexural analysis of a section with NSM FRP reinforcement is based on force equilibrium and strain compatibility, as shown for a rectangular section in Figure 15.3. The balanced amount of FRP reinforcement, A_{fb}, is defined as the area of FRP at which the concrete and FRP fail simultaneously. Depending on FRP reinforcement, A_f, the flexural behavior can be classified as

- *Balanced failure*: if $A_f = A_{f,b}$, failure will occur by FRP failure with the FRP strain at the effective strain ($\varepsilon_{fe} = 0.7 * \varepsilon_{frpu}$) and concrete failure ($\varepsilon_{cu} = 0.003$) simultaneously.
- *Understrengthened section*: if $A_f < A_{f,b}$, failure will occur by FRP failure ($\varepsilon_{fe} = 0.7 * \varepsilon_{frpu}$) before concrete failure ($\varepsilon_{cu} < 0.003$).
- *Overstrengthened section*: if $A_f > A_{f,b}$, failure will occur by concrete failure ($\varepsilon_{cu} = 0.003$) before FRP failure ($\varepsilon_f < \varepsilon_{fe}$).

To guard against brittle failure, it is assumed that in all three cases, the internal steel reinforcement will have reached the yield strain before FRP failure or concrete crushing. This assumption shall be checked by the designer.

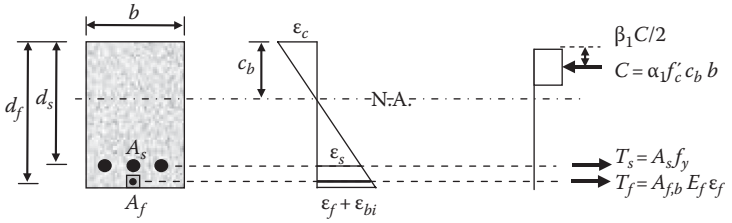

FIGURE 15.3 Strain compatibility and force equilibrium in a non-prestressed section.

Balanced Condition

At the balanced condition, the compression strain in the concrete ε_c is at the crushing strain ε_{cu} = 0.003 and the tensile strain in the FRP, ε_f, is at the effective strain (ε_{fe} = 0.7 * ε_{frpu}). Based on strain compatibility and force equilibrium equations for a rectangular section, the depth of the neutral axis, c_b, and the balanced FRP reinforcement, $A_{f,b}$, can be calculated by Equations 15.6 and 15.7.

$$c_b = \frac{\varepsilon_{cu}}{\varepsilon_{fe} + \varepsilon_{bi} + \varepsilon_{cu}} \cdot d_f \tag{15.6}$$

$$A_{f,b} = \frac{\alpha_1 f_c' b c_b - A_s f_y}{E_f \varepsilon_{fe}} \tag{15.7}$$

Understrengthened Section

In an understrengthened section ($A_f < A_{f,b}$), the FRP strain ε_f reaches its ultimate design strain, ε_{fe}, with compression strain in the concrete $\varepsilon_c < \varepsilon_{cu}$ or 0.003. The strain profile and forces in a rectangular section are shown in Figure 15.3. For this case, α_1 and β_1 are the mean stress factor and centroid factor of the parabolic concrete stress–strain curve when the concrete strain at top fiber does not reach its ultimate strain (Collins and Mitchell 1987).

$$\frac{f_c}{f_c'} = 2\frac{\varepsilon_c}{\varepsilon_c'} - \left(\frac{\varepsilon_c}{\varepsilon_c'}\right)^2 \tag{15.8a}$$

$$\varepsilon_c' = 2\frac{f_c'}{5500\sqrt{f_c'}} \tag{15.8b}$$

$$\alpha_1\beta_1 = \frac{\varepsilon_c}{\varepsilon_c'} - \frac{\varepsilon_c^2}{3\varepsilon_c'^2} \tag{15.9a}$$

$$\beta_1 = \frac{4 - (\varepsilon_c/\varepsilon_c')}{6 - (2\varepsilon_c/\varepsilon_c')} \tag{15.9b}$$

To determine the neutral axis depth, c, an iterative approach is required by assuming the concrete strain at top fiber, ε_c, and revising it until the force equilibrium and strain compatibility equations are satisfied (Figure 15.3). The nominal moment for this case is given in Equation 15.10.

$$M_n = A_s f_y \left(d_s - \beta_1 \frac{c}{2}\right) + A_f E_f \varepsilon_{fe} \left(d_f - \frac{\beta_1 c}{2}\right) \tag{15.10}$$

Overstrengthened Member

In an overstrengthened section ($A_f > A_{f,b}$), the compression strain in the concrete, ε_c, reaches the ultimate strain, ε_{cu} ($\varepsilon_c = \varepsilon_{cu}$ = 0.003) before FRP strain ε_f reaches its ultimate design strain, ε_{fe} ($\varepsilon_f < \varepsilon_{fe}$). The nominal moment for this case is calculated using Equation 15.11:

$$M_n = A_s f_y \left(d_s - \frac{\beta_1 c}{2}\right) + A_f E_f \varepsilon_f \left(d_f - \frac{\beta_1 c}{2}\right) \tag{15.11}$$

The analysis presented in this section is based on the rectangular section, and therefore if the cross-sectional area of the members is different, appropriate derivations based on the force equilibrium and strain compatibility shall be carried.

Example 15.1: Moment in a Non-Prestressed Section

This section shows the calculation procedure for the nominal moment of an RC slab strengthened with non-prestressed NSM FRP reinforcement. Figure 15.4 is the cross section of a slab pedestrian bridge, and the typical geometric and material properties are summarized as follows:

- Concrete: b = 1000 mm, h = 300 mm, $f_c' = 30$ MPa
- Steel: A_s = 800 mm^2, E_s = 200,000 MPa, f_{sy} = 400 MPa, d_s = 254 mm
- FRP: A_f = 120.0 mm^2 (4–6 mm diameter rods), E_f = 140 GPa, ε_{frpu} = 0.0150, d_f = 295 mm

Step 1. Determine nominal moment of the unstrengthened member

$$\alpha_1 = 0.85 - 0.0015 f_c' = 0.80$$

$$\beta_1 = 0.97 - 0.0035 f_c' = 0.895$$

$$\beta_1 c = \frac{A_s f_y}{\alpha_1 f_c' b} = \frac{(800)(400)}{(0.805)(30)(1000)} = 13.25 \text{ mm}$$

$$M_n = A_s f_y \left(d_s - \frac{\beta_1 c}{2} \right) = (800)(400)\left(254 - \frac{13.25}{2} \right) = 79.20 \text{ kN} \cdot \text{m}$$

Step 2. Determine failure mode of the section
Effective FRP strain, $\varepsilon_{fe} = 0.7 * \varepsilon_{frpu} = 0.7 * (0.015) = 0.0105$
FRP strain, $\varepsilon_f = \varepsilon_{fe} = 0.0105$
Concrete strain, $\varepsilon_{cu} = 0.003$
Initial strain, $\varepsilon_{bi} = 0$

$$c_b = \frac{\varepsilon_{cu}}{\varepsilon_{fe} + \varepsilon_{bi} + \varepsilon_{cu}} d_f = \frac{0.003}{0.0105 + 0 + 0.003} (295) = 65.5 \text{ mm}$$

$$A_{f,b} = \frac{\alpha_1 f_c' b c_b - A_s f_y}{E_f \varepsilon_{fe}}$$

$$= \frac{(0.805)(30)(1{,}000)(65.5) - (800)(400)}{(140{,}000)(0.0105)} = 858 \text{ mm}^2$$

$$A_f = 120 \text{ mm}^2 < 858 \text{ mm}^2$$

Understrengthened section (FRP failure mode)

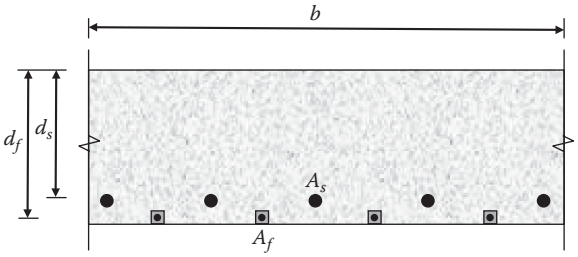

FIGURE 15.4 Typical cross section of concrete slab.

Step 3. Determine nominal moment of the strengthened member
Use trial and error to find "c" while satisfying force equilibrium and strain compatibility.
Assume strain in concrete at top fiber, $\varepsilon_c = 0.002$

$$\varepsilon_c' = 2\frac{f_c'}{5500\sqrt{f_c'}} = 0.002$$

$$\alpha_1\beta_1 = \frac{\varepsilon_c}{\varepsilon_c'} - \frac{\varepsilon_c^2}{3\varepsilon_c'^2} = \frac{0.002}{0.002} - \frac{1}{3}\left(\frac{0.002}{0.002}\right)^2 = 0.67$$

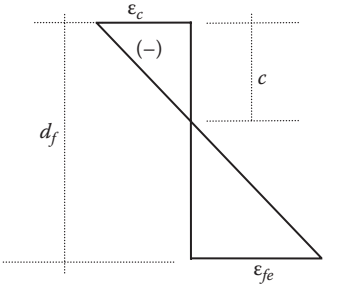

$$\beta_1 = \frac{4-(\varepsilon_c/\varepsilon_c')}{6-(2\varepsilon_c/\varepsilon_c')} = \frac{4-(0.002/0.002)}{6-2(0.002/0.002)} = 0.75$$

$$c = \frac{\varepsilon_c}{\varepsilon_{fe}+\varepsilon_c}d_f = \frac{0.002}{0.105+0.002}(295) = 47.2\text{ mm}$$

Force equilibrium condition

$$\begin{array}{llll} C_c = & \alpha_1 b_1 f_c' c b & = (0.67)(30)(47.2)(1{,}000) & = \underline{948.7\text{ kN}} \\ T_s = & A_s f_{sy} & = (800)(400) & = 320\text{ kN} \\ T_f = & A_f E_f \varepsilon_{fe} & = (120)(140{,}000)(0.0105) & = 176.4\text{ kN} \\ T_s + T_f & & & = \underline{496.4\text{ kN}} \end{array} \quad \neq C_c \quad \text{Revise}$$

Select $\varepsilon_c = 0.0015$

$$\frac{\varepsilon_c}{\varepsilon_c'} = 0.75 \quad \alpha_1\beta_1 = 0.563 \quad \beta_1 = 0.722 \quad c = 36.9\text{ mm} \quad C_c = 623\text{ kN} \quad \neq T_s + T_f \quad \text{Revise}$$

Select $\varepsilon_c = 0.00130$

$$\frac{\varepsilon_c}{\varepsilon_c'} = 0.65 \quad \alpha_1\beta_1 = 0.509 \quad \beta_1 = 0.713 \quad c = 32.5\text{ mm} \quad C_c = 496.3\text{ kN} \quad = T_s + T_f \quad OK$$

The nominal moment is calculated using Equation 15.10:

$$M_n = A_s f_y\left(d_s - \beta_1\frac{c}{2}\right) + A_f E_f \varepsilon_{fe}\left(d_f - \frac{\beta_1 c}{2}\right)$$

$$M_n = 320\left(254 - \frac{0.713\times 32.5}{2}\right) + 176.4\left(295 - \frac{0.713\times 32.5}{2}\right)$$

$$= 127.5\text{ kN}\cdot\text{m} \quad (60\%\text{ increase in capacity})$$

PRESTRESSED NSM STRENGTHENING

General

The fundamental concept of a prestressed NSM FRP-strengthened member is to improve the serviceability (cracking, deflection) and moment by providing an active "prestressing" force to the concrete element (Figure 15.5). The tensile stress at the concrete bottom face at mid-span under service loads is reduced or changed into compressive stress due to the effect of prestressing force, as shown in Figure 15.5. By using prestressed NSM strengthening, open cracks shall close, and the deflection of the member is reduced.

Prestressing Stresses

The allowable stresses for prestressed NSM FRP reinforcement shall be taken similar to those prescribed by ACI 440.4R-04. For CFRP, the maximum allowable stress is 60%–65% of the ultimate tensile strength of the FRP reinforcement. Regarding prestress losses, there are limited data for FRP reinforcement in epoxy medium, and as such, the designer should consult the current literature for these values.

Service Stresses

The serviceability condition for a prestressed NSM FRP-strengthened member requires the calculation of stresses under service loads to ensure they are within permissible values in design guides such as ACI 440.4-04. The stresses at a section are given as

$$\sigma = +\frac{P}{A} + \frac{Pe}{S} + \frac{M}{S} \tag{15.12}$$

where

σ is the stress in the concrete at distance y from centroidal axis, MPa
P is the prestress force in the NSM FRP reinforcement, N
M is the moment due to service loads, N·mm
e is the eccentricity measured from centroidal axis, mm
A is the cross-sectional area, mm^2
S is the section modulus, mm^3

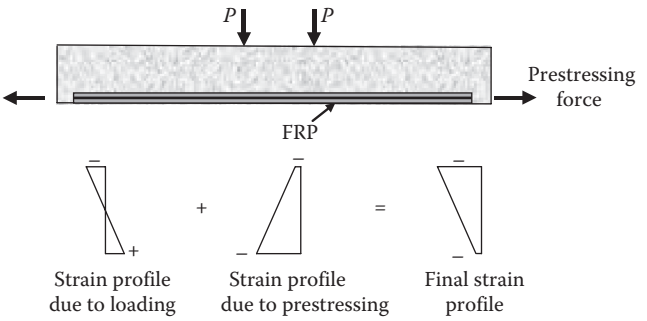

FIGURE 15.5 Stresses in a prestressed NSM FRP strengthening system.

Example 15.2: Flexural Stresses in an NSM Prestressed Slab

Compute the stresses in the prestressed NSM FRP-strengthened RC slab in Example 15.1. The slab is carrying a service moment of 60 kN·m. The slab is prestressed with four 6 mm diameter CFRP bars each stressed to 40% ultimate after losses. The CFRP bars have ultimate strength f_{frpu} = 2100 MPa, modulus of elasticity, E_{frp} = 140 GPa, and rupture strain = 0.015. Concrete strength, $f'_c = 30\,\text{MPa}$.

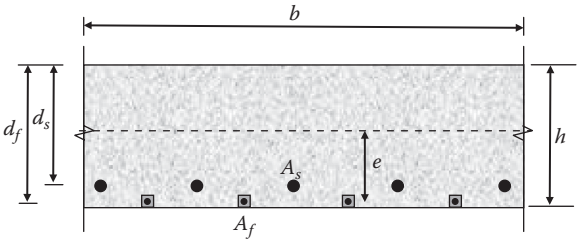

Solution

$$P_f = (0.4) f_{frpu} A_f = 0.40 \times 2100 \times 120 = 101\,\text{kN}$$

$$e = 295 - \frac{300}{2} = 145\,\text{mm}$$

$$A = bh = 300 \times 1000 = 300 \times 10^3\,\text{mm}^2$$

$$S = \frac{bh^2}{6} = \frac{1000 \times 300^2}{6} = 15 \times 10^6\,\text{mm}^3$$

Stresses in the concrete under service loads

$$\frac{P}{A} = \frac{100 \times 10^3}{300 \times 10^3} = 0.33\,\text{MPa}$$

$$\frac{Pe}{S} = \frac{(100 \times 10^3)(145)}{15 \times 10^6} = 0.966\,\text{MPa}$$

$$\frac{M}{S} = \frac{(60 \times 10^6)}{15 \times 10^6} = 4.0\,\text{MPa}$$

The stresses in the concrete at the top and bottom fibers under service loading are thus:

$$\text{top:} \quad \sigma_T = -0.33 + 0.966 - 4.0 = -3.36\,\text{MPa}$$

$$\leq 0.6 f'_c = 0.6 \times 40 = 24\,\text{MPa} \qquad \text{OK}$$

$$\text{bottom:} \quad \sigma_B = -0.33 - 0.966 + 4.0 = +2.7\,\text{MPa}$$

$$\leq 0.5\sqrt{f'_c} = 0.5\sqrt{30} = 2.75\,\text{MPa} \qquad \text{OK}$$

The concrete stresses in both extreme fibers are within permissible limits under service loads. The allowable stresses are specified in design guides, for example, ACI 440.4R (2004).

Cracking Moment

The cracking moment, M_{CR}, is calculated with the extreme tensile fiber stress in the concrete set equal to the modulus of rupture, $f_r = 0.6\sqrt{f_c'}$, as follows:

$$M_{CR} = \left(-\frac{P}{A} - \frac{Pe}{S_t} + 0.6\lambda\sqrt{f_c'} \right) S_t \tag{15.13}$$

where S_t is the section modulus at tension face, mm^3.

Example 15.3: Cracking Moment in NSM Prestressed Slab

Compute the cracking moment for the slab in Example 15.2.

$$M_{CR} = \left[-(-0.33) - (-0.966) + 0.6\sqrt{30} \right] (15 \times 10^6)$$

$$= 68\,\text{kN} \cdot \text{m}$$

$$= 68\,\text{kN} \cdot \text{m} > 60\,\text{kN} \cdot \text{m} \ (\text{service})$$

Flexural Strength

The flexural strength of a prestressed NSM FRP-strengthened section is determined by satisfying the force equilibrium and strain compatibility while accounting for the initial condition due to the prestressing effects. Figure 15.6 shows a prestressed rectangular section.

The strain compatibility is used to compute the stress in the NSM FRP at ultimate (f_{fu}).
Strain in tendon at ultimate

$$\varepsilon_{fu} = \varepsilon_{f,pres} + (\varepsilon_{f,c} + \varepsilon_{f,load}) < \varepsilon_{fe} \tag{15.14}$$

$$\varepsilon_{fe} = 0.7 * \varepsilon_{frpu}$$

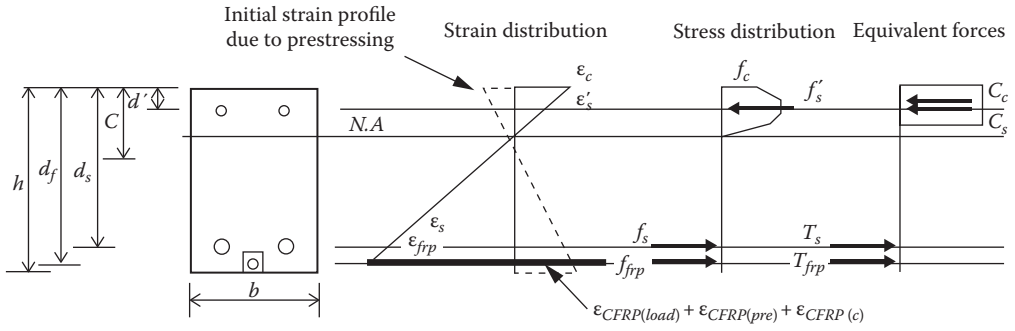

FIGURE 15.6 Strain compatibility and force equilibrium in a prestressed section.

From strain diagram at ultimate

$$\varepsilon_{f,load} = \varepsilon_{cu}\left(\frac{d_f}{c} - 1\right) \tag{15.15}$$

From equilibrium

$$A_f f_{fu} + A_s f_y = \alpha_1 f_c' ab \tag{15.16}$$

The solution proceeds by iteration to satisfy Equations 15.14 through 15.16. The nominal moment of an NSM prestressed section is calculated, ignoring the compression steel, using Equation 15.17:

$$M_n = A_s f_y (d_s - c) + A_{frp} E_{frp} (\varepsilon_{f,pres} + \varepsilon_{f,c} + \varepsilon_{f,load})(d_f - c) \tag{15.17}$$

where

A_s is the area of the tension steel reinforcement
A_{frp} is the area of the FRP reinforcement
b is the beam width
c is the depth of neutral axis
f_y is the stress in the tension steel reinforcement
M_n is the nominal bending moment
$\varepsilon_{f,pres}$ is the strain in NSM FRP due to initial prestressing force
$\varepsilon_{f,c}$ is the strain in NSM FRP at decompression in concrete at level of bar
$\varepsilon_{f,load}$ is the strain in NSM FRP due to loading by compatibility of strain

Example 15.4: Flexural Strength of NSM Prestressed Slab

Compute the ultimate moment of the NSM prestressed slab in Example 15.2. The CFRP bars have ultimate strength f_{frpu} = 2100 MPa, modulus of elasticity, E_{frp} = 140 GPa, and rupture strain = 0.015. Concrete strength, f_c' = 30 MPa. The prestress level after losses is $f_{pe} = 40\% f_{frpu}$.

Solution:

$$A = 300{,}000\,\text{mm}^2; \quad I = 22.5\times10^8\,\text{mm}^4; \quad e = 145\,\text{mm}$$

$A = 300{,}000\,\text{mm}^2$ $I = 22.5\times10^8\,\text{mm}^4$ $e = 145\,\text{mm}$

$P = 0.40\times2{,}100\times120 = 100\,\text{kN}$ $E_c = 5{,}500\sqrt{f_c'} = 5{,}500\sqrt{30} = 30{,}125\,\text{MPa}$

Total FRP strain $\varepsilon_{fu} = \varepsilon_{f,pres} + \varepsilon_{f,c} + \varepsilon_{f,load}$

a. $\varepsilon_{f,pres}$ = FRP strain due to prestressing

$$= \frac{f_{pe}}{E_f} = \frac{0.4\times2100}{140\times10^3} = 6000\times10^{-6}$$

b. $\varepsilon_{f,c}$ = concrete strain at level of FRP tendon due to prestressing

$$\sigma = \frac{P}{A} + \frac{Pe^2}{I}$$

$$= \frac{(-100\times10^3)}{300\times10^3} + \frac{(-100\times10^3)(145)^2}{22.5\times10^8} = -1.26\,\text{MPa}$$

$$\therefore \varepsilon_{f,c} = \frac{f_{ce}}{E_c} = \frac{1.26}{30125} = 42\times10^{-6}$$

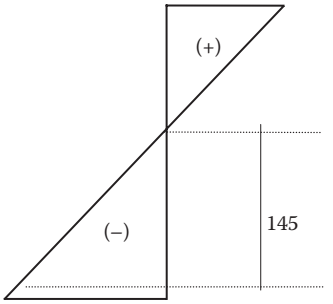

c. $\varepsilon_{f,load}$ = concrete strain at level of tendon at ultimate

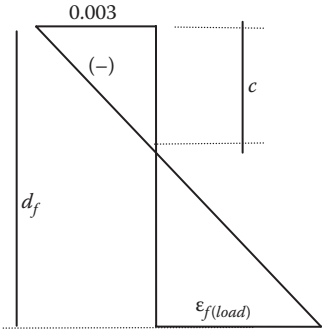

Assume $f_f = f_{fe} = 0.7\times2100 = 1470\,\text{MPa}$

$$c = \frac{A_f f_f + A_s f_y}{\alpha_1\beta_1 f_c' b} = \frac{120\times1470 + 800\times400}{0.80\times0.895\times30\times1000} = 23\,\text{mm}$$

$$\varepsilon_f = 0.003\times\frac{(295-23)}{23} = 0.035 > 0.0105 \quad (=\varepsilon_{fe})$$

For design, the maximum FRP strain = $0.7*\varepsilon_{frpu} = 0.7*0.015 = 0.0105$ or 10,500 με

$$\varepsilon_{fu} = \varepsilon_{f,pres} + \varepsilon_{f,c} + \varepsilon_{f,load}$$

$$10{,}500\times10^{-6} = (6000 + 42 + \varepsilon_{f,load})\times10^{-6}$$

$$\varepsilon_{f,load} = 4458\times10^{-6} = 0.00446$$

The two unknowns "c" and "ε_c" are to be determined by trial and error approach as follows:

$$\text{Assume } \varepsilon_c = 1000\,\mu\varepsilon \quad \alpha_1\beta_1 = 0.4167 \quad \beta_1 = 0.7 \quad c = 54.0\,\text{mm}$$

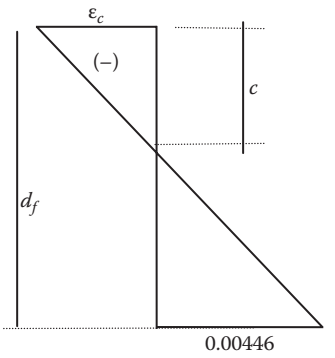

$$\begin{aligned} C_c &= \alpha_1\beta_1 f_c' b &&= \underline{675{,}613\,\text{N}} \\ T_s &= A_s f_y &&= 320{,}000\,\text{N} \\ T_f &= A_f f_{fe} &&= 176{,}000\,\text{N} \\ T_s + T_f &&&= \underline{496{,}000\,\text{N}} \end{aligned} \quad \neq C_c \quad \text{Revise}$$

$$\text{Select } \varepsilon_c = 800\,\mu\varepsilon \quad \alpha_1\beta_1 = 0.4167 \quad \beta_1 = 0.7 \quad c = 54.0\,\text{mm}$$

$$C_c = \alpha_1\beta_1 f_c' b = \underline{466{,}793\,\text{N}} \quad \neq T_s + T_f \quad \text{Revise}$$

$$\text{Select } \underline{\varepsilon_c = 830\,\mu\varepsilon} \quad \alpha_1\beta_1 = 0.357 \quad \beta_1 = 0.69 \quad c = 46.3\,\text{mm} \quad \beta_1 c = 32\,\text{mm}$$

$$C_c = \alpha_1\beta_1 f_c' b = \underline{496{,}726\,\text{N}} \quad \neq T_s + T_f \quad \text{OK}$$

The nominal moment is calculated as follows:

$$\begin{aligned} M_n &= A_s f_y \left(d_s - \frac{\beta_1 c}{2} \right) + A_f E_f \varepsilon_f \left(d_f - \frac{\beta_1 c}{2} \right) \\ &= 320 \left(254 - \frac{32}{2} \right) + 176.4 \left(295 - \frac{32}{2} \right) = 125.40\,\text{kN} \cdot \text{m} \end{aligned}$$

Comparing with the example in Example 15.1, the nominal moment of the prestressed section is slightly smaller than the non-prestressed section. However, the curvature (ε_c/c) for the prestressed section is $18 \times 10^{+6}$, which is half that for the non-prestressed section ($40 \times 10^{+6}$).

SERVICEABILITY REQUIREMENTS

The serviceability (cracking and deflection) for an NSM-strengthened member shall satisfy the applicable provisions in existing design guidelines. For example, ACI 440.2R (2008) limits the service stress in concrete to 45% of the compressive strength and the service stress in the internal steel and 80% of the yield strength of the reinforcement. The fatigue stress and creep-rupture limits shall be based on ACI 440.2R (2008), which specifies the stresses in a CFRP reinforcement under service loads to be below 55% of the ultimate strength of the CFRP.

SHEAR DESIGN

There are very limited data on the shear behavior of NSM FRP-strengthened members (De Lorenzis and Teng 2007). The effective strain in the NSM FRP reinforcement, mounted on the sides of the member, can be conservatively taken as an EB face FRP plies following the procedure described in ACI 440.2R (2008). The design engineer shall review the suitability of provisions in ACI 440.2R (2008) for EB FRP laminates and ACI 440.1R (2006) for internal FRP stirrups. The designer shall consult the published literature on shear strengthening as they become available.

CONCLUDING REMARKS

NSM FRP reinforcement is recently used for the rehabilitation and strengthening of concrete structures. This chapter has focused primarily on the flexural behavior of concrete members strengthened with non-prestressed and prestressed NSM FRP reinforcement. Many research areas are still needed including serviceability criteria, bond and development, shear strength, fire resistance and protection, external prestressing and devices, etc. For this emerging technology to become widespread, specific provisions addressing NSM reinforcement shall be included in international guidelines and specifications.

REFERENCES

ACI (2004). Prestressed concrete structures with FRP tendons, ACI 440.4R-04, American Concrete Institute, Farmington Hills, MI, 35pp.

ACI (2006). Guide for the design and construction of structural concrete reinforced with FRP bars, ACI 440.1R-06, American Concrete Institute, Farmington Hills, MI, 44pp.

ACI (2008). Guide for the design and construction of externally bonded FRP systems for strengthening concrete structures, ACI 440.2R-08, American Concrete Institute, Farmington Hills, MI, 80pp.

Asplund, S.O. (1949). Strengthening bridge slabs with grouted reinforcement, American Concrete Institute (ACI), *Structural Journal*, 20(4), 397–406.

Badawi, M. and Soudki, K.A. (2006). Strengthening of RC beams with prestressed near surface mounted CFRP rods, *Third International Conference IIFC Composites in Civil Engineering*, December 13–15, Miami, FL.

Badawi, M., Wahab, N., and Soudki, K.A. (2011). Evaluation of the transfer length of prestressed near surface mounted CFRP rods in concrete, *Journal of Building and Construction Materials*, 25(3), 1474–1479.

CNR (2004). *Guide for the Design and Construction of Externally Bonded FRP Systems for Strengthening Existing Structures, CNR-DT 200/2004*. CNR—Advisory Committee on Technical Recommendations for Construction, Rome, Italy, 144pp.

Collins, M.P. and Mitchell, D. (1987). Prestressed concrete basics, Canadian Prestressed Concrete Institute (CPCI), Ottawa, Ontario, Canada, 614pp.

De Lorenzis, L. and Teng, J.G. (2007). Near-surface mounted FRP reinforcement: An emerging technique for strengthening structures, *Composites Part B*, 38(2), 119–143.

El-Hacha, R. and Rizkalla, S.H. (2004). Near-surface-mounted fiber-reinforced polymer reinforcements for flexural strengthening of concrete structures, *ACI Structural Journal*, 101(5), 717–726.

fib (2001). Externally bonded FRP reinforcement for RC structures—Bulletin 14, International Federation for Structural Concrete (fib), Lausanne, Switzerland, 130pp.

Hassan, T. and Rizkalla, S. (2003). Investigation of bond in concrete structures strengthened with near surface mounted carbon fiber reinforced polymer strips, *ASCE Journal of Composite for Construction*, 7(3), 248–257.

Hassan, T.K. and Rizkalla, S.H. (2004). Bond mechanism of near-surface-mounted fiber-reinforced polymer bars for flexural strengthening of concrete structures, *ACI Structural Journal*, 101(6), 830–839.

ISIS (2008). FRP rehabilitation of reinforced concrete structures, Design Manual No. 4, Version 2, ISIS Canada, Toronto, Ontario, Canada.

Lorenzis, L. and Nanni, A. (2002). Bond between near-surface mounted fiber-reinforced polymer rods and concrete in structural strengthening, *ACI Structural Journal*, 99(2), 123–132.

SIA166 (2004). Klebebewehrungen (Externally bonded reinforcement), Schweizerischer Ingenieur- und Architektenverein—SIA, Zurich, Switzerland, 44pp.

TR55 (2004). Design guidance for strengthening concrete structures using fibre composite materials, 2nd edition, Technical Report No. 55 of the Concrete Society, London, U.K., 102pp.

16 Confinement of Reinforced Concrete Columns

Kerstin Lang and Andrin Herwig

CONTENTS

INTRODUCTION

This chapter deals with the confinement of reinforced concrete members under compression, such as columns, using fiber-reinforced plastics (FRP). In general, confinement acts to increase the compressive strength and ultimate compressive strain of concrete by creating a three-dimensional state of stress in the concrete. This increase in compressive strength and ultimate compressive strain of concrete leads to an increase in bending moment and rotational capacity of the concrete member under compression, which is of major importance for structures subjected to seismic action. In general, the increase in strength is much less significant than the increase in ductility. Recent earthquakes have shown again and again that many columns in existing buildings have insufficient transverse reinforcement leading to major damage of the columns or even collapse (Figure 16.1). The need to upgrade columns has become more and more evident (Priestley and Seible, 1995). Traditional external confinement techniques are steel jackets or hoops. However, steel yields at a tensile strain of only 0.002 and then exerts an almost constant confining pressure, whereas FRP shows an elastic behavior up to failure, usually at strains of more than 0.01. The confining action therefore increases continuously during loading. Furthermore, due to its lightweight, FRP is more convenient to apply and it is not prone to corrosion. In the last couple of years, the use of FRP to confine existing reinforced concrete columns has become increasingly popular for the reasons mentioned earlier. Experimental studies have shown, in fact, that the confinement of columns using FRP can be very efficient, especially for circular columns (Seible et al., 1997; Rochette and Labossière, 2000; Matthys et al., 2005; Gosh and Sheikh, 2007).

Further effects of FRP confinement, in addition to the increase in compressive strength and strain already mentioned, are

- Increase in shear capacity
- Prevention of lap-splice failure
- Prevention of buckling of longitudinal reinforcement

FIGURE 16.1 Damaged reinforced concrete columns with insufficient transverse reinforcement (pictures taken after the earthquake in Gujarat, 2001).

FRP confinement is usually produced using a hand lay-up by laying up successive layers of fiber sheets or fabrics and impregnating them with a liquid polymer resin. The fibers are predominantly orientated transversely to the column axis. After the curing process is complete, the layers and the resin form a composite shell (Figure 16.2). Other methods exist using, for example, precured FRP strips wound around the column.

The aim of this chapter is to familiarize the reader with the concept of confining reinforced concrete columns using FRP, with a discussion of some of the earlier-mentioned effects. First, compressive stress–strain relationships for circular concrete columns confined with FRP are introduced. Several procedures are shown that allow the prediction of the stress–strain relationship. In the next section, the

(a) (b)

FIGURE 16.2 FRP wrapping of (a) a circular and (b) a rectangular column.

implications of partial wrapping, rectangular, and oval cross sections are presented. It is then shown how the increase in compressive strength and ultimate compressive strain leads to an increase in lateral displacement capacity. Some suggestions on the confinement in the lap-splice regions are given. Finally, a worked example is given for the design of FRP confinement of a square reinforced concrete column to increase the load-carrying capacity and the ductility under seismic action.

Relevant design guidelines for the external confinement of reinforced concrete columns using FRP are the fib Bulletin 14 (2001), the ACI committee report ACI 440.2R-08 (2008), the ISIS Canada design manual no. 4 (2001), and the CNR advisory committee recommendations CNR-DT 200/2004 (2004). For more detailed information on this subject, the reader can also refer to the textbooks of Bank (2006), Teng et al. (2002), and Hollaway and Teng (2008).

STRESS–STRAIN RELATIONSHIP FOR CIRCULAR COLUMNS

When a column is subjected to axial compression, the concrete wants to expand laterally. If the column is confined with FRP, the expansion of the concrete is opposed by the FRP, which in turn is strained. If we consider a circular column, for which the confinement is uniform around the perimeter, the lateral confining stress σ_l can be determined as follows (Figure 16.3):

$$\sigma_l = \frac{2t_f}{d}\sigma_f = \frac{1}{2}\rho_f E_f \varepsilon_f \text{ with } \rho_f = \frac{4t_f}{d} \tag{16.1}$$

where

σ_f, t_f, E_f, ε_f, and ρ_f are the tensile stress, the thickness, the modulus of elasticity, the strain, and the volumetric ratio of the FRP confinement

d is the diameter of the column

The theoretical maximum confining stress f_l is given when the FRP confinement has reached its tensile strength f_f. Experiments, however, have shown that the FRP jacket often ruptures before the ultimate tensile strain of the FRP material ε_{fu} is reached. Possible reasons are the triaxial state of stress of the wrapping, the quality of execution, the curved shape of the wrapping, and the size effect when applying multiple layers. A reduction factor between 0.5 and 0.7 therefore seems appropriate (Lam and Teng, 2003a; Karam and Tabbara, 2005). The actual maximum confining stress $f_{l,a}$ is therefore given by

$$f_{l,a} = \frac{1}{2}\rho_f E_f \varepsilon_{f,rup} = \frac{2t_f}{d} E_f \varepsilon_{f,rup} \text{ with } \varepsilon_{f,rup} \approx 0.5 \div 0.7\varepsilon_{fu} \tag{16.2}$$

where $\varepsilon_{f,rup}$ is the actual rupture strain of the FRP confinement.

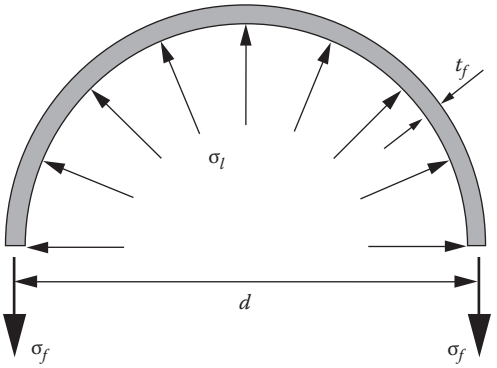

FIGURE 16.3 Lateral confining stress.

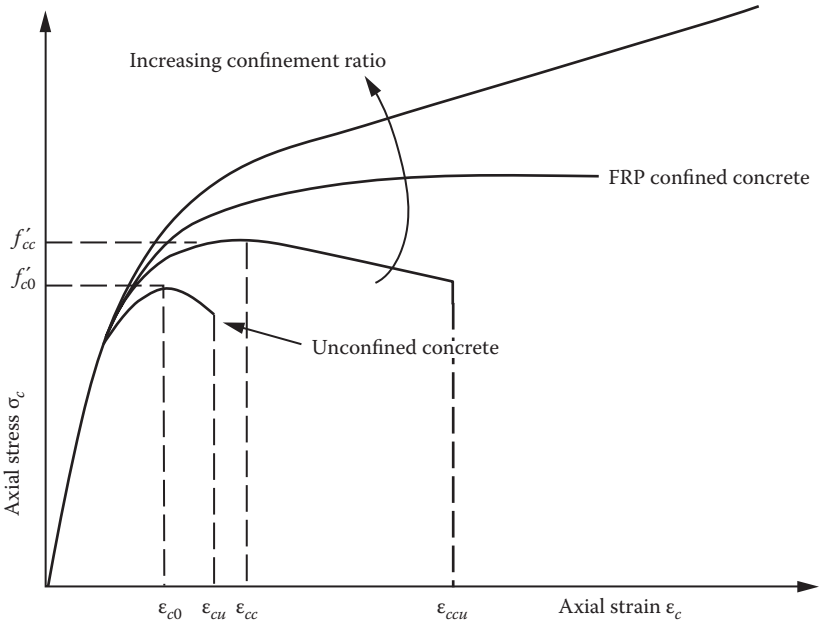

FIGURE 16.4 Schematic of compressive stress–strain relationships for unconfined concrete and FRP-confined concrete.

Figure 16.4 shows schematically the stress–strain relationship of FRP-confined concrete with the most important parameters indicated. At small axial strains, the stress–strain curve corresponds to the stress–strain curve of unconfined concrete. Only at higher axial strains, when the concrete behavior becomes more nonlinear, does the effect of the confinement become evident by increasing the compressive strength f'_{cc} and the ultimate axial compressive strain ε_{ccu} of the confined concrete with respect to the compressive strength f'_{c0} and the ultimate axial compressive strain ε_{cu} of the unconfined concrete. In fact, the higher the confinement ratio, the higher the compressive strength f'_{cc} and ultimate axial compressive strain ε_{ccu} of the confined concrete. For well-confined columns, the stress–strain relationship is continuously increasing such that the compressive strength f'_{cc} is reached at the point of ultimate axial compressive strain ε_{ccu}. For columns with a rather low confinement ratio, the compressive strength f'_{cc} is reached at an axial compressive strain $\varepsilon_{cc} < \varepsilon_{ccu}$ beyond which the strength decreases with strain.

The compressive strength of confined concrete is often expressed in the following form (Mirmiran and Shahawy, 1997):

$$\frac{f'_{cc}}{f'_{c0}} = 1 + k_1 \left(\frac{f_{l,a}}{f'_{c0}} \right) \tag{16.3}$$

where

f'_{cc} and f'_{c0} are the compressive strengths of confined and unconfined concrete respectively

k_1 is the so-called effectiveness coefficient

$f_{l,a}$ is the actual maximum confining stress that can be calculated using Equation 16.2

This equation was first proposed by Richart et al. (1928). Lam and Teng (2002) proposed a value of $k_1 = 3.3$, which was also adopted by the ISIS Canada design manual no. 4 (2001) and ACI 440.2R-08 (2008).

Mander et al. (1988) suggested a nonlinear relationship:

$$\frac{f'_{cc}}{f'_{c0}} = 2.254\sqrt{1+7.94\frac{f_{l,a}}{f'_{c0}}} - 2\frac{f_{l,a}}{f'_{c0}} - 1.254 \tag{16.4}$$

Even though this formulation was derived for steel-confined concrete, it is now widely accepted for FRP-confined concrete and was recently introduced in the fib Bulletin 14 (2001).

For the axial compressive strain ε_{cc} at the compressive strength f'_{cc}, Richart et al. (1929) suggested the following relationship:

$$\frac{\varepsilon_{cc}}{\varepsilon_{c0}} = 1 + k_2\frac{f_{l,a}}{f'_{c0}} \tag{16.5}$$

where

ε_{c0} is the axial compressive strain of the unconfined concrete at its compressive strength f'_{c0}

k_2 is the strain enhancement coefficient

They also suggested the use of $k_2 = 5k_1$, which leads to the following expression:

$$\frac{\varepsilon_{cc}}{\varepsilon_{c0}} = 1 + 5\left(\frac{f'_{cc}}{f'_{c0}} - 1\right) \tag{16.6}$$

This relationship to calculate ε_{cc} is also used by the stress–strain model proposed by Mander et al. (1988) for steel-confined concrete and was introduced in the fib Bulletin 14 (2001).

To determine the ultimate axial compressive strain of confined concrete ε_{ccu}, Seible et al. (1995) suggested the following relationship:

$$\varepsilon_{ccu} = 0.004 + \frac{2.5\rho_f f_f \varepsilon_{f,rup}}{f'_{cc}} \tag{16.7}$$

This practical formula is adopted by the fib Bulletin 14 (2001), whereas the ISIS Canada design manual no. 4 (2001) does not give any recommendation to evaluate ε_{ccu}. Lam and Teng (2003a) suggested an alternative expression to calculate ε_{ccu} based on a best-fitting trend line for available test data:

$$\frac{\varepsilon_{ccu}}{\varepsilon_{c0}} = 1.75 + 12\left(\frac{f_{l,a}}{f'_{c0}}\right)\left(\frac{\varepsilon_{f,rup}}{\varepsilon_{c0}}\right)^{0.45} \tag{16.8}$$

Equation 16.8 was introduced in ACI 440.2R-08 (2008) in a slightly modified form with the factor 1.5 instead of 1.75.

Knowledge of the ultimate axial compressive strain of confined concrete is in fact very important for the seismic retrofitting of reinforced concrete columns as will be seen later on.

For the design of FRP confinement, the values of compressive strength f'_{cc}, axial compressive strain ε_{cc} at the compressive strength f'_{cc}, and ultimate axial compressive strain ε_{ccu} of the confined concrete are usually enough. However, in cases where the full stress–strain relationship is of interest, a plenitude of models is available. The proposed models differ depending on their objective. Design-oriented models are usually rather simple and are expressed in closed form, whereas

analysis-oriented models aim at describing the complete stress–strain relationship using an incremental iterative procedure (Teng and Lam, 2004). As it is not possible to give a complete overview of all the available models, only one example is given for each category, and the reader is referred to Teng and Lam (2004) for a more complete listing of the available models. For the design-oriented models, the model developed by Lam and Teng (2003a) is introduced. It is based on the assumptions that the stress–strain relationship consists of a parabolic first portion and a straight-line second portion, and that the initial slope of the parabola is the same as that for unconfined concrete. For the parabolic first portion, the stress–strain relationship is given by the following relationship:

$$\sigma_c = E_c\varepsilon_c - \frac{(E_c - E_2)^2}{4f_0}\varepsilon_c^2 \quad \text{for } 0 \le \varepsilon_c \le \varepsilon_t \tag{16.9}$$

where

σ_c and ε_c are the current compressive stress and strain of the concrete respectively
E_c is the elastic modulus of concrete
E_2 is the slope of the linear second portion
f_0 is the stress at the intercept between the parabolic first portion and the straight-line second portion
ε_t is the corresponding strain given by

$$\varepsilon_t = \frac{2f_0}{E_c - E_2} \tag{16.10}$$

The slope of the linear second portion is given by

$$E_2 = \frac{f_{cc}' - f_0}{\varepsilon_{ccu}} \tag{16.11}$$

For the straight-line second portion, the stress–strain relationship is given by the following relationship:

$$\sigma_c = f_0 + E_2\varepsilon_c \quad \text{for } \varepsilon_t \le \varepsilon_c \le \varepsilon_{ccu} \tag{16.12}$$

This model is defined by three parameters: the compressive strength of confined concrete f_{cc}', the ultimate axial compressive strain of confined concrete ε_{ccu}, and the stress at the intercept between the parabolic portion and the straight-line portion f_0. f_{cc}' and ε_{ccu} can be calculated using Equations 16.3 and 16.8, whereas the stress at the intercept between the parabolic portion and the straight-line portion f_0 is taken to equal f_{c0}':

$$f_0 = f_{c0}' \tag{16.13}$$

It is important to note that the model proposed by Lam and Teng is valid only for sufficiently confined columns, that is, the actual confinement ratio $f_{l,a}/f_{c0}' \ge 0.07$.

As an example for the analysis-oriented models, the model proposed by Spoelstra and Monti (1999) is introduced. Their model is based on the model proposed by Mander et al. (1988) for steel-confined concrete, which they modified to take into account the increased confining effect during loading due to the elastic nature of the FRP confinement. In fact, the interaction between the

concrete core and the confining FRP is considered at every strain increment leading to an iterative procedure. The stress–strain relationship is given in the following form, based on the formulation by Popovics (1973):

$$\sigma_c = \frac{f'_{cc} x r}{r - 1 + x^r}$$

$$\text{with } x = \frac{\varepsilon_c}{\varepsilon_{cc}}, \quad r = \frac{E_c}{E_c - E_{sec}}, \quad \text{and} \quad E_{sec} = \frac{f'_{cc}}{\varepsilon_{cc}} \tag{16.14}$$

The compressive strength of the confined concrete f'_{cc} is calculated using Equation 16.4, and the axial compressive strain ε_{cc} at the compressive strength f'_{cc} of the confined concrete is calculated using Equation 16.6. To express the dependency of the lateral strain ε_l on the current axial compressive strain ε_c, the constitutive model for unconfined concrete developed by Pantazopoulou and Mills (1995) is used:

$$\varepsilon_l = \frac{E_c \varepsilon_c - \sigma_c}{2\beta\sigma_c} \tag{16.15}$$

The constant β is a property of concrete and can be expressed in a simplified form as a function of the compressive strength of the unconfined concrete f'_{c0}:

$$\beta = \frac{5700}{\sqrt{|f'_{c0}|}} - 500 \tag{16.16}$$

From Equation 16.15, the tensile strain in the FRP confinement can be deduced (for axially loaded cylinders: $\varepsilon_f = \varepsilon_l$) and, hence, the corresponding lateral confining stress σ_l can be calculated using Equation 16.1. This updated value of σ_l can be again used to calculate a new estimate of ε_l leading to an iterative procedure until σ_l converges to the correct value. The whole procedure is then repeated for the next increment of ε_c (Figure 16.5):

Even though the model uses an iterative procedure, the convergence is usually very fast.

INFLUENCE OF NONUNIFORM CONFINING STRESS

Columns with noncircular cross sections, such as rectangular ones, are widely used. Due to the low confinement bending stiffness, the confining pressure around the perimeter and within the cross section is nonuniform leading to a variation of the compressive strength of the confined concrete over the cross section.

Furthermore, columns may be wrapped continuously using FRP sheets or partially with discrete hoops using FRP straps.

The nonuniform confining stress for the strength calculation can be considered by the introduction of an effectiveness factor k_e, which is given as follows:

$$k_e = k_p k_s \tag{16.17}$$

where

k_p takes into account the effect of partial wrapping ($k_p \leq 1.0$)

k_s is the shape factor for the effect of rectangular or elliptical cross sections ($k_s \leq 1.0$)

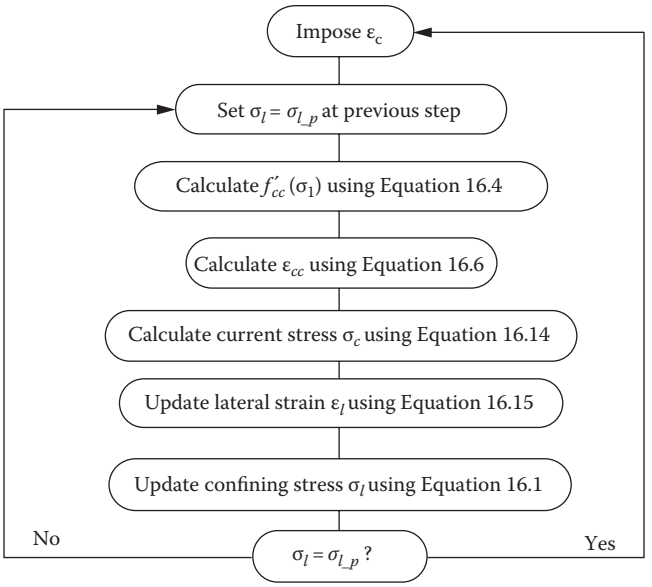

FIGURE 16.5 Iterative procedure used for the model by Spoelstra and Monti. (From Spoelstra, M.R. and Monti, G., *ASCE J. Compos. Constr.*, 3(3), 143, 1999.)

Hence, Equation 16.2 adopts the following form to calculate $f_{l,a}$:

$$f_{l,a} = k_e \frac{2t_f}{d} E_f \varepsilon_{f,rup} \tag{16.18}$$

Partially Wrapped Columns

In partially wrapped columns, there exist both confined and unconfined zones over the height of the column (Figure 16.6).

According to fib Bulletin 14 (2001), the confinement between two FRP hoops due to arching action is taken into account by the factor k_p, which can be calculated as follows:

$$k_p = \frac{A_e}{A_c} = \frac{(1-(s'/2d))^2}{1-\rho_{sc}} \approx \left(1-\frac{s'}{2d}\right)^2 \tag{16.19}$$

where

$\rho_{sc} = A_{s,l}/A_c$ is the cross-sectional area ratio of longitudinal steel reinforcement
s' is the clear spacing between the hoops
A_e is the effectively confined area

$$A_e = \frac{\pi}{4}\left(d-\frac{s'}{2}\right)^2 \tag{16.20}$$

Rectangular Columns

A parabolic arching action is assumed for the concrete core for square or rectangular cross sections with rounded corners where only a part of the cross section is confined. The concept

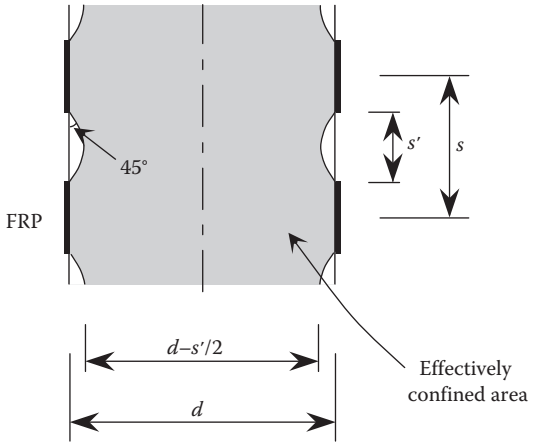

FIGURE 16.6 Longitudinal cut through a partially wrapped column. (After fib, Externally bonded FRP reinforcement for RC structures, International Federation for Structural Concrete, Bulletin 14, Lausanne, Switzerland, 2001.)

for the calculation of the effectively confined area was proposed by Mander et al. (1988). The effectively confined area is illustrated in Figure 16.8, but the initial slopes of the parabolas are equal to 45° instead of arctan (*b*/*h*). The shape factor k_s for the confined compressive strength is

$$k_s = 1 - \frac{(b-2r_c)^2 + (d-2r_c)^2}{3A_g(1-\rho_{sc})} \tag{16.21}$$

where A_g is the gross area of the column section with rounded corners given by

$$A_g = bh - (4-\pi)r_c^2 \tag{16.22}$$

The actual maximum confining stress $f_{l,a}$ in the fib Bulletin 14 is based on the model by Mander et al. (1988) and considers the two principal directions separately with *d* equal to the dimensions of the cross section in the direction considered. For a detailed description, the reader is referred to Mander et al. (1988).

Karam and Tabbara (2005) give an alternative for the calculation of the shape factor for the confined compressive stress. They propose a shape factor based on a mechanical model, which is verified by numerical simulations. Figure 16.7 shows the upper right quadrant of a rectangular column with a short side *b*, a long side *h*, and a corner radius r_c. The concrete is assumed to be subjected to an average confining stress at its middle sections with σ_b acting along the short side and σ_h acting along the long side. The relationship between σ_b, σ_h, and the FRP tensile stress σ_f is obtained by establishing the equilibrium of forces acting on the column quadrant in the horizontal and vertical directions:

$$t_f\sigma_f = \frac{b}{2}\sigma_b = \frac{h}{2}\sigma_h \tag{16.23}$$

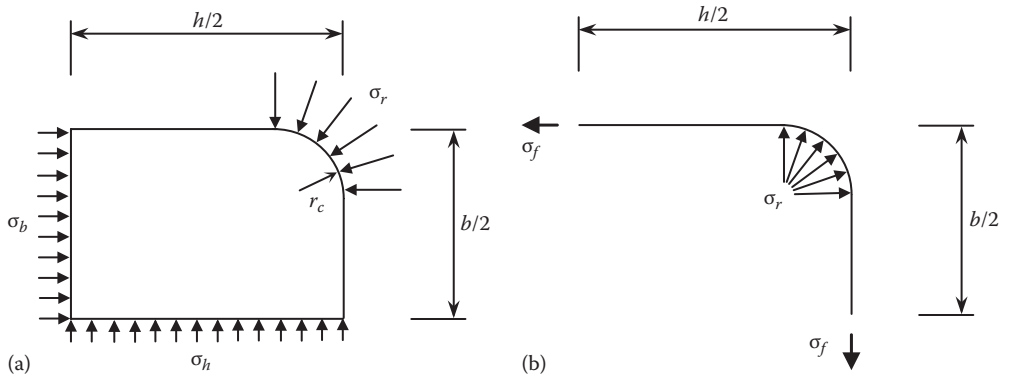

FIGURE 16.7 Free-body diagram of upper right quadrant according to Karam and Tabbara. (a) Forces acting on the concrete, (b) forces acting on the confinement. (From Karam, G. and Tabbara, M., *ASCE J. Compos. Constr.*, 9(5), 388, 2005.)

The equilibrium of the forces acting on the confinement gives

$$t_f \sigma_f = r_c \sigma_r \tag{16.24}$$

Using Equations 16.23 and 16.24, the following relationships can be given:

$$\frac{\sigma_r}{\sigma_b} = \frac{b}{2r_c} \tag{16.25}$$

and

$$\frac{\sigma_h}{\sigma_b} = \frac{b}{h} \tag{16.26}$$

A shape factor is defined by dividing the average confining stress over the whole cross section by the maximum confinement stress attained at the corners. It can then be calculated from Equations 16.24 through 16.26 as

$$k_s = \frac{\sigma_b + \sigma_h}{2} \frac{1}{\sigma_r} = \frac{r_c}{b}\left(1 + \frac{b}{h}\right) \tag{16.27}$$

To calculate the actual maximum confining stress $f_{l,a}$, again, an equivalent diameter has to determined. Karam and Tabbara do not give suggestions for the determination of this value.

Also based on the parabolic action, Lam and Teng (2003b) proposed another model to calculate the effectively confined area. The model allows for the calculation of the confined compressive strength as well as the ultimate axial compression strain ε_{ccu}.

The confined compressive strength is calculated with the shape factor k_{s1} and the ultimate axial compression strain with the shape factor k_{s2}. The effectively confined area is contained by four parabolas as illustrated in Figure 16.8. The initial slopes of the parabolas are the same as the adjacent diagonal lines.

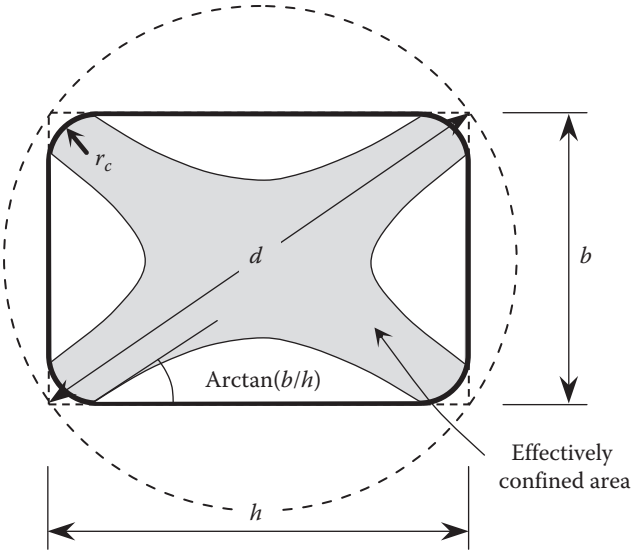

FIGURE 16.8 Effectively confined concrete section. (After Hollaway, L.C. and Teng, J.G. (eds.), *Strengthening and Rehabilitation of Civil Infrastructures Using Fibre-Reinforced Polymer* (*FRP*) *Composites*, Woodhead Publishing Limited, Cambridge, U.K., 2008.)

The shape factor k_{s1} for the confined compressive strength is

$$k_{s1} = \left(\frac{b}{h}\right)^2 \frac{A_e}{A_c} \tag{16.28}$$

with

$$\frac{A_e}{A_c} = \frac{1 - \left(\frac{b}{h}(h-2r_c)^2 + \frac{h}{b}(b-2r_c)^2 \Big/ 3A_g\right) - \rho_{sc}}{1-\rho_{sc}} \tag{16.29}$$

The actual maximum confining stress $f_{l,a}$ is calculated with an equivalent diameter

$$d = \sqrt{h^2 + b^2} \tag{16.30}$$

Equation 16.18 takes the following form:

$$f_{l,a} = k_e \frac{2t_f}{\sqrt{h^2+b^2}} E_f \varepsilon_{f,rup} \tag{16.31}$$

Finally, the confined compressive strength is calculated using Equation 16.3.

The ultimate axial compression strain is calculated with the shape factor k_{s2}:

$$k_{s2} = \left(\frac{h}{b}\right)^{0.5} \frac{A_e}{A_c} \tag{16.32}$$

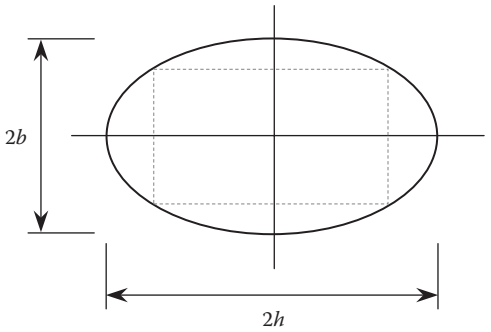

FIGURE 16.9 Elliptical cross section with the definition of the axes.

$f_{l,a}$ is given by

$$f_{l,a} = k_{s2} \frac{2t_f}{\sqrt{h^2 + b^2}} E_f \varepsilon_{f,rup} \tag{16.33}$$

This concept is also adopted by ACI 440.2R-08 (2008).

Strength of Confined Elliptical Columns

Rectangular columns may be transformed into elliptical columns for more effective confinement. Tests showed that the confinement effectiveness decreases as the aspect ratio (h/b) increases.

The shape factor k_s according to Teng et al. (2002) is given as

$$k_s = \left(\frac{b}{h}\right)^2 \tag{16.34}$$

where h and b are the major and the minor axes, respectively, of the elliptical cross section according to Figure 16.9.

The effectiveness factor k_e is calculated with Equation 16.17. The actual maximum confining stress $f_{l,a}$ is calculated with Equation 16.18 using the equivalent diameter

$$d = \frac{4hb}{\left[1.5(h+b) - \sqrt{hb}\right]} \tag{16.35}$$

$$f_{l,a} = k_e \frac{2t_f \left[1.5(h+b) - \sqrt{hb}\right]}{4hb} E_f \varepsilon_{f,rup}. \tag{16.36}$$

SEISMIC LOADING

For seismic loading, the lateral displacement capacity of a structure is of primary importance. The deformation capacity of a whole structure (building or bridge) depends on the deformation capacity of the individual members (walls, columns, etc.). In the following, the lateral displacement capacity of a column is considered (Figure 16.10). The procedure outlined to determine the lateral

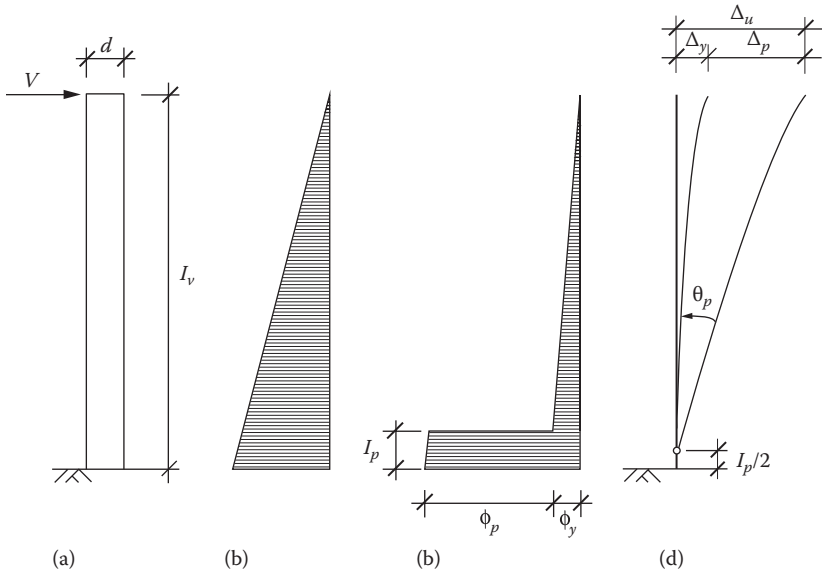

FIGURE 16.10 Deformation of a column under horizontal force. (a) Column, (b) moments, (c) curvatures, and (d) deflections. (After Paulay, T. and Priestley, M.J.N., *Seismic Design of Reinforced Concrete and Masonry Buildings*, John Wiley & Sons, Inc., New York, 1992.)

displacement capacity of a confined column follows the procedure proposed by Paulay and Priestley (1992) for buildings, and Priestley et al. (1996) for bridges.

The lateral displacement capacity of a column under a horizontal force depends on its rotational capacity, which in return is a function of its section-curvature ductility. Considering the column in Figure 16.10, the total displacement Δ_u at the top of the column due to the horizontal force V is composed of an elastic part, referred to as yield displacement Δ_y, and a plastic displacement Δ_p:

$$\Delta_u = \Delta_y + \Delta_p \tag{16.37}$$

The displacement ductility $\mu\Delta$ of the column is defined as

$$\mu_\Delta = \frac{\Delta_u}{\Delta_y} \tag{16.38}$$

The yield displacement can be calculated using elastic theory:

$$\Delta_y = \frac{V l_v^3}{3E_c I_e} \tag{16.39}$$

where

I_e is the effective moment of inertia of the cracked section

l_v is the shear span of the column, that is, the distance from the base of the column to the point where the bending moment M is zero: $l_v = M/V$

In the case of a cantilever, as shown in Figure 16.10, the shear span l_v is equal to the height of the column. When rotations are prohibited at both ends of the column (fixed end conditions), the shear

span l_v is equal to half the height of the column. For this case, the yield displacement calculated with Equation 16.39 corresponds to the displacement at mid-height of the column.

From the yield displacement Δ_y, the curvature at yield ϕ_y can be deduced:

$$\phi_y = \frac{M_y}{E_c I_e} = \frac{V l_v}{E_c I_e} = \frac{3\Delta_y}{l_v^2} \tag{16.40}$$

where M_y is the yield moment. Based on numerical investigations, Priestley (2003) observed that the yield curvature ϕ_y is quasi-independent of the loading conditions. He therefore proposed simple formulae to calculate the yield curvature ϕ_y as functions of the yield strain of the steel reinforcement ε_y:

$$\phi_y = 2.25\frac{\varepsilon_y}{d} \quad \text{for circular columns} \tag{16.41}$$

$$\phi_y = 2.10\frac{\varepsilon_y}{a} \quad \text{for rectangular columns} \tag{16.42}$$

where a is the width of the rectangular column in the direction considered.

For a column subjected to horizontal forces, the plastic deformation is usually concentrated in one region, the plastic hinge region, with a length l_p, whereas the rest of the column remains elastic. The plastic hinge rotation θ_p can be calculated as a function of the plastic curvature ϕ_p:

$$\theta_p = \phi_p l_p = (\phi_u - \phi_y) l_p \tag{16.43}$$

where ϕ_y and ϕ_u are the yield curvature and the ultimate curvature, respectively. This assumes that the variation of plastic curvature in the plastic hinge region is rather small. The ultimate curvature can be determined from the ultimate compressive strain of confined concrete using section analysis:

$$\phi_u = \frac{\varepsilon_{ccu}}{c_u} \tag{16.44}$$

where c_u is the depth of the neutral axis. From the plastic hinge rotation θ_p, the plastic lateral displacement Δ_p at the top of the column can be determined assuming that the plastic hinge is concentrated at a height $l_p/2$ from the base:

$$\Delta_p = \Delta_u - \Delta_y = \theta_p\left(l_v - \frac{l_p}{2}\right) = (\phi_u - \phi_y) l_p\left(l_v - \frac{l_p}{2}\right) \tag{16.45}$$

Thus, a relationship between displacement ductility μ_Δ and the curvature ductility μ_ϕ is obtained:

$$\mu_\phi = \frac{\phi_u}{\phi_y} = \frac{(\mu_\Delta - 1)}{3(l_p/l_v)(1 - 0.5(l_p/l_v))} + 1 \tag{16.46}$$

In order to use Equation 16.46, the plastic hinge length l_p needs to be determined. Paulay and Priestley (1992) suggested the following equation to estimate l_p for a column confined with internal transverse steel reinforcement:

$$l_p = 0.08l_v + 0.022 f_y d_l \geq 0.044 f_y d_l \tag{16.47}$$

where

f_y is the yield strength of the internal longitudinal steel reinforcement (in MPa)
d_l is the diameter of the longitudinal steel reinforcing bar

Bank (2006) suggested to use the lower limit to calculate the plastic hinge length for columns confined with FRP wraps:

$$l_p = 0.044 f_y d_l \tag{16.48}$$

By considering Equations 16.44 and 16.46, it now becomes evident why an increase in the ultimate axial compressive strain is so important for seismic loading: Increasing the ultimate axial compressive strain ε_{ccu}, by confining the column with FRP, increases the plastic hinge rotation θ_p and hence the displacement ductility μ_Δ of the column. It should be noted that the increase in displacement capacity is realized only if a premature shear failure of the column as well as lap-splice failure is prevented (Seible et al., 1997). In general, confining FRP wraps also act to increase the shear capacity and prevent lap-splice failure. The effect on lap-splices is discussed in the next section. For more information on shear strengthening, see Chapter 15 of this book.

LAP-SPLICES

Lap-splices of longitudinal column reinforcement in existing structures are often arranged at the base of the columns due to ease of execution. The lack of adequate seismic design codes has not inhibited this type of arrangement. However, inelastic deformations occur predominantly at the base of the columns. This leads to lap-splice failure. As a consequence, flexural strength and energy absorption degrade rapidly. Lap-splice failure can be prevented by an appropriate confinement (Figure 16.11).

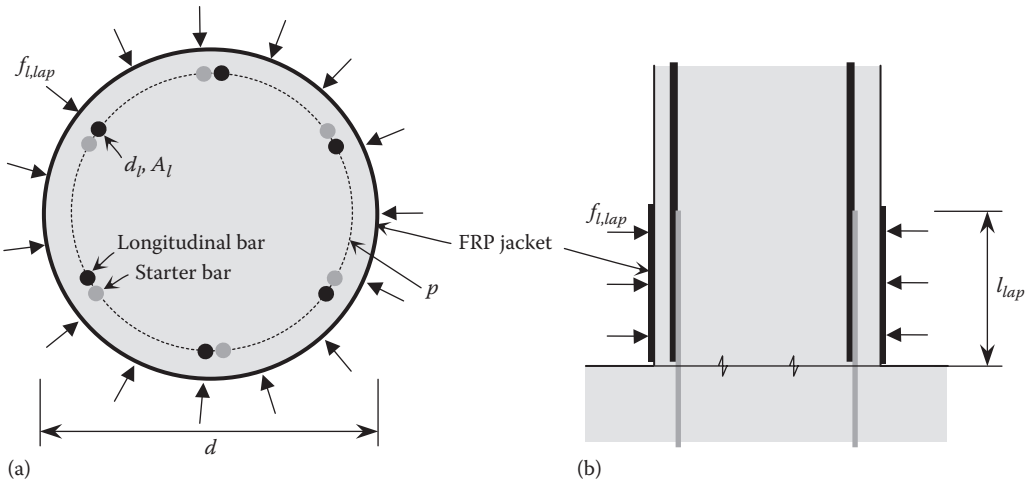

FIGURE 16.11 (a) Column cross section and (b) elevation in the lap-splice region.

Experiments on lap-spliced columns indicate that a critical radial dilatation strain of about 0.001 exists (Priestley and Seible, 1995). Therefore, the strain of the FRP jacket due to the dilatation of the lap-splices needs to be limited to a maximum value of 0.001. Thus, from Equation 16.1,

$$\varepsilon_{f,lap} = 0.001 = \frac{df_{l,lap}}{2E_f t_{f,lap}} \tag{16.49}$$

Rearranging Equation 16.49 and ignoring the confining pressure due to existing spirals or ties, the required jacket thickness $t_{f,lap}$ for circular columns becomes

$$t_{f,lap} = 500\frac{df_{l,lap}}{E_f} \tag{16.50}$$

To calculate the required lateral confining pressure $f_{l,lap}$ to be provided by the jacket, Seible et al. (1997) suggest the following equation:

$$f_{l,lap} = \frac{A_l f_y}{\left[p/(2n) + 2(d_l + c)\right] l_{lap}} \tag{16.51}$$

where

c is the thickness of the concrete cover
n the number of longitudinal bars
p the circumference at the level of longitudinal bars (see Figure 16.11)
A_l the area of a single longitudinal bar
f_y and d_l yield strength and diameter of longitudinal bars
l_{lap} the length of the lap-splice

In general, the ultimate tensile strains of FRP confinement materials are larger than the critical strain for lap-splice failure $\varepsilon_{f,lap}$ and therefore not determinant for the dimensioning.

Equation 16.50 was developed for circular columns. Where rectangular columns containing lap-splices are to be retrofitted, oval bolsters are generally added to the region to be wrapped in order to develop a confining pressure that also reaches the lap-splices at the side faces of the column. Without such bolsters, lap-splice failure may be prevented only for the corner bars.

WORKED EXAMPLE

This example demonstrates the design of an FRP confinement for a square column for a seismic retrofit. Consider the building in Figure 16.12 with only columns at the ground floor. The columns have a square section of 400 mm × 400 mm and a height of 2.5 m. The vertical loads acting on each column due to life and dead loads are 1000 kN each. The transverse reinforcement of the column has a very wide spacing of s = 240 mm and hence the rotational ductility of the column is rather limited. The material properties are given in Table 16.1. The task is to confine the columns using CFRP wraps for a displacement ductility of $\mu_\Delta = 4$.

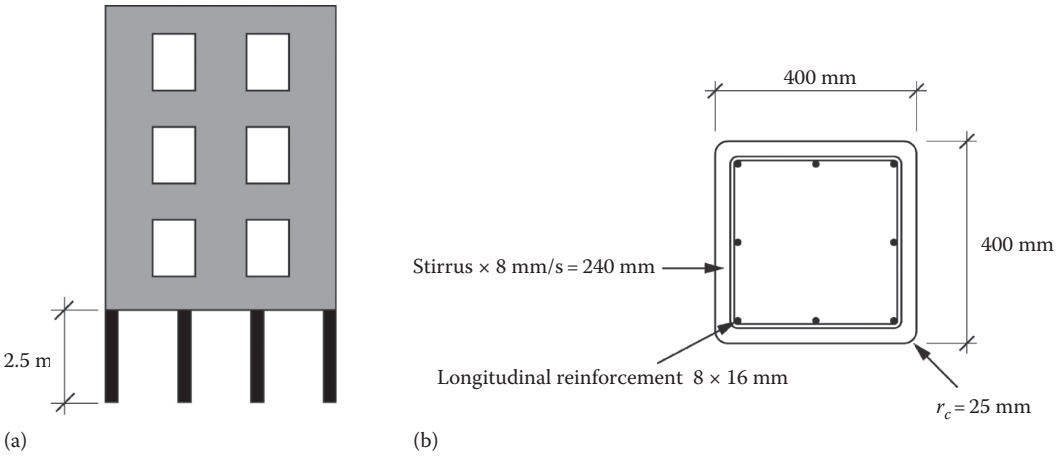

FIGURE 16.12 Example of a square reinforced concrete column to be retrofitted with FRP wraps: (a) example of columns at ground floor and (b) section and reinforcement of example column.

TABLE 16.1
Material Properties

Concrete properties	Compressive strength f'_{c0}	20 MPa
	Axial strain at f'_{c0}, ε_{c0}	0.002
Reinforcing steel properties	Yield strength f_y	450 MPa
	Yield strain ε_y	0.0022
Properties of CFRP wrap	Elastic modulus E_f	140 GPa
	Tensile strength f_f	1870 MPa
	Thickness of one layer $t_{f,1}$	0.125 mm
	Ratio $\varepsilon_{f,rup}/\varepsilon_{fu}$	0.7

From the required displacement ductility, the first step is to calculate the required curvature ductility. To do this, the plastic hinge length has to be calculated using Equation 16.48:

$$l_p = 0.044 f_y d_l = 0.044(500)(16) = 352 \text{ mm}.$$

It can be assumed that the columns at the ground floor have fixed ends at top and bottom and hence the shear span l_v = 1.25 m from Figure 16.12. The required curvature ductility can then be determined using Equation 16.46:

$$\mu_\phi = \frac{(\mu_\Delta - 1)}{3(l_p/l_v)(1 - 0.5(l_p/l_v))} + 1 = \frac{(4-1)}{3(0.352/1.25)(1 - 0.5(0.352/1.25))} + 1 = 5.13$$

Using Equation 16.42, the yield curvature of the section is

$$\phi_y = 2.10 \frac{\varepsilon_y}{a} = 2.10 \frac{0.0022}{0.4} = 0.012 \text{ m}^{-1}$$

And hence the required ultimate curvature

$$\phi_u = \mu_\phi \phi_y = 5.13(0.012) = 0.06 \text{ m}^{-1}$$

From section analysis, it can be found that the depth of the neutral axis at ultimate conditions of the unconfined column c_u = 162 mm, taking into account the acting normal force of 1000 kN. In the following, it is assumed that the value remains the same for the confined column, and therefore from Equation 16.44, the required ultimate strain of the column becomes

$$\varepsilon_{ccu} = \phi_u c_u = 0.06(0.162) = 0.01$$

Having found the required ultimate strain of the column, the number of layers required to ensure the rotational capacity can be determined. This can be done using, for example, the equations proposed by Lam and Teng (2003a,b) and solving for the actual required confining stress $f_{l,a}$.

From Equation 16.22,

$$A_g = bh - (4-\pi) r_c^2 = 400^2 - (4-\pi)25^2 = 159{,}463 \text{ mm}^2$$

$$\rho_{sc} = \frac{8(201)}{159{,}463} = 0.01$$

Using Equation 16.29,

$$\frac{A_e}{A_c} = \frac{1-\rho_{sc} - 2(b-2r_c)^2/3A_g}{1-\rho_{sc}} = \frac{1-0.01-2(400-2\times25)^2/3(159{,}463)}{1-0.01} = 0.48$$

And from Equations 16.28 and 16.32,

$$k_{s2} = k_{s1} = \frac{A_e}{A_c} = 0.48$$

$$\varepsilon_{f,rup} = 0.7\varepsilon_{fu} = 0.7\frac{f_f}{E_f} = 0.7\frac{1{,}870}{140{,}000} = 0.0093$$

Finally, using Equation 16.8 and solving for $f_{l,a}$,

$$f_{l,a} = \left(\frac{\varepsilon_{ccu}}{\varepsilon_{c0}} - 1.75\right)\frac{f'_{c0}}{12k_{s2}}\left(\frac{\varepsilon_{c0}}{\varepsilon_{f,rup}}\right)^{0.45} = \left(\frac{0.01}{0.002} - 1.75\right)\frac{20}{12(0.48)}\left(\frac{0.002}{0.0093}\right)^{0.45} = 5.6 \text{ MPa}$$

From Equation 16.31, the required thickness of the FRP confinement can be determined:

$$t_f = \frac{\sqrt{2}bf_{l,a}}{2E_f\varepsilon_{f,rup}} = \frac{\sqrt{2}(400)(5)(6)}{2(140{,}000)(0.0093)} = 1.22 \text{ mm}.$$

With a thickness of 1 layer of 0.125 mm, 10 layers of CFRP wrap are needed to secure a displacement ductility of the column of $\mu_\Delta = 4$.

The axial strength enhancement of the column can be calculated using Equation 16.3 since

$$k_{s1}\frac{f_{l,a}}{f'_{c0}} = 0.48\frac{5.6}{20} = 0.13 \geq 0.07$$

$$\frac{f'_{cc}}{f'_{c0}} = 1 + 3.3k_{s1}\frac{f_{l,a}}{f'_{c0}} = 1 + 3.3(0.48)\frac{5.6}{20} = 1.44$$

Note that the shape factor k_{s1} is added in the equation since it is not yet included in $f_{l,a}$.

And, therefore,

$$f'_{cc} = 1.44f'_{c0} = 28.9 \text{ MPa}$$

For the design of the CFRP confinement, the earlier calculated parameters are enough. The complete stress–strain relationship is usually not required. However, our readers should note that Figure 16.13 shows the stress–strain relationships for the unconfined and the confined example column using the earlier presented models of Lam and Teng (2003b) and Spoelstra and Monti (1999).

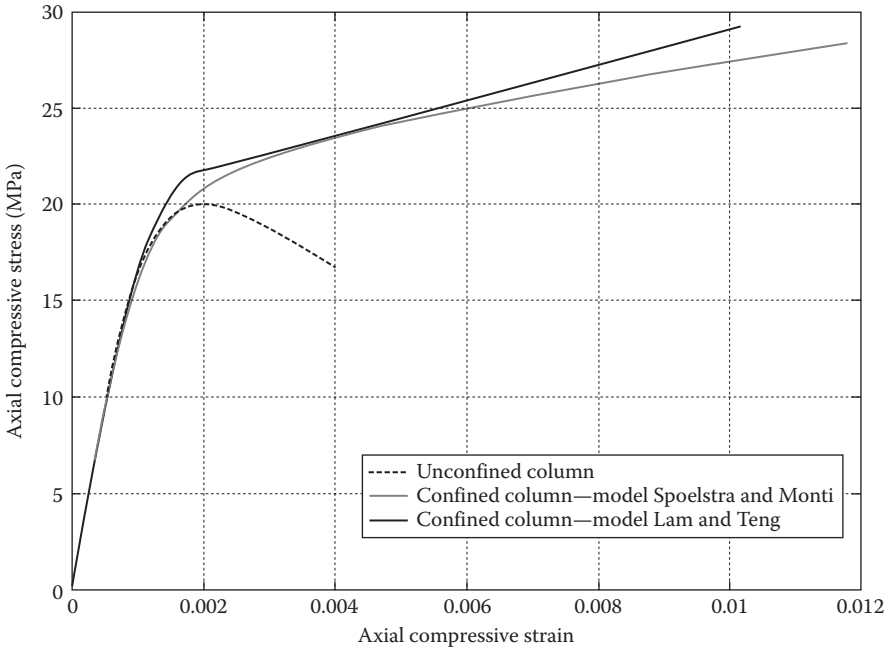

FIGURE 16.13 Stress–strain relationships for unconfined and confined example columns.

Notations

Latin Letters

A_c concrete area of column section
A_e effectively confined area of column section
A_g gross area of column section
A_l area of one longitudinal reinforcing bar
$A_{s,l}$ total area of longitudinal reinforcing bars
a dimension of the rectangular column in the direction considered
b short side of rectangular cross section, minor axis of elliptical cross section
c thickness of the concrete cover
c_u depth of neutral axis
d diameter of column
d_l diameter of longitudinal steel reinforcing bar
E_c elastic modulus of concrete
E_2 slope of linear second portion of Lam and Teng model
E_f modulus of elasticity of FRP confinement
f_0 stress at intercept between parabolic first portion and straight-line second portion of Lam and Teng model
f'_{c0} compressive strength of unconfined concrete
f'_{cc} compressive strength of confined concrete
f_f tensile strength of FRP confinement
f_l theoretical maximum confining stress
$f_{l,a}$ actual maximum confining stress
$f_{l,lap}$ required confining stress to prevent lap-splice failure
f_y yield strength of steel reinforcement
h long side of rectangular column, major axis of elliptical cross section
I_e effective moment of inertia of cracked section
k_1 effectiveness coefficient
k_2 strain enhancement coefficient
k_e effectiveness factor
k_p factor for partial wrapping
k_s shape factor for rectangular or elliptical cross sections
k_{s1} shape factor for rectangular cross sections for the compressive strength
k_{s2} shape factor for rectangular cross sections for the ultimate strain
l_{lap} lap-splice length
l_p plastic hinge length
l_v shear span
M_y yield moment
n number of longitudinal reinforcing bars
p circumference at the level of longitudinal bars
r_c corner radius
s spacing between the hoops
s' clear spacing between the hoops
t_f thickness of FRP confinement
$t_{f,lap}$ required jacket thickness for lap-splices
V horizontal force

Greek Letters

β constant depending on the property of concrete
Δ_p plastic displacement

Δ_u total displacement
Δ_y yield displacement
ε_c axial compressive strain of concrete
ε_{c0} axial compressive strain at the compressive strength of unconfined concrete
ε_{cu} ultimate axial compressive strain of unconfined concrete
ε_{cc} axial compressive strain at the compressive strength of confined concrete
ε_{ccu} ultimate axial compressive strain of confined concrete
ε_f strain of FRP confinement
$\varepsilon_{f,lap}$ maximum radial dilatation strain for lap-splices
ε_{fu} ultimate tensile strain of FRP material
$\varepsilon_{f,rup}$ actual rupture strain of FRP confinement
ε_l lateral strain
ε_t strain at intercept between parabolic first portion and straight-line second portion of Lam and Teng model
μ_Δ displacement ductility
μ_ε strain ductility
μ_ϕ curvature ductility
ρ_f volumetric ratio of FRP confinement, also called confinement ratio
ρ_{sc} cross-sectional area ratio of longitudinal steel reinforcement
σ_b average confining stress at middle section acting along the short side
σ_c compressive stress of concrete
σ_f tensile stress of FRP confinement
σ_h average confining stress at middle section acting along the long side
σ_l lateral confining stress
θ_p plastic hinge rotation
ϕ_p plastic curvature
ϕ_u ultimate curvature
ϕ_y yield curvature

REFERENCES

ACI (2008), Guide for the design and construction of externally bonded FRP systems for strengthening concrete structures, ACI 440.2R-08, American Concrete Institute, Farmington Hills, MI.

Bank L.C. (2006), *Composites for Construction—Structural Design with FRP Materials*, John Wiley & Sons, Inc., Hoboken, NJ.

CNR-DT 200 (2004), Guide for the design and construction of externally bonded FRP systems for strengthening existing structures—Materials RC and PC structures, masonry structures, National Research Council, Advisory committee on technical recommendations for construction, Rome, Italy.

fib (2001), Externally bonded FRP reinforcement for RC structures, International Federation for Structural Concrete, Bulletin 14, Lausanne, Switzerland.

Gosh K.K., Sheikh S.A. (2007), Seismic upgrade with carbon fiber-reinforced polymer of columns containing lap-spliced reinforcing bars, *ACI Structural Journal*, 104(2), 227–236.

Hollaway L.C., Teng J.G. (eds.) (2008), *Strengthening and Rehabilitation of Civil Infrastructures Using Fibre-Reinforced Polymer (FRP) Composites*, Woodhead Publishing Limited, Cambridge, U.K.

ISIS (2001), Strengthening reinforced concrete structures with externally-bonded fibre reinforced polymers, Design manual no. 4, ISIS, Winnipeg, Manitoba, Canada.

Karam G., Tabbara M. (2005), Confinement effectiveness in rectangular concrete columns with fiber reinforced polymer wraps, *ASCE Journal of Composites for Construction*, 9(5), 388–396.

Lam L., Teng J.G. (2002), Strength models for FRP-confined concrete, *ASCE Journal of Structural Engineering*, 128(5), 612–623.

Lam L., Teng J.G. (2003a), Design-oriented stress-strain model for FRP-confined concrete, *Construction and Building Material*, 17, 471–489.

Lam L., Teng J.G. (2003b), Design-oriented stress-strain model for FRP-confined concrete in rectangular columns, *Journal of Reinforced Plastics and Composites*, 22(13), 1149–1186.

Mander J.B., Priestley M.J.N., Park R. (1988), Theoretical stress–strain model for confined concrete, *ASCE Journal of Structural Engineering*, 114(8), 1804–1826.

Matthys S., Toutanji G., Audenaert K., Taerwe L. (2005), Axial load behaviour of large-scale columns confined with fibre-reinforced polymer composites, *ACI Structural Journal*, 102(2), 258–267.

Mirmiran A., Shahawy M. (1997), Behaviour of concrete columns confined by fibre composites, *ASCE Journal of Structural Engineering*, 123(5), 583–590.

Pantazopoulou S.J., Mills R.H. (1995), Microstructural aspects of the mechanical response of plain concrete, *ACI Material Journal*, 92 (November–December), 605–616.

Paulay T., Priestley M.J.N. (1992), *Seismic Design of Reinforced Concrete and Masonry Buildings*, John Wiley & Sons, Inc., New York.

Popovics S. (1973), Numerical approach to the complete stress–strain relation for concrete, *Cement and Concrete Research*, 3(5), 583–599.

Priestley M.J.N. (2003), *Myths and Fallacies in Earthquake Engineering*, Revisited, IUSS Press, Pavia, Italy.

Priestley M.J.N., Seible F. (1995), Design of seismic retrofit measures for concrete and masonry structures, *Construction and Building Materials*, 9(6), 365–377.

Priestley M.J.N., Seible F., Calvi G.M. (1996), *Seismic Design and Retrofit of Bridges*, John Wiley & Sons, Inc., New York.

Richart F.E., Brandtzaeg A., Brown R.L. (1928), A study of the failure of concrete under combined compressive stresses, University of Illinois, Engineering Experimental Station, Urbana, IL.

Richart F.E., Brandtzaeg A., Brown R.L. (1929), The failure of plain and spirally reinforced concrete in compression, University of Illinois, Engineering Experimental Station, Urbana, IL.

Rochette P., Labossière P. (2000), Axial testing of rectangular column models confined with composites, *ASCE Journal of Composites for Construction*, 4(3), 129–136.

Seible F., Burgueno R., Abdallah M.G., Nuismer R. (1995), Advanced composite carbon shell systems for bridge columns under seismic loads, Progress in research and practice. In *Proceedings of National Seismic Conference on Bridges and Highways*, San Diego, CA.

Seible F., Priestley M.J.N., Hegemeier G.A., Innamorato D. (1997), Seismic retrofit of RC columns with continuous carbon fiber jackets, *ASCE Journal of Composites for Construction*, 1(2), 52–62.

Spoelstra M.R., Monti G. (1999), FRP-confined concrete model, *ASCE Journal of Composites for Construction*, 3(3), 143–150.

Teng J.G., Chen J.F., Smith S.T., Lam L. (2002), *FRP Strengthened RC Structures*, John Wiley & Sons, Ltd., Chichester, U.K.

Teng J.G., Lam L. (2004), Behaviour and modeling of fibre reinforced polymer-confined concrete, *ASCE Journal of Structural Engineering*, 130(11), 1713–1723.

17 Strengthening of Masonry and Metallic Structures

Kerstin Lang and Ann Schumacher

CONTENTS

MASONRY STRUCTURES

Introduction

Masonry is one of the oldest building materials in the world. A large number of buildings around the world are made from unreinforced masonry, among which there are many historical monuments of great cultural value. Due to differences in the origin, no single uniform unreinforced masonry type exists, but a plenitude of different types. These can be differentiated by different types of units: clay brick, sandstone, natural stone or concrete, and different types of mortar: lime or cement, and different types of assemblages. Thus, when speaking about masonry, we speak in fact about very different materials, and statements are very difficult to generalize. However, for design purposes, it is common practice to simplify the material to an orthotropic material.

Unreinforced masonry is characterized by a very low tensile strength in comparison to its compressive strength, which makes it susceptible to horizontal forces such as those induced by an earthquake. Since many existing masonry buildings were designed and constructed without any considerations of horizontal forces, they show an insufficient resistance against horizontal forces, and strengthening is required. Traditional strengthening techniques such as steel plates and reinforced concrete overlays, or even additional reinforced concrete elements, have a high impact on the behavior of the building structure due to their weight and stiffness. They are usually also rather obtrusive and therefore not well suited for historical buildings.

In the last 10–15 years, the use of fiber-reinforced polymer (FRP) to strengthen masonry structures has become increasingly popular. The advantages of using FRP to strengthen the structures in comparison to traditional strengthening techniques are its low weight so that the dynamic response of the structure remains unchanged, minimal impact (FRP laminates are rather unobtrusive), and its insusceptibility to corrosion. However, the disadvantages of using FRP at the moment are the lack of appropriate design procedures and an insufficient knowledge of the materials' long-term durability (Hollaway and Teng, 2008). The only design guidelines available for the strengthening of masonry are the Italian guideline CNR-DT 200 (2004) and a draft of the ACI committee 440 (2004).

In general, FRP strengthening is applied to provide tensile strength to the masonry structure. Various different FRP strengthening techniques for unreinforced masonry exist. These can be roughly divided into two categories:

1. *Externally bonded FRP laminates*: This technique uses either FRP sheets using a wet lay-up technique or pre-cured FRP laminates bonded onto the masonry surface with an adhesive. The orientation of the laminates can be horizontal, vertical, diagonal, or in a grid pattern; they can be applied on one side or on both sides.
2. *Near-surface-mounted reinforcement* (*NSR*): This technique uses FRP strips that are bonded with adhesives into grooves or slots cut to a shallow depth in the masonry surface. The effects are similar to externally bonded FRP.

Unbonded FRP is seldom used to strengthen masonry, and in these rare cases, it is primarily used to ensure the integrity of a building (Triantafillou and Fardis, 1997).

FRP strengthening can have various objectives. It can be applied to improve the in-plane behavior of walls, that is, to increase the load-carrying and deformation capacity of the wall. It can be applied to improve the out-of-plane behavior of walls by improving the links to the orthogonal walls, thus increasing the bending moment capacity. It can be used to confine masonry columns or to strengthen arches and vaults. Finally, it can be used to improve the integrity of the whole structure.

In the following, an introduction to the strengthening of unreinforced masonry walls using externally bonded FRP sheets and laminates to improve the in-plane and out-of-plane behavior is given. The methods of analysis presented follow the Italian guideline CNR-DT 200 (2004). For more background information on the methods of analysis, the reader is referred to the chapter on strengthening of masonry structures by De Lorenzis in Hollaway and Teng (2008).

However, no consideration is given here to the NSR technique, strengthening of arches and vaults, and confinement of masonry columns. For more information on these strengthening types, the reader is again referred to the corresponding chapter in Hollaway and Teng (2008).

General

Independent of the objective of the strengthening, whether FRP is applied to improve the in-plane or the out-of-plane behavior, the following failure mechanisms of FRP-strengthened masonry are encountered (Hollaway and Teng, 2008):

1. *Masonry compression failure*: This failure mode usually occurs for high FRP reinforcement ratios and high-strength materials such as carbon FRP (CFRP). It is desirable as it shows a rather "ductile" behavior (Triantafillou, 1998), similar to concrete compression failure for concrete strengthened with FRP.
2. *Rupture of FRP laminates in tension*: This usually occurs with a low FRP reinforcement ratio and low strength materials such as GFRP. Similar to FRP tensile failure for concrete strengthened with FRP, the resulting failure mechanism is less "ductile" than masonry compression failure but still shows some deformation capacity and is therefore acceptable (Triantafillou, 1998).

3. *Masonry shear failure*: This failure mode is characterized by 45° cracks (flexural shear) or cracks along bed joints (sliding shear). It usually occurs for low FRP reinforcement ratios. Flexural shear is very brittle and should therefore be circumvented with an appropriate design.
4. *Bond failure*: This failure mode usually occurs for an intermediate FRP reinforcement ratio and is therefore the most common failure type. As in the case of reinforced concrete structures, debonding usually starts at the location of stress concentrations at cracks, or at the end of the laminates.

Bond Behavior

Bond behavior means the behavior at the interface of the FRP system and the masonry surface. This behavior is of great importance because it greatly influences the overall behavior of the FRP-strengthened masonry wall. Similar to concrete structures, bond failure is usually brittle and therefore undesirable. Any design should therefore aim for a bond strength greater than that at concrete compression failure or at rupture of FRP laminates in tension. The main principle of bond behavior of FRP on masonry is similar to the bond behavior of FRP on concrete surfaces, even though the actual problem is more complicated due to the fact that the FRP is bonded onto a nonuniform surface made of units and mortar joints. In addition, masonry exists in many different forms (natural stone masonry, clay brick masonry, concrete block masonry, etc.), which makes any generalization difficult. However, the following principles are still valid (Hollaway and Teng, 2008):

- The maximum tensile force that can be transmitted increases with increasing bond length.
- Debonding normally occurs in the masonry since the tensile strength of the adhesive is larger than the tensile strength of masonry.
- Two debonding mechanisms exist: debonding at the end of the laminate or debonding at a crack and/or mortar joint due to high shear and normal stresses at these locations.

In practice, design against debonding is done in a simplified manner, similar to that proposed for concrete structures. Two approaches exist: (1) calculation of minimum required bond length and the corresponding debonding force and (2) introduction of a bond reduction factor k_b.

The first approach is adopted by the Italian guideline CNR-DT 200 (2004). To calculate the maximum force that can be anchored, a procedure similar to the model developed by Holzenkämpfer (1994) and modified by Neubauer and Rostasy (1997) for concrete structures is proposed. According to this procedure, the maximum bond strength $f_{b,\max}$ can be calculated from the fracture energy G_f:

$$f_{b,\max} = \sqrt{\frac{2E_{frp}G_f}{t_{frp}}} \tag{17.1}$$

where

E_{frp} and t_{frp} are the modulus of elasticity and the thickness of FRP laminates, respectively
G_f is the fracture energy that can be determined as follows:

$$G_f = c_1\sqrt{f_{mx}f_{mt}} \tag{17.2}$$

where

f_{mx} is the compressive strength of masonry orthogonal to the mortar bed joint
f_{mt} is the tensile strength of masonry orthogonal to the mortar bed joint

Reasonable results can be obtained assuming that $f_{mt} = 0.10 f_{mx}$. c_1 is an experimentally determined coefficient and can be assumed to be equal to 0.015 in the absence of appropriate test results. On the basis of recent studies, Nardone et al. (2008) proposed values of 0.045 for FRP strips applied on natural stone masonry and 0.03 for FRP strips applied on clay brick masonry.

For the maximum bond strength to be realized, the optimal bond length l_e has to be guaranteed:

$$l_e = \sqrt{\frac{E_{frp} t_{frp}}{2 f_{mt}}} \tag{17.3}$$

For a bond length $l_b < l_e$, the effective bond strength f_b can be determined as follows:

$$f_b = f_{b,\max} \frac{l_b}{l_e}\left(2 - \frac{l_b}{l_e}\right) \tag{17.4}$$

The effective strength of the FRP laminate $f_{frp,e}$ is given by the minimum of the tensile strength of the FRP laminate $f_{frp,u}$ and the bond strength f_b:

$$f_{frp,e} = \min(f_b, f_{frp,u}) \tag{17.5}$$

It should be noted that all the equations are given with characteristic values of the material properties. For the design, appropriate partial factors for the material and the model need to be introduced depending on the respective design guideline.

The second approach to design against debonding introduces an empirical bond reduction factor k_b to limit the stress and strain in the FRP laminate:

$$f_{frp,e} = k_b f_{frp,u} \tag{17.6}$$

$$\varepsilon_{frp,e} = k_b \varepsilon_{frp,u} \tag{17.7}$$

where

$f_{frp,e}$ and $\varepsilon_{frp,e}$ are the effective useable FRP strength and strain
$f_{frp,u}$ and $\varepsilon_{frp,u}$ are the tensile strength and ultimate tensile strain of the FRP laminate, respectively

For a minimum anchor length of 300 mm, Garbin et al. (2007) proposed values for k_b between 0.45 and 0.65 for externally bonded FRP laminates based on a limited number of test results. It is in fact the main disadvantage of this approach that till today there are not enough data available to clearly determine k_b.

Strengthening for In-Plane Behavior

Experimental results have shown that unreinforced masonry walls strengthened with FRP laminates show an increased load-carrying and deformation capacity as well as a more uniform crack distribution (Schwegler, 1995; Elgawady, 2004; Moon et al., 2007).

One of the first works on FRP-strengthened masonry walls was carried out by Schwegler (1995). With the aid of full-scale tests on 3.6 m × 2.0 m masonry walls, two strengthening techniques with FRP were investigated. The first technique employed CFRP laminates bonded diagonally onto the masonry walls and anchored to the adjoining upper and lower concrete slabs. The second technique used woven polyester fabrics applied over the entire wall surface. In contrast to the CFRP laminates,

these fabrics were not anchored onto the concrete slabs. The strengthened walls were tested cyclic-statically, and the results compared with an unstrengthened reference wall. The tests showed an increase in load-carrying capacity of a factor 4 for the walls strengthened with CFRP laminates and a factor 1.5 for the walls strengthened with the woven fabrics. The deformation capacity was more than doubled in the case of the CFRP laminates. Schwegler (1995) also showed that stress fields in combination with appropriate failure conditions are well suited to estimate the load-carrying capacity of the walls strengthened with FRP.

In the meantime, more research work has been done on the in-plane behavior of masonry walls strengthened with various types of FRP, for example, Triantafillou (1998), Zhao et al. (2003), Elgawady (2004), and Marcari et al. (2007) to mention a few, allowing the establishment of simple design procedures.

Generally, two in-plane mechanisms are distinguished for masonry walls. The first mechanism is dominated by a flexural behavior under the combined action of bending and compression, and the second mechanism is dominated by shear. In the first case where the behavior is dominated by flexure, strengthening techniques usually comprise of vertically oriented FRP laminates located in the tension regions. The design procedure in the Italian guidelines CNR-DT 200 (2004) is analogous to that for reinforced concrete assuming that sections remain plane with a linear strain distribution.

Considering the masonry wall strengthened with FRP in Figure 17.1, the equilibrium and compatibility equations can be written as follows:

$$N = \alpha c_u t_w \beta f_{mx} - A_{frp,b} \varepsilon_{frp} E_{frp} \tag{17.8}$$

$$M = \alpha c_u t_w \beta f_{mx} \left(\frac{l_w}{2} - \frac{\alpha c_u}{2} \right) + A_{frp,b} \varepsilon_{frp} E_{frp} \left(d - \frac{l_w}{2} \right) \tag{17.9}$$

$$\frac{\varepsilon_m}{\varepsilon_{frp}} = \frac{c_u}{d - c_u} \tag{17.10}$$

where

c_u is the depth of the neutral axis
f_{mx} is the compressive strength of masonry orthogonal to the mortar bed
$A_{frp,b}$, ε_{frp}, and E_{frp} are the area, the strain, and the modulus of elasticity of the FRP laminates in the tension zone, respectively
ε_m is the compressive strain of the most compressed fiber of the masonry section
t_w and l_w are the thickness and the length of the masonry wall, respectively
d is the distance between the most compressed fiber of the masonry section and the centroid of the vertical FRP laminates
α and β are two coefficients that describe the equivalent stress block
M and N are the applied bending moment and axial load, respectively

Failure takes place either due to the failure of the FRP laminates, or by concrete crushing, depending on whether the tensile strain in the FRP laminates ε_{frp} first reaches the effective useable FRP strain $\varepsilon_{frp,e}$ or the compressive strain in the masonry ε_m first reaches the ultimate compressive strain of masonry ε_{mu}. The FRP reinforcement ratio at which the effective useable FRP strain in the laminate $\varepsilon_{frp,e}$ is reached at the same time as the ultimate compressive strain of masonry ε_{mu} is often referred to as a balanced FRP reinforcement ratio ρ_b. In the case of the FRP-strengthened wall in Figure 17.1, the FRP reinforcement ratio ρ_{frp} is defined as follows:

$$\rho_{frp} = \frac{A_{frp,b}}{dt_w} = \frac{2b_{frp}t_{frp}}{dt_w} \tag{17.11}$$

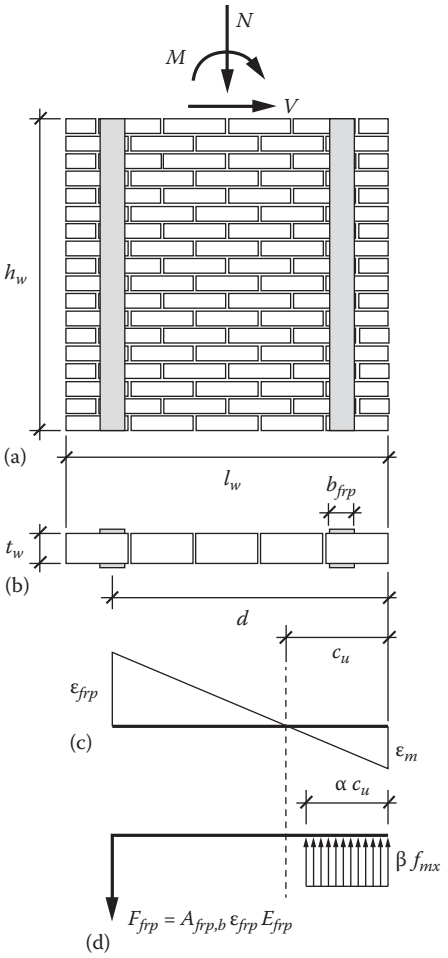

FIGURE 17.1 Masonry wall under combined in-plane bending and compression: (a) wall with forces, (b) wall section, (c) internal stress distribution, and (d) internal strain distribution.

where b_{frp} and t_{frp} are the width and the thickness of the FRP laminates. For a balanced FRP reinforcement ratio ρ_b, the strain distribution in the wall section is defined and the position of the neutral axis c_u therefore known:

$$c_u = \frac{\varepsilon_{mu}}{\varepsilon_{mu} + \varepsilon_{frp,e}} d \tag{17.12}$$

Considering Equations 17.8 and 17.12, the balanced FRP reinforcement ratio ρ_b is then given by

$$\rho_b = \frac{f_{mx}}{f_{frp,e}} \left(\alpha\beta \frac{\varepsilon_{mu}}{\varepsilon_{mu} + \varepsilon_{frp,e}} - \frac{N}{d t_w f_{mx}} \right) \tag{17.13}$$

When $\rho_{frp} > \rho_b$, failure takes place by concrete crushing. In this case, the stress distribution in the compression zone is given by an equivalent stress block with a uniform compressive strength of βf_{mx} distributed over an equivalent compression zone with a length equal to αc_u. The value for α normally lies between 0.6 and 0.8 and the value for β between 0.8 and 0.9. In order to inhibit bond failure, the effective useable FRP strain is used (cf. section provided earlier). The bending moment resistance of the wall section strengthened with FRP can be found based on Equations 17.8 through 17.10.

When $\rho_{frp} < \rho_b$, failure takes place by the rupture of FRP laminates in tension or debonding. In this case, the stress distribution in the compressive zone does not correspond to ultimate conditions, and hence the coefficients α and β have to be derived for the appropriate stress distribution first. This is usually an iterative procedure.

If it is the case that the in-plane behavior is dominated by shear, possible strengthening laminate patterns are vertical, horizontal, and/or diagonal. The appropriate pattern and design of FRP laminates can be found using stress fields as proposed by Schwegler (1995), where the FRP laminates take the tensile forces and the masonry the compressive forces. This is in fact the most general model that takes into account all possible failure mechanisms. The Italian guideline CNR-DT 200 (2004) proposes a simplified method to design FRP strengthening for shear based on a truss analogy. The shear capacity V_R of a masonry wall strengthened with FRP can be found from the sum of the masonry contribution $V_{R,m}$ and FRP contribution $V_{R,frp}$:

$$V_R = V_{R,m} + V_{R,frp} \tag{17.14}$$

The contribution of masonry $V_{R,m}$ to the shear capacity can be calculated as follows:

$$V_{R,m} = dt_w f_{mv} \tag{17.15}$$

where

d is the distance between the most compressed fiber of the masonry section and the centroid of the vertical FRP laminates

t_w is the thickness of the masonry wall

f_{mv} is the shear strength of masonry and can be determined according to Eurocode 6 (2005):

$$f_{mv} = f_{mv0} + 0.4\sigma_n \tag{17.16}$$

where

σ_n is the acting normal stress

f_{mv0} is the characteristic shear strength of masonry in the absence of normal stresses

The contribution of FRP $V_{R,frp}$ to the shear capacity can be calculated by considering a 45° truss analogy:

$$V_{R,frp} = 0.6\frac{dA_{frp,s}f_{frp,e}}{s} \tag{17.17}$$

where

$A_{frp,s}$ is the area of FRP laminates parallel to the direction of the shear force

s is the center-to-center spacing of the FRP laminates

The 45° truss analogy assumes that the FRP laminates are applied parallel to the mortar bed joints for shear and orthogonal to the mortar bed joints for flexure. If no flexural reinforcement is needed, and FRP laminates are applied only for shear strengthening, they are often applied diagonally. The Italian guideline CNR-DT 200 (2004) does not give a formula for the determination of the contribution of FRP to the shear capacity for diagonal laminates. A possible formulation can be found in Nardone et al. (2008).

The upper limit for the shear capacity of the wall V_R is given by failure of the compression strut:

$$V_R \le 0.3dt_w f_{my} \tag{17.18}$$

where f_{my} is the compressive strength of masonry parallel to the mortar bed joint. In the absence of appropriate test results, a reasonable assumption is $f_{my} = 0.5f_{mx}$, f_{mx} being the compressive strength of masonry orthogonal to the mortar bed joint.

As a final remark on the strengthening for in-plane behavior, the reader should note that it is recommended to apply FRP strengthening on both sides of the wall for optimal results (Schwegler, 1995).

Strengthening for Out-of-Plane Behavior

The out-of-plane collapse mechanism is the predominant failure mechanism for unreinforced masonry buildings subjected to seismic loading. The reasons for this are insufficient connections between the wall excited orthogonal to its plane and the adjoining structural elements (floors, roofs, and walls). Depending on the boundary conditions, the following out-of-plane collapse mechanisms occur:

- Overturning
- Vertical and horizontal bending

Overturning of a wall panel is critical when the wall is not connected to orthogonal walls and not restrained at the top. Figure 17.2a shows a simple overturning collapse mechanism with a hinge at the bottom of the wall. This collapse mechanism can be prevented by applying horizontal FRP laminates at the top of the wall that are anchored to the orthogonal walls. The tensile force F_{frp} for which the FRP laminates and the anchorage need to be designed for can be obtained from simple equilibrium considerations:

$$F_{frp} = \frac{1}{2h_{frp}}(Qh_w - (N + G_w)t_w) \tag{17.19}$$

where

h_{frp} is the height of the applied FRP laminates
Q is the horizontal force due to seismic loading
h_w, t_w, and G_w are the height, thickness, and self-weight of the wall, respectively
N is the axial load acting on top of the wall

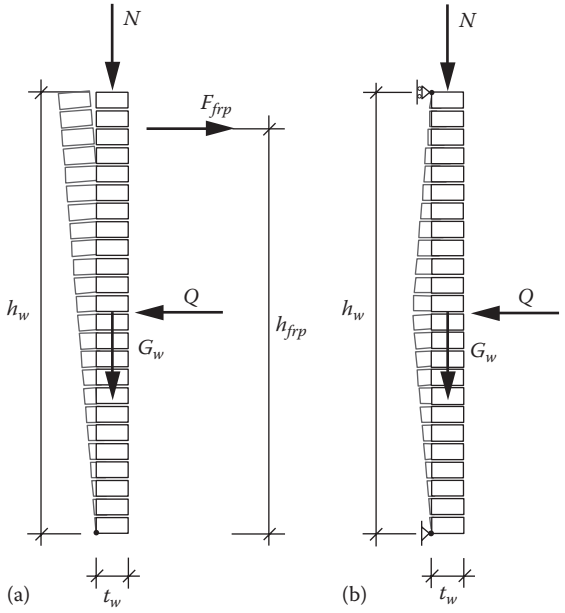

FIGURE 17.2 Out-of-plane collapse mechanisms (a) by simple overturning and (b) by vertical bending.

If the wall is restrained at the top, or the wall is well connected to orthogonal walls, collapse due to horizontal loading will take place by vertical or horizontal bending, respectively. This collapse mechanism can be prevented by applying FRP laminates on the tension side with the fibers aligned in the direction of the principal tensile stress (Hollaway and Teng, 2008). Similar to the flexural in-plane behavior, the design procedure is analogous to reinforced concrete where the compressive stresses are taken by the masonry and the tensile stresses by the FRP laminates. Again the Italian guideline CNR-DT 200 (2004) proposes a rectangular stress block for masonry under compression with a uniform compressive strength. For the calculation of the effective strength of the FRP laminates, either the bond length can be calculated or a bond reduction factor can be used. The FRP laminates must be designed such that

$$M_R \geq M \tag{17.20}$$

where
M_R is the bending moment resistance of the wall section
M is the applied bending moment due to seismic action

As for the overturning collapse mechanism, M can be found from equilibrium conditions (Figure 17.2b).

METALLIC STRUCTURES

Introduction

Fiber-reinforced polymer (FRP) strengthening is a proven technique for extending the life of metallic structures. FRP strengthening allows existing metallic structures to be upgraded when they no longer possess adequate structural strength or stiffness. Some reasons for strengthening a metallic structure include

- Increasing the shear, flexural, or axial load-carrying capacity of a structure
- Extending the fatigue life of a structure
- Replacing material lost to or changed due to corrosion, impact, or thermal loading
- Increasing the strength of connections between metallic members
- Stiffening the structure to reduce deflection and increase buckling capacity

Compared with FRP strengthening of concrete structures, FRP-strengthened metallic structures within the domain of civil infrastructure is a younger field for which research and the investigation of practical applications are still in progress. Although the reasons for using FRP to rehabilitate or strengthen a metallic or concrete structure may be similar, the way in which the FRP works with an existing metallic structure can often be very different to how it works with a concrete structure, which will lead to different degradation, failure modes, and analysis techniques (Hollaway and Teng, 2008). Specifically, unlike FRP strengthening of a reinforced concrete beam where tensile flexural cracking is usually acceptable, the application of FRP to a metallic member, in particular one that exhibits brittle behavior, will be done with the aim of reducing the normal stresses, in order to decrease the likelihood of failure at the tensile fiber. Furthermore, contrary to what usually occurs in a reinforced concrete beam, delamination of FRP reinforcement from a metallic element usually does not occur in the substrate, but either in the adhesive, the metal/adhesive, or adhesive/FRP interfaces, or in the FRP.

Structural adhesive joints have been applied successfully in other industries such as the aerospace industry, where bonded composite patches are regularly used to repair aluminum structures. Although the underlying requirements for a successful adhesive joint are similar for aerospace and infrastructure strengthening, the two applications require different configurations and materials.

For example, infrastructure strengthening uses greater thicknesses of FRP, resulting in considerably higher peeling stresses within the adhesive joint. Furthermore, the joint is formed in situ and not under controlled factory conditions, which is mostly the case for aerospace strengthening (Hollaway and Teng, 2008).

At present, there exists only limited information on externally bonded FRP strengthening of metallic civil engineering structures as compared with FRP strengthening of reinforced concrete structures. Some of the more recent guidelines and overview documents include the following:

- The CIRIA report *Strengthening Metallic Structures Using Externally Bonded Fibre-Reinforced Polymers*, which includes case histories (Cadei et al., 2004)
- The Italian guidelines (also in English) *Guidelines for the Design and Construction of Externally Bonded FRP Systems for Strengthening Existing Structures* (CNR-DT 202, 2005)
- Chapter 8, "Strengthening of metallic structures with fibre-reinforced polymer (FRP) composites," in the book *Strengthening and Rehabilitation of Civil Infrastructure Using Fibre-Reinforced Polymer (FRP) Composites* (Hollaway and Teng, 2008)
- The papers "State-of-the-art review on FRP strengthened steel structures" (Zhao and Zhang, 2007), "Retrofit of steel structures using fibre-reinforced polymers (FRP): state-of-the-art" (Shaat et al., 2004), and "Progress in the technique of upgrading metallic structures with advanced polymer composites" (Hollaway and Cadei, 2002).

Important Considerations

Nature of Substrate Material

Metallic materials used in structural applications have evolved over the past two centuries. An understanding of the metallic structure and the nature of the material is important before strengthening can be planned, since each material has its own characteristics that determine how externally bonded FRP should be used (Cadei et al., 2004).

Cast iron, also referred to gray cast iron, was used extensively in the construction of bridges and buildings, starting in the late eighteenth century. After being cast, gray cast iron is cooled slowly, which allows the graphite to form discrete flakes that act as stress raisers. Cast iron can be characterized as brittle, weak in tension, and sensitive to fatigue loading. Ductile cast iron, on the other hand, is a modern material used in tunnel linings, pipes, truss, or frame nodes, and possesses similar properties to carbon steel.

Wrought iron replaced cast iron as a structural material between the mid-1840s and early 1850s (Cadei et al., 2004). Due to its superior tensile strength, it was used in truss and girder bridges, as well as roof trusses. Wrought iron is more ductile than cast iron; however, its material properties also differ substantially from steel.

The material properties and structural behavior of carbon (modern) steel are well documented in codes and guidelines. The material is characterized by linear-elastic behavior up to yield, followed by ductile plastic strain, usually accompanied by strain hardening, up to rupture.

Maximizing the Efficiency of the FRP Strengthening

A metallic member or structure has been efficiently strengthened when a significant portion of the tensile strength of the FRP is utilized. This can be achieved by ensuring a transfer of dead load into the FRP during strengthening, by using high-modulus FRP (in particular for brittle material), and, for a ductile material, allowing the substrate to yield.

In the former case, if the strengthening material is simply bonded to the structure under permanent loading (e.g., dead load), it will carry only live loads applied to the structure after it has been strengthened. This is less critical in the case of ductile metals, where the load is redistributed to the FRP as the metal yields. For brittle materials such as cast iron, however, it is important for the

FRP to carry load immediately upon strengthening, since the stresses due to the dead load may be a significant proportion of the metal's ultimate strength. In order to transfer part of the dead load stress from the metallic structure into the FRP, two methods can be used: (1) to prestress the FRP prior to bonding and (2) to relieve the structure partly of its dead load stresses during strengthening by, for example, load-relief jacking. More information on these two methods can be found in Cadei et al. (2004).

A higher FRP-to-metal modular ratio allows the FRP to develop greater stress when the composite section is loaded and results in a more efficient strengthened section (Hollaway and Teng, 2008). This is particularly important for brittle metals such as brittle cast iron with a relatively low ultimate strain. A ductile metal such as steel, on the other hand, can be allowed to yield and develop a large strain. In this case, a lower modulus FRP can be used, since the strain capacity of the FRP will be mobilized after the steel has yielded.

Temperature Effects

The differential thermal expansion between the metallic substrate and the FRP strengthening can lead to significant stresses in the adhesive layer and must be considered in the design. Furthermore, the relatively good thermal conductivity of metallic materials as compared with other structural materials conventionally strengthened with FRPs such as reinforced concrete must also be taken into account. Since the adhesive loses considerable strength at temperatures approaching its glass transition temperature (T_g), care must be taken that the operating temperature remains a margin of approximately 10°C–20°C below T_g (Cadei et al., 2004). When a large area of the metallic structure is covered with FRP strengthening, the heat flow and temperature distribution of the structure may be affected, which must be taken into account when assessing the operating temperature of the structure.

Strengthening Tensile Elements

Strengthening of tensile elements can be done to restore the load-bearing capacity of partially corroded elements, as well as to increase the strength of undamaged elements. As described in the Italian guideline (CNR-DT 202, 2005), the failure of tensile elements strengthened using FRP materials occurs due to failure of the metallic substrate or FRP reinforcement, or due to debonding. The latter failure mode, debonding, will be discussed in the "Evaluation of Debonding Strength" section. In the simple case of symmetric strengthening (e.g., two opposing faces of a tensile element), for restoring the load-bearing capacity of damaged elements, the strengthening must be calculated such that

$$2A_f f_f \geq A_s f_s \tag{17.21}$$

where

A_f is the cross-sectional area of the FRP
f_f is the tensile strength of the FRP
A_s is the cross-sectional area of the metallic substrate
f_s is the yielding stress of the ductile material or the failure stress of the brittle material

In the case of strengthening of an undamaged element, the normal stress in the metallic substrate and the FRP, as well as the subsequent check, taking into account the difference in thermal expansion of the two materials, is given by

$$\sigma_s = \frac{(N + 2E_f A_f(\alpha_f - \alpha_s)\Delta T)E_s}{2E_f A_f + E_s A_s} \leq f_s \tag{17.22}$$

$$\sigma_f = \frac{(N + 2E_s A_s(\alpha_s - \alpha_f)\Delta T)E_f}{2E_f A_f + E_s A_s} \leq f_f \tag{17.23}$$

where

σ_s and σ_f are the normal stresses in the metallic substrate and FRP, respectively
N is the tension load applied to the element
E_f and A_f are the modulus of elasticity and the cross-sectional area of the FRP, respectively
E_s and A_s are the modulus of elasticity and the cross-sectional area of the metallic substrate, respectively
α_f and α_s are the coefficient of thermal expansion of the FRP and metallic substrate, respectively
ΔT is the change in temperature after the strengthening application

Equations 17.21 through 17.23 do not include partial factors that are required in the design of these members.

Strengthening Flexural Elements

The potential failure modes of a metallic beam strengthened in flexure using externally bonded FRP are shown in Figure 17.3 that include the following:

- Tensile failure of the metallic beam or the FRP; the former can be either fracture or yielding depending on the material
- Compression failure of the metallic beam (local buckling or yielding)
- Shear failure of the metallic beam
- Buckling of the metallic beam (axial or lateral-torsional)
- Debonding of the FRP

Debonding will be discussed in more detail in the "Evaluation of Debonding Strength" section.

A detailed description of the earlier listed failure modes as affected by, for example, the substrate material is given in CNR-DT 202 (2005).

A sectional analysis is a first step in designing the flexural strengthening for a metallic beam, followed by the determination of the adhesive joint capacity based on a bond analysis. The latter step is addressed in the next section. For the sectional analysis of a flexurally strengthened metallic beam, the following assumptions must be made:

- Full composite action between the FRP and the metallic beam, that is, no slip
- Plane section remain plane
- The FRP plate and adhesive are thin as compared with the metallic beam
- The stiffness of the adhesive layer is negligible

The meaning of the former two assumptions is well known. The third assumption allows the FRP and adhesive to be simplified into a single fiber, acting at the extreme outer fiber of the metallic beam. The last assumption is based on the small elastic modulus and small thickness of the adhesive when compared with the metallic beam.

When carrying out a sectional analysis, it is necessary to take into account the stresses existing in the structure at the time of strengthening. Some of these may be due to permanent loads, temperature (or other environmental loads), temporary work loads, and support settlements. In calculating the flexural capacity of the beam, a conventional plane section analysis is used whereby the composite FRP and metallic section are analyzed using a transformed section. In fixing the neutral axes of the sections, attention must be paid to the shift in the neutral axis that is caused by the

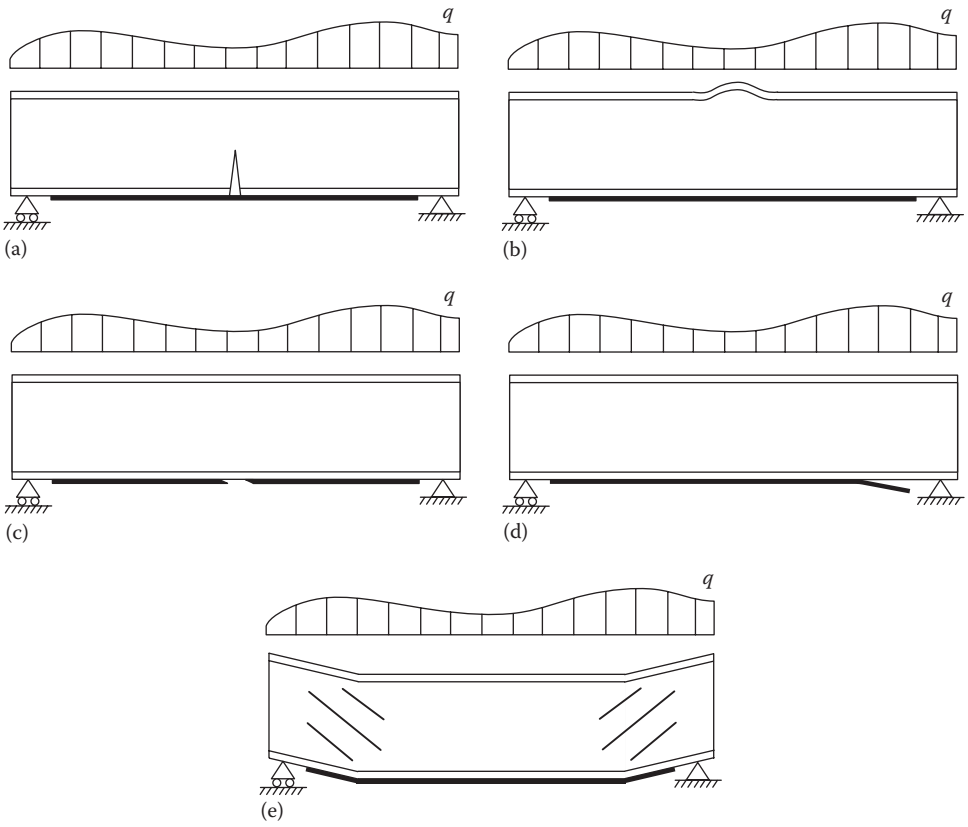

FIGURE 17.3 Failure modes of a metallic beam strengthened with FRP and loaded in flexure. (a) Tension failure of substrate, (b) local buckling of strengthened member, (c) tension failure of strengthening, (d) debonding, and (e) shear failure.

application of the strengthening at the extreme fiber of the beam. Once the strain distribution across the cross section has been found, the appropriate stress–strain relationship, dependent on the type of material, is used to evaluate the stresses at each fiber of the cross section (refer to Figure 17.4). Equilibrium of the resultant forces in the direction of the beam axis can subsequently be checked, and, once determined, the flexural capacity of the beam can be calculated.

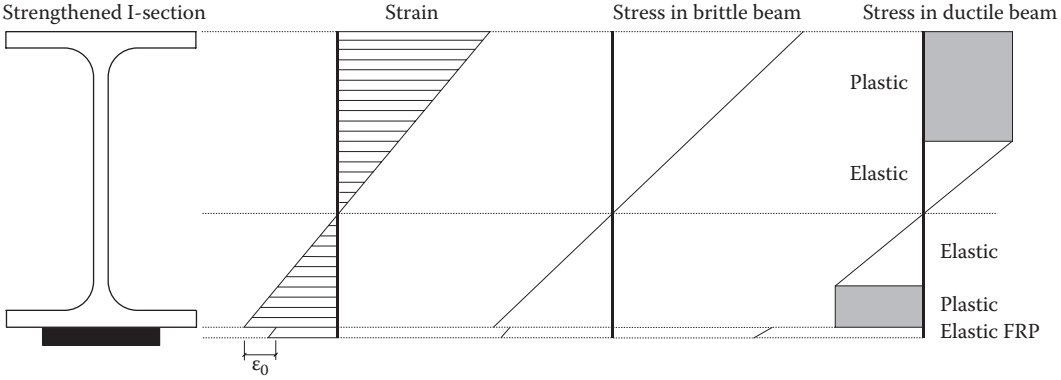

FIGURE 17.4 Flexural strain and stress distributions of a brittle and ductile metallic I-beam loaded prior to strengthening.

As can be seen in Figure 17.4, the stress distribution across the section will depend on the type of material. In the case of brittle metallic beams (e.g., cast iron), the stress distribution will remain elastic, and the capacity of the section will be governed by the extreme fiber strain. As pointed out by Stratford in Hollaway and Teng (2008), unlike concrete structures, a cracked section is normally not permitted in metallic structures, since the energy released by crack formation will usually lead to catastrophic failure of the adhesive joint. In the case of ductile materials (e.g., steel) or ductile systems (steel–concrete composite sections), part of the cross section will yield, while the central fibers of the cross section will remain elastic. Since the FRP strengthening will change the initial cross-sectional stress distribution in the beam, the slenderness of the beam and the associated strain limitations as well as global and local buckling must be checked.

Evaluation of Debonding Strength

In the calculation guidance given in the two previous sections, the metallic tensile and flexural members were considered to act fully compositely with the adhesive and FRP. However, due to high stress concentrations that also develop in the adhesive, the so-called debonding of the reinforcement from the metallic element leading to a sudden and substantial reduction in the load-carrying capacity of the element may occur and must be considered separately.

As shown in Figure 17.5, debonding of a strengthened metallic element can take place at the interfaces, in the substrate, in the adhesive, or in the reinforcement. Debonding in a strengthened metallic member usually occurs (from weakest to strongest) in the adhesive (cohesive failure), in the FRP, or at the interface. As stated earlier, this differs from a reinforced concrete member where debonding mostly occurs in the weak substrate material, that is, the concrete.

There are generally two approaches that can be used to assess the debonding strength of the adhesive layer: an elastic, stress-based approach, and a fracture mechanics approach. The fracture mechanics approach, while more generally appropriate from a theoretical point of view (CNR-DT 202, 2005), and already widespread in the calculation of aerospace applications, has yet to be refined and improved for structural engineering purposes (Buyukozturk et al., 2004). More information on the fracture mechanics approach can be found in Cadei et al. (2004).

In the stress-based approach, the debonding strength can be calculated by evaluating the local longitudinal shear (τ) and the transverse (normal) peeling stress (σ) concentrations that develop in the adhesive layer where there are discontinuities in the adhesive, substrate, or strengthening material. Figure 17.6 illustrates an example of shear and peeling stress distributions in the adhesive near the end of an FRP plate. Numerous analysis methods for determining these stresses have been proposed in the literature and vary with respect to the approximations on which they are based. The majority of these methods, referred to as approximate or lower-order solutions, give simple solutions based on the assumption of constant shear and peeling stresses through the thickness of the adhesive (e.g., Roberts, 1989; Saadatmanesh and Malek, 1997; Taljsten, 1997;

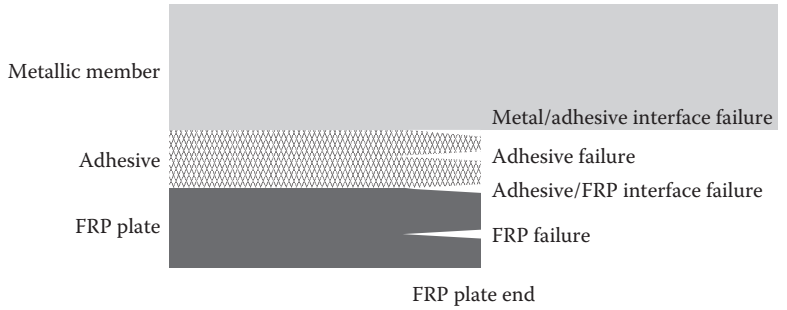

FIGURE 17.5 Possible locations of debonding at FRP plate end.

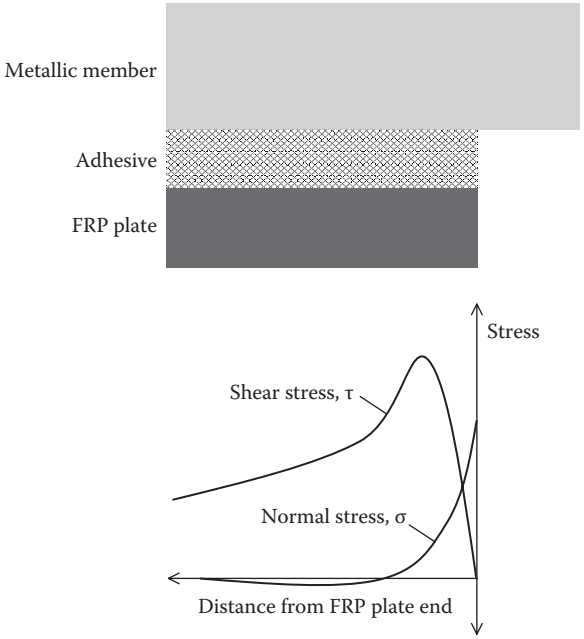

FIGURE 17.6 Shear and peeling (normal) stresses in the adhesive, near the end of the FRP plate.

Smith and Teng, 2001). Although global equilibrium requirements are satisfied, lower-order solutions do not satisfy the local zero shear stress boundary condition at the end of the plate (Hollaway and Teng, 2008). The so-called higher-order methods, on the other hand, take into account one or more of the stress variations across the adhesive thickness and therefore satisfy the zero shear stress boundary condition as is shown in Figure 17.6 (e.g., Rabinovitch and Frostig, 2000; Shen et al., 2001; Yang and Ye, 2005). Both methods, lower- and higher-order, give results that are very similar except within a small zone near the end of the adhesive layer, the zone being approximately the size of one adhesive layer (Buyukozturk et al., 2004). In the case of irregular geometry or loading, the earlier-described analysis methods are, in most cases, not applicable. For these situations, finite element models can be used to predict the local shear and peeling stresses, although care must be taken in selecting the appropriate mesh densities in the areas of high stress concentrations (Teng et al., 2002).

Failure of the adhesive joint will occur at the location of maximum principal stress derived from the shear and peeling stresses described earlier. Although the maximum shear and peeling stresses do not coincide (Figure 17.6), for simplicity, they can be assumed to occur at the same location. The maximum principal stress, σ_1, as given in Cadei et al. (2004) and CNR-DT 202 (2005), is

$$\sigma_1 = \frac{\sigma}{2} + \sqrt{\left(\frac{\sigma}{2}\right)^2 + \tau^2} \leq \sigma' \tag{17.24}$$

where

σ is the peeling stress

τ is the shear stress

σ' is the characteristic strength of the adhesive system, including any representative substrate preparation

Equation 17.24 does not include either partial load or partial material factors, which would be needed in the case of design. The characteristic strength of the adhesive system is obtained through a single or double lap-shear test. Since the results from the lap-shear test are reported as an average shear stress over the entire bonded area, the results must be back-analyzed using an elastic stress analysis in order to obtain the peak stress that causes bond failure, that is, σ'. Back-analyses of adhesive stress distributions in single and double lap-shear specimens are given in Cadei et al. (2004).

Strengthening of Fatigue-Sensitive Details

A limited amount of work has been done in the area of strengthening of metallic structures subjected to fatigue loading or rehabilitating fatigue-damaged metallic members. Of the work that has been carried out, emphasis has been placed on notched, nonwelded (e.g., riveted) details (Bassetti, 2001; Tavakkolizadeh and Saadatmanesh, 2003; Taljsten et al., 2009). The most comprehensive design guidance at present can be found in CNR-DT 202 (2005), which lists two possible fatigue failure modes in FRP-strengthened metallic members:

1. Fatigue delamination of the FRP
2. Fatigue damage of the metallic substrate

CNR-DT 202 (2005) underlines the importance of prestressing the FRP plates prior to bonding in the case of strengthening for fatigue, since the compressive stresses introduced into the member by the prestressed plate reduce significantly the stress ratio acting on the detail in question. A reduction in the stress ratio produces a decrease in the crack propagation rate, in some cases up to crack arrest.

Notations

Latin Letters

A_f cross-sectional area of FRP
$A_{frp,b}$ area of FRP laminates in the tension zone
$A_{frp,s}$ area of FRP laminates parallel to the direction of the shear force
A_s cross-sectional area of metallic substrate
A_w area of masonry wall section
b_{frp} width of FRP laminate
c_1 experimentally determined coefficient
c_u depth of neutral axis
d distance between the most compressed fiber of the masonry section and the centroid of the vertical FRP laminates
E_f modulus of elasticity of FRP
E_{frp} modulus of elasticity of FRP laminate
E_s modulus of elasticity of metallic substrate
F_{frp} tensile force of FRP laminate
f_b effective bond strength
$f_{b,max}$ maximum bond strength
f_f tensile strength of FRP
$f_{frp,e}$ effective strength of FRP laminate
$f_{frp,u}$ tensile strength of FRP laminate
f_{mt} tensile strength of masonry orthogonal to the mortar bed joint

f_{mx} compressive strength of masonry orthogonal to the mortar bed joint
f_{my} compressive strength of masonry parallel to the mortar bed joint
f_{mv} shear strength of masonry
f_{mv0} characteristic shear strength of masonry in the absence of normal stresses
f_s yielding stress of ductile metallic material or failure stress of brittle material
G_f fracture energy
G_w self-weight of masonry wall
h_{frp} height of the application of the horizontal FRP laminates
h_w height of masonry wall
k_b bond reduction factor
l_b bond length
l_e optimal bond length
l_w Length of masonry wall
M applied bending moment due to seismic loading
M_R bending moment resistance of the masonry wall strengthened with FRP
N applied axial load acting on top of the wall; tension load in metallic element
Q horizontal force due to seismic loading
s center-to-center spacing of the FRP laminates
T temperature
T_g glass transition temperature
t_{frp} thickness of FRP laminate
t_w thickness of the masonry wall
V_R shear capacity of masonry wall strengthened with FRP
$V_{R,m}$ masonry contribution to shear capacity of masonry wall strengthened with FRP
$V_{R,frp}$ FRP contribution to shear capacity of masonry wall strengthened with FRP

Greek Letters

α, β coefficients that describe the equivalent stress block
α_f coefficient of thermal expansion of FRP
α_s coefficient of thermal expansion of metallic substrate
ε_{frp} tensile strain in FRP laminate
$\varepsilon_{frp,e}$ effective useable tensile strain of FRP laminate
$\varepsilon_{frp,u}$ ultimate tensile strain of FRP laminate
ε_m compressive strain of the most compressed fiber of masonry section
ε_{mu} ultimate compressive strain of masonry
ρ_b balanced FRP reinforcement ratio
ρ_{frp} FRP reinforcement ratio
σ_s normal stress in metallic substrate, local transverse peeling (normal) stress in adhesive
σ_f normal stress in FRP
σ_n acting normal stress
σ_1 maximum principal stress
σ' characteristic strength of adhesive system
τ local longitudinal shear stress in adhesive

REFERENCES

ACI 440.ZR Draft (2004), Guide for the design and construction of externally bonded FRP system for strengthening unreinforced masonry structures, ACI Committee 440, Farmington Hills, MI.

Bassetti A. (2001), Lamelles précontraintes en fibres de carbone pour le renforcement de ponts rivetés endommagés par fatigue, Dissertation No. 2440, EPFL, Lausanne, Switzerland.

Buyukozturk O., Gunes O., Karaca E. (2004), Progress on understanding debonding problems in reinforced concrete and steel members strengthened using FRP composites, *Construction and Building Materials*, 18, 9–19.

Cadei J.M.C., Stratford T.J., Hollaway L.C., Duckett W.G. (2004), Strengthening metallic structures using externally bonded fibre-reinforced polymers, Report C595, CIRIA, London, U.K.

CNR-DT 200 (2004), Guide for the design and construction of externally bonded FRP systems for strengthening existing structures—Materials RC and PC structures, masonry structures, Italian National Research Council, Advisory Committee on Technical Recommendations for Construction, Rome, Italy.

CNR-DT 202 (2005), Guidelines for the design and construction of externally bonded FRP systems for strengthening structures—Metallic structures, Italian National Research Council, Advisory Committee on Technical Recommendations for Construction, Rome, Italy.

Elgawady M. (2004), Seismic in-plane behaviour of URM walls upgraded with composites, Dissertation No. 3111, EPFL, Lausanne, Switzerland.

Eurocode 6 (2005), *Design of Masonry Structures*, Comité Euro-International du Béton, Lausanne, Switzerland.

Garbin E., Galati N., Nanni A., Modena C., Valluzzi M.R. (2007), Provisional design guidelines for the strengthening of masonry structures subject to in-plane loading, *Proceedings of Tenth North American Masonry Conference*, St. Louis, MO.

Hollaway L.C., Cadei J. (2002), Progress in the technique of upgrading metallic structures with advanced polymer composites, *Progress in Structural Engineering and Materials*, 4(2), 131–148.

Hollaway L.C., Teng J.G. (ed.) (2008), *Strengthening and Rehabilitation of Civil Infrastructures Using Fibre-Reinforced Polymer (FRP) Composites*, Woodhead Publishing Limited, Cambridge, U.K.

Holzenkämpfer P. (1994), Ingenieurmodelle des Verbundes geklebter Bewehrung für Betonbauteile, PhD thesis, TU Braunschweig (in German), Braunschweig, Germany.

Marcari G., Manfredi G., Prota A., Pecce M. (2007), In-plane shear performance of masonry walls strengthened with FRP, *Composite Part B*, 38(7–8), 887–901.

Moon F.L., Yi T., Leon R.T., Kahn L.F. (2007), Testing of a full-scale unreinforced masonry building following seismic strengthening. *ASCE Journal of Structural Engineering*, 133(9), 1215–1226.

Nardone F., Prota A., Manfredi G. (2008), Design criteria for FRP seismic strengthening of masonry walls, *Proceedings 14th World Conference on Earthquake Engineering*, Beijing, People's Republic of China.

Neubauer U., Rostasy F.S. (1997), Design aspects of concrete structures strengthened with externally bonded CFRP-plates, *Proceedings Seventh International Conference on Structural Faults and Repair*, Edinburgh, U.K.

Rabinovitch O., Frostig Y. (2000), Closed-form higher-order analysis of beams strengthened with FRP strips, *Journal of Composites for Construction-ASCE*, 4, 65–74.

Roberts T.M. (1989), Approximate analysis of shear and normal stress concentrations in the adhesive layer of plated RC beams, *The Structural Engineer*, 67(12), 229–233.

Saadatmanesh H., Malek A.M. (1997), Prediction of shear and peeling stresses at the plate ends of beams strengthened with FRP plates, *Proceedings of 3rd International Symposium Non-Metallic (FRP) Reinforcement for Concrete Structures*, Vol. 1, JCI, Tokyo, Japan, pp. 42–56.

Schwegler G. (1995), Strengthening of masonry in seismic regions using FRP (in German), Empa report No. 229, Dübendorf, Switzerland.

Shaat A., Schnerch D., Fam A., Rizkalla S. (2004), Retrofit of steel structures using fiber-reinforced polymers (FRP): State-of-the-art, *Proceedings of Transportation Research Board (TRB) Annual Meeting*, CD-ROM, San Antonio, TX.

Shen H.S., Teng J.G., Yang J. (2001), Interfacial stresses in beams and slabs bonded with thin plate, *Journal of Engineering Mechanics-ASCE*, 127(4), 399–406.

Smith S.T., Teng J.G. (2001), Interfacial stresses in plated beams, *Engineering Structures*, 23(7), 857–871.

Taljsten B. (1997), Strengthening of beams by plate bonding, *Journal of Materials in Civil Engineering-ASCE*, 9(4), 206–212.

Taljsten B., Skodborg Hansen C., Wittrup Schmidt J. (2009), Strengthening of old metallic structures in fatigue with prestressed and non-prestressed CFRP laminates, *Construction and Building Materials*, 23, 1665–1677.

Tavakkolizadeh M., Saadatmanesh H. (2003), Fatigue strength of steel girders strengthened with carbon fiber reinforced polymer patch, *Journal of Structural Engineering-ASCE*, 129(2), 186–196.

Teng J.G., Zhang J.W., Smith S.T. (2002), Interfacial stresses in reinforced concrete beams bonded with a soffit plate: A finite element study, *Construction and Building Materials*, 16, 1–14.

Triantafillou T.C. (1998), Strengthening of masonry structures using epoxy-bonded FRP laminates, *Journal of Composites in Construction*, 2(2), 96–103.

Triantafillou T.C., Fardis M.N. (1997), Strengthening of historic masonry structures with composite materials, *Materials and Structures-ASCE*, 30, 486–496.

Yang J., Ye, J. (2005), Closed-form rigorous solution for the interfacial stresses in plated beams using a two-stage method, *Proceedings of the International Symposium on Bond Behaviour of FRP in Structures (BBFS 2005)*, Chen and Teng (eds.), Hong Kong, People's Republic of China.

Zhao X.-L., Zhang L. (2007), State-of-the-art review on FRP strengthened steel structures, *Engineering Structures*, 29, 1808–1823.

Zhao T., Zhang C.J., Xie J. (2003), Experimental study on earthquake strengthening of brick walls with continuous carbon fibre sheet, *Masonry International*, 16, 21–25.

18 Externally Bonded FRP Composite and Viscoelastic Materials for Mitigating Vibrations of Floor Systems

Arya Ebrahimpour and Marco P. Schoen

CONTENTS

INTRODUCTION

Floor system vibration control may be achieved using passive, semi-active, and active systems. Typical passive dampers include tuned mass dampers (TMDs). A semi-active damper can be produced by making one of the parameters of a passive damper active such as controlling the variable tuning of a TMD with computer and instrumentation system. Fully active systems make use of sensors and actuators controlled by a computer system to produce forces that counteract externally applied forces (Breukelman and Haskett, 2001).

Another form of passive control is achieved using viscoelastic (VE) materials. VE materials have been used to reduce the response of structures due to seismic and/or wind excitations. Seattle's 76-story Columbia Center currently uses VE material, as did the World Trade Center in New York City. These dampers absorb the "punch" of unusual as well as normal winds, thus reducing the perceived sway in the upper floors of the buildings (Caldwell, 1986). Chang et al. (1995) used VE dampers in conducting shake-table studies on a 2/5-scale five-story steel structure model subjected to mild and strong earthquake motions. More recently, Aref and Jung (2006) have developed the use of advanced composite panels with VE interface layers for (1) attenuating floor accelerations in hospital buildings and (2) seismic energy dissipation by incorporating such panels in the structural framing system.

This chapter examines floor vibration control through the use of two mechanisms: a VE material is applied to increase damping and an FRP material is applied to increase stiffness, while also constraining the VE material. The VE material will function as an energy absorber, and the FRP material will provide additional stiffness to the member and at the same time increase the energy storage capability of the VE material. These materials are lightweight and could be easily attached to floor systems without requiring temporary bracings. They can conform to contours even with obstacles present. Compared to steel retrofit, the installation and labor costs may offset the high material costs associated with the advanced fiber composites. The "Viscoelastic Materials" section provides an overview of VE materials. The "Retrofitting Wood Floors" and "Retrofitting Composite Steel–Concrete Floors" sections present applications of VE and FRP for retrofitting wood and steel–concrete floors, respectively. The "Application Problem" section presents a practical problem; similar approaches may be taken by practicing engineers to retrofit existing floor systems with excessive vibrations.

VISCOELASTIC MATERIALS

We can distinguish VE materials from most other structural engineering materials quite easily using Hook's law, which prescribes a linear relationship between the stress and the strain. For elastic materials, often the compliance is used, that is, $\varepsilon = J\sigma$, where ε is the strain, J the compliance, and σ the stress. Therefore, the elastic compliance is the inverse of Young's Modulus E. This behavior as detailed and defined by Hook's law is in contrast to viscous material, which is characterized by shear stress. The shear stress can be defined by the viscosity μ, which will affect the stress as follows:

$$\tau = \mu \frac{d\varepsilon}{dt}$$

The viscosity can be described by considering two plates at a distance d, having a surface area A, and a fluid of viscosity μ between the plates. The plates move relative to each other with a velocity v. Then the plates resist this motion with a force

$$F = \frac{\mu A}{d} v \tag{18.1}$$

In general, for any material, there will always be some deviation from Hook's law. Materials that possess elastic and viscous characteristics are called VE materials. To be more precise, if the material's stress and strain, in addition to the modulus of elasticity, depend on time, the material has a VE property. This characteristic can be observed, for example, if one holds the stress of a material constant, while the strain is measured and indicates a continuous increase with time, commonly referred to creep. The inverse is also true; if one keeps the strain constant, the stress of VE materials will decrease, also called relaxation. It is worthwhile to note that the effective stiffness depends on the rate of the application of the load.

Viscoelasticity is also a function of temperature. Most structural materials such as steel and aluminum at room temperature do not deviate much from the linear prescription of Hook's law, while elevated temperatures will increase the material's VE properties. On the other hand, wood or synthetic polymers do not require elevated temperatures to behave in a VE manner.

Kelvin–Voigt Model

There are a number of different models to quantify viscoelasticity, among them the Maxwell model, the Kelvin–Voigt model, and standard linear solid model. In this section, we will restrict our attention to the Kelvin–Voigt model. Consider the spring–damper system in Figure 18.1. The total stress

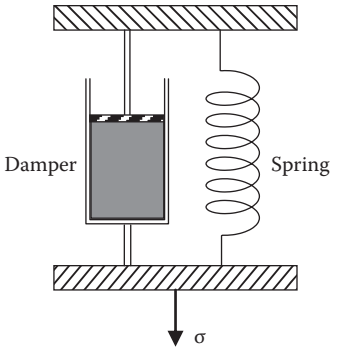

FIGURE 18.1 Kelvin–Voigt element for modeling viscoelastic materials.

σ is distributed between the damper σ_1 and the spring σ_2. We know that $\sigma_1 = \mu(d\varepsilon_1/dt)$ and $\sigma_2 = \varepsilon_1 E$. Therefore, we have $\sigma_1 = \mu(d\varepsilon_1/dt) + \varepsilon_2 E$. Assuming this is the result of a creep test, we can solve this differential equation and obtain

$$\varepsilon(t) = \frac{\sigma}{\mu}\left[1 - \exp\left(\frac{Et}{\mu}\right)\right] \tag{18.2}$$

Dynamic Modulus

In structural dynamic analysis, the measurement parameters showing the polymer's potential damping capability are the loss factor, η, and storage modulus, G', both functions of frequency and temperature. For VE materials, G' is the real part, of the complex dynamic modulus G^* and the loss modulus G'' is the imaginary part, as shown in Equation 18.3. G', G'', and G^* are also related to η, as shown in Equations 18.4 and 18.5 (Gibson, 1994). The storage modulus represents the elastic properties of the material while the loss modulus represents the material damping, both moduli being frequency and temperature dependent.

$$G^* = G' + iG'' \tag{18.3}$$

$$\eta = \frac{G''}{G'} \tag{18.4}$$

$$G^* = G'(1 + i\eta) \tag{18.5}$$

The loss factor, η, can also be determined from nomographs provided by manufacturers of the VE materials. Figure 18.2 shows a nomograph for the 3M damping polymer 110 (3M, 1999). To obtain the loss factor, a line should be drawn horizontally from the desired application frequency to the desired application temperature line. From this intersection point, a vertical line should be extended that intersects both the loss factor and storage modulus G' curves. The loss factor and the storage modulus are then found by extending horizontal lines from the intersections to the left axis. For computational purposes, at a given frequency and temperature, the storage modulus G' may be viewed as the shear modulus of elasticity G used for elastic isotropic material.

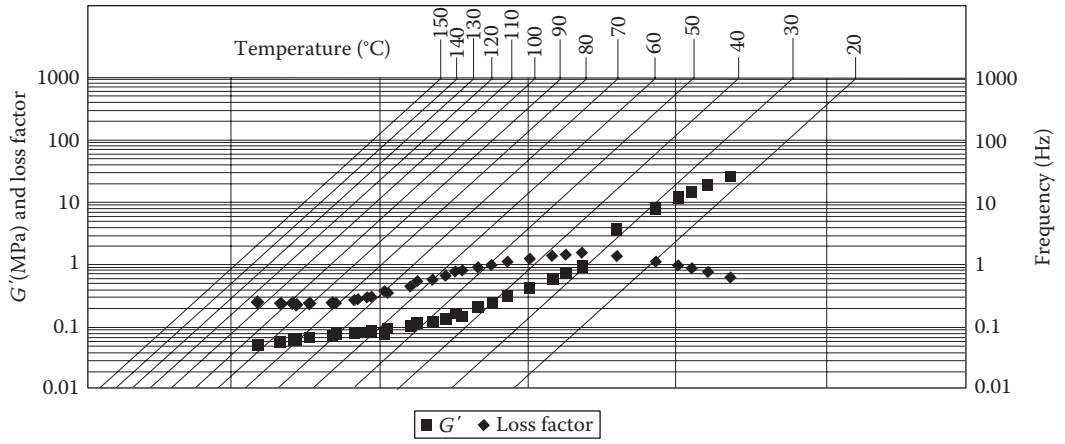

FIGURE 18.2 3M™ Viscoelastic damping polymer 110 nomograph. (From 3M, *Viscoelastic Damping Polymers 110- 120- 130-*, Bonding Systems Division, St. Paul, MN, 1999.)

RETROFITTING WOOD FLOORS

Martell (2002) and Ebrahimpour and Martell (2003) carried out experimental and analytical work to investigate the effects of advanced materials on the vibration responses of laboratory wood floors. Narrow 2 ft (0.61 m) by 16 ft (4.88 m) simply supported floors were constructed using two 2 × 8 (38 mm × 184 mm) wood joists, spaced at 16 in. (406 mm) on center, and oriented strand board sheathing. The bottom of each joist in one of the floors was retrofitted with one constrained 0.25 in. (6.4 mm) thick layer of VE material (3M Damping Polymer 130) and a 0.25 in. (6.4 mm) thick laminate of carbon fiber–reinforced polymer and epoxy (CFRP/epoxy). The CFRP/epoxy laminate consists of three layers of SIKA's CFRP strips bonded together by two layers of SIKADUR 30 epoxy adhesives. Thin layers of PLIOGRIP structural polyurethane adhesive (Ashland Specialty Chemical Company, Covington, Kentucky) were used to bond the VE layer to the bottom of the joist and the CFRP/epoxy laminate. This retrofit scheme represents high damping with some increase in stiffness.

Dynamic tests involved mass-drop test and tests involving one person performing standard heel-drop (Murray, 1979), walking across the floor, and in-place walking. Both acceleration– and displacement–time data were recorded. The mass-drop test is ideal for experimentally measuring the floor damping using the log-decrement method (Foschi et al., 1995). A small sand bag was dropped onto the center of the floor from a height of approximately 1 in. (25 mm), and the resulting free vibration response was measured. Figure 18.3 shows the free vibration responses before and after both types of retrofit. In Figure 18.3, for

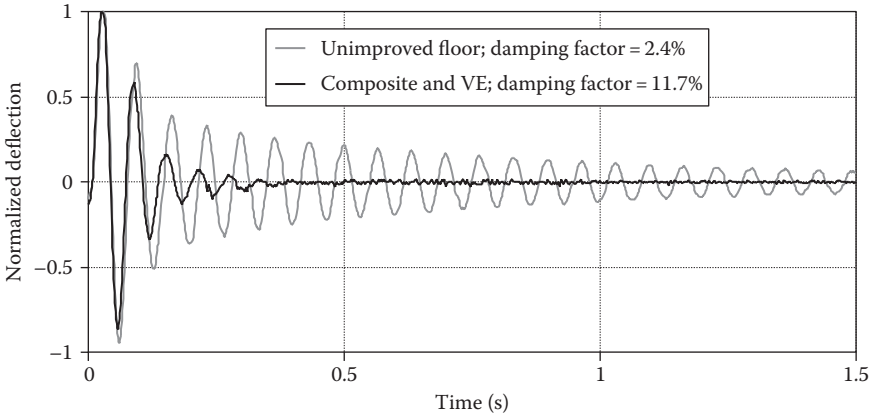

FIGURE 18.3 Wood floor mass-drop displacement responses.

the purpose of comparison, all maximum displacements were adjusted (normalized) to be one unit. The average measured equivalent damping, ζ_m, for the unmodified floor was 2.4% while the retrofit with FRP composite and constrained VE material resulted in an average damping value of 11.7%.

The damping model developed by Ungar and Kerwin (1962) was used in this project. The system loss factor, η, could be expressed in terms of the summation of the product of the individual element loss factors and the fraction of the strain energy stored in each element, as shown in Equation 18.6.

$$\eta = \frac{\sum_{i=1}^{n} \eta_i U_i}{\sum_{i=1}^{n} U_i} \tag{18.6}$$

where

η_i is the damping loss factor for element i
n is the total number of elements
U_i is the strain energy stored in element i at maximum vibratory displacement

For small damping, the equivalent viscous damping ratio of the system, ζ, is related to loss factor as $\zeta = \eta/2$.

Using Equation 18.6, the predicted equivalent viscous damping for the floor retrofitted with composite and VE materials is 14.3%, compared to the measured value of 11.7%. The difference in damping values may be due to damage to the VE layer caused by the adhesive, that is, the VE layer may have lost its high damping property on both sides of the constrained layer. Martell (2002) provided a practical example problem; a similar and more detailed example problem will be given in the "Application Problem" section.

RETROFITTING COMPOSITE STEEL–CONCRETE FLOORS

Wiegman and Ebrahimpour (2004) and Wiegman (2005) studied the vibrations in steel–concrete beams, but with more precision and better control on repeatability. A shake table was used to test the floor beams at low levels of acceleration. All tests were done in order to find the average damping ratio and loss factor for each case.

In determining damping using the forced vibration, Gibson (1992) listed two methods; these are (1) stress–strain hysteresis loop using a fixed frequency oscillation and (2) changing the excitation frequency and plotting the response magnitude versus the frequency. The second method was used in which the specimens are subjected to vibrations using the sine sweep method over a frequency range with constant acceleration. Damping in the specimens can be related to the sharpness of resonance or the width of the resonant peak of dynamic magnification factor versus frequency ratio, that is, the half-power bandwidth method. This method commonly uses the dynamic magnitude factor (*DMF*) representing the forced vibration amplitude over the static amplitude (Tedesco et al., 1999). However, the experimental setup used in this study is represented by an oscillating support problem. The base or support (shake table) is oscillating, thus causing a motion in the beam specimen. The motion that is transmitted to the specimen due to the excitation of the base is the transmissibility ratio (*TR*). The *TR* and the *DMF* are related, as shown in Equation 18.7.

$$TR = DMF\sqrt{1 + (2\zeta r)^2} \tag{18.7}$$

For r near unity and very small ζ, as experimentally determined for the retrofitted composite floor beam ($\zeta_{max} < 0.016$), the *TR* and the *DMF* are almost equal. As an example, for $r = 1$ and $\zeta = 0.016$,

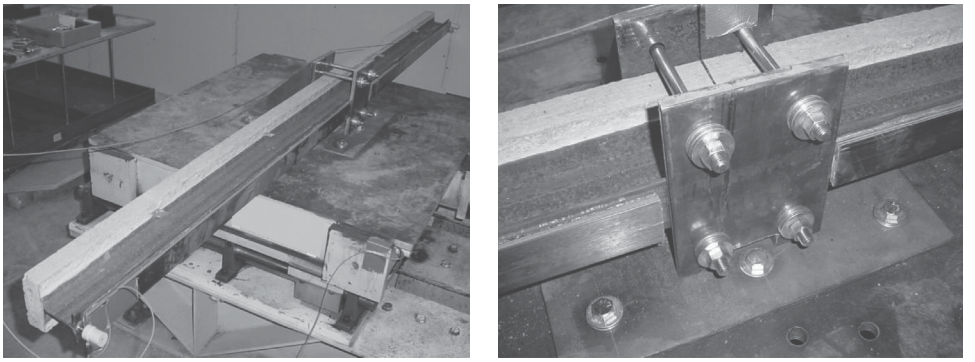

(a) (b)

FIGURE 18.4 (a) Composite steel–concrete beam with constrained VE and CFRP; (b) close-up view of the beam.

the ratio of *TR* to *DMF* is 1.0005. The *TR* was used to estimate the specimen damping values. In testing using the sine sweep method, the shake-table displacement and load limits were the factors that influenced the size of the floor beam specimens. Test floor beams were designed to comply with constraints of the shake table. In order to determine the overall damping loss factor of the retrofitted beams, the loss factor for each material needed to be determined. Individual beams of each material (except VE) were constructed for testing. A steel–concrete floor beam without constrained VE and CFRP was also constructed. The beam specimens were tested in a double cantilever position in the horizontal shake table, as shown in Figure 18.4.

One of the unique contributions of this project is testing at low acceleration levels representative of those seen in floor systems. The recommended peak acceleration levels that humans can tolerate without annoyance are 0.5 *%g* for office activities, 1.5 *%g* for activities near dance floors, etc., and 5 *%g* for aerobic activities. Tests were performed at five different acceleration levels: 0.5, 1, 2, 5, and 10 *%g*. For each specimen, three tests of the double-cantilevered beams were performed at each acceleration level. The test beams were vibrated over a range of frequencies surrounding the natural frequency of the beams. A range was selected that was large enough to allow for the half-power bandwidth method to be used while at the same time allowing for a very dense resolution of data points.

The shake-table control software reported the frequency and acceleration level (in acceleration of gravity, *g*). These data were then imported into a preprogrammed spreadsheet to automatically calculate the loss factor for each beam. Figure 18.5 is a plot of the damping loss factor data points

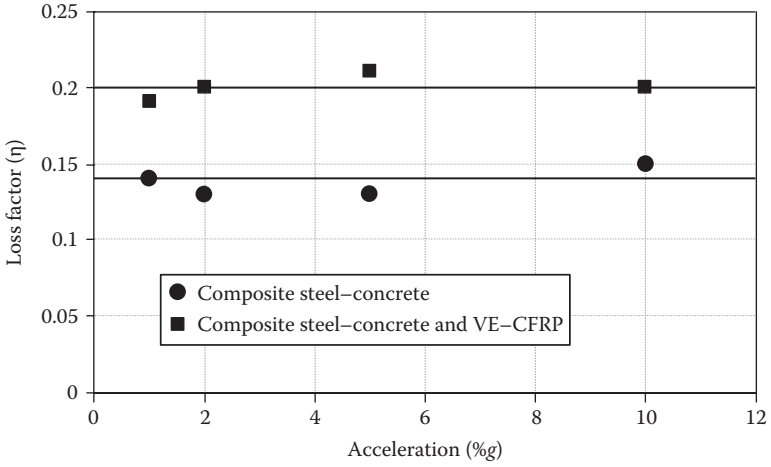

FIGURE 18.5 Loss factor data and mean (solid lines) versus acceleration.

TABLE 18.1
Mean Values of Loss Factors η

Beam	*H*
CFRP	0.017
Concrete	0.013
Steel	0.004
Composite steel–concrete	0.014
Composite steel–concrete with constrained VE and CFRP	0.020

TABLE 18.2
Loss Factors, η, Produced by Computer Model and Experimentally

Floor Beam	ANSYS	Experimental
Composite steel–concrete	0.008	0.014
Composite steel–concrete with constrained VE and CFRP	0.019	0.020

and horizontal lines representing the average values for the plain and retrofitted composite beams. Table 18.1 shows that the CFRP has a larger damping than the concrete and steel. The loss factors for the VE materials are found in nomographs provided by the manufacturer (3M, 1999). For normal temperature and low frequencies, the VE material used had a loss factor of about 1.

In order to test the Ungar–Kerwin model (Equation 18.6) at low acceleration levels considered here, computer models of each of the three composite beams were developed using ANSYS finite element program (ANSYS, 2006). This was done in order to obtain the element strain energy (U_i) required for calculating the overall damping loss factor (η) of Equation 18.6. The loss factors obtained were then compared to the results obtained experimentally. The strain energy along with the element material type were extracted from ANSYS and placed into a spreadsheet and were sorted by material number. The strain energy for each material and the corresponding loss factor were used in Equation 18.6 to determine the overall system loss factor, as shown in Table 18.2.

In comparing the model results with those obtained experimentally, there are some differences (see Table 18.2). Experimentally, the plain composite beam produced a loss factor much larger than the value calculated from computer modeling. This is probably due to sources of damping present in the experimental specimen (e.g., friction between steel and concrete). Considering the cases in Table 18.2, one may conclude that the finite element predictions of the damping loss factors for the plain composite beam and the constrained composite beam are either conservative or almost the same.

APPLICATION PROBLEM

Using a finite element program, simplified models of the problematic floors can be obtained with and without retrofitting. Strain energy data can be extracted for each element in order to solve for the overall damping loss factor using the Ungar–Kerwin model. The loss factors combined with the floor system dimensions and loads may be entered in a commercial floor vibration analysis program to verify that the retrofitted floor meets the recommended acceptance criteria for human comfort.

Floor vibrations due to walking was selected for the application example. This relationship is represented in simplified form as (Murray et al., 2003)

$$\frac{a_p}{g} = \frac{P_o \exp(-0.35 f_n)}{\zeta W} \leq \frac{a_o}{g} \tag{18.8}$$

where

q_p/g is the predicted peak acceleration as a fraction of gravity (g)
a_o/g is the acceleration ratio limit from recommended peak acceleration limits for human activity vibration
P_o is the constant force representing the excitation with recommended values equal to 65 lb (0.26 kN) for floors and 92 lb (0.41 kN) for footbridges
f_n is the natural frequency of floor system
ζ is the damping ratio
W is the effective weight of floor

Floor Example

Murray et al. (2003) presented an example floor system that was also used in this chapter. This floor system is shown in Figure 18.6. In this example, a damping ratio (ζ) of 0.03 was recommended and, when applied in Equation 18.8, produces an acceleration level that satisfies the acceptance criterion for human comfort. Murray et al. recommend that ζ of 0.03 be used for floors with nonstructural components and furnishings, but with only small demountable partitions, typical of many modular office areas. However, if the floor has few nonstructural components (ceilings, ducts, partitions, etc.) as can occur in open work areas and churches, a value of 0.02 is recommended for ζ. It was assumed that the example floor system meets the second case (i.e., has low damping of $\zeta = 0.02$), that is, when applied to Equation 18.8, it produces an acceleration level that does not meet the minimum recommended value. The floor system of Figure 18.6 is an interior bay and is constructed of four W18 × 35 beams supported by two W21 × 50 girders. The concrete slab has a total thickness of 5.25 in. (133 mm). However, because of the corrugated steel form, the concrete deck has a continuous thickness of 3.25 in. (83 mm) with 2 in. (51 mm) ribs. The concrete properties given for this example include weight of concrete of w_c = 110 pcf (17.3 kN/m^3) and 28 day compressive strength of $f_c' = 4000$ psi (27.6 MPa). A 11 psf (527 Pa) live load is specified along with a 4 psf (192 Pa) mechanical equipment and ceiling load.

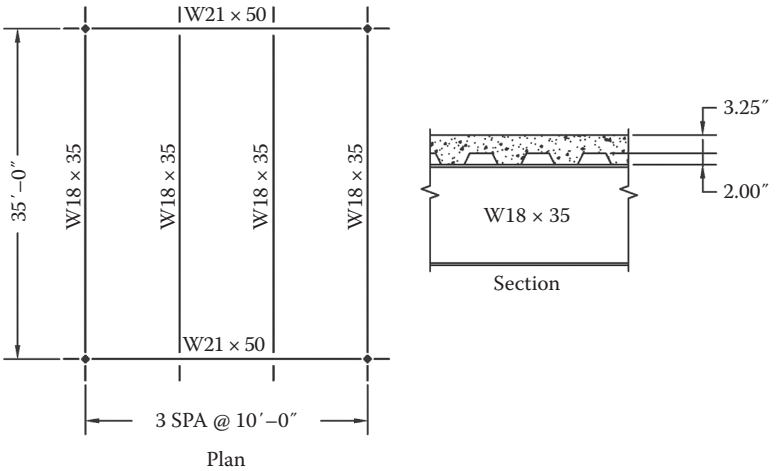

FIGURE 18.6 Interior bay floor framing plan (1 in. = 25.4 mm and 1ft = 0.305 m).

Finite Element Models

In order to avoid modeling the entire floor bay all at once, with four beams and two girders, a simplified method was devised. Using ANSYS, a single beam and a single girder were each modeled and analyzed separately. The strain energy data for each material in both the beam and girder were then combined in the Ungar–Kerwin equation (Equation 18.9) to determine the overall loss factor of the floor system.

$$\eta = \frac{\sum_{i=1}^{n} \eta_i (N(U_b)_i + (U_g)_i)}{\sum_{i=1}^{n} (N(U_b)_i + (U_g)_i)} \tag{18.9}$$

where

N is the number of beams
$(U_b)_i$ is the strain stored in beam element i
$(U_g)_i$ is the strain stored in girder element i

The assumption was made that the deflected shape of the floor system under the gravity load matches the first mode of vibration, and thus the structural damping corresponds to the first mode of vibration. In order to model the floor system, it is necessary to determine how the load will be transmitted to the structural elements of the floor. Using the general rules of $(L_2/L_1) \geq 2$, where L_1 is the length of the girder between each connected beam and L_2 is the length of each beam, the floor is considered one way. The beams are each spaced 10 ft (3.04 m) apart giving a tributary area of 10 ft (3.05 m) by 35 ft (10.67 m).

In order to more closely model the concrete floor in ANSYS, the top 3.25 in. (83 mm) of concrete supported by each beam has an effective slab width of 10 ft (120 in. or 3.04 m) and the bottom 2 in. (51 mm) has an effective slab width of 5 ft (60 in. or 1.52 m) due to the ribs. Figure 18.7 shows the model beam and slab dimensions. Note that the flange thickness dimensions differ slightly from those presented in any steel section manual due to the simplification of the model; the flanges are slightly thicker in the model in order to maintain the given moment of inertia. The ANSYS SOLID45 element was used to model both the plain and retrofitted beams and girders. The beams

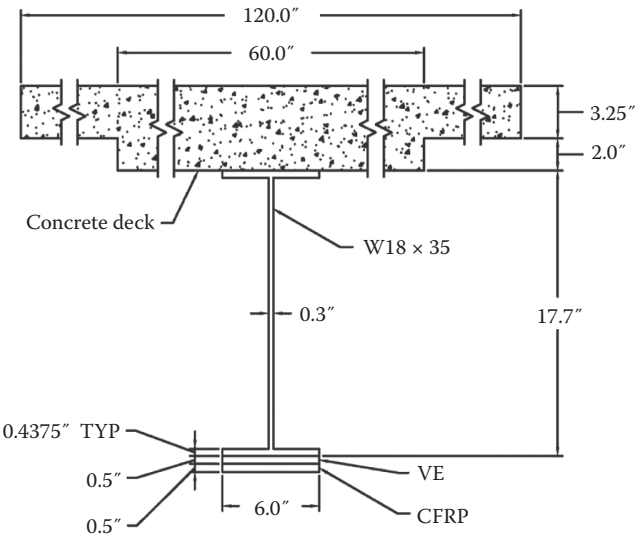

FIGURE 18.7 Dimensions of beam and slab as modeled (1 in. = 25.4 mm).

and girders were modeled separately in order to keep the number of nodes under the 32,000-node limit while still maintaining the best possible aspect ratio. Beams and girders were modeled as simply supported beams.

The beam was modeled under dead load (by assigning material densities and acceleration of gravity) and applied surface pressure representing the live load, the load due to steel deck form, and the mechanical and ceiling loads. In order to correspond with the given example, the girder was modeled under live and mechanical loads along with the weight of the entire bay applied as a pressure on the tributary area. To account for the necessary stiffness, as recommended by Murray et al. (2003), the girder effective slab width was calculated by the smaller of $0.4L_g$ or L_j, where L_g is girder length of 30 ft (9.15 m) and L_j is beam length of 35 ft (10.67 m). Therefore, for the girder, the effective slab width is 144 in. (3.66 m) for the top 3.25 in. (83 mm) of concrete and 72 in. (1.83 m) for the bottom 2 in. (51 mm) of concrete. Since the weight of the bay is included as pressure on the girder model, no density was assigned to the concrete in the girder model. Dimensions for the modeled girder and slab are shown in Figure 18.8.

The beam and girder (plain beam and plain girder) were first modeled without any retrofit applied. A retrofit of attached VE and CFRP was applied in 0.25 in. (6.4 mm) layers each to both the beam and the girder. This was done again with 0.5 in. (12.7 mm) layers of each material and with 0.75 in. (19.1 mm) layers to finally arrive at the necessary damping ratio. Table 18.3 presents the ANSYS strain energy values for each material for the beams and girders modeled. The 0.25, 0.5, and 0.75 in. designations on the retrofit beams and girders refer to the thickness of each of the retrofit VE and CFRP layers (e.g., the 0.5 in. retrofit beam consists of 0.5 in. of VE and 0.5 in. of CFRP attached to the beam, as shown in Figure 18.7).

Individual material loss factors from different sources have been utilized in calculating the overall loss factor for comparison purposes. Bachmann et al. (1995) present individual material damping ratios (converted to loss factors, η_i, for purposes of this discussion) for different structural materials including reinforced concrete with small stress intensity (uncracked) and steel. Murray recommends damping ratios (converted to η) indicative of many concrete-slab on steel-joist office floors as presented previously. Murray's values include damping derived from other sources (ceilings, ducts, partitions, etc.) and not just the floor structure itself (Murray et al., 2003). Values were obtained experimentally, for each material (concrete, steel, and CFRP) for several acceleration levels, as

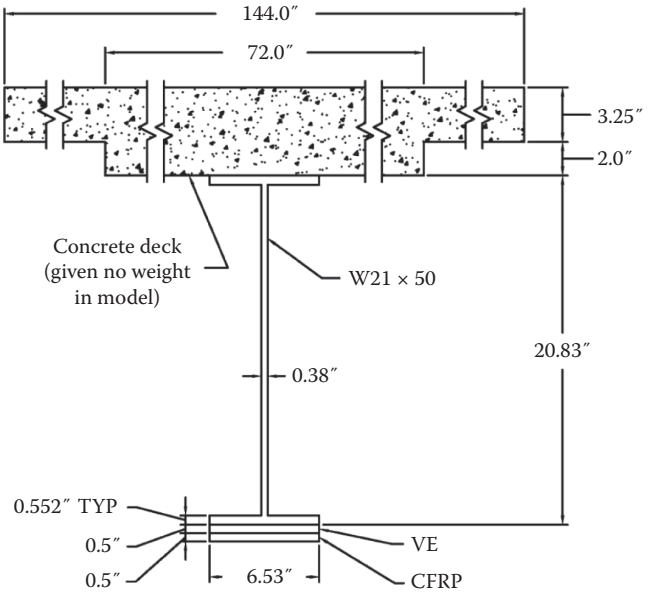

FIGURE 18.8 Dimensions of girder and slab as modeled (1 in. = 25.4 mm).

TABLE 18.3
Material Strain Energy U_i (lb·in.)

Material	Plain Beam	Plain Girder	0.25 in. Retrofit Beam	0.25 in. Retrofit Girder	0.5 in. Retrofit Beam	0.5 in. Retrofit Girder	0.75 in. Retrofit Girder	0.75 in. Retrofit Girder
Concrete	610	3,465	579	3,360	574	3,355	580	3,372
Steel	2,351	8,178	1,875	6,950	1,823	6,919	1,881	7,104
VE	0	0	68	214	169	446	202	479
CFRP	0	0	185	432	116	225	62	108
Total	2,962	11,643	2,706	10,956	2,681	10,945	2,725	11,062

1 lb in. = 0.113 N·m and 1 in. = 25.4 mm.

TABLE 18.4
Material Loss Factors η_i

Material	Bachmann Low	Bachmann High	Murray	Experimental
Concrete	0.014	0.020	0.040	0.013
Steel	0.002	0.004	0.040	0.004
VE	—	—	—	1.000[a]
CFRP	—	—	—	0.017

[a] From the manufacturer (3M, *Viscoelastic Damping Polymers 110- 120- 130-*, Bonding Systems Division, St. Paul, MN, 1999.)

presented previously. The η_i values presented here for each material are an average of those values. Both the Bachmann and experimental values provide the damping created by the structural elements themselves only (i.e., steel, concrete, VE, and CFRP) and not outside sources. A comparison of the η_i values is presented in Table 18.4. The experimental η_i values of this research project for steel and concrete compare well with those presented by Bachmann et al.

One beam and one girder were modeled; however, in order to more closely match the Design Guide (Murray et al., 2003) example floor, the strain energy from more than one beam was required to calculate the floor system loss factor. Thus, the number of beams, *N*, used in Equation 18.9 was 3.

Comparison of Results

Several combinations of plain and retrofit beam and girder strain energies were calculated using Equation 18.9 to determine the floor system loss factors that corresponded with the minimum retrofit required to pass the acceptance criteria for human comfort. Table 18.5 lists the beam and girder combinations along with the calculated overall loss factors. Using Bachmann (or present experimental) data, the 0.75 in. retrofit beam and 0.75 in. retrofit girder combination is one choice of achieving the required damping. Again, notice that the experimental values compare very well with the Bachmann et al. values. Using the Murray's data, the floor nearly satisfies the criteria for human comfort using the 0.25 in. retrofit beam and 0.25 in. retrofit girder combination.

For later comparison, the deflection and natural frequency for each beam and girder have been calculated and listed in Table 18.4. The beam and girder deflection data were obtained from the finite element analysis, but the fundamental natural frequencies were calculated using Equation 18.10.

TABLE 18.5
Overall Floor System Loss Factors η

Floor System	Bachmann Low	Bachmann High	Murray	Experimental
Plain beam and plain girder	0.005	0.008	0.040	0.006
0.25 in. Retrofit beam and plain girder	0.016	0.019	0.049	0.017
Plain beam and 0.25in. retrofit girder	0.016	0.019	0.050	0.018
0.25in. Retrofit beam and 0.25 in. retrofit girder	0.028	0.031	0.060	0.029
0.5 in. Retrofit beam and plain girder	0.031	0.034	0.064	0.032
Plain beam and 0.5 in. retrofit girder	0.028	0.031	0.061	0.029
0.5 in. Retrofit beam and 0.5 in. retrofit girder	0.056	0.059	0.087	0.057
0.75 in. Retrofit beam and plain girder	0.034	0.039	0.069	0.037
Plain beam and 0.75 in. retrofit girder	0.029	0.032	0.063	0.031
0.75 in. Retrofit beam and 0.75 in. retrofit girder	0.062	0.065	0.094	0.063

1 in. = 25.4 mm.

TABLE 18.6
Estimated Natural Frequency, f_n, for the Floor System

Floor System	Natural Frequency (Hz)
Plain beam and plain girder	3.72
0.25 in. Retrofit beam and plain girder	3.80
Plain beam and 0.25 in. retrofit girder	3.79
0.25 in. Retrofit beam and 0.25 in. retrofit girder	3.87
0.5 in. Retrofit beam and plain girder	3.81
Plain beam and 0.5 in. retrofit girder	3.79
0.5 in. Retrofit beam and 0.5 in. retrofit girder	3.89
0.75 in. Retrofit beam and plain girder	3.80
Plain beam and 0.75 in. retrofit girder	3.78
0.75 in. Retrofit beam and 0.75 in. retrofit girder	3.86

1 in. = 25.4 mm.

The fundamental natural frequency of the entire floor system is calculated using a form of the Dunkerley relationship (Equation 18.11). Table 18.6 lists the floor system natural frequencies.

$$f_n = 0.18\sqrt{\frac{g}{\Delta}} \tag{18.10}$$

$$\frac{1}{f_n^2} = \frac{1}{f_{nj}^2} + \frac{1}{f_{ng}^2} \tag{18.11}$$

where

Δ is the member mid-span deflection relative to its supports due to weight supported
f_{nj} is the beam or joist panel mode frequency, Hz
f_{ng} is the girder panel mode frequency, Hz

In terms of changing the natural frequency, there appears to be an optimum amount of retrofit that should be added. Thicker retrofits do not increase the natural frequency of the beam, the girder, or the floor as can be seen in Table 18.6. In order to determine if a floor system will meet the acceptance criteria for human comfort, the floor system must be evaluated for its natural frequency and acceleration. To accomplish this, AISC Design Guide 11 "Floor Vibrations Due to Human Activity" outlines a floor evaluation procedure. The computer program FLOORVIB2 was used for these calculations (FLOORVIB2, 1997). The floor evaluation calculation procedure is based on Equations 18.8 and 18.11.

The only way to include the effects of the added VE and CFRP materials was to change the damping values in the FLOORVIB2 program. Because the retrofit materials or dimensions cannot be entered into the program, the stiffness, weight, and subsequently the natural frequency of the floor system do not change. However, these changes are small and can be ignored. FLOORVIB2 calculates the natural frequency of the floor panel to be 4.03 Hz, which is close to the ANSYS value of 3.72 Hz (See Table 18.6).

The damping for the plain floor system along with the retrofitted floor systems was presented previously in Table 18.5 as η. Upon assigning the damping ratios, the system is evaluated as satisfying the vibration criterion. Table 18.7 contains the calculated damping ratios (ζ) for the plain floor, the 0.25 in. retrofit floor, the 0.5 in. retrofit floor, and the 0.75 in. retrofit floor. The 0.25 in. retrofit on beam and girder provides the damping necessary to meet the acceptance criteria given the Murray individual material damping values (i.e., $\zeta = 0.02$ individually for steel and concrete). The Bachmann and the present experimental individual material damping values require the 0.75 in. retrofit on both beam and girder to satisfy the criterion. The difference between the necessary retrofit thickness required by the Murray and Bachmann values indeed indicates damping due to other sources (i.e., office equipment, carpet, partitions, etc.), which are not included in the damping model.

As a part of the system evaluation, the maximum response acceleration of the floor system (in *%g*) is also given in Table 18.7 for comparison with the recommended 0.5 *%g* limit for offices. Criterion is satisfied when the system response acceleration is less than the 0.5 *%g* limit. To be consistent with the given example, the natural frequency of 4.03 Hz is used in calculating each of the acceleration levels in all floors considered in Table 18.7. Table 18.7 shows that the acceleration responses (in parentheses) for both the 0.25 in. retrofit with Murray's values and the 0.75 in. retrofit with Bachmann (or experimental) data satisfy the comfort criteria of being less than 0.5 *%g*. Each of these acceleration levels when plotted at the natural frequency of the floor panel can be shown in

TABLE 18.7
Floor System Damping Ratio, ζ, and Acceleration Responses (in parentheses) %*g*

Floor System	Bachmann Low	Bachmann High	Murray	Experimental
Plain beam and plain girder	0.003 (5.658)	0.004 (3.548)	0.020 (0.721)	0.003 (4.390)
0.25 in. Retrofit beam and 0.25 in. retrofit girder	0.014 (1.035)	0.015 (0.937)	0.030 (0.482)	0.015 (0.989)
0.5 in. Retrofit beam and 0.5 in. retrofit girder	0.028 (0.518)	0.029 (0.492)	0.044 (0.330)	0.029 (0.506)
0.75 in. Retrofit beam and 0.75 in. retrofit girder	0.031 (0.467)	0.032 (0.446)	0.047 (0.307)	0.032 (0.458)

1 in. = 25.4 mm.

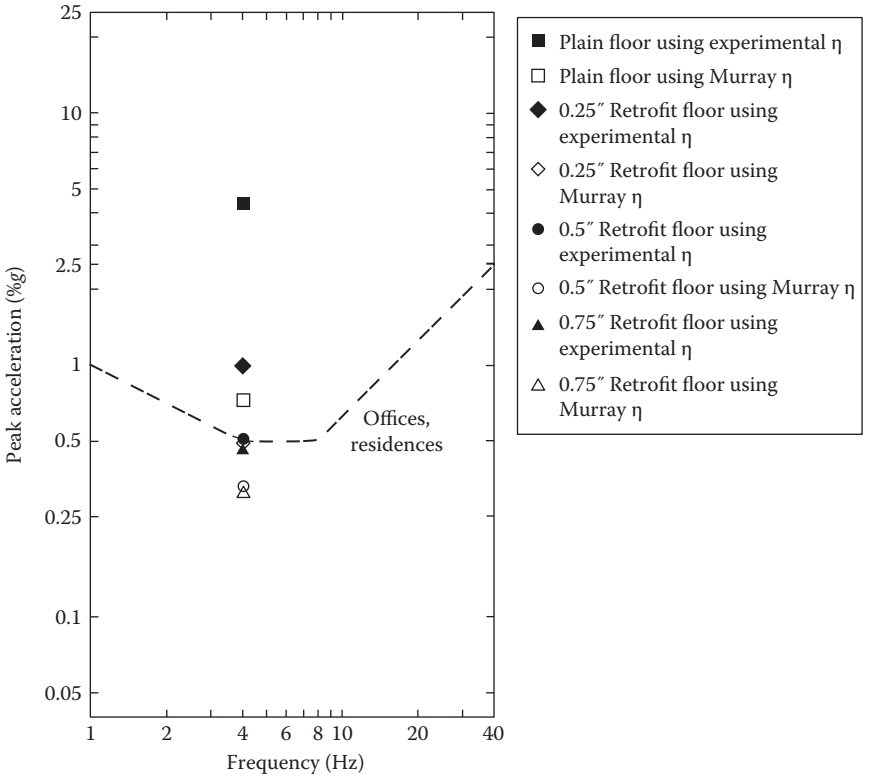

FIGURE 18.9 Acceptance criteria for human comfort chart showing effects of retrofit (1 in. = 25.4 mm).

the AISC's human comfort chart in Figure 18.9. Only Murray and experimental values are shown in the chart due to the proximity of values. The responses based on experimental values are almost at the same locations as those obtained from the Bachmann data.

Summary of Steps in Retrofitting a Floor System

The following steps may be used in a trial and error process coupled with cost–benefit analysis for an optimum retrofit option.

1. Model the floor system's individual beams and girders using a commercial finite element package (e.g., ANSYS) capable of determining strain energy in individual materials (steel, concrete, etc.).
2. Using the recommended damping values given in Table 18.4 and Ungar–Kerwin equation (Equation 18.9), determine the overall loss factors η of the floor system and thus the equivalent viscous damping ratio $\zeta = \eta/2$.
3. Using Equation 18.11, calculate the approximate value of the system natural frequency.
4. Using Equation 18.8 (or another appropriate relationship), calculate the predicted peak acceleration of the floor system under certain activity (walking, etc.) as a fraction of the acceleration of gravity (g). Then, use a vibration acceptance chart (e.g., Figure 18.9 or another appropriate chart) to determine the degree to which the floor system is vulnerable to human-induced vibrations. This results in a point on the vibration perception chart (see Figure 18.9) for the existing (not retrofitted) floor system.

5. Using trial and error and the same finite element software, try various thicknesses of the VE and FRP materials. Following steps 2–4 above, for each option, determine the new location (again a point) in the vibration perception chart. Considering the retrofit options that pass the perception criterion, using cost–benefit analysis, determine which option is best suitable for the project under consideration.

SUMMARY AND CONCLUSIONS

This chapter presented a type of passive floor vibration control through the use of combination of FRP composite and constrained VE materials. In addition, simplified computer models were provided by which practicing engineers may model a floor system in order to determine the amount of retrofit needed to mitigate excessive floor vibrations. The properties of VE materials were presented, followed by application for retrofitting wood floors. Detailed work on steel–concrete floors was presented next. A shake table was used to test composite steel–concrete beams at low acceleration levels representative of those seen in floor systems.

An example of a steel beam and concrete-slab floor panel was used to show the applicability of an FRP/VE retrofit. Using ANSYS, simplified versions of a beam and a girder were developed. The strain energy values were used to determine the overall floor system's damping loss factor. With the aid of a commercial floor vibration program, several VE/CFRP retrofits were considered. Using the shake-table experimental data (or Bachmann's data) and Murray's higher damping values, two different retrofit schemes were suggested that satisfied the maximum acceleration limit for an office floor.

REFERENCES

3M (1999), *Viscoelastic Damping Polymers 110- 120- 130-*, Bonding Systems Division, St. Paul, MN.

ANSYS (2006), *ANSYS 10.0 Documentation*, ANSYS Inc., Canonsburg, PA.

Aref, A. J. and Jung, W.-Y. (2006), Advanced composite panels for seismic and vibration mitigation of existing structures, *Journal of Engineering Materials and Technology*, 128(4), 618–632.

Bachmann, H. et al. (1995), *Vibration Problems in Structures: Practical Guidelines*, Birkhauser Verlag, Berlin, Germany, p. 166.

Breukelman, B. and Haskett, T. (December 2001), Good vibrations, *Civil Engineering—ASCE*, 71(12), 55–59.

Caldwell, D. B. (1986), Viscoelastic damping devices proving effective in tall buildings, *Engineering Journal—American Institute of Steel Construction*, 23(4), 148–150.

Chang, K. C., Soong, T. T., Oh, S.-T., and Lai, M. L. (October1995), Seismic behavior of steel frame with added viscoelastic dampers, *Journal of Structural Engineering—American Society of Civil Engineers*, 121(10), 1418–1426.

Ebrahimpour, A. and Martell, J. L. (2003), Retrofitting floors with advanced materials to mitigate occupant-induced vibrations, *Proceedings*, *Structures Congress 2003, ASCE*, Washington, DC, May 29–June 1.

FLOORVIB2 (1997), *User's Manual*, Version 1.0, Structural Engineers Inc., Radford, VA.

Foschi, R. O., Neumann, G. A., Yao, F., and Folz, B. (1995), Floor vibration due to occupants and reliability-based design guidelines, *Canadian Journal of Civil Engineering*, 22, 471–479.

Gibson, R. F. (1992), Damping characteristics of composite materials and structures, *Journal of Materials Engineering and Performance*, 1(1), 11–20.

Gibson, R. F. (1994), *Principles of Composite Material Mechanics*, McGraw-Hill Inc., New York, pp. 402–408.

Martell, J. L. (2002), Experimental and analytical study on mitigating floor vibrations using advanced materials, MS thesis, College of Engineering, Idaho State University, Pocatello, ID.

Murray, T. M. (November1979), Acceptability criterion for occupant-induced floor vibrations. *Sound and Vibration*, 13(11), 24–30.

Murray, T. M., Allen, D. E., and Ungar, E. E. (2003), *Floor Vibrations Due to Human Activity*, Steel Design Guide Series 11, American Institutes of Steel Construction, Chicago, IL, 69p.

Tedesco, J. W., McDougal, W. G., and Ross, C. A. (1999), *Structural Dynamics: Theory and Applications*, Addison Wesley Longman, Menlo Park, CA.

Ungar, E. E. and Kerwin, E. M., Jr. (1962), Loss factors of viscoelastic systems in terms of strain energy, *Journal of the Acoustical Society of America*, 34(2), 954–958.

Wiegman, B. and Ebrahimpour, A. (2004), Shake table study of steel–concrete floor beams with constrained treatment, *Proceedings*, *46th Idaho Academy of Science Meeting*, Pocatello, ID, March 25–27.

Wiegman, B. (2005), Experimental study of steel–concrete floor beams with constrained treatment, MS thesis, College of Engineering, Idaho State University, Pocatello, ID.

19 Durability

Luke S. Lee and Hector Estrada

CONTENTS

INTRODUCTION

Durability issues regarding externally bonded fiber-reinforced polymer (FRP) composites in civil infrastructure continue to cast doubt about the effectiveness and long-term performance of FRP-rehabilitated components. For several decades, researchers have engaged in identifying degradation mechanisms and predicting the time-dependent response of FRP composite materials under multiple exposure conditions in order to characterize the effectiveness, or ineffectiveness, of the material in environments indicative of civil infrastructure (Bank et al. 1995, Liao et al. 1998, Weitsman and Elahi 2000, Karbhari 2007).

The attractiveness of FRP composites as construction materials is derived from a set of advantages in terms of material properties and use in field applications, which include (1) high strength-to-weight and stiffness-to-weight ratios, (2) enhanced fatigue life, (3) corrosion resistance, and (4) potential lower life cycle costs (see Chapter 6). The lightweight of the material and a variety of available manufacturing processes are especially advantageous for construction purposes, particularly where these materials can be fabricated in highly uncontrolled environments (Karbhari 2007), such as in wet lay-up for flexural strengthening using externally bonded CFRP composites, as shown in Figure 19.1. A rehabilitation strategy, such as flexural strengthening of an RC bridge girder with FRP composites, can be performed without interference of the intended operation of the structure, that is, no interference with traffic. Although significant advantages are realized with FRP composites for strengthening and repair, questions regarding the effectiveness of using FRP composites remain, particularly in long-term properties.

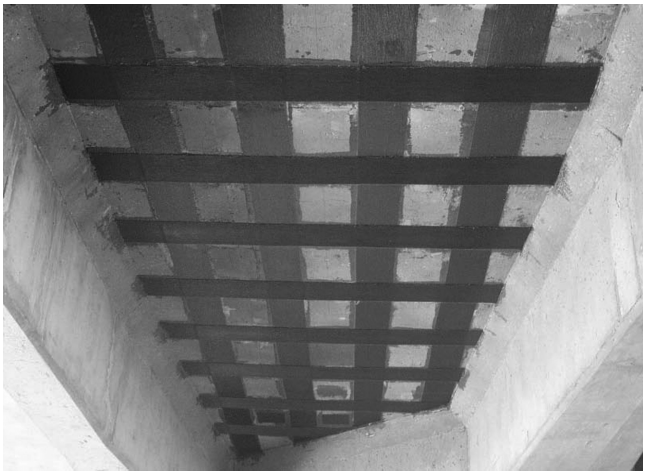

FIGURE 19.1 Bridge deck rehabilitation with externally bonded CFRP composites.

It is widely known that externally bonded FRP composites can be utilized to increase the capacity of existing and/or deficient infrastructure systems and components. However, the uncharacterized durability of the FRP composite material and the long-term performance of rehabilitated infrastructure systems remain the primary obstacle in widespread acceptance of the material for civil engineering systems.

Composite materials have been successfully developed and adapted in aerospace, automotive, industrial, electrical, military, sporting, and marine industries. However, the loading conditions, environment, and manufacturing/construction techniques for civil infrastructure are significantly different, particularly long-term performance (Karbhari et al. 2003). Furthermore, the expectation for useful service life can be 50 years or more.

The expected service life and stationary nature of civil infrastructure presents a unique challenge to the issue of durability where environmental conditions can be singular or involve a multitude of exposures. One of the advantages of externally bonded FRP composites is that potential benefits exist for a diverse number of applications where the material can be used to strengthen or retrofit an existing structure; some of these applications include (1) flexural and shear strengthening of reinforced concrete structure; (2) use of FRP materials as structural liners (Lee et al. 2002) or as crack arrestors (O'Donoghue and Zhuang 1999) in above- and belowground piping components; (3) FRP materials bonded to steel members as stiffeners and crack overlays to increase fatigue performance (Fawzia et al. 2006, Zhao and Zhang 2007); (4) FRP composites bonded to external surfaces of RC columns as a barrier to prevent the migration of chlorides and thus slow the onset of corrosion of the steel (Herrador and Karbhari 2004); and (5) FRP composites bonded to vehicles and structures for blast protection and mitigation (Buchan and Chen 2007). Due to the diverse number of applications, the FRP composite material itself is likely to be subject to multiple harsh, changing conditions over its expected life. These environments can be categorized as follows (Bank et al. 1995, Liao et al. 1999, Karbhari et al. 2003):

- Moisture/solution
- Alkaline environment
- Thermal effects
- Fatigue
- Creep/relaxation
- UV radiation

The contribution of FRP composite material durability research, in the context of civil infrastructure, is to characterize the time-dependent changes in material properties and utilize this information to efficiently design rehabilitation strategies that successfully extend the service life of existing structural components and systems. The durability of the FRP composite material is an integral part in estimating the remaining service life of FRP-rehabilitated structures. An ability to estimate the service life of an FRP-rehabilitated component provides a means to quantify the influence of local material degradation mechanisms on the ability of a structural component to continue performing its intended function.

This chapter emphasizes durability issues associated with externally bonded FRP composites and discusses approaches to predict remaining service life using material-level predictions. Therefore, the goal of this chapter is to examine issues affecting the durability of FRP-rehabilitated components in the built environment and consider the influence of composite material durability on the performance of rehabilitated structural component in terms of service life. In order to accomplish the goal of this chapter, an overview of the damage mechanisms of composite materials associated with each of the aforementioned environmental conditions is discussed. Then, a framework for probabilistic service life estimation of FRP-rehabilitated components is presented as a means to integrate prediction models of the composite material in order to quantify the reliability of FRP-rehabilitated components over time.

DURABILITY ISSUES

The diverse number of applications and the harsh changing conditions characteristic of the built environment make a complete durability characterization of FRP materials in civil infrastructure a challenging prospect. Over the past three decades, researchers have engaged in the investigation of damage mechanisms and degradation behavior of FRP composites subject to a variety of exposure conditions that are singular or synergistic. A number of publications are readily available that detail the material performance of the FRP composites in the built environment. Some reviews regarding durability are listed here, but is by no means exhaustive (Bank et al. 1995, Liao et al. 1998, Weitsman and Elahi 2000, Karbhari 2007). This section provides a summary of known FRP composite responses to anticipated environmental exposures of externally bonded composites in civil infrastructure.

Moisture/Solution

When exposed to moisture or solution, the polymer matrix of a composite is known to undergo reversible and irreversible changes via hydrolysis, plasticization, saponification, and other mechanisms (Liao et al. 1998, Karbhari et al. 2003). In particular, the absorption of moisture causes plasticization, which is characterized by a decrease in the glass transition temperature, T_g, and mechanical properties of the polymer matrix. This is primarily caused by the interruption of Van der Waals bonds between polymer chains (Bank et al. 1995, Silva and Biscaia 2008) and contributes to the decrease in matrix-dominated properties of a composite. This behavior has been observed in epoxy, polyester, and vinylester resins, which are the most often used in composite materials for construction (Browning et al. 1977, Bank et al. 1995, Liao et al. 1998, Karbhari 2007).

Other influences of moisture include the swelling of the matrix region, which can induce stresses similar to thermal responses and result in microcracking in the matrix, again leading to a decrease in matrix-dominated properties (Kajorncheappungam et al. 2002). In some instances, the moisture can wick along the fiber matrix interface and induce interphase cracking that results in debonding between fiber and matrix (Weitsman and Elahi 2000). Debonding between fiber and matrix can lead to premature failure of the composite in the fiber direction and loss of load transfer across fibers. Furthermore, glass fibers are known to degrade when exposed to moisture. This degradation is initiated by moisture extracting ions resulting in a potential loss of thermo-mechanical properties of the

fibers (Bank et al. 1995, Kajorncheappungam et al. 2002). Also since aramid fibers are polymers, they can absorb moisture, which can eventually result in fibrillation of the fibers. On the other hand, carbon fibers do not absorb moisture and are resistant to chemical attack making them particularly robust in changing environmental conditions characteristic of civil infrastructure (Liao et al. 1998).

Alkaline Environment

With the high usage of FRP composites to restore reinforced concrete structures, externally bonded composites will likely come in contact with water contaminated with concrete, the solution of which can have pH values as high as 13.5 (Karbhari et al. 2003). The influence of the alkaline environment depends on the matrix and fibers used in the composites. Glass fibers are particularly susceptible to alkaline attack, inducing greater levels of irreversible damage, which are characterized by high levels of fiber surface degradation and pitting. When exposed to alkaline environments, glass fibers can also undergo leaching, where alkali ions diffuse out of the glass structure essentially dissolving the fiber (Silva and Biscaia 2008). Alkaline solutions also cause degradation of the resin and interphase (Chu et al. 2004).

Temperature Effects

An increased viscoelastic response is observed for composite materials exposed to elevated temperatures where softening of resins or adhesives occurs. In addition, the softening of the polymer is associated with a reduction in mechanical properties and increased rates of moisture diffusion, which can accelerate damage mechanisms of the polymer (Karbhari et al. 2003). Some elevated temperature effects can be beneficial, such as post-cure of resins; however, with the combination of high temperatures and moisture immersion, the residual effects of post-cure can be negated by rapid deterioration (Karbhari and Abanilla 2007). Furthermore, when composite materials are exposed to high temperatures (>100°C), the matrix softens leading to distortion, buckling, and potentially failure of load-bearing elements. At temperatures in the range of 250°C–400°C, near the pyrolysis temperature of the matrix, ignition of the composite can occur (Mouritz 2007).

FRP composites exposed to freezing conditions can result in matrix hardening, matrix microcracking, and fiber–matrix bond degradation. Freeze–thaw conditions can accelerate the degradation of composite properties especially when coupled with expansion and contraction associated with the absorption of moisture and/or salt deposits (Karbhari et al. 2003).

UV Radiation

Polymers used in outdoor applications are susceptible to photo-initiated oxidation leading to surfaced degradation (Chin et al. 1997). While this degradation is usually confined to the top few micrometers of the surface, flaws from the surface can cause stress concentrations and result in premature fracture (Karbhari et al. 2003). UV radiation is a component of the natural weathering process and is often accompanied by changes in temperature, moisture, chemical agents, and microorganisms (Liao et al. 1998). To protect against UV radiation, FRP composites are typically protected by a coating or gel coat, which serves as a sacrificial layer to prevent the FRP composite from being directly exposed to UV (Karbhari et al. 2003). The protective coating requires routine maintenance because it is not resistant to UV radiation degradation.

Fatigue

Fatigue of externally bonded FRP composites includes mechanical fatigue, where a periodic mechanical load is applied, and environmental fatigue, which involves temperature cycles (i.e., hot–cold, freeze–thaw) or chemical cycles (i.e., moisture, seasonal road treatments, oxidation, NO_x effects)

(Liao et al. 1998, Karbhari et al. 2003). Mechanical fatigue in composites is progressive and accumulative in nature, as opposed to crack growth behavior observed in metals. Under fatigue loads, composites can experience microcracking, delamination, fiber fracture, and fiber/matrix debonding (Zhou et al. 2007). In general, it has been observed that composites with higher modulus fibers display greater fatigue resistance; hence, carbon fibers exhibit slower stiffness and strength degradation under mechanical fatigue (Zhou et al. 2007).

Creep and Relaxation

Creep mostly affects matrix-dependent properties, which makes FRP composite materials more susceptible to creep because resins and adhesives are integral to composite manufacturing and construction (Morgan et al. 2001). The occurrence of creep in polymeric composites can be attributed to a combination of bulk material strain and microflaw initiation (such as fiber–matrix debonding and cracking); both of the mechanisms are time-dependent due to the viscoelastic nature of the polymer (Barnes and Garden 1999). Aramid and glass fibers are known to have higher susceptibility to creep rupture at lower stress levels than carbon fibers (Karbhari et al. 2003). Of particular importance is the creep behavior of under-cured resins, since a majority of externally bonded FRP composite applications rely on ambient cure. Under-cured composites have a higher susceptibility to creep and microcrack initiation at the early stages of service.

Bond Durability

While external bonding of FRP composites significantly increase the load-bearing capacity of existing structures (Stallings et al. 2000), questions regarding long-term durability have hindered widespread adoption of this material in infrastructure applications. In particular, the long-term performance of the bond between FRP and substrate is unknown, yet it significantly influences the failure behavior of a repaired structure because any failure in the stress transmission zone would render the advantageous properties of FRP composites useless.

The increase in load-bearing capacity of RC members with externally bonded FRP composites is well documented in the literature (Stallings et al. 2000, Teng et al. 2003). Traditional beam bending failure is initiated as stresses in the tension zone reach the yield strength of the material or when compressive stresses reach the compressive strength of the material. However, for members strengthened with externally bonded FRP composites for flexure and shear (Figure 19.2), debonding of the FRP composite from the substrate material can lead to brittle failure of the structure. FRP-strengthened RC members are susceptible to additional failure modes besides conventional concrete compression failure or fracture of the FRP material (Ueda and Dai 2005), including (1) plate-ended failure or concrete cover delamination, (2) anchorage failure, and (3) midspan debonding, where interface debonding initiates from the tips of flexural cracks (Smith and Teng 2002, Ueda and Dai 2005, Toutanji et al. 2007). While conventional failure modes would allow the rehabilitated

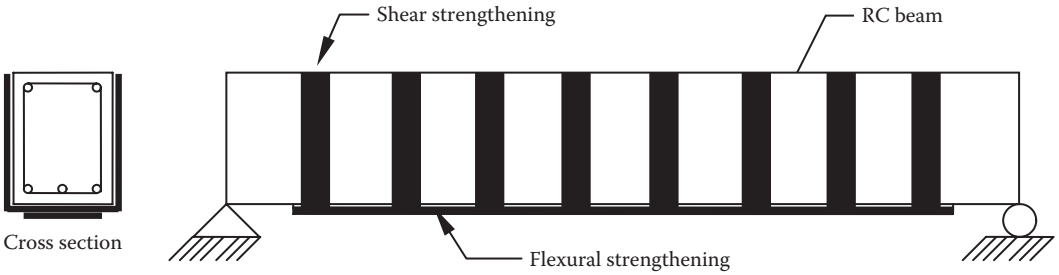

FIGURE 19.2 Schematic of RC beam strengthened with FRP composites.

structure to achieve its projected capacity, a bond failure of the FRP-rehabilitated component results in premature brittle failure (Davalos et al. 2006).

While considerable effort is being placed on the development of codes and guidelines for FRP rehabilitation (*fib* 2001, ACI 2002) that consider the as-built integrity of the rehabilitated structure, the long-term effectiveness and durability of the rehabilitation component remain relatively unknown. Extensive research has been conducted on modeling and predicting bond failure of as-built FRP composites bonded to concrete structures (Smith and Teng 2002, Teng et al. 2003, Sharma et al. 2006); however, information regarding the time-dependent behavior of FRP bonding systems is limited. Time-dependent bond performance is critical in rehabilitation because it directly impacts the safety of all structures repaired with externally bonded FRP composites and will ultimately alter the criteria used to design the rehabilitation component. Myers (2007) provides a good review of durability studies emphasizing the bond integrity of externally bonded FRP composites.

Characterizing the time-dependent durability of the interface bond from substrate material to the FRP composite is critical since organic polymers are typically used as the adhesive to transfer shear stresses between the two components (Toutanji et al. 2007). In addition, the integrity of the bond is likely to change as a function of environment since the composite, the polymer bond layer, and the substrate are three different materials, and interfacial stresses develop as permanent damage accumulates. The role of temperature and moisture on the bond performance of FRP composites to concrete is of particular concern since mismatches in coefficients of thermal expansion and moisture expansion can lead to the development of interfacial stresses that reduce the overall capacity of the bond. Most of the literature on durability of the bond has emphasized synergistic effects of moisture and temperature, but not the adverse effect of these environmental conditions.

Polymers, when exposed to moisture, are susceptible to the physical effects of plasticization and swelling, which can lead to the development of microcracks as well as increasing the creep compliance, affecting the performance of the rehabilitated structure over time. The microcracks in the bond layer provide a path through which more aggressive solutions (like saline solutions from deicing salts) can diffuse between the interfaces of the bond layer and substrate or the bond layer and FRP composite (Al-Dulaijan et al. 2001). For epoxy adhesives used to bond prefabricated FRP composites to surfaces, the presence of hydrophilic groups in the adhesive is known to cause degradation in mechanical properties due to moisture uptake because these groups react with water to form weak hydrogen bonds (Yang et al. 2008). The influence of moisture has been observed to significantly decrease tensile strength and tensile modulus of epoxy adhesives, with retentions of initial tensile strength at 57% and initial tensile modulus at 63% when immersed in water at 23°C. In cases where moisture is coupled with elevated temperatures, the degradation in mechanical properties of the adhesive was observed to increase with only 31% and 31.7% retention of initial tensile strength and tensile modulus, respectively (Yang et al. 2008).

Freeze–thaw cycles have been observed to accelerate the bond degradation in the presence of moisture with progressive damage leading to decreases in load-carrying capacity and reductions in the length of the cohesive stress transfer zone between FRP composite and structure (Silva and Biscaia 2008, Subramanian et al. 2008). Bond durability studies with freeze–thaw cycling coupled with moisture have observed that the decrease in the strength of rehabilitated components is associated with the degradation of the concrete rather than the FRP material (Myers 2007).

Characterizing bond durability may require evaluation beyond traditional limit state approaches, since moisture-affected debonding can result in material decohesion and interface separation (Silva and Biscaia 2008).

SERVICE LIFE ESTIMATION

Durability evaluation of FRP composite materials involves exposing specimen to environments varying in terms of temperature, moisture level, chemical solution, stress levels, and time. While a number of research programs (CERF, HITEC, and Caltrans) have been conducted in recent years

to evaluate the long-term changes in material properties (such as tensile modulus, tensile strength, interlaminar shear strength, flexural strength, and modulus), understanding the influence of material durability on the long-term performance of FRP-rehabilitated structural components and the design of the rehabilitation is relatively unknown. Furthermore, the influence of the surrounding environment on the long-term performance of an FRP-rehabilitated structural component is unknown, and the influence of durability on structural safety is unknown.

The quality of an FRP rehabilitation has implications on the ability of the structure to perform as required, that is, accommodate increased load demands and/or avoid a specific failure mode. The variation in material parameters of the applied FRP composite and degradation of material properties over time provide a level of uncertainty about the ability of the structure to perform as intended over the expected design life. Design safety margins are directly affected by variation in material properties (Plevris et al. 1995), while issues related to durability and aging of materials in an FRP-strengthened structure limit its service life. An understanding of the reliability, capacity, and remaining service life helps to determine if an FRP rehabilitation is able to perform as material degrades.

Material degradation models can be integrated into life cycle performance models as proposed by Hastak et al. (2003) and Frangopol et al. (2003). A general framework for evaluating life cycle performance of a component is shown in Figure 19.3 and is discussed in more detail in Chapter 6.

The durability data at the material level can be used to develop performance curves (as illustrated in Figure 19.4) for representative structural components in order to ascertain how the safety of the structure degrades, in terms of failure probability, as the bond between FRP and composite degrades over time. For the hypothetical situation shown in Figure 19.4, a structural member's performance or safety can be related to a level of damage, which is detectable and known at the as-built state. As the structure serves its intended function, a time-dependent decrease in component performance can occur due to weathering, aging, fatigue, etc. When a specified performance limit is reached, a maintenance or rehabilitation strategy is selected. If FRP rehabilitation is selected for the structure following construction and manufacturing, the increase in capacity can be estimated according to design formulations and a performance level after rehabilitation. The rate of performance degradation, a, b, or c will depend on the selection of constituent materials for the composite,

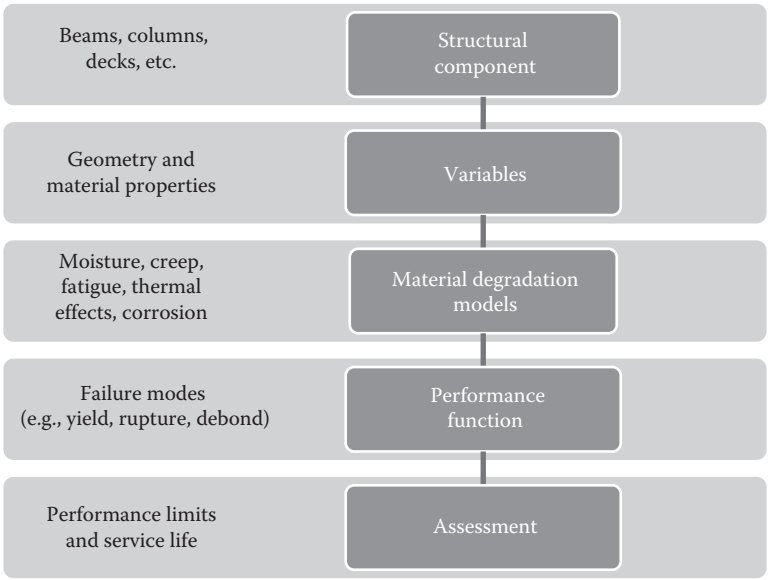

FIGURE 19.3 Overview of service life estimation approach.

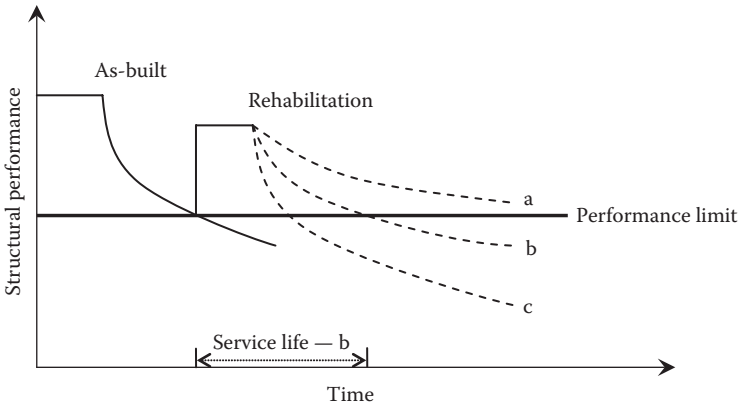

FIGURE 19.4 Schematic of structural performance for an FRP-rehabilitated component.

quality of rehabilitation, environment of the structure (i.e., cold regions, marine environments, wet, desert, etc.), as well as the degradation of other materials that are part of the rehabilitated structure. Performance curves developed from this durability data will aid engineers in determining appropriate levels of FRP rehabilitation to ascertain a specific level of safety and desired service life extension.

Not only does an estimate of the service life of a rehabilitated component provide a quantitative measure of durability, but it also provides the basis for establishing appropriate inspection intervals and evaluation of life cycle costs for purposes of decision making with regard to material selection, replacement, repair, or FRP rehabilitation design based on a specified life extension. The estimation of the remaining service life not only provides a means to assess the criticality of existing structures, but can also act as a design tool to determine adequate levels of rehabilitation with respect to the reliability of the system and desired extension of service life for an existing deficient structure. As a general rule, a methodology for estimating the remaining service life of a system must be able to incorporate unbiased field observations (e.g., nondestructive test data) such that a correlation between field measurements and life prediction exists.

Probabilistic Approach to Service Life Estimation

There are many sources of variability in FRP composites when used in any application, but there are even more sources of variability in rehabilitation applications given that the composite is manufactured on-site. Variation in mechanical properties (e.g., ultimate tensile strength and modulus of elasticity) and geometry (thickness and fiber orientation) can cause significant deviations from the intended design performance of FRP rehabilitation and increase the probability of failure, or adversely affect the safety of the structure. The use of a probabilistic approach to service life estimation allows for the development of predictive models at a structural level that can integrate material-level predictive models and the variability of composite material properties; this is especially critical in cases where wet lay-up techniques are used to construct the externally bonded composite (Atadero et al. 2005).

Quantification of the uncertainty caused by different types of variation and their impact on performance is critical in decision making and materials selection, and most importantly in establishing the safety (reliability) of the structure. One technique for quantifying all uncertainties associated with the variations is the use of the reliability index, β. This is part of structural reliability methods and is based on materials, loading, and configuration of the structure (Atadero et al. 2005). A number of approximation techniques such as mean value, second moment first-order and second-order

methods are well established and available to calculate β (Melchers 1999). The failure probability, p_f, of a structural component is related to β through the standard normal distribution, Φ, as follows:

$$p_f = \Phi(-\beta) \tag{19.1}$$

Higher values of β indicate a higher degree of structural reliability or safety for a given limit state, which can be quantified and presented in equation form. The basic structural reliability problem considers a load effect defined by S and resisted by resistance, R. These are both described by probability distribution functions f_S and f_R, respectively. In general, R is a function of random variables describing material properties and cross-section geometry, while S is a function of random variables describing applied loads, material densities, and geometry of the structure (Melchers 1999). The probability of failure of a structural component or member is defined as the probability that a limit state or performance function will be violated and can be formulated as

$$p_f = P\left[g(R,S) \le 0\right] \tag{19.2}$$

where

$g(R,S)$ is defined as the performance function

probability of failure, p_f, is the probability that the performance function is less than or equal to zero

Evaluation of the probability of failure utilizes measures of marginal probability density functions f_R and f_S for R and S, respectively, and a joint probability density function $f_{RS}(r,s)$. Definitions and explanations for density functions and joint density functions are available in standard probability theory texts (Rosenkrantz 1997). The failure probability of the performance function is defined as follows (Melchers 1999):

$$p_f = P\left[g(R,S) \le 0\right] = \dagger \int_{R-S \le 0} f_{RS}(r,s)drds \tag{19.3}$$

The generalized reliability problem requires the grouping of random variables into resistance and load functions, with the resistance, R being a function of random variables, X_i, representing material properties and dimensions:

$$R(X_i) \quad \text{for } i = 1,\ldots,n \text{ number of random variables}$$

Similarly, the load, S, on a structure is a function of random variables, X_i, representing applied loads, material densities, and possibly geometry of the structure.

$$S(X_i) \quad \text{for } i = 1,\ldots,n \text{ number of random variables}$$

The performance function of the reliability problem is then conveniently expressed as a function of all relevant basic random variables:

$$Z = g(R,S) = g(X_1,\ldots,X_n) = g(\vec{X}) \tag{19.4}$$

where $\vec{X}$ is the vector of random variables with probability distributions, $f_{\vec{X}}(\vec{x})$. With the performance function or limit state function in terms of n random variables, the calculation for the probability of failure is formulated as

$$p_f = P\left[g(\vec{X}) \le 0\right] = \int \cdots \int_{g(\vec{X})\le 0} f_{\vec{X}}(\vec{x})d\vec{x} \tag{19.5}$$

where $f_{\vec{X}}(\vec{x})$ is the joint probability density function for the n-dimensional vector, $\vec{X}$, of random variables in the performance function. As in the basic reliability formulation, the region of integration $g(\vec{X}) \le 0$ defines the failure domain or "unsafe" region and $g(\vec{X}) > 0$ is the "safe" region. Typically, the solution for the earlier integral is determined numerically, using Monte Carlo simulations, or by avoiding the integration problem with a transformation of the density function, $f_{\vec{X}}(\vec{x})$, to a multi-normal probability density function and approximating the probability of failure. Methods that incorporate the latter include first-order second moment method, first-order reliability methods (FORMs), and second-order reliability methods (SORMs).

Component Service Life

By utilizing time-dependent variables in reliability analysis, it is possible to calculate the change in reliability index as a function of time, $\beta(t)$. Specifically, time dependence may be introduced from predictions for degradation of material parameters such as loss in steel corrosion or, in the case of CFRP composites, potential degradation of mechanical properties due to environmental exposure. Formulation of a time-dependent reliability analysis for service life estimation of FRP-rehabilitated components requires identification of the following: (1) identification of random variables and statistical descriptions; (2) selection of appropriate material degradation models; and (3) application of failure modes to define appropriate limit state equations. The emphasis of the service life estimation should be placed on structural components (beams, columns, slabs, etc.) according to Richard et al. (2007) since (1) a performance measure for an entire structure provides little value with respect to the selection of maintenance and repair actions and (2) if needed, each of the component service life analyses can be included into a framework for overall structural performance using a fault-tree approach.

Random Variables

The random variables of a rehabilitated component can be separated into resistance and demand variables. The resistance variables of a component are those material and geometric properties that contribute toward the capacity of a structural component. The demand variables represent the required capacity for a particular limit state and are associated with the applied loads on the structure.

The most important aspect of a random variable is its characteristic statistical properties (i.e., mean, variance, and probabilistic distribution parameters), which are used to describe the variation of the property. For instance, composites fabricated using the wet lay-up process are susceptible to large variations in mechanical properties due to the nature of the manual process, with coefficients of variation observed to be as high as 13% for both tensile strength and tensile modulus (Atadero et al. 2005).

Material Degradation Models

The time dependence and predictive basis for component behavior are directly attributed to models based on durability tests at the material level. Bank et al. (1995) provide a summary of predictive models for a particular material characteristic of FRP composites, which includes mechanics-based, chemical-based, accelerated, and long-term verification models. Of these, accelerated aging models are the most commonly used for predictive modeling.

Accelerated aging tests typically involve the exposure of the composite material to elevated temperatures and moisture, where the elevated temperature acts as a forcing function in a time–temperature superposition approach (Gentry et al. 2002, Karbhari and Abanilla 2007). An Arrhenius

relationship has been used by investigators to predict long-term performance of polymer-based composites where moisture diffusion is Fickian. This method relates the material performance to temperature in an inverse logarithmic form, over time, that is, time–temperature superposition. The prediction of material properties using an Arrhenius method results in equations of the following form (Karbhari and Abanilla 2007):

$$P(t) = \frac{P_o}{100}\left[A\ln(t) + B\right]\dagger \quad \text{for } t > 0 \tag{19.6}$$

where

$P(t)$ and P_o are performance attributes or material properties at time t and 0, respectively
A is a constant denoting degradation rate
B is a constant reflecting the early effects of post-cure

This is a semiempirical mechanism-based modeling approach. The model uses relevant known and observed phenomena to capture the first-order effects of interest thought parameters A and B, which should be obtained using a minimum series of short-term accelerated tests. To accelerate these tests, an environmental chamber is typically used, where the specimens can be subjected to changing moisture and temperature as a function of time. To model the effect of temperature and moisture transport in composites, the transport properties discussed in Chapter 4 can be used.

While FRP composites are the primary focus in this durability discussion, it should be noted that degradation models for other materials within a component can be included in the framework for service life prediction (i.e., loss of area due to steel corrosion) in order to asses combined effects.

The selection of material degradation models or inclusion of empirical data should reflect the environment where the rehabilitation is to take effect. For instance, where combination of high temperature and high humidity are anticipated, prediction models developed from moisture and temperatures would be considered most appropriate for the constituent materials selected in the rehabilitation.

Application

The development of a service life estimate for an FRP-rehabilitated component depends on the environment, loading conditions, and limit states of the structure. A number of service life prediction examples and methodologies are readily available in the literature that deals with structures where steel components or reinforcement is corroding (Ahmmad and Melchers 1994, Frangopol et al. 2003, Lee et al. 2010). In this section, the application of the service life–based procedure is highlighted for FRP composites externally bonded to structural components.

Atadero et al. (2004) applied a mean value, first-order reliability approach to compare the influence of variation in material properties of wet lay-up, field-manufactured CFRP composites. An Arrhenius rate model was used to predict the deterioration of CFRP composite tensile strength and tensile modulus. The CFRP rehabilitation, using field-measured properties, was designed for a simply supported beam with an anticipated increase in live load of 50%, which is based on Example 14.3—Flexural Strengthening of an interior beam in ACI 440R-02. Three designs using wet lay-up manufactured CFRP properties and variation were integrated with the probabilistic approach with statistical properties characteristic of one-layer and two-layer field-manufactured composites. It was observed that the initial reliability and overall durability of the component decreased with increasing coefficients of variation for as-built material properties with similar geometric cross-sectional areas of CFRP. Table 19.1 and Figure 19.5 summarize reliability results, and time-dependent performance observed (Atadero et al. 2004).

Lee et al. (2010) utilized a time-dependent FORM in order to compare the performance of FRP piping components subject to moisture versus steel pipes subject to corrosion. The influences of fiber volume fraction of the composite and material degradation were considered for hoop strength

TABLE 19.1
Reliability Index Results with Associated Geometry and Tensile Modulus

Design	*X*-Section Area of CFRP (cm^2)	Modulus Mean (GPa)	Modulus COV (%)	Reliability Index (β)			
				0 Year	1 Year	5 Years	10 Years
1B	3.328	70.36	13.42	3.32	3.247	3.215	3.201
2A	4.462	65.78	11	3.46	3.389	3.358	3.345
2B	3.343	78.96	9.12	3.42	3.345	3.313	3.299

Source: Atadero, R.A. et al., Effect of variability of composite properties on wet layup based rehabilitation of concrete structures, in *Proceedings of the ASC-ASTM D30 Joint 19th Annual Technical Conference*, Atlanta, GA, October 17–20, 2004.

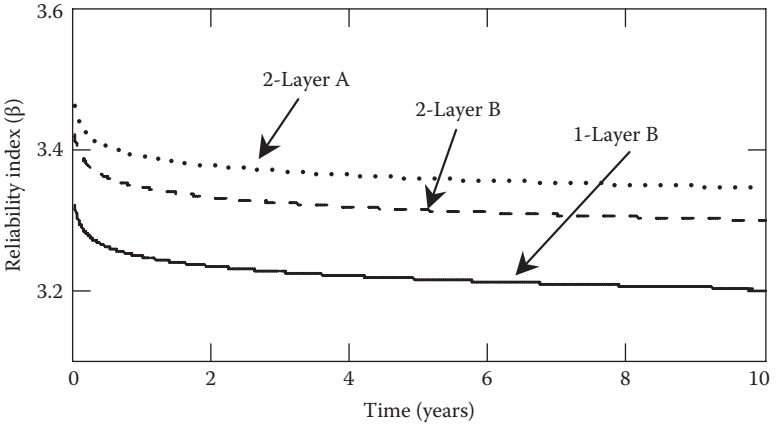

FIGURE 19.5 Time-dependent reliability of CFRP-strengthened RC beam. (From Atadero, R.A. et al., Effect of variability of composite properties on wet layup based rehabilitation of concrete structures, in *Proceedings of the ASC-ASTM D30 Joint 19th Annual Technical Conference*, Atlanta, GA, October 17–20, 2004.)

in an FRP piping component. The study was an extension of the time-dependent reliability analysis conducted by Ahmmad and Melchers (1994), who evaluated the lifetime performance of steel pipes subject to corrosion using a FORM. In the FRP composite pipe analysis, Arrhenius rate models for CFRP material degradation were used to model tensile modulus and ultimate strength. As shown in Figure 19.6, the fiber volume fraction achieved during manufacture will determine if a CFRP pipe can exceed the performance of a steel pipe over its lifetime.

Both studies illustrate the use of probability-based predictive approaches for an initial approximation to long-term performance of externally bonded FRP composites. These examples also demonstrate a potential tool for decision making with respect to design, selection of materials, and selection of manufacturing processes. However, these examples have considered only a single performance function or limit state with respect to component behavior (i.e., moment capacity in the case of the beam and hoop stress for the pipe) and considered only degradation of FRP composite as opposed to combined degradation models. A full characterization of the influence of FRP material durability requires consideration of multiple limit states simultaneously as well as multiple degradation models for the various materials present in the structural component. It is important to note that the predictive methodologies are only as robust as the predictive material deterioration models developed from durability characterization at the material level and, most importantly, the properties used to calibrate these models (Richard et al. 2007).

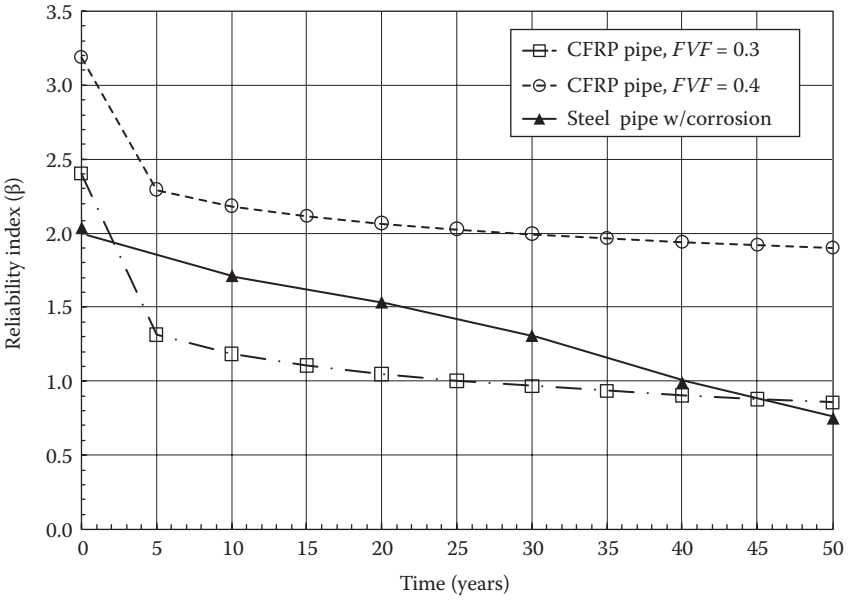

FIGURE 19.6 Time-dependent reliability results of CFRP-rehabilitated pipe vs. steel pipe with corrosion. (From Lee, L.S. et al., *ASCE J. Compos. Constr.*, 14(3), 272, 2010.)

CONCLUSIONS

In this chapter, issues regarding the durability of an FRP-rehabilitated component were described at the material level as well as an approach to predict time-dependent performance in terms of failure probability. The uncharacterized durability of FRP composite systems continues to hinder the adoption of polymer-based composites in civil infrastructure.

As externally bonded reinforcement, FRP composites are intended to enhance the useful life of structures constructed of traditional civil materials (i.e., steel, concrete, and timber). Research in the durability of FRP composite materials has evolved from single exposure to an emphasis on synergistic conditions that evaluate the combined effects of moisture, temperature, physical aging, and fatigue effects. The lack of established testing procedures and acceptance criteria for material and bond durability has led to challenges with regard to integrating research into design practices, which often leads to overly conservative designs with the use of "knockdown" factors. As time-dependent models of material performance emerge, the overall response of an FRP rehabilitation in a specific environment can be readily assessed to select an appropriate design, anticipate maintenance actions, and estimate life cycle costs. The availability of predictive models for material behavior is particularly important as materials continue to evolve (e.g., nanocomposites, fillers, natural fibers) and are introduced to infrastructure applications.

REFERENCES

ACI—American Concrete Institute (2002), *Guide for the Design and Construction of Externally Bonded FRP Systems for Strengthening Concrete Structures*, ACI 440.2R-02, Emerging Technology Series, Reported by ACI Committee 440, Farmington Hills, MI, October, First Printing.

Ahmmad M and Melchers R E (1994), Probabilistic analysis of underground pipelines subject to combined stresses and corrosion, *Engineering Structures*, 19(12), 988–994.

Al-Dulaijan S U, Al-Zahrani M M, Nanni A, Bakis C E, and Boothby T E (2001), Effect of environmental precondition on bond of FRP reinforcement to concrete, *Journal of Reinforced Plastics and Composites*, 20(10), 881–900.

Atadero R A, Lee L S, and Karbhari V M (2004), Effect of variability of composite properties on wet layup based rehabilitation of concrete structures, in *Proceedings of the ASC-ASTM D30 Joint 19th Annual Technical Conference*, Atlanta, GA, October 17–20, 2004.

Atadero R A, Lee L, and Karbhari V M (2005), Consideration of material variability in reliability analysis of FRP strengthened bridge decks, *Composite Structures*, 70, 430–443.

Bank L C, Gentry T L, and Barkatt A R (1995), Accelerated test methods to determine the long-term behavior of FRP composite structures: Environmental effects, *Journal of Reinforced Plastics and Composites*, 14, 559–587.

Barnes R and Garden H N (1995), Time-dependent behaviour and fatigue, in Holloway L C and Leeming M B (eds.), *Strengthening of Reinforced Concrete Structures—Using Externally-Bonded FRP Composites in Structural and Civil Engineering*, Cambridge, U.K.: Woodhead Publishing Ltd., pp. 183–221.

Browning C E, Husman G E, and Whitney J M (1977), Moisture effects in epoxy matrix composites, in *Proceedings of the Fourth Composite Materials: Testing and Design Conference*, American Society of Testing and Materials, Special Technical Publication 617, Valley Forge, PA, 16 pp.

Buchan P A and Chen J (2007), Blast resistance of FRP composites and polymer strengthened concrete masonry structures—A state-of-the-art review, *Composites Part B*, 38, 509–522.

Chin J W, Nguyen T, and Aouadi K (1997), Effects of environmental exposure on fiber-reinforced plastic (FRP) materials used in construction, *Journal of Composites, Technology and Research*, 19(4), 205–213.

Chu W, Wu L, and Karbhari V M (2004), Durability evaluation of moderate temperature cured E-glass/vinylester systems, *Composite Structures*, 66, 367–376.

Davalos J F, Kodkani S S, and Ray I (2006), Fracture mechanics method for mode-I interface evaluation of FRP bonded to concrete substrates, *Journal of Materials in Civil Engineering*, 18(5), 732–742.

Fawzia S, Al-Mahaidi, and Zhao X-L (2006). Experimental and finite element analysis of a double strap joint between steel plates and normal modulus CFRP, *Composite Structures*, 75, 156–162.

fib, International Federation for Structural Concrete (2001), Externally bonded FRP reinforcement for RC structures, Technical Report, Bulletin 14, Task Group 9.3.

Frangopol D M, Bruhwiler E, Faber M H, and Adey B (eds.) (2003), *Life-Cycle Performance of Deteriorating Structures: Assessment, Design, and Management*, American Society of Civil Engineers, ASCE Publications, Reston, VA.

Gentry T R, Bank L C, Thompson B P, and Russell J S (2002), An accelerated-test-based specification for fiber reinforced plastics for structural systems, in *Proceedings of the Second International Conference on Durability of Fiber Reinforced Polymer (FRP) Composites for Construction*, Montreal, Quebec, Canada, May 29–31, 12 pp.

Hastak M, Mirmiran A, and Deepak R (2003), A framework for life-cycle costs assessment of composites in construction, *Journal of Reinforced Plastics and Composites*, 22(15), 1409–1430.

Herrador M F and Karbhari V M (2004), Corrosion mitigation—Can composite wraps serve as an effective mechanism?, in *Proceedings of the 36th International SAMPE Technical Conference—Materials and Processing: Sailing into the Future*, San Diego, CA, pp. 429–443.

Kajorncheappungam S, Gupta R K, and GangaRao H V S (2002), Effect of aging environment on degradation of glass-reinforced epoxy, *Journal of Composites for Construction*, 6(1), 61–69.

Karbhari V M (ed.) (2007), *Durability of Composites for Civil Structural Applications*, Cambridge, U.K.: Woodhead Publishing Ltd.

Karbhari V M and Abanilla A (2007), Design factors, reliability, and durability prediction of wet lay-up carbon/epoxy used in external strengthening, *Composites Part B*, 38, 10–23.

Karbhari V M, Chin J W, Hunston D L, Benmokrane B, Juska T, Morgan R, Lesko J J, Sorathia U, and Reynaud D (2003), Durability gap analysis for fiber-reinforced polymer composites in civil infrastructure, *Journal of Composites for Construction*, 7(3), 238–247.

Lee D G, Chin W S, Kwon J W, and Yoo A K (2002), Repair of underground pipes with resin transfer molding, *Composite Structures*, 57, 62–77.

Lee L S, Estrada H, and Baumert M (May/June 2010), Time dependent reliability of FRP rehabilitated piping, *ASCE Journal of Composites for Construction*, 14(3), 272–279.

Liao K, Schultheisz C R, and Hunston D L (1999), Effects of environmental aging on the properties of pultruded GFRP, *Composites Part B: Engineering*, 30(5), 485–493.

Liao K, Schultheisz C R, Hunston D L, and Brinson L C (1998), Long-term durability of fiber-reinforced polymer–matrix composite materials for infrastructure applications: A review, *Journal of Advanced Materials*, 30(4), 3–40.

Melchers R (1999), *Structural Reliability Analysis and Prediction*, Chichester, U.K.: John Wiley & Sons.

Morgan R, Dunn C, and Edwards C (2001), Effects of creep and relaxation, in *Gap Analysis for Durability of Fiber Reinforced Polymer Composites in Civil Infrastructure*, CERF Report #40578, Washington, DC, pp. 52–59.

Mouritz A P (2007), Durability of composites exposed to elevated temperature and fire, in Karbhari V (ed.), *Durability of Composites for Civil Structural Applications*, Cambridge, U.K.: Woodhead Publishing Ltd., pp. 98–125.

Myers J J (2007), Durability of external fiber-reinforced polymer strengthening systems, in Karbhari V (ed.), *Durability of Composites for Civil Structural Applications*, Cambridge, U.K.: Woodhead Publishing Ltd., pp. 247–283.

O'Donoghue P E and Zhuang Z (1999), A finite element model for crack arrestor design in gas pipelines, *Fatigue & Fracture of Engineering Materials and Structures*, 22, 59–66.

Plevris N, Triantafillou T C, and Veneziano D (1995), Reliability of RC members strengthened with CFRP laminates, *Journal of Structural Engineering*, 121(7), 1037–1044.

Richard D, Hong T, Hastak M, Mirmiran A, and Salem O (2007), Life-cycle performance model for composites in construction, *Composites Part B*, 38, 236–246.

Rosenkrantz W A (1997), *Introduction to Probability and Statistics for Scientists and Engineers*, New York: McGraw-Hill.

Sharma S K, Ali M S, Goldar D, and Sikdar P K (2006), Plate-concrete interfacial bond strength of FRP and metallic plated concrete specimens, *Composites Part B*, 37, 54–63.

Silva M A G and Biscaia H (2008), Degradation of bond between FRP and RC beams, *Composite Structures*, 85, 164–174.

Smith S T and Teng J G (2002), FRP-strengthened RC beams—I: Review of debonding strength models, *Engineering Structures*, 24(4), 385–395.

Stallings J M, Tedesco J W, El-Mihilmy M, and McCauley M (2000), Field performance of FRP bridge repairs, *Journal of Bridge Engineering*, 5(2), 107–113.

Subramaniam K V, Ali-Ahmad M, and Ghosn M (2008), Freeze-thaw degradation of FRP-concrete interface: Impact on cohesive fracture response, *Engineering Fracture Mechanics*, 75(13), 3924–3940.

Teng J G, Chen J F, Smith S T, and Lam L (2003), Behavior and strength of FRP-strengthened RC structures: A state-of-the-art review, *Structures and Buildings*, 156(1), 51–62.

Toutanji H, Saxena P, Zhao L, and Ooi T (2007), Prediction of interfacial bond failure of FRP-concrete surface, *Journal of Composites for Construction*, 11(4), 427–436.

Ueda T and Dai J (2005), Interface bond between FRP sheets and concrete substrates: Properties, numerical modeling and roles in member behavior, *Progress in Structural Engineering and Materials*, 7, 27–43.

Weitsman Y J and Elahi M (2000), Effects of fluids on the deformation, strength, and durability of polymeric composites—An overview, *Mechanics of Time-Dependent Materials*, 4, 107–126.

Yang Q, Xian G, and Karbhari V M (2008), Hygrothermal ageing of an epoxy adhesive used in FRP strengthening of concrete, *Journal of Applied Polymer Science*, 107, 2607–2617.

Zhao X-L and Zhang L (2007), State-of-the-art-review on FRP strengthened steel structures, *Engineering Structures*, 29, 1808–1823.

Zhou A, Post N, Pingry R, Cain J, Lesko J J, and Case S W (2007), Durability of composites under fatigue loads, in Karbhari V (ed.), *Durability of Composites for Civil Structural Applications*, Cambridge, U.K.: Woodhead Publishing Ltd., pp. 126–149.

Part IV

FRP Composites for Reinforcement of Concrete Structures

Nestore Galati and Gustavo Tumialan

20 Introduction

Julio F. Davalos and Yi Chen

CONTENTS

HISTORICAL BACKGROUND

The degradation of steel reinforced concrete (RC) structures is a critical issue of worldwide concern, due to high maintenance requirements and resulting in shorter service lives of concrete facilities. In the United States, the average age of the approximately 600,000 bridges in the interstate highway system is 45 years old. About one-fifth of those bridges are classified as structurally or functionally deficient. It is estimated that the repair cost for existing highway bridges is more than $50 billion, and $1–3 trillion for all concrete structures. In Canada, about 40% of bridges above 40 years of life and numerous multistory parking garages are structurally deficient. The cost of repair of parking garages alone in Canada is estimated at more than $6 billion and over $74 billion for all concrete structures. In Europe, the estimated annual cost of concrete repair is about £1 billion (Balendran and Leung 2003, Nkurunziza et al. 2005).

Corrosion of steel reinforcement is the major cause of deterioration of existing RC structures. Combined effects of moisture, temperature, and chlorides reduce the alkalinity of concrete and exacerbate the corrosion of steel reinforcement, especially for concrete structures subjected to aggressive environments, such as marine structures and bridges and parking garages exposed to deicing salts. As the corrosion of steel bars develops, the resultant products on bar surfaces lead to volumes that are two to five times larger than the original steel. This volume increase causes cracks and spalling of concrete, which facilitate the migration of chemical ions, especially chlorides. In turn, the ingress of chemicals and moisture leads to further corrosion of the steel reinforcement.

To address the corrosion problem of steel reinforcement, engineers have turned to various techniques such as galvanized coatings, electro-static-spray fusion-bonded (powdered resin) coatings, epoxy coatings, cathodic protection, and polymer-impregnated concrete. Despite all these efforts, the steel corrosion has not been completely overcome. The epoxy-coated steel bars have captured about 15% of the North American market. But field and research data indicated that the commonly used epoxy-coated reinforcing bars have not provided a final solution to the corrosion problem of

reinforcement in concrete (Clear et al. 1995). In recent years, fiber-reinforced polymer or plastic (FRP) reinforcements have been increasingly used in concrete structures due to their resistance to corrosion, high strength-to-weight ratio, good fatigue properties, and ease of handling.

APPLICATIONS OF FRP REINFORCEMENT

FRP composite products have been widely used in the aerospace, marine, and corrosion-exposed industries since the 1940s, and the use of FRP reinforcement for concrete structures can be traced back to the mid-1950s (ACI 440 1996). But initially, FRP bars were used as reinforcement for polymer concrete due to their close compatibility of thermal expansions, unlike the mismatch between steel and polymer concrete. FRP bars were not considered as a viable solution to address the corrosion problem of steel and were not commercially available until the 1970s. The increase use of FRP bars started in the 1980s, when FRP were applied as reinforcing materials in concrete structures that required special performance characteristics, such as nonmagnetic properties, or for use in areas that were subjected to adverse environments or chemical attacks. Before the 1990s, the primary FRP reinforcements were still limited to applications such as marine structures, as shown in Figure 20.1a, magnetic resonance imaging (MRI) installations (Figure 20.1b), large transformer foundation pads, and airport runways and electronic laboratories.

The world's first highway bridge using FRP reinforcement was built in Germany in 1986 (ACI 440 2003). Since then, bridges reinforced with FRP have been constructed throughout Europe, Japan, and North America. There are more than 100 demonstration and commercial projects of FRP reinforcement applications in Japan. Glass FRP (GFRP) bars have been commercially employed in over 40 structures in North America (ACI 440 2003).

Recently, FRP bars have also been used for the rehabilitation of existing structures, such as near-surface mounting (NSM) and strengthening of masonry structures, as shown in Figure 20.2. The use of NSM FRP bars is a promising technology for increasing flexural and shear strength of deficient RC members. Advantages of using NSM FRP bars with respect to externally bonded FRP laminates are the possibility of anchoring the reinforcement into adjacent RC members, and less installation time. This technique becomes particularly attractive for the flexural strengthening of negative moment regions of slabs and decks, where external reinforcement would be subjected to mechanical and environmental damage, and the required protective cover would interfere with the presence of finishes.

The common forms of FRP products used as reinforcement in concrete structures can be classified as (Figure 20.3) follows: (1) one-dimensional forms such as bars, tendons, rods, tubes, strands, cables, and ropes; (2) two-dimensional forms such as grids, fabrics, and gratings; and (3) three-dimensional

(a) (b)

FIGURE 20.1 Application of FRP bars. (a) Sea wall restoration and (b) MRI room foundation. (Courtesy of Hughes Brothers, Inc., Seward, NE, http://www.hughesbros.com.)

(a) (b)

FIGURE 20.2 New application of FRP bars in civil engineering. (a) NSM and (b) masonry strengthening. (Courtesy of Hughes Brothers, Inc., Seward, NE, http://www.hughesbros.com.)

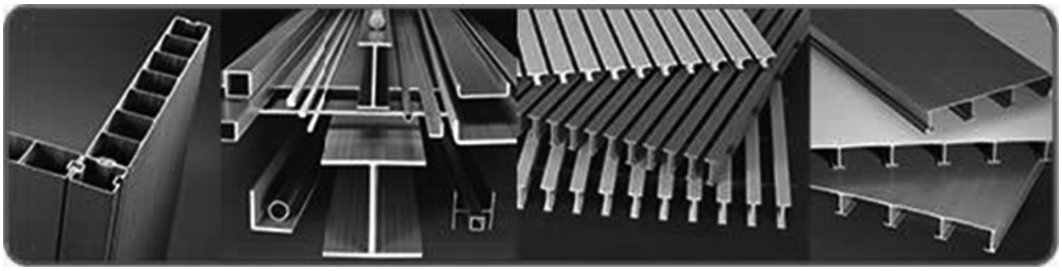

FIGURE 20.3 Common forms of FRP products. (Courtesy of Strongwell Corporation, Bristol, VA, www.strongwell.com/products/pultruded-prod/overview.)

forms such as 3-D fabrics. Fibers typically used for FRP reinforcements of concrete are glass, carbon, and aramid, and the most commonly used resins are vinyl ester, epoxy, and polyester.

HISTORICAL DESIGN GUIDES

Several design codes and guidelines for concrete structures reinforced with FRP have been recently published in Japan, North America, and Europe, as listed in Table 20.1. To formulate design methods for FRP RC structures, usually two approaches can be adopted. The first is to develop completely new methods and the second is to adapt the existing ones. At present, most design guidelines for FRP RC structures are adapted from existing conventional design guidelines, based on established knowledge. They are intended to supplement existing codes and guidelines for steel RC structures, to provide engineers and building officials with assistance for the specification, design, and construction of concrete reinforced with FRP bars. Thus, throughout most of the design guidelines, provisions for existing designs of steel RC structures are often cited. As such, current guidelines are based on the implicit assumption that the users are familiar with design codes for steel RC structures. Also, due to limited available information on the behavior of FRP reinforcements and lack of sufficient application experience, current design guides are conservative and often provide provisions only for selected applications.

It is well established that the properties and characteristics of FRP reinforcement differ significantly from those of conventional steel. So the underlying assumption in current design guidelines based on similarity with conventional design methods may not be effectively applicable. The design codes for concrete structures reinforced with steel are based on more than 100 years of experience

TABLE 20.1
Design Guidelines and Codes for Concrete Structures Reinforced with FRP Materials

Country	Publisher	Year	Codes and Guidelines
Japan	Japan Society of Civil Engineers (JSCE)	1997	*Recommendation for Design and Construction of Concrete Structures Using Continuous Fiber Reinforced Materials*
Norway	The Foundation for Scientific and Industrial Research at the Norwegian Institute of Technology (SINTEF)	1998	*EUROCRETE Modifications to NS3473 When Using FRP Reinforcement*
United Kingdom	Institute of Structural Engineers (ISE)	1999	*Interim Guidance on the Design of Reinforced Concrete Structures Using Fibre Composite Reinforcement*
Canada	Canadian Standards Association (CSA-S6)	2000	*Section 16: Fiber-Reinforced Structures, Canadian Highway Bridge Design Code*
Canada	Intelligent Sensing for Innovative Structures (ISIS)	2001	*Reinforcing Concrete Structures with Fiber Reinforced Polymers* (*Design Manual No. 3*)
	Canadian Standards Association (CSA-S806)	2002	*Design and Construction of Building Components with Fiber-Reinforced Polymers*
United States of America	American Concrete Institute Committee 440 (ACI 440)	2003	*Guide for the Design and Construction of Concrete Reinforced with FRP Bars*

and consist of combinations of basic principles and simple rules of thumb. Often, engineers are given no guidance on how conventional requirements were formulated and how to modify existing provisions for FRP reinforcing materials. Moreover, there remain many topics that are still being investigated, and therefore, published design guidelines need to be reevaluated from time to time to reflect up-to-date knowledge and confidence gained through research, field applications, and product developments.

Of all codes and guidelines listed in Table 20.1, only those published by CAN/CSA-S806 and CAN/CSA-S6 are national standards. The others are guidelines proposed by organizations such as the American Concrete Institute (ACI) and Japan Society of Civil Engineers (JSCE). Moreover, guidelines proposed by SINTEF and ISE are in the format of comments and modifications to existing design codes for steel RC structures.

The first design guidelines for FRP-reinforced and prestressed concrete buildings were established by JSCE in 1993. These guidelines were published in Japanese in 1995, and 2 years later, the English version was available (JSCE 1997). Since then, the JSCE design equations and methods have often been cited by other guidelines. This document included recommendations for design and construction, quality specifications, standard test methods, and necessary data for using FRP. The recommendations provided general requirements for the design of concrete structures using FRP, including structures where FRP is used together with steel reinforcement. The corresponding conventional design guideline for this recommendation was the "Standard Specification for Design and Construction of Concrete Structures" of JSCE, whose provisions were to be followed if no changes were necessary when including FRP reinforcement.

In the document proposed by SINTEF (1998), the Norwegian Standard NS3473 containing design rules for conventional concrete structures was extensively cited in regard to the use of FRP reinforcement. The main purpose of the comments with reference to NS3473 was to identify all sections that needed modifications to incorporate FRP reinforcement, pointing out the problems and/or indicating possible solutions for a future code development. The comments were based on published international literature and reported results of the Eurocrete project. The guides provided by ISE (1999) were in a similar format to the one by SINTEF. Suggested changes were made to the British design codes: BS 8110 "Structural Use of Concrete" and BS 5400: "Part 4 Code of Practice

for Design of Concrete Bridges." In addition, background for those changes and future work was included in the document. But the designs of prestressing concrete and seismic application were not covered by the comments of SINTEF or ISE.

In 2000, the first edition of the Canadian Highway Bridge Design Code included a section on fiber-reinforced structures (CSA-S6 2000). Provisions in that section were mainly for bridge components with FRP such as prestressed and non-prestressed concrete beams and slabs, fiber-reinforced concrete (FRC) deck slabs, stressed wood decks, and barrier walls.

In 2001, the ACI Committee 440 published recommendations on the engineering and construction of concrete reinforced with FRP bars. Then the revised version (ACI 440.1R-03) was released in 2003. This guideline for FRP RC was consistent with ACI 318-95 "Building Code Requirements for Structural Concrete and Commentary." In addition to flexural and shear design, the guide included descriptions on the history and use of FRP reinforcement, and the unique material properties of FRP reinforcement. A quality standard and designation system for FRP reinforcement materials was proposed, and design examples and areas of future research were also listed. But this guideline addressed only non-prestressed concrete with FRP reinforcement and did not include the use of FRP in combination with steel reinforcements. Also test methods and material specifications to support design and construction guidelines were not included.

In 2001, a design manual (ISIS 2001) was published by the Canadian Network of Centers of Excellence on Intelligent Sensing for Innovative Structures. This manual provided design equations and guidelines that can be easily used for the design of FRP RC structures. Design examples and empirical design charts were also included. The background and specific material properties of FRP reinforcement were also discussed. Moreover, the document included information on several types of commercially available FRP reinforcements. But this manual was mainly intended for the design of FRP RC beams. The designs of prestressed concrete with FRP, concrete with FRP in combination with steel, and FRP-reinforced structures under fire, and seismic design of FRP-reinforced structures were not included.

In 2002, the Canadian Standards Association (CSA) published a design guideline for FRP RC structures (CSA-S806 2002), which was approved in 2004 as a national standard for Canada. The standard CSA-S806 covered the design of concrete components reinforced or prestressed with FRP, the design of concrete components with surface-bonded FRP, the design of FRC and FRP combined composite cladding, and seismic design. This guide was consistent with the National Building Code of Canada.

Conservative designs are common to all current design guidelines for FRP RC structures, and their provisions may lead to uneconomic designs. There is a pressing need for standardizing FRP products and test methods. A review of the earlier design guides also showed that the design of columns, prestressed structures, and structures subject to seismic and fire loads is not covered in most design documents. Additional information on FRP reinforcements, more experience with field applications, and new research contributions are all needed for further developments of design guidelines.

LIMITATIONS

Compared to steel, FRP materials offer distinct advantages for concrete reinforcement, such as resistance to corrosion, high strength-to-weight ratio, and ease of handling. But their disadvantages, as listed in Table 20.2, limit the range of reinforcement applications in concrete structures. The advantages and disadvantages of FRP materials also influence changes in conventional designs. Due to its relative low cost, GFRP is the most widely used composite material in civil engineering, but it also presents disadvantages and limitations in relation to carbon composites (CFRP), as noted in Table 20.2. There is also limited use of FRP in certain applications mainly due to disadvantages of the material.

TABLE 20.2
Disadvantages of FRP as Reinforcement for Concrete Structures

Properties	Disadvantages
Glass transition temperature	The glass transition temperature (T_g) of FRP is in the range of 65°C–150°C. Beyond T_g, the flexural, shear, and bond strength will be significantly reduced
Thermal expansion	The coefficients of transverse thermal expansion of FRP are much larger than that of concrete
Linear elastic behavior up to failure	Unlike steel, FRP has no yielding before tensile failure. So the failure of FRP-reinforced concrete structures is brittle either due to concrete crushing or reinforcement rupture
Young's modulus	The typical Young's modulus for FRP ranges from one-fourth to three-fourth of that of steel reinforcement. The Young modulus of GFRP is only one-fourth of that of steel
Shear strength	Since polymer matrix governs the shear strength, FRP usually has very low shear capacity. The transverse shear strength is about 25% of the tensile strength, while the interlaminar shear strength is only about 10% of the tensile strength
Creep rupture and fatigue	FRP materials are susceptible to creep rupture and fatigue failure
Compressive behavior	Compressive strength and stiffness of FRP is lower than its tensile strength and stiffness. FRP reinforcement is more susceptible to buckling than steel under compression
Durability	FRP, especially GFRP, is susceptible to attack by moisture, elevated temperature, and alkaline solutions
The tensile strength of bent portion	A reduction of 40%–50% of ultimate strength is specified in bent portions of FRP
Shear lag	Tensile strength is dependent on bar diameter. Smaller-diameter bars are more efficient

Structures under Fire

FRP reinforcement is not recommended in structures for which fire resistance is essential to maintain structural integrity, because of its low glass transition temperature, T_g, as shown in Table 20.2. Though the lack of available oxygen would inhibit the burning of FRP when embedded in concrete, at temperatures close to T_g, the resin becomes soft and the mechanical properties of FRP are significantly reduced, resulting in decreased shear transfer and flexural and bond strengths, and leading to increases in crack width and deflection.

Design guidelines proposed by ACI 440, ISIS, and CSA-S6 do not cover the design of structures subjected to fire. Other design guidelines (JSCE 1997, SINTEF 1998, ISE 1999, CSA-S806 2002) require to follow special precautions and assessments when dealing with fire performance of FRP-reinforced structures. The limit on concrete cover was adopted by some design guidelines (JSCE 1997, CSA-S806 2002) to achieve fire protection of the structure, based on fire resistance of FRP, fire temperature and duration, and size of concrete aggregate. Recent test results (Nadjai et al. 2005) showed that the fire response of FRP RC beams depended mainly on the concrete cover, which supported the approach adopted by design guides. No detailed information was provided in JSCE (1997) for the fire protection of FRP-reinforced structures, but it was suggested that if necessary, additional fire-proofing layers should be considered. In CSA-S806 (2002), charts adapted from Kodur and Baingo (1998) were used to establish the fire resistance of FRP RC slabs for a given critical temperature specified by the manufacturer. ISE (1999) suggested that the design of FRP-reinforced structures under fire should be based on either direct application of results of fire tests or fire engineering analysis.

TABLE 20.3
Temperatures at Which Fibers Begin to Degrade

Bar Type	GFRP	CFRP	AFRP
Temperature (°C)	980	1650	175

The behavior of FRP RC structures under fire is not well understood, and several investigations are still examining this topic. The test results by Katz et al. (1998, 1999) showed that bond strength of FRP can be reduced by up to 40% at 100°C and up to 90% at 200°C. Sakashita et al. (1997) showed that when the temperature of FRP reinforcement reached 250°C–350°C, FRP-reinforced beams under sustained load failed by reinforcement rupture. One recent study (Abbasi and Hogg 2005) proposed a service-life prediction model for high-temperature performance of concrete beams reinforced with GFRP bars.

From the literature, continuous fibers usually begin to degrade at temperatures, as listed in Table 20.3. So in case of fire, provided that both the end-regions of the FRP reinforcement are kept cool and end-anchorages are maintained, the safety of the structure may not be significantly affected since the tensile strength of FRP mainly depends on the integrity of the fibers. But the member will then behave in a manner similar to one with disbonded reinforcement, such as in post-tensioning, due to softening of the resin. Collapse may occur when the temperature of the FRP fibers reaches the level at which they begin to degrade. This temperature will be about 1000°C for glass fibers and approximately 1700°C for carbon fibers, as shown in Table 20.3. Due to the unique properties of FRP and failure mechanisms of FRP-reinforced structures under fire, the guidelines to be observed in design can be summarized as (1) the reinforcement should be continuous between ends; (2) the temperature at the member ends should remain below the T_g of the resin matrix during a fire; and (3) the concrete cover must be sufficient to maintain a low temperature of bars so that the fibers will not begin to degrade significantly. Also the design of FRP-reinforced structures under fire can be based on the following two distinct criteria (ISE 1999): (1) the temperature at the surface of the reinforcement reaching T_g and (2) the temperature at the bar reaching a level at which fibers start to degrade to a significant extent. The choice of one of these criteria will depend on the anchorage conditions for the bars. Further research work is needed to address this important topic.

Members under Compression

The compressive strength of FRP bars depends on the fiber type, volume fraction, and manufacturing process and is usually much lower than the tensile strength, as shown in Table 20.4. It is generally agreed that the compressive stiffness ranges from 77% to 97% of the tensile stiffness. Since

TABLE 20.4
Compressive Strengths of FRP Bars (as Percentages of Ultimate Tensile Strengths)

Bar Type	Kobayashi and Fujisaki (1995) (%)	Chaallal and Benmokrane (1993) (%)	Wu (1990); Mallick (1988) (%)
CFRP	30–50		78
GFRP	30–40	75	55
AFRP	10		20

the compressive strength and modulus of FRP bars are subject to significant variations and are significantly lower than their tensile strength and modulus, most design guidelines do not recommend the use of FRP for compression reinforcement or in compression members, due to lack of sufficient experience for such applications. When FRP reinforcement is used in the compression zone of concrete, its contribution is often neglected in design. Also appropriate confinement may need to be considered for FRP bars within the compression zone to prevent axial instability and minimize the relatively high transverse thermal expansion effect.

Some test results (Alsayed et al. 1999) indicated that replacing the longitudinal steel bars in concrete columns by equivalent GFRP bars reduced the axial capacity of the column by 13%, but current column design equations from ACI 318 overestimated their capacity by 12%. A study by Mirmiran et al. (2001) showed that the current design slenderness limit should be reduced from 22 to 17 for concrete columns when FRP is used as reinforcement instead of steel. It was also suggested that the stiffness formulas and reduction factors from ACI 318 needed to be adjusted by including modular-ratio or combined modular-ratio and eccentricity-ratio for FRP RC columns. According to limited literature available, there is potential for the use of FRP bars in concrete columns, but more test results are needed to formulate appropriate design equations specific for FRP.

Non-Ductile Behavior

Due to its nearly linear elastic behavior to rupture, FRP reinforcement is currently not recommended for moment frames or zones where moment redistribution is required. At present, the moment redistribution of FRP RC members is not considered in design, due mainly to lack of experience with such applications. Some test results by Tezuka et al. (1995) showed that continuous beams exhibited a maximum moment redistribution of about 10%. Due to the large strain capacity of FRP, the section at failure tends to have high curvatures. And although no plastic deformation occurs with FRP, the higher rotation capacity may introduce some moment redistribution in continuous members. More research is needed in this area to define and justify moment redistribution capacity of FRP-reinforced structures that may allow more economic design solutions.

Also due to the absence of yielding of FRP under tensile load, some design guidelines (ISE 1999) did not recommend the use of FRP in members possibly subjected to significant stress reversals, such as for structures under seismic loads. The lack of energy absorption by plastic deformation may make FRP reinforcement unsuitable for use in such situations. In some design guidelines, it was prescribed that the seismic design for FRP RC structures should follow the provisions in conventional design, but in such case, the corresponding deformation beyond flexural yielding exhibited by equivalent steel RC should be ignored. In CSA-S806 (2002), to allow for the lack of hysteretic behavior in dissipating seismic energy through inelastic action when using FRP materials, the seismic base shear design is to be determined using a force modification factor of 1.5. Nehdi and Said (2004) investigated the behavior of FRP RC under seismic loading. They tested two full-scale beam–column joint specimens reinforced with steel and GFRP, respectively, in order to investigate their performance in the event of an earthquake. The control steel-reinforced specimen was detailed according to the Canadian Code recommendations, and the GFRP-reinforced specimen was detailed following a similar scheme but using a GFRP grid. The behavior of the two specimens under reversed cyclic loading, their load–storey drift envelope relationship, and energy dissipation ability were compared. The GFRP-reinforced specimen showed a predominantly elastic behavior up to failure. Though its energy dissipation was low, its performance was considered acceptable in terms of total storey drift demand.

To ensure enough deformation before ultimate failure of FRP-reinforced structures, CSA-S806 (2002) prescribed that FRP reinforcement used in structural components should have ultimate failure strain larger than 1.2%. To this end, some design guidelines (CSA-S6 2001, ISIS 2001)

incorporated a combination of strength and deformation in the deformability factor, which is used to ensure enough ductility of FRP RC members. Additional research is needed to study the use of FRP in seismic design of RC structures.

Durability Performance

In conventional design guidelines, the strength of steel reinforcement in concrete is assumed unaffected throughout the design life of the structure. But the properties of FRP reinforcement are subjected to changes with time. FRP bars offer excellent resistance to corrosion induced by chloride ions, but are susceptible to attack by various environments, particularly GFRP bars, including moisture, elevated temperature, alkaline or acidic solutions, and ultraviolet light. For example, test results have shown reductions in tensile properties of FRP bars (Table 20.5) due to exposure to aqueous solutions with high pH values. To account for this degradation, current guidelines usually prescribe design material properties by multiplying the short-term properties of materials with reduction factors. The idea is to base the design on expected properties at the end of the product design life, but overconservative factors are typically applied because realistic service-life degradation factors are not available. Moreover, due to the lack of long-term data, design guidelines even limit the use of FRP in certain applications. The role of the polymer matrix that protects and binds the fibers is critical in achieving adequate durability. Thus, for example, CSA-S6 (2000) recommended that the matrices of FRP reinforcements should comprise only thermosetting polymers. Some design guidelines (ISE 1999, CSA-S806 2002) specifically prohibited the use of polyester resins for FRP materials embedded in concrete. This is due to the lower durability performance of polyester resin in alkaline environment. In CSA-S806 (2002), it is also prescribed that the FRP reinforcing materials should be made of carbon, glass, or aramid fibers and vinyl ester or epoxy resins.

In addition, some guidelines allow the use of GFRP as primary reinforcement in concrete only if the durability performance of the GFRP under expected tensile strain can be demonstrated. Further, it is recommended that GFRP reinforcement used in prestressed concrete beams and slabs, if permitted, be not in direct contact with concrete. In CSA-S806 (2002), GFRP can be used for nonstructural purposes such as partition walls, cladding, slabs on grade, and lining of floors and walls. The use of GFRP for flexural reinforcement of prestressed concrete is not permitted. When the GFRP is used for structural purposes, the tensile stress under sustained factored loads should not exceed 30% of its tensile strength. Similarly, in ACI 440, the limit of sustained stress level for GFRP bar is 20% of its design strength. Such limitations are due to concerns with durability performance in alkaline environment, based on conservative applications of available test results.

Recently, the present authors and their collaborators at West Virginia University have carried out a comprehensive study on the durability of FRP bars (Chen et al. 2006, 2007, Davalos et al. 2012). Service-life prediction procedures were developed for GFRP bars in concrete environment, leading to the possible adoption of material reduction factors in design and indicating that the current limit of sustained stress level for GFRP bars in design guides can be relaxed.

TABLE 20.5
Property Reductions of FRP Bars Due to Aqueous Solutions with High pH

Tensile Properties	GFRP (%)	AFRP (%)	CFRP (%)
Tensile strength	0–75	10–50	0–20
Tensile stiffness	0–20	0–20	0–20

Shear Lag

Unlike steel, FRP bars exhibit more pronounced nonuniform far-field axial stress, termed shear lag, resulting in reduced average axial strength as the bar diameter increases. CSA-S806 (2002) prescribed that the cross-sectional area of round and rectangular bars shall not exceed 500 mm^2 (i.e., the diameter should be less than 25 mm for round bar). For prestressing tendons, the cross-sectional area shall not be larger than 300 mm^2. This provision is to minimize the shear-lag effect in FRP reinforcement.

Transverse Thermal Expansion

It is well known that the coefficients of thermal expansion (CTEs) of FRP bars are different in the longitudinal and transverse directions. The longitudinal CTE, depending on fibers, is lower than that of concrete and even negative (as in the case of CFRP), while the transverse CTE, depending on matrices, is about 3–10 times that of concrete. Therefore, thermal fluctuations can lead to mismatch of thermal expansions between FRP and concrete, resulting in bond degradation and even concrete cracking. CSA-S806 (2002) prescribed that the transverse CTE of FRP for structural components should not be larger than 40×10^{-6}/°C.

But some test results and theoretical analyses (Masmoudi et al. 2005) found that cracking is not induced due to the mismatch of thermal expansion between GFRP bar and concrete, as long as the concrete cover is thicker than 1.9 times the bar diameter. Field applications have confirmed that there is no visible fragmentation of concrete cover due to FRP thermal expansion despite small depths of cover (CSA-S6 2000). This may be due to FRP reinforcement usually having very low transverse elastic modulus (dominated by the matrix), which may not induce enough stress to cause tensile cracking of surrounding concrete.

A recent study (Galati et al. 2006) found that a 200 h temperature exposure at 70°C resulted in a 16% maximum bond strength reduction of GFRP bars. The study carried out by Davalos et al. (2008) found that 30 days of daily thermal cycles from –20°C to 80°C caused about 4%–18% reduction in pullout bond strength of carbon and glass FRP bars, with more severe reductions for GFRP, while the reduction of bond strength was mainly due to the near-surface degradation of FRP bars than to microcracking of surrounding concrete.

According to published results, the design limits used for FRP bars due to thermal expansion effects can be relaxed, but the induced bond strength reduction needs to be appropriately addressed.

Other Limitations

Besides the earlier limitations related to specific properties of FRP reinforcement, concerns with high initial cost, lack of unified products and test methods, and lack of sufficient design and application experiences are recognized as major obstacles for its acceptance on a broader scale in civil engineering. From current reports, the cost of GFRP bars is about 1.6–1.8 times of epoxy-coated steel or galvanized steel. The increase in total cost for bridge construction using GFRP bars is about 2.5%–4%. But both construction labor and maintenance costs can be reduced significantly by using FRP bars. It is expected that the use of FRP bars instead of steel will reduce the long-term maintenance costs by over 80%. With new advances in manufacturing technology, the cost of FRP reinforcement is expected to be reduced. There is an urgent need to establish agreement for standardizing FRP products and test methods between technical organizations and manufacturers. Unlike steel, there are currently no accepted standards for properties of FRP materials that depend on the type and quantity of fibers, resins, additives, and processing methods. The broad variety of FRP reinforcements produced by different manufacturers, and the lack of product standards and standard test methods have been obstacles for allowing relative comparisons of research results and developing unified design guides. With further research results and more complete design guides for FRP reinforcements, the design and application experiences will be advanced rapidly.

SPECIAL ATTENTION TO CONSTRUCTION PRACTICE

It is recognized that FRP reinforcing bars are susceptible to surface damage, which may significantly reduce their strength and durability performance. To avoid damage of FRP bars, they should be handled, stored, and placed more carefully than steel bars are. Special attention to construction practices of FRP RC members are briefly noted in the following text.

FRP reinforcement should not be stored on the ground; exposure to high temperature, chemical substances, and ultraviolet rays should be avoided. Cutting of FRP bars should be done with a high-speed grinding cutter or a fine-blade saw. Any cut ends should be immediately protected by a suitable resin coat or other approved methods. Carbon fiber reinforcement may be damaged by lightning and should be insulated from possible lightning strikes.

To avoid undesirable displacements, FRP reinforcement should be properly secured and supported by chairs when the concrete is placed. Due to its low stiffness and density (the density is lower than concrete), the FRP reinforcement may float or bend excessively during the casting of concrete. Coated tie wire, plastic or nylon ties, or plastic snap ties and plastic chairs, but not metal wire, should be used to tie and support the reinforcement. A plastic vibrator, instead of a conventional vibrator, should be used when casting concrete. Bending of FRP bars usually should be carried out before the resin is fully cured. Some guidelines also impose a limit on the bending curvature of FRP reinforcement (for a circular bent, the bending-diameter over the bar-diameter ratio should be no less than 4). Bending of FRP reinforcement on site for bars containing cured thermoset matrices should be avoided. Because thermosetting polymers are highly cross-linked, heating the bar is not allowed as it would lead to decomposition of the resin. Some design guidelines (CSA-S6 2000) prescribed that concrete reinforced with FRP should be moist-cured and not heat-cured, or autoclaved. During curing, the vapor temperature should stay below 40°C. This limitation is given to ensure that the temperature at the reinforcement is below glass transition temperature, T_g.

REFERENCES

Abbasi, A. and Hogg, P.J., A model for predicting the properties of the constituents of a glass fibre rebar reinforced concrete beam at elevated temperatures simulating a fire test, *Composites Part B*, 36, 384–393, 2005.

ACI 440, *State-of-the-Art Report on Fiber Reinforced Plastic (FRP) Reinforcement for Concrete Structures*, American Concrete Institute, Farmington Hills, MI, 1996.

ACI 440, *Guide for the Design and Construction of Concrete Reinforced with FRP Bars*, American Concrete Institute, Farmington Hills, MI, 2003.

Alsayed, S.H., Al-Salloum, Y.A., Almusallam, T.H., and Amjad, A.M., Concrete columns reinforced by glass fiber reinforced polymer rods, *ACI SP188*, 10, 103–112, 1999.

Balendran, R.V. and Leung, H.Y., Flexural behavior of concrete beams internally reinforced with GFRP rods and steel rebars, *Structural Survey*, 21(40), 146–157, 2003.

Chaallal, O. and Benmokrane, B., Physical and mechanical performance of an innovative glass-fiber-reinforced plastic rod for concrete and grouted anchorages, *Canadian Journal of Civil Engineering*, 20(2), 254–268, 1993.

Chen, Y., Davalos, J.F., and Ray, I., Durability prediction for GFRP reinforcing bars using short-term data of accelerated aging tests, *ASCE Journal of Composites for Construction*, 10(4), 279–286, 2006.

Chen, Y., Davalos, J.F., Ray, I., and Kim, H.Y., Accelerated aging tests for evaluations of durability performance of FRP reinforcing bars for concrete structures, *Journal of Composite Structures*, 78(1), 101–111, 2007.

Clear, K.C., Hartt, W.H., McIntyre, J., and Lee, S.K., Performance of epoxy-coated reinforcing steel in highway bridges, Transportation Research Board, NCHRP Report 370, Washington, DC, 1995.

Davalos, J.F., Chen, Y., and Ray, I., Long-term durability prediction models for GFRP bars in concrete environment, *Journal of Composite Materials*, 46(16), 1899–1914, 2012.

Davalos, J.F., Chen, Y., and Ray, I., Effect of FRP bar behavior on durability of interface bond with concrete, *Cement and Concrete Composites*, 30(8), 722–730, 2008.

Galati, N., Nanni, A., Dharani, L.R., Focacci, F., and Aiello, M.A., Thermal effects on bond between FRP rebar and concrete, *Composites Part A: Applied Science and Manufacturing*, 37(8), 1223–1230, 2006.

Katz, A., Berman, N., and Bank, L.C., Effect of cyclic loading and elevated temperature on the bond properties of FRP rebars, *International Conference on the Durability of Fiber Reinforced Polymer Composites for Construction*, Sherbrooke, Quebec, Canada, pp. 403–413, 1998.

Katz, A., Berman, N., and Bank, L.C., Effect of high temperature on bond strength of FRP rebars, *ASCE Journal of Composites for Construction*, 3(2), 73–81, 1999.

Kobayashi, K. and Fujisaki, T., Compressive behavior of FRP reinforcement in non-prestressed concrete members, in *Non-Metallic (FRP) Reinforcement for Concrete Structures*, L. Taerwe (ed.), E & FN Spon, London, U.K., pp. 267–274, 1995.

Kodur, V.K.R. and Baingo, D., Fire resistance of FRP reinforced concrete slabs, IRC Internal Report No. 758, Institute for Research in Construction, National Research Council of Canada, Ottawa, Ontario, Canada, 1998.

Mallick, P.K., *Fiber-Reinforced Composites: Materials, Manufacturing, and Design*, Marcel Dekker Inc., New York, 1993.

Masmoudi, R., Zaidi, A., and Gérard, P., Transverse thermal expansion of FRP bars embedded in concrete, *Journal of Composites for Construction*, 9(5), 377–387, 2005.

Mirmiran, A., Yuan, W., and Chen, X., Design for slenderness in concrete columns internally reinforced with fiber-reinforced polymer bars, *ACI Structural Journal*, 98(1), 116–125, 2001.

Nadjai1, A., Talamona1, D., and Faris, A., Fire performance of concrete beams reinforced with FRP bars, *Proceedings of the International Symposium on Bond Behaviour of FRP in Structures*, International Institute for FRP in Construction, Hong Kong, People's Republic of China, pp. 401–410, 2005.

Nehdi, M.L. and Said, A.M., Use of FRP for RC frames in seismic zones: Part II. Performance of steel-free GFRP-reinforced beam-column joints, *Applied Composite Materials*, 11(4), 227–245, 2004.

Nkurunziza, G., Debaiky, A., Cousin, P., and Benmokrane, B., Durability of GFRP bars: A critical review of the literature, *Progress in Structural Engineering and Materials*, 7(4), 194–209, 2005.

Sakashita, M. et al., Deflection of continuous fiber reinforced concrete beams subjected to loaded heating, *Non-Metallic (FRP) Reinforcement for Concrete Structures, Proceedings of the Third International Symposium*, Sapporo, Japan, Vol. 2, pp. 51–58, 1997.

Tezuka, M., Ochiai, M., Tottori, S., and Sato, R., Experimental study on moment redistribution of continuous beams reinforced or pretensioned with fiber reinforced plastic, in *Non-Metallic (FRP) Reinforcement for Concrete Structures*, L. Taerwe (ed.), E & FN Spon, London, U.K., pp. 387–394, 1995.

Wu, W.P., Thermomechanical properties of fiber reinforced plastic (FRP) bars, PhD Dissertation, West Virginia University, Morgantown, WV, 1990.

21 Material Characteristics

Stijn Matthys

CONTENTS

INTRODUCTION

Advanced composites—under the form of fiber-reinforced polymers (FRPs)—have gained considerable interest in construction practice worldwide as structural reinforcement. Originally, these FRP materials have been developed in the space and aircraft industry in the 1940s, when fibers with high strength and stiffness and low density became available. Since then, FRPs have become an important material group in several sectors of the industry. In the 1970s, research and development of FRP reinforcement for concrete construction started gradually in North America, Europe, and Japan. The first commercial products became available in the late 1970s, followed by the first practical applications in the early 1980s (see also Chapters 12 and 20) [1–6]. Nowadays, FRP reinforcement for concrete has become commercially of considerable importance, especially to strengthen existing structures. Also the momentum in the use of FRP materials for new reinforced and prestressed concrete is increasing [7,8].

FRP materials consist of a high number of small, continuous, directionalized, nonmetallic fibers with advanced characteristics, embedded in a polymer matrix. Used as a structural reinforcement for concrete, FRP elements are mostly based on glass (GFRP), carbon (CFRP), or aramid (AFRP) fibers in combination with a thermoset resin such as epoxy, vinylester, or unsaturated polyester. Fiber volume fractions up to about 60%–70% are common. As they occupy the largest volume fraction and share the major portion of the acting load, fibers are the principal stress-bearing constituent, while the resin transfers stresses among fibers and protects them. An enlarged view of a carbon FRP is shown in Figure 21.1.

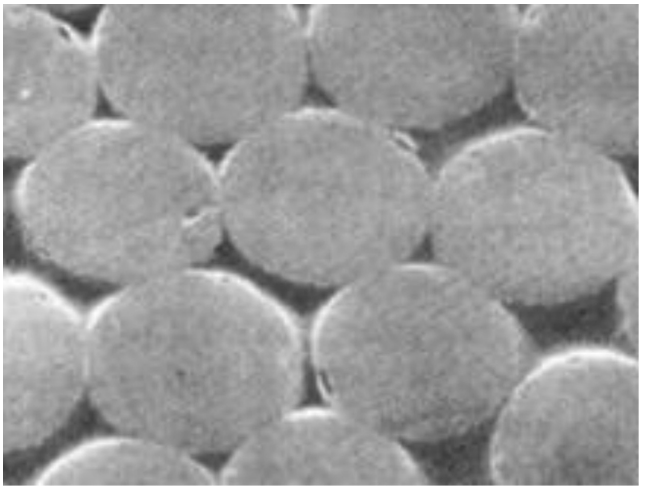

FIGURE 21.1 Enlarged view of a CFRP element.

FRP REINFORCEMENT SYSTEMS FOR CONCRETE

FRP elements for reinforcing concrete members are made available in the form of bars, tendons, ropes, grids, strips, profiles, or other possible shapes among which permanent formwork. Several manufacturing methods exist for the production of FRP composites, among which lay-up techniques, molding techniques (e.g., injection, compression, resin transfer, vacuum bag, and autoclave molding), pultrusion, filament winding, braiding, or weaving. Often used for FRP reinforcement is pultrusion [5,6]. Some typical FRP elements are illustrated in Figure 21.2. For new structures, they are used to reinforce and prestress concrete elements. In the repair sector, they are used to strengthen existing structures, for example, by means of external post-tensioning, externally bonded reinforcement, near-surface-mounted reinforcement, or in combination with shotcrete. Also they are used as stay cables, ground anchors, structural shapes, etc. Often, the FRP reinforcement may come as a system, like, for example, in the case of FRP prestressing reinforcement. Hereby, the system contains the FRP prestressing wires or cables, as well as a specific anchorage for gripping (see the "Multiaxial Strength" section).

FRP reinforcement forms a group of products rather than being one reinforcement type, as its characteristics depend on fiber and resin type and properties, volume fractions, production parameters, shape, and surface texture. The stress–strain behavior of some FRP elements, compared with reinforcing and prestressing steel, is shown in Figure 21.3. Similar to the behavior of the fibers and unlike steel, FRP do not experience any yield but rather a linear elastic behavior nearly up to failure. The modulus of elasticity ranges between about 50 and 250 GPa and is for most FRP elements lower than steel. At the other hand, FRPs are characterized by a high tensile strength, which is close or higher than that of prestressing steel. Being an anisotropic material, the mechanical properties of unidirectional (linear) FRP elements in transverse direction are inferior to those parallel to the fibers.

The application of FRP reinforcement is, due to the often high material cost, related to the utilization of the specific material properties of FRP. Therefore, it is used as a specific alternative for common steel reinforcement, rather than a general substitute for it. Compared to steel, favorable material properties of FRP reinforcement are thus:

- High axial strength
- Low weight
- Excellent corrosion resistance and nonsusceptibility to a wide range of aggressive media
- Electromagnetic neutrality
- Excellent fatigue characteristics for CFRP and AFRP
- Low axial coefficient of thermal expansion (CTE)

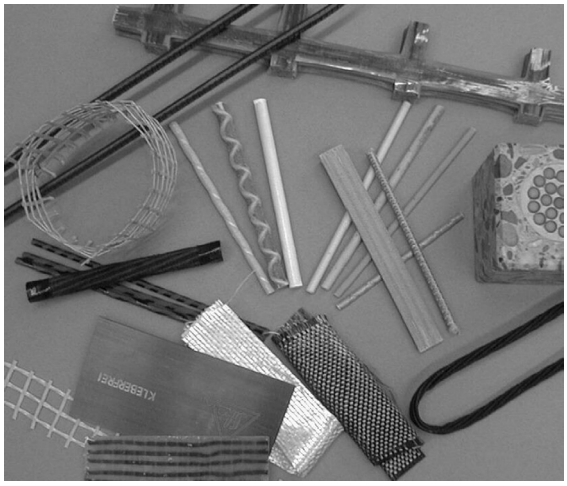

FIGURE 21.2 Examples of various FRP reinforcing elements.

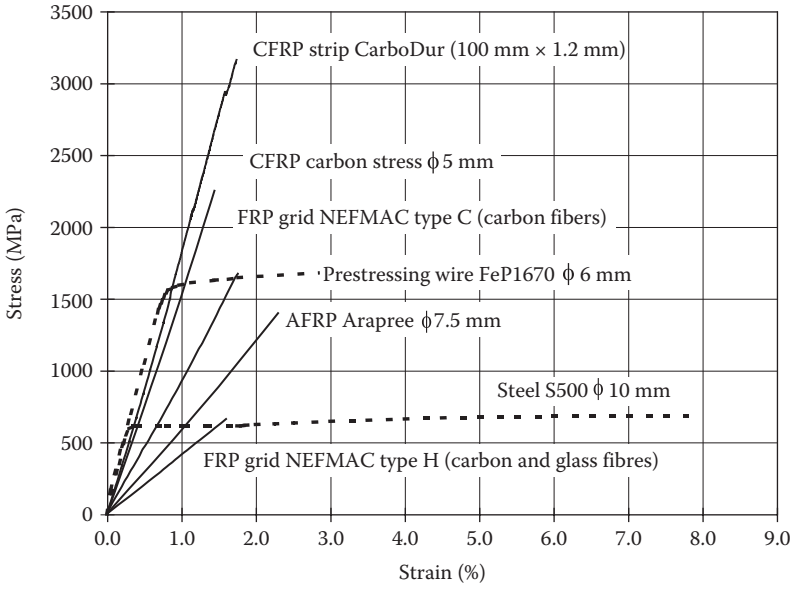

FIGURE 21.3 Stress–strain behavior of some FRP elements compared to steel.

Material properties that are regarded as a disadvantage for the use of structural FRP reinforcement include the following:

- Relatively low failure strain
- High ratio of axial-to-transverse strength
- Relatively low long-term to short-term static strength for GFRP and AFRP
- Specific durability issues (ultraviolet (UV) light, alkalis) may apply for mainly GFRP and AFRP

CONCRETE

Before going more into detail on the material properties of FRP reinforcement and its constituents, in the framework of this book, also a brief discussion is given on the material properties of concrete. For more detailed information, reference is made to standard works on concrete, such as [9–12].

General

Concrete is a carefully proportioned combination of aggregates, sand, cement, and water, sometimes in combination with specific fillers or additives. The concrete is manufactured by mixing these components and to cast the fresh concrete in a formwork that shapes the concrete element. The casting is done on site—with on-site mixing or with ready mixed concrete brought on site—or in a precasting plant. Hardening of the concrete is due to the chemical reaction between the hydraulic cement and the water, in forming cement stone and binding all the constituents together. In the case only small size aggregates are used (e.g., sand)—with a maximum size of 4 mm—the term cement mortar is used instead of concrete.

Concrete can only be formed thanks to the cement, which acts as hydraulic binder. A hydraulic binder is a substance that sets and hardens after combining with water and which retains strength and stability after hardening, even under water. Several types of cement exist, as well as other hydraulic or non-hydraulic binders. Portland cement or Portland cement blends are most commonly used for concrete.

The large freedom in forming and shaping concrete, the construction possibility for small- and (very) large-scale elements and structures, the good fire resistance, the low maintenance costs, and the attractive cost prize compared to other building materials explain the worldwide popularity of concrete construction. As such, the use of concrete has a long tradition—whereas cement mortar was first used by the Romans, among which in the form of concrete for the in-fill of masonry walls. The developments of modern era cement date from the late eighteenth century and continued in the nineteenth century. One of the milestones was the first production of Portland cement in 1824 by Joseph Aspdin [13]. Although concrete construction may be regarded by many as not sophisticated, the use of proper concrete technology and construction detailing is important to obtain good quality and durability of concrete structures.

Some Basic Characteristics of Hardened Concrete

Strength and Stress–Strain Behavior

Hardened concrete can be regarded as artificial stone and is extremely strong in compression. The compressive strength is typically in the range of 30–60 MPa, though today it is possible to make high-strength concretes with a compressive strength well above 100 MPa. On the other hand, concrete has little tensile strength, which equals typically about 10% of the compression strength. The stress–strain behavior of concrete under short-term loading conditions is illustrated in Figure 21.4. The modulus of elasticity of concrete is in the range of 30,000–40,000 MPa. Some strength classes of concrete are given in Table 21.1 (based on [12]), in terms of the mean compressive strength f_{cm} at 28 days (tested on cylinders with diameter 150 mm and length 300 mm), characteristic value of the compressive cylinder strength f_{ck}, mean tensile strength f_{ctm} under concentric loading, and tangent modulus of elasticity E_{ci}.

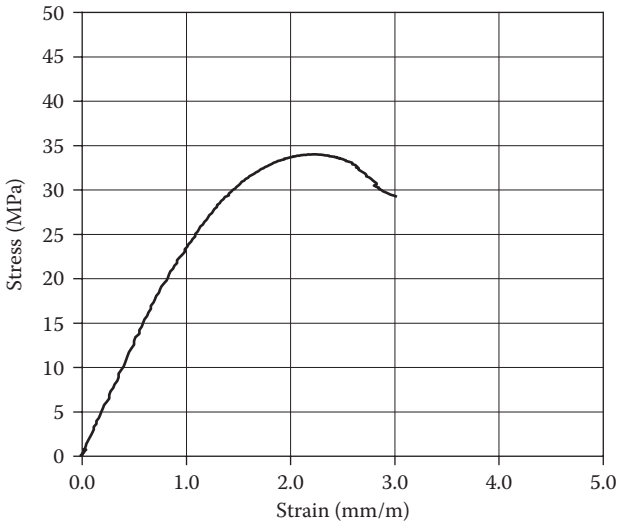

FIGURE 21.4 Stress–strain behavior of concrete.

TABLE 21.1
Some Strength Classes of Concrete

Concrete Grade	C12	C20	C30	C40	C50	C60	C70	C80
f_{cm} (MPa)	20	28	38	48	58	68	78	88
f_{ck} (MPa)	12	20	30	40	50	60	70	80
f_{ctm} (MPa)	1.6	2.2	2.9	3.5	4.1	4.6	5.1	5.6
E_{ci} (GPa)	27	30	34	36	39	41	43	44

Concrete Types and Density

The density of hardened concrete is generally 2400 kg/m^3, though by the choice of aggregates or production techniques also "lightweight concrete" (about 1600 kg/m^3; lightweight concrete is, e.g., used in relation to improved thermal isolation) and "heavy concrete" (about 3300 kg/m^3; heavy concrete is, e.g., used for better shielding against radioactive radiation) can be made. To obtain a dense structure, typically the concrete needs proper vibration during casting. This is no longer the case for "self-compacting concrete," developed in the 1980s, and especially used in precasting plants [14].

Creep and Shrinkage Deformations

Concrete can be regarded as a pseudo viscoelastic material. Though mainly a solid material, due to the complex structure of the cement stone, which contains pores, to some extent a viscous behavior is obtained. The main consequences of the viscoelastic behavior are the long-term deformations of concrete, by means of creep (concrete shortening under constant load) and shrinkage (reduction in concrete volume due to mainly evaporation of water). The order of magnitude of the creep and shrinkage deformation of concrete on the long term is 1 mm/m.

Thermal Properties

The CTE of concrete is between 8 and 12 × 10^{-6}/°C for ambient temperatures. In reality, the CTE is temperature dependent and increases at elevated temperatures. The CTE of concrete is very similar to that of steel (about 10 × 10^{-6}/°C).

At elevated temperatures below 100°C, there is no significant influence on most of the material properties of concrete. Beyond 100°C, free water in the concrete starts evaporating. Extensive structural changes start at temperatures beyond about 500°C, with the decomposition of certain components in the concrete. Strength reductions of the concrete below 80% of the initial strength are generally obtained for temperatures beyond 200°C–300°C. Because of the relative high temperature resistance and, in addition to that, a low thermal conductivity, concrete structures have a good fire resistance. In addition, special concrete compositions have been developed, to obtain a good fire resistance up to temperatures of 1400°C.

At low temperatures (below zero), the compressive strength increases considerably and is strongly dependent on the humidity content of the concrete. Also, a more brittle material behavior is obtained. Freeze–thaw cycles, especially in the presence of water and deicing salts, have an adverse effect on the strength properties of concrete.

Chemical Durability

Being an artificial stone, concrete can generally be regarded as a durable material. Nevertheless, several specific durability issues apply to the concrete or the steel inside the concrete. The durability relates to a combination of both physical (e.g., cracking) and chemical aspects. The latter includes the influence of acids, salts, sulfates, or chlorides. The most common durability problems in relation with concrete are [9–12,15] thus:

- Vulnerability of the concrete to strong acids, which have the tendency to dissolve limestone (part of the cement stone). A special form of acid attack of concrete is biogenic corrosion of concrete, whereas a combination of anaerobic and aerobic bacteria leads to the formation of sulfuric acid, which further deteriorates the concrete.
- Sulfate attack, for example, by the formation of ettringite, which results in damaging expansive phenomena.
- Aggregate expansion due to alkali–silica reaction, whereas alkali-sensitive aggregates in combination with humidity and a sufficiently high alkali content in the concrete, yields the formation of expansive alkali–silica gel.

Problems in relation to steel corrosion inside the concrete are thus:

- Carbonation of the concrete that results in a depassivation of the reinforcing steel (pH < 9), so that the electrochemical corrosion process of steel may occur (depending on the availability of oxygen and moisture).
- Ingress of chlorides that may lead to steel corrosion, often in the form of pitting corrosion.

To avoid durability problems, certain code prescriptions apply, which basically aim to have a high compactness of the concrete, sufficient concrete cover, chemical purity of the constituent materials, and a limitation of cracking. To avoid steel-related durability problems in concrete structures, also the use of FRP reinforcement is of considerable interest.

Concrete Reinforcement

Given the high compressive strength of concrete, in structural bearing elements, the use of concrete is especially functional for taking compression forces. However, as most structures are subjected to both compression and tension forces, the tension zones of the concrete member is reinforced with tensile elements. Reinforced concrete elements are generally cracked under service conditions, which results in a reduced stiffness (higher deformations than uncracked concrete) and crack openings that need to be limited to avoid corrosion of steel reinforcement. By prestressing the concrete, the concrete section acts completely in compression under service conditions and is free of cracks. The prestressing forces to pre- or post-tension concrete are obtained through prestressing wires, strands, or tendons. These are subjected to a tensile force, prior to casting the concrete in pre-tensioned concrete or after the concrete has cured in post-tensioned concrete.

Reinforcing and prestressing elements for concrete are generally made from steel. One of the most important alternatives for reinforcing steel is FRP reinforcement. The stress–strain behavior of these reinforcing elements is given in Figure 21.3. Typical strengths of steel rebars, expressed as the characteristic value of the yield strength, are in the range of 220–520 MPa (grade 500 MPa is often used in Europe, and grades 60 ksi [420 MPa] and 75 ksi [520 MPa] in North America). For prestressing steel, higher tensile strength grades of steel are used, with a characteristic value of the tensile strength up to 1860 MPa. The modulus of elasticity of the steel is about 200 GPa. Properties of the FRP reinforcement are further discussed in the following.

FRP CONSTITUENT MATERIALS

General

FRP materials are composites that consist of organic or inorganic fibers embedded in a matrix. The matrix, sometimes referred to as binder, is a polymer resin, often with some fillers and additives of various nature.

The suitability of FRP materials as load-bearing component is related to the efficient use of small fibers with high strength and stiffness by embedding them in a relatively ductile polymer binder. The small-diameter fibers achieve their strong material properties due to the highly oriented and pure (defect free) microstructure of the fibers. The binder or matrix allows for a good transfer of forces between the fibers as well as a smooth transfer of load from a broken fiber to nearby intact fibers. Hence, by virtue of the matrix, local stress concentrations decrease and a higher unidirectional composite strength can be achieved. In addition, the matrix protects the fibers to a certain extent against mechanical damage and environmental attack.

Several FRP products have become available as structural reinforcement in construction. These systems, designed to act as a composite in an optimum way, are based on different fiber configurations, types of constituent materials, application techniques, etc. As the components of a system are carefully chosen to interact jointly, each product is relative unique.

In the following, the constituent materials of FRP are discussed [16–23].

Fibers

Various fibers (sometimes referred to as filaments) are commercially available, with a wide range of material properties. In continuous lengths and with small diameter, relatively stiff and strong fibers are very efficient to reinforce polymer matrix materials, allowing efficient load transfer between the fibers and hence utilizing the excellent fiber properties. The suitability of the fibers mainly depends on the composite properties that are needed. For FRP concrete reinforcement, this means that selection is related to characteristics such as corrosion resistance, high tensile strength, sufficient failure strain, fatigue resistance, and dimensional stability. With this respect, mainly three types of fibers are currently used for FRP reinforcement in concrete construction: glass, carbon, and aramid. These fibers have a tensile strength that is higher than that of steel and are linear elastic up to tensile failure. The physical and mechanical properties vary considerably between the different fiber types and may vary significantly for a given type of fiber as well. Some typical properties are given in Table 21.2. The tensile stress–strain behavior of the fibers is shown in Figure 21.5.

Glass Fibers

To reinforce polymer matrix materials, glass fibers are most commonly used. Also for FRP rebars, glass fiber is often utilized. Glass fibers are made of silicon oxide with the addition of small amounts of other oxides and are formed by extruding molten glass and fiber stretching. As glass fibers are very surface active and hydrophilic, individual fibers are generally coated by a sizing agent immediately after fiber forming. The sizing also acts to minimize abrasion damage and to aid coupling

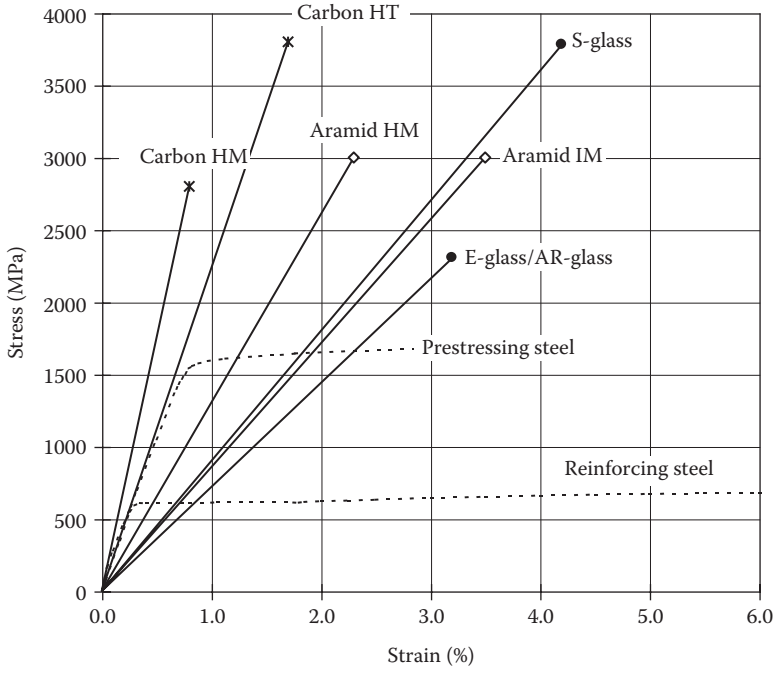

FIGURE 21.5 Stress–strain behavior of fibers.

with polymer matrices. Depending on their chemical composition, glass fibers can be divided into groups. Most general purpose and widely used are E-glass fibers, which are based on calcium-aluminoborosilicate glass. These low-cost fibers have a good electrical resistance and strength. S-glass is a magnesium-aluminosilicate formulation, which has higher strength, stiffness, and thermal stability. C-glass has a soda-lime-borosilicate composition that is used for its higher chemical stability against acids. Alkali-resistant (AR) glass fibers contain a considerable amount of zirconium oxide to increase resistance against alkalis from cement matrices.

Yet characterized by high tensile strength, good electrical resistivity, good thermal resistance, and low price (especially E-glass fibers), glass fibers are known to degrade in the presence of water, acid, and alkaline solutions. Also, they exhibit a considerable creep or stress rupture behavior, meaning that the tensile strength gradually decreases under constant stress. Given the low durability of glass fibers, it is important to select a suitable and protective matrix. The use of AR-glass fibers with higher chemical resistance is of interest as well.

Carbon Fibers

Carbon and graphite fibers are produced from polyacrylonitrile (PAN), pitch, or rayon. Isotropic pitch and rayon are used to produce low-modulus carbon fibers (fiber E-modulus of about 50,000 N/mm^2). High-modulus/high-strength carbon and graphite fibers (Table 21.2), more of interest for FRP reinforcement, are made from PAN or liquid crystalline pitch. PAN fibers are obtained by separating a chain of carbon atoms from polyacrylonitrile through heating and oxidation. Pitch fibers are fabricated by using refined petroleum or coal pitch that is passed through a thin nozzle and stabilized by heating. The molecular structure consists of graphene (hexagonal) layer networks ordered in two or three dimensions. The former is defined as carbon, the latter as graphite. Typically, graphite has a higher tensile modulus than carbon. Although this difference, the term carbon fiber is often used irrespective of the graphitization.

Carbon fibers are the stiffest and strongest reinforcing fibers for polymer composites. They are very resistant against creep and fatigue and have a very good chemical, UV light, and moisture resistance. Hence, carbon fibers are very durable and have excellent mechanical properties. As the fibers are electrically conducting, they can give galvanic corrosion in contact with metals. The wetting of the fibers by resins is not easy, so that surface treatments are normally needed. In this respect, carbon fibers are often provided with an epoxy size treatment that protects the fibers against abrasion (improved handling) and offers an epoxy matrix compatible interface. Compared to glass fibers, carbon fibers are much more expensive (at least 10 times more expensive than E-glass).

TABLE 21.2
Typical Properties of Fibers

Fiber Type	Tensile Strength (MPa)	Modulus of Elasticity (GPa)	Ultimate Strain (%)	Density (kg/m^3)	Fiber Diameter (μm)
E-glass[a]	1800–3500	70–75	2.0–3.5	2500–2600	5–25
S-glass	3400–4800	85–100	3.5–5.0	2500–2600	5–25
Carbon—Pitch HM	3000–3500	400–800	0.4–1.5	1900–2100	9–18
Carbon—PAN HM	2500–4000	350–700	0.4–0.8	1800–2000	5–8
Carbon—PAN HT	3500–5000	200–260	1.2–1.8	1700–1800	5–8
Aramid—IM	2700–4500	60–80	4.0–4.8	1400–1450	12–15
Aramid—HM	2700–4500	115–130	2.5–3.5	1400–1450	12–15
Basalt	1850–4800	70–110	2.5–3.5	2500–2900	6–13

IM, intermediate modulus; HM, high modulus; HT, high tensile strength.

[a] Properties of AR-glass are similar to E-glass, though the density may be somewhat lower.

Aramid Fibers

Aromatic polyamide or aramid fibers are produced from para-phenylene-terephthalamide by extrusion as a liquid crystal polymer and by fiber stretching. These organic fibers have an anisotropic fibrillar structure. In the fiber axis direction, they consist of aligned molecular chains with strong covalent bond. In transverse direction, these chains are cross-linked by weaker hydrogen bridges, so that higher tensile strength and stiffness are obtained in the longitudinal direction. Besides the high tensile strength, aramid fibers show high energy absorption and toughness (as no other fibers), good vibration damping and fatigue resistance, low thermal conductivity, good thermal stability, moderate to fairly good chemical resistance, low compressive strength, and moderate adhesive properties. The aramid fibers respond elastically in tension but exhibit nonlinear and ductile behavior under compression.

With respect to durability, aramid fibers generally exhibit a low or moderate resistance against acids, a moderate resistance against alkalis, and a poor resistance against UV radiation. Due to the interaction of water with the polymer structure, they are sensitive to moisture as well. Because of these aspects, the fibers should be embedded in a matrix that is carefully chosen to provide additional protection. To improve the bond between fibers and matrix, surface treatments may be used. The cost prize of aramid fibers is similar to that of carbon fibers.

Whereas aramid and carbon fibers are anisotropic, which yield different values of mechanical and thermal characteristics in the longitudinal and transverse directions, glass fibers have a more isotropic behavior [24].

Other Fibers of Interest

Whereas glass, carbon, and aramid are most commonly used to reinforce polymer matrix composites, also other fibers may be of interest. Such a fiber, with increasing interest to apply in concrete construction, is basalt [25]. Some material properties of basalt fiber are given in Table 21.2. Basalt is a volcanic rock, from which fibers can be drawn by melting (melting point above 1400°C) crushed basalt stone—giving a single ingredient rock melt—and fiber winding. Mechanical properties of basalt fibers are very similar or sometimes better than those of glass fibers. Properties of the basalt fiber generally depend on the source of the basalt rock and the production process. Thanks to improved production facilities and quality control, today basalt fibers are industrially available with high quality and low variability. Basalt fibers have high fire resistance and are much cheaper than carbon fibers (yet more expensive than E-glass). The use of basalt FRP reinforcement is currently in the research and development phase.

An emerging new fiber in the composite industry is the carbon nanotube. Nanotubes are cylindrical carbon molecules, with a diameter in the order of a few nanometers. They can be single- or multiwalled. These nanofibers have novel properties including ultra-high strength and stiffness, can undergo plastic deformations at high strain levels, and have very high toughness [26]. There is an increasing interest in carbon nanotubes in various industries, among which is the composite industry. The possible use of nanotube fibers or particles for FRP reinforcement is yet in an early research stage.

Other developments in the composite industry, with respect to high-performance structural fibers for advanced polymer matrix composites, are ongoing [27,28] and are of interest for FRP reinforcement as well. An example of a relative new organic high-strength fiber is poly phenylene benzobisoxazole (PBO). The strength and modulus of elasticity of PBO fibers can be higher than aramid and carbon; in addition, they have high-impact tolerance and energy absorption, high creep resistance, and high fire resistance. The application of PBO-based FRP composite reinforcement is mentioned in, for example, [29].

Polymer Matrices

The polymer matrix of an FRP material consists of a resin binder (polymer binder) and normally some fillers and additives. Primarily, the matrix has to bind the fibers together, provide lateral

support to the fibers, protect the fibers from their surroundings, offer a load transfer medium, and may beneficially influence some FRP material properties. In addition, the matrix selection is also important with respect to composite processability and cost.

Polymer matrices can be either based on thermosetting or thermoplastic polymers. Thermosetting resins, when cured, are characterized by a high degree of cross-linking of molecules (polymerization) so that it solidifies or "sets" irreversibly. Upon heating, these cured resins show no melting (at high temperature, decomposition occurs). On the other hand, thermoplastic polymers are characterized by more linear macromolecules and can be repeatedly softened when heated and hardened when cooled.

Thermosetting polymer matrices allow for a good fiber wet-out without applying high pressure or temperature, which makes them very attractive with respect to processability. Compared to thermoplastics, thermosets also offer better thermal stability and chemical resistance, as well as reduced creep and stress relaxation. Disadvantages are their limited storage life and failure strain. Because thermoplastic polymers are more ductile and tough, they have higher impact strength, fracture resistance, and microcracking resistance than thermosetting polymers. Other potential advantages of thermoplastics are the post-formability, the shorter fabrication time, and the long storage life. However, as they are very viscous, incorporation of continuous fibers to thermoplastic matrices and hence composite production are difficult.

Polymer matrix materials are highly viscoelastic. Upon loading, they exhibit elastic deformations, while under constant load, slow viscous deformations occur. At increased temperature, low loading rates or long-term loading, their response tends to be more ductile, while low temperature and high loading rate result in a rigid and more brittle behavior. The mechanical properties of the polymer materials drop drastically when reaching the glass transition temperature T_g. At this temperature, the polymer softens, meaning that it changes from a hard (often brittle) solid state to a more rubber-like (soft and tough) solid state. Upon further heating, thermoplastics reach a highly viscous liquid state before decomposition, while thermosets degrade (char at very high temperature) before rubbery flow can be achieved.

For structural fiber composites, among which FRP reinforcement for concrete, unsaturated polyester, vinyl ester, and epoxy are often used as polymer binder. From these thermosetting resins, polyesters are the most general purpose and frequently applied, given the good processability, fairly good properties, and low cost. Vinyl esters process essentially like polyesters, but provide improved mechanical and chemical performance. Epoxy resins are more expensive than polyesters and vinyl esters, but are largely used in high-performance composites as they generally have the best mechanical properties, good adhesion properties, and excellent resistance to chemicals and solvents. Some typical properties of these polymers, according to [18], are given in Table 21.3.

TABLE 21.3
Typical Properties of Resins According to Ref. [18]

Resin Type	Tensile Strength (MPa)	Modulus of Elasticity (GPa)	Density (kg/m³)	Cure Shrinkage (%)
Polyester	35–104	2.1–3.5	1100–1400	5–12
Vinyl ester	73–81	3.0–3.5	1100–1300	5–10
Epoxy	55–130	2.8–4.1	1200–1300	1–5

Source: Triantafillou, T., Ed., Fiber-reinforced polymer reinforcement for concrete structures, in *Proc. FRPRCS-8 Symposium*, Patras, Greece, 2007, pp. 564–595.

Unsaturated Polyester

Thermosetting polyesters consist of an unsaturated ester polymer (a condensation polymerization product of difunctional acids and glycols), dissolved in a cross-linking monomer such as styrene (or other vinyl unsaturated monomer). By adding a free-radical initiator (for elevated temperature cure) or a promoter (for room temperature cure), a nonreversible chain polymerization reaction is initiated that yields a cross-linked styrene–polyester copolymer (cured polyester resin). To prevent premature cure during the storage of the unsaturated polyester, an inhibitor may be added.

Polyester resins can be formulated to provide a wide variety of properties. Formulations that result in a higher cross-link density improve stiffness, glass transition temperature, and thermal stability, but lower ductility. Given their low cost, good properties (Table 21.3), reasonable chemical resistance, good processability (low viscosity, fast cure time), and dimensional stability, polyesters are widely used for polymer matrix materials. The main disadvantage of polyesters is their high volumetric cure shrinkage, which promotes residual stresses in the composite.

Vinyl Ester

Vinyl esters are produced from an unsaturated carboxylic acid (usually methacrylic acid) and an epoxy resin (usually produced from bisphenol A and epichlorohydrin). Like unsaturated polyester, they are mixed with styrene for cross-linking. Hence, vinyl esters process and cure essentially as polyesters.

Compared to polyesters, vinyl esters have better chemical and temperature resistance, but are more expensive. As their molecular structure is characterized by fewer cross-links, they are more resilient, which makes them easier to handle during processing and provides higher fracture toughness. Furthermore, their chemical structure promotes hydrogen bonds with the surface of glass fibers, resulting in excellent wet-out and good adhesion with these fibers. As epoxy resins are used for the production, vinyl esters exhibit improved heat resistance and thermal stability, although tensile strength is not significantly influenced. Like unsaturated polyester, they exhibit low viscosity and short curing time, as well as the disadvantage of a high volumetric shrinkage during cure.

Epoxy

Epoxy resins are made of low-molecular-weight organic liquid resins containing epoxide groups (rings of two carbon and one oxygen atom). The most widely used epoxy resins are based on epichlorohydrin and bisphenol A. Epoxy resins are often modified using other products to improve characteristics. The formulation may include mixing of diluents to reduce viscosity and flexibilizers to improve impact strength of the cured epoxy. The cross-linking or curing of the epoxy is initiated by adding a hardener. The latter is a reactive curing agent of the amine, anhydride, or Lewis acid type. Cross-linking is achieved by the epoxide groups, as well as by hydroxyl groups if available. For amine type of curing agents, hydrogen atoms in the amine groups react with the epoxide groups of the bisphenol A, enabling the epoxy molecules to cross-link in a three-dimensional network.

Due to the diversity of input materials, epoxy resins have a very wide range of mechanical and physical properties, as well as processing conditions. As a result, they are the most versatile polymer binder for fiber composites, although more expensive than polyester and vinyl ester resins. Main advantages of epoxies are the excellent strength, the good creep resistance, the strong adhesion to fibers, the good resistance to chemicals and solvents, and the low cure shrinkage. Disadvantages are the relative high cost, the long curing time, and the need for careful processing to maintain moisture resistance.

Other Resins of Interest

As discussed earlier, the use of thermoplastic matrices may offer several advantages, though the FRP production is difficult with respect to impregnation and fiber wetting. This is mainly due to the high viscosity of thermoplastics at processing temperature. In [23], the following thermoplastic matrices are mentioned in relation to FRP reinforcement. Polyether ether ketone (PEEK) is the most common thermoplastic resin for high performance applications. It has high fracture toughness,

which is important for damage tolerance of composites. PEEK has very low water absorption (about 0.5% by weight) at room temperature. Polyphenylene sulfide (PPS) is a thermoplastic with very good chemical resistance. Polysulfone (PSUL) is a thermoplastic with very high elongation to failure and excellent stability under hot and wet conditions. The development of thermoplastic-based FRP reinforcement is mainly of interest for (on-site) bendable FRP rebars. The use of thermoplastic FRP reinforcement has been investigated by, for example, [30–32].

Other new developments with respect to resins focus on high heat-resistant FRP bars. For these types of bars, the glass transition temperature of the resin should be sufficiently high (e.g., higher than 200°C). Herewith, phenol-based resins are of interest. Behavior of FRP reinforcement with phenol resin is discussed in [33]. In [34], the use of an inorganic matrix is proposed, which is a low-viscosity resin prepared by blending aluminosilicate powder with a water-based activator. In comparison to epoxy, the inorganic matrix has the advantages of high resistance to fire, resistance to UV radiation, good workability, and no emission of odors or toxins during construction or curing.

Fillers and Additives

Fillers may be used not only to reduce matrix costs but also to control shrinkage, improve certain material properties, improve the load transfer capability of the matrix, control the thixotropy of the resin, etc. They are available in a variety of forms. Examples of some fillers are clay (alumina silicate), calcium carbonate, wollastonite, and glass microspheres.

To enhance the resistance of the matrix and to improve processing of FRP manufacturing, additives of various nature may be used, such as UV inhibitors, flame retardants, antioxidants, initiators (catalysts), wetting agents, color pigments, and mold release materials.

FRP MATERIAL CHARACTERISTICS

General

With regard to the use, design, and detailing of FRPs for reinforcing and strengthening concrete structures and to gain a fundamental understanding in the structural behavior, knowledge of the material characteristics of FRP is required. In the following sections, the physical and mechanical properties of FRP reinforcement are provided. A comparison between the main properties (order of magnitude) of FRP, fiber, epoxy, concrete, and steel is given in Table 21.4.

TABLE 21.4
Typical Properties (Order of Magnitude) of FRP, Fiber, Epoxy, Concrete, and Steel

Property	FRP[a]	Fiber[a]	Epoxy	Concrete	Steel
Comprehensive strength (MPa)	125–2400	—	55–100	25–150	200–2000
Tensile strength (MPa)	400–3000	1800–5000	9–20	1–6	200–2000
E-modulus (GPA)	35–500	60–800	0.5–20	25–50	≈200
CTE (10^{-6}/°C)	≈0 (longitudinal) 25–35 (transverse)	−6.0 to 5.0 (longitudinal) ≈ 45[b] (transverse)	25–30	8–12	≈10
Density (kg/m^3)	1300–2200	1400–2600	1200–1300	≈2400	≈7800
Poisson ratio	0.25–0.35	0.25–0.35	≈0.30	0.15–0.20	0.30

CTE, coefficient of thermal expansion.

[a] FRP based on glass, carbon, or aramid fiber with epoxy matrix.

[b] For aramid fiber (for carbon and glass, the transverse CTE is similar to the longitudinal CTE).

It is important to note that FRP can be designed and manufactured to coincide with specific requirements for its use as structural reinforcement. Indeed, the choice of the fibers and polymer matrix in relation to the applied volume fractions is deterministic for the constitutive behavior of FRP reinforcement. Furthermore, the material properties will be influenced by the production process, including dimensional effects and quality control during manufacturing. With respect to their use as structural reinforcement, FRP properties also relate to the level and duration of loading and to environmental effects such as temperature and humidity. Given these aspects, the material characteristics in the following are described on an overall basis, whereas for additional product-specific information, further reference is made to the manufacturers.

In structural engineering, normally the materials dealt with are basically (quasi-)isotropic. This is no longer the case for FRP materials, which are orthotropic due to the mostly unidirectional orientation of the continuous fibers. Because of the anisotropy, the various possibilities with respect to constituent materials, and the influence of the production process, properties of FRP materials depend on various factors. Therefore, material properties are preferably determined on the final products and by means of standard test methods. Recommendations for material testing and characterization of FRP for reinforcing and strengthening concrete structures are becoming more and more available [35–37]. For unified standards on FRP material testing, reference can also be made to work in progress by the International Standards Organization (ISO), Subcommittee ISO/TC71/SC6, on "Non Traditional Reinforcing Materials for Concrete."

FRP Type and Dimensions

As a first characterization, the type and the dimensions of the FRP reinforcement are of interest to know. These data deal with fiber type, polymer matrix, fiber orientation(s), nominal cross-sectional dimensions, length, and surface texture. The definition of the nominal cross section may differ and can be as follows. As FRP is generally produced with small tolerances on the dimensions, the nominal cross section is generally taken in relation to the global cross-sectional dimensions. Alternatively, referring to the continuous fibers as the principal stress-bearing component, an equivalent dry fiber cross section is sometimes used. The later is obtained as the ratio of the fiber mass per length (kilogram of fibers per unit length*) and the fiber density. For FRP with multiple fiber directions, where a different amount of fibers per unit length is applied in different fiber directions, the definition of the nominal dry fiber cross section always relates to the specified fiber direction, or more than one nominal cross section (or nominal thickness) may be given depending on the fiber direction.

As design verifications are based on equilibrium of forces, the definition of the nominal cross section (as far as used in a consistent way) does not influence the outcome of the design. However, if data sheets of FRP products are compared, the possible difference in defining the nominal cross section should be taken in mind. Indeed, the equivalent dry fiber cross section is considerably lower than the global cross section of the FRP, yielding higher values of the modulus of elasticity and the tensile strength. This is schematically illustrated in Figure 21.6, which shows how the stress–strain behavior, derived from load–strain tensile testing results, has a different appearance upon the definition of the nominal cross section. As demonstrated in, for example, Figure 21.8, the FRP properties differ significantly from the properties of the fibers. Hence, it may be recommended to refer to the global cross-sectional area, instead of the equivalent dry fiber cross section, in defining the nominal cross section of the FRP. This is to derive stress–strain curves which represent the actual composite behavior in a better way.

The surface texture of the FRP may range considerably between the different FRP products commercially available, for example, sand-coated surface, helicoidal indentations in the polymer-rich outer layer, and helicoidally winded yarn on the surface. Some examples of different surface

* In the textile industry, often reference is made to the unit tex. This is the weight in grams of 1000 m of yarn.

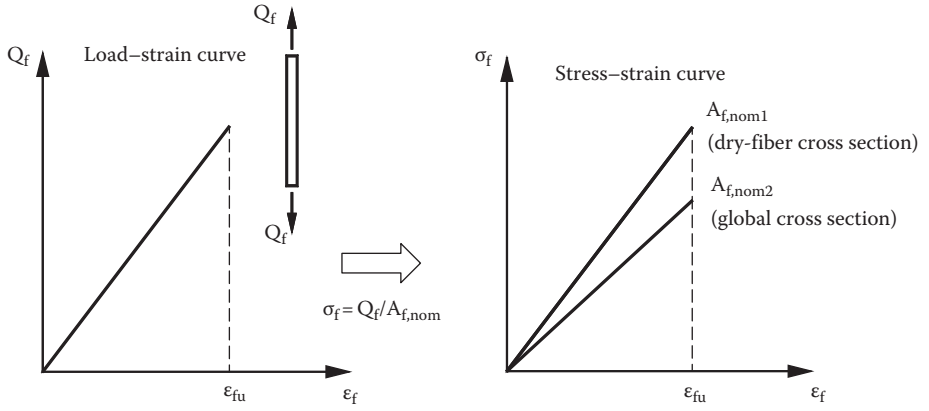

FIGURE 21.6 Influence of the definition of the nominal cross section.

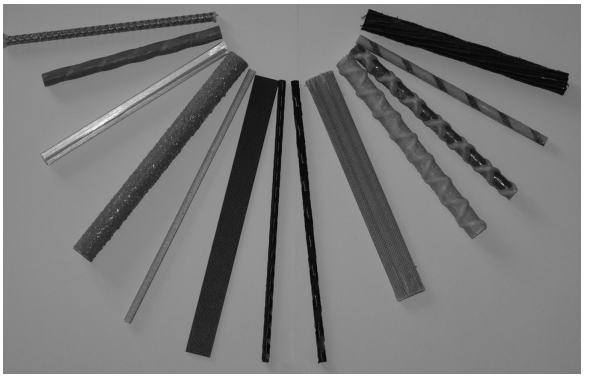

FIGURE 21.7 Examples of FRP bars with different surface texture.

textures are illustrated in Figure 21.7. The surface texture roughness is manufactured in such a way to obtain a good bond between the concrete and the FRP.

Physical Properties

Constituent Material Fractions and Density

FRP elements consist of fibers and a matrix, which are provided in certain quantities. The fraction of a constituent can be defined as the ratio of the constituent quantity to the total quantity of the composite. Constituent material fractions can be given either by mass (weight) or by volume. The mass fractions are obtained from tests. As the volume equals the mass divided by the density, the volume fraction follows from the mass fraction as

$$v_i = \frac{\rho_f}{\rho_i} m_i \tag{21.1}$$

where, v_i and m_i are, respectively, the volume and the mass fraction of constituent i. The density ρ_f of the fiber composite may be derived by applying the rule of mixture, often used for predicting unidirectional continuous fiber composite properties. Hereby, the composite property is estimated

as the sum of the constituent responses weighted by the component volume fractions. Accordingly, the density is given as

$$\rho_f = \sum \rho_i v_i \tag{21.2}$$

Or, also, from Equation 21.1 and given the fact that Σv_i equals 1

$$\rho_f = \frac{1}{\sum (m_i/\rho_i)} \tag{21.3}$$

Typically, the density of FRP reinforcement equals 1300–2200 kg/m^3. Compared to steel, FRP is about four times lighter.

Coefficient of Thermal Expansion

The CTE of steel and concrete is about the same and equal roughly to 10×10^{-6}/°C. As a result, thermal stresses at the bond interface of the steel reinforcement and the concrete are generally not significant. Values of the CTE for FRP reinforcement are mentioned in Table 21.5. Given the anisotropy, different values are obtained in the longitudinal and transverse directions. Compared to the value for concrete, the longitudinal CTE of FRP may differ significantly. As a result, temperature changes may unfavorably influence the bond between the FRP and the concrete. An even larger difference may be found for the transverse CTE. For internal reinforcement, a high transverse CTE may induce longitudinal cracking of the concrete cover for very shallow covers. In the case of external reinforcement, the transverse thermal expansion is of no influence as it is not restrained.

Glass Transition Temperature

The glass transition temperature T_g is of particular importance, as it reflects the change of molecular mobility of polymer materials. This change significantly influences the mechanical properties of a composite material when subjected to an elevated temperature (see further). At the glass transition temperature, the amorphous regions of polymers change from hard (glass like) to rubbery (viscous) or vice versa. Compared to the fibers, the glass transition temperature of the matrix is lower, so that the latter is deterministic for the behavior of FRP elements at elevated temperature. For factory-processed FRP elements, the matrix generally has a T_g in the range of 130°C–140°C. The T_g of cold-cured (ambient-cured) adhesives/saturating resins may be lower (in the range of about 50°C–80°C for epoxy).

Moisture Absorption and Chemical Stability

With regard to the durability of fiber composite materials, the chemical stability of FRP elements and their constituent materials subjected to moist, solvents, alkalis, acids, or UV light is of interest. Generally,

TABLE 21.5
Coefficient of Thermal Expansion

FRP Type	Longitudinal CTE (10^{-6}/°C)	Transverse CTE (10^{-6}/°C)
AFRP	≈–2	≈30
CFRP	≈0	≈25
GFRP	≈5	≈25

it can be assumed that moisture absorption and chemical reactions may occur over time, resulting in a certain material degradation. The rate and significance of the deterioration are to be evaluated against the envisaged service life and will depend on both mechanical and environmental loading. Although specific durability problems may arise, such as degradation of glass fibers under alkaline environment, fiber composite materials generally have a good to excellent durability in various environments. A more detailed discussion on durability and long-term behavior is given in the sections "Environmental Durability" and "Mechanical Behavior under Sustained and Cyclic Loading" of this chapter.

Mechanical Properties and Behavior under Short-Term Loading

Tensile Strength and Stress–Strain Behavior

FRP elements primarily act as tensile reinforcement, so that the tensile stress–strain behavior is of basic interest for design. Given the mechanical characteristics and volume fractions of the constituent materials, it is possible to estimate the basic properties of unidirectional FRP elements based on the rule of mixture simplification. The FRP tensile stress (based on the global cross section) is given as

$$\begin{aligned}\sigma_f &= \sigma_{fib} v_{fib} + \sigma_{mat} v_{mat} \\ &= \sigma_{fib} v_{fib} + \sigma_{mat} (1 - v_{fib})\end{aligned} \tag{21.4}$$

where the fiber and matrix stress are taken at the same strain level, hence assuming that fibers, matrix, and fiber composite undergo identical axial strain. The modulus of elasticity and Poisson ratio are obtained as

$$E_f = E_{fib} v_{fib} + E_{mat} (1 - v_{fib}) \tag{21.5}$$

$$\nu_f = \nu_{fib} v_{fib} + \nu_{mat} (1 - v_{fib}) \tag{21.6}$$

The stress–strain behavior of FRP, with σ_f according to Equation 21.4, is shown in Figure 21.8a. As the fibers are the main tensile stress-bearing element and as the fiber volume fraction is relatively high, the axial response of the FRP in tension is basically a reflection of that of the fibers. Compared to the fibers, the axial strength and modulus of elasticity of the FRP are lower. As the rule of mixture is an approximation of the micro-mechanical behavior of fiber composites, a more detailed prediction of the stress–strain behavior (especially near ultimate load) should be obtained through tensile testing, for example, according to [35–39]. Reflecting the fiber and matrix characteristics as well as microstructural aspects such as fiber diameter, distribution and parallelism of fibers, local defects, volume fractions, and fiber–matrix interfacial properties, the stress–strain behavior of FRP (as generally obtained through tensile testing) is shown in Figure 21.8b. Under increasing tensile load, it appears that the FRP stress–strain response stiffens and hence is not perfectly linear elastic. This is because the fibers are initially lightly crimped and not fully aligned, so that they straighten and become more effective under higher loads. Near ultimate load, the stiffness decreases again, as fibers start to fracture. Due to the load transfer from broken to intact fibers by the matrix, this does not immediately result in FRP fracture. Eventually, the FRP fails by fiber fracture and/or fiber delamination. Based on Equation 21.4 and because the contribution of the matrix to the axial strength is generally negligible, the axial FRP tensile strength equals about

$$f_f \approx f_{fib} v_{fib} \tag{21.7}$$

with, f_f and f_{fib} the tensile strength of the FRP and the fibers, respectively.

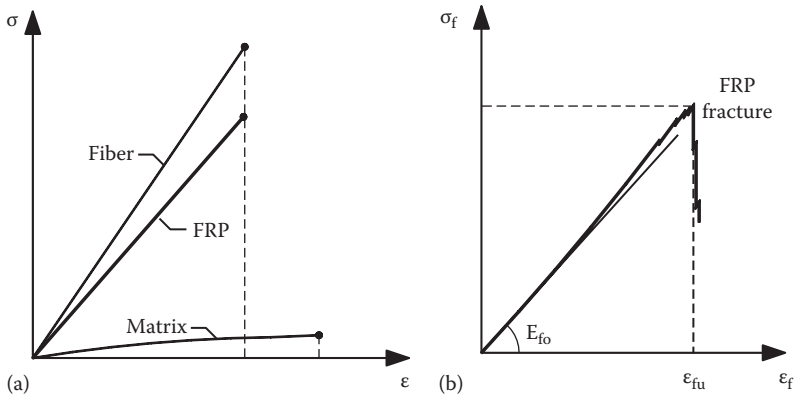

FIGURE 21.8 Tensile stress–strain behavior: (a) rule of mixture, (b) actual.

TABLE 21.6
Typical Tensile Properties of FRP

FRP Type	Tensile Strength, f_f (MPa)	Modulus of Elasticity, E_f (GPa)	Ultimate Strain, ε_{fu} (%)
CFRP	600–3000	80–500	0.5–1.8
GFRP	400–1600	30–60	1.2–3.7
AFRP	600–2500	30–125	1.8–4.0

In Table 21.6, typical values of the tensile strength, modulus of elasticity, and ultimate strain of FRP products are given. In Figure 21.3, the stress–strain behavior of some FRP elements is compared with steel. Both Table 21.6 and Figure 21.3 refer to the short-term static strength of straight specimens under normal laboratory conditions. For bended FRP elements, a reduced tensile strength is applicable. Due to stress concentrations and micro-buckling in the bend region, the tensile strength may be up to about 50% of the tensile strength of a straight bar. The influence on the strength (and stiffness) of aspects such as sustained loading, temperature, moisture, and UV radiation is discussed in the "Environmental Durability" and "Mechanical Behavior under Sustained and Cyclic Loading" sections.

Compressive Strength and Modulus of Elasticity

The compressive strength and modulus of elasticity of FRP elements are smaller than their counterparts in tension. A poor compressive strength is especially obtained for AFRP, while GFRP has a moderate and CFRP has a fairly high compressive strength. Indicative values, obtained from tests on FRP bars, are reported in Table 21.7 [22]. In [40], even lower values of the compressive strength are mentioned (10% for AFRP, 30% for GFRP and CFRP).

As concrete members generally have to be reinforced or strengthened in the tension region, the compressive strength of FRP is often of no relevance. Nevertheless, it may occur that certain zones of the FRP, normally subjected to tension, are also subjected to compression. This depends on the load distribution and the member configuration. Few information on the behavior of concrete members with FRP compression reinforcement is available. In [40,41], it has been demonstrated that FRP can be feasible as reinforcement in a compression region. On the other hand, given the generally low values for compressive strength and stiffness, most design guides recommend to neglect the contribution of FRP as compression reinforcement in the design. This design recommendation should however be considered with care, in case the FRP is subjected to both compressive and tensile strain

TABLE 21.7
Compressive Properties

FRP Type	$f_{f,comp}/f_{f,tens}$	$E_{f,comp}/E_{f,tens}$
CFRP	0.78	0.85
GFRP	0.55	0.80
AFRP	0.20	1.00

Source: ACI, Guide for the design and construction of structural concrete reinforced with FRP bars, ACI Report 440.1R-06, American Concrete Institute, ACI Committee 440, Detroit, MI, 2006.

(compression–tension cyclic loading). Indeed, the FRP tensile capacity will be adversely affected if FRP compression damage mechanisms start to occur.

Multiaxial Strength

Although primarily subjected to axial tension, the application of FRP requires transfer of the tensile force to the concrete and the complete FRP cross section. Due to this load transfer, mainly shear stresses are generated, which act on the interior of the FRP as well as on the bond interface. In general, the shear strength of the FRP is superior to that of the concrete. For FRP rebars with large diameter or FRP systems with a high number of plies, the interlaminar shear strength may become critical.

As the shear and transverse strength of unidirectional FRP elements mainly depend on the matrix, these strengths are low compared to the axial tensile strength. As a result, FRP elements are generally very vulnerable to, for example, gripping forces and direct impact loading. Also the dowel action of FRP rebars in concrete will be limited. By orienting fibers also in the off-axis direction(s), the multiaxial strength properties can be significantly improved. For FRP bars, this can be done by braiding or winding fibers transverse to the main fibers. In layered FRP systems, fibers in multiple directions can be introduced. Generally, by introducing additional fibers in the off-axis direction, at the same time, the strength in the main direction will be reduced. Given the low FRP strength with respect to gripping, special anchorage provisions are required when tensile testing is performed or for prestressing applications. Test results may highly depend on the way of testing, so that the use of standard tests is very important. Anchorage systems for FRP have been developed or investigated by several authors, among which [42–51].

Environmental Durability

The durability and long-term behavior of concrete structures reinforced or strengthened with FRP basically depend on the concrete structure, the FRP reinforcement, as well as the bond interaction. This section deals with the most important aspects regarding the durability of FRP composites. The long-term behavior under sustained or cyclic loading is discussed in the following section.

Temperature and Fire

Although fibers exhibit relatively high thermal stability, polymer resins are strongly affected by temperature. As a result, the material properties of FRP are influenced by temperature and decrease drastically when reaching the glass transition temperature T_g. In the event of fire, sufficient concrete cover should be available so that the glass transition temperature is reached only after the required time span. For external reinforcement systems, fire protections systems may be required.

More details on the influence of elevated temperature and fire on the mechanical properties of fibers and fiber composites are provided in [20,52,53].

Thermal Stresses and Freeze–Thaw Action

Subjected to a temperature change ΔT, thermal stresses are initiated in the FRP and the concrete. These stresses are due to the—by virtue of the bond interface—restraint difference in thermal expansion. In the interface, thermal bond stresses are generated, which may become critical for high values of ΔT [54]. Moreover, small defects such as microcracks and voids are generally present in the bond layer, which may further deteriorate under thermal cycling. The most critical condition is obtained in the case of wet freeze–thaw action, where also the expansion of freezing water is involved.

Durability with respect to wet freeze–thaw action has been investigated experimentally in [54–60]. Based on these tests, the following can be concluded:

- Tension tests on GFRP bars subjected to 141 freeze–thaw cycles under salt or alkaline immersion [55] revealed no strength loss in salt immersion and up to 15% strength loss in alkaline solution. The stiffness reduced up to 5% in salt immersion and up to 13% in alkaline solution. The order of magnitude of the strength and stiffness loss of the same immersion tests, without freeze–thaw cycling, was mostly similar. Hence, indicating a relatively small influence of the freeze–thaw action.
- A similar conclusion "environmental combined cycles did not produce significant damage in conditioned composites and residual physic-mechanical properties did not show a decrease in all cases" is drawn in [56], based on environmental durability tests on two types of GFRP rod and three types of CFRP rod.
- Also with respect to external reinforcement and bond to concrete, authors have generally found no negative effects [54,57–60]. Or if any, it is concluded that it relates to the freeze–thaw resistance of the concrete, rather than the FRP.

Influence of Moisture

Whereas carbon and glass fibers are relatively inert to water, damage may occur to the resin–glass fiber interface of GFRP due to the intrusion of moisture. In a similar way, a negative effect on the tensile strength and resin–fiber interface of AFRP may be expected, as aramid fibers tend to absorb moisture up to 4% by weight (8% if stored under water) [20]. Matrix materials absorb moisture as well, resulting in a reduction of the glass transition temperature and a stiffening of the resin. To deal with the negative influence of moisture, permeability and allowable water absorption of matrices are generally restricted.

Natural (outdoor exposure) and accelerated weathering tests (wet–dry cycles at a certain temperature) taking into account both fresh and salt water are reported in [57]. These tests indicate no tensile strength reduction of CFRP, whereas GFRP and AFRP show a significant decrease in the tensile strength. After 10,000 h wet–dry cycles at 65°C (assumed equivalent to about 50 years of exposure) and based on limited test results, a 35% and 30% tensile strength reduction was found for AFRP and GFRP, respectively. These test results should however be considered with caution as no indication was given on the T_g value. In [55], no tensile strength loss and minor stiffness loss are found after salt immersion of GFRP bars in ambient conditions. For CFRP to concrete bond in direct pull-off tensile testing, no negative influence of wet–dry cycles was found [57]. Results from moisture exposure test with and without applied stress and in combination with UV radiation have shown tensile strength loss of 0%–20% in CFRP, 0%–30% in AFRP, and 0%–40% in GFRP [61,62]. Outdoor exposure (close to the ocean) of FRP specimens gave no significant change of tensile strength or modulus of any of the tested GFRP, AFRP, and CFRP bars [63].

Chemical Resistance

The chemical resistance of FRP materials against acids, alkalis, and organic solvents mainly depends on the type of fiber, the resin system, and the mechanical loading (which may cause matrix microcracking), whereas increased temperature is used as a means to accelerate testing.

In general, FRP materials appear to have a good to excellent chemical resistance against chemical attack, although specific problems may occur.

Glass and aramid fibers generally have a low acid resistance, whereas the alkali resistance is moderate for aramid fibers and generally low for glass fibers. Carbon fibers have high chemical resistance. With respect to the resins, vinyl esters show superior resistance compared to polyesters, while epoxies are regarded to be very inert.

For concrete construction applications, given the alkaline environment of concrete, mainly the alkali resistance is of importance:

- Extensive deterioration in mechanical properties has been found for GFRP in alkaline solutions, especially at elevated temperatures and high mechanical stresses [64–66]. AFRP materials are less affected by alkaline solutions than GFRP. Nevertheless, combined with high tensile stresses, the lifetime of AFRP may considerably shorten [65,67]. CFRP with a proper fiber–resin system does not exhibit significant durability problems [56,64].
- For GFRP bars in a stressed and unstressed situation, losses up to 75% and 20% have been reported in literature, for tensile strength and stiffness, respectively [56,64–70]. For AFRP bars exposed to elevated-temperature alkaline solutions either with or without applied tensile stress, losses up to 50% and 20% have been reported in literature, for tensile strength and stiffness, respectively [65,67,71–73]. However, it is important to note that these generalized figures of strength and stiffness loss are to be considered with care, as often no or little information is available on the constituents of these bars. Some of these test results likely refer to fiber–resin systems that are not yet optimized. It is therefore important to consider product-specific test data instead of generalized data, where possible.
- Vinyl ester has a better resistance against alkaline environment than polyester [56,66]. Epoxy is regarded to be fairly inert [19]. In a recent study [56], the use of thermoplastic resin revealed to be a promising approach in terms of long-term potential degradation of E-glass fiber-based GFRP bars.
- Exposure to natural concrete environment appears considerably less severe than exposure to alkaline solutions (which simulate the concrete pore solution) [67].

UV Radiation

UV rays are known to affect fiber composites, although the effects are mainly limited to the surface of the composite [74]. Tests on fibers [75] demonstrated almost no tensile strength reduction for carbon fibers, while glass and especially aramid fibers appear susceptible to UV radiation. The tensile strength of matrix materials is only affected in a limited way [75], although color changes and reduced light transmissibility may occur. These latter aspects may be perceived by the public as an indication of loss of integrity of the composite. UV radiation on the surface of a composite may also lead to, for example, increased moisture absorption. Degradation due to UV light is of concern only in the case of external FRP reinforcement and can be solved by appropriate additives to resin systems or by protective paint.

Mechanical Behavior under Sustained and Cyclic Loading

FRP Creep and Creep Rupture

FRP reinforcement combines elastic fibers, which have excellent resistance to creep, with a viscoelastic polymer matrix, which may show significant creep deformations. Consequently, FRP creep will be mainly due to the creep of the matrix and the time-dependent growth of fiber–matrix debonding and resin microcracking [76]. As FRP tensile members normally have a high degree of fiber orientation, large fiber volume fractions, and a high ratio of fiber over matrix stiffness, the tensile force shared by the matrix is extremely low. Because of this and provided that the glass

transition temperature is well above the service temperature, FRP creep is generally negligible. Tests on FRP rods, at load levels in the range of 70%–90% of the tensile capacity, are reported in [77]. No significant creep was found for CFRP. For GFRP almost no and for AFRP very small creep was found; however, sudden jumps in the creep strain occurred after some time, which may correspond to the onset and growth of microstructural damage prior to creep rupture.

Whereas creep basically influences the long-term deformations, sustained stresses may also reduce the short-term tensile strength of FRP. This phenomenon, which occurs for most structural materials, is referred to as creep or stress rupture. The higher the sustained stress, the lower the endurance time (time under constant load after which creep rupture occurs). For low sustained loads, creep rupture may become irrelevant. Generally, CFRP can withstand stress levels up to at least 80% of its short-term strength, while considerably lower stress levels apply for AFRP (about 50% on a 50 year basis) and GFRP (about 30% on a 50 year basis) [20,77–79]. The permissible stress level can strongly depend on the fiber/resin system, the alignment of the fibers, and the fiber volume fraction. In addition, creep rupture is generally adversely influenced by the environmental conditions discussed in the previous section. In [76], based on a review of creep tests, it is suggested that the sustained stress in an adhesive joint should be limited to 25% of the short-term strength. Experimental tests reported in [77], on 6 mm FRP bars made of GFRP, AFRP, and CFRP, indicate a linear relationship between creep rupture strength and the logarithm of time (test data available for up to 100 h). Assuming that this linear trend on a logarithmic time scale can be extrapolated, the ratio of the creep rupture strength after 50 years over the short-term tensile strength was found to be 0.29, 0.47, and 0.93, for GFRP, AFRP, and CFRP, respectively. In [78], for commercial twisted CFRP and AFRP bars with an epoxy matrix, estimated values at 50 years of 0.79 and 0.66 have been found, for CFRP and AFRP, respectively. Creep rupture strength of GFRP bars with vinyl ester matrix has been investigated in [79]. An extrapolated value of 0.55 has been found for the creep rupture strength ratio after 50 years.

Relaxation

To be able to account for prestressing losses in the design of FRP prestressed concrete, it is important to know the relaxation (loss of tensile stress in a tensile element kept at a constant length) of FRP prestressing elements. Carbon and glass fibers show almost no relaxation, while aramid fibers have significant relaxation. In addition, the viscoelastic polymer matrix will be subjected to relaxation as well. Hence, the lower the fiber volume, the more pronounced the relaxation.

The amount of relaxation has been demonstrated to be very dependent on the environment (temperature, moisture, alkaline solution). The higher the temperature, the greater the relaxation rate. In [20], results of relaxation tests are reported. For CFRP stressed at 80% of its characteristic tensile strength, superior relaxation is obtained compared to prestressing steel. The relaxation of GFRP stressed at 50% of its characteristic tensile strength appeared somewhat higher than prestressing steel (low relaxation class) tensioned at 60%, whereas the measured GFRP relaxation loss was equal to about 2% after 1000 h. The relaxation of AFRP is significantly higher compared to GFRP and CFRP and is found equal to about 10% at 1000 h. According to [80], relaxation after 1000 h can be estimated as 1.8%–2.0% for GFRP tendons, 0.5%–1.0% for CFRP tendons, and 5.0%–8.0% for AFRP tendons, depending on the initial tensile stress. Relaxation of GFRP, CFRP, and AFRP tendons after 50 years of loading can be estimated as 4.0%–14.0%, 2.0%–10.0%, and 11.0%–25.0%, respectively.

Prestressing losses due to relaxation of FRP, especially for AFRP, has only a limited influence on the design. Indeed, the prestressing loss due to shrinkage and creep of the concrete is equivalent with the ratio of the modulus of elasticity E_p/E_c (with, E_p the E-modulus of the prestressing element and E_c the E-modulus of concrete). E_p/E_c equals about six in the case of prestressing steel and only about three in the case of AFRP. Hence, the prestressing loss due to shrinkage and creep is, in the case of AFRP, only half of that for prestressing steel. This means that the higher prestressing loss due to relaxation of AFRP is compensated by a lower prestressing loss due to concrete shrinkage and creep.

Cyclic Loading

If a material is subjected to a large number of load cycles, growth of internal or surface flaws may occur, resulting in a reduced mechanical strength compared to the short-term static strength. The phenomenon is generally referred to as fatigue. High-modulus fiber composites have superior fatigue resistance, as has been demonstrated in research for aerospace applications. The cyclic tension fatigue of resin-impregnated fibers (fiber volume of about 60%) loaded under ambient laboratory conditions in tension–tension with a minimum to maximum stress ratio ($\sigma_{min}/\sigma_{max}$) of 0.1 is given in Table 21.8, based on a review of data conducted in [22]. The values in Table 21.8 represent the average downward slope of the test results in a plot of the maximum stress versus the logarithm of the number of cycles at failure (whereby $\sigma_{min}/\sigma_{max} = 0.1$). In terms of stress range $\Delta\sigma$ ($= \sigma_{max} - \sigma_{min}$) versus number of load cycles until failure (S–N curves), the fatigue strength of unidirectional AFRP and CFRP exceeds that of prestressing steel, while that of GFRP is lower [20]. The fatigue strength of CFRP is higher than that for AFRP. Some values are given in Table 21.9. As the fatigue limit of the matrix is lower than that of the fibers, fatigue failure is usually governed by damage in the matrix and at the fiber–matrix interface [76]. Consequently, the influence of environmental exposure on the fatigue behavior is basically related to the sensitivity of the matrix against environmental conditions. Furthermore, as high-modulus fibers and large fiber volume fractions result in low matrix strains, this has a beneficial influence on the fatigue resistance. Deformations (such as ribs or wraps to increase bond behavior of FRP) may adversely affect the fatigue strength compared to flat composite specimens. These deformations can induce local stress concentrations that significantly affect the performance of a GFRP bar under fatigue loading [81]. In [82], based on fatigue testing of CFRP, indications have been found that the fatigue resistance decreases with increasing loading frequency.

TABLE 21.8
Fatigue Strength of Fiber Polymer Composites (for $\sigma_{min}/\sigma_{max} = 0.1$)

FRP Type	Degradation of Initial Static Strength per Decade of Logarithmic Fatigue Lifetime
CFRP	≈5%
GFRP	≈10%
AFRP	≈5%–6%

TABLE 21.9
Fatigue Strength of Reinforcement after 2.10^6 Cycles

Type	σ_{max}/f_{tk}[a]	$\Delta\sigma$[b] (MPa)
Prestressing steel	~0.60	~200
E-glass/polyester (rod)	~0.50	~60
E-glass/epoxy (rod)	~0.50	~75
Aramid/vinylester (rod)	~0.60	~235
Carbon/vinylester (rod)	~0.60	>350
Carbon/epoxy (strand)	~0.60	~310

[a] Applied maximum stress as a function of the characteristic tensile strength of the reinforcement.
[b] Stress range yielding fatigue failure at 2.10^6 cycles.

Regarding concrete to FRP bond, also the fatigue performance of the polymer as such is of importance. In [76], it is concluded that the stress range of cold cured epoxies, not subjected to service temperatures above 45°C, should be limited to 4 MPa. As bond shear stresses in the serviceability limit state of concrete structures are considerably lower than the concrete shear strength (which also equals about 4 MPa), effect of fatigue on the bond may be limited. Cyclic loading bond test on deformed GFRP bars have been reported in [83–85], using different GFRP types, environments, and test configurations. The obtained test results gave different trends and indicated that bond strength can either increase, decrease, or remain the same after cyclic loading. Further investigations on the bond strength may be required.

Residual Strength after Sustained or Cyclic Loading

Knowing the creep rupture and fatigue resistance, permissible stress levels can be applied for the design to avoid creep rupture or fatigue failure. These permissible stress levels should however also take into consideration that at the end of the service life, sufficient residual strength is required. Few studies on residual strength after sustained or cyclic loading can be found in the literature [20,86–88]. Tentatively it may be concluded that FRP reinforcement has a high strength retention after sustained or cyclic loading. It is only for situations close to creep rupture or fatigue failure that the residual tensile strength is considerably lower than the short-term static strength.

BEHAVIORAL ASPECTS

Given the properties of FRP reinforcement, some overall observations with respect to the expected behavior of concrete elements reinforced with FRP can be made as follows:

1. Given their excellent corrosion resistance, FRP materials offer a strong potential in enhancing sustainability of concrete structures. From a materials point of view, this requires that the FRP elements are designed and manufactured properly and hence that the durability is considered explicitly in the development of specific FRP reinforcing elements.
2. Given the high strength of FRP, relatively small cross-sectional areas are needed to reinforce or strengthen concrete elements with respect to the ultimate limit state (strength considerations).
3. On the other hand, to fulfill serviceability criteria, sufficient flexural stiffness should be available. Once cracked, the stiffness of a reinforced concrete section significantly depends on the stiffness of the reinforcement. Due to the small cross-sectional area needed for strength considerations and the generally lower modulus of elasticity of most FRP materials in comparison with steel, serviceability problems may arise when the design is based on the ultimate limit state only.
4. By prestressing, serviceability criteria can easily be satisfied and the FRP strength can be utilized in a more optimum way. Furthermore, it can be noted that a low modulus of elasticity of the FRP prestressing reinforcement is beneficial in terms of long-term prestressing losses due to creep and shrinkage of the concrete. On the other hand, as the transverse strength of FRP is considerably lower than its axial strength, special anchorage devices have to be used for FRP prestressing.
5. Given the linear elastic behavior of FRP reinforcement up to failure, energy dissipation in concrete members with FRP may be significantly different compared to steel-reinforced concrete elements. Properly designed FRP-reinforced or -strengthened members will exhibit large deformability before failure and/or a high safety margin between the ultimate and the service load. In specific situations, additional ductility measures may be required [89] (e.g., FRP confinement of columns for seismic strengthening).

6. Fire resistance of polymeric matrix-based FRP is limited. In the case of internal reinforcement, this involves the use of sufficient concrete cover protection.
7. The advanced material properties of FRP and the fact that FRP products are available in a variety of forms, characteristics, and shapes create opportunities for the novel use of FRP in terms of efficient construction materials and techniques, with respect to both internal or external reinforcement for concrete structures.

CONCLUSIONS

The design and application of FRP to reinforce concrete structures require adequate knowledge of FRP materials and their characteristics. From the overview presented in this chapter, it follows that FRP reinforcement forms a group of materials, with high-performance characteristics that strongly depend on the assembly of constituent materials. From the literature overview on physical and mechanical characteristics of fibers, matrices, and fiber composites, it can be concluded that FRP reinforcement is generally very strong and durable. Nevertheless, like any structural material, their performance may be negatively influenced by certain environmental and loading conditions. Evaluating the properties of AFRP, CFRP, and GFRP, CFRP will exhibit generally the best performance. Nevertheless, also AFRP and GFRP have strong potentials to be used as FRP reinforcement, in addition to alternative materials currently under investigation.

REFERENCES

1. ACI, FRP around the world, *ACI Concrete International*, 21(10), 1999.
2. Taerwe, L. and Matthys, S., FRP reinforcement for concrete structures: State-of-the-art, in *Proceedings of the 1999 IABSE Symposium on Structures for the Future—The Search for Quality*, Rio de Janeiro, Brazil, 1999, pp. 578–585.
3. Taerwe, L. and Matthys, S., FRP for concrete construction: Activities in Europe, *ACI Concrete International*, 21(10), 33–36, 1999.
4. Matthys, S. and Taerwe, L., Use of advanced composites in concrete construction, in *Proceedings of the International Conference on Technology Watch and Innovation in the Construction Industry*, Brussels, Belgium, 2000, pp. 177–184.
5. Clarke, J.L., Ed., *Alternative Materials for the Reinforcement and Prestressing of Concrete*, Chapman & Hall, London, U.K., 1993.
6. Nanni, A., Ed., *Fibre-Reinforced-Plastic (FRP) Reinforcement for Concrete Structures: Properties and Applications, Developments in Civil Engineering 42*, Elsevier Science, Amsterdam, the Netherlands, 1993.
7. Rizkalla, S. and Nanni, A., Eds., *Field Applications of FRP Reinforcement: Case Studies*, ACI SP-215, American Concrete Institute, Farmington Hills, MI, 2003.
8. Triantafillou, T., Ed., Fiber-reinforced polymer reinforcement for concrete structures, in *Proceedings of the FRPRCS-8 Symposium*, Patras, Greece, 2007, pp. 564–595.
9. Neville, A.M., *Properties of Concrete*, 3rd edn., John Wiley & Sons, New York, 1981.
10. Hewlett, P.C., *Lea's Chemistry of Cement and Concrete*, 4th edn., Arnold, London, U.K., 1998.
11. MacGregor, J.G. and Wight, J.K., *Reinforced Concrete: Mechanics and Design*, 4th edn., Pearson Prentice Hall, Upper Saddle River, NJ, 2006.
12. Comité Euro-International du Béton, *CEB-FIP Model Code 1990—Design Code*, Thomas Telford, London, U.K., 1993.
13. Portland Cement Association, *Principles of Quality of Concrete*, John Wiley & sons, New York, 1975.
14. De Schutter, G., Bartos, P.J.M., Domone, P., and Gibbs, J., *Self-Compacting Concrete*, Whittles Publishing, Caithness, U.K., 2007.
15. Mays, G., Ed., *Durability of Concrete Structures: Investigation, Repair, Protection*, Spon, London, U.K., 1992.

16. Matthys, S., Material characteristics, FRP EBR systems and techniques, in Structural Behaviour and Design of Concrete Members Strengthened with Externally Bonded FRP Reinforcement, Ph.D. thesis, Ghent University, Ghent, Belgium, 2000, http://hdl.handle.net/1854/3679.
17. Bakis, E.B., FRP reinforcement: Materials and manufacturing, in *Fibre-Reinforced-Plastic (FRP) Reinforcement for Concrete Structures: Properties and Applications, Developments in Civil Engineering 42*, Nanni, A., Ed., Elsevier Science, Amsterdam, the Netherlands, 1993, pp. 13–58.
18. Malek, A.M. and Saadatmanesh, H., Physical and mechanical properties of typical fibres and resins, in *Proceedings of the 1st International Conference on Composites in Infrastructure*, Saadatmanesh, H. and Ehsani, M.R., Eds., University of Arizona, Tucson, AZ, 1996, pp. 68–79.
19. Hutchinson, A.R. and Quinn, J., Materials, in *Strengthening of Reinforced Concrete Structures Using Externally Bonded FRP Composites in Structural and Civil Engineering*, Hollaway, L.C. and Leeming, M.B., Eds., Woodhead Publishing, London, U.K., 1999, pp. 46–82 (Chapter 3).
20. Rostásy, F.S., Ed., Evaluation of potentials and production technologies of FRP, Report No. BREU 1-92, BRITE Project 4142/BREU-CT 91 0515, Fibre Composite Elements and Techniques as Non-Metallic Reinforcement of Concrete, 1992.
21. ACI, State-of-the-art report on fibre reinforced plastic reinforcement for concrete structures, ACI Report 440R-96, American Concrete Institute, ACI Committee 440, Detroit, MI, 1996.
22. ACI, Guide for the design and construction of structural concrete reinforced with FRP bars, ACI Report 440.1R-06, American Concrete Institute, ACI Committee 440, Detroit, MI, 2006.
23. fib, FRP reinforcement in reinforced concrete structures (Technical report on the design and use of fibre reinforced polymer (FRP) reinforcement in reinforced concrete structures), fib Bulletin, International Federation for Structural Concrete, fib Task Group 9.3, Lausanne, Switzerland, 2007, 160pp.
24. Gay, D., Hoa, S.V., and Tsai, S.W., *Composite Materials—Design and Applications*, CRC Press, Boca Raton, FL, 2003.
25. Tierens, M., Verkennend onderzoek naar het gebruik van basaltvezels voor de versterking van betonconstructies (Feasibility study on the use of basalt fibres for reinforcement of concrete structures), in Dutch, Master dissertation (supervisor Matthys, S), Ghent University, Faculty of Engineering, Ghent, Belgium, 2007.
26. Coleman, J.N., Khan, U., Blau, W.J., and Gun'ko, Y.K., Small but strong: A review of the mechanical properties of carbon nanotube-polymer composites, *Carbon*, 44(9), 1624–1652, 2006.
27. Hearle, J.W.S., Ed., *High Performance Fibres*, Woodhead Publishing, London, U.K., 2001.
28. National Research Council, *High-Performance Structural Fibres for Advanced Polymer Matrix Composites*, Committee on High-Performance Structural Fibres for Advanced Polymer Matrix Composites, National Materials Advisory Board, National Academic Press, Washington, DC, 2005.
29. Wu, Z.S., Iwashita, K., Hayashi, K., Higuchi, T., Murakami, S., and Koseki, Y., Strengthening prestressed-concrete girders with externally prestressed PBO fiber reinforced polymer sheets, *Journal of Reinforced Plastics and Composites*, 22(14), 1269–1286, 2003.
30. Imjai, T., Guadagnini, M., and Pilakoutas K., Use of thermoplastic FRP composites as shear reinforcement for concrete structures, in *Proceedings of the 3rd International Conference on Advanced Composites in Construction*, University of Bath, Bath, U.K., 2007, pp. 273–281.
31. Vanderpool, D.R., Micelli, F., and Nanni, A., Thermoplastic rebar: Performance and applications, in *Proceedings of the CCC 2001, Composites in Construction*, Figuerias, J., Juvandes L., and Furia, R., Eds., Porto, Portugal, 2001, pp. 153–157.
32. Fukushima, T., Sakayama, K., and Hashimoto, S., Dynamic behaviours of continuous carbon and glass fiber reinforced thermoplastics (CFRP and GFRP) for recyclable non-metallic reinforcements for concrete structures, in *Proceedings of the 3rd International Symposium on Non-Metallic (FRP) Reinforcement for Concrete Structures*, Japan Concrete Institute, Sapporo, Japan, 1997, Vol. 2, pp. 235–241.
33. Sumida, A., Mutsuyoshi, H., and Pandey, G.R., Development of new heat-resisting FRP bars, in *Proceedings of the 8th International Symposium on Fiber-Reinforced Polymer Reinforcement for Concrete Structures*, Triantafillou, T., Ed., University of Patras, Patras, Greece, 2007, pp. 438–439.
34. Toutanji, H., Zhao, L., and Zhang, Y., Flexural behavior of reinforced concrete beams externally strengthened with CFRP sheets bonded with an inorganic matrix, *Engineering Structures*, 28(4), 557–566, 2006.
35. ACI, Guide test methods for fiber-reinforced polymers (FRPs) for reinforcing or strengthening concrete structures, ACI Report 440.3R-06, American Concrete Institute, ACI Committee 440, Detroit, MI, 2004.
36. JSCE, Test methods for continuous fibre reinforcing materials, in *Recommendation for Design and Construction of Concrete Structures using Continuous Fibre Reinforcing Materials, Concrete Engineering Series 23*, Machida, A., Ed., Japan Society of Civil Engineers, Tokyo, Japan, 1997, pp. 91–167.
37. BUtgb, Gelijmde wapening (Bonded reinforcement), in Dutch, Technical approval and certification guide no. G0026, Belgian Union for Technical Approvals in the Construction Sector, Brussels, Belgium, 2004.

38. ASTM, *Standard Test Method for Tensile Properties of Polymer Matrix Composite Materials*, D 3039/D 3039M, Book of ASTM Standards, Vol. 15.03, American Society for Testing and Materials (ASTM), Philadelphia, PA, 2006.
39. CEN, Plastics. Determination of tensile properties. Test conditions for unidirectional fibre-reinforced plastic composites, EN ISO 527:5, Comité Européen de Normalisation (CEN), Brussels, Belgium, 1997.
40. Kobayashi, K. and Fujisaki, T., Compressive behaviour of FRP reinforcement in non-prestressed concrete members, in *Proceedings of the 2nd International Symposium on Non-Metallic (FRP) Reinforcement for Concrete Structures*, Taerwe, L., Ed., Ghent, Belgium, 1995, pp. 267–274.
41. Deuring, M., Verstärken von Stahlbeton mit gespannten Faserverbund-werkstoffen (Strengthening of reinforced concrete with prestressed FRP), in German, EMPA Bericht No. 224, Swiss Federal Laboratories for Materials Testing and Research, Dübendorf, Switzerland, 1993.
42. Al-Mayah, A., Soudki, K.A., and Plumtree, A., Development and Assessment of a New CFRP rod-anchor system for prestressed concrete, *Applied Composite Materials*, 13(5), 321–334, 2006.
43. Yu, P., Silva, P. F., and Nanni, A., Innovative mechanical device for the post-tensioning of glass fiber reinforced polymer bars for masonry type retrofit applications, *Journal Experimental Mechanics*, 44, (3), 272–277, 2004.
44. Al-Mayah, A., Soudki, K., and Plumtree, A., Mechanical behaviour of CFRP rod anchors under tensile loading, *Journal of Composites for Construction*, 5, 128–135, 2001.
45. Pincheira, J.A. and Woyak, J.P., Anchorage of carbon fiber reinforced polymer (CFRP) tendons using cold-swaged sleeves, *PCI Journal*, 46, 100–111, 2001.
46. Sayed-Ahmed, E.Y. and Shrive, N.G., A new steel anchorage system for post-tensioned applications using carbon fibre reinforced plastic tendons, *Canadian Journal of Civil Engineering*, 25, 113–127, 1998.
47. Kerstens, G.M., Bennenk, W., and Camp, J.W., Prestressing with carbon composite rods: A numerical method for developing reusable prestressing systems, *ACI Structural Journal*, 95, 43–50, 1998.
48. Nanni, A., Bakis, C.E., O'Neil, E.F., and Dixon, T.O., Performance of FRP tendon-anchorage systems for prestressed concrete structures, *PCI Journal*, 41(1), 34–44, 1996.
49. Meier, U. and Farshad, M., Connecting high-performance carbon-fiber-reinforced polymer cables of suspension and cable-stayed bridges through the use of gradient materials, *Journal of Computer-Aided Materials Design*, 3, 379–384, 1996.
50. Scheibe, M. and Rostasy, F.S., Aspects of laboratory testing to determine mechanical properties of FRP, in *Proceedings of the 2nd International Symposium on Non-Metallic (FRP) Reinforcement for Concrete Structures*, Taerwe, L., Ed., Ghent, Belgium, 1995, pp. 116–123.
51. Erki, M.A. and Rizkalla, S.H., Anchorages for FRP reinforcement, *Concrete International*, 15(6), 54–59, 1993.
52. Blontrock, H., Taerwe, L., and Matthys, S., Properties of fibre reinforced plastics at elevated temperatures with regard to fire resistance of reinforced concrete members, in *Proceedings of the 4th International Symposium on Fibre Reinforced Polymer Reinforcement for Reinforced Concrete Structures*, Dolan, C.W., Rizkalla, S.H., and Nanni, A., Eds., American Concrete Institute, Detroit, MI, 1999, pp. 43–54.
53. Wang, Y.C., Wong, P.M.H., and Kodur, V., Mechanical properties of fibre reinforced polymer reinforcing bars at elevated temperatures, NRCC-47020, National Research Council, Ottawa, Ontario, Canada, 2003.
54. Kaiser, H., Bewehren von Stahlbeton mit kohlenstoffaserverstärkten Epoxidharzen (CFRP reinforcement for reinforced concrete), in German, Ph.D thesis, Technical University of Zürich, Zürich, Switzerland, 1989.
55. Vijay, P.V., GangaRao, H.V.S., and Kalluri, R., Hygrothermal response of GFRP bars under different conditioning schemes, in *Proceedings of the 1st International Conference on Durability of Fibre Reinforced Polymer (FRP) Composites for Construction*, Benmokrane, B. and Rahman, H., Eds., Sherbrooke, Quebec, Canada, 1998, pp. 243–252.
56. Micelli, F. and Nanni, A., Durability of FRP rods for concrete structures, *Construction and Building Materials*, 18(7), 491–503, 2004.
57. Yagi, K., Tanaka, T., Sakai, H., and Otaguro, H., Durability of carbon fiber sheet for repair and retrofitting, in *Proceedings of the 3rd International Symposium on Non-Metallic (FRP) Reinforcement for Concrete Structures*, Japan Concrete Institute, Sapporo, Japan, 1997, Vol. 2, pp. 259–266.
58. Tysl, S.R., Imbrogno, M., and Miller, B.D., Effect of surface delamination on the freeze-thaw durability of CFRP-reinforced concrete beams, in *Proceedings of the 1st International Conference on Durability of Fibre Reinforced Polymer (FRP) Composites for Construction*, Benmokrane, B. and Rahman, H., Eds., Sherbrooke, Quebec, Canada, 1998, pp. 317–324.
59. Toutanji, H. and Rey, F., Durability characteristics of concrete columns wrapped with FRP tow sheets, in *Proceedings of 3rd International Symposium on Non-Metallic (FRP) Reinforcement for Concrete Structures*, Japan Concrete Institute, Sapporo, Japan, 1997, Vol. 2, pp. 251–258.

60. Green, M.F., Bisby, L.A., Fam, A.Z., and Kodur, V.K.R., FRP confined concrete columns: Behaviour under extreme conditions, *Cement and Concrete Composites*, 28(10), 928–937, 2006.
61. Sasaki, I., Nishizaki, I., Sakamoto, H., Katawaki, K., And Kawamoto, Y., Durability evaluation of FRP cables by exposure tests, in *Proceedings of the 3rd International Symposium on Non-Metallic (FRP) Reinforcement for Concrete Structures*, Japan Concrete Institute, Sapporo, Japan, 1997, Vol. 2, pp. 131–137.
62. Uomoto, T., Durability of FRP as reinforcement for concrete structures, in *Proceedings of the 3rd International Conference on Advanced Composite Materials in Bridges and Structures*, Humar, J.L. and Razaqpur, A.G., Eds., Canadian Society for Civil Engineering, Montreal, Québec, Canada, 2000, pp. 3–17.
63. Tomosawa, F. and Nakatsuji, T., Evaluation of the ACM reinforcement durability by exposure test, in *Proceedings of the 3rd International Symposium on Non-Metallic (FRP) Reinforcement for Concrete Structures*, Japan Concrete Institute, Sapporo, Japan, 1997, Vol. 2, pp. 139–146.
64. Porter, M.L., Mehus, J., Young, K.A., O'neil, E.F., and Barnes, B.A., Ageing for fibre reinforcement in concrete, in *Proceedings of the 3rd International Symposium on Non-Metallic (FRP) Reinforcement for Concrete Structures*, Japan Concrete Institute, Sapporo, Japan, 1997, Vol. 2, pp. 59–66.
65. Uomoto, T. and Nishimura, T., Development of new alkali resistant hybrid AGFRP rod, in *Proceedings of the 3rd International Symposium on Non-Metallic (FRP) Reinforcement for Concrete Structures*, Japan Concrete Institute, Sapporo, Japan, 1997, Vol. 2, pp. 67–74.
66. Gangarao, H.V.S. and Vijay, P.V., Ageing of structural composites under varying environmental conditions, in *Proceedings of the 3rd International Symposium on Non-Metallic (FRP) Reinforcement for Concrete Structures*, Japan Concrete Institute, Sapporo, Japan, 1997, Vol. 2, pp. 91–98.
67. Scheibe, M. and Rostasy, F.S., Stress-rupture behaviour of AFRP-bars in concrete and under natural environment, in *Proceedings of the 2nd International Conference on Fibre Composites in Infrastructure*, Tucson, AZ, 1998, Vol. 2, pp. 138–151.
68. Bank, L.C. and Puterman, M., Microscopic study of surface degradation of glass fiber-reinforced polymer rods embedded in concrete castings subjected to environmental conditioning, in *High Temperature and Environmental Effects on Polymeric Composites*, ASTM STP 1302, Gates, T.S. and Zureick, A.-H., Eds., ASTM International, West Conshohocken, Pa., 1997, Vol. 2, pp. 191–205.
69. Porter, M.L. and Barnes, B.A., Accelerated aging degradation of glass fiber composites, in *Proceedings of the 2nd International Conference on Composites in Infrastructure*, Saadatmanesh, H. and Eshani, M.R., Eds., University of Arizona, Tucson, AZ, 1998, Vol. 2, pp. 446–459.
70. Tannous, F.E. and Saadatmanesh, H., Durability of AR-glass fiber reinforced plastic bars, *Journal of Composites for Construction*, 3(1), 12–19, 1999.
71. Sen, R., Shahawy, M., Rosas, J., and Sukumar, S., Durability of aramid pretensioned elements in a marine environment, *ACI Structural Journal*, 95(5), 578–587, 1998.
72. Takewaka, K. and Khin, M., Deterioration of stress-rupture of FRP rods in alkaline solution simulating as concrete environment, in *Proceedings of the 2nd International Conference on Advanced Composite Materials in Bridges and Structures*, El-Badry, M.M., Ed., Canadian Society for Civil Engineering, Montreal, Québec, Canada, 1996, pp. 649–664.
73. Gerritse, A., Durability criteria for non-metallic tendons in an alkaline environment, in *Proceedings of the 1st International Conference on Advanced Composite Materials in Bridges and Structures*, Canadian Society of Civil Engineers, Sherbrooke, Quebec, Canada, 1992, pp. 129–137.
74. Bank, L.C. and Gentry, T.R., Accelerated test methods to determine the long-term behavior of FRP composite structures: Environmental effects, *Journal of Reinforced Plastic and Composites*, 14, 558–587, 1995.
75. Kato, Y., Nishimura, T., and Uomoto, T., The effect of ultraviolet rays to FRP rods, in *Proceedings of the 1st International Conference on Durability of Fibre Reinforced Polymer (FRP) Composites for Construction*, Benmokrane, B. and Rahman, H., Eds., Sherbrooke, Quebec, Canada, 1998, pp. 487–497.
76. Barnes, R.A. and Garden, H.N., Time-dependent behaviour and fatigue, in *Strengthening of Reinforced Concrete Structures Using Externally Bonded FRP Composites in Structural and Civil Engineering*, Hollaway, L.C. and Leeming, M.B., Eds., Woodhead Publishing, London, U.K., 1999, pp. 183–221 (Chapter 7).
77. Yamaguchi, T., Nishimura, T., and Uomoto, T., Creep model of FRP rods based on fibre damaging rate, in *Proceedings of the 1st International Conference on Durability of Fibre Reinforced Polymer (FRP) Composites for Construction*, Benmokrane, B. and Rahman, H., Eds., Sherbrooke, Quebec, Canada, 1998, pp. 427–437.

78. Ando, N., Matsukawa, H., Hattori, A., and Mashima, A., Experimental studies on the long-term tensile properties of FRP tendons, in *Proceedings of the 3rd International Symposium on Non-Metallic (FRP) Reinforcement for Concrete Structures*, Japan Concrete Institute, Sapporo, Japan, 1997, Vol. 2, pp. 203–210.
79. Seki, H., Sekijima, K., and Konno, T., Test method on creep of continuous fiber reinforcing materials, in *Proceedings of the 3rd International Symposium on Non-Metallic (FRP) Reinforcement for Concrete Structures*, Japan Concrete Institute, Sapporo, Japan, 1997, Vol. 2, pp. 95–202.
80. Balazs, G.L. and Borosnyoi, A., Long-term behaviour of FRP, in *Proceedings of the International Workshop on Composites in Construction: A Reality*, Cosenza, E., Manfredi, G., and Nanni, A., Eds., American Society of Civil Engineers, Reston, VA, 2001, pp. 84–91.
81. Katz, A., Effect of helical wrapping on fatigue resistance of GFRP, *Journal of Composites for Construction*, 2(3), 121–125, 1998.
82. Adimi, R., Rahman, H., Benmokrane, B., and Kobayashi, K., Effect of temperature and loading frequency on the fatigue life of a CFRP bar in concrete, in *Proceedings of the 2nd International Conference on Composites in Infrastructure*, Tucson, AZ, 1998, Vol. 2, pp. 203–210.
83. Katz, A., Bond to concrete of FRP rebars after cyclic loading, *Journal of Composites for Construction*, 4(3), 137–144, 2000.
84. Bakis, C.E., Al-Dulaijan, S.U., Nanni, A., Boothby, T.E., and Al-Zahrani, M.M., Effect of cyclic loading on bond behavior of GFRP rods embedded in concrete beams, *Journal of Composites Technology and Research*, 20(1), 29–37, 1998.
85. Sippel, T.M. and Mayer, U., Bond behavior of FRP strands under short-term, reversed and cyclic loading, in *Proceedings of the 2nd International Conference on Advanced Composite Materials in Bridges and Structures*, El-Badry, M.M., Ed., Canadian Society for Civil Engineering, Montreal, Québec, Canada, 1996, pp. 837–844.
86. Guedes, R.M., Durability of polymer matrix composites: Viscoelastic effect on static and fatigue loading, *Composites Science and Technology*, 67(11–12), 2574–2583, 2007.
87. Michaelov, G. and Kihl, D.P., Comparative study of nonlinear damage accumulation models in stochastic fatigue of FRP laminates, *Journal of Structural Engineering*, 127(3), 314–323, 2001.
88. Yao, W.X. and Himmel, N., A new cumulative fatigue damage model for fibre-reinforced plastics, *Composites Science and Technology*, 60(1), 59–64, 2000.
89. Naaman, A.E. and Jeong, S.M., Structural ductility of concrete beams prestressed with FRP tendons, in *Proceedings of the 2nd International Symposium on Non-Metallic (FRP) Reinforcement for Concrete Structures*, Taerwe L., Ed., *RILEM Proceedings 29*, Spon, London, U.K., 1995, pp. 379–386.

22 Design Procedures

Luke A. Bisby, Brea Williams, and Ching Chiaw Choo

CONTENTS

INTRODUCTION

The ultimate goal of expanding the base of fiber-reinforced polymer (FRP) material and behavioral knowledge is the development and calibration of design codes for use by practicing engineers. These documents serve to link research with practical applications and to eventually enable design engineers to produce durable and sustainable infrastructure systems.

To safely and efficiently design concrete members reinforced with FRP, it is crucial to understand the fundamental behavior of FRP materials and how this differs from conventional steel

reinforcement. Several of the unique material properties of FRPs and FRP-reinforced concrete (RC) members, and their implications on design procedures, are the following:

- *Linear elastic behavior*: Conventional steel reinforcement typically displays elastic–plastic behavior. Thus, when steel reinforcement in RC members yields, large deformations are often possible with little loss in load-carrying capacity, and this provides warning of structural failure as evidenced by extensive cracking and deflection. FRP materials used as internal reinforcement for concrete are typically linear elastic to failure, with no yielding, and the failure of RC members reinforced with FRPs can thus be comparatively sudden. To compensate for the relative absence of clear warnings of failure, FRP-reinforced RC members are often designed for a desired "deformability" and a higher reserve of strength. As discussed later, serviceability requirements often govern the design of FRP RC members in any case, and the strength is consequently much higher than that required to satisfy the ultimate limit state.
- *Comparatively low stiffness*: Currently available FRP reinforcing bars have elastic moduli that are considerably lower than steel reinforcing bars. This results in smaller post-cracking stiffness of FRP RC flexural members that can lead to larger deflections than that would be encountered with conventionally reinforced designs. Consequently, service deflections must be checked as they often govern the design in flexural reinforcing applications. Low stiffness reinforcement can also result in larger crack widths under service loads and may compromise the concrete's contribution to shear strength (through aggregate interlock) in shear reinforcing applications.
- *Relatively low compressive modulus*: Steel reinforcement displays equal stiffness in both tension and compression, allowing the use of steel reinforcing bars in both tensile and compressive applications. FRP materials typically display compressive moduli that are considerably less than their tensile values. FRP reinforcement is thus not currently recommended for use in compression.
- *Corrosion resistance*: The standard crack width limitations of ACI 318 (ACI, 2005) that apply to steel-reinforced RC members can, in certain cases, be relaxed for FRP-reinforced members because electrochemical corrosion of reinforcement is not a concern in the latter case. Accordingly, larger crack widths are often permitted in FRP RC members (although the reader will note that relaxed crack width limitations may be inappropriate in cases where widths are limited for aesthetic reasons or to ensure shear strength of concrete).
- *Diverse nature of FRP constituents and characteristics*: Manufacturers offer a wide range of fibers, resins, additives, curing techniques, and surface finishes for FRP reinforcing materials. Quality control and manufacturing processes can also affect FRP product performance, as can assorted durability considerations (see Chapter 10). With the current diversity of available products and properties, and ongoing development expected in the future, available design documents tend to suggest conservative approaches for the design of FRP RC. It is expected that this conservatism will relax in the years to come, as additional research and field performance data become available.

Many organizations have developed design codes and/or guidelines for the use of internal FRP reinforcement in RC members. These include the American Concrete Institute (ACI, 2004, 2006), the Canadian Standards Association (CSA, 2002, 2006), the Japan Society of Civil Engineers (JSCE, 1997), the International Federation for Structural Concrete (Fib, 2005), the British Institution of Civil Engineers (BISE, 1999), the Italian National Research Council (CNR, 2006), the Norwegian Standards agency (NS, 2003), and Intelligent Sensing for Innovative Structures Canada (ISIS, 2001, 2006).

While numerous codes and guidelines are currently available, this chapter outlines design procedures on the basis of those currently recommended by Committee 440 of the ACI, in the document ACI 440.1R-06, "Guide for the Design and Construction of Concrete Reinforced with FRP Bars" (ACI, 2006). ACI 440.1 uses strength-based design and draws from the related ACI document for the

design of conventionally reinforced concrete structures, ACI 318-05, "Building Code Requirements for Structural Concrete and Commentary" (ACI, 2005) as the philosophical basis of its design approaches for FRP RC members. ACI 440.1 applies limit state design principles, where an FRP RC member is first designed for strength and then checked for fatigue endurance, creep rupture limits, and satisfaction of various serviceability criteria (which often govern the design).

The reader will note that the following information is not a design code and does not purport to exhaustively cover all of the important information in this area. Rather, the goal herein is to provide a general understanding and awareness of the philosophies and approaches currently used in typical design of FRP RC elements in North America. Clearly, the ACI 440.1 source document (or the specific design code that is applicable in a given region) must be consulted prior to embarking on an actual design.

Following the lead of ACI 440.1 (ACI, 2006), the design considerations discussed herein include the following:

- Design material properties
- Design for flexure
- Serviceability criteria
- Creep rupture and fatigue
- Design for shear
- Development and splices of reinforcement

DESIGN MATERIAL PROPERTIES

Because of the wide variety of currently available FRP reinforcing products, generalized values for their mechanical properties cannot always be provided. Whereas typical yield strengths of different grades of steel reinforcement are widely accepted and standardized, for FRP reinforcement, the designer must often use material properties provided by the FRP bar manufacturer (or determined through testing by a certified laboratory). Specification documents are emerging however (e.g., ISIS, 2006), and it is hoped that in time, these will lead to standardization of FRP reinforcing bar properties across most manufacturers.

Material properties provided by reputable FRP bar manufacturers typically represent guaranteed initial values. With time and exposure to the environment, the mechanical properties of FRP reinforcement may decrease due to a variety of interrelated factors. To account for this potential degradation, the mechanical properties of FRP reinforcing bars are typically reduced, as shown in Equations 22.1 and 22.2 from ACI 440.1 (ACI, 2006). These equations require that the tensile strength and rupture strain be reduced to account for environmental effects using an environmental reduction factor, C_E. The modulus of elasticity (E_f) is apparently indirectly assumed not to be affected.

Table 22.1 shows the ACI 440.1-suggested environmental reduction factors used to convert the manufacturers' guaranteed mechanical properties to the design mechanical properties.

TABLE 22.1
Environmental Reduction Factors, C_E

	Type of Fiber		
Exposure Condition	**Carbon**	**Glass**	**Aramid**
Concrete not exposed to earth and weather	1.0	0.8	0.9
Concrete exposed to earth and weather	0.9	0.7	0.8

Source: ACI, *Guide for the Design and Construction of Concrete Reinforced with FRP Bars*, ACI 440.1R-06, American Concrete Institute, Farmington Hills, MI, 2006.

These values are considered conservative estimates based on the available research and are influenced by the durability of each bar type under various exposure conditions, as discussed in Chapter 10. For instance, carbon FRP (CFRP) bars are considered to be more resistant to environmental degradation within concrete than glass FRP (GFRP) bars, as reflected in the higher C_E value suggested for CFRP. Although small-range temperature effects are implicitly included in the environmental reduction factors, it is not recommended that FRP bars be subjected to environments where the temperature might exceed the glass transition temperature (T_g) of the bar's polymer resin, due to the anticipated severe loss of bond strength at these temperatures (Katz et al., 1999). Thus, the design tensile strength of FRP reinforcing bars is given by

$$f_{fu} = C_E f_{fu}^* \tag{22.1}$$

where

f_{fu} is the design tensile strength of FRP reinforcement, considering reductions due to environmental effects (MPa)

C_E is the environmental reduction factor, as reproduced in Table 22.1

f_{fu}^* is the guaranteed tensile strength of FRP reinforcement, as provided by the FRP manufacturer (MPa)

The guaranteed tensile strength is taken as the mean tensile strength determined from a sample of standard test specimens minus three times the standard deviation of the sample strengths.

Similarly, the design tensile rupture strain of an FRP bar is

$$\varepsilon_{fu} = C_E \varepsilon_{fu}^* \tag{22.2}$$

where

ε_{fu} is the design rupture strain of FRP reinforcement, considering reductions due to environmental effects

ε_{fu}^* is the guaranteed rupture strain of FRP reinforcement, as provided by the FRP manufacturer

The guaranteed rupture strain is the mean rupture strain determined from a sample of standard test specimens minus three times the standard deviation of the sample strains.

In addition to considering environmental effects, the FRP bar geometry must also be accounted for in the design properties. Bent FRP bars, such as those used as lateral and shear reinforcement in concrete, display significantly reduced tensile strength at the bend location(s) due to transverse stresses and stress concentrations that arise at the bend locations. The available research data (Ehsani et al., 1995) indicate that the tensile strength developed at the bend of a GFRP bar is a function of the geometry of the bend, the tail length, and the concrete strength. Adapting a design recommendation from the JSCE (1997), ACI 440.1 suggests the following tensile strength of a bent FRP bar, f_{fb} (in the absence of specific test data on a particular bent bar configuration):

$$f_{fb} = \left(0.05\frac{r_b}{d_b} + 0.3\right) f_{fu} \le f_{fu} \tag{22.3}$$

where

f_{fb} is the strength of the bent portion of an FRP bar (MPa)

r_b is the internal radius of the FRP bar bend (mm)

d_b is the diameter of the FRP bar (mm)

f_{fu} is the design tensile strength of the FRP bar, accounting for environmental reductions (MPa)

FLEXURAL DESIGN

The design of FRP RC members for flexure uses similar standard assumptions and follows similar methodologies as are used in the design of conventional steel RC members, although allowances must be made to account for the unique material characteristics of FRP.

Design Assumptions

The following standard assumptions are typical for the design of both steel and FRP RC members according to ACI procedures (ACI, 2005, 2006, 2011):

- Perfect bond exists between the reinforcement and the concrete
- Plane sections before bending remain plane after bending (i.e., strain compatibility holds)
- The maximum useable compressive strain in the concrete is 0.003
- Cracked concrete has no strength in tension

An additional assumption is required in the case of FRP RC members in bending, namely,

- FRP behavior is linear elastic to failure

Potential Failure Modes

In the flexural design of steel RC members, under-reinforced sections are preferred since this ensures that the steel reinforcement yields in tension before the concrete crushes in compression and provides considerable warning prior to member failure. In FRP RC, rupture of the FRP reinforcement in tension prior to concrete crushing is invariably sudden and provides little warning. In general, FRP RC members exhibit less ductility than steel RC members. Existing guidelines for flexural design of FRP RC typically prefer concrete crushing prior to FRP rupture. This failure mode is more desirable because the member will exhibit some plastic behavior prior to failure (Nanni, 1993). In addition, because the modulus of FRP bars is less than steel reinforcement, FRP RC members may exhibit large deflections prior to failure, and some codes (e.g., ISIS, 2006) have used the concept of flexural "deformability" to ensure that adequate warning is provided prior to failure.

While concrete crushing is a more desirable failure mode, ACI 440.1 (ACI, 2006) allows designs on the basis of either FRP rupture prior to concrete crushing, or concrete crushing prior to FRP rupture, provided that both the strength and serviceability requirements specified in the code are satisfied. However, higher strength reserves (i.e., smaller strength reduction factors) are used in the former case to account for the lack of ductility/deformability exhibited by flexural members that are designed to fail by rupture of the FRP reinforcement (see the following text).

Flexural Design Equations

Basic Capacity Equation

As is typical for limit state flexural design procedures in RC, the basic capacity condition that must be satisfied in the design of FRP RC members is (ACI, 2006) thus:

$$\phi M_n \geq M_u \tag{22.4}$$

where

ϕ is the strength reduction factor, as discussed in the "Design Flexural Capacity: Strength Section Reduction Factors" section

M_n is the nominal moment capacity of FRP RC member (N·mm)

M_u is the factored (ultimate) moment expected to act on a section, as determined using load factors suggested by ACI 318 (N·mm)

The nominal moment capacity of an FRP RC section can be calculated using traditional methods for steel RC members by assuming a failure mode and subsequently applying strain compatibility and force equilibrium to determine the section's capacity (as outlined in the following sections). The assumed failure mode must be verified. Satisfaction of Equation (22.4) is the first step in the safe design of an FRP RC structural member.

Balanced Reinforcement Ratio and Assumed Failure Mode

To assume a failure mode for a given FRP RC section, the balanced FRP reinforcement ratio must first be determined and compared to the reinforcement ratio provided in the section. It is important to recognize that the balanced FRP reinforcement ratio for FRP RC sections has a different meaning than the balanced reinforcement ratio for conventional steel RC sections. When the balanced reinforcement ratio is provided in an FRP-reinforced section, the FRP is assumed to fail in tension simultaneously with the concrete crushing in compression. Below the balanced FRP reinforcement ratio, the FRP is assumed to rupture before concrete crushing, and above the balanced FRP reinforcement ratio, the concrete is assumed to crush prior to FRP failure. Equations 22.5 and 22.6 define the FRP reinforcement ratio (ρ_f) and the balanced FRP reinforcement ratio (ρ_{fb}), respectively. For a rectangular concrete section, the FRP reinforcement ratio is defined similarly as the familiar steel reinforcement ratio:

$$\rho_f = \frac{A_f}{bd} \tag{22.5}$$

where

A_f is the area of FRP reinforcement (mm^2)
b is the width of rectangular concrete section (mm)
d is the distance from extreme compression fiber to centroid of tensile reinforcement (mm)

The balanced FRP reinforcement ratio is found using strain compatibility, equilibrium of cross-sectional forces, and by assuming an equivalent rectangular compressive stress block in the concrete (in the same manner as is commonly done for conventional RC design) (ACI, 2006):

$$\rho_{fb} = 0.85\beta_1 \frac{f'_c}{f_{fu}} \frac{E_f \varepsilon_{cu}}{E_f \varepsilon_{cu} + f_{fu}} \tag{22.6}$$

where

β_1 is the stress block factor taken as 0.85 for concrete strength, f'_c, up to and including 30 MPa. Above this threshold, the factor is reduced by 0.05 for every 7 MPa increase in strength. This value should not be taken less than 0.65
f'_c is the specified compressive strength of concrete (MPa)
E_f is the guaranteed modulus of elasticity of FRP, as specified by the manufacturer (MPa)
ε_{cu} is the ultimate strain in concrete = 0.003 according to ACI design procedures (ACI, 2005, 2011)

Because FRP reinforcing bars are linear elastic and typically have ultimate tensile strengths several times those of typical mild steel reinforcement, the balanced reinforcement ratio for FRP RC members is typically much lower than the balanced reinforcement ratio for an equivalent steel RC member.

Nominal Flexural Capacity

The flexural capacity of an FRP RC section must be calculated on the basis of one of the three possible failure modes: (a) failure by concrete crushing, (b) balanced failure, and (c) failure by FRP rupture. The assumed stress and strain distributions associated with each of these cases are illustrated in Figure 22.1 and are used to derive design equations for the first and third failure modes.

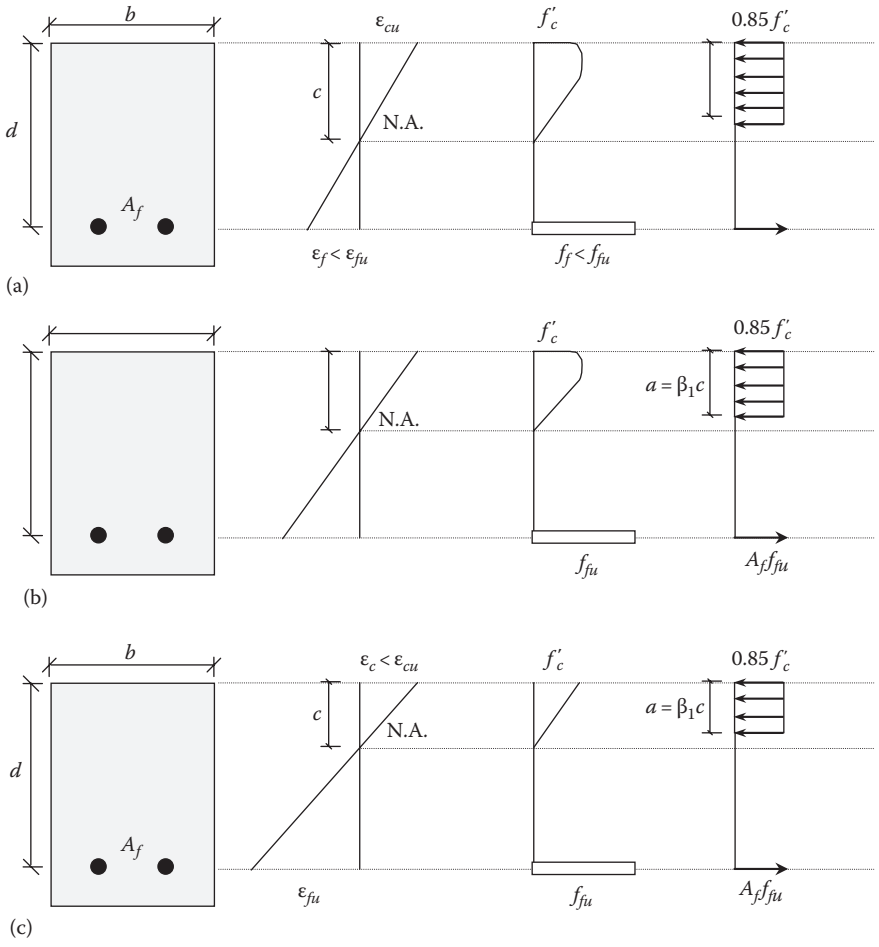

FIGURE 22.1 Strain and stress distributions at various failure conditions: (a) concrete crushing, (b) balanced failure, and (c) FRP rupture.

Concrete Crushing Failure ($\rho_f > \rho_{fb}$)

When $\rho_f > \rho_{fb}$, concrete crushing is the governing failure mode, and the equivalent stress block may be used to represent the stress distribution in the compression zone. The tensile and compressive forces in the FRP reinforcement and concrete are respectively

$$T = A_f f_f \tag{22.7}$$

and

$$C = 0.85 f'_c ab \tag{22.8}$$

Since the stress in the FRP reinforcement is less than ultimate, it must be expressed as a function of its location within the section. Using strain compatibility gives (refer to Figure 22.1a)

$$f_f = E_f \varepsilon_{cu} \frac{\beta_1 d - a}{a} \tag{22.9}$$

Substituting Equation 22.9 into 22.7), and Equating to 22.8, the stress in the FRP at failure is (ACI, 2006)

$$f_f = \left(\sqrt{\frac{(E_f \varepsilon_{cu})^2}{4} + \frac{0.85\beta_1 f_c'}{\rho_f} E_f \varepsilon_{cu}} - 0.5 E_f \varepsilon_{cu} \right) \leq f_{fu} \tag{22.10}$$

The earlier expression can subsequently be used to determine the depth of the equivalent concrete stress block, a:

$$a = \frac{A_f f_f}{0.85 f_c' b} \tag{22.11}$$

and the flexural capacity of the section, M_n,

$$M_n = A_f f_f \left(d - \frac{a}{2} \right) \tag{22.12}$$

or

$$M_n = \rho_f f_f \left(1 - 0.59 \frac{\rho_f f_f}{f_c'} \right) b d^2 \tag{22.13}$$

Example 22.1

Nominal flexural capacity when concrete crushing failure governs

Problem

Determine the nominal flexural capacity of a simply supported concrete beam of normal-density concrete with f_c' of 25 MPa. Due to architectural constraints, the beam must be 250 mm wide by 450 mm deep. GFRP reinforcement is to be used, with a guaranteed tensile strength of 620 MPa, a tensile elastic modulus of 44.8 GPa, and a guaranteed rupture strain of 0.014. Three 20 mm-nominal diameter GFRP bars (A_f = 300 mm^2 per bar) are provided as flexural reinforcement. The beam has an internal exposure condition.

Step 1: Determine the design tensile properties of the FRP

Because the GFRP will be used to reinforce an interior beam, the exposure factor, C_E, from Table 22.1 is 0.80. Applying Equations 22.1 and 22.2 gives the design tensile properties for the GFRP bars as

$$\begin{aligned} f_{fu} &= C_E f_{fu}^* \\ &= 0.80\,(620\,\text{MPa}) \\ &= 496\,\text{MPa} \end{aligned}$$

$$\begin{aligned} \varepsilon_{fu} &= C_E \varepsilon_{fu}^* \\ &= 0.80\,(0.014) \\ &= 0.0112 \end{aligned}$$

Step 2: Compute the FRP reinforcement ratio
As an initial estimate, assume 40 mm cover and 10 mm-diameter bars for shear reinforcement. The resulting depth to the tensile reinforcement is

$$\begin{aligned} d &= h - \text{cover} - \text{stirrup} - \frac{d_b}{2} \\ &= 450\text{mm} - 40\text{mm} - 10\text{mm} - \frac{20\text{mm}}{2} \\ &= 390\text{mm} \end{aligned}$$

Applying Equation 22.5, the corresponding FRP reinforcement ratio is

$$\begin{aligned} \rho_f &= \frac{A_f}{bd} \\ &= \frac{3(300\text{mm}^2)}{250\text{mm}(390\text{mm})} \\ &= 0.0092 \end{aligned}$$

Step 3: Determine the stress level in the FRP reinforcement
Applying Equation 22.10, the stress in the FRP reinforcement when the concrete crushes (i.e., when the concrete compression fiber reaches a compressive strain of 0.003) is

$$\begin{aligned} f_f &= \left(\sqrt{\frac{(E_f\varepsilon_{cu})^2}{4} + \frac{0.85\beta_1 f_c'}{\rho_f} E_f\varepsilon_{cu}} - 0.5E_f\varepsilon_{cu} \right) \\ &= \left(\sqrt{\frac{(44.8\times10^3\,\text{MPa}(0.003))^2}{4} + \frac{0.85(0.85)(25\,\text{MPa})}{0.0092} 44.8\times10^3\,\text{MPa}(0.003)} \right. \\ &\quad \left. -0.5(44.8\times10^3\,\text{MPa})(0.003) \right) \\ &= 451\text{MPa} < f_{fu} = 496\,\text{MPa} \end{aligned}$$

Note that the actual stress in the FRP at failure is less than the rupture strength of the reinforcement; therefore, concrete crushing is the governing failure mode, as assumed. This can also be verified by checking the FRP reinforcement ratio against the balanced FRP reinforcement ratio.

Step 4: Determine the balanced FRP reinforcement ratio
Applying Equation 22.6, the balanced FRP reinforcement ratio for this rectangular section is

$$\begin{aligned} \rho_{fb} &= 0.85\beta_1 \frac{f_c'}{f_{fu}} \frac{E_f\varepsilon_{cu}}{E_f\varepsilon_{cu} + f_{fu}} \\ &= 0.85(0.85)\left(\frac{25\,\text{MPa}}{496\,\text{MPa}}\right)\left(\frac{44.8\times10^3\,\text{MPa}(0.003)}{44.8\times10^3\,\text{MPa}(0.003) + 496\,\text{MPa}}\right) \\ &= 0.0078 \end{aligned}$$

The actual FRP reinforcement ratio, $\rho_f = 0.0092$, is greater than the balanced ratio, $\rho_{fb} = 0.0078$, confirming that the concrete crushes before tensile rupture of the FRP.

Step 5: Compute the nominal flexural capacity
Using Equation 22.13, the flexural capacity of the section is

$$M_n = \rho_f f_f \left(1 - 0.59\frac{\rho_f f_f}{f'_c}\right) bd^2$$

$$= 0.0092(451\,\text{MPa})\left(1 - 0.59\frac{(0.0092)(451\,\text{MPa})}{25\,\text{MPa}}\right)\frac{(250\,\text{mm})(390\,\text{mm})^2}{1\times10^6}$$

$$= 142\,\text{kN}\cdot\text{m} \Leftarrow$$

FRP Rupture Failure ($\rho_f < \rho_{fb}$)
When FRP rupture is the governing failure mode, the assumed maximum concrete compressive strain of 0.003 may not actually be achieved in the concrete at failure. As a result, the equivalent rectangular stress block assumed at failure (which is typically appropriate to assume in the design of conventional under-reinforced concrete sections, or FRP RC sections that fail by concrete crushing) may not be applicable. The result is a situation in which, strictly speaking, modified stress block factors would be required, and two additional unknowns (i.e., stress block parameters α_1 and β_1) are introduced. Since four unknowns are thus involved in the resulting analysis (ε_c, c, α_1, β_1), simplified equations have been developed and adopted by ACI 440.1 (ACI, 2006) to allow conservative estimation of the neutral axis depth, c, and the nominal moment capacity of the section, as shown in the following:

$$c_b = \left(\frac{\varepsilon_{cu}}{\varepsilon_{cu} + \varepsilon_{fu}}\right) d \tag{22.14}$$

where c_b is the distance from extreme compression fiber to the neutral axis at the balanced strain condition (Figure 22.1b). Thus, the following equation can be used to approximate the nominal flexural capacity when concrete strains are less than ultimate at the rupture of the FRP reinforcement.

$$M_n = A_f f_{fu}\left(d - \frac{\beta_1 c_b}{2}\right) \tag{22.15}$$

In Equation 22.15, the product $\beta_1 c_b$ is the maximum possible value for $\beta_1 c$, thus providing a conservative estimate of the nominal moment capacity.

Example 22.2

Nominal flexural resistance when FRP rupture governs

Problem
Using the same beam geometry and dimensions as in Example 22.1, calculate the nominal flexural capacity when two 20 mm-diameter GFRP bars are provided as tensile reinforcement.

Step 1: Determine the design tensile properties of the FRP
From Example 22.1, the design tensile strength is 496 MPa, and the design rupture strain is 0.0112.

Step 2: Compute the FRP reinforcement ratio
Applying Equation 22.5,the corresponding FRP reinforcement ratio is

$$\rho_f = \frac{A_f}{bd}$$

$$= \frac{2(300\,\text{mm}^2)}{(250\,\text{mm})(390\,\text{mm})}$$

$$= 0.0062$$

The geometry of the section is the same as in the previous example; therefore, the balanced FRP reinforcement ratio is 0.0078. Since the actual $\rho_f = 0.0062 < \rho_{fb} = 0.0078$, FRP rupture occurs before crushing of the compression concrete.

Step 3: Determine the location of the neutral axis of a balanced section
Applying Equation 22.14, the neutral axis depth for an equivalent balanced section is

$$\begin{aligned} c_b &= \left(\frac{\varepsilon_{cu}}{\varepsilon_{cu}+\varepsilon_{fu}}\right)d \\ &= \left(\frac{0.003}{0.003+0.0112}\right)(390\,\text{mm}) \\ &= 82\,\text{mm} \end{aligned}$$

Step 4: Compute the nominal flexural capacity of the section
Using Equation 22.15, the simplified conservative estimate of the nominal flexural capacity of the section is

$$\begin{aligned} M_n &= A_f f_{fu}\left(d-\frac{\beta_1 c_b}{2}\right) \\ &= 2(300\,\text{mm}^2)(496\,\text{MPa})\left(390\,\text{mm}-\frac{(0.85)(82\,\text{mm})}{2}\right)/1\times10^6 \\ &= 106\,\text{kN}\cdot\text{m} \Leftarrow \end{aligned}$$

Design Flexural Capacity: Strength Reduction Factors

To compensate for the relative lack of ductility exhibited by most FRP RC flexural members, conservative strength reduction factors must be applied to the nominal moment capacities discussed previously. This is identical to the approach used for conventional steel RC design. For instance, when failure is initiated by concrete crushing, as is the case in the design of an over-reinforced conventional steel RC flexural member, ACI 318 (ACI, 2011) recommends a strength reduction factor, ϕ, of 0.65. A similar philosophy can be applied to FRP RC members and is suggested by ACI 440.1 (ACI, 2006). When failure by concrete crushing governs, the strength reduction factor for FRP RC members in flexure is 0.65. However, when failure is by the even less ductile failure mode of FRP rupture, ACI 440.1 recommends that a further reduction of strength be applied, leading to a reduction factor, ϕ, of 0.55.

In addition, ACI 440.1 recognizes that, in practice, concrete members may not be constructed exactly as per the engineer's design due to human error or other unavoidable factors. For instance, a concrete mix with a higher strength may actually be used in constructing an FRP RC member that was originally designed to fail by concrete crushing. If this occurs, the member may actually fail due to the less desirable failure mode of FRP rupture rather than the assumed failure mode of concrete crushing. In part to account for such possibilities, a flexural reduction factor transition region is recommended between FRP rupture and concrete crushing failure modes as illustrated in Figure 22.2 and described by Equation 22.16. FRP RC members with FRP reinforcement ratios less than 40% greater than the balanced reinforcement ratio are designed using a strength reduction factor somewhat less than 0.7 (ACI, 2006).

$$\phi = \begin{cases} 0.55 & \text{when } \rho_f \le \rho_{fb} \\ 0.3+0.25\dfrac{\rho_f}{\rho_{fb}} & \text{when } \rho_{fb} < \rho_f < 1.4\rho_{fb} \\ 0.65 & \text{when } \rho_f \ge 1.4\rho_{fb} \end{cases} \tag{22.16}$$

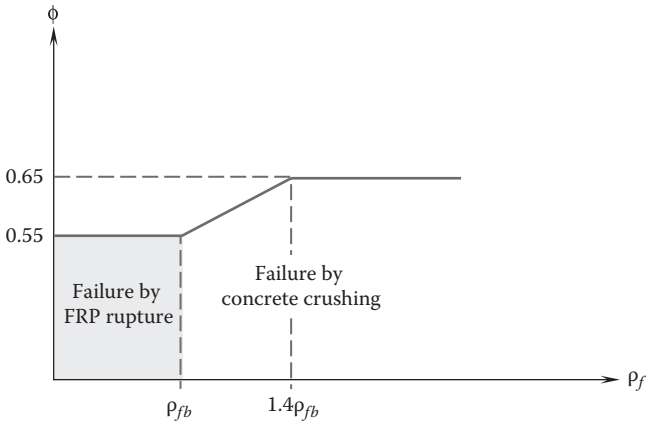

FIGURE 22.2 Flexural strength reduction factor, ϕ, as a function of FRP reinforcement ratio, ρ_f.

Example 22.3

Flexural design strength (using reduction factors)

Problem
Determine the design flexural capacities for the beams described in Examples 22.1 and 22.2.

Step 1: Determine the applicable region of Figure 22.2 (i.e., FRP rupture, transition region, or concrete crushing)

From example 22.1

$$\rho_{fb} = 0.0078 < \rho_f = 0.0092 < 1.4\rho_{fb} = 0.0109$$

Therefore, the strength reduction factor falls in the transition region between φ = 0.55 and φ = 0.65.

From example 22.2

$$\rho_f = 0.0062 < \rho_{fb} = 0.0078$$

Therefore, the strength reduction factor falls in the "FRP rupture" region where φ = 0.55.

Step 2: Calculate the strength reduction factor

For Example 22.1, the strength reduction factor in the transition region is determined using Equation 22.16:

$$\varphi = 0.3 + 0.25\frac{\rho_f}{\rho_{fb}}$$

$$= 0.3 + 0.25\left(\frac{0.0092}{0.0078}\right) = 0.59$$

For Example 22.2, the strength reduction factor when FRP rupture occurs is 0.55.

Step 3: Calculate the flexural capacities

The flexural capacities of each of the beams in the previous examples are thus:

Example 22.1

$$\varphi M_n = (0.59)(142\ \text{kN} \cdot \text{m}) = 84\ \text{kN} \cdot \text{m} \Leftarrow$$

Example 22.2

$$\varphi M_n = (0.55)(110\ \text{kN} \cdot \text{m}) = 61\ \text{kN} \cdot \text{m} \Leftarrow$$

Minimum FRP Reinforcement

When FRP rupture is the governing failure mode, a minimum amount of FRP reinforcement is required to ensure that failure will not occur when the concrete cracks in tension under first loading beyond cracking the cracking moment. ACI 318 (ACI, 2005, 2011) uses this philosophy for steel RC members, and its equation, shown as follows, can therefore be modified for use in FRP RC design.

$$A_{s,\min} = \frac{\sqrt{f_c'}}{4f_y} b_w d \geq \frac{1.4}{f_{fy}} b_w d \tag{22.17a}$$

Whereas ACI 318 uses a strength reduction factor of 0.9 when failure occurs due to tension-controlled failure (i.e., steel yielding), ACI 440.1 uses a reduction factor of 0.55 when FRP rupture governs. Thus, multiplying the earlier ACI 318 equation by a factor of 0.90/0.55 = 1.64 provides an equation for the minimum amount of FRP reinforcement.

$$A_{f,\min} = \frac{0.41\sqrt{f_c'}}{f_{fu}} b_w d \geq \frac{2.29}{f_{fu}} b_w d \tag{22.17b}$$

This equation need not be checked when concrete crushing is the governing failure mode, since the minimum FRP reinforcement area is automatically satisfied.

Example 22.4

Minimum FRP reinforcement

Problem

Determine the minimum area of FRP reinforcement for the beam described in Example 22.1.

Applying Equation 22.17b,

$$\begin{aligned} A_{f\,\min} &= \frac{0.41\sqrt{f_c'}}{f_{fu}} b_w d \\ &= \left(\frac{0.41\sqrt{25\ \text{MPa}}}{496\ \text{MPa}} \right) (250\ \text{mm})(390\ \text{mm}) \\ &= 403\ \text{mm}^2 \end{aligned}$$

$$A_{f,\min} \geq \frac{2.29}{f_{fu}} b_w d$$

$$= \left(\frac{2.29}{496\ \text{MPa}} \right) (250\ \text{mm})(390\ \text{mm})$$

$$= 450\ \text{mm}^2 \Leftarrow$$

Therefore, the minimum area of FRP reinforcement in the section is 450 mm^2, which is satisfied by the three 20 mm-diameter bars that are provided.

Other Important Issues

Multiple Layers of FRP Reinforcement

When performing a flexural design with tensile steel reinforcement in multiple layers, all of the tensile reinforcement is typically assumed to yield at ultimate conditions (i.e., it is "lumped"), and the total tensile force in the cross section can in most cases reasonably be assumed to act at the centroid of the different layers. Because FRP reinforcement demonstrates linear elastic behavior with no yielding, the strain and stress at each different reinforcement layer must be determined individually as a function of its distance from the neutral axis. The strain in the outermost layer of FRP reinforcement governs in determining the mode of failure, since it would rupture first, and strain compatibility is used to determine the other FRP strains and hence the flexural capacity of the section. A similar concept applies when different types or grades of FRP bars are used within the same cross section. This essentially means that lumping of tensile reinforcement should not be permitted in the design or analysis of FRP RC flexural members.

Example 22.5

Flexural analysis with multiple layers of FRP reinforcement

Problem

Determine the nominal flexural capacity of a concrete beam reinforced in bending with two layers of GFRP reinforcement. The beam is 250 mm wide, 450 mm deep, and is to be constructed from concrete with $f_c' = 25$ MPa. The GFRP reinforcement is the same product as that used in Example 22.1. Assume that the beam is reinforced with 16 mm-nominal diameter bars ($A_f = 200$ mm^2 per bar) in two layers, as shown in Figure 22.3.

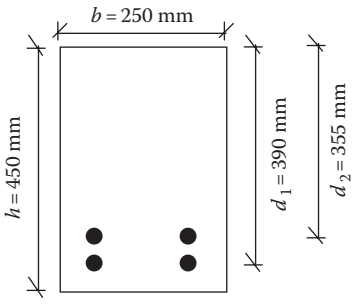

FIGURE 22.3 FRP RC beam with multiple reinforcement layers.

Step 1: Compute the FRP reinforcement ratio
Since the reinforcement ratio equation requires the depth to the FRP reinforcement, *d*, as an input, we begin by computing the approximate FRP reinforcement ratio using the average depth to the two layers (373 mm). Note that if FRP rupture governs, then the average depth must not be used in the calculation of the flexural capacity.

$$\rho_f = \frac{A_f}{bd}$$

$$= \frac{4(200\ \text{mm}^2)}{(250\ \text{mm})(373\ \text{mm})}$$

$$= 0.0086$$

Step 2: Determine the balanced FRP reinforcement ratio
From Example 22.1, it is already known that the balanced reinforcement ratio for this section is 0.0078. Since ρ_f is greater than ρ_{fb}, the section should fail due to concrete crushing (this will be verified later).

Step 3: Determine the location of the neutral axis of the section
ACI 440.1 (ACI, 2006) requires that design with multiple layers of FRP reinforcement be performed using strain compatibility. Thus, the simplifying equation for the stress in the FRP reinforcement at failure, Equation (22.10), cannot be applied in this case. Rather, first principles must be used.

The tension and compression forces existing in the section are determined using Equations 22.7 through 22.9. Note that the stress in the FRP reinforcement should be less than its design ultimate stress, since concrete crushing should govern based on Step 2 given earlier.

$$T = \sum A_f f_f = \sum A_f E_f \varepsilon_{cu} \frac{\beta_1 d - a}{a}$$

$$= 2(200\ \text{mm}^2)(44.8 \times 10^3\ \text{MPa})(0.003)\left(\frac{0.85(390\ \text{mm}) - a}{a}\right)$$

$$+ 2(200\ \text{mm}^2)(44.8 \times 10^3\ \text{MPa})(0.003)\left(\frac{0.85(355\ \text{mm}) - a}{a}\right)$$

$$= 53760\frac{332 - a}{a} + 53760\frac{302 - a}{a}$$

$$C = (0.85)(25\ \text{MPa})a(250\ \text{mm})$$

$$= (5313)a$$

Equating the two forces and solving the resulting quadratic equation for the depth of the equivalent rectangular compressive stress block, *a*, yield a stress block depth of 71 mm.

Step 4: Compute the stress level in each FRP layer
Successive application of Equation 22.9 leads to the following stress values in the FRP:

Layer 1

$$f_f = E_f \varepsilon_{cu} \frac{\beta_1 d - a}{a}$$

$$= (44.8 \times 10^3\ \text{MPa})(0.003)\left(\frac{(0.85)(390\ \text{mm}) - 71\text{mm}}{71\text{mm}}\right) = 493\ \text{MPa} < f_{fu} = 496\ \text{MPa}$$

Layer 2

$$f_f = E_f \varepsilon_{cu} \frac{\beta_1 d - a}{a}$$

$$= (44.8 \times 10^3 \text{ MPa})(0.003)\left(\frac{0.85(355\text{mm}) - 71\text{mm}}{71\text{mm}}\right) = 437 \text{ MPa} < f_{fu} = 496 \text{ MPa}$$

Step 5: Compute the nominal flexural capacity
Using Equation 22.12, the nominal flexural capacity of the section can be calculated as the sum of each of the FRP layer's moment capacity contribution calculated about the compressive force resultant:

$$M_n = \sum A_f f_f \left(d - \frac{a}{2}\right)$$

$$= 2(200\text{mm}^2)(493 \text{ MPa})\left(390\text{mm} - \frac{(0.85)(71\text{mm})}{2}\right)$$

$$+ 2(200\text{mm}^2)(437 \text{ MPa})\left(355\text{mm} - \frac{(0.85)(71\text{mm})}{2}\right)$$

$$= 128 \text{ kN} \cdot \text{m} \Leftarrow$$

FRPs as Compression Reinforcement

Due to the relatively low compressive strength of FRP as compared to its tensile strength, it is recommended that the strength of any FRP bar in compression should be ignored. In addition, based on currently available research, FRP bars cannot be efficiently used as longitudinal reinforcement in RC columns, and their use in compressive applications is not typically permitted.

Moment Redistribution

Due to the linear elastic behavior of FRP, plastic hinges are not typically expected to form in FRP RC members, and moment redistribution cannot therefore be relied upon in the design of continuous structural members. Additional research is required in this area.

Design for Serviceability

Under limit state design philosophies, it is essential to verify that members satisfy both strength and serviceability requirements; this is particularly critical in the case of FRP RC members. In the case of steel-RC members, design for strength capacity very often governs the final flexural reinforcement design selected for a particular member. However, because FRP-reinforced members typically have comparatively low flexural rigidities after cracking (as a consequence of the lower stiffness of the FRP reinforcing bars as compared with conventional reinforcing steel), deflections of FRP-reinforced members under service loads will often control the selection of the tensile reinforcement.

In designing to meet applicable serviceability criteria for cracking and deflections, ACI 318 (ACI, 2005) provides the basis for the fundamental equations currently suggested by ACI 440.1 (ACI, 2006) for the design of serviceable FRP RC members, obviously with appropriate modifications to account for the unique behavior of FRP reinforcement. If an FRP RC section is designed to fail by concrete crushing, it will typically satisfy crack width and deflection criteria.

Cracking

Crack width limits for steel RC were established largely on the basis of the susceptibility of conventional reinforcing bars to corrosion (in addition to aesthetics and shear considerations). Since FRP materials do not corrode electrochemically, these limits may, in some cases, be relaxed. However, in cases where a combination of steel and FRP reinforcement is used, the most critical crack width criterion must be applied.

ACI 440.1 (ACI, 2006) recommends following allowable crack width limits suggested for FRP reinforcement in concrete by the CSA (2002)—these are 0.5 mm for exterior exposure and 0.7 mm for interior exposure. If the FRP RC structural member is to be located in a destructive environment, then these crack widths should be reduced accordingly. Similarly, if the structural member is designed for a short service life where aesthetics is a secondary concern, then the crack width limitations need not be applied.

ACI 440.1 uses a similar approach as adopted by ACI 318 (ACI, 2005) to approximate the maximum probable crack width for an FRP RC member. The equation, which was developed for steel RC members, is independent of reinforcement type, but for the case of FRP reinforcement, it must be modified by a bond quality coefficient, k_b. This bond coefficient is intended to account for the bond properties of the FRP reinforcement as compared with conventional steel reinforcing bars. The maximum probably crack width, w, in mm, is given by

$$w = 2\frac{f_f}{E_f}\beta k_b\sqrt{d_c^2 + \left(\frac{s}{2}\right)^2} \tag{22.18}$$

where

- β is the ratio of the distance from the neutral axis to the extreme tension fiber to the distance from the neutral axis to the centroid of the tensile reinforcement
- d_c is the thickness of the concrete cover measured from the extreme tension fiber to the center of the closest reinforcing bar (mm)
- s is the spacing of longitudinal bars (mm)

In some cases, FRP bars may have a bond superior to that of steel bars, in which case the bond coefficient, k_b, may be smaller than 1.0. In other cases, the bond may be inferior, in which case k_b is greater than 1.0. ACI 440.1 notes that average k_b values determined from research on various types of FRP reinforcing bars with various types of surface treatments to enhance bond range from 0.60 to 1.72. When k_b is not known through testing for the specific FRP reinforcement being contemplated for use, the bond coefficient can, according to ACI 440.1, be assumed as 1.4. However, this assumption does not apply either to smooth bars or to FRP grids since further research and analysis are required to quantify k_b for these types of FRP reinforcement.

Example 22.6

Checking crack width limitations

Problem

Determine whether the beam of Example 22.1 satisfies the maximum crack width limits of ACI 440.1. Assume that the service moments due to dead and live loads are 10 kN·m and 20 kN·m, respectively.

Step 1: Compute the total service moment on the beam

$$\begin{aligned} M_{\text{S-TOTAL}} &= M_{\text{S-DEAD}} + M_{\text{S-LIVE}} \\ &= 10\ \text{kN}\cdot\text{m} + 20\ \text{kN}\cdot\text{m} \\ &= 30\ \text{kN}\cdot\text{m} \end{aligned}$$

Step 2: Determine the modular ratio of the FRP with respect to the concrete, n_f

$$E_f = 44.8 \times 10^3 \text{ MPa}$$

$$E_c = 4{,}700\sqrt{f'_c} = 4{,}700\sqrt{25 \text{ MPa}} = 23{,}500 \text{ MPa}$$

$$n_f = \frac{E_f}{E_c} = \frac{44.8 \times 10^3 \text{ MPa}}{23{,}500 \text{ MPa}} = 1.9$$

Step 3: Calculate the depth to the neutral axis
From basic mechanics, and assuming linear elastic material behavior at service load levels, the location of the neutral axis under service loads, *c*, can be determined as

$$c = \left(\sqrt{(\rho_f n_f)^2 + 2\rho_f n_f} - \rho_f n_f\right) d$$

$$= \left(\sqrt{(0.0092(1.9))^2 + 2(0.0092)(1.9)} - 0.0092(1.9)\right)(390 \text{ mm})$$

$$= 66 \text{ mm}$$

Step 4: Determine the stress in the FRP reinforcement under service loads
The stress in the FRP can be determined by rearranging the expression for the existing moment in the section. Since the calculation is at service load levels, the ACI equivalent stress block does not apply. Rather, the compressive stress distribution is assumed to be triangular, with its centroid at a depth of *c/3*. Therefore,

$$M = A_f f_f \left(d - \frac{c}{3}\right)$$

$$f_f = \frac{M}{A_f\left(d - \frac{c}{3}\right)}$$

$$= \frac{30 \times 10^6 \text{ N} \cdot \text{mm}}{3(300 \text{ mm}^2)\left(390 \text{ mm} - \frac{66 \text{ mm}}{3}\right)}$$

$$= 90.6 \text{ MPa}$$

Step 5: Compute the remaining factors in the crack width formula

$$\beta = \frac{h - c}{d - c}$$

$$= \frac{450 \text{ mm} - 66 \text{ mm}}{390 \text{ mm} - 66 \text{ mm}}$$

$$= 1.19$$

$$d_c = h - d$$

$$= 450 \text{ mm} - 390 \text{ mm}$$

$$= 60 \text{ mm}$$

s = [beam width − cover both sides − stirrups both sides − 2 × (bar diameter/2)]/(# of bars − 1)

$$s = \frac{250\,\text{mm} - 2(40\,\text{mm}) - 2(10\,\text{mm}) - 2\left(\frac{20\,\text{mm}}{2}\right)}{3-1} = 65\,\text{mm}$$

Step 6: Obtain predicted maximum crack width and compare with allowable crack width
From Equation 22.18, the maximum likely crack width in the beam is

$$\begin{aligned} w &= 2\frac{f_f}{E_f}\beta k_b\sqrt{d_c^2 + \left(\frac{s}{2}\right)^2} \\ &= (2)\left(\frac{90.4\,\text{MPa}}{44.8\times10^3\,\text{MPa}}\right)(1.19)(1.4)\sqrt{60^2 + \left(\frac{65}{2}\right)^2} \\ &= 0.46\,\text{mm} < 0.7\,\text{mm} \Leftarrow \end{aligned}$$

If a beam does not satisfy crack width requirements, the reinforcement design can be modified by increasing the area of the individual bars or by providing additional bars (i.e., by increasing the flexural rigidity of the member).

In the current case, with three 20 mm-nominal diameter bars, crack width criteria are satisfied.

Deflection

In ACI 318 (ACI, 2005, 2011), adequate control of deflections for flexural members under service load conditions can be achieved by requiring minimum section depths and by limiting the allowable deflections. ACI 440.1 (ACI, 2006) uses the ACI 318 minimum member thickness for deflection control equations as a guide for determining member dimensions for FRP RC members and also *requires that an explicit calculation of deflection be made* as a final check. Note that deflections due to seismic or other dynamic loads are not considered herein.

Recommended Minimum Thickness

Table 22.2 provides suggested ratios of length to depth for flexural members. Satisfaction of these requirements provides an initial estimate of the member proportions necessary to satisfy explicit deflection requirements for design, but does not ensure that all deflection requirements will be met. The values in Table 22.2 are based on the research by Ospina et al. (2001) and assume a maximum total service load deflection of less than $L/240$, and assumed reinforcement ratios of $2.0\rho_{fb}$ and $3.0\rho_{fb}$ for slabs and beams, respectively.

TABLE 22.2
Recommended Minimum Member Thickness (Non-Prestressed Beams and One-Way Slabs)

	Minimum Thickness (h)			
	Simply Supported	**One End Continuous**	**Both Ends Continuous**	**Cantilever**
One-way slabs	$L/13$	$L/17$	$L/22$	$L/5.5$
Beams	$L/10$	$L/12$	$L/16$	$L/4$

Source: ACI, *Guide for the Design and Construction of Concrete Reinforced with FRP Bars*, ACI 440.1R-06, American Concrete Institute, Farmington Hills, MI, 2006.

Calculating Deflections in FRP RC Members: Effective Moment of Inertia

The first step in determining the deflection of a flexural member under service loads is to calculate its effective moment of inertia, I_e, at those load levels. When an FRP RC section is uncracked, it behaves according to its gross moment of inertia, I_g. For a rectangular section, this can be approximated using elementary mechanics as

$$I_g = \frac{bh^3}{12} \tag{22.19}$$

where M_{cr} is the cracking moment of the RC member.

Again, based on elastic analysis, the cracked moment of inertia of an FRP RC section can be approximated as

$$I_{cr} = \frac{bd^3}{3}k^3 + n_f A_f d^2 (1-k)^2 \tag{22.20}$$

where

$$k = \sqrt{2\rho_f n_f + (\rho_f n_f)^2} - \rho_f n_f \tag{22.21}$$

For a steel RC member, it has been shown that a section subjected to service load levels (provided the loads are greater than the cracking moment) has a flexural stiffness, E_cI, lying somewhere between E_cI_g and E_cI_{cr}, and that the flexural stiffness varies with the magnitude of the applied moment, M_a. This applies also to FRP RC members, although modifications are required to account for the unique bond characteristics and lower modulus of elasticity of typical FRP reinforcing bars. ACI 318 has adopted the following equation for the stiffness of a steel RC section at service load levels (Branson, 1977):

$$I_e = \left(\frac{M_{cr}}{M_a}\right)^3 I_g + \left[1 - \left(\frac{M_{cr}}{M_a}\right)^3\right] I_g \le I_g \tag{22.22}$$

For FRP RC members, research has shown that Equation 22.22 tends to overestimate the effective moment of inertia, likely because of differences in the tension stiffening behavior of FRP RC members, and ACI 440.1 has consequently suggested a modified version of the equation to account for this:

$$I_e = \left(\frac{M_{cr}}{M_a}\right)^3 \beta_d I_g + \left[1 - \left(\frac{M_{cr}}{M_a}\right)^3\right] I_g \le I_g \tag{22.23}$$

where β_d is a factor to account for reduced tension stiffening with FRP reinforcement and is given by

$$\beta_d = \frac{1}{5}\frac{\rho_f}{\rho_{fb}} \le 1.0 \tag{22.24}$$

In those cases where M_a is less than M_{cr}, the uncracked section properties should be used. In cases where M_a is only slightly less than M_{cr}, it is conservative to apply Equation 22.23, as shrinkage and temperature would likely contribute to cracking of the section (in these cases, M_a should be taken as M_{cr}).

Example 22.7

Effective Moment of Inertia

Problem
Determine the effective moment of inertia of the 250 mm wide, 450 mm deep FRP RC beam of Example 22.1. The member is reinforced with three 20 mm-diameter GFRP bars, and the concrete has a compressive strength of 25 MPa. The service live load on the beam is 15 kN/m, and the service dead load on the beam is 10 kN/m over a 4.0 m simply supported span.

Step 1: Calculate the key reinforcement properties for the beam
From Example 22.1, the following values are already known:

$$A_f = 3(300\text{ mm}^2) = 900\text{ mm}^2$$

$$d = 390\text{ mm}$$

$$\rho_f = 0.0092$$

$$\rho_{fb} = 0.0078$$

From Example 22.6, the modular ratio is already known:

$$n_f = 1.9$$

Step 2: Determine the service moment applied to the section at midspan
The service moments due to the dead load and live loads are

$$M_{DL} = \frac{10\text{ kN}(4.0\text{ m})^2}{8} = 20.0\text{ kN}\cdot\text{m} \quad \text{and} \quad M_{LL} = \frac{15\text{ kN}(4.0\text{ m})^2}{8} = 30.0\text{ kN}\cdot\text{m}$$

giving a total midspan applied service moment of 50 kN·m.

Step 3: Calculate the cracking moment of the section
From ACI 318 (ACI, 2005, 2011), the rupture strength of the concrete, f_r, is taken as

$$\begin{aligned} f_r &= 0.62\sqrt{f'_c} \\ &= 0.62\sqrt{25\text{ MPa}} \\ &= 3.1\text{ MPa} \end{aligned} \tag{22.25}$$

The gross moment of inertia of the beam's cross section is (Equation 22.19)

$$I_g = \frac{(250\text{ mm})(450\text{ mm})^3}{12}$$

$$= 1.9\times10^9\text{ mm}^4$$

The cracking moment of a concrete section, based on elementary mechanics, is

$$M_{cr} = \frac{f_r I_g}{y_t}$$
$$= \frac{(3.1\text{ MPa})(1.9\times10^{9}\text{ mm}^4)}{(450\text{ mm}/2)}$$
$$= 26.2\times10^{6}\text{ N}\cdot\text{mm}$$
$$= 26\text{ kN}\cdot\text{m} \qquad (22.26)$$

Since M_{cr} (26 kN·m) is exceeded by (M_a = 30 kN·m), the effective moment of inertia of the cracked FRP RC section must be determined.

Step 4: Calculate the moment of inertia of the fully cracked cross section
To compute the fully cracked moment of inertia, the ratio of the depth of the neutral axis to the depth of the FRP reinforcement, k, must be determined from Equation 22.21.

$$k = \sqrt{2\rho_f n_f + (\rho_f n_f)^2} - \rho_f n_f$$
$$= \sqrt{2(0.0092)(1.9) + (0.0092(1.9))^2} - 0.0092(1.9)$$
$$= 0.17$$

From Equation 22.20, the fully cracked moment of inertia is

$$I_{cr} = \frac{bd^3}{3}k^3 + n_f A_f d^2 (1-k)^2$$
$$= \left(\frac{250\text{ mm}\,(390\text{ mm})^3}{3}\right)(0.17)^3 + 1.9\,(900\text{ mm}^2)(390\text{ mm})^2(1-0.17)^2$$
$$= 203\times10^{6}\text{ mm}^4$$

Step 5: Determine the effective moment of inertia of the cracked section
The coefficient β_d is required from Equation 22.24:

$$\beta_d = \frac{1}{5}\frac{\rho_f}{\rho_{fb}} \le 1.0$$
$$= \left(\frac{1}{5}\right)\left(\frac{0.0092}{0.0078}\right)$$
$$= 0.236 \le 1.0$$

Finally, the effective moment of inertia for the FRP-reinforced section is (Equation 22.23)

$$I_e = \left(\frac{M_{cr}}{M_a}\right)^3 \beta_d I_g + \left[1-\left(\frac{M_{cr}}{M_a}\right)^3\right] I_{cr}$$
$$= \left(\frac{26.2\text{ kN}\cdot\text{m}}{30.0\text{ kN}\cdot\text{m}}\right)^3 (0.236)(1.9\times10^{9}\text{mm}^4) + \left[1-\left(\frac{26.2\text{ kN}\cdot\text{m}}{30.0\text{ kN}\cdot\text{m}}\right)^3\right](203\times10^{6}\text{mm}^4)$$
$$= 417\times10^{6}\text{ mm}^4 \Leftarrow$$

Once the effective moment of inertia of a section is known, the immediate and long-term deflections may be calculated and then checked against the prescribed deflection limits; it is essential to check both types of deflections in an FRP RC. Because of the comparatively low elastic modulus of FRP reinforcing bars, initial short-term deflections of FRP-reinforced members can be up to three to four times those of steel RC members of the same flexural design capacity, and long-term deflections may be two to three times the immediate deflections.

Immediate short-term deflections can be determined using standard structural analysis procedures along with the effective moment of inertia of the cracked section calculated previously. Long-term deflections, however, require modifications to the equations presented by ACI 318 to account for the effect of concrete compressive stress levels, the different bond characteristics of FRP bars, and larger initial deflections in FRP-reinforced members. A detailed discussion of deflection calculations is considered beyond the scope of the current document, and the reader is referred to ACI440.1 (ACI, 2006) for additional information and references to relevant research.

Creep Rupture and Fatigue Limits

As discussed in Chapter 10, the effects of sustained load (creep) and repeated load cycles (fatigue) are potentially important in influencing the long-term performance of FRP RC members. As such, the maximum stress and stress ranges experienced at service load levels must be limited to avoid inducing failure in FRP RC members by creep rupture or fatigue. The maximum allowable stress in FRP RC members at service load levels is conservatively taken by ACI 440.1 as (ACI, 2006)

- $0.20f_{fu}$ for GFRP reinforcement
- $0.30f_{fu}$ for aramid FRP reinforcement
- $0.55f_{fu}$ for CFRP reinforcement

These currently recommended values represent conservative limits based on the results of available research studies, and they may be increased in the future as more complete data become available.

Since the earlier FRP stress limits are imposed at service load levels, in which FRP RC members are typically within their elastic range of behavior, a simple elastic analysis based on strain compatibility can be used to determine the member stresses. Figure 22.4 depicts the assumed strain and stress conditions under assumed linear elastic conditions at service load levels for a cracked FRP RC member.

Therefore, the stress in the FRP reinforcement under sustained loads, f_{fs}, can be taken as

$$f_{fs} = M_s \frac{n_f d(1-k)}{I_{cr}} \tag{22.27}$$

where

M_s is the moment due to the dead load and the sustained portion of the live load

I_{cr} is the cracked moment of inertia

k is the depth to the elastic neutral axis that can be determined using Equations 22.20 and 22.21

As long as the value derived from Equation 22.27 is less than the maximum allowable stress for the FRP reinforcement, failure of the FRP reinforcement by creep rupture should be prevented based on available data. Should a member be subjected to cyclic loading, the same maximum stress limits apply. In this case, however, the stress in the FRP should be calculated with Equation 22.27, but with M_s taken as the moment due to sustained loads plus the maximum moments due to a fatigue loading cycle.

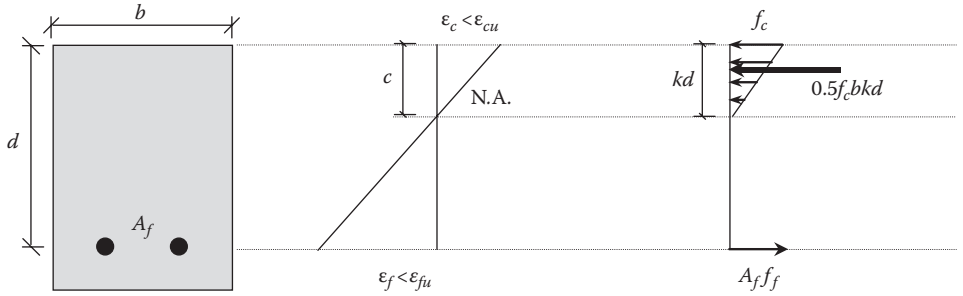

FIGURE 22.4 Elastic strain and stress diagrams in an FRP RC section in flexure.

Example 22.8

Creep rupture limits

Problem
Check whether the beam of Example 22.7 satisfies ACI 440.1 allowable FRP reinforcement stress limits to prevent creep rupture. Assume that 20% of the live load is sustained.

Step 1: Calculate the moment due to sustained loading
First, determine the uniformly distributed load due to sustained loading, which is the sum of the dead load on the beam plus the sustained portion of the live load.

$$\begin{aligned} w_{sustained} &= w_{DL} + \%_{sustained} w_{LL} \\ &= 10\ \text{kN/m} + (0.20)(15\ \text{kN/m}) \\ &= 13\ \text{kN/m} \end{aligned}$$

$$\begin{aligned} M_s &= \frac{w_{sustained} l^2}{8} \\ &= \frac{(13\ \text{kN/m})(4.0\ \text{m})^2}{8} \\ &= 26\ \text{kN} \cdot \text{m} \end{aligned}$$

Step 2: Calculate the sustained stress level in the GFRP reinforcement
From Example 22.7, it is known that for this section, k is 0.17, I_{cr} is 203 × 10^6 mm^4, n_f is 1.9, and d is 390 mm. Using Equation 22.27, the stress level in the FRP is

$$\begin{aligned} f_{fs} &= M_s \frac{n_f d (1-k)}{I_{cr}} \\ &= (26 \times 10^6\ \text{N} \cdot \text{mm}) \left(\frac{1.9 (390\ \text{mm})(1-0.17)}{203 \times 10^6\ \text{mm}^4} \right) \\ &= 79\ \text{MPa} \end{aligned}$$

Step 3: Check against maximum stress limits
The maximum allowable stress for GFRP according to ACI 440.1 (ACI, 2006) is 0.20 f_{fu} = 0.20 (496 MPa) = 99 MPa, which is greater than the actual sustained service stress in the FRP reinforcement in this case (79 MPa). Therefore, the section satisfies creep rupture stress limitations.

SHEAR DESIGN

General Considerations

As with ACI 440.1 flexural design procedures with FRP reinforcement, the procedures for shear design with internal FRP reinforcement are essentially derived from those suggested by ACI 318 for steel RC members. This approach is typical of the various available codes for the shear design of FRP RC members around the world (e.g., ISIS, 2001). However, shear design procedures with FRP reinforcement must account for the different behavior of the FRP as compared with steel reinforcement. The important differences include the comparatively low tensile elastic modulus of currently available FRPs, their high strength and linear elastic behavior, and, very importantly, their significantly reduced tensile strength at bends and low dowel resistance, all of which must be accounted for in any design.

It is important to recognize that the use of FRP reinforcing bars as primary flexural reinforcement alters the cracking behavior of concrete members, such that the shear design of FRP RC members should be performed using the procedures described herein, regardless of whether the shear reinforcement is steel or FRP (or in cases such as slabs where shear reinforcement is not typically present). Thus, ACI 440.1 (ACI, 2006) treats shear design for the following cases:

- FRP flexurally reinforced concrete beams
- FRP-reinforced one-way concrete slabs
- The use of FRP stirrups as shear reinforcement
- The punching shear capacity of FRP-reinforced two-way concrete slabs

Shear Design Equations

Basic Capacity Equations

ACI 440.1 bases its shear design approach on the strength design method outlined in ACI 318 (ACI, 2005, 2011) for steel RC, where the shear resistance of an RC section is taken as the sum of the shear strength contribution from the concrete, V_c, plus the shear strength contribution from the shear reinforcement, V_s (which in the conventional case is from steel ties or stirrups); thus, provided that shear crushing of the web concrete is avoided (see discussion later),

$$V_u = V_c + V_s \quad \text{for steel shear reinforcement; or} \tag{22.28}$$

$$V_u = V_c + V_f \quad \text{for FRP shear reinforcement} \tag{22.29}$$

ACI 440.1 also states that the typical strength reduction factor of 0.75 for reducing nominal shear capacity of steel RC members should also be used for FRP reinforcement and that the following equation must be satisfied (again using a limit state design philosophy):

$$\varphi V_n \geq V_u \tag{22.30}$$

where

φ is the strength reduction factor of 0.75 for shear
V_n is the nominal shear capacity of FRP RC member (N)
V_u is the factored (ultimate) shear expected to act on a section, as determined using load factors suggested by ACI 318 (N)

Shear Strength Contribution from the Concrete (V_c)

The shear strength provided by the concrete in an FRP RC member is typically less than that of an equivalent steel RC member. Since FRP has a lower axial stiffness, less concrete is required to resist the forces that develop in FRP flexural reinforcement, and the result is a smaller depth to the

neutral axis than for a steel RC member, with a corresponding reduction in shear strength. With a smaller compressive section and wider crack widths in an FRP RC member, the shear resistance provided by aggregate interlock and the compressed concrete, V_{cf}, is typically smaller for the FRP-reinforced case.

Furthermore, because FRP bars have low strength and stiffness in the transverse direction (i.e., due to their anisotropy), it is reasonably assumed that the contribution of FRP flexural reinforcement to the concrete shear strength through dowel action is significantly less than that of an equivalent area of steel flexural reinforcement (although it is not well known and additional research is needed in this area). With these considerations in mind, the shear strength contribution of the concrete in an FRP RC member can be taken as (ACI, 2006)

$$V_c = \frac{2}{5}\sqrt{f_c'}\, b_w c \quad \text{or} \quad = \frac{2}{5}\sqrt{f_c'}\, b_w k d \tag{22.31}$$

where for the simplest case of a singly reinforced rectangular concrete member,

$$k = \sqrt{2\rho_f n_f + (\rho_f n_f)^2} - \rho_f n_f \tag{22.32}$$

Note that the maximum allowable shear contribution of the concrete must be avoided to prevent shear crushing of the web concrete. ACI 440.1 recommends, as in ACI 318, that

$$V_c \le 0.29\sqrt{f_c'}\, b_w d \tag{22.33}$$

Shear Strength Contribution from Steel or FRP Shear Reinforcement (V_s or V_f)

If conventional shear reinforcement is provided in the form of steep stirrups, the shear strength contribution from this internal steel reinforcement, V_s, can be calculated using normal procedures as suggested in ACI 318 (ACI, 2005, 2011). If FRP reinforcing bars are used to provide internal shear reinforcement, the shear strength contribution of the FRP stirrups, V_f, can be derived by modifying the ACI 318 equations for steel shear reinforcement; thus,

$$V_f = \frac{A_{fv} f_{fv} d}{s} \tag{22.34}$$

where

A_{fv} is the amount of FRP shear reinforcement within spacing, s (mm^2)
s is the spacing of stirrups or continuous spirals (mm^2)

$$f_{fv} = 0.004 E_f \le f_{fb}\ \text{MPa} \tag{22.35}$$

Equation 22.35 shows that the tensile strength of the stirrups for shear design, f_{fv}, is limited (often severely) to control shear crack widths that would otherwise compromise aggregate interlock and the shear capacity of the concrete section. In addition, the shear strength of the FRP stirrups is further limited to less than the tensile capacity of the stirrup at its bends, f_{fb} (recall Equation 22.3). Some existing codes for concrete design with FRP reinforcement (e.g., CSA, 2006) take a more conservative approach, limiting the maximum FRP strain to values as low as 0.002 under service loads. However, the maximum allowable value (under design ultimate loads) of 0.004 is justified by ACI 440.1 as the strain that maintains aggregate interlock and consequently provides for an acceptable shear resistance contribution from the concrete.

Therefore, in the design of concrete members reinforced for shear with FRP bars, spirals, or stirrups, the required area or spacing of FRP stirrups (placed perpendicular to the longitudinal axis of the member) can be determined using (ACI, 2006)

$$\frac{A_{fv}}{s} = \frac{V_u - \varphi V_c}{\varphi f_{fv} d} \tag{22.36}$$

ACI 440.1 also allows the use of inclined internal shear reinforcement, and the reader should consult the source document for information in this area.

Minimum Shear Reinforcement

As is the case for steel RC members, a minimum amount of shear reinforcement is required when the applied shear is greater than $\varphi V_c/2$. This limit is enforced to provide adequate reserve strength after cracking, thus guarding against brittle shear failure. ACI 440.1 recommends a minimum FRP shear reinforcement of

$$A_{fv,\min} = \frac{0.35 b_w s}{f_{fv}} \tag{22.37}$$

where
b_w and s are in mm
f_{fv} is in MPa

The earlier equation is valid for both steel and FRP shear reinforcement. However, when applied to FRP shear reinforcement, it provides a more conservative result (ACI, 2006).

Detailing and Spacing of FRP Stirrups

FRP reinforcing bars are anisotropic and have comparatively poor transverse properties. Therefore, several special detailing requirements are needed in the design of FRP RC members, particularly when bent FRP reinforcing bars or spirals are used as shear reinforcement. Figure 22.5 summarizes the key detailing requirements recommended by ACI 440.1 for FRP stirrups.

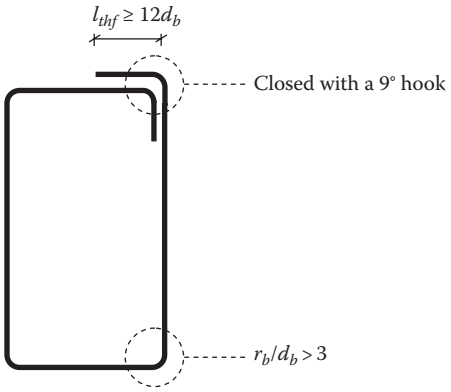

FIGURE 22.5 Selected stirrup detailing requirements from ACI 440.1. (From ACI, *Guide for the Design and Construction of Concrete Reinforced with FRP Bars*, ACI 440.1R-06, American Concrete Institute, Farmington Hills, MI, 2006.)

Sharp bending of the FRP bars causes stress concentrations and can result in the failure of the bar at axial stresses as low as 50% of their ultimate uniaxial tensile strength. Sharp bends must therefore be avoided to prevent severe strength loss. ACI 440.1 recommends that the minimum bend radius be taken as three times the bar diameter. In addition, a minimum tail length, l_{thf}, of 12 times the bar diameter is recommended to ensure that the tensile force in the FRP reinforcement is transferred to the concrete.

As is the case for conventionally reinforced concrete members designed for shear, the maximum allowable stirrup spacing required by ACI 440.1 is the lesser of *d/2* or 600 mm (where stirrups are required). This requirement is needed to ensure that all potential shear cracks are intercepted by at least one stirrup.

Example 22.9

Shear design

Problem

The beam in Example 22.1 is subject to a service dead load of 10 kN/m and a service live load of 15 kN/m over a 7.0 m simply supported span. Determine whether shear reinforcement is required at the critical section. If yes, design to provide the required shear capacity using 10 mm-nominal diameter GFRP closed stirrups (A_f per bar = 100 mm^2), oriented vertically, with the same properties used in Example 22.1.

Step 1: Determine the factored load on the beam

The factored uniformly distributed load on the beam, using ACI 318 load factors (ACI, 2005, 2011), is

$$\begin{aligned} w_f &= \alpha_D D L + \alpha_L L L \\ &= 1.4(10\ \text{kN/m}) + 1.7(15\ \text{kN/m}) \\ &= 39.5\ \text{kN/m} \end{aligned}$$

Step 2: Determine the shear demand at the critical section

The critical section occurs at a distance, *d*, from the support; therefore,

$$\begin{aligned} V_u &= \frac{w_u L}{2} - w_u d \\ &= \frac{39.5\ \text{kN/m}\ (7.0\ \text{m})}{2} - 39.5\ \text{kN/m}\ (0.39\ \text{m}) \\ &= 123\ \text{kN} \end{aligned}$$

where *d* is known from Example 22.1.

Step 3: Calculate the shear strength contribution from the concrete

From Equation 22.21 and known from previous examples, *k* is

$$\begin{aligned} k &= \sqrt{2\rho_f n_f + (\rho_f n_f)^2} - \rho_f n_f \\ &= \sqrt{2(0.0092)(1.9) + (0.0092(1.9))^2} - 0.0092(1.9) \\ &= 0.17 \end{aligned}$$

Applying Equation 22.31, the concrete shear contribution is

$$V_{cf} = \frac{2}{5}\sqrt{f_c'}\,b_w kd$$

$$= \left(\frac{2}{5}\right)\sqrt{25\ \text{MPa}}\,(250\ \text{mm})(0.17)(390\ \text{mm})$$

$$= 33\ \text{kN}$$

Since the concrete contribution to the shear capacity (33 kN) is less than the shear demand (123 kN), shear reinforcement is required (i.e., the applied shear is greater than $\varphi V_c/2$).

Step 4: Calculate the allowable stress in the stirrup at the bend
From Equation 22.3, and assuming the minimum allowable bend radius, $r_b/d_b = 3.0$, according to Figure 22.5, the allowable stress at the stirrup bend is

$$f_{fb} = \left(0.05\frac{r_b}{d_b} + 0.3\right) f_{fu}$$

$$= (0.05(3) + 0.3)(496\ \text{MPa})$$

$$= 223\ \text{MPa}$$

Step 5: Determine the allowable design stress in the FRP reinforcement to maintain aggregate interlock
Equation 22.35 limits the design stress, f_{fv}, to $0.004E_f = 179$ MPa. Since this is less than the attainable strength at the stirrup bend, 223 MPa, the lower stress limit of 179 MPa governs.

Step 6: Compute the required minimum spacing of the FRP stirrups based on shear demand
Rearranging Equation 22.34, the required FRP stirrup spacing at the critical section is

$$s = \frac{\varphi A_{fv} f_{fv} d}{V_u - \varphi V_{cf}}$$

$$= \frac{0.85\,(2\,(100\ \text{mm}^2))(179\ \text{MPa})(390\ \text{mm})}{122.8\times10^3\ \text{N} - 0.85\,(33.2\times10^3\ \text{N})}$$

$$= 126\ \text{mm}$$

Therefore, for strength requirements, assume stirrups spaced at 100 mm.

Step 7: Check minimum shear reinforcement area
Rearranging Equation 22.37, the required spacing to meet minimum reinforcement requirements is

$$s = \frac{A_{fv} f_{fv}}{0.35 b_w}$$

$$= \frac{(2\,(100\ \text{mm}^2))(179\ \text{MPa})}{0.35\,(250\ \text{mm})}$$

$$= 410\ \text{mm}$$

The provided stirrup spacing (100 mm) is less than that required for minimum shear reinforcement (410 mm); therefore, the stirrups should be spaced at 100 mm. Before specifying this spacing in a design, however, the detailing requirements must also be met.

Step 8: Check detailing and general spacing requirements
Step 4 indicated that a minimum stirrup radius to bar diameter ratio of 3.0 would be used in the current example. The minimum tail length required is $12 \times d_b$, which is 120 mm. To ensure that cracks are intercepted by at least one stirrup, the maximum spacing limit is $d/2$, or 195 mm in this case. Therefore, a spacing of 100 mm will be used.

Therefore, all of the strength and detailing requirements are satisfied if 10 mm-diameter GFRP bars are used at 100 mm spacing. ⇐

Shear Strength of Two-Way FRP RC Slabs

Research has demonstrated that punching shear failure in FRP RC slabs is sudden and brittle. The shear capacity of such a system may be enhanced by increasing the stiffness of the upper FRP layer in the slab, which also leads to reduced deflections at ultimate. Punching shear resistance may be made less brittle by the use of FRP grid reinforcement, rather than FRP bars, since grids continue to absorb energy after initial failure and thus limit the sudden and brittle nature of failure (Ospina et al., 2003).

The punching shear resistance of two-way FRP-reinforced slabs can be expressed using a modified form of the ACI 318 (ACI, 2005, 2011) punching shear equation, or

$$V_c = \frac{4}{5} k \sqrt{f_c'}\, b_o d \tag{22.38}$$

where

k is defined in Equation 22.32

b_o is the perimeter of the critical section for the slab or footing, taken as the same shape as the supporting column or concentrated applied load, and as described in Figure 22.6 (mm).

TEMPERATURE AND SHRINKAGE REINFORCEMENT

As in the case of conventional steel RC design, temperature and shrinkage reinforcement is reinforcement that is included in a member in addition to the reinforcement provided for flexural strength and serviceability requirements. The main purpose of this reinforcement is to limit crack widths due to fluctuations in temperature and shrinkage strains. Longitudinal cracking is controlled by the flexural reinforcement. Therefore, cracking parallel to a member's span must be controlled by temperature and shrinkage reinforcement that is placed transversely.

At this time, no experimental data are available to determine the minimum required area of FRP reinforcement to adequately control shrinkage and temperature cracks. Thus, the recommendations of ACI 318 have been adopted by ACI 440.1 with modifications to account for the specific properties of FRP reinforcement. ACI 440.1 should be consulted for additional guidance in this regard.

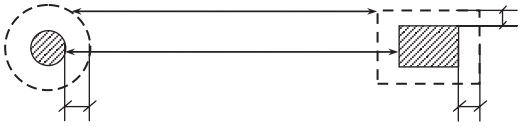

FIGURE 22.6 Definition of critical perimeter for punching shear resistance.

DEVELOPMENT LENGTH OF REINFORCEMENT

An adequate development length for tensile reinforcement (either steel or FRP) is fundamental to transferring tensile forces from the concrete to the reinforcing bar. Force is transferred from the concrete to the reinforcement through bond stresses that are aligned along the longitudinal axis of the bar. The quality of bond between different currently available FRP reinforcing bars and concrete is complex, and is apparently a function of the FRP type, the elastic modulus, the surface configuration (i.e., geometry and any surface treatments or coatings), and the cross-sectional shape of the FRP bar. What follows is a summary of the current development length recommendations of ACI 440.1 (ACI, 2006).

Development of Stress in Straight Bars

Force is assumed to be transferred from the concrete to the FRP through an average bond stress that acts over the basic development length of the FRP bar, l_e. The developable stress in an FRP bar, f_{fe}, over its development length, l_e, is

$$f_{fe} = \frac{0.083\sqrt{f'_c}}{\alpha}\left(13.6\frac{l_e}{d_b} + \frac{C}{d_b}\frac{l_e}{d_b} + 340\right) \le f_{fu} \tag{22.39}$$

where

- α is the factor to account for bar location. For bars with more than 300 mm concrete cast below them, this factor may be taken as 1.5; otherwise it is equal to 1.0
- d_b is the bar diameter (mm)
- C is the lesser of cover to center of bar, or one-half of center to center spacing of bars (mm)

The term C/d_b should not be taken greater than 3.5.

For the purposes of design, ACI 440.1 states that the maximum achievable bar stress should be assumed to vary linearly from zero at the end of the bar, to the value predicted by Equation 22.39 at a distance $20d_b$ from the end of the bar. Beyond development lengths of $20d_b$, Equation 22.39 can be used to approximate the force that can be developed in an FRP bar. However, because Equation 22.39 was derived based on a limited number of tests, development lengths less than $20d_b$ are not recommended, and the applicability of the equation is questionable beyond development lengths of $100d_b$ due to a paucity of test data.

The designer must check that the moment capacity at the end of the provided embedment length is adequate to develop the FRP bar forces needed to resist the applied moment at that location. If this is not the case, the designer must either increase the embedment length, increase the number of bars in the section, or recalculate the nominal moment capacity accounting for bond failure.

It may also be possible to hook the FRP bar to increase the stress that can be developed. However, very little data are available in this area, and rational guidance cannot be given at this time. The reader will recall that bends in FRP bars tend to reduce the force that can be developed, so that equations for hooked steel bars are not applicable to FRP bars. Furthermore, since currently available thermosetting polymer matrix FRP bars cannot be bent on site, use of hooked bars may be problematic in many applications. While additional research is required in this area, ACI 440.1 does provide recommendations for the development length of bent FRP bars based on a study by Ehsani et al. (1996). The reader should consult the source document for additional information, although in no case is the development length permitted to be below 230 mm or $12d_b$.

In cases where bond limits the stress that can be developed in a bar, failure of the section is caused by either concrete crushing (if f_{fe} is greater than f_f determined from Equation 22.10) or bond failure (if f_{fe} is less than f_f determined from Equation 22.10); therefore,

- Where f_{fe} (Equation 22.40) > f_f (Equation 22.10) ⇒ Apply Equation 22.12 for moment capacity
- Where f_{fe} (Equation 22.40) < f_f (Equation 22.10) ⇒ Apply Equation 22.14 for moment capacity with f_{fe} substituted for f_{fu} and f_{fe}/E_f substituted for ε_{fu} in Equation 22.13. A strength reduction factor of 0.55 is recommended in this case.

Example 22.10

Development stress in straight bars

Problem

A simply supported concrete beam with an interior exposure and a width of 225 mm, height 400 mm, and concrete compressive strength of 25 MPa is supported by a 200 mm thick block wall at each end and spans a distance of 3.0 m from center-to-center of the supports.

The beam is reinforced with three 16 mm-diameter CFRP bars in flexure. Assume that 10 mm-diameter FRP stirrups are used for shear reinforcement and that 25 mm of clear cover is provided. The manufacturer of the CFRP reports that the guaranteed tensile strength of the CFRP is 1655 MPa, with a modulus of elasticity of 138 GPa and a guaranteed rupture strain of 0.012.

Check that the required bar stress can be developed and that bond is sufficient.

Step 1: Determine the design tensile properties of the FRP reinforcing bars

Since the CFRP is being used in an interior exposure, the exposure factor, C_E, from Table 22.1 is taken as 1.0. Applying Equations 22.1 and 22.2 produces design tensile properties of

$$\begin{aligned} f_{fu} &= C_E f_{fu}^* \\ &= 1.0\,(1655\ \text{MPa}) \\ &= 1655\ \text{MPa} \end{aligned}$$

Step 2: Calculate the section properties

The distance to the centroid of the FRP reinforcement is

$$\begin{aligned} d &= 400\ \text{mm} - 25\ \text{mm} - 10\ \text{mm} - \frac{16\ \text{mm}}{2} \\ &= 357\ \text{mm} \end{aligned}$$

The reinforcement ratio, ρ_f, for the section is

$$\begin{aligned} \rho_f &= \frac{A_f}{bd} \\ &= \frac{600\ \text{mm}^2}{(225\ \text{mm})(357\ \text{mm})} \\ &= 0.0075 \end{aligned}$$

Step 3: Determine the value of C for Equation 22.39

Spacing of bars = (beam width − 2 × cover − d_b)/(Number of bars − 1)
= (225 mm − 2(25 mm) − 16 mm)/(3 − 1)
= 80 mm
C = 1/2 (spacing of bars)
= 1/2 (80 mm)
= 40 mm ⇐ governs

or

= cover-to-center of bar
= 25 mm + 10 mm + 16 mm/2
= 43 mm

Step 4: Calculate developable bar stress for the given embedded length of bar, l_e
The developable bar stress at midspan of the beam (with $l_e = l/2 = 1.5$ m) is found by applying Equation 22.39.

$$f_{fe} = \frac{0.083\sqrt{f'_c}}{\alpha}\left(13.6\frac{l_e}{d_b} + \frac{C}{d_b}\frac{l_e}{d_b} + 340\right) \le f_{fu}$$

$$= \frac{0.083\sqrt{25\ \text{MPa}}}{1.0}\left(13.6\frac{1500\ \text{mm}}{16\ \text{mm}} + \frac{40\ \text{mm}}{16\ \text{mm}}\frac{1500\ \text{mm}}{16\ \text{mm}} + 340\right) \le 1655\ \text{MPa}$$

$$= 767\ \text{MPa} \le 1655\ \text{MPa}$$

Step 5: Determine the required bar stress for flexural strength at the critical section
The bar stress required for flexural strength is obtained from Equation 22.10.

$$f_f = \left(\sqrt{\frac{(E_f\varepsilon_{cu})^2}{4} + \frac{0.85\beta_1 f'_c}{\rho_f}E_f\varepsilon_{cu}} - 0.5E_f\varepsilon_{cu}\right)$$

$$= \left(\sqrt{\frac{(137.9\times10^3\ \text{MPa})(0.0035))^2}{4} + \left(\frac{(0.85)(0.81)(25\ \text{MPa})}{0.0075}\right)(137.9\times10^3\ \text{MPa})(0.0035)} - (0.5)(137.9\times10^3\ \text{MPa})(0.0035)\right)$$

$$= 838\ \text{MPa} \le 1655\ \text{MPa}$$

The actual stress in the FRP is less than the rupture strength of the material; therefore, concrete crushing is the governing failure mode provided that bond failure does not occur due to insufficient development length.

Step 6: Compare developable and required bar stresses
The developable bar stress (767 MPa) is less than that required for flexural strength (838 MPa). Therefore, the development length is insufficient to develop the necessary stress in the FRP reinforcement to resist the design moment in the section. Ideally, the length of the bars could be increased; however, if it is assumed that the beam in the current example is of fixed length and this cannot be done, we must instead increase the number of bars to 4 (or recalculate the moment capacity accounting for bond failure as previously discussed).

Step 7: Calculate the new developable bar stress based on four bars

Spacing of bars = (beam width − 2 × cover − d_b)/(Number of bars − 1)
= (225 mm − 2(25 mm) − 16 mm)/(4 − 1)
= 53 mm
C = 1/2 (53 mm) = 26.5 mm

$$f_{fe} = \frac{0.083\sqrt{25\ \text{MPa}}}{1.0}\left(13.6\frac{1500\ \text{mm}}{16\ \text{mm}} + \frac{26.5\ \text{mm}}{16\ \text{mm}}\frac{1500\ \text{mm}}{16\ \text{mm}} + 340\right) \le 1655\ \text{MPa}$$

$$= 734\ \text{MPa} \le 1655\ \text{MPa}$$

Step 8: Calculate the new required bar stress for adequate moment capacity

$$\rho_f = \frac{800\ \text{mm}^2}{225\ \text{mm} \times 357\ \text{mm}}$$

$$= 0.010$$

$$f_f = \begin{pmatrix} \sqrt{\frac{(137.9\times10^3\ \text{MPa})(0.0035)^2}{4} + \frac{0.85(0.81)(25\ \text{MPa})}{0.010}(137.9\times10^3)(0.0035)} \\ -0.5(137.9\times10^3\ \text{MPa})(0.0035) \end{pmatrix}$$

$$= 702\ \text{MPa} \le 1655\ \text{MPa}$$

Step 9: Compare revised developable and required bar stresses
The developable bar stress (734 MPa) is greater than that required for flexural strength (704 MPa). Therefore, the development length is adequate. ⇐

Development Length of Positive Moment Reinforcement

For straight bars, ACI 440.1 states that the stress to be developed should be the minimum of

- the ultimate stress, f_{fu}
- the developable stress, f_{fe}
- the stress in the FRP at failure, f_f

The development length, l_d, for straight bars is defined as the bond length required to develop f_{fr} and is given by the following equation (ACI, 2006):

$$l_d = \frac{\left(\alpha f_{fr} / 0.083\sqrt{f_c'}\right) - 340}{13.6 + (C/d_b)} d_b \tag{22.40}$$

where f_{fr} is the minimum of f_f (Equation 22.10) and f_{fe} (Equation 22.39).

Based on a modification of the requirements of ACI 318 for development length of steel reinforcement (ACI, 2005), the available development length must also satisfy the following modified form of the ACI 318-05 equation:

$$l_d \le \frac{\varphi M_n}{V_u} + l_a \tag{22.41}$$

where

M_n is the nominal moment strength assuming that all reinforcement at the section is stressed to the bar stress, f_{fr} (N · mm)

V_u is the factored shear force at the section (N)

l_a is the embedment length of bar beyond center of support, or the larger of effective member depth or $12d_b$ when at a point of inflection (mm)

The first term in Equation 22.42 may be increased by 30% when the ends of the reinforcement are confined by a compressive reaction.

Example 22.11

Development length of flexural reinforcement

Problem

Determine whether the development length of the four 10 mm-diameter CFRP bars in Example 22.11 is sufficient.

The service dead load on the beam is 20 kN/m, and the service live load is 30 kN/m.

Step 1: Section properties

From Example 22.10, it is known that

$$d = 357 \text{ mm}$$

$$\rho_f = 0.010$$

$$C = 25.5 \text{ mm}$$

$$f_f = 702 \text{ MPa}$$

$$f_{fe} = 734 \text{ MPa}$$

Step 2: Determine development length, l_d

Since f_f (702 MPa) is less than f_{fe} (734 MPa), f_{fr} becomes 702 MPa.

From Equation 22.39,

$$l_d = \frac{(\alpha f_{fr} / 0.083\sqrt{f_c'}) - 340}{13.6 + (C / d_b)} d_b$$

$$= \frac{(1.0)(702 \text{ MPa}) / 0.083\sqrt{25 \text{ MPa}}) - 340}{13.6 + (25.5 \text{ mm} / 16 \text{ mm})} (16 \text{ mm})$$

$$= 1423 \text{ mm}$$

$$= 1.42 \text{ m}$$

Step 3: Calculate the nominal moment strength and factored shear at the section

From Equation 22.13, the moment strength with $f_f = f_{fr}$

$$M_n = \rho_f f_f \left(1 - 0.59 \frac{\rho_f f_f}{f_c'}\right) bd^2$$

$$= 0.010 (702 \text{ MPa}) \left(1 - 0.59 \frac{0.010 (702 \text{ MPa})}{25 \text{ MPa}}\right) (225 \text{ mm}) (357 \text{ mm}^2)$$

$$= 168 \text{ kN} \cdot \text{m}$$

The factored shear demand at the middle of the block wall is

$$V_u = \frac{w_f L}{2}$$
$$= \frac{(1.4(20\ \text{kN/m}) + 1.7(30\ \text{kN/m}))(3\ \text{m})}{2}$$
$$= 119\ \text{kN}$$

Step 4: Determine the length of bar available for development
The available development length is the lesser of the following two expressions:

$$(1)\ l_d \le \frac{L}{2} + l_a$$
$$\le \frac{3.0\ \text{m}}{2} + 0.2\ \text{m}$$
$$\le 1.70\ \text{m}$$

$$(2)\ l_d \le \frac{1.3M_n}{V_u} + l_a$$
$$\le \frac{1.3(168\ \text{kN} \cdot \text{m})}{118.5\ \text{kN}} + 0.2\ \text{m}$$
$$\le 2.04\ \text{m}$$

The first limitation governs; therefore, the available development length is 1.70 m, which is greater than the required 1.42 m. ⇐

Tension Lap Splices

ACI 318 requires a steel splice length of $1.0l_d$ and $1.3l_d$ for Class A and B splices, respectively. This classification is not applicable to FRP reinforcement as it is typically not necessary to develop the full stress capacity of the bar. Instead, all FRP bar splices are conservatively classified as Class B splices by ACI 440.1, with a recommended development length of $1.3l_d$.

FINAL REMARKS

Reinforcing concrete sections with FRP bars represents the synthesis of high-performance materials with infrastructure engineering. New design procedures must be developed to ensure that the engineer is provided with a system performing safely at its optimum capacity. For the engineer designing with internal FRP reinforcing materials, an appreciation of the fundamental behavioral differences between FRP and steel is essential for safe, efficient designs. As stated at the beginning of this chapter, a full review of ACI 440.1R-06 "Guide for the Design and Construction of Concrete Reinforced with FRP Bars" (ACI, 2006) is recommended for a more in-depth background of the design equations presented herein. With these fundamentals in hand, design engineers will have the ability to produce efficient, durable, safe, and innovative structures.

REFERENCES

ACI. (2004a), *Prestressing Concrete Structures with FRP Tendons*, ACI 440.4R-04, American Concrete Institute, Farmington Hills, MI.

ACI. (2004b), *Guide Test Methods for Fiber-Reinforced Polymers (FRPs) for Reinforcing or Strengthening Concrete Structures*, ACI 440.3R-04, American Concrete Institute, Farmington Hills, MI.

ACI. (2005), *Building Code Requirements for Structural Concrete*, ACI 318M-05, American Concrete Institute, Farmington Hills, MI.

ACI. (2006), *Guide for the Design and Construction of Concrete Reinforced with FRP Bars*, ACI 440.1R-06, American Concrete Institute, Farmington Hills, MI.

ACI. (2011), *Building Code Requirements for Structural Concrete (ACI 318-11) and Commentary*, American Concrete Institute, Farmington Hills, MI.

BISE. (1999), *Interim Guidance on the Design of Reinforced Structures Using Fibre Composite Reinforcement*, British Institution of Structural Engineers, Seto Ltd., London, U.K.

Branson, D. E. (1977), *Deformation of Concrete Structures*, McGraw-Hill Book Co., New York, 546 pp.

CNR DT. (2006), Istruzioni per la Progettazione, l'Esecuzione ed il Controllo di Strutture realizzate con Calcestruzzo armato mediante Barre di Materiale Composito Fibrorinforzato (draft in Italian).

CSA. (2002), *Design and Construction of Building Components with Fibre Reinforced Polymers*, CAN/CSA S806-02, Canadian Standards Association, Ottawa, Ontario, Canada.

CSA. (2006), *Canadian Highway Bridge Design Code*, CAN/CSA-S6-06, Canadian Standards Association (CSA) International, Toronto, Ontario, Canada.

Ehsani, M. R., Saadatmanesh, H., and Tao, S. (1995), Bond of hooked glass fiber reinforced plastic (GFRP) reinforcing bars to concrete, *ACI Materials Journal*, 92(4), 391–400.

Ehsani, M. R., Saadatmanesh, H., and Tao, S. (1996), Bond behavior and design recommendations for fiberglass reinforcing bars, *Proceedings of the First International Conference on Composites in Infrastructure (ICCI-96)*, H. Saadatmanesh and M. R. Ehsani (eds.), Tucson, AZ, pp. 466–476.

Fib. (2005), *FRP Reinforcement for RC Structures—Technical Report on the Design and use of Fibre Reinforced Polymer Reinforcement (FRP) for Reinforced Concrete Structures*, Task Group 9.3 FRP (fibre reinforced polymer) reinforcement for concrete structures (draft), Federal Institute of Technology, Lausanne, Switzerland.

ISIS. (2001), *ISIS Design Manual No. 3. Reinforcing Concrete Structures with Fibre Reinforced Polymers*, Intelligent Sensing for Innovative Structures Canada, Winnipeg, MB.

ISIS. (2006), *Specifications for Product Certification of Fibre Reinforced Polymers (FRPs) as Internal Reinforcement in Concrete Structures*, ISIS Product Certification of FRP Materials, Product Certification #1, Intelligent Sensing for Innovative Structures Canada, Winnipeg, MB.

JSCE. (1997), Recommendation for design and construction of concrete structures using continuous fiber reinforcing materials, *Concrete Engineering Series No. 23*, Japan Society of Civil Engineers, Tokyo, Japan, 325 pp.

Katz, A., Berman, N., and Bank, L. C. (1999), Effect of high temperature on bond strength of FRP rebars, *Journal of Composites for Construction*, 3(2), 73–81.

Nanni, A. (1993), Flexural behavior and design of reinforced concrete using FRP rods, *Journal of Structural Engineering*, 119(11), 3344–3359.

Norwegian Standard. (1998), NS 3473. Prosjektering av betongkonstruksjoner-Beregnings-og konstruksjonsregler.

Ospina, C. E., Alexander, S., and Cheng, J. J. (2001), Behaviour of concrete slabs with fibre-reinforced polymer reinforcement, *Structural Engineering Report No. 242*, Department of Civil and Environmental Engineering, University of Alberta, Alberta, Canada, 355 pp.

Ospina, C. E., Alexander, S. D. B., and Cheng, J. J. R. (2003), Punching of two-way concrete slabs with fiber-reinforced polymer reinforcing bars or grids, *ACI Structural Journal*, 100(5), 589–598.

23 FRP Prestressed Concrete

Khaled Soudki

CONTENTS

INTRODUCTION

In prestressed concrete, internal stresses are initially introduced so that the subsequent stresses resulting from superimposed loads are counteracted to a desired degree. Prestressing is applied by means of high-strength tendons in tension passing through concrete. This can be achieved in two ways, main distinction between the two methods being whether the tendon is tensioned before or after concrete is cast, hence terms pretensioned and post-tensioned (Campbell and Soudki, 1996).

Pretensioning: Tendon tensioned before casting of the concrete

- A number of individual tendons are stretched, then the concrete is cast around the tendons and the tendons are cut after concrete hardens
- Prestressing force introduced by bond
- Precast plant operation (mass production)

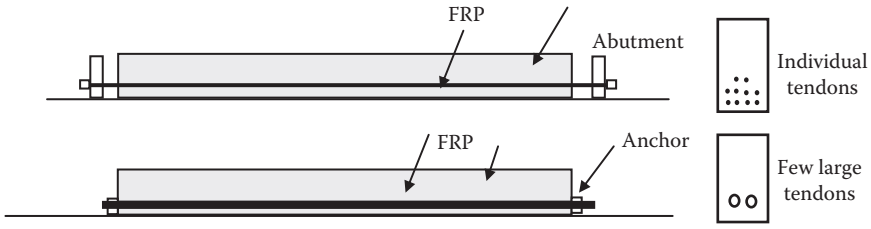

FIGURE 23.1 Pre-tensioned vs. post-tensioned construction.

Post-tensioning: Tendon tensioned after concrete is cast

- Tendons are located freely inside ducts and stressed at ends of the concrete member (from one or both sides simultaneously) after concrete attains enough strength (specified at release)
- Prestress force provided by anchor
- Tendons are either grouted (bonded section) not grouted (unbonded section) after anchoring
- In situ operation (can obtain any profile) (Figure 23.1)

Fiber reinforced polymer (FRP) tendons are composite materials consisting of synthetic or organic high-strength fibers impregnated in a resin matrix. FRP tendons with their corrosion resistance and excellent mechanical properties are promising alternative to steel tendons for prestressed concrete industry. Their use for prestressed concrete, demonstrated in research and field applications, has been limited due to the lack of a universal anchor system to grip the FRP tendon.

Design guidelines and codes for FRP reinforced and prestressed concrete have been developed by several organizations, including the American Concrete Institute (ACI), Canadian Standards Association (CSA), the Japan Society of Civil Engineers (JSCE), the International Federation for Structural Concrete (fib), and Intelligent Sensing for Innovative Structures (ISIS) Canada (JSCE, 1997; ACI, 2004, 2006; ISIS, 2005; CSA, 2006).

This chapter outlines the design procedures currently recommended by Committee 440 of the American Concrete Institute in the document ACI 440.4R-04, *Prestressed Concrete Structures with FRP Tendons* (ACI, 2004). The design considerations discussed in this chapter include

- Tendon and anchor systems
- Jacking stresses
- Flexural service stresses
- Flexural strength
- Serviceability criteria
- Shear design
- Transfer length and development

The author recognizes that the procedures in the guidelines are conservative and will be revised as the development of FRP technology and research gaps are addressed.

FRP TENDONS AND ANCHORS

FRP Tendons

The FRP tendons used for prestressed construction are classified according to the type of fiber into three categories: aramid FRP (AFRP), carbon FRP (CFRP), and glass FRP (GFRP). Figure 23.2 shows the typical FRP tendons and their stress–strain relationships.

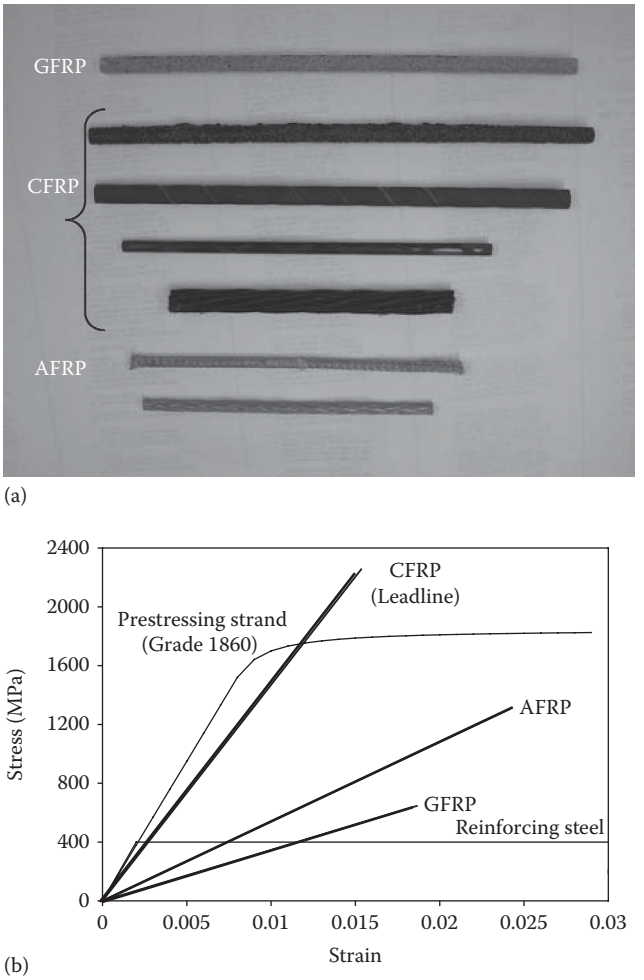

FIGURE 23.2 Typical (a) FRP tendons and their (b) stress–strain relationship.

Aramid FRP (*AFRP*): AFRP tendons are available commercially in four main types: Arapree (Italy), Fibra (Japan), Technora (Japan), and Parafil (United Kingdom). They are manufactured in various shapes such as braided, spiral wound, and flat rods.

Carbon FRP (*CFRP*): CFRP tendons are available commercially as Leadline (CFRP) and Carbon Fiber Composite Cable (CFCC), both of Japan, and Aslan200™ tendons, of the United States. Carbon fibers are characterized by their high longitudinal tensile strength and their high modulus of elasticity. CFRPs are available in the form of bars, multiwire strands, ropes, and cables.

Glass FRP (*GFRP*): GFRP tendons are commercially available as Isorod (Canada), Aslan100 (the United States), and Plalloy (Japan). GFRPs are characterized by their low modulus of elasticity and their low transverse shear resistance. GFRP tendons are not recommended as prestressing tendons (ACI 440.4R, 2004) but are used in nonprestressed applications (Table 23.1).

Anchorage Systems

FRP tendons are strong in the longitudinal direction (direction of the fibers) but weak in the transverse direction (ratio of longitudinal to transverse strength as high as 30:1). Thus, they are highly

TABLE 23.1
FRP Tendons Properties

Tendons	Specific Gravity	Tensile Strength (MPa)	Tensile Modulus (GPa)	Ultimate Elongation (mm/mm)	Coefficient Therm. Exp (10^{-6}/°C)	Relaxation % Loss from Jacking
GFRP	2.40	1379–1724	48–62	0.03–0.045	10.0	—
CFRP	1.50	2000–2610	142–165	0.01–0.015	0.0	2–3
AFRP	1.25	1200–2100	50–74	0.02–0.026	−2.0	6–15
Steel	7.90	1100–1862	186–200	>0.04	11.7	3

susceptible to premature failures at the anchorage zone during the gripping process. This makes the use of conventional anchoring systems for gripping steel strands (e.g., toothed steel wedges and threading) not possible for FRP tendons. Various types of anchors are available for FRP tendons, usually recommended by the manufacturer, and are classified based on their gripping mechanisms as described next (see Figure 23.3):

1. *Clamp anchor*: Consists of grooved steel plates held together by bolts clamping the sleeve-encased FRP rod and transferring the force by shear-friction mechanism.
2. *Plug and cone anchor*: Consists of a socket housing and conical spike used to anchor Parafil ropes held by a compressive force, generated by inserting the spike into the barrel, together with friction forces developed between the rope and the socket.
3. *Resin sleeve anchor*: The FRP tendon is embedded in resin filling a metallic housing and the tendon is gripped by a bond between the rod and the filling material.
4. *Resin potted anchor*: Is similar to the resin sleeve anchor except that the profile of the inner surface of the socket is conical with a constant taper.
5. *Metal overlay anchor*: Is attached to the ends of the FRP rod during the manufacturing process by means of die molding and the rod is gripped by a typical wedge anchor.
6. *Split wedge anchor*: Consists of a number of wedges (two to six) fitted into a barrel. The FRP wedge anchor includes a soft metal sleeve encasing the rod to protect it from notching and a variable profile of inner surface of the barrel.

FLEXURAL DESIGN

FRP tendons exhibit linear elastic response to rupture without yielding and, thus, have a pronounced effect on the flexural design philosophy. Flexural design includes requirements for flexural service stresses and flexural strength. Service stresses are determined using techniques similar to steel prestressed concrete. Flexural strength is determined based on force equilibrium and compatibility of strains (bonded section) or deformations (unbonded section) accounting for the FRP tendon properties. Therefore, the design is by satisfying service stress and strength requirements. If the stress requirements are met but the strength capacity is not satisfied, then nonprestressed FRP reinforcement can be used to increase the strength of the member.

General

FRP prestressed beams exhibit a bilinear load-deflection response, which is distinctly different from a steel prestressed beam, as shown in Figure 23.4. The precracking behavior is identical to beams with steel strands at the same level of prestress. Postcracking behavior, however, is significantly different: FRP prestressed beams exhibit larger deformation and wider crack widths than beams with steel due to the lower elastic modulus of FRP tendons.

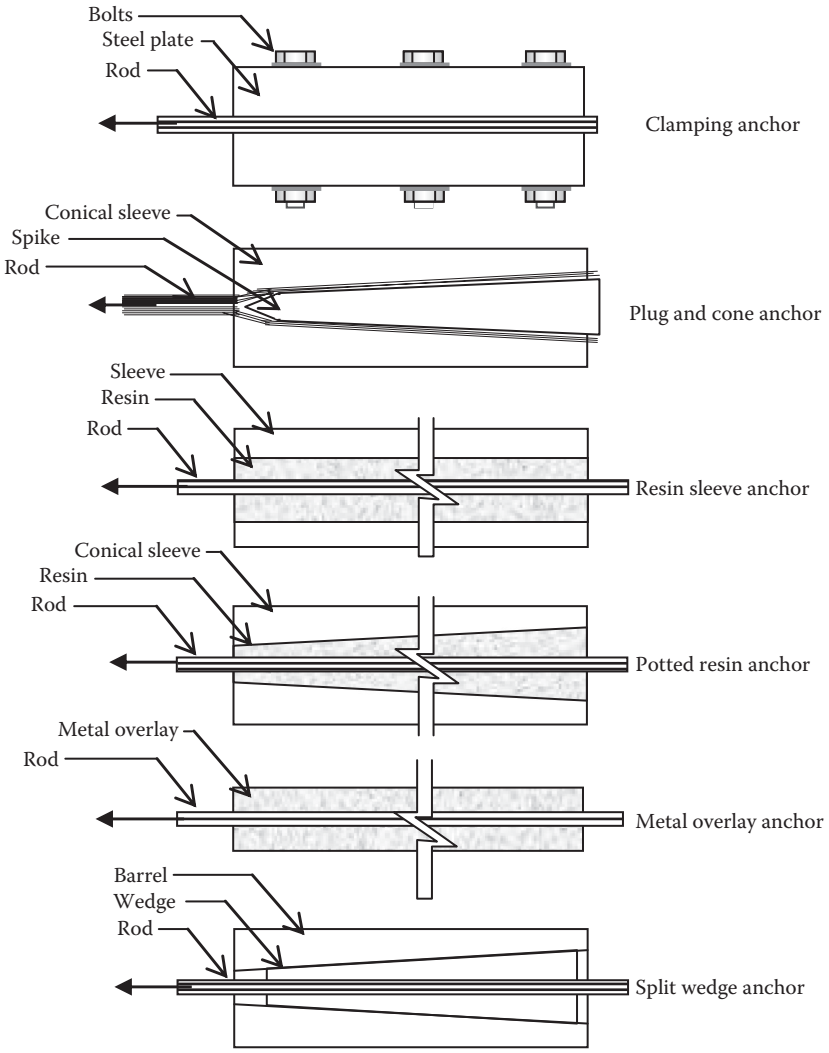

FIGURE 23.3 Typical anchors for FRP tendons.

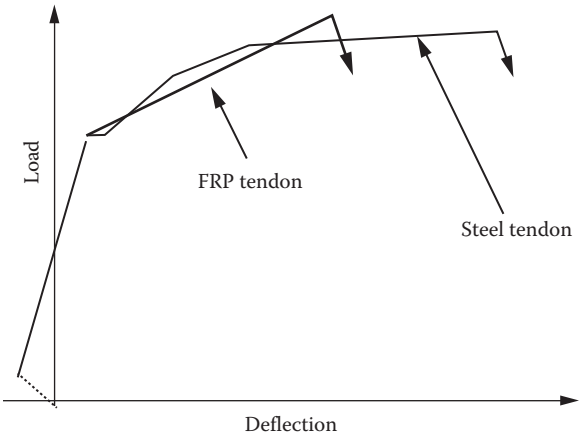

FIGURE 23.4 Typical load-deflection curves of beams prestressed with FRP and steel tendons.

TABLE 23.2
Allowable Tendon Stresses

	Aramid	Carbon
Allowable jacking stresses	$0.50 f_{pu}$	$0.65 f_{pu}$
Allowable stress at transfer	$0.40 f_{pu}$	$0.60 f_{pu}$

Source: ACI, *Prestressed Concrete Structures with FRP Tendons*, ACI 440.4R-04, American Concrete Institute, Farmington Hills, MI, 2004, 35pp.

Concrete beams with steel are generally designed as under-reinforced so that steel yields prior to concrete failure, thus providing a ductile failure. Failure of concrete beams with FRP will occur either by tensile rupture of the FRP tendon or crushing of the concrete. Tensile failure occurs when the tendon farthest from the neutral axis ruptures before concrete fails. This type of failure is brittle when compared to a similar beam with steel tendons. The crushing failure mode occurs when concrete strain reaches ultimate before rupture strain in the FRP tendon. This is comparable to over-reinforced concrete beams with steel, which is also a brittle mode.

Jacking Stresses

The allowable jacking stresses for FRP tendons based on ACI 440.4R-04 are given in Table 23.2. These prestress values are established to be consistent with the extrapolated creep-rupture data, for CFRP and AFRP tendons to give a predicted stress of 70% and 55% for CFRP and AFRP tendons for 100 years of service life.

Prestress losses (immediate and time-dependent) reduce the stresses in the FRP tendon. The jacking stress is reduced immediately upon transfer to stress at transfer by

- Friction losses (FR)
- Anchorage slip (SLIP)
- Elastic shortening (ES)

The tendon stress at transfer is further reduced over long-time period to result in the tendon stress at service (after all losses) by

- Creep of concrete (CR)
- Shrinkage of concrete (SH)
- Relaxation of tendon (REL)

These prestress losses, except relaxation of tendon, can be determined similar to steel prestressed tendons. Their values are less than those for steel due to the lower FRP modulus of elasticity. Tendon relaxation losses (range from 3% to 14%) may be computed based on the method given in ACI-440.4R-04.

When a FRP tendon is harped, localized curvature stress in the tendon is developed, leading to a high-stress concentration in the tendon. Due to the elastic behavior of FRP up to failure, the increase in stress at the curved points may lead to premature failure at the harped locations. This amount of stress must be accounted for in determining the tendon strength. The following equation is adopted by ACI 440.4R-04 for the localized stress f:

$$f = \frac{E_f R_t}{R} \tag{23.1}$$

where

R_t is the radius of the tendon
R is the radius of curvature of the harp point
E_f is the modulus of the tendon material

TABLE 23.3
Allowable Concrete Stresses

Allowable stresses at transfer of prestress (before losses)	
(a) Extreme fiber stress in compression	$0.60 f'_{ci}$
(b) Extreme fiber stress in tension except for (c)	$0.25 \sqrt{f'_{ci}}$
(c) Extreme fiber stress in tension at ends	$0.5 \sqrt{f'_{ci}}$
Allowable stresses under service loads (following losses)	
(a) Extreme fiber stress in compression due to prestress plus sustained loads	$0.45 f'_c$
(b) Extreme fiber stress in compression due to prestress plus total loads	$0.60 f'_c$
(c) Extreme fiber stress in precompressed tensile zone	$0.5 \sqrt{f'_c}$

Source: Constructed from various sources.

Flexural Service Stresses

Design for serviceability requires calculation of stresses under various load conditions and comparison of these stresses with permissible values specified in design codes. Allowable concrete service stresses as specified by ACI 440.4-04 are found in Table 23.3. The stresses in concrete at a section can be computed from the relationship

$$\sigma = + \frac{P}{A} + \frac{Pey}{I} + \frac{My}{I} \tag{23.2}$$

where

σ is the stress at distance y from centroidal axis (MPa)
P is the prestress force (N)
M is the Moment due to specified loads (N mm)
e is the eccentricity measured from centroidal axis (mm)
A is the cross-sectional area (mm^2)
I is the second moment of area of section (mm^4)

Example 23.1

Flexural stresses in a pretensioned concrete beam

Compute the stresses at midspan in a pretensioned concrete beam of shown section. The beam is simply supported over a 12.0 m span. It carries a dead load of 4.0 kN/m in addition to self-weight and a live load of 3.4 kN/m. The beam is prestressed with four 12.7 mm diameter CFRP tendons each stressed initially to 65% ultimate. After losses, the prestress level is 50% ultimate. The CFRP tendon used has ultimate strength f_{pu} = 2068 MPa, modulus of elasticity, E_p = 124 GPa, rupture strain = 0.017. Concrete strengths are f'_{ci} = 30 MPa and f'_c = 40 MPa.

Solution:

$$P_f = 500 \times 0.50 \times 2068 = 517\,\text{kN}$$

$$e = \frac{600}{2} - 75 = 225\,\text{mm}$$

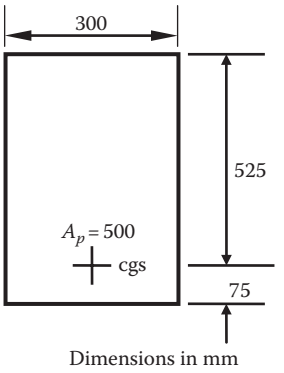

$$I = \frac{bh^3}{12} = \frac{300 \times 600^3}{12} = 5400 \times 10^6 \text{ mm}^4$$

$$A = bh = 300 \times 600 = 180 \times 10^3 \text{ mm}^2$$

$$y_T = y_B = \frac{600}{2} = 300 \text{ mm} \quad \text{(rectangular section)} S_B = S_T = \frac{5400 \times 10^6}{300} 18 \times 10^6 \text{ mm}^3$$

Self-weight of section = 0.30 × 0.600 × 23.5 = 4.23 kN/m
Superimposed dead load = 4.00 kN/m
Live load = 3.40 kN/m
Therefore, specified load = 11.63 kN/m

$$\text{Maximum bending moment due to specified load} = \frac{wl^2}{8} = \frac{11.63 \times 12^2}{8} = 209 \text{ kNm}$$

$$\text{Maximum bending moment due to sustained load} = 209 \times \frac{8.23}{11.63} = 148 \text{ kNm}$$

Note that we are considering specified loads, so load factors are unity in this case.

Stresses at midspan under specified loading are

Top:

$$\sigma_T = \frac{(-517 \times 10^3)}{180 \times 10^3} + \frac{(-517 \times 10^3)(+225)(-600/2)}{5400 \times 10^6} + \frac{(+209 \times 10^6)(-600/2)}{5400 \times 10^6}$$

$$= -2.87 + 6.46 - 11.6$$

$$= -8.0 \text{ MPa} \le 0.6 f'_c = 0.6 \times 40 = 24 \text{ MPa OK}$$

Bottom:

$$\sigma_B = \frac{(-517 \times 10^3)}{180 \times 10^3} + \frac{(-517 \times 10^3)(+225)(+600/2)}{5400 \times 10^6} + \frac{(+209 \times 10^6)(+600/2)}{5400 \times 10^6}$$

$$= -2.87 - 6.46 + 11.6$$

$$= +2.27 \text{ MPa} \le 0.5\sqrt{f'_c} = 0.5\sqrt{40} = 3.16 \text{ MPa OK}$$

Check also compressive stress at top fiber due to sustained loading:

$$\sigma_T = -2.87 + 6.46 - 11.60 \times \frac{148}{209}$$

$$= -2.87 + 6.46 - 8.21$$

$$= -4.62 \text{ MPa} \le 0.45 f_c' = 0.45 \times 40 = 18 \text{ MPa OK}$$

The stresses at midspan of the beam in both extreme fibers are within the permissible limits under both specified and sustained loads.

Cracking Moment

The factored flexural resistance of a prestressed section should be at least 1.5 times the cracking moment. This ensures that complete failure does not occur when a section cracks. Therefore, we must be able to calculate the cracking moment, M_{CR}.

The section cracks, and thus M_{CR} is attained, when the extreme tensile fiber stress in the concrete reaches the modulus of rupture, $f_r = 0.6\sqrt{f_c'}$.

Hence, for cracking in a homogeneous section, setting the stress in the extreme tension fiber at $y = y_t$, equal to the modulus of rupture, gives

$$M_{CR} = \left(-\frac{P}{A} - \frac{Pey_t}{I} + 0.6\lambda\sqrt{f_c'} \right) \frac{I}{y_t} \tag{23.3}$$

Example 23.2

Cracking moment in a pretensioned concrete beam
Compute the cracking moment for the beam in Example 23.1.
Extreme tension fiber at midspan is at the bottom of beam

$$M_{CR} = \left[-(-2.873) - (-6.46) + 0.6\sqrt{40} \right] \frac{5400 \times 10^6}{300}$$

$$= 236 \times 10^6 \text{ N mm}$$

$$= 236 \text{ kN m} > 209 \text{ kN m (applied)}$$

Note there is no cracking under specified load. This is expected since the tensile stress at the midspan section under specified load was less than the permissible value.

Flexural Strength

The capacity condition that must be satisfied in the design of FRP prestressed concrete members:

$$\varphi \cdot M_n \ge M_u \tag{23.4}$$

where

φ is the strength reduction factor
M_n is the nominal flexural capacity of FRP-reinforced concrete member
M_u is the ultimate moment determined using load factors suggested by ACI 318-02

The strength reduction factors, φ, are based on the failure mode (ACI 440.4R-04):

- Tension controlled, φ = 0.70 for aramid and φ = 0.85 for carbon
- Compression-controlled, φ = 0.65 (carbon or aramid)

Bonded Section

The strength design for prestressed beams with FRP tendons is based on the concept of a balanced reinforcement ratio, ρ_b, the reinforcement ratio at which concrete fails in compression at the same time FRP tendon ruptures. ACI 440.4R-04 classifies the flexural behavior of FRP prestressed beam depending on the reinforcement ratio into three groups:

1. *Balanced failure*: If $\rho = \rho_b$, failure will occur by rupture of the tendon ($\varepsilon_p = \varepsilon_{pu}$) and crushing of the concrete ($\varepsilon_{cu} = 0.003$) simultaneously.
2. *Tension failure*: If $\rho < \rho_b$, the member is under-reinforced and will fail by rupture of the tendon ($\varepsilon_p = \varepsilon_{pu}$) with concrete below crushing strain ($\varepsilon_{cu} = 0.003$).
3. *Compression failure*: If $\rho > \rho_b$, concrete fails by crushing in compression ($\varepsilon_{cu} = 0.003$) prior to rupture of tendon ($\varepsilon_p < \varepsilon_{pu}$).

The flexural resistance proceeds rationally using strain compatibility approach and force equilibrium of the section utilizing the material characteristics of FRP and concrete.

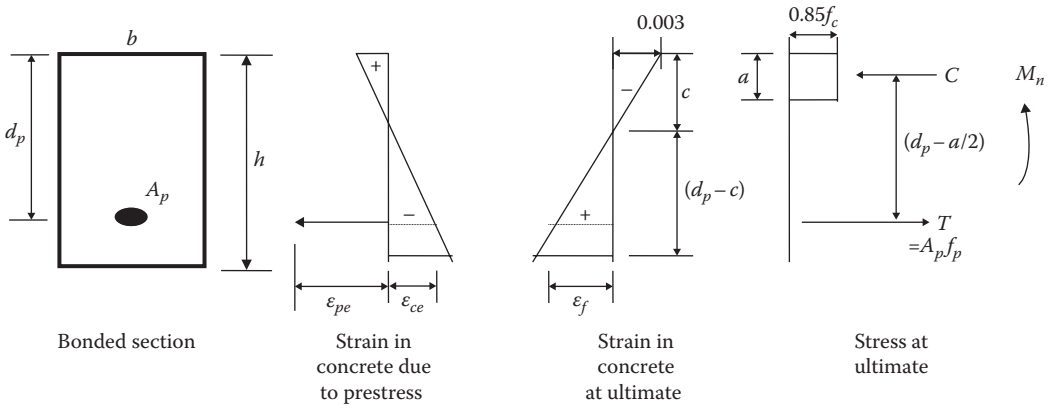

The strain compatibility is used to compute the stress in the FRP tendon at ultimate (f_p).

$$\text{Strain in tendon at ultimate } \varepsilon_p = \varepsilon_{pe} + (\varepsilon_{ce} + \varepsilon_f) \tag{23.5}$$

From strain diagram at ultimate,

$$\varepsilon_f = \varepsilon_u \left(\frac{d_p}{c} - 1 \right) \tag{23.6}$$

For equilibrium $T = C$,

$$A_p f_p = 0.85 f'_c ab \tag{23.7}$$

$$\therefore c = \frac{a}{\beta_1} = \frac{A_p f_p}{0.85 f_c' \beta_1 b} \tag{23.8}$$

$$\beta_1 = 0.85 - 0.05\frac{(f_c' - 27.5)}{6.9} > 0.65$$

$$\text{giving } \varepsilon_{cu} = \varepsilon_u \left(\frac{0.85 f_c' \beta_1}{\rho_p f_{ps}} - 1 \right) \quad \text{where } \rho_p = \frac{A_p}{b d_p} \tag{23.9}$$

$$\text{Hence, } \varepsilon_p = \varepsilon_{pe} + \varepsilon_{ce} + \varepsilon_f \left(\frac{0.85 f_c' \beta_1}{\rho_p f_p} - 1 \right) \tag{23.10}$$

The unknowns in this equation are ε_p and f_p. These two terms are also related by the stress–strain curve for FRP tendon, which is linear ($f_p = E_p\, \varepsilon_p$). The solution proceeds by iteration to find f_p.

Having found f_p, the flexural resistance of the section is given by

$$M_n = T\left(d_p - \frac{a}{2}\right) = A_p f_p \left(d_p - \frac{a}{2}\right) \tag{23.11}$$

If tension failure (or balanced failure) controls, the analysis is simplified by setting $f_p = f_{pu}$ and solving for "a" from force equilibrium without iteration and determining M_n as earlier.

The aforementioned derivation assumes a single layer of FRP tendons. The analysis of a section with multiple layers of tendons is presented elsewhere (ACI 440.4R-04).

Example 23.3

Flexural strength of pretensioned concrete beam (bonded)

Compute the ultimate moment of the rectangular section used in Example 23.2 assuming a bonded section. The CFRP tendon used has ultimate strength f_{pu} = 2068 MPa, modulus of elasticity, E_p = 124 GPa, rupture strain = 0.017. The specified concrete strength is $f_c' = 40\ \text{MPa}$.

The prestress level after losses is f_{pe} = 50% f_{pu}.

Solution:

A = 180,000 mm^2

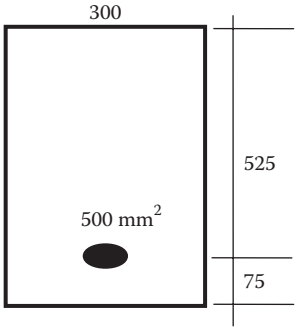

$I = 5400 \times 10^6$
e = 225 mm

$$P = 0.50 \times 2068 \times 500 = 517 \times 10^3 \text{ N} \qquad \beta_1 = 0.85 - 0.05\frac{(40 - 27.5)}{6.9} = 0.76$$

$$E_c = 4{,}500\sqrt{f'_c} = 4{,}500\sqrt{40} = 28{,}460 \text{ MPa}$$

(a) ε_{pe} = FRP strain due to prestressing

$$= \frac{f_{pe}}{E_{ps}} = \frac{0.5 \times 2068}{124 \times 10^3} = 8338 \times 10^{-6}$$

(b) ε_{ce} = concrete strain at level of FRP tendon due to prestressing

$$\sigma = \frac{P}{A} + \frac{Pey}{I}$$

$$= \frac{(-517 \times 10^3)}{180 \times 10^3} + \frac{(-517 \times 10^3)(225)(225)}{5400 \times 10^6} = -7.7 \text{ MPa}$$

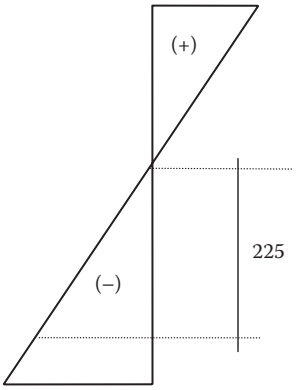

$$\varepsilon_{ce} = \frac{f_{ce}}{E_c} = \frac{7.7}{28460} = 271 \times 10^{-6}$$

(c) ε_f = concrete strain at level of tendon at ultimate

Assume $f_p = f_{pu} = 2068$ MPa

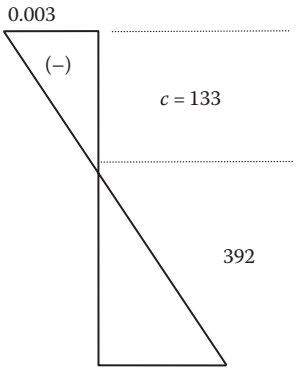

$$a = \frac{A_p f_p}{0.85 f'_c b} = \frac{500 \times 2068}{0.85 \times 40 \times 300} = 101\,\text{mm}$$

$$c = \frac{a}{\beta_1} = \frac{101}{0.76} = 133\,\text{mm} \qquad \therefore \varepsilon_f = 0.003 \times \frac{133}{392} = 8842 \times 10^{-6}$$

Total FRP strain $\varepsilon_{pu} = \varepsilon_{pe} + \varepsilon_f + \varepsilon_{cu}$

$$\varepsilon_{pu} = (8338 + 271 + 8842)10^{-6}$$

$$= 17451 \times 10^{-6} = 0.0175$$

$$\therefore f_p = E_p \varepsilon_{pu} = 124{,}000 \times 0.0175 = 2{,}163\,\text{MPa} > 2{,}068\,\text{MPa} \Rightarrow \text{tension failure}\ f_p = 2068\,\text{MPa}$$

The neutral axis depth, c = 133 mm (and depth of compression block, a = 101 mm), is the same as given earlier. The flexural strength of the section:

$$M_n = A_p f_p \left(\frac{d-a}{2}\right) = 500 \times 2068 \left(525 - \frac{101}{2}\right) = 490\,\text{kNm}$$

Unbonded Section

The behavior of beams post-tensioned with unbonded FRP tendons conceptually differs from that if the tendons were bonded to concrete. Due to the absence of bond, the stress in the unbonded tendon remains constant throughout the span length between the anchorages. The stress is based on the deformation of the whole member and not on section strain compatibility between the tendons and the surrounding concrete. The analysis of the section with unbonded tendons is reduced to that of a section with bonded tendons by applying a reduction coefficient, Ω, to the strain values, as follows:

$$\Omega = \frac{(\Delta\varepsilon_{cp})_{\text{unbonded}}}{(\Delta\varepsilon_{cp})_{\text{bonded}}} \tag{23.12}$$

The values of the strain reduction coefficient, Ω, are given in ACI 440.4R-04 as

- $\Omega = 1.5/(L/d_p)$ (one-point loading)
- $\Omega = 3.0/(L/d_p)$ (two-point or uniform loading)

To determine the flexural strength of beams post-tensioned with unbonded FRP tendons, it is necessary to predict the stress in the prestressing tendons at ultimate, f_p, using the following:

$$f_p = f_{pe} + \Delta f_p = f_{pe} + \Omega E_p \varepsilon_{cu} \left(\frac{d_p}{c_u} - 1\right) \tag{23.13}$$

where f_{pe} is the effective prestress due to the prestress force and dead load moment and Δf_p is the increased stress caused by additional loading to reach the ultimate moment resistance. Thus, the flexural resistance of the section is given by

$$M_n = T\left(d_p - \frac{a}{2}\right) = A_p f_p \left(d_p - \frac{a}{2}\right) \tag{23.14}$$

where

$$a = \frac{A_p f_p}{0.85 f_c' b}$$

Example 23.4

Flexural resistance of post-tensioned concrete beam (unbonded)

Calculate the nominal strength of a post-tensioned beam identical to that in Example 23.3 but with CFRP tendons unbonded in the section. The analysis proceeds as follows:

$$f_{pu} = 2{,}068 \text{ MPa}\ E_p = 124{,}000 \text{ MPa}$$

Beam span = 12.0 m

Solution:

Strain reduction factor:

$$\Omega = \frac{3.0}{L/d_p} = \frac{3.0}{12{,}000/525} = 0.13$$

Stress in FRP tendon at failure:

$$f_p = f_{pe} + \Omega E_p \varepsilon_{cu}\left(\frac{d_p}{c_u} - 1\right) = 0.5(2{,}068) + 0.13 \times 124{,}000 \times 0.003\left(\frac{525}{c_u} - 1\right)$$

$$f_p = 1034 + 48.3\left(\frac{525}{c_u} - 1\right) \tag{23.15}$$

Equilibrium of forces:

$$A_p f_p = 0.85 f_c' ab \Rightarrow 500 f_p = 0.85(40)(300)(0.76)c_u \Rightarrow f_p = 15.5 c_u \tag{23.16}$$

Substituting Equation 23.16 into 23.15 yields the following quadratic equation:

$$c_u^2 - 63.6 c_u - 1636 = 0$$

$$c_u = 83 \text{ mm} \quad \text{and} \quad a = \beta_1 c_u = 63 \text{ mm}$$

$$f_p = 15.5 c_u = 15.5(83) = 1286 \text{ MPa}$$

$$M_n = A_p f_p \left(d_p - \frac{a}{2} \right) = 500 \times 1286 \left(525 - \frac{63}{2} \right) = 317 \text{ kN m}$$

Recall that the strength of a bonded section, M = 490 kN m. Thus, the efficiency of the unbonded section versus a similar beam with bonded tendons is 317/490 = 0.64.

Example 23.5

Adequacy of prestressed concrete beam in Examples 23.3 and 23.4
Evaluate the flexural adequacy of the prestressed beams with bonded and unbonded sections in Examples 23.3 and 23.4. The analysis is as follows:

1. Ultimate moments
   ϕ = 0.85 for carbon FRP—tension controlled failure
   Case 1: bonded section, $M_r = \phi M_n$ = 0.85 (490) = 417 kN m
   Case 2: unbonded section, $M_r = \phi M_n$ = 0.85 (317) = 270 kN m
2. Minimum reinforcement (cracking moment):
   Case 1: bonded section, $\frac{M_r}{M_{cr}} = \frac{416}{236} = 1.76 > 1.5$ OK

   Case 2: unbonded section, $\frac{M_r}{M_{cr}} = \frac{270}{236} = 1.14 < 1.5$ NG
3. Factored loads
   We also require the flexural resistance of the section to be greater than the moment due to design load (i.e., factored loads). According to ACI 318-02, the design load is given by:

$$U = 1.2D + 1.6L$$

$$= 1.20 \times 4.23 + 1.6 \times 7.4 = 16.9 \text{ kN/m}$$

$$\text{design moment } (M_f) = \frac{16.90 \times 12^2}{8} = 304 \text{ kN m}$$

   Case 1: bonded section, M_r = 416 kN m > M_f = 304 kN m OK
   Case 2: unbonded section, M_r = 270 kN m < M_f = 304 kN m N.G
   Therefore, for case 2 (unbonded section), we must add nonprestressed bonded FRP to guard against cracking and to increase the flexural strength of the unbonded section.

SERVICEABILITY REQUIREMENTS

Deflection

Deflection in a prestressed member is classified as camber (or the upward deflection) due to prestressing and deflection (or the downward deflection) due to self-weight and service loads. A designer must ensure that deflections, both short term and long term, are within the permissible values prescribed in codes. The procedure for calculating the deflection for FRP prestressed concrete is outlined in ACI 440.4R-04. The key points are given next.

Immediate deflections, occurring at the time load is applied, are calculated based on mechanics of materials. If the section is uncracked, the deflection is calculated using gross moment of inertia. Following cracking, a modified effective moment of inertia I_e is used as

$$I_{eff} = \left(\frac{M_{cr}}{M_a} \right)^3 \beta_d I_g + \left(1 - \left(\frac{M_{cr}}{M_a} \right)^3 \right) I_{cr} < I_g \tag{23.17}$$

$$\beta_d = 0.5\left[\frac{E_p}{E_s} + 1\right] \tag{23.18}$$

where

I_{eff} is the effective moment of inertia
I_g is the gross moment of inertia
I_{cr} is the cracked moment of inertia
M_{cr} is the cracking moment
M_a is the unfactored live load moment
β_d is the factor to soften effective moment of inertia

The long-term deflections occur after load has been sustained for a long time as a result of creep and shrinkage of concrete, and relaxation of tendon. Long-term deflections are calculated individually and adjusted using multiplier factors similar to conventional prestressed members. The multipliers for FRP tendons range from 1.00 to 4.10 at erection and final conditions.

Example 23.6

Moment of inertia of prestressed beam

Determine the effective moment of inertia of the prestressed beam of Example 23.3 for an applied service moment of M_a = 209 kN m (case 1) and M_a = 300 kN m (case 2).

CFRP tendon has ultimate strength f_{pu} = 2068 MPa, modulus of elasticity, E_p = 124 GPa, and rupture strain = 0.017. The effective prestress, f_{pe} = 50% f_{pu} and concrete strength is $f'_c = 40$ MPa.

Solution:

The effective prestress, f_{pe} = 50% f_{pu} = 1034 MPa
Area of prestress tendons, A_p = 500 mm² (4 – 12.7 mm diameter)

$$\rho = \frac{A_p}{bd} = \frac{500}{300 \times 525} = 0.0031$$

$$n = \frac{E_{frp}}{E_c} = \frac{124{,}000}{4{,}500\sqrt{40}} = \frac{124{,}000}{28{,}460} = 4.36$$

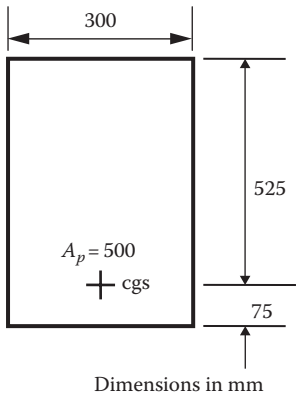

Gross moment of inertia:

$$I_g = \frac{bh^3}{12} = \frac{300 \times 600^3}{12} = 5400 \times 10^6 \text{ mm}^4$$

Cracked moment of inertia:

$$k = \sqrt{(\rho n)^2 + 2\left(1 - \frac{f_{pe}}{f_{pu}}\right)(\rho n)} - (\rho n)$$

$$= \sqrt{(4.36 \times 0.0031)^2 + 2(1 - 0.5)(4.36 \times 0.0031)} - (4.36)(0.0031)$$

$$= 0.104$$

$$I_{cr} = \frac{b(kd)^3}{3} + nA_p(d - kd)^2$$

$$= \frac{300(0.1 \times 525)^3}{3} + 4.36 \times 500(525 - 0.1 \times 525)^2$$

$$= 501 \times 10^6 \text{ mm}^4$$

Effective moment of inertia depends on the level of applied service moment (vs. cracking moment):
Cracking moment, M_{cr} (Example 23.2) = 236 kN m

$$\beta_d = 0.5\left[\frac{E_p}{E_s} + 1\right] = 0.5\left[\frac{124{,}000}{200{,}000} + 1\right] = 0.81$$

Case 1: (Example 23.7) M_a = 209 kN m < M_{cr}
Therefore, take $I = I_g$ in deflection calculations, that is, full section effective under service load.

Case 2: M_a = 300 kN m > M_{cr}

$$\frac{M_{cr}}{M_a} = \frac{236}{300} = 0.78$$

$$I_{eff} = \left(\frac{M_{cr}}{M_a}\right)^3 \beta_d I_g + \left(1 - \left(\frac{M_{cr}}{M_a}\right)^3\right) I_{cr}$$

$$= (0.78)^3 \times 0.81 \times 5400 \times 10^6 + (1 - 0.78^3) \times 501 \times 10^6 = (2075 + 263) \times 10^6$$

$$= 2338 \times 10^6 \text{ mm}^4$$

Once the effective moment of inertia is known, the immediate and long-term deflections can be calculated using conventional methods and must be checked against permissible limits.

Crack Width

Crack width requirements of ACI 318-02 are proposed to be used with FRP prestressed beams, provided the stress term is scaled by the ratio of modulus of elasticity of FRP to that for steel.

Fatigue

Fatigue of FRP prestressed beams is evaluated by comparing the obtained stress range in the prestressed tendon under cyclic loading to that obtained from S–N curves for FRP tendon. Fatigue should not be a problem in FRP prestressed beams since the service cyclic stresses are usually small (ACI 440.4R-04). If the prestressed member remains uncracked under service loads, the fatigue of the tendon-anchor system will not be critical. In cracked prestressed concrete beams, fatigue may

become significant with increased tendon stress at cracks in pretensioned beams, fretting fatigue in post-tensioned beams, and fatigue of tendon-anchor system.

TRANSFER AND DEVELOPMENT LENGTH

The development requirements for prestressing FRP tendons are intended to provide bond integrity for the strength of the member. The transfer length of the tendon is the distance over which the tendon must be bonded to the concrete to develop the effective prestress f_{pe} in the tendon. The flexural bond length represents the additional length over which the tendon must be bonded so that a stress f_p may develop in the tendon at nominal strength of the member.

The expression for development length λ_d for a tendon of diameter, d_b, may be written as two terms, transfer length and flexural bond length:

$$\ell_d = k_1 f_{pe} d_b + k_2 (f_p - f_{pe}) d_b \tag{23.19}$$

where

d_b is the tendon diameter
f_{pe} is the effective prestress in the tendon
f_p is the stress in the tendon at failure of the section
k_1 k_2 are the constants that vary with FRP type. ACI 440.4R-04 proposes k_1 = 1/3 and k_2 = 3/4 for CFRP tendon.

The transfer length of FRP tendon is a function of the perimeter configuration area and surface condition of the FRP, the stress in the FRP, and the method used to transfer the FRP force to the concrete. The mechanism of bond differs between FRP and steel strands. FRP material is derived from a different proprietary manufacturing process and has unique and characteristic surface texture. The surface configuration of FRP tendons varies greatly when compared with steel strands. It is likely that the differences in FRP tendon surface and tendon design characteristics will influence the bond performance and affect the development length requirements. In general, most FRP tendons have linear elastic behavior to failure and exhibit transfer lengths shorter than that of steel. Tendons with treated rough surface can have appreciably shorter transfer length than untreated tendons. Gentle release of tendon will permit a shorter transfer length than abruptly cutting the tendons. Higher initial prestress in tendon leads to larger transfer length. The typical values for transfer and development lengths for FRP tendons are given in Table 23.4.

TABLE 23.4
Typical Transfer Length and Development Length for Various FRP Tendons (Constructed from Various Sources)

Material	Type	Diameter (mm)	Young's Modulus (GPa)	Tensile Strength (MPa)	f_{pi}/f_{pu}	L_t/d_b	L_d/d_b
Aramid	Arapree	10.00	127.5	2447	0.5–0.7	16–50	100
	FIBRA	10.40	48.30	1434	0.4–0.6	20–50	90
	Technora	7.40	68.60	1724	0.6	43	112
Glass	S-2 glass	9.52	48.30	1379	0.3–0.5	28–37	—
Carbon	Leadline	7.93	149.6	1980	0.5–0.7	50–80	175
	CFCC	8.30	137	2220	0.5–0.7	50	n.a.
Steel	7 wire	12.70	200	1860	0.75	50–60	106

SHEAR DESIGN

There are limited data on the shear behavior of FRP prestressed beams. The shear design in prestressed concrete is determined using the same approach as for reinforced concrete that conservatively modifies ACI318-02 (ACI, 2002) expressions to account for the special properties of FRP stirrups. The shear strength is taken as the sum of three components: V_c representing the concrete contribution, V_{frp} the FRP stirrups contribution, and V_p vertical component of the prestress force in the tendon. The shear equation is as follows:

$$V_n = V_c + V_{frp} + V_p \tag{23.20}$$

The approach for shear design and detailing requirements for FRP shear stirrups can be found in Chapter 9, which is based on the ACI 440.1R-06 guide. V_p is found as in steel prestressed beams.

DUCTILITY AND DEFORMABILITY

Ductility indices are commonly given in terms of curvature, rotation, or deflection as follows:

$$\mu_\varphi = \frac{\phi_u}{\phi_y},\ \mu_\varphi = \frac{\theta_u}{\theta_y},\ \text{or}\ \ \mu_\phi = \frac{\Delta_u}{\Delta_y} \tag{23.21}$$

where

μ is the ductility index
ϕ_y ϕ_u is the curvature at yield and ultimate condition
θ_y θ_u is the rotation at yield and ultimate condition
Δ_y Δ_u is the deflection at yield and ultimate condition

Since FRP tendons are characterized by their linear elastic behavior with lower strain at failure, the conventional definition of ductility is not applicable for FRP prestressed concrete. Several alternative definitions for ductility or deformability index were proposed in the literature:

- The ratio of deformation at ultimate to that under service or cracking load
- The ratio of total energy to elastic energy using unloading path of load-deflection
- The ratio of the curvatures under ultimate and service loads and the formula for deformability index, *DI,* is as follows (ACI 440.4R-04):

$$DI = \frac{(d - kd)\varepsilon_{pu}}{(d - (a/\beta_1))\varepsilon_{ps}} \tag{23.22}$$

To obtain high deformability in a FRP prestressed beam, the designer may reduce the initial tendon strain, thus providing more tendon strain reserve for safety against brittle failure. Also, the ductility of FRP prestressed members can be improved by partial prestressing, confinement by stirrups or fiber reinforcement, layered tendon, or using unbonded tendons. Conceptually, the later configuration with FRP tendons is very attractive since the stresses in unbonded tendons do not reach ultimate at concrete failure.

FINAL REMARKS

Prestressed concrete with FRP tendons represents the most efficient way of using the high-performance materials in civil engineering structures. While there has been significant progress achieved with respect to guidelines for FRP prestressed concrete members, a number of research

and development areas are still needed, including commercial tendon-anchorage systems, fire resistance and protection, shear strength, bond and development protocols, stressing procedures, external prestressing devices, prestressed circular tanks, tendon replacement for repair, are examples of FRP prestressed research areas (ACI 440.4R-04).

A design engineer must be aware of the fundamental differences between FRP and steel prestressed concrete to achieve an efficient and safe design. Review of ACI 440.4R-04, *Prestressed Concrete Structures with FRP Tendons* (ACI, 2004) is recommended for a more in-depth background of the design equations presented herein. Other guides and codes, in preparation by fib and ISIS Canada, should also be consulted to provide additional information on the use of these innovative materials.

REFERENCES

ACI (2002), *Building Code Requirements for Structural Concrete,* 318M-02, American Concrete Institute, Farmington Hills, MI, 443 pp.

ACI (2004), *Prestressed Concrete Structures with FRP Tendons,* ACI 440.4R-04, American Concrete Institute, Farmington Hills, MI, 35 pp.

ACI (2006), *Guide for the Design and Construction of Structural Concrete Reinforced with FRP Bars,* ACI 440.1R-06, American Concrete Institute, Farmington Hills, MI, 44 pp.

Campbell T.I. and Soudki, K.A. 1996. *Prestressed Concrete—Notes and Examples*, Kingston, Ontario Canada.

CAN/CSA-S6-06 (2006), *Canadian Highway Bridge Design Code*, Clause 16, Canadian Standards Association (CSA) International, Toronto, Ontario, Canada.

ISIS Canada (2005), *Prestressing Concrete Structures with Fiber Reinforced Polymers,* Draft Design Manual No. 5, ISIS Canada Network of Centers of Excellence, Winnipeg, Manitoba, Canada.

Japan Society of Civil Engineers (JSCE) (1997), Recommendation for design and construction of concrete structures using continuous fiber reinforcing materials, *Concrete Engineering Series* No. 23, 325 pp.

24 Concrete Columns Reinforced Internally with Fiber Reinforced Polymer Bars

Ching Chiaw Choo and Issam Harik

CONTENT

INTRODUCTION

The strength interaction ($P_n - M_n$) behavior of concrete columns reinforced internally with fiber reinforced polymer (FRP) bars is quantified herein based on *ultimate strength* approach by considering stress equilibrium, strain compatibility, and material constitutive laws. The study shows that rupturing of FRP bars in concrete columns is probable, prior to concrete reaching its ultimate strain and strength, resulting in sudden and explosive-type failure. Design recommendations are provided herein in particular to preventing tensile rupture of FRP bars in these columns. More stringent design requirements than are discussed here will have to be considered such as when long-term and sustained loadings are present.

STRENGTH INTERACTION OF CONCRETE COLUMNS

A structural design of a concrete column is quite a complicated process. The evaluation, however, of a given column section and reinforcement is quite straightforward. Because columns rarely carry axial load alone, such as when loads applied off center, moments induced at joints, etc., column strength evaluation must account for direct axial load and flexure. As such the concrete column strength diagram is typically a plot of interactions between axial load and flexural capacities, in which the abscissa (i.e., the x- or horizontal axis) often shows the bending moment or flexural strength whereas the ordinate (i.e., the y- or vertical axis) represents the axial strength of a concrete column.

The strength evaluation process is illustrated in Figure 24.1 for one particular strain distribution, where a location of the neutral axis is selected, the corresponding strains, stresses, and forces of reinforcements and concrete can be calculated appropriately to determine the axial load capacity, P_n and bending moment capacity, $M_n = P_n \cdot e$, about the plastic centroid of the cross section [1].

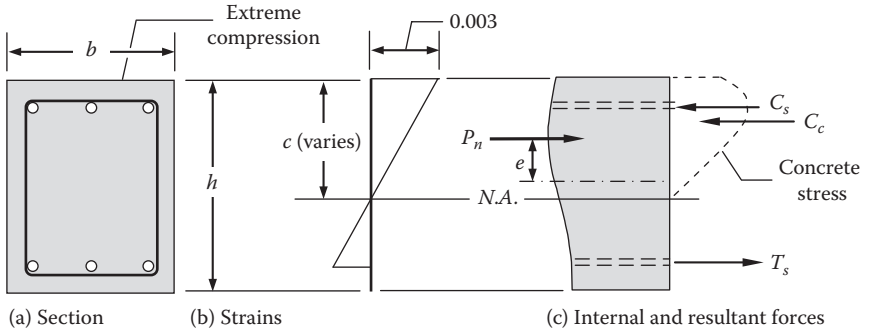

FIGURE 24.1 Calculation of P_n and M_n: (a) column cross section, (b) strain distribution, and (c) internal resultants.

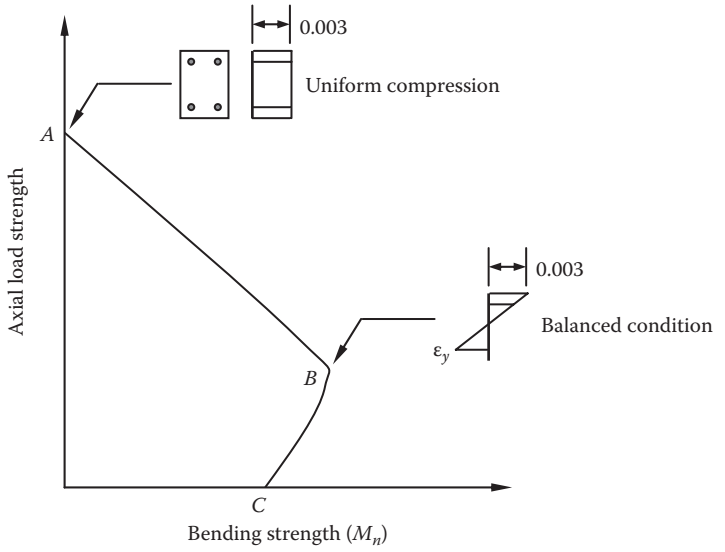

FIGURE 24.2 Strength interaction diagram.

These values of P_n and M_n represent one point on the interaction diagram. Additional points on the interaction diagram can be generated by repeating aforementioned procedures with additional locations of the neutral axis or other depths c, each yielding a unique set of P_n and M_n. The ultimate or maximum compressive strain at the outermost extreme compression fiber of concrete is generally set to be 0.003 per ACI 318-11 Code [2].

Figure 24.2 shows a typical nominal strength interaction for a tied concrete column reinforced with conventional steel reinforcement. Several points in the interaction curve for a steel reinforced concrete column are highly distinguishable: (1) Point ***A***—*pure axial load*. This represents the largest nominal axial load the column can carry, without moment and (2) Point ***B***—*balanced condition*. This point corresponds to a strain distribution with concrete reaching maximum strain value of 0.003 at the extreme compression fiber on one face, and a tensile strain of steel reaching yield strain, ε_y, at the extreme tensile layer farthest from the extreme compression fiber of concrete; and (3) Point ***C***—*pure flexure*. This point represents the nominal flexural capacity of the column, without the presence of an axial load.

STRENGTH INTERACTION BEHAVIOR OF CONCRETE COLUMNS INTERNALLY REINFORCED WITH FIBER REINFORCED POLYMER BARS

Testing of full-scale reinforced concrete columns internally reinforced with glass reinforced polymer (GFRP) bars under axial load showed that these columns behaved very similar to that of conventional steel reinforced concrete columns and demonstrated that the use of longitudinal GFRP bars did not have an adverse effect on the performance of the columns [3]. Under pure axial load condition, the failure of the GFRP reinforced concrete columns was initiated by the crushing of the concrete, with the axial strains measured being much higher than those observed in the steel RC columns [3].

Strength interaction behavior of concrete columns internally reinforced with FRP bars was investigated using *ultimate strength* approach by considering stress equilibrium, strain compatibility, and the material constitutive laws of concrete and FRP bar, similar to the approach used for steel RC columns, and the following observations were made with reference to Figure 24.3 [4]:

- The moment resistance, in most cases, of a FRP reinforced concrete column, which lacks a *balanced* point, increases as axial load increases from pure axial load to pure flexure; unlike a steel reinforced concrete column that exhibits a simultaneous reduction in moment and axial load resistances from *balanced condition* to pure flexure (see Figure 24.2). This is especially apparent as the amount of FRP or reinforcement ratio (ρ_f) in the column increases.
- Depending upon the ultimate or maximum usable tensile strain, ε_{fut}, of the FRP type considered, e.g., GFRP bars in Figure 24.3b, tensile rupture of the FRP bar—termed *brittle tension* failure—could occur prior to concrete reaching its maximum usable strain, ε_{cu}, and hence not allowing concrete to attain its maximum usable strength.
- While conceivably FRP bars could experience compression rupture, such failure is deemed less likely compared to *brittle tension* failure as the ultimate or maximum

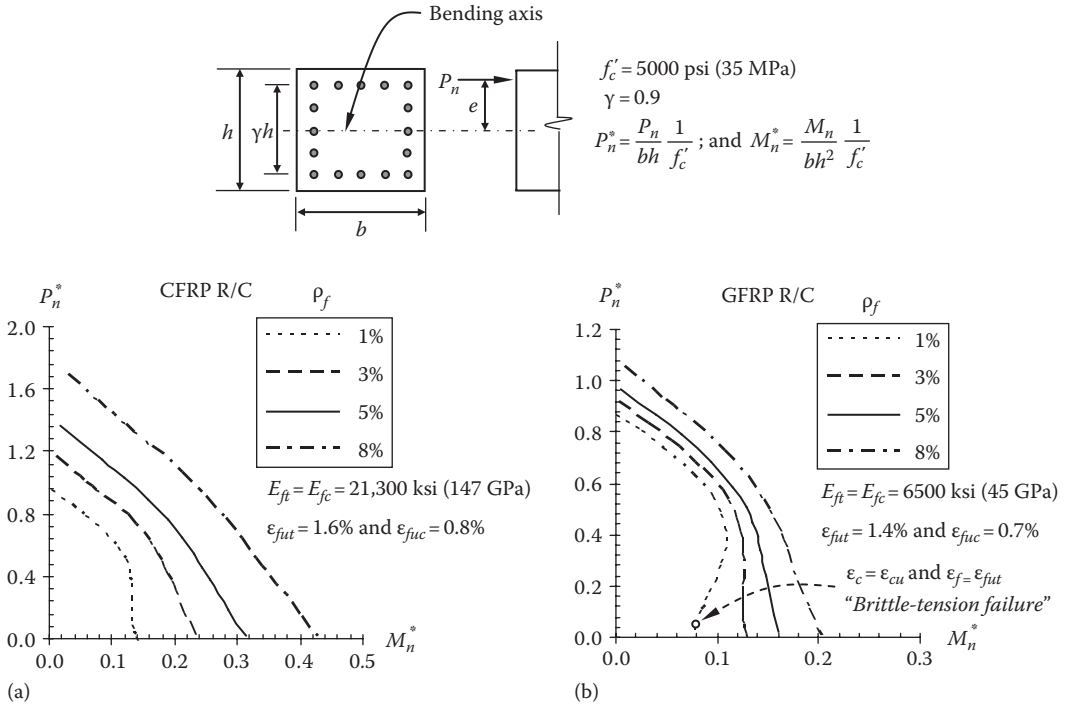

FIGURE 24.3 Strength interaction behavior of (a) CFRP RC columns and (b) GFRP RC columns. (From Choo, C.C. et al., *ACI Struct. J.*, 103(3), 452, 2006. With permission.)

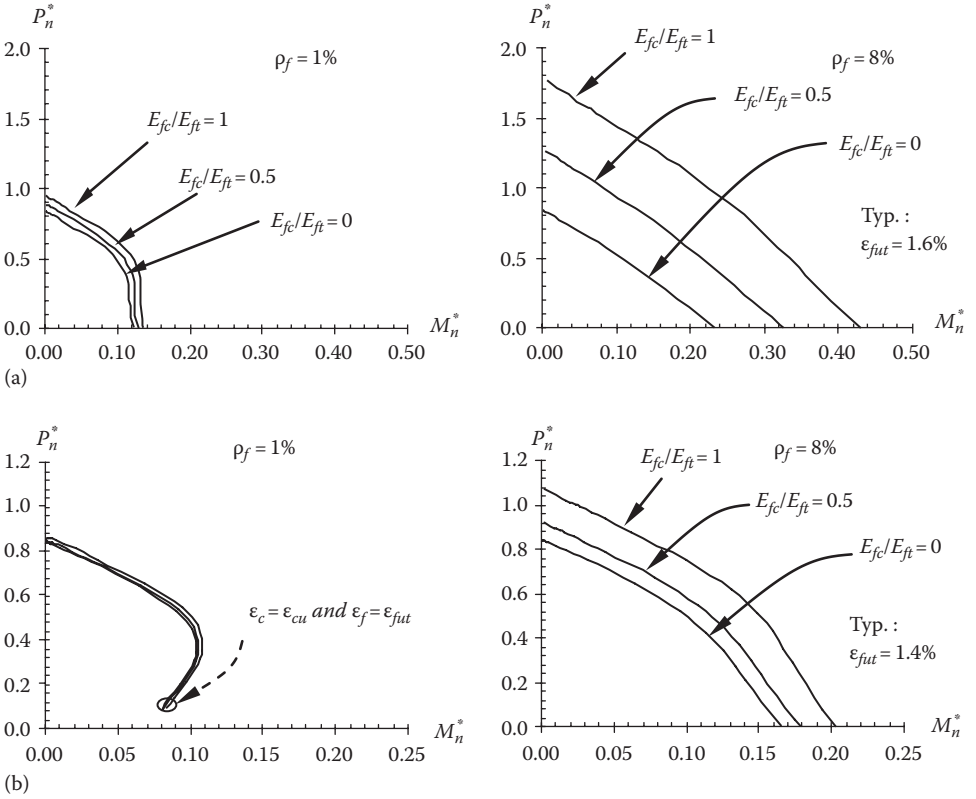

FIGURE 24.4 Effect of compression moduli to tension moduli ratios (E_{fc}/E_{ft}) on cross-sectional strengths of column reinforced with CFRP and GFRP bars. (a) CFRP RC column cross sections, E_{ft} = 21,300 ksi (147 GPa). (b) GFRP RC column cross sections, E_{ft} = 6,500 ksi (45 GPa). (From Choo, C.C. et al., *ACI Struct. J.*, 103(3), 452, 2006. With permission.)

usable compression strain, ε_{fuc}, of the FRP is often much larger than the ultimate or maximum usable compression strain of concrete. Nonetheless, this failure mode should be checked if FRP were to be used in concrete columns.

Due to the anisotropic and nonhomogeneous nature of FRP, it is difficult to obtain accurately the compression properties of the material. Reportedly, FRP reinforcements generally have lower compressive strength and stiffness compared to their tensile counterparts. In Figure 24.3, the $\varepsilon_{fuc} = 0.5\varepsilon_{fut}$ (i.e., $> \varepsilon_{cu} = 0.003$) did not cause FRP rupture in compression. On the one hand, lower stiffness in compression resulted in reduction in strength interaction of FRP RC columns to a certain degree as illustrated in Figure 24.4. Hence, it has been suggested that neglecting the contribution of compression reinforcement, a practice that is common in concrete design, may be conservative when defining the strength interaction of these columns [4].

DESIGN OF FRP REINFORCED CONCRETE COLUMNS

The primary concern of using FRP as the only longitudinal reinforcement type in a concrete column may have been the potentially explosive and catastrophic nature of the column if its failure was initiated by rupturing of these internal FRP bars. Such failure is perceived to be lack of warning, which is highly undesirable. Rupturing of FRP bars is conceivably probable as demonstrated in Figures 24.3b and 24.4b, where it occurs prior to concrete crushing or reaching its ultimate strain.

For FRP reinforced concrete columns, failure initiated by concrete crushing may be the preferred mode, as it has been demonstrated in flexural members reinforced with FRP bars exhibiting concrete crushing that a more progressive and less catastrophic failure was exhibited [5,6].

To prevent *brittle tension* failure, a FRP reinforced concrete column will need to be provided with a certain amount of reinforcement [7]; as shown in Figure 24.3b, a GFRP reinforced concrete column with a reinforcement ratio, $\rho_f = A_f/A_g$, of 1% experienced *brittle tension* failure at a certain level of axial load on the strength interaction but no such failure in the ones with higher reinforcement ratios, 3% or more. A FRP reinforced concrete column can be safeguarded from *brittle tension* failure if the amount of reinforcement or reinforcement ratio provided, ρ_f, is greater than a *certain* minimum, $\rho_{f\min}$, and this minimum may be greater than the 1% set in the ACI 318 Code for steel reinforced concrete columns [7].

The design aids of Figure 24.5a to f, combined appropriately with the different adjustment factors to account for type of concrete, FRP bars and their layout, allow one to quickly estimate the

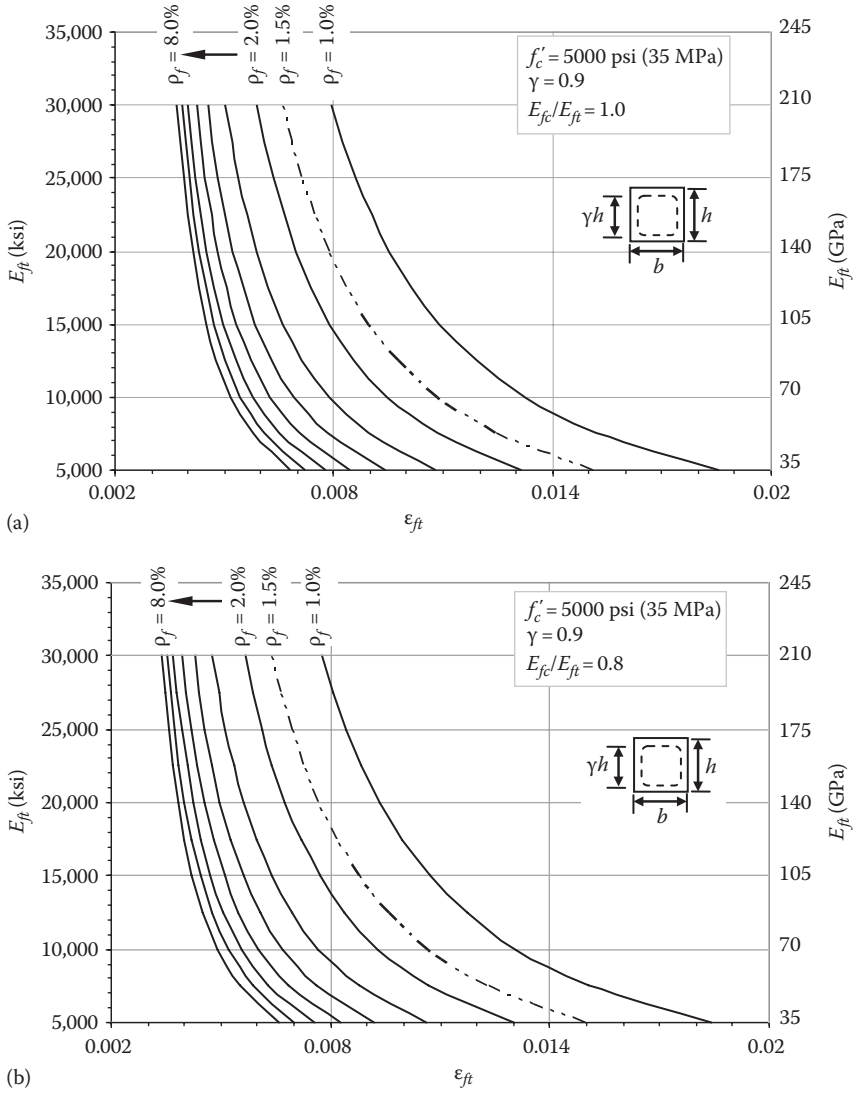

FIGURE 24.5 Tensile elastic modulus–tensile strain (E_{ft}–ε_{ft}) interaction diagrams for rectangular concrete columns reinforced with FRP bars of different modular ratio, E_{fc}/E_{ft} (a) 1.0, (b) 0.8, respectively.

(*continued*)

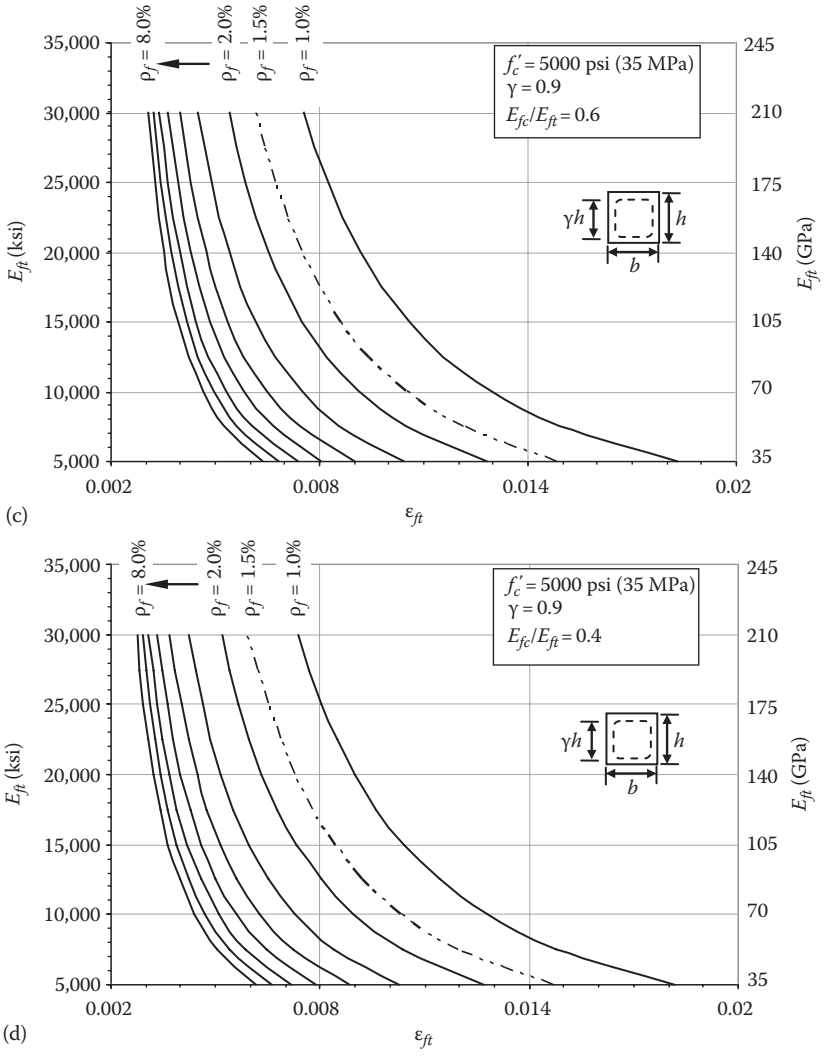

FIGURE 24.5 (continued) Tensile elastic modulus–tensile strain (E_{ft}–ε_{ft}) interaction diagrams for rectangular concrete columns reinforced with FRP bars of different modular ratio, E_{fc}/E_{ft} (c) 0.6, (d) 0.4, respectively.

$\rho_{f\min}$ of rectangular-shape column cross sections reinforced with FRP [7]. The aids are generated by estimating the maximum tensile strain for a particular type of FRP, ε_{ft}, that could develop for a given concrete and layout, corresponding to the pure flexure condition [7]. The range of FRP considered in these aide covers most available ones commercially [7]. If a concrete column is provided with a ρ_f greater than or equal to the certain minimum, $\rho_{f\,\min}$, determined from these aids, then *brittle tension* failure of the concrete column can be averted. Should the computed $\rho_{f\,\min}$ be less than 1%, it is recommended then to take $\rho_{f\,\min}$ equal to 1% similar to the one specified for steel reinforced concrete column per ACI 318 Code [7].

To estimate $\rho_{f\,\min}$, one would need the stiffness (i.e., tensile and compressive Young's moduli, E_{ft} and E_{fc}) and maximum usable or ultimate tensile strain, ε_{fut}, of the FRP bar used in the design of a reinforced concrete column. Since the tensile strain, ε_{ft}, of the FRP would be a function of the type of concrete and layout of these bars, the maximum usable or ultimate tensile strain, ε_{fut}, which is

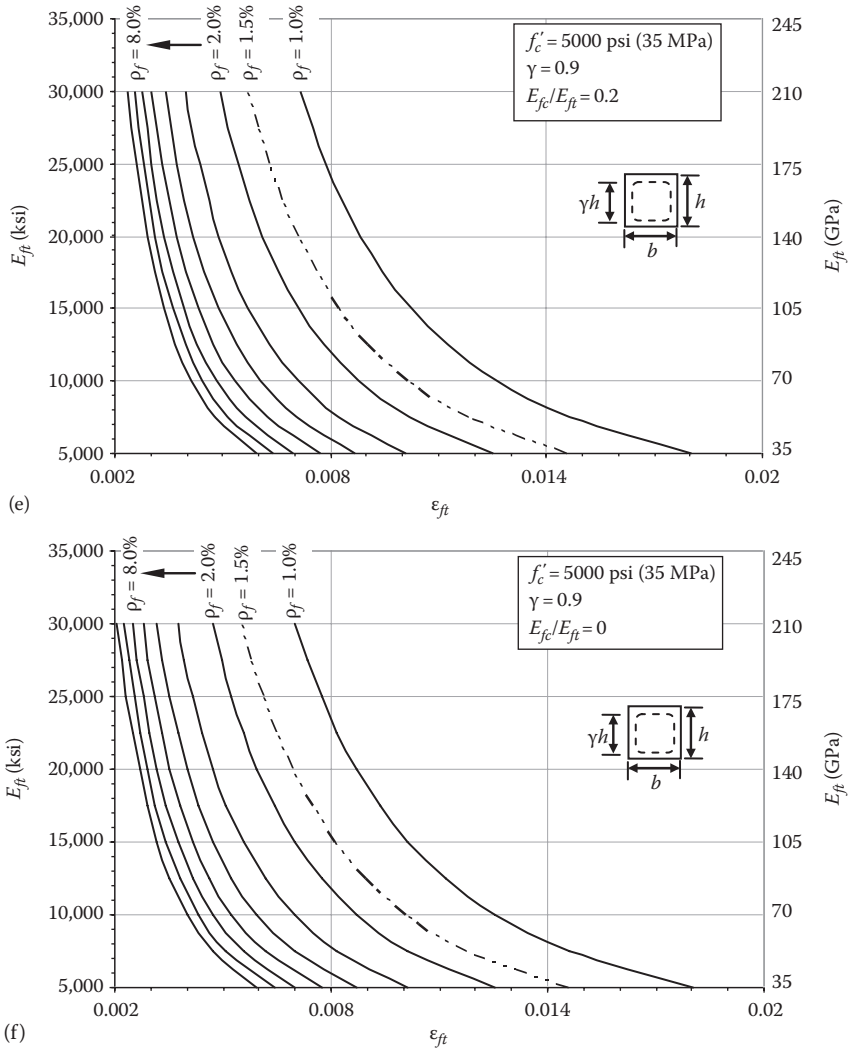

FIGURE 24.5 (continued) Tensile elastic modulus–tensile strain (E_{ft}–ε_{ft}) interaction diagrams for rectangular concrete columns reinforced with FRP bars of different modular ratio, E_{fc}/E_{ft} (e) 0.2, and (f) 0.0, respectively. (From Choo, C.C. et al., *ACI Struct. J.*, 103(3), 460, 2006. With permission.)

typically provided by the manufacturer, must first be modified as follows, in order to estimate $\rho_{f\min}$ using one of the aids in Figure 24.5 [7]:

$$\varepsilon^*_{fut} = \alpha_c \times \alpha_\gamma \times \varepsilon_{fut} \tag{24.1}$$

α_c and α_γ shown in Equation 24.1 are factors to account for concrete strength, f'_c, other than 35 MPa or 5000 psi and the layout of FRP bars, γ, as defined in Figure 24.5, respectively [7].

As pointed out earlier, the default value of α_c is 1.0 when f'_c is equal to 35 MPa or 5000 psi, or otherwise computed using the following expressions for others [7]:

When 21 MPa ≤ f_c' < 35 MPa or 3000 psi ≤ f_c' < 5000 psi:

$$\alpha_c = \left(\frac{21 - 0.2f_c'}{14}\right) \geq 1.0 \quad \text{or} \quad \alpha_c = \frac{3000 - 0.2f_c'}{2000} \geq 1.0 \tag{24.2}$$

When 35 MPa ≤ f_c' < 55 MPa or 5000 psi ≤ f_c' < 8000 psi:

$$\alpha_c = \left(\frac{25.25 - 0.15f_c'}{20}\right) \leq 1.0 \quad \text{or} \quad \alpha_c = \frac{3750 - 0.15f_c'}{3000} \leq 1.0 \tag{24.3}$$

The default value of α_γ is 1.0 when γ is equal to 0.9, or otherwise computed using the following expression for others [7]:

When $0.45 \leq \gamma \leq 0.9$:

$$\alpha_\gamma = 1.5 - 0.556\gamma \geq 1.0 \tag{24.4}$$

It should be noted that Figure 24.5 is derived by assuming that FRP reinforcement is uniformly distributed on all end faces of a rectangular column cross section. Therefore, the use of Figure 24.5 to estimate the minimum reinforcement ratio, $\rho_{f\min}$, of a rectangular column cross section with FRP reinforcement only at the two end faces should be conservative.

Example

A square, tie, short concrete (f_c' = 5500 psi or 38.5 MPa) column of 24 in. × 24 in. with bars uniform distributed on all faces is to the reinforced with GFRP bars with the following properties (provided by the manufacturer):

Tensile modulus of elasticity, E_{ft} = 6500 ksi (45.5 GPa)

Maximum/ultimate tensile strain, ε_{fut} = 1.4% (0.014)

For design, conservatively assume $E_{fc} = 0.6\ E_{ft}$ and $\varepsilon_{fuc} = 0.5\varepsilon_{fut}$ (unless these properties are also provided). The minimum reinforced ratio, $\rho_{f\min}$, required for this column cross section will be?

Solution

Since $\varepsilon_{fuc} = 0.5\varepsilon_{fut} = 0.5 \times 0.014 = 0.007 > \varepsilon_{cu} = 0.003$ (maximum usable concrete compression strain per ACI 318 Code), therefore *premature compression* rupture of GFRP bars is unlikely.

Modification factor α_c for f_c' = 5500 (38.5 MPa) > 5000 psi (35 MPa):

From Equation 24.3, $\alpha_c = \dfrac{3750 - 0.15(5500)}{3000} = 0.975$

A reasonable 2.5 in. of concrete cover measuring from the surface to the centroid of reinforcing bars is assumed per ACI 318 requirements gives

$$\gamma = \frac{24 - 2(2.5)}{24} = 0.792, \text{ say } 0.8 \quad \text{OK}$$

Therefore, modification factor α_γ for $\gamma = 0.8 < 0.9$.

From Equation 24.4, $\alpha_\gamma = 1.5 - 0.556(0.8) = 1.06$

Hence, the adjusted ultimate tensile strain of GFRP bars to be used in concrete column design is, from Equation 24.1,

$$\varepsilon_{fut}^* \alpha_c \times \alpha_\gamma \times \varepsilon_{fut} = 0.975 \times 1.06 \times 0.014 = 0.0145$$

Setting the adjusted value $\varepsilon^{*}_{fut} = 0.0145 = \varepsilon_{ft}$ and giving that the moduli of elasticity ratio is

$$\frac{E_{fc}}{E_{ft}} = \frac{3900\ \text{ksi}}{6500\ \text{ksi}} = 0.6$$

The estimated $\rho_{f\min}$ is approximately 1.4%, obtained from Figure 24.5c. Therefore, if ρ_f provided $\geq \rho_{f\min} = 1.4\%$ (or $0.014A_g$), then brittle tension failure should be prevented.

SLENDERNESS EFFECT

A parametric study of slender FRP reinforced concrete columns showed that these types of columns may be more susceptible to instability failure than steel reinforced concrete columns [8]. The design practice of using moment magnification factors appears to applicable to FRP reinforced concrete columns; however, it is recommended that the slenderness limit of 22 for steel reinforced concrete columns bent in single curvature be reduced to 17 for FRP reinforced concrete columns [8].

NOTATIONS

A_f	total area of FRP bars in a column cross section
A_g	column cross section area = $b \times h$
E_f	elastic modulus of FRP bars
E_{fc}	elastic modulus of FRP bars in compression
E_{ft}	elastic modulus of FRP bars in tension
f_c'	concrete compression strength
M_n	nominal moment
P_n	nominal axial load
α_c	strain modification factor dependent on f_c'
α_γ	strain modification factor dependent on γ
ε_{cu}	ultimate or maximum usable concrete compression strain (= 0.003 per ACI 318–08)
ε_{fc}	compression strain developed in the FRP bars
ε_{ft}	tensile strain developed in the FRP bars
ε_{fuc}	ultimate/maximum usable compression strain of FRP bars
ε_{fut}	ultimate/maximum usable tensile strain of FRP bars
γ	ratio of distance between centroid of outer layers of rebars to height of rectangular column cross section in the direction of bending
ρ	reinforcement ratio (= A_s/bh) for steel reinforced concrete columns
ρ_f	reinforcement ratio (= A_f/bh) for FRP reinforced concrete columns
$\rho_{f\min}$	minimum reinforcement ratio for FRP reinforced concrete columns

REFERENCES

1. Wight, J.K. and MacGregor, J.G. *Reinforced Concrete: Mechanics & Design*, 5th edn., Pearson Prentice Hall: Upper Saddle River, NJ, 2009.
2. ACI Committee 318, *Building Code Requirements for Structural Concrete* (ACI 318-11) and *Commentary* (ACI 318R-11), American Concrete Institution, Farmington Hills, MI, 2008.
3. De Luca, A., Matta, F., and Nanni, A. Behavior of full-scale glass fiber-reinforced polymer reinforced concrete columns under axial load, *ACI Structural Journal*, 107(5), 589–596, September–October 2010.
4. Choo, C.C., Harik, I., and Gesund, H. Strength of rectangular concrete columns reinforced with fiber-reinforced polymer bars, *ACI Structural Journal*, 103(3), 452–459, May–June 2006.

5. Nanni, A. Flexural behavior and design of reinforced concrete using FRP rods, *ASCE Journal of Structural Engineering*, 119(11), 3344–3359, 1993.
6. GangaRao, H.V.S. and Vijay, P.V. Design of concrete members reinforced with GFRP bars, *Proceedings of the Third International Symposium on Non-Metallic (FRP) Reinforcement for Concrete Structures (FRPRCS-3)*, Japan Concrete Institute, Sapporo, Japan, Vol. 1, 1997, pp. 143–150.
7. Choo, C.C., Harik, I., and Gesund, H. Minimum reinforced ratio for fiber-reinforced polymer reinforced concrete rectangular columns, *ACI Structural Journal*, 103(3), 460–466, May–June 2006.
8. Mirmiran, A., Yuan, W., and Chen, X. Design for slenderness in concrete columns internally reinforced with fiber-reinforced polymer bars, *ACI Structural Journal*, 98(1), 116–125, January–February 2001.

25 Codes and Standards

Brahim Benmokrane, Ahmed K. El-Sayed, and Ehab El-Salakawy

CONTENTS

INTRODUCTION

A number of committee activities from professional organizations around the world address the use of FRP materials in civil structures. These activities have resulted in publishing several codes and standards relevant to FRP as primary reinforcement for structural concrete. FRP codes and standards have been in development since the 1980s. Due to the different properties of FRP materials in comparison to conventional steel bars, FRP warrants separate treatment in these specifications. FRP materials have relatively low modulus of elasticity and are characterized by high tensile strength only in the direction of the reinforcing fibers. Furthermore, FRP materials do not yield; rather, they are elastic until failure without showing any ductile performance.

The brisk development of design guides and codes around the world speeds the insertion of FRP reinforcements in construction practice. Codes allow structures containing FRP materials to be designed, built, and operated with safety and confidence (Bakis et al. 2002). This chapter summarizes the international activities relevant to the development of FRP standards and codes with emphasis on the activities established in Japan, Canada, the United States, and Europe. This chapter describes the codes and standards pertinent to the use of FRP materials for the reinforcement of new structures and for the repair and retrofit of existing structures.

JAPANESE STANDARDS

Efforts to develop guidelines and recommendations for the design and construction of concrete members internally or externally reinforced with FRP materials started in Japan in the 1980s. The first research committee on continuous fiber reinforced materials was established in 1989 by the Japan Society of Civil Engineers (JSCE). Design recommendations developed by this

committee were first published in Japanese in 1996 and then in English in 1997 (JSCE 1997). Parallel to JSCE, other research committees have been established by the Architectural Institute of Japan (AIJ) and the Building Research Institute (BRI), resulting in various publications. The FRP design recommendations by these committees are presented in this section.

JSCE Design Recommendations

Two FRP design guidelines were issued by the JSCE. The first guide, *Recommendation for Design and Construction of Concrete Structures Using Continuous Fiber Reinforcing Materials*, was published in 1997 (JSCE 1997). The recommendation includes a set of guidelines for practical design and construction methods together with the standard test methods and specifications. Most of the FRP-specified properties are determined based on tests described in the recommendation. The recommendation was prepared to provide design provisions consistent with the *JSCE Standard Specification for Design and Construction of Concrete Structures* (JSCE 1986a,b). The design part of the recommendation is based on the limit state design method in which ultimate, serviceability and fatigue limit states are examined. The construction part in the recommendation deals with issues such as FRP storage and handling, assembly and placement of FRP reinforcements, precautions in concrete placing and tendon jacking, and quality control.

The second FRP guide developed by JSCE, *Recommendations for Upgrading of Concrete Structures with Use of Continuous Fiber Sheets*, was published in 2001 (JSCE 2001). These recommendations consist of design and construction standards for the upgrading of existing concrete structures using FRP sheets with the aim of improving their strength and durability. The types of continuous fiber covered by these recommendations are carbon and aramid fibers, with which Japan has considerable experience. These recommendations include equations for evaluating the effects of FRP sheets on flexural capacity, shear capacity, and ultimate deformations of columns. They also include standards for upgrading process and materials, detailed inspection of existing concrete structures, upgrading work, and maintenance of upgraded concrete structures. Test methods are also prescribed to determine the properties of FRP sheets.

Building Research Institute Design Guidelines

Parallel to the work of JSCE, a task committee on FRP reinforced concrete building structures was established in 1993. The committee was organized by the BRI, Japanese Ministry of Construction. The work of this committee resulted in the publication of *Design Guidelines of FRP Reinforced Concrete Building Structures* as part of research and development project on *Effective Use of Advanced Construction Materials* (Sonobe et al. 1997). These guidelines are intended for building structures and describe design concept for nonprestressed concrete elements reinforced with FRP bars. They adopt a limit state-based design method with specific provisions somewhat different from those of JSCE recommendation (JSCE 1997). The guidelines also include structural requirements and testing methods for the tensile and bond strength of FRP bars.

CANADIAN STANDARDS

There are two Canadian design codes concerning the design of FRP-reinforced concrete structures: the *Canadian Highway Bridge Design Code* (CHBDC) (CAN/CSA S6), which includes a section for fiber-reinforced structures, and the building code CAN/CSA S806; *Design and Construction of Building Components with Fiber-Reinforced Polymers*. Both the two codes are developed by the Canadian Standards Association (CSA). In 2010, the Canadian Standard Association (CSA) published its standard for the specification of FRP: Specification for Fiber-Reinforced Polymer (CAN/CSA S807-10).

CAN/CSA-S807-10

This standard covers the manufacturing process requirements of FRP bars or bars that are part of a grid for use in nonprestressed internal reinforcement of concrete components of structures (e.g., bridges, buildings, and marine structures). This standard covers FRP bars having nominally circular or square cross section. This standard does not include FRP bars made of more than one type of fiber. In this standard, FRPs are classified on the basis of their fibers, strength, stiffness, and durability.

Canadian Highway Bridge Design Code, CSA-S6-06

The first edition of the CHBDC was published in 2000. The code includes a section, Section 16, on *Fiber-Reinforced Structures*. These include structures with FRP and fiber-reinforced concrete. The fiber reinforcement provisions of Section 16 apply to fully, or partially, prestressed concrete beams and slabs, nonprestressed concrete beams, slabs, and deck slabs, fiber-reinforced concrete deck slabs of slab-on-girder bridges, stressed wood decks, and barrier walls (Bakht et al. 2000).

In 2006, the second edition of the CHBDC was published, which also included Section 16 on *Fiber-Reinforced Structures*. In the second edition of the CHBDC, a lot of revisions have been made on the design provisions for fiber-reinforced structures reflecting the considerable research and successful applications that have been done during the period between the two editions. Furthermore, the second edition provides new design provisions for FRP applications not covered by the first edition of the CHBDC. Among the new design provisions are those for glass FRP as both primary reinforcement and tendons in concrete; and for rehabilitation of concrete and timber structures with externally bonded FRP systems or near-surface-mounted reinforcement (Mufti et al. 2007). In 2010, this design code was updated with the Supplement No. 1 (S6S1-10), where some design aspects were refined (especially the shear design of FRP-reinforced concrete members), the material safety factors were updated, and the minimum FRP-reinforcing bar diameters for bridge decks applications were revised.

Canadian Building Code, CSA-S806-12

The CSA in collaboration with Public Works and Government Services Canada undertook the task of developing a standard for design of buildings with FRP components. This standard, titled, S806-12: *Design and Construction of Building Components with Fiber-Reinforced Polymers*, was published in 2012. The S806 code contains design provisions for building components composed of FRP and also for building components reinforced with FRP. The code covers general design requirements, limit states design, the properties of FRP components and reinforcing materials, the design of concrete components with FRP reinforcement, the design of concrete components prestressed with FRP, the design of concrete components with surface-bonded FRP, the design of fiber-reinforced concrete/FRP composite cladding, and seismic design and construction. It also provides the first punching-shear design provisions in the Canadian Standards for FRP-reinforced concrete slabs. The S806 code includes annexes that provide test procedures relevant to FRP materials.

U.S. DESIGN GUIDES AND STANDARDS

The American Concrete Institute (ACI), and its Committee 440 "FRP Reinforcement" with ten different subcommittees, addresses FRP composites in concrete. Committee 440 was established in 1991 and since that date the committee has published several guides and reports. Among these guides are *Guide for the Design and Construction of Structural Concrete Reinforced with FRP Bars* (ACI 440.1R-06), *Prestressing Concrete Structures with FRP Tendons* (ACI 440.4R-04), and *Guide for the Design and Construction of Externally Bonded FRP Systems for Strengthening Concrete Structures* (ACI 440.2R-08). These three documents are highlighted next.

ACI 440.5-08 Standard

This specification covers cast-in-place structural concrete reinforced with fiber-reinforced polymer (FRP) bars except where other provisions are specified in the contract documents.

ACI 440.6-08 Standard

This specification describes permitted constituent materials, limits on constituent volumes, and minimum performance requirements for carbon and glass FRP bars to be used as reinforcement for nonprestressed concrete. This specification covers only carbon and glass FRP bars excluding the following cases: FRP bars made of more than one fiber type (hybrid FRP), pultruded FRP bars with no external surface enhancement (that is, plain or smooth bars) to facilitate bond with concrete, hollow FRP bars, and plain FRP bars used as dowels (that is, devices that transfer shear across concrete joints) where the intended function requires slip of the dowel. Further, this specification does not cover FRP bars when used for external and near-surface-mounted strengthening applications.

ACI 440.1R-06 Design Guidelines

The first version of this document *Guide for the Design and Construction of Structural Concrete Reinforced with FRP Bars* (ACI 440.1R) was published in 2001, followed by the second revision in 2003. Committee 440 recently produced the third revision of this document (ACI 440.1R-06). The ACI 440.1R-06 document provides recommendations for the design and construction of FRP-reinforced concrete structures. The document only addresses nonprestressed FRP reinforcement and offers general information on the history and use of FRP reinforcement. It provides also a description of the unique material properties of FRP and guidelines for the construction and design of structural concrete members reinforced with FRP bars. The design philosophy considered in this guide is based on limit state design principles in that an FRP-reinforced concrete member is designed based on its required strength and then checked for fatigue endurance, creep rupture endurance, and serviceability criteria. The load factors given in ACI 318-05, *Building Code Requirements for Structural Concrete and Commentary*, are used to determine the required strength of a concrete member reinforced with FRP.

ACI 440.4R-04 (Reapproved in 2011) Design Guidelines

This guide, *Prestressing Concrete Structures with FRP Tendons* (ACI 440.4R-04), was published in 2004. It offers general information on the history and use of FRP for prestressing applications and a description of the material properties of FRP. The guide focuses on the current state of design, development, and research needed to characterize and ensure the performance of FRP as prestressing reinforcement in concrete structures. The design recommendations provided by the guide include the current developments that cover the basic understanding of flexure and axial prestressed members, FRP shear reinforcement, bond of FRP tendons, and unbonded or external FRP tendons for prestressing applications. Only aramid and carbon fibers are recommended in this guide. Therefore, the emphasis of the guide is on flexural members in concrete buildings and bridges pretensioned with aramid or carbon FRP tendons. The design guidelines are pertinent to fully prestressed members, with no attempt being made to address partially prestressed members.

ACI 440.2R-08 Design Guidelines

This document, *Guide for the Design and Construction of Externally Bonded FRP Systems for Strengthening Concrete Structures* (ACI 440.2R-08), was published in 2008, providing general information on the history and use of FRP strengthening systems; a description of the unique material properties of FRP; and committee recommendations on the engineering, construction, and inspection of FRP systems used to strengthen concrete structures. Information on material

properties, design, installation, quality control, and maintenance of FRP systems used as external reinforcement is presented in the guide. This information can be used to select an FRP system for increasing the strength and stiffness of reinforced concrete beams or the ductility of columns, and other applications. The guide applies only to FRP strengthening systems used as additional tensile reinforcement. It is currently not recommended to use these systems as compressive reinforcement. The design recommendations presented in the guide are based on limit states design principles in accordance with ACI 318-99 strength and serviceability requirements, using the load factors stated in ACI 318-99. The strength reduction factors required by AC I318-99 are also used.

EUROPEAN DESIGN GUIDES

In December 1993, the EUROCRETE project started in Europe and ended in 1997. This pan-European research program was established with the aim of developing FRP rebars for concrete and many areas of interest were examined. More work on the development of unified guidelines for Europe started by establishing FIB (Fédération International du Béton/International Federation for Structural Concrete) Task Group 9.3, *FRP Reinforcement for Concrete Structures*. The work started in CEB (Comité Euro-International du Béton) Task Group 3.10 in September 1996 which converted, with the merger of CEB and FIB in June 1998, into FIB Task Group 9.3, under the supervision of Commission 9 *Reinforcing and Prestressing Materials and Systems*. Task group 9.3 is divided into subgroups on material testing and characterization, reinforced concrete, prestressed concrete, externally bonded reinforcement, and marketing and applications. The main objective of the task group is to elaborate design guidelines for the use of FRP reinforcement in accordance with the design format of the CEB-FIB Model Code and Eurocode2.

Two reports have been produced by FIB Task Group 9.3. The first report, *Externally Bonded FRP Reinforcement for RC Structures,* was published in 2001 (FIB Bulletin No. 14 2001). The bulletin gives detailed design guidelines on the use of externally bonded FRP reinforcement for the repair and strengthening of concrete structures, the practical execution and quality control. The second report, *FRP Reinforcement for RC Structures,* was published in 2006 (FIB 2006). The bulletin deals with design aspects and state-of-the-art knowledge on FRP materials, their properties and characterization, as well as its use for RC structures. The two FIB bulletins, however, are regarded as progress reports because it is not the aim of the bulletins to cover all aspects of RC with FRP composites. In addition, several of the topics presented are the subject of ongoing research and development, and the details of various modeling approaches may be subjected to future revisions (Taerwe and Matthys 2001).

Various other national design guidelines have been published by individual countries across Europe. One of the early initiatives to develop guidelines followed from the work done by the EUROCRETE project, which has been included in interim guidelines published by the British Institution of Structural Engineers (1999) and SINTEF Norway (Thorenfeldt 1998). These documents provide recommendations on the use of FRP reinforcement for RC, with respect to the British and Norwegian standards, respectively. Similar design guidelines have been published in Italy. The Italian design recommendations for externally bonded FRP reinforcement for concrete structures (CNR-DT 200/2004) were published in 2004, whereas the Italian design recommendations for design and construction of concrete structures reinforced with FRP bars (CNR-DT 203/2006) were published in 2006.

REFERENCES

ACI Committee 318, (1999), *Building Code Requirements for Structural Concrete and Commentary*, ACI 318-99/ACI 318R-99, American Concrete Institute, Farmington Hills, MI, p. 391.

ACI Committee 440, (2001), *Guide for the Design and Construction of Concrete Reinforced with FRP Bars*, ACI 440.1R-01, American Concrete Institute, Farmington Hills, MI, p. 41.

ACI Committee 440, (2002), *Guide for the Design and Construction of Externally Bonded FRP Systems for Strengthening Concrete Structures*, ACI 440.2R-02, American Concrete Institute, Farmington Hills, MI, p. 45.

ACI Committee 440, (2003), *Guide for the Design and Construction of Concrete Reinforced with FRP Bars*, ACI 440.1R-03, American Concrete Institute, Farmington Hills, MI, p. 41.

ACI Committee 440, (2004), *Prestressing Concrete Structures with FRP Tendons*, ACI 440.4R-04, American Concrete Institute, Farmington Hills, MI, p. 35.

ACI Committee 318, (2005), *Building Code Requirements for Structural Concrete and Commentary*, ACI 318-05/ACI 318R-05, American Concrete Institute, Farmington Hills, MI, p. 430.

ACI Committee 440, (2006), *Guide for the Design and Construction of Structural Concrete Reinforced with FRP Bars*, ACI 440.1R-06, American Concrete Institute, Farmington Hills, MI, p. 44.

ACI Committee 440, (2008), *Specification for Construction with Fiber-Reinforced Polymer Reinforcing Bars*, ACI 440.5-08, American Concrete Institute, Farmington Hills, MI, p. 5.

ACI Committee 440, (2008), *Specification for Carbon and Glass Fiber-Reinforced Polymer Bar Materials for Concrete Reinforcement*, ACI 440.6-06, American Concrete Institute, Farmington Hills, MI, p. 6.

Bakht, B. et al., (2000), Canadian bridge design code provisions for fiber-reinforced structures, *Journal of Composites for Construction*, 4(1), 3–15.

Bakis, C. E. et al., (2002), Fiber-reinforced polymer composites for construction: State-of-the-art review, *Journal of Composites for Construction*, 6(2), 73–87.

Canadian Standards Association, (2000), *Canadian Highway Bridge Design Code*, CAN/CSA-S6-00, Rexdale, Ontario, Canada, p. 734.

Canadian Standards Association, (2002), *Design and Construction of Building Components with Fiber Reinforced Polymers*, CAN/CSA-S806-02, Rexdale, Ontario, Canada, p. 177.

Canadian Standards Association, (2006), *Canadian Highway Bridge Design Code*, CAN/CSA-S6-06, Rexdale, Ontario, Canada, p. 733.

Canadian Standards Association, (2010), *Specification for Fibre-Reinforced Polymers*, CAN/CSA-S807-10, Rexdale, Ontario, Canada, p. 27.

CNR-DT 200/2004, (2004), *Guide for the Design and Construction of Externally Bonded FRP Systems for Strengthening Existing Structures*, National Research Council, Rome, Italy, p. 144.

CNR-DT 203/2006, (2006), *Guide for the Design and Construction of Concrete Structures Reinforced with Fiber-Reinforced Polymer Bar*, National Research Council, Rome, Italy, p. 35.

Fédération Internationale du Béton (FIB), (2001), *Externally Bonded FRP Reinforcement for RC Structures*, Lausanne, Switzerland, p. 138.

Fédération Internationale du Béton (FIB), (2006), *FRP Reinforcement for RC Structures*, Lausanne, Switzerland, p. 157.

Institution of Structural Engineers, (1999), *Interim Guidance on the Design of Reinforced Concrete Structures Using Fiber Composite Reinforcement*, Reference No. 319, Institution of Structural Engineers, London, U.K., p. 116.

Japan Society of Civil Engineers, JSCE, (1986a), *Standard Specification for Design and Construction of Concrete Structures: Part 1. Design*, SP 1, Japan Society of Civil Engineers, Tokyo, Japan.

Japan Society of Civil Engineers, JSCE, (1986b), *Standard Specification for Design and Construction of Concrete Structures: Part 2. Construction*, SP 2, Japan Society of Civil Engineers, Tokyo, Japan.

Japan Society of Civil Engineers, JSCE, (1997), *Recommendation for Design and Construction of Concrete Structures Using Continuous Fiber Reinforcing Materials*, Concrete Engineering Series 23, Japan Society of Civil Engineers, Tokyo, Japan, p. 325.

Japan Society of Civil Engineers, JSCE, (2001), *Recommendations for Upgrading of Concrete Structures with Use of Continuous Fiber Sheets*, Concrete Engineering Series 41, Japan Society of Civil Engineers, Tokyo, Japan, p. 256.

Mufti, A. et al., (2007), New Canadian highway bridge design code design provisions for fiber-reinforced structures, *Canadian Journal of Civil Engineering*, 34(3), 267–283.

Sonobe, Y. et al., (1997), Design guidelines of FRP-reinforced concrete building structures, *Journal of Composites for Construction*, 1(3), 90–115.

Taerwe, L. and Matthys, S. (2001), Use and design of FRP reinforcement for concrete construction: FIB task group 9.3 and other activities in Europe, *Proceedings of the International Conference on Composites in Construction (CCC 2001)*, Porto, Portugal, pp. 393–401.

Thorenfeldt, E. (1998), Modifications to NS3473 when using fiber-reinforced plastic (FRP) reinforcement, SINTEF Report STF22 A98741, Trondheim, Norway.

26 Specific Durability Issues

Luke A. Bisby, Brea Williams, and Pedram Sadeghian

CONTENTS

INTRODUCTION

A primary advantage of fiber reinforced polymer (FRP) reinforcing bars, rods, tendons, and grids for use as internal reinforcement for concrete structural elements is their inherent resistance to electrochemical corrosion. Indeed, corrosion of conventional steel reinforcement in concrete structures is one of the key factors responsible for the widespread deterioration of infrastructure currently evident around the world, and FRPs are now seen as promising materials in helping to address this daunting problem. However, FRP-reinforcing bars in concrete are not immune to long-term degradation—they are susceptible to varying degrees of physical and mechanical damage in the presence of assorted harmful environments and chemicals. It is, thus, essential when contemplating the use of FRP reinforcement in any specific concrete-reinforcing application to remain cognizant of the potentially damaging effects that might arise from exposure to moisture, high temperatures, low temperatures, thermal cycling, alkaline, acidic, saline, or otherwise harmful solutions, cyclic loading, sustained loading, and ultraviolet radiation. Because the term "durability" is not easily defined, in this chapter it is defined as the ability of an FRP element *to resist cracking, oxidation, chemical degradation, delamination, wear, and/or the effects of foreign object damage for a specified period of time, under the appropriate load conditions, under specified environmental conditions* (Karbhari et al., 2003).

While FRP materials have been used widely, and have a proven durability track record in many aerospace, automotive, and marine applications, they have only in the last 15–20 years been seriously considered for internal reinforcement of concrete. Since most reinforced concrete structures are designed with service lives of more than 40 years, the long-term durability of FRP-reinforcing materials in concrete represents a crucial research need. Indeed, recent research needs surveys and workshops that have focused specifically on FRP materials for infrastructure applications have identified durability and long-term performance data of FRP-reinforcing

materials for concrete as critical research needs that must be addressed to enable the confident use of these materials (Harries et al., 2003; Karbhari et al., 2003; Porter and Harries, 2005). The durability of FRP materials for construction applications has also been the specific focus of at least four international scientific conferences (Benmokrane and Rahman, 1998; Benmokrane and El-Salakawy, 2002, 2007, 2011). A detailed summary of the various approaches taken by existing design documents to account for the durability of FRP reinforced concrete (RC) structures has been presented by Ceroni et al. (2006).

The sections that follow briefly outline the pertinent issues and current state of the art with respect to the durability of FRP materials used as internal reinforcement for concrete. It is important to recognize that FRP-reinforcing materials are constantly evolving, as new and superior component materials and manufacturing processes are developed, and research is ongoing in this area. Much of the information presented in this chapter has been adapted and summarized from information presented previously by Chin et al. (1997), Liao et al. (1998), Benmokrane et al. (2002), Karbhari et al. (2003), Benmokrane (2007), ACI (2006), and Karbhari (2007). The interested reader is encouraged to consult these source documents for more detailed information.

OVERVIEW OF DURABILITY CONCERNS

All engineering materials are subject to mechanical and/or physical deterioration with time, load, and exposure to various temperatures and environments, and FRPs are no different. It is important while reviewing the material presented in this chapter, however, to recognize that FRP materials are in general less susceptible to most common durability concerns than other materials such as timber or steel.

The strength, stiffness, and bond properties of a specific FRP-reinforcing material may increase, decrease, or remain the same depending on its constituent materials and the combination of physical and chemical exposure conditions to which it is subjected. Factors that influence the durability performance of FRP products include the matrix and fiber type, the fiber volume fraction, the manufacturing process, the presence of matrix additives and/or fillers, the installation procedures, and the short- and long-term loading and chemical and environmental exposure conditions. The individual constituent materials used in the fabrication of an FRP must be chosen based on both short-term performance and long-term durability requirements. Good quality assurance and quality control during manufacturing, handling, storage, and installation are critical in ensuring the durability of a FRP component or an FRP-reinforced concrete member.

Clearly, the task of accurately predicting the durability of an FRP material in any given environment is a complicated and time-consuming task. In the case of FRP materials used as internal reinforcement for concrete structures (which are most commonly bars or grids with continuous uniaxial reinforcing fibers), the uniaxial tensile properties (strength and elastic modulus) of FRP bars, and the FRP-to-concrete bond characteristics, are the most important parameters. This is because these properties are crucial for the FRP reinforcement to transfer and carry tensile loads induced in the structure—these properties are, thus, the focus of the discussions that follow.

When FRP bars, rods, grids, or tendons are used as internal reinforcement for concrete, special attention should be paid to the environmental, chemical, and physical factors shown in Figure 26.1.

The degree to which each of the listed factors in Figure 26.1 may be a concern depends on the specific application being considered, the timing and geographic location of the project, the age (or expected service life) of the structure, the specific formulation and properties of the FRP reinforcement, and the quality of the installation and construction methods. In addition, synergies may (and often do) exist between specific physical and environmental/chemical effects, and these may exacerbate potential damage in some instances. This is of particular concern when moisture, alkalinity, and stress act together; as is often the case for FRP reinforcement in concrete. Each of these factors is treated separately in the following sections, although documented synergies are discussed where appropriate.

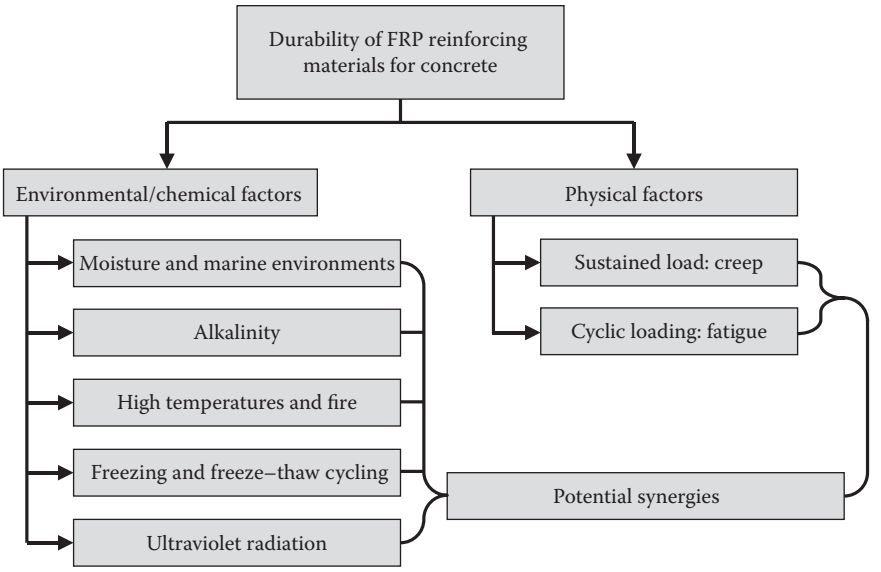

FIGURE 26.1 Potentially harmful long-term factors for FRP-reinforcing materials in concrete.

Moisture and Marine Environments

Because of their corrosion resistant properties, FRP-reinforcing materials are often proposed as an alternative to steel reinforcement for concrete structures in moist and/or marine environments, where corrosion of conventional reinforcing steel might otherwise cause problems. While the concrete cover to the reinforcement that would typically be provided in these situations does allow for some initial measure of protection against moisture and other potentially harmful solutions, all concrete is permeable (and almost inevitably becomes cracked). Thus, the reinforcement will, in all cases, eventually be exposed to moisture and assorted chemicals in solution in its surrounding environment.

The rate of degradation of FRP composites exposed to wet environments is thought to be related to the rate of sorption of the fluid into the polymer matrix (Micelli and Nanni, 2004). All polymer resins absorb moisture. This may cause damaging physical, thermal, mechanical, and/or chemical changes. Depending on the severity and duration of the exposure, absorption of moisture can cause both reversible and irreversible changes in the chemical structure of the polymer matrix, and hence the physical structure of the FRP reinforcement. The amount of absorption depends on the type and concentration of liquid, the type of polymer matrix and its chemical composition and degree of cure (all of which influence the amount of covalent cross-linking between individual polymer chains), the fiber type and fiber–resin interface characteristics (which are related largely to the fiber sizing chemistry), the manufacturing methods used, the ambient temperature, the applied stress level, the extent of preexisting damage (matrix cracking), and the presence (or absence) of protective coatings. Clearly, moisture absorption in FRPs is an extremely complex topic that cannot be covered in exhaustive detail in this chapter. The reader is referred to the excellent review of absorption kinetics presented by Weitsman and Elahi (2000) and to various other research papers dealing with this topic (Benmokrane et al., 2002; Uomoto et al., 2002; Karbhari et al., 2003).

It appears that the main effects of moisture absorption on FRPs are hydrolysis (causing plasticization) and a reduction in the glass transition temperature of the polymer matrix. Thus, the matrix-dominated properties (i.e., flexural, shear, and bond) are more affected than those that are dominated by the fibers (i.e., longitudinal strength and stiffness). In cases where the longitudinal strength and stiffness are affected, the effects on strength are more significant than on stiffness.

Fracture toughness may also be affected by moisture absorption, although the effects may be positive or negative (Weitsman and Elahi, 2000).

Synergies are known to exist between moisture absorption effects and the effects of sustained stress and elevated temperatures, where higher sustained levels of stress and higher temperatures contribute to increased moisture absorption. These synergies remain incompletely understood, however, and additional research is required. Sustained load appears to play a major role in moisture diffusion, likely due to stress-induced microcracking of the polymer matrix, which increases its bulk permeability. In addition to moisture absorption into the matrix, moisture can wick along fibers from matrix cracks and cut ends of reinforcing bars and can subsequently damage the fiber–resin interface causing a loss of structural integrity of the FRP. It has been suggested in the past that cut ends of FRP bars should be treated with a sealant before being placed in concrete, although FRP-reinforcing bar manufacturers typically do not require such treatment.

In the specific case of glass fibers, moisture that penetrates to the fibers can extract ions from the fiber and eventually can cause etching and pitting of the fibers. This can result in degradation of tensile strength and elastic modulus of the FRP. The composition of the glass fibers (e.g., E-glass vs. alkali resistant (AR) glass) is also known to be a potentially important factor, with AR-glass providing superior performance, particularly in alkaline environments within concrete. Aramid fibers absorb moisture, which can cause fibrillation and swelling of the fibers and reductions in compressive, shear, and bond properties. Certain chemicals such as sodium hydroxide and hydrochloric acid can cause dramatic hydrolysis of aramid fibers and should, thus, be avoided. Carbon fibers are apparently not affected by exposure to moist environments (Sen et al., 1998), although it is important to recall that most matrices are affected by moisture, and thus, carbon FRPs do experience slight degradation due to moisture attack (Benmokrane et al., 2007).

FRP bars can be protected against moisture by appropriate selection of matrix materials or the use of protective coatings. Karbhari et al. (2003) state that an uncracked resin-rich surface must exist on FRP components to provide adequate long-term protection for the fibers—the approach that appears to be used in the FRP-reinforcing bar industry when E-glass fibers are used. Furthermore, the importance of adequate resin curing must not be overlooked, and additional research is required to adequately understand the influence of cure kinetics on moisture uptake by polymers used as matrices in the manufacture of FRP-reinforcing bars (Karbhari et al., 2003). Recent developments in the FRP rebar industry have focused on using low-permeability matrices, specialized fillers, suitable sizing chemistry, and strictly controlled manufacturing processes (Benmokrane et al., 2007).

The presence of salt in solution has also been studied to shed light on the durability of FRP-reinforcing bars in marine environments. Salt solutions have been shown to not necessarily make a significant difference in the strength and stiffness of FRP bars in comparison to the same exposure solutions without salt. However, testing on carbon FRP composites has indicated that decreases in strength and the amount of moisture uptake are greater when the exposure solution is salt water as opposed to fresh water (Rege and Lakkad, 1983).

Recently, Robert and Benmokrane (2013) have investigated the mechanical, durability, and microstructural characterization of unstressed GFRP reinforcing bars exposed to concrete environment and saline solutions under accelerating conditions. These conditionings were used to simulate the effect of seawater or deicing salts on GFRP bars. The pre- and post-exposure tensile strengths of the bars were used for long-term property predictions based on the Arrhenius theory. The results revealed no significant differences in the durability of the concrete-wrapped GFRP bars, whether immersed in salt solution or tap water and the very high long-term durability of the GFRP bars in salt solution. According to the predictions, even after a service life of 100 years, the tensile-strength retention of the tested GFRP bar would still be 70% and 77% for mean annual temperatures of 50°C (the mean annual temperature and the marine environment of the Middle East and warm regions) and 10°C (mean average temperature of northern regions), respectively, which are higher than the design tensile strength according to the ACI 440.1R (ACI, 2003).

Alkalinity

When FRP bars are used as reinforcement for concrete, their durability in the highly alkaline environment inside concrete must be evaluated. The pore water that is present within concrete is known to have a very high pH; sometimes as high as 13.5 (Karbhari et al., 2003). This is a concern primarily for glass FRP systems, since researchers have shown without question that bare glass fibers suffer severe degradation of mechanical properties under exposure to highly alkaline solutions. However, when FRP bars are embedded within concrete, damage to an FRP's fibers depends also on the protection provided by its polymer matrix, as well as the presence of alkalis, the level of applied stress, and the temperature. These factors and their interrelationships are seen as critically important, and they have, thus, received a large amount of research attention.

Glass FRPs may potentially be damaged by the alkaline environment within concrete through several interrelated mechanisms. When able to penetrate into a glass FRP-reinforcing bar and attack the glass fibers, alkaline solutions result in embrittlement of the individual fibers (causing a reduction in tensile properties) and contribute to damage at the fiber–resin interface (resulting in damage to both the longitudinal and transverse properties). This is due to a complex combination of mechanisms involving chemical attack on the fibers and growth of hydration products on the surface of the fibers (called hydroxylation). It is worth noting that sorption rates appear to be higher (by a factor of two) for alkaline solutions than for saline solutions or tap water (Vijay and GangaRao, 1999).

The effect of applied stress during exposure to alkalinity is also known to be important (Benmokrane et al., 2002; Micelli and Nanni, 2004), particularly with respect to creep rupture of the glass FRP bars, which is discussed in the "Creep and Relaxation" section. Higher levels of applied stress appear to exacerbate alkalinity induced degradation (Benmokrane et al., 2002), as do higher temperatures and longer exposure times (ACI, 2003).

The use of a polymer matrix as a binder and protective coating around glass fibers provides protection for the fibers in FRP-reinforcing bars, and the degree to which this is true is a key factor in the alkali resistance of glass FRP bars in concrete. However, migration of highly alkaline solutions and alkali salts is always possible through the resin. The potential for this migration is enhanced by the presence of stress, which causes the development of microcracks in the matrix as discussed previously, and elevated temperature, which increases sorption rates.

A large volume of data is available from short-term tests on bare glass fibers in highly alkaline environments that have been used to extrapolate their long-term performance. In the case of glass FRP bars in concrete, however, the performance is related not only to the chemical deterioration of the fibers but also to the matrix properties and a combination of complex and incompletely understood mechanisms as noted previously. There is no evidence that the available test data on glass fibers are directly applicable to glass FRP bars in concrete, and extrapolation of the results of short-term tests to field conditions is not possible without in-service performance data. A step in this direction was taken by ISIS Canada (ISIS, 2005). In this study, researchers removed samples of glass FRP-reinforcing bars from concrete structures after up to eight years of service in five different bridge decks from across Canada, and studied these samples for evidence of deterioration. Test results revealed that the alkaline environment within the concrete bridge decks did not appear to have had any detrimental effect on the FRP materials. Specifically, the researchers found no evidence of debonding, microcracking, void formation, glass fiber degradation, delamination, deterioration of glass transition temperature, chemical degradation of the resin, or hydrolysis. These data are encouraging and compellingly suggest that simulated durability testing of glass FRP bars in alkaline solutions may not be representative of their true in-service performance.

In terms of the ability of various resins to protect glass fibers from alkalinity within concrete, the consensus within the research community appears to be that vinyl ester resins have superior resistance to moisture and alkalinity ingress in comparison with other common resins such as epoxies or polyesters. Polyesters in particular should not be used for the fabrication of FRP-reinforcing bars (Micelli and Nanni, 2004). Vinylester resins appear to be tougher and more resistant to

microcracking, resulting in minimal diffusion through the matrix, and they are resistant also to various acids and other solutions.

The type of glass fiber used also appears to be an important factor in the alkali resistance of GFRP bars. Alkali-resistant (AR-glass) fibers are available and can significantly improve the performance of glass fibers in highly alkaline environments, although they are considerably more costly than standard E-glass fibers and may not be required if adequate protection can be provided by the matrix (Benmokrane et al., 2002). Tensile strength reductions ranging from 0% to 75% of initial values have been reported for glass FRP bars exposed to various combinations of pH, alkalinity, temperature, and sustained stress. Observed tensile stiffness reductions range between 0% and 20% (ACI, 2003).

Only limited data are available on the durability of aramid and carbon FRP-reinforcing bars in alkaline environments. With respect to aramid FRPs, tensile strength and stiffness have been reported to decrease between 10%–50% and 0%–20% of initial values, respectively, in elevated temperature alkaline solutions either with or without tensile stress (Benmokrane, 2007). In the case of carbon FRPs, strength and stiffness have both been reported to decrease between 0% and 20% (Benmokrane, 2007).

Clearly, the durability of FRP bars in alkaline environments, particularly in combination with elevated temperature and applied stress, remains incompletely understood. As such, conservatism in design is advised when using FRP-reinforcing bars within concrete until more complete information is available. Results from particular testing programs reported in the literature vary tremendously according to differences in the test methods and materials used. Further research is needed in this area, as are uniformly accepted, rational, conservative, and reproducible test methods.

High Temperatures and Fire

Perhaps the most widely implemented application of FRP-reinforcing materials to date is as reinforcement in reinforced concrete bridge decks. While fire is not a serious concern in these applications (although there have been several high-profile bridge failures due to fire in recent years), elevated temperatures must be expected in tropical or desert climates, and may be encountered even in temperate zones during the summer months. FRP materials are particularly sensitive to the effects of elevated temperatures, and most suffer severe degradation of mechanical and/or bond properties at temperatures approaching their glass transition temperature, T_g (Bisby et al., 2005). In addition, all organic polymer matrix materials will combust at sufficiently high temperatures, and most release unacceptable amounts of dense, black, toxic smoke (Sorathia et al., 1992). The residual performance of heated FRPs can also be cause for concern. However, thermal cycling of FRP-reinforcing materials within the typical range of service temperatures does not appear to cause appreciable damage, other than minimal amounts of matrix microcracking resulting from differential thermal expansion between the fibers and the matrix.

A comprehensive review of the performance of FRP materials at high temperature is given by Bisby et al. (2005). FRPs display high-temperature behavior that is drastically different than concrete or steel. All polymer matrix composites will burn if subjected to a sufficiently high heat flux. In addition, commonly used matrix materials such as polyester, vinylester, and epoxy support combustion and evolve large quantities of dense black smoke (Sorathia et al., 1992). Compared with unreinforced polymers, thick FRPs have advantages with regard to their involvement in fire in that the noncombustible fibers displace polymer resin making less fuel available for the fire. Also, when the outermost layers of a composite lose their resin due to combustion, the remaining fibers and resin char act as an insulating layer for the underlying material (Sorathia et al., 2001). However, these advantages are not particularly helpful when FRP materials are used as unexposed internal reinforcement for concrete. While the FRPs are protected against combustion by the concrete cover,

research has shown (Katz et al., 1999) that loss of bond at temperatures exceeding T_g of the polymer matrix is likely to be the critical factor during fire in these applications.

It is well established that the mechanical properties of FRPs deteriorate with increasing temperature. The critical temperature is commonly taken to be the glass transition temperature of the polymer matrix, which is in the range of 65°C–140°C for matrices currently used in infrastructure applications. Degradation in both strength and stiffness may be observed even before T_g is reached (Blontrock et al., 1999). Beyond T_g, the elastic modulus of a polymer is drastically reduced due to changes in its molecular structure. Because of the anisotropy of unidirectional FRP materials, the transverse, shear, and bond properties are much more affected by elevated temperatures than the longitudinal strength and stiffness. It is, thus, important that an FRP component not be exposed to temperatures close to or above T_g during normal operating conditions.

Several research projects have been reported studying the high-temperature mechanical properties FRP materials and their constituent materials (Bisby et al., 2005). Degradation of mechanical properties at high temperature is governed by the properties of the polymer matrix near T_g, since commonly available fibers are relatively more resistant to thermal effects. Carbon fibers are insensitive to elevated temperatures, showing no deterioration in strength or stiffness up to at least 1000°C. Glass and aramid fibers experience significant deterioration of strength at high temperature, with glass fibers experiencing a 20%–60% reduction in strength at 600°C, and aramid experiencing similar reductions at 300°C (Bisby, 2003).

Carbon, glass, and aramid FRP composites show diminished strength and stiffness properties with increasing temperature, although there is a great deal of scatter in the available test data (as should be expected given the wide range of possible matrix formulations, fiber orientations, and fiber volume fractions). Tensile strength reductions as high as 80% can be expected at temperatures of 300°C. Other properties more directly affected by shear transfer through the resin, such as shear, bending, and bond strength, are reduced significantly at temperatures approaching T_g. The bond between FRP and concrete, which is severely affected at only slightly elevated temperatures, is essential to transfer loads from the concrete through the polymer matrix into the FRP reinforcement. Changes in the mechanical properties of the matrix material at temperatures above T_g have the potential to cause loss of bond at only modestly increased temperatures, resulting in loss of interaction between FRP and concrete. Limited research on the bond properties of FRP-reinforcing bars for concrete at elevated temperature has been reported (Katz et al., 1999; Galati et al., 2004). Dramatic decreases in bond strength, to values of about 10% of room temperature strength, have been observed at temperatures of between 100°C and 200°C. Limited information is available on the post-fire residual strength and stiffness of FRP materials for use in infrastructure applications (Bisby and Foster, 2007), although additional research is required to determine allowable exposure temperatures and post-fire repairability of FRPs and FRP-reinforced concrete members.

The temperature at which a polymer matrix will ignite, the flame spread characteristics, and the amount and toxicity of smoke produced are all dependent on its particular formulation (Nelson, 1995). Combustion gases from burning FRPs create a toxicity hazard for humans and can be highly corrosive to equipment and electronics. Sorathia et al. (1992) studied the smoke generation and toxicity characteristics of a variety of FRP materials for use in marine and offshore applications. The results demonstrated that thermosetting resins commonly used in structural FRPs generate unacceptable quantities of smoke, they have relatively poor flame spread characteristics, and they generate varying quantities of carbon monoxide, hydrogen fluoride, hydrogen chloride, hydrogen sulfide, and hydrogen cyanide, all of which are potentially harmful compounds. While there exist various resin additives that can enhance the ability of polymer materials to resist ignition, flame spread, and smoke generation, these additives tend to diminish mechanical properties, discouraging their use in structural applications (Nelson, 1995). The level of hazard in internal FRP-reinforcing applications is low, however, because the FRPs are protected by the concrete cover and the volume of FRPs is small.

Because of the susceptibility of FRPs to elevated temperatures, many existing design guidelines (e.g., ACI, 2006) state that the use of FRP reinforcement is not recommended for structures in which fire resistance is essential to maintain structural integrity. Exposure to elevated temperatures for a prolonged period of time is also a concern with respect to exacerbation of moisture absorption and alkalinity effects, as discussed previously. Finally, it is worth noting that short-term exposure to mildly increased temperatures may actually be beneficial to some FRPs, since it may provide a slight post-cure of the polymer matrix, thus improving performance.

Freezing and Freeze–Thaw Cycling

In cold climates, freezing temperatures and freezing and thawing cycles can be expected for FRP-reinforced concrete elements when used in exterior applications, such as bridge deck or concrete pavement reinforcement. Freezing and freeze–thaw cycling have the potential to affect the durability performance of FRP-reinforcing materials through changes that may occur in material behavior at low temperatures, differential thermal expansion between polymer matrix and fiber components or between concrete and FRP materials, and may result in damage to the FRP, the concrete, or the FRP–concrete interface.

Exposure to subzero temperatures can result in the development of residual stresses in an FRP that can cause matrix microcracking and fiber matrix bond degradation (Karbhari et al., 2003). This is a result of the combined effects of matrix stiffening and differential thermal expansion between the polymer and the reinforcing fibers (typical polymer matrices have coefficients of thermal expansion that are an order of magnitude different than those of common fibers). Microcracks may grow under repeated freezing–thawing cycles to form transverse matrix cracks and result in fiber/matrix debonding, subsequently affecting FRP stiffness, strength, dimensional stability, fatigue resistance, and presumably moisture absorption and resistance to alkalinity. Freeze–thaw cycling in the presence of salts is thought to be a more severe exposure due to the formation and expansion of salt crystals (Karbhari et al., 2003). Unidirectional tensile strengths of FRP materials have been shown to decrease at temperatures down to −40°C, whereas the transverse (matrix dominated) strength may actually increase due to matrix hardening (ACI, 2003). Increasing freeze/thaw cycles have been shown to result in increased severity and density of matrix cracks, an increase in matrix brittleness, and a decrease in the tensile strength (Benmokrane et al., 2007).

The coefficients of thermal expansion of various currently available FRP bars can vary widely, both from product to product and when comparing longitudinal versus transverse behavior. The longitudinal coefficient of thermal expansion of glass FRPs is similar to that of concrete, so the potential for the development a damaging bond stresses due to differential thermal expansion is, in most cases, minimal. However, carbon and aramid FRP bars have longitudinal coefficients of thermal expansion that are typically an order of magnitude different than that of concrete, and while there is apparently no evidence that this has been a problem in the field, the potential exists for the development of differential thermal strains under large changes in temperature. The coefficients of thermal expansion of FRP bars in the transverse direction are typically much greater than that of concrete, leading to concerns that changes in temperature could cause splitting failures of the concrete cover. For this reason, some design guidelines (e.g., ISIS, 2001; ACI, 2003, 2006) specify minimum concrete covers to the FRP reinforcement that are based, in part, on preventing thermally induced cover cracking and splitting failures.

Ultraviolet Radiation

The effects of ultraviolet (UV) radiation on the durability of FRP bars are potentially important in applications where FRP bars are used as external reinforcement (e.g., in external post-tensioning) or when FRP bars are left in the sun for prolonged periods of time during storage or prior to installation on a construction site. For standard applications involving the use of FRP bars as internal

reinforcement for concrete, the effects of UV radiation are not important, provided that adequate care is taken during storage and installation.

While carbon and glass fibers are insensitive to UV radiation, direct exposure to UV light is damaging to most polymer matrix materials and to aramid fibers (Micelli and Nanni, 2004). UV radiation causes degradation of polymer constituents through a mechanism known as photodegradation, in which UV radiation within a certain range of specific wavelengths can break bonds between polymer chains. This typically results in discoloration, surface oxidation, embrittlement, and microcracking of the polymer matrix (Karbhari et al., 2003), which can significantly reduce the mechanical properties of FRPs in some cases. It should be noted that UV radiation can penetrate only the outer surface of most FRP materials, and that direct UV degradation is typically confined to a relatively thin layer near the surface of an FRP component. However, such surface flaws can cause stress concentrations that may result in failure at much lower loads than unexposed specimens (Karbhari, 2007). Surface flaws are also important in that they increase the susceptibility of FRPs to damage resulting from other mechanisms such as moisture or alkalinity.

The effects of UV radiation appear to be exacerbated by other factors such as temperature, moisture, abrasion, and thermal cycling (Karbhari et al., 2003). Results of test programs indicate a great deal of uncertainty and variability in the methods used and the results obtained. For instance, combined UV and moisture exposure tests on FRP bars, with and without applied tensile stress, have shown tensile strength reductions of 0%–20% in CFRP, 0%–30% in AFRP, and 0%–40% in GFRP. However, another study of GFRP, AFRP, and CFRP bars kept outdoors for a prolonged period of time showed no significant change of the tensile mechanical properties (Benmokrane, 2007).

Protection of FRP components that will be exposed to UV radiation is most commonly accomplished through the use of UV-resistant paints, coatings, or sacrificial surfaces, although these are not typically required for FRP-reinforcing bars for concrete. When FRP bars are used as external reinforcement for concrete, they should be protected, typically within some type of UV-resistant duct or sheathing. As a final comment in this regard, polymeric resins are currently under development that are resistant to UV degradation through the incorporation of specialized fillers such as nanoclays.

Creep and Relaxation

Given that most reinforced concrete structures are designed with service lives of at least several decades, FRP-reinforcing materials in concrete structures can be expected to be required to resist some level of sustained load for a prolonged duration. While typical reinforcing fibers of glass, carbon, and aramid are not expected to creep significantly, typical organic polymer matrices are known to experience significant creep and/or relaxation under sustained load. For FRP-reinforced concrete structures, creep is a potentially important topic since it can result in rupture of an FRP material at loads significantly less than ultimate. Glass fibers in particular are susceptible to a combined physical/chemical phenomenon known as creep rupture under sustained load (sometimes called stress rupture or stress corrosion). Carbon fibers exhibit little to no chemically induced strength degradation. Plain aramid and glass fibers, however, are known to be highly susceptible to alkali-induced strength degradation (Karbhari et al., 2003).

The creep behavior of a particular FRP material depends on its constituents and its fabrication in addition to the type and level of applied loading. To complicate matters further, until recently no standard test methods were available for creep testing of FRP-reinforcing materials for concrete, and, thus, relatively little information is available with which to make generalizations about the performance of FRPs under sustained loads.

Creep and relaxation depend largely on the properties and performance of the polymer matrix (Karbhari et al., 2003). Thus, it is essential to use an appropriate matrix material and to ensure that care is taken during the fabrication and curing process, as is the case for essentially all durability

considerations. Various damage mechanisms, including stress rupture of the fibers, fiber–matrix interface damage, and matrix and fiber cracking, are all involved, depending on the environmental conditions and stress levels to which the FRP component is subjected (Benmokrane, 2007).

Clearly, as the ratio of the sustained tensile stress to the ultimate strength of the FRP increases, the endurance time (i.e., the time to failure under sustained load) is expected to decrease. The endurance time is also synergistically affected by other environmental conditions such as elevated temperature, UV exposure, alkalinity, moisture, and freezing–thaw cycling. Based on the limited information available, carbon fibers appear to be the least susceptible to creep rupture, whereas aramid fibers are moderately susceptible, and glass fibers are the most susceptible. Various authors have presented short-term creep data that have subsequently been extrapolated to give creep rupture stress limits up to lifetimes of 50 or 100 years. These data, for FRP bars in air at room temperature, suggest 50 year creep rupture strengths of 29%–55%, 47%–66%, and 79%–93% of the initial tensile strength of the materials for glass, aramid, and carbon FRPs, respectively (Ando et al., 1997; Seki et al., 1997; Yamaguchi et al., 1997; Greenwood, 2002). Excellent reviews on the creep properties of FRPs are available by Liao et al. (1998) and Benmokrane (2007).

Cyclic Loading and Fatigue

Many civil engineering structures, particularly bridges but also some buildings and industrial structures, are subjected to repeated cycles of loading and unloading (fatigue). These cyclic loads may result from moving loads (i.e., traffic), thermal effects (such as differential thermal expansion), or assorted chemical effects (Karbhari et al., 2003), and can cause failure of structural components under stress levels that may be considerably less than ultimate static strengths. The ability of FRP materials, and of FRP reinforced concrete members, to withstand repeated load cycles must therefore be evaluated to ensure long and healthy service lives.

Most of the available data on the fatigue performance of specific FRP materials is from the aerospace industry; only very limited long-term fatigue data are available for pultruded FRP-reinforcing bars, and a review is provided by Liao et al. (1998). The composition of the polymer matrix appears to play a more significant role than the type of fiber when considering fatigue effects in FRPs, since most fibers are relatively insensitive to fatigue effects. Thus, good fatigue performance in FRPs depends largely on the toughness of the matrix and its ability to resist cracking, both of which are also related to other durability damage mechanisms discussed previously.

Carbon FRPs appear to have the best fatigue performance among the three most commonly used FRPs types in infrastructure applications. The strength of carbon FRPs is typically between 50% and 70% of initial static strength after one million load cycles (ACI, 2003). Some specific reports of data to 10 million cycles for carbon FRPs indicated a continued downward trend of 5%–8% strength decrease per decade of logarithmic lifetime (Curtis, 1989). Glass FRPs have also demonstrated good fatigue performance for reinforcement of concrete structures, typically experiencing 10%–12% losses in initial strength per decade of logarithmic lifetime. Aramid fibers display excellent fatigue performance, with strength degradation of only 5%–6% per decade of logarithmic lifetime. For aramid FRP bars for concrete applications, fatigue strengths have been reported in the range of 54%–73% of initial bar strengths after two million cycles (ACI, 2003; Karbhari et al., 2003; Benmokrane, 2007).

Elevated temperatures, humidity, and the presence of moisture or corrosive fluids degrade the fatigue performance of FRP materials, although it is difficult on the basis of the information available in the literature to arrive at conclusive results, since data from individual test programs are related to the test methods used and the specific fiber/matrix combination. Other potentially important factors include alkalinity, the surface deformation of the bars, stress ratio, stress intensity, the gripping mechanism used, and the presence of encasing concrete.

Because carbon fibers are relatively resistant to environmental degradation due to other effects (as discussed previously), the fatigue life of carbon FRPs is relatively unaffected by moisture and

temperature exposures to be expected within concrete structures, unless the resin or fiber/resin interface is degraded by the environment. However, results from one specific study found that the fatigue strength of CFRP bars encased in concrete decreased when the environmental temperature increased from 20°C to 40°C (Adimi et al., 1998). It was also found that higher loading frequencies resulted in lower fatigue lives due to increased bar temperatures resulting from sliding friction. For glass FRPs, other environmental factors appear to play a pivotal role in determining the long-term fatigue behavior, although again it is difficult to separate the effects of the various damage mechanisms. Moisture, alkaline, and acidic solutions may seriously degrade the fatigue performance of glass FRP composites due to reductions in the strength and stiffness of the glass fibers and damage to the polymer matrix and fiber matrix interface, as previously described. Because aramid FRP bars are in some cases susceptible to degradation from moisture and elevated temperature, these exposures also appear to degrade their long-term fatigue performance.

The presence of deformations on the surface of FRP bars, rod, or tendons, which are added to improve the bond strength of the FRP-reinforcing materials to concrete, has been observed for glass FRP bars to decrease their fatigue performance (Katz, 1998), likely due to local transverse and longitudinal stress concentrations induced by the deformations. In applications involving prestressing with FRPs, stress concentrations at anchorages, or movement and friction at cracks, can contribute to reduced fatigue performance—these factors should, thus, be given appropriate consideration where appropriate.

While additional research on the fatigue performance of FRP reinforcement for concrete, it should be noted that the fatigue performance of FRP-reinforcing materials and FRP-reinforced concrete members appears to be at least as good as conventional reinforcing steel or reinforced concrete members provided that other forms of environmental degradation are prevented.

Bond Durability

The aforementioned discussions have highlighted the fact that most durability concerns associated with the use of FRP bars as internal reinforcement for concrete result from damage to the polymer matrix due to a number of complex and interrelated factors. It is worth noting that the bond of FRP reinforcement, which is critical for adequate structural performance, relies heavily on the matrix-dominated transfer of shear and transverse forces at the interface between the FRP bar and the concrete, and between individual fibers within the FRP bar (ACI, 2003). This is in contrast to the tensile mechanical properties of FRP bars, which are governed largely by the performance of the (typically more durable) fibers. The specific durability of the FRP-concrete bond under exposure to many of the exposure conditions discussed earlier has, thus, received some research attention.

Direct pullout tests on carbon FRP and glass FRP bars after exposure to natural environmental exposures have not indicated significant decreases in bond strength over periods of up to 2 years (Clarke and Sheard, 1998; Sen et al., 1998). Testing after shorter but more severe laboratory exposures has given increasing or decreasing bond strength trends for GFRP bars subjected to wet, elevated temperature, and/or alkaline environments in concrete (ACI, 2003). Similar testing on carbon and aramid FRP bars has yielded similar results, which is not surprising given the matrix-dominated nature of the FRP-concrete bond.

The effect of fatigue loading on the bond of glass FRP-reinforcing bars has been studied using bond tests in concrete (ACI, 2003). The results, from tests on different materials and using slightly different methodologies, have indicated that bond strength can either increase, decrease, or remain the same following cyclic loading. Further research is required in this area. Again, conservatism is recommended until more complete information is available.

Recently, Robert and Benmokrane (2010) have performed an experimental investigation on the durability of the bond between GFRP bars and concrete, specifically as it relates to the degradation of the GFRP-bar surface and the behavior of the bar–concrete interface. The GFRP bars were embedded in concrete and exposed to tap water at 23°C, 40°C, and 50°C to accelerate potential

degradation. The bond strengths before and after exposure were considered as a measure of the durability of the bond between the GFRP bars and concrete. The results showed that aging did not significantly affect the durability of the bar–concrete interface under the conditions used in this study.

As mentioned previously, cracking of the concrete cover may occur due to differential thermal expansion or moisture-induced swelling and can seriously degrade the bond strength of FRP bars in concrete. Sufficient measures must be taken to prevent such cracking in field applications, which usually means providing adequate concrete cover over the FRP bars (as specified in most available design recommendations).

SUSTAINED STRESS LIMITS

To account for long-term degradation of mechanical properties of FRP-reinforcing bars in concrete, sustained stress levels should typically be limited (sometimes severely) during the design of FRP-reinforced concrete components. Various different sustained stress limits have been suggested in the literature for different types of FRP-reinforcing materials; typical examples are presented in Table 26.1. The variability and (and sometimes disagreement) that has been observed in durability related studies is evident in the suggested stress limits, although there appears to be a reasonable consensus that carbon FRPs are least susceptible to durability effects, while glass is most susceptible. Most codes also incorporate either material resistance factors (e.g., CSA, 2006) or environmental reduction factors (e.g., ACI, 2006), which are applied to the mechanical properties of FRP-reinforcing bars, in part to account for their susceptibility to environmental degradation.

DURABILITY TEST METHODS

Durability testing of FRP-reinforcing bars for concrete is currently a rapidly evolving field. Numerous test methods, environments, and exposures have been used and/or proposed for studying the durability of FRP materials and systems for reinforcement of concrete, and there currently appears to be little consensus among researchers in this area. Clearly, a significant research effort is required to fill the existing knowledge gaps with respect to the durability of FRP bars for concrete. To ensure that the data obtained by various researchers are both useful and comparable, appropriate test methods and protocols are required (Karbhari et al., 2003). A step in this direction has been taken by Committee 440 of the American Concrete Institute with the publication of ACI 440.3R: Guide Test Methods for Fiber-Reinforced Polymers (FRPs) for Reinforcing or Strengthening Concrete Structures (ACI, 2012). Included in this document are suggested test methods for studying the alkali resistance of

TABLE 26.1
Sustained Stress Limits Proposed by Various Documents for the Use of FRP Reinforcing Bars in Concrete

	Suggested Sustained Stress Limit for Design (% of Ultimate)		
Document	**GFRP**	**CFRP**	**AFRP**
ACI 440.1R-06 (ACI, 2006)	20	55	30
CAN/CSA S6-06 (CSA, 2006)	25	65	35
TR 55 (Concrete Society, 2004)	45	65	40
Karbhari et al. (2003)	25	40	30

FRP bars, tensile fatigue of FRP bars, creep-rupture of FRP bars, and long-term relaxation of FRP bars. Similar durability test methods are also suggested for creep, relaxation, fatigue, and alkali resistance of FRP bars in the Canadian design code CSA S806: Design and Construction of Building Components with Fiber-Reinforced Polymers (CSA, 2012).

ISIS Canada has recently published a product certification document on Specifications for Product Certification of Fibre Reinforced Polymers (ISIS, 2006). The scope of the specifications deals with FRPs as internal reinforcement in concrete components of structures, such as bridges, buildings, and marine structures. The reader is referred to the source document for additional information.

Many researchers are selecting very high temperatures (up to 80°C) to get the maximum rate of aging to evaluate the durability of GFRP reinforcing bars. But the use of very high temperature of aging could lead to over degradation of the polymer matrix and underestimation of the durability of GFRP materials. It is for these reasons that standardized test methods for the accelerated test for alkali resistance of FRP reinforcing bars were established. According to ACI 440.3R (ACI, 2012) and CSA S806 (CSA, 2012), the temperature of aging shall be equal to 60°C (Robert et al., 2010).

SUMMARY AND CONCLUSIONS

This chapter gives a brief and limited overview of the current state of knowledge with respect to those factors and environments that are currently considered important for the long-term durability of FRP-reinforcing materials for internal reinforcement of concrete structures. It is clear from the preceding discussions that many issues regarding the durability of these materials remain unresolved, and that a considerable research effort will be required to fill all of the remaining gaps in knowledge. This is particularly true with respect to potential synergies that may exist among the various environmental/chemical and physical factors discussed herein.

It is critically important to recognize in the context of this chapter that FRP materials, while potentially susceptible to various forms of environmental degradation, are highly durable materials in comparison with conventional materials such as concrete, timber, or steel. All engineering materials deteriorate with time, repeated loading, and environmental exposure, and the task of the engineer is to account for these weaknesses in ways that best take advantage of the materials' properties. FRP materials appear to be very well suited to concrete-reinforcing applications, and they have a bright future in a number of specific applications.

As FRP technology advances, new and more durable materials can be expected to be available for use in concrete-reinforcing applications. As we have seen, the durability of FRP-reinforcing materials depends largely on the ability of the polymer matrix to protect the fibers and the fiber–matrix interface from distress. Emerging technologies in polymer science (the use of nanoclay fillers to significantly reduce matrix permeability, for instance) can be expected to further improve the durability of FRP materials in the years to come.

REFERENCES

ACI. 2003. *ACI 440.1R-03: Guide for the Design and Construction of Structural Concrete Reinforced with FRP Bars*. American Concrete Institute, Farmington Hills, MI.

ACI. 2006. *ACI 440.1R-06: Guide for the Design and Construction of Structural Concrete Reinforced with FRP Bars*. American Concrete Institute, Farmington Hills, MI.

ACI. 2012. *ACI 440.3R-12: Guide Test Methods for Fiber-Reinforced Polymers (FRPs) for Reinforcing or Strengthening Concrete and Masonry Structures*. American Concrete Institute, Farmington Hills, MI.

Adimi, R., Rahman, H., Benmokrane, B., and Kobayashi, K. 1998. Effect of temperature and loading frequency on the fatigue life of a CFRP rebar in concrete. *Proceedings of the 2nd International Conference on Composites in Infrastructure (ICCI-98)*, Tucson, AZ, Vol. 2, pp. 203–210.

Ando, N., Matsukawa, H., Hattori, A., and Mashima, A. 1997. Experimental studies on the long-term tensile properties of FRP tendons. *Proceedings of the 3rd International Symposium on Non-Metallic (FRP) Reinforcement for Concrete Structures (FRPRCS-3)*, Japan Concrete Institute, Sapporo, Japan, Vol. 2, pp. 203–210.

Benmokrane, B. 2007. Durability of FRP, In: ACI Committee 440C (Ed.), *State-of-the-Art Report*. American Concrete Institute, Farmington Hills, MI, pp. 56–63.

Benmokrane, B. and El-Salakawy, H., Eds. 2002. Durability and field applications of fiber-reinforced polymer (FRP) composites for construction. *Proceedings of CDCC'02 International Conference*, Sherbrooke, Québec, Canada, pp. 1–692.

Benmokrane, B. and El-Salakawy, H., Eds. 2007. Durability and field applications of fiber-reinforced polymer (FRP) composites for construction. *Proceedings of CDCC'07 International Conference*, Sherbrooke, Québec, Canada, pp. 1–569.

Benmokrane, B. and Rahman, H., Eds. 1998. Durability and field applications of fiber-reinforced polymer (FRP) composites for construction. *Proceedings of CDCC'98 International Conference*, Sherbrooke, Québec, Canada, pp. 1–706.

Benmokrane, B. and El-Salakawy, E., Eds. 2011. Durability and sustainability of fiber reinforced polymer (FRP) composites for construction and rehabilitation. *Proceedings of CDCC'11 International Conference*, Québec City, Québec, Canada, pp. 1–692.

Benmokrane, B., Robert, M., and Youssef, T. 2007. Reinforcement of concrete using fibre-reinforced polymer composites. In: Karbhari, V.M., (Ed.), *Durability of Composites for Civil Structural Applications*. Woodhead Publishing Limited, Cambridge, England, Chapter 11, pp. 225–246.

Benmokrane, B., Wang, P., Ton-That, T.M., Rahman, H., and Robert, J.-F. 2002. Durability of glass fiber-reinforced polymer reinforcing bars in concrete environment. *Journal of Composites for Construction*, 6(3): 143–153.

Bisby, L.A. 2003. Fire behaviour of FRP-reinforced concrete. Ph.D. thesis, Queen's University, Kingston, Ontario, Canada.

Bisby, L.A. and Foster, S.K. 2007. High temperature residual bond properties of FRP systems for concrete. *Proceedings of the 3rd International Conference on Durability and Field Applications of Fiber-Reinforced Polymer (FRP) Composites for Construction (CDCC'07)*, Québec City, Québec, Canada, p. 8.

Bisby, L.A., Green, M.F., and Kodur, V.K.R. 2005. Response to fire of concrete structures that incorporate FRP. *Progress in Structural Engineering and Materials*, 7: 136–149.

Blontrock, H., Taerwe, L., and Matthys, S. 1999. Properties of fibre reinforced plastics at elevated temperatures with regard to fire resistance of reinforced concrete members. *Proceedings of the 4th International Symposium on Non-Metallic (FRP) Reinforcement for Concrete Structures*, Baltimore, MD, pp. 43–54.

Ceroni, F., Cosenza, E., Gaetano, M., and Pecce, M. 2006. Durability issues of FRP rebars in reinforced concrete members. *Cement and Concrete Composites*, 28: 857–868.

Chin, J.W., Nguyen, T., and Aouadi, K. 1997. Effects of environmental exposure on fiber-reinforced plastic (FRP) materials used in construction. *Journal of Composites Technology and Research*, 19(4): 205–213.

Clarke, J.L. and Sheard, P. 1998. Designing durable FRP reinforced concrete structures. *Proceedings of the 1st International Conference on Durability of Fiber Reinforced Polymer Composites for Infrastructure (CDCC'98)*, Sherbrooke, Québec, Canada, pp. 13–24.

Concrete Society. 2004. Technical report no. 55: Design guidance for strengthening concrete structures using fibre composite materials. The Concrete Society, Crowthome, U.K.

CSA. 2012. *CAN/CSA S806-12: Design and Construction of Building Components with Fibre Reinforced Polymers*. Canadian Standards Association, Ottawa, Ontario, Canada.

CSA. 2006. *CAN/CSA S6-06: Canadian Highway Bridge Design Code*. Canadian Standards Association, Ottawa, Ontario, Canada.

Curtis, P.T. 1989. The fatigue behavior of fibrous composite materials. *Journal of Strain Analysis*, 24(4): 235–244.

Galati, N., Vollintine, B., Nanni, A., Dharani, L.R., and Aiello, M.A. 2004. Thermal effects on bond between FRP rebars and concrete. *Proceedings of Advanced Polymer Composites for Structural Applications in Construction (ACIC'04)*, Cambridge, U.K. Woodhead Publishing Ltd., Surrey, U.K., pp. 501–508.

Greenwood, M. 2002. Creep-rupture testing to predict long-term performance. *Proceedings of the 2nd International Conference on Durability of Fibre Reinforced Polymer (FRP) Composites for Construction (CDCC'02)*, Montreal, Québec, Canada, pp. 212.

Harries, K., Porter, M., and Busel, J. 2003. FRP materials and concrete: Research needs. *Concrete International*, 25(10): 69–74.

ISIS. 2001. *ISIS Design Manual No. 3. Reinforcing Concrete Structures with Fibre Reinforced Polymers*. Intelligent Sensing for Innovative Structures Canada, Winnipeg, Manitoba, Canada.

ISIS. 2005. *Excellent Performance of GFRP in Concrete*. Intelligent Sensing for Innovative Structures Canada, Winnipeg, Manitoba, Canada, http://www.isiscanada.com/latest/latest.htm#GFRP, accessed August 6, 2005.

ISIS. 2006. *Specifications for Product Certification of Fibre Reinforced Polymers (FRPs) as Internal Reinforcement in Concrete Structures*. ISIS Product Certification of FRP Materials, Product Certification #1, ISIS Canada, Winnipeg, Manitoba, Canada.

Karbhari, V.M., Ed. 2007. *Durability of Composites for Civil Structural Applications*. Woodhead Publishing Limited, Cambridge, England.

Karbhari, V.M., Chin, J.W., Hunston, D., Benmokrane, B., Juska, T., Morgan, R., Lesko, J.J., Sorathia, U., and Reynaud, D. 2003. Durability gap analysis for fiber reinforced composites in civil infrastructure. *Journal of Composites for Construction*, 7(3): 238–247.

Katz, A. 1998. Effect of helical wrapping on fatigue resistance of GFRP. *Journal of Composites for Construction*, 2(3): 121–125.

Katz, A., Berman, N., and Bank, L.C. 1999. Effect high temperature on the bond strength of FRP rebars. *Journal of Composites for Construction*, 3(2): 73–81.

Liao, K., Schultheisz, C.R., Hunston, D.L., and Brinson, L.C. 1998. Long-term durability of fiber-reinforced polymer-matrix composite materials for infrastructure applications: A review. *Journal of Advanced Materials*, 30(4): 3–40.

Micelli, F. and Nanni, A. 2004. Durability of FRP rods for concrete structures. *Construction and Building Materials*, 18: 491–503.

Nelson, G.L. 1995. Fire and polymers: An overview. *Proceedings of Fire and Polymers II*, ACS Symposium Series 599, American Chemical Society, Washington, DC, pp. 1–26.

Porter, M.L. and Harries, K.A. 2005. *Workshop on Research in FRP Composites in Concrete Construction*. San Francisco, CA, October 2004. Final Report submitted to the National Science Foundation, Washington, DC.

Rege, S.K. and Lakkad, S.C. 1983. Effect of salt water on mechanical properties of fiber reinforced plastics. *Fiber Science and Technology*, 19: 317–328.

Robert, M. and Benmokrane, B. 2010. Effect of aging on bond of GFRP bars embedded in concrete. *Cement and Concrete Composites*, 32(6): 461–467.

Robert, M. and Benmokrane, B. 2013. Combined effects of saline solution and moist concrete on long-term durability of GFRP reinforcing bars. *Construction and Building Materials*, 38: 274–284.

Robert, M., Wang, P., Cousin, P., and Benmokrane, B. 2010. Temperature as an accelerating factor for long-term durability testing of FRPs: Should there be any limitations? *Journal of Composites for Construction*, 14(4): 361–367.

Seki, H., Sekijima, K., and Konno, T. 1997. Test method on creep of continuous fiber reinforcing materials. *Proceedings of the 3rd International Symposium on Non-Metallic (FRP) Reinforcement for Concrete Structures (FRPRCS-3)*, Sapporo, Japan, Vol. 2, pp. 195–202.

Sen, R., Shahawy, M., Sukumar, S., and Rosas, J. 1998. Durability of carbon pretensioned elements in a marine environment. *ACI Structural Journal*, 95(6): 716–724.

Sorathia, U., Dapp, T., and Beck, C. 1992. Fire performance of composites. *Materials Engineering*, 109(9): 10–12.

Sorathia, U., Ohlemiller, T., Lyon, R., Riffle, J., and Schultz, N. 2001. Chapter 9: Effects of fire. *Gap Analysis for Durability of Fibre Reinforced Polymer Composites in Civil Infrastructure*. American Society of Civil Engineers, New York, pp. 100–121.

Uomoto, T., Mutsuyoshi, H., Katsuki, F., and Misra, S. 2002. Use of fiber reinforced polymer composites as reinforcing material for concrete. *Journal of Materials in Civil Engineering*, 14(3): 191–209.

Vijay, P.V. and GangaRao, H.V.S. 1999. Development of fiber reinforced plastics for highway application: Aging behavior of concrete beams reinforced with GFRP bars. CFC-WVU Report No. 99-265 (WVDOHRP #T-699-FRP1).

Weitsman, Y.J. and Elahi, M. 2000. Effects of fluids on deformation, strength and durability of polymeric composites—An overview. *Mechanics of Time-Dependent Materials*, 4: 107–126.

Yamaguchi, T., Kato, Y., Nishimura, T., and Uomoto, T. 1997. Creep rupture of FRP rods made of aramid, carbon, and glass fibers. *Proceedings of the 3rd International Symposium on Non-Metallic (FRP) Reinforcement for Concrete Structures*, Sapporo, Japan, Vol. 2, pp. 179–186.

27 Quality Assurance/Quality Control, Maintenance, and Repair

Ehab El-Salakawy

CONTENTS

QUALITY ASSURANCE AND QUALITY CONTROL: AN OVERVIEW

Quality control (QC) is a system of routine technical activities to measure and control the quality of a product or service as it is being developed. The QC system is designed to provide consistent checks to ensure data correctness, and completeness; identify and address errors and omissions; and record all QC activities.

In engineering and manufacturing, QC is involved in developing systems to ensure products or services are designed and produced to meet or exceed customer requirements. These systems are often developed in conjunction with other business and engineering disciplines using a cross-functional approach.

Quality assurance (QA) is the activity of providing evidence needed to establish adequate confidence among customers and other stakeholders that a product or service will satisfy given requirements for quality. QA assures the existence and effectiveness of procedures that attempt to make sure, in advance, that the expected levels of quality will be reached. QA, in general, includes the regulation of the quality of raw materials, assemblies, products, and components; services related to production; and management, production, and inspection processes. It also includes QC, which comprises those QA actions related to the physical characteristics of a material, structure, component, or system that provide a means to control the quality of the material, structure, component, or system to predetermined requirements.

Composite materials are made of fibers embedded in a polymeric resin known as fiber-reinforced polymers, FRP. In a composite material, fibers are the main source of strength and stiffness while the polymer resin is environmentally resistant. The combination of fibers and resin results in a

composite material with mechanical properties and durability better than either of its constituents alone. In addition to these two main components, resin fillers and additives are used to reduce the volume of the used polymer to reduce the cost without excessively degrading the composite properties. However, the main properties of the FRP reinforcement for concrete structures such as the tensile strength, mechanical relaxation, toughness, fatigue resistance, dimensional stability, and electrical and magnetic properties are highly dependent on the manufacturing process and the quality of the raw materials (ACI Committee 440 2007, ISIS Canada 2007, Khennane and Melchers 2000). Therefore, it is essential that the FRP reinforcement manufacturers have a standardized QC program that includes routine sampling, inspection, and testing of all constituent materials and the final FRP product.

In addition, the structures' owner or end-user may require to perform QA testing and inspection of the materials and manufacturing facilities to provide adequate confidence the FRP reinforcement, being supplied for a specific project, is in accordance with relevant specifications and that the properties of the FRP product delivered to the project site are in complete agreement with those reported in the qualification tests and the manufacturer's QC tests reports.

During the last decade, one major obstacle faced the wide acceptance of the FRP composites, especially reinforcing bars, as reinforcement for concrete structures was the lack of specifications for FRP product certification. Recently, the Canadian Network of Centers of Excellence on Intelligent Sensing for Innovative Structures, ISIS Canada, has taken the initiative to produce such a document (ISIS Canada 2006). This specifications document covers FRP internal reinforcing bars or grids made of glass, carbon, and aramid fibers in matrices of isophthalic polyester, vinylester, and epoxy resins. It includes procedures for qualification testing of FRP reinforcement for their mechanical, physical, and durability properties related to both short- and long-term performance as well as methods of reporting, certification, handling, and storage.

MAINTENANCE AND REPAIR OF FRP-REINFORCED CONCRETE STRUCTURES

Background

A successful maintenance program is the key to the long-term preservation of any structure. Regular inspections and accurate record-keeping are essential. Biannual inspections, occurring ideally in the spring and fall, include the identification of all kinds of problems, such as excessive cracking, cover separation and spalling, concrete fractures, and leaking at joints, rusting of bearings, etc. Records should be kept in the form of a permanent maintenance log that describes routine maintenance tasks and records the date a problem is first noted, when it was corrected, and the treatment method. The location of the work and the type and manufacturer of the repair material should be noted in the log.

Although FRP internal reinforcement seems to be a promising solution for steel corrosion-related problems, concrete structures reinforced with FRP reinforcement, for many reasons, still need maintenance, routine inspection and repair. Among these reasons are

1. Premature concrete deterioration due to
   a. Poor quality coarse aggregate, for example, with a high shale content, which results in serious scaling after short time in service
   b. Freeze–thaw damage, sulfate attack, and alkali-aggregate reactions causing cracking and spalling of concrete cover
   c. Concrete erosion in hydraulic structures
   d. Chemical attack in sewage treatment facilities
2. The possibility of deterioration of FRP reinforcement due to uncertainty of long-term performance, particularly in severe civil infrastructure environmental conditions (Benmokrane et al. 2002)

FIGURE 27.1 Problems caused by vehicle hitting the guardrail.

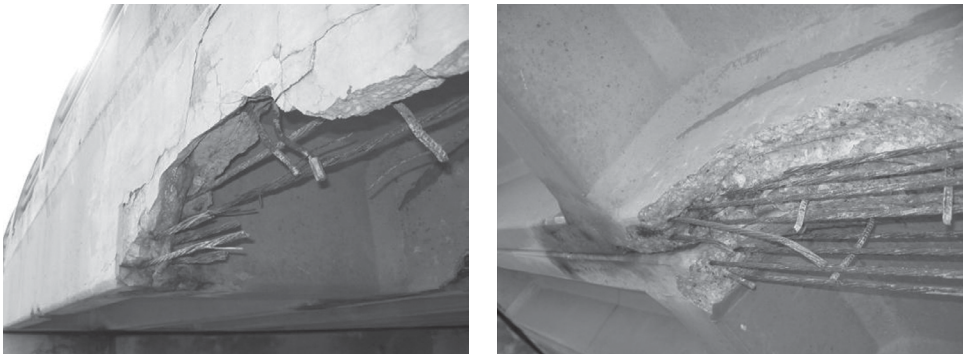

FIGURE 27.2 Problems caused by vehicle hitting a girder.

3. Structural damage due to service conditions, for example, in a bridge, a vehicle impact can cause the following damage to the bridge deck:
   a. Cracked/fractured concrete due to snow blow impact on deck joints, curbs, and railings
   b. Accident damage to curbs, railings, and concrete barriers (Figure 27.1)
   c. Accident damage to superstructure elements, such as bridge girders, from impact of over-height vehicles (Figure 27.2)

Also, the service conditions include foundation movement, malfunction bearings, and deck joints in a bridge, overloaded structures, and inadequate maintenance (Figure 27.3).

FIGURE 27.3 Problems caused by expansion joints.

4. Design errors, poor construction practices and workmanship, and improper design details
5. Need for future structural modifications to accommodate changes in level of service such as bridge widening and strengthening, or change in use or occupancy for building structures

The damaged areas may be identified by surface tapping or by suitable nondestructive testing methods. Repairs can be classified into two categories. First is the easy repair where there is a light damage (normally limited to the concrete cover zone) that does not affect the structural integrity, for which cosmetic repairs are acceptable. Second is the complex repair where there is an extensive damage (contamination, spalling, and delamination have progressed into the concrete layer that surrounds and encases the reinforcing assembly) that significantly affects the structural performance. At the locations of light damaged areas, the concrete section may be locally patched by replacing the damaged concrete. For extensively damaged areas, some or all the reinforcement needs to be replaced. In the later case, the concrete section and reinforcement may be partially or fully replaced based on the extent of damage in both surface and thickness directions. For example, in a bridge deck slab and due to the use of de-icing salts, the concrete slab may suffer damaged over large areas on the top surface only. Therefore, the suitable repair method is to replace the top reinforcement assembly at the damaged locations. In other situations, for example due to a vehicle impact to the bridge barrier, the damaged to the deck slab is localized in a small area. Replacing the full concrete section and adding new reinforcement may represent the best repair method in this case.

Concrete Removal/Demolition

In most repair cases, if not all, concrete demolition or removal close to or around the internal reinforcement in damaged areas is necessary. There are a number of methods for concrete removal/demolition. These methods range from scrabbling that can be used for concrete surface preparation and patches, to sawing, which is used for the full-depth removal of a given area.

For light damaged areas that can be repaired by local patches, it is normally required to remove only the concrete cover. The work involves removal to a depth less than the cover depth of the top FRP reinforcement and thus no work between, around, or under the reinforcing assembly is included in the task. For small thickness removal, one of the used techniques to is by scrabbling the concrete surface. A scrabbler uses pneumatically driven bits to impact the surface to remove concrete to a depth of between 1.0 and 6.0 mm. Scrabblers vary in size from large, self-propelled machines that can only work on large horizontal surfaces to small, hand-held tools for use in restricted, vertical or irregular surfaces. For bigger thickness, the scrabbling process can be used in repeated paths to achieve the required depth. However, this is an inefficient use of this method, and the only effective way to achieve bigger thickness, especially when large areas are involved, is by using a concrete milling machine. A milling machine removes concrete by the impact of numerous bits mounted on a rotating drum, as shown in Figure 27.4. Milling machines can only be used on horizontal surfaces such as bridge decks and concrete pavements. They should be used very carefully when removing concrete above FRP reinforcement since severe damage can occur when milling teeth cut or snag the FRP bars or grids.

For extensive damaged areas, the work involved is challenging to some extent, as it involves the removal of concrete surrounding the FRP reinforcement without damaging the bars, cracking the substrate concrete, or damaging the bond between FRP reinforcement and concrete in areas where the concrete is not to be removed. Three different methods for concrete removal can be identified: nonexplosive controlled demolition agents (or expansive agents), jackhammers, and hydro-demolition. The first two methods are known as labor-intensive techniques because they are greatly dependant on workmanship. While the latter is known as equipment-intensive method since the machines are doing most of the job. All of these techniques may be used to remove cover and matrix concrete in a single operation or may be used to remove only matrix concrete following a more specialized and

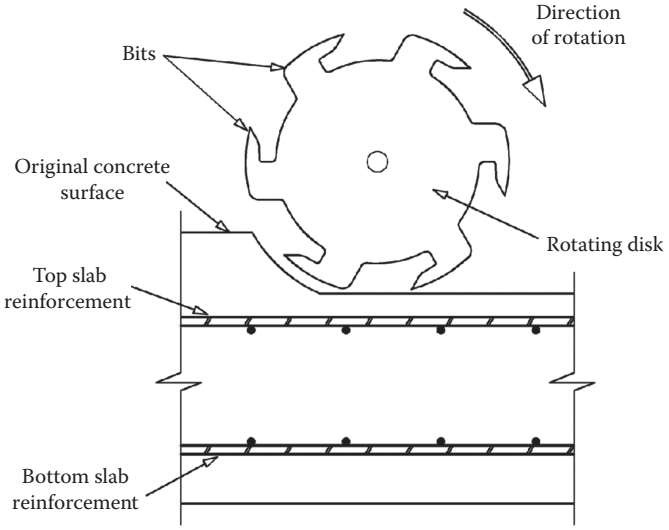

FIGURE 27.4 Milling machine on a reinforced concrete section.

high-production method, such as milling, has been used to remove the cover concrete. The three methods are described briefly in the following sections.

Nonexplosive Controlled Demolition Agents

This technique provides 500 kg/cm^3 of expansive strength when mixed with water. The process is simple; water should be mixed with the product and then poured into holes in which the mix will expand causing the reinforced concrete to crack. The main advantages of this technique are (Dexpan 2007, DTI 2007)

- Cracks reinforced concrete safely and quietly
- Safer and more efficient than blasting, diamond sawing, and jack-hammering
- It works without noise, vibration, dust by providing silent expansive cracking
- No special permit, insurance, training, or equipment needed

It is essential with this technique to properly design the hole-drilling pattern and orientation. This will minimize consumption of the demolishing agent by cutting into desired sizes. In shallow concrete section, such as bridge deck slabs, it is recommended to use inclined rather perpendicular holes to the concrete surface, so that the vertical components of the expansive forces cause the concrete above the holes to fracture. Also, for better results, it is important not to use the expansive agent in high temperatures and protect the filled holes from direct sunlight so that blowing-out can be avoided.

After the expansive agent is poured into holes drilled in concrete, the expansive stress gradually increases with time to reach more than 60,000 kN/m^2 in 24 h at room temperature. As the expansive agent generates its expansive stress, the concrete undergoes a process of crack initiation, crack propagation, and crack widening. When multiple holes are filled with the expansive agent, which are properly adjacent to each other, the cracks from one hole propagate to connect with the neighboring holes. Figure 27.5 shows demonstrating photos of the use of expansive demolition agent.

Hydro-Demolition

Hydro-demolition applies an extremely high-pressure (80–240 MPa) water jet to destroy the cement matrix of the concrete and liberate the coarse aggregate over a large continuous area. The equipment needed to generate the pressure and focus the water jet on the concrete to be removed is expensive and complex. The equipment can be adjusted to remove concrete to almost any depth, as shown

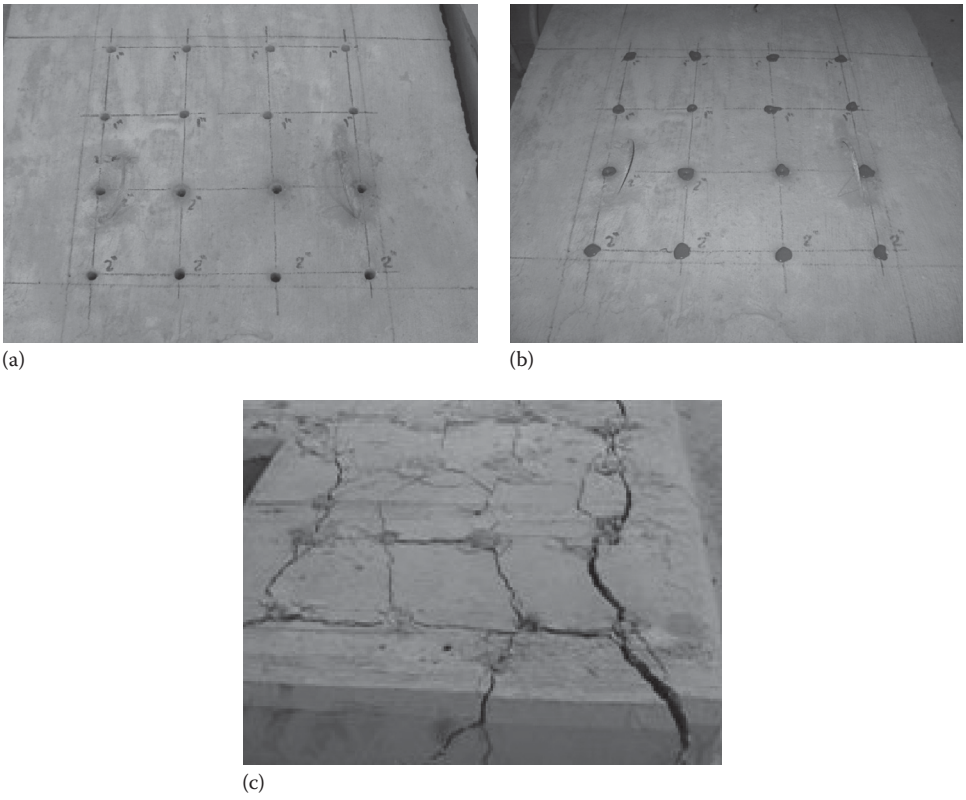

FIGURE 27.5 Demonstrating photos of the use of an expansive demolition agent. (a) Holes drilled on a marked grid. (b) Holes filled with grout. (c) Concrete splitting.

in Figure 27.6, by applying a constant amount of energy to the concrete in a manner that causes all material with less than the required strength to be removed regardless of depth. The pressure and flow rates as well as jet characteristics should be carefully adjusted so that the demolition will not result in tearing apart the GFRP bars or remove the coating layer that normally provides the required bond strength and protect the fibers from adverse environments. The International Concrete Repair Institute (ICRI) recently published technical guideline on the use of hydro-demolition for concrete removal and surface preparation (ICRI 2004).

There are many advantages to using hydro-demolition in concrete removal. These advantages include the following (Rampat Hydro 2007):

- A rough, irregular surface profile can be created to provide a good mechanical bond for a subsequent application of repair materials
- Surface micro-fracturing (bruising) may be minimized
- Exposed aggregates are not fractured, split, or damaged
- Undesirable strength and deteriorated concrete is selectively removed
- Dust and vibration of the surrounding structural elements can be minimized

Jackhammers

The jackhammer is the most common method for concrete removal in rehabilitation work, especially in bridges. The jackhammer is a hand-held tool powered by compressed air to deliver a series of high-frequency blows that fracture the concrete in a small, easily controlled area, as shown in Figure 27.7. The efficiency of jackhammer depends on two factors: the size (weight: 4–55 kg) of

(a)

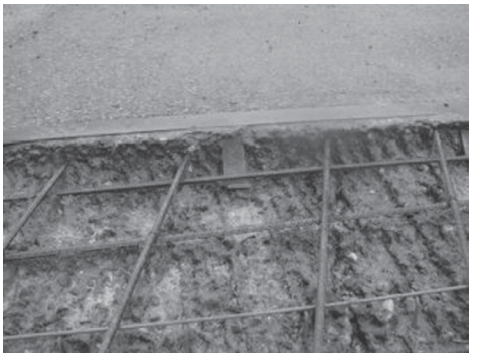

(b)

(c)

FIGURE 27.6 Hydro-demolition of concrete. (a) Exposing the coarse aggregate using scarification. (b) Removal of concrete around the reinforcing bars. (c) Full depth removal of a slab.

(a)

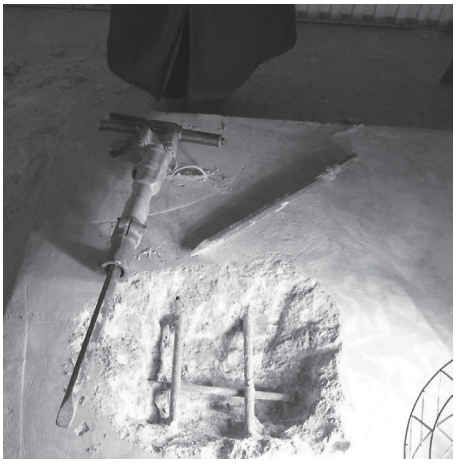

(b)

FIGURE 27.7 Jackhammer to expose the reinforcement. (a) Jackhammering. (b) Exposed reinforcement.

the breaker and the skill of the operator. Heavier hammers are more productive/destructive because they are able to impart more energy with each blow. Hammers can be powered by a variety of energy sources including hydraulic pressure, gasoline engine, or electric motor.

Hydraulic hammers are attached to a compressor through a set of hoses to pump a pressurized fluid to actuate the tool. While the power supply for gas and electric hammers is attached to the instrument. Therefore, for similar production efficiency, gas and electric hammers are generally

heavier than the hydraulic-operated ones. However, these later units are self-contained and require no additional support equipment, which is suitable in situations where access is restricted.

One of the obstacles for using jackhammers is to determine the location of GFRP bars in a concrete element. Since GFRP bars have a low hardness compared to steel bars, a jackhammer operator should be very cautious during the removal of concrete to prevent or minimize FRP bar damage. Allowing the jackhammer to rest on a GFRP bar would easily nick or fully cut through the bar. Investigations are currently underway to apply the ground penetrating radar (GPR) technology to locate the FRP reinforcement embedded in concrete. If the GPR gives a satisfactory results, the use of jackhammers in removing concrete in such structures will be one of the most efficient and economical techniques.

Repair of a Concrete Bridge Deck Slab: Field Application

Concrete bridge decks deteriorate faster than any other bridge component because of direct exposure to environment, de-icing chemicals, and ever-increasing traffic loads. The use of non corrodible FRP composites as reinforcement for concrete bridge decks provides a potential for increased service life, economic, and environmental benefits (Benmokrane and El-Salakawy 2002, 2007, Nanni and Faza 2002, Steffen et al. 2001). On the other hand, since glass FRP bar/grid is more economical than the other available types (carbon and aramid) of FRP reinforcement, it is more attractive for infrastructure applications and to the construction industry. Therefore, most of the recent field applications of FRP composites in concrete structures have been utilizing GFRP bars in bridge deck slabs (Benmokrane et al. 2007, El-Salakawy et al. 2003, 2005).

Considering that these field applications have been in service for a relatively short period with no corrosion-related deterioration, very few field examples for the repair of FRP-reinforced concrete structures are available in the literature. One of these examples was reported by Deitz et al. (2000) that involved removal and demolishing of concrete in a reinforced concrete bridge deck slabs. In this project, two of the aforementioned demolition schemes, jackhammers and hydro-demolition, have been used and evaluated. Two concrete mock bridge decks were constructed as slabs on grade: one reinforced with GFRP bars and the other was reinforced with epoxy-coated steel (ECS) for comparison purposes. The concrete dimensions and spacing of reinforcing bars in all directions for the two slabs were identical.

In the following sections, the applications of the two methods in removing concrete from GFRP- or ESC- reinforced bridge decks are highlighted.

Jackhammer

A jackhammer was used to dig two holes, one in each mock bridge decks. In the bridge deck reinforced with ECS bars, a pachometer was used to detect the location of the steel reinforcement. This allowed the jackhammer operator to avoid the bars from the beginning of the concrete removal process. A pachometer could not be used to determine the location of GFRP bars in a bridge deck. Therefore, a jackhammer operator has to find the location of the bars while removing concrete, often damaging bars in the process.

The authors (Deitz et al. 2000) also made another observation that the ECS bars can be used as a guide for the jackhammer during concrete removal. Since the ECS bars are stiff enough, the jackhammer operator often wedged the tip of the jackhammer against the ECS bar when removing concrete around it. This did little more to the bar than scratch the epoxy coating. GFRP bars could not be used as a guide during concrete removal. First, the GFRP bars were not stiff enough to firmly wedge the tip of the jackhammer. Second, the use of a GFRP bar as a jackhammer guide resulted in damage to the bar, often removing surface deformations and/or sand-coating layer.

To minimize the damage to the GFRP bars, the operator would have to jackhammer until a bar in each horizontal direction was found. Once the bars were found, the operator could estimate the location of adjacent bars based on the reinforcement spacing, if available. In every test case

performed on the mock bridge deck the operator would inflict damage to the GFRP bar before realizing that the hammer was resting on the bar. After the first bar was located the operator was better able to avoid the other bars.

They also observed that it was very difficult for the operator to remove concrete near the surface of the GFRP bar. When the jackhammer would shake, the point of the jackhammer would slip, changing position. Often the change in position would move the tip of the jackhammer directly on the bar resulting in substantial damage.

Though damage to the ECS bars also occurred, in most cases it was limited to removal of the epoxy coating and small nicks. Most of the damage done to the mock deck reinforced with ECS bars could be corrected by applying a new epoxy coating to the nicked surfaces, assuming that all of the damaged surfaces are easily detected.

The authors (Deitz et al. 2000) concluded that the use of jackhammers is a viable method for removing of concrete from a deck reinforced with GFRP bars and they provided the following steps as a guide in the concrete removal procedure:

Step 1: Locate a GFRP bar in each of the two horizontal directions. Remove concrete in thin layers until at least one bar in each direction is exposed.
Step 2: Using the bars found in Step 1 as a guide, mark positions of adjacent bars based on the spacing in the bridge plans.
Step 3: Remove the concrete around and underneath the bars while taking precautions to avoid resting the tip of the hammer on the GFRP bars. During the procedure, the operator should avoid using the GFRP bars as a guide for the jackhammer because this will remove surface deformations.

Hydro-Demolition

The hydro-demolition equipment used in the study consisted of the apparatus that removes the concrete and a semi-trailer to produce the required hydraulic pressure. Water at high pressure was released under the base of the apparatus breaking up and removing concrete in the mock deck slab reinforced with ECS. The authors (Deitz et al. 2000) observed that during the removal process the water moved sand and gravel around with the water at high speed. This act as an abrasive, removing the epoxy coating from ECS bars. Therefore, they recommended that following the concrete removal, the steel bars should be re-coated with epoxy to provide long-term reinforcement protection.

To evaluate the hydro-demolition process as a concrete demolition scheme for bridge decks reinforced with GFRP, an individual loose GFRP bar was placed under the machine while it was in operation. The abrasive action of the sand and gravel extensively damaged the GFRP bar. They concluded that hydro-demolition should not be considered a viable option for the repair of bridge decks reinforced with GFRP bars. However, there are other factors such as water jet pressure that should be investigated before reaching a sound conclusion.

GUIDELINES FOR THE REPAIR OF FRP-REINFORCED CONCRETE STRUCTURES

There is a lack of research data and field experience regarding the repair of FRP-reinforced concrete structures. Consequently, no guidelines for the repair of such structures are currently available. However, for FRP material to be considered as a conventional construction material used in a large scale, some level of comfort should be given to the owners that concrete structures reinforced with FRP materials can be repaired. The issue of providing guidelines and recommendations to repair, rehabilitate, or extend an existing concrete structure reinforced with FRP internal reinforcement has been raised by officials from the Ministries of Transportation and DOTs, which

own the majority of concrete structures reinforced with FRP internal reinforcement in Canada and United States, namely, bridges (deck slabs) and continuously reinforced concrete pavements (CRCP). From the owners' perspective, every bridge or overpass will require some kind of repair due to various kinds of damage as stated in the "Background" section. They are also concerned about the need for future structural modifications to accommodate changes in level of service such as bridge widening or strengthening.

ISIS Canada has already taken the initiative to provide such guidelines and formed two-joint committees with more than 30 experts in the FRP field: one is based in Manitoba and the other in Quebec.

Based on the recommendations of this joint committee, two important issues are identified when considering the repair of such structures reinforced with FRP bars. The first issue is to investigate the feasibility and economics of repairing FRP-reinforced concrete by replacing damaged concrete. This requires investigating the available various techniques for concrete demolition and their effect on the existing FRP bars in terms of mechanical, bond, and durability properties. The second issue is related to the structural behavior and durability performance of FRP-reinforced concrete elements after being extended or widened (rehabilitated). Research is currently on going at the University of Manitoba to provide the essentially needed data to be able to introduce adequate guidelines.

REFERENCES

ACI Committee 440. (2007). *State of the Art Report on Fiber Reinforced Plastic (FRP) Reinforcement for Concrete Structures*. ACI 440.R-07, American Concrete Institute, Farmington Hills, MI.

Benmokrane, B. and El-Salakawy, E., Eds. (2002). Durability of fibre reinforced polymer (FRP) composites for construction. *Proceedings of the 2nd International Conference*, University of Sherbrooke, Sherbrooke, QC, p. 715.

Benmokrane, B. and El-Salakawy, E., Eds. (2007). Durability and field applications of fibre-reinforced polymer (FRP) composites for construction. *Proceedings of the 3rd International Conference*, University of Sherbrooke, Sherbrooke, QC, 569 p.

Benmokrane, B., El-Salakawy, E.F., El-Ragaby, A., and El-Gamal, S. (2007). Performance evaluation of innovative concrete bridges reinforced with FRP bars. *Canadian Journal of Civil Engineering*, 34(3), 298–310.

Benmokrane, B., Wang, P., Ton-That, T.M., Rahman, H., and Robert, J-F. (2002). Durability of GFRP reinforcing bars in concrete. *Journal of Composites for Construction*, ASCE, 6(3), 143–155.

Bradberry, T.E. (2001). Concrete bridge decks reinforced with fiber reinforced polymer bars. Transportation Research Record 1770, Transportation Research Board, National Research Council, Washington, DC, pp. 94–104.

Deitz, D., Harik, I.E., and Gesund, H. (2000). *GFRP Reinforced Concrete Bridge Decks*. Research Report KTC-00-9, Kentucky Transportation Center, College of Engineering, University of Kentucky, Lexington, KY, 164pp.

Dexpan Non-Explosive Controlled Demolition Agents. (2007). http://www.archerusa.com/Product_Dexpan_En1.html (accessed on January 18, 2007).

DTI Demolition Technologies Incorporated. (2007). http://demolitiontechnologies.com (accessed on January 18, 2007).

El-Salakawy, E., Benmokrane, B., and Desgagné, G. (2003). FRP composite bars for the concrete deck slab of Wotton Bridge. *Canadian Journal of Civil Engineering,* 30(5), 861–870.

El-Salakawy, E.F., Benmokrane, B., El-Ragaby, A., and Nadeau, D. (2005). Field investigation on the first bridge deck slab reinforced with glass FRP bars constructed in Canada. *ASCE Journal of Composites for Construction*, 9(6), 470–479.

International Concrete Repair Institute (ICRI). (2004). *Guide for the Preparation of Concrete Surfaces for Repair Using Hydro-demolition Methods*. Technical Guideline No. 03737, Des Plaines, IL. http://www.icri.org/index.asp

ISIS Canada. (2006). *Specifications for Product Certification of Fibre Reinforced Polymers (FRP) as Internal Reinforcement in Concrete Structures*. ISIS Product Certification of FRP Materials, Product Certification # 1, ISIS Canada Research Network, Winnipeg, Manitoba, Canada.

ISIS Canada. (2007). *Reinforcing Concrete Structures with Fibre Reinforced Polymers*. Design Manual No.3, ISIS-M03-07, ISIS Canada Research Network, Winnipeg, Manitoba, Canada.

Khennane, A. and Melchers, R.E. (2000). *Fiber Reinforced Polymers for Infrastructure Applications: Durability and Life Prediction: A Review*. Research report No. 192.06.2000, Department of Civil, Surveying and Environmental Engineering, The University of Newcastle, Newcastle, Australia.

Nanni, A. and Faza, S. (2002). Designing and constructing with FRP bars: An emerging technology. *American Concrete Institute* (*ACI*) *Concrete International*, 24(11), 53–58.

Rampat Hydro. (2007). http://www.rampart-hydro.com (accessed on January 12, 2007).

Steffen, R.E., Trunfio, J.P., and Bowman, M.M. (2001). Performance of a bridge deck reinforced with CFRP grids in Rollinsford, New Hampshire, USA. In: Figueiras, J., Juvandes, L., and Furia, R. (eds.), *Proceedings, FRP Composites in Construction*, Porto, Portugal, Europe, pp. 671–676.

Part V

Hybrid FRP Composite Systems

Amir Mirmiran and Amir Fam

28 Introduction

Amir Fam and Amir Mirmiran

CONTENTS

GENERAL

There is a great demand for bridge components, piling, poles, highway overhead sign structures, and other structural components in corrosive environments to be made of materials that are more durable in comparison to traditional construction materials. More effective systems are also desired to accelerate the construction process and utilize the merits of constituent materials intelligently. The new systems will have to withstand corrosive environments such as the splash zone in the case of marine piles, where they would be alternately submerged and exposed (Stapleman 1997). Similarly, highway overhead sign structures, poles, and bridge piers would have to retain their integrity in cold regions where salt is used for deicing the roads. Fiber reinforced polymers (FRP) have been widely used in recent years for rehabilitation and strengthening of existing structures to increase their flexural, shear, and axial load resistance as well as improve their ductility. However, their use to date in new construction has been limited to a number of demonstration projects around the world, where FRPs have been used in the form of bar and tendon reinforcement in concrete structures as replacements for steel reinforcement due to their high strength-to-weight ratio and corrosion-resistant characteristics. FRPs may also be used in the form of structurally integrated stay-in-place formwork for concrete structures in a hybrid manner that maximizes the advantages of both FRP and concrete while simplifying the construction procedure and reducing the erection time. In the last few years, a number of such hybrid systems have been developed; a brief review of some of these systems is presented below.

Triantafillou and coworkers proposed a novel beam system that consisted of a rectangular glass-FRP (GFRP) box beam with a carbon-FRP (CFRP) laminate bonded to its tension side and a concrete layer cast on top of its compression side. In this system, it is assumed that compression is taken by concrete, tension is taken by the CFRP laminate, and the GFRP box section resists shear. Deskovic et al. (1995) showed that the system could be optimized by uncoupling the most critical failure modes and correlating them to the material properties of each component.

Hall and Mottram (1998) proposed a novel slab system that consists of a concrete slab cast onto a pultruded FRP panel with a flat continuous base and T-up stands used as shear connectors. The FRP panels in this case serve as permanent formwork and reinforcement for the slab. The system relies on mechanical bond between concrete and the studs to transfer the horizontal shear. The general behavior was shown to be linear elastic in the serviceability range.

Concrete-filled FRP tube is another application of the concept of structurally integrated stay-in-place form that could be used as piles in marine environments to replace reinforced, prestressed, concrete-filled steel tubes and timber piles commonly used in these environments (Mirmiran and Shahawy 1995, Parvathaneni et al. 1996, Seible 1996, Fam and Rizkalla 2000). The same concept

has also been proposed for bridge columns and piers in seismic zones because of the enhanced ductility due to concrete confinement (Seible et al. 1998). Although the beneficial effects of concrete confinement are less pronounced in the presence of bending, as compared to a case of pure axial loading, other advantages such as utilization of the prefabricated FRP tubes as stay-in-place form work, ease of fabrication, and speed of erection still make this system attractive. Studies on hollow GFRP tubes have shown that thin FRP tubes would fail prematurely by local buckling under flexural loading before reaching their full strength (Polyzois et al. 1999). It is, therefore, believed that concrete filling adds tremendous structural value to the FRP tubes.

APPLICATIONS AND CONFIGURATIONS

Figure 28.1 illustrates the different potential applications of the stay-in-place system as piles, bridge columns and piers, overhead sign structures, poles, traffic signs and traffic lights, pipes, and bridge girders. The system can be utilized through different cross-sectional configurations, as shown in Figure 28.2, which may be classified as "closed forms" or "open forms." Closed forms include totally filled round tubes, as shown in Figure 28.2a (Mirmiran and Shahawy 1996, Seible 1996, Fam and Rizkalla 2002), or partially filled tubes as in Figure 28.2b–d (Fam and Rizkalla 2002). The hole in the latter could be maintained by nonstructural sections such as PVC or cardboard tubes or alternatively by another FRP tube for additional strength. The inner tube could be concentric with respect to the outer one for axi-symmetric geometry and loading or could be eccentric to allow for more concrete in the compression zone of the section, depending on the nature of loading. Rectangular FRP tubes may also be totally filled, as shown in Figure 28.2e (Mirmiran et al. 1998, Fam et al. 2005), or partially filled, as shown in Figure 28.2f–h (Fam et al. 2005).

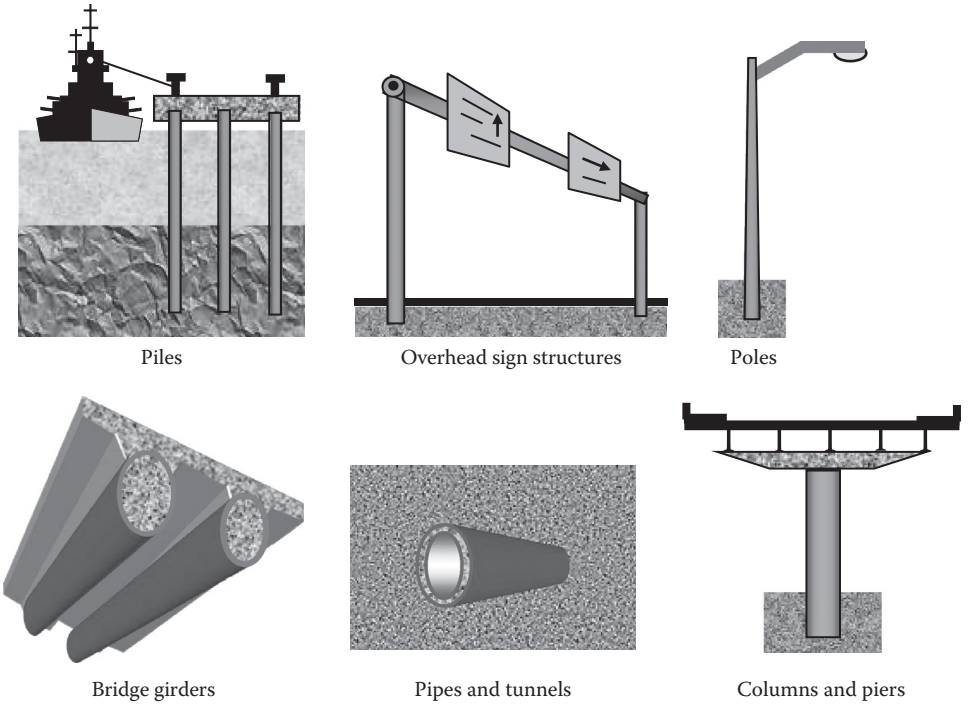

FIGURE 28.1 Potential applications of the concrete-filled FRP tubes. (From Fam, A.Z. and Rizkalla, S.H., Hybrid FRP/concrete structural members, in *Proceedings of the ACUN-2 International Conference on Composites in Transportation Industry*, University of New South Wales, Sydney, New South Wales, Australia, 2000.)

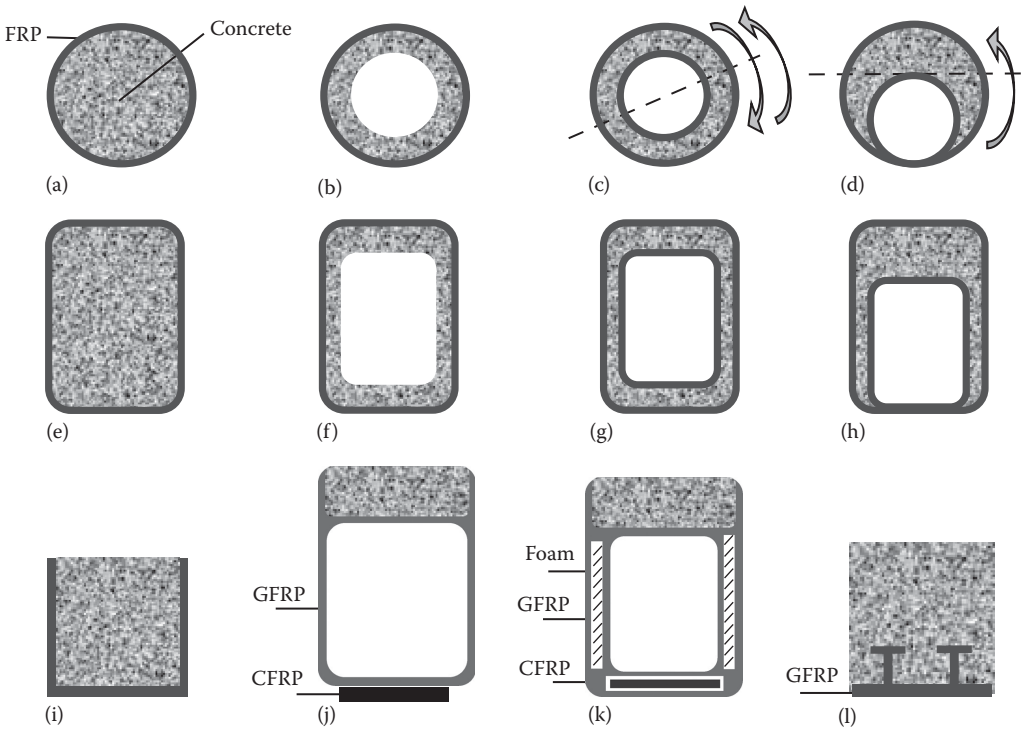

FIGURE 28.2 Different configurations of FRP structurally integrated stay-in-place formwork for concrete members. Concrete filled FRP tube (CFFT): (a) round CFFT, (b) round CFFT with a central hole, (c) round, double-skin concentric CFFT, (d) round, double-skin eccentric CFFT, (e) rectangular CFFT, (f) rectangular CFFT with a central hole, (g) rectangular double-skin concentric CFFT, (h) rectangular double-skin eccentric CFFT, (i) open u-shape form, (j) rectangular tube with a top concrete layer and a bottom CFRP layer, (k) hybrid section with a stiffened web, and (l) ribbed-plate form.

Open forms may include a box section with an open side, as shown in Figure 28.2i (Fardis and Khalili 1981). Concrete may also be placed outside the closed FRP section for compressive resistance, while the FRP section is used to resist shear, as shown in Figure 28.2j and k (Triantafillou and Meier 1992, Canning et al. 1999). The FRP section may also serve as formwork for slabs, as shown in Figure 28.2l (Hall and Mottram 1998). Conventional reinforcements or prestressing may also be added to the system (Parvathaneni et al. 1996, Cole et al. 2005). Additional case studies and field applications are presented in a later chapter.

ADVANTAGES AND LIMITATIONS OF THE SYSTEM

The most common characteristics of the integrated hybrid systems are as follows:

- FRP shape acts as permanent form for concrete; hence, will save the cost of formworks involved in conventional cast-in-place or pre-cast industries.
- Main reinforcement for concrete is provided externally by the FRP shape, even though additional reinforcement of other types of materials such as steel may be provided internally. In concrete-filled FRP tubes, the tube acts as reinforcement for both shear and flexure, utilizing the multidirection fiber orientation. This would save the time and cost involved in conventional construction in assembling longitudinal bars together with stirrups. The closed composite shells also provide passive confinement to the concrete, which significantly improves the strength and ductility.

- Depending on the nature of loading, the capacity and performance of the system may depend on the composite action between the concrete and FRP shape. For example, under axial loads, it is desired not to have the FRP tube bonded to the concrete core, while under bending, it is essential to provide the full composite action.
- The system lends itself to optimization based on material properties of each component. The hybrid system provides the designers with several flexible parameters, which can be controlled to achieve optimum design in individual applications including type of fibers, orientation of the fibers, number of layers in the composite shell, and the concrete wall thickness.
- The contained concrete, in case of concrete-filled tubes, is protected from moisture intrusion that could otherwise deteriorate the concrete core.

It is important to also note the limitations of the system. Fire is a concern in building applications, and measures must be taken to achieve appropriate rating using fire-retardant resins and coatings or cover materials. Vandalism and graffiti are also of concern in outdoor applications, such as bridges, and measures must be taken either to limit access to the FRP or to paint and texture the FRP similar to the concrete surface. Finally, when the FRP form is in direct contact with water, it must be protected against moisture intrusion through the use of appropriate resin mix.

REFERENCES

Canning, L., Hollaway, L., and Thorne, A.M. (1999) Manufacture, testing and numerical analysis of an innovative polymer composite/concrete structural unit, *Proceedings of the Institution of Civil Engineers: Structures and Buildings*, Paper 11826, 134: 231–241.

Cole, B., Mandal, S., and Fam, A. (2005) Effect of longitudinal reinforcement and prestressing on flexural performance of concrete-filled FRP tubes, *Proceedings of the 3rd International Conference on Construction Materials, ConMat'05*, Vancouver, Canada, pp. 22–24.

Deskovic, N. and Triantafillou, T.C. (1995) Innovative design of FRP combined with concrete: Short-term behavior, *Journal of Structural Engineering*, 121(7): 1069–1078.

Fam, A.Z. and Rizkalla, S.H. (2000) Hybrid FRP/concrete structural members, *Proceedings of the ACUN-2 International Conference on Composites in Transportation Industry*, University of New South Wales, Sydney, New South Wales, Australia, Sydney, Australia, pp. 191–197.

Fam, A.Z. and Rizkalla, S.H. (2002) Flexural behaviour of concrete-filled fiber-reinforced polymer circular tubes, *ASCE Journal of Composites for Construction*, 6(2): 123–132.

Fam, A., Schnerch, D., and Rizkalla, S. (2005) Rectangular filament-wound GFRP tubes filled with concrete under flexural and axial loading: Experimental investigation, *ASCE Journal of Composites for Construction*, 9(1): 25–33.

Fardis, M.N. and Khalili, H. (1981) Concrete encased in fiberglass-reinforced plastics, *ACI Structural Journal*, Title no. 78-38, November–December, 440–446.

Hall, J.E. and Mottram, J.T. (1998) Combined FRP reinforcement and permanent formwork for concrete members, *Journal of Composites for Construction*, 2(2): 78–86.

Mirmiran, A. and Shahawy, M. (1995) A novel FRP-concrete composite construction for the infrastructure, *Proceedings of the ASCE Structures Congress XIII*, Boston, MA, pp. 1663–1666.

Mirmiran, A. and Shahawy, M. (1996) A new concrete-filled hollow FRP composite column, *Composites Part B: Engineering*, 27B(3–4): 263–268.

Mirmiran, A., Shahawy, M., Samaan, M., El Echary, H., Mastrapa, J.C., and Pico, O. (1998) Effect of column parameters on FRP-confined concrete, *Journal of Composites for Construction*, 2(4): 175–185.

Parvathaneni, H.K, Iyer, S.L., and Greenwood, M. (1996) Design and construction of test mooring pile using superprestressing, *Proceedings of the Advanced Composite Materials in Bridges and Structures*, Montreal, Quebec, Canada, pp. 313–324.

Polyzois, D., Ibrahim, S., and Raftoyiannis, I.G. (1999) Performance of fiber-reinforced plastic tapered poles under lateral loading, *Journal of Composite Materials*, 33(10): 941–960.

Seible, F. (1996) Advanced composites materials for bridges in the 21st century, *Proceedings of the Advanced Composite Materials in Bridges and Structures*, Montreal, Quebec, Canada, pp. 17–30.

Seible, F. (1998) Innovative designs for pedestrian bridges, *Proceedings of the Developments in Short and Medium Span Bridge Engineering '98*, Calgary, Alberta, Canada.

Seible, F., Karbhari, V., Burgueno, R., and Staberg, E. (1998) Modular advanced composite bridge system for short and medium span bridges, *Proceedings of the Developments in Short and Medium Span Bridge Engineering '98*, Calgary, Alberta, Canada.

Stapleman, J. (1997) Pile on the abuse. *Composites Technology*, September/October 1997, 3 pp.

Triantafillou, T.C. and Meier, U. (1992) Innovative design of FRP combined with concrete, In: K.W. Neale and P. Labossiere, (eds.), *Proceedings of the Advanced Composite Materials in Bridges and Structures*, Canadian Society for Civil Engineering, Sherbrooke, Quebec, Canada, pp. 491–499.

29 Material Characteristics and Fabrication Methods

Amir Fam and Amir Mirmiran

CONTENTS

FRP COMPONENT

The FRP component of the integrated system has to accommodate the concrete, act as reinforcement in one or more directions, and in some cases provide confinement for concrete at the same time. Therefore, the FRP product may be in the form of thin shells (laminates) with large surface area of different shapes, including both closed tubes and box sections and also open forms. The following sections briefly review some of the fundamentals of the FRP materials including their physical and mechanical properties, as well as manufacturing processes with emphasis on thin laminates in particular.

FRP Laminates

FRP refers to composite materials consisting of two phases including a dispersed phase, reinforcement, and a continuous phase, matrix (Daniel and Ishai 1994). The dispersed phase is usually continuous-fiber reinforcement, which is the backbone of the material that determines its stiffness and strength in the direction of the fibers. The matrix phase provides protection and support for the sensitive fibers as well as facilitates local stress transfer from one fiber to another. The continuous fibers can be all parallel (unidirectional continuous fiber composites), oriented at right angle to each other (cross ply or woven fabric continuous fiber composites), or oriented along several directions (multidirectional continuous fiber composites).

A lamina or a ply is a plane or curved layer of unidirectional fibers or woven fabric embedded in a matrix. The lamina is considered an orthotropic material with principal material axes (1, 2, and 3), as shown in Figure 29.1a. A laminate is made up of two or more unidirectional laminae or plies stacked together at various orientations. Since the principal material axes differ from ply to another, it is more convenient to analyze laminates using a common fixed system of coordinates (x, y, and z),

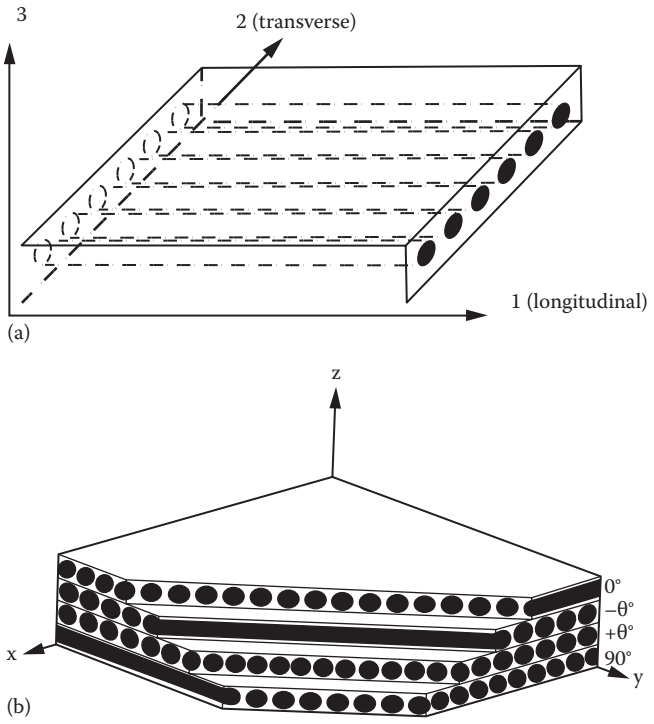

FIGURE 29.1 (a) Unidirectional lamina and principal coordinate axes. (b) Multidirectional laminate and reference coordinate system. (From Daniel, I.M. and Ishai, O., *Engineering Mechanics of Composite Materials*, Oxford University Press, New York, 1994.)

as shown in Figure 29.1b. The orientation of a ply is given by the angle between *x*-axis and principal axis-1 of the ply. The configuration of the laminate indicating its ply composition and exact location or sequence of various plies is called stacking sequence. A laminate is considered symmetric when for each layer on one side of the middle surface there is a corresponding layer at an equal distance from that reference plane on the other side with identical thickness, orientation, and properties. A laminate is called balanced when it consists of pairs of layers with identical thickness and elastic properties but with $+\theta$ and $-\theta$ orientations.

Given details and structure of the laminate in terms of number of layers, fiber orientation in each layer, thickness of individual layers, fiber and resin types and mechanical properties, as well as fiber volume fraction, the classical lamination theory is typically used to analyze FRP laminates (Daniel and Ishai 1994). The theory provides equivalent mechanical properties of the laminate in the major directions and predicts the strength under different loading conditions.

Types of Fibers and Matrices

A large variety of fibers are available as reinforcement for composites. The desirable characteristics of most fibers are high strength, high stiffness, and relatively low density (Daniel and Ishai 1994). Because of its high tensile strength and lower cost, glass is the most commonly used fiber in low to medium performance composites. However, glass fibers have relatively low stiffness and fatigue endurance, and rapid property degradation with exposure to severe hygrothermal conditions. Aramid fibers have higher stiffness and lower density, but they are limited by very low compressive strength and high moisture absorption. Boron fibers, not widely used at present, are useful in local stiffening applications because of their high stiffness. Carbon (graphite) fibers come in many types with a range of stiffnesses and strengths. In general, carbon fibers have the advantage of

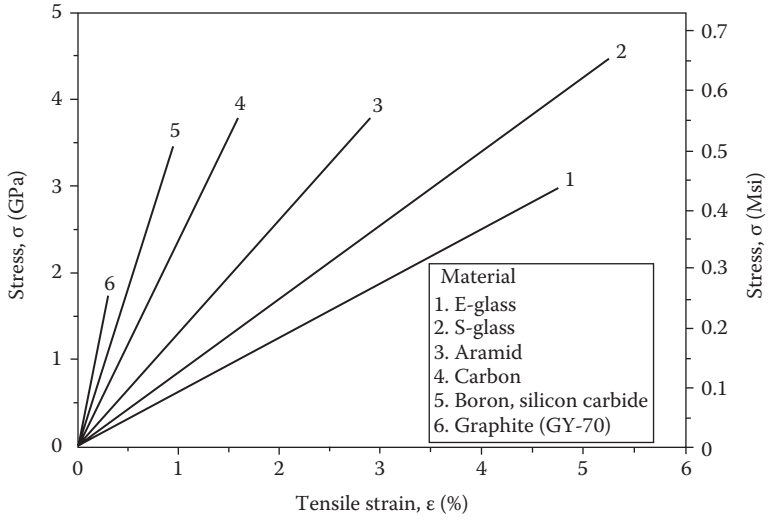

FIGURE 29.2 Stress–strain curves of typical reinforcing fibers.

high strength and stiffness, but also cost higher. Most fibers behave linearly to failure, as shown in Figure 29.2. The basis of the superior performance of composites lies in the high specific strength (strength to density ratio) and high specific stiffness (modulus to density ratio). These two properties are controlled by the fibers.

Polymeric matrices may be thermoset (epoxy, polyimide, or polyester) or thermoplastic (poly-ether-ether-ketone, or polysulfone). The most highly developed of these are epoxies. They can be formulated with a range of stiffnesses, as shown in Figure 29.3. There are two types of epoxies, those cured at low temperature and used in components exposed to low or moderate temperature variations, and those cured at a higher temperature and used in higher performance components exposed to high temperature and moisture variations. Polyesters are used in quick-curing systems for commercial products, whereas polyimide matrices are used for high-temperature applications.

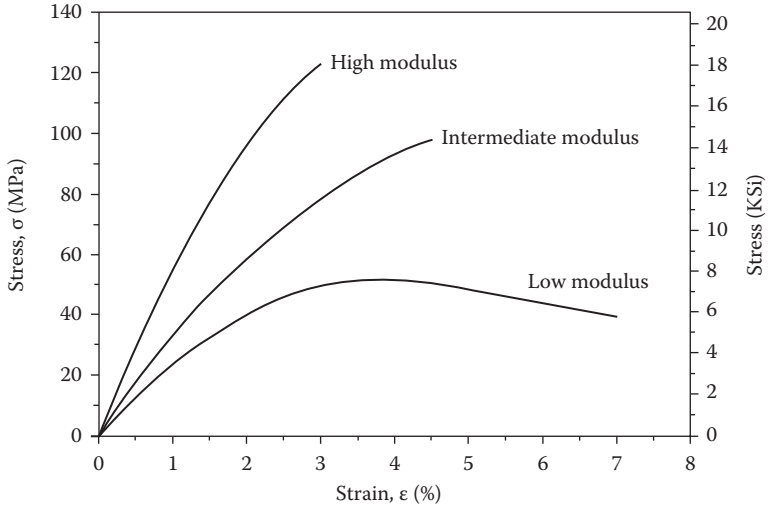

FIGURE 29.3 Stress–strain curves of epoxy matrix resins of different moduli.

Mechanical Properties of FRP Laminates

The basic characteristics of a unidirectional single lamina such as its elastic modulus and strength in the axial and transverse directions are determined using coupon tests. These properties are then used as input for the classical lamination theory to determine the equivalent elastic modulus and strength of a laminate composed of layers at different angles. Figure 29.4 shows the specimen geometry for determination of tensile properties of unidirectional lamina in both directions (ASTM specification D3039-76 1989). Six plies are used for the longitudinal specimen and eight plies for the transverse one. Figure 29.5 shows the specimen geometry for determination of compressive strength of unidirectional lamina (ASTM D-3410-87). The coupon is 15–20 plies thick. The tensile strength of the overall laminate in the axial direction can also be determined experimentally by a method proposed by Fam and Rizkalla (2001) for cylindrical tubes, where a longitudinal curved strip is cut from the FRP tube. Since stress concentration at the grip can severely influence the strength of FRP coupons, the scheme shown in Figure 29.6a is used for gripping. The two ends of the FRP strip are embedded inside hollow steel tubes, 300 mm long each, for gripping and epoxy resin is then cast in the tubes. The size of the part of the FRP coupon between the two steel tubes is 150 mm × 25 mm. The hoop strength and stiffness of an FRP tube could also be evaluated using a split-disk test, as shown in Figure 29.6b. A 25 mm wide ring is cut from the tube and tested in tension using two semicircular stiff steel plates of a similar curvature to that of the GFRP tube. It should, however, be noted that these methods could slightly underestimate the real strength of the laminate due to the discontinuity at the free edges. A study by Mandal (2004) has shown that providing a rather short (25 mm) length between the gripping devices of longitudinal coupons would provide more accurate and representative modulus and tensile strength, compared to the standard ASTM D3039-76 coupon, for filament-wound tubes with fibers oriented at slight angles relative to the longitudinal axis.

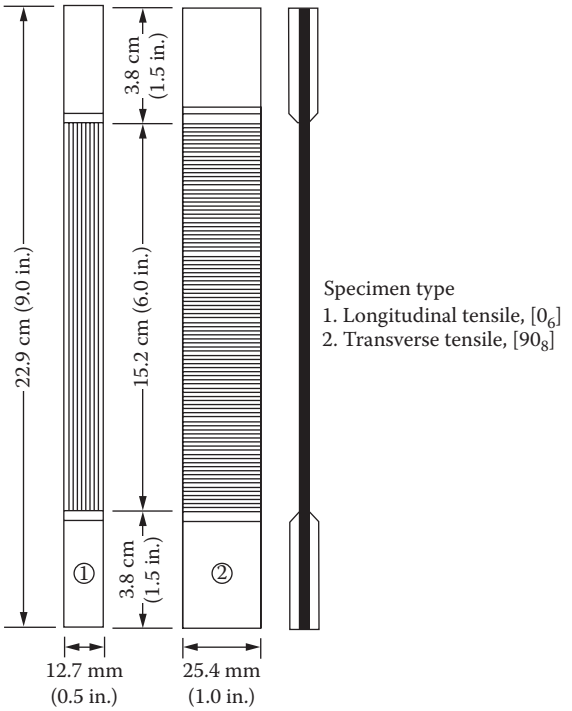

FIGURE 29.4 Specimens geometries for determination of tensile properties of unidirectional lamina.

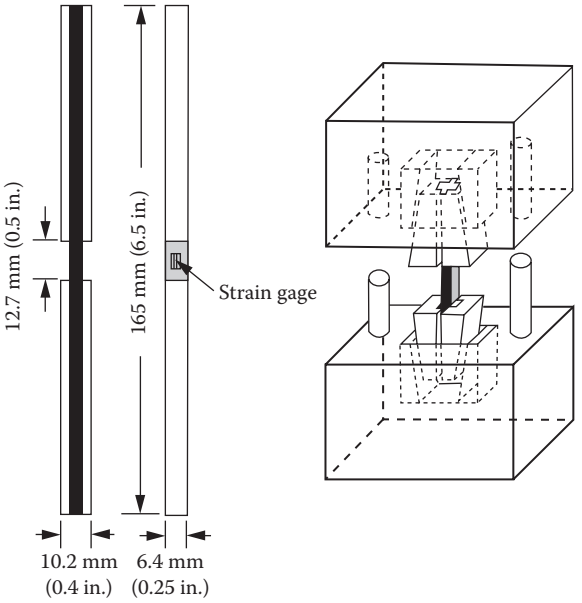

FIGURE 29.5 Compression specimen and fixture.

Fabrication Processes

The most commonly used fabrication processes of FRP-closed sections are the filament winding and pultrusion processes. In some cases, the centrifugal casting method is also used. The open molding method is normally used for FRP open sections.

Filament Winding

Filament winding was invented in 1946 and incorporated into missile applications in the 1950s (Daniel and Ishai 1994). The technique is generally used to produce hollow symmetrical products such as pipes, tanks, rocket motors, or any element not containing concave geometry. A mandrel of the required shape is rotated on its axis, and wound with a continuous filament of reinforcement, which is passed through a resin bath immediately before contact with the laminate. When fully wound with resin-wetted reinforcement, the lay-up is cured, on or off the mandrel, as shown in Figure 29.7. The reinforcement in many cases consists of a band of several roving. The band may be positioned perpendicular to the axis of the mandrel (circumferential winding) or inclined at an angle relative to the axis (helical winding). The process is capable of great flexibility in type, mix, density, and direction of winding, and normally high fiber volume fractions (60%–75%) are obtained. Winding can be done with fibers, which are impregnated with resin during the winding process (wet winding), or with fibers encapsulated in a semihardened resin (prepreg winding). The part may also be wound dry, and then impregnated under pressure. Additional reinforcement in the form of mat or fabric may be applied in alternating layers with the filament wound roving or tape to enhance axial strength. Filament winders are typically computer-controlled (Carrino et al. 1998). Winder sizes range from small tabletop to giant machines capable of winding parts of up to 9 m diameter and 46 m length. The mandrel must be stiff enough to avoid sagging and must possess dimensional accuracy and smooth surface to facilitate extraction of the wound parts. The mandrel may be made collapsible, or may be made of fiberglass, wood, rubber or salt, the latter of which can be dissolved for part removal. For unlimited lengths, continuous winding over a short mandrel is used, whereby the machine will continue to wind, as the wound part advances and cures (Stapleman 1997).

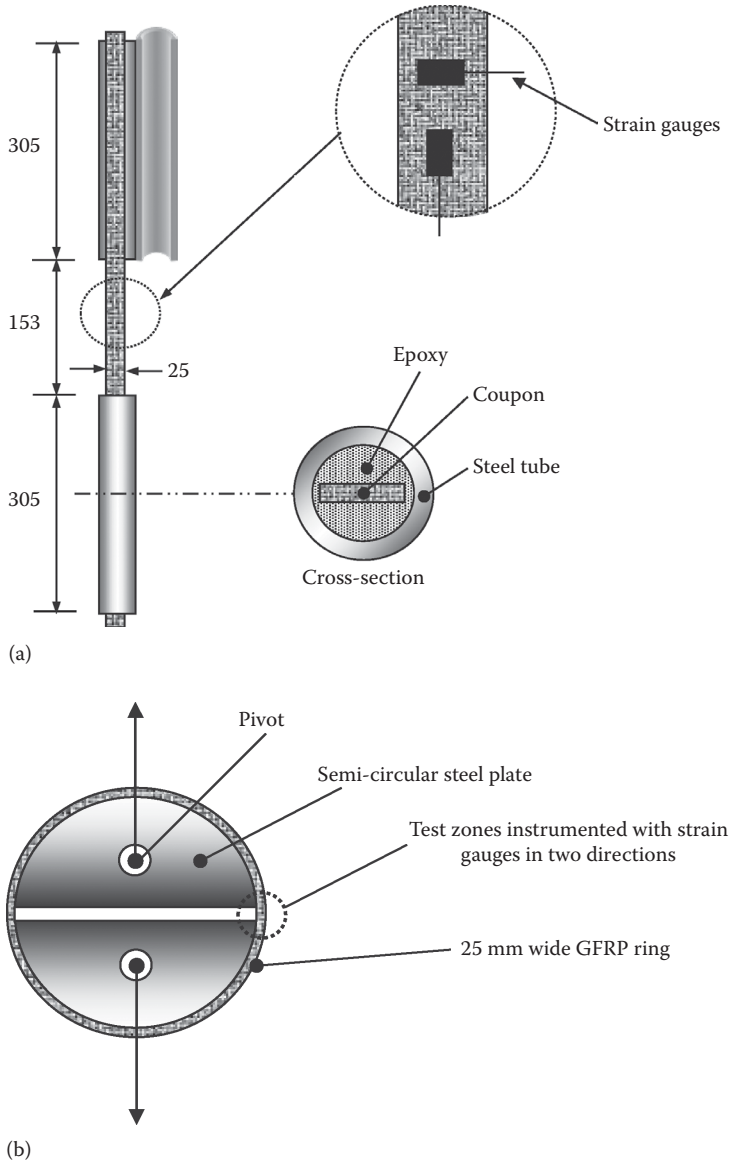

FIGURE 29.6 (a) Details of tension coupon for properties in the axial direction. (From Fam, A.Z. and Rizkalla, S.H., *ACI Struct. J.*, 98(3), 280, 2001.) (b) Details of split-disk tension test for properties in the hoop direction.

Open Molding

In this method, fibers and resin are applied to a single surface mould, as shown in Figure 29.8. The process includes hand lay-up and vacuum bagging. In the hand lay-up method, the reinforcement is a woven fabric, continuous or chopped mat, or combination of both. The reinforcement can be preimpregnated with resin and then placed on the mold or mandrel, or it can be preplaced and then saturated with resin by spray or pressure rollers. In either case, the saturated reinforcement must be consolidated to remove trapped air. The resin is usually cured chemically, but can also be heat cured by various means, including heater bars, steam heated mandrels, and heating ovens.

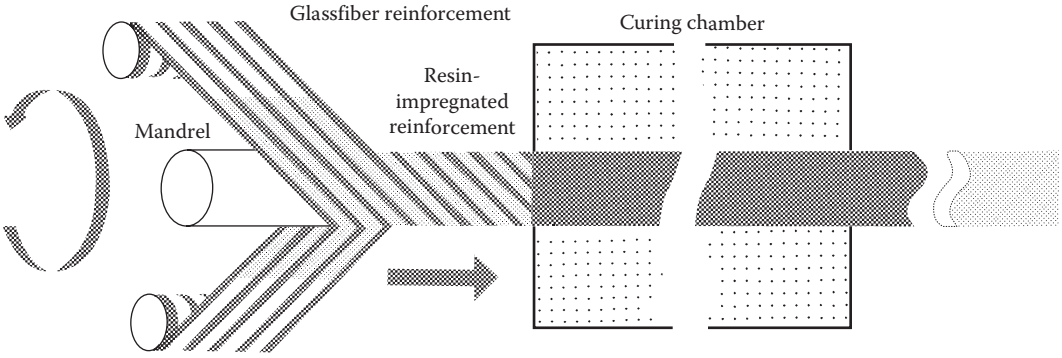

FIGURE 29.7 Schematic of the filament winding process. (From Murphy, J., *Reinforced Plastic Handbook*, 2nd edn., Elsevier Science Ltd., Amsterdam, the Netherlands, 1998.)

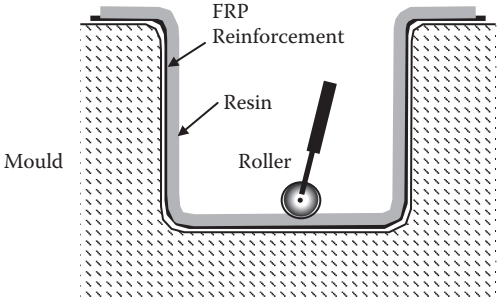

FIGURE 29.8 Molding by hand lay-up. (From Murphy, J., *Reinforced Plastic Handbook*, 2nd edn., Elsevier Science Ltd., Amsterdam, the Netherlands, 1998.)

Centrifugal Casting

This method is suited to the production of hollow parts such as pipes. Fiber reinforcement in the form of chopped roving mixed with resin is sprayed inside a mandrel rotating at high speed, as shown in Figure 29.9. The centrifugal force helps the resin to impregnate the reinforcement while minimizing the void ratio.

Pultrusion

Pultrusion is used for continuous production of all types of profiles. Continuous fiber reinforcement in the form of roving or mat/roving is drawn through a resin bath, as shown in Figure 29.10. The resin-impregnated fibers are then assembled by a forming guide and pulled through a heated die for shaping and compaction, as well as initiating the curing. The profile is pulled through the die at a constant speed. The process is suitable for complex hollow or solid profiles. It should be noted,

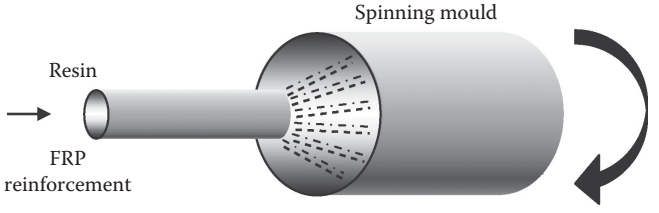

FIGURE 29.9 Centrifugal casting of reinforced plastics. (From Murphy, J., *Reinforced Plastic Handbook*, 2nd edn., Elsevier Science Ltd., Amsterdam, the Netherlands, 1998.)

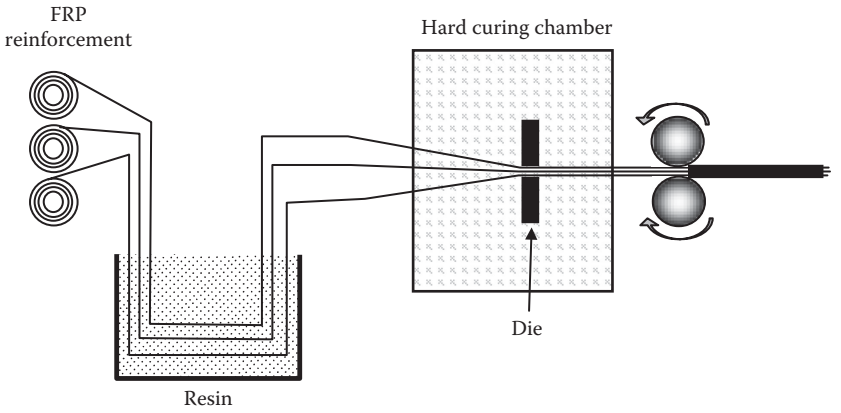

FIGURE 29.10 Schematic of the pultrusion process. (From Murphy, J., *Reinforced Plastic Handbook*, 2nd edn., Elsevier Science Ltd., Amsterdam, the Netherlands, 1998.)

TABLE 29.1
Sample of a Concrete Mix Using Expansive Component

Material	Quantity/m³	Units
Cement	403	kg
CONEX (expansive material)	44	kg
Sand	829	kg
Stone	916	kg
Water	149	L
Water reducer (Polyheed 997)	2235	mL
SUPER (Rheobuild 2500)	2500	mL
Air (MBVR)	134	mL

however, that if unidirectional fibers are used such that fibers are oriented mainly in the longitudinal direction, it may lack strength in the transverse direction.

CONCRETE COMPONENT

Concrete component may be plain, reinforced, or prestressed. While any conventional concrete mix may be used, it is possible to use shrinkage compensating admixture to improve bond with FRP in confined sections. Table 29.1 provides a sample concrete mix. On the other hand, recent studies into the long-term behavior of FRP-confined concrete columns has found shrinkage of concrete core in concrete filled tubes to be quite negligible, as the core is essentially sealed from the drying environment (Naguib and Mirmiran 2002). Additional measures such as shear connectors or sand-coated FRP surface may be taken to improve bond between FRP and concrete.

REFERENCES

ASTM D3039/D3039M-95a. (1989) Standard test method for tensile properties of polymer matrix composite materials.

ASTM D3410/D3410M-95. (1995) Standard test method for compressive properties of polymer matrix composite materials with unsupported gage section by shear loading.

Carrino, L., Moroni, G., and Turchetta, S. (1998) CAD/CAM for robotic filament winding process design, *Proceedings of the ECCM-8, European Conference on Composite Materials*, Vol. 2, I. Crivelli Visconti (ed.), Brazil, June 3–6, pp. 615–622.

Daniel, I. M. and Ishai, O. (1994) *Engineering Mechanics of Composite Materials*, Oxford University Press, New York.

Fam, A. Z. and Rizkalla, S. H. (2001) Behavior of axially loaded concrete-filled circular fiber reinforced polymer tubes, *ACI Structural Journal*, 98(3): 280–289.

Mandal, S. K. (2004) Prestressed concrete-filled fibre reinforced polymer (FRP) tubes, M.Sc. thesis, Queen's University, Kingston, Ontario, Canada, p. 204.

Murphy, J. (1998) *Reinforced Plastic Handbook*, 2nd edn., Elsevier Science Ltd., Amsterdam, the Netherlands.

Naguib, W. and Mirmiran, A. (2002) Time-dependent behavior of FRP-confined concrete columns, *ACI Structural Journal*, 99(2): 142–148.

Stapleman, J. (1997) Pile on the abuse, *Composite Technology*, 3.

30 Construction Considerations of Hybrid Members

Amir Fam and Amir Mirmiran

CONTENTS

CONCRETING

The FRP structural form, whether it is a closed or open form, may or may not be designed to support the weight of fresh concrete, depending on the project and availability of shoring systems. FRP tubes may be filled with concrete in a vertical, inclined, or horizontal position. Care must be taken to support the weight of fresh concrete until it hardens; otherwise, excessive deformation, sagging, or distortion of the tube may occur. Support platforms and shoring may be provided for hybrid slabs and beams, if necessary. Concrete may be pumped or poured in place. Some fabricators prefer to pressure pump the concrete fill into the FRP tubes, uphill against gravity as a means of eliminating air voids. As in any other application, concrete may be consolidated using electric air-powered mechanical vibrators that may be hand held or mounted on the form or the rack.

In tubular forms, plugs or caps may be necessary to contain the wet concrete at the bottom. They may be held in place with lag screws and further reinforced by means of attaching metal bands to the end of the tube to engage and further hold the plug in place. End plugs may also be installed to provide a smooth and square end surface for concrete. Caps that fit over the end of the tube can be made of metal, plastic, or FRP material. Caps should be of an adequately strong material and fit snugly. Caps and plugs can be removed or left in place, depending on the application. Quality control for concreting may follow the same procedures recommended by the ACI.

BOND BETWEEN CONCRETE AND FRP

Composite action and load transfer between FRP and concrete depends on their interface bond. It is only for passive confinement applications that the bond does not play an important role. Since natural bond between FRP and concrete is almost nonexistent, the following methods have been proposed to achieve the required bond strength:

- Mechanical interlock or shear connectors can be provided by forming circumferential ridges or a grid work of pockets on the inside of the tubular member (Mirmiran et al. 1998, Seible et al. 1998). Other researchers have applied a layer of coarse silica sand over

the inner surface of the tubes, applied over an epoxy coating (Fam and Rizkalla 2002). These methods will allow the wet concrete to extend into and lock with the FRP shell when cured. It is not recommended to roughen the inner FRP wall, exposing glass reinforcement, as a means of creating a mechanical lock. There is concern that the chemistry of the cement will negatively react with the exposed glass and cause failure of the FRP element over time.

- Chemical bond between concrete and FRP may be achieved using special concrete adhesives. The drawbacks of this method include the cost and difficulty of application.
- Some fabricators suggest the use of shrinkage reducing admixtures to keep the concrete engaged with the FRP form in tubular sections.

PROTECTIVE COATING OF FRP

In some applications, a durable finish may be required for stay-in-place FRP forms, especially when exposed to ultraviolet (UV) rays. This type of exposure over time, without a coating, may lead to the breakdown of the FRP shell and potentially structural failure. Coatings are also applied for aesthetic reasons, mainly to maintain more permanent color and/or gloss. When properly applied, a normal coating will protect the structure for many years. When adhesion is properly established with the FRP substrate, the coating material cannot be easily taken off the product. Proper surface preparation is vital to the longevity of the coating system. The coating material will perform only as well as the preparation. In-line treatments that are effective such as corona and other arc-type surface effectants are also available before final cure of the FRP.

Since the FRP substrate exhibits low expansion and contraction, the success and longevity of the coating depend on the material itself and on the quality of the surface preparation to maximize adhesion. FRP forms are manufactured by different methods and require different methods of surface preparation. Gentle sanding may be sufficient to roughen the resin surface to promote a mechanical lock with the coating material. Blasting with sand or metal shot is another method of scaring the surface to promote mechanical lock with the coating material. Care must be taken not to penetrate the resin-rich surface and expose the fiber reinforcement or surface veils. This will cause fiber blooming and will make for a rough surface finish that will have a negative effect on the life of the coating material. All sanded surfaces must be thoroughly washed; otherwise, the coating may peel off. High-pressure water spray is an effective method of surface preparation on some types of FRP forms. Water alone will not properly remove mold release agents or other contaminants. Solvent wipes may also be an effective method of surface preparation for removing fatty acids and other mold release agents. Acetone, xylene, mineral spirits may be used. It is best to wipe the surface just prior to the paint application where possible.

The service environment often determines the most appropriate coating material for use on stay-in-place FRP forms. Waterborne acrylic paints are useful for light abrasive duty, full sun exposure, and mid/low gloss. Urethane enamel is useful for good abrasion resistance, full sun exposure, good adhesion, high gloss, and good color retention. Engineered siloxane is excellent for abrasion resistance, full sun exposure, good gloss, and good for partial or full saltwater submersion. Finally, epoxy also provides good adhesion, but poor UV protection.

Usually, one heavy coat with a minimum of 2 mils dry film thickness and a maximum of 4 mils is sufficient in most environments. Coating may be applied using paint brushes, rollers, or spray-up equipment. In larger projects, coating may be applied using a high-volume low-pressure spray gun. Sufficient curing time must be allowed before shipping and handling. Special care must be given not to scratch or mar the finished surface during handling and transportation.

REFERENCES

Fam, A. Z. and Rizkalla, S. H. (2002) Flexural behaviour of concrete-filled fiber-reinforced polymer circular tubes, *Journal of Composites for Construction*, 6(2): 123–132.

Mirmiran, A., Shahawy, M., Samaan, M., El Echary, H., Mastrapa, J. C., and Pico, O. (1998) Effect of column parameters on FRP-confined concrete, *Journal of Composites for Construction*, 2(4): 175–185.

Seible, F., Karbhari, V., Burgueno, R., and Staberg, E. (1998) Modular advanced composite bridge system for short and medium span bridges, *Proceedings of the Developments in Short and Medium Span Bridge Engineering '98*, Calgary, Alberta, Canada.

31 Axial Hybrid Members

Amir Fam and Amir Mirmiran

CONTENTS

GENERAL

The commonly known structural systems for FRP/concrete axial members involve mainly FRP closed sections, including both circular and rectangular configurations, as shown in Figure 31.1a and e. An important aspect in the design of these types of members is the design of the FRP shell component itself. The FRP shell acts as the formwork required to support the fresh concrete and also acts as the reinforcement at the same time. Special care should be allocated to the laminate structure and fiber architecture of the shell. For example, an FRP shell required for a circular column would contain more fibers oriented in the hoop direction for confinement, whereas a shell used for flexural member would contain more fibers in the axial direction for flexural strength. This chapter addresses the different aspects of axial members in terms of design considerations and behavior, based on the work done by different researchers.

DESIGN CONSIDERATIONS

This section provides guidance for the design of concrete-filled FRP tubes as axial members, with more emphasis on members with round FRP tubes. The confinement effects are addressed, including the available analytical models developed to predict the behavior of confined concrete.

Axial Members with Round FRP Tubes

Concrete-filled FRP tubes with round cross sections are more popular than the rectangular ones due to their higher confinement effectiveness. Also, the totally filled tubes are the most commonly used due to the fact that the entire cross section is utilized in compression. However, in some cases,

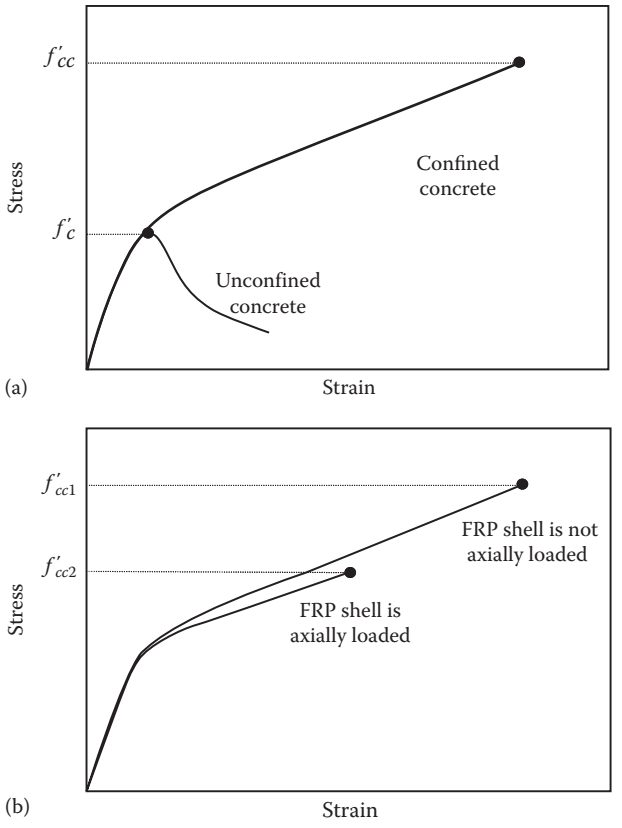

FIGURE 31.1 Confinement effect of FRP tubes on stress–strain behavior of concrete. (a) Stress–strain response of FRP-confined concrete. (b) Effects of loading the FRP shell in the axial direction on the stress–strain response.

partially filled tubes with central holes are used to reduce the self-weight of the member, as in large diameter piles. In principle, the FRP shells required for this type of members need to be designed to provide the maximum strength and stiffness in the transverse direction for optimum confinement of concrete.

Stress–Strain Curve of FRP-Confined Concrete

Studies have shown that the stress–strain curve of FRP-confined concrete is bilinear with curved transition zone near the peak unconfined concrete strength, as shown in Figure 31.1a (Mirmiran and Shahawy 1997). From a structural point of view, the optimum confinement mechanism takes place when only the concrete core is axially loaded and the FRP shell is fully utilized for confinement under hoop tensile stresses. However, in practical applications, this is not always achievable due to the fact that friction, adhesion, and surface irregularities provide some axial load transfer to the shell (Fam and Rizkalla 2001a,b). Figure 31.1b shows the typical stress–strain curves for concrete confined with FRP shell under two loading conditions, including axially loaded core only and axially loaded core and shell. Fam and Rizkalla (2001b) have shown that for the case of concrete-filled FRP tube with only the concrete core is axially loaded, the level of the confinement pressure σ_R, which controls the axial strength and stiffness of confined concrete, is significantly affected by stiffness of the tube in the hoop direction ($E_s t/R$) as given by Equation 31.1, where E_s is the effective elastic modulus of the tube in the hoop direction, t is the thickness of the tube, and R is the radius. The confinement pressure is also function of the lateral expansion of the concrete core in terms of

Poisson's ratio υ_c, which is a variable during the loading history. E_c is the elastic modulus of the concrete core and ε_{cc} is the axial strain.

$$\sigma_R = \frac{\upsilon_c}{(R/E_s t)+(1-\upsilon_c/E_c)}\varepsilon_{cc} \tag{31.1}$$

Effect of Loading the FRP Shell

Loading the FRP shell in the axial direction has two negative effects. The first effect is reducing the strength of the FRP shell in the hoop direction, which explains the reduction in the ultimate confined strength from f'_{cc1} to f'_{cc2} in Figure 31.1b. This is attributed to the biaxial state of stress developed in the FRP shell, as shown in Figure 31.2. In this case, the biaxial failure envelope is established for the FRP shell, using a failure criterion such as Tsai-Wu, and the combination of axial compressive stress and hoop tensile stress is compared to the failure envelope to detect failure. The second effect is the expansion of the shell outward under axial compression due to its own Poisson's ratio. This expansion reduces the confinement pressure at the interface between the shell and the concrete core. Fam and Rizkalla (2001b) have shown that the confinement pressure σ_R in the case of axial load applied to both the tube and the core can be given by a similar expression to that in Equation 31.1, except that the numerator is $(\upsilon_c - \upsilon_s)$ instead of υ_c, where υ_s is Poisson's ratio of the shell. This effect is reflected in the slightly lower stiffness of the curve given in Figure 31.1b.

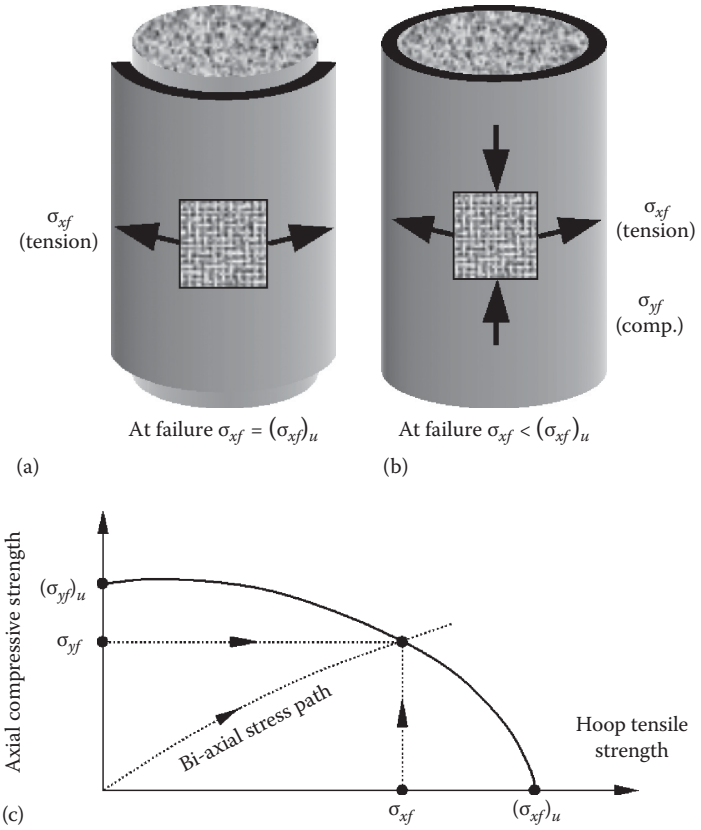

FIGURE 31.2 Effect of the axial loading condition on the strength of FRP shell. (a) Only core is axially loaded. (b) Both core and shell are axially loaded. (c) Biaxial stress failure envelop. (From Fam, A.Z. and Rizkalla, S.H., *ACI Struct. J.*, 98(3), 280, 2001a.)

As mentioned before, axial loading of the FRP shell cannot be avoided in most cases. Therefore, the laminate design of the tube could be controlled to produce the minimum Poisson's ratio. Some analytical models can account for the effect of loading the shell axially, on the predicted response of confined concrete (Fam and Rizkalla 2001b).

Effect of Central Holes

Providing central holes inside the concrete core reduces the self-weight of the member, but it also reduces the confinement effectiveness by reducing the confining pressure and consequently the confinement ratio as evident from Equation 31.2 (Fam and Rizkalla 2001b). The equation shows that the larger the radius of the inner hole, R_i with respect to the outer radius R_o, the lower the confinement pressure σ_R.

$$\sigma_R = \frac{(R_o - R_i)\upsilon_c}{\left(R_o^2/E_s t\right) + R_o\left(R_o^2 + R_i^2/R_o^2 - R_i^2\right) - \upsilon_c/E_c}\varepsilon_{cc} \tag{31.2}$$

Figure 31.3 shows the reduction of confined strength with increasing the size of the central hole. It was also shown that the confinement effectiveness can be improved for the partially filled FRP tubes if the central hole in the concrete core is maintained by another FRP tube Fam and Rizkalla 2001a,b). Some analytical models can account for the effect of the size of the hole on the predicted response of the confined concrete (Fam and Rizkalla 2001b).

Confinement Models

Different analytical models have been developed to predict the stress–strain response of confined concrete using FRP round shells. All these models recognize the fact that confining pressure is variable and is a direct function of the interaction between the expanding concrete core and the FRP shells with linear characteristics (i.e., passive confinement). This is totally different from steel confined concrete, where the confining pressure is stable once the steel yields.

There are a number of available confinement models, some of which predict the entire stress–strain relationship for confined concrete, whereas the others may only predict the peak strength and the confinement effectiveness (Harries et al. 1998). Some of these models are based on dilation

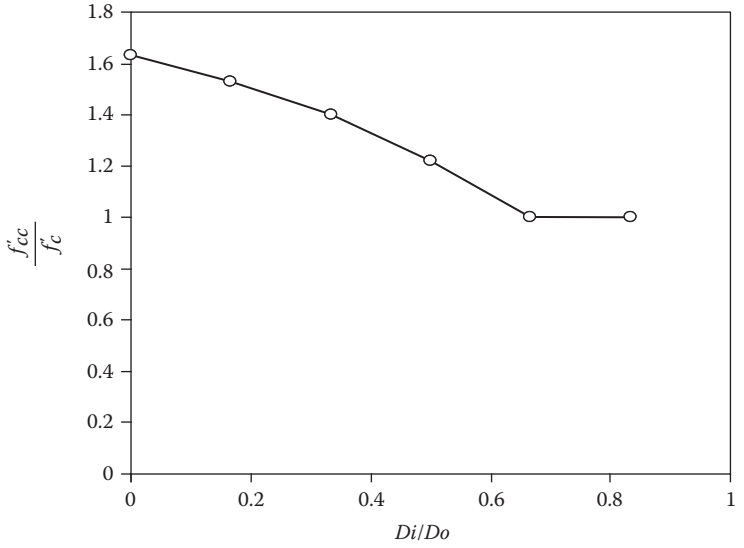

FIGURE 31.3 Variation of confinement ratio and confinement effectiveness with void size. (From Fam, A.Z. and Rizkalla, S.H., *ACI Struct. J.*, 98(4), 251, 2001b.)

relationship for confined concrete (Samaan et al. 1998), modified Ahmad and Shah's model (Saafi et al. 1999, Toutanji 1999) or modified Mander's model, using different relationships between lateral and axial strains (Spoelstra and Monti 1999, Fam and Rizkalla 2001b) or the energy-balanced technique (Parent and Labossiere 1997). Other models have also been developed that are based on octahedral stress theory for triaxial stress state by Gerstle (Becque 2000). Recognizing the passive nature of confinement with FRP, a number of models have been developed as early as 1995 (Mirmiran and Shahawy 1995), using an active confinement model (such as Mander's model) in an iterative-incremental scheme and with different assumed shapes of Poisson's ratio or rate of dilation. Spoelstra and Monti (1999) have developed a different variation of the same technique.

Studies by Naguib and Mirmiran (2002) have shown the significant effect of strain rate on the level of confinement provided by FRP tube or jacket. This could potentially affect the comparison of various confinement tests. Also, recent studies by Mandal et al. (2005) have shown that the confinement effectiveness of FRP jackets is highly dependent on the original unconfined strength of concrete, f_c', and generally, it reduces as f_c' is increased. This effect is usually not accounted for in most of the existing models. Mandal et al. (2005) have proposed a model that accounts for both low and high strength concrete. Several researchers (Picher et al. 1996, Mirmiran et al. 2000) have utilized plasticity models such as Drucker-Prager in finite element analysis to predict the level of confinement in fiber-wrapped concrete or concrete-filled FRP tubes.

Axial Strength of the Member

The strength of the axial member in this case is based on the strength of the confined concrete and can be calculated from the following equation:

$$P_{\max} = A_c f_{cc1}' \quad \text{(for axially loaded concrete core only)} \tag{31.3}$$

$$P_{\max} = A_c f_{cc2}' + A_f \sigma_{fy} \quad \text{(for axially loaded concrete core and shell)} \tag{31.4}$$

where

$P_{\max}$ is the axial load capacity of the member
A_c is the area of the concrete cross section
f_{cc1}' is the strength of confined concrete when the FRP shell is not axially loaded
f_{cc2}' is the strength of confined concrete when the FRP shell is axially loaded
A_f is the area of the FRP shell cross section
σ_{fy} is the compressive stress level in the FRP shell in the axial direction when it fractures

Values of f_{cc1}' and f_{cc2}' can be predicted using the confinement models presented in the "Confinement Models" section.

Axial Members with Rectangular FRP Tubes

Studies have shown that the confinement effect in rectangular sections is insignificant unless the radius of the round corners is large, compared to the size of the column (Mirmiran et al. 1998, Picher et al. 1996). In the absence of reliable information regarding the confinement effects in rectangular sections, it is reasonable to use the unconfined concrete strength f_c' in Equations 31.3 and 31.4 to predict the strength of the column.

Slenderness Effects

Slenderness effect in intermediate and long compression members must be accounted for by considering the additional bending moments resulting from the P-δ effect. In this case, the member is treated as a beam-column element.

SUMMARY OF THE EXPERIMENTAL WORK ON AXIAL MEMBERS

With the development of different FRP manufacturing technologies such as the filament winding techniques, tubular FRP sections of various shapes and laminate structures became available for the construction industry. FRP jackets, other than being much lighter than steel jackets and noncorrosive, provide other advantages from the structural point of view. Its low modulus of elasticity forces concrete to take most of the axial load, therefore, allowing the shell to be utilized more in the hoop direction, which could prevent premature failure due to outward local buckling in the axial direction. Unlike steel jackets, the FRP expansion in the hoop direction under axial load, due to Poisson's ratio effect, can be controlled by carefully selecting the laminate structure, such that its expansion is less than that of concrete at the early stage of loading, which results in eliminating any separation or delay of the confinement process. Finally, the orthotropic laminate structure of FRP shells allows uncoupling of the two fiber orientations for design optimization (Shahawy and Mirmiran 1998).

Attempts for confining concrete with nonmetallic shells started in the late 1970s. In 1978, Kurt suggested using commercially available plastic pipes (PVC or ABS) filled with concrete. Kurt reported that the increase in concrete core compressive strength was 3.25 times the confining pressure. For a slenderness ratio less than 20, failure of such columns was by shear, at 45°. Because the plastic materials were neither very strong nor very stiff, the increase in concrete strength due to confinement was small.

Fardis and Khalili (1981) reported about concrete encased in fiberglass-reinforced plastic, which is believed to be one of the earliest attempts to utilize structural composites for confinement. They pointed out few interesting facts, which are considered fundamentals in FRP-confined concrete behavior:

1. The role of hoop fibers is to confine the concrete, whereas that of axial fibers is to take any tension caused by bending and to improve buckling resistance by increasing the flexural rigidity.
2. The hoop stiffness of the FRP casing controls lateral strains and microcracking in the concrete core.
3. Failure of the system is governed by failure of the shell in the hoop direction.

Although the authors wrapped the cylinders with GFRP cloth impregnated with resin, they proposed casting concrete in filament wound tubes to achieve about 80% fiber volume fraction, rather than 50%, in the composite shell. The study concluded that confinement using FRP jackets resulted in a very high increase in strength and ductility. A 1.9 mm thick GFRP jacket increased both the strength and ductility of the 102 mm diameter concrete cylinder by 5 and 8.5 times, respectively.

In 1997, Mirmiran and Shahawy reported the results of twenty-four 152.5 × 305 mm concrete-filled GFRP tubes and six plain concrete specimens. The average unconfined concrete strength was 30 MPa. Three jacket thicknesses, 1.3, 2.1, and 3.0 mm were considered by using 6, 10, and 14 plies. The shells were filament-wound angle plies of polyester resin and unidirectional E-glass fibers at ± 15° winding angle. Interaction between the jacket and the concrete in the axial direction was prevented. Figure 31.6 shows the stress–strain curves of both the plain and confined concrete with different jacket thicknesses. The behavior indicates significant improvement in strength and ductility. The response consists of three distinct regions. In the first region, behavior is similar to plain concrete, since lateral expansion of the core is insignificant. With the increase of microcracks, a transition zone is observed where the tube exerts a lateral pressure on the core to counteract the stiffness degradation of concrete. Finally, a third region is recognized, where the tube is fully activated and the stiffness is stabilized around a constant rate. The response in this region is mainly dependent on the stiffness of the tube while the ultimate peak strength is dependent on the hoop strength of the shell.

Kanathrana and Lu (1998) and Fam (2000) showed that when FRP pultruded tubes are used as concrete-filled specimens under compression, the tubes would split immediately once the concrete starts to increase in volume at the unconfined concrete strength level due to the lack of stiffness in the hoop direction. They also pointed out the advantages of filament-wound tubes in this regard.

Fam and Rizkalla (2001a) tested eleven concrete-filled FRP tubes and one concrete-filled steel tube. The study included totally and partially filled FRP tubes with central hole. All the stubs had the tubes loaded in the axial direction. The study showed that the larger the size of the inner hole, the lower the confinement effect; however, if the central hole includes an inner FRP tube, the confinement is improved. The study also showed that loading the tube axially reduces the confinement effect.

Comparison of FRP-Confined Concrete and Steel-Confined Concrete

The stress–strain behavior of concrete-filled GFRP tubes is compared to that of concrete-filled steel tubes in Figure 31.4 (Samaan et al. 1998). Because of its high modulus, the steel jacket starts to confine the concrete at low load levels if only loaded in the hoop direction. A small lateral strain in concrete is needed to develop significant hoop stresses and result in a noticeable confining pressure. On the other hand, FRP-confined concrete is insensitive to small lateral expansion; therefore, it behaves very similar to unconfined plain concrete up to a load level near the unconfined strength. This is attributed to the low hoop modulus of FRP, especially GFRP jackets. As the unconfined strength is approached, major microcracking develops and high lateral expansion occurs resulting in activation of the FRP jacket, which induces passive confining pressure, continuously increasing due to the linear characteristics of the FRP. Once the jacket reaches the hoop strength, it ruptures and the concrete fails. This is totally different from the behavior of the steel jacket, which induces a constant confining pressure and develops an active confinement state, independent of the lateral expansion of concrete, once the steel yields.

Another way of comparing steel-confined concrete to FRP-confined concrete is to examine the volumetric strain as well as the dilation behavior (Samaan et al. 1998). For unconfined concrete, the volumetric strain reflects compaction and volume reduction at the beginning, due to bond cracks closure. Poisson's ratio at this stage is constant, 0.15–0.2. At about 0.5 f_c', Poisson's ratio increases due to lateral expansion resulting from initiation of micro cracking, until it reaches 0.5

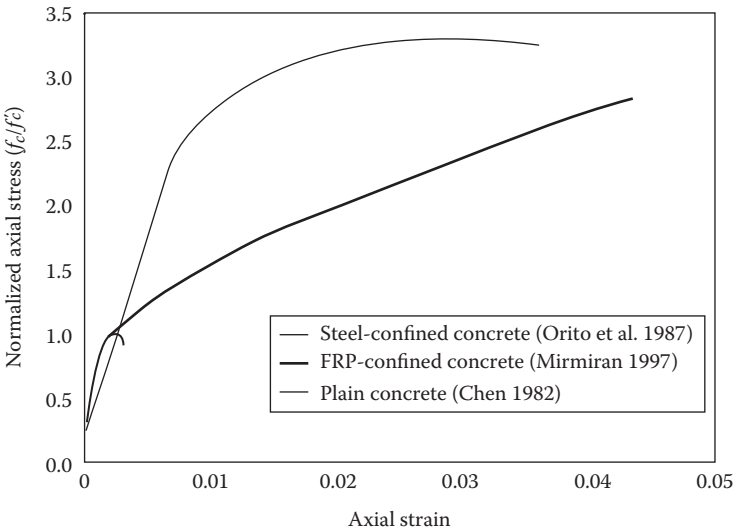

FIGURE 31.4 Stress–strain response of FRP-confined versus steel-confined concrete. (From Samaan, M. et al., *J. Struct. Eng.*, 124(9), 1025, 1998.)

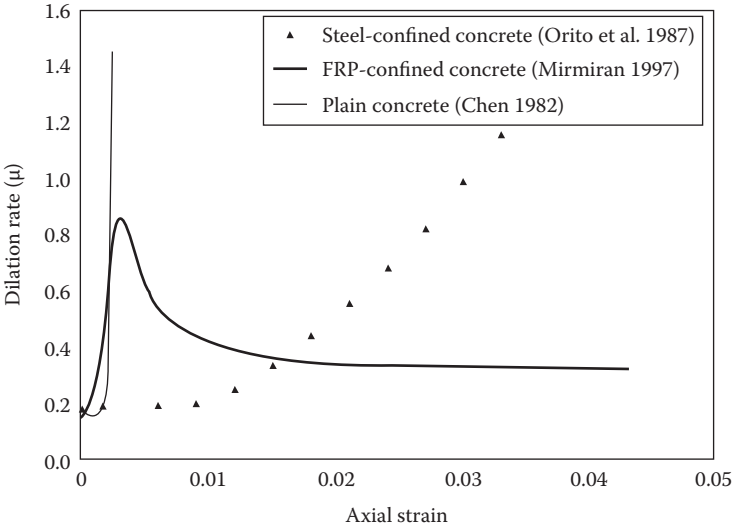

FIGURE 31.5 Dilation curves of FRP-confined concrete versus steel-confined concrete. (From Samaan, M. et al., *J. Struct. Eng.*, 124(9), 1025, 1998.)

at load stage of about 0.9 f_c'. At this point the concrete reached its minimum possible bulk, and starts to increase in volume rapidly, where Poisson's ratio can reach more than 0.7 (Avram et al. 1981). For steel-confined concrete, the steel shell effectively confines the concrete and controls the dilation as long as it is elastic. Once it is yielded, concrete dilation becomes unstable. The dilation rate of FRP-confined concrete, on the other hand, displays a totally different and unique response. Despite some volume expansion beyond the critical stress, the linearly increasing hoop stress of FRP not only reduces the volume expansion and reverses its direction but also reduces its peak value according to the amount and stiffness of the fiber composites. The dilation ratio, μ, represents the rate of change of lateral strain with respect to axial strain. Figure 31.5 shows that all three curves starts at dilation ratio equal the Poisson's ratio of concrete. The dilation response of FRP-confined concrete, even though it behaves similar to unconfined concrete at the beginning, it reaches a peak value, after which it decreases and finally stabilizes. The peak and final dilation ratios both depend on the stiffness of the FRP jacket as shown by Mirmiran and Shahawy (1997).

Effect of Geometry and Configuration of Cross Section

Mirmiran et al. (1998) reported testing of twelve 152.5 × 152.5 × 305 mm concrete-filled GFRP tubes with square cross sections, including round corners with 6.35 mm radius. The tubes were filament-wound E-glass with polyester resin, wound at ± 75° with respect to the vertical axis. Three different wall thicknesses were considered including 1.45, 2.21, and 2.97 mm, using 6, 10, and 14 plies. The average unconfined concrete strength was 40 MPa. Only the concrete core was loaded in axial compression. Figure 31.6 shows the load axial-strain of the square specimens, compared to 152.5 mm diameter circular specimens with the same jacket structure but using 30 MPa concrete. The curves are normalized with respect to the peak strength and corresponding strain of the respective unconfined concrete. Unlike circular sections, the ultimate strength of square sections is lower than their peak strength and stabilizes at about 70% of the peak, unconfined strength, irrespective of the tube thickness. The circular specimens failed by rupture of fibers near midheight in the hoop direction whereas, in square tubes, the specimens failed due to stress concentration at the corners. Similar observations were also reported by Fam et al. (2005).

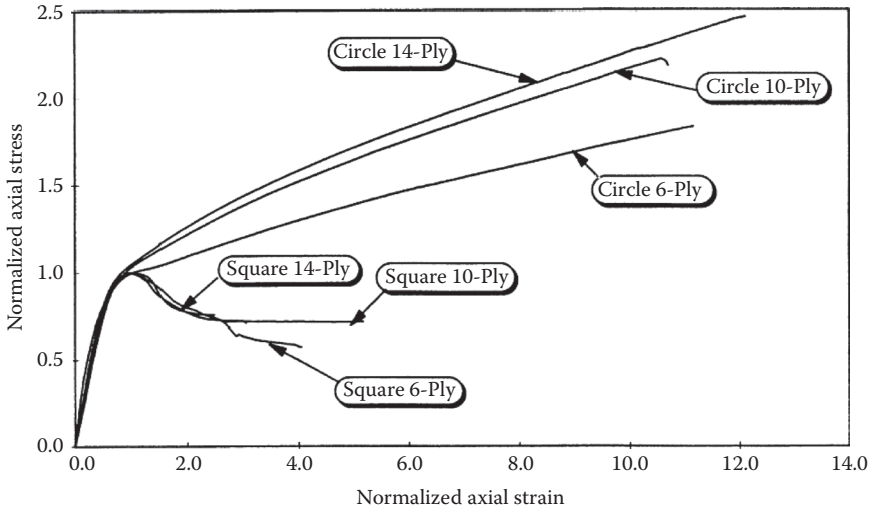

FIGURE 31.6 Normalized stress–strain curves of concrete-filled GFRP circulate and square tubes. (From Mirmiran, A. et al., *J. Compos. Constr.*, ASCE, 2(4), 175, 1998. With permission.)

Picher et al. (1996) reported the results of CFRP-confined 152 × 152 × 500 mm square columns, and 152 × 203 × 500 mm rectangular columns. The specimens included a 5, 25, 38, and 75 mm radius at the corners. Although, the columns were wrapped with CFRP sheets rather than being cast in prefabricated tubes, they showed a similar behavior to that reported by Mirmiran et al. (1998). In all cases, confinement improved the ductility. For the most effective configurations, square specimens strength was increased by up to 20%. The behavior showed an initial slope, which follows the unconfined concrete slope, up to the unconfined strength, and then shows a plastic zone with large ductility. Failure occurs when the sheets fail at or near the corners due to stress concentration. Figure 31.7 shows the effect of the radius at corners on the behavior of specimens having the same number of CFRP layers. Increasing the radius causes the behavior of the square columns to become gradually similar to that of confined cylinders ($D/R = 2$).

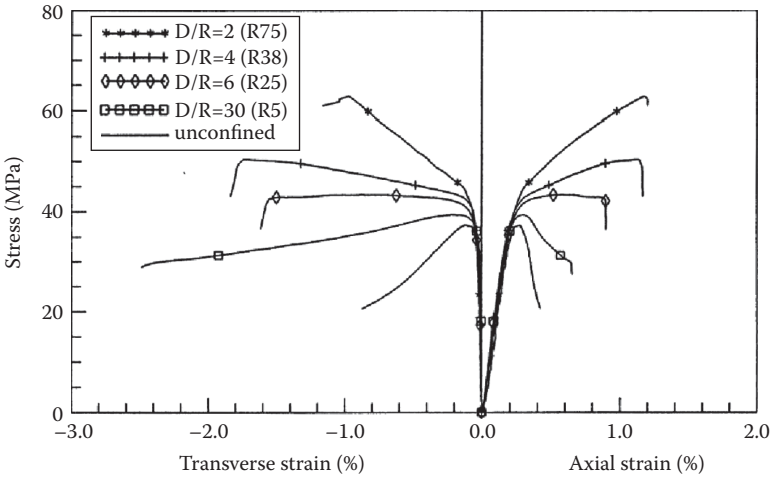

FIGURE 31.7 Effect of corner radius on CFRP-confined square columns. (From Picher, F. et al., Confinement of concrete cylinders with CFRP, *Proceeding of the First International Conference on Composites in Infrastructure* (*ICCI'96*), Tucson, AZ, pp. 829–841, 1996.)

Effect of Slenderness and Eccentricity of Load

Kurt (1978) examined the length effect on concrete-filled plastic (PVC and ABS) tubes under compression. Although the tubes were not FRP materials, but rather plastics, it is considered analogous to a case of low modulus composites. He showed that slenderness effect becomes important when the slenderness ratio is greater than 20.

Mirmiran et al. (1998) tested 24 concrete-filled 152.5 mm diameter cylindrical tubes with three GFRP tube thicknesses of 1.45, 2.21, and 2.97 mm and four different lengths including 305, 457, 610, and 762 mm to provide (*L*/*D*) ratios of 2:1 to 5:1. The unconfined concrete strength was 44.8 MPa. Although some local buckling was observed, shear failure was noted as the primary mode of failure for the tubes. No overall buckling as a result of slenderness was noticeable, as the length effects were insignificant within the range of (*L*/*D*) ratios studied. However, the ultimate strength was somewhat affected by the length. For a 5:1 (*L*/*D*) ratio, the strength was reduced by about 20%.

Recent studies (Mirmiran et al. 2000, Yuan and Mirmiran 2001) have identified a slenderness limit of 11 for concrete-filled FRP tubes, rather than the current limit of 22 set for conventional steel-reinforced concrete columns bent in single curvature with equal end moments. A higher slenderness limit may be expected for concrete-filled aramid FRP tubes. The same study also suggests lowering the stiffness reduction factor in the moment magnification method of ACI 318 for concrete-filled FRP tubes based on the modulus of elasticity of the FRP tube in the axial direction.

Sustained Loading

A recent study by Naguib and Mirmiran (2002) has shown the creep of concrete core in concrete-filled FRP tubes to be much lower than that estimated by the ACI 209 models. This was attributed to sealing of concrete core by the tube, effect of lateral confinement, and most importantly, the stress re-distribution that takes place between concrete and the FRP tube in the axial direction. As the stiffness of the tube increases relative to that of concrete core, a larger stress re-distribution occurs over time, yielding a lower creep coefficient for the concrete core.

Bond Effects

The bond between the FRP jacket and the concrete core can be achieved by using an adhesive such as epoxy, as in case of fiber-wrapped concrete, a series of mechanical shear connectors as in concrete-filled tubes with internal ribs, or by using an expansive agent in the concrete to produce higher friction with the shell as a result of the radial stresses produced from expansion (Figure 31.8).

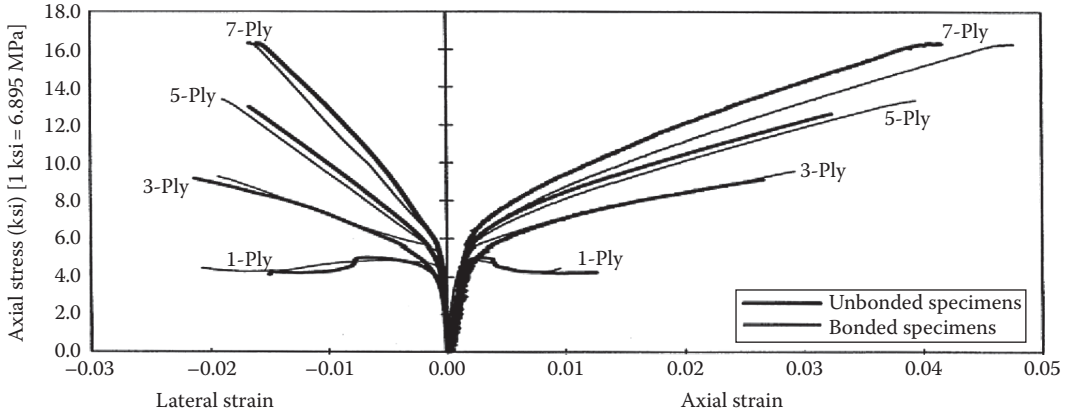

FIGURE 31.8 Effect of bond condition on the response of concrete-filled GFRP tubes with different numbers of layers. (From Mirmiran, A. et al., *J. Compos. Constr.*, ASCE, 2(4), 175, 1998. With permission.)

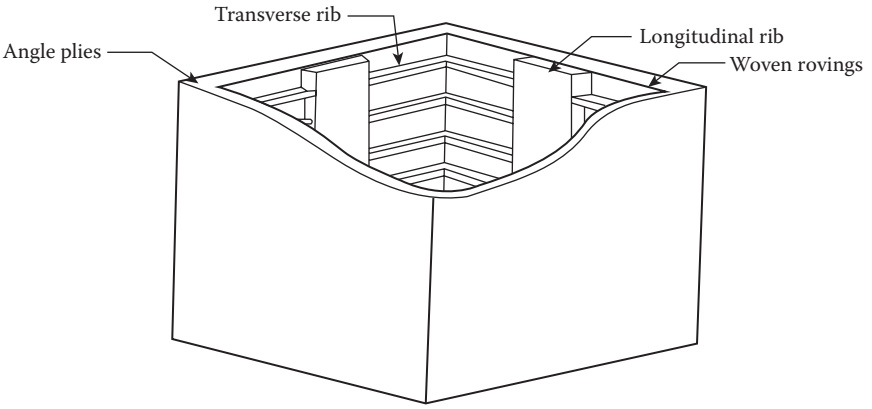

FIGURE 31.9 GFRP tube with shear connector ribs. (From Mirmiran, A. et al., *J. Compos. Constr.*, ASCE, 2(4), 175, 1998. With permission.)

In 1998, Mirmiran et al. introduced a square tube with shear connector ribs in the inner surface of the tube, as shown in Figure 31.9. The 178 × 178 × 305 mm tubes were made using a special collapsible mandrel. The ribs were made using special polyester paste consisting of polyester resin, 1% by volume chopped glass fibers, and 1.5% catalyst. The longitudinal and transverse ribs were 42 and 19 mm wide respectively, and 6.4 mm thick. The tubes consisted of 15 plies of ± 75° E-glass/polyester. The tubes were filled with 18.6 MPa concrete and tested in compression. Although the square tube with the ribs did not achieve the same effectiveness of circular tubes, the ribs helped improve the load-carrying capacity by distributing the confining pressure more effectively around the circumference of the tube, thus minimizing the stress concentrations at the corners. The longitudinal ribs act as stringers and help the tube resist axial and lateral loads. They also divide the shell into small panels, thus increasing the buckling and compressive resistance. Moreover, they help arrest the growth of cracks in the shell by accepting tensile loads that the shell can no longer carry. The horizontal ribs help maintain the cross-sectional shape of the skin, provides end restrains for the longitudinal ribs, and finally acts with the shell in resisting hoop stresses. This study concluded that mechanical bond significantly improves the performance of the section.

REFERENCES

Avram, C., Facaoaru, I., Mirsu, O., Filimon, I., and Tertea, I. (1981) *Concrete Strength and Strains*, Elsevier Scientific Publishing Company, New York.

Becque, J. (2000) Analytical modeling of concrete columns confined by FRP, Master's thesis, The University of Manitoba, Winnipeg, Manitoba, Canada.

Fam, A.Z. (2000) Concrete-filled fiber reinforced polymer tubes for axial and flexural structural members, PhD thesis, The University of Manitoba, Winnipeg, Manitoba, Canada, p. 261.

Fam, A.Z. and Rizkalla, S.H. (2001a) Behavior of axially loaded concrete-filled circular fiber reinforced polymer tubes, *ACI Structural Journal*, 98(3): 280–289.

Fam, A.Z. and Rizkalla, S.H. (2001b) Confinement model for axially loaded concrete confined by FRP tubes, *ACI Structural Journal*, 98(4): 251–461.

Fam, A., Schnerch, D., and Rizkalla, S. (2005) Rectangular filament-wound GFRP tubes filled with concrete under flexural and axial loading: Experimental investigation, *Journal of Composites for Construction*, ASCE, 9(1): 25–33.

Fardis, M.N. and Khalili, H. (1981) Concrete encased in fiberglass-reinforced plastic, *ACI Structural Journal*, 78–38, 440–446.

Harries, K.A., Kestner, J., Pessiki, S., Sause, R., and Ricles, J. (1998) Axial behavior of reinforced concrete columns retrofit with FRPC jackets, *Second International Conference on Composites in Infrastructure*, Tuscon, AZ, pp. 411–425.

Kanatharana, J. and Lu, L.W. (1998) Strength and ductility of concrete columns reinforced by FRP tubes, In: H. Saadatmanesh and M.R. Ehsani, (eds.), *Proceeding of the First International Conference on Composites in Infrastructure ICCI'96*, Tucson, AZ, pp. 370–384.

Kurt, C.E. (1978) Concrete filled structural plastic columns, *Journal of the Structural Division*, 104(ST1): 55–63.

Mandal, S., Hoskin, A., and Fam, A. (2005) Influence of concrete strength on confinement effectiveness of fiber-reinforced polymer circular jackets, *ACI Structural Journal*, 102(3): 383–392.

Mirmiran, A. and Shahawy, M. (1995) A novel FRP-concrete composite construction for the infrastructure, *Proceedings of the ASCE Structures Congress XIII*, Boston, MA, pp. 1663–1666.

Mirmiran, A. and Shahawy, M. (1997) Behavior of concrete columns confined by fiber composites, *Journal of Structural Engineering*, ASCE, 123(5), 583–590.

Mirmiran, A., Shahawy, M., and Beitleman, T. (2001) Slenderness limit for hybrid FRP-concrete columns, *Journal of Composites for Construction*, ASCE, 5(1): 26–34.

Mirmiran, A., Shahawy, M., Samaan, M., El Echary, H., Mastrapa, J.C., and Pico, O. (1998) Effect of column parameters on FRP-confined concrete, *Journal of Composites for Construction*, ASCE, 2(4): 175–185.

Naguib, W. and Mirmiran, A. (2002) Time-dependent behavior of FRP-confined concrete columns, *Structural Journal*, American Concrete Institute (ACI), 99(2): 142–148.

Parent, S. and Labossiere, P, Finite *Element Analysis of Reinforced Concrete Columns Confined with Composite Materials*, Paper, University of Sherbrooke, Quebec, Canada.

Picher, F., Rochette, P., and Labossiere, P. (1996) Confinement of concrete cylinders with CFRP, *Proceeding of the First International Conference on Composites in Infrastructure (ICCI'96)*, Tucson, AZ, pp. 829–841.

Saafi, M., Toutanji, H., and Li, Z. (1999) Behavior of concrete columns confined with fiber reinforced polymer tubes, *ACI Materials Journal*, 96(4): 500–509.

Samaan, M., Mirmiran, A., and Shahawy, M. (1998) Model of concrete confined by fiber composites, *Journal of Structural Engineering*, 124(9): 1025–1032.

Shahawy, M. and Mirmiran, A. (1998) Hybrid FRP-Concrete Beam-Columns, *Proceeding of ICCE/5 Fifth International Conference on Composites Engineering*, Las Vegas, NV, July 5–11, pp. 619–620.

Spoelstra, M. and Monti, G. (1999) FRP-confined concrete model, *Journal of Composites for Construction,* ASCE, 3(3): 143–150.

Toutanji, H. (1999) Stress-strain characteristics of concrete columns externally confined with advanced fiber composite sheets, *ACI Materials Journal*, 96(3): 397–404.

Yuan, W. and Mirmiran, A. (2001) Buckling analysis of concrete-filled FRP tubes, *International Journal of Structural Stability and Dynamics*, World Scientific, 1(3): 367–383.

32 Flexural and Axial/Flexural Hybrid Members

Amir Fam and Amir Mirmiran

CONTENTS

GENERAL

Hybrid structural members, including concrete-filled FRP tubular sections, have great potential for beam and beam-column applications. Although the beneficial effects of confinement of concrete are significantly reduced in bending as compared to axially loaded members, other advantages such as utilization of the FRP shells as stay-in-place formwork, ease of fabrication, and speed of erection still make this system attractive. All the configurations shown in Figure 28.2 can be utilized in flexural members. In principle, the rule of the concrete is to resist the compressive stresses, while the FRP component is to resist the tensile stresses. However, in thin FRP-closed sections, the concrete has another important rule, mainly supporting the FRP shell in the compression side to avoid premature local buckling failure. In fact, this function of the concrete core gives the concrete-filled FRP tubular sections a major advantage over the hollow FRP ones, as indicated from a study by Fam and Rizkalla (2002). For example, the flexural strength of a filament wound FRP tube was increased by 212% by filling the tube with concrete. The same study has also shown that the higher the stiffness or the thickness-to-diameter ratio of the tube, the lower the gain in flexural strength and stiffness, resulting from concrete filling.

The following sections cover the different aspects of the behavior of hybrid FRP/concrete members as beams and beam-column members, including design considerations and structural behavior.

DESIGN CONSIDERATIONS

For flexural analysis, the fundamental principles include equilibrium of forces on the cross section, compatibility of strains, and constitutive behavior of the materials. Regardless of the cross-sectional configuration, the same fundamental design philosophy is applied. Design and analysis of flexural members, including concrete-filled round FRP tubes, except for prestressed members, can be reasonably based on the unconfined concrete strength f_c', as will be discussed in the "Confinement Effect in Bending" section. Figure 32.1 summarizes the flexural analysis for a case of concrete-filled FRP tube. Ultimate moment capacity of the section can be estimated by allowing the constituent materials to reach their ultimate strength. This includes the FRP shell in tension, FRP shell in compression, whichever reaches its ultimate strength first. In the case of concrete-filled FRP tubes, normally tension failures are governing; where the shell ruptures in the tension side, however, it could be possible to achieve compression failure in tubes with thicker or stiffer shells (Burgueno et al. 1998, Mirmiran et al. 1999). Due to the partial confinement in the compression zone, the ductility of concrete is improved and compression failure is likely to occur in the tube before crushing of concrete. The procedure described in Figure 32.1 can also be applied for other configurations, including rectangular cross sections. The equilibrium and strain compatibility method can be applied through the layer-by-layer method, which is suited for complicated geometry, and also allows using realistic functions for the compressive stress distribution in the compression zone (Fam 2000). It should also be noted that complete bond between the FRP and concrete is essential in order to use this method of analysis.

Fam and Rizkalla (2002) have shown that the flexural strength and stiffness of concrete-filled FRP tubes are governed not only by the reinforcement ratio but also by the laminate structure of the tube. The reinforcement ratio is defined by the ratio of the cross-sectional area of the tube to that of the concrete core. For large diameter D-to-thickness t ratios, the reinforcement ratio ρ can be approximated as follows:

$$\rho = \frac{4t}{D} \tag{32.1}$$

Figure 32.2 shows the variation of the flexural strength with the reinforcement ratio ρ. The graph was established using the strain compatibility approach, described in Figure 32.1. The variation is given for four different laminate structures of the FRP tube, which has fibers oriented in the axial and hoop directions with various proportions designated as (1:3), (1:1), (3:1), and (9:1). A (1:3) laminate indicates that 25% of the fibers oriented in the axial direction and 75% in the hoop direction. For a given laminate structure, increasing the wall thickness could change the failure mode from tension to compression. Similarly, for a given wall thickness (or reinforcement ratio), changing the laminate structure by increasing the stiffness in the axial direction could change the failure mode from tension to compression. Figure 32.2 also shows that the balanced reinforcement ratio, which results in failure of the tube in tension and compression simultaneously, is dependent on the

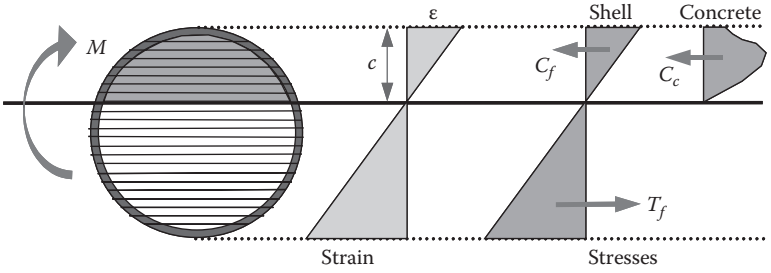

FIGURE 32.1 Flexural analysis of concrete-filled FRP tube.

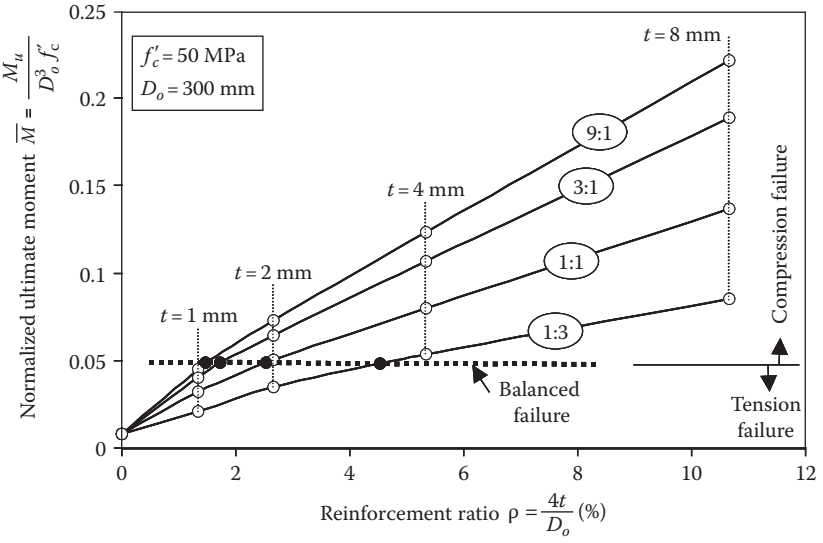

FIGURE 32.2 Variation of the flexural strength with reinforcement ratio for concrete-filled FRP circular. (From Fam, A.Z. and Rizkalla, S.H., *ASCE Journal of Composites for Construction*, 6, 2, 123–132, 2002.)

laminate structure of the tube. Generally, the balanced reinforcement ratio is reduced as the tube becomes stiffer in the axial direction.

In the presence of axial compressive loads in addition to bending moments, the same fundamental principles, including equilibrium of forces on the cross section, compatibility of strains, and constitutive behavior of the materials, still apply for the design or analysis of these sections. However, there are two main differences in this case as compared to flexural members: the additional external axial compression load, which would be included in the equilibrium of forces, and the more significant effect of confinement on the constitutive relationship of concrete in round FRP tubes.

Constitutive Behavior and Material Properties

For the FRP component, the linear stress–strain relationship in both tension and compression can be used. The ultimate tensile and compressive strength as well as the elastic modulus are obtained for the given laminate structure in the longitudinal direction using the classical lamination theory.

For concrete in compression, the layer-by-layer approach facilitates using sophisticated nonlinear functions for the stress distribution such as parabolic, trapezoidal, or other polynomials; however, the equivalent stress block can also be used with the appropriate parameters, according to the geometry of the compression zone. In the case of axial/flexural round members, the stress–strain curve of the confined concrete can be used due to the significant confinement effects in this case. This is attributed to the additional axial load, which shifts the neutral axis toward the tension side. In this case, a large part of the concrete section is under compression and the confinement effect is significant. The stress–strain response of the confined concrete can be obtained analytically using the models described in the "Confinement Models" section in Chapter 31. The axial compression-bending moment interaction diagram can be established for a given section using equilibrium, strain compatibility, and material constitutive relationships and can be used for design purposes. Figure 32.3 shows the effect of ignoring the confinement effects on the predicted interaction diagram of concrete-filled FRP circular tube. Large errors could be encountered with the predicted axial strength, whereas almost no error on the predicted pure flexural strength if confinement effects are ignored.

For the concrete in tension, the tension-stiffening effects can be ignored when calculating the ultimate flexural strength; however, in serviceability analysis and deflection calculations, the tension stiffening could be significant. Fam (2000) has shown that the constitutive relationship proposed by

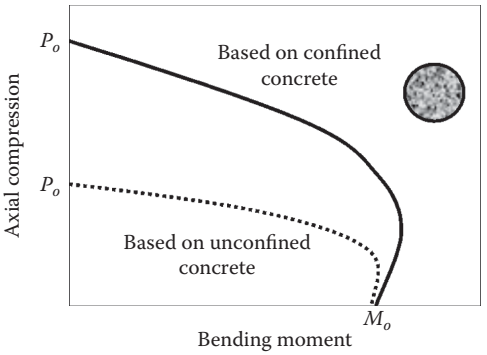

FIGURE 32.3 Effect of ignoring the confinement of concrete on the predicted interaction diagram.

Collins and Mitchell (1997), given in Equation 32.1, can be used for concrete-filled FRP tubes with a bond factor α_1 of 0.3 for smooth tubes. However, this factor is highly dependent on the nature of the inner surface of the tube. The function in Equation 32.1 can be approximately integrated with the area of concrete in tension. More research is needed to study the behavior of concrete in tension in concrete-filled FRP tubes:

$$f_c = \frac{\alpha_1 \alpha_2 f_{cr}}{1 + \sqrt{500\,\varepsilon_{cf}}} \tag{32.2}$$

where

f_c is the tensile stress level
f_{cr} is the cracking strength of concrete
α_2 is the loading factor, 1.0 for short-term monotonic loading and 0.7 for sustained or repeated loading
ε_{cf} is the tensile strain level after cracking

Confinement Effect in Bending

Concrete confinement in noncircular-closed FRP shells such as rectangular tubes is insignificant even under pure compression. In fact, even in the case of round FRP tubes filled with concrete and subjected to pure bending, experimental and analytical studies (Fam 2000) have shown that the effect of confinement of concrete in the compression zone is insignificant, especially in the case of tension failure, for several reasons:

1. By comparing the axial strain versus the lateral strain behavior of the FRP tube in the compression zone of a beam to that of an identical FRP tube confining a concrete core under axial compression, as shown in Figure 32.4a, we see that the behavior is bilinear for axial members, which indicates a significant increase in lateral strains due to confinement. On the other hand, lateral strains in the beam increase at a constant rate, which represents more or less Poisson's ratio of the tube.
2. The compression zone of the section is relatively small and the strain profile is also linear, as compared to the uniform distribution in columns.
3. Failure normally takes place in the tension side, for tubes with moderate stiffness and wall thickness, by rupture of the tube before the full stress–strain curve of concrete is developed in the compression side. At this point, the additional part of the stress block, resulting from any possible confinement, is relatively small and is integrated over a much smaller part of the compression zone, as shown in Figure 32.4b and c.

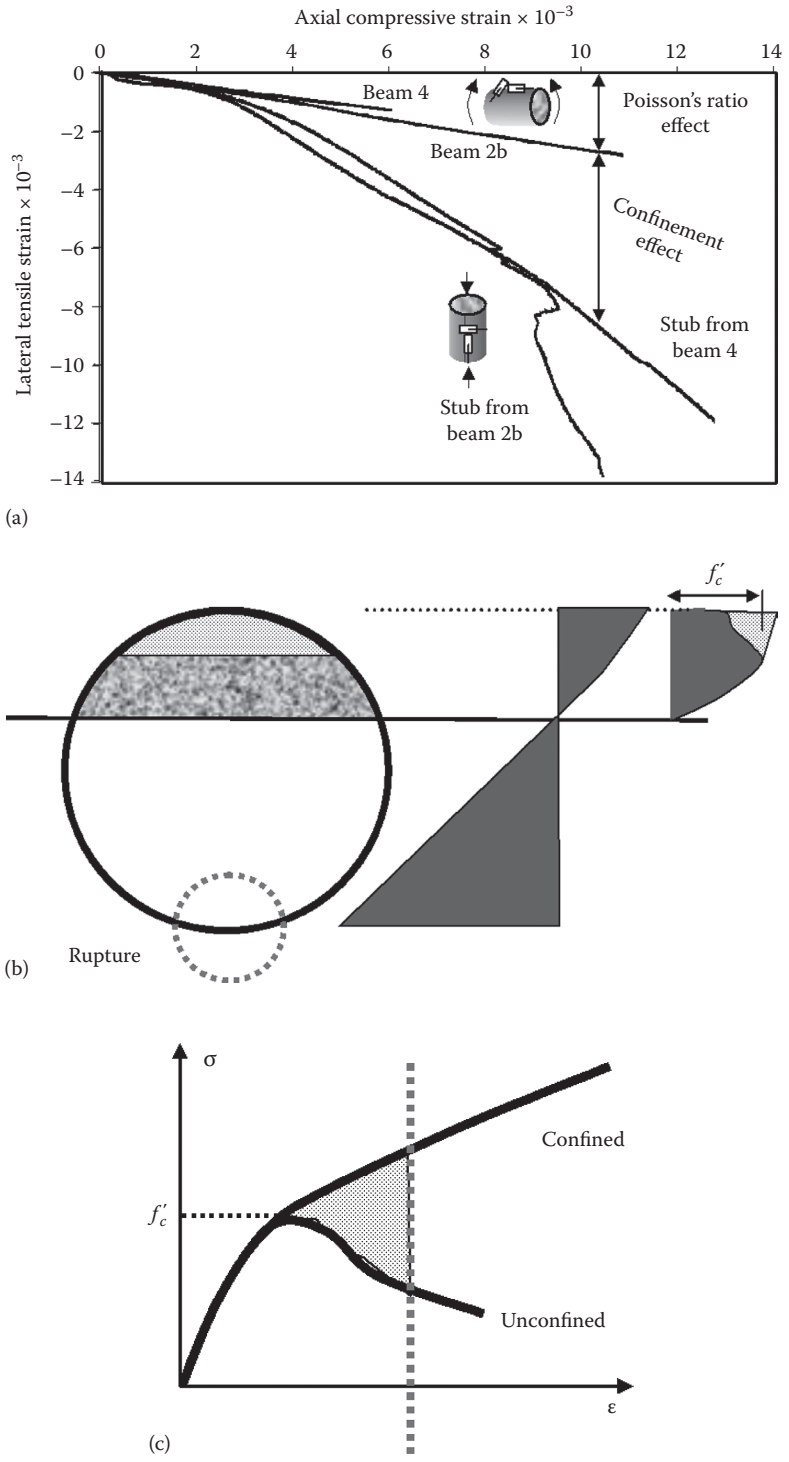

FIGURE 32.4 Insignificant confinement effects on bending: (a) variation of lateral tensile strain with axial compressive strain in tube, (b) compression zone strains and stresses in concrete-filled tube using unconfined and confined concrete models, and (c) unconfined and confined concrete stress–strain curves. (From Fam, A.Z., Concrete-filled fiber reinforced polymer tubes for axial and flexural structural members, PhD. thesis, University of Manitoba, Winnipeg, Manitoba, Canada, p. 261, 2000.)

Bond between FRP and Concrete

The key to the efficiency of hybrid FRP/concrete systems in flexure is to ensure a composite section behavior. The FRP component should be fully bonded to the concrete and slip should be avoided. This can be achieved by mechanical interlock between deformed FRP surface and concrete. In the case of smooth FRP tubes, it has been shown that bond can be enhanced by creating a rough surface. This can be achieved by applying epoxy coating and a layer of coarse silica sand to the inner surface (Fam 2000). Other different methods such as adhesive bond can also be used. The use of expansive concrete also enhances the bond. More research is still needed in the area of bond in hybrid systems and a simple, yet more effective and cost-efficient technique needs to be developed.

Cracking Strength

The cracking moment of the flexural member can be calculated based on the cracking strength of concrete given by the ACI code. However, in the case of concrete-filled FRP round tubes using concrete with shrinkage-reducing admixtures, it has been observed that this method would underestimate the cracking moment (Fam and Rizkalla 2002). This is attributed to the confinement effects due to the expansion of concrete, which results in a state of "chemical prestressing" of the concrete.

Optimization of Flexural Members

When the section is subjected to pure bending, the amount of concrete in the cross section can be optimized in order to reduce the self-weight of the member. Figure 32.5a shows the load-deflection behavior of GFRP tube totally and partially filled with concrete and tested in bending (Fam and Rizkalla 2002). Figure 32.5a indicates that the self-weight of the member can be significantly reduced with insignificant reduction in strength and stiffness. It was also observed that the neutral axis depth is stable during the loading history. This phenomenon can be utilized in optimization, as shown in Figure 32.5b, where the compression zone depth can be estimated from analysis based on totally filled tube and a voided core can be provided, such that its size is limited by the depth of the compression zone. The same concept can be also applied for rectangular sections (Triantafillou and Meier 1992, Canning et al. 1999).

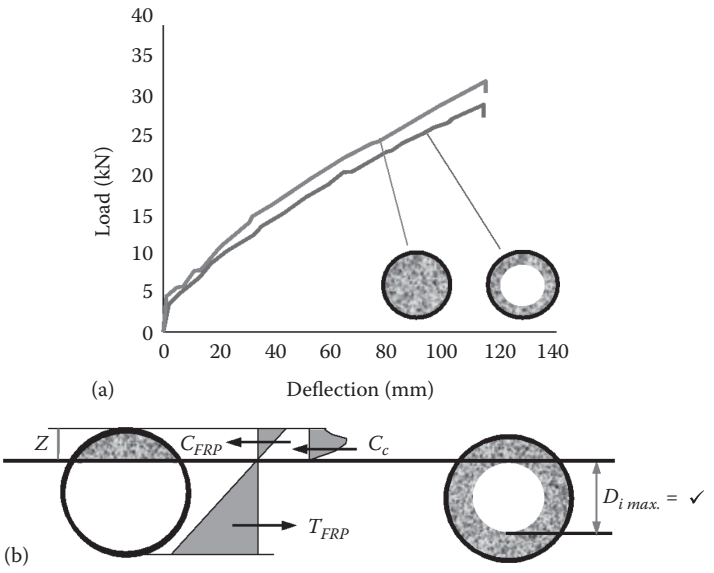

FIGURE 32.5 Optimization of cross section of flexural members: (a) load deflection responses and (b) stress and strain distribution over the cross-section of totally and partially filled tubes. (From Fam, A.Z., Concrete-filled fiber reinforced polymer tubes for axial and flexural structural members, PhD thesis, University of Manitoba, Winnipeg, Manitoba, Canada, p. 261, 2000.)

Prestressed Elements

Super prestressing refers to the prestressed-confined concrete (Parvathaneni et al. 1996). Taking advantage of the higher strength of confined concrete, the prestressing level could be increased to a higher level compared to that used for conventional unconfined concrete. In this case, the additional axial compressive stress acting on the shell due to the prestressing should be accounted for in the design of the shell. Mirmiran et al. (1999) have evaluated the effect of longitudinal prestressing of concrete-filled FRP tubes on their stiffness and strength. Two benefits may be recognized by prestressing concrete-filled FRP tubes: (1) improving stiffness and, therefore, serviceability of the system and (2) incorporating the prestress as a redundant system for the external reinforcement. Mandal (2004) has tested large-scale (326 mm diameter) pretensioned and post-tensioned concrete-filled FRP tubes in flexure and compared their behavior to a conventional prestressed member with spiral steel reinforcement. The study pointed out the superior performance of the FRP tubes compared to the steel spiral as it confines more concrete area and contributes strength and stiffness in the longitudinal direction. The study also showed that modeling the flexural behavior using unconfined concrete model will grossly underestimate the strength as the concrete appears to have very high level of confinement as a result of prestressing.

Hysteretic Behavior of Concrete-Filled FRP Tubes

A number of research investigations have focused on studying the performance of concrete-filled FRP tubes under cyclic loading. The studies can be divided into three areas:

1. Effect of cyclic loading and unloading on the FRP-confined concrete: This study is being carried out by Shao and Mirmiran at the North Carolina State University to develop the complete model for FRP-confined concrete under unloading and reloading. A parallel study is being carried out by Chen and coworkers at Tsinghua University and the Ministry of Building Construction in China.
2. Seismic behavior of concrete-filled tubes with or without internal reinforcement at the member level: This study is being carried out by Shao and Mirmiran at the North Carolina State University on a number of specimens under constant axial load and cyclic lateral load in a four-point bending test.
3. Seismic behavior of concrete-filled tubes with or without internal reinforcement at connection level: Yamakawa et al. (1999) have tested carbon and aramid FRP tubes with internal steel reinforcement under cyclic lateral loads. Seible et al. (1998) have tested carbon shells with or without mild steel reinforcement inside the tube. The focus was again at the connection with the footing. Fan et al. (2000) at the Tongji University in China have reported a ductility of 10 for concrete-filled FRP tubes with internal mild steel reinforcement. Currently, Shao and Mirmiran at the North Carolina State University are working on the modeling and testing of low-cycle fatigue of concrete-filled FRP tubes at the connection with the footing.

Sustained Loading

Recent experimental and analytical investigations by Naguib and Mirmiran (2001) have shown that creep effects reduce the flexural stiffness of concrete-filled FRP tubes. However, ultimate strength is not significantly altered. Slow rate of loading and short-term creep at 70% of static capacity may cause premature rupture of the tube. Fiber analysis of CFFT beam columns by discretizing the section into filled and hollow FRP tubes can adequately simulate the flexural creep behavior. Isochronous sustained stress–creep strain curves may be used as constitutive nonlinear relationship for creep analysis in flexure. Creep deflection of beam columns is much less than that of beams mainly because

axial compressive loads tend to retard cracking of concrete and tensile creep of FRP tube. The stiffness ratio of FRP tube with respect to concrete core has a pronounced effect on creep deflection of concrete-filled FRP beam columns. As the stiffness ratio increases, creep deflections decrease. However, there exists a threshold beyond which stiffer tubes do not provide additional benefit.

SUMMARY OF EXPERIMENTAL WORK ON AXIAL/FLEXURAL MEMBERS

The following sections provide a summary of the different experimental programs related to the behavior of beams and beam-column members. The main applications were intended for bridge columns and girder as well as for piles.

Concrete-Filled FRP Tubular Sections for Bridge Girders and Piers

In 1996, Seible introduced the concrete-filled carbon shell concept for new bridge systems, in which a filament wound CFRP shell is filled with lightweight concrete and used as a girder or a column. The shell is envisioned to replace the reinforcing steel and formwork, provide better seismic response, more durability, and greater speed of erection. Two different criteria were adopted for bridge columns, as shown in Figure 32.6: the ductile design concept with steel starter bars at foundation level, and the strength design concept with the shell extended into foundation, in which the response is essentially elastic. In the first system, it was verified that short development lengths of the bars are required due to the high confinement. In the second system, the behavior was linear elastic up to failure, which occurred at only 52% of the column capacity due to stress concentration at the footing level. The observed excellent response of those columns led to the development of complete bridge systems. Figure 32.7a shows the dual-tied arch bridge, which is proposed to cover a 61 m span. The arch comprises concrete-filled CFRP segments, the tie girder consists of post-tensioned concrete-filled CFRP tube, and the cross beams are CFRP tubes placed in a link-and-log system over the beams with only the joints being concrete-filled. Figure 5.7b shows an alternative system utilizing a carbon shell space truss with post-tensioned truss members.

In 1998, Seible et al. also proposed using the carbon shell system for short and medium span girder bridges, as shown in Figure 32.8. Conventional RC or new FRP decks are connected to the girders through rebars or special FRP dowel connections (Zhao et al. 1997). The CFRP shells are round or square filament wound with hoop (90°) and longitudinal (±10°) fibers. A special mandrel is used to produce helical ribs on the inside of the shell for better bond with concrete. The typical span-to-depth ratio in this system is 17–20, including the 150 mm deck, and higher ratios can be achieved with post-tensioning or continuous girder action (Seible 1996). Studies by Seible et al. (1997), Burgueno et al. (1998), and Davol et al. (2001) have shown that the design is stiffness driven with the material strength not fully utilized, and an optimal diameter to thickness ratio can be found to satisfy a span length requirement. Also different lamination architectures of the tube can modify the performance of the complete system. A series of four beam tests using four-point loads were performed on concrete-filled CFRP tubes including both circular sections and square sections with corner radius equal to 1/3 the depth. The capacity of the square tube was 25% higher than that of the circular one, while the stiffness was 50% higher. It should be noted however that a square section has a larger concrete and CFRP cross-sectional areas compared to a round section of the same size. The beam with thicker wall failed in compression. Full-scale testing (Karbahri et al. 1998) was also conducted on the carbon shell system, including full-scale beam–slab assemblies. At 3.3 times the service load, degradation was gradually observed as the beam–slab interface slipped. The stiffness and moment capacity of the beam–slab unit were increased compared to the single girder. Also the strains along the compression side were reduced; therefore, the compression failure mode of the single girder was not expected in the beam–slab system unless the system becomes uncoupled.

The carbon shell system was also proposed by Seible (1998) for pedestrian bridges. The Scripps Crossing bridge at LaJolla, California, was used to demonstrate the new concepts. The adopted

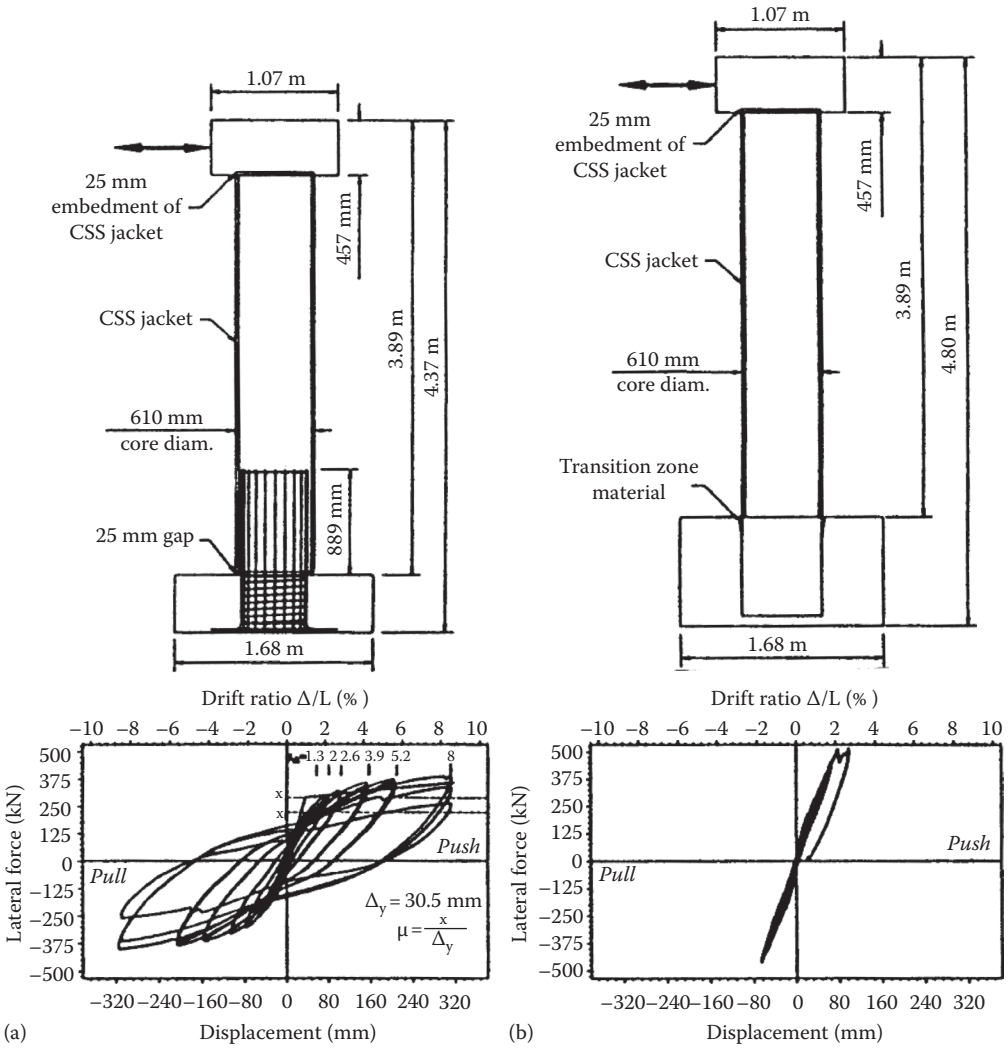

FIGURE 32.6 Carbon shell column systems. (a) Ductile design concept. (b) Strength design concept. (From Seible, F., Advanced composites materials for bridges in the 21st century, *Proceedings of the Advanced Composite Materials in Bridges and Structures*, Montreal, Quebec, Canada, pp. 17–30, 1996.)

design solution consists of a cable-stayed 42.3 m long bridge with a single eccentric 18.3 m long pylon and a slender super structure. Figure 32.9a shows the conventional design of the super structure. Subsequent to the completion of the bridge, alternative designs were developed. The cross-sectional geometry of the conventional design was almost preserved by utilizing the carbon shell system for the exterior girders with a GFRP bridge deck spanning between the longitudinal girders, as shown in Figure 32.9b, or concrete deck, as shown in Figure 32.9c. Cable stays can be anchored to the carbon shell girders. While the stiffness of all three super structures is almost identical, weight savings of the FRP superstructure with GFRP deck resulted in factors of 2–3 compared to the concrete super structure. For a single cable plane and wider cable spacing, the use of a central larger carbon shell and precast concrete deck was also investigated, as shown in Figure 32.9d. Although the study demonstrated the advantages of weight reduction using FRP bridge design (ratio of dead-to-live loads of 1.0 compared to 2.3 for conventional design), it also pointed out that other design aspects such as the aerodynamic stability and vibrations under live load become more critical and need to be addressed. The study also concluded that, generally, it is difficult for the FRP bridge

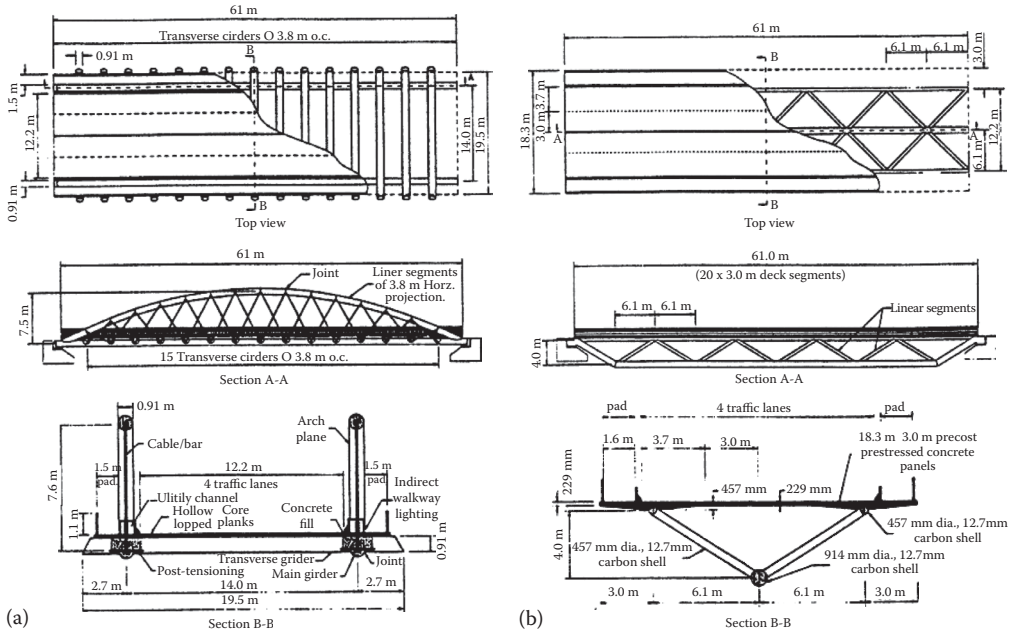

FIGURE 32.7 Carbon shell bridge systems. (a) Shallow dual tied arch. (b) Space truss. (From Seible, F., Advanced composites materials for bridges in the 21st century, *Proceedings of the Advanced Composite Materials in Bridges and Structures*, Montreal, Quebec, Canada, pp. 17–30, 1996.)

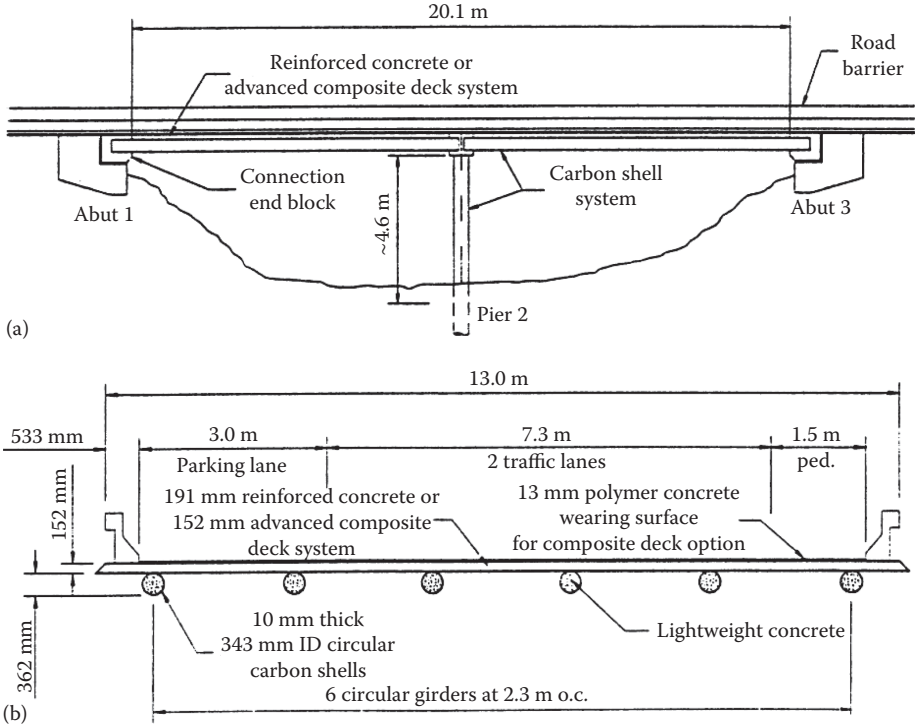

FIGURE 32.8 Carbon shell girder-type bridge system. (a) Longitudinal section. (b) Transverse section. (From Seible, F. et al., Design issues with carbon fiber composite reinforced concrete structures, *Proceedings of the Third International Symposium, Non-Metallic (FRP) Reinforcement for Concrete Structures*, Vol. 2, Sapporo, Japan, October, pp. 89–112, 1997.)

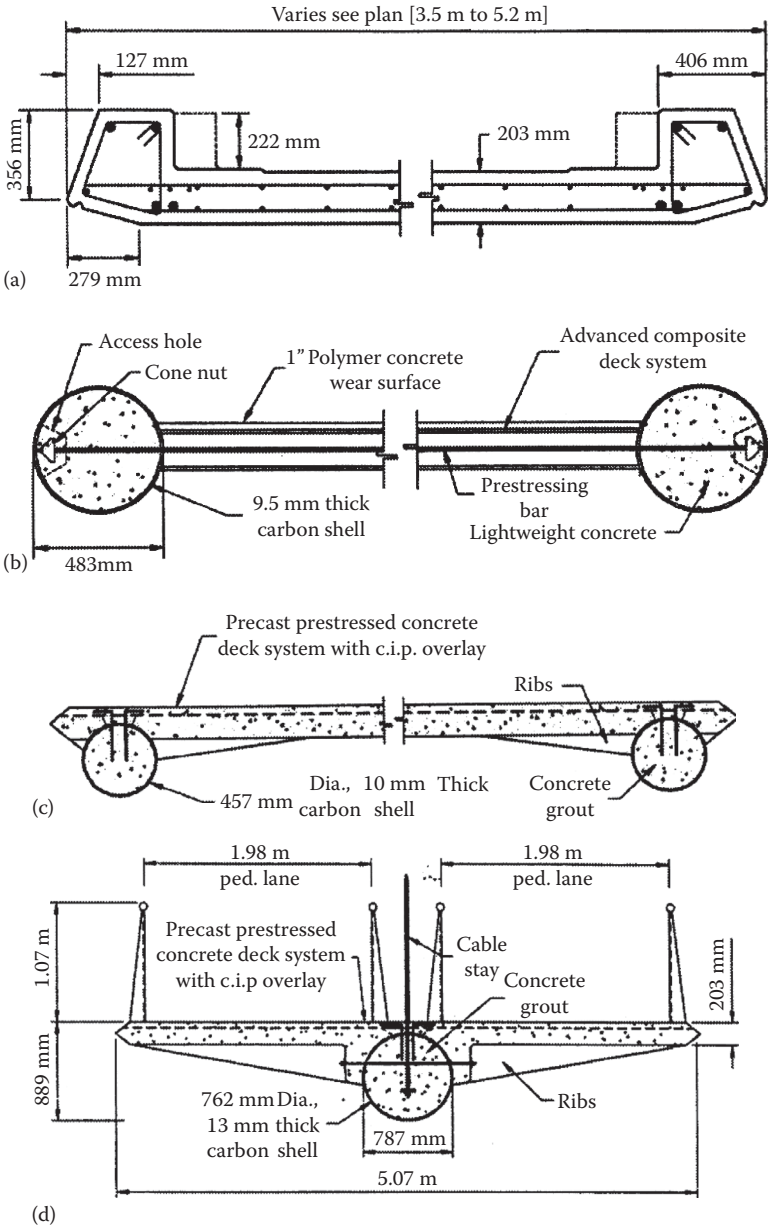

FIGURE 32.9 Proposed systems for pedestrian bridges super structure utilizing carbon shell concept. (a) Conventional ("as built") design. (b) Advanced composite design alternate. (c) Hybrid design alternate. (d) Single cable plane carbon shell concept. (From Seible, F., Innovative designs for pedestrian bridges, *Proceedings of the Developments in Short and Medium Span Bridge Engineering '98*, Calgary, Alberta, Canada, 1998.)

design system to compete with conventional designs; however, hybrid solutions, which utilize conventional concrete decks with carbon shell girders, provide cost-competitive solutions.

Concrete-Filled FRP Tubular Sections for Piles

In 1999, Mirmiran and Shahawy investigated the behavior of a 13.7 in. diameter over-reinforced and a 14.5 in. diameter under-reinforced concrete-filled FRP tubes. The motivation was to develop a new piling system for the Florida DOT, which has sponsored a detailed study since 1994.

It is believed that the FRP tubes protect the concrete core and alleviate the problems of moisture intrusion and permeability of concrete. The wall thicknesses of the FRP tubes were 0.5 and 0.26 in. for the over- and under-reinforced concrete-filled FRP tubes, respectively. The tubes were tested under increasing bending and fixed axial loads ranging from 0 to 600 kip. The moment-curvature response was bilinear for the two types of specimens, with the transition point between the two slopes corresponding to major cracking of concrete. While the first slope is approximately the same for both types, the second slope is considerably larger for the over-reinforced specimen. The ultimate deflections of the over-reinforced specimens were about 0.5–0.75 those of the under-reinforced specimens, whereas their strengths were 1.25–4 times higher. The effect of secondary moments was less for the over-reinforced sections (Shahawy and Mirmiran 1998).

Fam and Rizkalla (2002) conducted a large experimental program to study the flexural behavior of hollow and concrete-filled FRP tubes. The study included tubes ranging from 89 to 942 mm in diameter and the span of the beams ranged from 1.07 to 10.4 m. The study investigated the effect of concrete filling, different configurations including tubes with central hole inside the concrete core to reduce the self-weight, and tubes with different laminate structures. Figure 32.10 shows the test setup of different size beams. The study concluded that concrete filling provides internal support to the tube, preventing local buckling, and also contributes to the internal forces, which increases the strength and stiffness. The study showed that the load-deflection behavior of such beams is almost bilinear, with the cracking load significantly small compared to the ultimate load. The stiffness after cracking is governed by the laminate structure as well as the diameter-to-thickness ratio of the tube. The study proved that filament-wound tubes are superior to pultruded ones, which failed prematurely by horizontal shear. Higher flexural strength-to-weight ratio was achieved by providing central hole inside the tube. The study has demonstrated that slip could occur between the concrete core and the tube and could reduce the strength and stiffness. Finally, the analytical phase of the study has demonstrated that the balanced reinforcement ratio of concrete-filled FRP tubes is dependent on

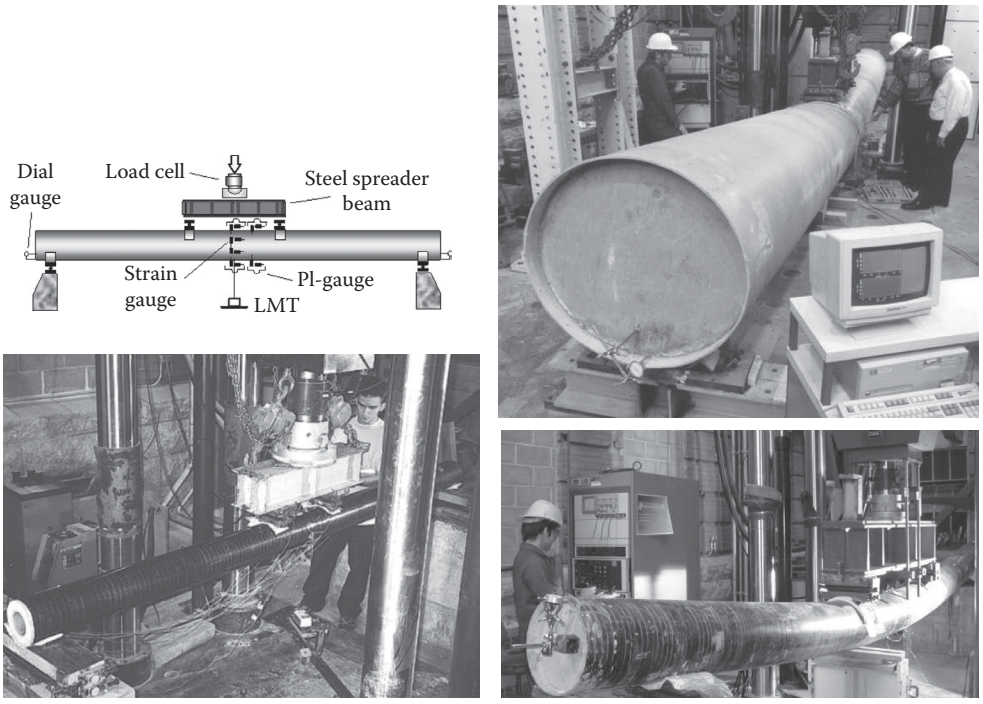

FIGURE 32.10 Test setup of concrete-filled FRP tubes as beams. (From Fam, A.Z., Concrete-filled fiber reinforced polymer tubes for axial and flexural structural members, PhD. thesis, University of Manitoba, Winnipeg, Manitoba, Canada, p. 261, 2000.)

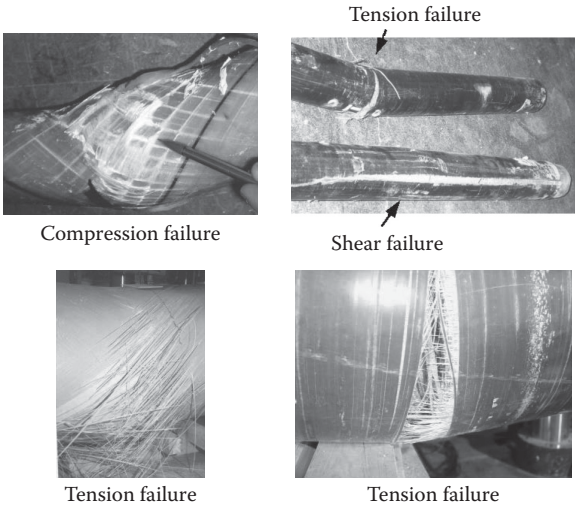

FIGURE 32.11 Failure modes of test beams. (From Fam, A.Z. and Rizkalla, S.H., *ASCE Journal of Composites for Construction*, 6, 2, 123–132, 2002.)

the laminate structure of the tube and generally is smaller for tubes with higher stiffness in the axial direction. Figure 32.11 shows the failure mode of beams failing in tension, compression, and shear.

Splices and Joints Involved in Concrete-Filled FRP Tubes

Different types of connections are involved with the hybrid structural systems. There are splices within the hybrid member itself due to the limited lengths that can be manufactured. In 1996, Parvathaneni and Iyer produced a 13.72 m pile using concrete-filled GFRP tubes. Three 4.57 m long filament-wound tubes were spliced using short steel tubing, 0.6 m long, which matched with the inside of the GFRP tubes. Concrete was then cast into the spliced tube.

There are also ductile connections within the hybrid member intended to provide plastic failure. The concrete-filled carbon shell bridge columns, shown in Figure 32.5a, can be connected to the foundation through short steel starter bars to produce more ductility as compared to carbon shells fixed into the foundation, which gives higher strength but less ductility (Seible et al. 1998). For girder-type bridges, it is proposed that the midspan section and the sections over the columns could be designed for full strength, whereas plastic hinges can be designed some distance away from the self-weight inflection points. Under overloads, an increase in moment will result in a hinge formation and a ductile system response. Since cracking may be concentrated in the joint and ordinary steel reinforcement could corrode, it is desired to develop a pseudo-ductile system with FRP rebars as connectors. Since FRP does not experience yielding like steel, ductility can only be achieved by other mechanisms such as slippage between the concrete and the rebars. However, the achieved ductility is only in one direction and the deformation and damage cannot be reversed, thus cyclic ductility demand for earthquake regions cannot be satisfied. Their anchorage lengths are chosen such that slippage occurs before they rupture (Wernli and Seible 1998). Special preparation is first done to the ends of the bars including sand blasting followed by painting with epoxy and dipping in sand. In addition, the rods at the ends can also have longitudinal cuts and splayed apart. The concept was investigated on a full-scale concrete-filled CFRP tube. 40 CFRP rods, 1.1 m long, were used at the connection and were arranged evenly in a circle. At both ends, the rods had at least 400 mm sanded, cut, and splayed with eight 200 mm long legs. The tube was tested in four-point bending. Numerical analysis accounting for the bond-slip behavior of the rods showed a ductile behavior. The initial stiffness of the moment-deflection response is slightly less than that of the tube and gradually decreases till the first rods start to slip entirely, resulting in the expected ductile

response. It was also proposed that any slip should be avoided during design service loads and that the mechanism should only be utilized for redistribution of loads before failure.

There are also connections between the hybrid element and other structural components such as deck slabs or columns. Connections between carbon shell girder and GFRP deck as well as two carbon shell girders over a column were developed by Seible et al. (1998). Zhao et al. (1997) showed that the dowel-type joint between carbon shell and composite deck using polymer concrete anchorage for the dowel in the deck has demonstrated higher shear transfer capacity than that between the carbon shell and ordinary reinforced concrete slabs, shown in Figure 32.9c and d.

Hybrid FRP/Concrete Rectangular Beam Sections

One of the earliest attempts to produce hybrid FRP/concrete beam elements was done by Fardis and Khalili (1981) as they proposed casting concrete into FRP boxes. They also pointed out the mechanical role of FRP and concrete as follows: (1) FRP carries the tensile forces in the tension zone; (2) It provides partial confinement of concrete in the compression zone, enhancing strength and ductility; (3) It carries part of the shear force in the beam through the two sides; and (4) The concrete core provides compressive strength and rigidity and prevents local buckling of the FRP casing. They also pointed out that adhesion between the concrete and FRP is not necessary provided that the FRP box is closed at the two ends and the unidirectional fibers at the bottom have adequate end anchorage, otherwise mechanical interlock can be introduced. Five FRP-encased concrete beams were constructed using 0, 5, or 10 layers of unidirectional GFRP reinforcement at the bottom. Wooden mold was used to build the three-sided GFRP boxes using hand layup. Concrete was cast after curing of the box, and after 28 days the top and two sides were covered with two layers of epoxy-wetted GFRP cloth. The beam without any unidirectional tension fibers was under-reinforced and failed by fracture of the GFRP cloth in tension. All other beams were over-reinforced and experienced ductile behavior with concrete failing in compression. Later, removal of the GFRP casing revealed that concrete was severely cracked in tension and shear and crushed at the top; however, the FRP on the three sides was still intact and provided confinement. As a result, unloading after failure led to almost total recovery of the deflection. The strength of all the beams tested was greater than that of typical conventional reinforced concrete beams of the same dimensions and ranging from over-reinforced to overly under-reinforced. This study proved that FRP-encased concrete beams are superior to reinforced concrete beams on a strength/material cost basis.

Triantafillou and Meier (1992), Deskovic et al. (1995), and Triantafillou (1995) presented an innovative hybrid box section suited for simply supported spans. The new system combines composite materials with low-cost construction material, concrete, to result in new concepts for the design of lightweight, corrosion immune and yet inexpensive beams with excellent damping and fatigue properties. A schematic illustration of the hybrid section is given in Figure 32.12. The section consists of GFRP pultruded box section with an upper layer of concrete in the compression side and a thin layer of CFRP in the tension side. The idea was initiated by considering the thin-walled GFRP pultruded box sections, which are considered to be the most efficient and widely used in structural applications, yet they suffer from some disadvantages. The compressive flange is considerably weaker than the tensile flange because GFRP has compressive strength about half its tensile strength and because of local buckling phenomena. Failure is usually catastrophic without warning because of the linear nature of the material. Finally, the relatively low stiffness of GFRP results in excessive use of composite materials to satisfy certain displacement requirements. In view of this, the new design is driven by the following considerations. First, the compression stresses in the section should be carried by a material with the highest compressive strength and stiffness to cost ratio, and therefore the GFRP flange could be eliminated and substituted by a layer of concrete. Second, another composite material with a failure strain less than that of GFRP could be added to the section's tension zone so that it will be the first element to fail, thus giving warning of an imminent collapse (pseudo-ductility). It should preferably also possess a high stiffness to increase the section rigidity. A thin layer of externally epoxy-bonded CFRP appears to be the best candidate material for this purpose as it will also enhance the member's

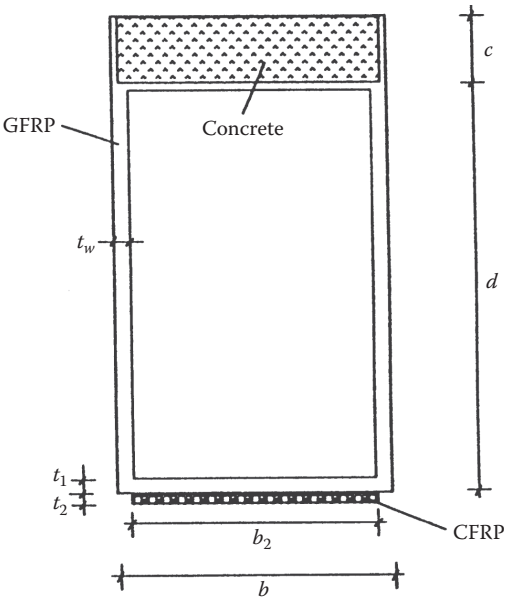

FIGURE 32.12 Hybrid concrete/GFRP/CFRP rectangular section. (From Triantafillou, T.C. and Meier, U., Innovative design of FRP combined with concrete, *Proceedings of the Advanced Composite Materials in Bridges and Structures*, Neale, K.W. and Labossiere, P. (eds.), Canadian Society for Civil Engineering, Montreal, Quebec, Canada, pp. 491–499, 1992.)

creep and fatigue behavior. Because the proposed design involves casting of concrete, part of the GFRP box section is extended to act as formwork for the wet concrete and to transfer the GFRP–concrete interface shear stresses. A good bond between the concrete and GFRP can be achieved by either using epoxy adhesive or providing mechanical deformations to the top GFRP surface.

A preliminary experimental program using small-scale specimens revealed that the desired failure sequence could hardly be achieved using standard pultruded GFRP profiles. Therefore, it was decided to fabricate the GFRP box sections using the filament winding technique. Prior to attaching the concrete or the CFRP layers, the beams were loaded elastically in three-point bending to establish their stiffness characteristics. Concrete layer was cast on top of the GFRP flange and bonded using epoxy adhesive in beam 1, steel shear connectors in beam 2 and beam 3 in order to enhance the shear transfer between the concrete and upper flange. Two pultruded CFRP straps were attached to the bottom flanges, near the corners, using adhesive. The beams were then reloaded to failure. Beam 1 failed by CFRP fracture, followed by GFRP–concrete interface debonding. Beams 2 and 3 failed in a pseudo-ductile mode, where the CFRP fractured, followed by crushing of concrete at a higher load level. Figure 32.13 shows the load-deflection behavior of the hybrid beam compared to a GFRP beam loaded to failure. The gradual failure, which starts by fracture of CFRP accompanied by the sudden drop of load and reduced stiffness, provides adequate warning before the complete failure. This pseudo-ductility is a major part of the innovation in this new system.

In 1999, Canning et al. proposed a similar hybrid system consisting of concrete section in the compressive region, GFRP composite sandwich foam core web section, and a GFRP tension flange interleaved with high-strength unidirectional carbon fiber tape. The beam was designed such that the neutral axis is situated at the soffit of the concrete to eliminate tensile stresses from concrete. Indents were placed in the vertical faces of the shuttering to enhance the bond with concrete. At early stages of the program, it was realized that buckling of the webs would be one of the critical modes of failure; therefore, an optimization study was performed to compare different configurations and the sandwich foam core was selected for its ease of fabrication. The beam was designed to fail in compression. During testing, bond between the concrete and the vertical GFRP shuttering

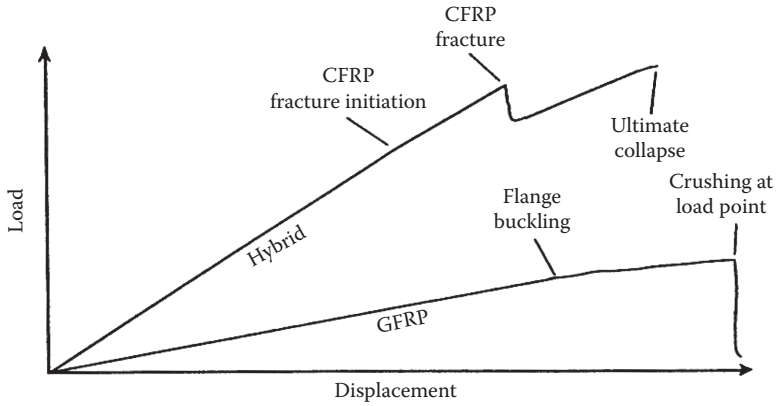

FIGURE 32.13 Load–deflection behavior of the hybrid beam compared to the GFRP beam. (From Triantafillou, T.C. and Meier, U., Innovative design of FRP combined with concrete, *Proceedings of the Advanced Composite Materials in Bridges and Structures*, Neale, K.W. and Labossiere, P. (eds.), Canadian Society for Civil Engineering, Montreal, Quebec, Canada, pp. 491–499, 1992.)

was failed but concrete continued to be held in position by the mechanical shear connectors in the vertical walls and a 1–2 mm slip occurred. Failure occurred when the concrete crushed in compression and as a result of the impact the webs failed by buckling in shear. The study concluded that (1) the hybrid beam had a similar ultimate bending capacity, half the flexural rigidity, and a weight reduction of about 75% compared to a singly reinforced concrete beam of the same dimensions with a 2% reinforcement ratio; (2) The production time of 24 h, including the vacuum process, is similar to reinforced concrete beams; (3) Up till 42% of the ultimate load, both adhesion and shear keys allowed full composite action, after that the adhesion bond failed and the shear key permitted high percentage of composite action with some slippage; (4) No buckling of the sandwich webs was observed; and (5) It is difficult to estimate the true cost of the product, as the fabrication techniques have not been finalized. The technology and materials used were adopted from aerospace industry.

Other Forms of Hybrid FRP/Concrete Sections

In Hall and Mottram (1998) presented a novel hybrid section combining GFRP "off-the-shelf" pultruded sections, commercially available as floor panels, with concrete. The GFRP sections act as tensile reinforcement and permanent formwork at the same time. Figure 32.14 shows a section of the GFRP reinforcing system having two T-up-stands and a continuous base. As the panels have smooth surface, the study included push-out bond tests of concrete cast around the panels as received, and concrete cast around the panels after coating with epoxy mortar. The unbonded specimen failed at the smooth interface, while the bonded one, concrete failed in the form of cone-shaped plug. A total of 12 beams were tested in four-point bending. Five different reinforcement arrangements were considered, as shown in Figure 32.14, including both bonded and unbonded conditions, normal and lightweight concrete, as well as steel fibers in the mix. The study concluded the following:

1. Plain reinforcement bond strength is similar to that quoted elsewhere for plain FRP rebars.
2. Conventional theoretical assumptions about reinforced concrete are still valid.
3. Beams behaved in a linear elastic manner for loading up to serviceability and continued to deform in a nonlinear manner to ultimate failure.
4. Failure was often by concrete in shear, no shear reinforcement was present, and the beams were over-reinforced in flexure.
5. To provide adequate bond, it will be necessary for plain reinforcement to be bonded by adhesive such as epoxy to concrete.

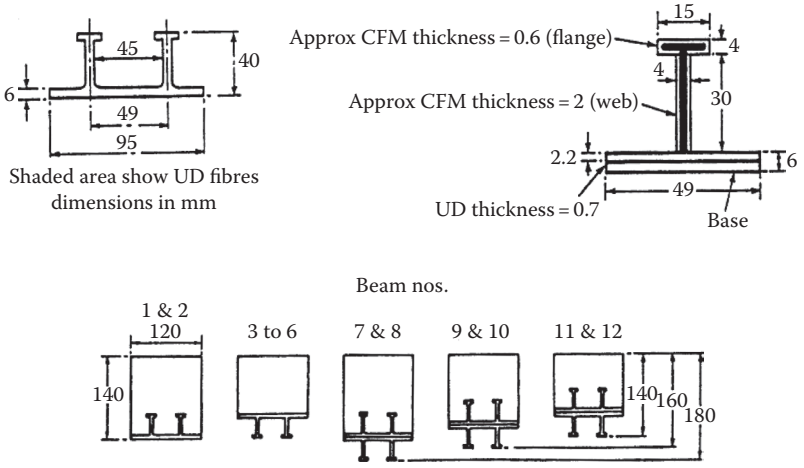

FIGURE 32.14 Hybrid rectangular beam cross sections. (From Hall, J.E. and Mottram, J.T., *J. Comp. Const*., 2(2), 78, 1998.)

REFERENCES

Burgueno, R., Davol, A., and Seible, F. (1998) The carbon shell system for modular bridge components, *Proceedings of the First International Conference on Composites in Infrastructure ICCI'96*, H. Saadatmanesh and M. R. Ehsani (eds.), Tucson, AZ , January, pp. 341–354.

Canning, L., Hollaway, L., and Thorne, A. M. (1999) Manufacture, testing and numerical analysis of an innovative polymer composite/concrete structural unit, *Proceedings of the Institution on Civil Engineerings Structures and Buildings*, Paper 11826, Boulder, CO, Vol. 134, August, pp. 231–241.

Collins, M. P. and Mitchell, D. (1997) *Prestressed Concrete Structures*, Response Publications, Montreal, Quebec, Canada.

Davol, A., Burgueno, R., and Seible, F. (2001) Flexural behavior of circular concrete filled FRP shell, *Journal of Structural Engineering*, 127(7): 810–817.

Deskovic, N. and Triantafillou, T. C. (1995) Innovative design of FRP combined with concrete: Short-term behavior, *Journal of Structural Engineering*, 121(7): 1069–1078.

Fam, A. Z. (2000) Concrete-filled fiber reinforced polymer tubes for axial and flexural structural members, Ph.D. thesis, University of Manitoba, Winnipeg, Manitoba, Canada, p. 261.

Fam, A. Z. and Rizkalla, S. H. (2002) Flexural behaviour of concrete-filled fiber-reinforced polymer circular tubes, *ASCE Journal of Composites for Construction*, 6(2): 123–132.

Fardis, M. N. and Khalili, H. (1981) Concrete encased in fiberglass-reinforced plastic, *ACI Structural Journal*, Title no. 78-38, November–December, 440–446.

Hall, J. E. and Mottram, J. T. (1998) Combined FRP reinforcement and permanent formwork for concrete members, *Journal of Composites for Construction*, 2(2), 78–86.

Karbhari, V. M., Seible, F., Burgueno, R., Davol, A., and Zho, L. (1998) Structural characterization of fiber-reinforced composite short-and medium-span bridge system, *Proceedings of the European Conference on Composite Materials (ECCM-8)*, I. Crivelli Visconti (ed.), Vol. 2, Naples, Italy, June 3–6, pp. 35–42.

Mandal, S. K. (2004) Prestressed concrete-filled fibre reinforced polymer (FRP) tubes, M.Sc. thesis, Queen's University, Kingston, Ontario, Canada, pp. 204.

Mirmiran, A. and Shahawy, M., and El Khoury, C. (1999) Comparison of over-reinforced and under-reinforced concrete-filled tubes, *Proceedings of the 13th Engineering Mechanics Conference*, ASCE, Baltimore, MD, CD-ROM.

Naguib, W. and Mirmiran, A. (2001) Time-dependent behavior of concrete-filled FRP tubes under sustained loading, *Proceedings of the Structures Congress*, ASCE, Washington, DC, May, CD-ROM.

Parvathaneni, Hari Kumar, I, Srinivasa, L., and Greenwood, M. (1996) Design and construction of test mooring pile using super prestressing, *Proceedings of the Advanced Composite Materials in Bridges and Structures*, Montreal, Quebec, Canada, pp. 313–324.

Seible, F. (1998) Innovative designs for pedestrian bridges, *Proceedings of the Developments in Short and Medium Span Bridge Engineering '98*, Calgary, Alberta, Canada.

Seible, F. (1996) Advanced composites materials for bridges in the 21st century, *Proceedings of the Advanced Composite Materials in Bridges and Structures*, Montreal, Quebec, Canada, pp. 17–30.

Seible, F., Karbhari, V., Burgueno, R., Davol, A., and Wernli, M. (1997) Design issues with carbon fiber composite reinforced concrete structures, *Proceedings of the Third International Symposium, Non-Metallic (FRP) Reinforcement for Concrete Structures*, Vol. 2, Sapporo, Japan, October, pp. 89–112.

Triantafillou, T. C. and Meier, U. (1992) Innovative design of FRP combined with concrete, *Proceedings of the Advanced Composite Materials in Bridges and Structures*, K. W. Neale and P. Labossiere (eds.), Canadian Society for Civil Engineering, Montreal, Quebec, Canada, pp. 491–499.

Triantafillou, T. C. (1995) An innovative application of composite materials in construction, *Proceedings of the First Israeli Workshop on Composite Materials for Civil Engineering Construction*, Haifa, Israel, May 28–29, pp. 17–20.

Wernli, M. and Seible, F. (1998) Ductile connections of modular bridge girders made of concrete filled FRP-tubes, *Proceedings of the First International Conference on Composites in Infrastructure ICCI'96*, H. Saadatmanesh and M. R. Ehsani (eds.), Tucson, AZ, January, pp. 356–367.

Yamakawa, T., Satoh, H., and Zhong, P. (1999) Seismic performance of hybrid RC circular columns confined in aramid fiber reinforced polymer tube, *Proceedings of the 4th International Symposium on Fiber-Reinforced-Plastic Reinforcement for Concrete Structures*, Rizkalla (ed.), American Concrete Institute, Detroit, MI, (under publication, received from the first author by mail).

Zhao, L., Karbhari, V., and Seible, F. (1997) *Experimental Investigation of Joint Response between Concrete-Filled Carbon Shell Girders and Composite Decks Using "Push-Out" Tests*, Report no. TR-97/16, Division of Structural Engineering, School of Engineering, University of California, San Diego, La Jolla, CA.

33 QA/QC, Maintenance, and Repair of Hybrid Structures

Amir Fam and Amir Mirmiran

CONTENTS

As with any new system, not only design and construction feasibility of structurally integrated FRP stay-in-place forms need to be addressed, but also their maintenance is of great importance. Possible repair schemes for various types of damages must be considered, and evaluation and diagnostic tools are needed to support decisions on repair strategy. However, there is very limited information available on maintenance and inspection of these systems. This chapter summarizes the available information.

INSPECTION

Inspection of structurally integrated FRP stay-in-place forms may be divided into three categories, as follows:

1. Construction inspection during and immediately after construction
2. Regular inspection during service life of the structure
3. Post-incident inspection, for example, after an earthquake or an impact accident

Each of the aforementioned types of inspection requires a different approach. Also, inspection of columns and above-ground piles is quite different from deep piles and covered surfaces of beams and slabs. The inspection may be visual or assisted with an instrument. Visual inspection often focuses on any discoloration or cracking of the FRP surface and cannot provide insight on the integrity of the concrete core. Since the state of concrete core is not readily visible from outside, nondestructive testing and evaluation (NDT or NDE) tools can help assess the health of a hybrid system, especially after an incident such as vehicle (or vessel) impact or a mild earthquake.

Two types of NDE can be envisioned: continuous health monitoring, as compared to frequent or regular monitoring. Continuous health monitoring systems require embedded gages within concrete and the FRP form as well as surface-mounted gages. The gages need to be placed at critical locations to monitor the axial and transverse strains in the concrete and the FRP form. The gages may be electrical resistance-type gages, fiber optic sensors, or vibrating wire gages. Of these, the electrical resistance-type gages are the least expensive. However, they tend to drift from the datum over time. It is, therefore, more appropriate to use either vibrating wire gages or fiber optic sensors.

The vibrating wire gages are often bulky. The fiber optic sensors are more conducive to FRP fabrication and can potentially be integrated into the manufacture of the FRP form. Recent advances in continuous or distributed fiber optic sensing (Gu et al. 2000) make them very efficient for FRP-concrete systems. The embedded system could be remotely monitored. Monitoring could also be automated to provide advance warning in case one of the control strain measurements exceeds its predetermined threshold value. Frequent or regular monitoring of stay-in-place systems may utilize one of the following methods.

Acoustic Emission

Both concrete and FRP release discrete bursts of acoustic emission (AE) energy when undergoing stress. AE sources in concrete may include cracking, friction due to aggregate interlock, and debonding between aggregate and mortar. AE sources in FRP may include debonding between matrix and fibers, matrix cracking, delamination, and fiber breakage. The integrated system may also emit signals as a result of debonding between FRP and concrete. Each type of damage often constitutes a certain energy level and amplitude. Feasibility and sensitivity of this method were examined by Mirmiran et al. (1999) for concrete-filled FRP tubes. They showed different sensitivity levels at different stages of the loading regime. A datum must be established for the structure so that regular AE monitoring could show the extent and location of damages. An important characteristic of AE signals is the presence of the Felicity or Kaiser effects. Felicity effect is the appearance of significant AE at a stress level below the previous maximum stress. Kaiser effect is the absence of any such detectable signal, until the previous maximum stress is exceeded. Therefore, for a structure with the Kaiser effect, the maximum stress level in the loading history can be easily established. Contrary to FRP, previous studies have shown concrete to exhibit the Kaiser effect for stress levels below 75%–85% of its ultimate strength. However, Mirmiran et al. (1999) showed that the Kaiser effect does not apply to concrete-filled FRP tubes, and therefore the previous maximum load level of the member may not be determined using the AE technique.

Ultrasonic Pulse Velocity and Ultrasonic Scanning

Unlike the AE tests, where one analyzes the signals emitted from within the structure under the applied loads, ultrasonic pulse velocity (UPV) evaluates the characteristics of a pulse signal as it travels through the structure. Since ultrasonic wave propagation depends on the extent of cracks in the section, damage assessment tools may be developed based on the variation of UPV. Such assessment tools can help quantify the extent and growth of cracks, or in general terms, progression of damage within the structure. Continuous UPV monitoring of a number of stub specimens has shown the concrete-filled FRP tubes to have higher sensitivity at lower stress ratios as compared to plain concrete (Mirmiran and Wei 2001). Repeated loading generally induces the same rate of change of UPV damage index as that of the initial loading on the virgin specimen. This phenomenon occurs irrespective of the stress ratio at which the specimen is unloaded or reloaded. A comparison of the UPV damage index with the normalized AE counts revealed that the two methods have different sensitivities at different stages of loading and could potentially complement each other as a hybrid damage assessment tool. Ultrasonic scanning has the potential of establishing damage contours for a member.

Electromagnetic Imaging

Feng et al. (2000) have developed a damage assessment tool using electromagnetic (EM) imaging technology for detecting voids and debonding between the FRP and the column, which may significantly weaken the structural performance of the column. This technology is based on the reflection analysis of a continuous EM wave sent toward and reflected from the layered FRP-adhesive-concrete medium.

Poor bonding conditions including voids and debonding will generate air gaps, which produce additional reflections of the EM wave. It should be noted that unlike the first two methods the EM method cannot assess the integrity of the concrete core.

Pile dynamic analyzer (PDA) could be used for evaluation of the concrete-filled FRP tubes during the driving process. The pile should also be instrumented with internal sensors and gages to ensure its structural integrity after the often-severe driving conditions. Inspection of below-ground portion of piles may require proof loading or ground penetrating radar (GPR).

MAINTENANCE AND REPAIRS

The repair strategy for structurally integrated FRP stay-in-place forms depends on the type and extent of damage, as well as its location. Damages may result from excessive axial or shear or flexural loading on the member, or direct impact of vessels or land vehicles on bridge pier column or the above-ground portion of the pile. Other forms of damages may include vandalism of the exterior surface of the FRP tube, fire, or environmental factors. The damage may be limited to either the concrete core or the FRP tube, or may extend to both. It is also possible that a structurally integrated FRP stay-in-place form may need to be strengthened to carry additional loads in flexure, axial, or shear.

The repair of damaged portion of the form must include a thorough examination of the core to ensure the survivability of the repair. It is possible to wrap the FRP tube with additional layers of fabric or precured shells similar to an existing concrete column. For beams and slabs, external bonding of plates or laminates can provide the necessary strength. Attention must be paid to surface preparation for the FRP form and its bond with the new layers of FRP. Wrap or bonding may be localized to strengthen or retrofit the weak portion of the member. Clearly, wrapping applies to columns or the above-ground portion of the piles, unless access is provided to the critical portions of the pile by jetting or digging around the pile. The wrap may be designed for shear or confinement strength. For axial/flexural strengthening or repair, the laminate must include fibers along the bending axis of the member with proper development length.

REFERENCES

Feng, M.Q., De, F.F., Kim, Y.J., and Diaz, R. (2000) Application of electromagnetic waves in damage detection of concrete structures, *Proceedings of the Smart Structures and Materials 2000: Smart Systems for Bridges, Structures, and Highways*, The International Society for Optical Engineering (SPIE), Vol. 3988, pp. 118–126.

Gu, X., Chen, Z., and Ansari, F. (2000) Method and theory for a multi-gauge distributed fiber optic crack sensor, *Journal of Intelligent Material Systems and Structures*, 10(4): 266–273.

Mirmiran, A., Shahawy, M., and El-Echary, H. (1999) Acoustic emission monitoring of hybrid FRP-concrete columns, *Journal of Engineering Mechanics*, 125(8): 899–905.

Mirmiran, A. and Wei, Y. (2000) Damage assessment of FRP-encased concrete using ultrasonic pulse velocity, *Journal of Engineering Mechanics*, 127(2): 126–135.

34 Examples and Case Studies

Amir Fam and Amir Mirmiran

CONTENTS

GENERAL

Stay-in-place FRP forms that are structurally integrated in the system have been used in a number of applications such as end-bearing or friction piles, fender piles, and structural supports for pier decks since late 1980s and early 1990s. FRP provides a solution for deteriorated piers and waterfront structures subjected to the harsh marine environment. The population growth of marine borers, strict environmental laws that limit the use of toxic treatments for wood, and prohibitions on traditional maintenance practices (lead-based primers, sandblasting, and solvent-based paints) have resulted in higher maintenance and replacement costs for traditional materials. Composite materials offer long-term and low-maintenance solutions. The use of composite piling in aggressive environments in certain instances has shown to be more economical than wood when life-cycle costs are considered. In this chapter, three available systems and their case studies or field applications are summarized.

PILE SYSTEMS AND APPLICATIONS

Different systems of concrete-filled FRP tubular piles currently available include hardcore pile, Lancaster composite pile, and compile composite pile. The following sections provide the details and field applications of these systems.

The hardcore composite pile is a cylindrical shell fabricated of high-strength FRP composite materials with a rubber-toughened, acrylic skin, which provides additional protection against abrasion, ultraviolet (UV) light, and chemicals. The tube is fabricated using vacuum-assisted resin transfer or infusion molding. The inner surface is textured to create a mechanical lock with a filler material, usually concrete. The piling is molded, shipped, and driven as a hollow shell and is then filled with concrete or other appropriate core material. The hardcore composite piling is in a range of 10–18 in. diameter and is fabricated using E-glass and vinyl ester resin. Also, hybrid glass/carbon fiber composite tubular piling with much higher stiffness is feasible. The hybrid pile uses carbon fibers in the axial direction for improved bending performance and E-glass fibers oriented along the circumference for economy. Hardcore also produces monopile technology with up to 6 ft. in diameter for specialty fender applications.

Hardcore piles can be driven with standard pile-driving equipment, including both vibratory and impact hammers. The piling is driven either open-ended or with a variety of driving shoes. A standard pipe pile-driving helmet or equivalent is used in most applications. When more aggressive soil conditions are encountered, it is recommended that the piles be filled with concrete prior to driving.

FIGURE 34.1 New Castle pier in Lewes, Delaware.

In some areas, installation may also be assisted by the use of jetting. Piles may be fabricated with integral jetting tubes to facilitate this installation technique.

New Castle Pier in Delaware was reconstructed using 12 and 18 in. diameter hollow composite tubes, driven over the remains of the original wood piling. The hollow tubes were then filled with concrete and used to anchor the new pressure-treated timber deck, as shown in Figure 34.1.

Another field application was a monopile of composite tube as a single 80 ft long 5 ft diameter pile, weighing only 14,000 lbs. The pile was installed for the Delaware River and Bay Authority at the Lewes, Delaware, ferry terminal, as shown in Figure 34.2. The pile driving was performed using a vibratory hammer and was faster than a typical steel monopile as the composite pile was fabricated in one continuous length, eliminating the need for field welding or splices. The pile was driven hollow and will not be filled with concrete. The monopile was tested for 240 kip force with a deflection of 31 in.

FIGURE 34.2 Hardcore monopile.

FIGURE 34.3 Bridge over Nottoway River in Virginia.

Lancaster Composites produces a Composite Post 40 (CP40) marine pile with a filament wound tube made by Ameron International. The tube is filled with "expansive" concrete, made using shrinkage reducing admixtures. Two of the field applications of the Lancaster Composites are listed next.

For a TEA-21 project, the Federal Highway Administration and Virginia DOT used Lancaster Composite piles on 4 bents of Route 40 Bridge over Nottoway River, as shown in Figure 34.3. The tubes were 14 m long with 0.6 m diameter and 6.4 mm wall thickness. The piles had a design capacity of 690 kN (Fam et al. 2003b).

At the U.S. Naval Facility Pier in Ingleside, Texas, Lancaster Composite piles with 325–356 mm diameters were used as vertical and batter piles for fender applications, as shown in Figure 34.4. The piles were designed with a factor of safety of 10 at a design capacity of 178 kN (Fam et al. 2003a).

Compile® is a specially designed concrete-filled fiber reinforced polymer tube by SDR Engineering. The tubes are manufactured with a special internal texture and minimal voids using the centrifugal casting technique. As part of a pilot study for the Florida Department of Transportation,

FIGURE 34.4 Fender piles.

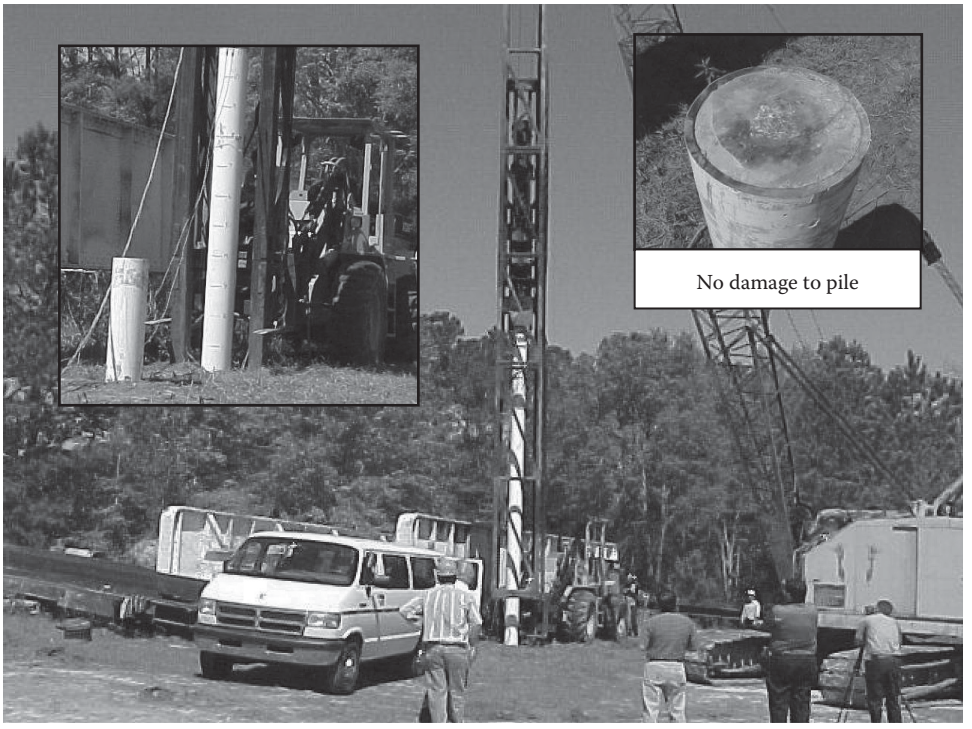

FIGURE 34.5 Compile® being driven as load-bearing piles in Florida.

a number of empty or concrete-filled FRP tubes, with or without field splices, were driven in March 2000, as shown in Figure 34.5. Field tests showed composite piles to be a feasible alternative for bridge substructure. No damage was observed at the top of the filled tube, nor in the tube–concrete interface, under more severe driving conditions than those allowed by current specifications for concrete piles (Mirmiran et al. 2002; Mirmiran and Shahawy 2003).

BRIDGE GIRDER APPLICATIONS

The research and development efforts on concrete-filled carbon-FRP tubes at the University of California, San Diego, have been implemented in a bridge demonstration project by the California Department of Transportation (Caltrans). One of the two parallel structures for the Kings Stormwater Channel Bridge (Figure 34.6) of Route 86 in Riverside County was designed with the modular

FIGURE 34.6 Kings Stormwater Channel Bridge, San Diego, California.

concrete-filled carbon shell system (CSS) construction concept (Seible et al. 1999). The bridge consists of a two-span, 20 m long and 13 m wide, continuous system with a beam-and-slab superstructure and a multicolumn intermediate pier. The superstructure is composed of six carbon/epoxy girders with 10 mm wall thickness and 0.34 m inside diameter filled on-site with lightweight concrete. The girders are connected compositely with cellular E-glass/vinylester FRP deck panels. The design was based on the characterization of concrete-filled carbon shell bridge components and assemblies (Karbhari et al. 2000). Continuing the carbon shell into the reinforced concrete elements and providing a conventional steel reinforcement anchorage allows connection of the carbon CFFT girders to the abutment end diaphragms and the center cap beam. The pier columns are conventional reinforced concrete pile extensions. After proof testing, the bridge was placed in service in July 2000. Long-term health monitoring of the Kings Stormwater Channel Bridge is being conducted by using permanent field monitoring instrumentation and a remote communication and data collection system (Zhao et al. 2001). Owner: California Department of Transportation. Structural Design: University of California, San Diego and California Department of Transportation. FRP Contractors: Alliant Techsystems, Inc. and Martin Marietta Materials, Inc. Service Date: May 2000.

REFERENCES

Fam, A., Greene, R., and Rizkalla, S. (2003a) Field applications of concrete-filled FRP tubes for marine piles, Field Application of FRP Reinforcement: Case Studies, ACI Special Publication, SP-215-9: 161–180.

Fam, A., Pando, M., Filtz, G., and Rizkalla, S. (2003b) Precast composite piles for the route 40 bridge in Virginia, *PCI Journal*, 48(3), 32–45.

Karbhari, V. M., Seible, F., Burgueño, R., Davol, R., Wernli, M., and Zhao, L. (2000) Structural characterization of fiber-reinforced composite short- and medium-span bridge systems, *Applied Composite Materials*, 7(2/3), 151–182.

Mirmiran, A. and Shahawy, M. (2003) Composite pile: A successful drive, *Concrete International*, 25(3), 89–94, 2003.

Mirmiran, A., Shao, Y., and Shahawy, M. (2002) Analysis and field tests on the performance of composite tubes under pile driving impact, *Composite Structures*, 55(2), 127–135.

Seible, F., Karbhari, V. M., and Burgueño, R. (1999) Kings stormwater channel and I-5/Gilman bridges, *Structural Engineering International, Journal of the International Association for Bridge and Structural Engineering*, 9(4), 250–253.

Zhao, L., Sikorsky, C. S., Seible, F., and Karbhari, V. M. (2001) Field monitoring of the kings stormwater channel advanced composite bridge, *Proceedings of the 6th Caltrans Seismic Research Workshop*, California Department of Transportation, Sacramento, CA.

Part VI

Nondestructive Testing and Evaluation

Sreenivas Alampalli and Glenn A. Washer

35 Introduction

Sreenivas Alampalli and Glenn A. Washer

CONTENTS

OVERVIEW

The aging bridge infrastructure presents a significant challenge to owners for maintaining the system in a cost-effective manner while ensuring safety and optimizing operational levels. New materials such as fiber reinforced polymer (FRP) materials have received considerable attention from bridge engineers to improve the durability of the infrastructure while reducing delays associated with the construction. Conventional inspection procedures are not sufficient to evaluate and quantify possible defects in these materials. This, combined with limited understanding and experience, is becoming a hindrance for successful application and optimization of components and structures made of FRPs. Thus, nondestructive evaluation technologies and structural health monitoring may play a big role in the future in assisting the infrastructure owners in condition assessment of structures that utilize FRPs. Part VI will focus on nondestructive evaluation (NDE) of FRP components used in bridge structures and reviews NDE techniques and inspection methodologies for FRP materials applied to civil structures. This field is rapidly progressing as the use of FRP materials becomes more widespread. The aging of FRP materials under realistic field conditions is still not well understood, and advanced NDE techniques will be required in the future to address in-service inspections.

NDE technologies also have a role in the quality assurance of FRP applications. Several approaches have been described in this chapter for evaluating debonding of an FRP laminate to a concrete or steel structure. Determining the strength of that bond in a nondestructive manner remains an elusive goal for both civil and aerospace structures. The evaluation of material properties of composite materials in a nondestructive manner has been explored by ultrasonic methods, but fieldable technologies are yet to emerge.

Overall, the application of NDE technologies for the evaluation of civil structures is a growing field, both in research laboratories and in practice. Table 35.1 indicates the NDE technologies discussed in this chapter and their primary application to various deterioration or damage modes in composites structures. This table illustrates that no single NDE technology is suitable for all failure or deterioration modes, and as is frequently the case, several technologies may need to be employed to achieve a comprehensive condition assessment of a particular structure or composite retrofit. It should also be noted that the table indicates the primary applications for the technologies; some of the techniques could be used for other deterioration modes if properly developed, but for various reasons, typically are not. For example, infrared thermography could be developed to detect broken fiber and fibrillation, but typically is not used for that purpose. At the same time, all the aforementioned NDE technologies mostly characterize local defects and do not give an indication of the strength or durability. Load testing is predominantly used for such applications. Future application of NDE technologies to composites used for civil infrastructure will improve the quality of construction, and as the existing infrastructure ages, help support effective repair and renovation of composite structures.

TABLE 35.1
Summary of NDE Technologies and Their Typical Applications

Technique	Moisture Absorption	UV Damage	Fibrillation Unraveling and Broken Fibers	Fiber Breakage	Loss of Mechanical Properties	Delamination of Composite From Substrate	Debonding Between Composite Layers	Bond Strength	Delaminations in Subsurface Concrete
Visual inspection	X	X	X						
Sounding						X	X		X
Infrared thermography						X	X		X
Microwaves						X	X		X
Ultrasonic pulse-echo			X		X	X	X		X
Acousto-ultrasonics			X		X	X	X		X
Guided waves			X		X	X	X	X	
Acoustic emission				X					

PART VI ORGANIZATION

Nondestructive testing and evaluation is a key component to evaluate structural health and is very useful for FRP structures from QA/QC at the manufacturing plant to inspection and maintenance phases of the structures to maintain the structure in safe and operational condition. Chapter 36 will discuss structural health in civil engineering concepts and applies them to FRP-related applications in bridge engineering.

Application of NDE to composite structures has developed in recent years primarily for aerospace applications of composites, where the operating environment and the maintenance aspects are very different from those experienced by civil structures. Hence, even though these methods are developed very well in aerospace industry, application and usefulness of these methodologies varies in bridge applications. Chapter 37 describes these issues related to FRP structures and where NDT methods are needed or useful. Visual inspection is still the primary procedure used for the inspection of bridges worldwide. This chapter briefly describes the visual inspection and sounding used for nondestructive evaluation of FRP structures. This chapter also describes the use of microwave methods for FRP components evaluation.

Chapter 38 describes the infrared thermography and microwave methods that are being used and widely explored for nondestructive evaluation of FRP components in bridges. Chapter 39 describes the acoustic methods. These chapters not only describe the methodologies but also give limitations of the procedures used.

As noted earlier, load testing is a commonly used NDT tool to evaluate in-service performance of FRP retrofits and new FRP installation, to evaluate the design assumptions used in analysis and design phases, to generate data for future research and calibration of analytical models, and to evaluate in-service performance. Chapter 40, at first, reviews the role of sensors, instrumentation, and software to provide general guidelines for bridge engineers unfamiliar with load testing. Then, it describes two case studies to illustrate the value of load testing as an NDT tool.

Composites are excellent candidates for use as active or smart materials. They have the potential to extend the performance of engineering systems well beyond what is possible with passive materials and Chapter 41 describes this smart composites concept.

36 Structural Health Monitoring

Sreenivas Alampalli and Mohammed M. Ettouney

CONTENTS

INTRODUCTION

Structural health monitoring (SHM) is often used to gain a better understanding of the structures, get durability data for research, and for decision making based on actual structural performance as opposed to analytical and theoretical analyses. This usually involves instrumenting the structure with sensors and measuring structural deformations and/or stresses under loads. According to Ettouney and Alampalli [1–3], the following are considered integral components of the SHM:

- Measurements and sensing
- Structural identification
- Damage/deterioration identification
- Decision making

Decision making is generally not considered integral to the SHM process. Ettouney and Alampalli [1–3] argued that any SHM project that does not incorporate decision-making/cost–benefit ideas in all its tasks cannot be a successful project and should not be pursued and introduced structural health in civil engineering (SHCE) concept (see Figure 36.1). For efficient and meaningful upkeep of structural health of our infrastructure inventory, decision making should be well integrated with SHM components. This section first covers the SHCE concepts and then applies it to FRP applications in bridge engineering.

STRUCTURAL HEALTH IN CIVIL ENGINEERING

This section briefly describes various phases of the SHCE, from the measurement phase to the decision-making phase [1–3]. All four phases are analogous to four bases in a baseball game. Every player starts at the home base and should return to the home base to score a run. Not returning to the home base by the end of the inning does not accomplish much except for certain individual player records. In a similar fashion, all SHCE programs start with a reason

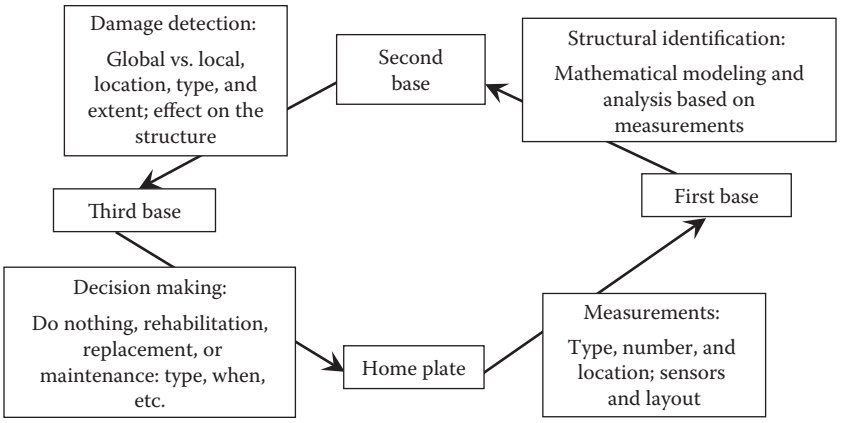

FIGURE 36.1 Baseball analogy of SHCE concept.

(requiring a decision) and should end with required information to make an appropriate decision (see Figure 36.1). If not, it may contribute to the knowledge base, but fail to reach the goal set for the individual SHCE project.

Measurement Phase

The first phase in SHCE is the measurement phase and forms the basis for the entire SHCE process. Measuring structural behavior will have two main goals. First, it is desirable to numerically identify the structural system and estimate the state of structural damage/condition, if any, to support the decision-making process. Often this requires structural measurements. The most obvious is selecting structural parameters which represent important structural response measures of interest. These include

1. Direct measurements: These relate to the structural performance and give an estimate of structural strength or failure condition directly. These include, but are not limited to, the following:
   a. Structural displacements
   b. Velocities
   c. Accelerations
   d. Structural deformation (e.g., strains)
   e. Inclinations
2. Indirect measurements: These include parameters that give the necessary information on structural parameters indirectly through some correlations.
   a. Measuring the acoustics of cable snapping in suspension bridges and then finding the location of the breaks in the cables by tracing the time of arrival of acoustic waves.
   b. Half-cell potential data from concrete columns can be correlated to corrosion rate.

In all situations, complete knowledge of the structural system is mandatory to collect successful and efficient measurements.

Structural Identification Phase

Once data from the measurement phase are obtained, transformation of this data to understand the structural properties is necessary. This is widely known as the structural identification problem.

The structure can be identified by several modes of information. For example, the structure can be identified by the distribution of stiffness throughout the structure, that is, the stiffness matrix of the structure. Identifying natural frequencies and mode shapes of a structure (modal analysis) is one of the popular structural identification methods.

Even with the existence of the large number of studies and methods for structural identification, it is wise to place structural identification in the context of the larger issue of engineering of structural health. A successful structural identification technique should be capable of addressing the needs of the SHCE problem. For example, if the SHCE problem on hand is the corrosion of reinforcing steel in a reinforced concrete bridge, the employed structural identification method should be capable of addressing the initiation and propagation of corrosion and structural deterioration due to corrosion. The choice of a particular method of structural identification should also depend on the type and degree of damage expected during a structure's life span (or the duration of the monitoring period).

Damage Detection Phase

The third phase in the SHCE is detection of damage that can occur/expected in the structural system. Damage monitoring of bridges is increasingly necessary as the effects of corrosion, ship traffic, earthquakes, and sadly, even terrorist actions continuously threaten the soundness of these vital structures. Two challenging problems present themselves. First, the number and location of structural monitoring measurements should ideally be kept to a minimum. Second, correlating the results of the measurements to a specific damage mechanism (e.g., hairline cracks and large localized strains) and damage location is difficult. The damage detection phase investigates the applicability and accuracy of different damage detection techniques to complex structures.

Decision-Making Phase

All data from the aforementioned three phases should answer the main reason why structural health monitoring was considered in the first place. These include questions such as:

- For a given damaged pattern in a structural component or a complete structural system, what is the reliability of such a component or a structure?
- What is the remaining service life before failure?
- Is the failure imminent?
- Are the assumptions used in design, construction, etc., valid?
- What loads are needed to cause failure?
- What are the predominant failure mechanisms under the expected loads of a structure's life?
- What type of actions (such as maintenance, rehabilitation, or replacement) are necessary and when?

FRP APPLICATIONS

It should be noted that even though these materials are embraced by several civil engineers in the recent past [4–9], these applications are still at their infancy [10,11]. Not much data on their service life, durability, maintainability, repairability, and life-cycle costs are yet available. Due to these reasons, several of the earlier applications are designed very conservatively [4,5,12–14]. More data are still needed for proper design, construction, and maintenance and for optimization of sections to make them more cost-effective. Hence, there is a strong need for structural health monitoring to document the in-service performance of bridges retrofitted with FRP materials under service loads. The following sections explore two main applications of FRPs in bridge structures. The basic use of each application is described along with a discussion on how SHCE can be utilized to maximize the benefits of the use of FRP in each application [15].

SHCE FOR FRP DECKS

One of the main applications of FRPs is the bridge decks application. The main reasons of using FRPs in bridge decks include the following:

- Lightweight: This offers higher live load capacity when they replace existing bridge decks and, thus, extend the service life of existing bridges avoiding expensive replacement of the entire structure.
- Noncorrosive properties: Most FRP materials are not subjected to corrosion due to deicing salts used on highways and bridge decks and, hence, the expected service life is higher than conventional materials such as steel and concrete.
- Shop-fabrication: Most FRP deck materials are shop fabricated and, hence, perceived to offer higher quality and economies. This will also tend to make the construction times shorter and, thus, required traffic closures and public inconvenience can be reduced.

As noted earlier, FRP bridge decks were first introduced to bridge applications on an experimental basis, in most cases to take advantage of their light weight, to replace deteriorated concrete bridge decks and increase the live load capacity of bridges. Until recently, most of the monitoring and research studies of these decks predominantly focused on bridge decks alone, with not much attention paid to the entire structure. The future use of FRP decks in bridge applications will depend on their practicality and cost-effectiveness as part of the entire bridge system. Hence, a system approach, instead of a component approach, is needed in studying these decks. Application of concepts of SHCE to FRP decks will yield a better understanding of the use of FRP decks for infrastructure applications. Figure 36.2 shows the performance and structural issues related to FRP decks. SHCE concepts can be of immense use in the following areas [15]:

1. Component health versus system health: FRP bridge decks are built using several components, such as:
   a. Top and bottom skins/plates, to resist stresses in axial/flexural compressive and tensile forces with a core to transmit shear between them (see Figure 36.3).
   b. Longitudinal and transverse joints and construction joints: manufacturing, construction, and transportation limitations dictate the size of the FRP deck segments, necessitating connections between segments (see Figures 36.4 through 36.6).
   c. Connections are required to attach the deck to the superstructure and the supports (see Figure 36.7).
   d. A wearing surface is added to provide a good riding surface (see Figure 36.8).

   There is limited information concerning the behavior of the entire system. This, coupled with the effect of in-service conditions on the behavior of FRP decks and the type of inspection they are subjected to, makes it important to design them for implementation in a service setting, that is, the actual deck rather than individual components. Thus, all these aspects become very important for structural health application involving an FRP deck [1,15]:
2. Material issues: FRP materials are engineerable materials and are not well understood by the engineering community. Several of the specific service-behavioral issues require careful consideration when using FRP bridge decks and should be studied. These include
   a. Fatigue: Even though there have been several studies done on fatigue effects of composite materials [16–19,28,29], the knowledge base still needs improvement to include the system behavior, behavior of connections, and correlation between the distress signs and state of the structure [11,15].
   b. Creep: This can have an important effect on the overall health of the deck, especially due to its strong correlation with fatigue behavior and causes [29].

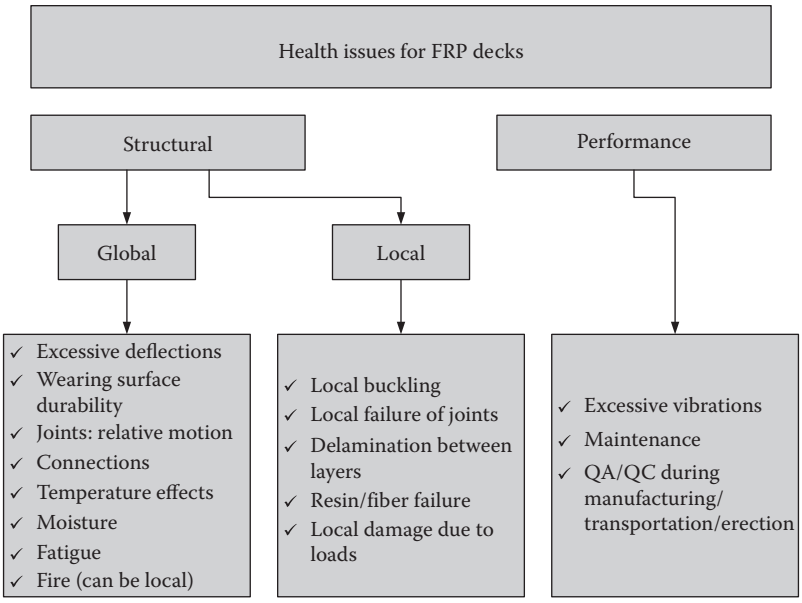

FIGURE 36.2 SHCE issues for FRP bridge decks.

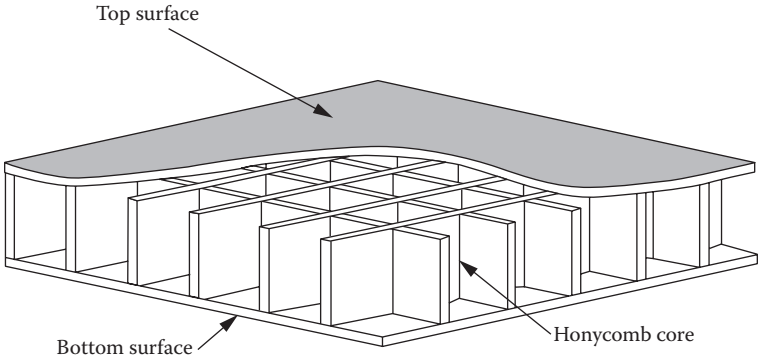

FIGURE 36.3 Schematic of a typical FRP deck with top and bottom skins and honeycomb core.

FIGURE 36.4 FRP bridge deck in New York State during installation.

FIGURE 36.5 FRP superstructure delivered to site before installation.

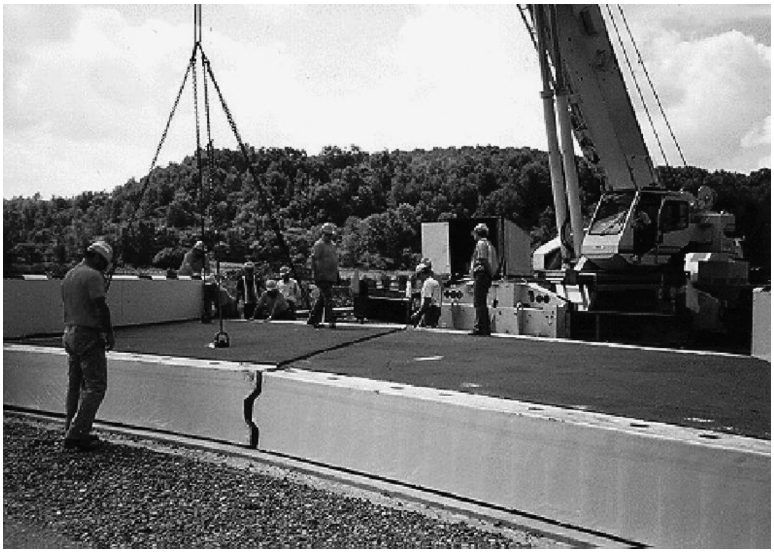

FIGURE 36.6 FRP superstructure showing shear-key to connect two sections.

c. Moisture: Exposure to moisture can have an adverse effect on FRP material, contrary to conventional wisdom [20]. This adverse effect can be easily mitigated through the judicial use of resin material and continued vigilance in monitoring the condition of the system under consideration. Moisture during curing of the resin is important, but moisture levels during the service life of the FRP bridge deck are also important. An effective SHCE strategy for moisture effects in FRP bridge decks can then involve the following program.
d. Temperature: Similar to the moisture situation, controlled curing temperature of the deck during manufacturing, freeze–thaw, and temperatures above the curing temperatures can lead to significant changes in expected performance of the FRP deck [21,22,30]. Finally, cyclic temperature changes (both range and number of cycles) can also have an effect on performance. Unfortunately, no comprehensive study is available for the FRP bridge decks.
e. Ultraviolet (UV): The UV effects on FRP bridge decks can have unwanted degradation effects on mechanical properties of the deck.

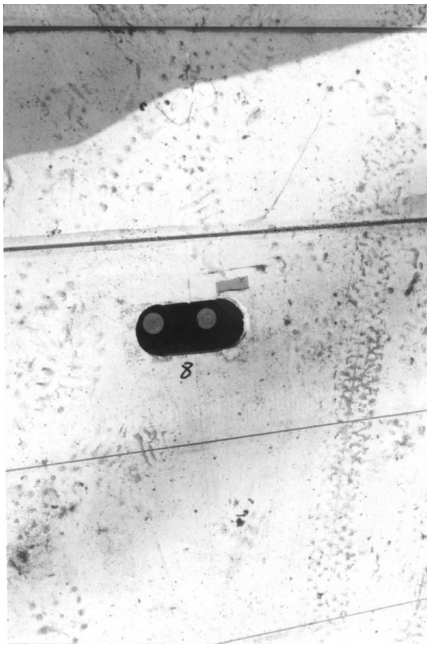

FIGURE 36.7 FRP deck during construction to show the connection with the girders.

FIGURE 36.8 Installation of wearing surface over an FRP deck.

f. Fire: Fire on FRP bridge decks can result from accidental fuel spill on the deck, intentional malicious acts, or any other number of sources. Thus, it is very important to study the impact of the fire on the FRP decks to assist the decision makers in the follow-up steps after the fire. When the FRP deck is subjected to a fire, the intense heat can adversely affect the mechanical properties of the FRP material to the extent that a structural collapse might ensue, either immediately or at a later time. There are very limited studies available on this topic [23].

3. Design issues: Most FRP decks available on the market are proprietary systems and are engineered to meet the demands. At present, no unified specifications exist to guide bridge owners for design and analysis of these decks. In several cases, the failure mechanisms are not well understood and require special attention. The specific information where SHCE programs can help includes, but are not limited to the following where not much of a knowledge base is yet available:
   a. Distribution factors
   b. Impact factors
   c. Stress fields and concentrations
   d. Allowances for creep, etc.
   e. Allowable strain limits for materials, components, and the entire system
4. Transportation issues: Transportation-related damages to the structure may not be visible and there are no nondestructive SHCE methods to detect most invisible damage suffered by the deck during transit. Temperature, moisture, and impact conditions may also have a direct effect on the performance and longevity of FRP materials. There are no data available on these issues to prepare specifications for transportation, storage, and handling. Hence, instrumenting and monitoring decks during transportation may shed some light on possible degradation/damages inflicted during transportation and reveal types of QA methods for the acceptance of a deck at the site. In order to facilitate the integration of transportation QA and any future SHCE for FRP decks, a standardized transportation report should be developed.
5. Erection issues: One of the advantages of FRP decks is that they may require light cranes and handling equipment and that facilitates a fast construction/erection process (see Figures 36.5 and 36.9). This phase starts with lifting the FRP deck from the vehicle that transported it from the plant to laying, aligning, and connecting it to appropriate bridge components. It ends with any testing required for acceptance of the structure. The handling of the deck as well as the environment (temperature, etc.) during the erection process may have a significant influence on the future durability and behavior of the FRP deck. Hence, this should be carefully considered and be an integral part of any successful SHCE program.
6. Inspection: Visual inspection along with limited nondestructive testing, such as coin tapping or hammering, is routinely used on concrete decks. Infrared thermography,

FIGURE 36.9 Sections of FRP deck delivered to construction site on a truck.

microwave, impact echo, and other advanced nondestructive testing methods are under investigation, but at present not much data are available. Automatic inspection methods, which rely on a set of sensors and measurements, are under investigation. Measuring different quantities, such as temperature, moisture, strains, or displacements, can be an integral part of an SHCE program. Different algorithms that utilize these types of measurements to identify the damages to the FRP deck must be developed and improved.

7. Maintenance: There is very little available information on the type and extent of maintenance required for FRP bridge decks. For long-term durability and life-cycle costs, the maintenance needs and schedules should be considered during the analysis, design, and manufacturing stages. Several of the issues identified by the owners of the FRP decks, based on their in-service experience, include:
   a. Failure of the wearing surface
   b. Delaminations in the face skin
   c. Warping at high temperatures due to expansion and contraction of the joints
   d. Failure of UV coatings or paint
   e. Leakage at the joints

Due to the experimental nature of the decks so far, these issues are new to bridge owners and there are no methods to detect premature failures such as those mentioned earlier. The major concern is the lack of knowledge base on remedial measures if any of the damages happen. Some of these damages may not affect the immediate use of the structure. But others, such as mechanical damage due to traffic or environment, snow plow operations, fire, and joint failure, require immediate attention if they affect the load carrying capacity of the bridge. Owners are also particularly interested in knowing the load rating of a bridge subjected to this type of damage and answers to questions such as: can one lane of the bridge be opened if the damage is in the other lane? Other issues will be the effect of any maintenance work on the durability of the entire system.

Hence, maintenance issues should be considered as part of an SCHE process and possible scenarios requiring maintenance, types of maintenance needed, and any necessary remedial actions should be properly investigated and documented. Installation of passive sensors, during fabrication/manufacturing, to detect moisture or delaminations is one way to account for some of these to initiate proper maintenance procedures in a timely fashion. Fiber optic sensors can be installed and strain/stress data can be collected cost-effectively during routine inspections, and maintenance cycles can be tied to the observed data. Since most of these decks are designed using finite element analysis, many of the "what if?" scenarios (such as the effect of expected mechanical or joint damage on load rating and traffic patterns) can be investigated, such that required maintenance procedures can be established from the beginning [14,23].

FRP WRAPPING

The other main bridge application of FRP is column wrapping. Generally speaking, the FRP wrapping process is to attach a thin layer (or layers) of FRP material to concrete bridge components. The benefits of FRP wrappings aim to extend the life of the structure by reducing the exposure to environmental conditions or giving additional ultimate capacity (see Figures 36.10 through 36.12). The main benefits of FRP wrapping are:

- Wrapping FRP layers around reinforced concrete columns can result in increased column strength due to the extra confinement that the FRP wrapping will induce in the column [24].
- If applied properly, the FRP layers can result in inhibiting corrosion in steel reinforcement [25] of columns (see Figure 36.10).

FIGURE 36.10 FRP wrapping to reduce exposure to road salt and inhibit corrosion.

- Strengthening and retrofitting deficient structural components can be accomplished using external application of FRP materials (see Figures 36.11 and 36.12). The FRP wraps can provide an extra tensile strength and/or extra stiffening measures to under-designed concrete components, such as bridge decks or bridge girders [26], as shown in Figure 36.11.
- Light weight of the materials makes it easier to use and needs lighter construction equipment compared to conventional repairs.
- The bridge components, such as concrete beams and pier caps, can be strengthened cost-effectively compared to conventional rehabilitation [27], as shown in Figure 36.12.

FIGURE 36.11 FRP wrapping of beams to increase flexural strength of bridge T-beams.

FIGURE 36.12 FRP laminates to increase stiffness of cap beams.

- The time needed for repairs is relatively less compared to conventional repairs and hence, inconvenience to the traveling public is minimized or avoided completely in some cases [26].
- Reduces the exposure to salt and moisture in cold climate areas where salt is used in winter for better traction on the road (Figure 36.10).

SHCE FOR FRP WRAPPING

Figure 36.13 shows the performance and structural issues related to FRP wrapping. SHCE concepts can be of immense use in the following areas:

1. Global structural performance: As mentioned earlier, the use of FRP wrappings can have an effect on the overall (global) structural behavior. It might be desired to monitor the effects of wrapping on such global performance. For example:
   a. Confinement: If the FRP wrappings are used to provide extra strength to a particular reinforced concrete column through increased confinement, it might be desirable to monitor such confinement on a medium or long-term basis. Such monitoring would measure the state of tri-axial strains in the concrete column. This type of monitoring can be of importance during a severe loading condition, such as a seismic event.
   b. Increased flexural stiffness/strength: Adhering FRP layers to the tension side of a flexural component (such as the underside of reinforced concrete bridge girders) is another use of FRP wrapping. It might be desirable to monitor the medium of long-term stiffness increases through the use of FRP wrapping. This can be accomplished by monitoring the static or dynamic displacements of the girders of interest. Such a medium or long-term monitoring project can assure the bridge manager of the adequacy of the FRP stiffening/strengthening effects.

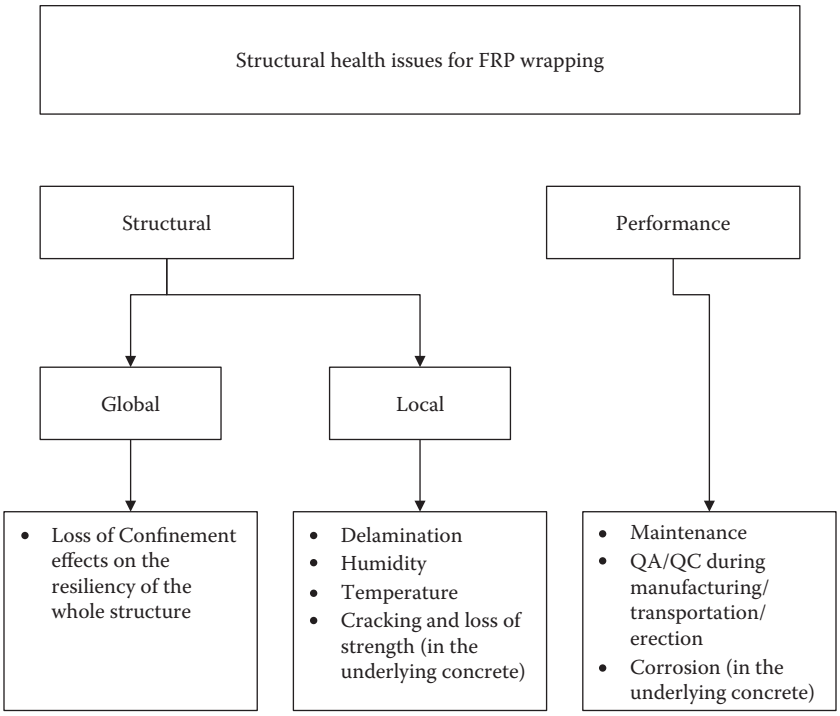

FIGURE 36.13 SHCE issues for FRP external application.

2. Local structural performance: As was mentioned earlier for bridge decks, FRP materials are engineerable materials and are not well understood by the engineering community. Some of the FRP wrapping local structural issues that can benefit from monitoring techniques are:
   a. Delamination: A typical FRP wrapping construct contains the FRP layers themselves and an adhesive material to connect it to the underlying concrete surface. Thus, proper condition of the adhesive material is essential for the FRP wrapping project to achieve its objectives. Delaminations (loss of adhesion between the FRP material and the underlying concrete) must be monitored and retrofitted as needed. Monitoring delaminations can be achieved by numerous NDT methods. Some of these methods are described in later portions of this section.
   b. Humidity: One of the uses of FRP wrapping is to inhibit corrosion in the underlying reinforced concrete construction. Because of this, it is of importance to monitor the humidity inside the wrapping material. Since FRP wrapping construction would preclude installing humidity sensors after the completion of the construction, it is essential to install such sensors during or before construction.
   c. Temperature: There can be a correlation between temperature and the corrosion rate in concrete columns that were wrapped by FRP layers. Because of this, it is important to monitor temperature in similar situations. This is particularly important in the long term. Since FRP wrapping construction would preclude installing temperature probes after the completion of the construction, it is essential to install temperature probes during construction.
   d. Loss of strength of the underlying concrete: If the concrete surface under the FRP layers cracked or lost its strength, the effectiveness of FRP material to meet its design objectives decreases. Concrete cracking can result from accidental impact, overloading, and corrosion of steel reinforcements among other reasons. Monitoring techniques for concrete cracking or loss of strength is similar to those of the aforementioned delaminations conditions.

3. Design: Similar to bridge decks, most FRP wrapping systems that are available to designers are proprietary systems and are engineered to meet the demands. Some areas where SHCE programs can help in providing a better design process (where there is a knowledge gap) include, but are not limited to, the following:
   a. Concrete-adhesive-FRP layers mechanics
   b. Ductile versus brittle behavior of the FRP wrapping construct
   c. Ultimate deformations under catastrophic loading
   d. Statistical properties of design parameters
4. Installation: Installation of the FRP wrappings is generally a manual process. Because of this, the quality of the installation can vary greatly, depending on the skill of the installers. The installation process as well as the environment (temperature, etc.) during the process may have a significant influence on the future durability and behavior of the FRP wrapping. Hence, the installation process should be carefully considered and be an integral part of any successful SHCE program. Environmental conditions during installation should be defined appropriately, as needed. Temperature, moisture, humidity, and laying of the adhesives and the FRP material itself should be considered during the design and the manufacturing processes and should be well documented. Any unexpected problems and the impromptu solutions might have an effect on future performance and strength; they should be reported in a timely fashion. All of this reporting, in a standardized fashion, will assist in developing a standardized erection procedure for the future. Nondestructive test methods should be developed or specified to make sure the FRP wrapping material was not damaged during the erection process. These data should be stored as this baseline information may be needed to develop future inspection and maintenance procedures.
5. Inspection: Visual inspection along with limited nondestructive testing, such as coin tapping or hammering, is routinely used on FRP wrapping projects. Infrared thermography, microwave, impact echo, and other advanced nondestructive testing methods are under investigation, but at present not much data are available. Automatic inspection methods, which rely on a set of sensors and measurements, are under investigation. Measuring different quantities, such as temperature, moisture, strains, or displacements, can be an integral part of an SHCE program. Different algorithms that utilize these types of measurements to identify the damages in the FRP wrapping construct must be developed and improved.
6. Maintenance: Maintenance issues for FRP wrapping constructs are similar to those of FRP bridge deck that was described earlier.

REFERENCES

1. Ettouney, M.M. and Alampalli, S. (2000). Engineering structural health. *Proceedings of the ASCE Structures Congress 2000*, Philadelphia, PA.
2. Ettouney, M. and Alampalli, S. (2002). Overview of structural health engineering. *Proceedings of the 2002 Structures Congress and Exposition*, Denver, CO, pp. 225–226.
3. Ettouney, M. and Alampalli, S. (2011). *Infrastructure Health in Civil Engineering* (Two-Volume Set). CRC Press, Boca Raton, FL.
4. Alampalli, S., O'Connor, J., and Yannotti, A. (2002). Fiber reinforced composites for the superstructure of a short-span rural bridge. *Journal of Composite Structures*, 58(1), 21–27.
5. Alampalli, S. and Kunin, J. (2003). Load testing of an FRP bridge deck on a truss bridge. *Journal of Applied Composite Materials*, 10(2), 85–102.
6. Burgueno, R., Karbhari, V.M., Seible, F., and Kolozs, R.T. (2001). Experimental dynamic characterization of an FRP composite bridge superstructure assembly. *Composite Structures*, 54, 427–444.
7. Chajes, M.J., Shenton, H.W., III, and Finch, W.W., Jr. (2001). Performance of fiber-reinforced polymer deck on steel girder bridge. *Transportation Research Record*, 1770, 105–112.
8. Shekar, V., Petro, S.H., and GangaRao, H.V.S. (2003). Fiber-reinforced polymer composite bridges in West Virginia. *Transportation Research Record*, 1819(2), 378–384.

9. Turner, M.K., Harries, K.A., and Petrou, M.F. (2003). In-situ structural evaluation of GFRP bridge deck system. *Proceedings of the 82nd Annual Meeting of Transportation Research Board*, CD-ROM, Washington, DC.
10. Aboutaha, R. (2004). Durability of wearing surfaces for FRP bridge decks. Research Report, NYSDOT Research Project, New York.
11. American Society of Civil Engineers, ASCE. (2001). Gap analysis for durability of fiber reinforced polymer composites in civil infrastructures. ASCE/CERF Report, Washington, DC.
12. Aref, A.J. and Chiewanichakorn, M. (2002). The analytical study of fiber reinforced polymer deck on an Old Truss Bridge. Report submitted to New York State Department of Transportation and Transportation Infrastructure Research Consortium, New York.
13. Chiewanichakorn, M., Aref, A.J., and Alampalli, S. (2003). Failure analysis of fiber-reinforced polymer bridge deck system. *Journal of Composites Technology and Research (ASTM)*, 25(2), 119–128.
14. Chiewanichakorn, M., Aref, A.J., and Alampalli, S. (2003). Structural behavioral study of an FRP deck system using FEA. *Proceedings of the National Workshop on Innovative Applications of Finite Element Modeling in Highway Structures*, New York.
15. Alampalli, S. and Ettouney, M.M. (2006). Long-term issues related to structural health of FRP bridge decks. *Journal of Bridge Structures: Assessment, Design and Construction*, 2(1), 1–11.
16. Dharan, C.K.H. (1975). Fatigue failure in graphite fiber and glass fiber polymer composites. *Journal of Material Science*, 10, 1665–1670.
17. Konur, O. and Matthews, F.L. (1989). Effect of the properties of the constituents on the fatigue performance of composites: A review. *Composites*, 20(4), 317–328.
18. Salvia, M. et al. (1997). Flexural behavior of UDGFRP experimental approach. *International Journal of Fatigue*, 19(3), 253–262.
19. Dutta, P.K., Kwon, S., and Lopez, A.R. (2002). Fatigue evaluation of FRP composite bridge deck systems under extreme temperatures. *Proceedings of the International Conference on Durability of FRP Composites for Construction*. Montreal, Quebec, Canada, Vol. 2, pp. 665–675.
20. Fried, N. (1967). Degradation of composite materials: The effect of water on glass reinforced plastics. *Proceedings of the 5th Symposium on Naval Mechanics*, Philadelphia, PA.
21. Gomez, J. and Casto, B. (1996). Freeze/thaw durability of composite materials. *Proceedings of the 1st International Conference on Composites in Infrastructures: Fiber Composites in Infrastructures*, Tucson, AZ.
22. Miyano, Y., Nakada, M., Yonemori, T., and Tsai, S.W. (1999). Time and temperature dependence of static, creep and fatigue behavior for FRP adhesive joints. *Proceedings of the 12th International Conference on Composite Materials*, Paris, France.
23. Alnahhal, W.-I., Chiewanichakorn, M., Aref, A.J., and Alampalli, A. (2006). Temporal thermal behavior and damage simulations of FRP deck. *Journal of Bridge Engineering (ASCE)*, 11(4), 452–464.
24. Priestley, M.J.N. and Seible, F. (1991). Seismic assessment and retrofit of bridges. Structural Systems Research Project, Report SSRP-91/103, University of California, San Diego, CA.
25. Alampalli, S. (2005). Effectiveness of FRP materials with alternative concrete removal strategies for reinforced concrete bridge column wrapping. *International Journal of Materials and Product Technology*, 23(3/4), 338–347.
26. Hag-Elsafi, O., Alampalli, S., and Kunin, J. (2004). In-service evaluation of a reinforced concrete T-beam bridge FRP strengthening system. *Journal of Composite Structures*, 64(2), 179–188.
27. Hag-Elsafi, O., Lund, R., and Alampalli, S. (2002). Strengthening of a bridge pier capbeam using bonded FRP composite plates. *Journal of Composite Structures*, 57(1–4), 393–403.
28. Chiewanichakorn, M., Aref, A.J., and Alampalli, S. (2007). Dynamic and fatigue response of a truss bridge with fiber reinforced polymer deck. *International Journal of Fatigue*, 29(8), 1475–1489.
29. Guedea, R.M. (Eds.) (2011). *Creep and Fatigue in Polymer Matrix Composites*, Woodhead Publishing Limited, Cambridge, UK.
30. Alnahhal, W.I., Chiewanichakorn, M., Aref, A.J., Kitane, Y., and Alampalli, S. (2007). Simulations of structural behavior of fiber-reinforced polymer bridge deck under thermal effects. *International Journal of Materials and Product Technology*, 28(1/2), 122–140.

37 Nondestructive Evaluation Methods for Composite Materials

General Overview, Visual Inspection, and Microwave Methods

Glenn A. Washer and Sreenivas Alampalli

CONTENTS

INTRODUCTION

Nondestructive evaluation (NDE) generally includes a family of instruments, procedures, and methods that can be applied to evaluate the in situ condition of a material or structure. These NDE technologies can range from the most obvious and simple, such as visual inspection, to extremely complex methods of using electromagnetic and acoustic waves to infer the physical properties of a material in situ. A list of common NDE technologies is included in Table 37.1, along with their primary applications. The technologies listed in this table are each a part of the American Society for Nondestructive Testing (ASNT) standard methods. These methods are traditional NDE technologies that have been developed primarily for application to metals. Many of these technologies are utilized in heavy manufacturing, aerospace, and the power generation industry. As shown in Table 37.1, the technologies and science related to NDE technologies have a broad range, and as a result, it is frequently difficult to differentiate between technologies and identify the most suitable

TABLE 37.1
Traditional NDE/NDT Technologies with Certification Available from ASNT

NDE Technique	ASNT Designation	Application
Visual inspection testing	VT	Surface conditions, general deterioration
Dye penetrant	PT	Reveals cracks in the surface of materials, typically metals
Ultrasonic testing	UT	Reflection of acoustic waves used to find subsurface defects in materials
Acoustic emission	AE	Detection and analysis of acoustic emissions generated from a defect under stress
Vibrational analysis	VA	Acoustic resonance measurement of objects and structures
Eddy current testing	ET	Reaction of induced currents in conductive materials
Magnetic particle testing	MT	Detection of magnetic flux leakage from surface-breaking cracks
Radiographic testing	RT	Imaging of material density using x-rays
Neutron radiographic testing	NR	Imaging of material density using neutrons
Infrared thermography	IR	Imaging of radiation emitted from solid bodies to infer surface temperature

technologies for a particular application. There are literally dozens of additional techniques, methods, and technologies for the NDE of structures that have been developed in recent years, but have not gained widespread use such that ASNT has provided certification. These include microwave and radar technologies, advanced acoustic wave techniques, and many others.

The increasing use of composite materials has resulted in increased research and development of NDE technologies for these materials. Many of the traditional NDE technologies, such as ultrasonic testing, acoustic emission, and of course visual testing, all can be adopted for application to the condition assessment and NDE of composite materials.

The application of NDE to fiber reinforced polymer (FRP) composite materials has developed in recent years primarily for aerospace applications. The condition assessment of composite structures in air and space craft have been developed with some success, though the deterioration modes that influence the behavior of composites over their service life remains a topic of research. As a result, NDE applications have been limited to a fairly small number, primarily focused on detection of adhesive failures that result in debonding between composite layers or between composite layers and substrates, and impact damage. The complex nature of polymer composites, combined with the fact that the application of composites to engineered structures is fairly new, has resulted in a limited understanding of what exactly an inspection of a composite structure should entail. There are a wide variety of material combinations of various carbon fibers, graphite fibers, glass, and polymers such as Aramid/Kevlar. Each of these fibers has their own performance characteristics, strength, stiffness, and environmental durability. Additionally, because the materials have come into wide use only in the last 10–20 years, a clear picture of what the critical deterioration modes and NDE requirements are has not fully developed. Experience with the effects of long-term environmental exposure on the properties, condition and performance of composites is limited. As such, it remains difficult to define specific conditions for which inspection and NDE should be applied for in-service condition assessment.

This and the next two sections will review several NDE techniques that have been applied to composites used in civil engineering applications. With relatively few exceptions, NDE applications have been limited to overlay applications. All composite structures, such as bridge beams manufactured entirely of FRP material, have received limited attention to date [1], as have embedded composites such as reinforcing bars in concrete decks. As a result, the focus of this section will be on the application of NDE technologies to composite overlay applications. Many of the examples presented concern the application of composites to bridges, though the techniques are equally viable for the inspection of other civil structures.

This section, at first, will discuss the general issues related to FRP applications for civil structures and possible deterioration and damages that need addressing. Then it discusses the visual inspection and microwave technologies. The next two sections describe thermographic methodologies and acoustic methods, respectively.

FRP APPLICATIONS FOR CIVIL STRUCTURES

Retrofitting

A common application of composite materials for civil structures is retrofitting existing structures to increase strength, the durability of a structure, and repair deficient materials. Retrofits of FRP material have been applied to both concrete and steel structures, for primary load bearing member and supports, and to columns. One of the most widespread applications of composite materials is to retrofit existing columns to improve earthquake resistance of a structure.

FRP retrofits can be applied under a variety of techniques. The fundamental principle of a retrofit is to bond FRP composite onto the surface of a concrete or steel structure to strengthen the structure. Several approaches can be used to apply a composite overlay. A hand layup process can involve cutting dry FRP fabric to length and then dipping the fabric into a resin bath. The heavy coated material is then applied to the surface of the structure and spread over the surface to flatten the fabric and remove entrapped air. Alternatively, the light resin may be applied to the surface of the concrete using a paint roller, then the fabric is spread over the surface and smoothed to remove entrapped air. The FRP may be pre-pregnated with resin and cured such that the laminate is a rigid plate or preformed shell that is then adhesively bonded to the surface of the concrete or steel.

Regardless of the manufacturing process, the retrofit of civil structures with composite materials usually shares the common characteristic of a bond to the surface of the existing structures. This bond is a critical factor in the performance of the retrofit because it is responsible for transferring stresses from the existing concrete or steel into the composite material. As a result, this bond has received much of the attention in terms of development of NDE techniques.

All-Composite Systems

All-composite systems for decks, cables, and main bridge members have been developed and applied to a number of bridges [2,25,26]. The all-composite systems are manufactured by a variety of methods including extrusion, pultrusion, and hand layup. Extruded composites are formed by forcing fibers and matrix materials through a die to form the desired cross section. Extruded composites can be formed in a variety of structural shapes consisting entirely of FRP. Pultrusion is a common manufacturing method for FRP cables and rods, and generally involves dipping fibers into a resin bath and then drawing the fibers through a die to form the desired cross section. Hand layup can be used to form structural shapes; this process involves placing FRP in successive plies around a mold of the desired shape. This process can be automated for wrapped tubes and tanks.

All-composite systems that have been applied to civil structures have received little attention in terms of NDE method development [1]. This is due in part to a lack of understanding of what the critical inspection task might be. How these all-composite systems will deteriorate under realistic field conditions is a developing field of understanding that has not yet reached a sufficient level to induce widespread research in the area. Additionally, the high cost of all-composite systems and their fairly limited use for civil structures has focused attention of researchers elsewhere.

DETERIORATION AND DAMAGE IN COMPOSITE MATERIALS

The selection of an appropriate NDE technique for a composite material relies in part on a full understanding of the damage that is to be detected. This is a particular challenge for composites in civil structures because there is only limited service experience with the material. Composites comprises

a resin and fibers of aramid, carbon, glass, or polyester. Each fiber material has its own characteristic of strength, modulus, and impact resistance. Each material also has its own resistance to chemical attack and age-related deterioration, making the long-term condition monitoring of the material a distinct challenge. Additionally, for composite retrofits, there is an adhesive layer that bonds the composite to the structure under repair, and this bond is essential to the effectiveness of the repair. The adhesive bond is the most obvious deterioration mechanism for civil applications and may have defects resulting from poor workmanship. As a result this bond has received much of the focus of research to date. Long-term deterioration due to aging, chemical changes in the material, and stress rupture phenomena are largely unexplored and may present unexpected challenges in the future. This section will briefly discuss the deterioration mechanism that may affect a composite in the field to provide a reader with a fuller understanding of the future outlook of condition assessment technologies for highway bridge applications.

Moisture

Organic polymer materials absorb moisture leading to changes in mechanical and chemical characteristics. The changes occur in the epoxy and polymer resins in the composite and can also affect the fibers themselves. Moisture that penetrates to the fiber–matrix interface can result in a loss of fiber–matrix bonding, and water may persist in this region even after the composite has been dried [3,4]. The presence of water molecules in the interface region results in a deterioration of interfacial bonds due to tensile stresses resulting from swelling. Water molecules can also wick along the fibers through capillary action, penetrating the composite material further. Additionally, the absorption of water by the matrix material results in hydrolysis and subsequently dissolution of polyester and vinyl-ester materials, with vinyl-ester being generally less susceptible to hydrolysis than polyesters [5]. This deterioration of the matrix materials leads to microcracking and weakening of the matrix, which may increase the penetration rate and depth of moisture [4]. In Aramid/Kevlar composites, the fibers themselves are susceptible to hydrolysis under certain conditions [6].

The intrusion of water into the composite can be addressed in part by using a resin-rich surface that provides a barrier against moisture intrusion, but this barrier must remain uncracked to provide effective protection [7]. Additionally, the resin itself may deteriorate with exposure to moisture over long periods of time, which would reduce its capacity to resist the intrusion of moisture. Most resins absorb moisture through diffusion processes, so resin-rich areas will retard the effects of moisture but not eliminate them. Moisture diffusing through the matrix can cause significant loss in strength of FRP composite materials [4]. This loss of strength may manifest in a change in stiffness properties of the material, and the composite action between the matrix and the fibers is lost such that stresses are no longer shared effectively between fibers.

UV Exposure

The ultraviolet components of solar radiation incident on the earth's surface are known to cause deterioration of composite materials by attacking the polymer matrix. The energy of photons in this band is comparable to the disassociation energies of the polymer's chemical bonds, such that photooxidation of the polymer can occur leading to degradation of the material properties [8]. However, the energy of the photons is typically not sufficient to penetrate the polymer significantly, and as such, UV degradation is generally considered a surface effect. Photooxidation can result in polymer chain scission that reduces the molecular weight of the polymer and loss in strength [8]. It can also result in polymer cross-linking, increasing the brittleness of the matrix and promoting microcracking [8]. The microcracking may act to increase the moisture intrusion into the composite material. Degradation of structural stiffness and load carrying capacity of carbon FRP (CFRP) and glass FRP (GFRP) retrofitted concrete beams exposed to hygrothermal and UV effects demonstrated significant losses of load capacity relative to control specimens in testing [9].

UV damage is sometimes accompanied by discoloration of the composite material, particularly in Aramid/Kevlar materials. The sacrificial coating layers of matrix materials can be used to protect FRP materials from UV damage [10]. However, the deterioration of the sacrificial layer over time may lead to cracking that allows the intrusion of water, and as such, these sacrificial layers may require maintenance to retain protective qualities [7].

Corners

A significant benefit of composite materials is the high tensile strength of the material. However, composites generally have low compressive strength. As a result, compressive bearing stress that may arise from wrapping FRP materials around corners can lead to fiber fracture and fibrillation and the splitting and fracturing of the fibrillar structure in the surface region [11]. Fibrillation is typically observable by visual inspection and individual and groups of fractured fibers may extend from the matrix surface. The low compressive resistance of FRPs requires that corners to be wrapped have relatively large radii, such that bearing stresses and stress concentrations are reduced [10]. The fibrillation of fibers extending from the surface of the material is significant because it results in a loss of strength since there are fewer continuous fibers available to share load. Additionally, the fibers protruding from the surface of the composite may compromise any resin coating that may have existed. As a result, the material is exposed to the environment such that moisture and other contaminants can be absorbed through the matrix and deteriorate the composite material.

Delamination, Debonding, and Spalling

Among the most often discussed defects in composite systems are delaminations. Delaminations can occur at interfaces between layers of the same material (i.e., between plies in a multi-ply laminate), between interfaces of different materials (i.e., a FRP laminate and the concrete surface—more accurately stated as "debonds"), between concrete repair materials and in situ concrete or within the concrete itself. Figure 37.1 shows a schematic diagram of a typical FRP laminate application commonly used for repair and strengthening of concrete structures. The laminate consists of a number of plies of FRP fabric joined with an epoxy resin and applied to the surface of a concrete structure.

When FRP retrofits are applied to concrete structures, areas where delaminated, spalled, or deteriorated concrete exist in the original structure, the damaged material is typically removed and a concrete repair material is applied to provide a level surface for applying the laminate. The laminate is applied with epoxy resin to the surface, a process that may result in areas where the laminate is debonded from the concrete surface. The debond may result from a lack of resin in the area, or a failure of the resin to bond to the concrete surface. For laminates that are rigid prior to applications,

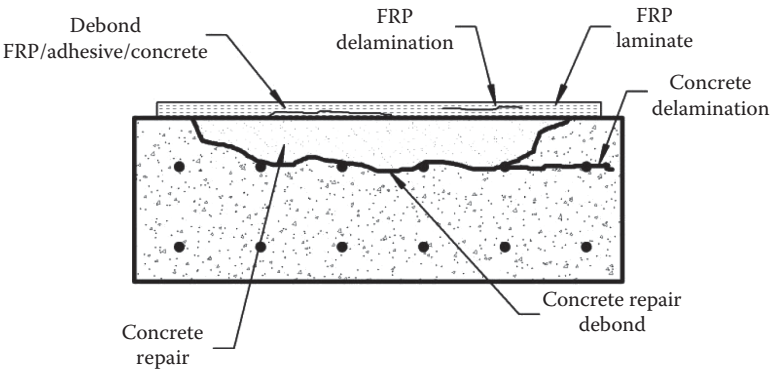

FIGURE 37.1 Schematic diagram of a typical FRP retrofit showing areas where potential debonds and delaminations may exist.

irregularities in the concrete surface may not be filled in completely by the adhesive used to bond the laminate to the surface. Surface deviations can also result in the laminate misalignment such that tensile stresses in the laminate act to straighten laminate and provide a normal force at the laminate/adhesive/concrete interface that could result in a debond [12]. Additionally, differences in thermal coefficients of expansion between the FRP material and the concrete may result in stresses that contribute to bond deterioration [11].

The concrete repair material may also debond from the original concrete substrate. This may be a result of poor construction methods that have failed to provide a bond between the repair materials and the substrate. The debond may also occur due to expansion of the corroding reinforcing steel that can create tensile stresses along the bond line between the repair and the substrate. The expansion of reinforcing steel can also result in subsurface delaminations in the concrete itself. These delaminations can propagate following the installation of the FRP laminate because the laminate repair does not interrupt the ongoing corrosion mechanism that may be present.

A layered composite material may also exhibit delaminations between the built-up layers. This may be caused by a lack of resin in an area or entrapped air, such that adjacent layers are unable to bond together. These types of defects may be insignificant in areas where the composite undergoes uniaxial tension, provided the delaminated area is small and there is sufficient bond to develop the strength of the material. However, the delaminated areas may provide an area where water can collect allowing for longer term exposure of the composite to damaging environmental effects. Additionally, multiple delaminations may join and grow over time, eventually undermining shear transfer between the composite layers.

Unraveling

Unraveling can occur when there is not good inter-layer adhesion in the composite lamina as a result of resin-starved areas, poor quality resin, or gelation of the resin between layer applications [11]. This deterioration mode can manifest in wrapping applications where out-of-plane forces exist, such as wrapped columns or areas where the FRP is wrapped around a corner. In composite laminates, interlaminar stresses arise at free-edges due to mismatch in elastic properties between plies. The classical laminated plate theory is not valid and a full three-dimensional state of stress is present. Potential debonding failure of laminated composites can be observed at the strips attached to the bottom of the beams strengthened with composite materials [24]. The deterioration mechanism would be characterized by large portions, up to a layer or more, of composite material unraveling from the balance of the material, as opposed to fibrillation, which is typically intended to characterize individual fibers breaking free from the matrix. This unraveling will obviously result in a loss of strength as broken fibers are no longer available to carry forces. Unraveling will also enable moisture to access the composite material, eliminating the benefit of a resin overlaying the composite to resist that intrusion. This will accelerate the deterioration of the composite material.

VISUAL INSPECTION

The most rudimentary method of inspecting composite reinforced structures is by visual inspection. Visual observations of condition provide fundamental data on the performance and condition of the material provided adequate procedures are utilized in the inspection process. A significant advantage of visual inspection is its low cost and simple application. Minimal training in detecting and documenting the deterioration modes such as unraveling, debonding at edges, UV damage, and absorption of moisture can enable an effective inspection to be conducted. Unfortunately, the methods are unable to detect subsurface deterioration, such as debonding between a composite overlay and the concrete substrate, or delaminations in the concrete overlaid with composite. A visual inspection can be combined with sounding (see Figure 37.2) to improve the inspector's ability to assess the condition of the composite. An in-depth visual inspection for a civil structure typically requires that the surface

FIGURE 37.2 Typical tools carried by a bridge inspector including a hammer.

of a structure being inspected be within an arms reach of the inspector. For bridges, this commonly requires specialized access equipment that can add significantly to the cost of the inspection.

Microcracking in the outer resin layers can be symptomatic of moisture absorption into the composite resulting in expansion of the resin and deterioration of the resin/fiber bond. Under severe situations, a general, widespread expansion of the matrix material or localized blistering may be evident due to water absorption. The appearance of moisture-induced deterioration of GFRP materials can be characterized by white lines appearing on the surface due to cracking between the glass fibers and the matrix [13].

The edge of composite laminate overlays presents a significant area for visual condition assessment. Loss of bonding between the composite materials and the concrete substrate may occur preferentially in this area due to the sudden change in structural stiffness represented by the edge of the composite and free edge stress effect. The variation in thermal expansion properties between the concrete and composite materials will also manifest in delamination that may initiate at this boundary. As a result, the edge of a composite laminate should be inspected to assess the condition of this interface and record incipient degradation.

For Aramid/Kevlar materials, discoloration of the materials may be indicative of photooxidation, that is, UV damage. This condition may exist in the top layers of a material, but it is generally believed that the depth to which this damage can be extended is limited by the relatively low energy of the photons causing the damage. However, UV damage in the surface layers may allow for the penetration of moisture into the composite materials, deteriorating the fiber-matrix bond and reducing the strength of the composite materials.

Sounding

A simple method for searching for delaminations and debonded areas is by mechanical sounding. This method consists of using a metal or plastic object to strike the surface of the composite material and listening to the tone of the impact. Delaminated areas can frequently be found located from their distinctive hollow tone. This method can also be used to find delaminations in concrete and delaminations between concrete repair materials and the original concrete.

Sounding has been implemented for aerospace structure utilizing a quarter, and hence, is commonly referred to as a coin-tap test. The low mass of a coin results in a high-pitched tone that

can reveal delaminations between layers of composite and possibly between the composite and the bonded substrate. For deeper features, a larger mass should be used such that the depth of the material is excited by the tapping. For composite retrofits on civil structures, a rock hammer or other suitable impact device may be used, though care should be taken to avoid damaging the composite material. The use of hammers allows for detection of features further from the surface, but near-surface features such as delaminations between layers of composites, may be obscured. A ¼–½ in. steel rod, approximately 6 in. in length, can also be used effectively in civil retrofit applications [14]. The advantage of using this type of device is that it is readily available, in that it can be formed from a piece of rebar and can provide both a high-mass and low-mass impactor depending on the orientation of the rod when impact is made.

Research has been conducted to evaluate the quantitative aspects of a tap-test for aerospace structures [15]. Areas of composite with embedded damage or debonds can be expected to have a lower stiffness than intact areas, and this lower stiffness results in the dull, low-frequency tone heard by an inspector. This effect can be measured using an accelerometer mounted on the tapping device. The accelerometer measures the width and amplitude of the impact pulse. The width of the pulse is sensitive to the stiffness of the material being impacted, whereas the amplitude of the pulse is sensitive to the velocity of the device during impact. Testing revealed that the pulse width was relatively insensitive to the velocity at impact, except for very low velocities, and this pulse width could be used to determine the structural stiffness of the material as well as reveal the location of subsurface defects.

MICROWAVE METHODS

Microwave technologies have also been applied to the detection of subsurface defects in composite repairs. One approach for implementing microwave techniques is to use an open-ended wave guide to transmit an electromagnetic wave that interacts with a material positioned in front of the wave guide [16]. Reflected waves from the material are detected by the probe and analyzed to determine various parameters related to the electronic properties of the materials. Subsurface defects such as delaminations can be detected through changes in these electronic properties.

The dielectric property of a material can be used to describe a materials' interaction with time-varying electromagnetic fields, such as microwaves. This property is commonly frequency dependent. The dielectric property of a material is a complex parameter that describes the polarization of a material in the presence of an electric field and the ability of the material to absorb energy. This parameter can be expressed relative to free-space by the following equation [17]:

$$\varepsilon_r = \frac{\varepsilon}{\varepsilon_o} = \varepsilon_r' - j\varepsilon_r'' \tag{37.1}$$

where

ε_r is the relative dielectric property of the material
ε is the absolute dielectric property of the material
ε_o is the dielectric property of free space
ε_r' is the relative permittivity of the material
ε_r'' is the relative loss factor

The dielectric property of a material depends on the constituent elements, proportions of the constituents, and inter-atomic bonding. For a layered material, such as a composite, the boundaries

between layers reflect and transmit microwaves in proportion to the contrast of the dielectric properties of the materials that form the boundary. As such, measurement of reflected wave properties can be used to infer information about materials at the boundaries. When an FRP composite has a delamination or is debonded from the concrete substrate, a boundary between the composite materials and air is created that provides a reflection due to the contrast in dielectric properties [18].

Given the frequency dependence of the dielectric properties of materials, systems can be designed to optimize contrast at boundaries of interest [17]. Various regions of the frequency spectrum have been assigned letter designations that provide a shorthand for describing the operating characteristics of a system. For example, the X-band refers to the portion of the spectrum from 8 to 12.4 GHz; the K-band refers to the portion from 18 to 26.5 GHz [17]. Waveguides and associated electronics operating within different portions of the spectrum can be relatively more or less sensitive to subsurface defects depending on the dielectric properties of the materials and anticipated depth [19]. As such, optimization of the operating frequency of a microwave system can provide improved sensitivity to subsurface defects [20].

Near-field microwave probes consist of reflectometers that transmit an incident wave and receive waves reflected from the material under test. The incident and reflected wave are combined within the waveguide and detected by a microwave detector that provides a DC voltage output that is proportional to the magnitude and/or phase of the reflected signal [16]. Changes in the DC voltage result from the probe passing over a region of material with different reflection characteristics, such as an area in which the FRP is debonded from the concrete substrate. This detection system can be combined with a spatial tracking device, such as a mechanical scanning system, to provide 2-D representation of voltage output that can show the area of a subsurface defect [16,21].

The near-field characteristics of the open-ended waveguide are such that the stand-off distance between the probe and the surface of the material can be optimized to maximize signals from subsurface defects [16,21]. In the near-field region, reactive (stored) fields dominate and as such, the distance between the radiator and the target can have significant effects on the field characteristics and system response. Additionally, the field interactions with material under test are complex and difficult to predict without the use of analytical and numerical models [17]. Fortunately, stand-off distances can be optimized using empirical techniques [16]. This is accomplished by measuring probe output voltages over a range of stand-off distances while the probe is directed at the FRP material that is sound (no debonds) and while the probe is directed at a debonded region. A multilayer electromagnetic formulation has also been developed that can be used to estimate appropriate stand-off distance based on electromagnetic theory [20,21].

Detection of interlayer debonds and delaminations using an open-ended rectangular waveguide probe has been accomplished in layered composite materials [20,22]. This approach is applicable to dielectric composite materials (i.e., nonconductive). Additional complexity is introduced when examining conductive materials such as carbon fiber reinforced polymer composites (CFRPs). For CFRPs, microwaves penetrate the composite material easily when the signal polarization and the fiber direction are orthogonal and reflect almost completely when the polarization and fiber direction are parallel [16]. This effect can be utilized to detect changes in standoff distance when parallel polarization is used.

Figure 37.3 shows a microwave system fielded to detect debonds in a CFRP overlay repair on a bridge structure [16]. The system consists of a scanner to control and record the spatial location of the microwave probe, a control module, microwave probe, and laptop computer. This system can be utilized for the detection of embedded debonds, as shown in Figure 37.4 [23]. In this figure, two subsurface embedded debonds detected by the microwave probe are shown on a 2-D image showing the location of the debonds within the scanned area.

FIGURE 37.3 On-site microwave inspection apparatus (scanner, laptop, control module, and microwave probe) for detecting disbands between CFRP laminates and a bridge member.

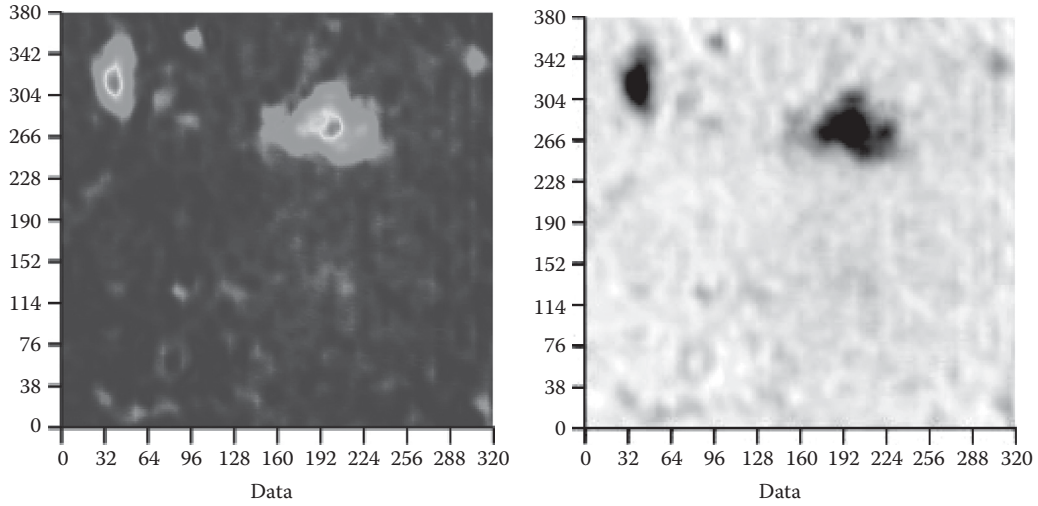

FIGURE 37.4 Microwave image of a CFRP laminate showing embedded disbands. (From Zoughi, R. and Nanni, A., Preservation of Missouri transportation infrastructure: Validation of FRP composite technology through field testing, MoDOT contract RI02-022, University of Missouri, Rolla, MO.)

REFERENCES

1. Duke, Jr., J.C., Case, S., and Lesko, J.J. (2003). NDE of FRP bridge beams and decks. *Proceedings of the Review of Quantitative Nondestructive Evaluation—American Institute of Physics Conference*, Melville, New York.
2. Keller, T. (2001). Recent all-composite and hybrid fibre reinforced polymer bridges and buildings. *Progress in Structural Engineering and Materials* 3(2): 132–140.
3. Kawagoe, M., Hashimoto, S., Nomiya, M., Morita, M., Qiu, J., Mizuno, W., and Kitano, H. (1999). Effect of water absorption and desorption on the interfacial degradation in a model composite of an aramid fibre and unsaturated polyester evaluated by Raman and FT infra-red microspectroscopy. *Journal of Raman Spectroscopy* 30: 913–918.

4. Hammami, A. and Al-Ghuilani, N. (2004). Durability and environmental degradation of glass–vinylester composites. *Polymer Composites* 25(6): 609–616.
5. Chin, J.W., Aouadi, K., Haight, M.R., Hughes, W.L., and Nguyen, T. (2001). Effects of water, salt solution and simulated concrete pore solution on the properties of composite matrix resins used in civil engineering applications. *Polymer Composites* 22(2): 282–297.
6. Yang, H.K. (1992). *Kevlar Aramid Fiber*. New York: Wiley & Sons.
7. Karbhari, V.M., Chin, J.W., Hunston, D., Benmokrane, B., Justka, T., Morgan, R., Lesko, J.J., Sorathia, U., and Reynaud, D. (2003). Durability gap analysis for fiber-reinforced polymer composites in civil infrastructure. *Journal of Composites for Construction* 7(3): 238–247.
8. Kumar, B.G., Singh, R.P., and Nakamura, T. (2002). Degradation of carbon fiber-reinforced epoxy composites by ultraviolet radiation and condensation. *Journal of Composite Materials* 36(24): 2713–2733.
9. Li, G., Pang, S., Helms, J., Mukai, D., Idekwe, S., and Alaywan, W. (2002). Stiffness degradation of FRP strengthened RC beams subjected to hygrothermal and aging attacks. *Journal of Composite Materials* 36(7): 795–812.
10. Hamilton, H.R. and Dolan, C.W. (2000). Durability of FRP reinforcements for concrete. *Progress in Structural Engineering and Materials* 2(2): 139–145.
11. Karbhari, V.M. (2001). Materials considerations in FRP rehabilitation of concrete structures. *Journal of Materials in Civil Engineering* 13(2): 90–97.
12. Mtenga, P.V., Parzych, J.G., and Limerick, R. (2001). Quality assurance of FRP retrofit using infrared thermography. *Proceedings of ASCE Structures Congress*, Washington, DC.
13. Nishizaki, I. and Meiarashi, S. (2002). Long-term deterioration of GFRP in water and moist environment. *Journal of Composites for Construction* 6(1): 21–27.
14. Washer, G.A. (2003). Nondestructive evaluation for highway bridges in the United States. *Proceedings of the International Symposium on Nondestructive Testing in Civil Engineering*, Berlin, Germany.
15. Hsu, D.K., Barnard, D.J., Peters, J.J., and Dayal, V. (2000). Physical basis of tap test as a quantitative imaging tool for composite structures on aircraft. *Review of Progress in Quantitative Nondestructive Evaluation* 19: 1857–1864.
16. Akuthota, B., Hughes, D., Zoughi, R., Myers, J., and Nanni, A. (2004). Near-field microwave detection of disbond in carbon fiber reinforced polymer composites used for strengthening cement-based structures and disbond repair verification. *Journal of Materials in Civil Engineering* 16(6): 540–546.
17. Zoughi, R. (2000). *Microwave Nondestructive Testing and Evaluation*. Boston, MA: Kluwer Academic Publisher.
18. Feng, M.Q., De Flaviis, F., and Kim, Y.J. (2002). Use of microwaves for damage detection in fiber reinforced polymer-wrapped concrete structures. *Journal of Engineering Mechanics* 126(2): 172–183.
19. Zoughi, R. and Bakhtiari, S. (1990). Microwave nondestructive detection and evaluation of disbonding and delamination in layered-dielectric-slabs. *IEEE Transactions on Instrumentation and Measurement* 39(6): 1059–1063.
20. Bakhtiari, S., Qaddoumi, N., Ganchev, S.I., and Zoughi, R. (1994). Microwave noncontact examination of disbond and thickness variation in stratified composite media. *IEEE Transactions on Microwave Theory and Techniques* 42(3): 389–395.
21. Hughes, D., Kazemi, M., Marler, K., Myers, J., Zoughi, R., and Nanni, A. (2001). Microwave detection of delaminations between fiber reinforced polymer (FRP) composite and hardened cement paste. *Proceedings of the Review of Progress in Quantitative Nondestructive Evaluation—American Institute of Physics Conference*, Brunswick, ME.
22. Ganchev, S.I., Qaddoumi, N., Ranu, E., and Zoughi, R. (1995). Microwave detection optimization of disbond in layered dielectrics with varying thickness. *IEEE Transactions on Instrumentation and Measurement* 34(4): 326–328.
23. Zoughi, R. and Nanni, A., Preservation of Missouri transportation infrastructure: Validation of FRP composite technology through field testing. MoDOT contract RI02-022, University of Missouri, Rolla, MO.
24. Alberski, T.C. (2000). The role of fiber prestress in improving damage resistance of composite laminates. PhD thesis, Rensselaer Polytechnic Institute, Troy, NY.
25. O'Connor, J., Aref, A., Alampalli, S., and Triandafilou, L. (2011). Strategic development and deployment of a composite bridge deck. *Advanced Composites in Construction Conference (ACIC)*, Warwick, U.K., September 2011.
26. Ettouney, M. and Alampalli, S. (2011). *Infrastructure Health in Civil Engineering: Applications and Management*. CRC Press, Boca Raton, FL.

38 Nondestructive Evaluation Methods for Composite Materials
Infrared Thermography

Glenn A. Washer and Sreenivas Alampalli

CONTENTS

INTRODUCTION

The application of infrared thermography for the inspection of civil structures has been increasing rapidly in recent years. The availability of thermoelectrically cooled thermal cameras and their increasing cost-effectiveness has contributed to this, as well as the improved camera technology and rugged, fieldable designs that are battery operated and highly portable. This section will provide an overview of several applications of thermal cameras, as well as some of the fundamental physical phenomena that contribute to the effectiveness of the method.

THEORY

The basic principle behind thermographic inspections of civil structures is that the flow of heat through the material being inspected is disrupted by the presence of a defect in the material. The disruption in heat flow manifests in an observable change in temperature at the surface of the material, which in turn is detected by an infrared camera and displayed on an image. While this seems a relatively simple approach, there are many complications encountered. First, there are typically several different materials comprising the structure being inspected. For example, a concrete structure has embedded steel rebar, typically has areas that are dirty, stained or wet, and may have coatings or other materials on the surface. Each of these materials have different thermal properties that create a high noise level in the image, that is, there appears to be thermal contrast between the materials that are not related to any defect or flaw. Second, the environmental

conditions surrounding the test, such as ambient temperature, thermal loading due to sunshine and wind, have significant effects on the thermal image that is produced. These environmental factors are difficult to define and vary over time. Finally, the temperature differences that result from subsurface defects can be small. This section provides an introduction to the theory behind thermographic inspections with the intention of illuminating some of the challenges faced in developing this technology.

Heat Flow

The rate of heat transfer across a solid in steady state can be expressed using the Fourier equation:

$$q_x = -kA_x \frac{dT}{dx} \tag{38.1}$$

where

A_x is the surface area normal to the direction of heat flow x
q_x is the rate of heat transfer in watts

The thermal conductivity, k, is a material property that is commonly expressed in watts per meter–degree Celsius ($\mathrm{w\,m^{-1}\,°C^{-1}}$) and represents the conduction rate for a gradient of 1°C. For homogenous materials, conduction is isotropic, but for materials such as fiber composites, conduction rates can vary significantly depending on direction. FRP composites typically have highly anisotropic conduction properties for the fiber themselves, as shown in Table 38.1. However, the resin matrix and epoxies used to bond composites are generally isotropic, mitigating the anisotropic conduction properties when viewed in a macroscopic sense, such as through a infrared camera when temperature variations across the viewing field are small.

The Fourier equation presents the most basic relationship for heat transfer in materials, representing a steady state in which heat transfer is independent of time. For realistic cases, the situation is typically more complicated by time-varying heat input and different thermal properties (e.g., k values) of materials making up the system being examined.

TABLE 38.1
Thermal Properties of Materials for Use in FRP Retrofitting of Concrete Beams

Material	Specific Heat ($\mathrm{J\,kg^{-1}\,°C^{-1}}$)	Density ($\mathrm{kg\,m^{-3}}$)	Thermal Conductivity ($\mathrm{W\,m^{-1}\,°C^{-1}}$)	Thermal Diffusivity ($\mathrm{m^2\,s^{-1}} \times 10^{-6}$)
Concrete	800	2400	1	0.53
CFRP	1200	1600	7	3.7
Epoxy resin	1700	1300	0.2	0.09
GFRP	1200	1900	0.38	0.17
Steel	440	7900	46	13
Air (defect)	700	1.2	0.024	33
Water	4180	1000	0.6	0.14

Source: Maldague, X.P., *Theory and Practice of Infrared Technology for Nondestructive Testing*, Wiley & Sons, New York, 2001.

For civil structures, particularly those exposed to the environment, convective heat transfer can play a significant role in the heat transfer. The convective heat transfer rate away from a surface can be expressed as:

$$q_c = h_c A_s (T_S - T_A) \tag{38.2}$$

where
q_c is the rate of heat transferred from the surface of area A_s
T_S is the surface temperature of the solid
T_A is the air temperature

The convective transfer coefficient, h_c, is typically an average value that depends on a number of factors, including the wind speed and air density. Of significance in this equation is the fact that for a large difference in temperature between the structure being inspected and the air temperature, the rate of convective heat transfer will be large. If the wind speed is high, the convective transfer coefficient will be high and the rate of transfer will also be high. The result of these effects is that the high rate of convective heat transfer can act to homogenize the surface temperature, masking subsurface defects. For this reason, procedures for applying infrared thermography under field conditions typically include provisions limiting the allowable wind speed during the inspection (ASTM D4788-03).

Transient Heat Flow

The fundamental theory of transient heat transfer in solids is provided by a diffusion equation that can be expressed in one dimension as [1]:

$$k\frac{\partial^2 T}{\partial x^2} - c\rho\frac{\partial T}{\partial t} = -H \tag{38.3}$$

where
T is the temperature
t is the time
x is the depth into a semi-infinite plate
H is the heat input from a source
c is the specific heat of the material
k is the thermal conductivity of the material
ρ is the density

This equation can be solved for the case of a semi-infinite plate whose surface temperature is suddenly increased and held constant, such that a transient heat flow is induced in the plate until equilibrium is reached [2,3]. This transient heat flow causes the temperatures within the plate to vary as a function of time according to the relation

$$(T_d - T_i) = (T_i - T_\infty) erf\left(\frac{x}{2\sqrt{\alpha t}}\right) \tag{38.4}$$

where
T_d is the temperature at any depth x in the plate
T_∞ is the applied constant surface temperature
T_i is the initial temperature of the solid
erf is the Gaussian error function
α is the thermal diffusivity of the materials

The thermal diffusivity of a material is the relationship between its thermal conductivity, density, and specific heat:

$$\alpha = \frac{k}{\rho c} \tag{38.5}$$

and describes how fast a material heats up and cools down under transient conditions. The equations can be examined qualitatively for the case of civil materials when some of the properties of materials involved, shown in Table 38.1, are examined. For example, concrete has a high specific heat, that is, it takes a great deal of energy to change the temperature of a given mass of concrete relative to steel. The thermal conductivity is also relatively low for concrete, indicating that the rate of heat flow through concrete will be relatively low and as a result the diffusivity is also low. Values of specific heat for GFRP and CFRP indicate that these materials also require large amounts of energy to be heated; carbon fibers have a significantly higher thermal conductivity than do glass fibers. However, the epoxy resins commonly used to bond the materials together have a very low thermal conductivity and diffusivity, and as a result the epoxy can cause thermal perturbations when heat is applied. It should be noted that the mass of FRP typically used for retrofitting civil structures is generally low relative to concrete and steel to which they are applied, and as a result heat relatively quickly (compared to the concrete to which they are attached) in practical situations. Also significant is the thermal properties of air, which has very high specific heat and extremely low thermal conductivity. As a result, during transient heating, thermal transfer is interrupted by the presence of air such as would be found at the interface of a subsurface delamination. Finally, the specific heat of concrete, epoxy, and FRPs is significantly lower than water, and as a result areas with varying moisture contents may heat and cool at different rates, making interpretation of thermal images more difficult. As the moisture within concrete and FRPs under field conditions can rarely be known, this introduces an additional complexity to the interpretation of images.

Emissivity

Infrared cameras can be used to infer temperature of a material but are in fact not thermometers but rather radiometers, which measure the electromagnetic radiation emitted or reflected from the surface of a material. The power of emitted radiation can be expressed by the Stefan–Boltzmann equation:

$$E = \varepsilon \sigma T^4 \tag{38.6}$$

where

E is the radiant energy emitted by a surface at all wavelengths
ε is the emissivity of the materials
σ is the Stefan–Boltzmann constant (5.67×10^{-8} W $(m^2\ K^4)^{-1}$)
T is the temperature in degrees Kelvin

The emissivity of a surface is the ratio of its emissive power relative to a black body. A black body absorbs all incident radiation regardless of wavelength and incident direction, such that there is no reflection and all of the radiation leaving the surface is emitted by the surface. As such, a black body is a perfect emitter and provides a useful comparison. For real materials, not all incident radiation is absorbed; some are reflected from the surface. Emissivity values are generally available such that the infrared radiation can be related to the temperature of the objects being observed. However, the emissivity of a material is a *surface property* that states the ability of the surface of an object to emit energy. The same material with different surface, e.g., painted concrete versus unpainted concrete, will appear to be at different temperatures when in fact the emissivity of the surface is different, but

the temperature is not. The surface roughness of a material will also have an effect on emissivity values with rough surfaces generally having higher emissivity than smooth surfaces.

An additional complication is that emission from a black body diffuses isotropically, that is, independent of direction. Charted values typically available represent the ratio of emitted power normal to the surface of the material; emitted radiation for a real material is dependent on direction, and as such the real emittance from a material may be different when the angle of observation is not normal.

APPLICATIONS TO COMPOSITE STRUCTURES

The most frequent application of infrared thermography for the inspection of composite structures is the detection and quantification of delaminations and debonds. This section will describe the application of active and passive thermal methods for the inspection of composite laminates applied to beam strengthening and column wrapping.

Passive Thermography

Passive methods of thermographic inspection can be applied to the detection of defects in FRP repairs where FRP is bonded to the surface of a concrete structure. For passive thermography, the temperature gradient required is supplied by the ambient environment, which include the surrounding air, and possibly sunshine, and the concrete structure itself. Concrete structures are typically massive in size and have relatively low thermal conductivity. As a result, the diurnal temperature changes of the ambient environment are out of phase with the diurnal temperature changes of the concrete. When daytime temperatures vary significantly from nighttime temperatures, the concrete will warm slowly through the course of the day through absorption of radiant energy from the sun and by convective heat transfer from warm air surrounding the concrete. However, this warming will lag significantly in time from the surrounding air, and as such there is an imposed thermal gradient. This effect is commonly used for the inspection of concrete bridge decks. For bridge decks, direct solar loading provides additional thermal gradient that improves the detectability of subsurface features.

The main advantage of this approach to thermal testing is that it requires minimal interaction with the structure under inspection. Thermal cameras can be used to view the thermal conditions from some distance, primarily determined by the required spatial resolution and atmospheric effects. This advantage can be undermined if the surface of the structure under inspection requires cleaning to provide constant thermal signature. The primary disadvantage of this approach is that it requires significant diurnal temperature variations to impose sufficient gradients, such that subsurface defects can be detected, typically in the range of 10°C. However, if there is direct radiant energy from the sun, it will provide a thermal gradient at lower diurnal temperature variations; the wind speed and relative humidity of the air surrounding the concrete will also affect the rate of heat transfer from the environment to the structure, and hence, the thermal gradient. As a result, passive techniques tend to be more qualitative than active methods where a better understanding of the thermal conditions during the test exists.

Figure 38.1 indicates a subsurface defect detected by passive thermography. In this case, the defect detected is in a debond between the concrete repair patch and a concrete box girder. The composite laminate was a multilayer carbon FRP applied with epoxy resin. Damaged concrete has been removed and repaired to provide a suitable surface for the application of the FRP laminate. The defect is approximately 40 mm deep into the concrete repair patch, but is clearly visible in the infrared image.

A large debonded area of FRP wrap surrounding a concrete column is shown in Figure 38.2 [4]. The large debonded area shown in the figure indicates the importance of quality control during the construction of FRP wraps. Figure 38.2 also illustrates the usefulness of thermal imaging as a rapid scanning method that requires minimal interaction with the structure being inspected.

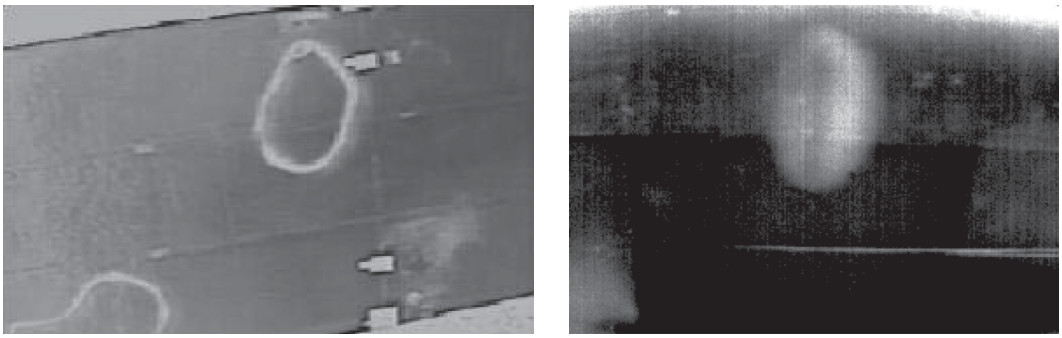

(a) (b)

FIGURE 38.1 Thermal images of a delaminated portion of carbon–fiber composite. (a) Video image showing area detected by a tap test and (b) IR image of the same area.

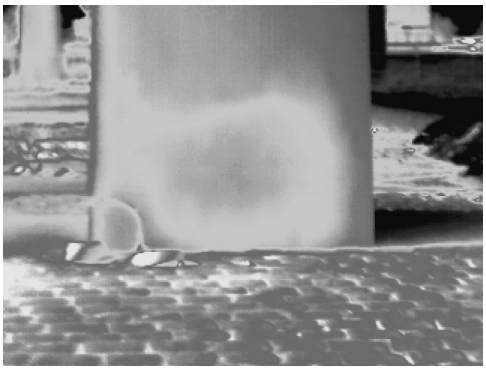

FIGURE 38.2 Thermographic images of a large debonded area in a FRP-wrapped bridge column.

Active Thermography

For the detection of debonding between FRP column wraps and underlying concrete materials, variations of pulsed active thermography have been applied [5,6]. For pulsed thermography, heat is applied to the surface under inspection for a short period of time, typically on the order of seconds to minutes for FRP materials in civil structures. The time of application of heat obviously depends on the heat source, typically a quartz halogen lighting fixture of some design, the anticipated depth of the defect, and the thermal diffusivity of the material under test. The heat source is then removed and the temperature decay at the surface is monitored over time as the heat applied at the surface diffuses into the material. Underlying delaminations between layers of the FRP wrap, or debonding between the overwrap and concrete substrate, can be detected due to the lack of heat transfer across the subsurface defect. As a result, the heat input from the external heating source is maintained slightly higher in the area directly above the delamination or debond. The contrast in an image created by the perturbation in heat transfer generally varies inversely with the cube of depth [5]:

$$c \approx \frac{1}{z^3} \tag{38.7}$$

where

c is the image contrast

z is the depth of the defect

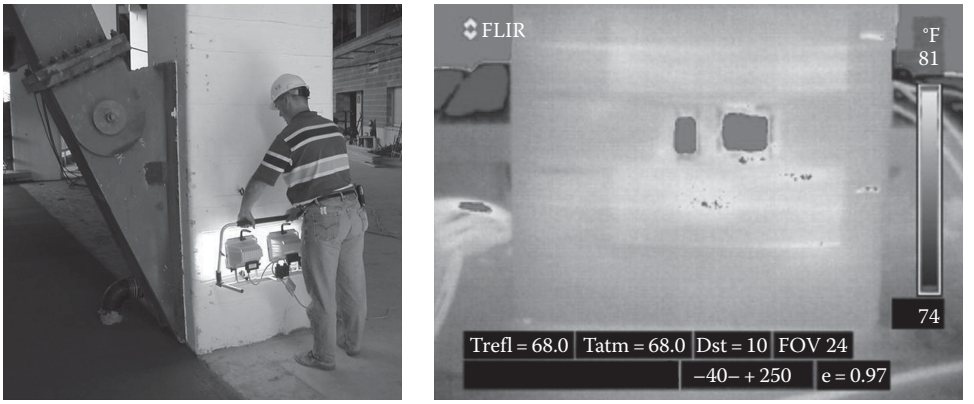

(a) (b)

FIGURE 38.3 Photographic and thermographic images of a hand-wrapped column with debonded areas: (a) heating of the column and (b) thermograph showing results from thermographic inspection. (Images courtesy of Wiss, Janney Elstner, Inc., Northbrook, IL.)

The time for this contrast to appear in the image generally varies with square of depth and depends on the diffusivity of material [5]:

$$t \approx \frac{z^2}{\alpha} \tag{38.8}$$

Figure 38.3 illustrates the application of thermography to a FRP hand-wrapped column. To perform the thermographic inspection, quartz heat lamps were used to provide a thermal gradient in the material, as shown in Figure 38.3a. Figure 38.3b shows the thermographic results clearly indicating the presence of debonded or delaminated areas of overwrapped FRP.

A consideration for the application of heat to the surface of the composite is generating uniform heat input such that the area of the composite being imaged is increased in a relatively consistent manner. A variety of heat input devices have been used for applying heat to the surface of a composite. A quartz halogen bulb is a typical heat source that is widely available in commercial devices such as work lights. Care should be taken to ensure that the heating is consistent as possible, as the induced temperature variations from inconsistent heating will result in a noisy image, making defects more difficult to detect. The thermal diffusivity of composite materials is commonly low such that heat applied to the surface takes some time to diffuse through the composite material. Generally, the higher the heat input to the surface, the larger the contrast above a defect will be.

Heat sources that have been used include heating blankets, heat guns, quartz heaters, and quartz halogen bulbs [7–10]. For the work by Hawkins, a special assembly was constructed that included several bulbs mounted on a wheeled assembly that maintain a constant distance between the lamps and the surface. Bulbs were spaced such that the areas between bulbs did not result in cool spots, and the assembly was driven by a clock motor such that a constant rate of heat application was obtained [6,10].

Cleaning

An important aspect of conducting thermal inspections of composite materials is cleaning [10]. The emissivity of a material is a surface property such that dust-covered material will emit radiation at a different rate than a clean surface and will absorb heat at a different rate as well. As such, it is important that the surface be clean of dust and other contaminants that may obscure images. For the case of civil structures, surface contamination can vary significantly across a single structure such

that cleaning of the structure may be required to ensure that effective inspections can be conducted. Washer (2009) provides detailed guidelines for thermographic inspection of concrete bridges based on a research project involving experimental studies and limited field testing [11–14].

REFERENCES

1. Spicer, J.M., Osiander, R. (2002). Active thermography. In: *Nondestructive Evaluation: Theory, Techniques and Applications*, P.J. Shull (ed.). New York: Marcel Dekker. Vol. 1, p. 841.
2. Lienhard, J.H. (1981). *A Heat Transfer Textbook*, Prentice Hall, Englewood Cliffs, NJ.
3. Starnes, M.A. (2002). Development of technical bases for using infrared thermography for nondestructive evaluation of fiber reinforced polymer composites bonded to concrete, PhD Thesis, Department of Civil and Environmental Engineering, Massachusetts Institute of Technology, Cambridge, MA.
4. Alampalli, S. (2001). Fiber reinforced polymers for rehabilitation of bridge columns, *Proceedings of the Fifth National Workshop on Bridge Research in Progress*, Minneapolis, MN, pp. 37–42.
5. Maldague, X.P. (2001). *Theory and Practice of Infrared Technology for Nondestructive Testing*. New York: Wiley & Sons.
6. Johnson, E.C., Nokes, J.P., Hawkins, G.F. (1999). NDE of composite seismic retrofits to bridges. *Nondestructive Characterization of Materials IX, AIP Conference Proceedings 497*, Sydney, New South Wales, Australia, pp. 367–372.
7. Mtenga, P.V., Parzych, J.G., Limerick, R. (2001). Quality assurance of FRP retrofit using infrared thermography. *Structures 2001, ASCE*.
8. Limerick, R., Mtenga, P., and Tawfiq, K. (2004). IRT evaluation of bond layer thickness for CFRP bonded to concrete, *16th World Conference on NDT*, Montreal, Quebec, Canada.
9. Halabe, U.B., Bangalore, G., Gangaroa, H.V.S., Klinkhachorn, P. (2003). Infrared scanning of FRP composite members. *Proceedings of Twenty-Ninth Review of Quantitative Nondestructive Evaluation*, Vol. 22, Bellingham, WA, pp. 1003–1010.
10. Hawkins, G.F., Johnson, E.C., Nokes, J.P. (2001). In-field monitoring of the durability of composite materials. Aerospace Report No. ATR-2001(7595)-1:20, Aerospace Corporation, Springfield, VA.
11. Washer, G.A., Fenwick, R. G., Bolleni, N.K. (2009). Development of hand-held thermographic inspection technologies, Report No. OR10-007, Final Report Missouri Department of Transportation, Jefferson City, MO.
12. Washer, G., Bolleni, N., Fenwick, R., Alampalli, S. (2008). Environmental factors for the thermographic inspection of highway bridges, *Structural Materials Technology (SMT): NDE/NDT for Highways and Bridges Topical Conference*, American Society for Nondestructive Testing, Oakland, CA, September 2008.
13. Washer, G., Fenwick, R., Bolleni, N., Harper, J., Alampalli, S. (2008). Thermal imaging for bridge inspection and maintenance, *10th International Bridge and Structure Management Conference*, Transportation Research Board Circular No. E-C128, Buffalo, NY, pp. 164–171, October 2008.
14. Washer, G., Fenwick, R., Bolleni, N. (2010). Effects of solar loading on infrared imaging of subsurface features in concrete. *Journal of Bridge Engineering*, ASCE, 15(4), 384–390.

39 Nondestructive Evaluation Methods for Composite Materials
Acoustic Methods

Glenn A. Washer and Paul Ziehl

CONTENTS

INTRODUCTION

The application of acoustic wave-based NDE methods is widespread in many engineering disciplines. For civil structures, a common application is ultrasonic testing that is used during the fabrication of metal structures. The method generally consists of launching a high-frequency acoustic wave from a transducer and detecting reflections that occur. Reflections resulting from internal discontinuities such as cracks, voids, and inclusions can be detected and analyzed to estimate the size, location, and shape of the discontinuity. This is the most fundamental application of ultrasonic testing, but many methods of monitoring the behavior of waves propagating in materials exist and have been applied for the nondestructive evaluation of FRP materials. This section will describe several approaches that have been utilized for the detection of defects in FRP-wrapped structures and for characterizing the material properties of FRP composites.

It is useful to first review the fundamental theory behind the propagation of elastic waves, that is, ultrasonic waves in solid materials. For the case of a homogeneous, linear-elastic anisotropic solid, the equation of motion can be expressed [1] as

$$c_{ijkl}\left(\frac{\partial^2 u_k}{\partial x_i \partial x_j}\right) = \rho \ddot{u} \tag{39.1}$$

where

σ_{ij} is the stress
c_{ijkl} are the second-order elastic constants
$\partial u_k / \partial x_l$ is the strain tensor expressed in terms of displacements, u_k and direction x_l
$\ddot{u}$ is the time differential of displacement (acceleration)
ρ is the density

For anisotropic materials, the number of elastic constants depends on the symmetry of the elastic properties. For an isotropic material, there are only two independent elastic constants according to the relations

$$c_{11} = c_{22} = c_{33} = \lambda + 2\mu \tag{39.2}$$

$$c_{12} = c_{13} = c_{23} = \lambda \tag{39.3}$$

$$c_{44} = c_{55} = c_{66} = \mu \tag{39.4}$$

where λ and μ are the Lamé constants.

The elastic constants can be related to the velocity of ultrasonic waves propagating through a material by the relations [1]

$$v_l = \sqrt{\frac{\lambda + 2\mu}{\rho}} \tag{39.5}$$

$$v_s = \sqrt{\frac{\mu}{\rho}} \tag{39.6}$$

where

v_l is the longitudinal wave velocity

v_s is the shear wave velocity in any direction in the isotropic material

The Lamé constants have direct relation to engineering constants Young's Modulus, E, shear modulus G, and Poisson's ratio, ν, according to the relations [1]

$$E = \frac{\mu(3\lambda + 2\mu)}{(\lambda + \mu)} \tag{39.7}$$

$$\upsilon = \frac{\lambda}{2(\lambda + \mu)} \tag{39.8}$$

$$G = \mu \tag{39.9}$$

These equations demonstrate the velocity of ultrasonic waves and can be used to determine the elastic constants of anisotropic and isotropic materials. The relationship between the wave velocity, modulus, and density of a solid material is used in a variety of engineering applications. The second-order elastic constant, c_{ij}, is infrequently of concern to civil engineers, as materials are typically considered to be isotropic, such that directionality of the constants loses meaning. Of course, for composite materials used in civil structure, there may be a high degree of anisotropy in the material, and vastly different elastic properties along fiber directions relative to perpendicular to the fiber direction. These equations have shown application to determine, for example, the effect of fiber direction on the velocity of ultrasonic waves [2].

Even the isotropic Lamé constants are difficult to determine under field conditions, as it requires measurement of both the longitudinal and shear wave velocities to determine their value. However, empirical relations can be drawn such that wave velocities can be used for qualitatively estimating the modulus of a material using the relationship

$$v_l \approx \sqrt{\frac{E}{\rho}} \tag{39.10}$$

which can be derived from a 1-D wave equation. This equation is useful for demonstrating that as a material's modulus decreases, the velocity decreases proportionally to the root of the modulus change. This effect is used in many qualitative applications, including pulse velocity measurements in concrete, where reductions in pulse velocity are correlated with damaged or deteriorating concrete.

Reflection-based ultrasonic techniques can be used to evaluate the quality of bond between the FRP overlay and the concrete surface. This method consists of launching a high-frequency ultrasonic wave into the surface of the FRP laminate. Reflections occur at the interface of the composite layer and the substrate due to the acoustic impedance mismatch between the two materials. The acoustic impedance of a material is related to the materials density and stiffness through the equation

$$z = \rho v_l \tag{39.11}$$

where z is the acoustic impedance of a material. When two materials are bonded together with an adhesive, such as an adhesively applied composite overlay, the impedance contrast between areas that are bonded and areas that are unbonded can be significant due to the low impedance of air (at the debond). The amplitude of reflections that occur at an interface is given by [3]

$$A_r = A_i\left(\frac{z_2 - z_1}{z_2 + z_1}\right) \tag{39.12}$$

where

A_r is the amplitude of the reflected wave
A_i is the amplitude of the incident wave
z_1 is the acoustic impedance of the material in which the wave is propagating as it approaches an interface
z_2 is the acoustic impedance of the material beyond the interface

As this equation shows, the amplitude of the reflected wave is proportional to the difference in acoustic impedances of the two materials that are bonded together.

This effect has been utilized by Bastianini et al. [4] to detect debonded areas between an aramid FRP (AFRP) and a cast iron beam. The AFRP was to be applied to a cast iron bridge structure in Venice, Italy, as a strengthening mechanism for the structure that was built in 1852. Due to the importance of the bond between the AFRP and the iron substrate, NDT methods were explored in the laboratory in preparation for the field installation of the strengthening scheme on the bridge. To evaluate ultrasonic methods of detecting debonds between the AFRP and the iron beam, a specimen with embedded, simulated defects was developed in the laboratory. The simulated defects were made by inserting a polyethylene foil between the AFRP surface of a 73 cm × 11.5 cm section of an iron beam removed from an iron bridge of the same type and era as that to be retrofitted. A schematic diagram of the simulated defects is shown in Figure 39.1, which illustrates six defects with dimensions as described in Table 39.1. Three of the simulated defects included an air bubble inserted between two layers of polyethylene foil as indicated in Table 39.1.

The sensitivity and spatial resolution of the ultrasonic approach was evaluated by generating C-scan images based on measurements made at each point in a 20 mm × 20 mm grid mesh, and applying false colors to either time-based or amplitude-based data. C-scan images are common in ultrasonic testing as a method of creating spatial images of ultrasonic data, either time, amplitude, frequency, or a derivative of these three fundamental wave properties. This allows for more rapid

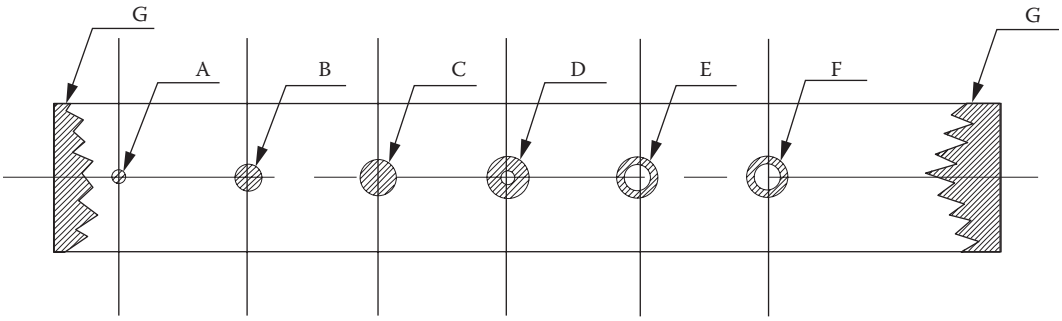

FIGURE 39.1 Schematic diagram of embedded debonds between a ARFP laminate and cast iron beam.

TABLE 39.1
Dimensions of Polyethene Foils Embedded at the ARFP–Iron Interface for Evaluating Ultrasonic Test Methods

Defect	Diameter (mm)	Thickness (mm)	Air-Filled Bubble Dimension (mm)
A	15	0.8	—
B	20	0.8	—
C	28	0.8	—
D	30	1.0	15
E	30	1.0	20
F	30	1.0	20
G	Detachment at ends due to improper handling		

interpretation of data and displays results in a manner that can be related spatially to the object under inspection.

Bastianini et al. [4] utilized three different ultrasonic approaches in detecting the embedded defect. First, a normal contact transducer with a center frequency of 2.0 MHz was used to generate a C-scan display. The color-coded amplitude measurements of reflections from the AFRP/iron bond interface are shown in Figure 39.2a. This allowed for relatively poor resolution of the embedded defects.

A second approach was used that included a delay line inserted in the beam path to extend the temporal location of reflections from the AFRP/iron interface. Delay lines are common in ultrasonic testing to resolve near-surface features, as the time required for the wave to pass through the delay line causes reflections to be detected later in time. This removes the reflected signals from the initial pulse that drives the sensor and allows amplifier circuits to dampen. The results for a 3.5 MHz transducer with a 25.4 mm delay line are shown in Figure 39.2b. This figure again shows the amplitude of the reflected signals, color-coded to provide a spatial image. Increased sensitivity was achieved using the delay line, in part due to the reduced noise levels experienced when the reflections being measured are moved away (in time) from the initial pulse. The delay-line transducers were also of higher frequency, which would be expected to result in resolution of smaller features due to the shorter resulting wavelength.

The third approach used by Bastianini et al. [3] involved a dual-element probe that includes two separate piezoelectric crystals in a single sensor. A dual-element probe transmits the ultrasonic pulse through one element and receives reflected waves through the second element. This has the effect of reducing the noise in the receiver circuits that result from the initial pulse. This provides

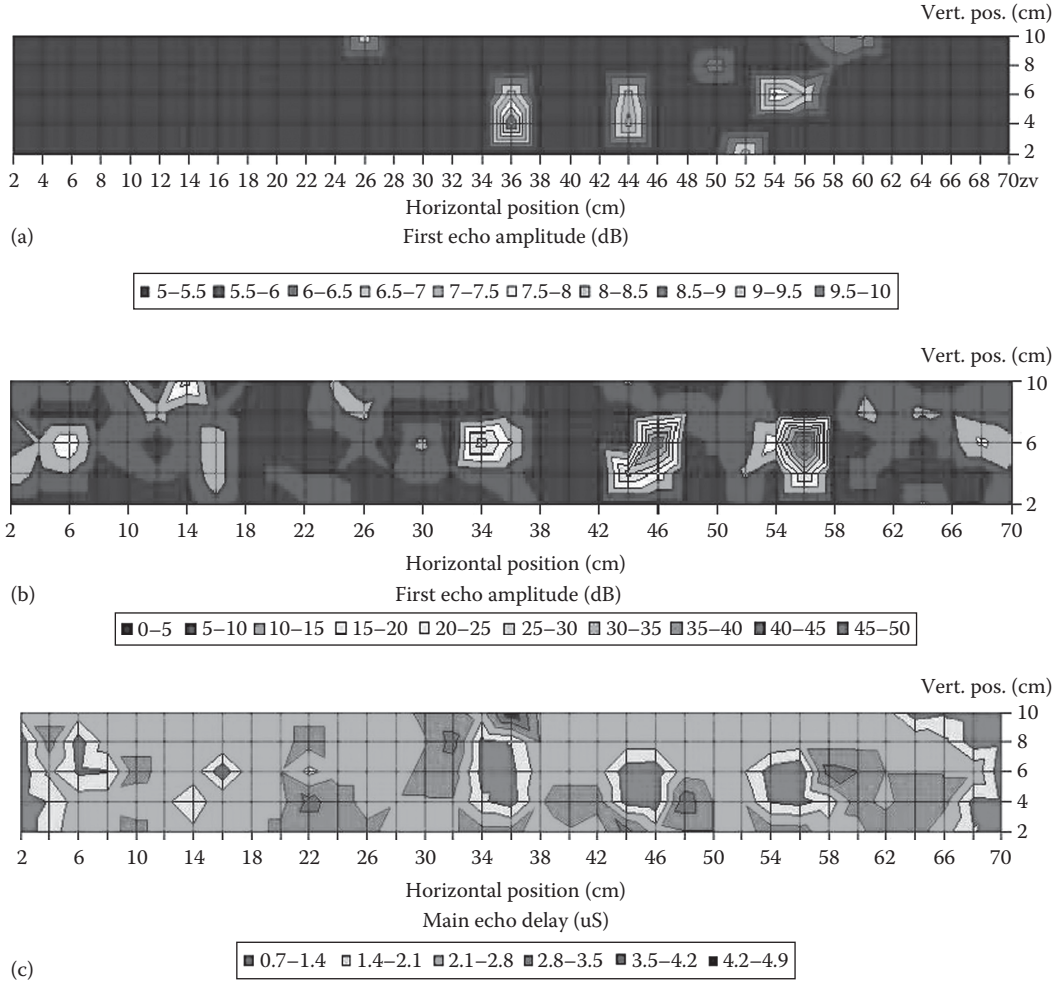

FIGURE 39.2 Ultrasonic C-scan images showing ultrasonic response to debonded AFRP applied to a cast iron beam. (a) Normal probe first-echo amplitude 2.2 MHz, (b) reflection amplitude using 1 in. delay line, 3.5 MHz probe, and (c) TOF response of dual element probe (4 MHz).

better resolution of near-surface features, and this type sensor is frequently used for the evaluation of coatings and for thickness measurement of thin plates. The improved sensitivity of this transducer allowed for a time-of-flight (TOF) measurement approach to be used in which the TOF to the most important reflection was plotted in the C-scan results shown in Figure 39.2c. The improved sensitivity of the dual-element probe provided many large-amplitude reflections due to multiple reflections in the case of well-bonded AFRP, and only one or two echoes referable to the probe-FRP and FRP-defect transitions are apparent in defective areas. This approach used a 4 MHz probe, and the increased resolution of the simulated defects is apparent in Figure 39.2c.

As Figure 39.2 illustrates, there are many approaches to conducting an ultrasonic inspection based on the reflection of ultrasonic waves. These approaches can be generally referred to as pulse-echo techniques, and there are a considerable number of commercially available instruments and transducers for conducting this type of inspection. The advantage of pulse-echo techniques is that the approach is relatively simple and robust, and the interpretation of data is also relatively simple. The primary disadvantage is that the technique requires contact with the surface of the specimen to achieve acoustic coupling, and the area inspected is essentially directly beneath the transducer. To evaluate a large structure is consequently very labor intensive and requires access to the entire

surface area to be inspected. Noncontact approaches have developed in recent years using either low-frequency, air-coupled ultrasound or laser ultrasonics, though the latter is not commonly available for field use.

There exists a myriad of other acoustic techniques that utilize ultrasonic waves to detect subsurface defects such as debonds and to evaluate material properties of FRP composites. The following sections review some of these approaches.

ACOUSTO-ULTRASONICS

An acousto-ultrasonic approach to evaluate the bond quality for composite overlays has also been demonstrated [5]. In this approach, the FRP composite overlay and a concrete substrate are modeled in as a layered media, and energy vectors of a propagating acoustic wave within the layers are predicted by a model that considers the frequency dependence of reflection coefficients. In this case, the reflection coefficients express the capacity of an acoustic energy to propagate within the layers, not simply between interfaces of material. As such, the propagating wavelength becomes a factor, that is, there is frequency dependence. The authors selected a frequency regime for an ultrasonic pulse, such that a debonded area of the FRP overlay (wrap) would produce a reduced amplitude signal as a wave propagated from a transmitter to a receiver.

A rolling transducer that operates without coupling is shown in Figure 39.3. A zero degree, longitudinal wave transmitter embedded in a rolling-wheel transducer is used to launch a 250 kHz acoustic wave. A receiving transducer in a separate wheel detects the acoustic wave propagating in the FRP. The transducer pair is mounted on a scanning bridge during the inspection to enable C-scans to be generated by plotting color-coded wave characteristics on a two-dimensional spatial image.

The received RF signals are shown in Figure 39.4 for an area that is bonded and an area that is debonded. The image shows the received wave packet from a 10 cycle tone burst in the transmitter, which is detected with higher amplitudes for bonded condition than for a debond. Figures 39.5 and 39.6 show a C-scan image of a partially debonded portion of FRP overlay, in which high-amplitude received signals are color-coded as dark green and low-amplitude received signals are assigned the red end of a color spectrum. The results shown are for a simulated defect generated by inserting a Teflon wafer between the concrete and the FRP overlay (wrap). A crack in the concrete is also apparent in the image.

A number of alternative approaches for acoustic-based NDE have been explored. The second-order elastic constants described in earlier equations have been measured using ultrasonic wave

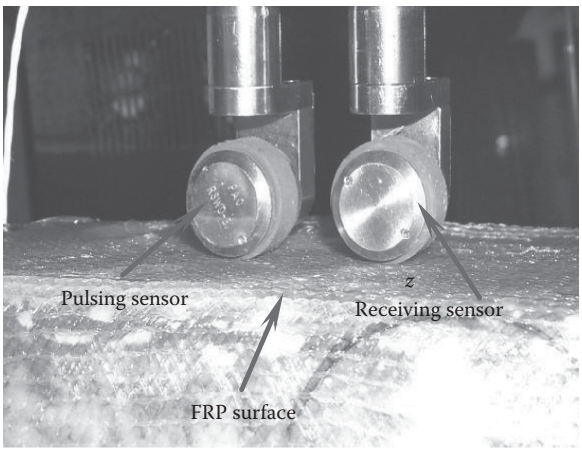

FIGURE 39.3 Detail of the rolling sensors during inspection of a FRP/concrete sample.

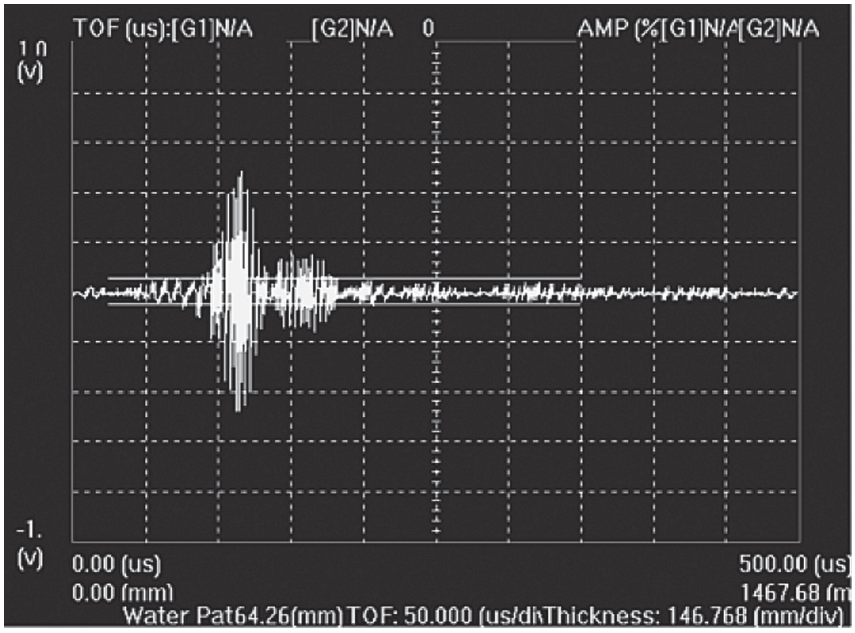

(a)

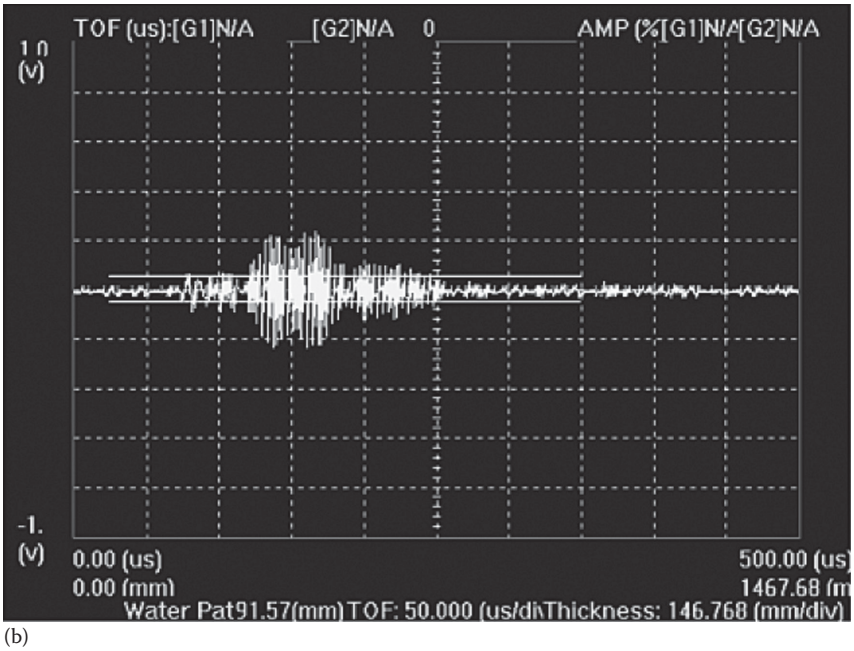

(b)

FIGURE 39.4 RF signals recorded with rolling sensors on an FRP/concrete sample: (a) Bonded area and (b) debonded area.

velocities and used to characterize pultruded composite members [6]. Longitudinal wave velocities in the axial and thru-thickness direction on a pultruded composite plate were used to determine the elastic constants corresponding to those directions, and comparison to values determined by mechanical testing were favorable. Ultrasonic measurements of this type have the potential to be applied for the quality control of composite materials or to measure degradation that manifest in changes in elastic properties of the composite material.

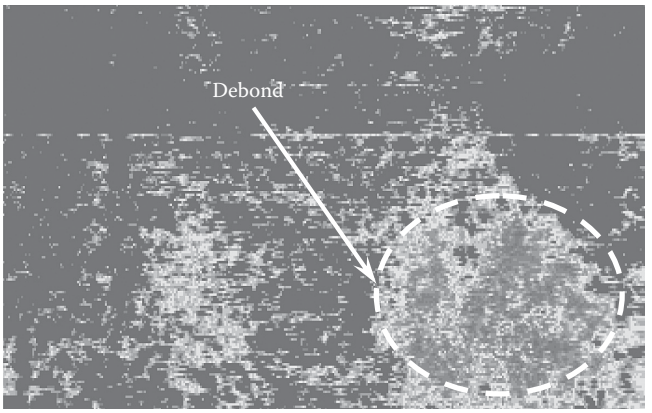

FIGURE 39.5 C-scan image of an FRP/concrete sample showing a debond between the FRP and concrete.

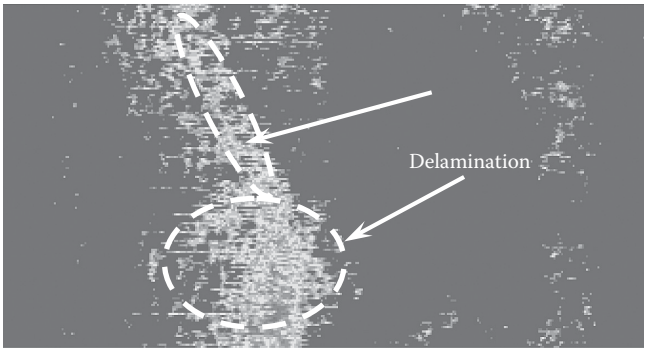

FIGURE 39.6 C-scan image of a FRP/Concrete sample showing a delamination inside the FRP and a crack in the concrete below the FRP wrap.

Rayleigh and Lamb Waves

Work has also been conducted to evaluate the use of Rayleigh waves for the NDE of FRP laminates and all-composite materials. A Rayleigh wave is a surface wave that induces an elliptical particle motion in a solid, with the majority of wave energy being concentrated with one wavelength of the surface such that [7]

$$d \approx \lambda = \frac{V_R}{F} \tag{39.13}$$

where
- d is the Rayleigh wave depth
- λ is the wave length
- V_R is the Rayleigh wave velocity
- F is the frequency

These wave modes are well suited for layered materials since the depth of penetration can be controlled by the frequency. The situation is more complex than suggested by the aforementioned equation for composite materials due to the effect of material and dispersion [8]. Dispersion is a phenomenon that results in wave velocities that vary as a function of frequency and is frequently associated with geometric shapes, such as plates or rods. If dispersion is present, a broadband waveform

will change shape as it propagates through the material, as higher frequency components of the wave travel at different velocities than low-frequency components. This makes velocity measurement difficult and requires more advanced signal processing schemes being adopted to characterize ultrasonic velocities as a function of wavelength.

Determining the dispersion relationship for a Rayleigh wave propagating in a pultruded composite has been used to monitor material degradation [8]. For this case, the dispersion results from the heterogeneous nature of the pultruded composite, and the relationship between the wavelength and the ultrasonic velocity has been used to detect deterioration resulting from exposure to heat and moisture. To provide a broadband ultrasonic pulse, a laser source was used to generate a thermoelastic pulse in the material. A laser interferometer that used the Doppler effect to measure out-of-plane particle velocity was used to detect the pulse. The detection scheme provided a broadband reception over a frequency range of 200 kHz–10 MHz.

This laser ultrasonic approach has several advantages over traditional methods. First, the approach is noncontact and eliminates difficulties introduced by the coupling layer required for traditional, piezoelectric ultrasonic transducers. Second, the generation and reception of ultrasonic pulses is broadband in nature, such that a single pulse contains a wide spectrum of wavelengths, whereas traditional ultrasonic transducers are typically narrow in bandwidth. Finally, there is the potential to develop laser ultrasonic systems that can scan large areas quickly by redirecting the laser light using mirrors.

Rayleigh wave velocities have also been used to monitor inter-laminar bonding of laminated FRP materials [7]. In this approach, a double-wedge sensor was used to initiate a Rayleigh wave in the surface layer of the CFRP. This sensor utilized a piezoelectric transducer initiate a pulse in an acrylic wedge coupled to a steel wedge. The steel wedge was pressed against the surface of the CFRP to initiate a Rayleigh wave in the material. Velocity measurements were made in pitch-catch arrangement, which utilizes a transmitting sensor and a separate receiving sensor. For this application, the wave velocity is determined by the time of flight of an ultrasonic pulse that is narrow band such that dispersive effects are less significant. Variations in velocity that resulted from resin-rich areas were measured and compared with bond thickness and strength [7].

Guided Lamb waves have also been used for the nondestructive evaluation of composite materials. Lamb waves are a plate mode of wave propagation that has geometric dispersion relationships. The elastic properties of the material, its density, and the plate thickness contribute to the specific dispersion relations for a given geometry. Lamb waves are useful for the plate geometry commonly used in FRP repairs and have been applied in the past to monitor materials' degradation for aerospace structures [9]. The stiffness, that is, modulus, of the composite material can be evaluated using Lamb waves if the density and plate thickness are known, and this effect has been used to determine the effects of long-term thermomechanical exposure [10]. The application of Lamb waves for civil FRP application has been limited, although for retrofit applications the Lamb wave approach would seem to be ideal.

In addition to its dependence on elastic properties, density, and plate thickness, dispersion relations depend on the boundary conditions of a plate. This effect has been explored as a means of using Lamb waves to investigate the quality and stiffness of the FRP/concrete bond [11,12]. This is accomplished by examining the dispersion relations for a Lamb wave propagating in the FRP composite. For this research, a laser ultrasonic system was used to provide broad bandwidth and enable the dispersion relationship to be determined without frequency bias [11,12]. The difference in the dispersion relations for a free (unbonded) FRP laminate plate and a plate bonded to a concrete substrate was explored. It was found that for a well-bonded FRP plate, an ultrasonic pulse traveled with a velocity approaching the Rayleigh wave velocity, while an unbonded plate exhibited multimode, Lamb-wave behavior.

Other acoustic approaches have been used to evaluate FRP materials. Ultrasonic pulse velocities measured in a through-transmission mode have been used to evaluate the integrity of FRP wrapped

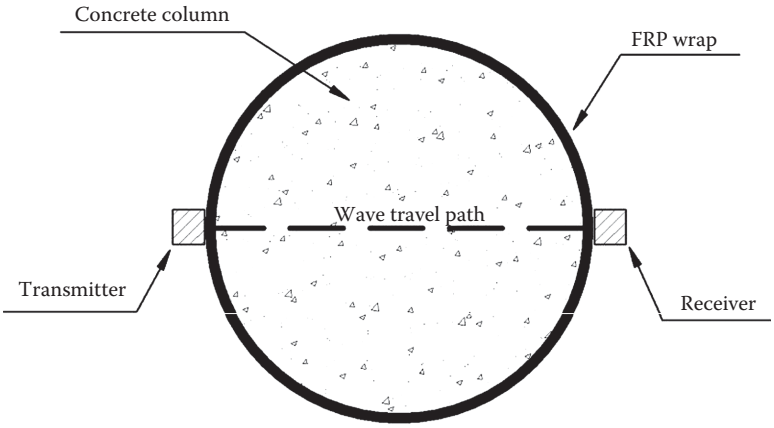

FIGURE 39.7 Schematic diagram of through-transmission ultrasonic approach for an FRP-wrapped column.

concrete columns tested to failure in the laboratory [13]. In through-transmission mode, an ultrasonic pulse is launched from one side of the object under inspection by the transmitter and received on the opposite side by the receiver, as shown in Figure 39.7. The transmitter and receiver are typically transducers of the same design such that they are interchangeable. The damage induced along the travel path of the wave manifests in reduced velocity, that is, increased travel time from the transmitter to the receiver. This technique is commonly applied for the qualitative measurement of deteriorated concrete. The advantage of this technique is that it is simple to apply and there is extensive experience in applying this technique to plain concrete structures. The primary disadvantage of this approach is that it requires simultaneous access to both sides of a structure. Additionally, it can be difficult to localize where, along the travel path of the wave, the damage has occurred.

ACOUSTIC EMISSION

The use of acoustic emission for monitoring and evaluation of composite structures has its background in the composite piping and pressure vessel industries. In those industries, acoustic emission has been used routinely for qualification of new vessels and for evaluation of in-service vessels since the early 1980s and it is standardized in ASME codes [14–16]. Standardized procedures for in-service evaluation have likewise been developed for composite aerial devices [17]. For civil engineering structures, it has been used for quality assurance of composite elements prior to field installation [18], as shown in Figure 39.8, and to detect ongoing damage of composite structures in the field [19–21].

The AE technique detects transient elastic waves that are generated by a number of sources in composite materials, including fiber breakage, matrix cracking, fiber-matrix debonding, and delamination within the composite material. It has also been used to detect delamination and debonding between composite strengthening systems and reinforced concrete beams [22]. The transient elastic waves are detected with piezoelectric sensor. Correlations can be made between several different received parameters, including signal strength, amplitude, and duration and the level of damage in the material or structure. Acoustic emission is most often used as a global method of evaluation. When damage is detected by acoustic emission, the source can often be located by a number of different techniques, including zonal location and triangulating between different sensors based on time-of-flight. If a more precise image of the damage is desired, more localized methods of assessment, such as ultrasonics, are frequently used for follow-up investigations.

The amount of acoustic emission generated is dependent on the degree of damage that is present and the loading history. Two important and related effects are the Kaiser effect and the Felicity

FIGURE 39.8 Composite bridge beams evaluated with acoustic emission for quality assurance prior to installation.

effect [23]. The Kaiser effect is a lack of acoustic emission during reloading to a level of load that was previously attained (Figure 39.9). The Felicity effect is the inverse of the Kaiser effect, or the presence of acoustic emission activity during reloading to a level of load that was previously attained. Research has shown that the presence of the Felicity effect is correlated to significant damage in composite structures and the stronger this effect the more significant the damage [24,25]. An ASME test procedure [14] has been developed that is based on this effect for the design of FRP pressure vessels [21].

This technique is in a sense destructive, because damage must occur for emission to be generated. However, the amount of damage that is necessary to generate AE is minute. In fact, the extreme

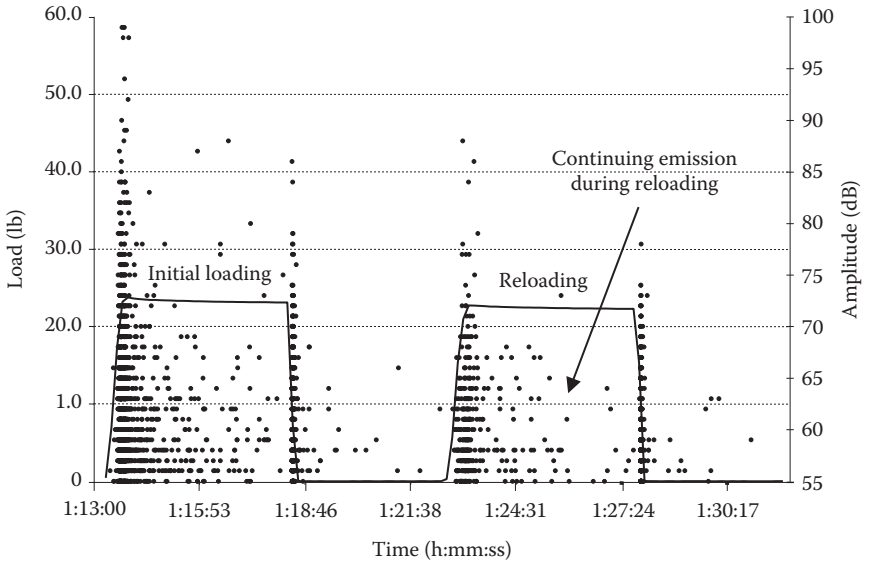

FIGURE 39.9 Example of the Felicity effect in reinforced concrete beam strengthened with composite materials.

sensitivity of the method is one of the considerations for applying it in a field environment because seemingly insignificant sources such as rain, wind-born debris, and even pedestrian traffic on a vehicular bridge can cause unwanted (sometimes referred to as "spurious") emission. The fact that damage must occur for AE to be generated does not generally limit the application of the technique because it is most often used to determine whether significant damage is present at or slightly above service-level loading. In the event that significant damage is not present, appreciable acoustic emission will not be generated provided the structure has been loaded to service levels previously. In the event that significant damage is present, the damage can be located and techniques for assessing the severity of the damage have been developed [26,27]. Similar methods have been reported for the evaluation of reinforced concrete structures and a recommended practice has been developed [28–30]. For composite civil systems, such as FRP decks and FRP strengthened reinforced concrete beams, similar protocols for assessing the severity of damage in the field are under development.

Acoustic emission is a useful laboratory tool for monitoring damage in test specimens during loading or load holds. The evaluation of damage caused by fatigue loading and the prediction of remaining service life have been the subject of laboratory investigations for composite piping [31]. The method has also been used to evaluate the damage caused by fatigue loading of a full-scale FRP honeycomb bridge specimen and to track the damage progression [20,32].

REFERENCES

1. Green, R.E. (1973). *Ultrasonic Investigation of Mechanical Properties*. Academic Press, New York.
2. Zimmer, J.E., Cost, J.R. (1970). Determination of the elastic constants of a unidirectional fiber composite using ultrasonic velocity measurements. *Journal of Acoustic Society of America*, 47(3): 795–803.
3. Sansalone, M.J., Streett, W.B. (1997). *Impact Echo: Nondestructive Evaluation of Concrete and Masonry*. Bullbrier Press, Jersey Shore, PA.
4. Bastianini, F., Ceriolo, L., Di Tommaso, A., Zaffaroni, G. (2004). Mechanical and nondestructive testing to verify the effectiveness of composite strengthening on historical cast iron bridge in Venice, Italy. *Journal of Materials in Civil Engineering*, 16(5): 407–413.
5. Godinez-Azcuaga, V.F., Gostautas, R.S., Finlayson, R.D., Miller, R., Trovillion, J. (2004). Nondestructive evaluation of FRP wrapped concrete columns and bridges. *Structural Materials Technology Conference*, Buffalo, New York.
6. Littles, J.W., Jacobs, L.J., Zurieck, A.H. (1998). Ultrasonic techniques to characterize pultruded composite members. *Journal of Composites for Construction*, 2(3): 126–131.
7. Zurn, B., Mantell, S.C. (2001). Nondestructive evaluation of laminated composites using Rayleigh waves. *Journal of Composite Materials*, 35(12): 1026–1044.
8. Dokun, O.D., Jacobs, L.J., Haj-Ali, R.M. (2000). Ultrasonic monitoring of material degradation in FRP composites. *Journal of Engineering Mechanics*, 126(7): 704–710.
9. Seale, M.D., Madaras, E.I. (1999). Lamb wave characterization of the effects of long-term thermal-mechanical aging on composite stiffness. *Acoustical Society of America*, 106(3): 1346–1352.
10. Seale, M.D.M., Eric, I. (2000). Lamb wave evaluation of the effects of thermal-mechanical aging on composite stiffness. *Journal of Composite Materials*, 34(1): 27–38.
11. Luangviai, K., Punurai, W., Jacobs, L. (2002). Guided lamb wave propagation in composite plate/concrete component. *Journal of Engineering Mechanics*, 128(12): 1337–1341.
12. Luangviai, K., Punurai, W., Jacobs, L.J. (2002). Guided wave technique to characterize repaired concrete. *American Institute of Physics*, 21: 1220–1226.
13. Mirmiran, A., Wei, Y. (2001). Damage assessment of FRP-encased concrete using ultrasonic pulse velocity. *Journal of Engineering Mechanics*, 127: 126–135.
14. ASME. (2011). *Reinforced Thermoset Plastic Corrosion Resistant Equipment*. RTP-1, ASME, New York.
15. ASME. (2013). *Section V—Nondestructive Examination*. American Society of Mechanical Engineers Boiler and Pressure Vessel Code, New York.
16. ASME. (2013). *Section X—Fiber-Reinforced Plastic Pressure Vessels*. American Society of Mechanical Engineers Boiler and Pressure Vessel Code, New York.
17. Ternowchek, S., Mitchell, J. (1992). *Advances in AE Technology for Testing of Aerial Devices*. American Society of Testing and Materials Special Technical Publication, Philadelphia, PA, pp. 68–82.

18. Ulloa, F., Medlock, R., Ziehl, P., Fowler, T. (2004). A hybrid FRP bridge for Texas. *Concrete International*, 26(5): 38–43.
19. Duke, J.C., Case, S., Lesko, J.J. (2003). NDE of FRP bridge beams and decks, in *Review of Quantitative Nondestructive Evaluation*, Thompson, D.O. and Chimenti, D.E (eds.), American Institute of Physics, Melville, New York, pp. 1178–1184.
20. Ziehl, P., Engelhardt, M., Fowler, T., Ulloa, F., Medlock, R., and Schell, E. (2009). Design and live load evaluation of a hybrid FRP/RC bridge superstructure system, *ASCE Journal of Bridge Engineering*, 14(5): 309–318.
21. Ziehl, P. and Pollock, A. (2012). Acoustic emission for civil structures, in *Acoustic Emission*, Sikroski, W. (ed.), Intech, Rijeka, Croatia, pp. 1–22.
22. Johnson, D., Shen, W., Finlayson, D. (2001). *Acoustic Emission Evaluation of Reinforced Concrete Bridge Beam with Graphite Composite Laminate*. Technical Report, Physical Acoustics Corporation, Princeton Junction, NJ.
23. ASTM. (2013). *Standard Terminology for Nondestructive Examinations*. ASTM E-1316-13a, American Society of Testing and Materials, Philadelphia, PA.
24. Fowler, T., Gray, G. (1979). *Development of an Acoustic Emission Test for FRP Equipment*. American Society of Civil Engineers Convention and Exposition, Boston, MA.
25. Fowler, T.J., Blessing, J.A., Conlisk, P.J. (1989). New directions in testing. *Proceedings of the Third International Symposium on Acoustic Emission from Composite Materials*, Paris, France.
26. CARP. (1987). Recommended practice for acoustic emission evaluation of fiber reinforced plastic (FRP) tanks and pressure vessels. The Committee on Acoustic Emission from Reinforced Plastics, The American Society for Nondestructive Testing (ASNT), Columbus, OH.
27. Fowler, T., Blessing, J., Strauser, F. (1992). Intensity analysis, *Proceedings of the Fourth International Symposium on Acoustic Emission of Composite Materials*, ASNT, Seattle, WA.
28. JSNDI. (2000). Recommended practice for in situ monitoring of concrete structures by acoustic emission. Japanese Society for Nondestructive Inspection, NDIS 2421, Tokyo, Japan, p. 6.
29. Ohtsu, M., Uchida, M., Okamoto, T., Yuyama, S. (2002). Damage assessment of reinforced concrete beams qualified by acoustic emission. *ACI Structural Journal*, 99(4), 411–417.
30. Columbo, S., Forde, M., Main, I., Shigeishi, M. (2005). Predicting the ultimate bending capacity of concrete beams from the relaxation ratio analysis of AE signals. *Construction and Building Materials*, 19: 746–754.
31. Ramirez, G., Ziehl, P., Fowler, T. (2004). Nondestructive evaluation of FRP design criteria with primary consideration to fatigue loading. *ASME Journal of Pressure Vessel Technology*, 126: 1–13.
32. Cole, T., Lopez, M., Ziehl, P. (2006). Fatigue behavior and nondestructive evaluation of full-scale fiber-reinforced polymer honeycomb bridge specimen. *Journal of Bridge Engineering*, 11(4): 420–429.

40 Load Testing of Bridge FRP Applications

Sreenivas Alampalli and Osman Hag-Elsafi

CONTENTS

INTRODUCTION

Long-term serviceability of the FRP retrofitted structure is not easy to predict analytically or in a laboratory because in-service conditions of bridges are far more severe than the laboratory environment and load-transfer and deterioration mechanisms cannot be accurately incorporated in analytical models. It is also extremely difficult to simulate environmental fluctuations, freeze–thaw cycles, deterioration, and vehicular traffic under laboratory conditions. For these reasons, evaluation of retrofitted bridge structures/elements is usually based on their in-service performance and behavior. Field testing using controlled loads predominantly is used for this purpose. Generally, these load tests are conducted at time intervals under similar loading conditions and structural behavior is monitored for changes. If no changes have been observed and the structure's behavior duplicated previous behavior, the effectiveness of the retrofit system could be concluded. Considerable care should be taken when planning testing to monitor in-service structural behavior as it may require instrumentation to survive exposure to severe and adverse weather conditions for a long time.

This chapter provides guidance on instrumentation as a tool to evaluate effectiveness and monitor in-service performance of FRP retrofit installations on bridges. It is intended to provide

general guidelines for bridge engineers, not familiar with instrumentation and testing, to strategically set up plans to evaluate effectiveness and monitor performance of FRP installations in common highway bridge FRP retrofit applications.

INSTRUMENTATION AND TESTING

Instrumentation and load testing is an integral part of bridge engineering that is conducted to obtain reliable information about structural parameters and structural responses to live loads. It is not an easy task to develop general guidelines for instrumentation and load testing of FRP retrofitted bridges because bridges are not identical and retrofit problems are not always similar. In this regard, the objective of this chapter is to consider the role of sensors and instrumentation in two common FRP bridge applications. They include testing an FRP slab bridge and a deteriorated T-beam bridge that has been strengthened using FRP laminates.

Sensors

Strain gages, inclinometers, load cells, linear variable displacement transducers (LVDTs), and demountable gages are the most commonly used sensors in testing and monitoring of FRP retrofit bridge applications. These sensors are discussed briefly in this section.

Strain gages: Strain gages are widely used in bridge testing, primarily to measure strains in such structural components as girders, rebars, and concrete decks. Measured data can then be employed to calculate physical parameters, evaluate bridge load capacity, and monitor structural safety. Environmental conditions may play important roles in bridge testing. For example, self-temperature compensating-type gages are generally preferred when wide temperature variations are expected. Gages are welded or attached with adhesives to the structure. Demountable/reusable strain gages are becoming popular during the last few years. These can be easy to mount and reduce installation time in the field. Two or four arm gages are also favored as they increase the signal to noise ratios, and several gage combinations are sometimes adopted to measure different components of strain (such as shear, bending, and axial). Normally, strain gages require DC input in the range 0–15 V and give outputs in the same range. Measured voltages are then converted to strains/stresses using appropriate engineering relations.

Inclinometers: Inclinometers are used to measure inclination of various bridge elements due to distresses in the bridge system. They are mainly used to evaluate fixity of bridge girders at supports and to monitor long-term movements of piers, abutments, and girders for general assessment of structural integrity. Normally, inclinometers require DC input in the range 5–15 V and give outputs in the same range. Measured voltages are then converted to inclinations using their sensitivity.

Load cells: Load cells are normally used in bridge testing to measure naturally or mechanically induced loads for which structures are being subjected. Again, conversion of output voltages to loads is direct and is accomplished in a similar manner to that for inclinometers.

Linear variable displacement transducers: LVDTs are physical devices used to measure deflections of bridge members by converting measured displacements to equivalent voltages, which can be recorded using data acquisition systems. Creation of a stable support to serve as a datum is a major problem when measuring deflections on bridges. Field measurement of deflections is not easy, even though they can be related to member stiffness more directly than other parameters such as stresses, strains, and inclinations. However, in field testing of bridges, this is not always practical and more than often not possible.

Sensor Selection

Selection of sensors and test planning require examination of the retrofitted structure and identification of the important response parameters to be measured. In this section, the authors share their experience and provide some guidelines for sensor selection.

1. *Purpose of the sensor*: Although many sensors work on similar principles, they are not equally effective in measurement of certain parameters.
2. *Test type*: Test type is an important factor since it is not always possible to use the same sensor in each test. Many of the commercially available inclinometers require longer response time to obtain stable data, therefore, sampling speed or load cycle time is important and should be given special consideration. Sensor selection depends on loading type and expected structural response in each test. In many cases, different installation procedures and adhesive types may be required, depending on whether static or dynamic load effects are measured, so that gages may survive structural response duration.
3. *Test environment*: Test environment plays a major role in choosing a sensor. Specially, when one considers the fact that many of the available sensors are designed for laboratory applications and may not sustain inclement weather conditions without proper protection. However, there are a few rugged sensors specially manufactured for use in variable or hostile environments, which are more suitable in bridge testing. If these sensors are unattainable, proper weatherproofing (against temperature, dust, water, wind, and vibration) should be specified to meet necessary requirements for sensor operation. Even though they are relatively expensive, rugged gages are a must in long-term monitoring. When weatherproofing is required, the entire measurement system, including connecting cables, should be properly protected.
4. *Data range and resolution*: Response range during the entire test period has to be estimated before the sensor selection is made. Accuracy of some sensors varies when used to measure data at different ranges. Some sensors behave linearly only for a small part of their operable range and may behave differently for positive and negative responses. Hence, the sensor's operating range and required accuracy should be chosen with the expected response range in mind.
5. *Response resolution*: Resolution is often coupled with data range. Normally, the minimum possible range has to be used to obtain maximum resolution. Most available instrumentation converts analog response to digital response using A/D converters into a fixed number of steps. For example, 20 με data range with 12 bit A/D gives a resolution of 0.078 με. When the same A/D used with 200 με range gives a resolution of 0.78 με. If expected structural response is less than 10 με, a sensor with a range close to 10 με should be chosen. At the same time, when the data range is around 200 με, and if a resolution of 0.078 με is required, an A/D with a greater number of steps has to be used.
6. *Loading conditions*: Some sensors do not operate effectively under certain types of loading. Each sensor takes a brief time (reaction time) to stabilize, depending on its principle of operation. For example, many LVDTs and inclinometers require longer reaction time compared to strain gages. If structural response changes faster than the sensor reaction time, accurate data cannot be collected even when high sampling speeds are used. If transient or dynamic response is to be measured, sensors with short reaction times should be chosen. Also, when long-term monitoring is planned, possible instrument drift should be determined.
7. *Technical skills available*: Sensor selection also depends on available technical skills. While a large number of sensors can be installed with relative ease, a few installations need more experience and technical skills in order to obtain reliable and consistent data. For example, some strain gages are manufactured and sold with cables, which eliminate

the necessity for field soldering and connections. However, they are relatively expensive compared to their counterparts without cables, a trade off for the time saved and the lesser need for gage installation expertise.

8. *Software and hardware compatibility*: It is very important to select sensors that are software and hardware compatible. The excitation voltage, output voltage, wiring scheme, overload handling conditions, and resetting time of the hardware and software should be considered when selecting a sensor. It is possible to obtain sensors of very high accuracy, but if the software and hardware are less reliable, it may be more economical to choose sensors with the same order of reliability. For example, hardware is manufactured with either a fixed output range or a capability to choose different ranges. If both systems have the same 12 bit A/D boards, the latter system will give better accuracy and resolution; therefore, the sensor data range may not be very important in this case.
9. *Structure type*: Type of test structure is also critical in choosing a proper sensor type in some cases. Different adhesives and bonding procedures have different effects on material types. Also, prevailing standards and specifications should be considered. In steel bridges, drilling holes for gage installations in tension zones of bridge girders may not be permitted. Strain gages are made with materials to match thermal conductivity of structural materials to increase accuracy and reliability of measured data.
10. *Miscellaneous*: The aforementioned guidelines do not cover the entire criteria for sensor selection. Several factors such as cable types, distance between test structure and instrumentation, cable lengths, surrounding environment, and electrical installations are also important in deciding the right sensors for the test. For example, if the cable lengths between instrumentation and sensors are very long, then sensors with built-in amplifiers should be considered to reduce noise/signal ratio. Use of wireless sensors may have potential to save installation time and costs in some cases.

In summary, relying on the aforementioned guidelines and good engineering judgment, a variety of sensors can be considered first and then the most appropriate ones based on application, accuracy, reliability, repeatability, and available instrumentation could be selected.

STATIC LOAD TESTS

This section describes some details on instrumentation selection, test procedure, and data processing for static load testing.

Instrumentation

A multiplexer is used to scan data from a group or from all sensors during a test, usually with one signal conditioner allocated for each sensor group. Although this practice is cost-effective, it may not be possible to set different excitation voltages, gains, and filters for individual channels. Also, when mixed types of sensors are employed, it may not always be possible to set optimum input voltages for individual sensors. For example, even when the same type of strain gage is used, when mounted on different materials, optimum input voltages depend on the individual material thermal conductivity characteristics. Before the test is started, data collection sequence has to be specified and parameters such as input voltage and gain for an individual or a group of channels have to be determined. Once all the circuitry is checked, zero readings are recorded.

Test Procedure

The structure is loaded in steps and data are collected at the end of each step in digital form, using an analog to digital "A/D" converter. Data are normally stored in a file. Then, the second load

increment is applied and collected data are appended to the previous file. This process is repeated for each load increment. After the final predetermined load is reached, the structure is unloaded by removing the loads, generally in reverse order, while recording the response. Data are monitored continuously to observe structural behavior and to note any permanent deformations under the applied loads. Such tests are repeated to eliminate random noise effect by averaging and checking for nonlinearities and permanency. Whenever possible during the test, zero readings (data recorded with no load on the structure) are recorded to correct for drifts and experimental bias. Reported strains usually range from 1 to 400 με and could be much lower than 1 με when monitoring is conducted during construction stages.

Data Processing

Once testing is completed, the data are normally sorted by channels using a computer program, and the generated data file is imported to a spreadsheet. Load effects are calculated after subtracting earlier recorded zero values from the data acquired at the end of each load step. Collected data are manipulated in the spreadsheet environment to account for gain and excitation voltages for each channel. Engineering parameters (such as maximum strains, stresses, and inclinations) of interest to the test are calculated by applying appropriate formulae.

The majority of available software does not provide online data display and analysis capabilities. If the results at any intermediate stage between load increments are required during the test, the test has to be stopped and the data imported to the spreadsheet environment to obtain desired values. Also, for relatively long test times, such factors as drift and environmental conditions may influence test data. However, many software do not have provisions to account for these factors.

INSTRUMENTATION SELECTION

With emerging technology, many new instrumentation, data-acquisition systems, and processing software are becoming available. Many of these systems are built for general testing purposes and offer a wide range of choices such as customized analysis procedures, controlled sampling speeds, and improved accuracy.

This section lists general guidelines and recommendations on features to be considered when purchasing a test system. Selection of appropriate features is often governed by available technical skills, frequency of testing, test type and conditions, and availability of funds.

Hardware

Commercially available data-acquisition and analysis systems can generally be divided into two main categories [1]: (1) Several independent instrumentation devices grouped together as a test and measurement system with display and computation capabilities, usually controlled by a personal computer. However, there are integrated systems as well in this category that are capable of interfacing with microcomputers and accessing their drives for additional data processing; and (2) Systems consisting of several add-on cards installed inside a computer and controlled by resident software packages, primarily to collect data from sensors. Such data can then be analyzed by a host computer. Normally, these systems have two modules of cards referred to as daughter and mother/master boards. The mother/master board resides inside the computer. The daughter board includes an A/D converter, usually housed in an external box, and is connected to the mother board through cables. This is done to protect the A/D converter from the computer electric noise and to increase signal/noise ratio by keeping it close to the sensors. These systems are relatively less expensive than the former ones. However, they are not easily expandable (expandability is limited by the number of boards that can be supported by the computer).

The maximum sampling speed for each channel is also very important when conducting dynamic tests. Required sampling speed can be calculated by multiplying desired maximum sampling speed/channel by the maximum number of channels. This number of channels should include any possible future expansion. If additional channels are added later on, by adding cards or by supplementing the system with one or more units, problems may arise if higher sampling speeds are desired and were not initially considered. Updating the system with add-on cards for high sampling rates is sometimes quite expensive.

Necessary sources of excitation depend on the type of sensors being used. Also, it is preferred to have both constant voltage and constant current for each channel and that the hardware be capable of detecting simple wiring connection errors. It is necessary, in some applications, to have few D/A conversion channels and interrupts as they may be needed for setting external triggers needed in bridge testing. The system should also be suitable to provide software selectable gains, filters, excitation voltages, and high speed, high volume data sampling.

Analog to digital converter selection should be based on required accuracy in test measurements, which also depends on data range and data resolution described earlier in the paper. Currently, A/D converters with 16 bit resolution (65,536 steps) and systems that use the entire A/D conversion range in selected data ranges are available on the market.

Test hardware should accommodate mixed types of sensors such as strain gages, LVDTs, and inclinometers although each one may have its own requirements. For example, strain gages require electric bridge completion circuits (depending on strain gage resistance and number of active arms).

Finally, systems should be able to communicate with host computers and other instrumentation using standard interfaces such as IEEE, RS-232, USB, and serial ports. This gives the flexibility to upgrade host computers in the future to meet changes in complexity of post-processing needs. It is also desirable to have high RAM "memory" for stand-alone instrumentation, especially during high-speed and high-volume data sampling.

Software

Software selection is also very important while choosing a data-acquisition system. For efficient interfacing and operation, the software should be user friendly, menu-driven with online help, and be compatible with the computer operating system in order to take full advantage of available storage and memory. Generally, the software should:

1. Provide real-time display and scan at various scanning speeds
2. Have the ability to support different test setups
3. Be able to adjust gains, filters, excitation voltages, etc., for each channel
4. Be able to save test setups and definitions together with collected data
5. Be able to save, recall, and replay the data and test setup
6. Provide pseudo channels to manipulate data from different channels using user-defined formulae for onsite real-time display
7. Provide intelligent trigger modes and sources
8. Have the capability to store data in local computer disk drives in real time during high-speed and high-volume data acquisition
9. Have auto-balancing features
10. Be able to provide alarm conditions to detect abnormalities in collected data
11. Have a built-in formulae library to solve rosette info, etc., online at the test site
12. Have provisions to account for gage drift, temperature, etc.
13. Have internal and external calibration functions
14. Provide overload protection
15. Record pre- and post-trigger data
16. Be able to export data in spreadsheet format

17. Save raw as well as processed data with formulae
18. Check test setup for inconsistencies
19. Save all or only requested channels data
20. Have good high-resolution graphics
21. Show data with time or with any other reference channel
22. Have auto-scaling features for display
23. Have an efficient filing system
24. Possess onsite printing and plotting capabilities
25. Allow for customization
26. Have provisions to write comments during each phase of the test
27. Generate test reports at the end of the test

Analysis

The data-acquisition system should be capable of onsite data analysis, that is, the software should be able to run analysis routines during data acquisition using an internal sensor calibration library or user-defined formulae to obtain physical parameters such as stresses/strains. It is more informative to have these physical quantities displayed rather than raw data, such as voltages, to control the test more efficiently. These quantities should be displayed using high-resolution graphics as the test progresses, and they could be extremely useful in bridge testing to make such decisions such as discontinuing loading whenever structural distress is observed.

Miscellaneous

For field data acquisition, the system selection criteria should include portability, reliable operation even in severe weather conditions, protection against dust and rough handling. It should also be weatherproof and be able to sustain problems associated with transportation. Finally, good technical support, documentation, and training facilities are also important factors, as personnel changes are anticipated in every organization. Therefore, it is good practice to have unified software and hardware standards for smooth transition and increased reliability. With the advancements in technology and more demanding needs expected in the future, selected systems should be easily upgradeable to meet these challenges.

CASE STUDIES

This section will briefly describe two case studies. The first case study describes the load testing performed on a new FRP slab bridge to determine the structural capacity immediately after the installation and then the periodic testing conducted to determine its in-service performance. The second case study describes the load testing of a T-beam bridge strengthened using FRP laminates to improve its structural capacity.

Slab Bridge Load Testing

In late 1998, New York replaced a deteriorated concrete slab bridge with an FRP superstructure to remove the load posting and prolong service life. At the time of the bridge construction, FRP materials were relatively new to bridge applications and there was no data on their in-service performance. The bridge was thus load-tested (see Figure 40.1) to verify the assumptions used during the design, monitor the in-service performance, and to collect data for further study of failure mechanisms and bridge behavior under service loads, thermal loads, and fire. A proof-load test [2,3] was conducted using strain gages, dial gages, and LVDTs (see Figures 40.1 through 40.3) before the bridge was opened to traffic to determine its actual load rating for comparison with its theoretical

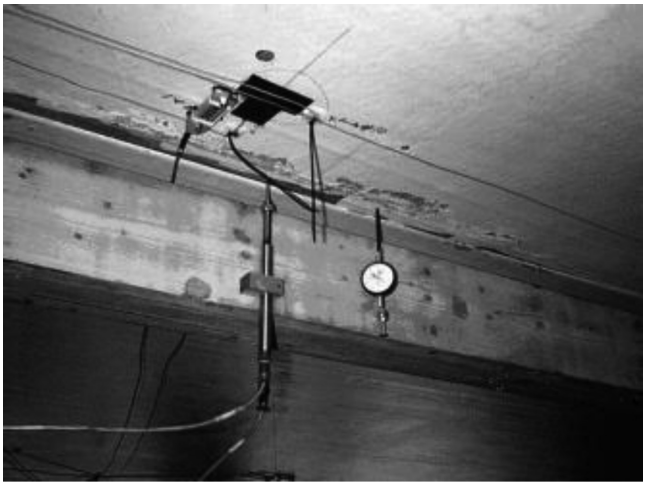

FIGURE 40.1 Strain gages, LVDT, and dial gages installed under an FRP slab bridge.

FIGURE 40.2 Proof-load testing of the FRP slab bridge.

load ratings, verify the integrity of the longitudinal shear-key, and establish baseline conditions for a future monitoring program. After the initial proof test was conducted, the load tests (see Figure 40.2) were repeated for three years to ensure that the structure was behaving satisfactorily and no degradation was noticed.

The FRP bridge superstructure is 7.8 m long and 10 m wide with a 30° skew. The superstructure was fabricated using E-glass/vinyl ester material and consists of two 61 cm deep, 5.03 m wide panels with vertical interior foam filled cells wrapped by E-glass fibers with top and bottom composite-fiber mats. A 9.5 mm thick polymer concrete wearing surface was used. More details can be found in Alampalli et al. [2]. Stress under service loads was conservatively limited to 20% of ultimate strength. The design was controlled by live-load deflection criteria which limited the maximum deflection to Span/800.

Four ten-wheel, loaded dump trucks, each closely resembling the AASHTO M-18 truck configuration, were used during the proof-load test [2]. The maximum strain recorded at any gage was 204 με, which was considerably less than the approximately 600 με predicted by the finite element analysis, indicating a significantly higher load capacity than anticipated (see Figure 40.4). The measured maximum deflection at midspan was less than 3.5 mm, which is considerably less than the

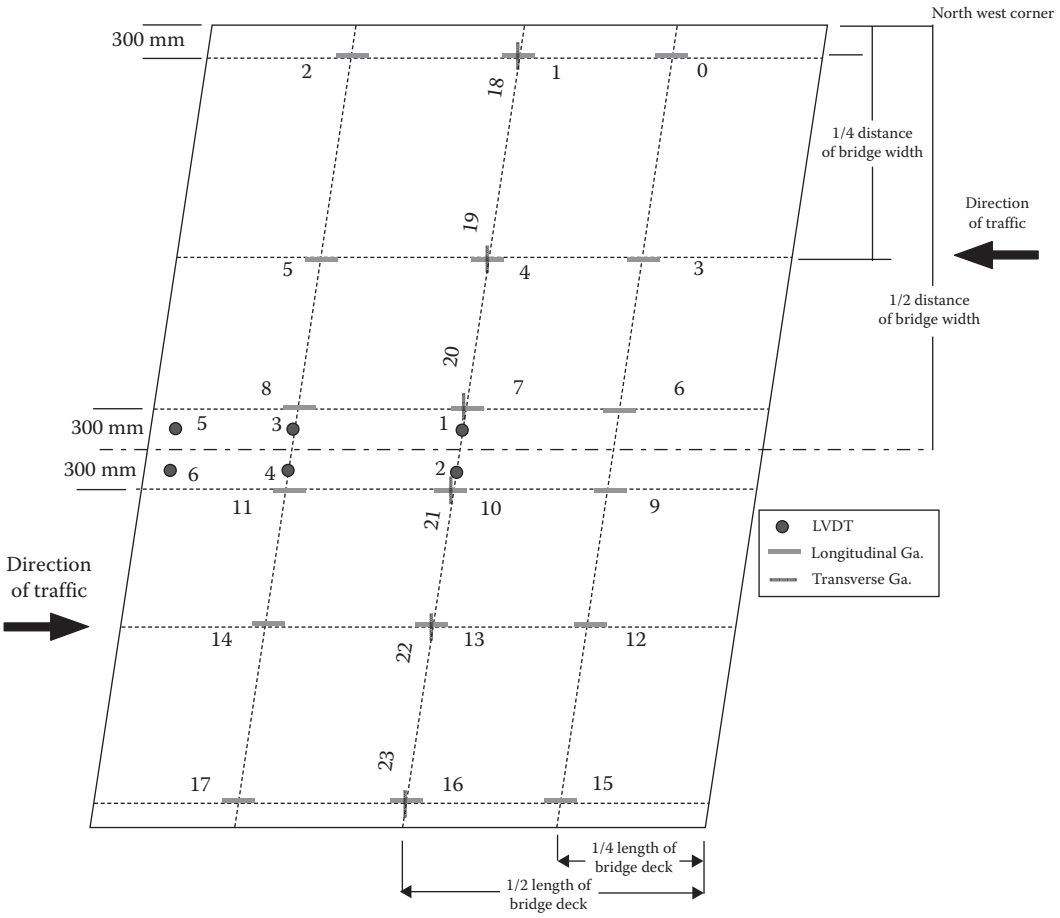

FIGURE 40.3 Sensor scheme for FRP slab bridge load testing.

Span/800 design limitation of 8.8 mm. The longitudinal joint along the centerline of the bridge was designed to carry the shear that developed along the plane resulting from the differential deflection of the two superstructure panels. The strain gages on both sides of the joint (1 vs. 2, 3 vs. 4, 5 vs. 6 in Figure 40.5) showed that the deflections and strains experienced by the gages on both sides of the joint are nearly the same, that is, the shear-key system is behaving as intended. The same was confirmed from the deflections measured using LVDTs [4].

The initial proof-load test was conducted during October 1998. Follow-up tests were conducted periodically over a period of several years [4]. The results indicated that the strain data from subsequent tests compare well to the initial proof-load test data, indicating that the FRP slab bridge and the shear-key are performing well without any structural/material problems (Figure 40.4). The impact factors calculated based on the truck driving at 5 and 55 mph were found to be as much as 50% and is similar to those documented in the literature for short span bridges.

These test data were used to generate calibrated finite element models of the bridge, which were used to further study the failure mechanisms, dynamic behavior, and the structural behavior under accidental damage and fire [5–7].

T-Beam Bridge Retrofit

A 70-year-old reinforced-concrete T-beam bridge in New York was retrofitted by the New York State Department of Transportation with an FRP composite laminates system. The bridge carries State Route

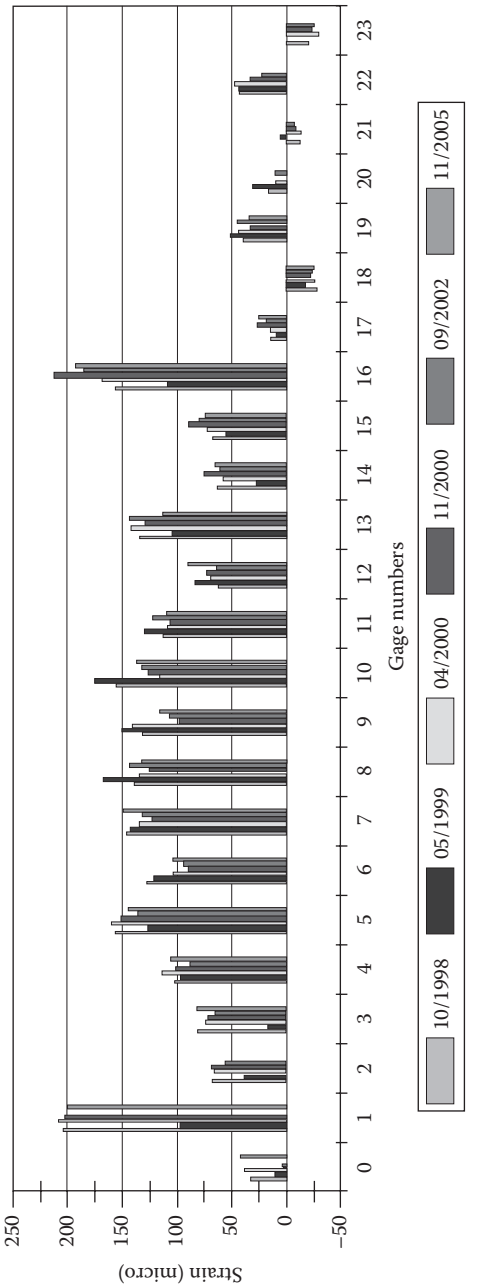

FIGURE 40.4 Strain data from the FRP slab bridge load tests.

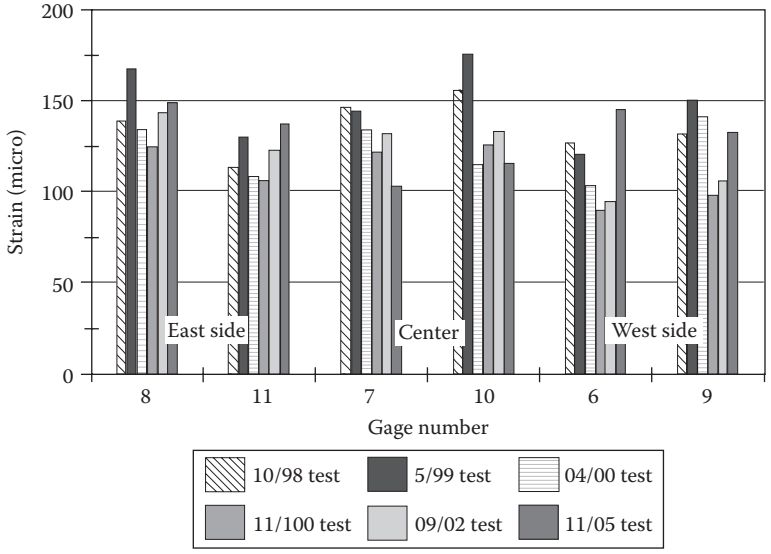

FIGURE 40.5 Strain data showing the FRP slab bridge shear-key effectiveness.

FIGURE 40.6 T-beam bridge side view.

378 over Wynanskill Creek in Rensselaer County (see Figure 40.6). The bridge is a 12.8 m long, 36.6 m wide, reinforced-concrete structure consisting of 26 T-beams. The bridge was retrofitted due to concerns over the integrity of the steel reinforcing and overall safety of the structure after observing damage to the beams and severe leakage of water contaminated with de-icing salts [8]. Design for shear and flexure was based on a laminates system compensating for an assumed 15% loss of the steel rebar area (Figures 40.7 and 40.8). The system consisted of FRP unidirectional carbon fibers having an ultimate strength of 3400 MPa and a guaranteed ultimate strain of 1.5%. In order to evaluate the effectiveness of the retrofit system and investigate its influence on the structural behavior of the bridge, the bridge was load tested before and after installation of the FRP laminates system [8,9].

Two lanes centered directly above beam 11 were loaded. Instrumenting 9 beams was judged to be adequate to reflect transverse live-load distribution (labeled 7–15 in Figure 40.8). For flexural evaluation, flexural steel and laminate strains were acquired at the midspan of these beams to provide information on live-load distribution. Three other locations on the center beam were also instrumented near the support to investigate the effect of the strengthening system on shear; and at quarter-span and

FIGURE 40.7 T-beams with FRP laminates.

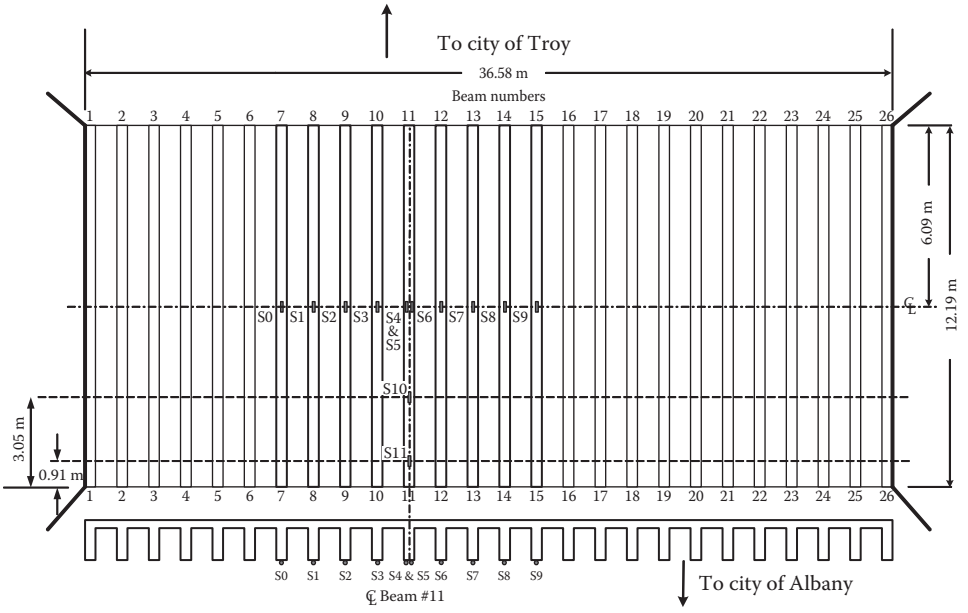

FIGURE 40.8 Strain gages on steel rebars.

midspan to assess laminate bond to concrete and laminate stresses. Locations of the instrumentation used to measure these strains on the steel rebars, concrete, and laminates are shown in Figures 40.8 through 40.10, respectively. Based on this plan, steel-reinforcement and laminate stresses, as well as effective flange width and position of the neutral axis on the center beam can be determined. Additionally, concrete shear stresses at one end of the center beam can also be determined.

Four trucks, each of the typical configuration shown in Figure 40.11 were used in the before and after installation load tests. Average weight of each of these trucks was approximately 196 kN. By assigning a unique letter, A through D, to each of the four trucks (see Figure 40.12), the testing was sequenced as follows: Truck A, Trucks A + C, Trucks A + B + C, Trucks A + B + C + D, Trucks B + C + D, Trucks B + D, Truck D. Based on prior analysis, the truck positions (3.66, 4.11, 4.42 m from each abutment) were determined to result in safe stress levels, assuming a

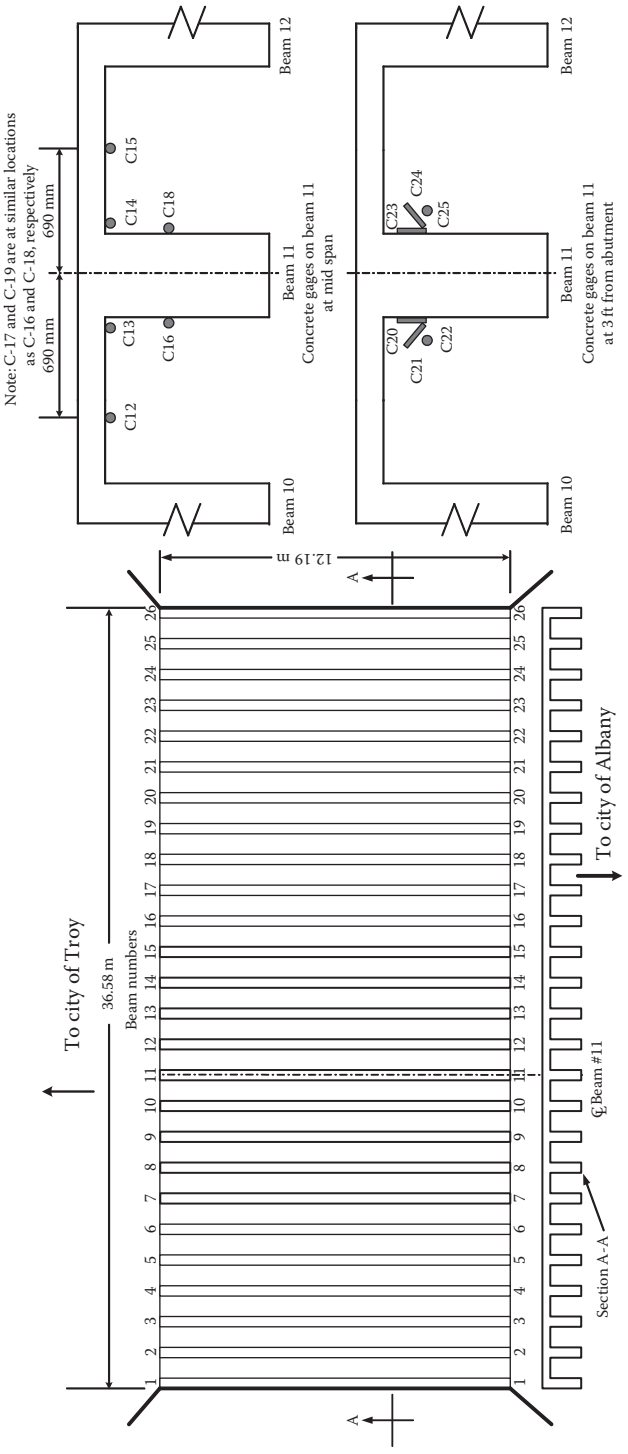

FIGURE 40.9 Strain gages on concrete.

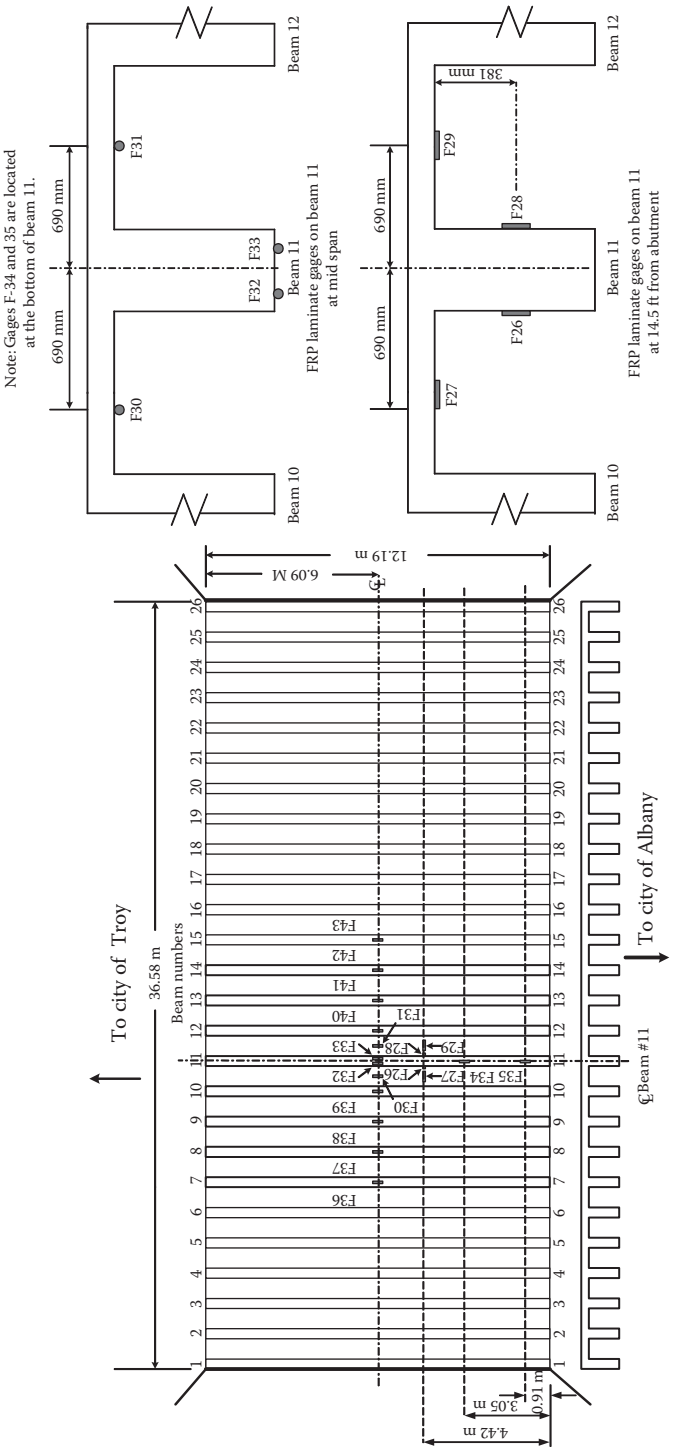

FIGURE 40.10 Strain gages on FRP laminates.

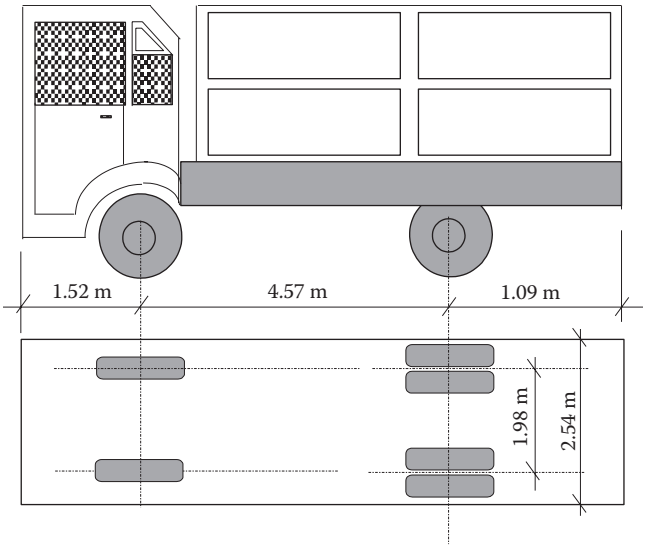

FIGURE 40.11 Typical truck used in load tests.

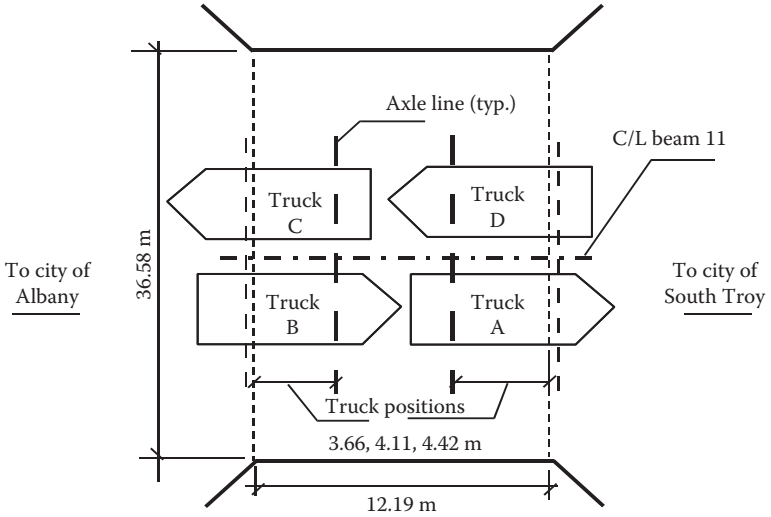

FIGURE 40.12 Truck positions for the load tests.

simply supported condition (see Figure 40.12). Since the actual strength of the structure was not known, three truck positions were marked to gradually increase applied moment on the bridge. Strains were continuously monitored during the tests to determine whether it was safe to advance the trucks to the next critical position. On this basis, in the after installation test, a new sequence was added in which trucks were parked back-to-back at 4.42 m positions to maximize load effects on the bridge.

Based on the before and after midspan moment vs. strain results, it was concluded that the system slightly improved flexural stiffness [8,9]. Maximum rebar stresses on the bridge for the three loading positions (Figure 40.13) showed a moderate decrease in stresses after installation of the retrofit system and indicated good agreement with analytical predictions. The T-beam structure was later tested to assess in service performance of the FRP retrofit system [10]. Load testing of bridge FRP applications may also be used for comparisons of deck systems, condition assessment, and risk management [11,12,13].

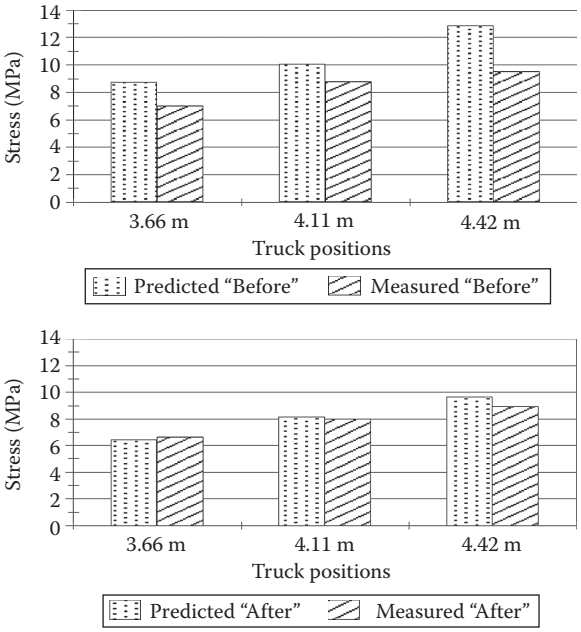

FIGURE 40.13 Rebar stresses before and after installation along with analytical predictions.

REFERENCES

1. Ashour, H.A., Al-Harami, A.A., and Rublah, A.A. Building a general purpose micro-computer based mechanical measurement system. *Experimental Techniques*, 17(3), 34–37 1993.
2. Alampalli, S., O'Connor, J., and Yannotti, A. Design, fabrication, construction, and testing of a FRP superstructure, Special Report 134, Transportation Research and Development Bureau, New York State Department of Transportation, Albany, NY, December 2000.
3. Alampalli, S., O'Connor, J., and Yannotti, A. Fiber reinforced composites for the superstructure of a short-span rural bridge. *Journal of Composite Structures*, 58(1), 21–27, 2002.
4. Alampalli, S., Schongar, G., and Greenberg, H. In-service performance of an FRP superstructure, Special Report 141, Transportation Research and Development Bureau, New York State Department of Transportation, Albany, NY, March 2004.
5. Aref, A. and Alampalli, S. Vibration characteristics of a fiber reinforced polymer bridge superstructure. *Journal of Composite Structures*, 52(3–4), 467–474, 2001.
6. Aref, A.J., Alampalli, S., and He, Y. Performance of a fiber reinforced polymer web core skew bridge superstructure: Field testing and finite element simulations. *Journal of Composite Structures*, 69(4), 491–499, 2005.
7. Chiewanichakorn, M., Aref, A., and Alampalli, S. Failure analysis of fiber-reinforced polymer bridge deck system. *Journal of Composites Technology and Research*, 25(2), 119–128, 2003.
8. Hag-Elsafi, O., Alampalli, S., and Kunin, J. Strengthening of Route 378 bridge over Wynantskill Creek in New York using FRP laminates, Special Report 135, Transportation Research and Development Bureau, New York State Department of Transportation, Albany, NY, March 2001.
9. Hag-Elsafi, O., Alampalli, S., and Kunin, J. Applications of FRP laminates for strengthening a reinforced-concrete T-beam bridge structure. *Journal of Composite Structures*, 52(3–4), 453–466, 2001.
10. Hag-Elsafi, O., Alampalli, S., and Kunin, J. In-service evaluation of a reinforced concrete T-beam bridge FRP strengthening system. *Journal of Composite Structures*, 64(2), 179–188, 2004.
11. Hag-Elsafi O., Albers W., and Alampalli, S. Dynamic analysis of the Bentley Creek Bridge with FRP deck. *Journal of Bridge Engineering*, ASCE, 17(2), 318–333, 2012.
12. Ettouney, M. and Alampalli, S. *Infrastructure Health in Civil Engineering: Theory and Components*. CRC Press, Boca Raton, FL, September 2011.
13. Ettouney, M. and Alampalli, S. *Infrastructure Health in Civil Engineering: Applications and Management*. CRC Press, Boca Raton, FL, September 2011.

41 Smart Composites

Dryver R. Huston

CONTENTS

INTRODUCTION

Composites are excellent candidates for use as active, or smart, materials. Such materials can sense and respond to environmental and internal states and have the potential to extend the performance of engineering systems well beyond what is possible with passive materials. The possibility of activating multiple physical mechanisms allows for creating a wide variety of high-performance smart composites. It is likely that with continued advancements, smart composites will see large increases in capabilities and usage in the future.

This chapter uses a relatively broad definition of smart composite materials, that is, composite materials that can sense, respond, and/or alter the operational state in response to external and internal stimuli. Figure 41.1 shows a classification of smart composites based on the degree of complexity of interactions between the material and the environment. *Level 1* materials sense the environment and internal states of the material, including damage. *Level 2* materials sense and respond to external stimuli. A typical response is mechanical actuation that causes the material to change shape. *Level 3* materials change state in response to stimuli. This includes self-healing, variable stiffness, and color changing materials [1].

ARCHITECTURES

Smart composite structural materials can have a variety of architectures. A globally homogeneous pattern is relatively simple to design and build. Figure 41.2 shows a smart composite with a homogeneous distribution of sensors with localized damage that is near to, but does not span the sensor. Figure 41.3 shows a smart composite with a grid-like distribution of sensors and with localized damage that spans the sensor. Grid patterns are a convenient method of providing a comprehensive composite sensing system [2]. More complicated arrangements of sensors are possible. For example, Figure 41.4 shows a smart composite structure with a hierarchical branching architecture and with local damage that also spans the sensors.

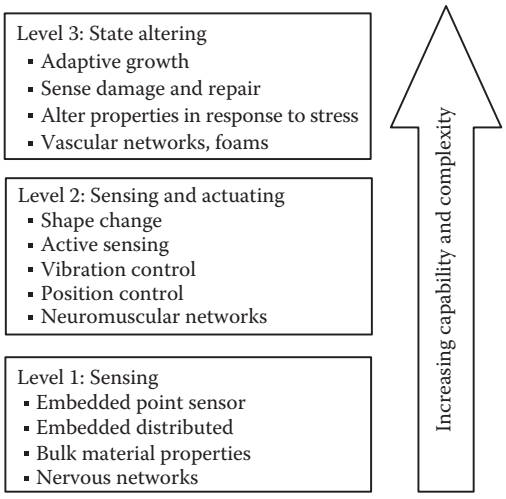

FIGURE 41.1 Classification of smart (active) materials technologies.

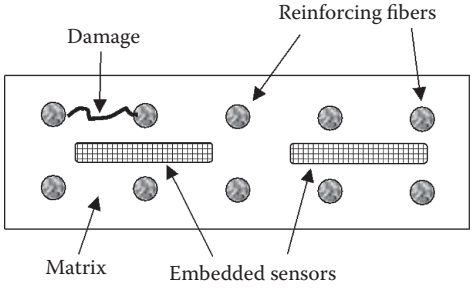

FIGURE 41.2 Homogeneous distribution architecture of sensors and with local damage possibly not being detected. (From Huston, D., *Structural Sensing, Health Monitoring and Performance Evaluation*, Taylor & Francis, Boca Raton, FL, 2011.)

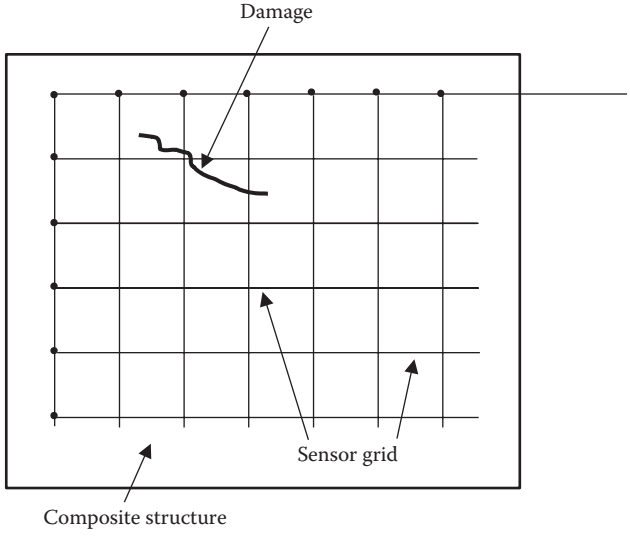

FIGURE 41.3 Distributed grid sensor architecture with local damage possibly being detected. (From Huston, D., *Structural Sensing, Health Monitoring and Performance Evaluation*, Taylor & Francis, Boca Raton, FL, 2011.)

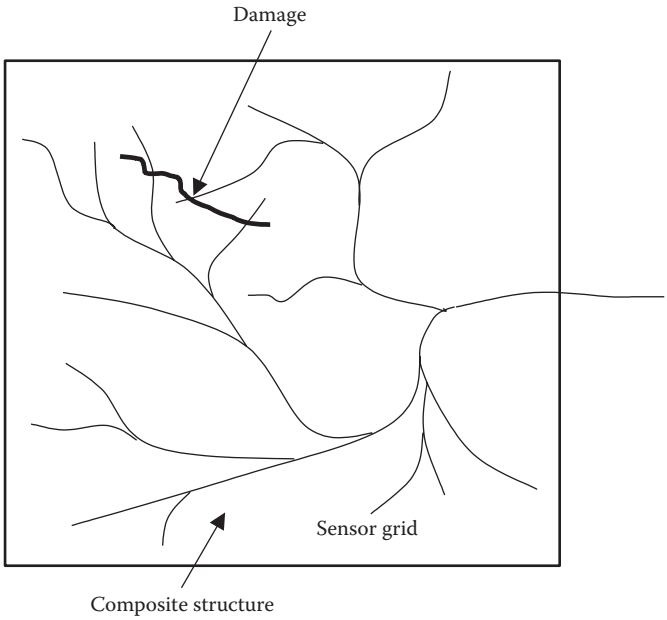

FIGURE 41.4 Branching sensor architecture and with local damage. (From Huston, D., *Structural Sensing, Health Monitoring and Performance Evaluation*, Taylor & Francis, Boca Raton, FL, 2011.)

COMPOSITES WITH SENSING CAPABILITIES

Composite structures with sensing capabilities are, in many respects, large-scale transducers that convert physical quantities of interest, that is, measurands, into signals that are collected and transmitted to interested users. Measurands of interest can include strain, stress, displacement, tilt, acceleration, temperature, electromagnetic parameters, fluid permeability, and more complex quantities, such as corrosion, cracking, and fatigue. For each of these measurands, a variety of sensors are available to transduce the information into an easily measured property, such as voltage, optical intensity, or direct digital readout. Inserting sensors and sensory materials directly into the composite structures is a straightforward approach to incorporating sensing capabilities into composite materials. Developments in nano- and microelectromechanical systems technologies are leading to smaller, less expensive yet better performing, integrated sensor systems [3]. The decreasing size of sensing systems makes them attractive for embedment. However, embedding sensors into composite structures does cause mechanical side effects, such as stress risers and the displacement of composite material [4].

Sensor geometric dimensionality is an important descriptive parameter (Figure 41.5). Sensors can measure over single, multiple, and fractional dimensions. Zero-dimensional (0-D) sensors have approximately zero dimensions of spatial coverage and are often called point sensors. These include foil strain gages, thermocouples, and accelerometers. When the spatial sensitivity extends beyond a point, the sensor becomes a distributed sensor (Figure 41.6). One-dimensional (1-D) distributed sensors measure along a line or a curve. Two-dimensional (2-D) distributed sensors measure over a distributed area or surface. Three-dimensional (3-D) sensors measure properties in 3-D volumes, usually with the aid of penetrating radiation and imaging techniques. Certain classes of distributed sensors can be viewed as having a fractional dimension. Between zero, one, two, and three dimensions are distributed linear sensors and arrays of point sensors. Such configurations can provide substantial coverage of an area or volume. Sensors with fractal geometry, such as the branching nervous system in vertebrates, are an intriguing possibility for smart composites.

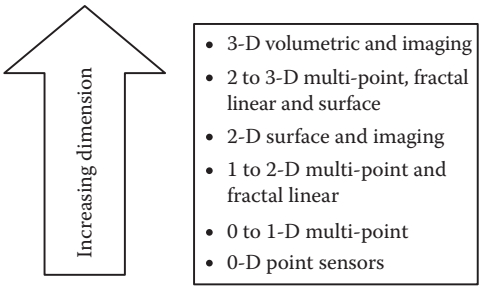

FIGURE 41.5 Geometric dimensionality of various sensor types. (From Huston, D., *Structural Sensing, Health Monitoring and Performance Evaluation*, Taylor & Francis, Boca Raton, FL, 2011.)

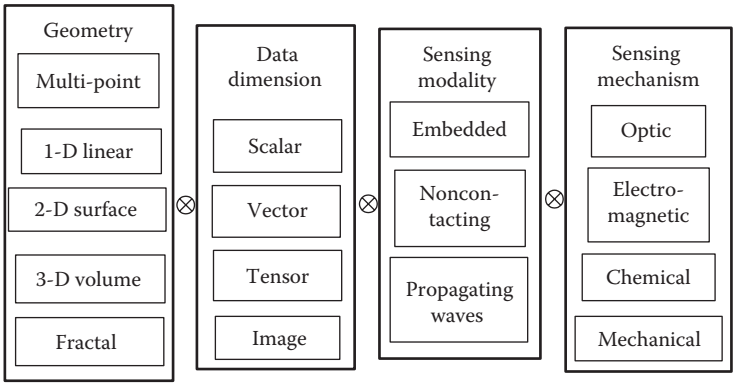

FIGURE 41.6 Classes of distributed sensors. (From Huston, D., *Structural Sensing, Health Monitoring and Performance Evaluation*, Taylor & Francis, Boca Raton, FL, 2011.)

SENSING WITH ELECTRICAL AND ELECTROMAGNETIC EFFECTS

Measurand induced change in electrical resistance can be exploited to make 0-D (point), 1-D, 2-D, and 3-D sensors. Resistance is a macroscopic quantity that depends on the local material resistivity, ρ, and the current flow patterns. Changes to the structural geometry, resistivity, and/or current flow patterns. Commonly used materials for resistance-based sensors include specialized alloys, such as Constantan and doped semiconductors [3,5]. Shape memory alloys, such as nitinol, undergo large resistivity changes that correspond to the large deformations characteristic of the phase change of the materials [6,7].

Using other electromagnetic effects can also form structural sensors. The ease of miniaturization is an advantage for many of these sensors. Capacitive sensors scale well with reduced size and are fairly common in MEMs sensors, such as accelerometers and acoustic emission transducers [8]. Variable reluctance sensors can measure air gaps with magnetic fields [9]. Piezoelectricity is a reciprocal strain–voltage effect in solids. The three main classes of piezoelectric transducers materials are (1) single crystal, such as natural or fused quartz, (2) polycrystalline piezoceramic, such as lead zirconate titanate (PZT), and (3) piezo polymers, including polyvinylidene fluoride (PVDF). Piezoelectric transducers can measure or produce transients, but have difficulty measuring or sustaining steady state and low-frequency effects.

Impedance testing is the measurement of the response of a system to harmonic excitation. Since the impedance of a system reflects the properties of a system, impedance testing can be useful for both sensing and diagnostics. Electromechanical impedance testing of structural composite systems often uses embedded or surface attached piezoelectric patches. Deviations from nominal impedances are indicative of structural changes, such as damage [10].

Specialized networks of piezoelectric transducers can detect damage in plate-like or elongated structural elements by measuring perturbations and changes to the transmissibility of ultrasound

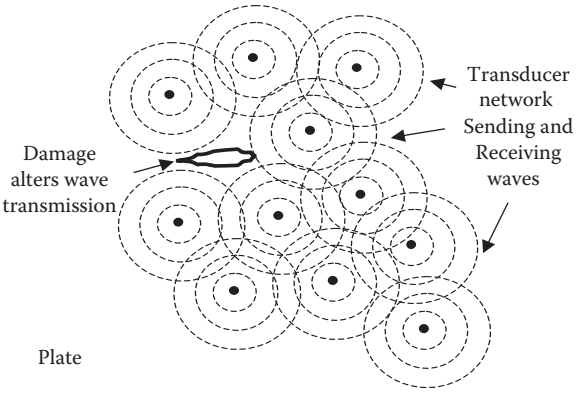

FIGURE 41.7 Piezoelectric sensor network detecting damage by transmission obstruction.

(usually Lamb) waves between transducers (Figure 41.7) [11,12]. These systems have the attractive property of being able to detect damage at remote distances in structures by taking advantage of elongated shapes that act as waveguides, i.e., plates or pipes. Integrated systems, such as the SMART (Stanford Material Receive and Transmit) Layer, are now available in a variety of forms. A difficulty with using piezoelectric sensor networks is that the requisite signal processing can be nontrivial. Under certain circumstances, it is possible to determine the effect that damage will have on elastic wave propagation from first principles. The piezoelectric sensor network method can be extended to more complex structures, such as honeycomb composite structures, stiffened panels, masonry panels and trusses [13].

Magnetostriction is similar to the piezoelectric effect. A magnetic field induces a strain in a solid and vice versa [14]. A principal distinction is that piezoelectric effects can be linear and magnetostrictive effects are inherently nonlinear.

It is possible to fabricate composite materials with bulk electric properties that are amenable to making an entire structural element act as a sensor. Metal wires can be embedded as a grid into a composite plate at an offset from the centroidal axis so that deflection in the plate induces strain in the wires, which transduces into a measurable resistance change and forms a distributed sensor [15]. The steel wires and rubber mesh in a tire may be configured to form a capacitive bulk strain sensor for the tire [16]. Carbon fibers and carbon particles embedded in composites form bulk electrical resistance sensors where the electrical resistivity increases with strain and damage [17].

SENSING WITH FIBER OPTICS

Fiber optic sensors use light as both a transduction and signal transmission mechanism. Fiber optic sensors are often considered in composite sensing applications because the optical fibers are small enough to be inserted into composite structures. However, it should be noted that most optical fibers have diameters on the order of 100 μm or more, which is often significantly larger than typical composite constituent particles and fibers. Optical effects that are useful for transduction include intensity modulation, modal domain interference, Bragg grating wavelength selective transmission and reflection, noncoherent white light interference, and Brillouin backscatter.

Intensity-based fiber optic sensors use mechanical effects to modulate transmitted or reflected light intensity. Light intensity can be detected easily with phototransistors, photoresistors, and photodiodes and can be used to make absolute intensity sensors that are useful in SHM [18].

Optical interference is a useful transduction mechanism for fiber optic sensors. When a beam of light is split into two parts, each of which is sent on a separate path, and then rejoined, interference patterns may form. A variation in the length of one of the paths causes the interference pattern to shift. Measuring interference pattern shifts can give very precise and accurate information about

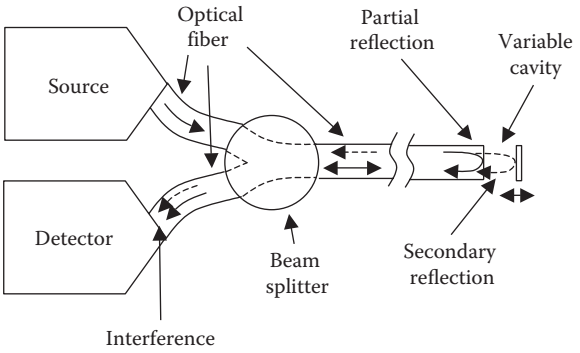

FIGURE 41.8 Fabry–Perot interferometer. (From Huston, D., *Structural Sensing, Health Monitoring and Performance Evaluation*, Taylor & Francis, Boca Raton, FL, 2011.)

changes in physical parameters that affect effective light path lengths. Both coherent (usually laser light) and incoherent (white or LED light) interferometry are useful for sensing applications.

There are several geometries of interferometers that produce interference patterns that are useful in fiber optic sensors [18]. The Fabry–Perot interferometer uses two parallel surfaces that are perpendicular to the light beam with the incident surface being a partial reflector and the second surface is a complete reflector (Figure 41.8) [19]. The two reflected beams are combined and sensed at a detector. The Fabry–Perot interferometers appear in embedment applications. For example, Benmokrane et al. embedded Fabry–Perot sensors to monitor fiber-reinforced polymer bridge decks [20].

Figure 41.9 shows a fiber optic version of a white light Michelson interferometer. The difference in the path lengths, ΔL, is

$$\Delta L = L_1 - L_2 \tag{41.1}$$

The light intensity received at the detector is a maximum if $\Delta L = 0$ (Figure 41.9). In terms of practical measurements, the system in Figure 41.9 is a bit too simple. The addition of second interferometer arms and a piezoelectric stage-mounted mirror creates a practical measurement tool [21].

The fiber optic Bragg grating (FOBG) strain gage uses the Bragg effect where an optical medium with a periodically varying index of refraction selectively reflects and transmits light at a wavelength, λ_B, that matches the index of refraction spacing λ_S (Figure 41.10) [22]

$$\lambda_B = \lambda_S \tag{41.2}$$

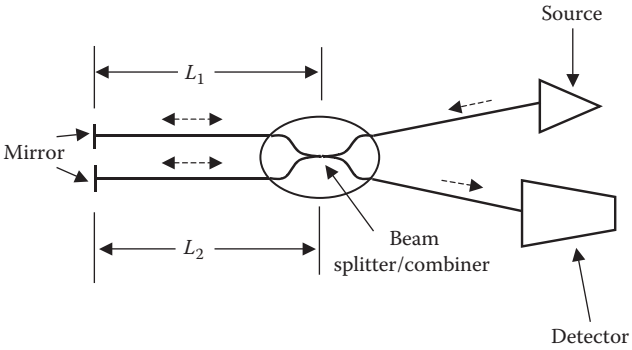

FIGURE 41.9 Simple version of fiber optic noncoherent white light interferometer. (From Huston, D., *Structural Sensing, Health Monitoring and Performance Evaluation*, Taylor & Francis, Boca Raton, FL, 2011.)

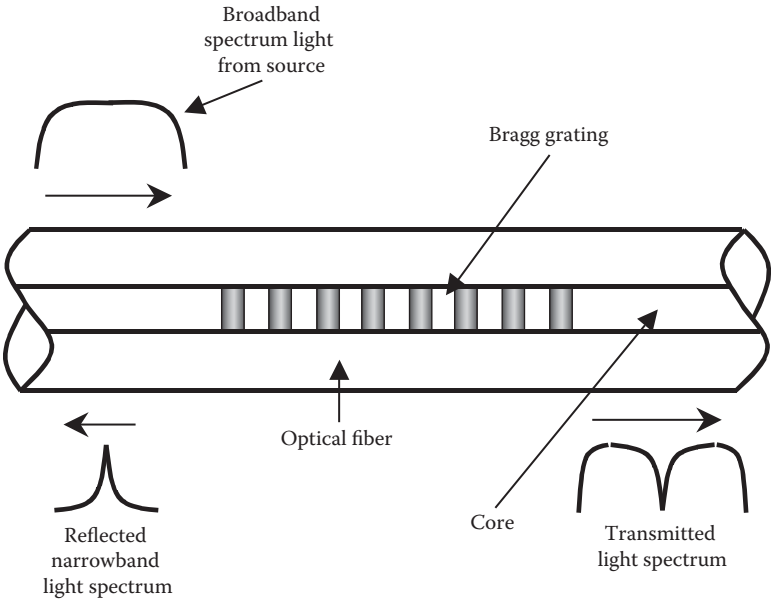

FIGURE 41.10 Operating principle of fiber optic Bragg grating. (From Udd, E., *Fiber Optic Smart Structures*, Wiley, New York, 1995.)

Strain and temperature changes in the fiber change the Bragg grating spacing and the wavelength of the reflected signal [23]

$$\frac{\Delta\lambda_B}{\lambda_B} = (1 - p_e)\varepsilon + (\alpha_\Lambda + \alpha_n)\Delta T \tag{41.3}$$

where

ε is the mechanical strain

ΔT is a temperature shift

p_e, α_Λ, and α_n are strain-optic, fiber thermal expansion, and thermal-optic coefficients, respectively

Since the reflected light is a wavelength-modulated signal, it is insensitive to intensity-based noise disturbances—in a manner similar to frequency modulated (FM) radio. The ability of an FOBG to selectively reflect a very narrow bandwidth of light enables placing several, if not many, Bragg gratings with different center wavelengths on the same cable for simultaneous multipoint strain measurement [24–26].

FOBGs are used in demanding applications, such as measuring strains in a complex airplane box structures under test, composite bridges, ship hull and mast strain measurements, and real-time measurements of a cryogenic fuel tanks [27–30]. The narrow diameter (typically 100–200 μm) of FOBGs makes them attractive for embedment applications, such as monitoring the performance of composite patches on aluminum aircraft structures, parachutes, metallic–intermetallic laminates, composite lap joints, composite load cells for bridge bearings, and filament wound composite pressure vessels [31–34]. An example of using multiple distributed fiber optic sensors for SHM is on the X-33 reusable launch vehicle [35]. This vehicle had cryogenic fuel tanks that were monitored with an array of FBGs for strain measurements, palladium hydride FBG hydrogen sensors, distributed Raman temperature sensors, and acoustic emission sensors.

The 1-D distributed sensors use curvilinear paths for both the sensor and signal transmission. In principle, 1-D sensors can be based on virtually any physical mechanism that transduces a signal as it propagates through a conductor along a linear or curvilinear geometry, i.e., electrical, optical, hydraulic, or pneumatic conductors. The sensing and communication media are co-located.

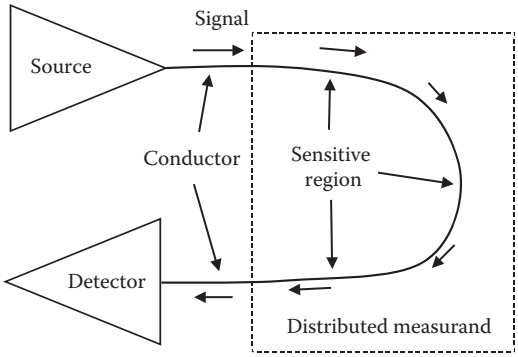

FIGURE 41.11 One-dimensional distributed sensor.

This enables measuring events along the path with position-dependent analog signal processing, such as weighted integration (Figure 41.11).

The 1-D distributed sensors are distinguished by the speed of signal transmission and transduction. In quasi-static sensors, the speed of information transmission through the sensor is faster than the time constants of signal transduction, that is, it is effectively instantaneous. In time-domain sensors, the time-of-flight of a signal through the sensor is significant and is measurable.

Tuning the physical placement to be sensitive to the desired physical effects and insensitive to others configures the sensitivity of a distributed 1-D sensor. Borrowing a term from radio engineering, this technique is known as tuning the antenna gain of the sensor [36]. Antenna gain tuning has been used for point load location, vehicle-type identification, and vibration mode shape identification [37]. The winding of optical fibers directly into filament-wound composite structures opens the possibility for interesting long gage distributed embedded fiber optic sensors for SHM. Wrapping the sensing fiber in radial or longitudinal directions produces a distributed sensor with circumferential and/or axial loading sensitivity.

High-speed distributed sensing uses the time of flight and reflection of an energy pulse as it propagates through a waveguide for the signal transduction mechanism. The most notable of these high-speed techniques is time domain reflectometry (TDR). Electrical and optical variants of TDR are common. Ultrasound versions are occasionally used. A propagating pulse reflects off of discontinuities and the bulk material of the waveguide [38]. Figure 41.12 is an idealized representative

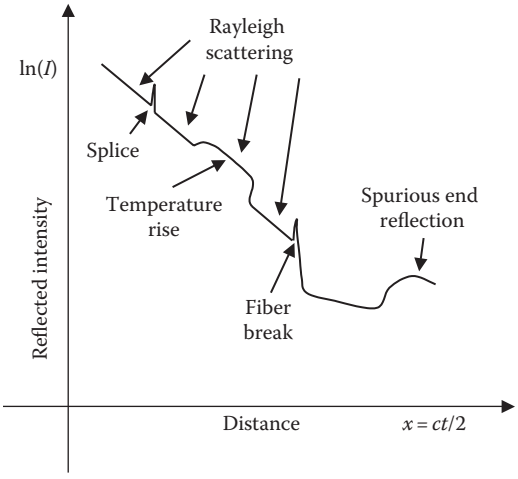

FIGURE 41.12 OTDR signal from an optical fiber with a splice joint, temperature variation, and break. (From Huston, D., *Structural Sensing, Health Monitoring and Performance Evaluation*, Taylor & Francis, Boca Raton, FL, 2011.)

optical OTDR signal including a portion where the amount of Rayleigh scattering backreflection is increased due to a temperature rise [39]. Spatial registration can be enhanced with the use of prepositioned reflectors along the length of the waveguide.

The OTDR effects described earlier use elastic scattering and reflection, that is, the light returns at the same wavelength as it was when launched. Inelastic and nonlinear effects, such as Raman and Brillouin scattering, can cause light to scatter at a wavelength that differs from the launch signal. Brillouin backscatter is where light is weakly scattered by interactions with acoustic phonons so that it is sensitive to both temperature and longitudinal strain [40]. Although the frequency shifts of Brillouin scattering are small, the relatively large amplitudes of the return signals tend to make it an attractive candidate for distributed temperature sensing applications [41]. Brillouin OTDR (BOTDR) test instruments are commercially available, but are somewhat expensive.

Fiber optic chemical sensors can be fabricated by exploiting optical interactions with chemical species—with and without the aid of activating reagents. Coupling light into and out of an optical chemical sensor is possible with a variety of techniques that include transmission and reflection, often with the use of a fiber optic waveguide. Evanescent surface waves can measure chemical reactions on surfaces, such as the outer reflective layer of a fiber optic waveguide. Flachsbarth et al. developed a moisture detection fiber optic sensor by embedding Reichart's dye embedded in custom formulated polymethacrylnitrile [42].

ADDITIONAL COMPOSITE SENSING TECHNIQUES

The use of continuity in hydraulic or pneumatic conductors is another possibility for distributed damage sensing in composites. Comparative vacuum monitoring (CVM) is a technique that can detect crack formation by measuring the differential pressure in segregated fluid conductor circuits [43]. When a crack grows to a sufficient size to breach both of the segregated circuits, the leak can be detected by differential pressure methods. Since the conductor circuits are readily mass-produced in a variety of patterns, including interdigitated arrays, and are lightweight, the CVM technique has generated considerable attention as a possible aircraft SHM system [44] (Figure 41.13).

Acoustic emission monitoring is the measurement of short-duration high-frequency elastic waves in solids due to incipient microcracks. Acoustic emission monitoring can indicate the level, progression, and location of microcracking structural damage. Event counting is routinely used for acceptance testing of composite and other high-performance parts, where a submaximal load is applied and the part is rejected if the number of acoustic emission events exceeds a preset threshold. Acoustic emission test instruments have become smaller and sufficiently easy to use that online instruments can be placed on structures for real-time assessments [45]. Embedded fiber optic sensors are another possible acoustic emission transduction mechanism.

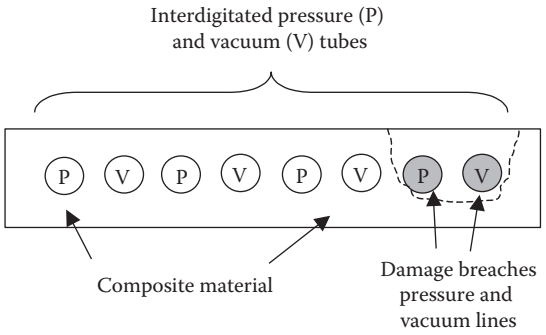

FIGURE 41.13 Comparative vacuum monitoring of damage in a composite. (From Wheatley, G. et al., Comparative vacuum monitoring as an alternative means of compliance, in *Structural Health Monitoring*, Palo Alto, CA, F.-K. Chang, ed., Destech, Lancaster, PA, 2003.)

CURE MONITORING OF COMPOSITES

The manufacture of many composite components involves curing in which chemical reactions alter the state of the composite to form an integrated material. Heating with pressure is a standard technique. Monitoring and controlling curing processes with integrating cure-monitoring sensors can improve quality control and economics of composite systems manufacture.

Thermosetting resins, such as epoxy, cure by transforming from a liquid to a solid by a chemical reaction that produces a three-dimensional network of covalently bonded molecular chains. The physical properties that change with cure include the dielectric coefficients, glass transition temperature, thermal stability, tensile modulus, chemical resistance, strain to failure, viscosity, dynamic modulus, and fracture toughness. Capacitive measurements of dielectric properties and ultrasound measurement of elastic properties are convenient methods of measuring the changes in polymer components with embedded sensors [46]. Polymer molecules contain dipoles and ions that align with an externally applied electric field. The combination of ionic mobility and dipolar motion determines the dielectric constant of the material [47]. The onset of cross-linking decreases dipolar mobility and the corresponding dielectric constant. Measuring the dielectric properties of a material typically involves a capacitance measurement, such as with a parallel plate capacitor, where the capacitance C (farads) is

$$C = \frac{\varepsilon_0 \varepsilon_r A}{d} \tag{41.4}$$

where

ε_r is the relative dielectric constant of the material in the gap (the curing composite)
ε_0 is the permittivity of air
A is the area of the electrodes
d is the distance between them

Since the elastic properties of resins change with cure, it is also possible to use ultrasonic techniques monitor cure in composite parts. Li and Menon monitored the cure of composite jackets used for retrofitting concrete structures such as bridge columns by measuring ultrasonic elastic wave transmission between embedded elastic (metal) waveguides [48]. As the resin cures from a liquid to solid, it can sustain waves, the between waveguide transmission increases and the along waveguide transmission decreases.

An example application of cure monitoring is a snowboard (Figure 41.14). Snowboards are high-performance structures used in winter sports. A snowboard is a multilayer laminate composite made of ultra high molecular weight (UHMW) plastic, glass fiber-reinforced polymer (GFRP), wood and ABS plastic that need to be manufactured economically with a minimum of variation and defects [49].

FIGURE 41.14 Top view of a snowboard. (From Pelczarski, N. and Huston, D., Cure monitoring of composite laminates used in the manufacture of snowboards, in *Smart Structures Process Control and Sensors for Manufacturing, Proceedings of SPIE*, Vol. 3993-26, Newport Beach, CA, 2000.)

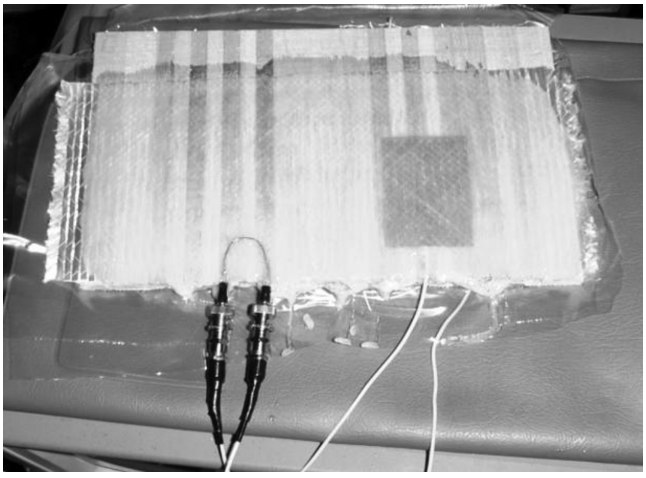

FIGURE 41.15 Waveguide and capacitance electrode in placement on a cured test sample. (From Pelczarski, N. and Huston, D., Cure monitoring of composite laminates used in the manufacture of snowboards, in *Smart Structures Process Control and Sensors for Manufacturing, Proceedings of SPIE*, Vol. 3993-26, Newport Beach, CA, 2000.)

Ultrasonic and dielectric snowboard cure monitoring systems were developed and evaluated for snowboard manufacturing (Figure 41.15). The ultrasonic system used two ultrasonic lead zirconate titanate (PZT) ceramic piezoelectric transducers (pinducers) that were coupled to a thin copper waveguide. The waveguides allow for the pinducer to remain outside of the curing epoxy and reusable. The dielectric transducer was a parallel plate capacitor that used the GFRP as an internal dielectric layer.

Figure 41.16 shows ultrasonic waveguide transmissibility versus time of cure with three distinct corners marked. Initially the transmissions increase up to corner 1. This increase is attributed to a decrease in the viscosity of the resin as it heats up. It is believed that cross-linking begins between corners 1 and 2. In the approach to corner 2, the resin changes into a gel, becomes able to support elastic waves, and energy leaks from the waveguide into the surrounding medium. As the process continues, larger amounts of ultrasonic energy leak into the hardening resin. Corner 2 represents the start of this phase. During solidification, the epoxy is capable of supporting ultrasonic waves because of the increased stiffness due to cross-linking. At corner 3, almost the entire wave energy leaks into the surrounding material.

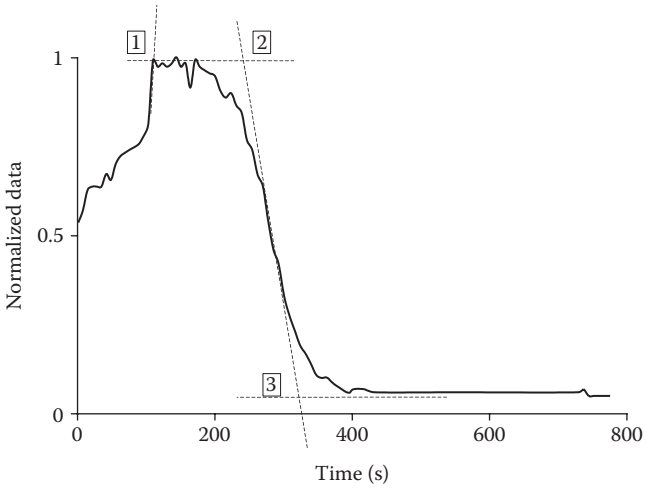

FIGURE 41.16 Ultrasound transmissibility versus curing time at 85°C with corners marked. (From Huston, D., *Structural Sensing, Health Monitoring and Performance Evaluation*, Taylor & Francis, Boca Raton, FL, 2011.)

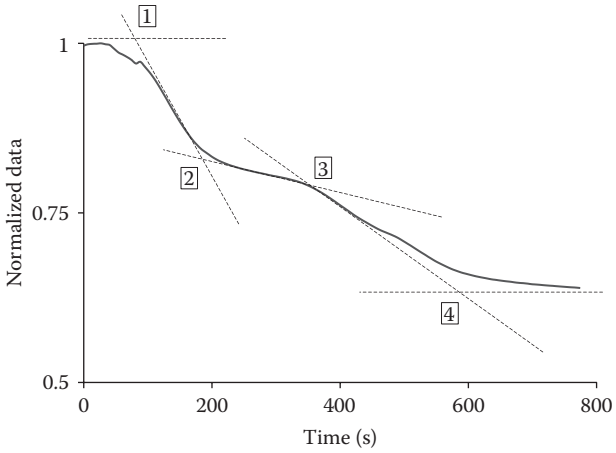

FIGURE 41.17 Capacitance plot with corner markers for sample cured at 85°C. (From Huston, D., *Structural Sensing, Health Monitoring and Performance Evaluation*, Taylor & Francis, Boca Raton, FL, 2011.)

The capacitance versus cure plots exhibit similar points of interest throughout the reaction (Figure 41.17). Initially, when the epoxy is in a low viscosity state, there is high dipolar mobility and correspondingly a measured high level of capacitance. As the gel state begins to form at corner 1, the capacitance drops. This is attributed to the onset of cross-links in the resin. Corners 1–2 suggest that the mobility of the dipoles is rapidly decreasing. Capacitance measurements appear to be extremely sensitive to this part of the reaction. At Corner 2, the change in capacitance slows dramatically, which suggests that the resin is no longer liquid-like. This can be correlated with ultrasonic data, where the viscosity increase is representative of the fall in signal amplitude from corner 2 to 3. During this period, the capacitance changes slightly, since the resin is in a solid phase. The capacitance corner 3 occurs consistently and can be useful for the detection of the end of cure. For the tests at 85°C, corners 1 and 2 occur at the same time as the ultrasonic data.

The repair of structures with composite patches is another area that is ripe for the application of smart structures technology. The quality and long-term durability of the repair depend in large part on the integrity of the adhesive bond between the patch and the structure. Patches with embedded strain and deformation sensors can be self-sensing systems that monitor the integrity of the repair patch and conceivably the progression, if any, of the underlying defect [50].

SHAPE-CHANGING COMPOSITES

Active structural systems that change shape or state in response to external or environmental stimuli are a bit more rare than sensing composites. The usage of these technologies is anticipated to increase in the future. Shape-change material classes include piezoelectric, magnetostrictive, shape memory alloy (SMA), and shape memory polymer (SMP). Piezoelectric and magnetostrictive materials undergo relatively small strains. SMA and SMP materials can undergo somewhat larger strains. Piezoelectric magnetostrictive material deformations tend to be zero-memory effects, which eases control issues. Shear lag models at the fiber level can describe many of the mechanics of SMA composites [51]. The memory nature of SMA and SMP materials complicates control and has hindered the routine engineering use of SMA and SMP in many applications. Nonetheless, many of these issues have been resolved through careful engineering design, with the result being high-performance shape-changing composite materials for aerospace, medical, and other applications [52]. Regardless of the size of material deformation, the overall deformation, the selective placement of active materials at specific locations enhances the deformation performance of the overall composite structure. An extreme case of using selective actuator placement to enhance deformation control is the tensegrity structure, which is composed of actuators and tendons that are organized on a mesoscale.

SELF-HEALING AND MATERIAL STATE ALTERATION COMPOSITE SYSTEMS

Self-healing engineered systems are not extremely common, but are beginning to appear in certain applications. If damage-prone composites can be made of active self-healing materials, then it may be possible to extend the performance envelope of cabling systems, possibly even with a weight reduction.

Passive self-healing systems exhibit a healing capability without active self-healing systems. Systems that break-in are an example. Shoes tend to fit better after being worn for a while. Journal bearings and other lubricated machine parts will wear-in during a start-up phase to achieve a smoother motion than is possible with standard manufacturing practices. Somewhat more sophisticated approaches are redundant parallel systems. Heavily loaded components can fail and transfer the load to a group of other components. Examples include parallel strand suspension bridge cables, multi-rivet joints, and fiber-reinforced composites.

Semiactive self-healing systems recover from damage by an alteration of operational parameters. Limping strategies are perhaps the most common of the semiactive approaches. If a system is damaged, it may continue to operate in a restricted range of behaviors. For example, a multi-engine airplane with an inoperable engine can still remain airborne by an appropriate alteration of flight control strategies.

Active self-healing systems change their properties in response to stress and damage. The work hardening of ductile metals has been used for centuries. Olex has developed a wiring insulation that turns into a ceramic when subjected to fire [53]. The ceramic insulation remains an insulator during and following a fire, but with degraded mechanical properties. The pre-embedment of capsules of liquid materials that are released when structural damage causes the rupture of the capsules is a self-healing mechanism for solids. Dry developed a series of technologies primarily related to the encapsulation and embedment of repair epoxies in concrete and masonry materials [54]. White developed a similar microencapsulation technique for self-repair in polymer composites [55]. Muntges et al. developed self-healing bolt systems where the bolts can sense a loosened state and attempt to retighten themselves [56]. Self-healing wire and cable insulation have also been demonstrated. Dakai et al. used transmission intensity sensing in fluid-filled fiber tubes that are used to transport self-repair epoxies to damage sites in composites to assess the occurrence of damage and fluid transport [57].

Examples of self-healing biological systems are seen in blood clotting, and a host of other processes. Biological self-healing is a complicated process that uses damage sensing, material transport and repair, and stops once the injured tissue has healed. It should be noted that healing uses many different materials and processes simultaneously, some of which promote activity while others inhibit activity.

Specialized composite materials can alter their operational state and condition on command. Altering the stiffness of a structural element on command can be advantageous in certain structural control applications. An approach developed by Bergamini et al. is to alter the amount of friction in shear layers in composite beams by means of electrostatic attraction across the friction layer [58]. Composite materials can be fitted with components that change color in a controllable manner. Barrett and Melkert demonstrated that small autonomous airplanes can be rendered virtually invisible by the addition of active electroluminescent materials to the skin [59].

POWER SUPPLY

Providing power to embedded sensors and actuators in composites is a significant engineering challenge. At least four possibilities exist:

1. *Embedded wires and sensors*: These are effective, but the routing of cables causes difficulties during fabrication and can weaken the structure.
2. *Wireless power transmission*: Near-field electromagnetic interactions can transmit power and data in what is often referred to as transformer mode. These systems can be useful in situations where it is convenient to have the sender and receiver in close proximity to one

another, but require a wireless noncontacting transmission link [64,65]. Far-field electromagnetic wave transmission of energy at lower levels is also possible, including the beaming of microwaves to rectennas [60].

3. *Onboard battery*: Batteries combined with efficient system design can produce sensors that may last for months or years without battery replacement or recharging. Eventually, onboard power needs to be replenished.
4. *Ambient energy harvesting*: An alternative to directly supplying power to the system is to harvest energy from the ambient environment. Energy harvesting is governed by the principles of thermodynamics, which essentially require differentials or gradients in energy levels for energy harvesting [61]. The larger the level of accessible energy gradients, the easier it is to harvest energy. Measurand-derived power is perhaps the simplest and most reliable method of powering a sensor. The possible sources of energy in the environment include wind, solar, ambient vibration, and thermal gradients [62]. Churchill et al. demonstrated a vibration energy system for powering wireless networks [63]. Solar power, if it can be conveniently harvested, is an excellent source of ambient energy.

CONCLUSIONS

Enabling technologies have been and are being developed that allow for the incorporation of smart elements into structural composites. These composites can actively sense, respond to, and sometime control the environment and internal states. Continued development of smart composites will likely result in the availability of very high performance structural systems.

REFERENCES

1. McKnight G, Henry C. (2005) Variable stiffness materials for reconfigurable surface applications. In: *Smart Structures and Materials 2005: Active Materials: Behavior and Mechanics*, *Proceedings of SPIE*, Vol. 5761, San Diego, CA.
2. Kiriker GR, Kang I, Lee W, Shinde V, Westheider B, Vesselin N, Schulz MJ, Shanov N, Sundearesand M, Ghosal A. (2005) Testing the analog processor of a structural neural system. In: *Smart Structures and Materials 2005: Smart Electronics, MEMS, BioMEMS, and Nanotechnology, Proceedings of SPIE*, Vol. 5763, San Diego, CA.
3. Hsu TR. (2002) *MEMS & Microsystems Design and Manufacture*. McGraw Hill, Boston, MA.
4. Schaaf K, Cook B, Ghezzo F, Starr A, Nemat-Nasser S. (2005) Mechanical properties of composite materials with integrated embedded sensor networks, In: *Smart Structures and Materials 2005: Sensors and Smart Structures Technologies for Civil, Mechanical, and Aerospace Systems, Proceedings of SPIE*, Vol. 5765, San Diego, CA.
5. Dally JW, Riley WF. (1991) *Experimental Stress Analysis*. McGraw-Hill, New York.
6. Ogisu T, Nomura M, Kikiukawa H, Takeda N. (1999) Development of a health monitoring system using embedded SMA foils in CFRP laminates. In: *Proceedings of the Second International Workshop on Structural Health Monitoring*, F.-K. Chang, ed., Stanford University, Stanford, CA. Technomic Publishing, Lancaster, PA.
7. Shiammoto A, Zhao H, Abèc H. (2005) Vibration characteristics in a smart bridge model using shape memory alloy fiber reinforced composite. In: *Smart Structures and Materials 2005: Active Materials: Behavior and Mechanics, Proceedings of SPIE*, Vol. 5761, San Diego, CA.
8. Acar C, Shkel AM. (2003) Comparative characterisation of low-g capacitive MEMs accelerometers. In: *Structural Health Monitoring 2003*, Palo Alto, CA, F.-K. Chang, ed. Destech, Lancaster, PA.
9. Arms S, Townsend CP. (1996) Differential variable reluctance transducer. U.S. Patent 5,497,147.
10. Rutherford AC, Park G, Sohn H, Farrar CR. (2004) Nonlinear feature identification of impedance-based structural health monitoring. In: *Smart Structures and Materials 2004: Smart Electronic, MEMS, BioMEMS, and Nanotechnology, Proceedings of SPIE*, Vol. 5389, San Diego, CA.
11. Wang CS, Chang FK. (1999) Built-in diagnostics for impact damage identification of composite structures. In: *Proceedings of the Second International Workshop on Structural Health Monitoring*, F.-K. Chang, ed. Stanford University, Stanford, CA (September 8–10, 1999). Technomic Publishing, Lancaster, PA.

12. Giurgiutiu V. (2003) Lamb wave generation with piezoelectric wafer active sensors for structural health monitoring. In: *Smart Structures and Materials 2003: Smart Structures and Integrated Systems, Proceedings of SPIE*, Vol. 5056, San Diego, CA.
13. Park J, Chang FK. (2003) Built-in detection of impact damage in multi-layered thick composite structures. In: *Structural Health Monitoring 2003*, Palo Alto, CA, F.-K. Chang, ed. Destech, Lancaster, PA.
14. Moon F. (1984) *Magneto-Solid Mechanics*. Wiley, New York.
15. Poh S, Baz A. (1996) Distributed sensor for rectangular plates. In: *Smart Sensing, Processing and Instrumentation, Proceedings of SPIE*, Vol. 2718, San Diego, CA.
16. Matsuzaki R, Todoroki A. (2004) Passive wireless strain monitoring of tire using capacitance change. In: *Smart Structures and Materials 2004: Sensors and Smart Structures Technologies for Civil, Mechanical and Aerospace Systems, Proceedings of SPIE*, Vol. 5391, San Diego, CA.
17. Inada H, Okuhara Y, Kumagai H. (2004) Experimental study on structural health monitoring of RC columns using self-diagnosis materials. In: *Smart Structures and Materials 2004: Sensors and Smart Structures Technologies for Civil, Mechanical and Aerospace Systems, Proceedings of SPIE*, Vol. 5391, San Diego, CA.
18. Udd E. (1991) *Fiber Optic Sensors*. Wiley, New York.
19. Claus RO, Gunther MF, Wang AB, Murphy KA, Sun D. (1993) Extrinsic Fabry–Perot sensor for structural evaluation. In: *Applications of Fiber Optic Sensors in Engineering Mechanics*, F. Ansari ed. ASCE, New York.
20. Benmokrane B, Quiriron M, El-Salakawy E, Debaikey A, Lackey T. (1993) Fabry–Perot sensors for the monitoring of FRP reinforced bridge decks. In: *Nondestructive Evaluation and Health Monitoring of Aerospace Materials and Composites III (2004)*, *Proceedings of SPIE*, Vol. 5393, San Diego, CA.
21. Inaudi D, Elamari A, Pflug L, Gisin N, Breguet J, Vurpillot S. (1994) Low-coherence deformation sensors for the monitoring of civil-engineering structures. *Sensors and Actuators A* 44: 125–130.
22. Dunphy J, Meltz G, Morey W. (1995) Optical fiber Bragg grating sensors: A candidate for smart structures applications. In: *Fiber Optic Smart Structures*, E. Udd, ed. Wiley-InterScience, New York, pp. 271–286.
23. Maher A, Chen B, Prohaska JD, Nawy EG, Snitzer E. (1994) Fiber optic sensor for measurement of strain in concrete structures. In: *New Experimental Techniques for Evaluating Concrete Material and Structural Performance*, D. Stevens and M. Issa, eds. ACI SP-143, Farmington Hills, MI.
24. Measures RM, Melle S, Liu K. (1992) Wavelength demodulated Bragg grating fiber optic sensing system for addressing smart structure critical issues. *Smart Materials and Structures* 1: 39–44.
25. Udd E. (1995) *Fiber Optic Smart Structures*. Wiley, New York.
26. Davis MA, Bellemore DG, Kersey AD, Putnam MA, Friebele EJ, Idriss RL, Kodinduma M. (1996) High sensor count Bragg grating instrumentation system for large-scale structural monitoring applications. In: *Smart Sensing, Processing and Instrumentation, Proceedings of SPIE*, Vol. 2718, San Diego, CA.
27. Cheng LK, Liu SY, Guan BO, Chung WH, Chan TH, Schaarsberg JJ, Oostijk BW, Tam HY. (2004) Dynamic load monitoring of the Tsing Ma bridge using a high-speed FBG sensor system. In: *Proceedings of the Second European Workshop on Structural Health Monitoring*, Munich, Germany. C Boller and WJ Staszewski, eds., DEStech, Lancaster, PA.
28. Kawiecki G, Pena J, Guemes A. (2004) Strain monitoring using FBG optical transducers in a mechanical test of an aeronautical structure. In: *Proceedings of the Second European Workshop on Structural Health Monitoring*, Munich, Germany. C Boller and WJ Staszewski, eds., DEStech, Lancaster, PA.
29. Foedinger R, Rea D, Sirkis J, Troll J, Grande R, Vandiver TL. (1999) Structural health monitoring and impact damage detection for filament wound composite pressure vessels. In: *Proceedings of the Second International Workshop on Structural Health Monitoring*, Stanford, CA, F.-K. Chang, ed. Technomic Publishing, Lancaster, PA.
30. Grant J. (2005) Distributed sensing of composite over-wrapped pressure vessel using fiber Bragg gratings at ambient and cryogenic temperatures. In: *Smart Structures and Materials 2005: Smart Sensor Technology and Measurement Systems, Proceedings of SPIE*, Vol. 5758, San Diego, CA.
31. Takeda S, Yamamoto T, Okabe Y, Takeda N. (2004) Debonding monitoring of a composite repair patch using small-diameter FBG sensors. In: *Smart Structures and Materials 2004: Smart Electronic, MEMS, BioMEMS, and Nanotechnology*, *Proceedings of SPIE*, Vol. 5389, San Diego, CA.
32. Li HC, Davis CE, Herszberg I, Mouritz AP, Galea SC. (2004) Application of fiber optic Bragg grating sensors for the detection of disbonds in bonded composite ship joints. In: *Proceedings of the Second European Workshop on Structural Health Monitoring*, Munich, Germany. C Boller and WJ Staszewski, eds., DEStech, Lancaster, PA.

33. Guemes A, Pintado JM, Frovel M, Menendez JM. (2004) FBG based SHM systems in monolithic composite structures for aerospace. In: *Proceedings of the Second European Workshop on Structural Health Monitoring*, Munich, Germany. C Boller and WJ Staszewski, eds., DEStech, Lancaster, PA.
34. Udd E, Schulz WL, Seim J, Corona-Bittick K, Dorr J, Slattery K, Laylor H, McGill G. (1999) Fiber optic smart bearing load structure. In: *Nondestructive Evaluation of Bridges and Highways III*, *Proceedings of SPIE*, Vol. 3587, Newport Beach, CA, S. Chase, ed. Bellingham, WA.
35. Melvin L, Childers B, Rogowski R, Prosser W, Moore J, Frogatt M, Allison S et al. (1997) Integrated vehicle health management for aerospace vehicles. In: *Structural Health Monitoring Current Status and Perspectives*, F.-K. Chang, ed. Technomic Publishing, Lancaster, PA.
36. Spillman Jr. W, Huston D. (1995) Scaling and antenna gain in integrating fiber optic sensors. *IEEE Journal of Lightwave Technology* 13(7): 1222–1230.
37. Huston DR, Spillman Jr. WB, Claus RO, Ayra V. (1996) Vehicle classification by pattern matching gage sensors. In: *Smart Structures and Materials, Proceedings of SPIE* 2718A-27, San Diego, CA.
38. Smith C. (1994) OTDR technology and optical sensors time domain reflectometry in environmental, infrastructure, and mining applications. U.S. Bureau of Mines, SP 19-94, Washington, DC.
39. Wanser KH, Haselhuhn M, LaFond M. (1993) High temperature distributed strain and temperature sensing using OTDR. In: *Applications of Fiber Optic Sensors in Engineering Mechanics*, F. Ansari ed., ASCE, New York.
40. Horiguchi T, Kurashima T, Koyamada Y. (1992) Measurement of temperature and strain distribution by Brillouim frequency shift in silica optical fibers. In: *Distributed and Multiplexed Fiber Optic Sensors II*, *Proceedings of SPIE*, Vol. 1797-01, Boston, MA.
41. Dakin JP. (1995) Distributed optical fiber sensors. In: *Fiber Optic Smart Structures*, E. Udd, ed. Wiley, New York.
42. Flachsbarth J, Brandes M, Kowalsky W, Johannes HH. (2004) Humidity sensor based on Reichart's dye prepared with eximer-laser. In: *Proceedings of the Second European Workshop on Structural Health Monitoring*, Munich, Germany. C Boller and WJ Staszewski, eds., DEStech, Lancaster, PA.
43. Davey KJ. (1998) Monitoring apparatus for monitoring impending faults in the integrity of a component or structure. U.S. Patent 5,770,794.
44. Wheatley G, Kollgaard J, Register J, Zaidi M. (2003) Comparative vacuum monitoring as an alternative means of compliance. In: *Structural Health Monitoring 2003*, Palo Alto, CA, F.-K. Chang, ed. Destech, Lancaster PA.
45. Carlos MR, Finlayson RD, Miller RK, Friesel MA, Klokus LL. (1999) Acoustic emission on-line monitoring systems (AEOLMS). In: *Proceedings of the Second International Workshop on Structural Health Monitoring*, F.-K. Chang, ed., Stanford, CA. Technomic Publishing, Lancaster, PA.
46. Oshima N, Inoue K, Motogi S, Fukuda T. (2003) Constructing of cure monitoring system with piezoelectric ceramics for composite laminate. In: *Smart Structures and Materials 2003: Smart Structures and Integrated Systems, Proceedings of SPIE*, Vol. 5056, San Diego, CA.
47. Jang BZ. (1994) *Advanced Polymer Composites*. ASM International, Materials Park, OH
48. Li Y, Menon S. (February 1998) Ultrasonic sensing of composite materials during the heat-cure cycle. *Sensors* 15(2): 5–10.
49. Pelczarski N, Huston D. (2000) Cure monitoring of composite laminates used in the manufacture of snowboards. In: *Smart Structures Process Control and Sensors for Manufacturing, Proceedings of SPIE*, Vol. 3993-26, Newport Beach, CA.
50. Wakha K, Samuels P, Pines DJ. (2005) A smart composite patch for the repair of aircraft structures. In: *Nondestructive Evaluation and Health Monitoring of Aerospace Materials, Composites, and Civil Infrastructure IV, Proceedings of SPIE*, Vol. 5767-45, San Diego, CA.
51. Murasawa G. (2005) Analytical model for predicting internal stress and deformation of shape memory alloy composite. In: *Smart Structures and Materials 2005: Active Materials: Behavior and Mechanics*, *Proceedings of SPIE*, Vol. 5761, San Diego, CA.
52. Arzbergera SC, Tupper ML, Lake MS, Barretta R, Mallicka K, Hazelton C, Francis W et al. (2005) Elastic memory composites (EMC) for deployable industrial and commercial applications. In: *Smart Structures and Materials 2005: Industrial and Commercial Applications of Smart Structures Technologies, Proceedings of SPIE*, Vol. 5762, San Diego, CA.
53. Alexander G, Cheng YB, Burford RP, Shanks R, Mansouri J, Barber KW, Rodrigo PD, Preston C. (2013) Ceramifying composition for fire protection. U.S. Patent 8,409,479.
54. Dry, C. (2003) Self-repairing reinforced matrix materials. U.S. Patent 6,527,849.
55. White SR, Sottos NR, Geubelle PH, Moore JS, Kessler MR, Sriram SR, Brown EN, Viswanathan S. (2001) Autonomic healing of polymer composites. *Nature* 409(6822): 794–797.

56. Muntges DE, Park G, Inman DJ. (2001) Self-healing bolted joint employing a shape memory actuator. In: *Smart Structures, Proceedings of SPIE*, Vol. 4327, Newport Beach, CA.
57. Dakai L, Mingshun H, Baoqi T, Hao Q. (1999) Research on some problems about optical fiber embedded in carbon fiber smart structures. In: *Proceedings of the Second International Workshop on Structural Health Monitoring*, Stanford, CA, F.-K. Chang, ed. Technomic Publishing, Lancaster, PA.
58. Bergamini A, Christen R, Motavalli M. (2005) Electrostatic tuning of the bending stiffness of simple, slender multilayer composite structures. In: *Smart Structures and Materials 2005: Damping and Isolation, Proceedings of SPIE*, Vol. 5760, San Diego, CA.
59. Barrett R, Melkert J. (2005) UAV visual signature suppression via adaptive material. In: *Smart Structures and Materials 2005: Industrial and Commercial Applications of Smart Structures Technologies, Proceedings of SPIE*, Vol. 5762, San Diego, CA.
60. Song KD, Yi WJ, Chu SH, Choi SH. (2003) Microwave-driven thunder materials. *Microwave and Optical Technology Letters* 36(5): 331–333.
61. Callen HB. (1960) *Thermodynamics*. Wiley, New York.
62. Sodano HA, Park G, Leo DJ, Inman DJ. (2003) Use of piezoelectric energy harvesting devices for charging batteries. In: *Smart Structures and Materials 2003: Smart Sensor Technology and Measurement Systems, Proceedings of SPIE*, Vol. 5050, San Diego, CA.
63. Churchill DL, Hamel MJ, Townsend CP, Arms SW. (2003) Strain energy harvesting for wireless sensor networks. In: *Smart Structures and Materials 2003: Smart Electronics, MEMS, BioMEMS, and Nanotechnology, Proceedings of SPIE*, Vol. 5055, San Diego, CA.
64. Chuang J, Thomson DJ, Bridges G. (2004) Wireless strain sensor based on resonant RF cavities. In: *Smart Structures and Materials 2004: Smart Electronic, MEMS, BioMEMS, and Nanotechnology, Proceedings of SPIE*, Vol. 5389, San Diego, CA.
65. Suster M, Ko WH, Young DJ. (2004) An optically powered wireless telemetry module for high-temperature MEMS sensing and communication. *Journal of Microelectromechanical Systems* 13(3): 536–541.
66. Huston D. (2011) *Structural Sensing, Health Monitoring and Performance Evaluation*., Boca Raton, FL: Taylor & Francis.

Part VII

Glossary

Robert L. Sierakowski

Appendix A: List of Books

Robert L. Sierakowski and Olesya I. Zhupanska

BOOKS

1. Abrate, S. Ed., *Impact Engineering of Composite Structures*, Springer, CISM, Udine, Italy, 2011.
2. Aboudi, J., *Mechanics of Composite Materials: A Unified Micromechanical Approach*, Elsevier, Amsterdam, the Netherlands, 1991.
3. Advanced Composite Thermoplastics (ACTP) Materials, *Polymer Composites*, Winona, MN, 1986.
4. Advincula, R.C., Brittain, W.J., Caster, K.C., and Rühe, J. Eds., *Polymer Brushes: Synthesis. Characterization. Applications*, Wiley & Sons, Chester, New York, 2004.
5. Agarwal, B.D. and Broutman, L.J., *Analysis and Performance of Fiber Composites*, 2nd edn., Wiley & Sons, Chester, New York, 1990.
6. Bahei-El-Din, Y. and Dvorak, G.J. Eds., *IUTAM Symposium on Transformation Problems in Composite and Active Materials*, Kluwer Academic Publishers, Dordrecht, the Netherlands, 1998.
7. Bakhvalov, N. and Panasenko, G., *Homogenisation: Averaging Processes in Periodic Media: Mathematical Problems in the Mechanics of Composite Materials*, Kluwer Academic Publishers, Dordrecht, the Netherlands, 1989.
8. Beland, S., *High Performance Thermoplastic Resins and Their Composites*, Noyes Publications, Park Ridge, NJ, 1990.
9. Berlin, A., Henrici-Olive, G., and Olive, S. Eds., *Principles of Polymer Composites*: *Properties and Applications*, Vol. 10, Springer-Verlag, New York, 1986.
10. Blain, W.R. and de Wilde, W.P., *Composite Materials: Design and Analysis*, 2nd edn., Springer-Verlag, Berlin, Germany, 1998.
11. Bogdanovich, A.E. and Pastore, C.M., *Mechanics of Textile and Laminated Composites*, Chapman & Hall, London, 1996, 575p.
12. Bogdanovich, A.E., *Non-Linear Dynamic Problems for Composite Cylindrical Shells*, Elsevier, London, 1993, 295p.
13. Bracke, P., Schurmans, H., and Verpoest, I., *Inorganic Fibers and Composite Materials*, Pergamon Press, Elmsford, New York, 1984.
14. Buckley, J.D. and Edie, D.D. Eds., *Carbon-Carbon Materials and Composites*, Noyes Publications, Park Ridge, NJ, 1993.
15. Bull, J.W. Ed., *Numerical Analysis and Modelling of Composite Materials*, Springer-Verlag, New York, 1995.
16. Bunsell, A.R. Ed., *Fibre Reinforcements for Composite Materials*, Composite Materials Series, Elsevier, Amsterdam, the Netherlands, 1988, p. 2.
17. Bunsell, A.R., Lamicq, A., and Massiah, A., *Developments in the Science and Technology of Composite Materials: ECCM3*, Springer-Verlag, Berlin, Germany, 1989.
18. Carlsson, L.A. Ed., *Thermoplastic Composite Materials*. Composite Materials Series, Vol. 7, Elsevier, Amsterdam, the Netherlands, 1991.
19. Carlsson, L.A., *Experimental Characterization of Advanced Composite Materials*, CRC Press, Boca Raton, FL, 1996.
20. Carlsson, L.A. and Pipes, R.B., *Experimental Characterization of Advanced Composite Materials*, 2nd edn., Prentice-Hall, Upper Saddle River, NJ, 1996.
21. Chawla, K.K., *Composite Materials*: *Science and Engineering*, Springer-Verlag, New York, 1987.
22. Chawla, K.K., *Composite Materials. Science and Engineering*, 2nd edn., Springer-Verlag, New York, 1998.
23. Cherkaev, A. and Kohn, R. Eds., *Topics in the Mathematical Modelling of Composite-Materials*, Birkhauser, Boston, MA, 1997.
24. Chung, D., *Composite Materials: Science and Applications: Functional Materials for Modern Technologies*, Springer-Verlag, London, U.K., 2003.
25. Clark, A.F., Reed, R.P., and Hartwig, G., *Nonmetallic Materials and Composites at Low Temperatures*, Plenum Press, New York, 1979, p. 1.

26. Clegg, D.W. and Collyer, A.A. Eds., *Mechanical Properties of Reinforced Thermoplastics*, Elsevier Applied Science, Barking, Essex, 1986.
27. Clyne, T.W. and Witners, P.J., *An Introduction to Metal Matrix Composites*, Cambridge University Press, Cambridge, London, U.K., 1993.
28. Cogswell, F.N., *Thermoplastic Aromatic Polymer Composites*, Butterworth Heinemann, Oxford, U.K., 1992.
29. Cole, J.M. and Berthelot, J.-M., *Composite Materials: Mechanical Behavior and Structural Analysis*, Springer-Verlag, New York, 1998.
30. Gay, D., *Composite Materials: Design and Applications*, CRC Press, Boca Raton, FL, 2002.
31. Daniel, I.M. and Ishai, O., *Engineering Mechanics of Composite Materials,* Oxford University Press, New York, 1994.
32. *Data Manual for Kevlar 49 Aramid*, E.I. Du Pont de Nemours and Co., Textile Fibers Department, DuPont Publication, Wilmington, DE, 1986.
33. Dvorak, G.J., *Inelastic Deformation of Composite Materials: IUTAM Symposium*, Troy, New York, May 29–June 1, 1990, Springer-Verlag, New York, 1991.
34. Ferry, J.D., *Viscoelastic Properties of Polymers*, 3rd edn., Wiley & Sons, Chester, New York, 1980.
35. Folkes, N.J., *Short Fibre Reinforced Thermoplastics*, Wiley & Sons, Chester, New York, 1992.
36. Friedrich, K. Ed., *Friction and Wear of Polymer Composites*, Composite Materials Series, Elsevier, Amsterdam, the Netherlands, 1986, p. 1.
37. Fuller, J., Gruninger, G., Schulte, K., Bunsell, A.R., and Massiah, A. *Developments in the Science and Technology of Composite Materials ECCM4*, Kluwer Academic Publishers, Dordrecht, the Netherlands, 1990.
38. Galasso, F.S., *High Modulus Fibers and Composites*, Gordon & Breach, New York, 1970.
39. Gandhi, M.V., *Smart Materials and Structures*, Chapman & Hall, London, U.K., 1992.
40. Gdoutos, E.E., Pilakoutas, K., and Rodopoulos, C.A. Eds., *Failure Analysis of Industrial Composite Materials*, McGraw-Hill, New York, 2000.
41. Gdoutos, E.E. and Marioli-Riga, Z.P., *Recent Advances in Composite Materials: In Honor of S.A. Paipetis*, Springer-Verlag, Berlin, Germany, 2003.
42. Gibson, L.J. and Ashby, M.F., *Cellular Solids: Structure & Properties*, Chapman & Hall, Pergamon Press, New York, 1988.
43. Gibson, R.F., *Principles of Composite Material Mechanics*, 3rd edn., CRC Press, Boca Raton, FL, 2011.
44. Gill, R.M., *Carbon Fibres in Composite Materials*, Iliffe Books, London, U.K., 1972.
45. Hilado, C.J., *Glass Reinforced Epoxy Systems, Part 2*, Technomic Publication, Lancaster, PA, 1982.
46. Gürdal, Z., Haftka, R.T., and Hajela, P., *Design and Optimization of Laminated Composite Materials*, Wiley & Sons, Chester, New York, 1999.
47. Hancox, N. and Meyer, R., *Design Data for Reinforced Plastics*, Chapman & Hall, London, U.K., 1994.
48. Hearle, J. Ed., *Atlas of Fibre Fracture and Damage to Textiles*, CRC Press, Boca Raton, FL, 1998.
49. Hearle, J.W.S., Grosberg, P., and Backer, S., *Structural Mechanics of Fibers, Yarns and Fabrics*, Wiley-InterScience, New York, 1969, p. 1.
50. Hench, L.H. and Ulrich, D.R. Eds., *Science of Ceramic Chemical Processing*, Wiley & Sons, Chester, New York, 1986.
51. Herakovich, C.T., *Mechanics of Fibrous Composites*, Wiley & Sons, Chester, New York, 1997.
52. Hilado, C.J. Ed., *Boron Reinforced Aluminum Systems*, Technomic Publication, Westport, CT, 1974.
53. Hilado, C.J. Ed., *Reinforced Phenolic, Polyester, Polyimide, and Polystyrene Systems*, Technomic Publication, Lancaster, PA, 1974.
54. Hilado, C.J. Ed., *Carbon Reinforced Epoxy Systems, Parts 1–5,* Materials Technology Series, Technomic Publication, Lancaster, PA, 1974–1984, pp. 1, 8, 9, 12, 13.
55. Hilado, C.J. Ed., *Glass Reinforced Polyester Systems*, Materials Technology Series, Technomic Publication, Lancaster, PA, 1984, p. 14.
56. Hoa, S.V. and Gauvin, R. Eds., *Composite Structures and Materials*, Springer-Verlag, New York, 2003.
57. Holzapfel, G.A., *Nonlinear Solid Mechanics: A Continuum Approach for Engineering*, Wiley & Sons, Chester, New York, 2000.
58. Hull, D. and Clyne, T.W., *Introduction to Composite Materials*, 2nd edn., Cambridge University Press, New York, 1996.
59. Hyer, M.W., *Stress Analysis of Fiber-Reinforced Composite Materials*, updated edition, DEStech Publishers, Lancaster, PA, 2009.
60. Ivanov, Y., Cheshkov, V., and Natova, M., *Polymer Composite Materials—Interface Phenomena & Processes*, Kluwer Academic Publishers, Dordrecht, the Netherlands, 2001.
61. Jones, R.M., *Mechanics of Composite Materials*, 2nd edn., Taylor & Francis, Philadelphia, PA, 1999.

62. Kachanov, L.M., *Delamination Buckling of Composite Materials*, Kluwer Academic Publishers, Dordrecht, the Netherlands, 1988.
63. Kalamkarov, A.L. and Kolpakov, A.G., *Analysis Design and Optimization of Composite Structures,* 2nd edn., Wiley & Sons, Chester, New York, 1997.
64. Kaminski, M.M., *Computational Mechanics of Composite Materials: Sensitivity, Randomness, and Multiscale Behaviour*, Springer-Verlag, New York, 2005.
65. Kardomateas, G.A. and Carlsson, L.A., *Structural and Failure Mechanics of Sandwich Composites,* Springer, New York, 2011.
66. Kaw, A.K., *Mechanics of Composite Materials*, CRC Press, Boca Raton, FL, 1997.
67. Khoo, I.-C., Simoni, F., and Umeton, C., *Novel Optical Materials and Applications*, Wiley & Sons, Chester, New York, 1996.
68. Kim, J.-K. and Mai, Y.-W., *Engineered Interfaces in Fiber Reinforced Composites*, Elsevier Applied Science, New York, 1998.
69. Kline, R.A., *Nondestructive Characterization of Composite Media*, Technomic Publication, Lancaster, PA, 1992.
70. Lee, S.M., *Dictionary of Composite Materials Technology*, CRC Press, Boca Raton, FL, 1995.
71. Margolis, J.M., *Advanced Thermoset Composites*, Van Nostrand Reinhold, New York, 1986.
72. McCrum, N.G., Buckley, C.P., and Bucknell, C.B., *Principles of Polymer Engineering*, Oxford University Press, Oxford, U.K., 1988.
73. Mileiko, S.T. Ed., *Metal and Ceramic Based Composites*, Composite Materials Series, Elsevier, Amsterdam, the Netherlands, 1997, p. 12.
74. Morley, J., *High Performance Fibre Composites*, Academic Press, New York, 1987.
75. Mota Soares, C.A., Mota Soares, C.M., and Freitas, M.J.M. Eds., *Mechanics of Composite Materials and Structures*, Kluwer Academic Publishers, Dordrecht, the Netherlands, 1999.
76. Nelson, W., *Accelerating Tests*, Wiley-InterScience, New York, 1990.
77. Nielsen, L.E., *Mechanical Properties of Polymers and Composites*, Marcel Dekker, New York, 1974, pp. 1, 2.
78. Parkyn, B., *Glass Reinforced Plastics*, CRC Press, Boca Raton, FL, 1970.
79. Partridge, I.K. Ed., *Advanced Composites*, Elsevier Applied Science, London, U.K., 1989.
80. Phillips, L.N., *Design with Advanced Composite Materials,* Springer-Verlag, Berlin, Germany, 1989.
81. Platti, G. Ed., *Advances in Composite Materials*, Elsevier Applied Science, Barking, Essex, 1978.
82. Ponte Castaneda, P., Telega, J.J., and Gambin, B. Eds., Nonlinear homogenization and its applications to composites, *Polycrystals and Smart Materials: Proceedings of the NATO Advanced Research Workshop*, Springer-Verlag, Berlin, Germany, 2004.
83. Prelas, M.A., Benedictus, A., Lin, L.-T.S., and Popovici, G. Eds., *Diamond Based Composites: And Related Materials*, Kluwer Academic Publishers, Dordrecht, the Netherlands, 1997.
84. Pyrz, R., *IUTAM Symposium on Microstructure-Property Interactions in Composite Materials*, Kluwer Academic Publishers, Dordrecht, the Netherlands, 1995.
85. Ranney, N.W., *Reinforced Composites from Polyester Resins*, Noyes Data, Park Ridge, NJ, 1972.
86. Rauwendaal, C., *Polymer Extrusion,* 4th edn., Hanser Gardner, Munich, Germany, 2001.
87. Read, B.E. and Dean, G.D., *The Determination of Dynamic Properties of Polymers and Composites*, Wiley & Sons, New York, 1978.
88. Reddy, J.N., *Mechanics of Composite Materials: Selected Works of Nicholas J. Pagano*, Kluwer Academic Publishers, Dordrecht, the Netherlands, 1994.
89. Reddy, J.N., *Mechanics of Laminated Composite Plates and Shells: Theory and Analysis*, 2nd edn., CRC Press, Boca Raton, FL, 2004.
90. Salmen, L. et al. Eds., *Composite Systems from Natural and Synthetic Polymers*, Materials Science Monographs, Elsevier, Amsterdam, the Netherlands, 1986, p. 36.
91. Saruhan, B., *Oxide-Based Fiber-Reinforced Ceramic-Matrix Composites: Principles and Materials*, Kluwer Academic Publishers, Dordrecht, the Netherlands, 2003.
92. Savage, G., *Carbon-Carbon Composites*, Chapman & Hall, London, U.K., 1993.
93. Scherer, G.W., *Relaxation in Glass and Composites*, Wiley & Sons, New York, 1986.
94. Serafini, T.T. Ed., *High Temperature Polymer Matrix Composites*, Noyes Data, Park Ridge, NJ, 1987.
95. Sheldon, R.P., *Composite Polymeric Materials*, Elsevier Application Science Publication, Barking, Essex, 1982.
96. Sierakowski, R.L. and Chaturvedi, S.K., *Dynamic Loading and Characterization of Fiber-Reinforced Composites,* Wiley & Sons, Chester, New York, 1997.

97. Sih, G.C. and Tamusz, V.P. Eds., *Fracture of Composite Materials*, Sijthoff & Noordhoff International Publishers, Alphen aan den Rijn, the Netherlands, March 1979.
98. Sih, G.S. and Chen, E.P., *Cracks in Composite Materials: A Compilation of Stress Solutions for Composite Systems with Cracks*, Martinus Nijhoff Publishers, The Hague, the Netherlands, 1981.
99. Singh, O.N. and Lakhtakia, A. Eds., *Electromagnetic Fields in Unconventional Materials and Structures,* Wiley & Sons, Chester, New York, 2000.
100. Gandhi, M.V. and Thompson, B.S., *Smart Materials and Structures*, Institute of Physics Publication, Bristol, England, 1992.
101. Sonneborn, R.H., *Fiberglass Reinforced Plastics*, Van Nostrand Reinhold, New York, 1954.
102. Springer, G.S. Ed., *Environmental Effects on Composite Materials*, Vol. 3, Technomic Publication, Lancaster, PA, 1984–1987.
103. Starr, T.F., *Glass-Fibre Databook*, Chapman & Hall, London, U.K., 1993.
104. Starr, T.F., *Databook of Thermoset Resins for Composites*, Elsevier Advanced Technology, Oxford, U.K., 1994.
105. Starr, T.F., *Glass-Fibre Directory and Databook*, Chapman & Hall, London, U.K., 1997; Summerscales, J., *Microstructural Characterization of Fibre-Reinforced Composites*, CRC Press, Boca Raton, FL, 1998.
106. Sun, C.T., *Mechanics of Aircraft Structures*, Wiley & Sons, Chester, New York, 1998.
107. Talreja, R. Ed., *Damage Mechanics of Composite Materials*, Elsevier, Amsterdam, the Netherlands, 1994.
108. Talreja, R. and Singh, C.V., *Damage and Failure of Composite Materials,* Cambridge University Press, Cambridge, England, U.K., 2012.
109. Tarnopol'skii, Y.M. and Kincis, T., *Static Test Methods for Composites*, Van Nostrand Reinhold, New York, 1985.
110. Taya, M. and Arsenault, R.J., *Metal Matrix Composites*, Pergamon Press, Elmsford, New York, 1989.
111. Taylor-Wilde, M., *A Practical Guide to Composites*, Multi-Sport Composites Ltd., Bolton, England, 1995.
112. Titow, W.V. and Lanham, B.J., *Reinforced Thermoplastics*, Halsted Press, New York, 1975.
113. Tong, L. and Soutis, C., *Recent Advances in Structural Joints and Repairs for Composite Materials*, Springer-Verlag, London, U.K., 2003.
114. Tuttle, M.E., *Structural Analysis of Polymeric Composite Materials*, Marcel Dekker, Hoboken, NJ, 2003.
115. Udd, E., *Fiber Optic Smart Structures*, Wiley & Sons, Chester, New York, 1995.
116. Uhlmann, D.R. and Ulrich, D.R. Eds., *Ultrastructure Processing of Advanced Materials*, Wiley & Sons, Chester, New York, 1992.
117. Vinson, J.R., *The Behavior of Shells Composed of Isotropic and Composite Materials*, Kluwer Academic Publishers, Dordrecht, the Netherlands, 1993.
118. Vinson, J.R. and Sierakowski, R.L., *The Behavior of Structures Composed of Composite Materials*, 2nd edn., Springer-Verlag, 2002.
119. Wang, Z.L. and Kang, Z.C., *Functional and Smart Materials: Structural Evolution and Structure Analysis*, Plenum Press, New York, 1998.
120. Watt, W., *New Fibres and Their Composites,* Royal Society, London, U.K., 1980.
121. Whitney, J.M., Daniel, I.M., and Pipes, R.B., *Experimental Mechanics of Fiber Reinforced Composite Materials,* Monograph No. 4, revised edition, Society for Experimental Mechanics, Prentice Hall, Englewood Cliffs, NJ, 1985.
122. Yang, H.H., *Kevlar Aramid Fiber*, Wiley & Sons, Chester, New York, 1993.
123. Zenkert, D. Ed., *An Introduction to Sandwich Construction*, EMAS Publishers, London, U.K., 1995.

PROCESSING AND MANUFACTURING

1. *Conference on Advanced Composite Technology*, T/C Publications, El Segundo, CA, 1978.
2. Advani, S.G., *Flow and Rheology in Polymer Composites Manufacturing*, Composite Materials Series, Vol. 10, Elsevier, Amsterdam, the Netherlands, 1994.
3. Astrom, B.T., *Manufacturing of Polymer Composites,* Chapman & Hall, London, U.K., 1997.
4. Benson, S., Cook, T., Trewin, E., and Turner, K.M. Eds., *Materials and Processing—Move into the 90's*, Elsevier, Amsterdam, the Netherlands, 1989.
5. Bhattacharyya, D. Ed., *Composite Sheet Forming*, Composite Materials Series, Vol. 11, Elsevier, Amsterdam, the Netherlands, 1997.
6. Campbell, F.C., *Manufacturing Processes for Advanced Composites*, Elsevier Advanced Technology, Oxford, U.K., 2003.
7. Carlsson, L.A. and Gillespie, J.W. Eds., *Processing and Fabrication Technology*, Delaware Composites Design Encyclopedia, Vol. 3, Technomic Publications, Lancaster, PA, 1990.
8. Ciriscioli, P.R. and Springer, G.S., *Smart Autoclave Cure of Composites*, Technomic Publications, Lancaster, PA, 1990.

9. Cogswell, F.N., *Thermoplastic Aromatic Polymer Composites: A Study of the Structure, Processing and Properties of Carbon Fibre Reinforced Polyetheretherketone and Related Materials*, Woodhead Publishers, Cambridge, U.K., 1992.
10. Delmonte, J., *Technology of Carbon and Graphite Fiber Composites*, Van Nostrand Reinhold, New York, 1981.
11. *DoD/NASA Structural Composites Fabrication Guide*, 2nd edn., Air Force Wright Patterson Aeronautics Lab, Dayton, OR, 1979.
12. Douglass, W.A., *Braiding and Braiding Machinery,* Centrex Publishers, Eindhoven, the Netherlands, 1964.
13. Gutowski, T.G. Ed., *Advanced Composites Manufacturing*, Wiley & Sons, Chester, New York, 1997.
14. Happey, F. Ed., *Contemporary Textile Engineering*, Academic Press, London, U.K., 1982.
15. Kaiser, R., *Technology Assessment of Advanced Composite Materials*, Argos Associations, Winchester, MA, 1978.
16. Ko, F.K., Pastore, C.M., and Head, A.A., *Handbook on Industrial Braiding,* Atkins & Pearce, Covington, KY, 1989.
17. Loewenstein, K.L., *The Manufacturing Technology of Continuous Glass Fibres,* 2nd edn., Elsevier, Amsterdam, the Netherlands, 1983.
18. Lord, P. and Mohamed, M., *Weaving: Conversion of Yarn to Fabric*, 2nd edn., Merrow Technical Library, Durham, England, 1982.
19. Mallick, P.K., *Fiber-Reinforced Composites: Materials, Manufacturing and Design*, 3rd edn., CRC Press, Boca Raton, FL, 2007.
20. Mallick, P.K., *Fiber-Reinforced Composites: Materials, Manufacturing, and Design*, 2nd edn., Marcel Dekker, New York, 1993.
21. Mazumdar, S.K., *Composites Manufacturing: Materials, Product, and Process Engineering*, CRC Press, Boca Raton, FL, 2002.
22. Moore, G.R. and Kline, D.E., *Properties and Processing of Polymers for Engineers*, Prentice-Hall, London, U.K., 1984.
23. Muccio, E.A., *Plastics Processing Technology,* ASM Publications, Materials Park, OH, 1994.
24. Parratt, N.J., *Fibre-Reinforced Materials Technology,* Van Nostrand Reinhold, New York, 1972.
25. National Technical Information Service, *Prepreg Composition, Processing and Applications*, 1973–1984, TIC Publications, El Segundo, CA, 1984.
26. Rosato, D.V. and Grove, C.S. Jr., *Filament Winding: Its Development, Manufacture, Applications and Design*, InterScience Publications, New York, 1964.
27. Schwartz, P., Rhodes, T., and Mohamed, M.H., *Fabric Forming Systems,* Noyes Publications, Park Ridge, NJ, 1982.
28. Schwartz, M.M., *Composite Materials, Vol. II: Processing, Fabrication, and Applications*, 1st edn., Prentice Hall, Upper Saddle River, NJ, 1993.
29. Seferis, J.C. and Nicolais, L. Eds., *The Role of the Polymeric Matrix in the Processing and Structural Properties of Composite Materials*, Plenum Press, New York, 1983.
30. Srivatsan, T.S. Ed., Machining of composite materials, *Proceedings of the ASM International Conference on Week'92 ASM Materials,*, Materials Park, OH, 1992.
31. Srivatsan, T.S., Bowden, D.M., and Lane, C.T. Eds., Machining of composite materials, Vol. II, *Proceedings of the ASM International Conference on ASM Materials Week*, Materials Park, OH, 1993.
32. Strong, A.B., *High Performance and Engineering Thermoplastic Composites*, Technomic Publications, Lancaster, PA, 1993.
33. Thomas, D.G.B., *An Introduction to Warp Knitting,* Merrow, Watford, U.K., 1971.
34. Wake, W.C. and Wooten, D.B. Eds., *Textile Reinforcement of Elastomers*, Elsevier Applied Science, Barking, Essex, 1982.
35. Weatherhead, R.G., *FRP Technology-Fibre Reinforced Resin Systems,* Elsevier Applied Science, Barking, Essex, 1980.

ASTM STP VOLUMES ON COMPOSITES

1. ASTM STP 427, Fiber-Strengthened Metallic Composites, 1967.
2. ASTM STP 438, Metal Matrix Composites, 1967.
3. ASTM STP 452, Interfaces in Composites, 1968.
4. ASTM STP 521, Analysis of Test Methods for High Modulus Fibers and Composites, 1973.
5. ASTM STP 524, Applications of Composite Materials, 1973.
6. ASTM STP 568, Foreign Impact Damage to Composites, 1975.
7. ASTM STP 569, Fatigue of Composite Materials, 1975.

8. ASTM STP 580, Composite Reliability, 1975.
9. ASTM STP 593, Fracture Mechanics of Composites, 1976.
10. ASTM STP 602, Environmental Effects on Advanced Composite Materials, 1976.
11. ASTM STP 636, Fatigue of Filamentary Composite Materials, 1977.
12. ASTM STP 638, Fatigue, 1977.
13. ASTM STP 658, Advanced Composite Materials: Environmental Effects, 1978.
14. ASTM STP 696, Nondestructive Evaluation and Flaw Criticality for Composite Materials, 1979.
15. ASTM STP 704, Commercial Opportunities for Advanced Composites, 1980.
16. ASTM STP 723, Fatigue of Fibrous Composite Materials, 1981.
17. ASTM STP 734, Test Methods and Design Allowables for Fibrous Composites, 1981.
18. ASTM STP 749, Joining of Composite Materials, 1981.
19. ASTM STP 768, Composites for Extreme Environments, 1982.
20. ASTM STP 772, Short Fiber Reinforced Composite Materials, 1982.
21. ASTM STP 775, Damage in Composite Materials, 1982.
22. ASTM STP 797, Composite Materials: Quality Assurance and Processing, 1982.
23. ASTM STP 831, Long-Term Behavior of Composites, 1983.
24. ASTM STP 836, Effects of Defects on Composite Materials, 1984.
25. ASTM STP 864, Recent Advances in Composites in the United States and Japan, 1985.
26. ASTM STP 873, High Modulus Fiber Composites in Ground Transportation and High Volume Applications, 1985.
27. ASTM STP 876, Delamination and Debonding of Materials, 1985.
28. ASTM STP 907, Composite Materials: Fatigue and Fracture, 1986.
29. ASTM STP 927, Fatigue in Mechanically Fastened Composite and Metallic Joints, 1986.
30. ASTM STP 936, Instrumented Impact Testing of Plastics and Composite Materials, 1987.
31. ASTM STP 937, Toughened Composites, 1987.
32. ASTM STP 948, Fractography of Modern Engineering Materials: Composites and Metals, 1987.
33. ASTM STP 964, Testing Technology of Metal Matrix Composites, 1988.
34. ASTM STP 1003, Testing Methods and Design Allowables for Fibrous Composites, 1989.
35. ASTM STP 1012, Composite Materials: Fatigue and Fracture, 1989.
36. ASTM STP 1032, Metal Matrix Composites: Testing, Analysis, and Failure, 1989.
37. ASTM STP 1044, Advances in Thermoplastic Matrix Composite Materials, 1989.
38. ASTM STP 1110, Composite Materials: Fatigue and Fracture, 1991.
39. ASTM STP 1128, Damage Detection in Composite Materials, 1992.
40. ASTM STP 1156, Composite Materials: Fatigue and Fracture, 1993.
41. ASTM STP 1174, High Temperature and Environmental Effects on Polymeric Composites, 1993.
42. ASTM STP 1178, Composite Materials for Implant Applications in the Human Body: Characterization and Testing, 1993.
43. ASTM STP 1208, Composite Materials: Testing and Design, 1993.
44. ASTM STP 1227, Composites Bonding, I994.
45. ASTM STP 1230, Composite Materials: Fatigue and Fracture, 1995.
46. ASTM STP 1242, Composite Materials: Testing and Design, 1997.
47. ASTM STP 1253, Life Prediction Methodology for Titanium Matrix Composites, 1996.
48. ASTM STP 1274, Composite Materials: Testing and Design, 1997.
49. ASTM STP 1285, Composite Materials: Fatigue and Fracture, 1997.
50. ASTM STP 1290, Fiber, Matrix, and Interface Properties, 1996.
51. ASTM STP 1302, High Temperature and Environmental Effects on Polymeric Composites, 1997.
52. ASTM STP 1309, Thermal and Mechanical Test Methods and Behavior of Continuous-Fiber Ceramic Composites, 1997.
53. ASTM STP 1330, Composite Materials: Fatigue and Fracture, 1998.
54. ASTM STP 1357, Time Dependent and Nonlinear Effects in Polymers and Composites, 2000.
55. ASTM STP 1369, Limitations of Test Methods for Plastics, 2000.
56. ASTM STP 1383, Composite Structures: Theory and Practice, 2000.
57. ASTM STP 1392, Mechanical, Thermal and Environmental Testing and Performance of Ceramic Composites and Components, 2001.
58. ASTM STP 1409, Fracture Resistance Testing of Monolithic and Composite Brittle Materials, 2002.
59. ASTM ATP 1416, Composite Materials: Testing, Design, and Acceptance Criteria, 2002.
60. ASTM STP 1436, Composite Materials: Testing and Design, 2003.
61. ASTM STP 1455, Joining and Repair of Composites Structures, 2005.

HANDBOOKS

1. Structural Plastics Research Council. *ASCE Structural Plastics Selection Manual*, Task Committee on Properties of Selected Plastics and Systems, Structural Plastics Research Council Publication, 1985.
2. ASTM Committee D-30 on High Modulus Fibers and Their Composites, *ASTM Standards and Literature References, for Composite Materials*, 2nd edn., ASTM, Philadelphia, PA, 1990.
3. Buckley, J.D. and Edie, D.D. Eds., *Carbon-Carbon Materials and Composites*, Noyes Publications, Park Ridge, NJ, 1993.
4. Bunsell, A.R. and Kelly, A. Eds., *Composite Materials: A Directory to European Research*, Butterworths, London, U.K., 1985.
5. Carlsson, L.A. and Pipes, R.B., *Experimental Characterization of Advanced Composite Materials*, 2nd edn., Prentice-Hall, Upper Saddle River, NJ, 1996.
6. Cheremisinoff, N.P. and Cheremisinoff, P.N., *Fiberglass-Reinforced Plastics Deskbook,* Ann Arbor Science, Ann Arbor, MI, 1978.
7. *Composite Materials Handbook-MIL 17, Volume 5: Ceramic Matrix Composites,* ASTM, Philadelphia, PA, 2002.
8. *Composite Materials Handbook-MIL 17, Volume 3: Material Usage, Design, and Analysis,* CRC Press, Boca Raton, FL, 1999.
9. *Composite Materials Handbook-MIL 17, Volume 2: Polymer Matrix Composites: Material Properties,* CRC Press, Boca Raton, FL, 2000.
10. *Composite Materials Handbook-MIL 17, Volume 1: Guidelines for Characterization of Structural Materials,* CRC Press, Boca Raton, FL, 1999.
11. ASTM International. Handbook Committee, *Engineered Materials Handbook Volume 1: Composites*, ASM International, Metals Park, OH, 1987.
12. *EPON Resin Structural Reference Manual*, Shell Chemical Co, Houston, TX, 1989.
13. *EXTREN Fiberglass Structural Shapes Design Manual*, Morrison Molded Fiber Glass Co, Bristol, VA, 1989.
14. Hagnauer, G. and Ilcewicz, L., Co-chairmen, *MIL-HDBK—l7,* in 3 Volumes, Technomic Publications, Lancaster, PA, 1997.
15. *ICI Fiberile Materials Handbook*, ICI Fiberite Technology Group, Tempe, AZ, 1991.
16. Kaelble, D.H., *CAD/CAM Handbook for Polymer Composite Reliability*, Vol. 1, Rockwell International, Thousand Oaks, CA, 1983.
17. Katz, H.S. and Milewski, I.V. Eds., *Handbook of Fillers for Plastics*, Van Nostrand Reinhold, New York, 1987.
18. Kelly, A. and Rabotnov, Y.N. Eds., *Handbook of Composites,* in 4 Volumes, Elsevier, Amsterdam, the Netherlands, 1983–1985.
19. Kutz, M., *Mechanical Engineers' Handbook*, 2nd edn., Wiley & Sons, Chester, New York, 1998.
20. Lee, S.M. Ed., Reference *Book for Composite Technology*, Vols. 1 and 2, Technomic Publications, Lancaster, PA, 1989.
21. Lee, S.M. Ed., *Dictionary of Composite Materials Technology*, Technomic Publications, Lancaster, PA, 1989.
22. Lee, S.M., *Handbook of Composite Reinforcements,* Wiley & Sons, Chester, New York, 1992.
23. Lubin, G. Ed., *Handbook on Fiberglass and Advanced Plastics Composites,* Van Nostrand Reinhold, New York, 1969.
24. Lubin, G. Ed., *Handbook on Fiberglass and Advanced Plastics Composites*, 2nd edn., RE Krieger Publications, Huntington, New York, 1975.
25. Lubin, G. Ed., *Handbook of Composites*, Van Nostrand Reinhold, New York, 1982.
26. Lynch, C.T. Ed., *CRC Handbook of Materials Science,* in 3 Volumes, CRC Press, Boca Raton, FL, 1974–1975.
27. Meyer, R.W., *Handbook of Pultrusion Technology,* Chapman and Hall, New York, 1985.
28. Milewski, I.V. and Katz, H.S. Eds., *Handbook of Reinforcements for Plastics,* Van Nostrand Reinhold, New York, 1987.
29. Mohr, J.G., Oleesky, S.S., Shook, G.D., and Meyer, L.S. Eds., *SPI Handbook of Technology and Engineering of Reinforced Plastics/Composites*, Van Nostrand Reinhold, New York, 1973.
30. Mohr, J.G., Oleesky, S.S., Shook, G.D., and Meyer, L.S. Eds., *SPI Handbook of Technology and Engineering of Reinforced Plastics/Composites*, Van Nostrand Reinhold, New York, 1973.
31. Nicholls, R.L. *Composite Construction Materials Handbook,* Prentice-Hall, Englewood Cliffs, NJ, 1976.
32. Neelakanta, P.S. Ed., *Handbook of Electromagnetic Materials Monolithic and Composite Versions and Their Applications*, CRC Press, Boca Raton, FL, 1996.
33. Oleesky, S.S. and Mohr, I.G., *Handbook of Reinforced Plastics of the Society of Plastics Industry, Inc,* Van Nostrand Reinhold, New York, 1964.
34. Packham, D.E., *Handbook of Adhesion,* 2nd edn., Wiley & Sons, Chester, New York, 2005.

35. Peters, S.T. Ed., *Handbook on Composites,* 2nd edn., Chapman & Hall, London, U.K., 1998.
36. *Phillystran Data Manual*, Owens-Corning Fiberglass Corporation, S-2 Glass Fiber, United Ropeworks, Toledo, OH, 1990.
37. Rollaway, L., *Handbook of Polymer Composites for Engineers,* Woodhead Publications, Cambridge, England, 1994.
38. Rosato, D.V. and Rosato, D.V. Eds., *Blow Molding Handbook: Technology, Performance, Markets. Economics: The Complete Blow Molding Operation*, Hanser Publications, Munich, Germany, 1989.
39. Rosato, D.V., DiMathia, D.P., Rosato, D.V., and Van Nostrand, R., *Designing with Plastics and Composites: A Handbook*, New York, 1991.
40. Rosato, D.V. and Rosato, D.V., *Injection Molding Handbook: The Complete Blow Molding Operation: Technology, Performance, Economics*, Chapman & Hall, New York, 1995.
41. Rosato, D.V., *Plastics Processing Data Handbook,* Chapman & Hall, New York, 1997.
42. Rubin, I.I. Ed., *Handbook of Plastic Materials and Technology*, Wiley & Sons, New York, 1990.
43. Sabnis, G.M. Ed., *Handbook of Composite Construction Engineering,* Van Nostrand Reinhold, New York, 1979.
44. Schwartz, M.M. Ed., *Fabrication of Composite Materials*, ASM, Metals Park, OH, 1975.
45. Schwartz, M.M., *Composite Materials Handbook*, McGraw-Hill, New York, 1984.
46. Schwartz, M.M. Ed., *Composite Materials Handbook,* McGraw-Hill, New York, 1992.
47. Starr, T.F., *Carbon and High Performance Fibers Directory and Databook*, Chapman & Hall, London, U.K., 1995.
48. *Thermoplastic Composite Materials Handbook*, ICI Thermoplastic Composites, Newark, DE, 1992.
49. Weeton, I.A., Peters, D.M., and Thomas, K.L. Eds., *Engineers' Guide to Composite Materials*, ASM, Metals Park, OH, 1986.
50. Woishnis, W.A. Ed., *Engineering Plastics and Composites*, ASM International, Materials Park, OH, 1993.

ENCYCLOPEDIAS

1. Bever, M.B. Ed., *Encyclopedia of Materials Science* and *Engineering*, in 8 Volumes, Pergamon Press, Oxford, England, 1984.
2. Mark, H.F. and Kroschwitz, J.I., *Encyclopedia of Polymer Science and Engineering,* 15 Volumes to date, 2nd edn., Wiley & Sons, New York, 1984–1996.
3. Grayson, M. Ed., *Encyclopedia of Composite Materials and Components*, Encyclopedia Reprint Series, Wiley-InterScience, New York, 1983.
4. Carlsson, L.A. and Gillespie, J.W. Eds., *Delaware Composites Design Encyclopedia,* in 6 Volumes, Technomic Publications, Lancaster, PA, 1989–1990.
5. Carlsson, L.A. and Gillespie, J.W. Eds., *Test Methods. Delaware Composites Design Encyclopedia*, Technomic Publications, Lancaster, PA, 1990, p. 6.
6. Clauses, H.R. Ed., *Encyclopedia/Handbook of Materials, Parts and Finishes*, Technomic Publications, Lancaster, PA, 1976.
7. Carlsson, L.A., Gillespie, J.W., and Zweben, C.H., *Delaware Composites Design Encyclopedia: Micromechanical Materials Model*, Vol. II, University of Delaware, CRC Press, Boca Raton, FL, 1990.
8. Grayson, M. Ed., *Encyclopedia of Composite Materials and Components,* Wiley & Sons, Chester, New York, 1983.
9. Kelly, A. Ed. *Concise Encyclopedia of Composite Materials*, Pergamon Press, Oxford, England, 1989.
10. Kelly, A. Ed., *Concise Encyclopedia of Composite Materials*, Revised edition, Pergamon Press, Oxford, England, 1994.
11. Kelly, A. and Zweben, C. Eds., *Comprehensive Composite Materials. Volume 1: Fiber Reinforcements and General Theory of Composites*, Elsevier Applied Science, Barking, Essex, 2000.
12. Lee, S.M. Ed., *International Encyclopedia of Composites*, Vol. 6, Wiley & Sons, Chester, New York, 1991.
13. Lee, S.M. Ed., *International Encyclopedia of Composites*, Vol. 5, Wiley & Sons, Chester, New York, 1991.
14. Lee, S.M. Ed., *International Encyclopedia of Composites*, Vol. 4, Wiley & Sons, Chester, New York, 1990.
15. Lee, S.M. Ed., *International Encyclopedia of Composites,* Vol. 3, Wiley & Sons, Chester, New York, 1990.
16. Lee, S.M. Ed., *International Encyclopedia of Composites*, Vol. 2, Wiley & Sons, Chester, New York, 1990.
17. Lee, S.M. Ed., *International Encyclopedia of Composites*, Vol. 1, Wiley & Sons, Chester, New York, 1989.
18. Mark, H.F., *Encyclopedia of Polymer Science and Engineering, Volume 3, Cellular Materials to Composites*, 2nd edn., Wiley & Son, Hoboken, NJ, 1985.
19. *Modern Plastics Encyclopedia*, McGraw-Hill, New York, 1999.
20. Rosato, D.V., *Plastics Encyclopedia and Dictionary*, Hanser Publications, Munich, Germany, 1993.

Appendix B: List of Journals

Robert L. Sierakowski and Alexander Bogdanovich

MAJOR JOURNALS

1. *Advanced Composites*
2. *Advanced Composites Bulletin*
3. *Advanced Composites Letters*
4. *Advanced Composite Materials (The official Journal of the Japan Society for Composite Materials)*
5. *An International Journal for the Science and Application of Composite Materials*
6. *Applied Composite Materials*
7. *Cement & Concrete Composites*
8. *Composites & Adhesives*
9. *Composites Design & Application*
10. *Composites Fabrication*
11. *Composite Interfaces*
12. *Composites Manufacturing*
13. *Composite Materials Science*
14. *Composite Material Technology*
15. *Composites Science and Technology*
16. *Composite Structures*
17. *Composites Technology*
18. *Composites Technology & Research*
19. *Composites Technology Review*
20. *Composites Part A: Applied Science and Manufacturing*
21. *Composites Part B: Engineering Fibre Science and Technology*
22. *High Performance Composites*
23. *International Journal of Cement Composites & Lightweight Concrete*
24. *Journal of Composite Materials*
25. *Journal of Composite Technology and Research*
26. *Journal of Composites in Construction*
27. *Journal of Reinforced Plastics and Composites*
28. *Journal of Thermoplastic Composite Materials*
29. *Mechanics of Composite Materials*
30. *Mechanics of Composite Materials and Structures*
31. *Plastics, Rubber, and Composites, Processing and Applications*
32. *Polymer Composites*
33. *Polymers & Polymer Composites*
34. *Reinforced Plastics*

JOURNALS WITH CONSIDERABLE NUMBER OF PUBLICATIONS ON COMPOSITES

1. *AIAA Journal*
2. *Applied Mechanics Reviews*
3. *British Plastics and Rubber*

4. *Computers & Structures*
5. *International Journal of Polymeric Materials*
6. *International Journal of Solids & Structures*
7. *Journal of Applied Mechanics*
8. *Journal of Applied Polymer Science*
9. *Journal of Engineering Materials and Technology*
10. *Journal of Materials Research*
11. *SAMPE Journal*
12. *SAMPE Quarterly*

OTHER RELATED PUBLICATIONS

1. *Aerospace Newsletters—Advanced Composite Materials*
2. *Advanced Ceramics Report*
3. ASCE Publications Home Page
4. *Aviation Week & Space Technology*
5. *Buyer's Guide 2004*
6. *Ceramic Bulletin*
7. *Composites*
8. *Composite Materials Handbook*
9. *Composites: An Insider's Technical Guide to Corporate America's Activities. 3rd edition*
10. *Composites* Online by Elsevier Science
11. *Composites News*
12. *Consulting Library (SRI International)*
13. *Continuous Fiber Ceramic Program Newsletter* (Department of Energy)
14. *Injection Molding Magazine*
15. *Journal of Electronic Materials*
16. *NDT Journal*
17. *NetComposites*
18. *Performance Composites—Newsletter*
19. *Space News*
20. *The Composite Corner*
21. *Universe Today*

Appendix C: List of Conferences' Proceedings and Symposiums

Robert L. Sierakowski and Olesya I. Zhupanska

INTERNATIONAL CONFERENCE ON COMPOSITE MATERIALS (ICCM)

1. *1st ICCM*, Geneva, Switzerland—Boston, MA, 1975
2. *2nd ICCM*, Toronto, Canada, 1978
3. *3rd ICCM*, Paris, France, 1980
4. *4th ICCM*, Tokyo, Japan, 1982
5. *5th ICCM*, San Diego, CA, 1985
6. *6th ICCM*, London, England, 1987
7. *7th ICCM*, Guangzhou, People's Republic of China, 1989
8. *8th ICCM*, Honolulu, Hawaii, 1991
9. *9th ICCM*, Madrid, Spain, 1993
10. *10th ICCM*, Whistler, British Columbia, Canada, 1995
11. *11th ICCM*, Gold Coast, Queensland, Australia, 1997
12. *12th ICCM*, Paris, France, 1999
13. *13th ICCM*, Beijing, China, 2001
14. *14th ICCM*, San Diego, CA, 2003
15. *15th ICCM*, Durban, South Africa, 2005
16. *16th ICCM*, Kyoto, Japan, 2007
17. *17th ICCM*, Edinburgh, Scotland, 2009
18. *18th ICCM*, Jeju Island, South Korea, 2011

ANNUAL CONFERENCE OF THE AMERICAN SOCIETY FOR COMPOSITES (ASC)

(Proceedings of all conferences published by Technomic Publishing, Lancaster, PA)

1. *ASC 1st Technical Conference*, Dayton, OH, 1986
2. *ASC 2nd Technical Conference*, Newark, DE, 1987
3. *ASC 3rd Technical Conference*, Seattle, WA, 1988
4. *ASC 4th Technical Conference*, Blacksburg, VI, 1989
5. *ASC 5th Technical Conference*, East Lansing, MI, 1990
6. *ASC 6th Technical Conference*, Albany, New York, 1991
7. *ASC 7th Technical Conference*, University Park, Pennsylvania, PA, 1992
8. *ASC 8th Technical Conference*, Cleveland, OH, 1993
9. *ASC 9th Technical Conference*, Newark, DE, 1994
10. *ASC 10th Technical Conference*, Santa Monica, CA, 1995
11. *ASC 11th Technical Conference*, Atlanta, GA, 1996
12. *ASC 12th Technical Conference*, Dearborn, MI, 1997
13. *ASC 13th Technical Conference*, Baltimore, MD, 1998
14. *ASC 14th Technical Conference*, Dayton, OH, 1999
15. *ASC 15th Technical Conference*, College Station, TX, 2000

16. *ASC 16th Technical Conference*, Blacksburg, VI, 2001
17. *ASC 17th Technical Conference*, West Lafayette, IN, 2002
18. *ASC 18th Technical Conference*, Gainesville, FL, 2003
19. *ASC 19th Technical Conference*, Atlanta, GA, 2004
20. *ASC 20th Technical Conference*, Philadelphia, PA, 2005
21. *ASC 21st Technical Conference*, Dearborn, MI, 2006
22. *ASC 22nd Technical Conference*, Seattle, WA, 2007
23. *ASC 23rd Technical Conference*, Memphis, TN, 2008
24. *ASC 24th Technical Conference*, Newark, DE, 2009
25. *ASC 25th Technical Conference*, Dayton, OH, 2010
26. *ASC 26th Technical Conference*, Montreal, Quebec, Canada, 2011
27. *ASC 27th Technical Conference*, Arlington, TX, 2012

EUROPEAN CONFERENCE ON COMPOSITE MATERIALS (ECCM)

1. *1st ECCM*, Bordeaux, France, 1985
2. *2nd ECCM*, London, England, 1987
3. *3rd ECCM*, Bordeaux, France, 1989
4. *4th ECCM*, Stuttgart, Germany, I990
5. *5th ECCM*, Bordeaux, France, 1992
6. *6th ECCM*, Bordeaux, France, 1993
7. *7th ECCM*, London, England, 1996
8. *8th ECCM*, Naples, Italy, 1998
9. *9th ECCM*, Brighton, U.K., 2000
10. *10th ECCM*, Brugge, Belgium, 2002
11. *11th ECCM*, Rhodes, Greece, 2004
12. *12th ECCM*, Biarritz, France, 2006
13. *13th ECCM*, Stockholm, Sweden, 2008
14. *14th ECCM*, Budapest, Hungary, 2010
15. *15th ECCM*, Venice, Italy, 2012

JAPAN–US CONFERENCE ON COMPOSITE MATERIALS (CCM)

1. *1st Japan–US CCM*, Tokyo, Japan, 1981
2. *2nd Japan–US CCM*, NASA Langley, Virginia, 1983
3. *3rd Japan–US CCM*, Tokyo, Japan, 1986
4. *4th Japan–US CCM*, Washington, DC, 1988
5. *5th Japan–US CCM*, Tama City, Japan, 1990
6. *6th Japan–US CCM*, Orlando, FL, 1992
7. *7th Japan–US CCM*, Kyoto, Japan, 1995
8. *8th Japan–US CCM*, Baltimore, MD, 1998
9. *9th Japan–US CCM*, Mishima, Japan, 2000
10. *10th Japan–US CCM*, Stanford, CA, 2002
11. *11th Japan–US CCM*, Yonezawa, Yamagata, Japan, 2004
12. *12th Japan–US CCM*, Yonezawa, Dearborn, MI, 2006
13. *13th Japan–US CCM*, Tokyo, Japan, 2008
14. *14th Japan–US CCM*, Dayton, OH, 2010
15. *15th Japan–US CCM*, Arlington TX, 2012

INTERNATIONAL CONFERENCE ON COMPOSITES ENGINEERING (ICCE)

1. *1st ICCE*, New Orleans, LA, 1994
2. *2nd ICCE*, New Orleans, LA, 1995
3. *3rd ICCE*, New Orleans, LA, 1996
4. *4th ICCE*, Big Island, Hawaii, 1997
5. *5th ICCE*, Las Vegas, NV, I998
6. *6th ICCE*, Orlando, FL, 1999
7. *7th ICCE*, Denver, CO, 2000
8. *8th ICCE*, Tenerife, Spain, 2001
9. *9th ICCE*, San Diego, CA, 2002
10. *10th ICCE*, New Orleans, LA, 2003
11. *11th ICCE*, Hilton Head, SC, 2004
12. *12th ICCE*, Tenerife, Spain, 2005

COMPOSITE MATERIALS: TESTING AND DESIGN CONFERENCE

1. *1st Composite Materials: Testing and Design Conference*, New Orleans, LA, 1969 (ASTM STP Publication 460)
2. *2nd Composite Materials: Testing and Design Conference*, Anaheim, CA, I971 (ASTM STP Publication 497)
3. *3rd Composite Materials: Testing and Design Conference*, Williamsburg, VI, 1973 (ASTM STP Publication 546)
4. *4th Composite Materials: Testing and Design Conference*, Valley Forge, PA, 1976 (ASTM STP Publication 617)
5. *5th Composite Materials: Testing and Design Conference*, New Orleans, LA, 1979 (ASTM STP Publication 674)
6. *6th Composite Materials: Testing and Design Conference*, New Orleans, LA, 1982 (ASTM STP Publication 787)
7. *7th Composite Materials: Testing and Design Conference*, Philadelphia, PA, 1986 (ASTM STP Publication 893)
8. *8th Composite Materials: Testing and Design Conference*, Washington, DC, 1988 (ASTM STP Publication 972)
9. *9th Composite Materials: Testing and Design Conference*, Philadelphia, PA, 1990 (ASTM STP Publication 1059)
10. *10th Composite Materials: Testing and Design Conference*, Philadelphia, PA, 1992 (ASTM STP Publication 1120)
11. *11th Composite Materials: Testing and Design Conference*, Atlanta, GA, 1993 (ASTM STP Publication 1120)
12. *12th Composite Materials: Testing and Design Conference*, Montreal, Quebec, Canada, 1994 (ASTM STP Publication 1274)
13. *13th Composite Materials: Testing and Design Conference*, Orlando, FL, 1996 (ASTM STP Publication 1242)
14. *14th Composite Materials: Testing and Design Conference*, Pittsburgh, PA, 2002 (ASTM STP Publication 1436)

Appendix D: List of Organizations

Robert L. Sierakowski and Alexander Bogdanovich

PROFESSIONAL SOCIETIES

1. AIAA American Institute of Aeronautics and Astronautics, Materials Technical Committee
2. American Ceramic Society
3. American Chemical Society, Chemical Abstracts Service
4. American Society of Civil Engineers
5. ASM International
6. ASME American Society of Mechanical Engineers
7. American Society for Nondestructive Testing Inc.
8. ASTM American Society for Testing Materials
9. American Welding Society
10. Australian Composite Structures Society
11. Belgian Ceramic Society
12. Brazilian Society of Metrology
13. Ceramic Society of Japan
14. Chinese Society of Theoretical and Applied Mechanics (CSTAM), China
15. Croatian Metrology Society
16. Czech Tribology Society
17. Czech Society for New Materials and Technologies
18. Euromech Society
19. Hellenic Society for Theoretical and Applied Mechanics
20. Institute of Measurement and Control Inc., New Zealand
21. Institution of Mechanical Engineers, IMechE, U.K.
22. Japan Society of Mechanical Engineers
23. Korean Society of Theoretical and Applied Mechanics
24. MRS Materials Research Society
25. Materials Research Society of India
26. Mexican Instrumentation Society
27. Royal Institution of Engineers, the Netherlands
28. Society of the Plastics Industry
29. SAMPE Society for the Advancement of Material and Process Engineering
30. SAE Society of Automotive Engineers
31. Society of Instrument and Control Engineers, Japan
32. SPIE—The International Society for Optical Engineering
33. SME Society of Manufacturing Engineers
34. Society of Materials Science, Japan
35. Slovene Mechanics Society, Slovenia
36. SPE Society of Plastics Engineers
37. TMS Minerals, Metals & Materials Society
38. Yugoslav Society of Mechanics

ASSOCIATION AND CONSORTIUMS

1. Aerospace Industries Assn. of America Inc. (AIA)
2. Aluminum Metal Matrix Consortium
3. American Composites Manufacturers Assn. (ACMA)
4. APFE
5. ASPLAR Brazil Association for Materials, Plastics & Composites
6. Association of Composites Manufacturers, Czech Republic
7. Asociación Nacional de las Industrias de Compuestos Moldeables y Plásticos Reforzados (ACP, Mexico)
8. Associazione Italiana di Meccanica Teorica ed Applicata (AIMETA), Italy
9. Associazione Italiana di Velocimetria Laser, Italy
10. Associação Portuguesa de Análise Experimental de Tensões (APAET), Portugal
11. Associação Portuguesa de Mecânica Teórica, Aplicada e Computacional, APMTAC
12. Association pour les Matériaux Composites (AMAC)
13. Association of Rotational Molders Intl.
14. Australasian Corrosion Assn. Inc.
15. Australian Nat. Committee for Theoretical and Applied Mechanics, Australian Acad. of Sciences
16. Automotive Composites Alliance
17. Automotive Composites Consortium (ACC)
18. AVENPLAR (Asociacion Venezolana de Plastico Reforzado), Venezuela
19. AVK—TV (Arbeitsgemeinschaft Verstärkte Kunststoffe—Technische Vereinigung), German Technical Assn. for Reinforced Plastics
20. British Plastics Federation
21. Canadian Association for Composite Structures and Materials (CACSMA)
22. Canadian Plastics Industry Assn. (CPIA)
23. Central European Association for Computational Mechanics (CEACM), Centro Nacional de Investigaciones Metalurgicas (CENIM), Madrid, Spain
24. Centro Español de Plásticos (CEP), Spain
25. Centro Materiali Compositi, Italy
26. CFA Composites Fabricators Association
27. Civil Engineering Research Foundation, CONMAT Council
28. Comisión Nacional de Energía Atómica (CNEA), Argentina
29. Composites Association of New Zealand
30. Composites Association of South Africa
31. Composites Engineering & Applications Center for Petroleum Exploration and Production
32. Composites Fabricators Association
33. Composites Institute of Australia Inc.
34. Composites Manufacturing Assn. of the Society of Manufacturing Engineers (CMAJSME)
35. Composites Processing Association, U.K.
36. Consiglio Nazionale delle Ricerche, CNR-MADESS, Italy
37. Cooperative Research Centre for Advanced Composite Structures Ltd. (CRC-ACS), Australia
38. Czech Association of Scientific and Technical Societies
39. EPTA European Pultrusion Technology Association
40. EMSz (Hungarian Assn. of Manufacturers of Reinforced Plastic Materials)
41. The Danish Plastics Federation, Denmark
42. EADS Deutschland GmbH, Germany
43. Egyptian Committee of Theoretical and Applied Mechanics
44. Électricité de France (EDF), France

45. ESD—The Engineering Society of Detroit
46. European Alliance for SMC
47. European Composites Industry Assn. (GPRMC)
48. Finnish National Committee on Mechanics
49. Georgian National Committee of Theoretical and Applied Mechanics, Georgia
50. Groupement de la Plasturgie Industrielle et des Composites (GPIC), France
51. Highway Innovative Technology Evaluation Center (HITEC)
52. IFP Swedish Institute for Fibre and Polymer Research
53. Industrial Fabrics Assn. Intl. (IFAI)
54. International Association for Hydromagnetic Phenomena and Applications, Japan
55. International Association for Vehicle System Dynamics
56. International Cast Polymer Alliance of the CFA
57. International Committee on Composite Materials (ICCM), Australia
58. International Measurement Confederation (IMEKO), Hungary
59. Instrumentation, Systems, and Automation Society (ISA)
60. Iran Composites Institute
61. IRACC International Research on Advanced Composites in Construction
62. ISIS Canada
63. Laboratório Nacional de Engenharia Civil (LNEC), Lisboa, Portugal
64. Maine Composites Alliance
65. Market Development Alliance of the FRP Composites Industry (MDA)
66. Mexican Academy of Technology
67. NanoScience and Technology Center, Chinese Academy of Sciences, Beijing, China
68. National Aerospace Laboratory of Japan
69. National Center for Advanced Technologies
70. National High Magnetic Field Laboratory, Florida St. University
71. National Metallurgical, National Academy of Ukraine
72. National Research Council Canada
73. New Jersey Center for Biomaterials
74. Norsk Kompositttforbund (NKF) (Norwegian Composite Industries Assn.)
75. Oak Ridge National Laboratory, Basic Energy Sciences, TN
76. Partnership for a New Generation of Vehicles
77. Personal Watercraft Industry Assn.
78. Plast- & Kemiforetagen, Kompositavdelningen (The Swedish Plastics and Chemicals Federation, Composites Group)
79. Pultrusion Industry Council
80. Radtech International North America
81. Russian National Committee on Theoretical and Applied Mechanics Russian Academy of Sciences
82. Reinforplast (Agoria), Belgium
83. Spanish Association of Composite Materials (AEMAC)
84. Suomen Muoviteollisuusliitto, Lujitemuovijaosto—Finska Platindustriforbundet Kompositavdelningen (Finnish Association of the Plastic Industry, Composites)
85. Turkish National Committee of Theoretical and Applied Mechanics
86. United States Advanced Ceramics Assn.
87. United States Council for Automotive Research (USCAR)
88. VKCN (Vereniging Voor de Thermohardende Kunststofindustrie) (Dutch Composites Industry Organization), the Netherlands
89. Vietnamese Association of Mechanics
90. World Academy of Ceramics

ACADEMIC RESEARCH CENTERS

1. Brigham Young University, Advanced Composites Manufacturing & Engineering Center
2. Chinese Academy of Sciences (ICCAS), Beijing, China
3. Concordia University, Center for Composites, Canada
4. Colorado State University, Composite Materials, Manufacture and Structures Laboratory
5. Drexel University, Department of Materials Engineering, Fibrous Materials Research Center
6. École Polytechnique de Montréal, Center for Applied Research on Polymers, Canada
7. École Polytechnique Montréal, Centre for Research in Computational Thermochemistry, Canada
8. Florida A&M University—Florida State University, Florida Advanced Center for Composite Technologies
9. Florida State University, Center for Materials Research and Technology (MARTECH)
10. Georgia Institute of Technology, Center for Polymer Processing Materials Science & Engineering Research
11. Greece Institute of Chemistry
12. Instituto de Engenharia Mecânica, IDMEC, Portugal
13. Institute of Magnetism, National Academy of Sciences of Ukraine
14. Institute of Metal Research, Chinese Academy of Sciences, China
15. Institute of Natural Fibres, Poznan, Poland
16. Instituto Tecnológico de Zacatepec, Mexico
17. Iowa State University, Center for Nondestructive Evaluation
18. Korea Advanced Institute of Science and Technology, Composite Materials Laboratory, Korea
19. Loughborough University, PUR (Polyurethane) Technology Centre of Excellence, England
20. MIT, Technology Laboratory for Advanced Composites, TELAC
21. Michigan Materials and Processing Institute (Consortium)
22. Michigan State University, Composite Materials & Structures Center Advanced Material Engineering Experiment Station, Technology Reinvestment Project
23. Nanyang Technological University, Biomedical Engineering Research Centre, Singapore
24. Northwestern University, Infrastructure Applications for Composite Materials
25. Nottingham University, Composites Research Group, England
26. Nottingham Trent University, Polymer Engineering Centre, England
27. Penn State University, Applied Research Lab
28. Rensselaer Polytechnic Institute, Center for Composite Materials & Structures
29. Russian Academy of Sciences, Laboratory of Reinforced Systems of Solid State Physics Institute, Russia
30. Shenyang National Laboratory for Materials Science, Institute of Applied Mechanics, China
31. Stanford University, Structures and Composites Laboratory
32. UCLA, Composites Product Development Laboratory
33. UNAM, Centre for Applied Sciences and Technological Development, Mexico
34. University of Alabama, Huntsville, Composite Design & Manufacturing Critiquing Center, Composite Materials Definitions
35. University of Alberta, Advanced Composite Material Engineering Group, Canada
36. University of Auckland, Centre for Advanced Composite Materials, New Zealand
37. University of California, Berkeley, Berkeley Composites Laboratory
38. University of California, San Diego, Composites and Aerostructures Laboratory
39. University of California, Santa Barbara, High Performance Composites Center
40. University of Central Florida, Advanced Materials Processing and Analysis Center (AMPAC)
41. University of Connecticut, Composite Processing Laboratory
42. University of Dayton, Center for Materials Diagnostics, OH

43. University of Dayton, Structural Integrity Division
44. University of Delaware, Center for Composite Materials (CCM)
45. University of Florida, Center for Advanced Composites
46. University of Idaho, Institute for Materials and Advanced Processes
47. University of Manchester, Institute of Science and Technology, Centre for Manufacture, England
48. University of Maryland, Composites Research Laboratory
49. University of Mississippi, Composite Materials Research Group
50. University of Missouri, Rolla, Engineering Education Center
51. University of Missouri, Rolla, Transportation Research Center on Advanced Materials and NAT Technologies
52. University of Newcastle upon Tyne, Centre for Composite Materials Engineering
53. University of Siegen, Institute of Mechanics and Control Engineering, Germany
54. University of Southern California, M.C. Gill Foundation Composites Center
55. University of Sydney, Center for Advanced Materials Technology, Australia
56. University of Texas, Center for Electromechanics
57. University of Utah, Advanced Materials Processing Laboratory, Department of Mechanical Engineering
58. University of Zlin, Institute of Physics and Material Engineering, Czech Republic.
59. Virginia Polytechnic Institute and State University, Science & Technology Center, Polymeric Adhesives & Composites
60. Virginia Polytechnic Institute and State University, Center for Composite Materials and Structures
61. Virginia Polytechnic Institute and State University, Fiber and Electro-Optics Research Center
62. VTT Technical Research Centre of Finland
63. Western Kentucky University, Materials Characterization Center
64. Wichita State University, Composites and Advanced Materials Laboratory

Appendix E: List of Typical Research Papers in Selected Areas

Robert L. Sierakowski and Alexander Bogdanovich

THEORY, MODELING, AND ANALYSIS OF COMPOSITE MATERIALS

1. Kelly, A. and Davies, G.J., The principles of the fiber reinforcement of metals, *Metallurgical Reviews*, 10(37), 1, 1965.
2. Rowlands, R.E., Flow and failure of biaxially loaded composites, *Inelastic Behavior of Composite Materials*, ASME-AMD, 13, 97, 1975.
3. Takeda, N. and Sierakowski, R.L., Localized impact problems of composite laminates, *The Shock and Vibration Digest*, 12, 3, 1980.
4. Abrate, S., Impact on laminated composites: Recent advances, *Applied Mechanics Reviews,* 47, 517, 1994.
5. Kaminski, M., On probabilistic fatigue models for composite materials, *International Journal of Fatigue,* 24, 477, 2002.
6. Zhang, Z. and Friedrich, K., Artificial neural networks applied to polymer composites: A review, *Composites Science and Technology,* 63, 2029, 2003.
7. Elder, D.J. et al., Review of delamination predictive methods for low speed impact of composite laminates, *Composite Structures,* 66, 677, 2004.
8. Jacob, G.C. et al., The effect of loading rate on the fracture toughness of fiber reinforced polymer composites, *Journal of Applied Polymer Science,* 96, 899, 2005.
9. Zhupanska, O.I. and Sierakowski, R.L., Effects of an electromagnetic field on the mechanical response of composites, *Journal of Composite Materials*, 41, 633, 2007.
10. Sierakowski, R.L., Telitchev, I.Y., and Zhupanska, O.I., On the impact response of electrified carbon fiber polymer matrix composites: Effects of electric current intensity and duration, *Composites Science and Technology*, 68, 639, 2008.
11. Tay, T.E., Liu, G., Tan, V.B.C., Sun, X.S., and Pham, D.C., Progressive failure analysis of composites, *Journal of Composite Materials*, 42, 1921, 2008.
12. Gibson, R.F., A review of recent research on mechanics of multifunctional composite materials and structures, *Composite Structures*, 92, 2793, 2010.

PROCESSING AND MANUFACTURING

1. Doyle, L.E., Reyser, C.S., Leach, I.L., and Schrader, G.F., *Manufacturing Processes and Materials for Engineers*, Prentice-Hall, New York, 1985, Chapter 2.
2. McMahon, P.E., Carbon fiber, evolving technology, in *Handbook on Composite Reinforcements,* Lee, S.M. (ed.), VCH Publications, New York, 1993, p. 70.
3. Yousefpour, A., Hojjati, M., and Immarigeon, J.P., Fusion bonding/welding of thermoplastic composites, *Journal of Thermoplastic Composite Materials*, 17, 303, 2004.
4. Hubert, P. and Poursartip, A., A review of flow and compaction modelling relevant to thermoset matrix laminate processing, *Journal of Reinforced Plastics and Composites*, 17, 286, 1998.
5. Lim, T.C. and Ramakrishna, S., Modelling of composite sheet forming: A review, *Composites Part A-Applied Science and Manufacturing*, 33, 515, 2002.
6. Njuguna, J. and Pielichowski, K., Recent developments in polyurethane-based conducting composites, *Journal of Materials Science,* 39, 4081, 2004.
7. Wang, Z., Liang, Z.Y., Wang, B., Zhang, C., and Kramer, L., Processing and property investigation of single-walled carbon nanotube (SWNT) buckypaper/epoxy resin matrix nanocomposites, *Composites Part A—Applied Science and Manufacturing*, 35, 1225, 2004.

PROPERTIES AND CHARACTERIZATION

1. Epstein, G., Testing of reinforced plastics, in *Handbook of Fiber-Glass and Advanced Plastic Composites,* Lubin, G. (ed.), Van Nostrand, Princeton, NJ, 1969, p. 639.
2. Bert, C.W., Static testing techniques for filament-wound composite materials, *Composites,* 5, 20, 1974.
3. Adams, D.F., Properties characterization-mechanical/physical/hygrothermal properties test methods, in *Reference Book for Composites Technology 2,* Lee, S.M. (ed.), Technomic Publications, Lancaster, PA, 1989, p. 49.
4. Adams, D.F. and Lewis, E.Q., Current status of composite material shear test methods, *SAMPE Journal*, 31, 32, 1995.
5. Kant, T. and Swaminathan, K., Estimation of transverse/interlaminar stresses in laminated composites—A selective review and survey of current developments, *Composite Structures*, 49, 65, 2000.
6. Zhou, G. and Sim, L.M., Damage detection and assessment in fibre-reinforced composite structures with embedded fibre optic sensors—Review, *Smart Materials & Structures*, 11, 925, 2002.
7. Kashtalyan, M.Y. and Soutis, C., Mechanisms of internal damage and their effect on the behavior and properties of cross-ply composite laminates, *International Applied Mechanics,* 38, 641, 2002.
8. Cheeseman, B.A. and Bogetti, T.A., Ballistic impact into fabric and compliant composite laminates, *Composite Structures,* 61, 161, 2003.
9. Andersons, J. and Konig, M., Dependence of fracture toughness of composite laminates on interface ply orientations and delamination growth direction, *Composites Science and Technology,* 64, 2139, 2004.
10. Jordan, J. et al., Experimental trends in polymer nanocomposites—A review, *Materials Science and Engineering A—Structural Materials Properties Microstructure and Processing*, 393, 1, 2005.
11. Chou, T.W., Gao, L.M., Thostenson, E.T., Zhang, Z.G., and Byun, J.H., An assessment of the science and technology of carbon nanotube-based fibers and composites, *Composites Science and Technology*, 70, 1, 2010.
12. Lu, W.B., Zu, M., Byun, J.H., Kim, B.S., and Chou, T.W., State of the art of carbon nanotube fibers: Opportunities and challenges, *Advanced Materials*, 24, 1805, 2012.

THEORY AND ANALYSIS OF COMPOSITE STRUCTURES

1. Anbartsumyan, S.A., Contributions to the theory of anisotropic layered shells, *Applied Mechanics Reviews,* 15, 245, 1962.
2. Sun, C.T. and Sierakowski, R.L., Studies on the dynamic impact of jet engine blades, *The 43rd Shock and Vibration Bulletin,* 4, 11, 1973.
3. Leissa, A.W., A review of laminated composite plate buckling, *Applied Mechanics Reviews,* 40, 575, 1987.
4. Noor, A.K., Burton, W.S., and Bert, C.W., Computational models for sandwich panels and shells, *Applied Mechanics Reviews*, 49, 155, 1996.
5. Tauchert, T.R. et al., Developments in thermopiezoelasticity with relevance to smart composite structures, *Composite Structures,* 48, 31, 2000.
6. Chopra, I., Review of state of art of smart structures and integrated systems, *AIAA Journal,* 40, 2145, 2002.
7. Mackerle, J., Smart materials and structures—A finite element approach—An addendum: A bibliography (1997–2002), *Modelling and Simulation in Materials Science and Engineering,* 11, 707, 2003.
8. Qatu, M.S., Sullivan, R.W., and Wang, W.C., Recent research advances on the dynamic analysis of composite shells: 2000–2009, *Composite Structures*, 93, 14, 2010.

JOINTS AND CONNECTIONS

1. Matthews, F.L., Kitty, P.F., and Goodwin, E.W., A review of the strength of joints in fibre-reinforced plastics. Part 2: Adhesively bonded joints, *Composites*, 13, 29, 1982.
2. Tsai, M. and Morton, J., An evaluation of analytical and numerical solutions to the single-lap joint, *International Journal of Solids Structures*, 31, 2537, 1994.
3. Camanho, P.P. and Matthews, F.L., Stress analysis and strength prediction of mechanically fastened joints in FRP: A review, *Composites Part A—Applied Science and Manufacturing,* 28, 529, 1997.
4. Ibrahim, R.A. and Pettit, C.L., Uncertainties and dynamic problems of bolted joints and other fasteners, *Journal of Sound and Vibration,* 279, 857, 2005.
5. Banea, M.D. and da Silva, L.F.M., Adhesively bonded joints in composite materials: An overview, *Proceedings of the Institution of Mechanical Engineers Part L—Journal of Materials- Design and Applications*, L1, 1, 2009.

DESIGNING WITH COMPOSITES

1. Chambers, R.E., Materials criteria for design, in *Structural Plastics Design Manual, ASCE Manual of Engineering Practice, 63*, ASCE, New York, 1984, Chapter 3.
2. Head, P.R. and Templeman, R.B., Application of limit state design principles to composite structural systems, in *Polymers and Polymer Composites in Construction,* Hollaway, L. (ed.), Thomas Telford Ltd., London, U.K., 1990, p. 73.
3. Sigmund, O. and Torquato, S., Design of smart composite materials using topology optimization, *Smart Materials & Structures*, 8, 365, 1999.
4. Lee, D.G. et al., Novel applications of composite structures to robots, machine tools and automobiles, *Composite Structures,* 66, 17, 2004.
5. You, C.S., Hwang, W., and Eom, S.Y., Design and fabrication of composite smart structures for communication, using structural resonance of radiated field, *Smart Materials & Structures,* 14, 441, 2005.

COMPOSITE APPLICATIONS

1. Yeung, Y.C.T. and Parker, B.E., Composite tension members for structural applications, in *Composite Structures,* Marshall, I.H. (ed.), Vol. 4, Elsevier, London, U.K., 1987, pp. 309–320.
2. Miller, A.G., Lovell, D.T., and Seferis, J.C., The evolution of an aerospace material: Influence of design, manufacturing and in-service performance, *Composite Structures*, 27, 193, 1994.
3. Liao, K. et al., Long-term durability of fiber-reinforced polymer-matrix composite materials for infrastructure applications: A review, *Journal of Advanced Materials*, 30, 3, 1998.
4. Ramakrishna, S. et al., Biomedical applications of polymer-composite materials: A review, *Composites Science and Technology,* 61, 1189, 2001.
5. Mouritz, A.P. et al., Review of advanced composite structures for naval ships and submarines, *Composite Structures,* 53, 21, 2001.
6. Bakis, C.E. et al., Fiber-reinforced polymer composites for construction—State-of-the-art review, *Journal of Composites for Construction,* 6, 73, 2002.
7. Teng, J.G. et al., Behaviour and strength of FRP-strengthened RC structures: A state-of-the-art review, *Proceedings of the Institution of Civil Engineers—Structures and Buildings*, 156, 51, 2003.
8. Herrador, M.F. and Karbhari, V.M., Composite jackets and corrosion of steel reinforcement—A critical review, *International Journal of Materials & Product Technology*, 21, 455, 2004.
9. Scholz, M.S. et al., The use of composite materials in modern orthopaedic medicine and prosthetic devices: A review, *Composites Science and Technology*, 71, 1791, 2011.
10. Bogdanovich, A.E. and Sierakowski, R.L., Composite materials and structures: Science, technology and applications. A compendium of books, review papers, and other sources of information, *Applied Mechanics Reviews*, 52 (2), Pt. 1, 351, 1999.

The International Handbook of

FRP COMPOSITES IN CIVIL ENGINEERING

"The latest development in nearly all aspects of FRP composites, their applications in civil engineering, and state-of-the-art technologies for nondestructive evaluation (NDE) and structural health monitoring (SHM) of FRP have been expounded in this comprehensive book, which is the result of collaboration among top experts from around the world. ... This book will enable FRP in civil engineering and lead it to a very bright future."

—From the Foreword by Prof. Dr. h.c. Urs Meier, EMPA
Swiss Federal Laboratories for Materials Science and Technology

"This handbook will bridge the gap of a lack of A-to-Z references, critical for development and construction of FRP composites civil infrastructure."

—Dr. Jayantha Epaarachchi
Centre of Excellence in Engineered Fibre Composites, University of Southern Queensland, Toowoomba, Australia

---

Fiber-reinforced polymer (FRP) composites have become an integral part of the construction industry because of their versatility, enhanced durability and resistance to fatigue and corrosion, high strength-to-weight ratio, accelerated construction, and lower maintenance and life-cycle costs. Applications include everything from bridge decks, bridge strengthening and repairs, and seismic retrofits to marine waterfront structures and sustainable, energy-efficient housing. ***The International Handbook of FRP Composites in Civil Engineering*** brings together a wealth of information on advances in materials, techniques, practices, nondestructive testing, and structural health monitoring of FRP composites, specifically for civil infrastructure.

With a focus on professional applications, the handbook supplies design guidelines and standards of practice from around the world. It also includes helpful design formulas, tables, and charts to provide immediate answers to common questions. Comprehensive yet concise, this is an invaluable reference for practicing engineers and construction professionals, as well as researchers and students. It offers ready-to-use information on how FRP composites can be more effectively utilized in new construction, repair and reconstruction, and architectural engineering.

2013

ISBN: 978-0-8493-2013-2
90000
9 780849 320132

CRC Press
Taylor & Francis Group
an **informa** business
www.crcpress.com

6000 Broken Sound Parkway, NW
Suite 300, Boca Raton, FL 33487
711 Third Avenue
New York, NY 10017
2 Park Square, Milton Park
Abingdon, Oxon OX14 4RN, UK

www.crcpress.com